Serbian Tribology Society

Faculty of Mechanical Engineering
University of Kragujevac

SERBIATRIB '11

12th International Conference on Tribology

11 – 13 May 2011, Kragujevac, Serbia

PROCEEDINGS

Serbian Tribology Society

Faculty of Mechanical Engineering
University of Kragujevac

SERBIATRIB '11

12th International Conference on Tribology

11 – 13 May 2011, Kragujevac, Serbia

PROCEEDINGS

EDITORS: Branko Ivković, Miroslav Babić, Slobodan Mitrović

SERBIATRIB '11

12th International Conference on Tribology – SERBIATRIB '11 PROCEEDINGS

ISBN: 978-86-86663-74-0

Editors:	**Branko Ivković**, Ph.D. Serbian Tribology Society **Miroslav Babić**, Ph.D. Faculty of Mechanical Engineering, University of Kragujevac **Slobodan Mitrović**, Ph.D. Faculty of Mechanical Engineering, University of Kragujevac
Publisher:	**Serbian Tribology Society** Sestre Janjić 6, 34000 Kragujevac, Serbia **Faculty of Mechanical Engineering, University of Kragujevac** Sestre Janjić 6, 34000 Kragujevac, Serbia
For the Publisher:	**Branko Ivković**, Ph.D., Serbian Tribology Society **Miroslav Babić**, Ph.D., Faculty of Mechanical Engineering
Technical editor:	**Slobodan Mitrović**, Ph.D. Faculty of Mechanical Engineering, University of Kragujevac
Printed by:	**SKVER**, 34000 Kragujevac, Serbia
Circulation:	100 copies

Copyright © 2011 by Serbian Tribology Society and Faculty of Mechanical Engineering

The publication of these Proceedings was financially supported by the Ministry of Science and Technological Development of the Republic of Serbia.

Supported by

Ministry of Science and Technological Development of the Republic of Serbia

CETR, Center for Tribology Inc, USA

CSM Instruments, Switzerland

International Scientific Committee

Nikolai Myshkin	V.A. Belyi Metal-Polymer Research Institute of National Academy of Sciences of Belarus (Belarus)
Konstantinos-Dionysios Bouzakis	Aristotle University of Thessaloniki (Greece)
Friedrich Franek	Vienna University of Technology (Austria)
Nyagol Manolov	Technical University of Sofia (Bulgaria)
Emilia Assenova	Technical University of Sofia (Bulgaria)
Mara Kandeva	Technical University of Sofia (Bulgaria)
Andrei Tudor	University Politehnica of Bucharest (Romania)
Niculae Napoleon Antonescu	Petroleum-Gas University of Ploiesti (Romania)
Mehmet Baki Karamiş	Erciyes University (Turkey)
Hakan Kaleli	Yildiz Technical University (Turkey)
Branko Ivković	Serbian Tribology Society (Serbia)
Aleksandar Rac	Serbian Tribology Society (Serbia)
Miroslav Babić	University of Kragujevac (Serbia)
Slobodan Mitrović	University of Kragujevac (Serbia)
Slobodan Tanasijević	University of Kragujevac (Serbia)
Aleksandar Vencl	University of Belgrade (Serbia)
Aleksandar Marinković	University of Belgrade (Serbia)
Dušan Stamenković	University of Niš (Serbia)
Miodrag Manić	University of Nis (Serbia)
Damir Kakaš	University of Novi Sad (Serbia)
Bogdan Sovilj	University of Novi Sad (Serbia)

Organising Committee

Presidents:

Miroslav Babić	University of Kragujevac (Serbia)
Branko Ivković	Serbian Tribology Society (Serbia)

Members:

Slobodan Mitrović	University of Kragujevac (Serbia)
Blaža Stojanović	University of Kragujevac (Serbia)
Aleksandar Vencl	University of Belgrade (Serbia)
Fatima Zivić	University of Kragujevac (Serbia)
Dragan Dzunić	University of Kragujevac (Serbia)
Marko Pantic	University of Kragujevac (Serbia)

Preface

The International Conference on Tribology – SERBIATRIB, is traditionally organized by the Serbian Tribology Society every two years, since 1989. The previous conferences were held in Kragujevac (1989, 1991, 1993, 1999, 2005 and 2007), Herceg Novi (1995), Kopaonik (1997) and Belgrade (2001, 2003 and 2009). This year the 12^{th} International Conference on Tribology – SERBIATRIB '11 takes place on 11-13 May 2011 in Kragujevac.

This Conference is organized by the Serbian Tribology Society (STS) and the University of Kragujevac, Faculty of Mechanical Engineering. Organizing Scientific Conferences, STS plays a significant role in helping engineers and researchers to introduce in the fundamentals of tribology and to present their experience, solutions and research results.

The scope of the 12^{th} International Conference on Tribology – SERBIATRIB '11 embraces the state of art and future trends in tribology research and application. The following two aspects of tribology practice require special attention. Firstly, the requirement for higher productivity of machinery means that machines must operate under higher loads and at higher speeds and temperatures, and that is why finding the right solutions for tribological processes is extremely important. Secondly, the good tribology knowledge can greatly contribute to the saving of material and energy.

The Conference program generally includes the following topics: fundamentals of friction and wear; tribological properties of solid materials; surface engineering and coating tribology; lubricants and lubrication; tribotesting and tribosystem monitoring; tribology in machine elements; tribology in manufacturing processes; tribology in transportation engineering; design and calculation of tribocontacts; sealing tribology; biotribology; nano and microtribology and other topics related to tribology.

All together 73 papers of authors from 18 countries (USA, Taiwan, Russia, Belarus, Ukraine, UK, Germany, Switzerland, India, Slovenia, Croatia, Bosnia & Herzegovina, Montenegro, Romania, Bulgaria, Greece, Turkey and Serbia) are published in the Proceedings. Approximately 32 papers were submitted by the foreign authors and app. 41 papers by the Serbian authors. All papers are classified into five chapters:

- Plenary lectures (4)
- Tribological properties of materials and coatings (29)
- Tribology in machine elements (14)
- Tribometry (20)
- Trenje, habanje i podmazivanje (5) – papers written in Serbian language

It was a great pleasure for us to organize this Conference and we hope that the Conference, bringing together specialists, research scientists and industrial technologists, and Proceedings will stimulate new ideas and concepts, promoting further advances in the field of tribology. The

Editors would like to thank the Scientific and the Organizing Committee and all those who have helped in making the Conference better. We would like to thank especially prof. Miroslav Babić and prof. Branko Ivković for the helpful suggestions and support.

The Conference is financially supported by the Ministry of Science and Technological Development of the Republic of Serbia, Center for Tribology Inc (CETR), CSM Instruments and Technology Transfer Center Hanover.

We wish to all participants a pleasant stay in Kragujevac and we are looking forward to seeing you all together at the 13th International Conference on Tribology – SERBIATRIB '13.

Kragujevac, May 2011 Editors

Contents

Plenary Lectures

Tribological Properties of Materials and Coating

Tribology of Machine Elements

Tribometry

Trenje, habanje i podmazivanje

Plenary Lectures

Serbian Tribology Society

SERBIATRIB '11

12th International Conference on Tribology

Faculty of Mechanical Engineering in Kragujevac

Kragujevac, Serbia, 11 – 13 May 2011

NANOTRIBOLOGY, NANOMECHANICS AND MATERIALS CHARACTERIZATION STUDIES AND APPLICATIONS TO BIO/NANOTECHNOLOGY AND BIOMIMETICS

Bharat Bhushan
Ohio Eminent Scholar and The Howard D. Winbigler Professor
Director, Nanoprobe Laboratory for Bio- & Nanotechnology and Biomimetics
The Ohio State University, Ohio, USA, bhushan.2@osu.edu

At most solid-solid interfaces of technological relevance, contact occurs at numerous asperities. A sharp atomic/friction force microscope (AFM/FFM) tip sliding on a surface simulates just one such contact. However, asperities come in all shapes and sizes which can be simulated using tips of different shapes and sizes. AFM/FFM techniques are commonly used for tribological studies of engineering surfaces at scales ranging from atomic- to microscales. Studies include surface characterization, adhesion, friction, scratching/wear, boundary lubrication, electrical resistance, surface potential, and capacitance mapping[1-5]. AFMs and their modifications are also used for nanomechanical characterization, which includes measurement and analysis of hardness, elastic modulus and viscoelastic properties, and in-situ localized deformation studies. State-of-the-art contact mechanics models have been developed and are used to analyze dry and wet contacting interfaces. The experimental data exhibit scale effects in adhesion, friction, wear, and mechanical properties, and a comprehensive model for scale effects due to adhesion/deformation and meniscus effects has been developed. Generally, coefficients of friction and wear rates on micro- and nanoscales are smaller, whereas hardness is greater. Therefore, micro/nanotribological studies may help define the regimes for ultra-low friction and near-zero wear. New lubrication strategies such as the use of self-assembled monolayers promise to be very versatile and effective at these scales.

Carbon nanotubes are being used for various nanotechnology applications. The mechanical strength of many of these devices critically relies on the nanotribology and nanomechanics of the CNTs. Various investigations of adhesion, friction, wear, and mechanics of MWNTs, SWNTs and MWNT arrays have been carried out [6]. For bio/nanotechnology applications, to improve adhesion between biomolecules and silicon based surfaces, chemical conjugation as well as surface patterning have been used [5]. Friction and wear studies of biomolecules show that these act as a lubricant but exhibit some wear resistance [5]. In the area of biomimetics [7], surface roughness present on Lotus and other leaves has been measured, and the surface films are characterized to understand the mechanisms responsible for superhydrophobicity (high contact angle), self-cleaning, and low adhesion. A model for surface-roughness-dependent contact angle has been developed, and optimum distributions have been developed for superhydrophobic surfaces [8,9]. Hierarchical structures of interest have been fabricated in the lab [4] using various fabrication techniques, and some of the surfaces show excellent performance superior to that of the Lotus leaf.

These fundamental nanotribological studies provide insight to the molecular origins of interfacial phenomena including adhesion, friction, wear, and lubrication. Friction and wear of lightly loaded micro/nano components are highly dependent on the surface interactions (few atomic layers). Nanotribological and nanomechanics studies are also valuable in the fundamental understanding of interfacial phenomena in macrostructures to provide a bridge between science and engineering. This talk will present an overview of nanotribological and nanomechanics studies and their applications.

REFERENCES

[1] Bhushan, B., Israelachvili, J.N., and Landman, U., "Nanotribology: Friction, Wear and Lubrication at the Atomic Scale," Nature 374, 607-616 (1995).

[2] Bhushan, B., Handbook of Micro/Nanotribology, 2nd ed., CRC Press, Boca Raton, Florida, 1999.

[3] Bhushan, B. et al.., Applied Scanning Probe Methods, Vol. 1-13, Springer, Heidelberg, Germany, 2004, '06, '07, '08, '09.

[4] Bhushan, B., Nanotribology and Nanomechanics – An Introduction, 2nd ed., Springer, Heidelberg, Germany, 2008.

[5] Bhushan, B., Springer Handbook of Nanotechnology, 2nd ed., Springer, Heidelberg, Germany, 2007.

[6] Bhushan, B. “Nanotribology of Carbon Nanotubes”, J. Phys.: Condens. Matter 20, 365214 (2008).

[7] Bhushan, B., “Biomimetics: Lessons from Nature - An Overview”, Phil. Trans. R. Soc. A 367, 1445-1486 (2009).

[8] Nosonovsky, M. and Bhushan, B., Multiscale Dissipative Mechanisms and Hierarchical Surfaces: Friction, Superhydrophobicity, and Biomimetics, Springer, Heidelberg, Germany, 2008.

[9] Bhushan, B. Jung, Y. C. and Koch, K., “Micro-, Nano-, and Hierarchical Structures for Superhydrophobicity, Self-Cleaning and Low Adhesion”, Phil. Trans. R. Soc. A 367, 1632-1672 (2009)

Serbian Tribology Society

SERBIATRIB '11

12th International Conference on Tribology

Faculty of Mechanical Engineering in Kragujevac

Kragujevac, Serbia, 11 – 13 May 2011

EQUIPMENTS AND MATERIALS FOR TRIBOTESTING IN OPEN SPACE ON ISL

N.K. Myshkin[1],
A.Ya. Grigoriev[1], V.L. Basiniuk[2], A.I. Mardasevich[2], V.G. Kudritsky[1], I.N. Кavaliova[1]
[1]Metal-Polymer Research Institite NASB, Belarus, mpri@mail.ru
[2]Joint Institute of Meschanical Engineering NASB, Belarus, bats@ncpmm.bas-net.by

Abstract: *The problems of hardware and methodology of ground-based and on-board tribotesting are discussed as well as the main features of space test equipment. New materials for space tribosystems are presented. The method of estimation and selection of equivalent conditions of space- and ground-based tribotestings is considered. The method is based on comparing the results of experiments in multidimensional feature space. Input and output parameters of the experiments are interpreted as coordinates of a point, representing conditions of tribosystems in the multidimensional space. Analysis of the distance between corresponding points allows one to solve the problem of selection of equivalence conditions of ground-based test and estimate uncontrolled parameters of space-born experiment).*

Keywords: *space tribology, experiment "Tribospace", on-board tribometer, tribotesting.*

1. INTRODUCTION

The current trend in technology of space apparatus is increasing of their service life. Friction units are one of the important components of mechanical part of orbital technique. Tooth gears, rolling and sliding bearings, cam mechanisms, guides, seals, docking units, locks, and other units operates in open space. Only on International Space laboratory there are more than 300 such tribosystems.

In the open space the tribosystems were exposed in operation to the high vacuum (on the Moon $p < 10^{-5}$ Pa), a broad range of temperature variations (from 100 to 400 K), IR, UV and X-Ray radiation, high energy ions and elementary particles, microgravitation, full absence of oxidizing atmosphere and so on.

All the factors can change the processes in the surface layers of materials, such as diffusion, degasification, sublimation; they modify the chemical composition, structure and behaviour, physical-mechanical properties, including the parameters of the dimensional stability, the conventional limits of elasticity and relaxation [1]. As a result the friction and wear performance in space is very much different from the ground conditions. This problem is well recognized and already in 1974 in the frame of "Luna-2" program the first experiment on investigation of friction and wear in open space was realized [2]. The friction simulator (FS) operated in open space 150 h was installed on the "Luna-22" space vehicle (Fig.1).

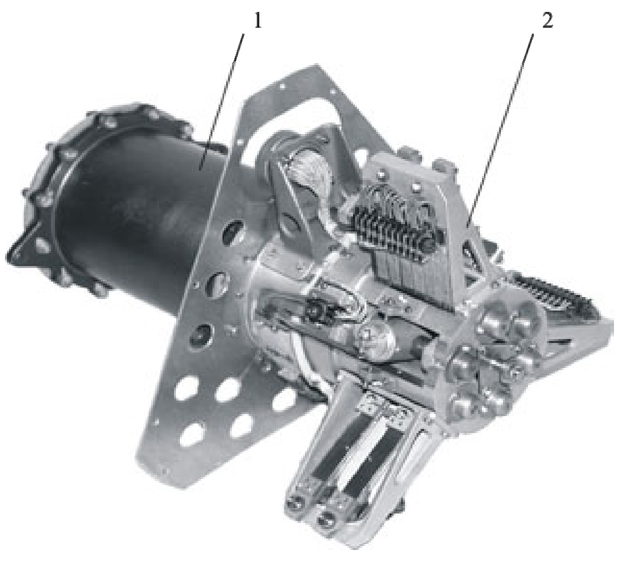

Figure 1. Space friction simulator used in "Luna-2" program: 1 – hermetic drive; 2 – friction units

Tester was driven from the electric motor via 5-stage reducing gear with maximum torque 10 Nm. Temperature on the surface of drive housing was measured by transducer as well as internal pressure in the housing. Friction torque was measured by electric current of the motor

The tested samples were based on solid lubricant coating ВНИИ НП-212 with MoS_2 covered an aluminum alloys ДТ16Т and АМГ-6. Tests were done in a ground laboratory, at the launching position of a spacecraft, and at the Moon orbit.

The following parameters were measured in operation: friction forces in start and steady rotation; current in driving motor; pressure in the sealed drive housing; temperature on the surface of driving and measuring housings. Due to limitation of experimental equipment wear of materials was not measured and tests were carried out at very low sliding speed (0.008 - 0.01 m/s).

Tests in space were run during 15 months being controlled from the ground. First operation cycle started 32 days after launching. At first seconds of operation the friction was the same as at the launching position. After 1.5 - 2 min the friction coefficient was 0.22 - 0.24 for bush-on-shaft and 0.15 - 0.16 for pin-on-disc. At the end of first test cycle it was 0.10 - 0.14 for bush-on shaft and 0.09 - 0.10 for pin-on-disc. The following conclusions about influence of space factors were made:

- Local atmosphere around the ship was found more favorable than ground vacuum chamber;
- Microgravity was also found favorable due to wear debris locking at the friction surfaces.

New possibilities in the field of space tribology will be opened after coupling of Russian science module to the International Space Lab (ISL). It is planned that new space experiment “Tribocosmos” will be curried out in cooperation of Russia and Belarus while studying advanced materials for friction and wear in the open space.

The aim is the experiment is the following:

- Development and testing of efficient materials and coatings for space applications;
- Studies in the effects of space environment on friction and wear of prospective materials and coatings;
- Studies in the similarity of data on the tests in space and on the ground;
- Development of testing methods and techniques for lifetime forecast up to 15 years for materials in sliding bearings and gears based on short-time tests;
- Creation of database on prospective materials, coatings and lubricants for space applications.

2. TEST EQUIPMENT FOR “TRIBOCOSMOS” EXPERIMENT

Test equipment [3] consists of two modules located in open space outside the ISL far from the engines. Orientation along the axes of ISL is not specified.

Tribotest module (TM) is designed as a pin-on-disc unit with 6 pins (3 on each side of disk) arranged at various radii of the sliding track. Normal load 0.1-30N, rotation velocity is up to 1000 rpm, on-line measurement of temperature, friction coefficient and wear.

Bearing module (BM) is designed as four bush-on-shaft units with an independent drive. Normal load is 10-100N, rotation velocity 6-1000 rpm. On-line measurement of friction coefficient and temperature should be provided.

The general view of developed equipment is presented in Fig. 2.

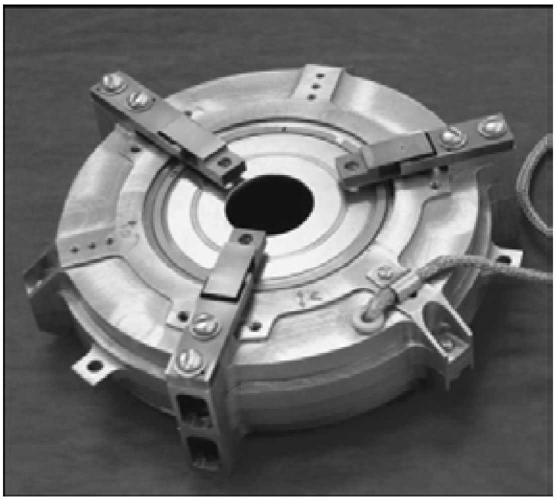

a

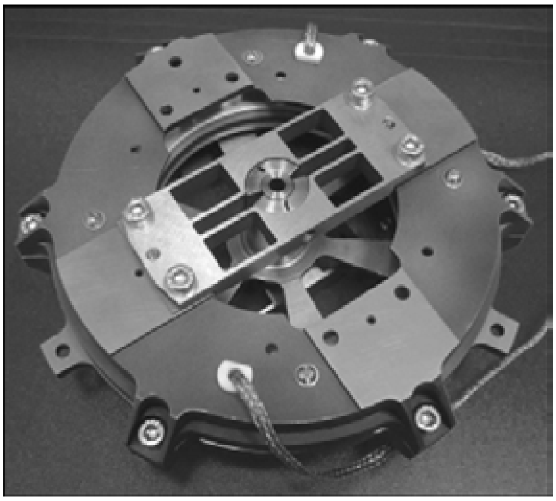

b

Figure 2. General view of tribotest (a) and bearing modules (b) for “Tribocosmos” experiment

For on-ground testing of materials in vacuum in a wide range of temperature special test equipment was developed. The general scheme of the test equipment and its photo are presented in Fig 3.

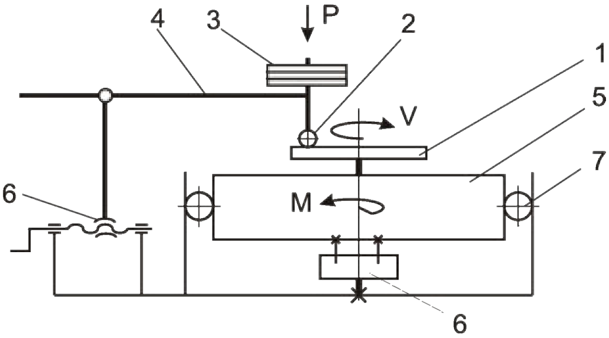

a

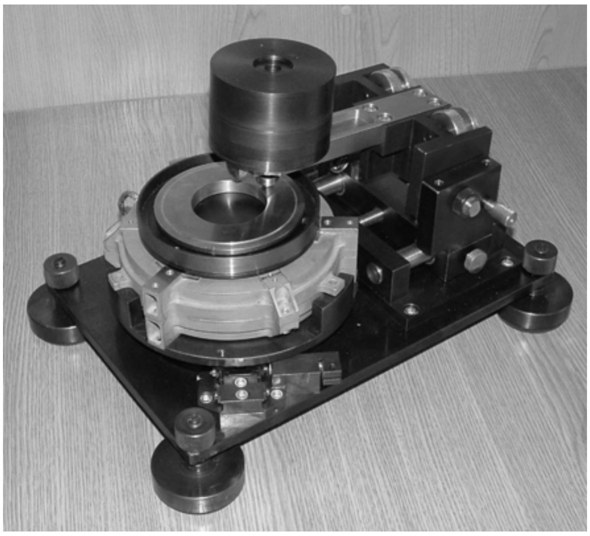

b

Figure 3. Scheme (a) and general view (b) of equipment for investigation of wear and friction of under conditions of space imitation

The device realizes sphere-plate geometry of testing with motion of test sample 1. Spherical indenter 2 is loaded by weight 3, located on lever 4. Sample 1 rotated by drive 5. The radius of wear track can be changed by drive-screw 6. Friction torque is maesured by torsion balance. For this aim drive 5 is installed on ball bearing 7. Friction torque is rotating the drive 5 being measured by detector 8.

Design of the device allows one to use it in normal ambient conditions and in vacuum of 10^{-3} Pa and temperature range from от 120 up to 420 K. The test equipment can be used for investigation dynamical parameters of direct-drive systems developed for TM and BM.

3. MATERIALS FOR SPACE TRIBOTESTS

Depending on application the following materials were developed [4]:

- gears, drive screws, threads and rolling bearings – ion-implanted self-lubricated coatings based on dyhalcohenides of Mo, W–S, Se and Co
- bearings, guides, and joints – gas-flame facings with the oxides and self-lubricating fillers
- electrical contacts, sliding bearings, joints – galvanic and electroless metal-polymer coatings Ni-P, Ni-P+SiO2, Ni-B + PTFE.

The structures of developed materials are presented in Fig. 4.

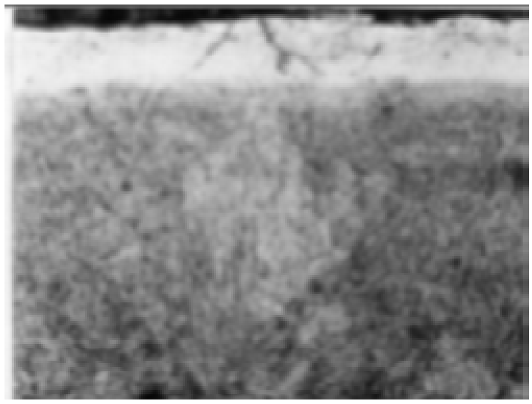

a

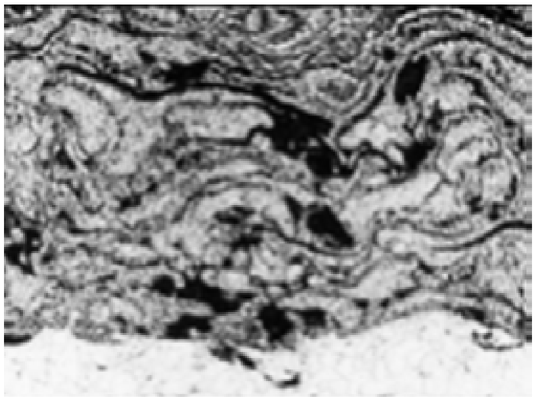

b

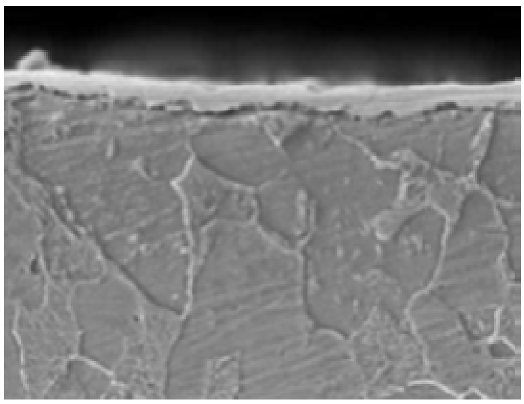

c

Figure 4. Materials for space tribotests: *a* – ion-implanted self-lubricated coating W-S on steel; *b* – gas-flame facings with the oxides and self-lubricating fillers; *c* – Ni-B coatings

4. METHODS OF TRIBOTESTING

The scheme of experiment is presented in Fig 5. It is planned to test all materials in the open space at the International Space Laboratory. In the same time all samples will be tested on the ground while imitating the space factors in similar test equipment. Ground-based tests will be carried out on extended program with realization all possible loads and velocities and registration of the additional parameters (measurement of wear, vibration and triboacoustic parametrs, analysis of wear debris and surface morphology). The purpose of ground-based tests is the extending parametrical space of experiment and obtaining data on influence space factors on friction and wear modes.

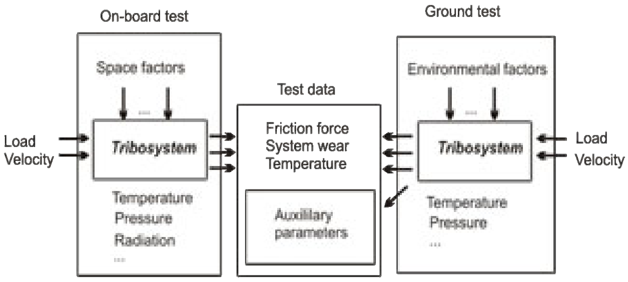

Figure 5. Scheme of friction test materials on space and ground-based conditions

Because some unknown acting space parameters the complexity of on-ground and on-board experiments arises. For solving the problem special method is developed [5].

The method is based on comparing the results of on-board and ground based experiments in multidimensional feature space. Input and output parameters of the experiments are interpreted as coordinates of a point, representing conditions of tribosystems in the multidimensional features space. Analysis of the distance between corresponding points allows us to solve the problem of selection of equivalence conditions of ground-based test and estimate uncontrolled parameters of space-born experiment.

5. CONCLUSIONS

International Space Lab “Tribocosmos” project is a real opportunity of accelerating the progress in space tribology. Combination of new generation of tribotesters on the orbit and ground with the possibility of on-line monitoring provides a unique chance of future fruitful applications. The major task in “Tribocosmos” project is bridging the gap between macroscopic data available and scientific advances in micro/nano.

International cooperation based on standard and reproducible measuring techniques is a milestone in “Tribocosmos” project. Final result of the project is foreseen mostly in prospective self-lubricating films and coatings as well as in development of novel in-situ monitoring techniques.

REFERENCES

[1] Yu.N. Drozdov, Seok-Sam Kim. Tribological behaviour of mechanical systems in the outer space, Journal of Friction and Wear, Vol 20, No 1, pp 8-14, 1999.

[2] V.M. Yarosh, A.A. Moisheev, M.A. Bronovets. Study of friction and wear of materials in open space at curcumlunar orbit, Journal of friction and wear, Vol. 24, No 6, pp. 41-49, 2003

[3] N.K. Myshkin, A.Ya. Grigoriev, V.L. Basiniuk et al. Equipment and methods for test materials on friction and wear in open space, in: *Proceedings of the IV Belorussian Space Congress*, 27-29.10.2009, Minsk, Vol. 1, pp. 58-62 (in Russian).

[4] V.L. Basiniuk, A.I. Mardosevich, N.K. Myshkin et al. Problems in development of composite materials for drives operated in extreme temperature conditions, in: *Proceedings of the IV Belorussian Space Congress*, 27-29.10.2009, Minsk, Vol. 1., pp. 69-73 (in Russian).

[5] N.K. Myshkin, A.Ya. Grigoriev, V.G. Kudritsky, A.P. Zozulya. Ground-based and on-board tribometers for test materials in space, Informatics, No 3, pp. 41-50, 2007 (in Russian)

Serbian Tribology Society

SERBIATRIB '11

12th International Conference on Tribology

Faculty of Mechanical Engineering in Kragujevac

Kragujevac, Serbia, 11 – 13 May 2011

OPTIMIZATION OF WET OR DRY MICRO-BLASTING ON PVD FILMS BY VARIOUS Al_2O_3 GRAIN SIZES FOR IMPROVING THE COATED TOOLS' CUTTING PERFORMANCE

K.-D. Bouzakis, A. Tsouknidas, G. Skordaris, E. Bouzakis, S. Makrimallakis, S. Gerardis, G. Katirtzoglou

Laboratory for Machine Tools and Manufacturing Engineering, Aristoteles University of Thessaloniki, Greece

Fraunhofer Project Center Coatings in Manufacturing, Centre for Research and Technology Hellas Thessaloniki, Greece, and Fraunhofer Institute for Production Technology, Aachen, Germany

bouzakis@eng.auth.gr

Abstract: *Micro-blasting on PVD coated tools is an effective technology for improving their cutting performance. Through micro-blasting, compressive stresses are induced into the film, thus increasing the coating hardness, but its brittleness too. Simultaneously, abrasion phenomena are activated, which may lead to roughness augmentation, film thickness decrease and substrate revelation. In this way, for a successful process conduct, it is pivotal to adapt, among others, the applied micro-blasting pressure to the employed medium, air or water. The paper deals with the optimization of wet or dry micro-blasting pressure by various* Al_2O_3 *grain sizes for improving the coated tool's wear resistance. The wear behaviour of coated and variously dry or wet micro-blasted tools was investigated in milling. Considering the grains' penetration kinematics into the coated tool surface and the film deformation mechanisms during dry or wet micro-blasting by fine or coarse sharp–edged* Al_2O_3 *grains, optimum process pressures can be determined.*

Keywords: *PVD coatings, micro-blasting, mechanical properties, brittleness, cutting edge radius, wear*

1. INTRODUCTION

Micro-blasting on PVD films is applied in the industry, as an efficient method for improving the performance of coated tools and machine elements [1,2,3,4,5,6,7]. By this process, residual compressive stresses are induced into the film structure, thus leading to coating hardness and strength properties improvement [8,9,10]. Micro-blasting parameters such as pressure and time have a pivotal effect on the coated tool cutting performance [2,6,7].The present paper introduces the potential for increasing the wear resistance of PVD TiAlN coated cemented carbide tools through dry or wet micro-blasting by Al_2O_3 abrasive grains of different diameters.

2. EXPERIMENTAL DETAILS

TiAlN films, with an Al/Ti ratio of 54/46 were deposited by a CEMECON C900 coating machine [11] on SPGN 120308 cemented carbide inserts of HW-K05/K20 ISO specifications. The film thickness on the tool rake was approximately 3.5 μm. A PVD process technology with high ionization sputtering and pulsing (HIS and HIP) was applied, leading to nano-structured, nano-laminated and nano-dispersed coating systems [11]. The deposition temperature was 450°C, the total gas pressure 570 mPa and the Ar and N_2 partial pressure amounted 450 mPa and 120 mPa respectively. The stress-strain curves were determined by analytical evaluation of related nanoindentation results, employing methods introduced in the literature [12].

Sharp-edged Al_2O_3 abrasives with average grain diameters of 10 μm and of 100 μm were used for conducting dry or wet micro-blasting on TiAlN films. Dry and water micro-blasting treatments were conducted by a DI12 machine and a NP10 one of WIWOX GmbH Surface Systems respectively. The working principle of the applied water micro-

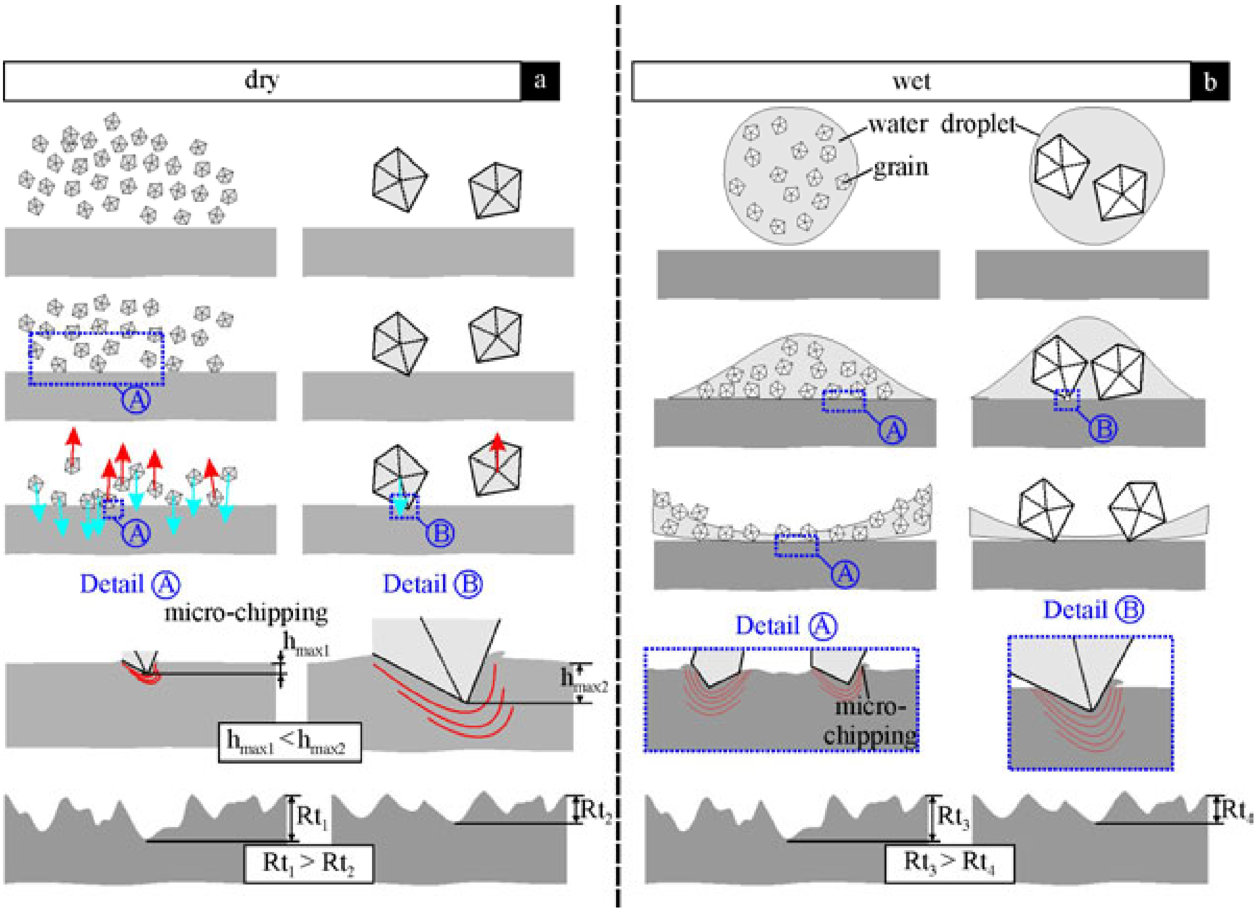

Figure 1. Effect of abrasive grains' size and their transport medium on the surface roughness in a) dry b) wet micro-blasting process.

blasting procedure is described in the literature [6]. Considering previous micro-blasting investigations published in [2,6,7], the distance between the nozzle and substrate was set to 100 mm and the process duration at 4 seconds. The air pressure was varied from 0.2 MPa up to 0.4 MPa, in steps of 0.1 MPa. The tool rake and flank were treated in separate micro-blasting procedures.

The nanoindentations were carried out by a FISCHERSCOPE H100 device. The roughness Rt of the coated specimens amounted approximately to 0.5 µm. For excluding the specimen roughness effect on the nanoindentation results accuracy, 30 measurements per nanoindentation were conducted for stabilizing the moving average of the indentation depth versus the indentation force [12]. To capture cutting edge radius and coating thickness distributions, white light scanning by a 3D confocal system µSURF of NANOFOCUS AG was employed. The milling investigations were carried out by a three-axis numerically controlled milling centre using the steel 42CrMo4 QT, hardened at approximately 300 HV.

3. RESULTS AND DISCUSSION

3.1 Abrasion mechanisms in wet and dry micro-blasting and developed film hardness

Figure 1 explains schematically the effect of dry or wet micro-blasting by fine Al_2O_3 grains of an average diameter of approximately 10 µm and by ten times larger in diameter as well, on the coated tools' surface integrity. In dry micro-blasting process (see figure 1a), a larger roughness Rt develops, if fine grains are employed. This can be explained by the repeated micro-chippings of the film's surface considering the large concentration of the fine particles, as it is schematically shown in this figure. Hence, due to the intense coating material removal, a smaller portion of the initial grain kinetic energy of the fine grains is consumed to deform plastically the coating, compared to the corresponding one by the coarser grains. In this way, coatings subjected to dry micro-blasting by Al_2O_3 grains of an average diameter of approximately 10 µm are expected to possess higher roughness and smaller nanohardness compared to micro-blasting by Al_2O_3 grains of ca. 100 µm average diameter, under the same conditions.

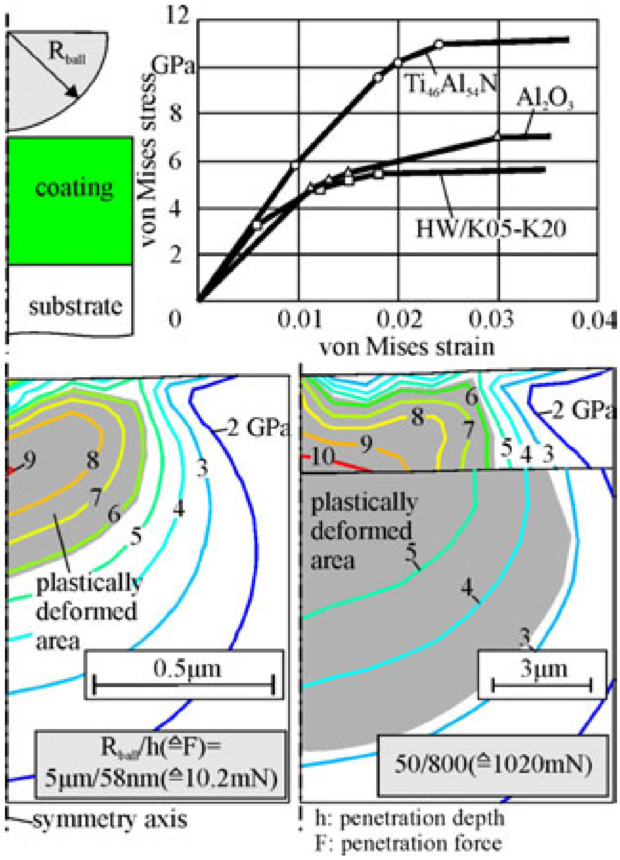

Figure 2. Developed von Mises stress fields during micro-blasting by different grain sizes

Related mechanisms appear in the case of wet micro-blasting, as it is illustrated in figure 1b [6]. Numerous fine abrasive grains are guided by water droplets at high density on the coated surface. These can cause more intense coating material removal through micro-chippings, for the same treatment duration compared to micro-blasting by coarse and less numerous grains per water droplet. On one hand, this happens, since the numerous small grains are dragged easier by the flowing water along the film surface, thus intensively deteriorating its roughness. On the other hand, the coarse grains are less affected by the flowing water and mainly deform the coating material. In this way, a larger portion of the initial grain kinetic energy of the coarse grains is consumed to deform plastically the coating, compared to the small ones. Thus, coatings subjected to wet micro-blasting by fine Al_2O_3 grains are expected to possess higher roughness and smaller nanohardness, compared to the corresponding ones, micro-blasted by coarser grains under the same conditions.

The abrasive effect exerted by dry blasting using Al_2O_3 particles is expected to be less intense for both, fine and coarse grain sizes compared to the corresponding one when a wet process is applied. In dry micro-blasting, the grains bounce from the coated surface after the impact almost perpendicular (see figure 1), thus affecting the film integrity slightly.

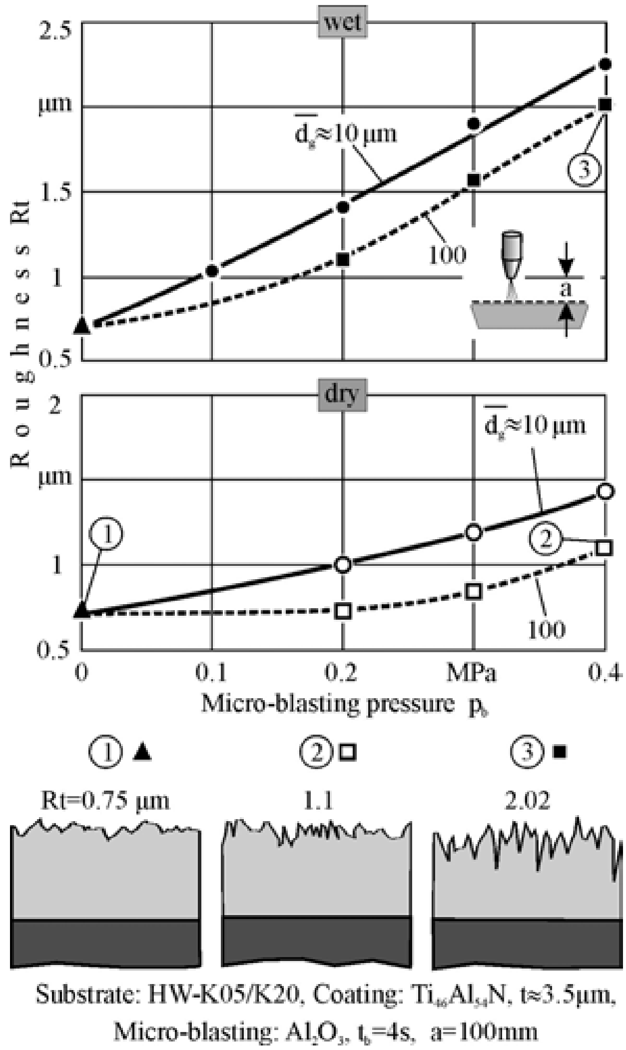

Figure 3. Roughness results on post-treated coatings by wet or dry micro-blasting via Al_2O_3 grains of different diameters, at various pressure

This effect results in larger coatings' nanohardness compared to wet micro-blasting, where the grains are dragged along the coating surface. In dry micro-basting process, the particles kinetic energy is mainly consumed to plastically deform the coating, while in the case of wet blasting, a portion of this energy is allocated to the described abrasive phenomena.

Insight into the coating and substrate deformation in micro-blasting by various grain sizes provides figure 2. The developed stress fields were calculated based on an already introduced FFM model [9], which simulates Al_2O_3 grains of 10 µm and 100 µm diameter. In the fine micro-blasting grain case, the penetration depth was only 58 nm corresponding to a maximum impact force of approximately 10.2 mN. If Al_2O_3 grains of an average diameter of 100 µm are employed, considering their mass relation to the 10 µm particles, over hundred times larger forces are expected. At such impact force levels, the penetration depth corresponds to much higher imprint depth.

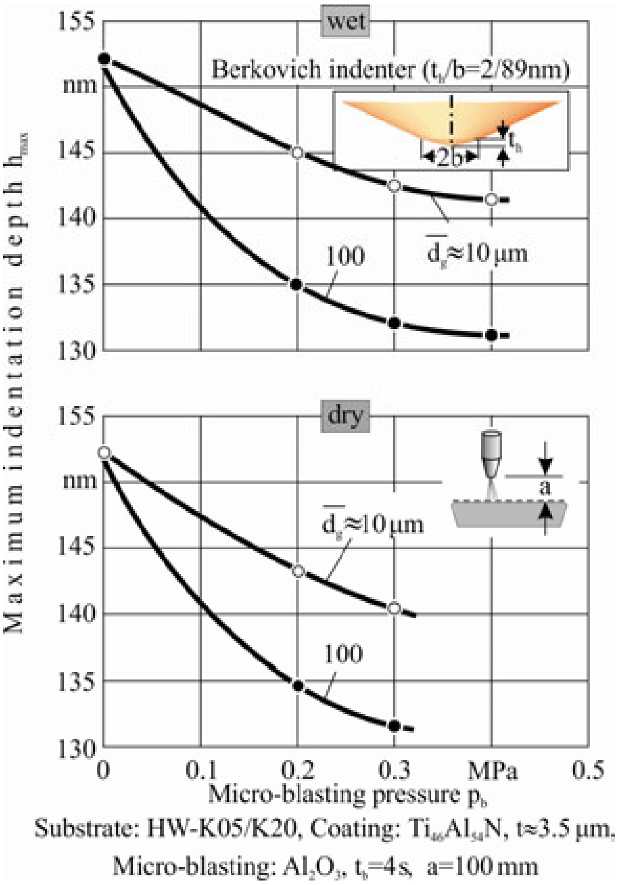

Figure 4. Nanoindentation results on post-treated coatings by wet or dry micro-blasting via Al_2O_3 grains of different diameters, at various pressures

In the demonstrated case, a grain of 100 µm diameter penetrates 800 nm into the film at an indentation force of 1020 mN. According to the FEM results, the coating is deformed plastically in both grain size cases. In the case of micro-blasting by the 10 µm grains, the substrate remains unaffected by the grain penetration. Moreover, at the larger grain size of 100 µm diameter, an extent region of the coating and the substrate is intensively deformed. Thus, the risk of a brittle coating failure and in this way substrate revelation after micro-blasting is higher, if coarser micro-blasting grains are used.

These assumptions can be validated considering the demonstrated results in figure 3. In both cases of wet and dry micro-blasting, when fine Al_2O_3 grains instead of coarse ones are used, a roughness increase develops on the film surface. Characteristic surface topomorphies before and after dry or wet micro-blasting at 0.4 MPa are displayed at the bottom figure part. In this way, it can be concluded that although the average coating's thickness remains practically invariable by blasting procedures at low pressures and process durations [2], the actual film thickness in individual micro-regions on rake and flank depends strongly on the developed integrity after micro-blasting. Thus, the augmentation of

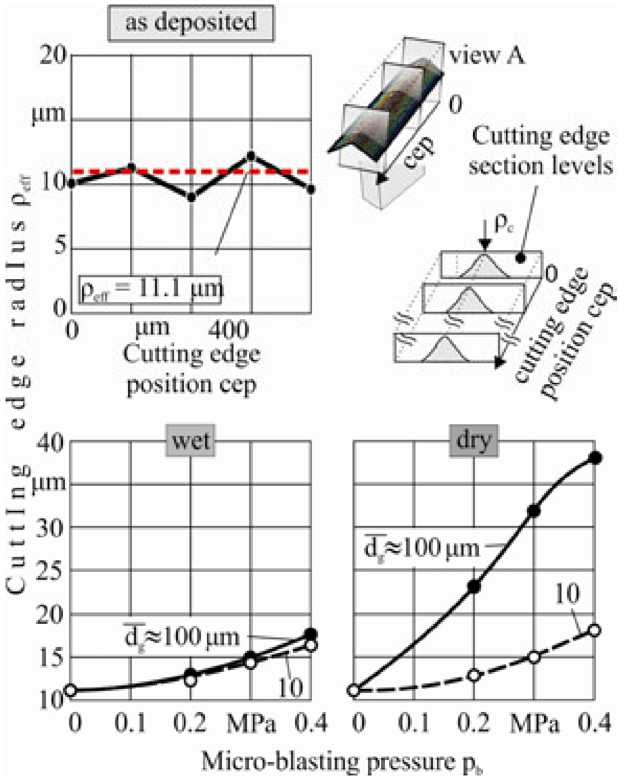

Figure 5. Cutting edge radius ρeff after wet or dry micro-blasting by various grain sizes at different pressures

micro-blasting pressure and duration may result in significant local coating thickness reductions, which may affect the micro-blasted coated tool's cutting performance.

Nanoindentations at a maximum load of 15 mN were conducted on coated inserts, subjected to wet or dry micro-blasting by fine (dg≈10 µm), or coarse (dg≈100 µm) Al_2O_3 grains at various pressures. The corresponding courses of the maximum indentation depth versus the micro-blasting pressure are presented in figure 4. In both wet and dry blasting processes, by increasing the micro-blasting pressure in the case of coarse Al_2O_3 grains, a diminution of the maximum indentation depth develops, thus improving the film hardness. Similar effects can be observed after micro-blasting by fine Al_2O_3 grains. A comparison of the achieved maximum indentation depths at various pressures confirms the hypothesis, that the more intense superficial coating deformation during wet micro-blasting by coarse Al_2O_3 grains leads to a larger hardness improvement, compared to the attained one by fine Al_2O_3 grains. Moreover, this phenomenon is even more intense in the case of dry blasted inserts.

It has to be pointed out that in the case of dry blasting at micro-blasting pressures over 0.3 MPa, coating damage and substrate revelation may take place, as it will be described in the next section.

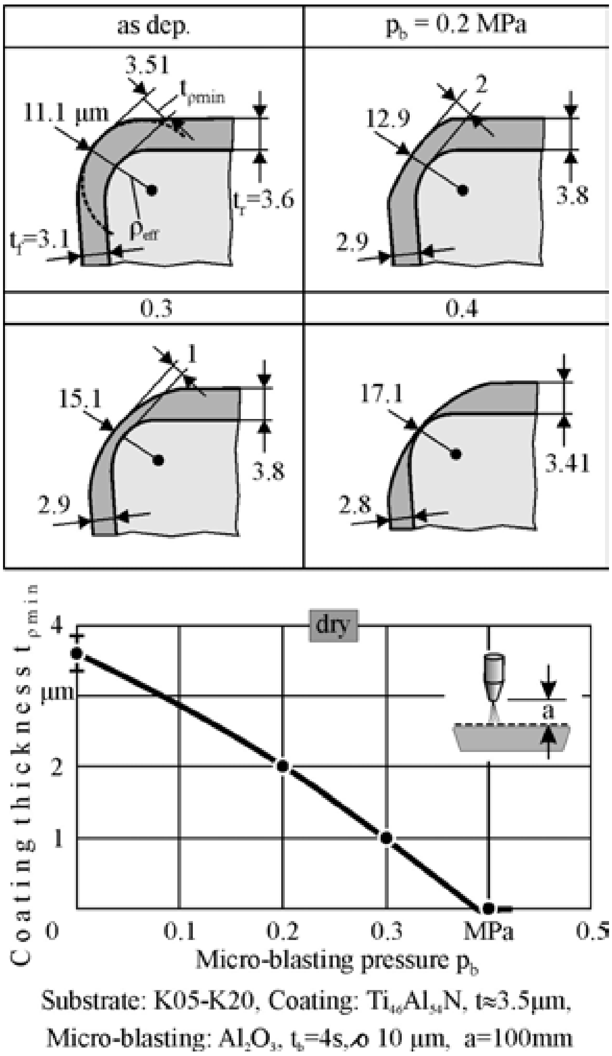

Figure 6. Cutting edge geometries and minimum coating thickness $t\rho_{min}$ after dry micro-blasting by fine grains at different pressures

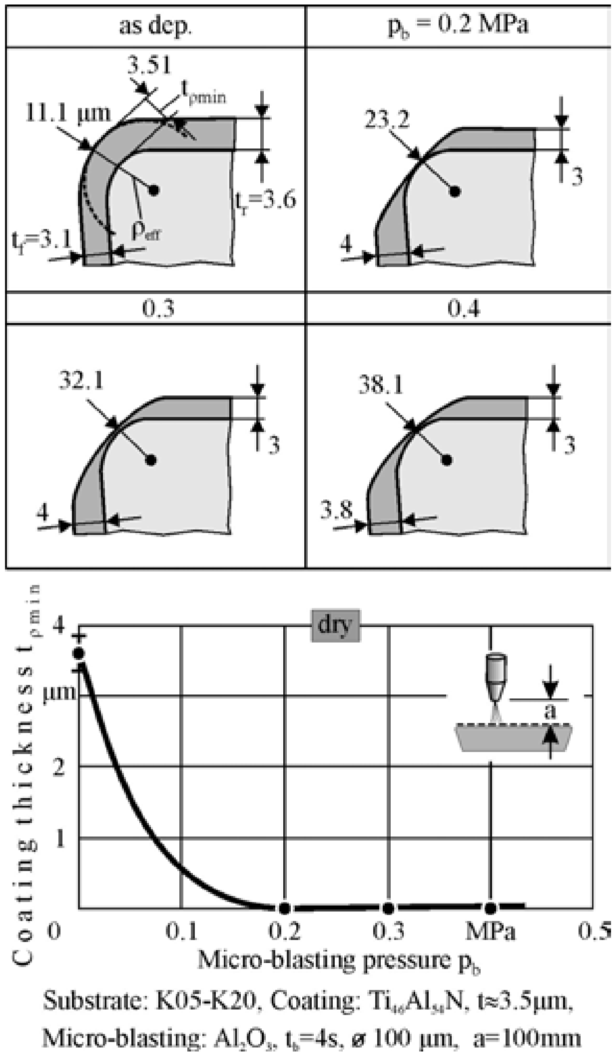

Figure 7. Cutting edge geometries and minimum coating thickness $t_{\rho min}$ after dry micro-blasting by coarse grains at different pressures

3.2 Effect of abrasive grains' size and blasting medium on the coated cutting edge geometry

For investigating the micro-blasting medium and grains' effects on the cutting edge roundness, confocal measurements along the cutting edges of variously wet and dry micro-blasted cutting inserts were conducted. In this way, successive cross sections of the cutting edges can be monitored and with their aid, the corresponding tool wedge radii as well as the average value and the fluctuations of the cutting edge roundness, before and after micro-blasting at various pressures can be estimated. A characteristic example, for the as deposited coating case is demonstrated in the upper part of figure 5. Moreover, the course of cutting edge radius versus the micro-blasting pressure, when fine or coarse Al_2O_3 grains are used, is shown at the bottom part of figure 5, for both, wet and dry blasting conditions. These results reveal that by increasing the micro-blasting pressure, when fine or coarse Al_2O_3 grains are used, an enlargement of the cutting edge radius develops. The cutting edge radius growth is visible at micro-blasting pressures over 0.2 MPa and it is more intense, when coarse Al_2O_3 grains are employed. This phenomenon amplifies even more in the case of dry blasting.

Taking into account the previous results, the coating thickness distributions along the cutting edge after dry micro-blasting at various pressures, were analytically determined. The calculated coated cutting edge cross section geometries after dry micro-blasting by fine and coarse grains at pressures of 0.2, 0.3 and 0.4MPa are monitored in figures 6 and 7 respectively. When fine grains are employed, the coating thickness $t_{\rho min}$ may diminish up to zero at approximately 0.4MPa. Thus, substrate revelations may develop. However, the application of coarse grains results in extent film damage near the cutting edges already at low micro-blasting pressure.

In figure 8, the effect of micro-blasting grain's transport medium on coating thickness distributions along the cutting edge is exhibited. When fine grains are used, the risk of coating thickness decrease and

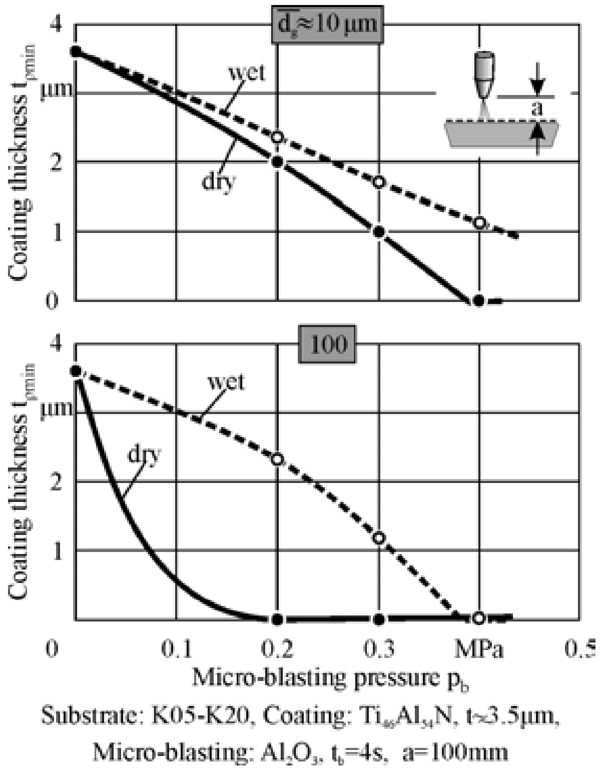

Figure 8. Minimum coating thickness t_{pmin} after wet or dry micro-blasting by fine or coarse grains at different pressures.

even more of a substrate revelation is more relevant in the case of dry micro-blasting compared to wet one at micro-blasting pressures over 0.3MPa. In the coarse grain case, the negative contribution of the dry micro-blasting on the coating thickness diminution along the cutting edge is visible. This was verified by SEM measurements for both Al_2O_3 grain sizes at pressures of 0.3 and 0.4MPa, as it is illustrated in figure 9.

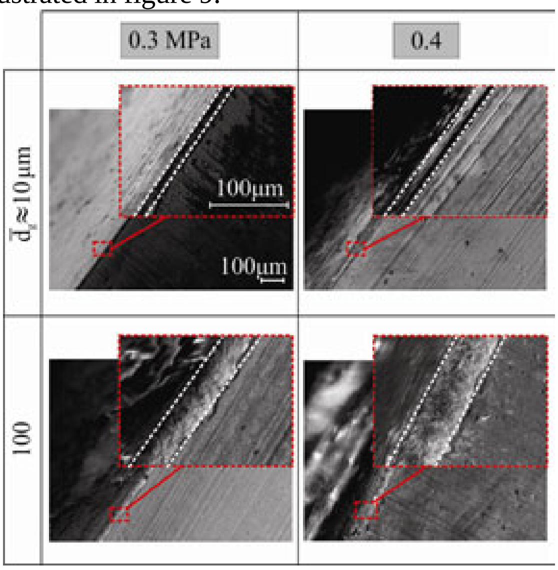

Figure 9. SEM micrographs of coated cutting edges after dry micro-blasting by fine or coarse grains at different pressures

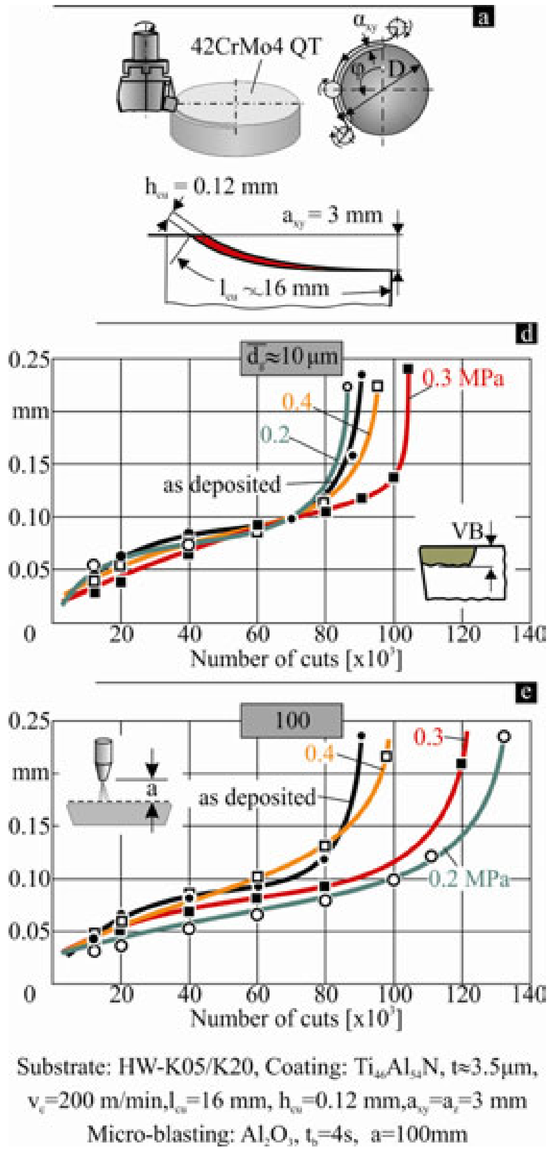

Figure 10. Flank wear development versus the number of cuts of wet micro-blasted coated inserts at various conditions.

It is evident that an increase of pressure results in a wider substrate exposure, especially when coarser grains are used.

3.3 Wear behaviour of coated tools with micro-blasted films in milling

As it has been previously described, on one hand, increased micro-blasting pressure results in enhanced film hardness. This improvement is more intense in the case of coarser Al_2O_3 grains and is restricted over a certain pressure (see figure 4). On the other hand, an increased micro-blasting pressure leads to an augmentation of the film brittleness [6,7].

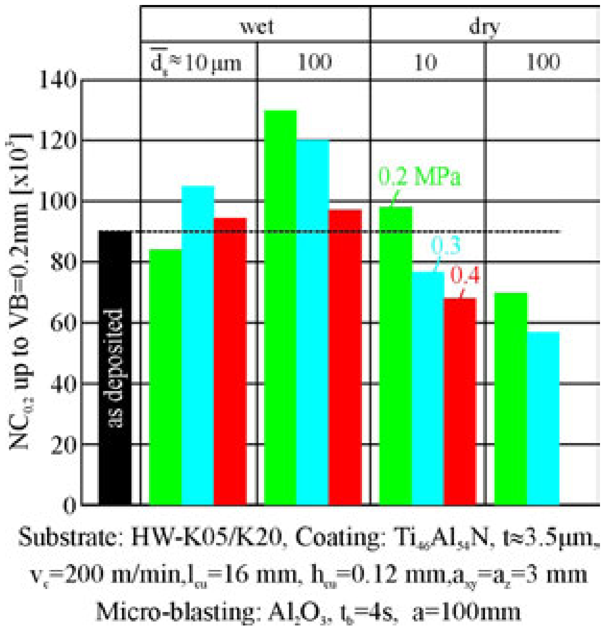

Figure 11. Comparison of flank wear development of coated tools subjected to wet or dry micro-blasting by fine or coarse grains at different pressures.

Furthermore, higher micro-blasting pressures resulted in increased cutting edge radius and simultaneously to a film thickness decrease on the cutting wedge, especially when dry blasting conditions are applied. This film thickness decrease is aggravated by the produced rough topomorphy of the micro-blasted surface, in particular when coarser Al_2O_3 grains are employed. Hence, micro-blasting on PVD films can be considered as an efficient method, if the balance between the described effects leads to improved tool life.

To determine the effect of wet micro-blasting conditions on the cutting performance of coated tools, milling investigations were conducted by a three-axis numerically controlled milling centre. The applied tool-workpiece system and the main characteristics of the undeformed chip geometry are illustrated in figure 10a. The flank wear development on coated inserts, which were wet micro-blasted by Al_2O_3 grains of average diameters of ca. 10 μm and 100 μm at various pressures, is demonstrated in figure 10b and 10c respectively. Cutting inserts wet micro-blasted with fine Al_2O_3 grains at 0.2MPa show a similar cutting performance with the as deposited coated tool, reaching a tool life of ca. 90 000 cuts up to a flank wear width of 0.2 mm. A cutting performance improvement of 105 000 cuts up to the same flank wear width is achieved after wet micro-blasting at a pressure of 0.3MPa because of the enhanced film hardness (see figure 4). At the higher micro-blasting pressure of 0.4MPa, local coating removals and substrate revelations as well as the increased film brittleness, despite the improved film hardness, reduce the tool life.

In the case of the coarse Al_2O_3 grains (see figure 10c), the micro-blasted tools at a pressure of 0.2 MPa exhibited the best cutting performance, reaching a tool life of approximately 130 000 cuts up to a flank wear width of 0.2 mm. A slight tool life reduction at 120 000 cuts up to the same flank wear of 0.2 mm was encountered at a pressure of 0.3 MPa. The treated tool at 0.4 MPa appears practically the same cutting performance, compared to milling with untreated inserts. Due to local coating removals, film brittleness augmentation and substrate revelations after wet micro-blasting at this pressure, the thermal barrier at the cutting edge roundness is locally damaged. Herewith, the substrate thermal and mechanical loads increase, thus contributing to cutting performance deterioration.

The achieved number of cuts up to a flank wear width of ca. 0.2 mm of coated tools subjected to micro-blasting by fine or coarse sharp-edged Al_2O_3 grains, employing different micro-blasting grain transport media is illustrated in figure 11. According to these results, wet micro-blasting, when coarse grains are used, contributes to coated tool cutting performance improvement. This enhancement depends on the applied micro-blasting pressure. Moreover, in the investigated cases, dry micro-blasting leads to tool wear behaviour improvement, only at low pressures and by fine grains.

4. CONCLUSION

In the present paper, the effect of wet and dry micro-blasting by Al_2O_3 abrasive grains of various diameters on PVD films' hardness, tool wedge geometry and cutting performance is introduced. Wet micro-blasting with coarse sharp-edged Al_20_3 grains may lead to a significant coated tool life increase. The applied micro-blasting pressure has to be adjusted with respect to the size of the used abrasive grains. Wet micro-blasting is a more efficient post treatment for enhancing the cutting performance of coated tools, compared to dry micro-blasting.

REFERENCES

[1] P.W. Gold, J. Loos, Wear resistance of PVD-coatings in roller bearings, Wear, Vol.253, No. 3-4, pp. 465-472, 2002.

[2] K. D. Bouzakis, S. Gerardis, G. Skordaris, G. Katirtzoglou, S. Makrimallakis, F. Klocke, E. Bouzakis, Effect of dry micro-blasting on PVD-film properties, cutting edge geometry and tool life in milling, Surface and Coatings Technology, Vol.204, No. 6-7, pp. 1081-1086, 2009.

[3] E. Bouzakis, Steigerung der Leistungsfähigkeit PVD-beschichteter Hartmetallwerk¬zeuge durch Strahlbehandlung, Dissertation, RWTH Aachen, 2008.

[4] F. Klocke, T. Schroeder, E. Bouzakis, A. Klein, Manipulation of coating and subsurface properties in reconditioning of WC-Co carbide cutting tools, Surface and Coatings Technology Vol. 202, No. 4-7, pp. 1194-1198, 2007.

[5] D. M. Kennedy, J. Vahey, D. Hanney, Micro shot blasting of machine tools for improving surface finish and reducing cutting forces in manufacturing, Materials and Design, Vol.26, No.3, pp. 203-208, 2005.

[6] K.-D. Bouzakis, E. Bouzakis, G. Skordaris, S. Makrimallakis, A. Tsouknidas, G. Katirtzoglou, S. Gerardis, Effect of PVD films wet micro-blasting by various Al_2O_3 grain sizes on the wear behaviour of coated tools, Surface and Coatings Technology, (2011) in press.

[7] K.-D. Bouzakis, G. Skordaris, E. Bouzakis, A. Tsouknidas, S. Makrimallakis, S. Gerardis, G. Katirtzoglou, Optimization of wet micro-blasting on PVD films with various grain materials for improving the coated tools' cutting performance, CIRP Annals - Manufacturing Technology, (2011) in press.

[8] M. Klaus, Ch. Genzel, H. Holzschuh, Residual stress depth profiling in complex hard coating systems by X-ray diffraction, Thin Solid Films, Vol.517, No. 3, pp. 1172-1176, 2008.

[9] K. D. Bouzakis, G. Skordaris, F. Klocke, E. Bouzakis, A FEM-based analytical-experimental method for determining strength properties gradation in coatings after micro-blasting, Surface and Coatings Technology, Vol. 203, No.19, pp. 2946-2953, 2009.

[10] C. Barbatti, J. Garcia, R. Pitonak, H. Pinto, A. Kostka, A. Di Prinzio, M.H. Staia, A.R. Pyzalla, Influence of micro-blasting on the microstructure and residual stresses of CVD κ-Al2O3 coatings, Surface and Coatings Technology, Vol.203, No. 24, pp. 3708-3717, 2009.

[11] CemeCon AG. Website, www.cemecon.de/index_eng.html (2010).

[12] K.-D. Bouzakis, N. Michailidis, S. Hadjiyiannis, G. Skordaris, G. Erkens, The effect of specimen roughness and indenter tip geometry on the determination accuracy of thin hard coatings stress-strain laws by nanoindentation, Materials Characterization, Vol. 49, No. 2, pp. 149-156. 2002.

Serbian Tribology Society

SERBIATRIB '11

12th International Conference on Tribology

Faculty of Mechanical Engineering in Kragujevac

Kragujevac, Serbia, 11 – 13 May 2011

NANOTECHNOLOGIES: APPLICATION OF AFM/MFM IN MATERIAL CHARACTERIZATION

Lidija Matija, Radivoje Mitrović, Đuro Koruga
Mechanical Engineering Faculty Belgrade

Abstract: *Nanotechnologies comprise techniques and methods used to study, design and manufacture nano devices, as a special way to organise atoms and molecules. Nanotechnology is revolutionizing many significant areas of engineering, biotechnology and medicine. One of the problems not known at macro scale and noticed at nanometer level, is derived from the increase of number of surface atoms in total number of nanostructure atoms. This, on one side, leads to great changes of physical and chemical characteristics of a material that can be favorable utilized, but on the other side, surface energy increase due to decrease of dimensions makes most of nano - structured materials to be thermodynamically unstable and metastable systems. One of the main challenges in production, characterization and processing of nanomaterials are overcoming the problem of high surface energy and prevention of growth of constituting particles of a nanomaterial, due to their constant tendency to lower high surface energy.*

Today, there are three main directions of nanosystems development: (1) physically oriented nanotechnologies, (2) chemically oriented nanotechnologies and (3) integrative physico-chemical oriented nanotechnologies. In scope of physically oriented nanotechnologies, three main techniques used for characterization of physically oriented systems are: STM (scanning tunneling microscope), AFM (atomic force microscope) and MFM (magnetic force microscope).

More and more often the question is raised whether the nanotechnology is a new technological revolution (the first - steam machine, the second - computers, the third - artificial intelligence) or not. A majority of experts think that it is, but some has an opinion that it is something more than previous technological revolutions, because in comparison to all others, it much more seriously and more obviously asks the question "What is a human"? Classification of scientific - technological revolutions can be done in different ways, but the most appropriate one is substitution of human activities by the machine. Nanotechnology can be considered as the fourth technological revolution that will enable creation of nano-systems as "self created" entities under the auspice of macroscopic nano-reactor (similar to the embryogenesis process), that will be able to create macroscopic systems capable to reproduce and enhance themselves in a completely new way. In such a new system, it is considered that manual, intellectual, routine and creative capabilities will be integrated, and should be complementary and compatible to human capabilities.

NANOTEHNOLOGIJE: PRIMENA AFM/MFM U KARAKTERIZACIJI MATERIJALA

Lidija Matija, Radivoje Mitrović, Đuro Koruga
Mašinski fakultet Univerziteta u Beogradu

Abstrakt: *Nanotehnologije obuhvataju tehnike i metode koje se koriste za proučavanje, projektovanje i izradu uređaja na nano nivou, kao posebne organizacije atoma i molekula. Nanotehnologija je do sada revolucionarizovala mnoge veoma važne oblasti inženjerstva, biotehnlogije i medicine. Jedan od problema koji je nepoznat na makroskali, a uočava se na nanometarskom nivou proističe iz porasta broja površinskih atoma u ukupnom broju atoma nanostruktura, što s jedne strane dovodi do velikih promena fizičkih i hemijskih svojstava materijala koje se mogu povoljno iskoristiti, ali na drugoj strani povećanje površinske energije usled smanjivanja dimenzija dovodi do toga da je većina nano – struktuiranih materijala termodinamički nestabilna i metastabilna. Prevazilaženje problema velike površinske energije i sprečavanje rasta gradivnih čestica nanomaterijala usled stalne tendencije da smanje veliku površinsku energiju jedan je od glavnih izazova u proizvodnji, karakterizaciji i obradi nanomaterijala.*

Danas postoje tri glavna pravca razvoja nanosistema: (1) fizički orijentisane nanotehnologije, (2) hemijski orijentisane nanotehnologije i (3) integralne fiziko-hemijski orijentisane nanotehnologije. U okviru fizičko orjentisanih nanotehnologija tri glavne tehnike koje se primenjuju za karakterizaciju fizičko orijentisanih sistema su: STM (skenirajući tunelski mikroskop), AFM (mikroskop međuatomskih sila) i MFM (mikroskop magnetnih sila).

Sve se češće postavlja pitanje da li je nanotehnologija nova tehnološka revolucija (prva-parna mašina, druga-kompjuteri, treća-veštačka inteligencija) ili ne. Većina stručnjaka misli da jeste, ali neki misle i da je ona nešto više od dosadašnjih tehnoloških revolucija, jer u odnosu na sve dosadšne ona mnogo ozbiljnije i očglednije postavlja pitanje "šta je čovek"?. Klasifikacija naučno-tehnoloških revolucija može se vršiti na različite načine, ali jedan od najprikladnijih je zamena ljudskih aktivnosti mašinskim. Nanotehnologiju možemo smatrati četvrtom tehnološkom revolucijom koja će omogućiti stavaranje nanosistema kao „samoniklih" tvorevina pod okriljem makroskopskog nano-reaktora (slično kao proces embriogeneze), koji će biti u mogućnosti da izgrade makroskopske sisteme sposobne da na jedan nov način reprodukuju i unapređuju sebe. U jednom takavom sistemu smatra se da biti integrisane manuelne, umne, rutnske i kreativne sposobnosti, koje u odnosu na ljudske treba da budu komplementarne i kompatibilne.

Ključne reči: *Nanotribologija, AFM, MFM, Materijali*

1. AFM/MFM: SKENIRAJUĆE MIKROSKOPIJE ATOMSKIH I MEĐUMOLEKULARNIH SILA

1.1 AFM

Skenirajuća mikroskopija atomskih sila (Atomic Force Microscopy – AFM) je metoda karakterizacije materijala pomoću lokalnog merenja međuatomskih sila. Lokalno (sondirajuće) merenje se ostvaruje pomoću nanokonzolnog senzora izrađenog iz konzolnog dela dužine oko 50-500 μm i konusnog ili piramidalnog dela koji se nalazi na kraju konzolnog dela i koji je usmeren u vertikalnom pravcu ka uzorku. Radijus vrha konusnog (piramidalnog) završetka se kreće od 7-90 nm i zavisi od namene senzora.

Rezolucija skenirajućih sondirajućih mikroskopa se danas kreće oko 1.0 pm, ili 10^{-12} m, što trenutno zadovoljava najstrožije zahteve nauke o materijalima, a time i nano-nauke. Rezolucija snimanja je u većoj meri ograničena uslovima kvaliteta pripreme uzorka (površine uzorka) koji u naučnoj literaturi ne dobija adekvatnu pažnju iako bi se moglo reći da je, posmatrajući pojedinačni doprinos svake od faza, priprema uzorka najznačajnija komponenta u procesu dobijanja snimka materijala u atomskoj rezoluciji.

Brojni su razlozi velikog uspeha i opšte prihvaćenosti metode AFM u nauci od kojih je većina povezana sa tehničkim rešenjima primenjenim u metodi. Ono što AFM izdvaja u odnosu na druge metode jeste *neinvazivnost* metode koja omogućava karakterizaciju uzoraka i u atomskoj rezoluciji bez unošenja poremećaja u strukturi. Iz ove osobine proističe i druga prednost AFM koja je mogućnost karakterizacije u uslovima kontrolisane atmosfere i karakterizacija u tečnostima, što su uslovi koji mogu *blisko odgovarati prirodnom okruženju*. Imajući u vidu pomenutu malu invazivnost dobijamo mogućnosti primene ove metode ne samo u tehnici nego i u biološkim i biomedicinskim istraživanjima koja pokazuju veliku osetljivost prema promeni uslova pod kojima se eksperiment odvija. Upravo se od primene AFM u biomedicini očekuje veliki pomak u razumevanju veze između strukture i funkcije sistema na molekularnom nivou.

Metoda AFM omogućava i snimanje u širokom opsegu uslova sredine. Tako je moguće podešavati temperaturu u širokom opsegu: od uslova hlađenja tečnim helijumom sve do nekoliko stotina stepeni na celzijusovoj skali. Moguće je izvršiti i prilagođenje atmosfere uvođenjem odgovarajućih gasova ali i snimanje u uslovima veoma visokog vakuuma (Ultra High Vacuum – UHV). Trenutno najnaprednija primena AFM (ali i tehnički najzahtevnija) se odnosi na mogućnosti snimanja u tečnoj sredini u kojoj je moguće u velikoj meri oponašati uslove realnih procesa, pogotovo u biološkim i biomedicinskim istraživanjima.

Na slici 1 je dat shematski prikaz principa rada mikroskopa međuatomskih i međumolekularnih sila. Uzorak koji se ispituje nalazi se na postolju koje pokrece piezoelektrični izvršni element koji ostvaruje kretanje uzorka u tri dimenzije: dve dimenzije ostvaruju ravansko skenirajuće kretanje – liniju po liniju, dok je treće, visinsko kretanje, diktirano informacijom koju generiše nanokonzola koja se nalazi u stalnoj interakciji sa uzorkom i pod uticajem je privlačno-odbojnih sila koje potiču od njihove interakcije. Poznavajući dinamičke osobine nanokonzolnog senzora i stepeni zakon promene međumolekularnih sila (Lenard-Džounsov potencijal) iz dobijene interakcije se dobijaju karakteristike ispitivanog materijala.

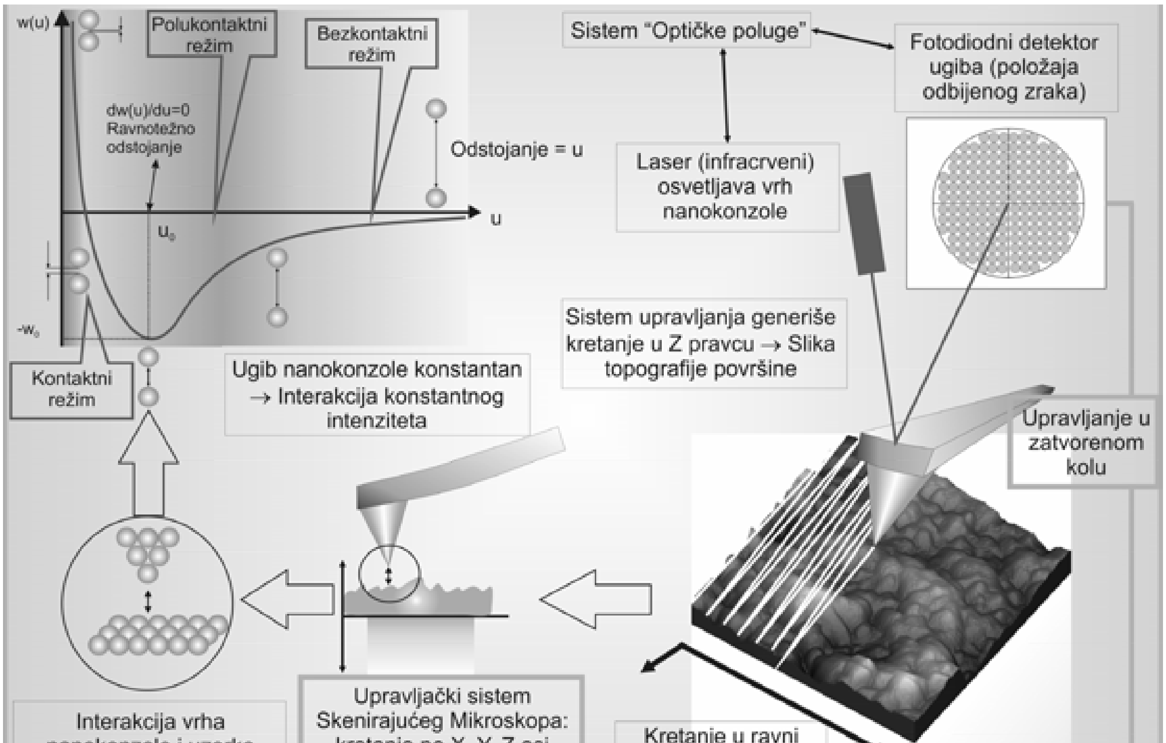

Slika 1. Shematski prikaz rada uređaja za merenje medjuatomskih i međumolekularnih sila (AFM).

Intenzitet privlačno-odbojnih sila zavisi od rastojanja između nanokonzole i uzorka koje određuje promenljiva kontura površine uzorka. Promene rastojanja generišu promene intenziteta sila koje savijaju nanokonzolu. Ugib nanokonzole se registruje pomoću ugla pod kojim se laserski zrak, usmeren na vrh nanokonzole, odbija ka fotodetektorskom senzoru čija je svaka tačka opremljena diodom osetljivom na svetlost, koja lasersku odbijenu svetlost pretvara u električni signal. Položaj odbijenog zraka, odnosno poznavanje pozicije diode koja prima odbijeni laserski zrak, omogućava stalno praćenje vertikalne pozicije (ugiba) nanokonzole. Informacija o ugibu se prenosi u korekcioni element koji grešku, nastalu promenom visine profila u odnosu na početnu ravnotežnu vrednost (određenu na početku snimanja) poništava tako što pomera uzorak u vertikalnom pravcu pomoću piezoelektričnog izvršnog elementa, kako bi se ugib nanokonzole stalno održavao na konstantnoj vrednosti (početna vrednost). Početna vrednost ugiba jeste ravnotežno stanje privlačnih međumolekularnih sila i sila otpora usled krutosti nanokonzolnog nosača senzora. Sva pomeranja piezoelektričnog organa uzrokovana su promenama na konturi površine uzorka tako da zapis vertikalnog pomeranja uzorka (piezoelektričnog izvršnog elementa) zapravo predstavlja zapis izgleda konture površine uzorka. Podaci za svaku liniju-presek uzorka se beleže u računaru, koji je nosilac funkcija upravljanja i obrade podataka, i na kraju se sve linije spajaju, čime se dobija 3D rekonstrukcija topografskog izgleda površine uzorka. Kako sila interakcije na zavisi od električne provodnosti uzorka to se mogu ispitivati i neprovodni materijali.

2.2 MFM

Mikroskopija magnetnih sila (Magnetic Force Microscopy – MFM) je metoda karakterizacije magnetnih struktura sa izraženom osetljivošću na komponente magnetnog polja čiji pravac odstupa od horizontalnog dakle poseduje ne-nultu komponentu u pravcu ose simetrije senzora. Za razliku od drugih metoda koje omogućavaju snimanje magnetnih osobina celokupne zapremine materijala, MFM pruža informacije o raspodeli nosilaca magnetnih osobina u tankom površinskom sloju materijala.

U metodi MFM se koristi „tehnika dva prolaza“ (prolaz senzora), kod koje se u „prvom prolazu“ prikupljaju informacije o topografiji uzorka dok se u „drugom prolazu“ vrši merenje magnetnih sila.

Dopunske tehnike zasnovane na MFM obuhvataju mapiranje magnetootpornosti (eng. Magnetoresistive Sensitivity Mapping – MSM) i visokofrekventnu MMS (eng. High Frequency MFM – HFMFM) kao i merenje magnetne disipacije (eng. Magnetic Dissipation Microscopy – MDM).

Kvalitativna MFM predstavlja proširenje dinamičkog režima rada MAS i osnovni režim rada MMS. Postupak merenja se sastoji iz istovremene akvizicije dva snimka, jednog kojime se određuje topografija (standardnim polukontaktnim režimom) i drugog kojime se određuju magnetne osobine. Slika 2. prikazuje primer snimka MMS.

Postupak drugog prolaza se izvodi tako što senzor, na osnovu informacije o topografskom profilu uzorka, formira odstojanje od uzorka (koje je podešljiva veličina koja se inicijalno zadaje) koje ima za zadatak da prostorno razdvoji uticaj van der Valsovih sila od uticaja magnetnih sila koje sporije opadaju sa rastojanjem.

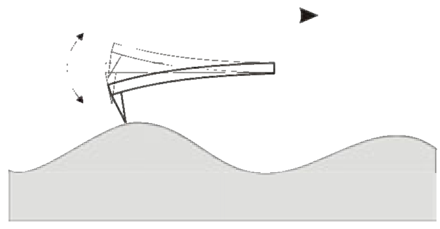

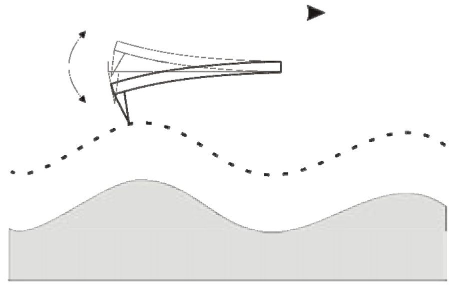

Slika 2. Ilustracija tehnike „dva prolaza“. Slika levo: u prvom prolazu senzor prenosi informaciju o topografiji površine uzorka. Slika desno: u drugom prolazu sistem upravljanja prati putanju koja je prethodno određena informacijom o profilu topografije, i na zadatoj visini održava odstojanje od uzorka opisujući identičan topografski profil. Formirano odstojanje omogućava fizičko filterovanje van der Valsovih sila uz registrovanje samo magnetnih sila.

Metoda MFM zahteva i upotrebu posebnih senzora čiji vrh sadrži feromagnetnu komponentu koja može primiti određen stepen magnetizacije koja se koristi u interakciji sa magnetnim poljem uzorka. Klasičan senzor poseduje vrh koji je obložen presvlakom izrađenom od tankog filma feromagnetnog materijala koji se sastoji iz sloja kobalta, debljine od oko 35-60 nm. Posledica prisustva feromagnetnog filma je povećanje radijusa zaobljenja vrha sonde i delimičan gubitak lateralne rezolucije koja trenutno iznosi oko 30-50 nm. Pitanje lateralne rezolucije predstavlja predmet razvoja tehničkog rešenja senzora tako da se očekuje da u bliskoj budućnosti lateralna rezolucija snimanja dostigne i manje vrednosti.

Osim klasičnih senzora (sa filmom feromagnetnog materijala) u upotrebi su i senzori na čijem se vrhu nalaze ugljenične nano-tube (UNT) prečnika oko 1.2 nm koje poseduju paramagnetska svojstva. Kao paramagnetni materijali, senzori sa UNT poseduju izuzetnu osetljivost na spoljašnje magnetno polje u koje unose minimalnu pertubaciju uz istovremeno pružanje vrhunske lateralne rezolucije. Očekuje se da ovi senzori budu unapređeni dodavanjem feromagnetnih komponenti u sastav ugljenične nanotube čime bi se značajno proširio opseg magnetnih interakcija između senzora i uzorka.

Konstanta krutosti mora biti dovoljno velika, kako bi obezbedila stabilnost u polukontaktnom režimu, ali i dovoljno mala kako bi nanokonzolni nosač imao visoku osetljivost na slabe magnetne sile (čije se merenje sprovodi u drugom prolazu). Specifikacije za konstante krutosti većine senzora se kreću u opsegu od 0.5-10.0 N/m. Skladištenje magnetnih nanokonzolnih senzora zahteva upotrebu odvlaživačke komore kojom se sprečava adhezija vlage i nečistoća na površinu senzora. Takođe, senzori se moraju zaštiti od dejstva vazduha i drugih oksidacionih sredstava koja mogu izmeniti fizičko-hemijska svojstva magnetnog filma. Neki proizvođači koriste zaštitu magnetnog filma slojem hroma debljine 20 nm koji omogućava veću mehaničku i magnetnu stabilnost i produženje radnog veka senzora. Ipak, uprkos prisustvu zaštitnog filma, većina proizvođača senzora i mikroskopa preporučuje čuvanje senzora u odvlaživačkim komorama.

Magnetnu silu određujemo, na osnovu energije interakcije između senzora i uzorka, sledećim izrazom:

$$F_{s-u} = \nabla E_{s-u} \tag{1}$$

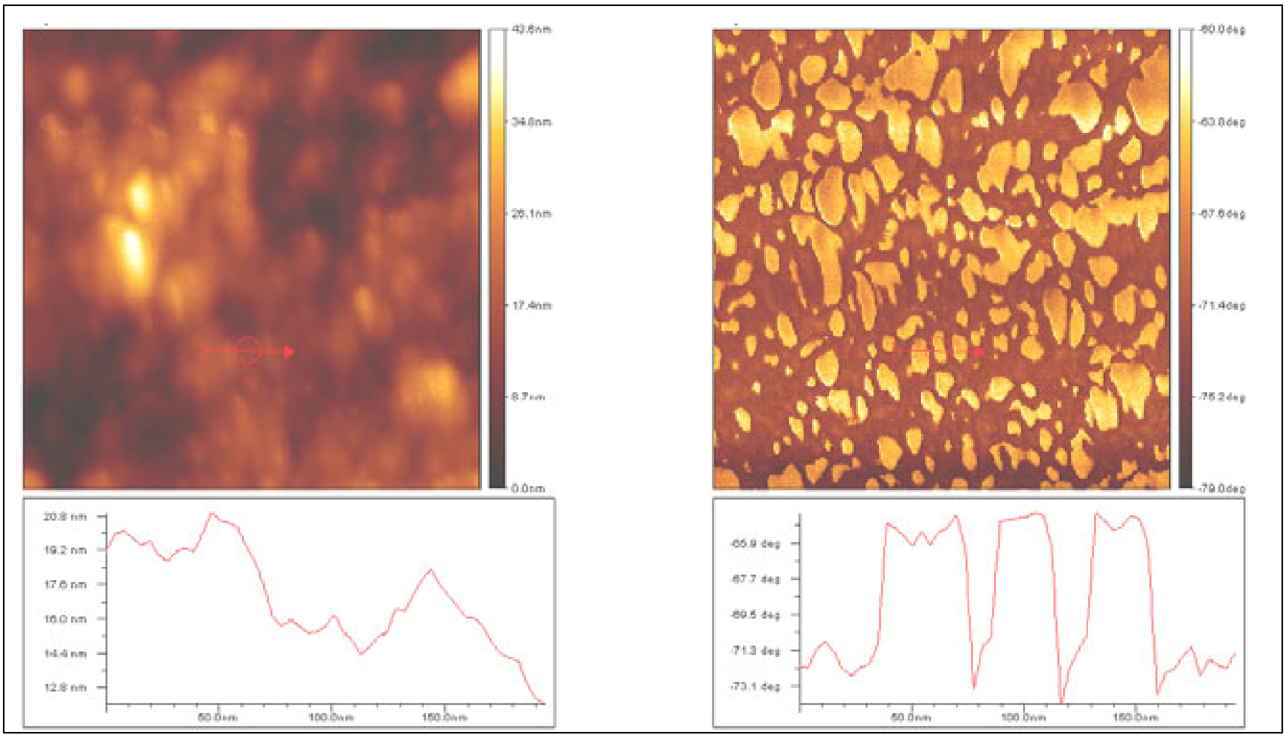

Slika 3. Ilustracija rezultata metode AFM. Snimani uzorak je hidrogel dopiran kobaltom. Površina snimanog uzorka je 1x1 μm. Slika levo: uporedni snimak topografije površine (čija maksimalna visina profila iznosi 43.6 nm) i magnetnih osobina (snimak gradijenta magnetnog polja). Slika desno: trodimeznionalan prikaz topografije i magnetizma na kome se uočava razdvajanje feromagnetne komponente (kobalt) od polimerne mreže (hidrogel) koja predstavlja nosač i pokazuje značajno slabiju reakciju na prisustvo magnetnog polja nanokonzolnog senzora

U praktičnoj primeni se interakcija senzor-uzorak aproksimira jednodimenzionalnim slučajem kod koga se razmatra samo komponenta u vertikalnom pravcu (z) a zanemaruju komponente u horizontalnim pravcima (x, y):

$$F_z = \frac{\partial}{\partial z} E_{s-u} \tag{2}$$

U slučaju postupka merenja magnetnih sila ova aproksimacija ima dodatnu opravdanost zato što se merenje magnetnih osobina vrši na odstojanju od uzorka čime se prosečan vremenski položaj oscilujuće sonde dodatno usklađuje sa pravcem upravnim na osu simetrije senzora. Osim toga, odstojanje doprinosi i prigušenju odstupanja od vertiklanog pravca nastalih promenama profila (usmerenja vektora normale na površinu materijala).

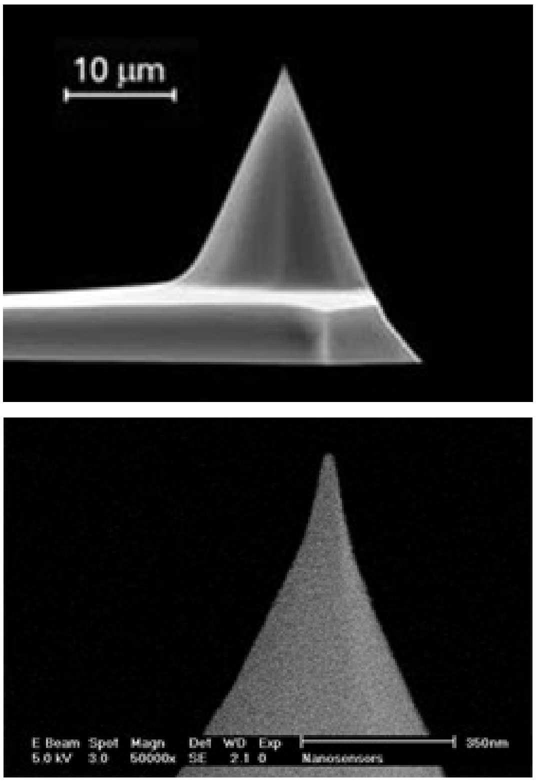

Slika 4. Snimci senzora koji se koriste u metodi MMS dobijeni skenirajućim elektronskim mikroskopom. Slika levo: senzor tipa NSC18/CoCr (proizvođač MikroMasch, Estonia). Garantovani radijus vrha senzora je manji od 90 nm. Slika desno: senzor tipa PPP-LM-MFMR-20 (proizvođač Nanosensors, Švjacarska). Garantovani radijus vrha senzora je manji od 35 nm.

2. ISPITIVANJE UGLJENIČNOG ČELIKA POMOĆU AFM/MFM

Pomoću AFM-a dobijamo topografiju površine uzorka vrlo visoke rezolucije i možemo uočiti i najmanje promene sve do 10 pm. Međutim, kod nekih materijala kao što su ugljenični čelici možemo videti popunjenost prostora materijalom pomoću AFM, kao što je to dato na slici 5 (levo), ali pomoću MFM (desno) vidimo da postoji izrazito smanjen gradijent magnetnog polja. Kako je gvožđe magnetik, a ugljenik dijamagnetik to iz uporedne analize zaključujemo da je granula veličine oko nekoliko stotina nanometara u stvari, ugljenična nanopartikula. Ostala, izrazito crna polja, na slici desno ukazuju na nehomogenost materijala (raspoređenosti ugljenika u čeliku). U slučaju da imamo ulegnuća u topografskoj slici AFM, a izraziti magnetizam na tom mestu na MFM tada mogu nastati dva slučaja: stanje Fe (jonsko) je različito ili se na tom mestu nalazi kiseonik (koji je kao molekul O_2 paramagnetik).

Uporedna topografska i magnetna karakterizacija ugljenične partikule veličine 250 nm u ugljeničnom čeliku data je na sl. 5. Pojava ovakve nehomogenosti može dovesti do pojave nano-pukotina koje pod dinamičkim opterećenjem se spajaju i postaju mikro pukotine i na kraju, makro pukotine. Sličan problem može nastati zbog prisustva kiseonika (molekularnog, O_2).

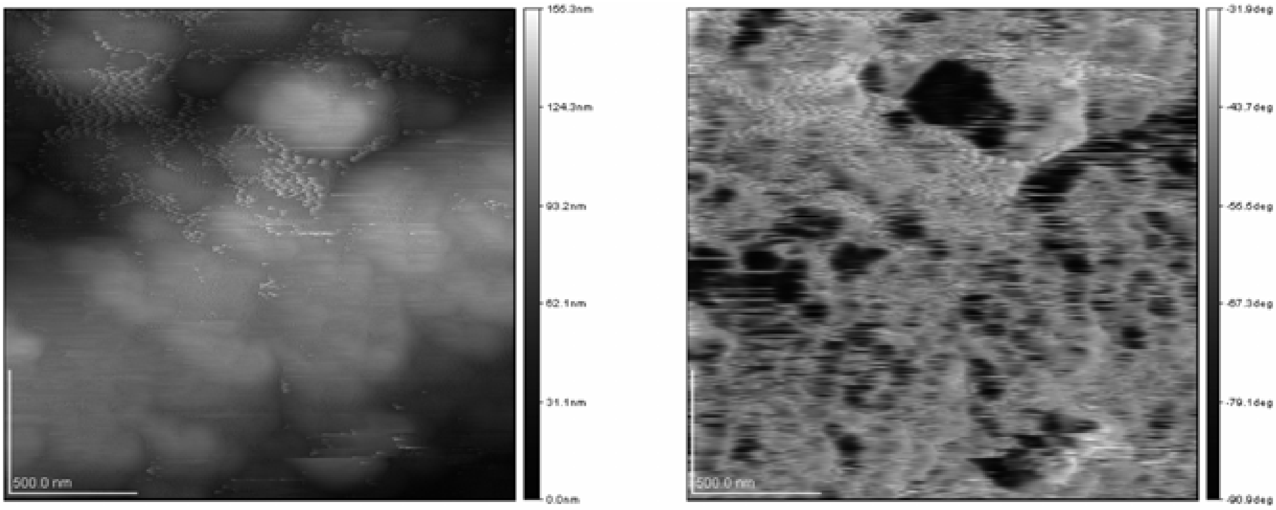

Slika 5. AFM/MFM iste površine za ugljenične čelike.

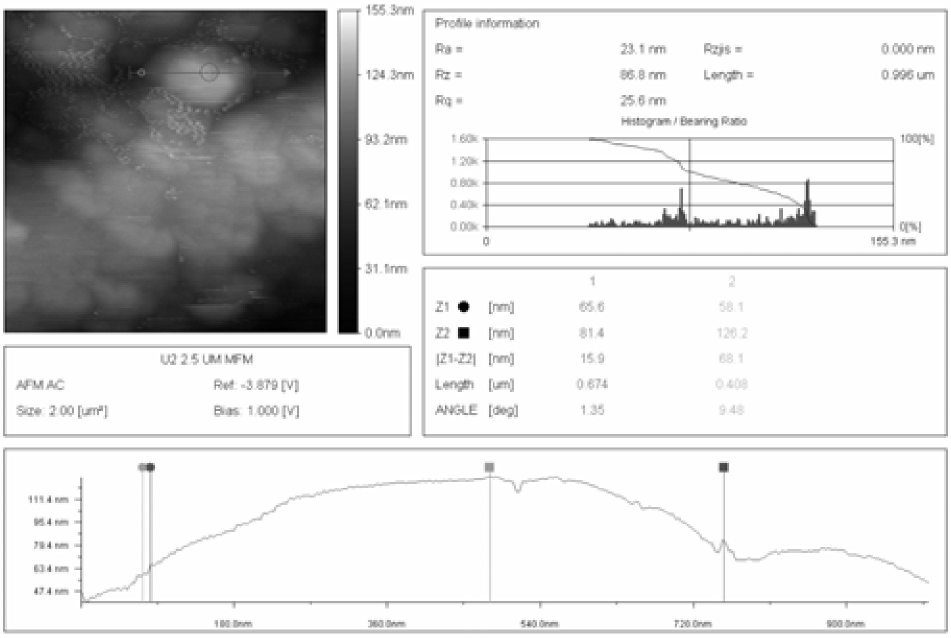

Slika 6. (a) Topografska karakterizacija ugljenične partikule u ugljeničnom čeliku

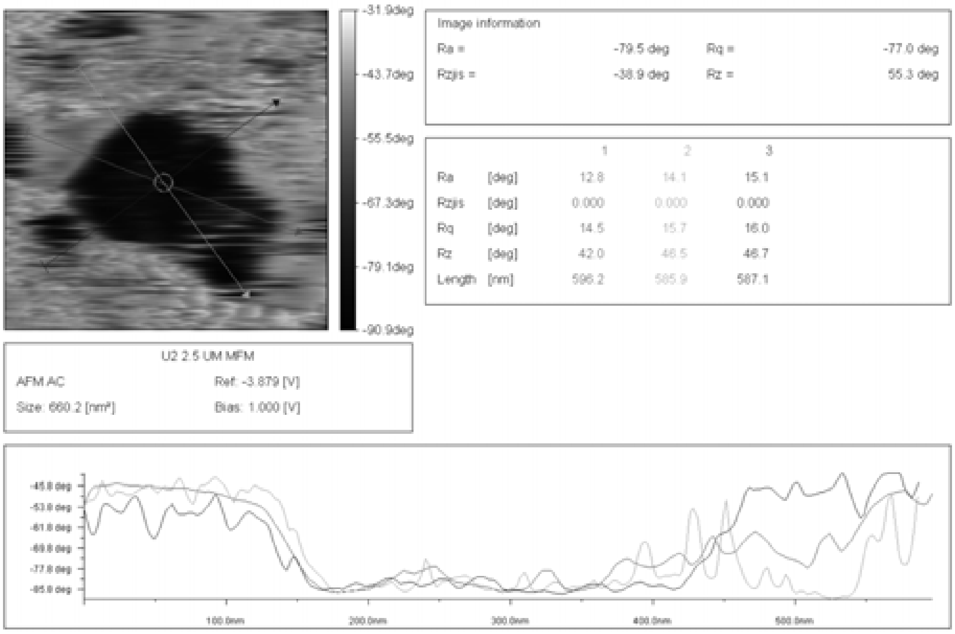

Slika 6. (b) Magnetna karakterizacija ugljenične partikule u ugljeničnom čeliku (pojava”magntenih rupa”)

3. ZAKLJUČAK:

Mikroskopija magnetnih sila (MFM) se koristi za snimanje gradijenta magnetnog polja i njegove distribucije po površini uzorka. MFM ima mogućnost snimanja magnetnog područja od svega nekoliko nanometara. MFM koristi tehniku dva prolaza, a detektovanje magnetnih sila se vrši u drugom prolazu. Varijacije MFM uključuju Magnetoresistive Sensitivity Mapping (MSM) i High Frequency MFM (HFMFM) kao i Magnetic Dissipation Microscopy (MDM). Navedene tehnike zahtevaju upotrebu kantilevera sa magnetnom presvlakom (Co-Cr). Ista presvlaka je formirana i na poleđini kantilevera zbog prevencije savijanja i povećanja refleksije laserskog snopa. Iako je kantilever namagnetisan prilikom proizvodnje, poželjno je i dodatno, naknadno, namagnetisavanje pomoću magneta. Vrednost namagnetisanja kantilevera je obično izmedju 50 i 100 nT. Konstanta elastičnosti i rezonantna frekvencija kantilevera obezbeđuju stabilnost u tapping modu i visoku osetljivost na slabe magnetne sile u drugom prolazu. Za čuvanje ovih kantilevera mora se koristiti specijalna posuda (odvlaživač) da bi vlažnost bila kontrolisana. Takođe, moraju se zaštiti od dejstva vazduha i kiselina.

Danas je nanotehnologija prisutna na svim renomiranim univerzitetima u svetu. Države poput SAD, Japana, Evropske Unije, Kine i Rusije ulažu velika sredstva u razvoj nanotehnologija. Mnoge svetske kompanije u svoj razvoj uvrstile su nanotehnologije, a neke su počele da i plasiraju nanotehnološke proizvode na tržište. U domenu zaštite od UV zračenja nanopartikule na bazi ZnO i TiO_2 pokazala su izrazite prednosti. Generalno, nanopartikule obezbeđuju i do deset puta bolju hemijsku reakciju nego klasični materijal, jer se povećava aktivna površina na kojima se odigrava hemijska reakcija. U razvijenim zemljama već postoje automobili bez brisača na šoferšajbnama, a razlog tome je nanotehnološko rešenje koje ne dozvoljava zadržavanje kišnih kapi ili prašine. Athezione sile su manje od smičućih sila na površini stakla, što se obezbeđuje nanoporama koje se golim okom ne primećuju. Slična situacija je i sa veoma otpornim premazima i tankim filmovima na habanje koji štite automobile i nedozvoljavaju stvaranje ogrebotna. Od nanotuba se prave prvi elektronski prekidači i sklopovi za potrebe nanoelektronike, a u mašinstvu užad čija je zatezna čvrstoća od 8-10 puta veća nego kod proizvoda od istog materijala i istog prečnika. Što se tiče tekstilne industije na pomolu je prava revolucija, jer se radi na razvoju tekstlnih vlakana koja će biti biokompatibilna i komlemetarna sa kožom, a koja će pored standardne funkcije koju imaju odevni pedmeti imati i ulogu biosenzornog sistema. Kako se na koži u triger zonama reprezentuju funkcije pojedinih organa tela to će se u budućnosti moći napraviti „intiligentna odeća" koja će izveštavati nosioca ili lekara (telemetrijski) o zdravstvenom stanju osobe koja nosi „nanotehnološku intiligentnu" odeću.

Nanotehnološka partikularna rešenja u oblasti instrmentacije i materijala je i dalje u usponu. Njihova primena je obično u poboljšanju postojećih klasičnih tehnoloških rešenja, ali se uočava i tendencijaja integralnog pristupa. Može se reći da su nanotehnologije danas u povoju, odnosno u eri „kamenog doba". U okviru većine postojećih tehnoloških disiplina nanotehnologije nalaze sve veću primenu, ali se polako formira i novi tehnološki pravac koji traga za nanositemskim rešenjima u kojima su integrisana organizaciona, energetska, informaciona i upravljačka rešenja. Za sada su domintna dva glavna pravca razvoja, jedan je *fizički* orjentisane nanotehnologije, a drugi *hemijski* orjentisane nanotehnologije. U bliskoj budućnosti očekje se, kao prvi korak, integracija ova dva prvca na „primtivnom" nivou, a zatim i njihova *sinergija*.

Integralni nanotehnološki pristup podrazumeva izbor samo-asemblirajućih materijala, pa zato nanomaterijal mora biti kodogen (slično kao DNK), bazični energetski izvor mora biti molekularni (sličan ATP), organizacijona struktura treba biti samo-organizujuća, što implicira da informaconi procesi trebaju imati dva kanala: klasični i kvantni. Nano-upravljanje mora biti imanentno sistemu, i po svom karakteru prirodno, što podrazumeva dvostruko: unutrašnje i spoljašnje, odnosno lokalno i globalno. U ovakvom pristupu biomimikra je neophodna, ali nanotehnološko rešenje u odnosu na biološko je kao let ptice i let aviona, oba sistema imaju krila, ali let je u osnovi različit. Ono što im je zajedničko je let kroz istu sredinu (vazduh), pa će zajedničko biološkim i nanotehnološkim sistemima biti *voda*. Makroskopska manifestacija nanotehnološkog sistema počivaće na viskozno-elastičnim svojstvima samo-asemblirajućeg kodogenog nanomaterijala. Voda postaje nezamnljiva unutrašnja aktivna radna supstanca, kao sredina nanotehnološkog sistema u kojoj su uronjeni visko-elastični kodogeni i samo-asemblirajući nanomaterijali.

REFERENCE:

[1] Matija, L., Nanotechnology: Artificial Versus Natural Self-Assembly, FME Transactions, Vol.32, pp.1-14, 2004

[2] Koruga,Dj. Hameroff,S., Withers,J., Loutfy,R., and Sundareshan,M., Fullerene C_{60}: History, Physics, Nanobiology, Nanotechnology, North.Holland (Elsevier), Amsterdam, 1993.

[3] Binnig,G., Rohrer,H., Scanning tunneling microscopy, Helvetica Physica Acta, 55: 726-735,1982.

[4] Kroto,H.W.,Heath,J.R.,O'Brein,S.C.O., Curl,R.F., Smally,R.E., C_{60} : Buckministrefullerene, Nature,318:162-163,1985.

[5] D. Kojić, R. Mitrović, L. Matija, Đ. Koruga: Magnetic Force Microscopy application in steel structure and milling process parameters evaluation, *Materials and Manufacturing Processes*, 532-2475, Volume 24, Issue 10, 2009, Pages 1168 – 1172.

[6] D. Kojić, L. Matija, Lj. Petrov, R. Mitrović, Dj. Koruga: Surface characterization of $Pb_{1-x}Mn_xTe$ alloy by Atomic Force Microscopy and Magnetic Force Mode, *Surface Engineering*, 0.1179/174329409X409369.

[7] M.Papić-Obradović, S. Miljković, L. Matija, J. Munćan, Đ.Koruga, Osnove nanomedicine: Embriologija, Farmakologija, Nanotehnologija, DonVas, Beograd, 2010.

[8] Matija, L, Kojić,D., Vasić,A., Bojović,B., Jovanović, T., Koruga,Đ., Uvod u nanotehnologije, DonVas-Nauka, beograd 2011.

Tribological Properties of Materials and Coatings

12th International Conference on Tribology – SERBIATRIB ’11

11 – 13 May 2011, Kragujevac, Serbia

Serbian Tribology Society

SERBIATRIB '11

12th International Conference on Tribology

Faculty of Mechanical Engineering in Kragujevac

Kragujevac, Serbia, 11 – 13 May 2011

WEAR-RESISTANCE OF ALUMINUM MATRIX MICROCOMPOSITE MATERIALS

Mara Kandeva [1], Lidia Vasileva [1], Rangel Rangelov [1], Silvia Simeonova [2]

[1] Technical University – Sofia, Bulgaria, kandeva@tu-sofia.bg , lsvelvi@yahoo.com, rafo@tu-sofia.bg
[2]Space Research and Nanomaterials Institute – Sofia, Bulgaria, svasseva@abv.bg

Abstract: *A procedure is developed for the study of wear of aluminum alloys AlSi7 obtained by casting, reinforced by TiC microparticles, submitted to thermal treatment or without it. Tribological study is realized under conditions of friction on counterbody with fixed abrasive. Experimental results were obtained for mass wear, wear rate, wear intensity and wear-resistance of the alloys with different contents in percentage of microparticles.*

Keywords: *tribology, composite aluminum alloys, microparticles, wear, wear-resistance.*

1. INTRODUCTION

Subject of tribotechnologies is the production and control of surface layers and coatings with physico-chemical and mechano-geometrical characteristics, which provide optimal regime of friction and wear in different exploitation conditions.

Composite materials with Al matrix are relatively new materials, the minimum specific weight and excellent mechanical and tribologcal properties of which make them unique for contact joints, especially for applications in aircraft industry and automotive industry.

The modern stage of advance of these materials is characterized by development of new kinds reinforcing and matrix components. A lot of studies are related to the influence of nature, size and contents in percentage of the disperse particles of silicon carbide, titanium carbide, tungsten carbide, titanium nitride, etc. [1],[2],[4],[5],[6].

A research team of the Department Material Science and Material Technology at the Technical University of Sofia works systematically on the development of technologies for obtaining micro- and nano-composite aluminum base materials, and on the study of their properties [3].

The purpose of the present research is development of the procedure and comparative study of wear and wear-resistance of aluminum alloys (*AlSi7*) with microparticles of titanium carbide (*TiC)* of the size 1.25 to 2.5 μm, without and with thermal treatment. The reinforcement of the aluminum alloy is realized by molding with different contents of microparticles in percentage of casting weight.

2. EXPERIMENTAL STUDY, RESULTS AND DISCUSSION

Wear and wear-resistance are studied for two groups of specimens – casted and treated thermally, reinforced with different contents of microparticles, which is one and the same for both groups of specimens. The study is carried out under conditions of dry friction against counterbody with fixed abrasive, keeping equal conditions of the experiment.

Table 1 shows some of the data and characteristics for both kinds of specimens.

Table 1. Characteristics of the composite materials

№	Code	% TiC	Micro-hardness	Technological data
1	Л-0	0 %		casted
2	Л-0,5	0,5 %		casted
3	Л-2	2 %		casted
4	Л-5	5 %		casted
5	Л-10	10 %		casted
6	Л-15	15 %		casted
7	ТО-0	0 %		treated thermally
8	ТО-0,5	0,5 %		treated thermally
9	ТО-2	2 %		treated thermally
10	ТО-5	5 %		treated thermally
11	ТО-10	10 %		treated thermally
12	ТО-15	15 %		treated thermally

2.1. Procedure and device for experimental study of abrasive wear

The study of wear is realized by means of pin-on-disk device in the Laboratory of Tribology at the Technical University of Sofia, Faculty of Machine Technologies. The procedure meets the requirements of the acting standards, especially the Bulgarian State Standard БДС 14289-77 (matching ISO) *Method for testing of abrasive wear at friction on fixed abrasive particles.*

The functional scheme of the device is given in Figure 1.

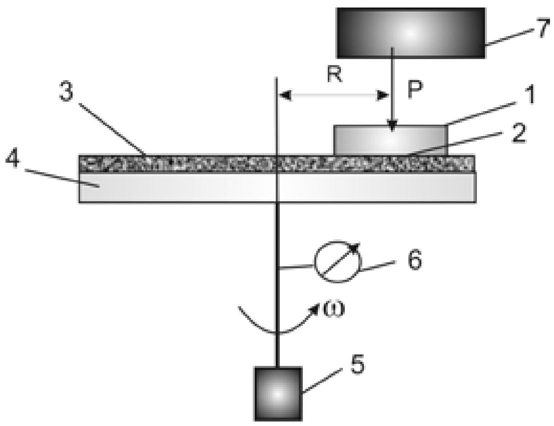

Figure 1. Functional drawing of the device for testing of abrasive wear

The specimen 1 (body) is of the form of parallelepiped with dimensions of the basis 10 x10 mm and height 25 mm. The counterbody 3 is abrasive surface, which is modeled by impregnated corundum with given characteristics – hardness of 60% higher of the microhardness of the surface layer of the tested material and given average size of the abrasive particles.

Coumterbody 3 is fixed on the horizontal carrier disk 4; it is replaced at each measurement. So, equal initial conditions of contact interaction are assured between the butt surface 2 of the tested specimen and the abrasive surface 3. Near the friction path is located the nozzle of a vacuum pump enabling the suction of the waste particles during wear.

The horizontal carrier disk 4 and the abrasive surface 3 rotate with constant speed $\omega = const$ around their vertical axis. The speed of rotation is given by the electrical motor 5; the number of cycles N, respectively the friction way L, are read by the counter 6. Specimen 1 is mounted properly in the loading head 7 providing by means of leverage system the required normal load P in the gravity center of specimen 1. The average sliding velocity during friction is given through variation of the distance R between the axis of disk 4 and the axis of specimen 1.

The testing procedure goes in the following sequence:

- The surfaces of all specimens prepared in equal form and dimensions are subjected to mechanical treatment of three stages – rough, grinding and polishing up to the achievement of equal roughness $Ra = 0{,}4 \div 0{,}6\ \mu m$. This is necessary and compulsory condition in order to provide equal initial conditions at the subsequent comparative study or specimens' wear-resistance.
- By choosing the most popular integral parameter „mass wear", we have to weight specimen's mass before and after a given friction way (number of cycles of interaction) using electronic balance of the type WPS 180/C/2 with accuracy up to 0,1 mg. Before each measurement by the balance, the specimens are cleaned by a solution neutralizing the static electricity.
- Specimen 1 is mounted in the loading head 7 in a given position. The normal central load P is given through the leverage system.

The basic parameters of the study are as follows:

- *absolute mass wear* m, $[mg]$ - the destroyed mass of the surface layer of the specimen as difference between the mass of the specimen before and after the specified time of contact interaction.
- *mass wear rate* $\dot{m}$ $[mg/\min]$ - the destroyed mass of the surface layer during one minute time.
- *wear intensity* i - the destroyed thickness of the surface layer in a unity of friction way. It is a dimensionless quantity; if expressed through the destroyed mass, it can be calculated by the formula:

$$i = \frac{m}{\rho . A_a . L} \left[\frac{kg.m^3}{kg.m^2.m} \right] \qquad (1)$$

where:

ρ is the material density of the specimen - $\rho = 2{,}7.10^3 \left| kg/m^3 \right|$;

A_a is the apparent contact area of the interaction.

L is the way of friction calculated by the corresponding number of cycles of contact interaction N using the formula:

$$L = 2\pi.R.N \quad [m] \qquad (2)$$

Here R is the distance between axis of rotation of the carrier disk and the center of mass of the specimen according to Figure 1.

- *absolute wear-resistance* I - a dimensionless quantity calculated as reciprocal value of wear intensity, i.e.

$$I = \frac{1}{i} = \frac{\rho . A_a . L}{m} \qquad (3)$$

- *nominal contact pressure* $p_a, [N/cm^2]$, i.e. the normal load distributed on unity apparent contact area of interaction A_a, so

$$p_a = \frac{P}{A_a} \qquad (4)$$

2.2. Experimental results

The described device and procedure have provided experimental results about wear, and wear rate depending on the number of cycles (friction time) at different contents of microparticles. Table 2 shows the parameters of the experimental study.

Table 2. Parameters of the experimental study

Apparent contact area A_a, $[m^2]$	1.10^{-4}
Nominal contact pressure p_a, $[N/m^2]$	$10{,}50.10^{-4}$
Average sliding velocity V, $[cm/s]$	15,96

Figures 2 and 3 show plots of the relationship of mass wear m and number of cycles N for various contents of microparticles of TiC in the case of casted (Figure 2) and thermally treated (Figure 3) Al alloys.

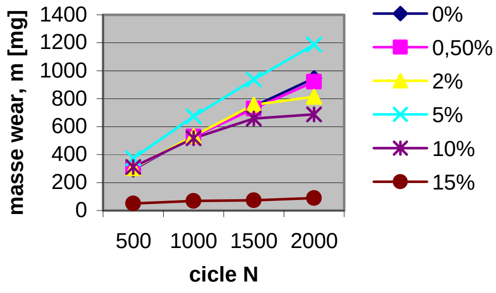

Figure 2. Mass wear versus number of cycles N at various % contents of TiC microparticles in the case of casted Al alloys

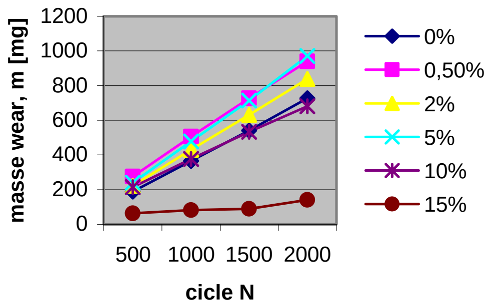

Figure 3. Mass wear versus number of cycles N at various % contents of TiC microparticles in the case of thermally treated Al alloys

Figures 4 and 5 show plots of the relationship of mass wear m and contents of microparticles of TiC in the case of casted (Figure 4) and thermally treated (Figure 5) Al alloys.

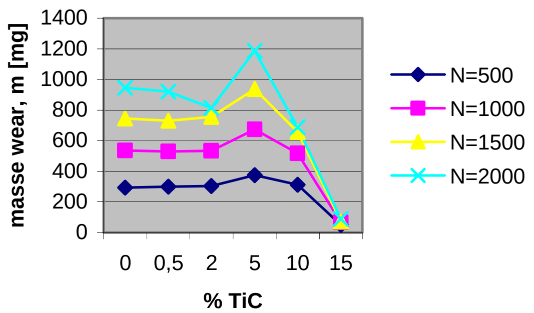

Figure 4. Mass wear versus % contents of TiC microparticles for different number of cycles N in the case of casted Al alloys

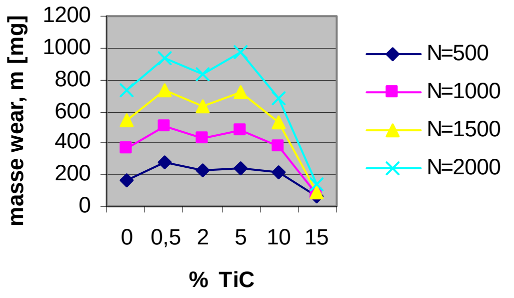

Figure 5. Mass wear versus % contents of TiC microparticles for different number of cycles N in the case of thermally treated Al alloys

Figure 6 show plots of the relationship of mass wear rate and contents of microparticles of TiC in the case of casted Al alloys specimens.

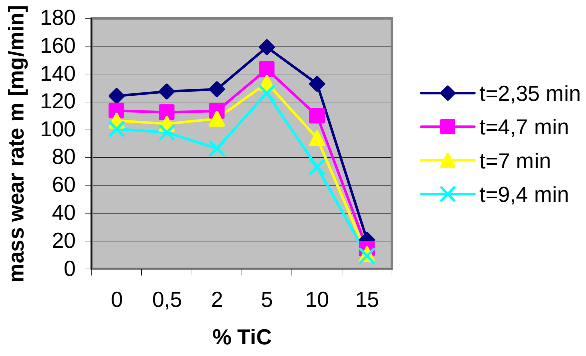

Figure 6. Mass wear rate $\dot{m}$ versus % contents of TiC microparticles for different time of wearing in the case of casted Al alloys

Table 3 gives the data about wear intensity and wear-resistance calculated according to equations (1) and (3) at $N = 2000$ cycles for all specimens

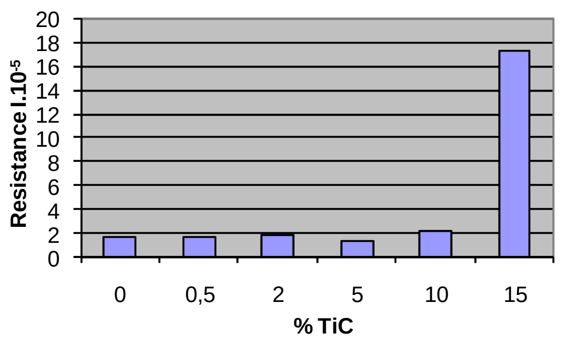

Figure 7. Diagram of wear-resistance at various % contents of TiC microparticles in the case of casted Al alloys

Table 3. Wear intensity i and wear-resistance I in the case of casted and thermally treated Al alloys

№	Code	Wear intensity i	Wear-resistance I
1	Л-0	$0{,}62.\ 10^{-5}$	$1{,}61.10^{5}$
2	Л-0,5	$0{,}6.\ 10^{-5}$	$1{,}67.10^{5}$
3	Л-2	$0{,}53.\ 10^{-5}$	$1{,}88.10^{5}$
4	Л-5	$0{,}78.\ 10^{-5}$	$1{,}28.10^{5}$
5	Л-10	$0{,}45.\ 10^{-5}$	$2{,}22.10^{5}$
6	Л-15	$0{,}06.\ 10^{-5}$	$17{,}24.10^{5}$
7	ТО-0	$0{,}48.\ 10^{-5}$	$2{,}1.10^{5}$
8	ТО-0,5	$0{,}62.\ 10^{-5}$	$1{,}62.10^{5}$
9	ТО-2	$0{,}55.\ 10^{-5}$	$1{,}81.10^{5}$
10	ТО-5	$0{,}64.\ 10^{-5}$	$1{,}57.10^{5}$
11	ТО-10	$0{,}45.\ 10^{-5}$	$2{,}24.10^{5}$
12	ТО-15	$0{,}092.\ 10^{-5}$	$10{,}86.10^{5}$

Figures 7 and 8 show diagrams of the wear-resistance for various % contents of TiC microparticles, respectively in the cases of casted (Figure 7) and thermally treated (Figure 8) Al alloys.

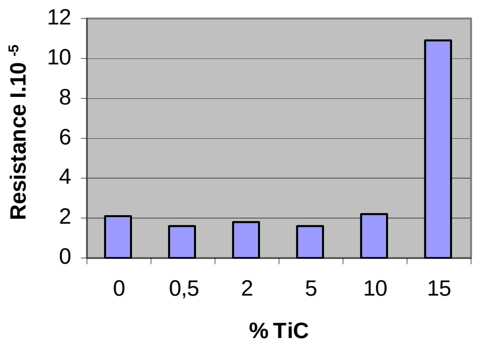

Figure 8. Diagram of wear-resistance at various % contents of TiC microparticles in the case of thermally treated Al alloys

2.3. Discussion on the experimental results

The analysis of the relationship mass wear versus friction way (number of cycles) shows clearly expressed linear proportionality (Figure 2 and Figure 3). Some kind of nonlinearity appears for casted non-thermally treated alloys with contents of microparticles 2% and 10% in the direction of wear decrease after $N = 1000$ cycles.

When the way of interaction corresponds to $N = 2000$ cycles and the wearing is in stationary regime, minimal wear values show casted specimens with 15% TiC - $m = 89\ mg$ (Figure 4).

At the same particle contents and $N = 2000$ cycles wear is about 1.6 times higher for thermally treated specimens, i.e. $m = 140{,}1\ mg$ (Figure 5).

The influence of the % contents of microparticles upon wear is ambiguous. In the case of casted alloys the presence of microparticles TiC with 0,5% and 2% contents does practically not influence the wear values. At 5% wear sharply grows up and at $N = 2000$ the value of wear $(m = 1187{,}2mg)$ is 1.25 times higher than that of casted specimen without microparticles $(m = 946{,}2mg)$- Figure 4. Strong decrease of wear is available at 15% TiC.

In the case thermally treated specimens (Figure 5) the minimal wear value is at 15% TiC $(m = 140{,}1mg)$, however this value is higher than that of the casted (non-thermally treated) alloys at the same % contents TiC $(m = 89mg)$.

Mass wear rate is a significant factor in the process of running-in in tribosystems; the higher rate assumes shortening of this period of adaptation and transition to stationary regime of operation. For casted specimens (Figure 6) at 15% TiC the wear rate is minimal - $\dot{m} = 9{,}4mg/\min$, and for thermally treated specimens our results showed $\dot{m} = 14{,}9mg/\min$.

Wear-resistance is a complex parameter of the contact interaction in tribosystems. It is highly sensitive to a lot of factors – structure, contents and properties of surface layers; structure and properties of counterbody; presence of lubricant layers, wear debris, aggressive environment; dynamic parameters – sliding velocity, frequencies, vibrations, etc. Even with fixed parameters of interaction, the factor „time" determines in various degree the value of wear, correspondingly the wear-resistance of different materials.

The analysis of the results in Table 3, Figures 7 and 8 demonstrates that the wear-resistance of casted specimens at 15% contents of TiC particles is the highest one $\left(I = 17{,}24.10^5\right)$ and is 1,6 times higher than that of thermally treated specimens with the same contents of microparticles.

3. CONCLUSION

- Procedure was developed and comparative study was carried out for wear and wear-resistance of composite aluminum alloys, casted without and with thermal treatment, reinforced by various contents of microparticles of TiC - 0,5%; 2%; 5%; 10%; 15%.
- Experimental results are obtained for the relationships of mass wear, wear rate, wear intensity and wear-resistance.
- The basic conclusion is that reinforcement of aluminum alloys by TiC microparticles leads to significant increase of their wear-resistance. The maximal wear-resistance in stationary regime of wearing showed casted non-thermally treated alloys reinforced by 15% microparticles contents. Maximal wear rate under the same conditions exhibited alloys with 5% microparticles contents.

The obtained results involve a complex future study of the tribological parameters of these alloys, having in view their operation under various exploitation conditions of interaction.

Acknowledgements:

1. The research team at department of Materials Science and Technology thanks to the Research Center at the Technical University of Sofia for the support and sponsoring of manufacturing and technological investigations of the new Al-Si matrix composites reinforced by micro TiC particles with Contract: №102 ni 123-5q2010/2011.

2. The tribological investigations are related to the first stage of the completion of the International Contract № ДНТС 02/12 in the scientific-technical collaboration between Romania and Bulgaria for 2010 in the topic „Tribotechnological study and qualification of composite materials and coatings lubricated by biodegradable fluids".

REFERENCES

[1] L. Vishniakov, V. Moroz, B. Sinaiskii, I. Romashko, V. Voropaev, V. Varchenko: Разработка и триботехнические свойства композиционных алюмоматричных материалов с частицами карбида кремния (Development and tribotechnical properties of Al matrix composite materials reinforced by SiC particles), Конструкційні іфункціональні матеріали (Construction and Functional Materials), Kiiv, 2009 (in Russian).

[2] T. Chernishova, L. Kobeleva, L. Bolotova: Дискретно армированные композиционные материалы с матрицами из алюминиевых сплавов и их трибологические свойства (Discrete reinforcement of Al matrix composite materials and their tribological properties), Металлы (Metals), № 6, pp. 85-98, 2001 (in Russian).

[3] L.Vasileva, R. Rangelov,I. Yankova, S. Simeonova, G, Avdeev, V.Yurukov, K. Petrov: Casting and Characterization of Al-Si Matrix Composites Reinforced by TiC Microparticles, Journal of Challenges in Higher Education and Research, Heron Press, vol. 9, Sofia, 2010.

[4] Y. Sahin: Preparation and some properties of SiC particle reinforced aluminum alloy composites, Materials and Design 24, pp 671-679, 2003.

[5] S. Zhang: Comparison of friction and wear performance of brake material dry sliding against two aluminum matrix composites reinforced with different SiC particles, Journal of Material Processing Technology 182, pp 122-127, 2007.

[6] T. Chernishova, L. Kobeleva, L. Bolotova, A. Panfilov: Алюмоматричные композиционные материалы антифрикционного назначения (Al matrix composite materials with antifriction use), Nauka, Moscow, pp.272-279, 2005 (in Russian).

Serbian Tribology Society

SERBIATRIB '11

12th International Conference on Tribology

Faculty of Mechanical Engineering in Kragujevac

Kragujevac, Serbia, 11 – 13 May 2011

ABOUT THE DEPOSITION OF SUPERALLOYS BY MEANS OF SUPERSONIC HVOF PROCESS

Iliyan Peichev [1], Mara Kandeva [2], Emilia Assenova [3], Viara Pojidaeva [4]

[1]Shumen – Passenger Autotransport Ltd , the city of Shumen, Bulgaria, iliqn_pei4ev@abv.bg
[2] Tribology Center - Technical University – Sofia, Bulgaria, kandeva@tu-sofia.bg
[3]The Society of Bulgarian Tribologists, Bulgaria, emiass@abv.bg
[4]University of Mining and Geology „St Ivan Rilsky" – Sofia, Bulgaria, vpojidaeva@abv.bg

Abstract: *The influence of the parameters of HVOF-technology on the quality of coatings obtained of three powder superalloys: 502 P, SX 199 and 6P50 WC has been studied in the paper. Experimental results about microhardness, porosity and roughness of the three coatings under three regimes of deposition have been obtained.Optimal parameters of the supersonic system of deposition "MICROJET-POWDER"have been found in relation to microhardness, porosity and roughness of the obtained coatings.*

Keywords: *tribology, superhard coatings, tribotechnologies, microhardness, roughness, porosity*

1. INTRODUCTION

Thermal deposition represents a complex of processes, where the introduced in the input material is heated and shooted in the form of independent particles or drops onto the given surface. The thermal deposition device generates heat necessary for the process by means of inflammable gases or electrical arcing.

During the heating, materials pass in plastic or melted state and are involved and accelerated to the basic surface in the stream or jet of gases under pressure. By their impact with the surface particles are deformed and build thin lamellas (splashes), which form contact bonds on the one hand with the roughness of the prepared surface, and, on the other hand – with the neighbouring lamellas.

The particles/drops cool during the impact with the surface and pile up a splash in laminar structure forming the deposited coating.

Figure 1 shows schematically the cross-section of the laminar structure of the deposited coating. It is a non-homogeneous structure containing a certain amount of pores and oxides in the case of metal deposition. The deposited material could be any fusible substance – metals, metal compounds, cements, oxides, polymers, etc. The source material can be given in the form of powder, wire or rod.

The forming contact bond between coating and basic surface could be mechanical, chemical and metallurgical, or combination of the three.

The properties of the deposited coating depend on the mutual action of different factors – source material, type and parameters of the used technological process, subsequent treatment of the deposited coating [1], [2].

The basic criterion for using a given material as a coating is the possibility that its particles are fusible or can transform in a state of high plasticity, deforming afterwards during the impact with the surface. The high temperatures combined with the possibility of regulation of composition, stream energy and its spatial configuration to the surface give a great variety of materials to form coatings of different characteristics.

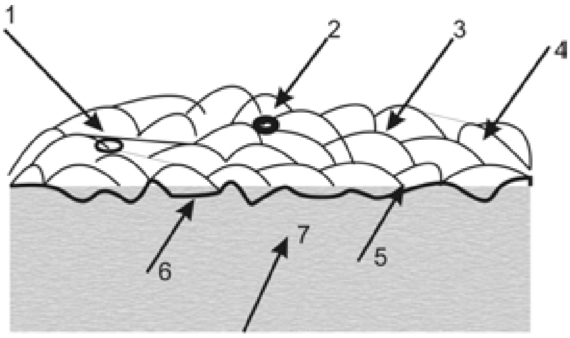

Figure 1. Typical cross-section of laminar structure of deposited coating

1 – pores; 2 – oxide inclusions; 3 – cohesion contacts between coating's parcticles; 4 – splashes (lamellas); 5 – adhesion contacts between surface and coating; 6 – roughnesses in the surface layer of the basic surface 7.

HVOF is one of the most recent methods in the tribotechnologies for thermal deposition of coatings. It represents a gas-flame supersonic process, where oxigen and combustible gas are used under high pressure.

Typical combustible gases are propane, propylene and hydrogene. The burning gas mixture is accelerated to supersonic velocity and the source powder material is injected in the flame.

HVOF technology minimizes the used thermal energy and maximizes the kinetic energy of the particles, so that coatings of high density, low porosity and high adhesion strength are obtained.

HVOF systems are compact, suitable for open-air usage; they are however mainly used in workshop conditions.

Wear-resistant coatings obtained by HVOF technology are widely used for improvement of the resource of contact elements, joints and systems, especially such of large size, in power engineering, industry, transport, etc.

The deposited HVOF coatings of superalloys are extremely important under conditions of high abrasion, erosion and cavitation [3], [4].

The paper aims investigation of the influence of the parametrs of HVOF-technology on the quality of coatings obtained from powder superalloys.

2.1. Experimental study

Coatings deposited by HVOF-technology obtained of three powder superalloys: 502P, SX199 and 6P50WC, have been studied.

Tables 1, 2 and 3 show the data about the chemical composition and physic-mechanical properties of those superalloys.

Table 1. Superalloy 502 P

№	Chemical composition	Specific weight	Melting point ^oC	Mohs' hardness
1.	Cr, 13,94 %	7,18	1850	9
2.	Si, 3,65 %		1414	7
3.	B, 2,52 %	2,3	2300	9
4.	Fe, 4,19 %	7,86	1535	4
5.	Ni, balance		1455	3,8
6.	Co, 0,03 %		1490	
7.	C, 0,59 %			

Table 2. Superalloy SX 199

№	Chemical composition	Specific weight	Melting point ^oC	Mohs' hardn ess
1.	Cr, 21 %	7,18	1850	9
2.	Ni, 7 %	8,9	1455	3,8
3.	$WC - Cr_3C_2 / C$ 6,1%	18,91	3370	9

Table 3. Superalloy 6P50W

№	Chemical composition	Specific weight	Melting point ^oC	Mohs' hardness
1.	Cr ,13,15 %	7,18	1850	9
2.	Si, 4,28 %		1414	7
3.	B, 2,87 %	2,3	2300	9
4.	Fe, 0,04 %	7,86	1535	4
5.	Ni, balance		1455	3,8
6.	Co, 0,04 %		1490	
7.	C, 0,58 %			
8.	W balance		3370	9

Briefly, the basic interactions between the components of the *superalloys* are:

- At high temperatures chrome (Cr) combines with carbon (C), silicon (Si) and boron (B) creating metalloids. With carbon it forms hard and churlish structure Cr_3C_2 of green color, which does not dissolve in acids. Chrome with atomic weight 52,01 and valency +VI, +III, +II has the isotopes 52, 53, 50, 54. The presence of impurities makes it brittle.

- At high temperatures boron (B) combines with variety of metals (Fe, Ni) forming borides. With carbon it forms boric carbide of great hardness.

- Nickel with atomic weight 58,69 and valency +II, +III has the isotopes 58, 60, 62, 61, 64. It enters the composition of superhard alloys, and exhibits ferromagnetic properties. Nickel is weakly attacked by acids; strong alkalis do not affect it. In oxidant media and high temperatures it combines with oxygen and forms hard oxides NiO of green color.

- Cobalt (Co) and iron (Fe), like nickel, show ferromagnetic properties and are used in the production of superhard alloys with magnetic properties.

- At high temperatures tungsten forms carbides with carbon: WC and W_2C of hardness similar to that of diamond.

The three superalloys 502 P, SX 199 and 6P50WC are obtained by agglomeration process with included phase of sintering. Grain size is in the interval 45+22,5µm. The superalloys sustain coating deposition by the supersonic HVOF process with the system MICROJET-POWDER GMA Belgium.

Coatings have been obtained at three basic technological deposition regimes. The characteristics microhardness, porosity and roughness are studied. The technological parameters are given in Table 4.

Table 4: Technological parameters

Parameters	Regime 1	Regime 2	Regime 3
C_3H_8 / O_2	45%/100%	55%/100%	55%/100%
Speed of deposition	5 diamonds 700 m/s	7 diamonds 1000 m/s	7 diamonds 1000 m/s
Distance orifice-surface	L = 80 mm	L =120 mm	L=160 mm
Angle of the jet	90^o	90^o	90^o
Air pressure	5 bar	5 bar	5 bar
N_2 pressure	4 bar	4 bar	4 bar
Rate of powder feed	1,5 tr/min	1,5 tr/min	1,5 tr/min
Average consumption of powder	22 g/min	22 g/min	22 g/min

2.2. Experimental results

Figures 2, 3 and 4 show graphically the relationship of microhardness in units HRC and coating thickness h [mkm] for each of the three coatings under technological regimes 1, 2 and 3.

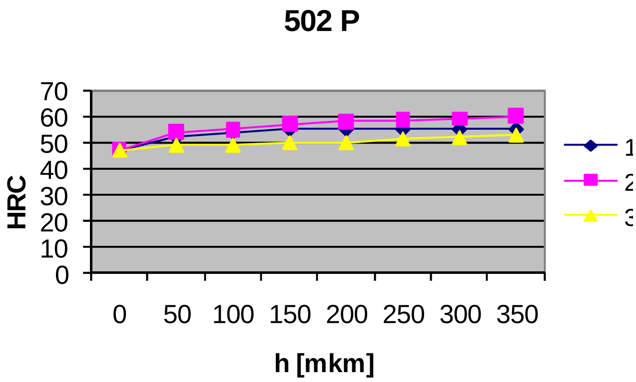

Figure 2. Microhardness versus thickness of the coating 502 P

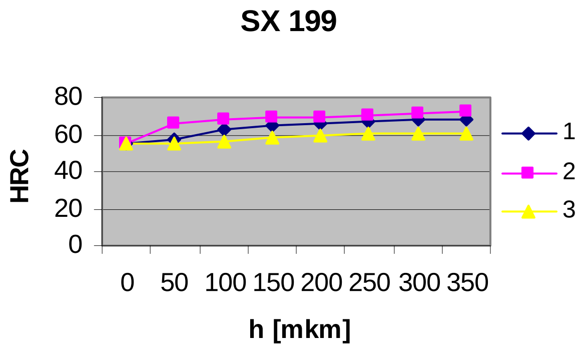

Figure 3. Microhardness versus thickness of the coating SX 199

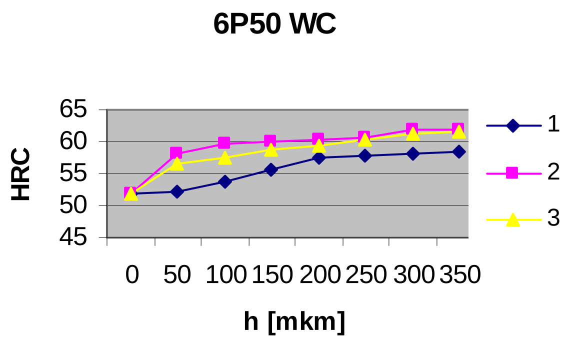

Figure 4. Microhardness versus thickness of the coating 6P50 WC

Figures 5, 6 and 7 give the results of porosity of the three coatings for the three technological regimes according to the data in Table 5.

Table 5. Porosity P

Regime	502 P	SX 199	6P 50W
1	3,7	3,55	3,25
2	2,5	2,3	1,55
3	4,7	4,55	3,8

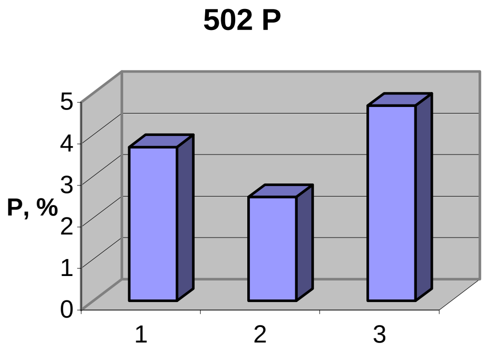

Figure 5. Variation of porosity of coating 502 P for the three technological regimes

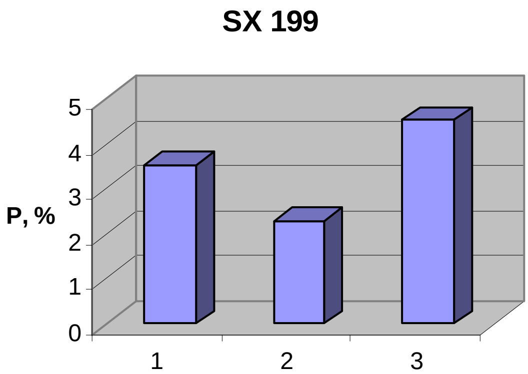

Figure 6. Variation of porosity of coating SX 199 for the three technological regimes

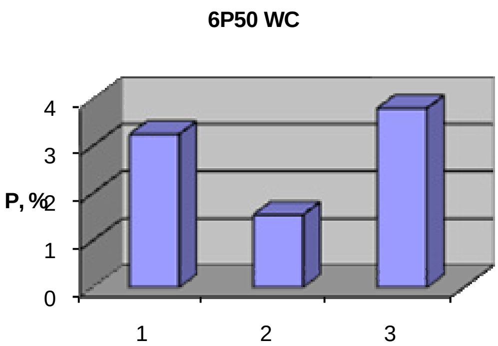

Figure 7. Variation of porosity of coating 6P50 WC for the three technological regimes

Results of roughness Ra study for the three coatings under the three regimes are given in Table 6, and as diagrams – in Figures 8, 9 and 10.

Table 6. Roughness Ra

Regime	502 P	SX 199	6P 50W
1	12 μm	9 μm	9 μm
2	7 μm	6 μm	7 μm
3	6,5 μm	8 μm	9 μm

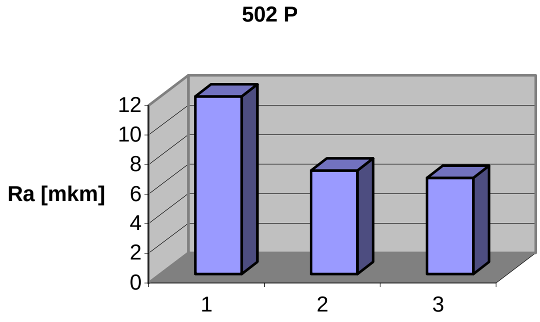

Figure 8. Variation of roughness of coating 502 P for the three technological regimes

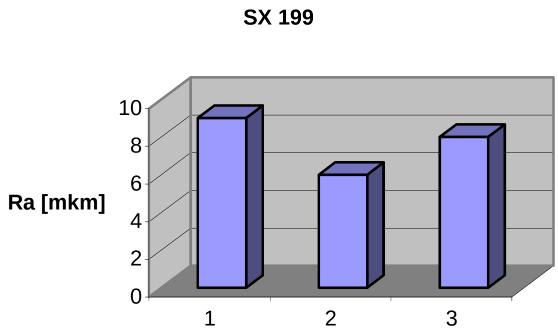

Figure 9. Variation of roughness of coating SX 199 for the three technological regimes

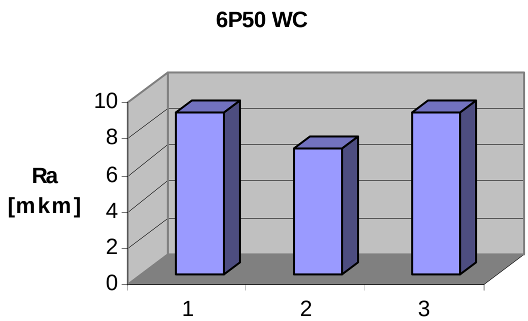

Figure 10. Variation of roughness of coating 6P50 WC for the three technological regimes

2.3. Results analysis

The analysis of the results of microhardness of the coatings in Figures 2, 3 and 4 has shown that evidently microhardness increases with increment of thickness h of the coatings of the three kinds under the three regimes. It has, however, different values and variation character. The maximum value is for h = 350 μm. For coatings *502 P* and *SX 199* the dependence is linear (Figures 2 and 3). The maximal hardness is for coating *SX 199* with the amount of 72 HRC at technological regime 2. This microhardness is obtained yet for the small coating thickness h = 100 μm, then it increases very slowly. The lowest microhardness is for h = 100 μm of coating *502 P*, namely 53 HRC under technological regime 3.

The relationship between microhardness of coating *6P50W* and thickness shows highly nonlinear form at the three regimes of deposition (Figure 4). The maximal microhardness 62 HRC appears for the coating with thickness h = 350 μm under regime 2, it is however lower than the microhardness of coating *SX 199* at the same regime.

Figures 5, 6 and 7 show diagrams of porosity P for the three coatings deposited at the three different regimes. All three coatings have their lowest porosity if obtained at technological regime 2. Minimal porosity shows coating *6P 50W*, namely P = 1,55. At the other two regimes the porosity is maximal for coating *502 P* obtained under regime 2; the value is P = 4,7 that is 3 times higher than the porosity of coating *6P 50W*. Coating *SX 199* obtained under regime 2 shows porosity close to that of coating *6P 50W*.

The diagrams of roughness Ra of the three coatings under the three regimes of deposition are given in Figures 8, 9 and 10 obtained according to the data in Table 6. The diapason of the obtained roughness is between 6 μm and 12 μm. The minimum Ra = 6 μm is for coating *SX 199* at regime 2, and the maximum Ra = 12 μm – for coating *502 P* obtained under regime 1.

Above analysis shows that optimum parameters of the supersonic system of deposition "MICROJET-POWDER" from the point of view of microhardness, porosity and roughness of the obtained coatings are as follows:

- C3H8-O2 =55%/100%
- distance between orifice and surface – L = 120 mm
- angle of the supersonic two phase jet related to the surface – 90^o
- air pressure of the compressor for cooling the system – 5 bar
- pressure of nitrogen in the batch feeding device – 4 bar
- rate of powder supply of the powder feeder – 1,5 tr/min
- average powder material consumption – 22 g/min.

CONCLUSION

- The paper studies coatings of three superalloys 502 P, SX 199 and 6P50 WC at three technological regimes of deposition.
- Experimental results about microhardness, porosity and roughness for the three kinds of coatings under the three technological regimes of deposition have been obtained.
- Optimal parameters of the supersonic system of deposition "MICROJET-POWDER" related to microhardness, porosity and roughness of the obtained coatings have been found.

The research will continue in the direction of the tribological characteristics of the coatings under conditions of interaction with fixed abrasive and hydro-abrasive, as well as under boundary friction and wear.

The investigation for above study is related to the first stage of the completion of the International Contract № ДНТС 02/12 in the scientific-technical collaboration between Romania and Bulgaria for 2010 in the topic „Tribotechnological study and qualification of composite materials and coatings lubricated by biodegradable fluids".

REFERENCES

[1] R.Schwetzke, H. Kreye: Microstructure and properties of coatings and WC deposited by different HVOF–systems, in: Proc. International Conference on Gas-Thermal Powder Deposition, Nice, France, pp. 187-192, 1998.

[2] L. Baldaev, L. Dimitrienko: Study of the possibility of replacement of galvanic chrome coatings by gas-thermal coatings deposited by means of supersonic gas-jet Top GUN-K, Moscow, 2009 (in Russian).

[3] L. Baldaev: Regeneration and reinforcement of machine details by the method of gas-thermal deposition, Ed. KXT, Moscow, 2004 (in Russian).

[4] I. Peichev, Application of supersonic technological processes /HVOF and Plasma/ for deposition of wear-resistant coatings. Corrosion and erosion protection in power plants, in: Tribological Journal, 01/2010, Sofia, pp. 101- 108 (in Bulgarian).

Serbian Tribology Society

SERBIATRIB '11

12th International Conference on Tribology

Faculty of Mechanical Engineering in Kragujevac

Kragujevac, Serbia, 11 – 13 May 2011

EULER'S LAW IN THE ASPECT OF THE GENERAL LAW OF CONTACT INTERACTION OF TRIBOLOGY

Mara Kandeva [1], Emilia Assenova [2], Yana Stoianova [1]
[1] Technical University –Sofia, Bulgaria, kandeva@tu-sofia.bg
[2]The Society of Bulgarian Tribologists, Bulgaria, emiass@abv.bg

Abstract: *The paper studiesEuler's law of friction between flexible thread and immovable cylindrical surface on the base of the contact interaction in tribology. Method and experimental procedure have been developed related to this study, so two improved forms of Euler's law taking into account the duration of the static contact between the flexible element and the fixed surface have been established.*

Keywords: *Tribomechanics, Law of contact interaction, friction force, Euler's law*

1. INTRODUCTION

The general law of contact interaction is a quantitative expression of the contact approach and the model of the functional atom related to all events in the behavior of contact systems. Roughly speaking, this law is the hearth of the interdisciplinary paradigm of tribology. Above facts are exemplified with the conduct of contact systems in different fields of nature, techniques and society [1]÷[5].

The paper aims to analyze and improve Euler's formula on friction between flexible element (a thread or wire) and immovable cylindrical or drum surface [6], [7] by the use of the potentialities of the general law of contact interaction.

This case is worth to be submitted to individual discussion, having in view that Euler's law is recognized as perfect success of mechanics in the field of friction between bodies [6], [7]. Moreover, Euler's law faultlessness is also adopted by the researchers in tribomechanics [8].

2. ANALYSIS

Let the flexible element (metal wire, polymer or textile thread) is put over immovable cylinder with hung equal loads P on both ends, then the initial (starting) friction force T according to Euler's law is calculated by the formula:

$$F = P.e^{\mu.\varphi} = P + T \qquad (1)$$

i.e.

$$T = P\left(e^{\mu.\varphi} - 1\right) \qquad (2)$$

where μ is the initial coefficient of friction, and φ - the enfold angle between thread and cylinder (Figure 1).

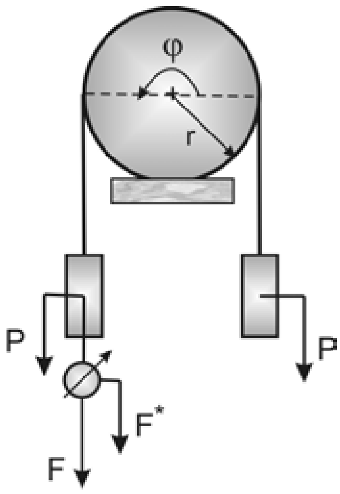

Figure 1. Scheme for the study of the initial friction force

According to equation (2) the friction force depends only on the material of the thread by means of μ, on the load P and the angle φ.

The initial friction force T as a reaction is in general function of the load P and the angle φ for each concrete thread for one and the same cylinder. The load P in that given case is force perturbation, and φ - geometrical perturbation. What is characteristic for Euler's law is that the force T does not depend on the radius r of the cylinder, on the direction of slipping, on the temperature and humidity of the environment, on the duration of the contact, etc.

2.1 Theoretical

Let look at the problem from the viewpoint of the general law of contact interaction in the form:

$$\frac{dR}{R} = \eta_1 \frac{dA_1}{A_1} + \eta_2 \frac{dA_2}{A_2} + ... + \eta_n \frac{dA_n}{A_n} = \sum_i^n \eta_i \frac{dA_i}{A_i} \quad (3)$$

Then the total reaction R is superimposed by the reactions caused by the perturbations A_i with communication potentials η_i.

The general law (3) for the case of Euler (2) has the form:

$$\frac{dT}{T} = \eta_1 \frac{dP}{P} + \eta_2 \frac{d\varphi}{\varphi} + \eta_3 \frac{dr}{r} + \eta_4 \frac{dt}{t} + ... \quad (4)$$

where t is the duration of static contact between thread and cylindrical surface. The communication potentials are obtained experimentally by the formulae:

$$\eta_1 = \frac{\Delta T}{T} : \frac{\Delta P}{P}\,; \varphi = const;\ r = const\,; t = const \quad (5)$$

$$\eta_2 = \frac{\Delta T}{T} : \frac{\Delta \varphi}{\varphi}\,; P = const;\ r = const\,; t = const \quad (6)$$

$$\eta_3 = \frac{\Delta T}{T} : \frac{\Delta R}{R}\,; P = const;\ \varphi = const\,; t = const \quad (7)$$

$$\eta_4 = \frac{\Delta T}{T} : \frac{\Delta t}{t}\,; P = const;\ \varphi = const\,; r = const \quad (8)$$

In order to find the partial communication potentials $\eta_1, \eta_2, \eta_3, \eta_4$ as per Euler's theoretical model, taking logarithm and differentiation of equation (2) is needed, i. e.:

$$\ell nT = \ell nP + \ell n\left(e^{\mu.\varphi} - 1\right)$$

$$\frac{dT}{T} = \frac{dP}{P} + \frac{d\left(e^{\mu.\varphi} - 1\right)}{e^{\mu.\varphi} - 1} = \frac{dP}{P} + \frac{e^{\mu.\varphi}}{e^{\mu.\varphi} - 1}.\mu.\varphi \frac{d\varphi}{\varphi} \quad (9)$$

Comparison of equations (9) and (4) gives:

$$\eta_1 = 1;\ \eta_2 = \mu.\varphi \frac{e^{\mu.\varphi}}{e^{\mu.\varphi} - 1}\,;\ \eta_3 = 0\,; \eta_4 = 0 \quad (10)$$

In the particular case when $e^{\mu.\varphi} >> 1$, (2) and (10) lead to:

$$T \approx P.e^{\mu.\varphi} \quad (11)$$

$$\eta_2 = \mu.\varphi \quad (12)$$

2.2 Experimental determination of the partial communication potentials

To find η_1, η_2, η_3 and η_4 in compliance with formulae (5), (6), (7) and (8) it is necessary to obtain experimentally the laws for the initial friction force T in the form:

$$T_1 = T_1(P),\ \varphi = const;\ r = const\,; t = const \quad (13)$$

$$T_2 = T_2(\varphi),\ P = const;\ r = const\,; t = const \quad (14)$$

$$T_3 = T_3(r),\ P = const;\ \varphi = const\,; t = const \quad (15)$$

$$T_4 = T_4(t),\ P = const;\ \varphi = const\,; r = const \quad (16)$$

Procedure for measuring the initial friction force

As per Figure 1 and Euler's law in the form

$$F = P.e^{\mu.\varphi}$$

as well as having in view that the force F is superimposed by the balancing load P and an additional tension force F^* read by the electronic dynamometer, i.e.

$$F = P + F^* = P + T$$

we obtain

$$T = F^* \quad (17)$$

This means that the friction force T is taken from the electronic dynamometer and is described by Euler's formula (2).

The present work allows Euler's formula to be verified for the initial friction force by means of comparing the theoretically and experimentally determined communication potentials. Because of the huge amount of experimental work, we consider below the communication potentials η_3 and η_4 only.

Determination of communication potential η_3

Initial friction of a textile thread on duralumin multi-stage cylinder with radii r_1, r_2, r_3, r_4, r_5 is being studied (Figure 2).

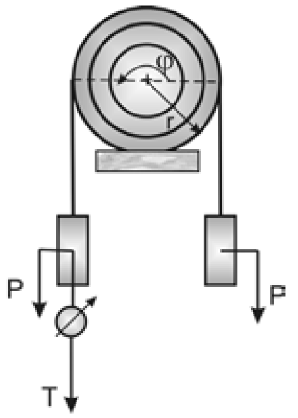

Figure 2. Scheme for the study of the initial friction force of multi-stage cylinder

Figure 3 shows the relationship of the initial friction force T and radius r for constant but different values of P and φ.

It is seen that in all these relations the force T has different values but remains constant and does not depend on r, that is why

$$\eta_3 = \frac{\Delta T_3}{T} : \frac{\Delta r}{r} = 0 \qquad (18)$$

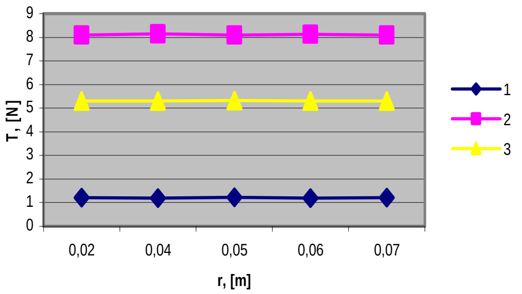

Figure 3. Relationship between initial friction force T and cylinder radius r:

1 - $P = 1{,}3\ N$, $\varphi = \pi$; 2 - $P = 1{,}3\ N$, $\varphi = 3\pi$; 3 - $P = 2{,}0\ N$, $\varphi = 5\pi$.

Determination of communication potential η_4

The reactive communication potential η_4 takes account of the influence of the duration t of the static contact between the thread and the surface upon the initial friction force T; the friction force increases with the duration t of the contact, i.e. $\eta_4 \neq 0$. The influence of t on the force T diminishes with the time.

We assume that this decrease follows the formula in the form:

$$T_4 = T_4^o . t^{k_1}; \ \eta_4 = c_1 t^{\alpha} \qquad (19)$$

and/or the exponential formula:

$$T_4 = T_4^o . e^{-k_{2t}}; \ \eta_4 = c_2 t^{-\beta t} \qquad (20)$$

2.2. Improved forms of Euler's law

The first case of the forms is presented here below. In order to obtain the actual law of initial force T_4 variation, we take the general law of contact interaction under assumption (19), because:

$$\eta_1 = 1; \ \eta_2 = \mu.\varphi; \ \eta_3 = 0; \ \eta_4 = c_1 t^{\alpha} \qquad (21)$$

Substitution of (21) in equation (4)

$$\frac{dT}{T} = \frac{dP}{P} + \mu.\varphi \frac{d\varphi}{\varphi} + c_1 t^{\alpha} \frac{dt}{t} \qquad (22)$$

then integration and taking antilogarithm of (22) lead to:

$$\ell n T = \ell n P + \mu.\varphi + \frac{c_1}{\alpha} t^{\alpha} = \ell n P + \mu.\varphi + c^* t^{\alpha}$$

$$T = P.e^{\mu.\varphi + c^* t^{\alpha}} \qquad (23)$$

Equation (23) represents the law of initial friction force after Euler at large enfold angles $e^{\mu.\varphi} >> 1$.

In the general case, according to (10) we have

$$\eta_2 = \mu.\varphi \frac{e^{\mu.\varphi}}{e^{\mu.\varphi} - 1}$$

Next after substitution in (4), integration and taking antilogarithm we obtain:

$$\frac{dT}{T} = \frac{dP}{P} + \mu.\varphi \frac{e^{\mu.\varphi}}{e^{\mu.\varphi} - 1} \frac{d\varphi}{\varphi} + c_1 t^{\alpha} \frac{dt}{t}$$

$$\ell n T = \ell n P + \ell n \left(e^{\mu.\varphi} - 1\right) + c^* t^{\alpha}$$

$$T = P\left(e^{\mu.\varphi} - 1\right) e^{c^* . t^{\alpha}} \qquad (24)$$

Equation (24) corresponds to the law of initial friction force after Euler in the general case of enfold' angles. The constants c^* and α are experimentally found through measurement of friction force and drawing the relationship $T = T(t)$ for several values of P and φ (See Figure 4).

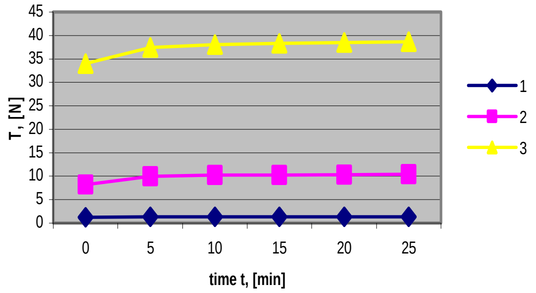

Figure 4. Relationship of friction force T and duration t of the static contact: 1- $P = 1{,}3\ N$, $\varphi = \pi$; 2 - $P = 1{,}3\ N$, $\varphi = 3\pi$; 3 - $P = 1{,}3\ N$, $\varphi = 5\pi$.

After processing the experimental data, the following values of the constants have been obtained:

$$c^* = 0{,}05;\quad \alpha = 0{,}2\,.$$

The coefficient of friction μ is determined according to Euler's formula in the form (2) by means of measurement of friction force T at the following conditions:

$$\varphi = \pi;\ P = 1{,}3\,\mathrm{N};\ r_1 = 20.10^{-3}\,\mathrm{m};\ t = 0,\ \mathrm{i.e.}$$

$$\mu = \frac{1}{\varphi}\ell n\frac{P+T}{P} \qquad (25)$$

For the case of that experiment the friction coefficient is $\mu = 0{,}21$.

A new moment is that the improved law of initial friction force in its two forms (23) and (24) takes into account the natural influence of contact upon the behavior of tribosystems related to the changes in the real area of interaction throughout time *t*.

3. CONCLUSION

The interdisciplinary paradigm of tribology presupposes availability of a general law of contact interaction. Above paper reveals the putting into operation of that general law in a particular law in the field of tribomechanics, namely Euler's law of friction between flexible element and cylindrical surface.

Following new elements are to be outlined in the present work:

- The classical communication potentials for Euler's law η_1, η_2, η_3 and η_4 are obtained following the universal procedure of the law of contact interaction.
- Experimental procedure has been developed for the study of the initial friction force and of the communication potential η_4 taking into account the effect of the duration of static contact.
- The law of variation of the communication potential η_4 is found and Euler's law on the initial friction force is obtained in two forms taking into account the effect of the duration of static contact.

The proposed procedure allows expanded study of the influence of supplementary external and internal factors on the contact system – humidity, temperature, surface layer roughness, nature of bodies, dynamic impacts, etc.

REFERENCES

[1] N. Manolov, M. Kandeva: *Overall Tribology*, Sv. Ivan Rilsky, Sofia, 2004 (in Bulgarian).

[2] N. Manolov, M. Kandeva: *Mechanics in Interdisciplinary Style*, „Sv. Ivan Rilsky", Sofia, 2004 (in Bulgarian).

[3] N. Manolov, M. Kandeva: *Interdisciplinary Paradigm of Tribology*, Technical University-Sofia, 2010 (in Bulgarian).

[4] M. Kandeva, N. Hristov, N. Tonchev, E. Assenova: Tribological Study of Cladded Bimetallic Coatings, *Solving Friction and Wear Problems, Proceedings of the 17th International Colloquium Tribology*, Esslingen, Germany, 19-21 January, 2010.

[5] M. Kandeva, E. Assenova, M. Manolova-Daneva: Triboecology as methodological centre of modern science, *Proceedings of the Intern. Conf. "ECOTRIB 2009"*, Pisa, Italy.

[6] N.I. Kolchin: *Machine Mechanics*, vol. 2, Mashinostroienie, Leningrad, 1972 (in Russian).

[7] V.F.Zhuravlev: History of the law of dry friction. *Doklady Physics*, vol.55, No. 7, 344-345, Springer Verlag, 2010.

[8] A.A.Nedostup, E.K.Orlov: Study of the static coefficient of friction of nfishing cordage on a friction gear drum. *Journal of Friction and Wear*, vol. 31, No. 4, 301-307, Springer Verlag, 2010.

Serbian Tribology Society

SERBIATRIB '11

12th International Conference on Tribology

Faculty of Mechanical Engineering in Kragujevac

Kragujevac, Serbia, 11 – 13 May 2011

INFLUENCE OF TIN ON THE STRUCTURE AND PROPERTIES OF SPHEROGRAPHITIC CAST IRON

Boriana Ivanova [1], Mara Kandeva [1], Zhulieta Kaleicheva [1], Rangel Rangelov [1]
[1] Technical University – Sofia, Bulgaria, kandeva@tu-sofia.bg

Abstract: *Spherographitic (high strength) cast iron is construction material with complex of properties, due to which it is different from the traditional Fe-C alloys. Its mechanical and tribological properties are determined by the structure – form and distribution of graphite inclusions, dispersity and composition of the metal base in the bulk and the surface layers. The paper aims study of the relationship between wearresistance and the amount of tin in spherographitic cast iron. Results are obtained about wear, wear rate and wearresistance of high strength cast iron with different concentration of Sn.*
The study is related to the first stage of the International Contract № ДНТС 02/12 of scientific-technical collaboration between Romania and Bulgaria for 2010 in the topic „Tribotechnological study and qualification of composite materials and coatings lubricated by biodegradable fluids" lead by Assoc. Prof. Mara Kandeva and financed by the Fund Scientific Research at the Bulgarian Ministry of Education and Science.

Keywords: *High strength cast iron, Sn influence, tribotechnologies, wearresistance*

1. INTRODUCTION

Cast irons are natural composite materials of steel metal base and imbedded graphite phase. Mechanical and tribologcal properties of cast iron are determined by its structure – form and distrubution of graphite inclusions, dispersity and structure of the metal base in bulk and surface layers. The various combinations of different microstructures of matrix and, on the other hand, the form, size and distrubution of graphite phases determine the great reserve of structures and properties of these alloys with huge application in industry.

Spherographitic (high strength) cast iron is construction material with a complex of properties, due to which it is different from the traditional Fe-C alloys. Spherographitic cast iron has very high tensile strength, high plasticity, lower sensitivity to stress concentration, good wearresistance and good casting properties.

Adding tin in greater amounts has anti-spheroidal action [1], [2], which requires some supplementary studies giving idea of the behavior of the material under operating and exploitation conditions.

The paper aims study of the relationship between wearresistance and the amount of tin in spherographitic cast iron.

2. ANALYSIS

Results obtained by the authors in previous studies have shown the influence of tin on the structure of the metal base for molded samples of spherographitic cast iron [3].

The paper proposes an investigation of wear on samples with different contents of Sn: 0,003 %, 0,01 %, 0,026 % and 0,062 % under conditions of fixed abrasive wear. Sample characteristics are given in Table 1.

Table 1. Chemical contents of the specimens

Chem. element [%] / Specimen №	0	1	2	3	4
Hardness [HB]	183	152	209	217	244
C	3.8	3.8	3.8	3.8	3.8
Mn	0.23	0.14	0.14	0.14	0.14
Si	1.84	1.28	1.28	1.28	1.28
P	0.037	0.02	0.02	0.02	0.02
S	0.008	0.017	0.017	0.017	0.017
Cr	0.036	0.01	0.01	0.01	0.01
Ni	0.027	0.013	0.013	0.013	0.013
Cu	0.088	0.012	0.012	0.012	0.012
Sn	0	0.003	0.01	0.026	0.062

2.1 Method and device for abrasive wear study

The study is realized using the procedure and device of the type „pin-disk" in the Laboratory of Tribology at the Technical University Sofia – Faculty of Machine Technology [4], [5]. The procedure follows the requirements of the acting standards, especially the Bulgarian State Standard БДС 14289-77 [6], which is harmonized to ISO.

The functional scheme of the device is given in Figure 1.

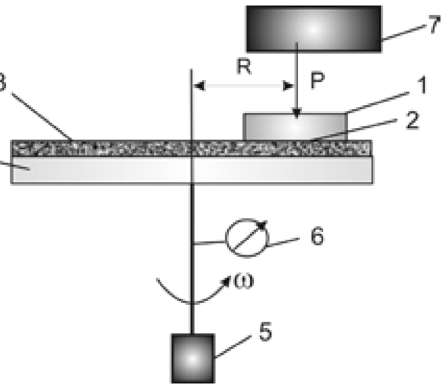

Figure 1. Functional scheme of the device for abrasive wear study

The specimen 1 (the body) has the form of parallelepiped with dimensions of the base 10x10 mm and height 25 mm. Counterbody 3 is the abrasive surface, which is being modeled by impregnated $A\ell_2O_3$ corundum with given characteristics – hardness 60% higher than the microhardness of the surface layer of the samples and definite average size of the abrasive particles.

Counterbody 3 is fixed on the supporting horizontal disk 4 and is changed at each measurement. This guaranties equal initial conditions of contact interaction between the butt surface 2 of the tested specimen and the abrasive surface 3. Near the friction path is the nozzle of a pump in order the wear waste be sucked during the process of wear.

The supporting horizontal disk 4 along with the abrasive surface 3 rotates with constant speed $\omega = const$ around its vertical axis. The rotational speed is given by a motor 5, and the number of cycles N, respectively the friction way L is read on the counter 6. The specimen 1 is fixed in the loading head 7 providing the desired normal load P in the center of gravity of the specimen 1 by a system of leverages. The average sliding speed is given and calculated by the variation of the distance R between the axes of disk 4 and specimen 1.

The procedure of the test represents the following:

1. The surfaces of all specimens, which are of equal form and size are subjected to mechanical treatment in three stages – rough treatment, grinding and polishing up to attaining equal roughness $Ra = 0{,}4 \div 0{,}6\ \mu m$. This is the necessary and obligatory condition to provide equal initial conditions in the comparative study of the wearresistance of the specimens.
2. Specimens' mass is measured before and after a given friction way (number of cycles of interaction) by means of electronic balance type WPS 180/C/2 with accuracy 0,1 mg. Before each measurement the specimens are cleaned by solution neutralizing the static electricity.
3. Specimen 1 is fixed in the loading head 7 in a given position and the central load P is set by means of the leverage system.

All specimens are tested at equal conditions: normal load in the center of the specimen, sliding speed and counterbody surface.

2.2 Basic parameters of the study

The basic parameters of the study are:

- *absolute mass wear* m, $[mg]$ - the destroyed mass of the surface layer of the specimen as difference between the specimen's mass before and after the given time t of contact interaction (number of cycles N).
- *mass wear rate* $\dot{m}$ $[mg/\min]$ - the destroyed mass of the surface layer in one minute time.
- *wear intensity* i - the destroyed thickness of the surface layer in a unit friction way. It is a dimensionless quantity, expressed by the destroyed mass and calculated by the formula:

$$i = \frac{m}{\rho . A_a . L} \quad \left[\frac{kg.m^3}{kg.m^2.m} \right] \qquad (1)$$

where:

ρ is the density of specimen's material - $\rho = 7{,}8.10^3 \left|kg/m^3\right|$;

A_a is the apparent contact area of interaction, in that particular case $A_a = 10.10^{-4} \left|m^2\right|$;

L is the friction way calculated by the corresponding number of cycles N of the contact interaction as per the formula:

$$L = 2\pi.R.N \quad [m] \tag{2}$$

Here R is the distance between the rotation axis of the supporting disk and the mass center of the specimen according to Figure 1.

- *absolute wearresistance* I - a dimensionless quantity calculated as reciprocal value of wear intensity, i. e.

$$I = \frac{1}{i} = \frac{\rho.A_a.L}{m} \tag{3}$$

- *nominal contact pressure* p_a, $\left|N/cm^2\right|$ which is the normal load distributed on unity apparent contact area of the interaction A_a, i.e.

$$p_a = \frac{P}{A_a} \tag{4}$$

For the given conditions of the experiment $p_a = 10{,}5 \left|N/cm^2\right|$

- *comparative index of wearresistance* ε_{ie} - represents the ratio between the wearresistance of the tested specimen I_i and the wearresistance of a sample specimen I_e, i.e. it is a dimensionless quantity, which shows how many times the wearresistance of the tested coating is higher than that of the sample specimen at equal conditions of contact interaction:

$$\varepsilon_{ie} = \frac{I_i}{I_e} \tag{5}$$

The sample specimen is a sample of basic cast iron.

2.3 Experimental results

The described procedure and device gave the possibility to obtain experimental results about the relationship of the mass wear m and the number of cycles N and about the dependence of the wear rate $\dot{m}$ on time t of the contact interaction, given in Tables 2 and 3 and graphically in Figures 2 and 3.

Table 2. Relationship between mass wear and number of cycles $m = m(N)$

Sn [%]	N 500	N 1000	N 1500	N 2000	N 2500	N 3000
0	55,0	46,5	34,5	29,3	24,0	23,9
0,003	16,2	15,4	14,2	14,6	14,85	14,9
0,01	46,4	32,4	20,3	18,4	16,8	16,5
0,026	37,4	37,1	36,7	35,7	34,6	33,9
0,062	36,3	24,2	19,0	15,5	12,7	12,6

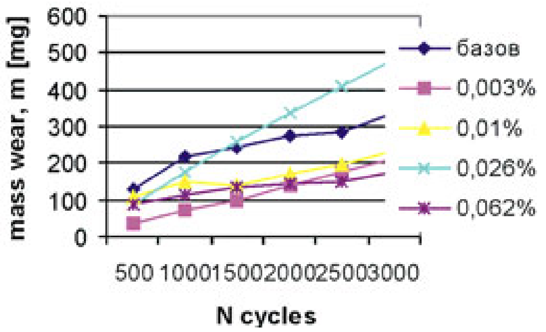

Figure 2. Relationship between mass wear m and number of cycles N (friction way)

Table 3. Relationship between wear rate $\dot{m}$ and time t

Sn [%]	t=2,35 [min]	t=4,7 [min]	t=7 [min]	t=9,4 [min]	t=11,7 [min]	t=14,1 [min]
0	55,0	46,5	34,5	29,3	24,0	23,9
0,003	16,2	15,4	14,2	14,6	14,85	14,9
0,01	46,4	32,4	20,3	18,4	16,8	16,5
0,026	37,4	37,1	36,7	35,7	34,6	33,9
0,062	36,3	24,2	19,0	15,5	12,7	12,6

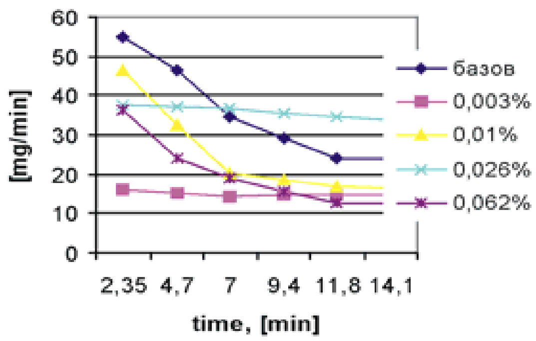

Figure 3. Relationship between wear rate $\dot{m}$ and time t

Table 4 gives experimental data about the variation of wear intensity i with time t calculated as per formula (1). Figure 4 shows this relationship graphically for all specimens.

Table 4. Relationship of wear intensity i on time t

Sn	0 %	0,003 %	0,01 %	0,026 %	0,062 %
t=2,35 [min]	0,25	0,07	0,21	0,17	0,17
t=4,7 [min]	0,42	0,14	0,30	0,34	0,22
t=7 [min]	0,47	0,19	0,28	0,50	0,26
t=9,4 [min]	0,53	0,27	0,34	0,67	0,28
t=11,75 [min]	0,55	0,34	0,38	0,77	0,29
t=14,1 [min]	0,66	0,42	0,45	0,90	0,34

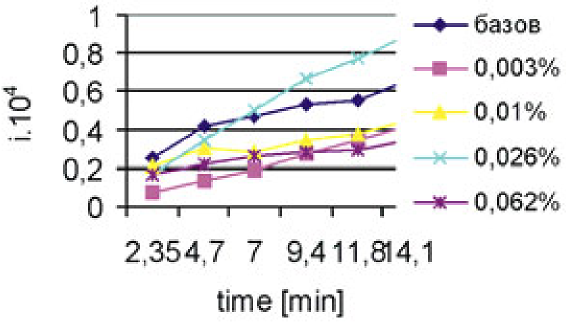

Figure 4. Variation of wear intensity i with time t

Table 5 shows the wearresistance I and the comparative index of wearresistance ε determined by formulae (3) and (5) for $N = 3000$ cycles, i.e. at friction way $L = 659{,}40\ [m]$. The data of Table 4 are presented graphically in Figure 5.

Table 5. Wearresistance I and comparative index of wearresistance ε

Sn [%]	I	$\varepsilon = \frac{I_i}{I_e}$
0	$1{,}5\ 10^4$	1
0,003	$2{,}4.\ 10^4$	1,6
0,01	$2{,}2.\ 10^4$	1,47
0,026	$1{,}1.\ 10^4$	0,73
0,062	$2{,}9.\ 10^4$	1,93≈2

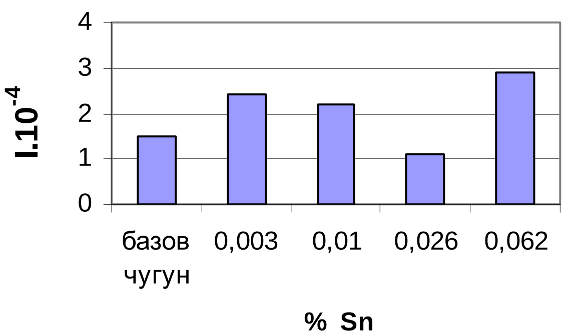

Figure 5. Chart of wearresistance I

3. ANALYSIS OF THE RESULTS, DISCUSSION AND CONCLUSIONS

The results in previous authors' investigation show that the various content of tin influences the hardness of the cast iron [3].

The obtained in this paper experimental results lead to following basic findings and conclusions:

- There is a direct dependence between hardness and wearresistance of cast iron in the frames of the tested Sn contents.
- Deviation of this dependence is found for specimen with Sn content of 0,026%. At the present stage of the study this fact can be taken as a result related to the non-homogeneity in the distribution of the graphite phase in the structure of the specimen. Wear and wearresistance are highly sensitive to the structure and the duration of wear. It is possible that at given stage of the wearing process, in the contact zone exists a structure with high graphite contents.
- Maximum wearresistance is observed for the specimen with Sn contents of 0,062%.
- The presence of Cu (0.008%) in the basic sample has greater influence on hardness than the amount of Sn (0.003) in sample № 1.

The obtained results would justify future systematic and complex investigations on tin by the authors, including also testing of high strength cast irons alloyed by Cu, Ni and Mo, which are produced in the factory of high strength cast irons „Osam" in the city of Lovetch, Bulgaria.

The study is related to the first stage of the International Contract № ДНТС 02/12 of scientific-technical collaboration between Romania and Bulgaria for 2010 in the topic „Tribotechnological study and qualification of composite materials and coatings lubricated by biodegradable fluids" lead by Assoc. Prof. Mara Kandeva and financed by the Fund Scientific Research at the Bulgarian Ministry of Education and Science.

REFERENCES

[1] Ya. E. Goldstein, V.G. Mizin, *Modifying and microalloying of cast iron and steel*, Moscow, Metalurgia, 1986 (in Russian).

[2] A. P. Lubchenko, *High Strength Cast Irons*, Moscow, Metalurgia, 1982 (in Russian).

[3] P. Dobrev, Zh. Kaleicheva, B. Saikova, *Microalloying of high strength cast iron by tin*, XIII National Conference «Metal Founding 2007», Lovetch, Machines, Technologies and Materials, Bulgaria (in Bulgarian).

[4] M. Kandeva, N. Hristov, N. Tonchev, E. Assenova, *Tribological Study of Cladded Bimetallic Coatings, Solving Friction and Wear Problems*, 17th International Colloquium Tribology, Esslingen, Germany, 19-21 January , 2010.

[5] M. Kandeva, D. Karastoyanov, *New methodological ideas and possibilities for study and qualifying of wearresistant coatings*, 26th International Scientific Conference, 65 Years Faculty of Machine Technology, 13-16 September, 2010, Sozopol, Bulgaria, c. 618-637

[6] БДС 14289-77 (Bulgarian State Standard) Method for testing on abrasive wear at friction upon fixed abrasive particles.

SERBIATRIB '11

Serbian Tribology Society

12th International Conference on Tribology

Faculty of Mechanical Engineering in Kragujevac

Kragujevac, Serbia, 11 – 13 May 2011

COMPLEX STUDY OF SURFACE LAYERS AND COATINGS

Mara Kandeva[1], Ilian Peichev[2], Nina Kostova[3], Kostadin Stoichkov[1]

[1]Technical University – Sofia, Bulgaria; kandeva@tu-sofia.bg;

[2]Shumen – Public Automotive Transport Ltd – the city of Shumen, Bulgaria; iliqn_pei4ev@abv.bg

[3]Institute of Catalysis, Bulgarian Academy of Sciences - Sofia

Abstract: *The paper presents theory and procedure for determination of the components of the communication potential η_1, η_2 and η_3, of their laws of variation and of the laws of linear wear for three typical situations and under three regimes of wear. The study is related to the first stage of the International Contract № ДНТС 02/12 of scientific-technical collaboration between Romania and Bulgaria for 2010 in the topic „Tribotechnological study and qualification of composite materials and coatings lubricated by biodegradable fluids".*

Keywords: *tribology theory and procedures, wear, coatings*

1. INTRODUCTION

As subject of machines' mechanics, the behavior of contact systems is described by one-parameter relationships with coefficient of proportionality between the external impact and the reactions in the joints related to friction, wear, lubrication, conductance, etc. contact processes [1], [2]. All these processes are based on contacts and contact interactions, thus the interdisciplinary science of tribology gives the central place and role to contact as a functional third body in the contact joints. This means that the contact as third body has to be presented through its individuality as complex distinct index in the law of contact interaction in general form, and, in particular, in the laws of friction, wear, etc. [3], [4].

This index is designated as communication (contact) potential η of the contact interaction in several papers of N. Manolov, M. Kandeva, et al. [4], [5], [6], [7].

According to the model of the functional atom, the interaction in contact joints and contact systems is described by the general law of contact interaction by the multiplication of three potentials: active potential λ, reactive potential δ and communication potential η in accordance with the equation:

$$\eta.\lambda.\delta = 1 \tag{1}$$

The same law (1) in its differential form has the form:

$$\frac{dR}{R} = \eta \frac{dA}{A} \tag{2}$$

where dA/A is the relative external perturbation acting on the joint; dR/R is its relative reflection; $\eta = \eta(A, R)$ is the communication potential.

In a first approximation the law in equation (2) can be presented in the form:

$$\frac{dR}{R} = \eta_3 . R^{1-\eta_1} A^{\eta_2 - 1} \frac{dA}{A} \tag{3}$$

So that in the general case the communication potential η is expressed by three indices η_3, η_1 and η_2.

The original item introduced by tribology in the study and qualification of contact joints is the triune non-dimensional essence of the communication potential by means of the indices η_3, η_1 and η_2.

The paper aims to propose a procedure for formulation of tribological laws of contact interaction during friction and wear, which take into account the triune parametric nature of the contact potential.

2. EXPOSE

The three components η_3, η_1 and η_2 of the communication potential η are non-dimensional quantities and have their own structure formed by the model of the functional atom. Figure 1 shows the structure of the communication potential η and its components in a flat and in a three-dimensional form.

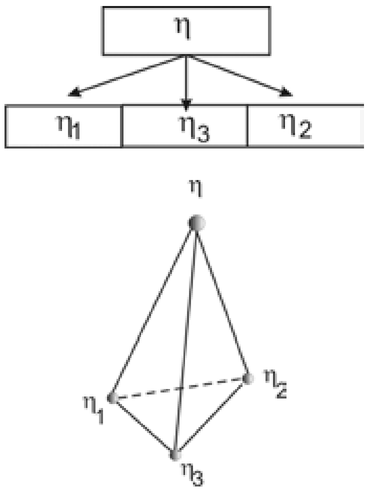

Figure 1. Structure of the communication potential in a flat and in a three-dimensional form

The parameter η_1 gives the reflection ability of contact, the parameter η_2 - the contact receptivity to external influence, and η_3 - the functional ability of contact as a third body in the tribosystem.

2.1 Communication components of wear during run-in, stationary and pathological regimes (Figure 2) [7]

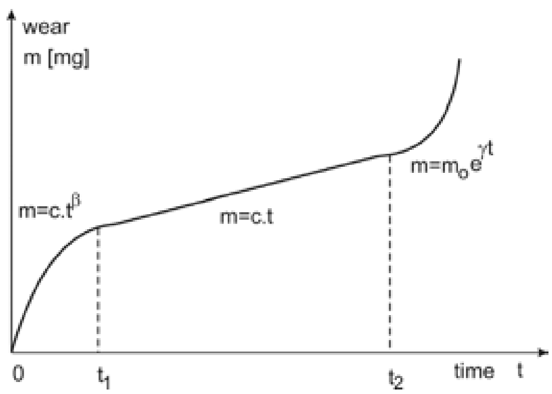

Figure 2. Curve of the three wear regimes – transient, stationary and pathological

The task is to calculate the components η_3, η_1 and η_2 of the communication potential η for the three regimes of wear and to present the obtained values in the form of Table 1.

Table 1.

Regime of wear	Transient regime $0 \le t \le t_1$		
Wear law	$m = c.t^{\beta}$, $\beta < 1$		
Components of η	$\eta_1 = 1$	$\eta_2 = 1$	$\eta_3 = \beta$

Regime of wear	Stationary regime $t_1 \le t \le t_2$		
Wear law	$m = c.t$		
Components of η	$\eta_1 = 1$	$\eta_2 = 1$	$\eta_3 = 1$

Regime of wear	Pathological regime $t > t_2$		
Wear law	$m = m_o e^{\gamma.t}$		
Components of η	$\eta_1 = 1$	$\eta_2 = 2$	$\eta_3 = \gamma$

a) Transient regime (running-in) $0 \le t \le t_1$

From equations

$$\frac{dm}{m} = \eta \frac{dt}{t} \quad \text{and} \quad m = c.t^{\beta} \tag{4}$$

follow

$$dm = c.\beta.t^{\beta-1}dt \text{ ; } \quad \frac{dm}{m} = \frac{c.\beta.t^{\beta-1}dt}{c.t^{\beta}} = \eta \frac{dt}{t}$$

Where from the communication potential is:

$$\eta = \beta < 1 \tag{5}$$

The law of contact interaction (2) is compared with its form (3), i.e.

$$\frac{dm}{m} = \eta \frac{dt}{t} = \beta \frac{dt}{t} = \eta_3.m^{1-\eta_1}t^{\eta_2-1}\frac{dt}{t} \tag{6}$$

For the components of η it follows:

$$\eta_3 = \beta < 1; \quad \eta_1 = 1; \quad \eta_2 = 1 \tag{7}$$

b) Stationary regime $t_1 \le t \le t_2$

From

$$\frac{dm}{m} = \eta \frac{dt}{t} \quad \text{and} \quad m = c.t \tag{8}$$

We obtain

$$\frac{dm}{m} = \frac{c.dt}{c.t} = \eta \frac{dt}{t}$$

or

$$\eta = 1 \tag{9}$$

Comparing (2) with (3) in this case gives:

$$\frac{dm}{m} = \eta\frac{dt}{t} = 1.\frac{dt}{t} = \eta_3.m^{1-\eta_1}.t^{\eta_2-1}\frac{dt}{t}$$

i.e. $\eta_3 = 1$; $\eta_1 = 1$; $\eta_2 = 1$ (10)

c) Pathological regime $t > t_2$

From $\dfrac{dm}{m} = \eta\dfrac{dt}{t}$ and $m = m_o e^{\gamma.t}$

follows $\dfrac{dm}{m} = \dfrac{m_o\gamma.e^{\gamma.t}dt}{m_o.e^{\gamma.t}} = \eta\dfrac{dt}{t}$

Hence

$$\eta = \gamma.t \tag{11}$$

The comparison of (2) and (3) gives:

$$\frac{dm}{m} = \eta\frac{dt}{t} = \gamma.t\frac{dt}{t} = \eta_3.m^{1-\eta_1}.t^{\eta_2-1}\frac{dt}{t}$$

or

$$\gamma.t = \eta_3.m^{\eta_1-1}.t^{\eta_2-1}$$

Then we can determine:

$$\eta_3 = \gamma;\ \eta_1 = 1;\quad \eta_2 = 2 \tag{12}$$

2.2 Theoretical study of contact wear of rough surface layers

In the considered general case the link between rough surface layers and the basic bodies is perfect (ideal) and is characterized by the components $\eta_1 = \eta_2 = 1$. So the dynamics in the process of wear is concentrated entirely in the dynamic processes in the contact as autonomous body by means of the variation in the parameter η_3.

If the current linear wear is designated by $h(t)$, where t is the duration of wear with fixed values of sliding velocity and nominal contact pressure, then in accordance with the law of contact interaction in the form (3) we obtain:

$$\frac{dh}{h} = \eta_3.h^{\eta_1}t^{\eta_2}\frac{dt}{t} \tag{13}$$

As in this case $\eta_1 = \eta_2 = 1$, it follows:

$$\frac{dh}{h} = \eta_3.h.dt \tag{14}$$

or

$$\frac{dh}{h^2} = \eta_3.dt \tag{15}$$

In a very short time interval $\Delta t = t_2 - t_1$ the component η_3 can be assumed as a constant, thus the integration of equation (15) in that narrow time interval leads to:

$$\int_{h_1}^{h_2}\frac{dh}{h^2} = \eta_3\int_{t_1}^{t_2}dt \tag{16}$$

or

$$-\frac{1}{h}\Bigg|_{h_1}^{h_2} = \eta_3(t_2 - t_1);\quad -\frac{1}{h_2} + \frac{1}{h_1} = \eta_3\Delta t\,,$$

i.e.

$$\eta_3^i = \frac{\Delta h_i}{\Delta t_i.(h_1.h_2)_i} \tag{17}$$

The law of variation of η_3 is determined by the graphical relationship $\eta_3 = \eta_3(t)$ drawn by the experimental data according to formula (17) by means of measurement of the difference in the linear wear $\Delta h_i = h_2 - h_1$ around the current moments t_i and the corresponding wear values h_1 and h_2 in the time intervals Δt_i around these moments.

The law of variation $\eta_3 = \eta_3(t)$ is determined by the experimental procedure described in an earlier publication [5].

The law of linear wear $h = h(t)$ is found by substitution of (17) in (16) and integration in arbitrary limits:

$$\int_{h_o}^{h}\frac{dh}{h^2} = \int_0^t\eta_3(t)dt \tag{18}$$

where $\eta_3(t)$ is the law of structural and functional change of contact as a third autonomous body in the regime of wear.

In the particular case

$$\eta_3 = k.t \tag{19}$$

and having in view (18), the law of linear wear takes the form:

$$-\frac{1}{h}\Bigg|_{h_o}^{h} = \frac{k.t^2}{2}\,;\ \frac{h-h_o}{hh_o} = \frac{k.t^2}{2}\,;\ h-h_o = \frac{h.h_o.k.t^2}{2}$$

Where from we obtain:

$$h(t) = \frac{h_o}{\left(1-\frac{h_o.k.t^2}{2}\right)} \tag{20}$$

2.3 Theory and procedure for the abrasive wear of tribological coatings

In the particular case when the abrasive is fixed on a plastic substrate, the components of the communication potential are $\eta_1 = 1$; $\eta_2 = 1$ and $\eta_3 = \eta_3(t)$, where η_1 characterizes the penetration of the reactive signal in the coating; η_2 - the penetration of the active signal in the coating; and η_3 characterizes the generative ability of the coating as separate object.

From the law of contact interaction in the form (3), where

$$\frac{dR}{R} = \frac{dh}{h} \text{ and } \frac{dA}{A} = \frac{dt}{t},$$

is obtained

$$\frac{dh}{h} = \eta_3 t \frac{dt}{t} \tag{21}$$

Integration is done in a very short interval $\Delta t_i = (t_2 - t_1)_i$

$$\int_{h_1}^{h_2} \frac{dh}{h} = \eta_3^i \int_{t_1}^{t_2} dt\,;\ \ell n\left(\frac{h_2}{h_1}\right)_i = \eta_3^i (t_2 - t_1)_i$$

or

$$\eta_3^i = \frac{1}{\Delta t_i}\ell n\left(\frac{h_2}{h_1}\right)_i \tag{22}$$

The law of variation of η_3 is determined by equation (22) in different intervals Δt_i by means of the experimentally obtained results.

After finding the law $\eta_3 = \eta_3(t)$ it is substituted again in formula (21) and is integrated in arbitrary limits from 0 to t, i. e. in the general case we obtain:

$$\int_{h_o}^{h} \frac{dh}{h} = \int_0^t \eta_3(t)dt = \psi(t) \tag{23}$$

Let consider the particular case $\eta_3 = k.t^{-\nu}$, where $\nu = const < 1$. After substitution in (23) and integration we have:

$$\int_{h_o}^{h} \frac{dh}{h} = \int_0^t k.t^{-\nu} dt\,;\ \ell n\frac{h}{h_o} = \frac{k.t^{1-\nu}}{1-\nu}$$

i.e.

$$h(t) = h_o.e^{\frac{k}{1-\nu}.t^{1-\nu}} \tag{24}$$

If we use development in Taylor series and neglect the small quantities of second and higher order, we obtain for the law of linear wear $h = h(t)$:

$$h(t) = h_o\left(1 + \frac{k}{1-\nu}.t^{1-\nu}\right) \tag{25}$$

3. CONCLUSION

Wear processes on fundamental level in tribology are analyzed through the non-dimensional communication potential η; they are described by the law of its variation $\eta = \eta(t)$ and the existing law of linear wear $h = h(t)$. If $\eta = const = 1$, the approach and the result of wear study is purely mechanical.

On the first essential level of tribology, contact wear is identified by the three components of the communication potential - η_1, η_2 and η_3. The values of these components are found through the selection of test conditions and the type of interaction in concrete contact joints and wear regimes.

The paper proposes theory and procedure for determination of the components of the на communication potential η_1, η_2 and η_3, of their laws of variation and the laws of linear wear in three typical situations and three regimes of wear.

The study in above paper is related to the first stage of the International Contract № ДНТС 02/12 of scientific-technical collaboration between Romania and Bulgaria for 2010 in the topic „Tribotechnological study and qualification of composite materials and coatings lubricated by biodegradable fluids" supported by the fund "Scientific Research" at the Bulgarian Ministry of Education and Science.

REFERENCES

[1] N.I. Kolchin: *Machine mechanics*, vol. 2, Mashinostroienie, Leningrad, 1972 (in Russian).

[2] V.E. Kanarchuk: *Fundamentals of machine reliability*, Naukova Dumka, Kiev, 1982 (in Russian).
[3] N. Manolov, M. Kandeva: *Overall Tribology*, Sv. Ivan Rilsky, Sofia, 2004 (in Bulgarian).
[4] M. Kandeva, E. Assenova, M. Manolova-Daneva: Triboecology as methodological centre of modern science, *Proceedings of the International Conference "ECOTRIB 2009"*, Pisa, Italy, 2009.
[5] N. Manolov, M. Kandeva: *Interdisciplinary Paradigm of Tribology*, Technical University-Sofia, 2010 (in Bulgarian).
[6] M. Kandeva, N. Hristov, N. Tonchev, E. Assenova: Tribological Study of Cladded Bimetallic Coatings, *Solving Friction and Wear Problems, Proceedings of the 17th International Colloquium Tribology*, Esslingen, Germany, 19-21 January, 2010.
[7] M. Kandeva: Study of wear of tribological coatings according to the law of contact interaction, *Proceedings of the 7th International Conference „BALKANTRIB'2011"*, Thessaloniki, Greece.

Serbian Tribology Society

SERBIATRIB '11

12th International Conference on Tribology

Faculty of Mechanical Engineering in Kragujevac

Kragujevac, Serbia, 11 – 13 May 2011

HEAT EXCHANGER TUBE TO TUBE SHEET JOINTS CORROSION BEHAVIOR

Madalin Iancu[1], Razvan George Ripeanu[2], Ioan Tudor[2]
[1]OMV PETROM S.A., Romania, madalin.iancu@petrom.com
[2]Petroleum-Gas University of Ploiesti, Romania, rrapeanu@upg-ploiesti.ro; itudor@upg-ploiesti.ro

Abstract: *Paper presents the studies made by the authors above the tube to tube sheet fittings of heat exchanger with fixed covers from hydrofining oil reforming unit. Tube fittings are critical zones for heat exchangers failures. On a device made from material tube and tube sheet at real joints dimensions were establish axial compression force and traction force at which tube is extracted from expanded joint. Were used two shapes joints with two types of fittings surfaces, one with smooth hole of tube sheet and other in which on boring surface we made a groove. From extracted expanded tube zones were made samples for corrosion tests in order to establish the corrosion rate, corrosion potential and corrosion current in working mediums such as hydrofining oil and industrial water at different temperatures.*
The corrosion rate values and the temperature influence are important to evaluate joints durability and also the results obtained shows that the boring tube sheet shape with a groove on hole tube shape presents a better corrosion behavior then the shape with smooth hole tube sheet.

Keywords: *tube to tube sheet fittings, stress, corrosion rate, hydrofining oil, temperature*

1. INTRODUCTION

Shell and tube heat exchangers are most commonly used in the process refinery industries due to a large ratio of heat transfer area to volume and weight. The tubes are the basic component of the heat exchanger, providing the heat transfer surface between one fluid flowing inside the tube and the other fluid flowing across the outside of the tubes. The tubes are held in place by being inserted into holes in the tube sheet and there either expanded into grooves cut into the holes or welded to the tube sheet were the tube protrudes from the surface. The main failures of heat exchangers are: - corrosion of tubes and jacket, tubes blockage and failures of tube to tube sheet joints. Paper presents the studies made by authors above the tube to tube sheet fittings of heat exchanger, type BEM as classified of Tubular Exchanger Manufacturers Association, with fixed covers from hydrofining oil reforming unit. In figure 1 is presented the catalytic reforming unit of hydrofining oil schema were heat exchanger has position "121-S1". Weldings between tubes and tube sheet is not recommended [2]. At studied heat exchanger the tube to tube sheet are expanded joints. The tubes and tube sheet, in addition to mechanical requirements, must withstand corrosive attack by both fluids in the heat exchanger and must be electrochemically compatible with the tube and all tube-side material [1, 3, 7].

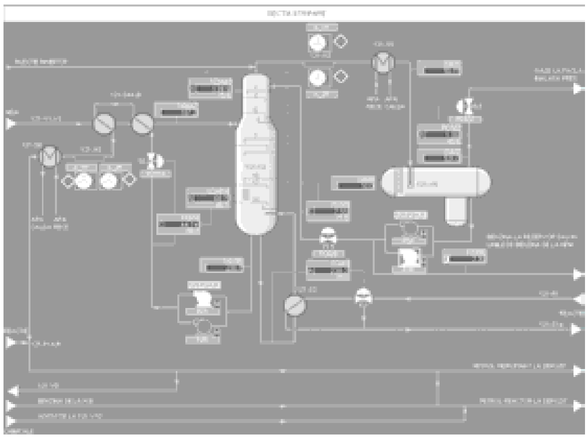

Figure 1. Catalytic reforming unit schema

At heat exchanger analyzed through the jacket is circulating hydrofining oil and through the tubes is circulating industrial water. In table 1 are presented the main working conditions.

Table 1. Main working conditions

Parameter	Jacket	Tubes
Maximum working pressure, MPa	1.15	0.65
Maximum temperature, ^{0}C	70	38
Minimum temperature, ^{0}C	50	30
Working medium	Hydrofining oil	Industrial water
Danger	Toxic, inflammable	-

The mechanical process of expanding of tube comprises two distinct phases, [2]:

a) *pre expanding of tube*, that preliminary flexible flare or / and elastic-plastic the tubular element (*TE*) until it comes in contact with the wall tube sheet hole (*TP*);

b) *proper expanding of tube*, additional enlargement mainly concerned elastic-plastic, residual *TE*, while broadening mainly flexible, reversible, the holes in *TP* as shown in figure 2, [2].

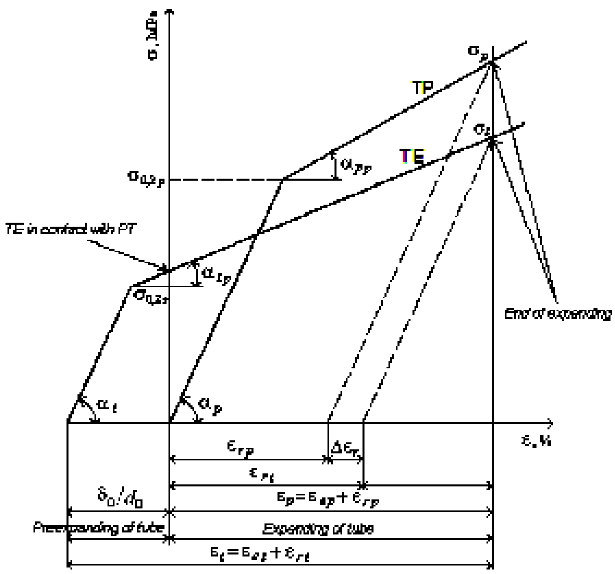

Figure 2. Typical characteristic curves of *TE* materials and, respectively, *TP* regarded as joint materials building plastic linear hardening

Pre expanding of tube phase corresponds to full depletion clearance of assembly $\delta_0 = 2\delta$ (fig.3), [2].

The main requirement of a tube-to tube sheet joint is better to resist the axial stress, compressive or tensile, applied to tube. This happens if tube-to-tube sheet joints, where tubes and tube sheet are made of steel, when the hoop stress in tube sheet is higher than in tubes [2].

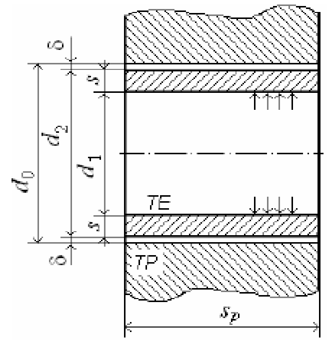

Figure 3. Tube to tube sheet schema

In order to better respect conditions of tension and compression in expanded tube to tube sheet joints the paper propose a different geometry of tube sheet which on boring surface we made a groove.

2. EXPERIMENTS

2.1 Tension and compression tests

To simulate the tube to tube sheet expanded joints were prepared samples at real joint dimensions. In figure 4 is presented the tube sheet sample with smooth hole tube sheet and in figure 5 the tube sheet sample which on boring surface we made a groove.

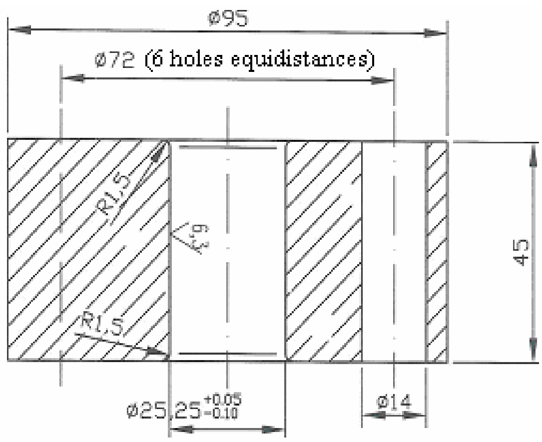

Figure 4. Tube sheet with smooth hole tube sheet

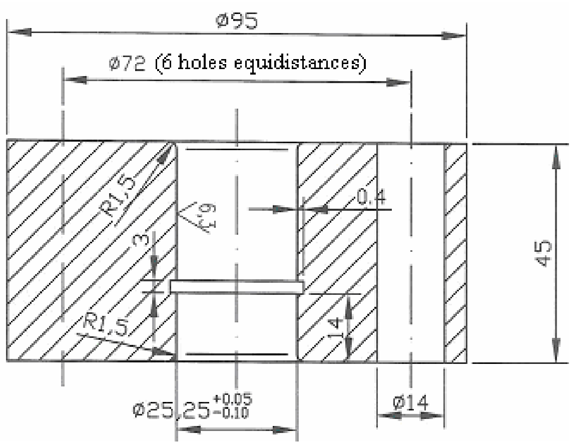

Figure 5. Tube sheet with a groove on boring surface

In figure 6 it is shown the tube samples dimensions.

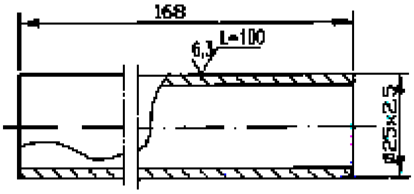

Figure 6. Tube sample construction

Tube sheet samples were made of steel type P355 NH, EN 10028 – 2:2009 and tubes of steel type P265 GH, SR EN 10217-5. The samples were extruded in similar conditions as real components.

The obtained assemblies were tested at tension and at compression. In figure 7 it is shown the tension variation vs. tube displacement in expanded joint with smooth hole tube sheet.

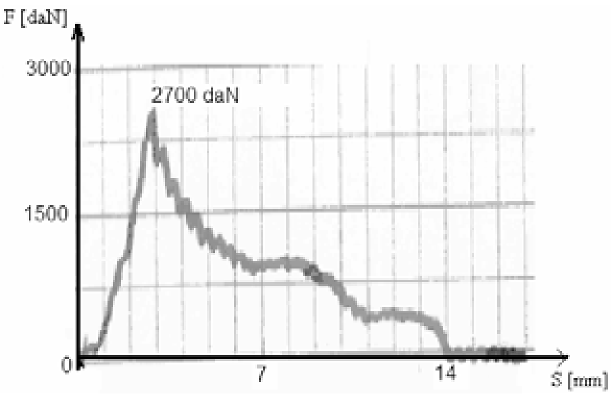

Figure 7. Tension variation vs. tube displacement in expanded joint with smooth hole tube sheet

In figure 8 it is presented the tension variation vs. tube displacement in expanded joint with a grove on tube sheet boring surface.

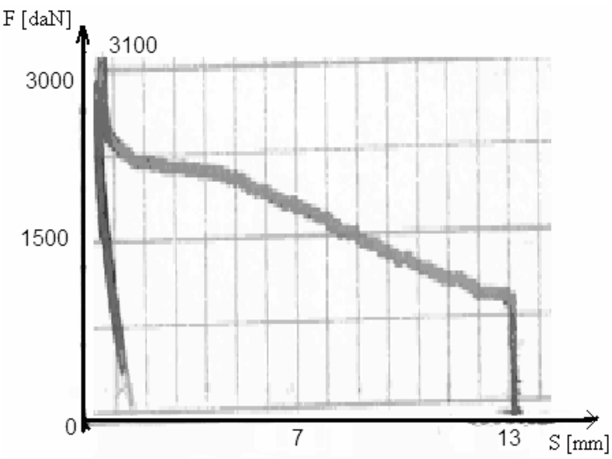

Figure 8. Tension force variation vs. tube displacement in expanded joint with a groove on boring surface

From figure 7 and 8 could be observed that the tension values were grater at expanded joint with tube sheet with a grove on boring surface. A similar behaviour was obtained at compression test. The maximum compression value obtained at expanded joint with smooth hole tube sheet was 3280 daN and at joint with a grove on tube sheet boring surface was 3350 daN.

The tension and compression results obtained confirm that model with a grove on tube sheet boring has an efforts better behavior.

Measuring the samples surfaces microgeometric parameters initial and after disassembling extruded joints by tension and by compression for the tubes that was in tube sheet with smooth hole tube sheet the roughness rise after compression and after tension than initial roughness. In table 2 are presented the roughness modifications for tubes.

Table 2. Tubes surface roughness modification

Tipe of extruded joint	Disassembling type	Roughness parameter modification, μm		
		Ra	*Rz*	*Rt*
Tubes for joint with smooth hole tube sheet	Tension	1.765	13.4	14.67
	Compression	0.445	-0.22	0.37
Tubes for joint with a grove on tube sheet boring surface	Tension	-0.051	-0.04	0.78
	Compression	-0.281	-1.96	-2.24

For the tubes that was in tube sheet with a groove on boring surface the roughness was smaller after compression and after tension than initial roughness. The tube sheet surface roughnesses were greater in case of disassembling by tension than in case of disassembling by compression for both tested geometries.

2.2 Corrosion tests

From both types expanded joints with tube sheet with smooth hole and with a grove on tube sheet boring surface were extracted samples from tube tubes active surfaces for corrosion tests. The samples were of steel type P265 GH, SR EN 10217-5. Also were tested samples extracted from tubes not used for expanded joints. Samples were named:

- "I" extracted from tubes not used for expanded joints:
- "5A" extracted from tubes from expanded joint with smooth hole tube sheet;
- "1A" extracted from tubes from expanded joint with a grove on tube sheet boring surface.

Working medium were industrial water with *pH*=7.18, *conductivity*=1524μS/cm, total solid deposition *TDS*=42mg/l and hydrofining oil with *pH*=5.55, *conductivity*=80pS/m, *sulphur*=1ppm.

Testing medium temperatures were 20, 40, 60 and 70^{0}C.

Samples have parallelepiped shapes and were machined without affecting tubes active surface.

At immersion corrosion tests the corrosion rate was obtained with relation, [3]:

$$v_{cor} = 8.76 \cdot \frac{m_f - m_i}{A \cdot \tau \cdot \gamma} \quad \text{, mm/year} \qquad (1)$$

Were m_f is sample final mass, g;

m_i- initial sample mass, g;

A- sample area, m^2;

τ- time, hours;

γ- specific weight, g/cm^3.

In figure 9 is presented the corrosion rate variation in time at temperature of 20^0C for tube samples immersed in industrial water.

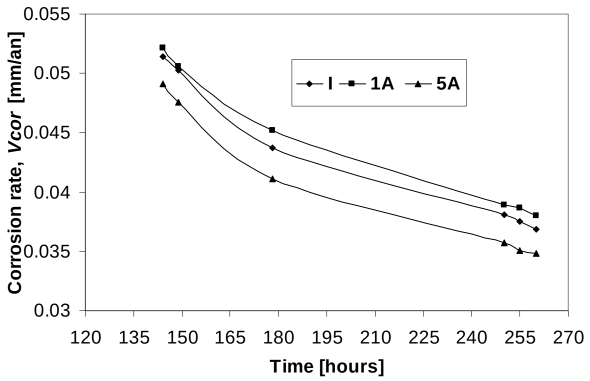

Figure 9. Corrosion rate at 20^0C in industrial water

In figure 10 it is shown the corrosion rate vs. time at temperature 40^0C, in figure 11 at 60^0C and in figure 12 at 70^0C in industrial water.

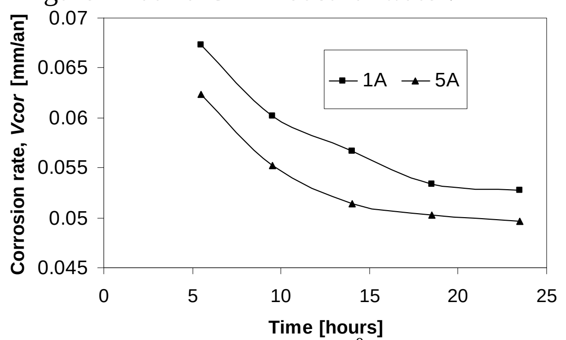

Figure 10. Corrosion rate at 40^0C in industrial water

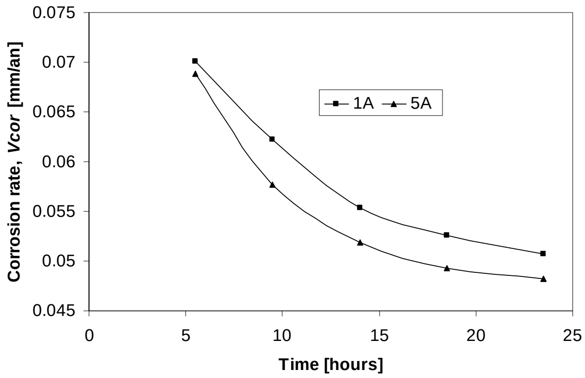

Figure 11. Corrosion rate at 60^0C in industrial water

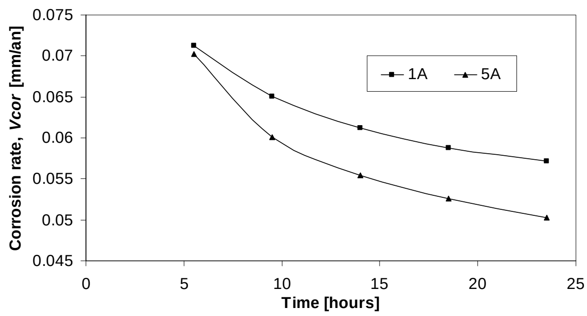

Figure 12. Corrosion rate at 70^0C in industrial water

From figures 9-12 could be observed that corrosion rate rise with temperature. Also the samples made from tube expanded joint with smooth hole tube sheet have a better corrosion behavior than samples made of tube with joint expanded having a grove on tube sheet boring surface.

In figure 13 it is presented the corrosion rate variation in time at temperature of 70^0C for tube samples immersed in hydrofining oil.

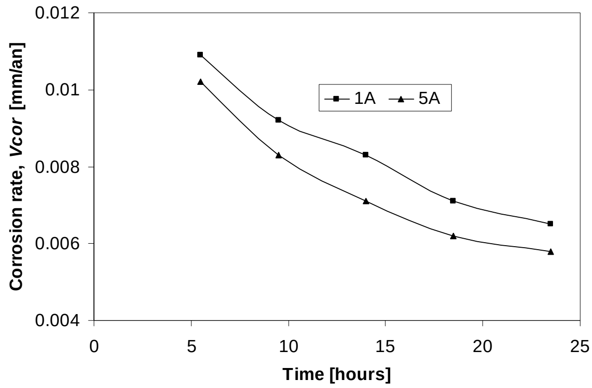

Figure 13. Corrosion rate at 70^0C in hydrofining oil

At temperatures of 20, 40 and 60^0C was observed a similar behaviour of corrosion rate at shown in figure 13. Could be observed that in hydrofining oil a better corrosion behaviour presents samples extracted from tube expanded joint with smooth hole tube sheet than samples extracted from tube expanded joint with a grove on tube sheet boring surface.

To establish electrochemical parameters, corrosion potential E_{corr}, corrosion current I_{corr} and corrosion rate v_{corr}, were extracted samples from tubes none extruded similar as from immersion corrosion tests. Specimens were machined with small cutting conditions and with cutting fluid in order to avoid the influence above metallographic structure at dimensions $\varnothing 16_{-0.1}$x3 mm. Active samples surface was polish with 500 Mesh abrasive papers.

There are several electrochemical techniques that can be used to evaluate the behavior of materials in aggressive medium such as [3, 4, 7]: potentiodynamic anodic, cathodic or both polarization measurements, galvanic corrosion measurements, potentiostatic measurements, linear polarization, pitting scans, Tafel plots measurements etc. Tafel plots technique quickly yields corrosion rate information. The linear portion of the anodic or cathodic polarization logarithm current vs. potential plot is extrapolated to intersect the corrosion potential line. This permits rapid, high accuracy measurement of extremely low corrosion rates. For this reason to determine electrochemical parameters we used this technique.

According to the mixed potential theory [3, 4, 7], any electrochemical reaction can be divided into two or more oxidation and reduction reactions, and can be no accumulation of electrical charge during the reaction. In a corroding system, corrosion of the metal and reduction of some species in solution is taking place at same rate and the net measurable current, i_{meas} is zero. Electrochemically, corrosion rate measurement is based on the determination of the oxidation current, i_{ox} at the corrosion potential, E_{corr}. This oxidation current is called the corrosion current, i_{corr}.

$$i_{meas} = i_{corr} - i_{red} = 0 \qquad at\ E_{corr} \tag{2}$$

The corrosion measurement system used was EG&G Princeton, New Jersey- model 350 that works together with compensator IR 351, [6,7,8,9].

Corrosion cell works with a saturated calomel reference electrode and specimen holder exposes 1 cm^2 of the specimen to the test solution. Using Tafel plots technique were determined the electrochemical parameters presented in table 3. Electrochemical tests were made according to ASTM G5-94, [5] and ASTM G1-90, [6]. The reference electrode was Calomel ($Pt/Hg/Hg_2Cl_2$). For tests at 40 and 60^0C was used a thermometer and a thermostatic plate were placed corrosion cell.

In figure 14 it is presented the electrochemical parameters obtained by Tafel technique sample “I” in industrial water at 20^0C.

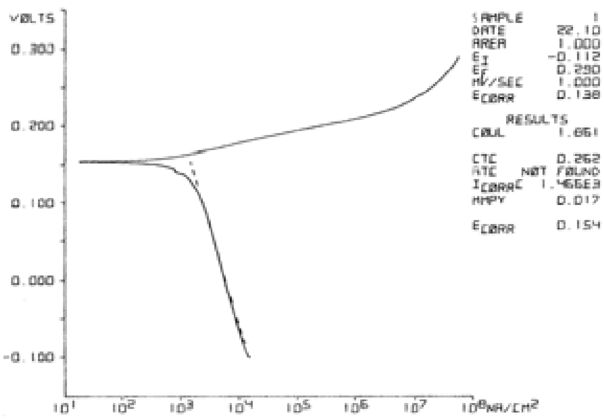

Figure 14. Electrochemical parameters obtained by Tafel technique sample *“I”* in industrial water at 20^0C

In table 3 are presented electrochemical parameters obtained for specimens extracted from non extruded tubes in industrial water.

Table 3. Electrochemical parameters

Temperature T, ^{0}C	Corrosion potential E_{cor}, V	Corrosion current I_{cor}, μA	Corrosion rate v_{cor}, mm/year
20	0.154	1.466	0.017
40	0.143	3.133	0.053
60	0.137	5.981	0.070

From values presented in table 3 we could observe that the corrosion current and corrosion rate rise with temperature. The obtained corrosion rate values by immersion are proximate with values obtained by electrochemical method.

3. CONCLUSION

Tube to tube extruded joints at heat exchangers represents a critical zone for stress and corrosion.

The tension and compression tests show that proposed model of tube sheet with a grove on boring surface improve the tube to tube sheet joint.

It is recommended to disassembling the extruded joints by tension because the obtained surfaces roughness is smaller than I case of disassembling extruded joints by compression.

Because the tube sheet with a grove on boring surface rise the stress in joints, more than smooth tube sheet surface, this modify the corrosion potential and the corrosion rate is greater.

The differences between corrosion rates for two models is not significant, nevertheless the number of groves and groves dimension must be reconsidered in order to obtain a uniform stress on the entire contact surface in the extruded joint.

REFERENCES

[1] K.J. Bell, A.C. Mueller: *Wolverine Engineering Data Book II*, www.wolverine.com, 2001.

[2] M. Iancu, A. Pupazescu, I. Tudor: Study on the state of stress and strain in tube-to tubular plate joints, Petroleum – Gas University of Ploieşti Bulletin, Technical Series, Vol. LXII, No.4B, pp.61-66, 2010.

[3] I. Tudor, R.G. Ripeanu: *Corrosion engineering*, Petroleum - Gas, Ploiesti, 2002.

[4] Application note 140, Princetown Applied Research Corporation, Princetown, AN 140-10M-5, 1978.

[5] ASTM G5-94.

[6] ASTM G1-90.

[7] Electrochemical Techniques for Corrosion, NACE Publication, Houston, U.S.A. 77027, 1978

SERBIATRIB '11

Serbian Tribology Society

12th International Conference on Tribology

Faculty of Mechanical Engineering in Kragujevac

Kragujevac, Serbia, 11 – 13 May 2011

FLOW BEHAVIOR OF EPDM RUBBER OF DIFFERENT HARDNESS VALUES UNDER AXYSYMETRIC COMPRESSIVE LOAD IN DRY WORKING CONDITION

Abhijit Mukhopadhyay[1], Moloy Sarkar[2]

[1]Mechanical Engineering, Jadavpur University, Kolkata, India, m_obiji@yahoo.com
[2]National Engineering Rubber, Kolkata,India

Abstract: *Rubber is very useful and suitable material for a wide varieties of engineering and other applications. It possesses large elasticity compared to metals, has greater damping capability, high internal friction and can accumulate energy greater than that of steel or other metals. During the deformation of rubber material, e.g., by compressive force, internal damping of the material leads to energy dissipation. This is the cause of hysteretic friction of rubber. Friction of rubber material is of great practical importance at the same time it has so many disadvantages too.*

Use of rubber as engineering material is not new. However in the recent time its application is gaining importance due to several reasons. One of such reasons is that recent researches on rubber material reveals its suitability for engineering application. Several researches are going on, though it is rather very difficult to predict the exact behavior of any viscoelastic material like rubber.

In the present work compression tests were carried out to determine the flow behavior of EPDM rubber of different hardness values. Flat MS platens were used to apply axysymetric compressive load on the specimen under dry working condition. The flow behavior like load –elongation curves, true stress – true strain curves and specific energy requirements were computed from the experimental data. Statical hysteresis and the loss factors were also obtained.

Experimental results revealed that the hardness values of EPDM rubber had significant effect on the flow behavior. The hardness, again, depends on the carbon black content. Thus it can be stated that the flow behavior can be governed by controlling the CB concentration in the EPDM rubber. The test may again be extended with different lubricants. The present work was conducted in the laboratory of Mechanical Engineering department utilizing the rubber samples obtained from National Engineering Rubber for the purpose.

Keywords**:** EPDM rubber, compression ,flow behavior, hysteresis, loss factor.

1.INTRODUCTION

Rubber is very useful and suitable material for a large and varied number of applications both engineering and others. It possesses large elasticity compared to metals, has good damping capability and can accumulate energy to a greater extent than that of steels. It has also got very high internal friction. During the deformation of rubber, particularly by compressive load , internal damping of rubber leads to energy dissipation. This is the cause of hysteretic friction of rubber. Friction of rubber as a material is of great practical importance in so far as the tires of automobiles, wiper blades, rubber seals, conveyor belts are concerned. However the increased friction in the die-work piece mating surfaces during rubber forming operations will lead to a phenomenon 'pancaking' or 'barreling' which is undesirable. This is particularly true during upsetting operations. Friction which leads to wear and abrasion is also undesirable. Rubber finds wide engineering and other applications with or without the use of some lubricant. Automobile tires ,rubber bushes, gasket, rubber spring insulated buildings, dock fenders, seals, bearings, sealants and sluices are some common examples of engineering applications. Some other areas are like water proof attires, bungee jump cords, high speed racing car tires and other sports accessories [1].

Rubber-metal springs are conveniently used in road and railway transport vehicles. Over metal springs they have the advantage like reduced weight, reduced cost, improved absorbing and damping capacity of shocks and overloads. In railway vehicles rubber-metal springs are used as primary and secondary suspensions, elastic supports of aggregates, buffers and draw gear applications [2].

Assembly and maintenance of rubber springs are comparatively simple. Rubber- metal contact is found in different other applications like vibration control, power transmission systems, seals and rubber pad forming processes[3].In rubber forming process one of the dies is made of rubber. This process has the advantage like low cost of tooling, ease of operation, reduced damage of the work material as well as has the capability to produce complex geometries [4].

It is thus clear that rubbers of different kind have wide industrial and other application potentials. The property requirements for rubber, particularly for engineering applications, are also varied and highly demanding. This necessitates the development of different grades of rubber and recent researches in different parts of the globe aim on the development of reinforcements with organophilic clay, carbon nanofibres, carbon nanotubes etc. Addition of white rice husk ash (WRHA), silica, carbon black in different quantities are also some examples in this regime of reinforcement to produce different vulcanizates [5,6].

Fundamental studies of the properties of rubber including tribological properties, the study of friction wear and lubrication, are not new. However the state of art knowledge in this field has many questions, many clarifications are also needed till date. Nowadays being fueled by the varied engineering application possibilities of rubber of different kinds a renewed interest is noticed in characterization including tribo-studies of different kinds of rubber [5]. Characterization of rubber, like any other metal, is also important to forecast the behavior during actual working of the same. It is not out of place to mention here that the properties of viscoelastic material like rubber are very complicated and there is hardly any model which can uniquely define such behavior. In tribological state tests friction and wear characteristics are of great importance. Friction behavior of rubber is also very complex. The viscoelastic characteristics greatly influence the friction of rubber [7].

Mechanical performance of different kinds of vulcanizates had been studied by many researchers. Thermal conductivity, stress-strain relationship, tensile stress, dynamic mechanical properties, elasticity, strength and so on are some few to be mentioned [1]. However, compression tests of EPDM rubber were hardly noticed.

Main objective of the present work is to study the flow behavior of EPDM rubber of different hardness values under compressive load and dry condition. This was done by evaluating the stress-strain relationship, specific energy calculation and finding out the loss factor.

2. THEORETICAL FRAMEWORK

Flow curve of any material can be established either by tension or compression test. Researches reveal that formability of material is lowest at tensile stress whether higher strains are developed during compression. Hence, compression is popular way to develop flow behavior, that is, flow stress – flow strain data, in metal forming applications [8].

During compression test a cylindrical or some times a rectangular specimen is squeezed by compressive load which is applied by some suitable device. The specimen is to be placed in between two parallel , flat platens to apply axysymetric load as shown in Figure 1.

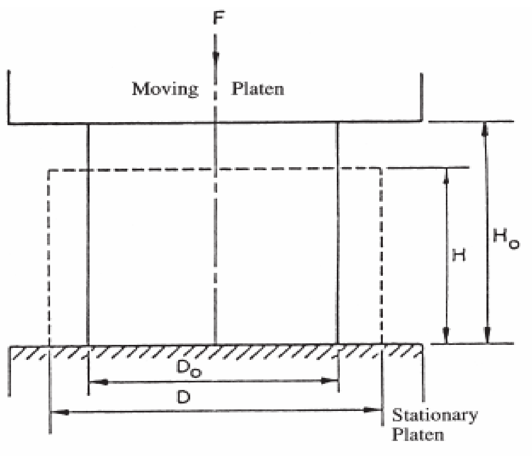

Figure 1. Homogenious compression of a solid cylindrical sample.

Throughout the test run the load and displacement, that is, the reduction in height values of the specimen are recorded. This data are utilized to find out various flow behavior of the material. Mathematically the stress and strain is expressed by the following relation:

$$\textit{Engineering stress} \quad s = \frac{P}{A_0}$$

and
$$\textit{True stress} \quad \sigma = \frac{P}{A}$$

whereas ,
$$\textit{Engineering strain} \quad = \frac{h - h_0}{h_0}$$

and
$$\textit{True strain} \quad = \ln\left(\frac{h}{h_o}\right)$$

True stress is the instantaneous load divided by the cross sectional area of the specimen at that instant, whereas, the engineering or conventional stress is the load divided by the original area of the specimen. Accordingly the true strain and engineering strain are also defined. In the above expressions 'h_o' is the original height and 'h' is the instantaneous height of the specimen[9].

Again we can define the strain rate as follows:

$$\textit{Engineering strain rate} \quad \dot{e} = -\frac{v}{h_o}$$

and
$$\textit{True strain rate} \quad \dot{\epsilon} = -\frac{v}{h}$$

where, 'v' is the travelling speed of the die. The negative sign indicates the case of compression. We shall ignore the sign during our entire calculation for the simplicity of the purpose.

At the room temperature the flow behavior of majority of the metals is generally independent of strain rate. However, if the metal is worked at recrystallization temperature zone , that is, if hot working is conducted then the flow behavior depends on the strain rate. So during working at ordinary or room temperature any speed of the cross head of the machine is permissible for metals[8]. But the behavior of viscoelastic materials are completely different from those of metals. Mechanically the rubber materials are elastic at high strain rates whereas at low strain rate they are viscous.. Some researchers also demonstrated that the flow behavior of rubber is strain rate sensitive even at ordinary temperature.It is also not out of place to mention that several experimental observations of rubbers are not yet explained properly. As an example, coefficient of friction of rubber changes after a speed change, known as "conditioning" as per Schallamach[10].

Compression test is also associated with some problems. When the specimen is compressed in between two flat platens, lateral flow of metal in an outward direction leads to the development of shearing stresses at the die-work contact surfaces. This surface shear is directed towards the centre and opposes the outward radial flow of metal. The metal at the mid height of the specimen can flow in an outward direction freely. The combined effect of these two phenomenon leads to the development of barrel shaped part, known as barreling or pan caking. This may lead to problems unless controlled accordingly with the application of lubricants. Lubricants will reduce frictional force at the tool/die-work piece interfaces[4,9].

In axysymetric homogeneous upsetting operation we may apply the concept of constancy of volume. Thus if a specimen of initial diameter 'd_o' and height 'h_o' is compressed to a diameter 'd' and height 'h' respectively then from the concept of volume constancy we may write:

Initial volume (Q_1) = Final volume (Q_2)

or
$$\frac{\pi d_0^2}{4} \cdot h_o = \frac{\pi d^2}{4} \cdot h$$

or
$$A_o h_o = Ah$$

or
$$A = \frac{A_o h_o}{h}$$

where A is the instantaneous area.

In case of compression of a rubber specimen if the surfaces are oil or grease lubricated then minimal resistance is offered to the lateral slippage both at the top and bottom dies. On the contrary if the surfaces are firmly bonded to the platens then no lateral slippage will take place. Bonded versus unbonded surfaces thus lead to the generation of different flow curves. In ruber specimen shape factor also plays an important role[11].

Due to barreling it may not be possible to obtain data which are truely indicative of the process. Firstly, the cross-sectional area changes along its height and secondly, energy is dissipated due to friction which (that is the extra energy) is to be supplied through an increased compressive force.

As mentioned earlier, with proper lubrication barreling can be reduced to a greater extent.

In case of viscoelastic materials like rubber an interesting characteristic is observed during compression and subsequent relaxation of applied loads. It is observed that the loading path and the unloading path are not equal during the application of load and successive relaxation of the same. This effect is called hysteresis. Figure 2 shows a typical load-elongation curve for rubber, where the clockwise loop , formed in between loading and unloading path, indicates the hysteresis. Hysteresis is the energy dissipation capacity of rubber. By virtue of this characteristic rubber can absorb shock and damp vibration which enables rubber to be used beneficially in ruber-metal springs and other engineering applications where shock loading and vibration are prominent.

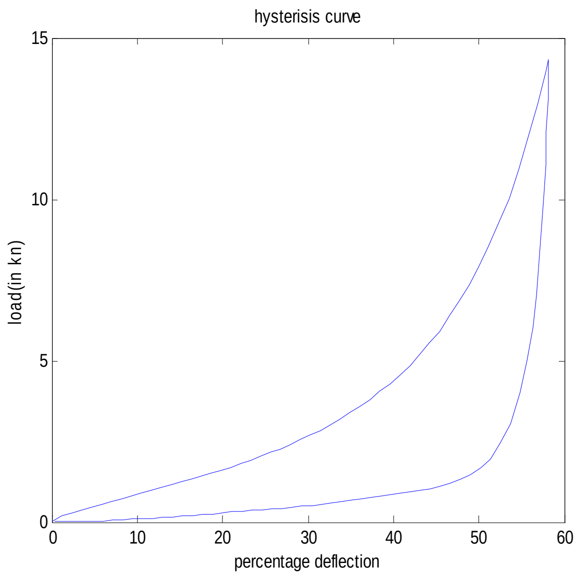

Figure 2. A typical hysteresis curve

When ruber specimen is compressed and then allowed to release subsequently it is observed that a fraction of energy which was put into the compressive specimen during loading is not recovered upon releae of load. The energy required to change the original shape of the specimen that is the strain energy is obtained from the area under the compression (loading) curve. Similarly energy released during relaxation (unloading) is also obtained from the area under the unloading curve. The difference gives the amount of hysteresis[2].

In case of compression of a viscoelastic material the exact nature of the curve is not kown as in case of purely plastic material the flow curve can be expressed in terms of well known power law equation $\sigma = K\varepsilon^n$. Hence the strain energy in case of rubber material is calculated using the Simpson's composite rule in this regard or by Trapizoidal rule[6]. The out line of such rule is mentioned below:

The interval of the curve [a, b] is subdivided into a number of small intervals 'n' ; 'n' being an even number. Simpson's rule is then applied to each subinterval and all such results are summed up. Thus,

$$\int_a^b f(x)dx \approx \frac{h}{3\left[f(x_0) + 2\sum_{j=1}^{\frac{n}{2}-1} f(x_{2j}) + 4\sum_{j=1}^{\frac{n}{2}} [f(x_{2j}-1) + f(x_n)]\right]}$$

Where, $x_j = a+jh$, for j = 0,1,2,……….(n-1),n

$$h = \frac{b-a}{n}$$

$x_o = a$, and $x_n = b$

Calculation of loss factor:

Loss factors may be calculated in several ways. To compare the loss properties of different materials a single method should be used. the Loss factor is obtained from the hysteresis loop by the following mathematical relation:

$$\eta = \frac{D}{2\pi U}$$

where, η = loss factor

D = energy dissipated per cycle

U = maximum strain energy per cycle

generally, $\eta < 1$: for material with lower loss

>1 : for material with high damping

All the calculations are done numerically using an indegeniously developed MATLAB code.

3. EXPERIMENTAL

3.1 EPDM rubber

Ethylene Propylene Diene Monomer rubber specimen were prepared in the laboratory of NEL(Rubber) using laboratory intermix and open mill in two steps. Theoretical proportions of the ingredients of EPDM rubber is as follows:

EPDM - 100 parts
ZnO - 5 parts
N-cyclohexyl-2-benzothiazole sulfonamide – 0.6 part
2 – mercapto benzothiazole – 0.6 part
Zn- dicyanatodiamine – 0.6 part
Zn- dibenzyl dithiocarbamate – 1.5 parts

Carbon black (CB) – in different portion depending on the hardness requirement e.g., 0,30,45,60 parts etc.

The actual recipe, however, is a trade secret and 'not disclosed grade'. The hardness differs with different proportion of CB contents.

3.2 Preparation of the test specimen

The basic ingredients, as mentioned, were first pre-mixed in a laboratory inter mix, type K4/2A-MK3, made by Alfred Herbert (net volume capacity 45 liters and fill factor approximately 0.6 to 0.75),for 6 minutes at a mixing temperature of 120^o -130^oC and at a ram pressure of 100 psi (7 kg/cm^2). Curatives were then added to the pre mixed materials on a two-roll laboratory mill (φ330 × φ150) at room temperature. The upper surfaces of both the roll is plated with hard chrome. A constant friction ratio of 1: 1.25 was maintained between the rolls. Total mixing time was approximately 10 minutes.

Processing characteristics including optimum cure time (t_{90}) and difference in torque ($\Delta M = M_h - M_l$) were then determined with the help of a rubber process analyser, Oscillating Disc Rheometre (Future Foundation, India made) being equipped with computer based data acquisition system and 'Rheosoft' software. M_h and M_l, high and low Mooney (torque) respectively, scorch time and optimum cure time (t_{90}) were noted. Approximately 10gm. of circular shaped sample were punched out from the uncured materials and placed between two rotating discs of the Rheometre at a constant temperature of 180^0C and at an arc of 3^0 for 6 minutes. The torque was monitored as a function of time. The time corresponding to the development of 90% of the maximum torque, that is, the optimum cure time (t_{90}) was measured from the corresponding rheographs.

The material, after qualifying the rheometric analysis, was entered in the molding press, which is a steam heated hydraulic press, made by Hydromech and Pneumatics pvt. Ltd., India. Molding of the samples were carried out in a die containing 9 cylindrical holes of Φ16.5 ±0.5 and h12.5 ±0.5 at a pressure of 3000psi and temperature 150^0C for 10 minutes as per IS: 3400 (part X)-1977. Silicon emulsion may have to be used in case the molten material sticks to the molding plates. The extra spew of materials were removed by scissor to give it the desired size.

3.3 Measurement of hardness

The hardness values of the specimen were measured according to IS:3400 (Part II) -1980 using a Shore (A) Durometer . TSE- Rubber Hardness Tester, SHR – Mark III –A ,sr.no.15718, made by Testing Machine, India, was used for the purpose. The machine was calibrated accordingly by Techno India. Indentations were made at several points on each specimen and the average value was then taken as a measure of hardness.

3.4 Measurement of the dimension of the specimens

Though the test specimens were produced using a dedicated mold for this purpose still it is very difficult to maintain exact dimensions of any viscoelastic material like rubber. Hence to cross check, the diameter and the height of each sample were measured using a Mitutoyo Digimatic Caliper (code no. 500-144, serial no. 0023360) equipped with SR44 battery. Measuring range of the instrument : 6 inch./ 150mm; resolution : 0.0005 inch/ 0.01mm; instrumental error : ± 0.02mm

3.5 Compression test

Test specimen was placed between two flat, axysymetric mild steel platens. Much care was taken to place the cylindrical specimen in between the platens and to place it perfectly at the centre. This is required to ensure an even force distribution on the face of the specimen. The required compressive load was provided by an Instron machine (model 8801; serial no. K 2342 with 'Dynacell' load cell, made in England. Maximum working pressure : 207 bar; dynamic load capacity : ± 100 KN). The machine is equipped with 8800 : Instron SAX V9.3 software based data acquisition system shown in Figure 3. Due to the want of a compression software , we utilized the fatigue cycle and only one cycle was utilized at a frequency of 0.005 Hz. The height of the cylindrical specimen was reduced by 65% for each sample. Each test was replicated twice to observe the repeatability of the process. The data of the compressive load followed by load relaxation were recorded and later utilized to plot the loading and unloading paths respectively. Following figure shows the compression test facility in Instron :

Figure 3. Instron (previous column) and associated computing system (above).

4. RESULTS AND DISCUSSIONS

Figures 4.1, 4.2 and 4.3 show the load-vs- % deflection , true stress-vs- % deflection and true stress-vs- true strain curves respectively of EPDM of different hardness under dry working condition. For all the EPDM with five different hardness experiments were replicated twice to establish the repeatability of the data and the test data thus generated reveal the representativeness of the experiments. Minor variations in test data were accepted considering the feasibility criterion of the experiments and the behavior of any viscoelastic material, discussed at length in the discussion section. Table 1 below indicates the different flow behavior values of EPDM rubber under dry working condition:

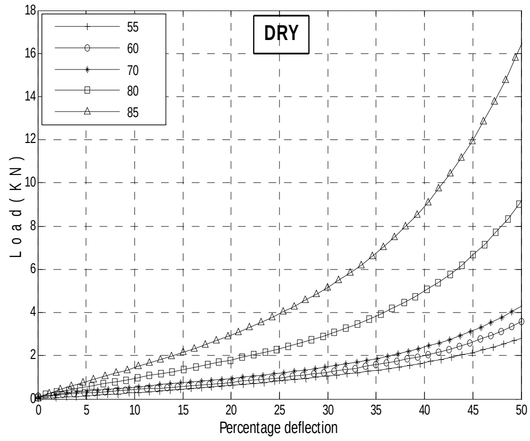

Figure 4.1. Load – % deflection curve

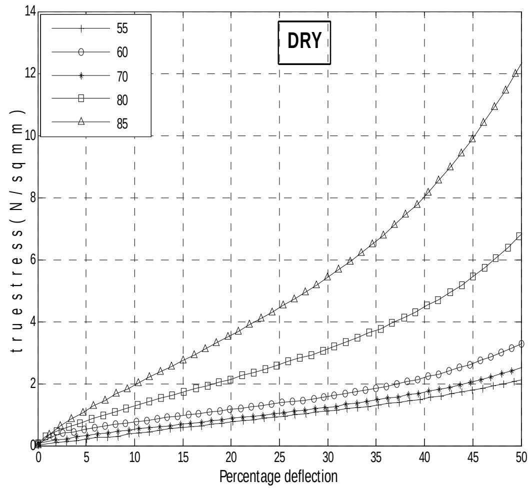

Figure 4.2. True stress- % deflection curve

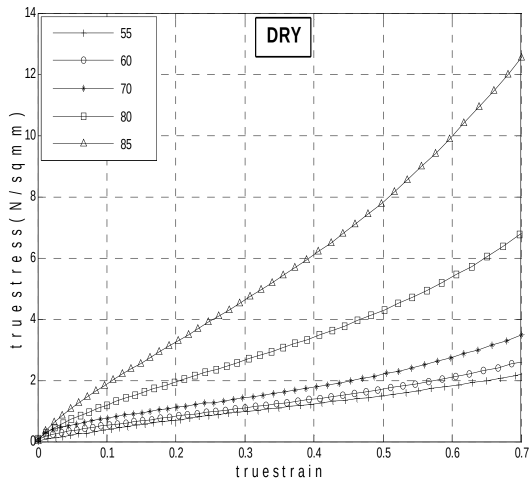

Figure 4.3. True stress-true strain curve

Table 1.

Hardness (Shore 'A')	Load (KN) at 50%	True stress (N/mm^2) at	True stress (N/mm^2)

	deflection	50% deflection	at true strain 0.7
55	2.71	2.08	2.16
60	3.35	2.41	2.53
70	4.05	3.15	3.47
80	9.03	5.95	6.75
85	16.57	10.00	12.53

The characteristic stress-strain curves for EPDM rubbers with different hardness are depicted in Figure 4.1. It is apparent from the curves that EPDM with hardness values of 55, 60 and 70 behave almost equally. However, reinforcing effect of 80 and 85 is significant. Reinforcing is generally done with different proportions of CB content (parts per hundred) . The observations are some how simlar with the test data of D.Felhos and J.Karger-Kocsis [5] where it reveals that EPDM 45 and EPDM 60 behave almost equally. In that test higher hardness values of EPDM were not considered. The present study also reveals that for low hardness values, e.g., upto 70, the nature of the stress-strain and stress-deflection curves are almost linear in nature. For hardness 80 and 85 linearity remains upto approximately 35% of deflection and 0.5 true strain respectively beyond which the curves are non-linear. For load – deflection ,however, the lower valued EPDM, upto 70, shows linearity upto 35 % and beyond this they are non-linear. For 80 and 85 non-linearity starts from approximately 25%.

In Figure 4.4 static hysteresis curves are shown.The corresponding values are tabulated in Table 2.

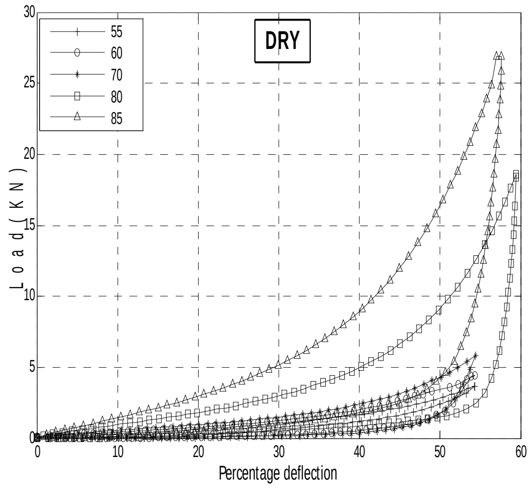

Figure 4.4. Static hysteresis curve

Table 2.

Shore ‘A’	Accumulated Work	Released Work	Absorbed Work	Max. Strain Energy	% Hysteresis	Loss Factor
55	58.67	38.95	19.72	9.108	33.61	0.344
60	71.85	19.48	52.37	9.988	72.88	0.834
70	95.34	21.60	73.74	14.035	77.33	0.835
80	278.6	168.1	110.5	46.016	39.66	0.382
85	481.0	380.4	100.6	71.361	20.90	0.224

The hysteretic component results from internal friction of the rubber which is very high and at the same time elastic modulus of rubber is very low. Thus , as per Grosch studies, friction of rubber is directly related to the internal friction and a bulk property. Though this conclusion is not unique, as the behavior of any viscoelastic material, unlike most other solids, is very complex. Such internal friction results in the energy dissipation. Thus hysteretic friction of rubber is caused by internal energy dissipation during the course of deformation. This leads to the property of damping which is very useful in various engineering application like rubber-metal springs in railway and other vehicles, automobile tires, vibration damper and many more.

There are various ways of finding out loss factor and they are not necessarily compatable. Thus any one method should be used as a comparator of the loss properties of materials. In the present work loss factor was calculated on the basis of the generated hysteresis loop. Value of the loss factor is generally below 1 for low loss and may be higher than 1 for very high damping.

Here, EPDM with lower shore hardness tends to have a higher loss factor than those with higher shore values. Result of EPDM 55 differs , may be due to eroneous and/or uncontrollable test or due to inherent defect in the sample itself. Rest of the results are in close agreement with the conclusion driven by Martinelli B.A.E.[7] based on his experimental results. The nature of the experimental hysteresis curves are in perfect theoretical shape, i.e.,the well known banana curve of hysteresis.

Difficulty arises in providing the same average contact pressure on the specimen surface. The actual contact stresses , thus, will differ from specimen to specimen. It is also very difficult to place the specimen between the flat platens in a manner which will assure perfect alignment of the axis of the specimen with that of the platens. Alignment of the two axes is an essential minimum for axysymetric compression. During the experiments much care was taken to maintain all these.

Generally it is also very difficult to deform the specimen maintaining homogenity during compression testing. This is due to the friction between the specimen surface and the platens. Layer of material , adjacent to the platens, will be prevented from sliding radially outwards; whereas the remaining material is forced to move radially outwards by the dead metal zone as the compression proceeds[4,8,9]. This gives rise to barreling or pan caking. As a result of such barreling fresh surface area which was initially on the cylindrical surface of the specimen will come in contact to the advancing platen surfaces. Hence lubrication of all the surfaces of the specimen is very much essential to reduce friction and ultimately barreling. In the present study, however, only dry condition was considered. It is planned to extend the study in very near future with different lubricants to address the issue.

The Instron machine which was utilized to conduct the experiments was a displacement controlled machine where the cross head, containing the specimen can move with a prefixed constant speed. Though in case of cold forming operation of metals strain rate sensitivity is not applicable. But for viscoelastic material like rubber strain rate is important at room temperature too. Therefore in the present experiments no conclusion is made regarding the strain rate sensitivity on the flow behavior of EPDM.

5. CONCLUSION

The stated experimental work was devoted to study the flow behavior of EPDM rubber of different hardness, which depends on the amount (parts per hundred) of CB. The test conditions were very difficult to be harmonized as it should be during real operationg conditions. However much care was taken to maintain the test conditions at par and based on the experimental data following conclusions were drawn:

- with increasing hardness of EPDM true stress values are increased and are non linear in nature.
- reinforcing effect of the CB content is less significant upto EPDM 70. Strong effect was noticed in case of EPDM 80 and 85 respectively.
- hysteresis, which gives rise very important property damping, was noticed for each specimen. At the test condition %- of hysteresis was highest for EPDM 70. All the EPDM showed low loss(loss factor being less than 1) and EPDM with lower hardness values exhibit higher loss factor.

The results , in general, are qualitatively in agreement with the literatures and related other works done by other researchers in this area.

Future work would be to study the effect of different lubricants as well as different working conditions on the characteristics of EPDM under compressive load and care will also be taken, in particular, to improve the accuracy of the test results.

ACKNOWLEDGEMENT

The present experimental work was carried out in the frame work of Mechanical Engineering department of the Jadavpur University, Kolkata, India. The authors wish to express their thanks to the faculty members, laboratory staff members and under graduate students who assisted in conducting the experiments and compiling the results. We are also thankful to NEL(Rubber), Kolkata, India, for their kind support in providing the work specimen.

REFERENCES

[1] N.S.M. El.Tayeb, Md. R. Nasir: Effect of soft carbon black on tribology of deprotenised and polyisoprene rubbers, Wear, Vol. 262 ,pp.350-361,2007.

[2] D. Stamenkovic, M. Milosevic: Friction at rubber-metal springs, in *Proceedings of the SERBIATRIB*, 13-15.05.2009, Belgrade,pp.215-219.

[3] E.L. Deladi, M.B. De Rooij, D.J. Schipper: Modellingof static friction in rubber-metal contact, Tribology International,Vol.40,pp.588-594,2007.

[4] S.Kalpakjian, S.R. Schmid:*Manufacturing processes for engineering materials,*Pearson, New York,2007.

[5] D. Felhos, J. Karger-Kocsis:Tribological testing of peroxide cured EPDM rubbers with different carbon black contents under dry sliding conditions against steel, Tribology International, Vol.41,pp.404-415,2008.

[6] H. Ismail, U.S. Ishiaku, E.S. Lu, Z.A. Md. Ishak: The fatigue and hysteresis bahaviour of filled epoxidized natural rubber compounds, International journal of Polymeric materials,Vol.39,pp.45-57,1998.

[7] A.E.B. Martinelli: *Rubber bearings for precision positioning systems*, M.S. thesis, Department of Mechanical Engineering, MIT, U.S.,2005.

[8] H. Sofuoglu, J. Rasty: Flow behavior of plasticine used in physical modeling of metal forming processes, Tribology International, Vol.33,pp.523-529,2000.

[9] G.E. Dieter: *Mechanical Metallurgy*,McGraw Hill, 3rd.(SI Metric) Edition,1988.
[10] K.C. Ludema: *Friction*,*Wear*,*Lubrication*,CRC Press, U.S.,1996.
[11] http://www.gallaghercorp.com/urethane/designguide/shape.shtml
[12] Mukhopadhyay Abhijit: Maintenance Tribology: A new paradigm in maintenance.SURVEY,management journal of IISWBM,Kolkata, Vol.50,3&4.pp.1-7.2010.
[13] Mukhopadhyay Abhijit: Review of the tribological state tests in some metal forming operation in industry. Communicated for publication to an international journal of tribology,Feb.,2011.

Serbian Tribology Society

SERBIATRIB '11

12th International Conference on Tribology

Faculty of Mechanical Engineering in Kragujevac

Kragujevac, Serbia, 11 – 13 May 2011

TRANSFERRED MATERIAL INFLUENCE ON ELASTOMER-PLASTOMER COUPLE BEHAVIOR IN DRY SLIDING

Geanina Podaru[1], Sorin Ciortan[2], Iulian Birsan[3]

[1]"Dunarea de Jos" University of Galati, Romania

geanina.podaru@ugal.ro; sorin.ciortan@ugal.ro; iulian.birsan@ugal.ro

Abstract: *The pneumatic drives' rods are subjected to specific inertia forces generated by speed and acceleration evolution during a working cycle. The sealing friction can be used to balance these forces effect. The polymeric materials, used as replacement for metals, offer lower weigth of the rod, leading to lower ineria forces. If a rubber lip-polymeric rod sealing system works in dry conditions, a transferred lip material film to the rod occur. The paper investigate the influence of this film on the tribological behavior and efficiency of the seal. The transferred material can improve the over-all drive's performances, especially in actuators case.*

Keywords: *pneumatic sealing, polymeric rods, rubber lip, dry sliding*

1. INTRODUCTION

During the pneumatic drives functioning, in reciprocating motion regime, the rod acceleration get high values at the ends of the strokes, Figure 1.

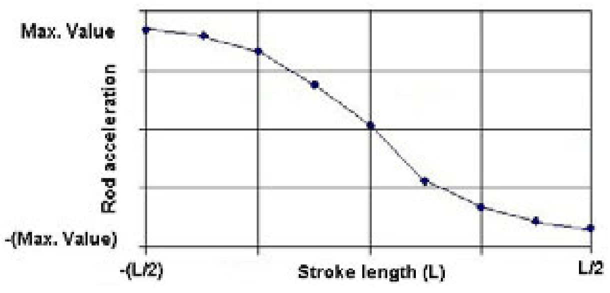

Figure 1. Rod acceleration values evolution during a stroke

Due to the rod weight, at the ends of the stroke the inertia forces can reach high values, leading to difficulties in precise positioning of the rod, especially in pneumatic actuators case. Different methods are used for inertia forces effects balancing, mainly based on the controlling of friction force values in the sealing system [1]. The drawback of the method is that the wear of the lip is accelerated, especially when the absence of the lubricant is required by environmental prescriptions.

A new approach of pneumatic drives' design is the use of polymeric materials [2]. These ones offer mechanical resistances comparable with metals, at much lower weight. Thus, the rod mass is lower, the inertia forces values being lower too.

The rod sealing systems used in pneumatic drives are rubber lip based and, if the rod is made by polymeric materials and the absence of lubricant is required, there are accomplished the conditions for the "third body" [3,4] appearance, as a transferred lip-to-rod material film.

The authors performed several investigations on the appearance and evolution of the transferred material film [5,6], the present paper being focused on the general evolution and influence of this "third body" on tribology and efficiency of the pneumatic drives' sealing system.

2. EXPERIMENTAL INVESTIGATIONS BASIS

In order to investigate the influence of transferred material film on seal's behaviour and performance a test rig was designed, as a pressurised enclosure where a polymeric rod is externally moved in reciprocating sliding. The sealing system is rubber lip based. The rig stands as a real pneumatic drive simulator, Figure 2.

The main functioning parameters, specific to pneumatic drives, can be monitored and recorded. Also, some of them are adjustable in a range of values, Table 1.

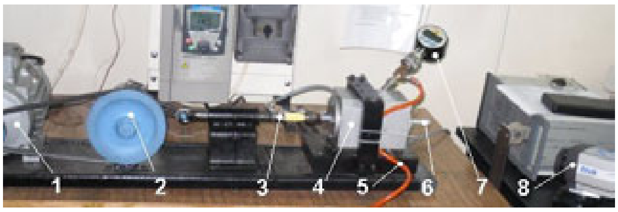

Figure 2. Pneumatic drives test rig: 1-electric drive; 2-eccentric; 3-stress gauge; 4-pressurised enclosure; 5-compressed air pipe; 6-polymeric rod; 7-pressure gauge; 8-thermographic & optical vision camera.

Table 1. Testing parameters

Parameter	Status	Range
Air pressure	Adjustable, recorded	6-8 bar
Sliding speed	Adjustable, recorded	105-472 strokes/min
Lip-rod tightening	Fixed	0.15 mm
Stroke length	Fixed	50 mm
Sealing friction force	Recorded	-
Sealing temperature	Recorded	-

As tested materials, were chosen silicone rubber for lip and polyetheretherketone (known under commercial name PEEK) for the rod.

Previous authors' research shows that the appearance and maintenance of transferred material film is possible only in a temperature domain, directly influenced by the rod material [6]. As consequence, a corresponding testing regime was chosen, in order to obtain the transferred material layer for the PEEK.

During the tests, the evolution of layer was optically monitored. The friction force and air pressure loss time evolutions were also recorded, Figure 3.

3. SEALING SYSTEM TRIBOLOGY IN PRESENCE OF TRANSFERRED FILM

Tribological analysis of a couple of materials covers two main aspects: friction evolution – as force or as coefficient and wear – as type or rate. Further, in this paper, the friction force and wear type is considered.

In dry sliding of polymers, especially when rubber is involved [7,8], stick-slip and adhesion phenomenon occur leading to the "third body" appearance, as a transferred material film.

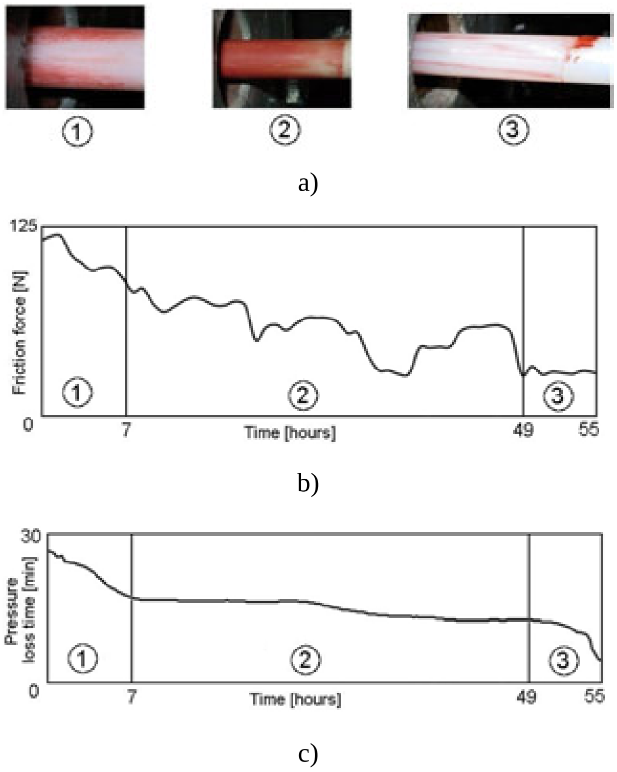

Figure 3. Friction force value evolution for PEEK rod, 7 bar air pressure, 210 stokes/min sliding speed (1-initial stage, transferred film formation; 2-stabilized stage, continuous transferred layer; 3-final stage, transferred layer discontinuity and sealing system failure): a) - layer evolution; b) – friction force evolution; c) – pressure loss time evolution.

The performed experiments shown that, in the beginning of the movement when the transferred film is not yet formed, the friction force value is high (area 1 in Figure 3b), leading to high contact temperatures. In this stage, the adhesion phenomenon leads to local transfer of the lip's material on the rod and it can be seen, in the corresponding optical image 1 in Figure 3a, that the layer is un-continuous, the initial deposits following a typical stick-slip pattern.

The transferred material layer, soon as it is full formed – optical image 2 in Figure 3a, acts as a lubricant leading to a decrease of friction force. This observation is in very well concordance with the literature [9]. A stabilized working regime of the sealing system is now reached, the transferred material layer compensating the wear of the lip-rod couple, area 2 in Figure 3b. Some variations of friction force value can be observed, caused by occasionally appearance of abrasive wear (due to hard debris detached – high values), but compensated by the transferred layer – low values.

Eventually, the quantity of material detached from the lip cannot be compensated, the transferred layer is expulsed by the pressure and the sealing fails – optical image 3 in Figure 3a and area 3 in Figure 3b.

In order to establish the dynamics of transferred layer evolution after its forming and the failure causes, some optical investigations were performed.

3.1 Rubber lip optical investigation

Taking into account that the main material source for the transferred layer is the lip [8,9], a closer look to this one is necesary, Figure 4.

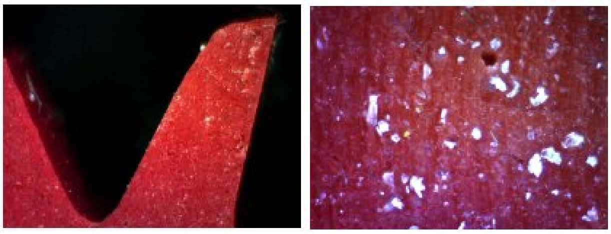

a) b)

Figure 4. Silicone rubber lip cross-section optical image: a) 30x magnification; b) 200x magnification

In Figure 4 can be identified the ingredients of the lip: the silicone rubber – as bulk base and silica particles, used as filler. Consequently, in the transferred layer both substances will be found.

Due to its physical properties, the rubber will act as a very viscous fluid, incorporating the hard silica particle. If the thickness of the transferred layer is higher than silica particles dimension, the contact between these ones and rod, respectively lip, is avoided, the abrasive wear of the system being avoided, Figure 5a.

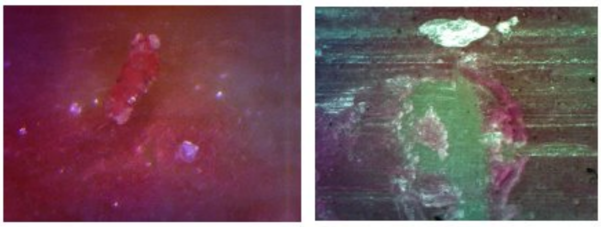

a) b)

Figure 5. Transferred material layer optical image: a) incorporated hard particles; b) hard debris generating layer rupture

During the seal functioning, due to high local temperatures, the transferred rubber material is subjected to a thermal hardening, becoming less fluid. At this time the enclosed hard particles acts as a sort of “crystallisation centres”, leading to layer ruptures and hard debris production, Figure 5b. These ones cannot anymore be incorporated into the material, generating ruptures into the layer.

The hard debris affects not only the transferred layer but also the lip, generating a massive detach of the material, Figure 6.

Eventually, due to thermal hardening and the action of hard debris, the transferred material layer cannot anymore compensate the wear of the lip. In this situation, the air pressure pushes out the layer material.

Figure 6. Abrasive wear of the lip due to hard debris

This elimination of the transferred material leads to quickly failure of the sealing system.

3.2 Polymeric rod optical investigation

During the seal’s working there are hard particles, detached from the lip or generated by hardening of the layer, which cannot be “isolated” into the layer material and reach to the rod surface, generating here abrasive wear tracks. In the early stabilized stage, when the transferred material has a viscous behaviour, the tracks on the rod’s surface are filled and covered, balancing this way the abrasive wear effects, Figure 7.

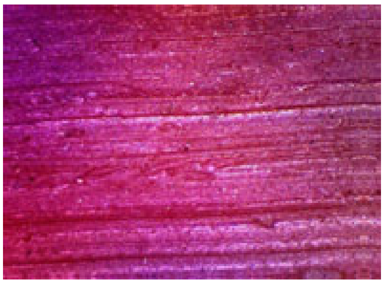

Figure 7. Abrasive wear tracks on the rod’s surface covered by transferred material

In the late stabilized stage, due to thermal hardening, the transferred material loses the capacity to compensate the abrasive wear, becoming fragile and developing large ruptures, Figure 8a. This way the rod surface is exposed to abrasive action of hard debris, either detached from the lip, either generated into the material layer, Figure 8b.

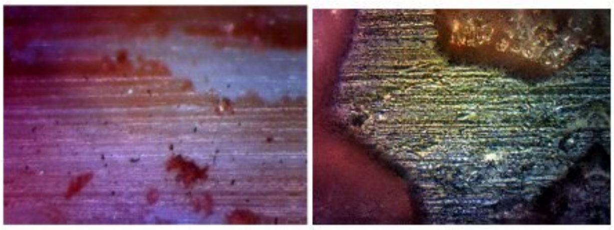

a) b)

Figure 8. Abrasive wear on the rod: a) layer rupture; b) wear tracks on the rod

The generated abrasive scars modify the rod's surface roughness, allowing the manifestation of internal friction phenomenon into the rubber [10], leading this way to rapidly degradation of the lip.

Taking into account all above presented, can be observed that, during the pneumatic drives' seals functioning in dry reciprocating sliding, the wear is both adhesive and abrasive.

In the beginning, before and in the early stage of transferred layer formation, the adhesive aspect of the wear is preponderant. After layer formation, due to hard debris (either filler particles detached from lip, either thermal hardened particles detached from the layer) the abrasive aspect of the wear become preponderant.

4. SEALING SYSTEM EFFICIENCY IN PRESENCE OF TRANSFERRED FILM

In order to investigate de effect of transferred material layer on seal's efficiency, the monitoring and recording of air pressure loses method was chosen [11]. During the tests was observed that time necessary for the air pressure to drop from nominal service value to minimum accepted value shows a continuous decrease, caused by sealing system wearing.

In the beginning, area 1 in Figure 3c, when the transferred layer is not yet formed, the pressure loss time have a high decrease rate. As soon the layer insulates the lip from the rod, the pressure loss time shows a constant, low decrease rate, area 2 in Figure 3c. Now all the modification occurred into the rod-lip couple tribology are compensate by the transferred material layer.

In the last working stage, area 3 in Figure 3c, the wear losses are too big, the layer cannot anymore compensate these and the system failure occur.

5. CONCLUSIONS

The influence of transferred material film on tribology and efficiency of pneumatic drives' sealing, based on polymeric rod-rubber lip couple working in dry sliding, was investigated.

Following the tests results, some conclusions can be drawn:

- the polymeric rod-rubber lip seal couple is a desirable designing solution for pneumatic drives;
- the transferred material layer have a considerable influence on tribology behaviour, of elastomer-plastomer couple in dry sliding contact, balancing the abrasive wear effects;
- the presence of transferred material layer leads to an improvement of the sealing system efficiency;
- the main influencing parameter of transferred material layer formation in dry sliding is the contact temperature;
- the elastomer-plastomer seal in dry sliding can be optimized by accurate controlling of the contact temperature, in order to avoid the thermal hardening of the transferred material.

REFERENCES

[1] Hasim I. Ali, Samsul Bahari B. Mohd Noor, S.M. Bashi, M.H.Marhaban: A Review of Pneumatic Actuators (Modeling and Control), Australian Journal of Basic and Applied Sciences, Vol. 3, No. 2, pp. 440-454, 2009.

[2] Pawel Kot: Pneumatic power servo-mechanism made from polymeric materials – analysis and optimization, Wydzial Mechaniczny, Politechnika Krakowska, Poland, 2009.

[3] A.K. Pogosian, K.V. Hovhannisyan, A.R. Isajanyan: Friction Transfer and Self-Lubrication of Polymers, Journal of Friction and Wear, Vol. 31, No. 1, pp. 81-88, 2010.

[4] B.J. Briscoe, S.K. Sinha: Wear of polymers, Proceedings Institution of Mechanical Engineers, Vol. 216, Part J, pp.401-413, 2002.

[5] G. Podaru, S. Ciortan: Optical methods based wear investigation of polymeric rods working in dry sliding, in: *Proceedings of The 11th International Conference on Tribology, ROTRIB'10*, 04-06.11.2010, Iasi, Paper RO-043.

[6] G. Podaru, I.G. Birsan, S. Ciortan, L. Deleanu: Friction generated heat and its effects in lubricantless pneumatic drives seals, in: *Proceedings of The 7th International Scientific Conference IRMES 2011*, 27-28.04.2011, Zlatibor.

[7] B.N.J. Persson: On the theory of rubber friction, Surface Science, No. 401, pp. 445-454, 1998.

[8] B.N.J. Persson: Theory of rubber friction and contact mechanics, Journal of Chemical Physics, Vol. 115, No. 8, pp. 3840-3861, 2001.

[9] A. Casoli, M. Brendle, J. Schultz, P. Auroy, G. Reiter: Friction of an elastomer sliding on polymeric model surfaces, Tribology Letters, Vol. 8, pp. 249-253, 2000.

[10] R.J. Pinnington: Rubber friction on rough and smooth surfaces, Wear, Vol. 267, pp. 1653-1664, 2009.

[11] Y. Yamaguchi: Tribology of plastic materials, their characteristics and applications to sliding components, Tribology Series, Vol. 16, pp. 295-361, 1990

Serbian Tribology Society

SERBIATRIB '11

12th International Conference on Tribology

Faculty of Mechanical Engineering in Kragujevac

Kragujevac, Serbia, 11 – 13 May 2011

INFLUENCE OF MICROSTRUCTURE, PRODUCED BY HEAT TREATMENT AND SEVER PLASTIC DEFORMATION, ON TRIBOLOGICAL PROPERTIES OF LOW-CARBON STEEL

V.I. Semenov[1], Song-Jeng Huang[2], L.Sh. Shuster[3], Po-Chou Lin[4]
[1, 3]Ufa State Aviation Technical University, Ufa, Russia, semenov-vi@rambler.ru
[2, 4]National Chung Cheng University, Taiwan, ROC, imehsj@gmail.com

Abstract: *This paper presents the results of tribological investigations conducted on steel 20 with the carbon content of up to 0.2%. The steel was studied in the three conditions: initial (hot-rolled), after heat-treatment (quenching+tempering) and after heat treatment with subsequent severe plastic deformation (SPD) performed by equal channel angular pressing technique (ECAP). It was stated that after various treatments the material acquires various structural conditions and possesses various strength properties and has a considerable difference in oxygen content in the surface layer. This influences the tribological properties during the contact with tool steel. The lowest values of adhesive bond shear strength, friction coefficient and wear rate are demonstrated in the material after martempering with subsequent SPD by ECAP technique. The surface of the investigated material after SPD treatment by the ECAP technique possesses a highest bearing capacity and requires more time for wearing-in in friction assemblies. Oxygen content increase in the form of metal oxides on the surface of low-carbon steels is accompanied by a decrease of the adhesive component of friction coefficient.*

Keywords: *Severe plastic deformation; adhesive bond shear strength; low-carbon steel; friction coefficient; wear rate; microstructure.*

1. INTRODUCTION

It is known that harder materials provide lower wear rate and friction coefficient [1]. There are various ways to enhance hardness of alloys by heat treatment [2, 3]. However, heat treatment may be an inefficient way to enhance hardness of many pure metals and low-carbon alloys. For such materials, various thermochemical [4-6] and surface plastic treatments [5-7] are used to enhance the strength of the surface of the materials under processing. The disadvantage of these techniques is that they results in a considerably shallow depth of the strengthened surface layer; that is why they may be used only for final treatment or for relatively simple and low-loaded parts in tribological pairs.

There are known papers on evaluation of the influence of microstructure and phase compositions of tool carbon steel on its tribological properties [5, 6, 8-10]. There tribological investigations were conducted on materials subjected to various treatments, which led to the changes of microstructure and phase composition of the materials.

Recently, the technology of effective and multiple strength enhancements retaining high technological plasticity, based on severe plastic deformation (SPD) techniques, has been developed. SPD enables to manufacture high-strength bulk billets out of metallic materials [11]. One of the SPD techniques is equal channel angular pressing (ECAP) [12], effected in several cycles of deformation. The principle of this ECAP strength enhancement technique is the maximum refinement of the grain structure to the sizes of submicrocrystalline- and nano-scale [13].

The SPD techniques considerably enlarge the field of application of such relatively cheap alloys as low-carbon steels. Therefore, complex comparative tribological investigations of low-carbon steel in various structural and phase conditions after heat and SPD treatments are of great research and practical interest.

2. MATERIAL AND METHODS OF INVESTIGATION

Low-carbon steel with the carbon content of up to 0.2% (percent by weight) was employed as material for present study. Samples after hot-rolling were taken as the initial condition. The dimensions of the samples are of 20 mm in diameter and of 100 mm in length.

In order to transform the investigated steel into the equilibrium condition and to release residual stresses, comprising quenching in water from the temperature of 880^{o} C with a subsequent tempering at the temperature of 600^{o} C and holding in a furnace at that temperature for 1.5 hour, was performed.

The ECAP scheme [14] shown in Fig. 1 was chosen for strain hardening of the initial material by SPD technique. ECAP was performed on a die-set with the angle of channel intersection of 120^{o} at a temperature of 400^{o}C, and with rotation of the billet along its longitudinal axis by 90^{o} after every cycle. The number of deformation cycles was four.

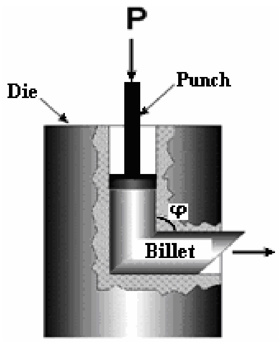

Figure 1. Scheme of a SPD technique – equal-channel angular pressing (ECAP).

The accumulated strain degree was calculated by the following formula [15, 16]:

$$\varepsilon = N \, \frac{2\cot(\varphi/2)}{\sqrt{3}}, \tag{1}$$

where ε is accumulated strain degree; N is the number of deformation cycles; φ is the angle of channel intersection.

The microstructure investigations were conducted with the help of optical metallography at different magnifications. The grain sizes were calculated by a secant line technique [17].

The techniques of evaluation of adhesive bond shear strength τ_n, determination of the adhesive component of the friction coefficient f_a [18] (Fig. 2, *a*) and evaluation of the friction coefficient f and wear rate J according to the scheme «block - on - disc» were employed for tribological studies [19] (Fig. 2, *b*).

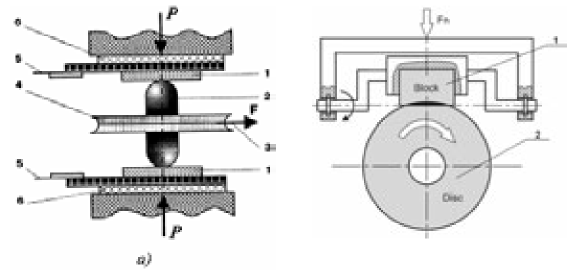

Figure 2. Schemes for tribological investigations: *a)* 1 - tested samples; 2 - spherical indenter; 3 – cable; 4 – disk groove; 5 – current conductor line; 6 – electrical insulating spacer [18]; *b)* 1 – tested sample; 2 – rotating steel disk.

The samples for evaluation of adhesive bond shear strength and determination of the adhesive component of the friction coefficient were prepared in the shape of discs of 20 mm in diameter and 5 mm in thickness and the spherical indenter with the sphere radius of 2.5 mm out of tool high-cutting steel *Fe – 6W – 5Mo*. Tests on determination of the adhesive bond shear strength were carried out at 20, 200 and 400^{o}C on a one-ball adhesiometer according to the scheme presented in Fig. 2, *a* [18]. The initial roughness of the contact surfaces of the samples for the test and the indenter were within 0.06 – 0.16 μm Ra.

The adhesive bond shear strength (τ_n) (MPa) was calculated with the help of the formula [18]:

$$\tau_n = 0.75 \times \frac{M}{\pi\left(\frac{d_{1,2}}{2}\right)^3}, \tag{2}$$

where τ_n is adhesive bond shear strength, *MPa*; $d_{1,2}$ are the diameters of the prints on the samples under investigation, *mm*; M – the indenter rotary moment, *N*mm*.

The adhesive component of the friction coefficient was calculated according to the following formula:

$$f_a = \frac{\tau_n}{p_r}, \tag{3}$$

where f_a is adhesive component of the friction coefficient; p_r – the normal pressure, *MPa, and*

$$p_r = \frac{P}{\pi \cdot \left(\frac{d_{1,2}}{2}\right)^2}, \tag{4}$$

where P – the compression force, *N*. P = Const = 2400 N for present test.

The samples in the shape of cubic blocks with the face of 12.7 mm were used for tests on the scheme «block-on-disc» (Fig. 2, *b*). The discs of 70 mm in diameter and with a thickness of 20 mm were prepared from tool high-cutting steel *Fe – 6W – 5Mo*. Three identical disks in accordance with numberous samples were prepared for testing. The initial roughness of the blocks and discs was in the range of 0.06 – 0.16 µm Ra. During testing the temperature of the tested sample was measured and variations of the temperature were recorded. The tests were carried out at room temperature on the tribometer *Timken* at a disc rotating speed of 1000rpm and a normal load of 5N for 15 min. The slide distance comprised 330000 cm. Every sample was weighed before and after testing in order to determine the wear rate. The geometric contact area was determined after testing. Then the wear rate was calculated according to the formula:

$$J = Q/qS_cL, \tag{5}$$

where J is wear rate value; Q – loss of weight, g; q – the material density, g/cm^3; S_c – the contact geometric area, cm^2; L – the slip distance, cm.

The wear of the discs fabricated from the tool high-cutting steel *Fe – 6W – 5Mo* and quenched to the hardness of HRC 58-65 was not taken into consideration due to its small value compared to the wear of the samples under testing.

The scanning electron microscope (SEM, Hitachi-S3500) with the add-on unit for Energy Dispersive Spectrometer (EDS) was used to conduct chemical analysis of the worn surface of the samples. The microhardness $H\mu$ was measured on the *Micromet-5101* at a load of 1.96 N with a holding of 15 sec.

Table 1. Surface analysis of steel 20 in various structural conditions

Treatment	Mean grain size, µm	Microhardness, MPA		Oxygen content, wt %	
		Before tests	After tests	Before tests	After tests
Hot-rolled (initial)	70	241	283	1.31	1.73
Heat treatment	50	265	307	1.51	1.82
Heat treatment + Severe Plastic Deformation (4 ECAP passes)	0.5	319	352	3.42	3.64

The microhardness measurement and the chemical analysis of the wearing surface with respect to the oxygen content were performed before and after the tests.

3. THE INVESTIGATION RESULTS

3.1 Measurement of microhardness and oxygen content of the sample surface

On the basis of microhardenss measurement and the chemical analysis of the worn surfaces with respect to the oxygen content, it was found that after tribological tests the microhardness of worn surfaces and the oxygen content of samples increase (referring to Table 1). Table 1 shows that the lowest values of the investigated parameters correspond to the initial (hot-rolled) condition of the material, and the highest values correspond to the condition of the material subjected to heat-treatment with subsequent severe plastic deformation by the ECAP technique.

As seen from the table 1, the material's structural condition influences significantly the increase of microhardeness and oxygen content on the surface of the low-carbon steel. Namely, the smaller is the mean grain size, the higher are the mentioned parameters. The material under consideration relates to hypoeutectoid steels, which possesses two structure components: ferrite and granular pearlite. The initial (hot-rolled) condition represents a coarse-grained ferrite-pearlite mixture (Fig. 3, *a*: ferrite – light grains, pearlite and carbide particles– dark grains). After heat-treatment (quenching after heating up to 880°C and subsequent tempering at 600°C) decrease of the initial carbide inhomogeneity and a certain mean grain size reduction were observed (Fig. 3*b*). After cyclic SPD by the ECAP technique the carbide phase is partially spheroidized, and areas in the shape of carbide net, decorating the boundaries of the ferrite grains, can be observed (Fig. 3, *c*)

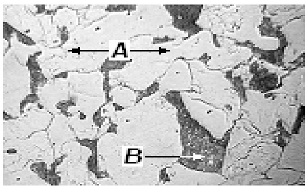

a) – in the initial condition, the mean grain size of 70 µm (x 500);

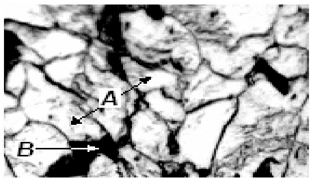

b) – after heat-treatment, the mean grain size of 50 µm (x 500);

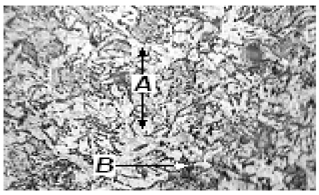

c) – after heat-treatment and 4 ECAP passes, the mean grain size of 0.5 µm (x 1000).

Figure 3. Steel 20 microstructure: A –ferrite; B – pearlite. In fig. 3, *c* pearlite is represented in the form of net on the boundaries of ferrite grains.

Fig. 4 represents surfaces of samples with different types of treatment before tribological tests. The surface areas, which were subjected to spectrographic analysis, are marked by rectangles

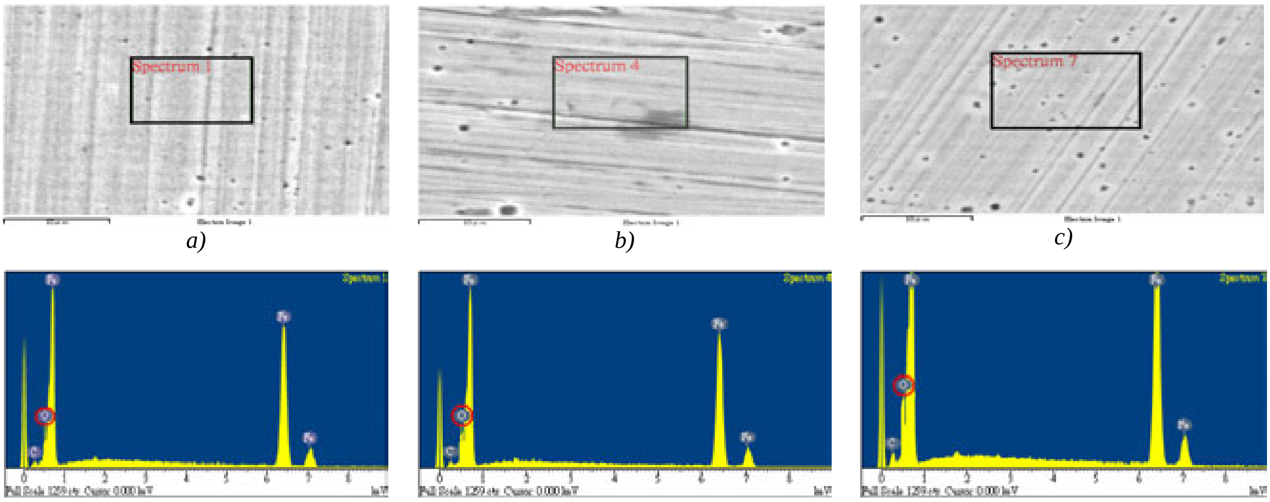

a) b) c) d) e) f)

Figure 4. Surfaces of samples with different types of treatment before tribological tests: *a)* – in the initial condition, the mean grain size of 70 µm; *b)* – after heat-treatment, the mean grain size of 50 µm; *c)* – after heat-treatment and 4 ECAP passes, the mean grain size of 0.5 µm; SEM - EDS spectrum: *d)* - in the initial condition; *e)* - after heat-treatment; *f)* - after heat-treatment and 4 ECAP passes. On the spectra there are displayed and marked oxygen peaks, corresponding to its content on the surface.

From the analysis of the obtained spectra it is observed that the biggest amount of oxygen in the form of oxides is revealed on the surface of the sample after heat-treatment and 4 ECAP passes (Fig. 4, *f*). Analogous spectra were obtained also on samples after performance of tribological tests.

It is known that severe plastic deformation, leading to grain structure refinement, is accompanied by increase of defect density and activation energy both inside the material and on its surface [13]. Moreover, in work [13] it is noted that there is an increase of diffusion rate in ultrafine-grained (UFG) materials, which contribute to energy reduction. Thus, we suppose that on the surface of UFG materials oxides are formed more intensively due to a higher diffusion rate of chemical elements form the environment, in particular, oxygen.

Analogous studies were performed on a magnesium AZ91D alloy [20] and on commercially pure titanium [21]. In all likelihood it is the common property of ultrafine grained (UFG) and nanostructured materials, grain boundaries of which contribute to a more active adsorption of oxygen on a metal surface with forming compounds with alloy components in the form of oxides. The numerical values of the oxygen content on the sample surface before and after tribological tests are shown in Table 1. It should be noted that after the tribological tests the oxygen content in the surface of all the samples increased as compared to the results obtained before the tests. These data associate with the results of other researchers [6, 10, 22 and others], and can be explained by the micro-structural changes on the surface under the action of normal pressures, friction forces and friction heating.

3.2 Tribological investigations according to the scheme "block-on-disc"

Fig. 5 represents characteristic areas of the worn surfaces on samples of low-carbon steel after different types of treatment with different microstructure.

Fig. 5 indicates that the worn surfaces in all the cases represent a combination of a metallic matrix in the form of a ferrite-pearlite mixture and oxides in different proportions, which depends on the type of treatment. Refering to table 1 and Fig. 4, *c*, it was found that on the worn surface of a sample with an ultrafine-grained structure after SPD by the ECAP technique there is a bigger amount of oxygen in the form of fine-dispersed oxides with mostly the same amount of iron and carbon compounds in the form of pearlites (Fig. 5, *c*). Contact interaction of the sample in the initial (hot-rolled) condition (Fig. 5, *a*) under the assumed test conditions, is accompanied by a more intensive adhering due to a less amount of oxides. Intensive adhering activates formation of adhesive bonds between the rotating disk made of tool steel and soft ferrite component. Subsequently, the failure of these bonds occurs under the action of friction forces. The pearlite phase with an increased carbon content (represented as dark parts in the photos) is located in the form of large fragments on the surface. After heat-treatment of steel samples (Fig. 5, *b*) pearlite agglomeration fragments of a smaller size are observed, but it does not have a considerable influence on friction forces

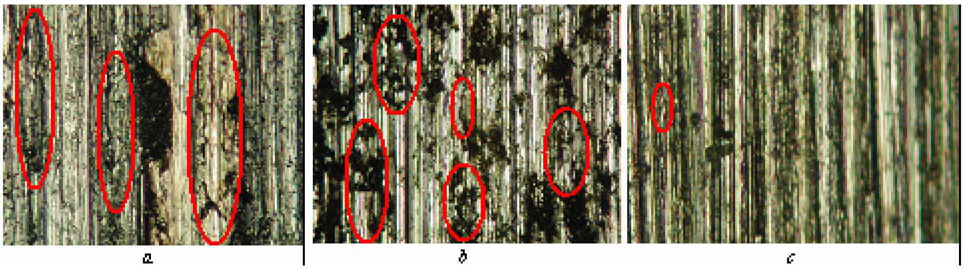

Figure 5. Worn surface on low-carbon steel after various types of treatment: *a* – sample in the initial condition (hot-rolled); *b* – samples after heat treatment (quenching and tempering); *c* – sample after ECAP and preceding heat treatment, x100.

Moreover it has been established that depending on the structure condition of low-carbon steel, and, consequently on the oxygen concentration on the surface there is observed different character of wearing in the contact zone. In Fig. 5, the areas of surface, where in the course of friction traces of spalling and pitting were observed, are marked. It can be observed in Fig. 5, *c*, the sample, subjected to ECAP processing has only a small area with spalling traces, while samples in the initial condition and after heat-treatment have more such areas, and they are roughly equal in their total surface area. However this fact requires further special inspection and investigation, as it is the basis for understanding the wear mechanism in low-carbon steels with different microstructure.

During the tribological testing the friction pair “low-carbon steel – tool steel” according to the scheme “block-on-disc” various characters of the friction coefficient changing with time were revealed in Fig. 6.

Severe plastic deformation by the ECAP technique leads to dispersion and a more uniform distribution of pearlite particles (Fig. 5, *c*), and also to hardening of the material due to structural constituents refinement.

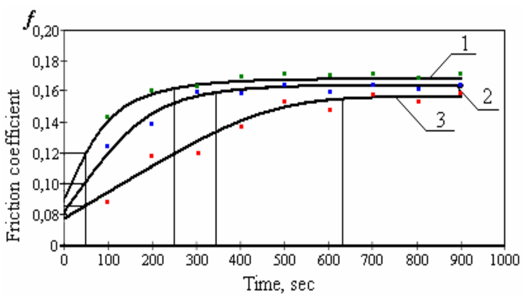

Figure 6. Dependence of the friction coefficient on testing time for the friction pair «low-carbon steel – tool steel *Fe – 6W – 5Mo* »: 1 – initial material (coarse-grained hot-rolled); 2 – material subjected to heat-treatment; 3 – material with ultrafine-grained structure after heat-treatment and SPD processing by ECAP technique.

Fig. 6 shows that the material with the ultrafine-grained structure after being subjected to heat treatment with subsequent severe plastic deformation (SPD) by ECAP technique has the lowest friction coefficient in the analized friction pair. Probably, friction conditions become more favorable due to the increase of strength and hardness of the low-carbon steel, and also to the uniform distribution of pearlite particles and larger oxygen content in the form of oxides and carbide particles on the surface. Such friction conditions, to an extent, can be compared to friction in a friction bearing [23]. As a result, the total value of the friction coefficient decreases. Thus we observe a complex formation of a “third body” [24], which consists of oxides, fine dispersion particles of pearlite and carbides. Besides, this wear test provides smoother transition to the established mode of friction that contributes to decrease of the wear rate. The bar chart in Fig. 7 shows the results of wear rate.

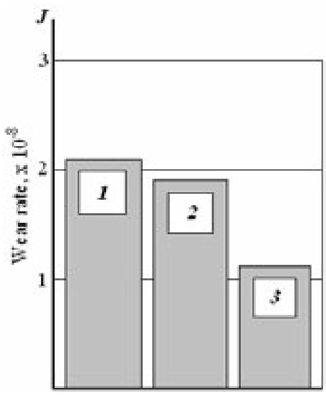

Figure 7. Wear rate o low-carbon steel depending on the structural condition of the material under investigation: 1 – initial material (coarse-grained hot-rolled); 2 – material subjected to heat-treatment; 3 – material with ultrafine-grained structure after heat-treatment and SPD processing by ECAP technique.

3.3 Adhesive bond shear strength evaluation

Fig. 8 shows the results of the tribological tests on determination of the adhesive bond shear strength τ_n depending on the pressure p_r during friction contact at various temperatures. These investigations proved the linear character of the dependence $\tau_n = f(p_r)$ both under the conditions of an elastic contact and plastic deformation at different temperatures θ. From these dependencies it follows that the adhesive component of the friction coefficient (f_a), which is calculated from the formula (3), increases with the growth of the temperature. The value f_a is calculated as a tangent of the angle of slope to the x-axis (i.e. a relation of adhesive bond shear strength (τ_n) to a normal pressure (p_r)).

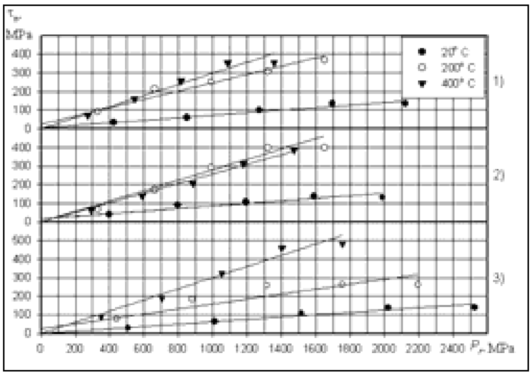

Figure 8. Dependence of the adhesive bond shear strength on the normal load in the tribological pair "low-carbon steel-tool steel *Fe – 6W – 5Mo* at various temperatures and during various treatment of the material under investigation: 1 – initial material (coarse-grained hot-rolled); 2 – material subjected to heat-treatment; 3 – material with ultrafine-grained structure after heat-treatment and SPD processing by ECAP technique.

The obtained temperature dependence of the adhesive component of the friction coefficient f_a for the friction pair under investigation is shown in Fig. 9. The curves in Fig. 9 are, plotted as a result of processing of data, represented in Fig. 8 and after calculation of f_a.

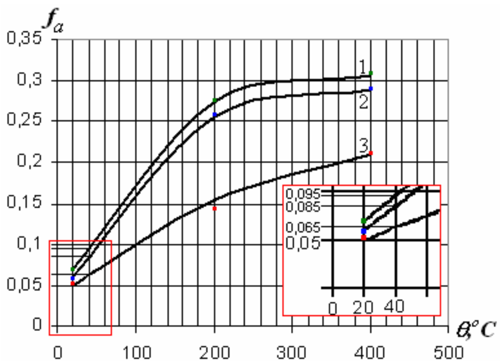

Figure 9. Changes in the adhesive component of the friction coefficient depending on the temperature: 1 – initial material (coarse-grained hot-rolled); 2 – material subjected to heat-treatment; 3 – material with ultrafine-grained structure after heat-treatment and SPD processing by ECAP technique. The right bottom corner represents a magnified and horizontally strained graph segment.

Fig. 8 and 9 show experimental dependencies of adhesion interaction parameters on pressure and temperature, which were typical of heavy loaded tribological pairs, and also of a contact of tool and treated material under conditions of mechanical treatment.

It has been found that the increase of adhesive bond strength is accompanied by the growth of normal pressure p_r on the contact. The best effect of abovementioned increase is observed in the samples with UFG structure after ECAP, which is probably connected with a more intense hardening of material due to deformation treatment in comparison to the other two conditions of the materials. It is known that with the increase of the temperature the bearing capacity of the contact gradually decreases [18]; as a result the adhesive component of the friction coefficient f_a increases (see Fig. 9).

However in the represented dependencies, it is seen that in low-carbon steel samples, subjected to heat treatment with a subsequent SPD by the ECAP technique, the adhesive component values of the friction coefficient are considerably lower within the whole investigated temperature range, comparing with the two other conditions. Data obtained for the initial sample and for the sample after heat treatment (without a subsequent SPD) do not differ significantly both by value and the character of the f_a variation. Probably it is predetermined by a slight difference of the mean grain size of the samples existing between the initial and heat treated conditions, and also by a very close oxygen content exhibiting within both materials of those conditions (see the Table 1). On the basis of the above mentioned suggestion, we suppose that the adhesive component of the friction coefficient f_a is directly connected with the structural condition of surface and with the oxygen content, because the oxide films (possessing high hardness) prevent the sample from a direct contact with the disc in one case, and from spherical indenter in another case.

3.4 Comparative evaluation of tribological investigation results of the two alternative techniques

Comparing the results given in Fig. 6 and Fig. 9, it can be noted that they are similar in the uprising area (left part of the graphs), and it can be supposed that the greatest contribution to the general changes in that integral value of the friction coefficient is introduced by its adhesive component. Probably it is connected with the low-carbon steels' tendency for strain hardening via structural grain refinement. A more flat area on the curve, corresponding to the investigated sample with a UFG structure after SPD treatment by ECAP technique, verifies that the sample has higher surface bearing capacity, but at the same time, this sample requires more time for wearing-in.

From the of temperature variation dynamics during temperature measurement in the process of tests of the block-on-disc scheme, it has been established that the maximum heating of the sample with the adopted conditions of test and dimensions of the samples and disks was at about 40 ± 1.5-2.0^{o}C. This temperature was achieved 50 seconds after the start of the tribological testing and practically did not change from then until the end of the tests.

In accordance with the known mechanical attraction friction theory [24] the integral friction coefficient value *(f)* is formed from the deformation (f_d) and adhesive (f_a) components. The deformation component of the friction coefficient is formed by resistance forces of the straining “bulge”, moving ahead of the irregularities intruded into the surface of a softer one of the contacting and slipping in relation to one another bodies. The value of the deformation component of the friction coefficient f_d depends on the number of intruded irregularities and their relative intrusion, which can be determined analytically [25] or experimentally as:

$$f_d = f - f_a \tag{5}$$

In order to compare the results of the investigations, represented in Fig. 6 and Fig. 9 a data cut-off, corresponding to the period of stabilization of the friction heating temperature (50 sec.) and the maximum value of the temperature after 50 sec (40C^o) was made in Fig. 6 with the following extrapolation of these data on curves, represented in Fig. 9. With the help of formula (5) the deformation component of the friction coefficient has been calculated.

Values of the total friction coefficient *(f)* and its adhesive component (f_a), obtained in comparable conditions on the basis of experimental data and represented in Fig. 6 and 9, showed that the deformation component (f_d) values are in the range 0.020 ± 10% regardless of the type of treatment and the structural condition of the samples. Thus it can be concluded that in the adopted testing conditions it is the adhesive component that has the biggest influence on the friction coefficient *(f)*.

4. CONCLUSIONS

1. Severe plastic deformation by equal channel angular pressing technique was shown to enhance efficiently the strength of the low-carbon steel due to its grain structural refinement that considerably influences the decrease in the friction coefficient and its adhesive component;
2. The increased oxygen content on the material surface after SPD compared to both initial condition and after heat-treatment contributes to stronger passivation of the surface due to the formation of oxide films, which together with strain hardening contributes to decrease in the friction coefficient in the specified temperature range and increase in wear resistance as well;
3. The surface of the investigated material after SPD treatment by the ECAP technique possesses a higher bearing capacity and requires more time for wearing-in in friction assemblies;
4. Oxygen content increase in the form of metal oxides on the surface of low-carbon steels is accompanied by an increase of the deformation component of friction coefficient.
5. The present wear mechanism of low-carbon steel with heat-treatment and processing by ECAP against tool steel *Fe – 6W – 5Mo* is suggested as the adhesive types

ACKNOWLEDGEMENTS

The authors express gratitude to Dr. S.V. Chertovskikh (Ufa State Aviation Technical University, Russia) and Prof. S.-G. Hwang (National University Formosa, Taiwan) for active participation in tribological investigations and processing of results.

The work was carried out within the frames of the joint Russian-Taiwan project No 07-08-92001 HHC_a, supported by RFBR, jointed with project NSC 96-2923-E-194 -001 -MY3 by NSC of Taiwan.

REFERENCES

[1] A.V. Chichinadze, E.M. Berliner, E.D. Brown et al., Friction, wear and lubrication (tribology and triboengineering), Mashinostroenie, Moscow, 2003

[2] Shabashov V.A., Korshunov L.G., Mukoseev A.G. et al. Deformation-induced phase transitions in a high-carbon steel // Materials Science and Engineering, 2003. Vol. A346. P. 196-197.

[3] Garnham J.E., Beynon J.H. Dry rolling-sliding wear of bainitic and pearlitic steels//Wear, 1992. Vol. 157, № 1. P. 81-109.

[4] G.S. Fox-Rabinovich, G.C. Weatherly, A.J. Kovalev, L.Sh. Shuster and others Nano-Crystaline FAD (Filtered Arc Depasited) TiALN PVD Coatings for High-Speed Machining Application//Intern. Conf. on Metallurgical Coatings and Thin Films. Progr. and abst. – San Diego, California, April 28 – May 2, 2003, p. 52.

[5] LuzhnovYu.M. and others. The Efficiency of the Friction of the “wheel-rail” – System/New Achievements in Tribology. 6th Intern. Symp.

"Insycont-02", September 2002, Krakow: Poland. P. 129-135.

[6] Johnson K.L. Contact Mechanics. Cambridge University Press, 1987. 452 p.

[7] L.G. Odintsov, Strengthening and finishing of parts via surface plastic deformation: Reference book, Mashinostroenie, Moscow, 1987.

[8] Yang Z.Y., Naylor M.G.S., and Rigney DA. Sliding wear of 304 and 310 stainless steels//Wear. 1985. Vol. 105. P. 73—86.

[9] Hornbogen E. Microstructure and Wear. — Metallurgical aspects of wear. — Bad Pyrmont, 1979. P. 23-49.

[10] Perez-Unzueta A. J, Beynon J. H. Microstructure and wear resistance of pearlitic rail steels//Wear, 1993. Vol. 162-164. P. 173-182.

[11] R.Z. Valiev The new trends in fabrication of bulk nanostructured materials by SPD processing, J. Mater. Sci., Vol. 42 (2007), pp. 1483-1490.

[12] G.I. Raab, F.F. Safin, T.C. Lowe, Y.T. Zhu, R.Z. Valiev Development of ECAP-Confomr to Produce Ultrafine-Grained Aluminum, Proc. of Ultrafine Grained Materials IV symposium held during the TMS 2006 Annual Meeting in San Antonio, Texas, USA, March 12-16, 2006, eds. Y. Zhu, T. Langdon, Z. Horita, M. Zehetbauer, S.L. Semiatin, T. Lowe (2006) pp. 171-177.

[13] R.Z. Valiev, T.G. Langdon Principles of equal-channel angular pressing as a processing tool for grain refinement, Progress in Materials Science, Vol. 51 (2006), pp. 881-981.

[14] R.Z. Valiev, Y. Estrin, Z. Horita, T.G. Langdon, M.J. Zehetbauer, Y.T. Zhu, Producing bulk ultrafine-grained materials by severe plastic deformation, J. Mate. 58 (2006) 33.

[15] V.M. Segal, V.I. Reznikov, A.E. Drobyshevskii, V.I. Kopylov et al., Plastic processing of metals by simple sear, Izvestia AN USSR Metals. 1 (1981) 115-123.

[16] Segal V.M. Equal channel angular extrusion: from macromechanics to structure formation //Mater. Sci. Eng. 1999. (A271). P. 322-333.

[17] S.A. Saltykov Stereometric Metallographic. Metallurgy, Moscow, 1976.

[18] V.V. Stolyarov, L.Sh. Shuster, M.Sh. Migranov, R.Z. Valiev, Y.T. Zhu Reduction of friction coefficient of ultrafine-grained CP titanium//Materials Science and Engineering A371, 2004. pp 313-317.

[19] ChichinadzeA.V. Evolution Method of the Carbon Friction Composite Materials Used in Multiple Disk Aviation Brakes//Tribologia. Warszawa. No. 1. 2000. Part I. P. 7-22; No. 2. 2000. Part II. P. 133-154; No. 1. 2001. Part III. P. 23-38.

[20] V.I. Semenov, Y.-R. Jeng, S.-J. Huang, Y.-Zh. Dao, S.-J. Hwang, L. Sh. Shuster, S. V. Chertovskikh, P.-Ch. Lin, Tribological properties of the AZ91D magnesium alloy, hardened with silicone carbide and by severe plastic deformation, J. of Fri. and Wear. 30 (2009) 194-198.

[21] V.V. Stolyarov, L.Sh. Shuster, S.V. Chertovskih Tribological behaviors of ultrafine-grained titanium alloys// Friction and lubrication in machines and mechanisms.-2006.-№10. – p. 11-19.

[22] A.S. Akhmatov, Molecular physics of boundary friction, State publishing House of physico-matematical literature, Moscow, 1963.

[23] Semenov A.P., Antifriction and antiseizure sliding bearings, Proc. III Int. Symposium of tribo-fatugue ISTF 2000, Beijing China Human University Press, China, (2000) 629-632.

[24] I.V. Kragelskii. Friction and wear. Mashinostroenie. Moscow, 1968.

[25] I.V. Kragelskii, M.N. Dobychin, V.S. Kombalov. Principles of friction and wear calculations. Mashinostroenie, Moscow, 1977.

SERBIATRIB '11

Serbian Tribology Society

12th International Conference on Tribology

Faculty of Mechanical Engineering in Kragujevac

Kragujevac, Serbia, 11 – 13 May 2011

EVALUATION OF THE SPREAD RANGE OF 3D PARAMETERS FOR COATED SURFACES

Lorena Deleanu[1], Alina Cantaragiu[1], Iulian Gabriel Bîrsan[1], Geanina Podaru[1], Constantin Georgescu[1]

[1]University "Dunarea de Jos", Galati, Romania, lorena.deleanu@ugal.ro

Abstract: *3D measurement on surface roughness could be used to assess the surface quality but the procedure is time-consuming and the better the equipment and its performances, the smaller the investigated surfaces. There were investigated the spread ranges for several 3D roughness parameters in order to use the information for establishing a less-time consuming, but acceptable set of measurements. The results pointed out there are some parameters with larger spread range (Sa, Sq, St)and others with narrower spread range (Ssk, Sku).*

Keywords: *spread range, 3D amplitude and functional parameters, surface topography, coating.*

1. INTRODUCTION

3D measurements of surface roughness could be used to assess the surface quality but the procedure is time-consuming and the better the equipment and its performances, the smaller the investigated surfaces. Modern 3D profilometry units evolved and are now capable of reaching a higher accuracy in measuring surface profilometry, but in the same time a smaller scale suppose a smaller area of investigation [1, 10].

Multiple measurements in different areas on the sample can produce results within a large range. This range is due to variations of the surface texture across the sample surface. Consequently, the results of any single measurement may not be representative of the overall surface quality [1].

A solution to statistically solve the problem of variation in the measured values is to do multiple measurements in different areas of the surface. The average surface texture will be described with good enough accuracy by the arithmetic average of the parameters. The number of measurements that are taken on a part is determined by the measured results and the part tolerances. How many measurements does one have to perform to be inside the recommended or imposed tolerances? How different could be the spread ranges for a particular parameter or a set of parameters?

The expectation of 3D measurement is that only one measurement (or at least a small number) should be sufficient for the analysis of a part, mainly due to the time needed per measurement. The large number of data points in one 3D measurement was hoped to give a statistically stable basis for the analysis of a surface [1, 3, 6, 7].

This study investigated the spread ranges for several 3D roughness parameters in order to use the information for establishing a less-time consuming, but acceptable set of measurements and for the assessment of the surface quality before and after deposition.

2. MEASURING METHODOLOGY

2.1 Materials

Commercially available 316L stainless steel specimens having the composition Fe + Cr: 18.00; Ni: 12.00; Mo: 2.50; Mn: 1.70; P: 0.04; C: 0.02; S: 0.01; Si: 0.15 (wt. %) were used as the substrate for a hard coating. The electrochemical process of deposition was performed in a small three-electrode cell on plate specimens. The process was carried out potentiostatically with a potentiostat/ galvanostat connected to a computer [2].

In this study there was used the following notation: sample 1 for the simple steel surface as grinded; samples 2 and 3 have TiO_2 coating, the first being obtained after 30 minutes, the second being obtained after 60 minutes (the coating parameters were kept constant).

Prior to make electrical contacts, the plates were mechanically polished using 600 and 1200 grit emery paper, organically degreased with acetone, etched in a 1:1 $HCl:H_2O$ solution for 60 seconds, chemical degreased with ethylic alcohol for few seconds and rinsed with distilled water. Then, the samples were activated by cathodisation at -1.1 V vs. SCE in a 0.1 M NaOH solution for 2 minutes and finally rinsed with doubly-distilled water. The deposition was performed at room temperature (23-25ºC) at -1.43 V potential vs. Ag/AgCl electrode. The deposited layer was then, heated in air at 400 ºC for 1 h in air to obtain crystalline TiO_2 film. The substrates were weighed prior the coating and after annealing to determine the amount of deposited TiO_2. Aspects of the investigated surfaces for Sample 2 and 3 are given in Figure 1 [2].

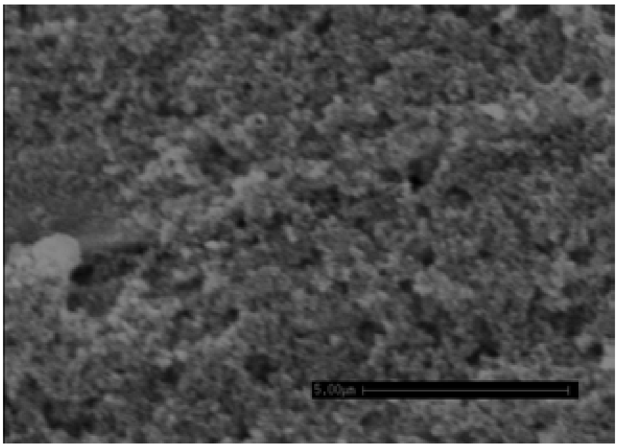

Sample 2

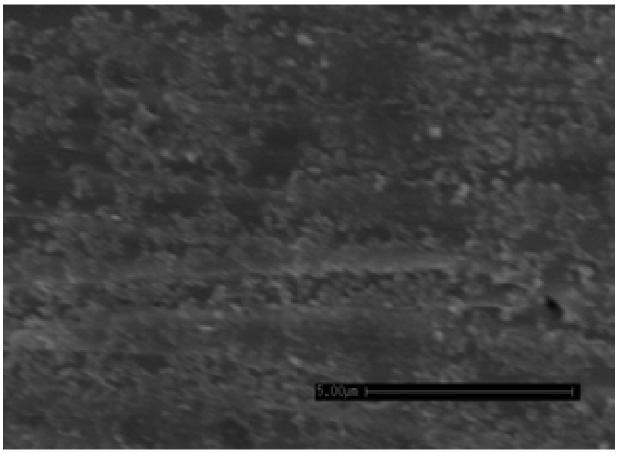

Sample 3

Figure 1. Surface of the coated samples

2.2 Measuring method

The 5 measurements for each sample were done with a contact profilometer, with the same set parameters: investigated areas: 500 μm x 500 μm (Fig. 2), 5 μm step between lines, the vertical range 500 μm, the scan speed was set at 35 μm/s and 200 points per scan line. All parameters are calculated from the raw profiles. Specialists talk about an actual measuring strategy.

Each of the discussed parameters are given as

$$Parameter\ Average\ value^{+\max value\ above\ the\ average\ (\%)}_{-min\ value\ below\ the\ average\ (\%)} \quad (1)$$

where the average value is calculated for 5 measurements and the max value above average is the maximum value among the five ones, the min value below the average is the minimum value among the same five values. The maximum and minimum spread from the average values spreads from are given in percentage as

$$As(\%) = max\ value\ above\ the\ average = \frac{As \cdot 100}{Av} \quad [\%] \quad (2)$$

$$Ai(\%) = min\ value\ above\ the\ average = \frac{Ai \cdot 100}{Av} \quad [\%] \quad (3)$$

where

$As = max\ value\ above\ the\ average - the\ average\ value$

$Ai = min\ value\ below\ the\ average - the\ average\ value$

$Av = \sum_{i=1}^{5} P_i$ is the average value for parameter P.

The following parameters were calculated as given by [9, 10] and discussed:

amplitude parameters:

- the roughness average, *Sa* [μm],
- the root mean square parameter, *Sq* [μm],
- the surface skewness, *Ssk* [-],
- the surface kurtosis, *Sku* [-],
- the peak-valley height, *Sy* [μm];

functional parameters

- the reduced summit height, *Spk* [μm],
- the core roughness depth, *Sk* [μm],
- the reduced valley depth, *Svk* [μm].

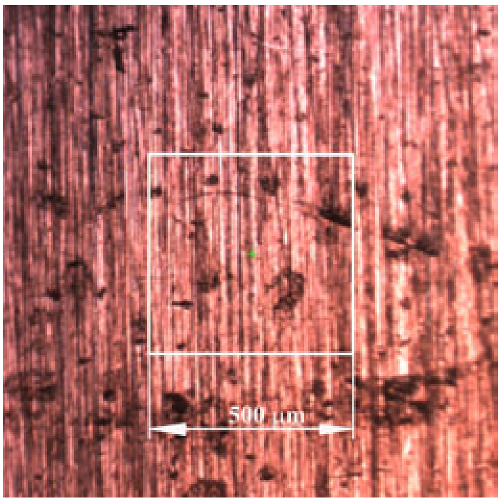

Figure 2. Example of the investigated area (measurement no 4 for Sample 1)

Figure 3 presents the measured values and the average of the amplitude parameters. Figure 4 presents the values of three functional parameters: *Svk*, *Sk* and *Spk*. In order to better estimate their values, for one measurement the column represents the sum (*Svk*+*Sk*+*Spk*). The Sample 1 has larger ranges for the three functional parameters, meaning the polishing process does not offer yet a uniform quality of the surface. It could be improved. The coated surfaces (Sample 2 and 3) have a more uniform distribution of these parameters but for sample 3 the values for *Sk* and *Spk* are larger than for those for Sample 2. It is possible to reflect the fact that the deposition follows the actual topography of the steel surface but emphasizing the heights (*Spk*) and enlarging the core zone (*Sk*). Thus, the coating does not cover the voids of the steel support.

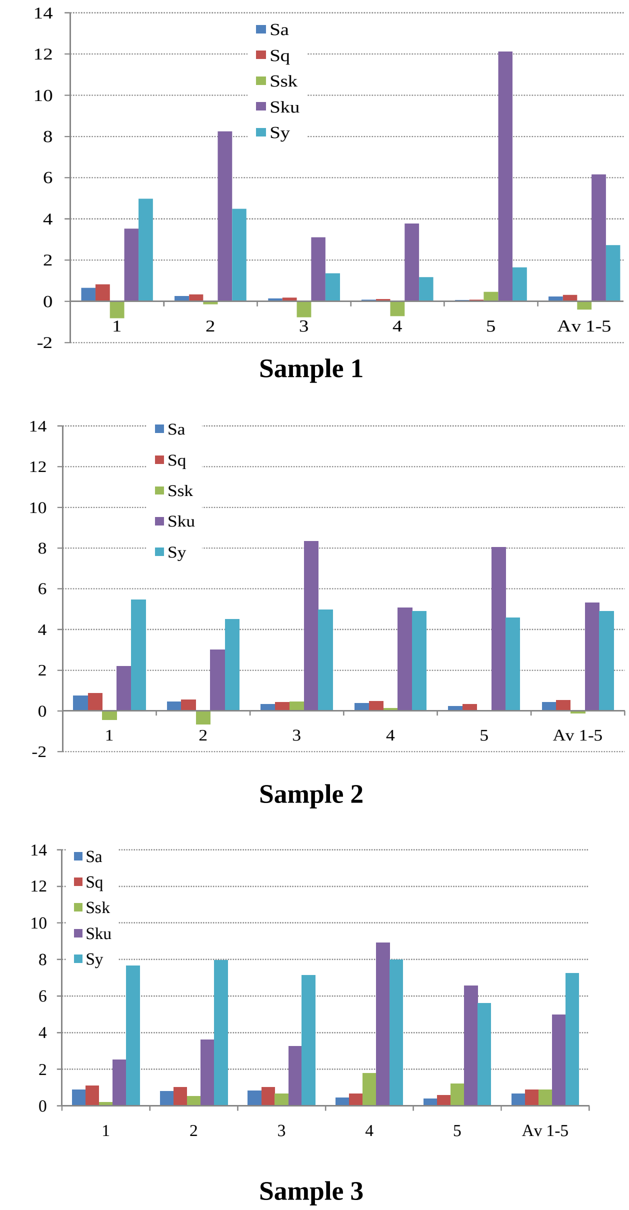

Figure 3. Several amplitude parameters for Samples 1, 2 and 3. Last parameter set was obtained as average of all 5 measurements.

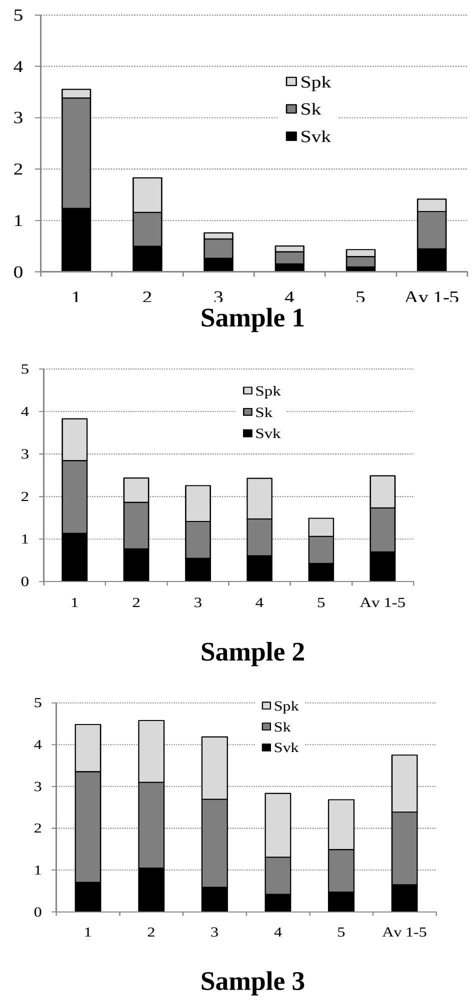

Figure 4. Functional parameters for Sample 1, 2 and 3. Last parameter (*Spk*+*Sk*+*Svk*) was obtained as average of all 5 measurements.

Surfaces with *Ssk*~0 have symmetric height distributions. Sample 2 has several measurements with *Ssk* <0, meaning, possibly, a bearing surface with holes. Sample 3 has *Ssk* >0 and it can be a flat surface with peaks. Values greater than 1.0 may indicate extreme holes or peaks on the surface (as, for instance, measurements 4 and 5 for Sample 3). Greater values than 3 for *Sku* indicate narrower height distributions.

There are two suggestions after noticing these characteristics of the coated surfaces:

- it is obviously necessary to have a polishing process of the coated surfaces in order to eliminate high and narrow peaks and to reduce *Spk* and *Sk*;
- mechanical test are necessary for assessing the wear of the coated surfaces

Figure 6 presents chromatographic images of the investigated surfaces. Each line is for the same sample, and includes one or two images for extreme values of some relevant parameters and one image close to the average values, at least for some of the investigated parameters.

Table 1. Amplitude parameters (average value from 5 measurements for each sample)

Sample 1	Sample 2	Sample 3
$Sa\ 0.243^{+0.41\,(+170.2\%)}_{-0.17\,(-73.6\%)}$	$Sa\ 0.430^{+0.32\,(+74.6\%)}_{-0.19\,(-44.7\%)}$	$Sa\ 0.681^{+0.22\,(+32.3\%)}_{-0.27\,(-40.2\%)}$
$Sq\ 0.310^{+0.52\,(+168.2\%)}_{-0.22\,(-72.9\%)}$	$Sq\ 0.528^{+0.34\,(+64.6\%)}_{-0.20\,(-39.5\%)}$	$Sq\ 0.880^{+0.23\,(+26.4\%)}_{-0.30\,(-34.8\%)}$
$Ssk\ -0.397^{+0.85\,(215.3\%)}_{-0.41\,(-104.9\%)}$	$Ssk\ -0.108^{+0.57\,(+514.8\%)}_{-0.55\,(-514.80\%)}$	$Ssk\ 0.887^{+091\,(+102.9\%)}_{-0.68\,(-77.0\%)}$
$Sku\ 6.15^{+5.95\,(+96.7\%)}_{-3.04\,(-49.9\%)}$	$Sku\ 5.334^{+3.00\,(+56.2\%)}_{-0.55\,(-58.6\%)}$	$Sku\ 4.982^{+3.93\,(78.9\%)}_{-2.44\,(-49.0\%)}$
$Sy\ 2.73^{+2.24\,(+82.0\%)}_{-1.54\,(-56.6\%)}$	$Sy\ 4.884^{+0.56\,(+11.6\%)}_{-0.55\,(-7.6\%)}$	$Sy\ 7.27^{+0.717\,(+9.86\%)}_{-1.66\,(-22.8\%)}$

Table 2. Functional parameters

Sample 1	Sample 2	Sample 3
$Spk\ 1.363^{+0.161\,(+11.8\%)}_{-0.231\,(-16.9\%)}$	$Spk\ 0.754^{+0.22\,(+29.9\%)}_{-0.33\,(-43.9\%)}$	$Spk\ 1.363^{+0.16\,(+11.86\%)}_{-0.23\,(-16.9\%)}$
$Sk\ 1.742^{+0.904\,(+51.9\%)}_{-0.857\,(-49.2\%)}$	$Sk\ 1.03^{+0.67\,(+65.1\%)}_{-0.39\,(-38.4\%)}$	$Sk\ 2.646^{+0.90\,(+51.9\%)}_{-0.85\,(-49.2\%)}$
$Svk\ 0.646^{+0.401\,(+62.1\%)}_{-0.224\,(-34.6\%)}$	$Svk\ -0.697^{+0.43\,(+62.8\%)}_{-0.26\,(-38.5\%)}$	$Svk\ -0.646^{+0.40\,(+62.1\%)}_{-0.22\,(-34.6\%)}$

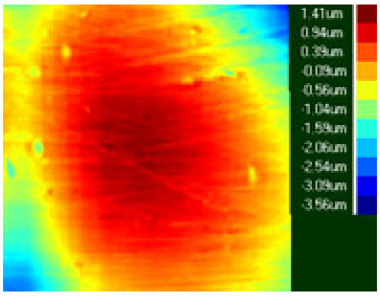

Measurement no. 1: the parameter values are different from the average ones

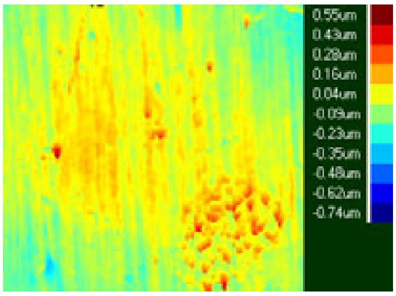

Measurement no. 5: the highest value for *Sku*

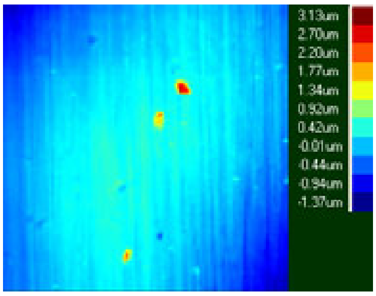

Measurement no. 2: the amplitude parameters are closer to the average ones, except *Sku* and *Sy*

Sample 1

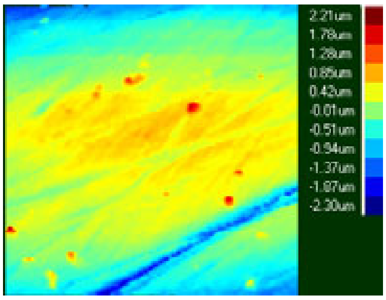

Measurement no. 2

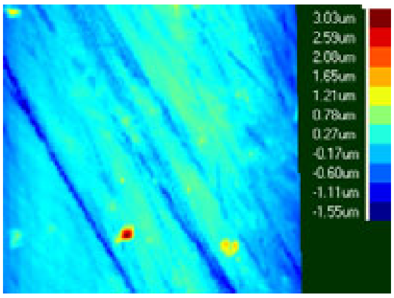

Measurement no. 5

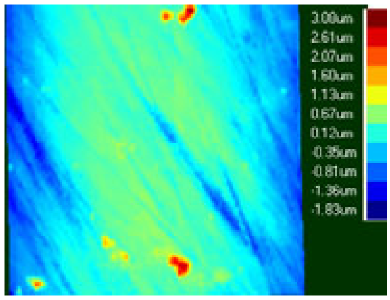

Measurement no. 4: closer values to the average ones, *Ssk* is negative for the average, but close to zero

Sample 2

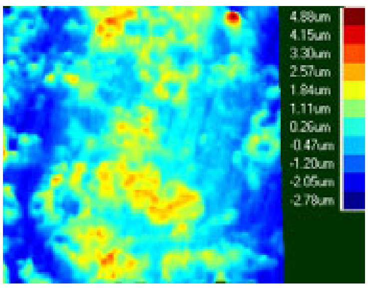

Measurement no. 1

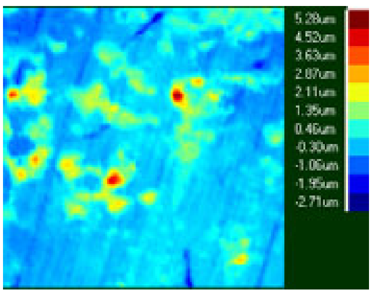

Measurement no. 4

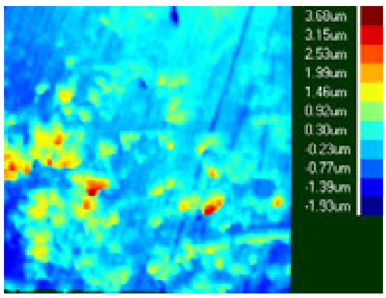

Measurement no. 5: closer values to average but not for *Sa* and *Sq* smaller than the average ones

Sample 3

Figure 5. Chromatic images of several investigated surfaces for each sample

Analysing the values given in Tables 1 and 2 one may notice that for the amplitude parameters, the spread ranges were reduced after coating, except *Ssk* that has the lowest average measured value for Sample 2 and then increasing for Sample 3. It is also this parameter that has the largest ranges of spread for all samples. Standards recommend for manufactured surfaces to have spread ranges around ±16%, but it is hard to obtained that for coatings (without further polishing process).

Figure 6 presents the spread ranges and the average value for each analysed parameter.

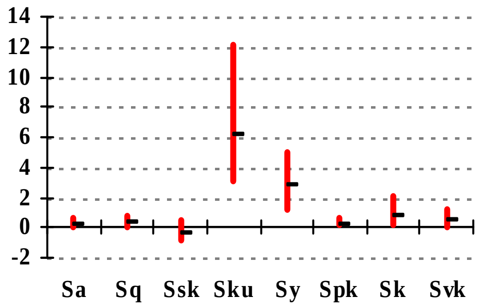

Sample 1

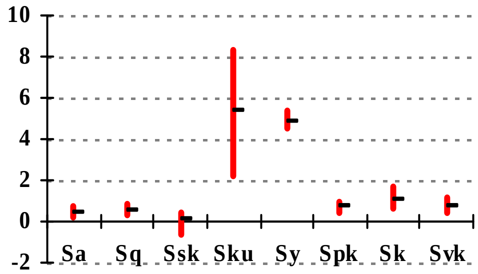

Sample 2

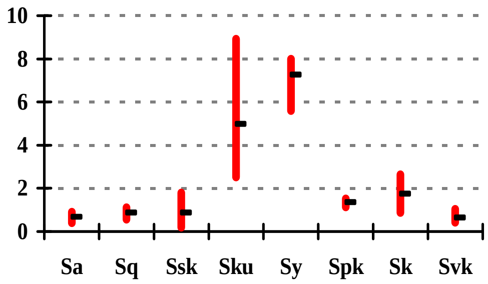

Sample 3

Figure 6. The spread ranges for each sample

3. CONCLUSION

Analysing the spread of the investigated parameters for Sample 1 the authors estimated that the polishing process could be improved in order to reduce the spread especially for *Sku*, *Sy* and *Sk*. There are few peaks but very high and narrow that could be eliminated by a better polishing, by changing the abrasive paper or even the method.

Investigating the spread of the measurements' values and their dependence on the covering process parameters will allow improving the coating technology and also the surface quality.

Therefore, it is most likely that some kind of rule (similar to the 16%) is needed to take account of the natural deviations that occur within a standard engineering surface.

If one will analyse only the amplitude parameters *Sa* and *Sq*, the conclusion does not reflect the actual quality of the surfaces. These two parameters are spread in similar ranges for all three types of surfaces. It is only possible to say that they have a slight trend to increase from values obtained for the uncoated surface.

The deposition process generates a non-uniform surface as one could see from Figures 1 and 5. It is necessary to study the surface quality after the final polishing process.

For Sample 2, the maximum value of *Sku* becomes lower but *Sy* remains with a maximum of 5.6 μm, but in a narrower range. *Spk* slightly increases, but the other two functional parameters slightly decrease in maximum values and the size of spread range.

Comparing Sample 1 and Sample 3, *Ssk* becomes positive, *Sy* increases meaning the deposition covers the high peaks, emphasis their heights. *Sk* is also increased meaning that the core of the topography is consolidated.

The coated samples (Sample 2 and Sample 3) have to bear a polishing process in order to become more uniform and without rare and sharp peaks.

The parameters could be grouped into two categories:

- **more robust**: *Sa* and *Sq* are good examples of parameters with small dispersions and they seems to be relatively insensitive to sampling.
- **less robust:** *Ssk* and especially *Sku* are parameters very sensitive to the number of measurements and have large dispersions.

The number of measurements needed for the calculation of a stable mean value depends to a large extent on which parameter is needed. It was found that it is often necessary to perform at least 5 measurements to obtain a stable mean value for many roughness parameters while others needed a larger number. The reason for this is that there is often one or a few measurements that diverge from the expected normally distributed result.

It can always be argued that this dispersion depends on the manufacturing process being unstable, resulting in a surface that is not equal at different places on a part. The point made here is that the investigated surfaces are typical engineering surfaces and the dispersions presented here will be the reality when measuring 3D surface roughness.

Therefore, it is most likely that some kind of rule (similar to the 16%) is needed to take account of the natural deviations that occur within a standard engineering surface.

Three functional surfaces have been measured in order to illustrate the comparison. The overall results showed that it was clear that single 3D surface measurements are not normally sufficient to statistically quantify a surface, the number of measurements required is usually below that required by 2D techniques. The required number is small but never the less this may be still too time-consuming in a production situation where contact measurement is the only option.

For coatings, an investigation on the surge=face topography could reveal especially the extreme values that could be than changed by an appropriate grinding process.

REFERENCES

[1] L. Blunt, X. Jiang, Advanced techniques for assessment surface topography, Elsevier, 2003.

[2] A. M. Cantaragiu, Biocompatible nanostructured coatings practical applications, PhD Report, pp. 80-88, 2009.

[3] A. Kakaboura, M. Fragouli, C. Rahiotis, N. Silikas, Evaluation of surface characteristics of dental composites using profilometry, scanning electron, atomic force microscopy and gloss-meter, J. Mater. Sci.: Mater Med., 18, pp. 155–163, 2007.

[4] Kulinich E.A., Khabas T.A., Vereshchagin V.I., The Effect of Nucleations on the Quality of Surface of Glass-Ceramic Denture Coatings, Glass and Ceramics, vol. 62, pp. 9-10, 2005.

[5] J. P. Rivière, C. Brin, J. P. Villain, Structure and topography modificationsof austenitic steel surfaces after friction in sliding contact, Materials Science & Processing. Applied Physics A, 76, pp. 277-283, 2003.

[6] E. S. Zanoria, T. R. Watkins, K. Breder, L. Riester, M. Bashkansky, J. Reintjes, J. G. Sun, W. A. Ellingson, P. J. Blau, Assessment of Techniques for Characterizing the Surface Quality of Ground Silicon Nitride, J. of Materials Engineering and Performance, vol. 7(4) August, pp. 533-544, 1998.

[7] K. J. Stout et al., The development of methods for the characterization of roughness on three dimensions, no. EUR 15178 EN of the Commission of the European Communities, Luxembourg, 1994.

[8] SR EN ISO 4288:2002 Geometrical product specifications (GPS) - Surface texture: Rules and procedures for the assessment of surface texture

[9] The Scanning Probe Image Processor SPIP™, Version 4.7 (2008).

[10] CETR, Evaluation of Mechanical Properties of Hard Coatings, http://www.cetr.com/

[11] SR EN ISO 4287:2003, SR EN ISO 4287:2003/ AC:2009 Geometrical product specifications (GPS). Surface texture: Profile method. Terms, definitions and surface texture parameters

SERBIATRIB '11

Serbian Tribology Society

12th International Conference on Tribology

Faculty of Mechanical Engineering in Kragujevac

Kragujevac, Serbia, 11 – 13 May 2011

THE TRIBOLOGICAL INVESTIGATIONS OF MULTICOMPONENT MULTILAYED ION-PLASMA COATINGS AVINIT

A. Sagalovych[1], V. Sagalovych[1], A. Kononyhin[1], V. Popov[1], A. Lubchenko[2], A. Olejnik[3]
[1]Scientific technological Corporation "FED", Kharkov, 61023, Ukraine
[2]Internation Solomon University, Kharkov, 61001, Ukraine
[3]State Enterprise "Malyshev Plant", Kharkov, 61037, Ukraine

Abstract: *The friction and wear characteristics of sliding friction in conditions of boundary lubrication for coatings, received by ion-plasma method on the heat resistant deformed alloy of АК4-1 type are investigated. Conducted tribological studies of improved designs of multi-component multi-layer coatings Avinit in fuel TS-1 media selecting coating materials for precision friction pairs of hydraulical units. Coatings are very effective in increasing the stability of the pair to bores cuffing teasers. Improved coatings have low friction coefficients (0.075 - 0.095) at loads up to 2.0 kN and showed high resistance to wear. More over relative stability increasing achieve 20-80 times, and contrabody wear decrease of 4-5 times.*

Keywords: *vacuum-plasma coatings, nanolayers and multilayers, coatings, tribology*

1. INTRODUCTION

Modern researches in the field of creation of new materials with record characteristics of wear resistance, roughness, a possibility to work in extreme conditions are connected with an area of nanotechnologies, which allow forming multi-component compositions with structural elements having sizes from several hundreds to units of nanometers. Such materials in comparison with materials of the same composition with a regular structure can have several times higher corresponding characteristics of tribological and other properties. It also concerns coatings – one of efficient methods of extension of possibilities of application of one or another material [1 - 7].

In works [8, 9] we have conducted researches on coating multi-component multilayer and nanolayer strengthening coatings on the basis of titanium, molybdenum and their compounds with nitrogen using methods of vacuum-plasma deposition. Multi-component multilayer coatings showed higher indexes of wear resistance and tribological characteristics compared with one-layer coatings on the basis of one compound.

In works [10, 11] there is described created by us experimentally-technological equipment - ***Avinit*** device for coating multilayer functional coatings.

Its **essential distinctive feature** is that the device allows to implement **complex** methods of coating functional coatings (plasmachemical CVD, vacuum-plasma PVD (vacuum-arc, magnetron), processes of ionic saturation, implantation and ion-beam processing of a surface), united within one technological cycle.

Substantial growth of a spectrum of the sources, caused by composite nature of used methods, allows to obtain coatings practically from any elements and alloys, high-melting oxides, carbides, nitrides, ceramic-metal compositions on the basis of high-melting metals and oxides, that essentially expands possibilities of creation of absolutely new materials and coatings of nodes and details with different functions, working in extreme conditions considering temperature, influence of corrosive mediums, mechanical loadings.

The **second distinctive feature** of ***Avinit*** device is a possibility **to pass on to nano-scale** for implementation of processes of controllable formation of multi-component nano- and microstructural coatings with the given characteristics.

It became possible thanks to the conducted radical reorganization of control over operation of all systems of technological equipment on the basis of the technology of open synchronization of operation of the systems of ion-stimulated deposition and diagnostics equipment of nano-scale coatings at the expense of introduction of new microprocessor supply systems to the equipment, synchronization and control over synthesis and diagnostics processes and development of a complex of controlling methods over technological parameters in the course of coating for purposeful control over the technological process.

There is a possibility to form multilayer structures containing a great number of layers of a various chemical compound (metal, nitride, carbide, oxide, etc.) being thick from units to hundreds of nanometers. These layers are put in ***Avinit*** device with usage of combined methods – PVD (vacuum-arc and magnetron sputtering) and CVD (gas-phase and plasmachemical sedimentation). The structure of layers is secured by programmed coordinated operation modes of sources of plasma (both PVD and CVD), working gases and high potential applied to a substrate.

A correct choice of individual materials of layers, methods of sedimentation and optimization of technological parameters create premises of synthesis of materials with a complex of unique properties, including exceptionally high hardness, durability, chemical stability, low coefficient of friction and raised wear resistance.

Within operational frameworks [11] a number of hardware and technological developments (application of advanced separating devices, improved diagnostics of plasma and gas flows, perfection of IR measurements (in an infrared range) of temperature fields of the covered products, perfection of mechanical and electronic systems of protection against microarcs and modernization of cathode nodes and management system) was implemented, that allowed to expand essentially possibilities of technology equipment and to provide coating of qualitative coatings on precision surfaces.

Coatings of ***"Avinit"*** type fall out on precision surfaces with high-class purity up to 12-13 class without lowering the class of purity of a surface. This is reached by a possibility to use efficient methods of cleaning a surface in developed technologies – cleaning in glow-discharge Ar, cleaning in two-stage vacuum-arc discharge and cleaning by metal ions under pressure above zero point of growth, and also prevention of damage of a surface by microarcs, for that in ***“Avinit”*** device there is a three-level system arc suppression, providing high quality of cleaning of a surface from oxides and other pollution without appearance of electrical breakdowns. Deposition happens at low temperatures, not exceeding temperatures of tempering of material of a basis, providing preservation of mechanical characteristics and absence of warpage of coated products.

The conducted reconstruction of technology equipment and the developed software solutions allowed to move to a qualitatively new level on further modification and perfection of constructions of functional coatings of ***Avinit*** type, stability of technologies and increase in control over their quality while coating such coatings for developed pairs of friction for possible use in details of precision friction pairs.

In this work the results of metallographic and tribological researches of improved coatings of ***Avinit*** type on the basis of Ti-Al-N system and on the basis of Mo-N system are presented.

2. METHODS OF RESEARCHES

2.1 METHOD OF OBTAINING COATINGS *“AVINIT”*

For obtaining multilayer coatings “***Avinit***” from solids in Ti-Al-N system a technological two-cathode circuit was used with simultaneous operation of two sources of sputtering which are allocated towards each other in the environment of reactionary gas with rotation of the sample around its axis, and for coating multilayer coatings based on the sequence of solid and soft layers (TiN-Ti, MoN–Mo systems), - a one-cathode circuit with continuous operation of a source of sputtering and impulse (periodic) submission of reactionary gas.

Coatings were put on samples of widely used in engine production and aggregate production materials from steel DIN 1.2379 (х12Ф1) with hardness 56 … 61HRC with precision surfaces (R_a = 0,016-0,021 microns (12-13 class of roughness) and on samples from aluminum alloy DIN 7980 (АК4-1).

2.2 METHOD OF METALLOGRAPHIC RESEARCHES

Metallographic researches and determination of parameters of materials (thickness of coatings, uniformity, deficiency and structure of the material) were done on microscope MMR-4. Microhardness of coatings was defined by means of microhardness tester PMT-3 under loading 50 H. Hardness of material was measured on the hardness tester by means of pressing a diamond tip by Rockwell method. Roughness of the surface of samples before and after coating was measured by profilometer-profilograph.

Measurements of microhardness and Young's modulus in multilayer and nano-layer coatings of ***Avinit*** type 1 … 3 microns were carried out with an instrument for measurement of nano-hardness by CSM company (Switzerland) (speed of loading 20,00 mH/min, max depth 100,00 nm under loading 0,6 H processing of results in Oliver–Far model).

Carrying out of researches of chemical individuality of a subsurface area of functional coatings was fulfilled with a method of mass-spectrometry of secondary ions (SIMS), electron X-ray microanalysis (EXMA), scanning electronic microscopy (SEM). Removal of profiles of change of chemical individuality of nano-layers of functional coatings was carried out by means of a method of mass-spectrometry of secondary ions (SIMS) on secondary-issue mass analyzer MA 7201M. The maximum depth of profiling is 5 microns. For sputtering the bundle of Ar^+ ions with energy 5–7 keV was used. Research of functional sections of a surface of samples was carried out by means of scanning electronic microscopy (SEM). Removal of space allocations of chemical elements was carried out by means of electron X-ray microanalysis (EXMA). Metallophysic measurements of the obtained coatings were carried out on scanning electronic microscope JSM T-300.

2.3 METHOD OF RESEARCH OF CHARACTERISTICS OF FRICTION AND WEAR

Tribological tests of antifriction, wear properties and seizure of samples with coatings were carried out by the machine of friction 2070 SMT-1 under the circuit "cube" - "roller" with a graduated loading in the range of loadings 1-20 MPa. Tests were done in the environment of TS-1fuel and in the environment of diesel fuel. For determination of seizure of surface layers of materials of pairs of friction loading was done from P_{min} to critical value of P_{cr} under which seizure happens.

In the process of tribological tests there were registered values of force of friction F_{fr}, normal loading N, contact pressure P, values of which helped to judge about mechanical losses in tribosystems. Friction coefficients were defined as $f = F_{fr} / N$.

3. EXPERIMENTAL RESULTS

One of indexes of multilayer coatings, in many respects defining their properties, is thickness of a separate layer. While a coating is being formed the necessary thickness of a layer is set by an operating time of a corresponding source, which demands knowledge of growth rate. Growth rate of a coating generally depends on capacity of a source of sputtering, distance from a source to a substrate, orientation and its position in relation to an axis of the direction diagram of an atomic flow of a source of sputtering, the form of the direction diagram, potential of displacement affecting the substrate. The substrate can be fixed, rotate around the fixed axis or make planetary motion.

In tab. 1 results of experiments on determination of growth rate of various coatings received both on fixed substrates, and on the substrates making planetary motion, are shown.

Table 1. Growth rate of coatings of various composition.

№ art.	Coating	Growth rate, V, micron/hour	Remarks
1	Ti	0,25	Planetary motion
2	Mo	0,2	-----x------
3	TiN	0,16	-----x------
4	MoN	0,14	-----x------
5	TiAlN	0,7	
6	TiN	0,9	Fixed position
7	MoN	0,7	-----x------

On the basis of the data about growth rate of coatings the data for several variants of nano-layer coatings were entered in the control program of ***Avinit*** device, namely:

- coatings Ti-TiN with the period of recurrence of 10 nanometers and thickness of separate nano-layers correspondingly 2 nanometers and 8 nanometers;
- coatings Mo-MoN with the period of recurrence of 20 nanometers and equal thickness of separate nano-layers;
- coatings TiN-AlN with the period of recurrence of 12 nanometers and thickness of separate nano-layers 4 and 8 nanometers.

Protocols of the automated monitoring system of these processes are presented in fig. 1.

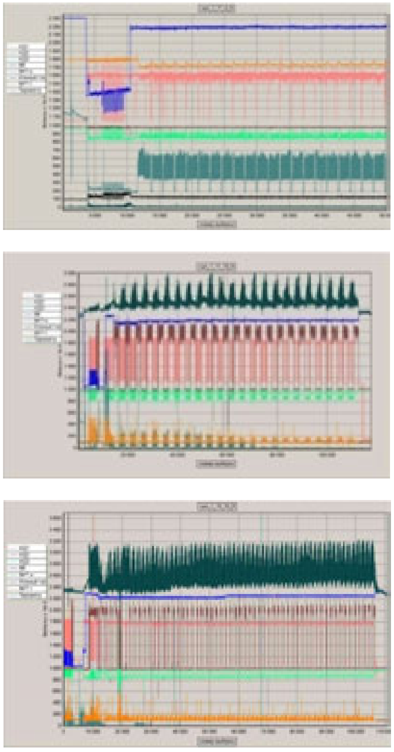

a) b) c)

Figure 1. Protocols of the automated monitoring system of the process of obtaining of coatings:
a) - Ti-TiN with the period of recurrence of 10 nanometers and thickness of separate nano-layers 2 nanometers and 8 nanometers;
b) - Mo-MoN with the period of recurrence of 20 nanometers and equal thickness of separate nano-layers;
c) - TiN-AlN with the period of recurrence of 12 nanometers and thickness of separate nano-layers 4 and 8 nanometers.

The composition and some characteristics of hardness, microhardness and roughness of the tested coatings received by means of various technological circuits, are shown in tabl. 2.
Comparing roughness of a substrate and coating shows that after coating samples with roughness equal to 12-13 classes of purity, roughness of the surface practically does not change, or there is an insignificant increase in the roughness which practically does not fall outside the limits of one class according to the classes of roughness of a surface.

The conducted X-ray researches of coatings of ***Avinit C/P 320-n1*** type showed that coatings in their composition have ~ 45 at % Al. The crystalline structure corresponded to TiN structure with grid parameter close to values of this connection. According to X-ray researches the size of areas of coherent scattering (ACS) in the coating made 32 nm. This value is well coordinated with the sizes separate nano-layers TiN and AlN (nano-layer growth rate for one turn ~ 35 nm), that confirms presence of a nano-layer structure according to the technological circuit of formation of coating.

In fig. 2 the results of electron X-ray microanalysis (EXMA) of ***Avinit*** coating *C/P 320-ms1* for three elements are shown: aluminum, iron and titan on the sample: ***Avinit*** *C/P 320-ms1* at scanning by an electronic bundle of the sample (diameter of an electronic probe Ø=30 nm, characteristic radiation is registered in the surface layer of a sample at the depth of 1 micron).

Table 2. Characteristics of samples

N art	Composition of coating	Initial parameters		Finite parameters		
		Hardness of a basis, HRC	Microhardness of the surface of a sample, $N_{v,}$ (MPa)	Thickness of coating, micron	Microhardness of the surface of a sample with coating, $N_{v,}$ (MPa)	Roughness, R_a, micron
1	Without coating	59 – 60	770 - 800			0,025 (12b)
2	TiN	59 – 60	770 - 800	1,0	1500-1900	0,040 (11c)
3	TiN-Ti	59 – 60	770 - 800	1,0	1300-1800	0,036 (12a)
4	MoN	59 – 60	770 - 800	1,0	2000-2300	0,040 (11c)
5	MoN-Mo	59 – 60	770 - 800	1,0	2000-2200	0,036 (12a)
6	TiN-AlN	59 – 60	770 - 800	1,0	2600-3500	0,025 (12b)
7	MoN (without a separator)	59 – 60	770 - 800	10,0	2000-2200	0,60 (8a)
8	TiN (without a separator)	59 – 60	770 - 800	12,0	1500-1800	0,70 (7c)

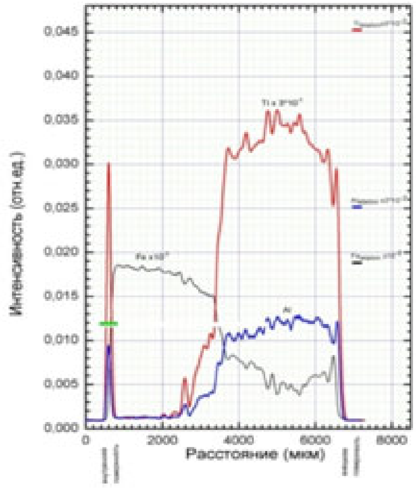

a)

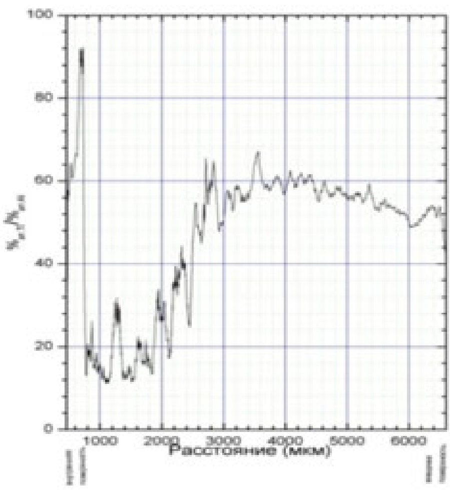

b)

Figure 2. Allocation of characteristic X-ray radiation of atoms of elements in coating ***Avinit*** *C/P 320-ms1 – à). % at. Ti / % at. Al – b).*

While scanning from the exterior surface to the interior one curves begin with peaks of intensity of titan and aluminum caused by characteristic radiation of these metals, placed on the exterior cylindrical part of a sample. Quantities of peaks of characteristic radiation Al and Ti with intensities of the same order are also observed on the conjunction of interior face and cylindrical surfaces. Allocations Al and Ti all over the analyzed surface are qualitatively close to each other.

In the surface with unaffected functional coating, despite existence of coating, there is observed characteristic Fe radiation, which intensity is much less, than that from Al and Ti. The type of dependence of a signal on Fe has an opposite character in comparison with them. In fig. 2b), where allocation of relation of quantity of atoms Ti to quantity of atoms Al is shown, it can be seen along the analysis line that the quantity of titan is a little bigger than that of aluminum.

Results of metallophysic measurings of coating ***Avinit*** *C/P 320-n1* on scattering electronic microscope JSM T-300 are shown in fig. 3, 4.

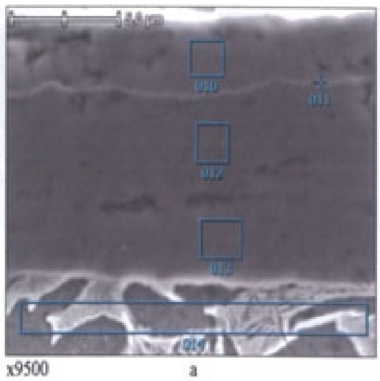

№ точки	N	Al	Ti	Mo	Всего,%
010	9,10	27,93	62,96		100
011	6,89	16,73	76,38		100
012	10,7	45,87	43,44		100
013	10,71	47,22	42,07		100
014		3,64	88,94	7,41	100

б

Figure 3. External view of coating ***Avinit*** *C/P 320-n1* (cross-sectional view) with marked zones of analysis–a); approximate chemical compound of analyzed zones–b).

Thickness of coating ~ 9 microns.

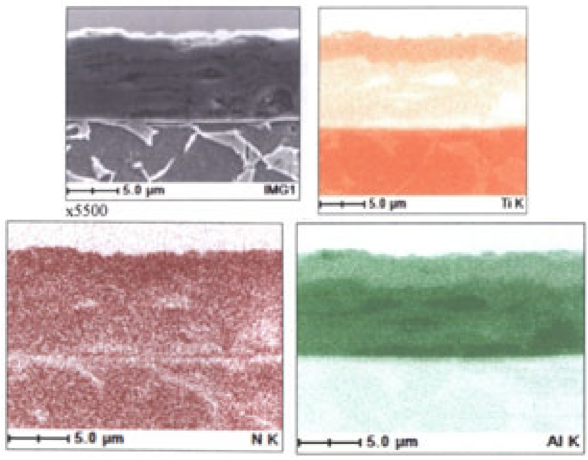

Figure 4. External view of coating ***Avinit*** *C/P 320-n1* (cross-sectional view) in a mode of mapping a part of coating. Bigger concentrations of elements correspond to more intensive coloring.

Thickness of thick non-filtered multilayer coatings ***Avinit*** *C/P 100-t10* and ***Avinit*** *C/P 220-t10* - 10 … 15 microns, Measured values of hardness of coatings of *Avinit C/P 320-ms1* type constituted not less than N_V = 3500 kNH/mm^2, coatings of ***Avinit*** *C/P 210-m1* type - not less than N_V = 2000-2500 kH/mm^2.

Thickness of thin multilayer and nano-layer coatings of ***Avinit*** *C/P 320-ms1* type and ***Avinit*** *C/P 210-m1* - 1 … 2 microns. For determination of microhardness of thin coatings (<4 microns) nano-hardness was measured with the help of nano indentation tester by CSM company (Switzerland) (loading rate 20,00 mH/min, max depth 100,00 nm at the level of loading - 0,6H), processing of results with usage of standard software on the basis of application of Oliver–Far model. The conducted measuring of microhardness and Young's modulus in coatings ***Avinit C/P 320-ms1*** with thickness of 1,4 microns resulted in the following values: N_v = 1600 – 2300 kH/mm^2, E = 250 - 300 GPa, coefficient of Poisson's ratio K = 0,30 (diagrams of loading are shown in fig. 5a).

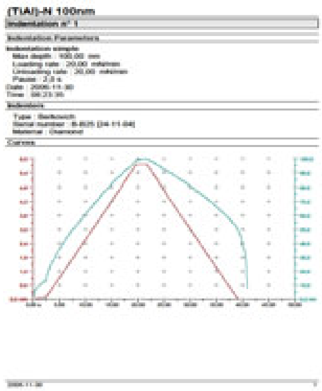

a)

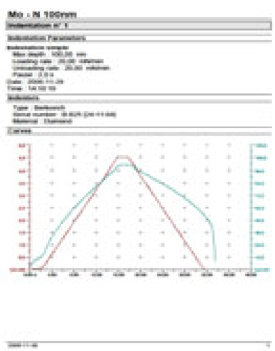

b)

Figure 5. Measurements of nano-hardness and Young's modulus
a) - coating ***Avinit C/P 320-ms1***, b) - coating ***Avinit C/P 210-m1.***

Similar measurements on coatings ***Avinit*** *C/P 210-m1* with thickness of 1,0 microns showed the following results - N_v = 1500 – 1800 kH/mm^2, E = 200 - 260 GPa, Poisson's ratio K = 0,30 (fig. 5b). It is necessary to mark that in model of Oliver-Far Young's modulus of coating and basis are assumed to be the same and consequently the calculated values can be a little lowered.

Metallographic researches of coatings of ***Avinit*** type with application of methods of mass-spectrometry of secondary ions (SIMS), electron X-ray microanalysis (EXMA), scanning electronic microscopy (SEM) were conducted.

In fig. 6a) for coating ***Avinit C/P 310-ms1*** dependences of currents of secondary ions Al $^+$, Ti $^+$ on sputtering time and correspondingly depths of a profile of allocation of components are shown.

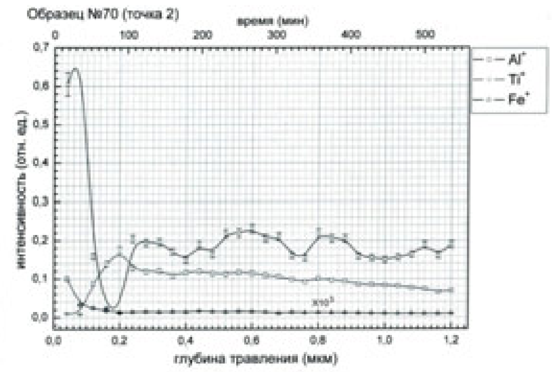

a)

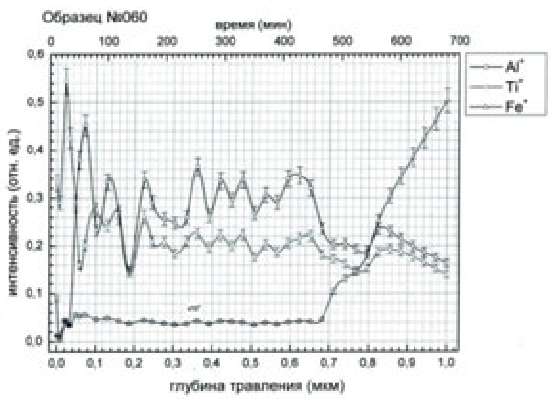

b)

Figure 6. Dependences of currents of secondary ions Al $^+$, Ti $^+$ on sputtering time
a) – coating Avinit C/P 310-ms1, b) - coating Avinit C/P 320-n1.

Change of the current of secondary ions for both experiments characterizes the change of concentration of corresponding elements deep into the sample in the process of sputtering of a subsurface area with a bundle of primary ions Ar$^+$. From the received dependences it follows that the exterior layer of coating has raised concentration of aluminum which with depth decreases. Similar dependences on profiles of allocation of aluminum and titan in a subsurface zone of the sample with functional coating ***Avinit C/P 320-n1*** are shown in fig. 6b). Synchronous changes of intensities of Al$^+$ and Ti$^+$ currents at depth ~ 1,8 microns from the surface are connected with technology of formation of coating.

Thus, experimental results confirm the possibility of low-temperature coating of highly rigid coatings ***Avinit C*** on the basis of nitrides of metals in the modes providing good adhesion to the material of a substrate (steel H12MF with precision surface R_a = 0,025 microns) without essential decrease in steel strength characteristics (<200ºC) and without deterioration of the class of purity of original surface.

4. RESULTS OF TRIBOLOGICAL TESTS

In fig. 1. the results of tribological tests (coating on coating) (“cube-roller” circuit) of multilayer coatings ***Avinit*** *C/P 320-ms1* (micro) and ***Avinit*** *C/P 510 μ1* with counterbodies with multilayer coatings ***Avinit*** *C/P 220-t10* and ***Avinit*** *C/P 100-t10 (*on the basis of *TiN-Ti)* with thickness of 10–15 microns, precipitated from non-filtered plasma flows.

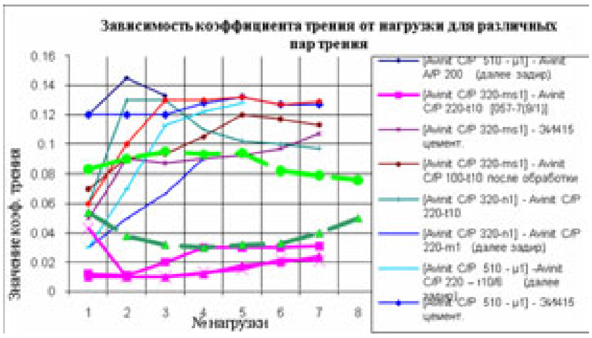

Figure 7. Dependence of coefficient of friction on loading.

In tabl. 3 values of weight wear of samples during 8 hours of wear tests of the tested pairs of friction with multilayer coatings ***Avinit*** are shown.

Table 3. Values of wear of samples in the course of wear tests during 8 hours.

Pair of friction	***Avinit C220-t (16 … 20)/10, ▼10 / Avinit C320-ms1***		
Wear, gr Time of tests 480 min.	***Avinit t (16 … 20)/10***	***Avinit C320-ms1***	total
	fixed	mobile	0,000 91
	0,00091	0	
	mobile	fixed	0,001 01
	0,00087	0,00014	

Presence of coatings essentially increases resistance of tribopairs against teasers, raising values of P_{cr} of teasers formation and practically preventing teasers formation.

Especially efficient are coatings on the basis of ***Avinit*** *C/P 220-t10* which have the highest values of P_{cr} and the lowest values of coefficient of friction. This is proven not only by maximum loading increase during tests, but also by a course of dependence of coefficients of friction on loading which after some loading increase up to 0.6-0.8 kN went down to the maximum loading 2 kN. Application of multilayer coatings (for example, ***Avinit*** *C/P 110* types *TiN-Ti)* leads to increase in P_{cr} in comparison with monolayer coatings (for example, ***Avinit*** *C/P 100* type *TiN).*

Coefficients of friction for all types of coatings have close enough values and with loadings more than 1,0 kN they are within 0,06 to 0,1. The lowest coefficient of friction had the pair of coating ***Avinit*** *C320-n1* - coating ***Avinit*** *C220-t20/10*. The value of coefficient of the pair of friction did not exceed 0,095 in all the range of loadings, and with the maximum loading it was 0,065, that corresponds to the minimum value received in this operation for pairs of friction with tested coatings.

All coatings in tests showed high resistance against wear which value did not exceed 0,8 microns. Value of wear on samples with coating fluctuates from 0.6 to 0.8 mm.

Pairs of friction which working surfaces have micro- and nano-layer coatings ***Avinit*** *C/P 320-ms1*, ***Avinit*** *C/P 320-n1*, ***Avinit*** *C/P 350-t20/10*, ***Avinit*** *C/P 220-t20/10*, ***Avinit*** *C/P 220-t16/10*, ***Avinit*** *C/P 220-t16/5*, tested in the conditions of boundary lubrication, are characterized by:

- high resistance against teasers formation; absence of secondary conformability; high enough stability in timing of the coefficient of friction while operating with invariable loading; essentially smaller distinction between "direct" and "reverse" pairs, in comparison with "basic" pair *bronze VB23NS / steel 30H3VA.*

The pair of friction ***Avinit*** *C/P 220-t16/10* / ***Avinit*** *C/P 320-n1* showed the best tribological characteristics in this work, namely: - friction coefficients (0,109 … 0,129) with durable operation under invariable loading are close enough to the "original" pair and are stable; - weight wear revealed after 8 hours of wear tests in "reverse" pairs, is less, than for the "original" pair a) minimum 12 times for the pair as a whole; b) minimum 2,5 times for a more solid sample of the pair; c) minimum 44 times for a softer sample of the pair;- for "direct" pairs after 8-hour tests by the used monitoring methods weight wear was not revealed.

5. CONCLUSION

There have been conducted metallographic and tribological researches of advanced constructions of multilayer coatings of ***Avinit*** type - coatings on the basis of Ti-Al-N system - ***Avinit*** *C/P 310-ms1*, ***Avinit*** *C/P 300-t10*, ***Avinit*** *C/P 100-t10*, ***Avinit*** *C/P 320-n1*, ***Avinit*** *C/P 350-t10* and coatings on the basis of Mo-N system - ***Avinit*** *C/P 210-m1* and ***Avinit*** *C/P 220-t10.* As tribological tests have shown, coating very effectively affects resistance of a pair to teasers, leading to increase in P_{cr} value of teasers formation.

Tested pairs with coatings had low coefficients of friction under loadings up to 2.0 kN. Pair ***Avinit***

*C/P 320-ms1 / **Avinit** C/P 220-t16/10* had the least coefficient of friction. Its value did not exceed 0,095 in all the range of loadings, and under the maximum loading was 0,075. In the tests all advanced coatings have showed high wear resistance which value did not exceed 0.8 microns.

Pair ***Avinit** C/P 320-n1 / **Avinit** C/P 220-t16/10* has shown the best combination of wear resistance and tribological properties**.** It had the least coefficient of friction and almost zero wear during 8 hours of tests.

REFERENCES

[1] S. Veprek, S. Reiprich: Concept for the design of novel superhard coatings, - Thin Solid Films V. 268, pp. 64-67, 1995.

[2] A.D.Korotayev, V.J.Moshkov and others.: Nanostructural and nanocomposite supersolid coatings, - Physical mesomechanics, V. 8, № 5, pp. 103-116, 2005.

[3] R. Haurt, J. Patscheider: From alloying to nanocomposites – improved performance of hard coatings,-Advanced Engineering Materials V. 2, № 5, pp. 247-259, 2000.

[4] S.Veprek: The search for novel, superhard materials, - J. Vac. Sci. Technol, A17 (5), pp. 2401-2420, 1999.

[5] J. Musil, P. Zeman, H.Hruby, P.H. Mayrhofer: ZrN/Cu nanocomposite film–a novel superhard material, - Surface and Coatings Technology V. 120-121, pp. 179-183, 1999.

[6] Sam Zhang, Yongqing Fu, Hejun Du ea: Magnetron sputtering of nanocomposite (Ti, Cr) CN/DLC coatings, - Surface and Coatings Technology V. 162, pp. 42-48, 2002.

[7] Veprek S., Veprek-Heijman M., Karvankova P., Prochazka J.: Different approaches to superhard coatings and nanocomposites, - Thin Solid Films V. 476, pp. 1-29, 2005.

[8] A.P.Lyubchenko, A.V.Sagalovich, V.V.Sagalovich and others: Research of characteristics of friction and wear of ion-plasma coatings received for aluminum alloy, - Physical engineering of a surface, V. 2, № 1-2, pp. 110-114, 2004.

[9] V.V.Popov, A.V.Sagalovich, S.F.Dudnik and others: Development of multicomponent coatings for increase in wear resistance of surfaces of pairs of friction in precision nodes, - Physical engineering of a surface, V. 5, № 3-4, pp. 154-165, 2007.

[10] A.V.Sagalovich, V.V.Sagalovich, S.F.Dudnik: Automated system of coating of functional nanocoatings, - Equipment and Instrument, V. 12, pp. 2-3, 2005.

[11] O.V.Sagalovich, O.V.Kononikhin, V.V.Popov and others: ***Avinit*** device for coating multilayer functional coatings, - Physical engineering of a surface, V. 8, pp. 336-347, 2010.

Serbian Tribology Society

SERBIATRIB '11

12th International Conference on Tribology

Faculty of Mechanical Engineering in Kragujevac

Kragujevac, Serbia, 11 – 13 May 2011

CORROSION BEHAVIOUR OF THE AS-CAST AND HEAT-TREATED ZA27 ALLOY

Biljana Bobić[1], Slobodan Mitrović[2], Miroslav Babić[2], Aleksandar Vencl[3], Ilija Bobić[4]

[1]R&D Center IHIS Techno-Experts, Belgrade, Serbia, biljanabobic@gmail.com

[2]Faculty of Mechanical Engineering,University of Kragujevac, Kragujevac, Serbia, boban@kg.ac.rs, babic@kg.ac.rs

[3] Faculty of Mechanical Engineering, University of Belgrade, Belgrade, Serbia, avencl@mas.bg.ac.rs

[4] Istitute of Nuclear Sciences ″Vinča″, University of Belgrade, Belgrade, Serbia, ilijab@vinca.rs

Abstract: *Corrosion behaviour of the as-cast and heat-treated ZA27 alloy was examined. The alloy was prepared by conventional melting and casting route and then thermally processed by applying T4 heat treatment regime (solutionizing at 370 °C for 3 hours followed by water quenching and natural aging). Corrosion rate of the as-cast and heat-treated ZA27 alloy was determined in 3.5 wt. % NaCl solution through immersion test using both weight loss method and polarization resistance measurements. It was shown that applied thermal treatment resulted in increased ductility of the heat-treatedalloy and had a small beneficial effect on the corrosion resistance of ZA27 alloy.*

Keywords: *ZA27 alloy, corrosion, heat treatment, microstructure, immersion test, polarization resistance*

1. INTRODUCTION

ZA27 alloy belongs to a group of zinc alloys with increased content of aluminium (ZA alloys) which have been used in technological applications for several decades. ZA27 alloy with a nominal aluminium content of 27 wt.% is distinguished with highest strength and lowest density of all ZA alloys [1]. The alloy has been shown to possess favorable combination of physical, mechanical and technological characteristics (low melting point, high strength, good castability, easy machinability) as well as excellent bearing capability, wear resistance and high corrosion resistance [1, 2]. ZA27 alloy has been used for pressure die castings and gravity castings wherever very high strength is required as well as in bearings and bushing applications as a replacement for bronze bearings because of its lower cost and equivalent or superior bearing performances [3].

During past two decades a few different approaches have been taken in order to improve physical, mechanical, tribological and corrosion properties of ZA27 alloy at room temperature: (a) addition of elements like Ni, Ti and Sr [4], (b) using different heat treatment regimes [4-7] and termomechanical treatments [8] (c) improvements in the alloy manufacturing techniques as is the use of thixoforming [9] or unidirectional solidification [10] and (d) production of composites with Al_2O_3, SiC and graphite particles [11-13].

Mechanical properties of ZA27 alloy can be influenced by thermal processing. It was reported [7] that ductility and structural stability of this alloy were markedly improved by applying T4 heat treatment. It was also shown that T4 regime had a beneficial effect on the tribological characteristics of the commercial ZA27 alloy [6], although it resulted in a minor reduction in hardness and tensile strength. In addition, T4 heat treatment is relatively cheap and easy to perform, thus providing time and energy savings.

Upon exposure to the corrosive environment many thermally processed alloys are subject to drastic changes. Possible effects of used heat treatments on the alloy performance in a corrosive medium are essential for a complete understanding of the alloy corrosion behavior [14].

Corrosion characteristics of the as-cast ZA27 alloy have been previously studied and reported in

[15, 16]. Aluminium presence in the alloy has a favourable effect on its corrosion behaviour [15, 16]. The alloy exibits high corrosion resistance in natural atmospheres and natural waters, soil etc. because of zinc ability to form a protective layer of corrosion products at the surface [14, 15], consisting mainly of zinc oxide, zinc hydroxide, simonkolleite or their mixtures. The most common form of corrosion encountered by ZA27 alloy in a variety of natural environments is general (uniform) corrosion [15]. This enables evaluation of the alloy mass loss per unit surface area that is evaluation of corrosion rate. Besides the weight loss method electrochemical polarization measurements have been frequently used in corrosion studies to assess the rate of uniform corrosion [14, 17]. Polarization resistance measurements provide the value of polarization resistance R_p enabling calculation of corrosion current (corrosion rate) according to the well-known Stern-Geary equation [18]. Appropriate values of anodic and cathodic Tafel slope have to be determined in separate experiments [14, 17]. However, it was shown that results of electrochemical measurements were not always in agreement with direct weight loss measurements [19] and weight loss method has been frequently used to confirm the results of electrochemical polarization tests.

Thermally processed (T4) ZA27 alloy is characterized by a good combination of tribological and mechanical properties [6] with ductility twice higher than the as-cast alloy [7] and can be used in producing machine parts where high ductility is required. However, there have been no results reported so far concerning the effect of T4 heat treatment on the corrosion performance of the ZA27 casting alloy. In view of the above, the aim of this work was to examine the influence of T4 heat treatment on the corrosion behaviour of ZA27 alloy. An attempt was also made to establish the correlation between microstructural parameters and corrosion properties of both as-cast and heat treated ZA27 alloy.

Within this work corrosion studies were carried out in neutral chloride solutions open to atmosphere because chloride ion is present in many corrosion environments and because of great influence of dissolved oxygen on the corrosion mechanism and kinetics of zinc and zinc alloys [20].

2. EXPERIMENTAL

2.1 Materials

Experiments were performed using zinc-aluminium alloy ZA27. Chemical composition of the alloy is in accordance with EN standard [21]. The alloy was prepared by conventional melting and casting route in Materials Science Laboratory in ″Vinca″ Institute. The alloy casting was performed at 570 °C in the steel mold preheated up to 100 °C. Prismatic castings (20 x 30 x 120 mm) were machine cut and samples for corrosion studies (20 x 30 x 6 mm) and microstructural examinations (4 mm in diameter and 8 mm in height) were obtained. The samples were subjected to heat treatment (T4 regime: solutionizing at 370 ˚C for 3 hours followed by water quenching and natural aging).

2.2 Corrosion tests

Immersion test and polarization resistance measurements were used to access corrosion behaviour of ZA27 alloy as-cast and heat treated. For both ZA27 alloys corrosion rates were determined and expressed as the corrosion penetration rate. All tests were performed in an approximately neutral NaCl solution (pH = 6.7) opened to atmospheric air and with same chloride concentration as in natural seawater (3.5 wt.% NaCl).

In immersion test samples of as-cast and heat treated ZA27 alloy were exposed in stagnant 3.5 wt. % NaCl solution at room temperature. Samples preparation and exposure were performed in accordance with ASTM G31 [22]. After dry ground samples were wet ground using progressively finer abrasive SiC paper (240, 360, 600 and 800 grit), washed in warm running water, rinsed with acetone and dried in the air. After weighing, the samples (in triplicate) were vertically exposed in the test solution. After 30 day exposure the samples were withdrawn from the test solution and rinsed with distilled water. Corrosion products were removed from the samples by chemical cleaning according to ASTM G1 [23]. The samples were then reweighed to determine their mass loss during exposure to NaCl solution.

Measurements of polarization resistance were carried out at room temperature using a cell for flat specimens with a contact area of 1 cm^2 between working electrode and electrolyte (3.5 wt. % NaCl, pH = 6.7). Platinum electrode was used as a counter electrode while saturated calomel electrode (SCE) was a reference electrode. Working electrode (as-cast and heat treated ZA27 alloy, respectively) was washed with acetone and distilled water before electrochemical polarization test. The test was conducted using Gamry Reference 600 Potentiostat and three measurements were performed for each working electrode, with good reproducibility. Prior to each polarization test, the electrode was permitted to stabilise for approximately 30 to 60 min in the test solution to make sure that steady state has been reached. The working electrode was then cathodically polarised from its open circuit potential *OCP* by 15 mV, which was immediately followed by a cathodic sweep over a 30 mV range at the 0.2 mV/s sweep rate.

2.3 Microstructural examination

Surface morphology and microstructure of the as-cast and heat treated samples of ZA27 alloy were examined before immersion test and after 30 day exposure in the test solution. The samples were analyzed by optical microscopy (OM) using Carl Zeiss optical microscope.

The samples for microstructural studies were prepared by wet grinding on progressively finer abrasive paper (240, 360, 600 and 800 grit SiC), with subsequent polishing with diamond paste (up to 2 µm particles size) on polishing cloth. Before their exposure to test solution (3.5 wt. % NaCl) the samples were rinsed with acetone and dried in the air. After exposure, the samples were wet ground and polished. Etching in 9 % v/v nitric acid was applied to reveal the samples microstructure.

3. RESULTS AND DISCUSSION

3.1 Corrosion rate

Immersion test. After 30 day exposure to quiescent NaCl solution surfaces of the test samples were covered with white powdered corrosion products. Corrosion has occured uniformly over the surface of exposed as-cast and heat treated samples. Corrosion products were removed by chemical cleaning and the samples were then reweighed to determine their mass loss during exposure to NaCl solution. On the basis of the samples mass loss the average penetration rate of corrosion (corrosion rate) was calculated using the following expression [23]:

$$C_R = \frac{K \cdot W}{A \cdot T \cdot D} \tag{1}$$

where C_R is corrosion rate (mm/year), K is a constant [22], W is sample mass loss (g), A is sample area (cm^2), T is time of exposure (hours) and D is density of ZA27 alloy (g/cm^3).

Calculated values of corrosion rate were 0.118 mm/year for the as-cast and 0.095 mm/year for the heat treated ZA27 alloy.

Polarization resistance measurements. Polarization curves in a small potential range near to *OCP* were obtained in the electrochemical polarization test for both as-cast and heat treated ZA27 alloy. Polarization resistance R_p was determined from the slope of experimental curve (dE/dj) at corrosion potential E_{corr} (Fig. 1a, b).

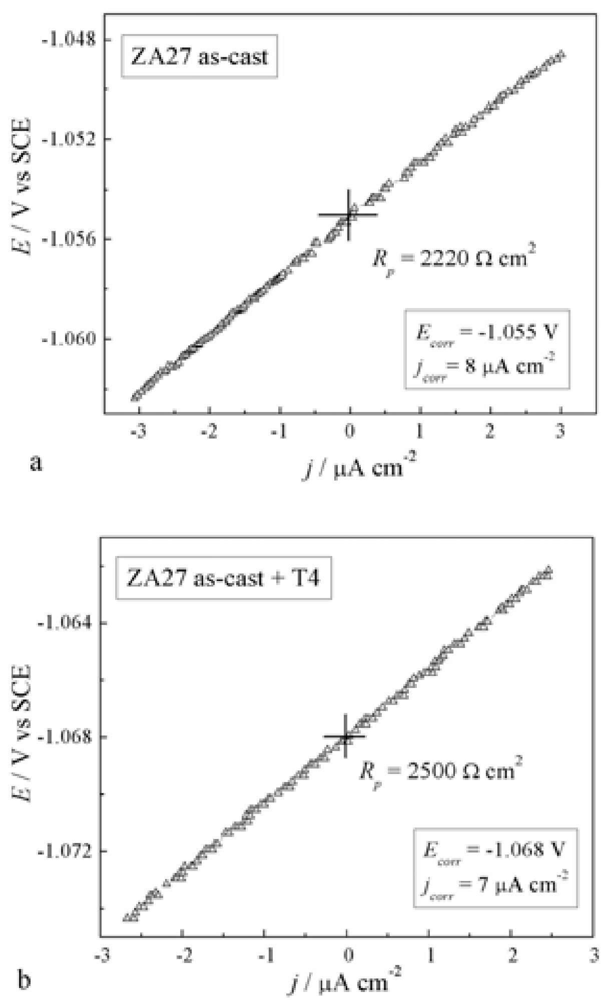

Figure 1. $E - j$ curves in 3.5 wt.% NaCl. (a) ZA27 alloy as-cast, (b) ZA27 alloy heat treated.

It can be seen that applied heat treatment resulted in increased value of R_p. Polarization resistance can be converted to corrosion current density j_{corr} using the Stern-Geary equation [18]:

$$j_{corr} = \frac{B}{R_p} \tag{2}$$

where B is a parameter dependent on the values of anodic b_a and cathodic Tafel slope b_c:

$$B = \frac{b_a \cdot b_c}{2.303 \cdot (b_a + b_c)} \tag{3}$$

Accordingly

$$j_{corr} = \frac{b_a \cdot b_c}{2.303 \cdot (b_a + b_c) \cdot R_p} \tag{4}$$

This expression was derived on the assumption that both anodic and cathodic reactions were charge-transfer controlled [14]. For a process that is controlled by diffusion of the cathode reactant and in which the anodic process is under activation control the modified Stern-Geary equation applies [14]:

$$j_{corr} = \frac{b_a}{2.303 \cdot R_p} \tag{5}$$

It has been recently reported [24] that corrosion of ZA27 alloy in chloride solutions takes place with charge-transfer controlled anodic reaction (alloy dissolution, with anodic Tafel slope b_a = 40 mV/dec), while cathodic reaction is under diffusion control of oxygen reduction. The value of anodic Tafel slope (b_a = 40 mV/dec) corresponds closely to values reported in literature for anodic dissolution of zinc [25]. Low solubility of oxygen (about 10^{-3} mol/dm^3) [14] in the test solution limits the transport of oxygen to the electrode surface and the cathodic reaction is under dominant diffusion control of oxygen reduction. When the reaction rate is entirely controlled by the rate of mass transport it no longer depends on potential [17] and the value of cathodic Tafel slope $b_c \rightarrow \infty$. Accordingly, the Eq. (5) was used to calculate corrosion current density. Calculated values were 8 µA/cm^2 for the as-cast and 7 µA/cm^2 for the heat treated ZA27 alloy.

Values of j_{corr} obtained on the basis of polarization resistance measurements (section 3.1) were converted into penetration rate C_R. Corrosion current density j_{corr} (µA/cm^2) and corrosion rate C_R (mm/year) are related by the following equation [23]:

$$C_R = K_i \cdot \frac{j_{corr}}{D} \cdot E_W \tag{6}$$

where K_i is a constant, E_W is equivalent weight of ZA27 alloy and D is as in Eq. (1). Calculated values of penetration rate were 0.099 mm/year for the as-cast alloy and 0.087 mm/year for heat treated ZA27 alloy. These results as well as the results of immersion test indicate to somewhat lower value of corrosion rate of heat treated ZA27 alloy in comparison to the as-cast alloy which means that applied heat treatment resulted in increased corrosion stability of ZA27 alloy. In addition, results of electrochemical measurements are in a very good agreement with results of gravimetric measurements.

Low values of corrosion rate obtained for as-cast and heat treated ZA27 alloy indicate to high corrosion resistance of both ZA27 alloys in neutral chloride solutions open to atmospheric air.

3.2 Microstructures

Corrosion behaviour of ZA27 alloy is determined by the alloy microstructure that is by chemical composition and distribution of the alloy phases [10, 19].

General surface appearance of the as-cast alloy is presented in Fig. 2a. Inclusions can be noticed in the alloy sample while porosity was not observed at this level of examination. The alloy was casted in metal mold (section 2.1) and hence subjected to rapid cooling. Solidification of the alloy in these conditions resulted in the alloy with dendritic microstructure as can be seen in Fig. 2b.

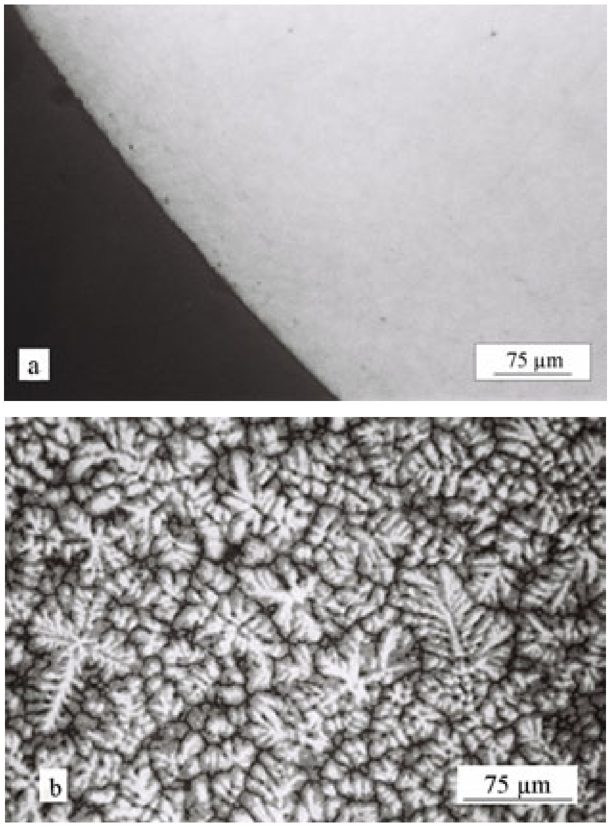

Figure 2. Microstructure of ZA27 alloy as-cast. (a) OM, polished, (b) OM, etched

Developed dendrites are complex (Fig. 2b), consisting of a core (α phase) and a periphery (a mixture of α phase and hexagonal η phase). The η phase is located into interdendritic regions. It was shown by SEM/EDS analysis [24] that dendritic cores are rich in aluminium; interdendritic phase is rich in zinc, while the composition of dendritic periphery is approximately equal to the chemical composition of ZA27 alloy. The SEM/EDS analysis has also indicated presence of intermetallic compound $CuZn_4$ (ε-phase) in interdendritic regions. It was reported that presence of ε phase had a beneficial effect on mechanical and wear properties of ZA27 alloy, particularly after certain heat treatment regimes [6].

The effect of corrosion on the microstructure of the as-cast sample after 30 days exposure in the test solution is shown in Fig. 3.

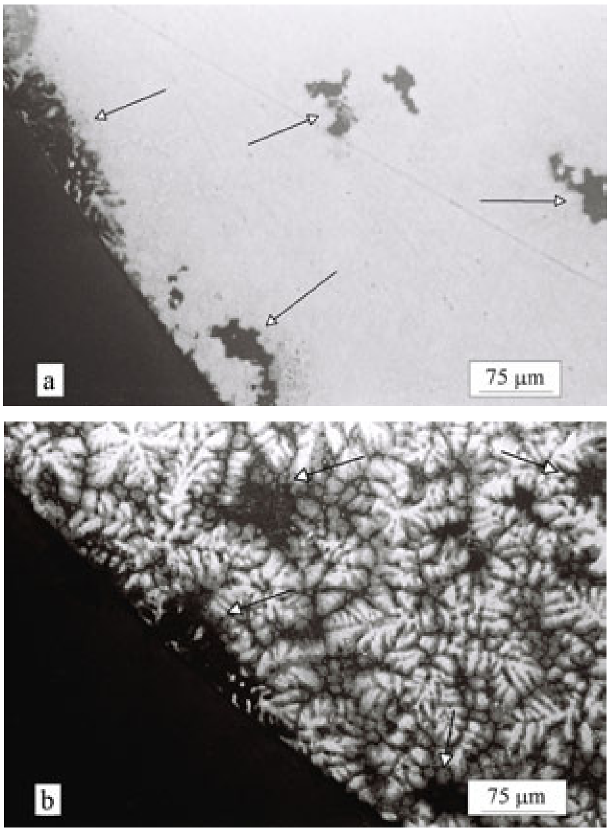

Figure 3. Microstructure of ZA27 alloy as-cast after 30 day exposure in 3.5 wt.% NaCl. (a) OM, polished, b) OM, etched.

It can be seen that corrosion has started on the edge of the sample and around inclusions (Fig. 3a). It was noticed [25] that corrosion of zinc and zinc alloys in salt solutions usually started at places where defects (scratches) or impurities were present. Corrosion process around inclusions in the as-cast sample mainly takes place laterally over the sample surface, which can be also seen on the etched sample (Fig. 3b). Destruction of *η* phase and *α* + *η* phase mixture regions has occured during corrosion process (Fig. 3b).

The T4 heat treatment that was applied within this work differs from the heat treatment regime recommended by standard [21] where furnace cooling instead of water quenching has been prescribed. It was shown earlier [7] that structure coarsening and appearance of *T′* phase ($Al_4Cu_3Zn_2$) took place during furnace cooling of ZA27 alloy. The *T′* phase is brittle and has a bad influence on ductility of ZA27 alloy. By using T4 regime within this work the appearance of *T′* phase in the heat treated samples was avoided which resulted in increased ductility of heat treated ZA27 alloy as was reported in [7].

Chemical composition of ZA27 alloy did not change after thermal processing while microstructure of heat treated ZA27 alloy remained dendritic although a significant morphological change took place as a result of T4 heat treatment. Solutionizing time (3 hours) was not enough for a complete homogenization i.e. for a complete destruction of dendritic cores and interdendritic *η* phase. The regions of *α* + *η* phase mixture were extended while dendritic cores (*α* phase region) and interdendritic regions (*η* phase) were reduced as can be seen in Fig.4b. A decrease in size of dendritic cores (α phase) and rounding off their edges happened, as well as the separation of individual dendritic cores into several smaller segments. Smaller dendritic cores were transformed into *α* + *η* phase mixture. During heating at 370 °C for 3 hours, there was an expansion of *β* phase at the expense of supersaturated *α* and *η* phases. After cooling, the newly created *β* phase was transformed into *α* + *η* phase mixture. According to the results presented in [7] the lattice parameter of *α* phase in the heat treated alloy was reduced comparing to the lattice parameter of α phase in the as-cast alloy as a consequence of zinc diffusion from the metastable *α* phase. Besides, it was shown by quantitative metallographic analysis [26] that volume fraction of *α* + *η* phase mixture was increased while both volume fractions of *α* and *η* phase were reduced in the heat treated ZA27 alloy in relation to the as-cast alloy. The effect of corrosion on the microstructure of heat treated ZA27 alloy is shown in Fig. 4a, b.

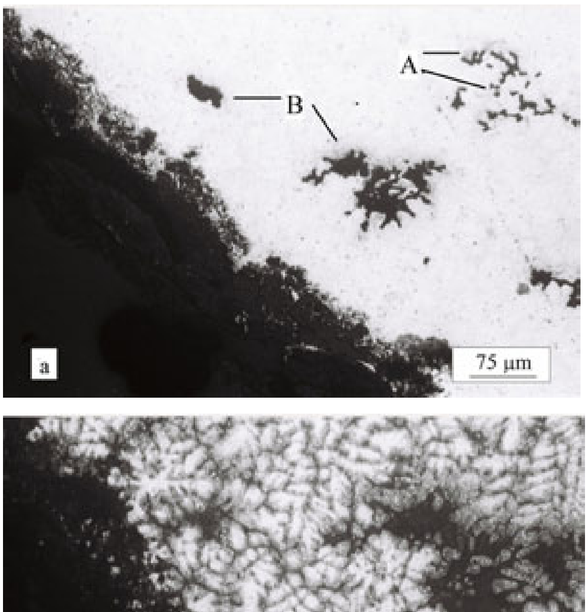

Figure 4. Microstructure of heat treated ZA27 alloy after 30 day exposure in 3.5 wt. % NaCl.
(a) OM, polished, (b) OM, etched.

Corrosion attack is observed on the sample edge (area of mechanical damage) and around some inclusions (Fig. 4a). As can be seen in Fig. 4b corrosion has occured in the region of $\alpha + \eta$ phase mixture and in the interdendritic η phase. Bright islands of α phase are surrounded by dark corrosion products. Appearance of microcracks in the heat treated samples was not observed after one month of exposure in corrosion environment which indicates increased ductility and thus, greater corrosion stability of heat treated ZA27 alloy.

Based on all results presented it could be concluded that applied heat treatment (T4) affected the microstructure of ZA27 alloy, as well as its corrosion resistance The alloy morphology was changed so that regions of $\alpha + \eta$ phase mixture were extended while dendritic cores (α phase region) and interdendritic regions (η phase) were reduced (Fig. 4b). The presence of microcracks was not observed in thermally processed ZA27 alloy neither before exposure to NaCl solution nor after 30 day exposure to this solution. This indicates an increase in ductility of the heat treated alloy. All these resulted in greater R_{p} value (Fig. 1b) and lower j_{corr} value of theat treated ZA27 alloy, namely in reduced corrosion rate. These results allow us to conclude that T4 heat treatment of ZA27 alloy has a small beneficial effect on its corrosion resistance which was the aim of this work.

4. CONCLUSIONS

On the basis of the results presented the following conclusions can be made:

1. Microstructure and corrosion resistance of ZA27 alloy was affected by T4 heat treatment.
2. Microstructure of heat treated ZA27 alloy remained dendritic after T4 heat treatment while corrosion process takes place through η phase and $\alpha + \eta$ phase mixture like in as-cast ZA27 alloy.
3. T4 heat treatment has shown small beneficial effect on the corrosion resistance of ZA27 alloy.
4. Low values of corrosion rate obtained for as-cast and heat treated ZA27 alloy ipoint out to high corrosion resistance of both ZA27 alloys in neutral chloride solutions open to atmospheric air.
5. Increased ductility and favourable corrosion properties of heat treated ZA27 alloy indicate its potential use in manufacturing machine parts like gears and worm gears.
6. Values of corrosion rate obtained in electrochemical polarization test are in accordance with results obtained by the weight loss method.

REFERENCES

[1] E. Gervais, R.J. Barnhurst, C.A. Loong, An Analysis of Selected Properties of ZA Alloys, JOM 11 (1985) 43–47.

[2] E.J. Kubel Jr., Adv. Metal Progress 7 (1987) 51–57.

[3] P.P. Lee, T. Savasakan, E. Laufer, Wear resistance and microstructure of Zn-Al-Si and Zn-Al-Cu alloys, Wear 117 (1987) 79–89.

[4] P. Choudhury, K. Das, S. Das, Evolution of as-cast and heat-treated microstructure of a commercial bearing alloy, Mater. Sci. Eng., A 398 (2005) 332–343.

[5] M.T. Jovanovic, I. Bobic, B. Djuric, N. Grahovac, N. Ilic, Microstructural and sliding wear behavior of a heat-treated zinc-based alloy, Tribol. Lett. 3 (2007) 173–184.

[6] M. Babic, A. Vencl, S. Mitrovic, I. Bobic, Influence of T4 Heat treatment on Tribological Behavior of ZA27 Alloy under Lubricated Sliding Condition, Tribol. Lett. 2 (2009) 125–134.

[7] I. Bobic, B. Djuric, M.T. Jovanovic, S. Zec, Improvement of Ductility of a Cast Zn–25Al–3Cu Alloy, Mater. Charact. 29 (1992) 277–283.

[8] H. Aashuri, Globular structure of ZA27 alloy by thermomechanical and semi-solid treatment, Mater. Sci. Eng., A 391 (2005) 77–85.

[9] T.J. Chen, Y. Hao, Y.D. Li, Effects of processing parameters on microstructure of thixoformed ZA27 alloy, Mater. Des. 28 (2007) 1279–1287.

[10] W.R. Osorio, C.M. Freire, A. Garcia, The effect of the dendritic microstructure on the corrosion resistance of Zn-Al alloys, J. Alloys Compd. 397 (2005) 179–191.

[11] I. Bobic, M.T. Jovanovic, N. Ilic, Microstructure and strength of ZA27 based composites reinforced with Al_2O_3 particles, Mater.Lett. 57 (2003) 1683–1688.

[12] Z.Q. Li, B.Y. Wu, S.Y. Zhang, Pretreatment process of SiC particles and fabrication technology of SiC particulate reinforced Zn-Al alloy matrix composite, Mater. Sci. Technol. 17 (2001) 954–960.

[13] S.C. Sharma, B.M. Girish, R. Kamath, B.M. Satish, Graphite particles reinforced ZA-27 alloy composite materials for journal bearing applications, Wear 219 (1998) 162–168.

[14] L.L. Shreir, R.A. Jarman, G.T. Burstein (Eds.), Corrosion, third ed., Butterworth-Heinemann, Oxford, 2000.

[15] F.C. Porter, Corrosion Resistance of Zinc and Zinc Alloys, ed. P. A. Schweitzer, Marcell Dekker, New York, 1994.

[16] R.J. Barnhurst, S. Belisle, Corrosion properties of Zamak and ZA alloys, Noranda Report, 1992.

[17] P.A Schweitzer, Fundamentals of Corrosion, Mechanisms, Causes and Preventive Methods, CRC Press, Taylor & Francis Group, Boca Raton, 2010.

[18] M. Stern, A.L. Geary, J. Electrochem. Soc. 104 (1957) 56.

[19] P. Choudhury, S. Das, Effect of microstructure on the corrosion behavior of a zinc-aluminium alloy, J. Mater. Sci. 40 (2005) 805–807.

[20] H. Dafydd, D.A. Worsley, H.N. McMurray, The kinetics and mechanism of cathodic oxygen reduction on zinc and zinc–aluminium alloy galvanized coating, Corros. Sci. 47 (2005) 3006–3018.

[21] BS EN 12844:1999 Zinc and zinc alloys. Castings. Specifications.

[22] ASTM G31–72 (2004) Standard Practice for Laboratory Immersion Corrosion Testing of Metals.

[23] ASTM G1–03 Standard Practice for Preparing, Cleaning and Evaluating Corrosion Test Specimens.

[24] B. Bobic, J. Bajat, Z. Acimovic-Pavlovic, M. Rakin, I. Bobic, The effect of T4 heat treatment on the microstructure and corrosion behaviour of Zn27Al1.5Cu0.02Mg alloy, Corros. Sci. 53 (2011) 409–417.

[25] X.G. Zhang, Corrosion and Electrochemistry of Zinc, Plenum Press, New York, 1996.

[26] I. Bobic, PhD Thesis, Belgrade, 2003.

Serbian Tribology Society

SERBIATRIB '11

12th International Conference on Tribology

Faculty of Mechanical Engineering in Kragujevac

Kragujevac, Serbia, 11 – 13 May 2011

ABRASIVE MATERIAL FOR ABRASIVE WATER JET CUTTING AND THEIR INFLUENCE ON CUT SURFACE QUALITY

Predrag Janković[1], Miroslav Radovanović[2], Jelena Baralić[3]

[1] University of Niš, Faculty of Mechanical Engineering, Serbia, jape@masfak.ni.ac.rs

[2]University of Niš, Faculty of Mechanical Engineering, Serbia, mirado@masfak.ni.ac.rs

[3]University of Kragujevac, Technical Faculty Čačak, Serbia, jbaralic@tfc.kg.ac.rs

Abstract: *The problem of cutting difficult-to-machine materials used in the aerospace industry, aircraft industry and automobile industry, led to the development and application of today the most attractive technology for contour cutting - Abrasive Water Jet Cutting.*

The use of the abrasive water jet cutting is based on the principle of erosion of the material uppon which the jet hits. Each of two components of the jet, i.e. the water and the abrasive material has a specific purpose. It is the primary purpose of the abrasive material within the jet stream to provide the erosive forces. It is the primary purpose of the water jet to deliver the abrasive material to the workpiece for the purpose of erosion. However the water jet also accelerates the abrasive material to a speed such that the impact and change in momentum of the abrasive material can perform its function.

Materials used for abrasives are generally characterized by high hardness, and moderate to high fracture toughness. This Paper presents types and properties of abrasive materials used in abrasive water jet cutting, as well the influence of abrasive mass flow rate on the cut surface quality.

Keywords: *Abrasive Materials, Abrasive Water Jet Cutting, Cut Surface Quality.*

1. INTRODUCTION

Each day reveals new materials that could be applied in different areas of mechanical engineering. In most of these materials processing by conventional methods is a major problem due to breakage and tool wear, uneconomical or even impossibility of processing, while the non-traditional manufacturing processes are applied without the usual restrictions on the mechanical properties and machinability of materials.

Advances in the automobile industry, material science, and space technology in 70's and 80's demanded and stimulated the outgrowth of new ideas and novel technologies in manufacturing. The first commercial water jet cutting system was built to cut laminated paper tubes in 1971. Since then, water jet technology has experienced a steady growth. In the early 80's, the idea of entraining abrasive into water jet was promoted by Hashish (1982) and commercial abrasive water jet (AWJ) systems became available in 1983.

The technology of water jet cutting uses either pure water or a mix of water and a fine abrasive material to form an abrasive water jet for use on harder workpieces. The list of materials that can be cut using a pure water jet includes Styrofoam, fiberglass, PVC, nylon, rubber and food products such as fish, meat, bread and cakes. With abrasive added to the water jet, virtually any material can be cut, including metals such as aluminum, carbon steel and stainless steel, high-nickel alloys and brittle materials such as marble, reinforced composites and honeycomb and sandwiched materials.

Modern machine shops now use abrasive water jet machines side by side with other traditional or non-traditional machine tools to cut 2D parts out of all kinds of materials and profit from the use because of their productivity, quick turn-around time, and relative low cost [1].

The aim of the Paper is to provide an overview to the influence of abrasive material, and especially abrasive mass flow rate on the cut surface quality by abrasive water jet cutting.

2. ABRASIVE WATER JET CUTTING TECHNOLOGY

According to a report from a market research company, abrasive water jet cutting is the fastest growing segment of the machine tool industry. So far there are more than 10,000 units of water jet machine tools in operation across the world, with the annual increase rate of more than 20% in the last few years.

Abrasive water jet machining is appropriate and cost effect for a number of procedures and materials and is applied in nearly all areas of modern industry. In the area of manufacturing, the water jet technique is used for: cutting of difficult-to-machine materials, milling and 3-D-shaping, turning, piercing and drilling.

At its basic, water flows from a pump, through plumbing, and out of a cutting head (Figure 1). The energy required for cutting materials is obtained by pressurizing water to high pressures and then forming a high-intensity cutting stream by focusing this water through a small orifice [2].

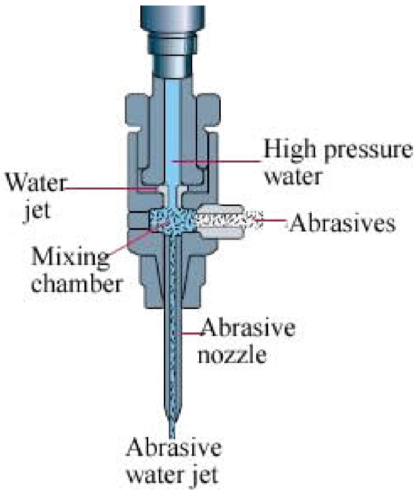

Figure 1. Abrasive water jet cutting head

Typical abrasive water jet cutting system provides an abrasive unit consisting primarily of an abrasive hopper, an abrasive feeder system, a pneumatically controlled on/off valve, and the specialized mixing chamber. The abrasive is first stored in the pressurized hopper and travels to a metering assembly, which controls the amount of particles fed to the nozzle (Figure 2). The abrasive is then introduced into the cutting stream in a special mixing chamber within the abrasive cutting head. After the cut, residual energy from the cutting stream is dissipated in a catcher tank, which stores the kerf material and spent abrasive [3].

The abrasive water jet differs from the pure water jet in just a few ways. In pure water jet, the supersonic stream erodes the material. In the abrasive water jet, the water jet stream accelerates abrasive particles and those particles, not the water, erode the material. The abrasive water jet is hundreds, if not thousands of times more powerful than a pure water jet. Both the water jet and the abrasive water jet have their place. Where the pure water jet cuts soft materials, the abrasive water jet cuts hard materials, such as metals, stone, composites and ceramics.

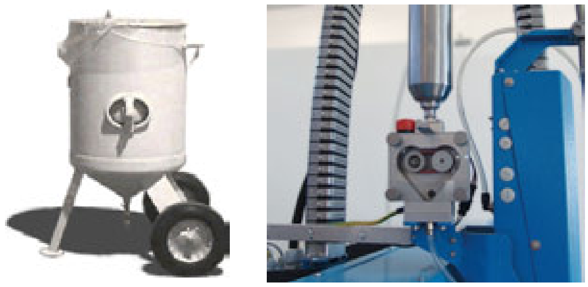

Figure 2. Abrasive hopper and feed-rate regulator

The abrasive water jet cutting process is characterized by a large number of process parameters [4] that determine efficiency, economy and quality. Typical parameter combinations used in abrasive water jet applications are give in Tab. 1.

Table 1. Typical process parameters of abrasive water jet cutting technology

Process parameter	*Value*
Workpiece material	any material up to about 250 mm
Operating pressure	240 - 410 MPa
Water jet nozzle diameter	0.25 - 0.46 mm
Abrasive water jet nozzle diameter	0.76 - 1.57 mm
Type of abrasive material	mineral garnet with # 60 - 120 mesh size
Abrasive flow rate	230 - 600 g/min
Water flow rate	1.9 - 3.8 l/min
Installation power	19 - 27 kW

Abrasive water jet cutting inherently is an environmentally friendly (green) process. Unlike traditional mechanical cutting systems, water jet cutting requires no cooling or lubricating oils, so there are no chemically contaminated chips to dispose of. Unlike thermal processes such as plasma or laser, water jet generates no noxious fumes during the cutting process [5].

3. CLASSIFICATION AND PROPERTIES OF ABRASIVE MATERIALS

Abrasives are those materials used in operations such as grinding, polishing, lapping, honing, pressure blasting or other similar process. Materials used for abrasives are generally characterized by high hardness, and moderate to high fracture toughness. Abrasives come in different particle or grit sizes depending on how much material needs to be removed.

The use of the abrasive materials with water jet for cutting is based on the principle of erosion of the material uppon which the jet hits [6]. Each hard abrasive particle acts like a single point cutting tool. Because of the size of the abrasive particles the impact on the workpiece of an individual particle is small but together the large total number of particles erode the material in significant volume.

Many different types of abrasive materials are used in the water jet cutting process, such as garnet, olivine, aluminium oxide, glass beads, copper slag and silica sand. Garnet, a hard, brittle crystalline mineral is the world standard abrasive for water jet cutting, with approximately 90% of all water jet cutting workshops using garnet.

The evaluation of an abrasive material for abrasive water-jet processes includes the following important parameters:

- *Material structure* - the chemical, physical and structural aspects of the abrasive material. Inclusions in the abrasive such as impurities have a tendency to be lighter and are usually ineffective for the cutting process, reducing the overall cutting ability of the abrasive.
- *Material hardness* - the hardness is decisive parameter for cutting efficiency. The hardness of an abrasive material is usually determined by Moh's hardness scratch test.
- *Mechanical behaviour* - the reaction of the abrasive grain on impact with the workpiece and the probability of the grain fracturing into smaller pieces.
- *Grain shape* - abrasive grain shapes can vary from near round and oval, to rectangular and triangular in shape. Abrasives with sharp, angular surfaces cut more effectively then other shapes.
- *Grain size distribution* - this is the range in the average size or diameter of the grain. It is important to have consistent grain size to maintain a uniform cutting action.

A markt report shows that most of the abrasive water jet workshops use garnet, followed by olivine mineral. In Table 2 are given mechanical properties and chemical composition of these two abrasive materials.

Garnet is hard, tough and inexpensive. A very small number of garnets are pure and flawless enough to be cut as gemstones. The majority of garnet mining is for massive garnet that is crushed and used to make abrasives. Garnet ranges in particle size from 0,2 to 0,5 milimeters. Different mesh (grit) sizes are used for different jobs. For example: #120 mesh – produces smooth surface; #80 mesh – most common, general purpose and #50 Mesh – cuts a little faster than #80, with slightly rougher surface.

Table 2. Mechanical properties and chemical composition of most common abrasive materials

	Garnet	Olivine
Mechanical properties		
Hardness [Moh's scale]	7 - 8	5.5
Specific weight [g/cm^3]	4.1	3.3
Grain shape	Edged	Angular
Chemical composition		
Silica (SiO_2) [%]	35.0	42.0
Iron (Fe_2O_3) [%]	31.0	7.0
Aluminium (Al_2O_3) [%]	21.0	0.5
Magnesium (MgO) [%]	8.0	48.0
Manganese (MnO) [%]	0.5	0.1
Calcium (CaO) [%]	1.5	0.1

4. EXPERIMENTAL STUDY ON INFLUENCE OF ABRASIVE FLOW RATE ON CUT SURFACE ROUGHNESS

Effects of abrasive feed rate on the cut surface roughness were experimentally investigated. The aim of this study is to investigate experimentally the quality of machined surfaces in terms of abrasive flow rate in AWJ-machined aluminium alloy (EN AW-6060). A series of water jet cutting experiments were conducted using a Bystronic abrasive water jet cutting system. It is equipped with a dual intensifier high output pump and a five axis robot positioning system, to cut 50 mm long slots on 700×300 mm test specimens of s = 6 mm and s = 10 mm thick.

The main process parameters varied in the cutting operation are the abrasive flow rate and cutting head feed rate (nozzle traverse rate). In this initial study the feed rate and abrasive flow rate was varied. For each level of the abrasive flow rate (q = 300 and 400 g/min), six levels of feed rates (v = 200, 300, 400, 500, 800 and 1000 mm/min) were used at a single level of water pressures of p = 400 MPa and a single level of impact angle of α = 90°. The other parameters were kept constant using the system standard configuration, that is, the water orifice diameter was d_0 = 0.30 mm, the abrasive nozzle diameter was d_A = 1.02 mm, the length of abrasive nozzle was l_A = 80 mm, and stand-off distance of z = 2 mm. The abrasive used was garnet sand with a mesh number of 80.

Whilst surface roughness is a common phenomenon in all machining operations, striation or waviness is a special feature of cuts with beam cutting technology, such as AWJ cutting. It is formed when the ratio between the available energy of the beam and the required energy of the destruction becomes comparatively small [7].

Abrasive water jet cutting belongs among complicated dynamical and stochastic processes with incomplete information about mechanism and side effects character. In AWJ cutting, the final cut surface roughness and the dimensional accuracy depend on the process parameters including the water pressure, the abrasive mesh number, the abrasive mass flow rate, the feed rate, and the orifice and abrasive nozzle diameters [8-9].

The cut surfaces produced by abrasive water jet cutting typically exhibit a smooth upper zone followed by a lower striated zone. Figure 3 shows the cut surface appearance obtained by cutting aluminium alloy using following abrasive water jet cutting parameters: water pressure of p = 400 MPa, material thickness of s = 10 mm, abrasive mass flow of q = 400 g/min, feed rate of v = 400 mm/min [10].

Figure 3. Cut surface generated in abrasive water jet cutting of aluminium alloy sample

In the present study, surface roughness as assessed by the centre-line average roughness Ra (according to standard ISO 4287:1997) was used in evaluating the cut quality. Surface roughness was measured at upper and lower region of the cut surface, and at the middle of the cut. These measurements were taken for each cut away from the ends of the slots to eliminate any effect of the cutting process at the jet entry and exit. The surface roughness was measured perpendicularly to the jet penetration axis, and parallel to the nozzle feed direction.

The cut surface has better quality at upper region (entrance area) of the jet. From the middle of the thickness downwards, the surface quality deterioration is observed. Surface quality deteriorates as the material thickness increase. As the penetration depth of abrasive water jet increases, the jet loses its energy due to the jet–material interaction, mutual particle impacts, etc. This situation results in rougher surface characteristics at the lower region of the cut surface. Figure 4 shows dependence of roughness average (Ra) at upper, middle and lower region of the cut surface of different feed rate values for material thickness of 10 mm.

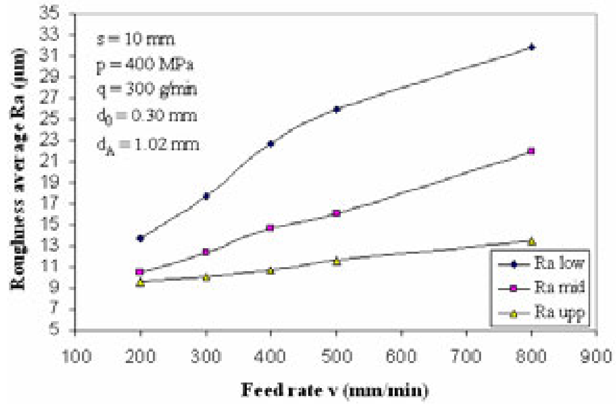

Figure 4. Roughness average Ra in dependence of feed rate when material thickness is 10 mm

The results of determining surface roughness at lower region of the cut surface with respect to the material thickness, feed rate and abrasive flow rate are graphically represented on Figure 5.

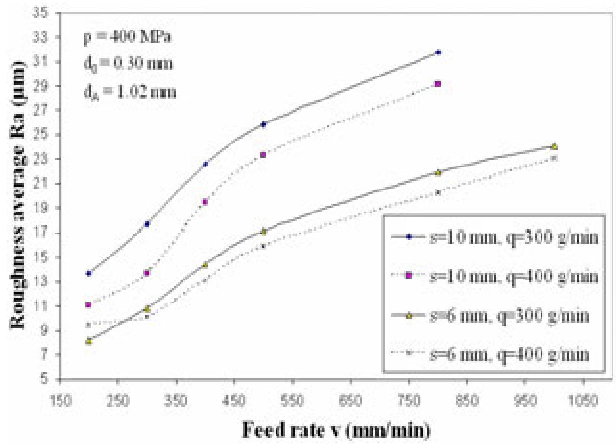

Figure 5. Roughness average Ra in dependence of material thickness, feed rate and abrasive flow rate

It can be noticed that the surface roughness significantly increases as the feed rate increase. This may be anticipated as increasing the feed rate allows less overlap machining action and fewer abrasive particles to impinge the surface, deteriorating surface quality [11].

The influence of abrasive flow rate is found to be less significant on surface roughness. The increase in the number of impacting particles contributes to the improved surface finish. A high number of abrasive particles involved in mixing increases the probability of particle collision that decreases the average diameter of the impacting particles, so the roughness decreases with an increase of the abrasive flow rate. These results are in accordance with the literature [12 - 14].

By literature review [15] the type of abrasive material, i.e. the hardness of the evaluated abrasives as a factor is not significant to average roughness by abrasive water jet cutting of aluminium (Fig. 6).

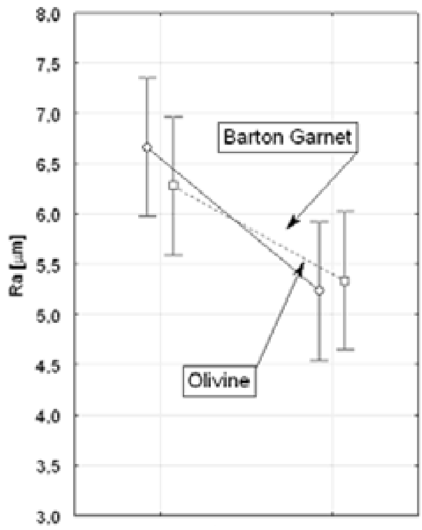

Figure 6. Plot of marginal means for abrasive flow rate of q = 300 g/min and q = 500 g/min, nozzle feed rate of v = 100 mm/min and two types of abrasive material

5. CONCLUSION

The flexibility and cool cutting characteristics of the abrasive water jet technique make it an important tool for cutting applications of new materials such as composites and sandwiched materials that are difficult to machine with traditional machining processes.

In abrasive water jet cutting the final cut surface roughness and the dimensional accuracy depend on the process parameters including the water pressure, the abrasive mesh number, the abrasive mass flow rate, the feed rate, and the orifice and abrasive nozzle diameters. Experimental study shows that, among others, the most important factors influencing the cut surface roughness of aluminium alloy are nozzle feed rate and abrasive mass flow rate.

ACKNOWLEDGMENTS

The authors would like to thank to the Ministry of Science and Technological Development of the Republic of Serbia. Paper is result of technological project TR35034 "The research of modern non-conventional technologies application in manufacturing companies with the aim of increase efficiency of use, product quality, reduces of costs and save energy and materials" which is supported by Ministry of Science and Technological Development of the Republic of Serbia.

REFERENCES

[1] J. Zeng, J. Olsen, C Olsen: The Abrasive Water Jet as a Precision Metal Cutting Tool. In: Proceedings of the 10th American Water Jet Conference, Houston, Texas, August 14-17, pp. 829-843, 1999.

[2] M. Radovanović: Characteristics of Abrasive Waterjet, 3th International Conference "Research and Development in Mechanical Industry"-RaDMI 2003, Herceg Novi, Serbia and Montenegro, pp. 469-473, 2003.

[3] http://www.k-cut.co.uk, K Cut 2011

[4] P. Janković, M. Radovanović: Parameters of Abrasive Waterjet Cutting Process, 6th International Conference ″Research and Development in Mechanical Industry″-RaDMI 2006, Budva, Montenegro, pp.343-346, 2006.

[5] J. Olsen: Green cutting with waterjets. 2008, http://www.thefabricator.com/article/ waterjetcutting/green-cutting-with-waterjets#.

[6] B. Nedić, J. Baralić: The Wear of the Focusing Tube and the Cut-Surface Quality, Tribology in industry, Vol. 32, No 2, pp. 38-43, 2010.

[7] L. Chen, E. Siores, W.C.K. Wong, High–pressure abrasive waterjet erosion process, Proc. Pacific Conf. on Manufacturing, Seoul, Korea, pp. 642–647, 1996.

[8] S. Hloch, S. Fabian: Qualitative analysis of AWJ factors affecting the surface roughness, Wissenschaftliche Beitraege 2006, TFH Wildau, Germany, pp. 113-119, 2006.

[9] A. Lebar, M. Junkar: Simulation of abrasive water jet cutting process, Modeling Simul. Mater. Sci. Eng. 12, pp. 1159-1170, 2004

[10] P. Janković, M. Radovanović: Kerf geometry by abrasive water jet cutting, Annals of the Oradea University, Fascicle of Management and Technological Engineering, Vol. VIII (XVIII), Oradea, pp. 1191-1196, 2009.

[11] P. Jankovic: Modeling of abrasive water jet cutting process and forming of technological processor, Doctoral dissertation, University of Nis (in Serbian), 2009.

[12] F. Chen, J. Wang, E. Lemma, E. Siores: Striation formation mechanism on the jet cutting surface, Journal Process Technol. 2003:141, pp. 213-218

[13] A. Momber, R. Kovacevic, R, Schüneman, et al: The influence of abrasive grain size distribution parameters on the abrasive water jet machining process. In:Rajukar K P (Eds) Proc. 25 th North American Manuf. Engrs, Dearborn, pp. 21-26, 1996.

[14] A. Akkurt: Cut front geometry characterization in cutting applications of brass wiht abrasive water jet, Journal of Material Engineering and Performance, published online: 14 July 2009

[15] S. Hloch, J. Mullerova, J. Valicek: Abrasive type influence on surface roughness at abrasive waterjet cutting, MTM internationa virtual journal, Vol 10-11, 2008.

Serbian Tribology Society

SERBIATRIB '11

12th International Conference on Tribology

Faculty of Mechanical Engineering in Kragujevac

Kragujevac, Serbia, 11 – 13 May 2011

SOME DEVELOPMENTS IN TRIBOANALYSIS OF COATED MACHINE COMPONENTS

Dr. Alexander A. Minewitsch[1]

[1]TTZH Tribologie & Hochtechnologie GmbH, Germany, alexander.minewitsch@ttzh.com

Abstract: *Surface engineering and coatings on surfaces of various auto- and machine components, bearings, piston rings, etc. have been since years proved to be a successful way of improving their performance.*

However, quality of coated triboelements remains to be a subject of complex triboanalysis, using sophisticated methods of tribotesting, micro- and nanoindentation, micro- and nanoscratch, measurements of coating thickness and surface roughness, e.g. using non-contact confocal optical profilometry and related surface metrology techniques and software. Very often a physicist dealing with creating of novel deposition techniques and analyzing influences of plasma and high energy particles bombarding the solid surfaces on the properties of surface engineered components and a tribophysical background of their better performance. In tribology terms, plasma surface engineering and physical vapour deposition of coatings is playing a role of a control method for friction and wear, which has to be based on observation or measurement of output tribological parameters, characterizing a tribocouple and very exact selection of input parameters, aiming to provide the conditions, which would be maximally adequate for a concrete application of surface engineered components.

The goal of present paper is to create some guidelines to selection of an optimal set of analytical techniques and configuration for some specific equipment for triboanalysis of engineered surfaces and coatings, assisting research scientist to formulate clear tasks for an experimental investigation, to obtain the best possible instrumentation and finally to be able to carry out experimental research and collect the experimental data giving the answers on principle questions of engineering of tribological surfaces.

Keywords: *surface engineering, triboanalysis, nano, micro indentation, scratch, roughness.*

1. SCHEMES OF TRIBOTESTING AND OPTIMAL CONFIGURATION OF TESTERS

Comprehensive testing of machines and equipment, is usually a multilevel and multiscale task [8, 15], involving the field tests, bench tests, tests of specific units and components, whereas the last would be always subdivided into natural tests of real components and simplified elements, modeling a real tribology contact. On the other hand, versatile tribology systems in various industries are making a scientist, practically in all situations to keep in a mind some friction and wear fundamentals, including the laws of friction, describing physically, chemically and mechanically a real contact between moving solids [9, 13, 14, 16]. Despite some mutual effects in hard discs of computers, watches, orthopedical implants, autos, airplanes, machine tools, pumps, wind energy plants, etc., modeling of a specific contact situation, requires different approaches and surface analyses vary from nanometer to micrometer scale.

Bench tests we are presently focusing on can involve both model and real test of coated details in one and the same tester, having as a limitation some overall dimensions only. So, it would an applicability of mean maximum sizes of coated machine components like 150-250 mm, which actually covers a lot of applications, starting from nanotechnology and microtechnology and expanding to classical mechanical engineering on a macrolevel.

The initial questions for preparing a configuration of a tribotester are as follows:

1. How to select a model test, corresponding to a real situation?

2. What are the input parameters? Are they controllable with a sufficient accuracy?
3. Which parameters can be monitored? What is possible in situ (or in vivo) and ex situ?
4. How to create an affordable solution? Why a cheap solution could turn to become extremely expensive?
5. Where is a compromise between a universal testing machine and a special machine, performing only one specific function?

Really, there is always one more question in the minds "to test it yourself", i.e. to find out and to buy a tester for own use, or to involve a partner or a service company, specialized on tribometry and triboanalysis routinely. Both approaches have their advantages and disadvantages and final decision of this question, dependent on a lot of variables, is beyond the present paper.

2. REALISTIC SCHEMATIZATION

Realistic schematization of a tribosystem could involve several geometries like "pin-on-disk", "pin-on-plate", "ball-on-disk", "ball-on-plate", "block-on-ring", "disk-on-disk", "parallel cylinders", "crossing cylinders", "4-ball" and some special ones, including various combinations of those mentioned above.


a) pin-on-disk

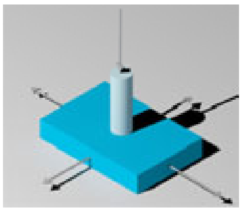
b) pin-on-plate

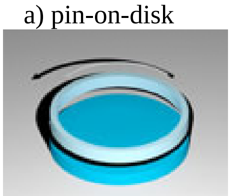
c) ring-on-disk


d) disk-on-disk

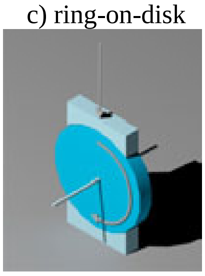

e) block-on-ring

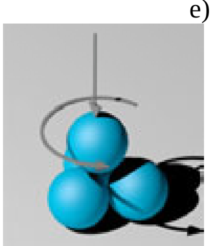
f) 4-ball

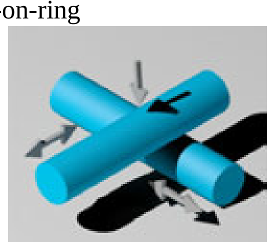
g) crossing cylinders

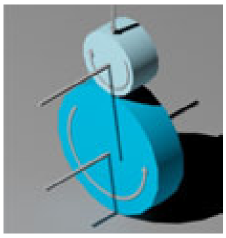
h) parallel cylinders

Figure 1. Several typical schemes of tribological contact

Additional specific features are coming with the different sizes of the samples concerned, with their relative positioning, with their overlapping on the contact. Turning from geometry only to the materials aspects and choosing which of the samples (or maybe all available ones) have to be coated and which thickness of coatings (measured in micrometers or nanometers) of plasma modified, galvanic and different layers have to be taken into consideration bring more variables to our task.

3. KINEMATICS AND TYPES OF THE TRIBOSYSTEMS

Using a number of drives for providing the required relative movements of samples and counterbodies involve rotary, linear and reciprocating movements and combinations thereof.

Kinematically complicated tribotests can implement a combination of movements of both upper and lower specimens, this way providing an adequate modeling of a real situation in a configuration of a tribometer. For example, a rather simple linear motion could be used in a tribometer for wear and fretting tests, scratch-tester, microindenter and / or nanoindenter, which could be considered as some specific cases of tribometers, but also in the butterfly wear-track tests. Of course, depending on the required input parameters, each specific tribometer has to be equipped with a specific drive, having its individual portrait like a "Speed versus Torque Characteristic" and often a high precision resolution on a micrometer level. An example of a tribometer, implementing linear reciprocating motion (having a possibility of fast changing of drives and this way providing its universality for testing under different of the aforementioned schemes, is shown on the Fig. 2).

Figure 2. Universal tribometer UMT

Some specific executions of these UMT / UNMT techniques have been described in the papers [17-18]. A variant of some tribotests with a more complicated kinematics have been developed in the paper [19] and obtained a name of a combinatorial approach in tribology. In case a physicist is concentrating on the “third body” for clarifying the influence of hard or soft coatings on performance of lubricating oils and greases some more specific testing techniques can be employed, as described in [20].

4. INPUT PARAMETERS

The most important parameters, characterizing a tribosystem are force (torque) and speed, which are fully predefining a choice of loading system and drive in a testing device. Of critical importance is a precision of measurements of these parameters, which is dependent on a concrete research project and requires a right selection of force and torque sensors, especially for a problem of distinguishing between several thin films, including those of nanometer thickness, determined by either their different compositions, or structures, or a combination of them both together with formation of some natural films, caused by the processes of friction and wear themselves. Load, measured in Newtons, milliNewtons, or microNewtons is actually considered to be a basic parameter only, while important related parameters are contact stress, impact force, oscillating load, etc. [9]. Parameters, related to sliding speed are average speed, rolling speed, spinning speed, impact speed, sliding/rolling ratio. Sliding distance (often given as a time of specific tests) can be in case of reciprocating tests characterized by amplitude (connected with a precision of positioning) and frequency. Relevance of the model bench tests is usually a subject of thorough analyses. It always remains of primarily importance in adequate experiments for reproducing the wear mechanisms of the field tests. Another aspect is reproducing a temperature level and environmental situation of the test materials and coatings.

The latter question is technically implemented using elevated and high temperature chambers (incl. devices and sensors for precise temperature measurements) for the tests under elevated (up to 175°C) and high temperatures (depending on techniques used up to 1000°C or even 1600°C), including those, running in the protective gases; chillers and special cooling devices for negative and low temperatures; vacuum chambers for the tests in vacuum (and alternatively in special gases); humidity chambers for the tests under the controlled atmospheres, circulating oils, etc.

5. OUTPUT PARAMETERS

Tribotests have since years demonstrated themselves to be much more complicated procedures, than only measuring friction and wear as performed in the mediaeval triboegineering. On the other side PC controlled input parameters being changed against time or sliding distance are causing the respective variations of the response in both open and closed engineering systems. So, the output parameters include measured forces and torques of friction, coefficient of friction COF, contact temperature, distribution of contact stresses and temperatures, changes of physical parameters of tribological surfaces and contacts. The latter aspect is connected with in situ (or in vivo) measurements of ECR (ESR) electrical contact resistance (electrical surface resistance) and remains an extremely sensitive method for catching a moment of breaking through of the deposited coatings and thin films. Supplementary is an AE acoustic emission analysis, bringing valuable semi-quantitative information about origin of damages on the contact between a PVD coating and a counterbody, on the interface between a coating and a substrate in the body of coatings and in the deeper deformed substrate layers, modified with nanometer scale films with a primarily goal of improvement of contact conditions on the engineered surfaces of various components. One of additional aspects in analyzing of the obtained results is software for processing and interpretation of the output parameters and their presentation in one of the forms, recognized by physicist, e.g. in the field of synergistic action of lubricating oils, modified with some more or less tribochemically aggressive additives and antifriction and anticorrosion PVD coatings, one of the popular interpretation of the results is a Stribeck curve (COF against ratio V/Fz – speed to normal load).

6. SOME CONCERNS ABOUT SELECTION OF A RELEVANT TEST

Relevant tribology test arranged in a bench top tribometer is a model, possibly repeating the prevailing wear mechanism of the real components and implementing the same type of contact, like point, linear or flat ones. This is not a must, that a complicated tribocontact, e.g. between a coated cutting edge, a metal chip and a machined workpiece has to be modeled using one scheme only. A detailed description of such practical situation can be done using several geometrical schemes and after collecting the results from several tribotests, e.g. “block-on-ring” plus “pin-on-disk” (alternatively “block-on-ring” plus ”pin-on-plate”), depending on a specific cutting tool type and geometry, etc. [4].

As nominated by STLE members in 2005 [21], tribotesting belongs to the ten greatest events in tribology history, as it is this helped to make tribology from a technological endeavor to an interdisciplinary science.

7. SURFACE CHARACTERIZATION

Characterization of coated surface includes measurement and determination first of all of their geometrical and mechanical properties. Geometrical properties are analyzed using contact and non-contact profilometers and AFM – atomic force microscopes and devices. Hardness on the nano-, micro- and macro-levels and determination of elasticity modulus are done using the indentation techniques, which in the case of evaluation of thin films and coatings could be performed in static and in dynamic modes, assisting to eliminate any influence of substrate on the results of the measurements.

8. PROFILOMETRY

Traditionally measured 2D parameters, such as Ra, Rz, Rq, Rmax, etc. employing well known contact techniques remain a complimentary to modern 3D surface topography analysis by means of chromatic confocal optical sensors and laser sensors. Submicrometer resolution in horizontal direction can go in this event down to 100 nm. Vertical range and respectively vertical resolution vary from 0,1 mm to 2,5 mm and from 2 nm to 40 nm for inductive (contact) sensors. Typical chromatic confocal (non-contact) sensors provide the resolution from 2 nm to 15 nm within larger vertical range from 460 µm to 3,7 mm. Laser non-contact sensors are giving a wider vertical range up to 10 mm, but worse resolution on a micrometer level. One of the popular models of optical profilometers NJ HP – 115 is demonstrated on the Fig. 3.

Figure 3. Optical profilometer NJ HP - 115

9. INDENTATION AND ELASTICITY MODULUS

Instrumented indentation is running according to ISO 14577 for measuring hardness, elasticity modulus, tensile and von Mises stresses, contact stiffness of various coatings and substrates. As described in [18], hardness tests as a part of tribotests and mechanical characterization involve a) wear tests for evaluation of coating friction and durability, b) scratch-hardness tests under constant load for scratch-resistance and microhardness measurement, c) scratch-adhesion tests under progressively increasing load for evaluation of the coating adhesion and scratch toughness properties, d) nano-indentation tests for coating nano-hardness and elastic modulus evaluation [18, 22].

10. MICRO-SCRATCH AND NANO-SCRATCH TESTS

Various physic-mechanical aspects of scratching have been described in [23], therefore we are dwelling here on some semi-standardized procedures only. According to DIN V ENV 1071 part 3 (compare DIN Fachbericht 39, p. 223ff) scratch test has to run with a diamond (Rockwell C), free of contaminations, tip radius 0,2 mm, opening angle 120°. Presence of contaminants have to be checked after 10 tests using an optical microscope, impurities are to be cleaned by methanol and fine brush, or a diamond tip have to be changed. Loading from zero to 100 N with a speed 1,67 N/s. Speed of scratching is 0,167 mm/s, measuring time 60 s, scratching distance 10 mm, distance between scratching tracks is minimum three times of lateral elongation of recognizable layer damages (max. 1 mm).

Environmental requirement include anti-vibration table, room temperature 22±5°, air humidity below 80% (to avoid condensation on samples and diamonds). Critical load would be determined measuring an acoustic noise level by means of a sound converter (resonance frequency 200 kHz and minimum level of frequency ca. 30 kHz). Parallel with the acoustic measurements, analysis of damages is made by an optical microscope. If the layers and substrates cannot be identified using optical light, then access to some more methods, as SEM, phase contrast, etc. have to be provided. Detection of cohesion failures, i.e. formation of the cracks within deposited layers could require magnification x500.

11. TOWARDS COMPREHENSIVE TRIBOANALYSIS OF COATED MACHINE COMPONENTS

Comprehensive triboanalysis requires full scale tribotests plus a number of methods for chemical, physical and mechanical characterization of contacting coatings and films, aiming to distinguish specific tribophysical phenomena, serving to a longer life of coated and modified components. Full scale characterization involves multi-sensing tests, multilevel analysis and multi-resolution estimation of the triboparameters.

REFERENCES

[1] K. Holmberg, A. Matthews: Coatings Tribology, Properties, Mechanisms, Techniques and Applications in Surface, Tribology and Interface Engineering, Second Edition, Vol. 56, Elsevier, Amsterdam, 2009, 560 p.

[2] J. Takadoum: Materials and Surface Engineering in Tribology, 2008, Wiley, 226 p. First published in France in 2007 by Hermes Science/Lavoisier: «Matériaux et surfaces en tribologie».

[3] Tribology of Diamond-Like Carbon Films, eds. Christophe Donnet, Ali Erdemir, Springer, 2008, 664 p.

[4] A.A. Minewitsch: Wear of cemented carbide cutting inserts with multilayer Ti-based PVD coatings, Surf. & Coat. Technol., 1992, v. 53, No. 2, p. 161-170.

[5] Hans Sjöström, A.A. Minewitsch: DLC coated bearings, In: “Modern Materials, Equipment and Technologies of hardening and recovery of machine elements”, Novopolotsk, Polotsk State University, 1999, p. 26-27 (In Russian).

[6] A.A. Minewitsch: Tribological Behaviour of Ti-B-Si-N CAE Coatings, 14th Int. Colloquium 13-15 January 2004 “Tribology and Lubrication Engineering”, vol. I, ed.: W.J. Bartz, Ostfildern,Technische Akademie Esslingen p. 573-578.

[7] A.A. Minewitsch: On Technological Heredity of Some PVD Coated Triboelements, Proc. 16th Int. Tribology Colloquium “Lubricants, Materials and Lubrication Engineering”, January 15-17, 2008, ed. Wilfried J. Bartz, Technische Akademie Esslingen, paper 21.12.

[8] Horst Czichos, Karl-Heinz Habig: Tribologie-Handbuch. Tribometrie, Tribomaterialien, Tribotechnik, Vieweg + Teubner Verlag, Wiesbaden, 2010, 757 S.

[9] G.W. Stachowiak, A.W. Batchelor, G.B. Stachowiak: Experimental Methods in Tribology, Elsevier, Amsterdam, 2004, 354 p.

[10] E.D. Braun: Methods and Devices for Tribotechnical Tests, In: Modern Tribology, ed. K.V. Frolov, Moscow, URSS, 2007, p. 367 – 414 (In Russian).

[11] E. Santner, H.-J. Böhmer, L. Deters et al.: Reibung und Verschleiß von Werkstoffen, Bauteilen und Konstruktionen. Tribologische Optimierung und Schadenbekämpfung, Kontakt & Studium, Band 602, Renningen, expert verlag, S. 232, 2004.

[12] B. Prakash: Tribotesting, In: Tribology in Engineering Design, B.V.A. Rao (Ed.), Institution of Engineers, India, p.152-165, 1993.

[13] Fundamentals of Friction: Macroscopic and Microscopic Processes, eds. I.L. Singer and H.M. Pollock, Kluwer, Dordrecht, 1992, 621 p.

[14] Nanotribology: Critical Assessment and Research Needs. Eds. S.M. Hsu and Z.C. Ying, Kluwer, Boston, 2003, 442 p.

[15] S. Hogmark, S. Jacobson: Hints and guidlines for tribotesting and evaluation, Lubr. Eng., 1992, v. 48, No. 5, p. 401-409.

[16] D. Tabor: Tribology and physics, J. Phys. D: Applied Phys., vol.25, No. 1A, p. A1-A2, 1992.

[17] N. Gitis, A. Minewitsch: Integrierte SPM für Nano-Tribologische Charakterisierung von Oberflächen, Tribologie & Schmierungstechnik, GFT Tribologie-Fachtagung, 26.-28. Sep. 2005, Göttingen, 2005.

[18] N. Gitis, A. Minewitsch: Tribomechanische Charakterisierung von Hartstoff-Beschichtungen im Nano-Mikrotester, GFT Tribologie-Fachtagung, 24.-26. Sep. 2007, Göttingen, Bd. II, S. 63/1-63/11, 2007.

[19] M. Eglin, A. Rossi, N.D. Spencer: A Combinatorial Approach to Elucidating Tribological Mechanisms, Tribology Letters, 15, 3, pp. 193-198, 2003.

[20] A.A. Minewitsch: Modern Equipment for Testing of Lubricants and Greases, Proc. of the VI Int. Conference “Lubricants Russia - 2010”, November 10-11, 2010, Renaissance Moscow Hotel

[21] Kathryn Carnes: The Ten Greates Events in Tribology History, Tribology & Lubrication Technology, June 2005, Vol. 61, No. 6, p. 38-47.

[22] A.A. Minewitsch, S.N. Dub: Mechanical properties of titanium nitride, produced by magnetron sputtering, J. Mater. Technol. Tool., No. 2, p. 35, 1996.

[23] Scratching of Materials & Applications, ed. Sujeet Sinha, Elsevier, Amsterdam, 2006, 319 p.

Serbian Tribology Society

SERBIATRIB '11

12th International Conference on Tribology

Faculty of Mechanical Engineering in Kragujevac

Kragujevac, Serbia, 11 – 13 May 2011

PLASMA NITRIDING AS TREATMENT FOR IMPROVEMENT OF WEAR PROPERTIES MACHINE PARTS

R. Gligorijevic[1], J.Jevtic[1], Dj. Borak[1]
[1]IMR Institute d.o.o, Serbia, imrkb@eunet.rs

Abstract: *Samles of hot work tool steel C.4751 (En-X37CrMoV51) from various previous heat treatments are nitrided in the glow discharge plasma of gas mixtures H_2 /N_2 at the temperatures from the interval (500-550)^o C with the durations of (6-30)h. Surface hardnesses of around 1100 HV O.3 and nitrided zone depths of (0.05-0.3)mm are achieved. Optimal choice of plasma nitriding parameter set has been achieved in order to form monophase γ'-Fe_4N compound layer on the surfaces of treated components. This layer is thinner than 10 um and it is nearly independent of process time duration. The plasma nitriding parameters set in order to get nitrided layer without any compound layer has been realised, too. The surface roughness of the treated components is slightly enhanced on both grounded and turned surfaces.*

Keywords: *Plasma nitriding,wear, tool steel*

1. INTRODUCTION

Tool steel C.4751 (Utop Mo 1, En-X37CrMoV51) to work in hot condition is very commonly used material for building tools for casting and extrusion. These material is often nitriding before using in such applications. Treatment with conventional gas nitriding in NH_3 lead to the formation of compound layer that is in terms of mechanical and thermal shock tends to cracking. Therefore, this type of layer must first be removed, so the operation requires additional processing which can be very hard, because the tools is often very complicated. Removal of the connective zone is significantly reduced resistance to adhesive wear of nitride devices, which causes problems related to the material. Technology plasma nitriding provides a satisfactory solution to these problems, and it mainly thanks to formation mono-phase thin compound layer type γ'-Fe_4N which is not porous and has sufficient resistance to cracking under conditions of mechanical and thermal shock.

The process of plasma nitriding belongs to the surface hardening group of steel and include the implantation energetic nitrogen ions in the surface layer that is thinner than 10 μm, where it is introduced into the deeper layers of the surface by diffusion process. Electric gas discharge at pressures of order mbar and serves as a source energetičih ions as an energy source for the implementation of high-temperature diffusion process. Basic data about unit where plasma nitriding is discussed in this paper gives enough details to work [1], while the manner of keeping the flow of plasma nitriding process conducted in a similar way to that which is detailed in article [2].

The main reasons for the application of plasma nitriding are: (i) to obtain high surface hardness, (ii) increase resistance to wear, (iii) improving the dynamic properties of materials, (iv) increase corrosion resistance (except stainless steel), (v) obtain surfaces that are resistant to softening effect even at temperatures slightly lower than the nitriding temperature, (vi) to obtain better surface layers of distortion and without dimensions changes of the components, and (vii) obtaining mono-phase nitride compound layer on the surface type ε or γ', and without obtaining nitride compound layers . The aim of this paper is to demonstrate the possibility of realizing some of the above-mentioned properties of tool steel C.4751 to work in hot condition.

2. EXPERIMENTAL

Samples of hot work tool steel C.4751, were heat treated to hardness of (400-500) HB, and they were shaped tiles measuring 50 x 10 mm. One of the base surface ones was polished to the roughness of Ra = 0.25 to 0.30 μm, while the other base grated to the roughness of Ra = 0.4-0.6 μm. The samples were nitrided, 5-30h, in a gas mixture H_2/N_2 different composition at temperatures in the range (500-550)^o C . After nitriding the samples were measured roughness, surface hardness, microhardnesses depth profile and was also made analysis of nitride zone microstructure.

3. RESULTS AND DISCUSSION

Figure 1 shows the microhardness-depth curves of samples plasma nitrided steel C.4751 in gas mixture H_2/N_2 at a temperature of 5000 ^{o}C and (60-30) h. Reached the surface hardness of about 1100 HV 0.5 and a depth of about 0.2mm. Figure 2 shows the microstructure of surface compound layer samples of steel C.4751 plasma nitrided in gas mixture H_2/N_2 . The nitrided layer consists only of the diffusion zone, and after such a long plasma nitriding of 25h at a temperature of 500 ^{0}C. The main mechanism for the formation of such layers can be explained is the sputtering of surface layers, ie. eject surface atoms into the vacuum as a result of interaction energetich beam of ions with the first few monoatomic layers of the sample that nitrided in plasma. By varying the process parameters, especially gas mixture actually varies the sputtering coefficient, given the fact that the coefficient of sputtering isfunction and energy and type oincident ions.

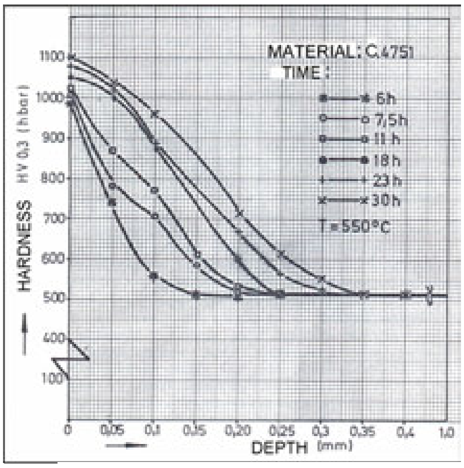

Figure 1. Microhardnesses depth profile of hot work toolsamples steel C .4751 plasma nitrided in gas mixture H_2/N_2.

The microstructure of the surface compound layer of steel samples C.4751 nitrided 6.5h in plasma gas mixture H_2/N_2 at a temperature of 500^0 C and the conditions under which non formation of diffusion zones,shows fig.3. This figure is as proof that the absence of compound layer can not be attributed to a simple spattering previously created compound layer, for example, at the end of the nitriding process, but that in our experiment shalt conditions under which there is a continuous straight balance between these two mutually opposing effects of growing connective zone and its degradation sputtering.

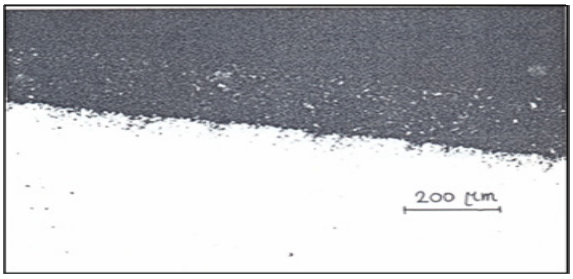

Figure 2. Microstructure of surface layer samples of steel C.4751 plasma nitrided 23h in gas mixture H_2/N_2 under the conditions formation diffusion zone-without compound layer

As a next and final argument to this statement serves Fig.4, showing the microstructure of surface compound layer samples from C 4751 plasma nitrided in the gas mixture H_2/N_2 for a period of 7.5h, at the temperature of 500 ^{0}C, but under conditions in which formed mono-phase compound layer type γ'-Fe $_4$N, a thickness of about 5 mm.

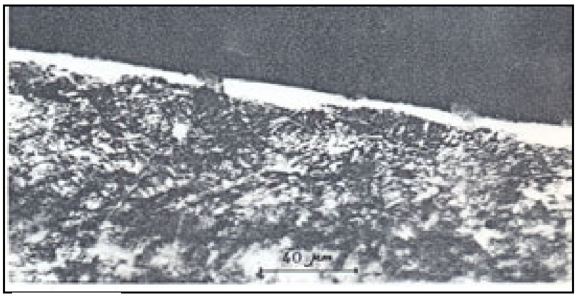

Figure 3. The microstructure of the surface layer of tool steel C.4751 samples plasma nitrided 6.5 h in gasmixture H_2/N_2 under the conditions of formation of diffusion zone only

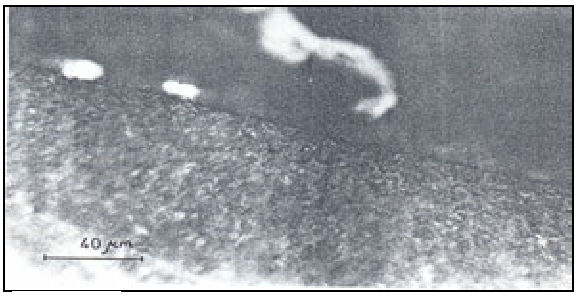

Figure 4. The microstructure of the surface layer of tool steel samples, C.4751, plasma nitrided 7.5h in gas mixture H_2/N_2 under condition formation mono-phase compound layer type γ'-Fe_4N

Roughness measurement results show that the surface quality of the samples plasma nitrided slightly lower than the initial state. Surface roughness Ra after nitriding is 0.30 to 0.45 μm to the previously ground surface (with an initial Ra = 0.25 to 0.30μm), and (0.6-0.8)μm previously grated surface (with initial Ra = (0.4 -0.6) μm). there was no significant differences in roughness between the nitrided surface with or without the mono-phase γ'- compound layer.

4. CONCLUSION

On the base obtained results it can be said:

1. The choice of plasma nitriding parameters enable formation g\` or e compound layer or nitridded zone without compound layer on the surface treated components.
2. Plasma nitrided samples of hot work tool steel in gas mixture H_2/N_2, give the compound layer which hardness is 1100 HV 0.3, and the depth of nitriding 0.05-0.3 mm. This compound layer-g\` give good resistance to wear, to corrosion resistance and resistance to softening at high temperature of tool.
3. The surface roughness of treated samples is slightly enhanced on both grounded and turned surfaces.

REFERENCES

[1] I. Terzic, M.Tosic "*Device for nitriding steel items in the plasma glow discharge"*, II Yugoslav Symposium 0 heat treatment and metal materials, just, 83, Proceedings, Part II, p. 153, Novi Sad 1983rd

[2] R. Gligorijevic, M.Tosic, I. Terzic, "*Carbonating nodular cast iron in plasma"*, II Yugoslav Symposium 0 heat treatment and metal materials, JUSTOM'83, Proceedings, Part II, p. 237, Novi Sad 1983rd.

Serbian Tribology Society

SERBIATRIB '11

12th International Conference on Tribology

Faculty of Mechanical Engineering in Kragujevac

Kragujevac, Serbia, 11 – 13 May 2011

DETERMINATION OF FRICTION IN BULK METAL FORMING PROCESSES

Kačmarčik[1] I., Movrin[1] D., Lužanin[1] O., Skakun[1] P., Plančak[1] M., Vilotić[1] D.

[1] Faculty of Technical Science, University of Novi Sad, Serbia, igorkac@uns.ac.rs

Abstract: *Consideration of tribological phenomena in bulk metal forming processes is very important as friction affects all relevant process parameters such as tool life, forming load and work, integrity of workpiece, quality of workpiece surface, material flow, etc. For the theoretical analysis of the metal forming process as well as for process modeling and simulation, knowledge of coefficient of friction (or friction factor) is indispensable. In metal forming operations in most cases two different friction laws are applied: Coulomb friction model and constant friction model. Evaluation of coefficient of friction is possible by different experimental trials such as backward extrusion, double cup extrusion test, forward bar extrusion, tube extrusion, etc. One of the most applied methods is ring compression test. The concept of this test is to observe and measure increase or decrease of the inner ring diameter during upsetting between two parallel plates. In case of low friction internal diameter increases, while if friction is high internal diameter decreases. Based upon this occurrence, friction calibration curves (FCCs) are created, which makes it possible to obtain coefficient of friction in every specific case.*

This paper is concerned with the possibilities to evaluate friction in metal forming processes. Different friction models are analyzed and assessed. Focus has been placed on the ring compression test and construction of friction curves. Our own modeling and experimental results are shown and analyzed.

Keywords: *metal forming, friction, ring compression test, FE modeling.*

1. INTRODUCTION

In metal forming processes friction is a very important variable which influences all relevant process parameters (force, load, work, temperature, material flow, etc) as well as quality of workpiece. Friction occurs due to relative motion between the tools or dies and workpiece material.

Many scientists have contributed to the research and explanation of physical phenomena which cause friction between two surfaces in relative motion. One of the most significant works is [1] in which authors developed their own approach known as "Adhesion Theory". They concluded that the true contact area between workpiece and tool/die contact is only a small percentage of the apparent contact area (Fig. 1).

Beside Bowden & Tabor's "Adhesion Theory", some other approaches to explain physical nature of friction have been elaborated, such as "Roughness Theory" and "Plowing Theory" [1], [2].

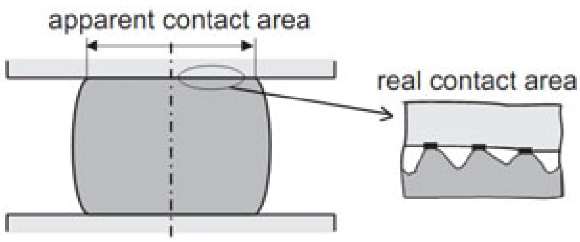

Figure 1. Real and apparent contact area

In recent time new technological developments, such as Scanning force microscope (SFM), contributed to the more sophisticated and more reliable investigation of friction in metal forming.

Characterization of friction (quantification of friction amount) is possible in different ways [3], [8]. Most common way is by Coulomb model:

$$\tau = \mu \cdot p \tag{1}$$

τ – tangential friction stress
μ - coefficient of friction
p – local normal pressure

Constant friction model proposes that friction stress is constant and proportional to the yield stress in pure shear "τ_{max}" and friction factor:

$$\tau = m \cdot \tau_{max} \quad (2)$$

Both models are insufficient for exact description of friction phenomenon as they do not take into account a number of other influential factors such as relative velocity, material properties, surface roughness, lubrication conditions and etc. However, due to their simplicity, they are commonly used for friction description in analytical or numerical modeling of metal forming processes [5], [7], [12].

Coefficient of friction (μ) and friction factor (m) can be obtained in different experimental trials which simulate real metal forming processes [5], [9], [12].

In further text, some of the most applied experimental methods to evaluate "μ" and "m" in bulk metal forming operations are presented [10], [13], [14].

2. EXPERIMENTAL TECHNIQUES FOR FRICTION MEASUREMENT IN BULK METAL FORMING

2.1 Forward bar extrusion (FBE)

In figure 2 schematic diagram of forward extrusion process is shown. Due to friction on the container wall, friction force F_c occurs.

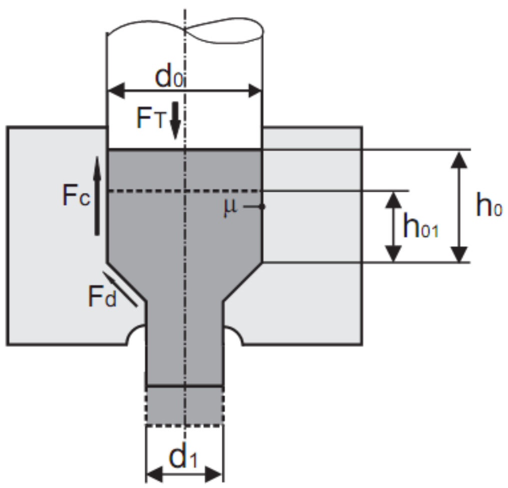

Figure 2. Forward bar extrusion

Total extrusion force is:

$$F_T = F_c + F_d + F_{dd} \quad (3)$$

F_c - friction force at the workpiece container interface

F_d – friction force at the conical die/workpiece interface

F_{dd} – deformation force in conical die

Friction force can be obtained as:

$$F_c = \tau \cdot \pi \cdot d_0 \cdot h_0 \quad (4)$$

τ – shear stress at the billet/container interface

$$\tau = \mu \cdot \sigma \quad (5)$$

σ – flow stress

With (5) equation (4) becomes:

$$F_c = \mu \cdot \sigma \cdot \pi \cdot d_0 \cdot h_0 \quad (6)$$

During steady state forward extrusion forces "F_d" and "F_{dd}" remain constant while friction force "F_c" decreases, as the length of the billet "h_0" decreases to "h_{01}". This means that equation (3) transforms to:

$$\Delta F_T = \Delta F_c + \Delta F_d + \Delta F_{dd} = \Delta F_c \quad (7)$$

(as ΔF_d and ΔF_{dd} are zero).

$$\Delta F_c = \Delta F_T = F_{T0} - F_{T1} \quad (8)$$

From the experimentally obtained diagram $F_T = f(\text{stroke})$ – Fig. 3. difference F_{T0} - F_{T1} can be obtained.

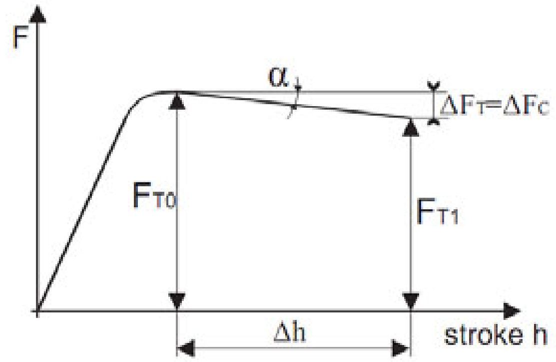

Figure 3. Load-stroke diagram

$$\Delta F_c = \Delta F_T = \mu \cdot \sigma \cdot \pi \cdot d_0 \cdot (h_0 - h_{01}) \quad (9)$$

From (9), coefficient of friction is:

$$\mu = \frac{\Delta F_T}{\sigma \cdot \pi \cdot d_0 \cdot \Delta h} = \frac{tg\alpha}{\sigma \pi \, d_0} \quad (10)$$

Coefficient of friction is proportional to the slope of load-stroke diagram in steady state phase.

2.2 Backward cup extrusion (BCE)

In backward extrusion, punch acts on the billet with the load F_1 (Fig. 4.). Billet material is extruded thought the gap between punch head and container, at which wall friction force F_f occurs. This force can be calculated as:

$$F_f = F_1 - F_2 \quad (11)$$

Friction force F_f is equal to:

$$F_f = \tau \cdot A = \mu \cdot \sigma \cdot A \tag{12}$$

σ – flow stress

A – contact area between container wall and billet.

From (11) and (12), coefficient of friction is:

$$\mu = \frac{F_f}{\sigma \cdot A} = \frac{F_1 - F_2}{\sigma \cdot A} \tag{13}$$

Forces at the punch head (F_1) and at the die bottom (F_2) are measured by separate load cells.

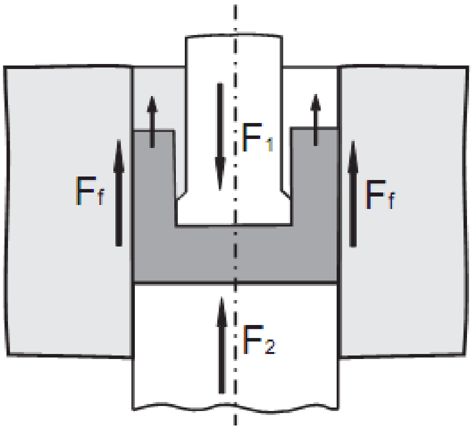

Figure 4. Backward cup extrusion

2.3 Backward extrusion with twist

There are a couple of variants of this test [9]. In one of them, workpece is deformed in backward extrusion process and then die with workpece is kept stationary, while the punch is rotated.

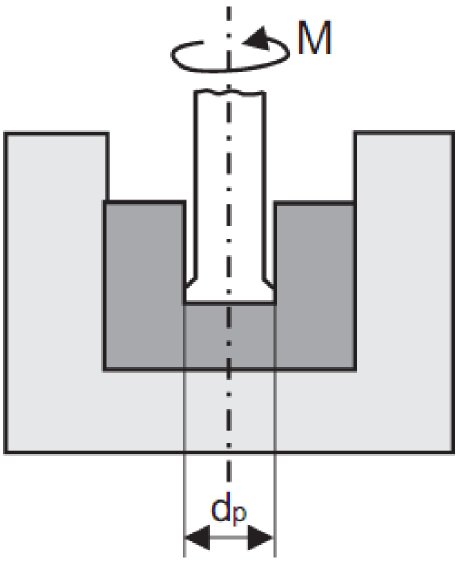

Figure 5. Backward extrusion with twist

Two different punches are used: one with and the other without land. While rotating, moments M_1 and M_2 are measured (each for every punch) and friction constant "m" can be obtained from:

$$m = \frac{2\sqrt{3}(M_1 - M_2)}{\pi \cdot d_p^2 \cdot h_c \cdot \sigma} \tag{14}$$

where d_p is the diameter of the punch, h_c is the length of the punch land and σ is flow stress of the material. The schematic of this process is shown in figure 5 [9].

3. RING COMPRESSION TEST

Ring compression test is a standard method to evaluate friction coefficient "μ" or friction factor "m" in bulk metal forming processes. Theoretical bases of this method was introduced by Male & Cockroft [4] and since then a number of authors have been involved in theoretical and experimental investigation on this issue [5], [6], [7], [12].

During ring compression between two parallel plates, two different situations can occur: in case of low friction internal diameter deforms outwards (Fig. 6a) and if the friction is high internal diameter decreases (Fig. 6b). Radius where no material flow takes place is known as neutral radius (r_n).

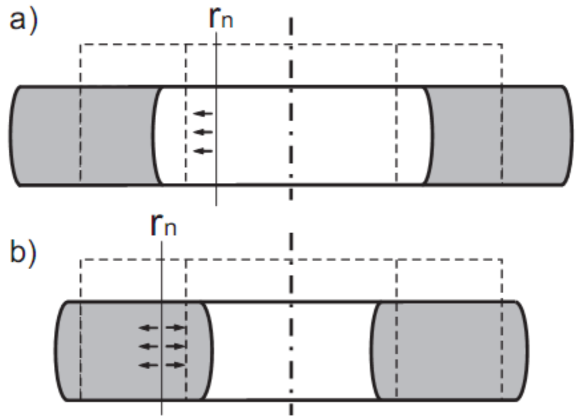

Figure 6. Material flow in low friction conditions (up) and high friction conditions (down)

By superimposing the experimentally obtained function $\varepsilon_d = f(\varepsilon_h)$ on the friction calibration curve (FCC), coefficient of friction (or friction factor) can be obtained ($\varepsilon_d = \frac{D_0 - D}{D_0} \cdot 100\%, \varepsilon_h = \frac{H_0 - H}{H_0} \cdot 100\%$).

Friction calibration diagram (curves) can be obtained in analytical and numerical way [6], [12]. Current paper presents FE modeling of ring compression test and subsequent construction of FCCs.

4. FE MODELING BY SIMUFACT FORMING 9.0

Simufact Forming 9.0 (SF 9.0) is a software solution capable of simulating almost all metal forming processes. It is developed by Simufact Engineering GmbH in Hamburg, Germany.

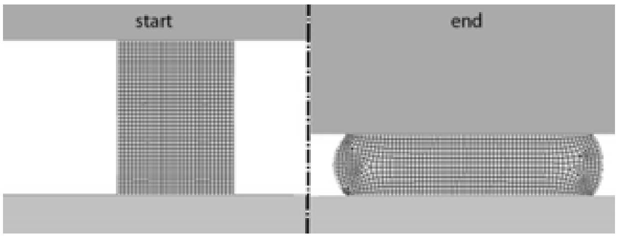

Figure 7. Ring between flat tools in Simufact Forming 9.0 (left: at beginning, right: at end of the process)

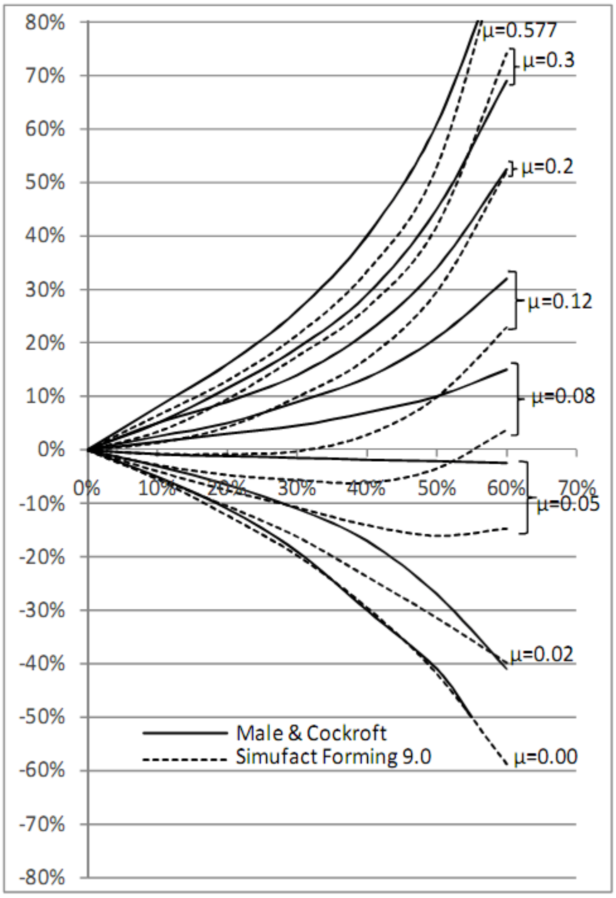

Figure 8. FCCs obtained by SF 9.0 simulation compared with Male & Cockroft curves

2D axisymmetric simulation of ring compression test with finite element solver was performed with SF 9.0 (Fig. 7). Ring with initial dimensions of 30x15x10mm (outer diameter, inner diameter, thickness) was used in simulation. This geometry ratio (6:3:2) is established as standard in most ring compression tests. Material of the billet was steel C1531 (C45) with stress-strain curve $\sigma = 289.671 + 668.779e^{0.3184}$. Upper and lower flat tool were set as rigid bodies, which means that no deformation of the tools takes place. Simulation was done at room temperature and Advanced Front Quad mesher was set to the billet with 0.25mm element size. Also, the remeshing process was not included. Total stroke of 7mm was conducted and results were attained for every 1mm of upper tool increment. After each increment, inner diameter of the ring was determined and deformation of the ring's thickness as well as deformation of the ring's inner radius was calculated. The total of 11 simulations were performed by varying Coulomb friction coefficient (μ) from μ = 0.00 to μ = 0.577. Obtained friction calibration curves are shown in Fig. 8. At the same figure, Male & Cockroft FC curves for 8 different coefficients of friction are given.

5. EXPERIMENT

Ring with dimensions 18:9:6mm was compressed in 6 increments to the final height of 2.4mm. Process was realized on Sack & Kieselbach hydraulic press of 6300kN. Two different kinds of lubrication were applied: (1) oil and (2) phosphate sulphate + MoS_2.

In Fig. 9. initial rings and rings after last increment for both lubrication cases are shown.

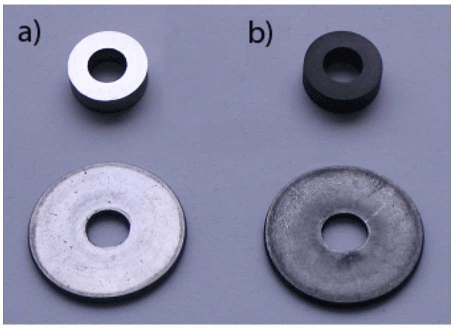

Figure 9. Rings before and after compression (a – oil; b – phosphate sulphate + MoS_2.)

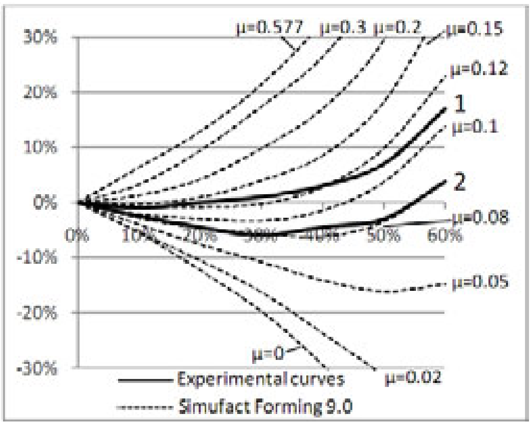

Figure 10. Determination of friction coefficient in experiments based upon FCCs obtained from SF 9.0. (1)-lubrication with oil, (2)-lubrication with phosphate sulphate + M_0S_2

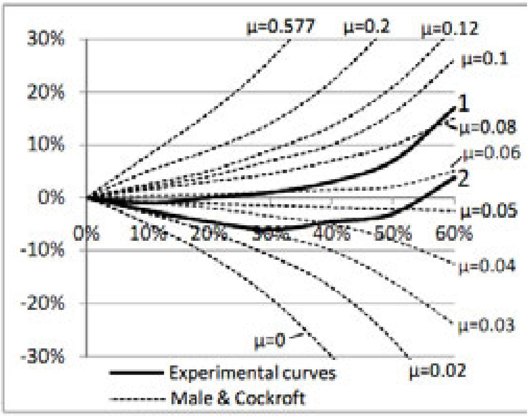

Figure 11. Determination of friction coefficient in experiments based upon FCCs from Male & Cockroft (1)-lubrication with oil, (2)-lubrication with phosphate sulphate + M_0S_2

Based upon measurement of "*Δh*" (height) and "*ΔD*" (internal diameter) after every increment, function ΔD = f(Δh) was established for both lubrication cases. Both curves are then superimposed on FCCs obtained by FE modelling with Simufact package (Fig. 10.) and Male & Cockroft friction calibration curves (Fig. 11.).

Coefficient of friction for both experimental cases, using SF – FC curves, are $\mu \approx 0.12$ (lubrica-ted with oil) and $\mu \approx 0.08$ (phosphate sulphate + M_0S_2) – Fig. 10. By using Male & Cockroft FC curves these values are: $\mu \approx 0.07$ (oil) and $\mu \approx 0.05$ (phosphate sulphate + M_0S_2).

It should be noted that all extracted "μ" magnitudes represent an average value, i.e. there is no exact match between experimentally obtained function ΔD = f(Δh) and corresponding curves in FCCs diagram (Male & Cockroft and Simufact FCCs).

6. CONCLUSIONS

Current paper elaborates possibilities to determine friction value in bulk metal forming operations. Some models to evaluate friction are described and focus is placed on ring compression test. Due to its simplicity this method is commonly applied for determination of coefficient of friction ("*μ*") and friction factor ("*m*").

In order to obtain "*μ*" ("*m*") by ring compression trial, friction calibration curves (FCCs) are needed. These curves can be obtained by theoretical analysis and by appropriate FE modelling.

In this work FCCs were determined by FE modelling, using Simufact Forming package.

Additionally, ring compression experiments are performed in order to verify FE-modelling results.

Comparison of FCCs obtained by SF 9.0 modelling and M&C FC curves shows a certain degree of discrepancies (Fig. 8.). These discrepancies are more apparent for "μ" values between 0.05 - 0.12, whereas for extreme low and extreme high friction values, differences between M&C and SF 9.0 FC curves are smaller.

As a consequence of those deviations, different "μ" values for the same ring compression experiments are obtained, depending which FC curves are used.

In further work on this subject, focus will be placed on the establishing of FCCs for specific deformation cases and under specific process conditions (pressure, temperature, velocity, material).

Also, assessment of different lubricants for cold bulk metal forming, using FC curves will be performed.

7. ACKNOWLEDGEMENT

This paper is a part of the investigation within the project EUREKA E!5005 financed by Serbian Ministry of Science and Technological Development. Authors are very grateful for the financial support.

REFERENCES

[1] Bowden, Tabor: Reibung und Schmierung fester Koerper, Springer Verlag, Berlin/Heidelberg, 1959.

[2] Kasperski I.W.: Reihung und Verlog, Veb Verlag Technik, Berlin 1971

[3] Schey J.: Metal deformation processes: Friction and Libricaion, Marcel Dekker INC, New York, 1970.

[4] Male A.T., Cockroft M.G.: A Method for the determination of the coefficient of friction on metals under conditions of bulk plastic deformation, Journal of the Institute of Metals, 1964-65, Vol. 93

[5] Burgdorf M.: Über die Ermittlung des Reib-wertes für Verfahren der Massivum-formung durch den Ringstauchversuch, Industrie Anzeiger, Nr. V, pp 15-20, 1967.

[6] Abdul N.A.: Friction determination during bulk plastic deformation of metals, Annals of the CIRP Vol. 30/1/, pp. 143-146, 1981.

[7] Sofuoglu H., Gedikli H.: Determination of friction coefficient encountered in large deformation processes, Tribology International 35 27-34, 2002

[8] Petersen S.B., Martins P.A.F., Bay N.: Friction in bulk metal forming: a general friction model vs. the law of constant friction, Journal of Material Processing Technology 66 pp. 186-194, 1997.

[9] Bay N., Wibom O., Nielsen J. Aa.: A new friction and lubrication test for cold forging, Annals of the CIRP Vol. 44/1/1995.

[10] Marinkovic V., Marinkovic T.: Odredjivanje koeficijenta trenja u procesima obrade istiskivanjem, 11th Int. conference on Tribology – Serbiatrib, 2009.

[11] Hawkyard J.B., Johnson W.: An analysis of the changes in geometry of a short hollow cylinder during axial compression, Int. J. Sci. Pergamon Press Ltd., Vol. 9, pp. 168-182, 1967.
[12] Sofuoglu H., Gedikli H.: Determination of friction coefficient encountered in large deformation processes, Tribology International 35 27-34, 2002.
[13] Fereshteh-Saniee F., Pillinger I., Hartley P.: Friction modeling for the physical simulation of the bulk metal forming processes, Journal of Material Processing Technology 153-154, pp. 151-156, 2004.
[14] Mielnik E.: Metalworking Science and Engineering, McGraw-Hill, 1991.
[15] Skakun P., Plancak M., Vilotic D., Milutinovic M., Movrin D., Luzanin O.: Comparative investigation of different lubricants for bulk metal forming operations, DEMI 2011, Banja Luka, accepted paper, 2011.
[16] Lange K.: Handbook of metal forming, SME, Dearborn, Michigan, 1994.

Serbian Tribology Society

SERBIATRIB '11

12th International Conference on Tribology

Faculty of Mechanical Engineering in Kragujevac

Kragujevac, Serbia, 11 – 13 May 2011

COMPARATIVE STUDY ON THE TRIBOLOGICAL BEHAVIOR OF METAL AND CERAMIC MODEL COATINGS

A. Mourlas[1], P. Psyllaki[1], A. Koutsomichalis[2], N.M. Vaxevanidis[3]

[1]Department of Mechanical Engineering, Technological Education Institute of Piraeus, Greece, amourlas@gdias.teipir.gr, psyllaki@teipir.gr

[2]Faculty of Aerospace Studies, Hellenic Air Force Academy, Dekelia Air Force Base Greece, akouts@eeogroup.gr

[3]Department of Mechanical Engineering Educators, School of Pedagogical and Technological Education (ASPETE), N. Heraklion Attikis Greece, vaxev@aspete.gr

Abstract: *The present study concerns parametric analysis on the tribological behaviour of two model coatings, one metallic and the other ceramic, deposited onto the same carbon steel substrate by Atmospheric Plasma Spraying (APS). The metallic coating, selected as a representative of ductile mechanical behaviour, was a CuNiIn, 200 μm thick. The ceramic coating, selected as a representative of brittle mechanical behaviour, was titanium oxide (TiO_2) of the same thickness. The influence of the normal load applied and of the counterbody on the evolution of the friction coefficient and the wear mechanisms was evaluated by testing the two model coatings against sliding in a ball-on-disc apparatus. The behaviour of the different tribosystems was correlated to the friction micro-mechanisms that are activated at the contact interface, during sliding.*

Keywords: *Atmospheric Plasma Spraying, Metallic Coatings, Ceramic Coatings, Parametric Analysis, Friction Coefficient, Wear Mechanisms.*

1. INTRODUCTION

Metallic and ceramic coatings deposited onto metallic substrates via thermal spraying techniques are widely used for anti-wear protection when mechanical components are subjected to frictional and/ or tribochemical loading [1-3].

Thermal spraying belongs to the class of semi-molten state coating techniques. It is a general term used for the description all the techniques consisting of the injection of the selected feedstock (e.g. powder, wire or liquid) into an area of high temperature, where the material to be deposited is heated, accelerated and directed onto the substrate surface. The coatings are formed by the immediate solidification on the surface of the substrate which is, in general, of much lower temperature (ambient temperature).

Among thermal spraying techniques, Atmospheric Plasma Spraying (APS) is a rather simple process from a practical point of view,

In Memory of Prof. G.P. Petropoulos (1959-2010)

basically consists of the injection of the selected powders into a direct current plasma jet, where they are molten, accelerated and directed onto the substrate surface.

Coatings are formed by the immediate solidification of the molten droplets on the substrate surface of lower temperature where they form the so-called splats. Due to this particular deposition process, atmospheric plasma sprayed coatings tend to have highly defective microstructures, with lamellar microcracks, un-molten particles, weak interfaces and voids between solidified splats [4]. The microstructure and consequently the mechanical properties of these coatings depend strongly on the spraying conditions, in particular on variables related to the injected powder particle size, as well as on the substrate's temperature and mechanical properties.

The present study is dealing with the tribological performance of a metallic and a ceramic APS coating, used as model coatings. Parametric analysis revealed as crucial factor for the behavior of the tribosystem, the metal to metal, or metal to ceramic nature of the coating/counterbody interface, during sliding.

2. EXPERIMENTAL PART

For an objective comparison, the two coatings were deposited onto the same common steel substrate, applying the deposition conditions suggested by the manufacturer of the commercial powders to be sprayed, and for duration sufficient to obtain 200 μm thick surface layers, for both the metallic and the ceramic coating. The metallic coating selected was CuNiIn and the ceramic one TiO_2. The microstructure of the ceramic coating obtained is shown in Figure. 1. The coating exhibits the typical microstructure of APS-deposited ceramic coatings characterized by pores and micro-voids, whilst its surface roughness is defined by the geometrical characteristics of the splats after solidification. Compared to that the metallic one is characterized by less porosity and surface roughness due to higher viscosity of the molten metallic feedstock.

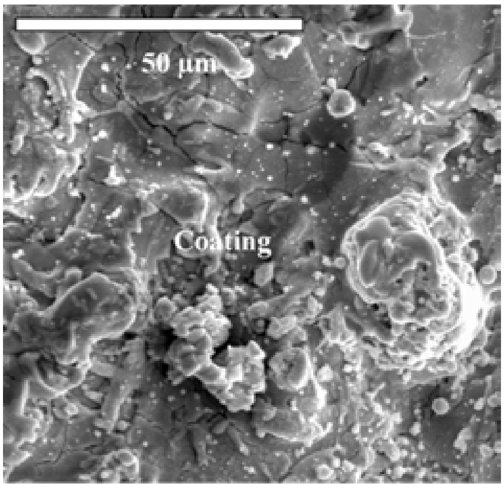

(a)

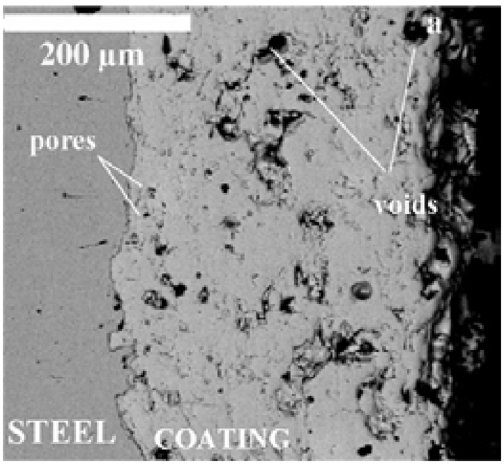

(b)

Figure 1. Characteristic micrographs of the ceramic coating (SEM images): (a) Top view, (b) Cross-section.

The influence of the normal load applied and of the counterbody on the evolution of the friction coefficient and the wear mechanisms was evaluated by testing the two model coatings against sliding in a ball-on-disc apparatus (CSM Instruments). Three series of tests per each coating were performed using Al_2O_3, Si_3N_4 and 100Cr6 steel ball counterbodies (Ø6) by applying normal loads of 1, 2.5 and 10 N. For all tests, the sliding velocity, the temperature and the relevant humidity were kept constant and equal to 0.5 $m.s^{-1}$, 20 ºC and 25 %, respectively.

3. RESULTS AND DISCUSSION

In the case of Al_2O_3 ball used as counterbody sliding against the ceramic APS coating, the friction coefficient was found to be constant, converging to an average value of 0,42±0,07 [5], for all the testing parameters. The evolution of friction coefficient as a function of the sliding distance, for all the normal loads applied, is presented in Figure 2.

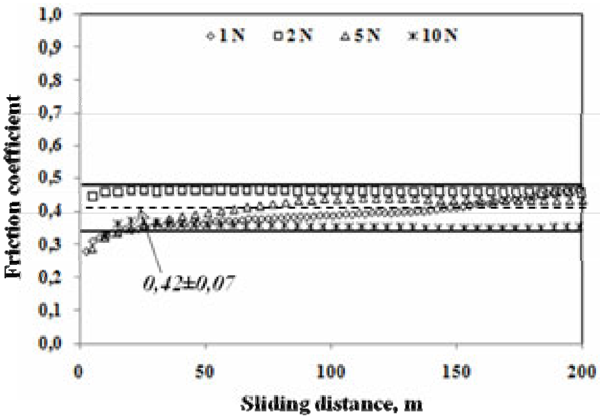

Figure 2. Evolution of friction coefficient for the tribosystem TiO_2/ Al_2O_3.

In the case of Al_2O_3 ball used as counterbody sliding against the metallic APS coating, the evolution of friction coefficient as a function of the sliding distance is shown in Figure 3. A different behaviour of the friction coefficient is observed. For the cases of the lower loads applied (1 and 2 N), the presence of three successive stages can be clearly distinguished and correlated to micro-phenomena taking place at the coating/ counterbody interface:

(a) In the first sliding stage, the friction coefficient tends to a value around 0.25, which is related to the initial wear of the metallic coating protrusions, via their plastic deformation at the micro-contact areas.

(b) In the second sliding stage, the friction coefficient increases to a value of around 0.40. This transition can be attributed to the increase of the real contact area that induces higher drag forces during sliding.

(c) In the last sliding stage, the friction coefficient remains practically constant, around an average value of 0.45 [6]. Such a behaviour can be explained by the intervention of the metallic debris remaining at the contact interface, where they are adherent after having been plastically deformed.

The duration of each stage depends on the normal load applied. The severe testing conditions in the cases of the higher loads (5 and 10 N), in the one hand diminish the duration of the first stage and, in the other hand accelerate the transition to the steady-state final sliding stage.

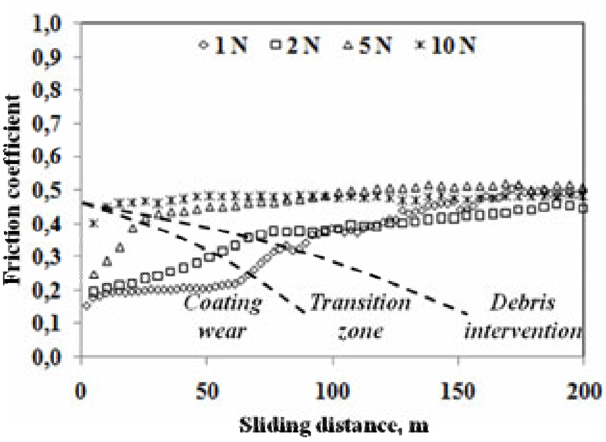

Figure 3. Evolution of friction coefficient for the tribosystem CuNiIn / Al_2O_3.

In the case of the steel (100Cr6) ball used as counterbody sliding against the metallic APS coating, the evolution of friction coefficient as a function of the sliding distance is shown in Figure 4. The strong influence of the normal load applied is obvious: for lower loads, higher friction coefficient values were recorded. A “parallel shift” of the curves corresponding to increasing values of normal load to lower values of friction coefficient can be clearly observed. The average values for each case are presented in Table 1.

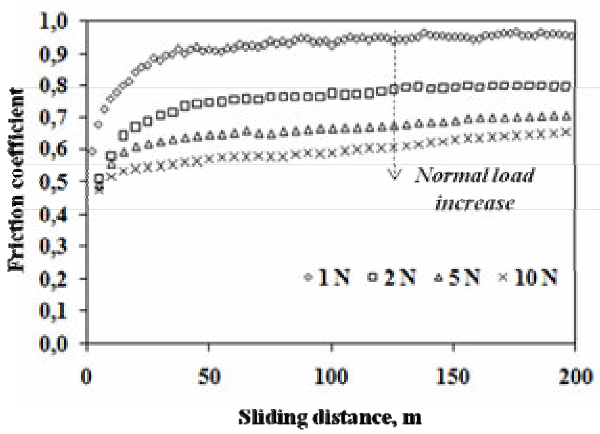

Figure 4. Evolution of friction coefficient for the tribosystem CuNiIn / 100Cr6.

Table 1. Average values of friction coefficient for the tribosystem CuNiIn / 100Cr6.

Normal load applied (N)	Average Friction Coefficient
1	0.92
2	0.72
5	0.64
10	0.55

For low applied load (1 N), the adhesion forces between the two metallic surfaces have a dominant role, inhibiting sliding. By increasing the normal load applied, the plastic deformation of the two bodies in contact, as well as the formation of a metallic debris interlayer, result in the diminution of the drag force developed at the interface and, consequently the reduction of the friction coefficient.

A similar trend of the influence of the applied load on the friction coefficient evolution was also observed in the case of the Si_3N_4 ball used as counterbody sliding against the ceramic APS coating (Figure 5). For every normal load applied, after a coverage of ~10 m sliding distance (running-in period), the friction coefficient attains a practically constant value (Table 2).

This behaviour of two brittle materials sliding vs. each other, can be attributed to the friction mechanism that is controlled by the micro-fracture taking place at the coatings protrusions, due to the coating roughness (Figure 1a). The influence of the surface topography is more pronounced in the case of the 1 N normal load, where significant fluctuations have been recorded. By applying higher normal loads, surface polishing takes place that facilitates relative sliding between the two ceramic bodies.

The differences observed relevant to case where Al_2O_3 ball was used as counterbody to the same ceramic coating, should be attributed to the different mechanical properties of the Si_3N_4 counterbody that alter the Hertz pressure and, consequently, modify wear micro-mechanisms.

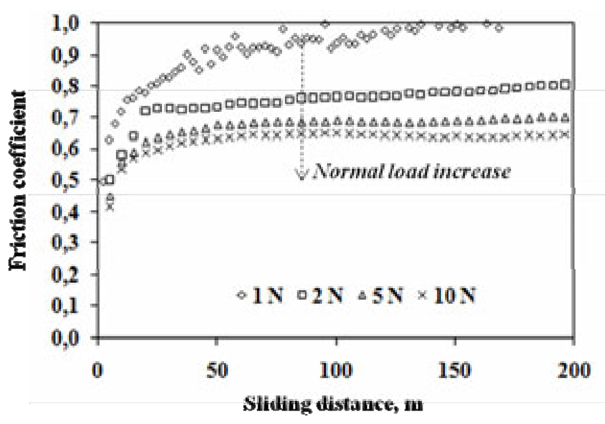

Figure 5. Evolution of friction coefficient for the tribosystem TiO_2 / Si_3N_4.

Table 2. Average values of friction coefficient for the tribosystem TiO_2/ Si_3N_4.

Normal load applied (N)	Average Friction Coefficient
1	0.98
2	0.77
5	0.69
10	0.64

Finally, in the two cases of metal to ceramic tribosystems (CuNiIn/ Si_3N_4 and TiO_2 / 100Cr6) similar behaviour has been recorded, exhibiting an opposite trend than all the previous systems (Figure 6). An increase of the normal load applied resulted in an increase on the friction coefficient recorded.

This macroscopically observed increase of the friction coefficient is due to the action of two competitive mechanisms; the ceramic body acts as a “plough” inserted into the metallic one and should overcome the plastic deformation of the latter at the front of the sliding track. Higher applied forces result in deeper penetration of the ceramic ball or the hard protrusion into the metallic body, affecting a larger volume that is plastically deformed; and thus, higher friction coefficient.

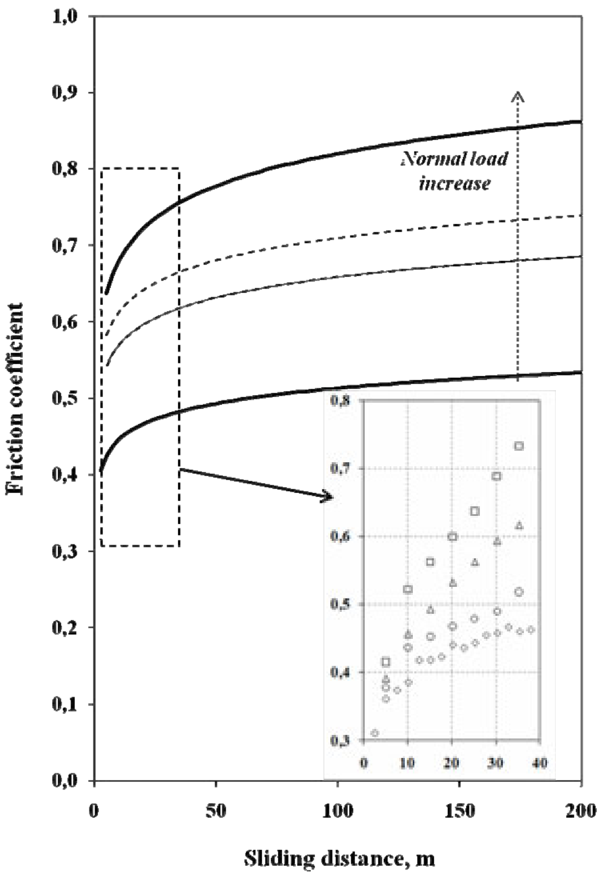

Figure 6. Evolution of friction coefficient for the metal to ceramic tribosystems: CuNiIn/ Si_3N_4 and TiO_2/ 10Cr6.

4. CONCLUSIONS

The sliding behaviour of two typical APS coatings, a metallic and a ceramic one, deposited onto steel substrate was studied. The parametric analysis, based on the classical friction micro-mechanisms activated during operation of several tribosystems, allowed distinguishing different performance of ceramic to ceramic, metal to metal and metal to ceramic systems. The dominant parameters influencing the friction coefficient values are the surface roughness of the brittle bodies, the plastic deformation of the ductile ones, as well as the intervention of wear debris remaining at the contact interface.

REFERENCES

[1] K.G. Budinski, Surface Engineering for Wear Resistance, Prentice Hall, NJ, 1988.

[2] L. Pawlowski, The Science and Engineering of Thermal Spray Coatings, Wiley, New York, 1995.

[3] A. Koutsomichalis, N. Vaxevanidis, G. Petropoulos, E. Xatzaki, A. Mourlas, S. Antoniou, Tribological Coatings for Aerospace Applications and the Case of WC-Co Plasma Spray Coatings, Tribology in Industry, Vol. 31, No 1-2, pp. 37-42, 2009.

[4] N.M. Vaxevanidis, D.E. Manolakos and G.P. Petropoulos, Surface integrity and tribology behavior of plasma sprayed alumina coatings on steel and aluminum substrates, Journal of the Balkan Tribological Association, Vol.12, No 1, pp.95-103, 2006.

[5] P. P. Psyllaki, M. Jeandin, D. I. Pantelis: Microstructure and wear mechanisms of thermal-sprayed alumina coatings, Materials Letters, Vol. 47, No 1-2, pp. 77-82, 2001.

[6] D. I. Pantelis, P. P. Psyllaki, N. Alexopoulos: Tribological behaviour of plasma-sprayed Al_2O_3 coatings under severe wear conditions, Wear, Vol. 237, No 2, pp. 197-204, 2000.

Serbian Tribology Society

SERBIATRIB '11

12th International Conference on Tribology

Faculty of Mechanical Engineering in Kragujevac

Kragujevac, Serbia, 11 – 13 May 2011

NANO CHARACTERIZATION OF HARD COATINGS WITH ADITIONAL ION IMPLANTATION

B Škorić[1], G. Favaro[2], D. Kakaš[3], A. Miletić[1], D. Ješić[3]

[1] University of Novi Sad, Faculty for Technical Sciences, Serbia, skoricb@uns.ac.rs

[2]CSM Instruments SA, Peseux, Switzerland

[3]University of Banja Luka, Faculty of Engineering, Bosnia and Herzegovina

Abstract: *In the paper are presented characteristics of hard coatings, type TiN, produced by classic technology PVD (physical vapour deposition) and IBAD (ion beam assisted deposition). Wear resistance and exchanges of friction coefficient was measured with on line test using special designed tribology equipment. Following the tests, the wear zone morphology and characteristics of surface layer structure as well as important properties were investigated. In the nanoindentation technique, hardness and Young's modulus can be determined by the Oliver and Pharr. Therefore, in recent years, a number of measurements have been made in which nanoindentation and AFM have been combined. Indentation was performed with CSM Nanohardness Tester. The results are analyzed in terms of load-displacement curves, hardness, Young's modulus, unloading stiffness and elastic recovery.The analysis of the indents was performed by Atomic Force Microscope. A variety of analytic techniques were used for characterization, such as scratch test, calo test, SEM, AFM, XRD and EDAX.*

Keywords: *nano, coating, super hard, ion implantation, wear.*

1. INTRODUCTION

The film deposition process exerts a number of effects such as crystallographic orientation, morphology, topography, densification of the films. The optimization procedure for coated parts could be more effective, knowing more about the fundamental physical and mechanical properties of a coating. In this research are present the results of a study of the relationship between the process, composition, microstructure and nanohardness.

A duplex surface treatment involves the sequential application of two surface technologies to produce a surface composition with combined properties[1]. A typical duplex process involves plasma nitriding and the coating treatment of materials. In the paper are presented characteristics of hard coatings deposited by PVD (physical vapour deposition) and IBAD (ion beam assisted deposition). The synthesis of the TiN film by IBAD has been performed by irradiation of Ar ions. Subsequent ion implantation was provided with N^{5+} ions. Ion implantation has the capabilities of producing new compositions and structures unattainable by conventional means. Implantation may result in changes in the surface properties of a material [1].

Thin hard coatings deposited by physical vapour deposition (PVD), e.g. titanium nitride (TiN) are frequently used to improve tribological performance in many engineering applications [2].

In many cases single coating cannot solve the wear problems [3].

Conventional TiN and correspondingly alloyed systems show high hardness and good adhesion strength. However, these coatings have poor cracking resistance especially in high speed machining. The duplex surface treatment was used to enhance adhesion strength and hardness of hard coatings.

In the nanoindentation technique, hardness and Young's modulus can be determined by the Oliver and Pharr method, where hardness (H) can be defined as: $H = \frac{P_{max}}{A}$, where P_{max} is maximum applied load, and A is contact area at maximum load. In nanoindentation, the Young's Modulus, E, can be obtained from:

$$\frac{1}{E_r}=\frac{1-\nu^2}{E}+\frac{1-\nu_i^2}{E_i},$$

where v_i=Poisson ratio of the diamond indenter (0.07) and Ei=Young's modulus of the diamond indenter.

This paper describes the use of the nanoindentation technique for determination of hardness and elastic modulus. The depth of nanopenetration provides an indirect measure of the area of contact at full load and thus hardness is obtained by dividing the maximum applied load with the contact area [4].

2. EXPERIMENTAL

The substrate material used was high speed steel type M2 Prior to deposition the substrate was mechanically polished to a surface roughness of 0.12 μm (R_a). The specimens were first austenized, quenched and then tempered to the final hardness of 850 HV. In order to produce good adhesion of the coating, the substrates were plasma nitrided at low pressure (1×10^{-3} Pa), prior to deposition of the coating. The PVD treatment was performed in a Balzers Sputron installation with rotating specimen. The deposition parameters were as follows: Base pressure in the chamber was 1×10^{-5} mbar. During etching, bias voltage was U_b=1 kV, current I_d=50 mA. During deposition substrate temperature was T_s=200 °C, partial pressure of Ar was $P_{Ar}= 1\times10^{-3}$ mbar and partial pressure of N_2 was $P_{N2}=3\times10^{-4}$ mbar. Prior to entering the deposition chamber the substrates were cleaned.

The IBAD system consists of an e-beam evaporation source for evaporating Ti metal and 5-cm-diameter Kaufman ion source for providing argon ion beam. Base pressure in the IBAD chamber was 1×10^{-6} mbar. The partial pressure of Ar during deposition was (3.1–6.6) $\times 10^{-6}$ mbar and partial pressure of N_2 was 6.0×10^{-6}–1.1×10^{-5} mbar. The ion energy (E_{Ar}=1.5–2 keV), ion beam incident angle (15°), and substrate temperature T_s=200 °C, were chosen as the processing variables. Deposition rate a_D=0.05–0.25 nm/s. Quartz crystal monitor was used to gauge the approximate thickness of the film. After deposition, the samples were irradiated with 120 keV, N^{5+} ions at room temperature (RT). The Ion Source is a multiply charged heavy ion injector, based on the electron cyclotron resonance effect (EC.R). The implanted fluencies were in the range from 0.6×10^{17} to 1×10^{17} ions/cm^2.

A pure titanium intermediate layer with a thickness of about 50nm has been deposited first for all the coatings to enhance the interfacial adhesion to the substrates.

The mechanical properties on coated samples were characterized using a Nanohardness Tester (NHT) developed by CSM Instruments, Nanoindentation testing was carried out with applied loads in the range of 10 to 20 mN. A Berkovich diamond indenter was used for all the measurements. The data was processed using proprietary software to produce load–displacement curves and the mechanical properties were calculated using the Oliver and Pharr method.

Scratch adhesion testing was performed using commercially available equipment (REVETEST CSEM) fitted with a Rockwell C diamond stylys (cone apex angle of 120^{o}C, tip radius 200 μm). Acoustic Emission (AE) is an important tool for the detection and characterization of failures in the framework of non-destructive testing. The analyzed AE signal was obtained by a scratching test designed for adherence evaluation. Detection of elastic waves generated as a result of the formation and propagation of micro cracks.

The tribological behavior of the coatings was studied by means of pin-on-ring contact configuration in dry sliding conditions, described elsewhere [5].

X-ray diffraction studies were undertaken in an attempt to determine the phases present, and perhaps an estimate of grain size from line broadening. The determination of phases was realized by X-ray diffraction using PHILIPS APD 1700 X-ray diffractometer. The X-ray sources were from CuKα with wavelength of 15.443 nm (40 kV, 40 mA) at speed 0.9°/min. The surface roughness was measured using stylus type (Talysurf Taylor Hobson) instruments. The most popular experimental XRD approach to the evaluation of residual stresses in polycrystalline materials is the $\sin^2\psi$ method. The method requires a θ-2θ scan for every ψ angle around the selected diffraction peak and, in order to emphasize the peak shifts.

3. RESULTS

The nitrogen to metal ratio (EDX), is stoichiometries for IBAD technology and something smaller from PVD (0.98). For sample with additional ion implantation, value is significantly different, smaller (0.89). It is possibly diffused from the layer of TiN to the interface.

All the results of nanohardness are obtained with the Oliver & Pharr method and using a supposed sample Poisson's ratio of 0.3 for modulus calculation The analysis of the indents was performed by Atomic Force Microscope (Figure 1).

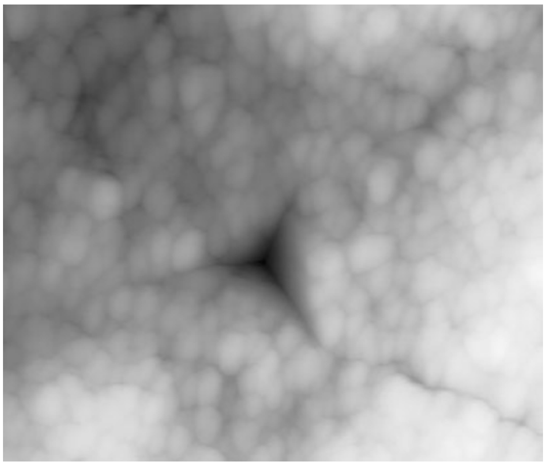

Figure 1. AFM image of crack paths from nanoidentation

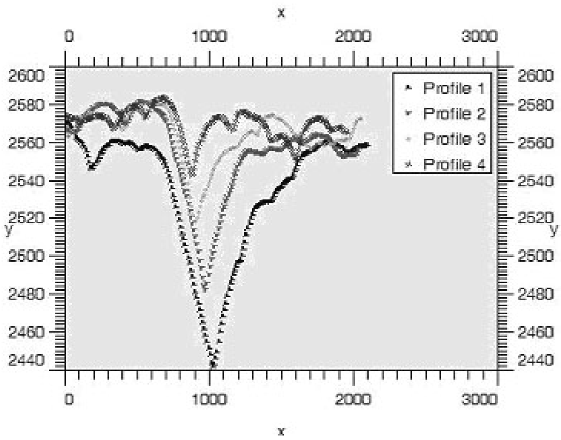

Figure 2. Cross section of the indentation

It can be seen, from cross section of an indent during indentation, that the indents are regularly shaped with the slightly concave edges tipically seen where is significant degree of elastic recovery.(Figure 2).

The nanohardness values and micro hardness are shown in Table 1.

Table 1. Surface mamohardness (load-10mN)

Unit	pn/IBAD	PVD	pn/PVD/II
GPa	21.6	32.6	42.6

For each adhesion measurement, the penetration (Pd), the residual penetration (Rd), the acoustic emission (AE) and the frictional force are recorded versus the normal load. The breakdown of the coatings was determined both by AE signal analysis and scanning electron microscopy. AE permits an earlier detection, because the shear stress is a maximum at certain depth beneath the surface, where a subsurface crack starts. Critical loads are presents in Table 2.

Table 2. Critical loads for different type of coatings

	pn/TiN(IBAD)	*pn/TiN(PVD)*
Lc1	-	23
Lc2	100	54
Lc3	138	108

The critical load Lc1 corresponds to the load inducing the first crack on the coating. No cracks were observed on sample 1.The critical load Lc2 corresponds to the load inducing the partial delamination of the coating. The critical load Lc3 corresponds to the load inducing the full delamination of the coating. In some places of hard coatings cohesive failure of the coating and the delamination of the coating were observed, (Figure 3).

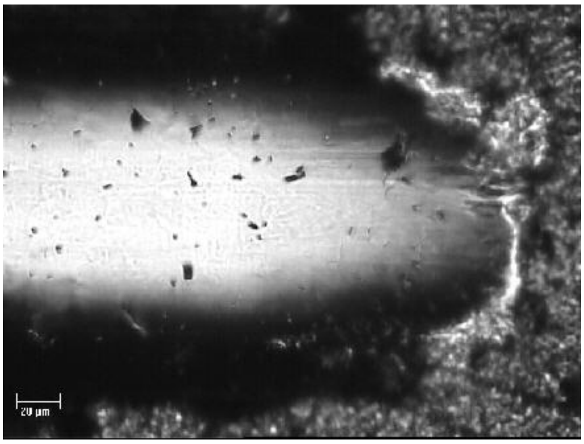

Figure 3. Delamination of coating

It was found that the plasma-nitriding process enhanced the coating to substrates adhesion. In some places of hard coatings cohesive failure of the coating and the delamination of the coating were observed, Figure 4.

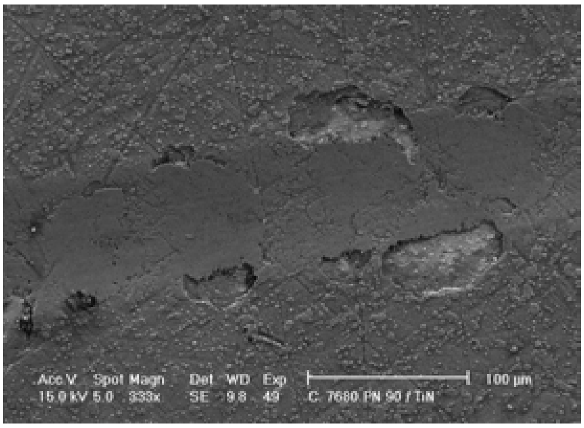

Figure 4. SEM morphology of scratch test pn/TiN(PVD).

The friction coefficient of sample with duplex coating with additional ion implantation, is presented in Figure 5.

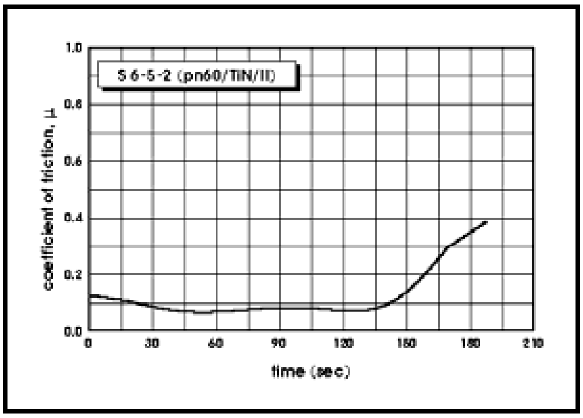

Figure 5. Friction Coefficient of pn/TiN/II.

The curves of friction coefficient are clearly reproducible and distinctively show a lower rise in friction coefficient for the composite (plasma nitrided/TiN) coated specimens and much lower for sample with additional ion implantation (under 0.1).

The reduction of strength, caused by high contact temperature, and high contact pressure in the contact zone, increases local deformability, thus produce enlarging of wear zone. When one considers the intimate contact of two sliding surfaces where hard particles are either present or formed during sliding, abrasive wear can occur as a consequence of both plastic deformation and fracture mechanisms. Damage to the coating surface is superficial (only a small polishing effect on TiN asperities can be seen and steel substrate is not exposed) by comparison with that inflicted by the other pin materials. At the worn zone are presented traces of adhered products of wear debris from counter-material. This adhered wear debris promotes new condition for wear at the tribological contact and influence on decreasing the wear and friction coefficient. When the steel counterface pin material is a softer material such as mild steel, under low-humidity conditions at low contact loads and speeds, the TiN wear mechanism reverts to regime with minimal damage to the coating, high steel wear and transfer of steel oxides to the TiN. As known, the sliding process is accompanied with the thermal effects. This is most common tribological contact condition and is often combined with high contact stress [6]. The significant part of the mechanical energy is converted into thermal energy. However, this thermal energy is inappropriate and the converted heat would be able to consider as a waste heat with negative environmental consequences.

The wear resistance of the TiN coating was obviously improved by the presence of a nitride interlayer. Such an improvements is probably due to the adequate bonding between the nitrided layer and substrate. Energy depressive analyze with X-ray (EDAX), of the transfer layer showed that the transfer layer consists of small amount of counter material (adhesive wear), Figure 6.

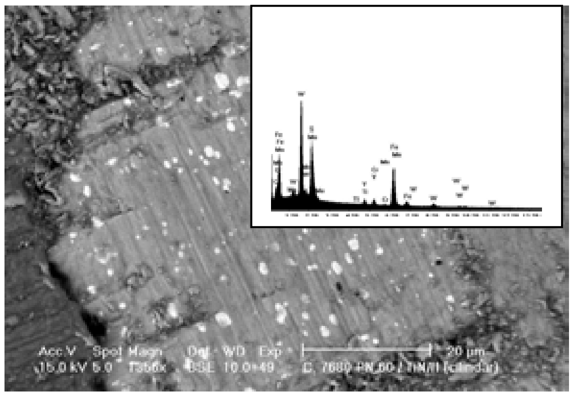

Figure 6. SEM micrograph of part with wear debris and EDAX image of wear debris.

Adhesive wear plays the predominant part in failure due to wear. Experience shows that every tribological system can be optimized by selecting the right coating.

The width of column, for plane (422), is derived from the width of the diffraction peaks (Scherrer formula):

$$t = \frac{0.9\lambda}{\beta \cos\frac{\theta}{\lambda} \cos\theta}$$

of TiN, (λ=0.154nm, θ=62.5^o and β=0.056rad), and it is 70 nm. Becouse of low deposition temperature, it is possible that another planes also have small width of columns.

The stress determination follows the conventional $\sin^2\psi$ method. Stress determination was performed using a PHILIPS XPert diffractometer. The (422) diffraction peak was recorded in a 2θ interval between 118^o and 130^o, with tilting angle: ψ_o^1=0°, ψ_o^2=18.75°, ψ_o^3=27.03°, ψ_o^4=33.83°, ψ_o^5=40°. A typical result for compact film, with residual stresses σ = -4.28Gpa, has TiN(PVD).

4. DISCUSION

A hardness increase is observed for implanted samples. This can be attributed to iron nitride formation in the near surface regions. The standard deviation of the results is relatively important due to the surface roughness of the samples. Because the thickness of the TiN coatings presented here is sufficiently large, which for all coatings is about 2900 nm (TiN-PVD), the hardness measurements will not be affected by the substrate, as in three times thinner (900 nm TiN-IBAD).

The individual values of E are the different for all measurements. The errors related to the measurements and estimations were different and for duplex coating with ion implantation is less than 4%. Good agreement could be achieved between the E_c values and nanohardness.

The topography of TiN coatings was investigated SEM (Figure 7).

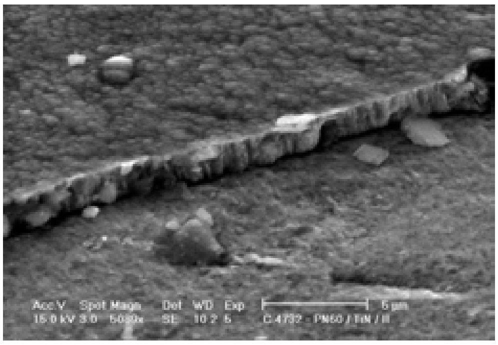

Figure 7. Surface morphology of coating with ion implantation.

The PVD coating process did not significantly change roughness. For the practical applications of IBAD coatings, it is important to know that the roughness of the surface decreased slightly after deposition (from Ra=0.19 μm to Ra=0.12 μm).

The formation of TiN by IBAD has its origin in a kinetically controlled growth. The nitrogen atoms occupy the octahedric sites in varying number according to the energy that these atoms possess to cross the potential barriers created by the surrounding titanium anions. The ion bombardment is believed to enhance the mobility of the atoms on the sample surface. The coating morphology was evaluated using the well-known structure zone model of Thornton. All observed morphologies, Figure 8, are believed to be from region of zone I (PVD) and from the border of region zone T (IBAD).

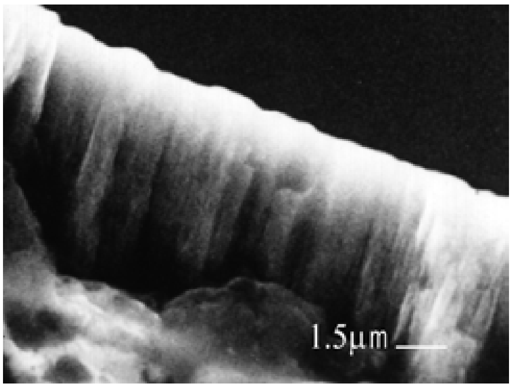

Figure 8. SEM of coating cross-section TiN(PVD).

It has been suggested [7], that the transition from open porous coatings with low micro hardness and rough surface, often in tensile stress to dense coatings films with greater micro hardness, smooth surface occurs at a well defined critical energy delivered to the growing film.

5. CONCLUSIONS

The experimental results indicated that the mechanical hardness is elevated by penetration of nitrogen, whereas the Young's modulus is significantly elevated. Nitrogen ion implantation leads to the formation of a highly wear resistant and hard surface layer.

Nitrogen implantation into hard TiN coatings increases the surface hardness and significantly reduces the tendency of the coatings to form micro cracks when subjected to loads or stresses.

The above findings show that deposition process and the resulting coating properties depend strongly on the additional ion bombardment.

The present coating method can produce dance structures, high hardness and the high critical load values can be achieved. Tribological tests confirm that these composite coatings are wear resistant and provide very low friction coefficient

REFERENCES

[1] S.Zheng Y.Sun, T.Bell and J.M. Smith, Mechanical properties microprobing of TiN coatings deposited by different techniques, The Fourth European Conference on Advanced Materials, p.p.177-184, 1995.

[2] V.Nelea, C.Ristoscu, C. Ghica, I. Mihailescu, P. Mille, 2000, Hydroxyapatite thin films growth by pulsed laser deposition: effects of the Ti alloys substrate passivation on the film properties by the insertion of a TiN buffer layer, *Sixth Conference on Optics*, Bucharest, Romania, p.p.247-252, 2000..

[3] W. Ensinger, Ion bombardment effects during deposition of nitride and metal films, Surface and Coatings Technology, 99, p.p. 1-13, 1998.

[4] M. Pharr, D.S. Harding, W.C. Oliver, in: M. Nastasi et al. Mechanical Properties and Deformation Behavior of Materials Having Ultra-Fine Microstructures, Kluwer, Dordrecht, p.p.449, 1993,

[5] B. Skoric, D. Kakas, Influence of plasma nitriding on mechanical and tribological properties of steel with subsequent PVD surface treatments Thin Solid Films, 317, p.p.486-489, 1988.

[6] Sekulić, M. , Jurkovič, Z. , Hadžistevič, M., Gostimirovič, M, The influence of mechanical properties of workpiece material on the main cutting force in face milling Metalurgija, 49,p.p.339-342, 2010.

[7] M. Griepentrog, at all, Properties of TiN hard coatings prepared by unbalanced magnetron sputtering and cathodic arc deposition using a uni- and bipolar pulsed bias voltage, Surface and Coatings Technology, 74-75, p.p.326-332,1995.

Serbian Tribology Society

SERBIATRIB '11

12th International Conference on Tribology

Faculty of Mechanical Engineering in Kragujevac

Kragujevac, Serbia, 11 – 13 May 2011

NANOSTRUCTURED AlN/TiN FILMS GROWN BY REACTIVE SPUTTERING OR ION IMPLANTATION OF Al/Ti MULTILAYERS

M. Milosavljević [1,3,*], D. Peruško[1], D. Pjević[1], M. Obradović[1], M. Mitrić[1], M. Čizmović[1], J. Kovač[2], P. Panjan[2] and C. Jeynes[3]

[1]VINČA Institute of Nuclear Sciences, Belgrade, Serbia
[2]Jožef Stefan Institute, Ljubljana, Slovenia
[3]University of Surrey Ion Beam Centre, Guildford ,United Kingdom
*Corresponding author, e-mail: momirm@vin.bg.ac.rs

Abstract: *A comparative study of AlN/TiN multilayers, grown by reactive sputtering of AlN and TiN, and by implantation of nitrogen into metallic Al/Ti multilayers, is presented. The (AlN/TiN)x5 and (Al/Ti)x5 multilayers with a total thickness of ~270 nm were deposited on Si(100). The Al/Ti structures were implanted with 200 keV N_2^+, to $1x10^{17}$ and $2x10^{17}$ at/cm^2, and AlN/TiN were irradiated with argon ions. It was found that sputter deposited AlN/TiN multilayers are well separated, with sharp interfaces and a nanocrystalline structure, remaining stable after argon ion irradiation. Nitrogen implantation of Al/Ti induced a pronounced intermixing, resulting in a graded multilayered structure, with different content of Al, Ti and N. In all cases nano-hardness increased with ion implantation fluence.*

Keywords: *AlN/TiN multilayers, reactive sputtering, ion irradiation, graded composition, nanocrystalline structure, nano-hardness*

1. INTRODUCTION

Nano-scaled multilayered coatings of metals and metal-nitrides offer numerous advantages over single component coatings, such as much higher hardness and strength due to a large number of interfaces, possibilities to form super lattices, graded composition, denser and less porous structures [1-4]. High strength nanolayered structures are also interesting as radiation protective materials, because of a large number of interfaces that act as obstacles to slip and sinks for radiation induced defects [5,6]. Multilayers composed of AlN/TiN provide the same performance at much lower thickness compared to thick single layers such as TiN or (Al,Ti)N, and have microstructural stability up to 1000^{o}C [7-9]. For very low thicknesses of individual layers (a few nm), these multilayers can form superlattices [8].

The use of ion beam processing in fabrication of thin film structures can be beneficial towards achieving better adhesion to the substrate, relaxing the interface stresses, increasing the film density and decreasing porosity. In this work we have studied the properties of TiN/AlN multilayers grown by reactive sputtering, and the changes induced upon irradiation with argon ions. We have also studied the formation of graded (AlTi)N multilayers by high fluence nitrogen ion implantation into Al/Ti multilayered structures.

2. EXPERIMENTAL DETAILS

Multilayered AlN/TiN and Al/Ti structures were deposited on Si(100) wafers, in a Balzers Sputtron II system, using 1.5 keV argon ions and 99.9% pure Al or Ti targets. The starting structures consisted of (AlN/TiN)x5 and (Al/Ti)x5, with a total thickness of ~270 nm. Depositions were done in a single vacuum run for each of the analyzed systems, switching from one target to the other. The base pressure in the chamber was around $1x10^{-6}$ mbar, and the argon partial pressure $1x10^{-3}$ mbar. For preparation of metal-nitride layers we used reactive sputtering, introducing high purity nitrogen in the vacuum chamber at a partial pressure of $3x10^{-4}$ mbar.

The (Al/Ti)x5/Si structures were implanted with 200 keV N_2^+ ions, to the fluences of $1x10^{17}$ and $2x10^{17}$ at/cm^2. The (AlN/TiN)x5/Si were irradiated with 200 keV Ar^+, to $5x10^{15}$ - $4x10^{16}$ ions/cm^2. All implantations were done at room temperature, with a beam current of ~ 1 μA/cm^2, to avoid beam heating of the samples The projected ion range in both cases was around mid-depth of the deposited structures, as calculated by TRIM [10].

Structural and compositional characterizations of the samples were done by Rutherford backscattering spectrometry (RBS), X-ray photoelectron spectroscopy (XPS), X-ray diffraction (XRD) and transmission electron microscopy (TEM). For RBS analysis a 1.5 MeV He^+ ion beam, generated by a 2 MV Tandetron accelerator from HV Europe was used [11]. Random RBS spectra at normal incidence to the sample surface were collected. The experimental data were analyzed with the NDF code [12]. XPS photoelectron spectroscopy analyses were carried out on the PHI-TFA XPS spectrometer produced by Physical Electronics Inc. Ion sputtering was performed with a 3 keV Ar^+ ion beam scanned over an area of 4 x 4 mm^2. The analyzed area was 0.4 mm in diameter. XPS spectra were excited by X-ray radiation from an Al-standard source. During depth profiling the samples were rotated to improve the depth resolution. For XRD analysis Cu K_α X-ray diffraction patterns were collected by Bruker D8 Advance Diffractometer. The step was 0.05^o and the time interval 10 s per step. TEM imaging was done on a Philips EM 400T microscope at 120 kV, the samples being prepared for cross-sectional analysis by ion beam thinning.

Nano-hardness measurements were done by the Vicker's method, using a pyramidal indenter with the top angle of 136^o. The applied load was 5 mN, so the indenter penetrates to around mid-depth of the multilayered structures. Due to a high influence of the substrate, the measured values of nano-hardness should be considered as relative.

3. RESULTS AND DISCUSSION

Elemental depth profiles obtained by XPS analysis of as-deposited (AlN/TiN)x5/Si sample and a sample implanted with argon to $4x10^{16}$ ions/cm^2, are shown in Fig. 1. Both depth profiles show well separated Al and Ti signals. The TiN layers are stoichiometric and the AlN layers are nitrogen rich, as was also determined by RBS. A build up of surface oxide is registered in the implanted sample. Ion irradiation causes an increased concentration of Ti in the second and third AlN layer up to about 5 at% and consequently decreases the concentration of Al and N in the same region. This suggests that some migration of Ti atoms occurred only in these AlN layers, located in the region where the highest radiation damage is deposited by the impact ions. Apart from this, the AlN and TiN layers remain well separated after ion irradiation.

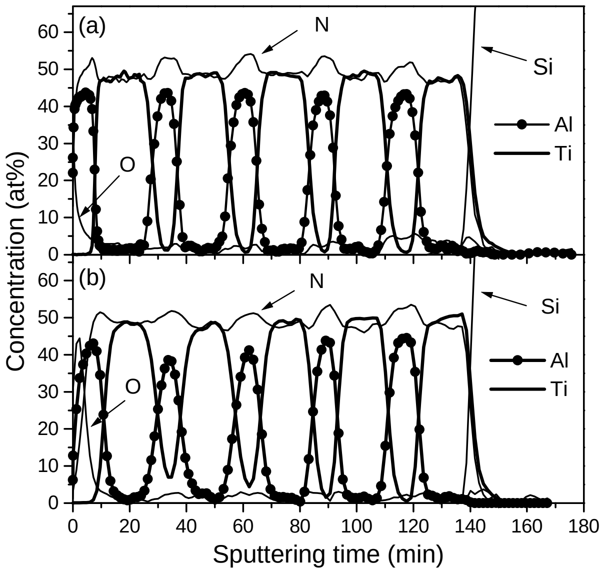

Figure 1. XPS depth profiles of (AlN/TiN)x5/Si: (a) as-deposited sample; (b) sample implanted with argon to $4x10^{16}$ ions/cm^2.

RBS analysis of (Al/Ti)x5/Si structures is presented in Fig. 2. Experimental spectra taken from an as-deposited sample and a sample implanted with nitrogen to $2x10^{17}$ at/cm^2 are shown in (a). It is seen that the initial as-deposited structure exhibits well separated Ti and Al signals from individual layers. After implantation the RBS yield arising from Ti and Al becomes lower and broader. We also observe a build up of backscattering yield arising from the implanted nitrogen, and a surface oxygen peak which increases after ion irradiation. Extracted depth profiles from sample implanted with nitrogen to $2x10^{17}$ at/cm^2 are shown in (b). The profiles show that Al and Ti become almost fully intermixed, especially at mid-depth of the structure, where a maximum concentration of nitrogen (~ 30 at%) was detected. Also, oxygen is detected at the surface, and there is a small fraction of argon, which was used as a sputtering gas and to clean the Si substrates before deposition.

XRD spectra taken from an as-deposited (Al/Ti)x5/Si, and from a sample implanted with nitrogen to $2x10^{17}$ at/cm^2, are shown in Fig. 3. Well defined Al and Ti diffraction peaks are seen in the as-deposited sample. In the implanted sample these peaks are shifted, their relative intensity is altered, and they become markedly broadened, suggesting the appearance of other phases. There is a number of possible reflections that can appear in the small 2Θ range from 35-40^{o}, which correspond to various Al-Ti intermetallic compounds and their nitrides. We have marked in the figure the positions that correspond to AlN, TiN, Ti_2AlN, Ti_3AlN and Ti_3Al phases. It is difficult to distinguish isolated peaks for each of these phases, though this analysis is in agreement with RBS results. The layers are fully intermixed, and the possible formed phases are intermetallic Al-Ti and metal-nitrides with various composition.

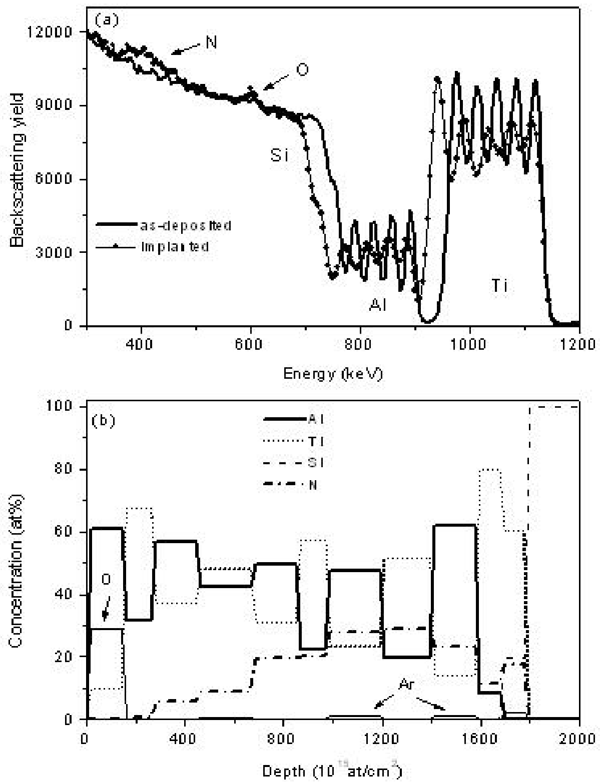

Figure 2. RBS analysis of (Al/Ti)x5/Si: (a) experimental spectra from an as-deposited sample and sample implanted with nitrogen to $2x10^{17}$ at/cm^2; (b) extracted depth profiles of the implanted sample.

The results of cross-sectional TEM analysis are shown in Figs. 4 & 5. Bright field image in (4a) was taken from as-deposited (AlN/TiN)x5/Si, and in (4b) after implantation of this structure with argon to $2x10^{16}$ ions/cm^2. Bright contrast corresponds to AlN layers and dark to TiN. In both cases the AlN and TiN layers are well separated, having a very fine nanocrystalline structure. Ion irradiation induces an enlargement of crystal grains in individual layers, from ~10 to ~20 nm. Also, some thickness increase is registered in the top three AlN/TiN bilayers, where the most damage is deposited and most of the Ar^+ ions are being stopped. Analysis of as-deposited (Ti/Al)x5/Si is shown in (5a), and of this structure implanted with nitrogen to $2x10^{17}$ at/cm^2 in (5b). White contrast is from Al layers and dark from Ti. Here we observe that initially well separated Al and Ti layers become fully intermixed after ion implantation. The mean grain size in the layers increases from ~30 to ~80 nm, and the contrast becomes unified in the region where most intermixing occurred. However, the multilayered nature of the structure is preserved.

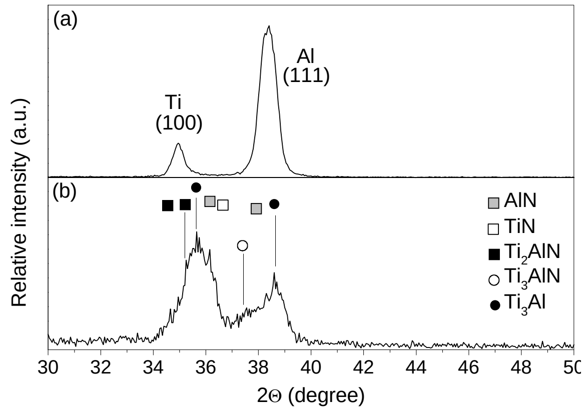

Figure 3. XRD spectra: (a) from as-deposited (Al/Ti)x5/Si; (b) sample implanted with nitrogen to $2x10^{17}$ at/cm^2.

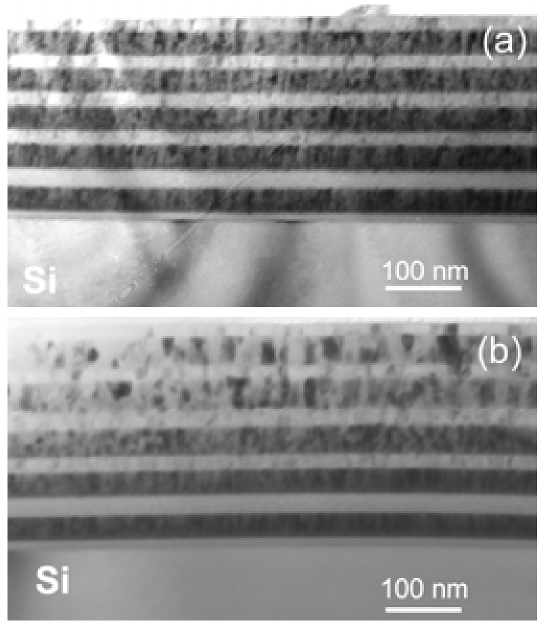

Figure 4. Bright field cross-sectional TEM images of: (a) as-deposited (AlN/TiN)x5/Si; (b) (AlN/TiN)x5/Si implanted with argon to $2x10^{16}$ ions/cm^2.

The results of nano-hardness measurements as a function of the irradiation fluence for both structures are plotted in Fig. 6. As a reference we have given the measured value for a single component TiN layer, deposited to a similar thickness. It is seen that in all cases the nano-hardness increases with the irradiation fluence. Nitrogen implanted Al/Ti structures do not reach the value measured for the TiN layer, obviously because the concentration of nitrogen was not sufficient for a complete formation of metal-nitrides. On the other hand, nano-hardness of the starting AlN/TiN structures is close to that of TiN, and for higher argon fluences it increases above the TiN reference value.

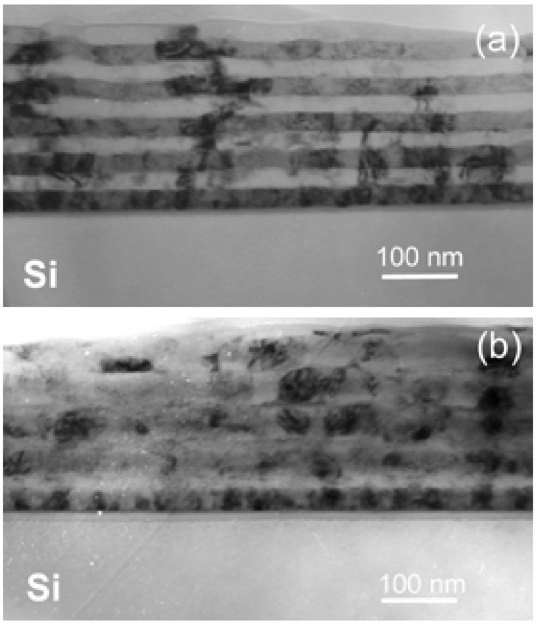

Figure 5. Bright field cross-sectional TEM images of: (a) as-deposited (Al/Ti)x5/Si; (b) (Al/Ti)x5/ implanted with nitrogen to $2x10^{17}$ at/cm^2.

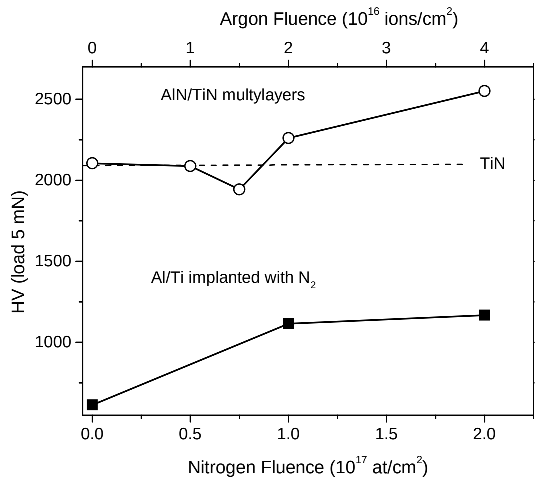

Figure 6. Nano-hardness as a function of the irradiation fluence for both (AlN/TiN)x5/Si and (Al/Ti)x5/Si structures.

There is a pronounced difference in the behavior of the two systems upon ion irradiation. The AlN/TiN layers are immiscible and stable at high temperatures [7-9]. Argon ion irradiation induced only minor structural changes, although their nano-hardness increased. The Al/Ti system is soluble and can form intermetallic compounds. Even much lighter nitrogen ions induced a totally intermixed structure. Implanted nitrogen can also interact with the target material and form metal nitrides. Multilayered structure is preserved after nitrogen implantation, but the layers have a graded composition, with different content of Al, Ti and N. The highest nitrogen concentration is around the projected ion range, while in the inner and outer regions mainly Al and Ti intermix. Because of a thorough intermixing, the resulting layers are tightly bound to each other. The measured nano-hardness did not reach the value of single component TiN, but it can be presumed that these tightly bound multilayers have a high friction and wear resistance.

4. CONCLUSION

The comparative study of sputter-deposited AlN/TiN multilayers and of nitrogen implanted Ti/Al multilayers showed a substantially different resulting structures. The sputter-deposited AlN/TiN multilayers are well separated, with a very fine nanocrystalline structure, and remain stable upon argon ion irradiation. Nitrogen implantation of Al/Ti system resulted in heavily intermixed graded multilayered structure, with different content of Al, Ti and N. In all cases nano-hardness increased with the ion implantation fluence.

ACKNOWLEDGEMENTS

We acknowledge the support from the Serbian Ministry of Education and Science (Project OI-171023), Slovenian Research Agency (Project P2-0082), and EU FP7 Project No 227012 SPIRIT.

REFERENCES

[1] W.D. Sproul, New Routes in the Preparation of Mechanically Hard Films, Science, Vol. 273, No. 5277, pp. 889-892, 1996.

[2] U. Helmersson, S. Todorova, S.A. Barnett, J.E. Sundgren, L.C. Markert, and J.E. Greene, Growth of single-crystal TiN/VN strained-layer superlattices with extremely high mechanical hardness, J. Appl. Phys., Vol 62, Iss. 2, pp. 481-484, 1987.

[3] D. Li, L.W. Lin, C.C. Cheng, V.P. Dravid, Y.W. Chung, M.S. Wong, and W.D. Sproul, Structure and hardness studies of CNx/TiN nanocomposite coatings, Appl. Phys. Lett., Vol. 68, No. 9, pp. 1211-1213, 1996.

[4] S. PalDey, S.C. Deevi, Single layer and multilayer wear resistant coatings of (Ti,Al)N: a review, Materialas Science and Engineering A, Vol 342, pp. 58-79, 2003.

[5] T. Höchbauer, A. Misra, K. Hattar, and R.G. Hoagland, Influence of interfaces on the storage of ion-implanted He in multilayered metallic composites, J. Appl. Phys., Vol. 98, Iss. 12, Art. No. 123516-1-7, 2005.

[6] A. Misra, M.J. Demkowicz,X. Zhang, and R.G. Hoagland, The radiation damage tolerance of ultra-high strength nanolayered composites, JOM Vol. 59, Iss. 9, pp. 62-65, 2007.

[7] A. Madan, I.W. Kim, S.C. Cheng, P. Yashar, V.P. Dravid, and S.A. Barnett, Stabilization of cubic AlN in epitaxial AlN/TiN superlattices, Phys. Rev. Lett., Vol. 78, Iss. 9, pp. 1743-1746, 1997.

[8] Y.Y. Wang, M.S. Wong, W.J. Chia, J. Rechner, and W.D. Sproul, Synthesis and characterization of highly textured polycrystalline AlN/TiN superlattice coatings, J. Vac. Sci. Technol. A Vol. 16, No. 6, pp. 3341-3347, 1998.

[9] D.G. Kim, T.Y. Seong, Y.J. Baik, Effects of annealing on the microstructures and mechanical properties of TiN/AlN nano-multilayer films prepared by ion-beam assisted deposition, Surface and Coatings Technology, Vol. 153, No. 1, pp. 79-83, 2002.

[10] J.F. Ziegler, J.P. Biersack, and U. Littmark: The Stopping and Range of Ions in Solids, Pergamon, New York, 1985.

[11] A. Simon, C. Jeynes, R.P. Webb, R. Finnis, Z. Tabatabaian, P.J. Sellin, M.H.B. Breese, D.F. Fellows, R. v-d Broek, R.M. Gwilliam, The new Surrey ion beam analysis facility, Nucl. Instrum. Meth. B Vol. 219-220, p.p. 405-409, 2004.

[12] N.P. Barradas, C. Jeynes, R.P. Webb, Simulated annealing analysis of Rutherford backscattering data Appl. Phys. Lett., Vol. 71, p.p. 291-293, 1997.; C. Jeynes, N.P. Barradas, P.K. Marriott,G. Boudreault, G.M. Jenkin, E. Wendler, and R.P. Webb, Elemental thin film depth profiles by ion beam analysis using simulated annealing - a new tool, J.Phys.D: Appl.Phys., Vol. 36, p.p. R97-R126. 2003.

Serbian Tribology Society

SERBIATRIB '11

12th International Conference on Tribology

Faculty of Mechanical Engineering in Kragujevac

Kragujevac, Serbia, 11 – 13 May 2011

INFLUENCE OF SLIDING SPEED AND SURFACE ROUGHNESS ON THE FRICTION COEFFICIENT AND WEAR OF TIN COATINGS DEPOSITED AT LOW TEMPERATURE

D. Kakaš[1], B. Škorić[1], P. Terek[1], L. Kovačević[1], A. Miletić[1], M. Vilotić[1], S. Mitrović[2], M. Babić[2],

[1] Faculty of Technical Sciences, University of Novi Sad, Serbia, terekpal@gmail.com

[2] Faculty of Mechanical Engineering, University of Kragujevac, Serbia, boban@kg.ac.rs

Abstract: *Wear behavior of TiN coatings during dry reciprocating sliding against an alumina ball was studied. The research focus was on the influence of sliding speed on friction and wear. In addition, the coatings of different surface roughness were tested in order to find the optimum one. The range of surface roughness analyzed in this research provides insight into a rarely studied domain of fine surface finish. The wear tests were conducted at low load with low sliding speeds in order to determine the wear behavior of TiN coatings in mild conditions. Low values of friction coefficient were obtained, ranging from 0.13 to 0.24. The decreasing trend of the friction coefficient and increasing trend of the wear rate with increase in the sliding speed were observed for the coatings of different surface roughness. The highest friction coefficient was found on the roughest specimen, while the smoothest specimen exhibited the highest wear rate. The different wear behavior is due to different wear mechanisms acting on specimens with different roughness. For the tests conditions and range of surface roughness studied, the coating with roughness of 20 nm has the optimum surface finish. This coating exhibited low friction coefficient and the lowest wear rate. No significant difference in wear behavior was found when sliding transversal and parallel to machining ridges.*

Keywords: *IBAD, TiN, reciprocating sliding, sliding speed, surface roughness*

1. INTRODUCTION

Their high hardness, good adhesion to steel substrates and good thermal and chemical stability make TiN coatings suitable for wear protection of various mechanical components. Although tribological properties of TiN coatings have been widely studied, there is still a number of possible application areas where behavior of TiN coatings during wear is to be investigated. Understanding of wear mechanisms occurring during contact of TiN with other materials plays a great role in expanding its exploitation field [1].

Tribological behavior of coated mechanical components depends on a great number of parameters. For a selected coating it depends on mechanical, physical and chemical properties of counter material, on surface roughness and working conditions (environment, contact geometry, contact pressure). In practice, it is not possible to theoretically link these factors to tribological response of coated elements. True tribological behavior can only be determined experimentally, [2], [3], [4].

Tribological studies of hard coatings are usually conducted by using sliding test with high normal loads and high sliding speeds. On the other hand, mechanical components are often wearing at rates of nanometers per hour. In addition, a number of applications where sliding occurs at low normal loads and low sliding speeds is constantly increasing [5], [6]. Therefore, in this research tribological properties were evaluated using low loads and low sliding speeds.

The coating tribological behavior was studied in reciprocating sliding under milli-Newton loads. Special consideration was given to the influence of sliding speed on a friction and wear of coatings with different surface roughness.

There are several parameters which are applied to quantify the wear performances of hard coatings. A worn volume is the one usually used, although this parameter is not as practical as wear rate [7] which was used in the present study.

2. MATERIALS AND EXPERIMENTAL

Studied coatings were prepared in an Ion Beam Assisted Deposition (IBAD) chamber with a base pressure of 1.5x10-6 mbar. The coatings were deposited at low temperatures around 50^0C. Carburizing steel (20MnCr5) disks were used as a substrate material. The substrates were prepared with three grades of surface roughness: Specimen 1 – substrate ground using 400 grit SiC paper; Specimen 2 - substrate ground using 1500 grit SiC paper; Specimen 3 - substrate polished using 1µm diamond paste.

Substrate hardness was measured by standard Vickers hardness test while coating hardness was assessed by using the "Fischerscope HM2000 S" Microhardness Measurement System.

Friction and wear behavior was evaluated by ball-on-plate nanotribometer. The reciprocating sliding tests were conducted in air at room temperature. An alumina ball with diameter of 1,5mm was used as a counterpart material. The wear tests were performed using the sliding speeds of 10, 15 and 25 mm/s and the applied normal load of 100 mN. A stroke length of 1 mm was used in all tests which were stopped after 3000 cycles. All tribo-tests were repeated two times.

Scanning electron microscope (SEM JEOL JSM 6460 LV) was applied to investigate morphology of worn zones. Specimen surface roughness and morphology of worn zones were evaluated by VEECO di-CPII atomic force microscope (AFM). All images were acquired in contact AFM mode using a symmetrically etched silicon-nitride probe. The scan size was 90x90 μm^2 while scan rate and set point were kept at 0.5 Hz and 225 nN respectively.

Worn volume "*V*" was determined by measuring the worn channels produced during reciprocating sliding and including the dimension of the alumina ball. The representative worn volume was calculated for a worn channel length of 90 µm, since all channels were imaged using 90x90 μm^2 scan sizes. Sliding distance "*s*" was calculated by multiplying the length of scanned area with the number of sliding cycles. The specific wear rate "*K*" was calculated for all regimes according to equitation (1)

$$K = \frac{V}{F \cdot s} \tag{1}$$

where "*F*" presents applied normal force, "s" sliding distance, and "*V*" worn volume which was calculated by equitation (2).

$$V = L \times \left(r^2 \times arcsin\left(\frac{x}{2r}\right) - \frac{x^2}{4tan(arcsin\left(\frac{x}{2r}\right))} \right) \tag{2}$$

where "*L*" presents worn channel length, "*r*" radius of alumina ball, and "*x*" worn channel width.

3. RESULTS AND DISCUSSION

The Vickers hardness of hardened steel substrates was measured prior to the deposition process. The surface hardness of 740HV features a material with high load bearing capacity, appropriate for hard coating substrate. The coating hardness was measured to a value of 1920HV, which is rarely achieved by deposition at nearly room temperature. The coating thickness of 1 µm was measured for all studied specimens. The thickness was assessed by SEM examination of specimen cross section.

The surface topography of as-deposited coatings was imaged by the AFM. The following values of average roughness were obtained: Specimen 1 Ra = 53 nm; Specimen 2 Ra = 20,1 nm and Specimen 3 Ra = 3,5 nm. These values correspond to the one usually obtained by fine grinding or honing. The fine surface finish used in the present study was rarely applied in previous studies of tribological behavior of TiN coatings during reciprocating sliding.

Figure 1 shows the friction vs. the sliding time curves of TiN coatings tested at a load of 100 mN with a sliding speed of 15 mm/s. The friction coefficient showed similar behavior for all specimens and for different regimes applied during testing. The beginning of the sliding was characterized by very low values of the friction coefficient (as low as 0.1). All friction curves exhibit two stages, running-in stage and steady-state stage. The typical transition stage is not evident. In the running-in stage the friction coefficient smoothly increases with sliding distance. The smooth increase of friction coefficient is a desirable property for the practical application of TiN coatings. In the steady-state stage the friction coefficient is oscillating around approximately constant value. This stage appears after deformation of asperities of contacting surfaces. The typical transition stage is absent; in the presented curves the transition stage is basically an extension of the running-in stage. The sliding distance at the running-in stage increased with decreasing the coating roughness. For the smoothest specimen the friction coefficient maintains its growing tendency (Figure 1c) even after reaching the maximum sliding distance used during the wear tests.

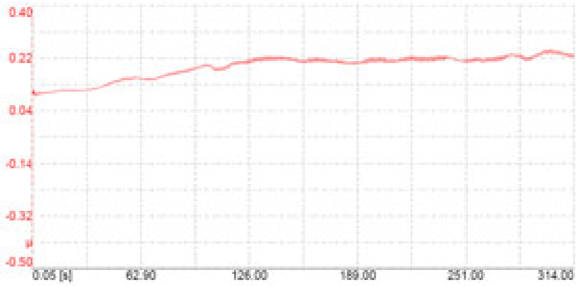

a)

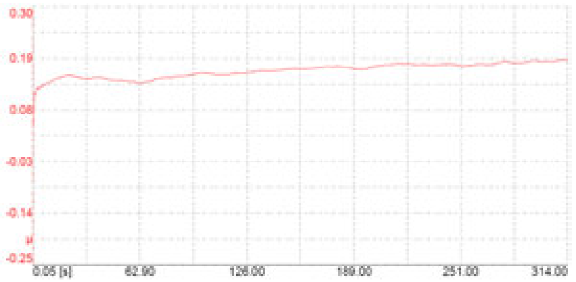

b)

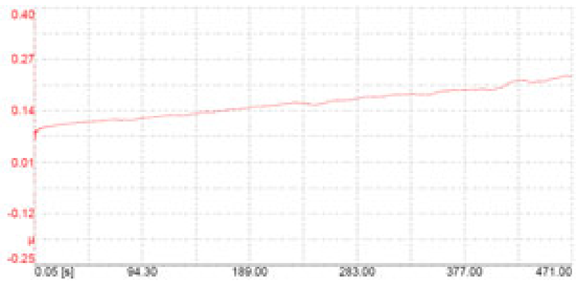

c)

Figure 1. Evolution of the friction coefficient for different specimens, v=15mm/s, F=100mN

Figure 2 summaries the friction coefficient of TiN coatings with different roughness in function of speed applied during the tribo-tests. The obtained low values of friction coefficient are typical for TiN coatings sliding against Al_2O_3 [8]. Low friction coefficient can be explained by the presence of an oxide tribolayer on the coating surface during sliding [10]. Formation of TiO_2 layer on TiN coating surface is common for sliding conditions used in the present study [15]. During reciprocating test with shorter stroke lengths temperature rises which favors tribochemical interaction between sliding pairs and surrounding atmosphere. The TiO_2 layer has low shear strength [11], [12] which leads to a low friction force [13], [14].

The friction coefficient decreases with increase in the sliding speed for all specimens (Figure 2). This is contrary to findings of S.Y. Yoon et al [9] who studied wear of TiN coatings. At higher sliding speed the tribolayer forms more easily [16], it increases in thickness and keeps the friction coefficient low. The smoother surfaces give a lower friction coefficient, see Figure 2. There was no significant difference in friction coefficient of Specimen 2 and Specimen 3. It appears that below a certain roughness, here Ra about 20 nm, the friction is less influenced by surface roughness. During sliding contact, asperities of two bodies in contact interact with each other. This interaction can results in plastic deformation of asperities of one or both bodies. For rougher surfaces higher energy is required for asperity deformation resulting in higher friction.

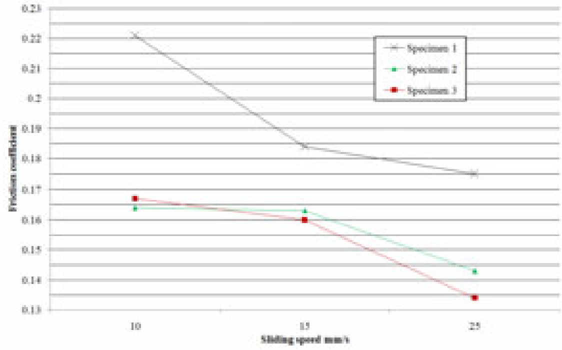

Figure 2. Friction coefficient of TiN coatings with different roughness in function of sliding speed

In addition to friction coefficient, wear loss is the other important parameter for practical application of hard coatings. The wear loss is often presented by worn volume. However, specific wear rate is more practical parameter for wear characterization. In order to calculate specific wear rates it is necessary to measure the worn channels. The accurate measurement of produced channels by optical or scanning electron microscopy is not an easy task (see Figure 3). In order to overcome this problem atomic force microscopy has been applied in the present study.

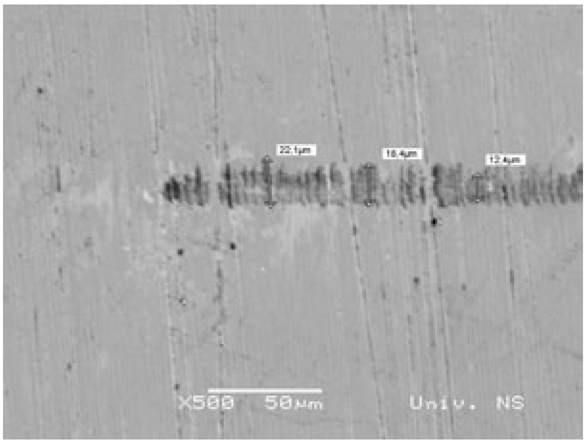

Figure 3. SEM micrograph of worn channel generated on Specimen 2, F=100mN, v=10mm/s

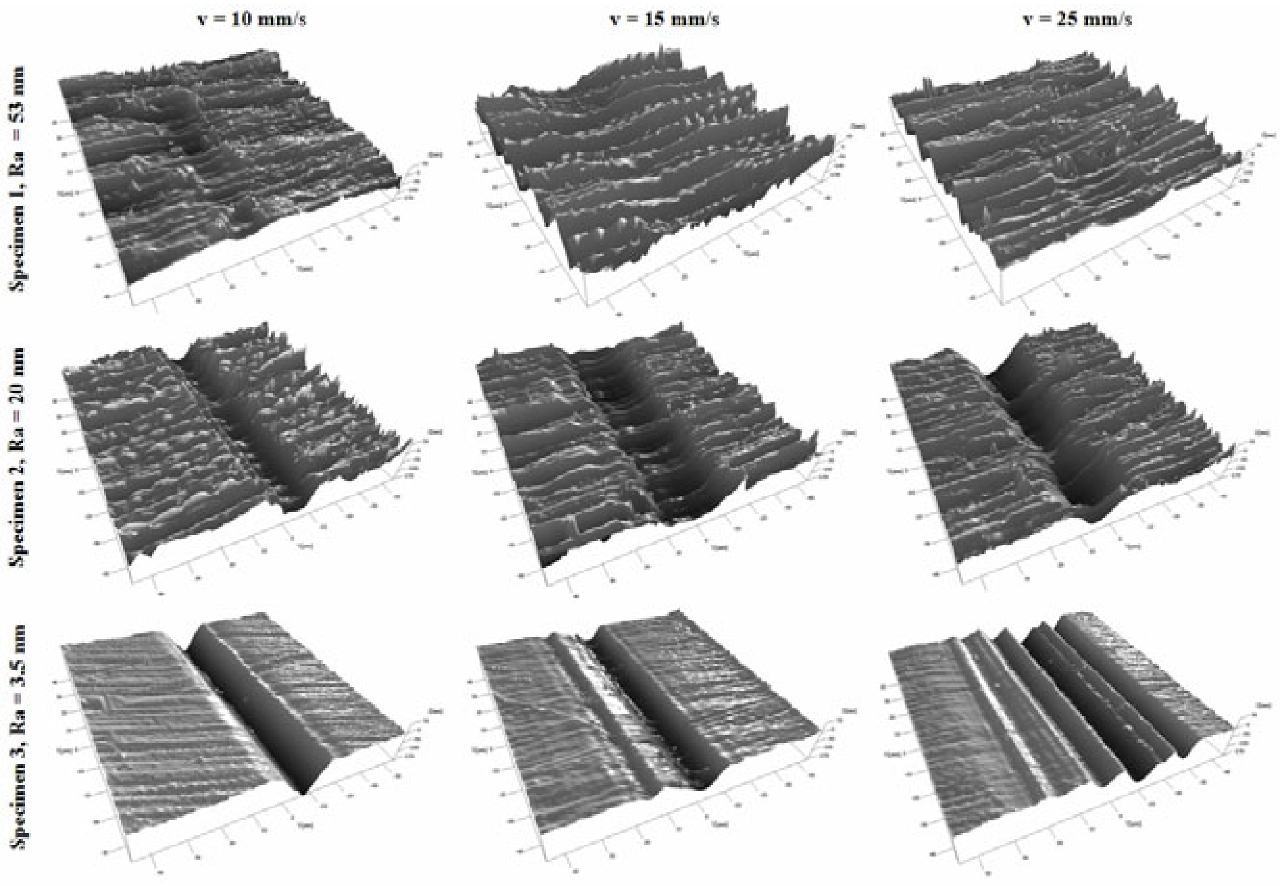

Figure 4. Morphology of the worn zones generated on TiN coatings of different roughness by reciprocating sliding with different sliding speeds

Figure 4 illustrates morphology of worn zones formed on all tested specimens by sliding with different speeds at load of 100 mN. The mild loading conditions applied did not produce any sign of hazardous wear. There were neither cracks, flakes nor fragmentation in the worn zones of studied specimens. This behavior can be attributed to high coating toughness which was confirmed by qualitative indentation tests conducted in our previous research [17]. The maximum wear track depth was around 150 nm which is far less from the coating thickness of 1 µm. The wear debris were not present inside the worn zones.

The machining ridges formed during specimen preparation were not worn away. Detailed analysis of areas inside and outside the wear tracks revealed drop in surface roughness. The maximum depth (R_{pv}) of the same machining ridges was lower inside the wear track. The machining ridges were flattened by plastic deformation and mild wear. The depth of worn channels was larger than the maximum depth of machining ridges. This suggests that machining ridges were pressed into the surface before being worn and plastically deformed.

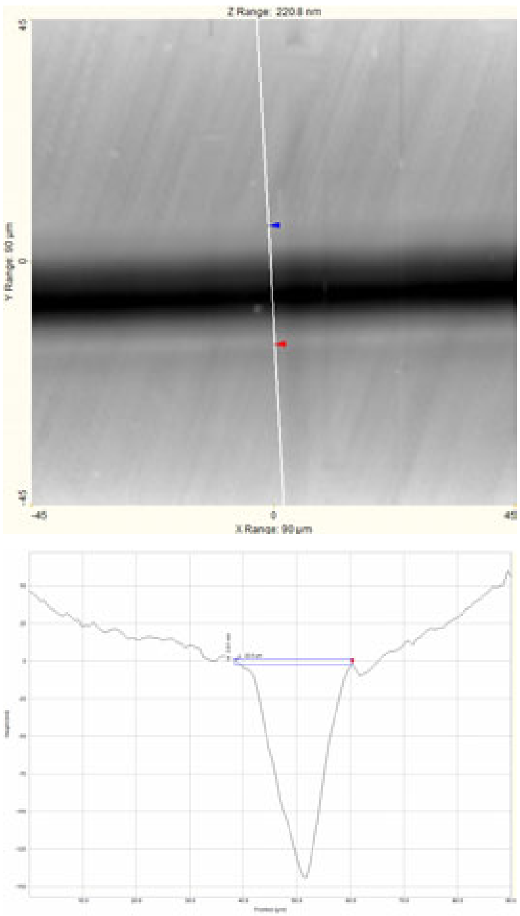

Figure 5. Measurement of wear track width

According to the SEM and AFM analyses there was no sign of wedge formation during wear. A wedge, which should be generated at the end of the wear track, forms when brittle coating is unable to absorb the load by its plastic deformation.

The worn zones produced during wear at different sliding speeds differ in size, morphology and roughness (Figure 4). Increase in the sliding speed led to increase in width and depth of wear tracks. The dimensions of worn channels were measured by applying appropriate image processing software. Figure 5 shows the measuring method applied. The conducted measurements provided the data for calculation of specific wear rates.

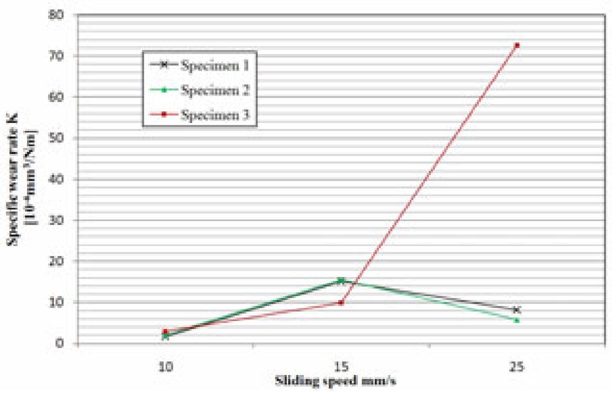

Figure 6. Specific wear rate of TiN coatings with different roughness in function of sliding speed

According to literature, a decrease of the wear rate with decrease in the friction coefficient should be expected [16], [17]. Nevertheless, such relationship cannot be taken as a rule of thumb for all material combinations in sliding contact [18], [19]. Figure 6 presents wear rates of coatings with different surface roughness in function of sliding speed applied during reciprocating sliding tests. The wear rate increases with increase in sliding speed and reaches a maximum of $72.3\text{x}10^{-6}$ mm^3/Nm at the smoothest specimen tested with sliding speed of 25 mm/s. The obtained wear rate values are comparable to those usually observed for TiN coatings sliding against Al_2O_3 [8]. The two rougher specimens (Specimen 1 and 2) behaved similarly during sliding wear tests and exhibited almost same values of specific wear rates. It appears that when sliding is conducted on surfaces of $R_a \approx 25$ - 50 nm the surface roughness does not affect the coating wear behavior significantly. In addition, for sliding speeds bellow 15 mm/s the wear rate is less affected by the surface roughness.

As already mentioned, the highest wear rate was calculated for the smoothest specimen. This value was significantly higher than wear rate values of other samples. Although the wear tracks formed on the smoothest sample tested with speed of 25 mm/s were the widest, they were also of the most irregular shape (Figure 4). The more the profile of the wear track deviate from the arc-like shape, the greater error is incorporated in calculation of the specific wear rate. Therefore, it is to believe that the actual wear rate of the Specimen 3 tested with 25 mm/s should be at least half of the calculated one. Since there is no great difference in the wear rate of the two rougher specimens, the high wear rate value determined for the smoothest specimen could be considered as the experimental scatter. However, the sliding tests were conducted two times, and both times the same results were obtained.

This result is contrary to usually observed increase of the wear rate with increase in the surface roughness [22]. Higher stresses, which are present on rougher surfaces, can lead to formation of cracks and flakes, coating fragmentation, formation of fatigue pits, and as a result to more severe wear. Neither of these defects was observed in the present study. The higher ware rate on the smoothest specimen can be explained in the following manner. During the test with the same applied load and the same sliding speed the same amount of energy is dissipated. On the rougher specimens the large amount of the energy is used for deformation of the machining ridges, while on the smoothest specimen almost all energy is used for formation of micro grooves present in the wear track of this specimen (see Figure 4). The difference in the wear rates was a consequence of different wear mechanisms acting on the tested specimens. While ridge deformation and mild abrasion were acting on the rougher specimens, abrasion was the dominant wear mechanism on the smoothest specimen.

According to the results of this investigation, for the conditions applied, the Specimen 2 has the optimum surface finish. This specimen exhibited low friction coefficient and the lowest wear rate. Although the polished specimen exhibits the lowest friction coefficient, the costs of its machining are not justified in term of high wear rate it displays in sliding wear. These findings are of practical importance for application of TiN coating as a wear resistant coating.

The roughest specimen was submitted to further examination of the relation between sliding direction and machining ridges. There was no significant difference in the friction coefficient when sliding transversal (0.221) and parallel (0.222) to the ridges. Such behavior is preferred in industrial applications as the relation between loading direction and machining ridges does not have to be considered during the designing stage of a particular part.

4. CONSLUSIONS

Tribological behavior of the TiN coatings of different roughness has been investigated on a reciprocating sliding against Al2O3 ball. The effect of sliding speed on the wear behavior of the coatings is discussed. The following conclusion can be drawn based on the experimental results:

- Low values of friction coefficient were obtained, ranging from 0.13 to 0.24. Low values of the friction coefficient are attributed to presence of titanium oxide inside the wear tracks.
- The friction coefficient of coatings with different roughness decreases with increase in sliding speed. The roughest specimen exhibited the maximal friction coefficient. For R_a below 20 nm the friction coefficient is less affected by surface roughness.
- Increase of wear rate with increase in sliding speed was observed. The highest value of wear rate was calculated for the smoothest specimen. There was no significant difference in wear behavior of specimens with average roughness between 20 and 50 nm. For this range of surface roughness, the wear rate is less affected by sliding speed applied during the tests.
- There was no sign of crack and flake formation, fragmentation or fatigue pit formation on any of tested specimens. The wear mechanism of the TiN coatings deposited on rough substrates was plastic deformation of machining ridges combined with mild abrasion, while abrasion was the dominant wear mechanism on the smoothest specimen.
- The specimen with average surface roughness of 20 nm has exhibited the best tribological behavior. The low friction coefficient was observed and the lowest wear rate was calculated for this specimen.
- The change of sliding direction relative to the direction of machining ridges does not influence the wear behavior significantly.

In order to construct wear maps, the future research will be oriented to studying the coatings deposited on substrates with wider range of surface roughness in tests with wider range of sliding speeds.

REFERENCES

[1] K. Holmberg, A. Mathews, H.Ronkainen, Coatings tribology – contact mechanisms and surface design, Tribology international, Vol. 31 pp. 107-120, 1998

[2] P. Hedenquist, S. Jacoson, S. Hogmark, Tribological laboratory evaluation of thin hard coatings, Surface and Coatings Technology Vol.97, pp.656-660, 1997

[3] S. Wilson, A.T. Alpas, Wear mechanism maps for TiN-coated high speed steel, Surface and Coatings Technology Vol.120–121, pp.519–527,1999

[4] W. Walkowiak, W. Precht, Influence of tribological conditions on the dry friction mechanism of PVD Zr–C:H hard coatings, Journal of Materials Processing Technology Vol.157–158, pp.451–455, 2004

[5] S. Achanta, D. Drees, J.P. Celis, Friction and nanowear of hard coatings in reciprocating sliding at milli-Newton loads, Wear Vol. 259, pp.719–729, 2005

[6] B. Bhushan, Applications of micro/nanotribology to magnetic storage devices and MEMS, Tribology International Vol. 28, pp.85–96,1995

[7] J.P. Celis, A system approach to the tribological testing of coated materials, Surface and Coatings Technology, Vol. 74-75, pp. 15-22,1995

[8] D. Klaffke, Tribological characterization of hard coatings with and without DLC top layer in fretting tests, Tribotest, Vol.12, pp. 29–46, 2006

[9] S.Y. Yoona, J.K. Kimb, K.H. Kima, A comparative study on tribological behavior of TiN and TiAlN coatings prepared by arc ion plating technique, Surface and Coatings Technology, Vol.161, pp.237–242, 2002

[10] D. Kakaš, B. Škorić, S. Mitrović, M. Babić, P. Terek, A. Miletić, M. Vilotić, Influence of Load and Sliding Speed on Friction Coefficient of IBAD Deposited TiN, Tribology in Industry, Vol. 31, No. 3&4, pp. 3-10, 2009

[11] X. Li, J. Lu, S. Yang, Effect of counterpart on the tribological behaviour and triboinduced phase transformation of Si, Tribology International, Vol.42, pp.628–633, 2009

[12] S. Wilson, A.T. Alpas, Tribo-layer formation during sliding wear of TiN coatings, Wear, Vol. 245, pp.223–229, 2000

[13] P. Harlin, P. Carlsson, U. Bexell, M. Olsson, Influence of surface roughness of PVD coatings on tribological performance in sliding contacts, Surface & Coatings Technology, Vol.201, pp.4253–4259, 2006

[14] M.N. Gardos, The tribo-oxidative behavior of rutile-forming substrates in: Proceedings of the Symposium Materials Research Society, 1989 pp. 325–338

[15] S. Kataria, N. Kumar, S. Dash, A.K. Tyagi, Tribological and deformation behaviour of titanium coating under different sliding contact conditions, Wear, Vol. 269, pp.797–803, 2010

[16] A. Öztruk, K.V. Ezirmik, K. Kazmanh, M. Ürgen, O.L. Eryilmaz, A. Erdemir, Comparative tribological behavior of TiN-, CrN- adn MoN-Cu nanocomposite coatings, Tribology International, Vol. 41, pp. 49-59, 2008

[17] D. Kakas et al., unpublished results

[18] N.P. Suh, N Saka., Mechanical properties of near-surface material in friciton and wear, Fundamentals of Tribology, 1980

[19] N.P. Suh, N. Saka, On the wear mechanisms and the wear equations, Fundamentals of Tribology, 1980

[20] S. Temel, Y., Alemdag Effects of pressure and sliding speed on the friction and wear properties of Al–40Zn–3Cu–2Si alloy: A comparative study with SAE 65 bronze, Materials Science and Engineering A, Vol. 496, pp.517–523, 2008

[21] Z.Z. Zhiping, Liang W.B., Microstructure and Dry-Sliding Wear Behavior of Thermal, Sprayed and Fused Ni-Based Coatings with the Addition of La2O3, Tribology Letters, Vol. 37, pp. 141–148 (2010)

[22] J. Jiang, R.D. Arnell, The effect of substrate surface roughness on the wear of DLC coatings, Wear, Vol. 239, pp, 1-9, 2000

Serbian Tribology Society

SERBIATRIB '11

12th International Conference on Tribology

Faculty of Mechanical Engineering in Kragujevac

Kragujevac, Serbia, 11 – 13 May 2011

TRIBOLOGICAL POTENCIAL OF HYBRID COMPOSITES BASED ON ZINC AND ALUMINIUM ALLOYS REINFORCED WITH SiC AND GRAPHITE PARTICLES

Slobodan Mitrović[1], Miroslav Babić[1], Blaža Stojanović[1], Nenad Miloradović[1]
[1] Universitu of Kragujevac, Faculty of Mechanical Engineering, Kragujevac, Serbia
boban@kg.ac.rs, babic@kg.ac.rs, blaza@kg.ac.rs, mnenad@kg.ac.rs

Abstract: *The paper reviews contemporary research in the area of hybrid composites based on zinc and aluminium alloys reinforced with SiC and graphite particles. Metal matrix composites (MMCs) based on ZA matrix are being increasingly applied as light-weight and wear resistant materials. Aluminium matrix composites with multiple reinforcements (hybrid AMCs) are finding increased applications because of improved mechanical and tribological properties and hence are better substitutes for single reinforced composites. The results of research show that the hybrid composites possess higher hardness, higher tensile strength, better wear resistance and lower coefficient of friction when compared to pure alloys.*

Keywords: *zinc and aluminium alloys, hybrid composites, tribological behavior*

1. INTRODUCTION

Metal matrix composites (MMCs) have attracted considerable attention recently because of their potential advantages over monolithic alloys. The MMCs are commonly reinforced with high strength, high modulus, and brittle ceramic phases, which may be in the form of fibre, whiskers, or particulates. The addition of ceramic reinforcement to a metal matrix improves strength and stiffness, but at the expense of ductility. Compared to the continuous fibre-reinforced composites, particulate-reinforced MMCs offer several advantages such as improved anisotropy, ease of fabrication, and lower cost.

Zinc–aluminium (ZA) alloys are important bearing materials, especially suitable for high-load and low-speed applications. Their main advantages are good tribo-mechanical properties, low weight, excellent foundry castability and fluidity, good machining properties, low initial cost, and environmental-friendly technology.

Good characteristics of ZA alloys have inspired researchers to reinforce them with different dispersed reinforcement materials (SiC, Al_2O_3, glass fibres, graphite and garnet) in order to obtain much more enhanced mechanical and tribological properties [1 - 18].

As a result, in the recent years, metal matrix composites (MMCs) based on ZA matrix are being increasingly applied as light-weight and wear resistant materials. MMCs have attracted considerable attention recently because of their potential advantages over monolithic alloys.

Aluminium matrix composites with multiple reinforcements (hybrid AMCs) are finding increased applications because of improved mechanical and tribological properties and hence are better substitutes for single reinforced composites.

Composites with combined reinforcement of SiC and Gr particulates are referred as Al–SiC–Gr hybrid composites. Thus, use of multiple reinforcements yields aluminium matrix hybrid composites to posses better tribological properties over composites with single reinforcement. However, reported studies [19 - 34] have indicated that efforts are scarce on parametric studies on the tribological behaviour of aluminium matrix hybrid composites. Consequently, an attempt is made here to study the influence of % reinforcement (SiC and Gr particulates), sliding speed, load and sliding distance on the tribological behavior of Al–SiC–Gr hybrid composites.

2. COMPOSITES BASED ON ZA ALLOYS

This chapter focuses on MMCs prepared with ZA27 (zinc–aluminium 27) alloy as the matrix and SiC and graphite particles as the reinforcement.

However, their broader application is limited. One of the major limitations of conventional ZA alloys, containing 8–28% Al, 1–3% Cu, and 0.05% Mg (ZA8, ZA12 and ZA27), is the deterioration of their mechanical and wear resistance properties at elevated temperatures (above 100°C) and their dimensional instability [1 - 4]. Thus, recent investigations have focused attention to development of modified version of the ZA27 alloy.

In addition, heat treatment of ZA alloys is one of the possible measures for their improvement. The effects of heat treatment on the microstructure, hardness, tensile properties, and tribological behaviour of ZA27 alloy were examined in [1,3]. Tests included the heating up to 370 °C for 3 or 5 h, quenching in water, and natural aging. The friction and wear behaviour of alloys were tested in contact with steel discs using combinations of three levels of load (10, 30, and 50 N) and three levels of linear sliding speeds (0.26, 0.50, and 1.00 m/s).

2.1 ZA27/graphite composite

In recent decades, many authors have reported that graphite in zinc aluminium alloys MMCs imparts improved tribological properties of the composites. However, the properties of Zn–Al alloy/graphite particulate composites have not been studied so extensively. It was found that the mechanical properties of the ZA27 zinc–aluminium alloy/graphite particulate composites are significantly changed by varying the amount of graphite.

Tribological tests showed that addition of graphite particles to the ZA27 alloy matrix improved the wear resistance of the composite, in spite of the significant decrease in hardness [5, 6].

Wear behaviour of tested ZA27/graphite composite samples in lubricated and dry sliding conditions is illustrated in Figure 1 (a and b) on the example of wear curves obtained in tests with 0.5 m/s of sliding speed for varying applied loads [2,4].

It could be noticed that wear of the composites with addition of the graphite particles is always significantly lower compare to the matrix ZA27 alloy.

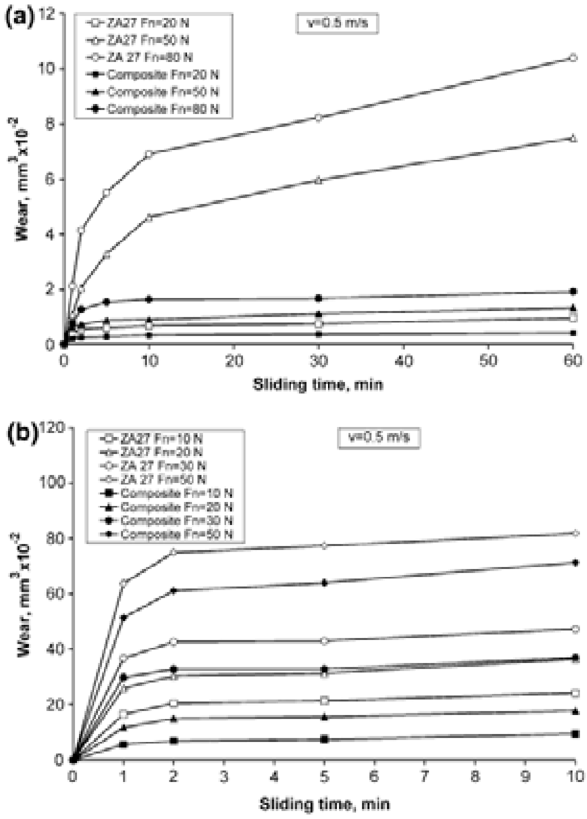

Figure 1. Wear curves of tested materials
a) Lubricated sliding, b) dry sliding [2, 4]

Figure 2 shows the wear rate of the tested materials as a function of applied load at different sliding speeds during lubricated sliding (a) and dry sliding (b) [2,4].

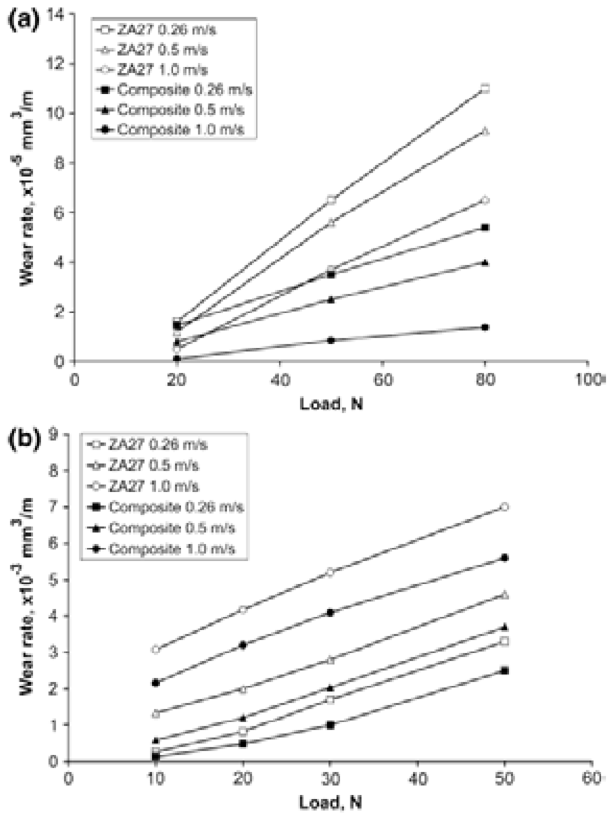

Figure 2. Wear volume vs. applied load
a) Lubricated sliding, b) dry sliding [2, 4]

The effect of sliding speed on the wear rate of the composite, as well as the matrix alloy specimens at different applied loads is presented in Figure 3 [2,4].

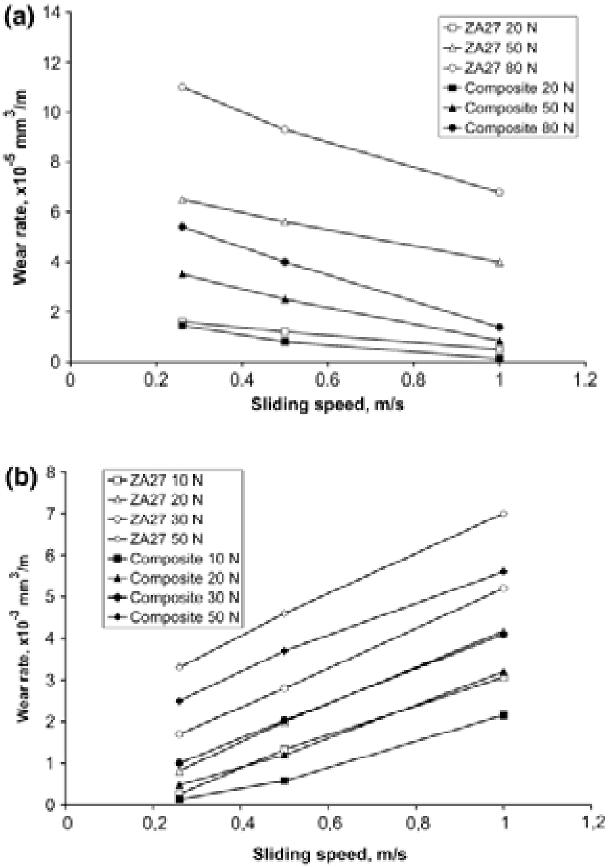

Figure 3. Wear curves of tested materials a) Lubricated sliding, b) dry sliding [2, 4]

The graphite particle reinforcing influenced significant tribological improvement of ZA27 matrix material. This improvement in conditions of dry sliding could be explained by tribo-influenced graphite film formation and its effect on friction and friction reduction. In conditions of lubricated sliding the positive tribological effects of graphite can be attributed to its influence on tribological characteristics of lubricating oil.

In [7,8], the effect of macroscopic graphite particles on damping behaviour of ZA27 alloy composites is investigated. ZA27 based MMCs have been prepared by the compo casting method with 0%, 4%, 6% and 8% of graphite particulate reinforcement. The damping behaviour, storage modulus and loss modulus of composite specimens are studied with varying percentages of graphite particulate, reinforced composites over a temperature range of 30–300 °C using a Dynamic Mechanical Analyzer

2.2 ZA27/SiC composite

The SiC-reinforced composites exhibit reduced wear rate when compared to unreinforced ZA27 alloy specimens during unlubricated [9] and lubricated sliding [10]. The wear rate decreased with increasing SiC content. The positive effects of silicon carbide toward improvement of the tribological behaviour of the ZA27 alloy was confirmed by Sharma et al. [9]. In mentioned research, the percentage of SiC was varied from 1-5% in steps of 2% by weight.

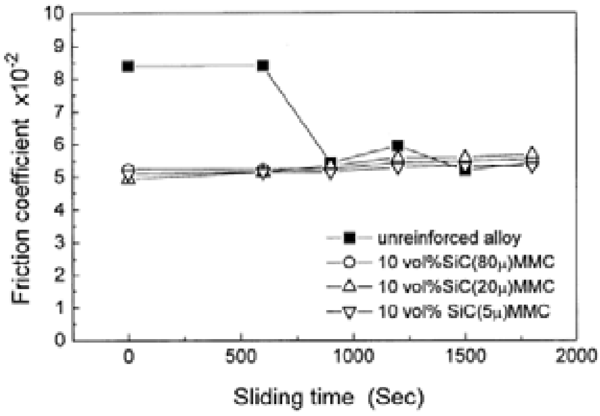

Figure 4. Friction coefficient *vs* sliding time for unreinforced ZA27 alloy and MMCs containing SiC particles of various sizes [10]

Also, reinforcement with SiC particles improved the abrasive wear response of matrix zinc-based alloys [11-13]. It has been noticed that the presence of SiC particles in ZA alloys leads to a substantial improvement in elastic modulus and hardness. Also, the wear resistance of ZA27 alloy is improved significantly by the alumina fibre reinforcement.

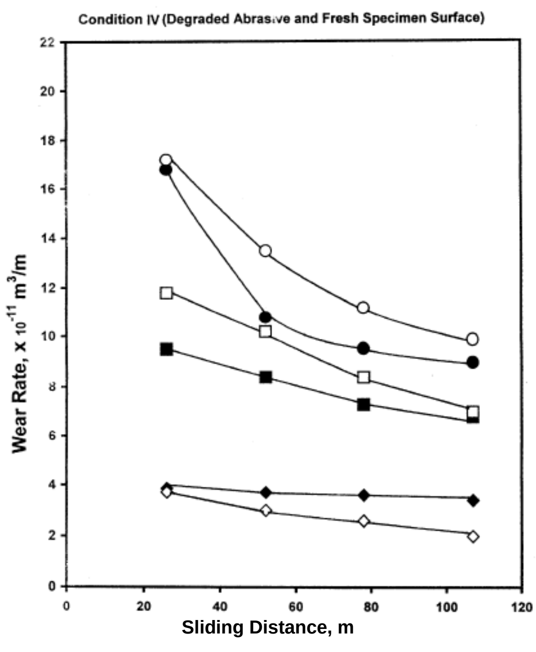

Figure 5. Wear rate of the specimens as a function of sliding distance at various applied loads in experimental condition (open symbols: composite, closed symbols: matrix alloy, ♦: 1N, ■: 3N, ▲: 5N, ●: 7 N [13]

According to Ranganath et al. [14], wear rate increases monotonically with load and decreases with an increase in wear speed.

Generally, the speed of forming of the protective tribolayers is directly dependent on the sliding speed, contact loads, and on the graphite content in the composite.

Prasad [13] conducted lubricated pin-on-disk wear test of zinc-based alloy reinforced with SiC particles and examined the effect of different amounts of graphite on tribological characteristics of lubricating oil in conditions of boundary lubrication. He prepared the series of SAE 40/graphite mixtures by mixing the graphite particles of 50–100 lm size in varying concentrations, ranging from 0 to 10 wt%. He found that positive effects of graphite additions to the lubricating oil, in decreasing the friction coefficient of tested composite in boundary lubrication, could be realized with the lower concentration of graphite (up to 4 wt%). The higher concentration of graphite in the lubricant mixture caused the reversed trend.

3. HYBRID COMPOSITES BASED ON ALUMINIUM ALLOYS

Hybrid composites represent the merging of two philosophies in tribological material design: hard particle reinforcement, for example by carbide particles; and soft particle reinforcement (and consequent lubrication), for example by graphite powder [33].

The tribological behaviour of self-lubricated aluminium/SiC/graphite hybrid composites with various amount of graphite addition synthesized by the semi-solid powder densification method has been studied by Ted Guo and Tsao [19]. Mixtures of 6061 aluminium powder (average powder size: 30 mm), SiC powder (average powder size: 45 mm) of 10 vol.%, and graphite powder (average powder size: 8 mm) of 2, 5 and 8 vol.% were investigated. Mechanical characteristics (hardness, coefficient of thermal expansion and fracture toughness) of tested materials decreased with the increase of graphite content.

The tribological tests lasts for 5 min under dry sliding condition, constant of 0.094 MPa and sliding speed of 1.09 m/s. The authors found that the seizure phenomenon which occurred with a monolithic aluminium alloy did not occur with the hybrid composites. The amount of graphite released on the wear surface increases as the graphite content increases, which reduces the friction coefficient, Figure 6.

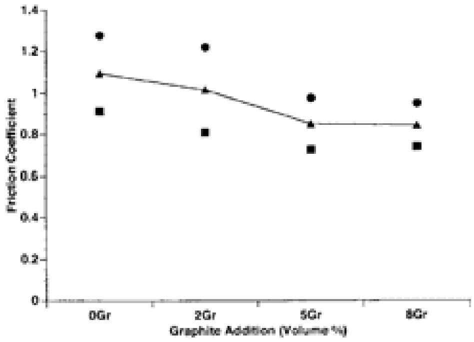

Figure 6. Variations of friction coefficient with the percentage of graphite addition [19]

Authors also concluded that wear becomes more stable, and wear debris particles become smaller as the graphite content increases, Figure 7.

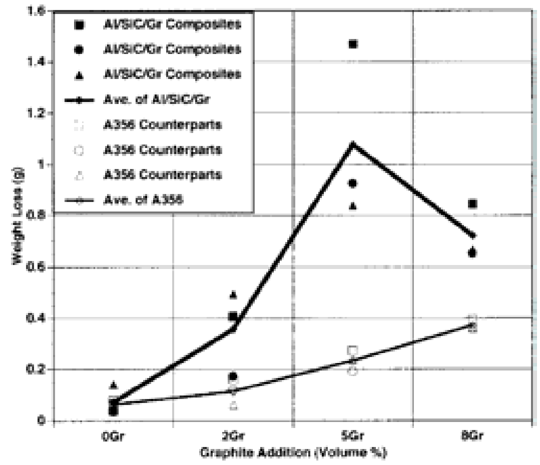

Figure 7. Weight loss of the composites and the counterparts for various graphite additions [19]

Basavarajappa et al. [20, 21, 22] investigated dry sliding wear behaviour of as cast aluminium alloy 2219, composite with SiC particles and composite with SiC particles and graphite. The composites were produced using the liquid metallurgy technique. SiC reinforcement content was 10 wt.% and average particle size of 25 μm for both composites, while the graphite content in the second composite was 3 wt.% and the average particle size of 45 μm.

The tribological tests were conducted with the load ranging from 10 to 40 N at a sliding speed of 1.53, 3, 4.6 and 6.1 m/s with a constant sliding distance of 5000 m.

It was found that the addition of SiC particles increases the wear resistance of the composites comparing to the matrix alloy. The wear resistance increase further with the composite containing SiC particles and graphite. The wear rate of the tested materials increased with increase of the sliding speed but for the both composite that increase was not as drastic as for matrix alloy, and yet the composite containing SiC and graphite showed the lowest increase, Figure 8.

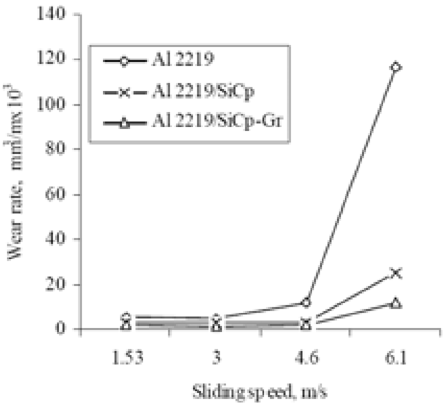

Figure 8. The wear rate variation with sliding speed for both composites and its matrix alloy [20, 21, 22]

Variation of wear rate with applied load for different composites and sliding speed of 3 m/s and sliding distance of 5000 m is presented in Figure 9.

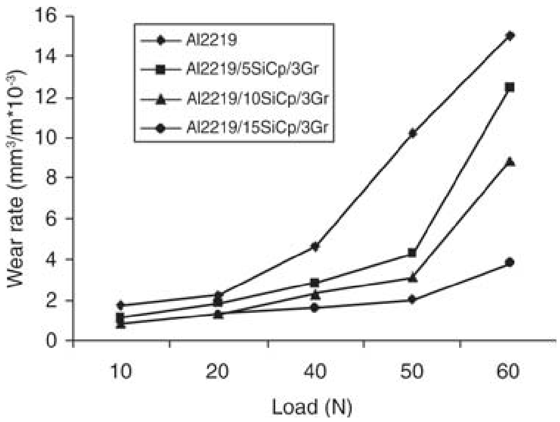

Figure 9. Variation of wear rate with applied load at a sliding speed of 3 m/s for a sliding distance of 5000 m [20, 21, 22]

Few investigations S. Suresha, BK. Sridhara [23,24,25] have been reported on the tribological behaviour of these composites with reinforcement percent above 10%. This study focuses on the influence of addition of graphite (Gr) particulates as a second reinforcement on the tribological behaviour of aluminium matrix composites reinforced with silicon carbide (SiC) particulates (Figure 10). Dry sliding wear tests have been performed to study the influence of Gr particulates, load, sliding speed and sliding distance on the wear of hybrid composite specimens with combined % reinforcement of 2.5%, 5%, 7.5% and 10% with equal weight % of SiC and Gr particulates. Experiments are also conducted on composites with reinforcement percent of SiC similar to hybrid composites for the sake of comparison. Load and sliding distance show a positive influence on wear implying increase of wear with increase of either load or sliding distance or both.

Sliding speed shows a negative influence on wear indicating decrease of wear with increase of speed. Interactions among load, sliding speed and sliding distance are noticed in hybrid composites and this may be attributed to the addition of Gr particulates. Such interactions are not present in composite reinforced with SiC alone.

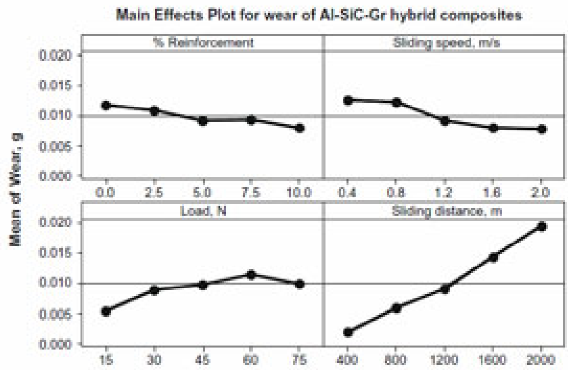

Figure 10. Main effect plot of effect of factors on wear of Al-SiC-Gr hybrid composites [23, 24, 25]

Authors A.R Riahi, A.T Alpas [26]. provide a systematic investigation of the role played by the tribo-layers that form on the contact surfaces during the sliding wear of graphitic cast aluminium matrix composites. The graphitic composites include A356 Al–10% SiC–4% Gr that are being developed for cylinder liner applications in cast aluminium engine blocks. It was shown that because of the thicker and more stable tribo-layers on the contact surfaces of graphitic composites, than that of non-graphitic composites and the A356 Al alloy, the graphitic composites displayed a transition from mild-to-severe wear at load and sliding speed combinations, which were considerably higher than those of the A356 aluminium alloy and the non-graphitic A356 Al–20% SiC composite (Figure 11). A negative effect of the hard constituents in the tribo-layers was the scuffing damage that they inflicted on the counterface.

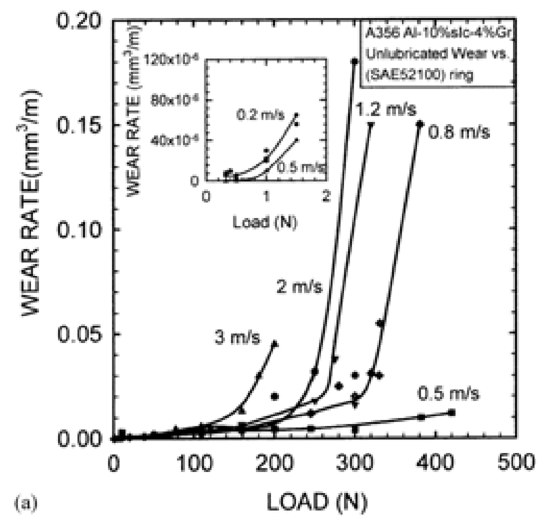

Figure 11. Wear volume vs. applied load [26]

The 40%SiC/5%Gr/Al composites with various-sizes graphite addition fabricated by squeeze casting technology and their friction and wear properties were investigated by Leng et al. in [27, 28, 29]. Results showed that, after the addition of graphite, the friction coefficient of composites decreased and the wear resistance increased by 170 to 340 times (Figure 12). In addition, wear resistance was improved with in-creasing of graphite particle size, which is attributed to the enhancement of integrity of lubrication tribo-layer composed of a complex mixture of iron oxides, graphite as well as fractured SiC particles and some fine particles containing aluminium.

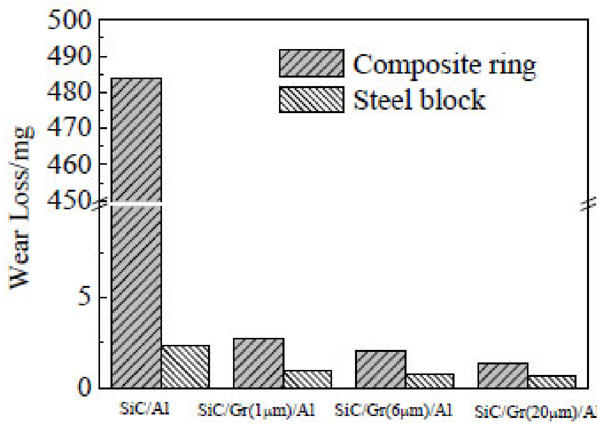

Figure 12. Wear loss of the composites and counterfaces of wear process for SiC/Al and SiC/Gr/Al [27, 28, 29]

The wear behaviour of A356 aluminium alloy matrix composites reinforced with 20 % SiC particles and 3 or 10 % graphite was investigated by Ames, Alpas [30]. The wear tests were performed using a block-on-ring (SAE 52100 steel) wear machine under dry sliding conditions within a load range of 1 to 441 N. The wear resistance of 3 % graphite-20 % SiC-A356 hybrid composite was comparable to 20 % SiC-A356 without graphite at low and medium loads. At loads below 20 N, both hybrid and 20 % SiC-A356 composites without graphite demonstrated wear rates up to 10 times lower than the unreinforced A356 alloy due to the load-carrying capacity of SiC particles. The wear resistance of 3 % graphite 20 % SiC-A356 was 1 to 2 times higher than 10 % graphite-containing hybrid composites at high loads. However, graphite addition reduced the counterface wear. The unreinforced A356 and 20 % SiC-A356 showed a transition from mild to severe wear at 95 N and 225 N, respectively. Hybrid composites with 3 % and 10 % graphite did not show such a transition over the entire load range, indicating that graphite improved the seizure resistance of the composites.

In study [31], Mahdavi applied a new method, namely In situ Powder Metallurgy (IPM) for the preparation of Al6061/SiC/Gr hybrid composites. By this method, the stir casting and the powder metallurgy synthesizing processes are combined into an integrated net shape forming process. 0–40 vol.% of SiC particles with an average size of 19 lm, along with 9 vol.% of uncoated Gr particles, were introduced to the molten 6061 aluminium alloy. The best wear resistance is achieved in the hybrid composite containing 20 vol.% SiC particles.

Effect of the SiC content on the volume loss and the wear rate of 9 vol.% Gr contained composites and unreinforced aluminium alloy is shown in Figure 13. It is seen that the dry sliding volume loss of all hybrid composites is lower than that of the base alloy. However, the volume loss and the wear rate of Al–9 vol.% Gr composite in higher than that of the base alloy and the hybrid composites.

Figure 13 eveals that the volume loss and the wear rate of hybrid composites are decreased by increasing the SiC content to 20 vol.%, and after that any increase in SiC content leads to their increases. The wear rate of the hybrid composite containing 20 vol.% SiC particles is about eight times lower than that of the base alloy sample.

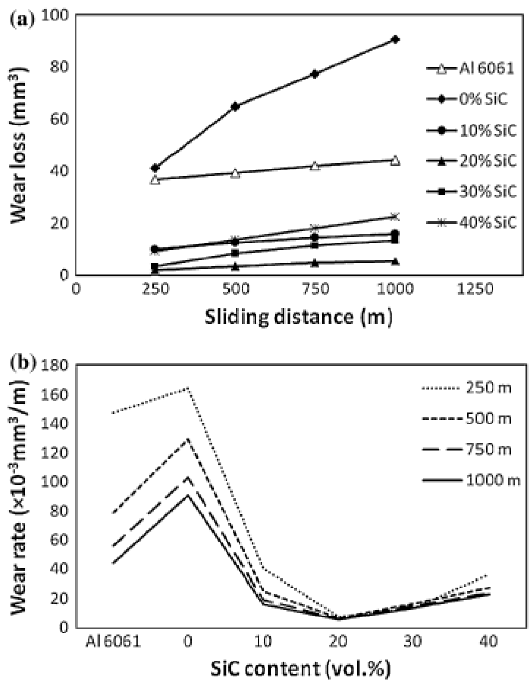

Figure 13. The variation of a wear loss with a)sliding distance and b) wear rate with SiC content for the hybrid composites containing 9 vol. % Gr particles [31]

Tribological investigation of these materials was just an initial one, with preliminary results and some more experiments to be done to completely understand their tribological behaviour. In order to achieve a higher confidence level in evaluating test results, three to four replicate tests were run for all the tested materials, Vencl et al. [32,33]. Obtained average values of the wear testing are presented in Figure 14. The highest value showed A356 aluminium alloy, then composite C1 (with Al2O3 particles), composite C2 (with SiC particles), and composite C3 showed the lowest wear (with SiC and graphite particles). These results are in correlation with the hardness values of the tested materials, except for the composite C3. The A356 aluminium alloys showed lower wear than it could be expected since it was not reinforced. Wear resistance of as cast A356 aluminium alloy is affected by silicon particles in the form of sticks that were created as a result of eutectic reaction during the alloy solidification.

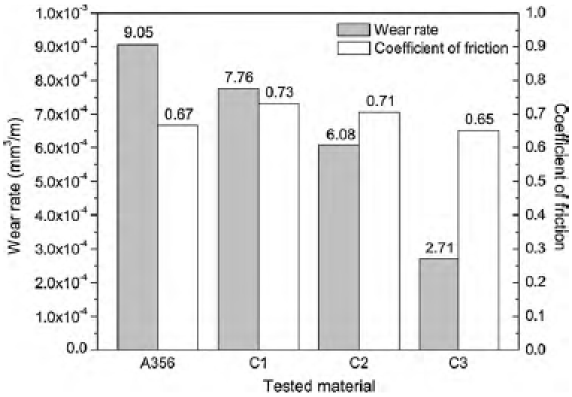

Figure 14. Wear rate and coefficient of friction values of heat treated (T6) A356 aluminium alloy, composite C1(with 10wt% Al_2O_3 particles), composite C2 (with 10wt% SiC particles), and composite C3 (with 10wt%SiC and 1wt% graphite particles) [32, 33]

4. CONCLUSION

Among the zinc-based foundry alloys, the zinc-aluminium (ZA) family of alloys has been used increasingly in past decades.

Interest for extending the practical application of zinc aluminium alloys is based on tribological, economical, and ecological reasons. These alloys are relatively cheap and can be processed efficiently with low energy consumption, without endangering the environment.

According to reviewed research, application of hybrid composites based on zinc and aluminium alloys reinforced with SiC and graphite particles will provide better tribological behaviour.

A combination of good properties, low cost and high workability has made them attractive for many applications.

ACKNOWLEDGEMENTS

The results of this article are realized through the national project TR-35021 financially supported by the Ministry of Science of the Republic of Serbia (Project Coordinator: Prof. Dr. Miroslav Babic)

REFERENCES

[1] M. Babic, A. Vencl, S. Mitrović, I. Bobić, Influence of T4 Heat Treatment on Tribological Behavior of Za27 Alloy Under Lubricated Sliding Condition, Tribology Letters, Vol.36, No.2, pp. 125-134, ISSN 1023-8883, 2009

[2] M. Babić, S. Mitrović, R. Ninković, Tribological Potencial of Zinc-Aluminium Alloys Improvement, Tribology in Industry, Vol.31, No.1&2, pp. 15-28, ISSN 0354-8996, 2009

[3] M. Babic, S. Mitrovic, B. Jeremic, The influence of heat treatment on the sliding wear behavior of a ZA-27 alloy, Tribology International, Vol.43, No.1-2, pp. 16-21, ISSN 0301-679, 2010

[4] M. Babic, S. Mitrovic, D. Dzunic, B. Jeremic, I. Bobic: Tribological Behavior of Composites Based on ZA-27 Alloy Reinforced with Graphite Particles Tribology Letters, Vol.37, No.2, pp. 401-410, ISSN 1023-8883, Doi 10.1007/s11249-009-9535-2, 2010

[5] Seah, K.H.W., Sharma, S.C., Girish, B.M., Lim, S.C.: Wear characteristics of as-cast ZA-27/graphite particulate composites. Mater Des 17(2), pp. 63–67, 1996

[6] Sharma, S.C., Girish, B.M., Kramath, R., Satish, B.M.: Graphite particles reinforced ZA-27 alloy composite materials for journal bearing applications. Wear 219, pp. 162–168, 1998

[7] B.M. Girish, K.R. Prakash , B.M. Satish, P.K. Jain, Phani Prabhakar: An investigation into the effects of graphite particles on the damping behavior of ZA-27 alloy composite material, Materials and Design 32, pp. 1050–1056, 2011

[8] WEI JN, SONG SH, HU KG, XIE WJ, MA ML, LI GM, HAN FS: Influence of macroscopic graphite particulates on the damping properties of Zn-Al eutectoid alloy, Sci China Ser G-Phys Mech Astron, vol. 52 no. 1 pp. 70-75, 2009

[9] Sharma, S.C., Girish, B.M., Kamath, R., Satish, B.M.: Effect of SiC particle reinforcement on the unlubricated sliding wear behavior of ZA-27 alloy composites. Wear 213, pp. 33–40, 1997

[10] Tjong, S.C., Chen, F.: Wear behavior of as-cast ZnAl27/SiC particulate metal-matrix composites under lubricated sliding condition. Metall Mater Trans A 28A, pp. 1951–1955, 1997

[11] Prasad, B.K.: Investigation into sliding wear performance of zinc based alloy reinforced with SiC particles in dry and lubricated conditions. Wear 262, pp. 262–273, 2007

[12] Prasad, B.K., Modi, O.P., Khaira, H.K.: High-stress abrasive wear behavior of a zinc-based alloy and its composite compared with a cast iron under varying track radius and load conditions. Mater Sci Eng A 381, pp. 343–354, 2004

[13] Prasad, B.K.: Abrasive wear characteristics of a zinc-based alloy and zinc-alloy/SiC composite. Wear 252(3–4), pp. 250–263, 2002

[14] G. Ranganath, S.C. Sharma, M. Krishna: Dry sliding wear of garnet reinforced zinc/aluminium

metal matrix composites, Wear 251, 1408-1413, 2001

[15] B. Bobić, S. Mitrovic, M. Babic, I. Bobić: Corrosion of Aluminium and Zinc-Aluminium Alloys Based Metal-Matrix Composites, Tribology in Industry, Vol.31, No.3&4, pp. 44-52, ISSN 0354-8996, 2009

[16] S. Mitrovic, M. Babic, F. Zivic, I. Bobic, D Dzunic: Nanotribology investigations of composites based on Za-27 alloy reinforced by Al2O3 particles, Tribology in Industry, Vol.30, No.1&2, pp. 33-39, ISSN 0354-8996, 2008

[17] I. Bobic, M. Babic, S. Mitrovic, Bobic B., M.T. Jovanovic: Rheological behavior of ZA27 alloy semi-solid slurries and Al2O3 particulate/ZA27 composite slurries, Tribology in Industry, Vol.30, No.1&2, pp. 47-54, ISSN 0354-8996, 2008

[18] M. Babić, S. Mitrović, I. Bobić: Tribological Properties of Composites with Substrate Made of the ZA-27 Alloy Reinforced by the Graphite Particles, Tribology in industry, Vol.29, No.3-4, pp. 3-8, ISSN 0354-8996, 2007

[19] M. L. Ted Guo, C. -Y. A. Tsao: Tribological behavior of self-lubricating aluminium/SiC/graphite hybrid composites synthesized by the semi-solid powder-densification method, Composites Science and Technology, Vol. 60, No. 1, pp. 65-74, 2000.

[20] S. Basavarajappa, G. Chandramohan, K. Mukund, M. Ashwin, M. Prabu: Dry sliding wear behavior of Al 2219/SiCp-Gr hybrid metal matrix composites, Journal of Materials Engineering and Performance, Vol. 15, No. 6, pp. 668-674, 2006.

[21] S. Basavarajappa, G. Chandramohan, A. Mahadevan: Influence of sliding speed on the dry sliding wear behaviour and the subsurface deformation on hybrid metal matrix composite. Wear, 262:1007–12, 2007

[22] S. Basavarajappa, G. Chandramohan: Dry sliding wear behavior of hybrid metal matrix composites, 1392-1320 Materials Science, Vol. 11, No. 3. 2005.

[23] S. Suresha, BK. Sridhara: Effect of addition of graphite particulates on the wear behavior in aluminium–silicon carbide–graphite composites. Mater Des ;31:1804–12, 2010

[24] S. Suresha, B.K. Sridhara: Wear characteristics of hybrid aluminium matrix composites reinforced with graphite and silicon carbide particulates Original Research Article Composites Science and Technology, Volume 70, Issue 11, Pages 1652-1659, October 2010

[25] S. Suresha, B.K. Sridhara: Effect of silicon carbide particulates on wear resistance of graphitic aluminium matrix composites, Materials & Design, Volume 31, Issue 9, Pages 4470-4477, October 2010

[26] AR. Riahi, AT. Alpas: The role of tribo-layers on the sliding wear behaviour of graphitic aluminum matrix composites. Wear;251:1396–407, 2001

[27] J. Leng, L. Jiang, G. Wu, S. Tian, G. Chen: Effect of Graphite Particle Reinforcement on Dry Sliding Wear of SiC/Gr/Al Composites, Rare Metal Materials and Engineering Volume 38, Issue 11, November 2009

[28] J. Leng, L. Jiang, Q. Zhang, G. Wu, D. Sun, Q. Zhou: Study of machinable SiC/Gr/Al composites Journal of Materials Science Volume 43, Number 19, 6495-6499, DOI: 10.1007/s10853-008-2974-6

[29] J. Leng, G. Wu, Q. Zhou, Z. Dou, X. Huang Mechanical properties of SiC/Gr/Al composites fabricated by squeeze casting technology Scripta Materialia, Volume 59, Issue 6, Pages 619-622, September 2008

[30] W. Ames, AT. Alpas: Wear mechanisms in hybrid composites of graphite-20% SiC in A356 aluminum alloy. Metall.Mater.Trans. A; 26: 85-98, 1995

[31] S. Mahdavi, F. Akhlaghi:Effect of SiC content on the processing, compaction behavior, and properties of Al6061/SiC/Gr hybrid composites, Journal of Materials Science, Volume 46, Number 5, 1502-1511, DOI: 10.1007/s10853-010-4954-x

[32] A.Vencl, I. Bobic, S. Arostegui, B. Bobic, A.Marinkovic, M. Babic: Structural, mechanical and tribological properties of A356 aluminium alloy reinforced with Al2O3, SiC and SiC + graphite particles, Journal of Alloys and Compounds, 506, pp. 631-639, 2010

[33] A.Vencl, A.Marinkovic: Influence of the solid lubricant particles reinforcement on composites tribological properties, 11th International Conference on Tribology, Belgrade, 2009.

[34] B. Bobic, S. Mitrovic, M. Babic, I. Bobic: Corrosion of Metal-Matrix Composites with Aluminium Alloy Substrate, Tribology in Industry, vol. 32, No. 1, pp. 3-11, 2010

Serbian Tribology Society

SERBIATRIB '11

12th International Conference on Tribology

Faculty of Mechanical Engineering in Kragujevac

Kragujevac, Serbia, 11 – 13 May 2011

INFLUENCE OF PREVIOUS MACHINING ON CHARACTERISTICS OF GALVANIC COATINGS

Bogdan Nedić[1], Desimir Jovanović [2], Gordana Lakić Globočki [3]

[1] Mašinski fakultet, Kragujevac, Srbija, nedic@kg.ac.rs
[2] Zastava oružje AD, Kragujevac, Srbija, zo.tehnologija@open.telekom.rs
[3] Mašinski fakultet, Banja Luka, Republika Srpska, BiH, gnm@urc.rs.ba

Abstract: *Galvanic coatings are applied to the base material surface in order to obtain some of the following characteristics: resistance to corrosion, chemical inertness, wear resistance, higher dimensions, lower coefficient of friction and a better aesthetic impression. Most studies of protective metal coatings focuses on the characterization of coatings and their links to the basic material, while very little is known about the effects of substrate on the characteristics of the coating. Surface finish has a great influence on determination of the physical and mechanical properties and structure of the surface layer. This paper presents the preliminary results of the surface topography changes depending on the thickness of Zn and Cr layer. The research was performed with samples of different hardness and different previous grinding.*

Keywords: *galvanic coatings, hardness, roughness, Zn coating, Cr coating*

1. INTRODUCTION

Creating metal coatings on the surface of another metal has a dual role, corrosion protection and changing characteristics of the metal surface, such as hardness, electrical conductivity, decoration and so on. Galvanic metal coatings have certain advantages over other coatings. They are resistant to mechanical damage, have good electrical and thermal conductivity and enable the connection of metal soldered together. But when the metal coatings are damaged, they can not simply be fixed, that makes them different from the organic coating.

The most important metal coatings, in terms of quantity in which they are applied, are the coatings of copper, nickel, zinc, chromium and tin. Coatings of precious metals (silver, cadmium, gold, rhodium, iridium, platinum and palladium) are used to a lesser extent but are important for special purposes.

Most studies in the field of galvanic coatings are focused on the characterization of coatings and their link with the basic material. The effect of processing procedure and conditions of pre-treatment and preparation of surfaces to which coatings are applied, technological heritage, is very little explored. Surface layers of machined surfaces obtained by different treatment processes and regimes may have a different structure, which only in the period of exploitation may be experienced. Therefore, it can be said that the characteristics of surface layers are formed as a result of different processing conditions in the technological chain of production of the finished part. The basic parameters that are inherited through the process of technological development can be divided into two groups. On the one hand there are parameters related to properties of materials: their composition, structure, stress state, etc.., while on the other hand are parameters related to macro and micro geometry of the surface (geometrical parameters). This indicates the complexity of the problem and the need for further studies.

Surface finish has a great influence on determining the physical - mechanical properties and structure of the surface layer. In this paper is investigation of the influence of the previous surface treatment and coating thickness on the changes of parameters of topography, in particular coating of chromium and zinc because they are most applicable to areas that are exposed to exploitation in extreme operating conditions, corrosive environment or high pressure and temperature.

2. GALVANIC COATING

Galvanic plating and metals are crystalline in nature. Therefore, the electrodeposition process is called crystallization. In the crystallization process - there are three independent processes:

1) formation of seeds (centers) or crystal nuclei,
2) crystal growth rate,
3) increase the speed of crystals on account of their merger.

These processes run in parallel. The creation and quality of metal coatings are influenced by many factors:

- concentration of metal ions,
- electrolyte composition,
- current density,
- mixing of the electrolyte,
- temperature of the electrolyte,
- state of the cathode surface, etc.

The concentration of ions significantly affects the quality of the coating, the composition of the electrolyte affect the properties and appearance of the coatings. Current density has a large impact on the formation rate of crystal nuclei, mixing is performed to maintain constant concentration of metal ions, the temperature plays a significant role in the speed of chemical reactions. Metals are polycrystalline particles, so the characteristics of the coating are affected by the structure of the substrate.

Electroplated coatings of zinc and chromium are most often changed, so in this work the attention is given to these coatings.

Zinc coatings are used for corrosion protection of machinery parts, steel plates, wire, etc.. located in different climate conditions, in closed environments with moderate humidity, at the polluted gases areas, flue gases area and in atmosphere containing sulfur vapor. These coatings are used to protect pipes, tanks and other parts, which are in contact with water at temperatures up to 70oC. Color of zinc coating is usually light gray, become dark during time, and therefore does not provide a decorative look. Zinc also protects the iron from corrosion when the coating is porous or damaged, because it forms a couple in which the iron is cathodically protected [3, 4].

Zinc belongs to the metals whose normal potential is more negative than the potential of iron, so zinc coating protects the iron not only mechanically but also electrochemically. The protective effect of the coating is interrupted only when the entire zinc layer is disrupted. Life of the protective effect of the coating depends on its thickness. For metal objects, which are used in relatively dry air in closed rooms, sufficient thickness of zinc coating of 10-15 μm. For items that are outside the room, in the air that is polluted by industrial gases, the thickness increases to 20 - 25 microns, and for articles intended for use in industrial environments, in terms of enhanced effects of moisture, sea water or water vapor, the thickness of zinc coating moving to 50 μm. Coating is more resistant if the zinc cleaner [1, 2, 3].

The hardness of metal coatings of zinc is 45 to 120 HB.

The thickness of coatings on parts of the weapon depends on the working conditions in which the part is used and usually is 5, 8, 12 to 25 microns, [SORS 2325]. Galvanic corrosion resistance of zinc coating can be improved by after-treatment - the application of phosphate or various types of chromate coatings: colorless – A, bluish – B, yellow - C, olives – D, and black - F coating. Chromate conversion coatings should not be applied to surfaces of elements that are in contact with flammable and explosive environments, [5, 6].

Requirements for quality zinc coatings are contained in the applicable standards and the most important are [5, 6, 7]:

The external appearance of galvanized zinc coating is defined by color that can be:

- Light-gray or silvery-white with blue gradient, shiny or matte,
- Silvery-gray or silvery-gray with blue or light-yellow hues,
- With olive olive of brown-green to dark green,
- With dark brown to black with green or blue-purple hue,
- With phosphate conversion coatings light-gray to dark gray.

Allowable defects of zinc coatings without post-processing are darker color of the coating on the inside surface elements, the presence of shiny and matte places on the same element, the absence of coating in blind holes, channels, and the like. at a depth of more than one diameter and in the openings that pass through the entire element at a depth greater than two diameters, slightly peeling in places of weld for molded parts, color change of coating after heating wit aim to the remove of hydrogen and the existence of traces of the inflow of water.

Unacceptable defects coatings without the occurrence of subsequent processing and dendrites and spongy coating, dark stripes on the edges of elements, (burned sites), uncovered places, except for points given to technical documentation, bubbles, layer removal and peeling of coating, appearance of grains and hard spots that interfere with the function of element, the black points and corrosion of zinc, traces of unwashed salts existence and mechanical damages of the coating.

The thickness of zinc coating is usually: 5, 8, 12 and 25 microns. Depending on the needs designer may define other values of thickness, allowing a greater thickness than the prescribed, if at the same time increasing the dimensions of the element does not affect its function. Smaller thickness of zinc coating is allowed on the inside surface, in holes and hollows, where the thickness of the coating must not be less than 60% of the prescribed level.

Adhesion. Galvanic zinc coatings shall not peel off of base metal and chromic or phosphate conversion coatings must not wash off from the zinc coating.

Corrosion resistance. Galvanic zinc coatings on steel must be corrosion resistant. When examining the chamber with a neutral salt fog 5% zinc coating without subsequent processing, does not allow the occurrence of red-brown dots (representing the corrosion of the base material) visible with the naked eye.

Chromium coatings in addition to zinc coatings are applied widely for galvanic coating of steel and its alloys [3].

Chromium is a very durable metal to various chemical agents. Soluble in hydrochloric and hot sulfuric acid. Unlike the nickel and silver, retains its color and shine. Change of the color of chromium occurs at temperatures above 500^{o}C.

Chromium coatings without a layer of copper and nickel under are used to increase surface hardness and resistance to mechanical wear of metals, to achieve the dimensions of parts, as well as anti-corrosive protection of wearing parts. Chromic coatings are commonly used in combination with a coating of nickel.

Chromic coatings with under layer of copper and nickel are used for protective-decorative coating and to increase the power of reflection of surface parts.

Electrolytic obtained chromium plating have specular gloss silver-steel color with bluish tint. Electrolytic chromium is possible to apply to almost all metals. Application of other metal parts on chromium parts can not be achieved, due to a high tendency towards passivity of chromium even in the air. Therefore, the potential of chromium plating in all known cases of is mere electrically positive than steel, so for iron and its alloys chromic coatings are only mechanical protectors.

Chromic coatings are void, even in thick areas, so plating for corrosion protection is done after the application of the under coatings on object surface of other metals, for example copper or nickel. Then the chromium layer protects only layer below it against mechanical damage and preserves the look of decorative items. The process of obtaining combined protective - decorative coatings, when the outer layer is of chromium, is called decorative chromium plating. It is widely used in protecting the outside of cars, measuring equipment and others. The thickness of the layer of chromium in this case does not exceed 1 μm, i.e. from 0.2 to 1.0 μm. To obtain a hard surface, often regenerated surfaces thickness range from 0.2 - 0.5 mm or more. Hard chromium coatings have potential in production of various tools, machine parts and printing rollers.

3. EXPERIMENTAL INVESTIGATIONS

The quality of metal coatings is major affected by the surface condition that it is applied to. Realized experiments in this paper had aim to determine the impact of previous treatment on the change of surface topography parameters of the deposition of electrolytic coatings of zinc and chromium.

For the purpose of testing the samples were made 15 x 6.3 x 10 mm (Figure 1). On samples from the front side were embedded serial numbers of the sample, and through lateral surfaces were drilled openings designed to mounting each sample individually for coating.

Samples are made of spring steel 67SiCr5 (Č4230). After the sample design, milling, heat treatment was done by improving the different hardness (Table 3).

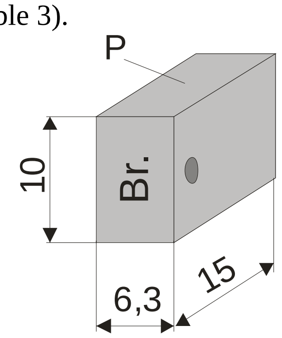

Figure 1. Samples

Grinding of samples was carried out with two regimes, A and B. Grinding of samples labeled A was performed with two passes with 0.02 mm depth and speed of 11 m/s and two passes with 0.01 mm and the speed of 22 m/s, and grinding of samples B was performed with two passes of depth 0.02 mm and speed 22 m/s. In this way they obtained different characteristics of the surface layer and the surface topography of various samples. Application of metal coatings was performed at the facility for electroplating factory "Zastava Arms", Kragujevac in production conditions, with different times in order to obtain different thicknesses of Zn (Table 1) and Cr (Table 2).

Zinc coating was carried out as follows:

I. alkaline degreasing without cyanides with industrial detergent,
II. rinse with water,
III. pickling in diluted hydrochloric acid in a 1:1 ratio,
IV. rinse with water,
V. electro-chemical coating of zinc,
VI. enlightening in 2% HNO3 for a period of 50 seconds,
VII. rinse with water,
VIII. blowing.
IX. temperature coating-room
X. strength of current I = 3 A/dm^2

Table 1. Terms of Zn application

Sample number	Thickness Zn, μm	Time, min	Power A/dm^2
2, 4, 11	< 6	8	3
10, 31, 34	6 - 10	16	3
5, 8, 13, 16, 22	10 - 15	25	3
6, 9, 17	>15	35	3

Chromium coatings are applied in the following way:

I. alkaline degreasing without cyanides with industrial detergent
II. rinse with water,
III. electro-chemical application of hard coating of chromium,
IV. enlightening in 2% HNO3 for a period of 50 seconds
V. rinse with water,
VI. coating temperature T = 55^{o}C
VII. strength of current I = 50 A/dm^2

Table 2. Terms of Cr application

Sample number	Thickness Cr, μm	Time, min	Power A/dm^2
15, 20, 25, 33, 24, 35	< 12	20	50
7, 18, 26, 28, 32, 36, 29, 37	> 12	30	50

Table 3 shows the data on the tested samples: marking of grinding, the hardness after heat treatment and obtained layer of Zn and Cr.

Coating thickness measurement was performed in a laboratory galvanizing area of factory "Zastava Arms" in Kragujevac. Samples with coatings of Zn in which the thickness were up to 4 μm were not further analyzed because it is the recommendation of the standard not to apply such thin zinc coatings.

Table 3. Hardness and thickness of Zn and Cr samples

Sample number	Grinding	Type coating	Hardness samples, HRC	Thickness μm
2	A	Zn	47,6	2
5	A	Zn	46,5	12
6	A	Zn	33	16
8	A	Zn	19,1	12
9	A	Zn	35,4	15
22	A	Zn	20,0	10
4	B	Zn	35,5	4
10	B	Zn	35,9	9
11	B	Zn	48,3	2
13	B	Zn	45,8	14
16	B	Zn	36,9	12.7
17	B	Zn	21,7	20
31	B	Zn	24,2	6.5
34	B	Zn	21,1	6
7	A	Cr	46,5	13.21
15	A	Cr	51,5	8.25
26	A	Cr	47,1	12,20
29	A	Cr	37,1	15.63
35	A	Cr	24,4	11.17
36	A	Cr	24,6	12.97
37	A	Cr	22,1	14.87
18	B	Cr	48,1	12.60
20	B	Cr	47,8	7.87
24	B	Cr	24,7	9.27
25	B	Cr	24,6	7.10
28	B	Cr	32,1	13.59
32	B	Cr	51,4	12.07
33	B	Cr	19,3	7.75

After grinding the samples, before applying the coatings, were measured hardness and surface topography parameters and the longitudinal and transverse direction. Measurements were taken at the surface of the sample P (Fig. 1). The appearance of ground surface of one of the samples before applying the coating is shown in figure 2. The value of the basic parameters of roughness in the longitudinal and transverse direction is approximately the same. Significant differences were observed in additional parameters, for example, uneven steps. Ra value ranges from 0.26 to 0.4 μm.

Realized tests were not possible to determine the dependence of the thickness of coatings of Zn and Cr from the previous grinding and the hardness of the samples. in order to establish the possible persistence of these depending on need extensive testing.

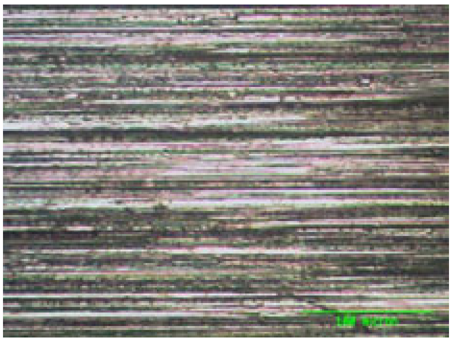

Figure 2. The appearance of ground surface of the sample before application of coatings

By measuring the parameters of the topography in the longitudinal and transverse direction it is shown that the coating changes the surface topography.

Applying Zn coatings leads to a deterioration of surface quality and roughness increases significantly. Class roughness of Zn coating can deteriorate for one, even for the two classes.

Figure 3 shows the topography of the sample surface 9 in the longitudinal direction before and after application of Zn. It can be concluded that the zinc coating thickness of 15 μm cause an increase of Ra twice.

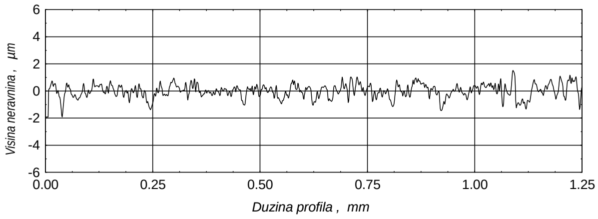

a) Before applying the coating, Ra = 0.392 μ m

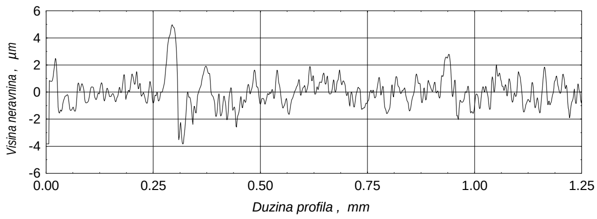

b) After application of Zn, Ra = 0.798 μ m

Figure 3. Profile of the sample 9

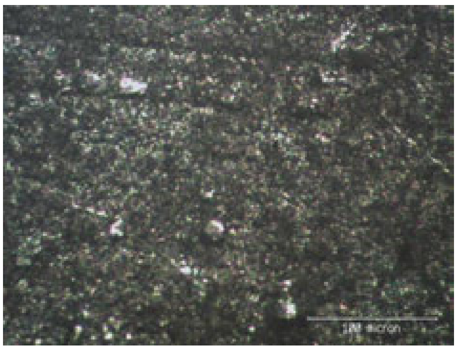

Figure 4. The appearance of the sample surface 9 after application of Zn

Realized testing did not determine dependence of coating thickness and surface topography changes. Figure 5 shows changes in the topography of the sample 31 with zinc coating thickness of 6.5 μm.

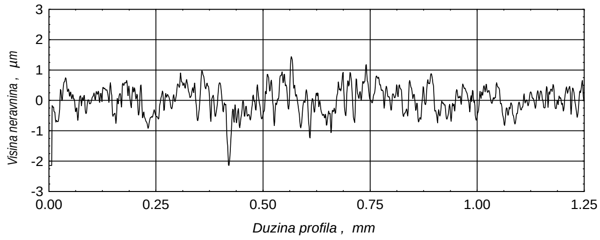

a) Before applying the coating, Ra=0,356 μm

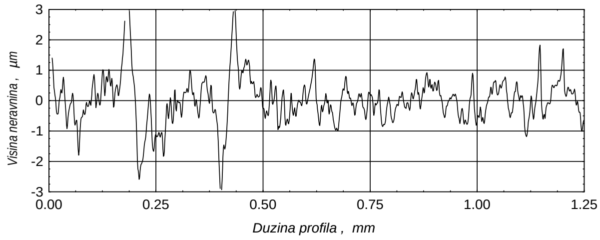

b) After application of Zn, Ra=0,566 μm

Figure 5. Profile of the sample 31

Figure 6. The appearance of the sample surface 31 after application of Zn

Table 4 shows the change in Ra due to the application of chrome plating.

Table 4. Change parameters Ra

Sample number	Grinding	Hardness samples, HRC	Thickness μm	Ra before μm	Ra after μm
7	**A**	46,5	13.21	0.3	0.35
15	**A**	51,5	8.25	0.278	029
26	**A**	47,1	12,20	0.384	0.356
29	**A**	37,1	15.63	0.404	0.38
35	**A**	24,4	11.17	0.43	0.439
37	**A**	22,1	14.87	0.322	0.418
18	**B**	48,1	12.60	0.226	0.32
20	**B**	47,8	7.87	1.84	1.86
24	**B**	24,7	9.27	0.268	0.363
25	**B**	24,6	7.10	0.47	0.439
28	**B**	32,1	13.59	0.295	0.305
32	**B**	51,4	12.07	0.29	0.302
33	**B**	19,3	7.75	0.304	0.305

From table 4 it can be concluded that applying a coating of chromium leads to minor changes - an increase of the surface topography parameter Ra. In Figure 5 is shown the profile of the sample 37 before and after application of chrome plating. It can be seen that there was an increase of height roughness parameters, but also a significant increase in steps prominence.

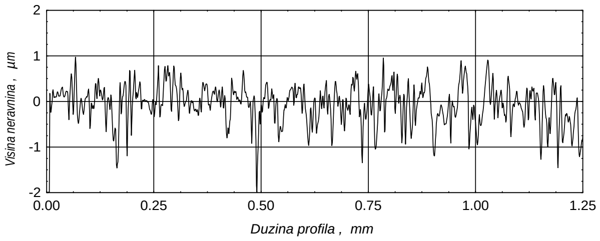

a) Before applying the coating Cr, Ra=0,322 μm

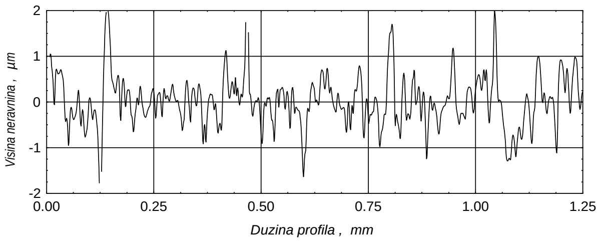

b) After application of Cr, Ra=0,418 μm

Figure 7. Profile of the sample 37

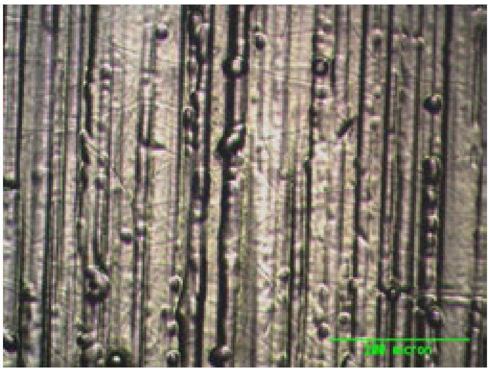

Figure 8. The appearance of the sample surface 37 after application of Cr (Ra=0,418 μm)

Figure 7 shows the surface appearance of the sample 33 on which is applied chrome coating thickness 7.75 μm. Comparing the appearance of this surface and the sample 37 with chrome coating thick 14.9μm it can be seen that sample 33 is clearly perceived the slightest traces of processing, while the sample 37 shallow bumps "flattening" - filled with chromium.

Figure 9. The appearance of the sample surface 33 after application of Cr (Ra=0,305 μm)

4. CONCLUSION

The main parameters that are inherited through the technological process of making the parameters related to properties of materials: their composition, structure, stress state, etc.., and parameters related to macro and mikrogeometry area (geometrical parameters).

Preliminary results of the surface topography changes depending on the type of Zn and Cr have shown that coating leads to significant changes in topography and that in order to establish the correlation very extensive research is required.

REFERENCES

[1] S. Đorđević, M. Maksimović, M. G. Pavlović, K. I. Popov, Galvanotehnika, Tehnička knjiga, Beograd, 1998.

[2] E. V. Proskurkin, V. A. Popovič, A. T. Moroz, Cinkovanie, “Metalurgija”, Moskva, 1988.

[3] H. G. Creutz, S. Martin, Plating and surface finishing, 1975.

[4] Volker Kunz, ZINTEK–TECHSEAL-TRI-COAT Catalouge, Trebur 2001.

[5] SRPS C.T7.111:1991

[6] SRPS C.T7.117:1991

[7] ISO 4539

Serbian Tribology Society

SERBIATRIB '11

12th International Conference on Tribology

Faculty of Mechanical Engineering in Kragujevac

Kragujevac, Serbia, 11 – 13 May 2011

INHOMOGENITIES OF PLASTIC DEFORMATION – SERRATIONS IN COMERCIAL Al-Mg ALLOYS

Lj.Radović[1], M.Nikačević[1], M.Popović[2], E.Romhanji[2], B.Jordović[3]
[1]Military Technical Institute, Belgrade, Serbia; ljmradovic@gmail.rs, banikac@ptt.rs
[2]Faculty of Technology and Metallurgy, Belgrade, Serbia, amiljana@tmf.bg.ac.rs, bendre@tmf.bg.ac.rs
[3]Technical Faculty Čačak, Serbia, bjordovic@tfc.kg.ac.rs

Abstract: *Plastic deformation of solid solutions is often accompanied by plastic instabilities due to dynamic strain aging (DSA) and dislocation interaction. The dislocation interactions lead to stress serrations and localized strain (deformation bands) in tensile tests, known as the Portevin-Le Chatelier (PLC) effect. The instable PLC deformation is closely connected with a localization of strain within the front of (propagating) deformation bands. These bands significantly limit the sheet formability leading to unacceptable surface roughness or premature fracture.*
The characteristics of serrated yielding of commercial Al-Mg sheets (3-6%Mg) have been studied using room temperature tensile testing. Tensile tests were performed at strain rates of $\dot{\varepsilon}_1 = 6.7\cdot10^{-4}\,s^{-1}$ *and* $\dot{\varepsilon}_2 = 6.7\cdot10^{-3}\,s^{-1}$. *The initiation of serrated flow was found to depend on Mg content as well as strain rate. The type of the serrations also, was governed by the strain rate and Mg content. The amplitude of the serrations (*$\Delta\sigma$*) increased with increasing strain and decreasing strain rate. The noticed dependence* $\Delta\sigma$ *of the Mg content reflects the role of Mg atoms in locking/pinning the dislocations. The strain rate showed no influence on the yield stress, while the general stress level and ultimate tensile stress have increased with decrease of strain rate. Therefore, it leads to increase the difference between ultimate and yield strength (*R_m-$R_{0.2}$*), and stronger work hardening effect, because of suppression of the dynamic recovery in Al-Mg alloys.*

Keywords: *Al-Mg alloys, serrated yielding, Mg content, strain rate, The Portevin-Le Chatelier effect (PLC).*

1. INTRODUCTION

Lightweight Al-Mg alloys have been widely used in many fields because of their optimal combination of strength, formability, corrosion resistance and weldability. However, their unstable plastic flow restricts theirs application. Unstable flow appears as a yield point elongation (or Lüders elongation) within the few percent of deformation, and discontinuous or serrated yielding at higher strains, tipical for industrial production. The Lüders elongation during uniaxial stretching causes the appearance of surface relief known as "A" ("flamboyant"), as discontinuous yielding causes the appearance yielding "B" ("parallel bands") type surface markings [1-4]. Both stretcher markings are harmful because they cause pronounced surface roughness.

Discontinuities in the flow stress as a manifestation of dynamic strain ageing, are commonly observed during deformation of f.c.c. solid-solution aluminum alloys under certain circumstances. It has been extensively investigated in aluminium alloys containing magnesium [5-10]. In the most accepted models serrated flow is related to the dynamic interaction between diffusing solute atoms and mobile dislocations, i.e. dynamic strain ageing (DSA). Solute atoms restrict the mobility of the dislocations and make dislocation rearrangement and annihilation more difficult. Mg atoms are particularly effective in this because of their large atomic size difference with aluminium. Solutes preferentially concentrate at dislocations due to the energetic interaction of the two sources of field, forming solute atmospheres at mobile dislocations and arrest them. When the applied force is raised high enough, the mobile dislocations break away from the atmospheres and advance to the other obstacles. Repetition of this process is manifested as the serrated flow observed in the stress-train curve. The amplitude of the serrations, defined as the stress change from the highest to the lowest points of the serration, is used for evaluated /the main measure of the serrated yielding.

Different serrations types can be identified from macroscopic stress-strain curves as a result of differences in microstructural strain localization./microstructure and testing condition. Researches classify serrations as type A, B, C D or E, which can occur sometimes simultaneously, depending on the testing condition [2,10-11]. Different types of serrations can overlap each other. Type A serrations are characterized by an abrupt rise of loads (stresses) above the general level of the load-extension (stress-strain) curve, type B are marked by fluctuations loads around the general level of curve, and type C serrations are characterized by fall of loads below the general level of curve. In many cases it is not clear to make distinction between B and C serrations. It seems that C serrations drop to lower stresses more abruptly than B serrations and A and B serrations do not occur under the some test conditions [6,9,12] More recently a laser scanning extensometer was used to identify serrations types based on deformation band propagation [13-15]. Detailed description of serrations types was done in ref 7.

In order to describe the amplitude of the serrations ($\Delta\sigma$), defined as the stress change from the highest to the lowest points of the serrations, has been investigated [6,16-20].

The strength of Al-Mg alloys arises from several factors. The Mg in solution provides solution hardening, and these alloys also have a significant Hall-Petch slope compared with other Al alloys, so grain size strengthening is important. The strain hardening significant contributes to the strength because of the high work hardening rate. Apart well known influence Mg content on the mechanical properties, it would be expected that Mg content has influence on deformation behaviour and the characteristics of serrated yielding. Further, it is known that deformation behaviour and mechanical properties of Al-Mg alloys are sensitive to strain rate.

The present paper is focused on some experimental observations of characteristics of serrated yielding in three commercial magnesium-containing aluminium alloys as function of deformation variables.

2. EXPERIMENTAL

To investigate the influence of Mg content and the strain rate on the deformation behaviour, three annealed commercial Al-Mg alloys, with average grain size of approximately 15 μm were tested. The chemical compositions of the alloys are:

AlMg3 (3.1 Mg, 0.03 Mn, 0.31 Fe, 0.09 Si); AlMg4.5Mn (4.55 Mg, 0.47 Mn, 0.42 Fe, 0.16 Si), AlMg6Mn (5.95 Mg, 0.54 Mn, 0.36 Fe, 0.12 Si).

Tensile tests were carried out at room temperature on a “Zwick” testing machine, using small ASTM tension specimen with a 25 mm gauge length. To investigate the influence of the strain rate on the mechanical properties and serrated yielding, different initial strain rates of $\dot{\varepsilon}_1 = 6.7 \cdot 10^{-4} s^{-1}$ and $\dot{\varepsilon}_2 = 6.7 \cdot 10^{-3} s^{-1}$ were applied.

3. RESULTS

The set of typical deformation curves of annealed Al-Mg alloys with grain size of about 15 μm, are shown in Figs. 1 and 2. Well developed serrations have been observed in all investigated alloys. The critical strain for serrated yielding ε_c=0, i.e. serrations began immediately after the Lüders elongation and continued until failure. The amplitude of the serrations beyond the Lüders strain increases with strain. During initial deformation at lower strain rate ($6{,}7\cdot10^{-4}s^{-1}$) A+B types of serrations were observed, and with increasing strain they changed to type B. This behaviour was observed in both AlMg3 and AlMg4.5 alloys. Type C was observed in AlMg6Mn alloy at the same strain rate (load falls below the general level of the curves).

With increasing strain rate, at strain rate of 6,7·10-3 s-1, in AlMg3 alloy the type A serrations were observed, while A, A+B and B serrations were observed in the other two alloys (Fig. 2). Despite that A and B serrations occur in both alloys, type A serration is less prominent in AlMg6Mn than in AlMg4.5Mn alloy, i.e. type B dominates in the AlMg6Mn alloy. The amplitude of the serrations steadily increases as a function of strain in all cases.

Apart from difference in the type of the serrations, there is also a difference in the amplitude of serrations, $\Delta\sigma$ (Fig. 3) shows the maximum amplitude of the serrations, $\Delta\sigma$, as a function of strain rate and Mg content. $\Delta\sigma$ depends strongly on both Mg content and strain rate. As the Mg content increases, amplitude of the serration raises almost linearly, while the increase of strain rate decreases it.

The effects of the strain rates and Mg content on the mechanical properties are shown in Fig. 4. Ultimate tensile strength slightly increases with decreasing strain rate and increases with increase in Mg content.

4. DISCUSSION

Lüders yielding and serrated flow were established to confirm the inhomogenous deformation during uniaxial tension. The Lüders yielding at the onset of plastic flow in the annealed condition in tested Al-Mg alloys indicates a low initial density of mobile dislocations. The Lüders yielding in substitutional alloys, like Al-Mg, occures when concentration of solutes atoms is enough to form atmosperes around the mobile dislocation and block them. To continue deformation the dislocation have to break away from these atmospheres and multiply.

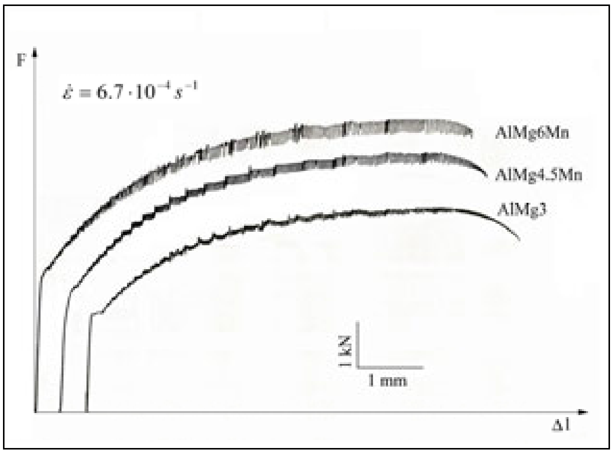

Figure 1. Deformation curves of Al-Mg alloys at strain rate $\dot{\varepsilon}_1 = 6.7 \cdot 10^{-4} s^{-1}$.

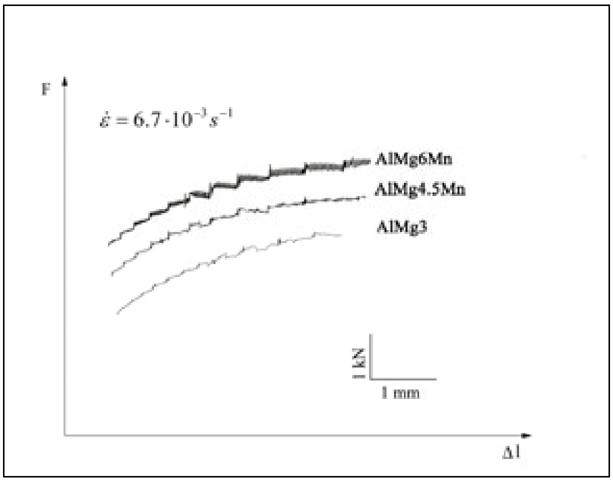

Figure 2. Deformation curves of Al-Mg alloys at strain rate $\dot{\varepsilon}_2 = 6.7 \cdot 10^{-3} s^{-1}$ - segment with serrations.

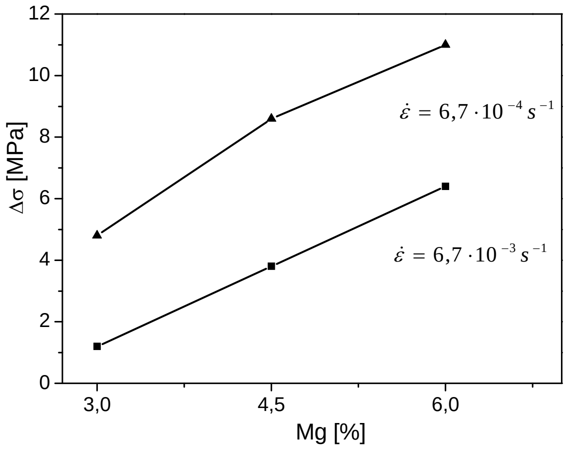

Figure 3. The influence of magnesium content and strain rate on amplitude of serrated yielding (Δσ).

So, the Lüders yielding fenomenon depends on relation between concentration of solute atoms and dislocation density [21], and become more pronounced with increasing of this relation [10].

The absence of Lüders yielding was observed only in AlMg6Mn alloy with coarse grains [22] at both strain rate (similar results was published earlier for AlMg6.5 alloy with grain size of 35-40μm ref. 12). This apparently is due to both the higher Mg content and large grains. The addition of Mg increases density of mobile dislocations, produced in activated dislocation sources [8,10]. This activation of dislocation sources is enhanced in large grains structures, together with the spreading of deformation to neighbouring grains. This suggest that the high density of dislocation in coarse grained AlMg6Mn alloy is sufficient to remove yield point (inhomogenities) observed in the other two alloys. The serrated yielding has occurred in all investigated alloys under the testing condition and also increases from AlMg3 to AlMg4.5Mn and than AlMg6Mn alloys (Figs 1 and 2). Mg content and strain rate affect the type and frequency of the serrations, but the influence of the grain size was not observed.

At low strain rate tests (~10-4s-1) type A+B and B serrations occure in both AlMg3 and AlMg4.5Mn alloys, but in AlMg6Mn alloy only C type occures. At higher strain rate (~10-3s-1), while the A type serration dominates in AlMg3 alloy, with further increase in Mg content type A become less prominent, resulting in the domination of type B serrations. This difference is related to the Mg content. Obviously, the increase of the Mg content as well as decrease of the strain rate lead to changes types of serration on the stress-strain curves from A→B→C. It seems that when the arrest mobile dislocation become more effectively, as a result of addition Mg and lower strain rate, it leads to change of types of serrations from A via B to C. C type of the serrations only fall below the general stress-strain dependence and it is considered that this type refer to the unlocking of dislocations from solute pinning and called “unlocking” serrations. On the other hand type A or B serrations refer to the locking of dislocations by solutes and called “locking” serrations. That kind of relationship has been found in ref. [9,12,20]. It seems that the most effective impede of dislocation and consequently the highest flow stress (Fig. 4) corresponds to the appearance of the type C of serrations, but/although the exact mechanism leading to either A and B or to C serrations are still hardly known.

The intensity of the serrated yielding, evaluated by the amplitude of the serration, has showed a relatively strong dependency of the Mg content and strain rate (Fig. 3). The moving dislocations are temporary held at obstacles, so Mg atoms than diffuse to these dislocations and arrest them. It was shown that both the mobile and forest dislocations densities increase with increasing Mg content [8,10 Horvath, Robinson]. Moreover, the increases of the mobile dislocation is higher than forest dislocation, because Mg enhanses strongly the multiplication of mobile dislocations. The addition of Mg decreases the mean free path for dislocation motion, so the dislocations intersect each other more frequently. Also, the addition of Mg suppresses the recovery of the Al-Mg alloys because the stocking fault energy decreases and cross-slip becomes more difficult [21]. This enhances strongly the multiplication of the mobile dislocations, leading to theirs higher density. The more dislocations temporary held at obstacles, the higher force is needed for dislocation unpinning, resulting in higher amplitude of the serrations on the stress-strain curve [1,5,10,20,23-25].

Strain rate analysis gives a good indication of the intensity of dynamic strain ageing, too. It is assumed to be due to lower rate of mobile dislocations, which is proportional to strain rate [21]. Therefore, the waiting time for the mobile dislocations at obstacles is longer which is manifested as an increase of the amplitude of the serrations. The mobile dislocations can be arrested more effectively by solute atoms at lower strain rate (~10^{-4} s^{-1}) than at higher (~10^{-3} s^{-1}), leading to the increase of the amplitude of the serrations.

It was found that the yield stress is rather strain rate independent in annealed Al-Mg alloys. On the other hand the ultimate strength exhibits inverse strain rate dependence. At higher strain rate the level of flow curves decreases. The minor influence the strain rate on the yield stress indicates that the concentration of the solutes /Mg atoms / in annealed Al-Mg alloys (3-6 wt.%Mg) is sufficient to form atmosphere and block mobile dislocations at the onset of the deformation and the stress for unpinning dislocation i.e. multiplication mobile dislocations is independent of the strain rate. The strength of the tested Al-Mg alloys in annealed condition is affected primarily by solution strengthening/hardening from the Mg (and/or other) atoms and grain size strengthening, according to the well known Hall-Petch relationship [21]. According to the previously reported results, the frictional stress σ_0 in the Petch equation, which reflects solution hardening due to Mg in solution, increases linearly with Mg content [23]. The addition of approximately 0.5wt. % Mn increases strength of AlMg4.5Mn and AlMg6Mn alloys, mainly due to solid solution strengthening.

5. CONCLUSIONS

Deformation behaviour has been investigated in three annealed commercial Al-Mg alloys (AlMg3, AlMg4.5Mn, and AlMg6Mn) at room temperature and strain rates of 6,7·10-4 s-1 and 6,7·10-3 s-1. Well developed serrations have been observed in all investigated alloys. The instable PLC deformation is closely connected with a localization of strain within the front of (propagating) deformation bands. These bands significantly limit the sheet formability leading to unacceptable surface roughness or premature fracture.

Serrations of A, B, A+B and C types were observed on stress-strain curves. The type and frequency of serrations were governed by Mg content and strain rate. While the A type serration dominates in AlMg3 alloy, further increase in Mg content decrease it, resulting in the domination of type B serrations in higher strain rate or tests C type in low strain rate tests in AlMg6Mn alloy.

The intensity of the serrated yielding, evaluated by the amplitude of the serrations/stress drop, ($\Delta\sigma$), increased with increasing strain and decreasing strain rate. The noticed dependence amplitude of the serrations of the Mg content reflects the role of Mg atoms in locking/pinning the dislocations.

REFERENCE

[1] Ildong Choi at al. Scripta Mat. Vol. 38, No.6, 1998, 887-892.

[2] H.Fujita and T.Tabata, Acta Met., Vol. 25, 1977, 793-800.

[3] D.J.Lloyd, Metall. Trans., Vol. 11A, 1980, 1287-1294.

[4] E.Romhanji et al., MJoM Metalurgija - Journal of Metalurgy, Vol 10 No 3, 2004, 205-216.

[5] Wei Wen, J.G.Morris, Mat.Sci.Eng A354, 2003, 279-285.

[6] E. Pink, A.Grinberg, Acta Metall. Vol.30, No, 1982, 2153-2160

[7] E.Pink, Acta Metall. Vol.37, No, 7, 1989, 1773-1781.

[8] G.Horváth, et al., Mat.Sci.Eng. A445-446, 2007, 186-192.

[9] Baohui Tian, Mat.Sci.Eng. A 349, 2003, 272-278.

[10] J.M.Robinson and M.P.Shaw, Mat.Sci.Eng., A174, 1994, 1-7

[11] E.Pink, W. Bernt and Monika Fellner, Scripta Met., Vol. 28, 1993, 1137-1142.

[12] E.Romhanji, M.Popovic, V.Radmilovic, Z.Metallkd. 90, 1999, 4, Carl Hanser Verlag. München, 305-310.

[13] A. Ziegebein et al., Comp. Mat. Sci. 19, 2000, 27-34.

[14] F.Chmelik at al. Mat.Sci.Eng. A 324, 2002, 200-207

[15] J.M.Reed, M.E.Walter, Mat.Sci.Eng. A359, 2003, 1-10.

[16] D. Thevenet, M. Mliha-Touati, A. Zeghloul, Mat. Sci.Eng. A266, 1999, 175–182.

[17] D. Thevenet, M. Mliha-Touati, A. Zeghloul, Mat. Sci.Eng., A291 (2000) 110–117.

[18] E. Pink a,1, R.J. Arsenault, Mat. Sci. Eng. A272, 1999, 57–62.

[19] L.P. Kubin, Y. Estrin, Acta Metall. 38 (1990) 697.

[20] Wei Wen, Yumin Zhao, J.G. Morris, Materials Science and Engineering A 392, 2005, 136–144.

[21] Dj. Drobnjak, Physical Metallurgy, Faculty of Technology and Metallurgy, Belgrade, 1988.

[22] Lj. Radovic, MSc Thesis, The influence of thermomechanical treatment and chemical composition on formability of Al-Mg alloys, Faculty of Technology and Metallurgy, Belgrade, 2008.

[23] G.B. Burger, A.K. Gupta, P.W. Jeffrez and D.J. Lloyd, Mat.Charact., 35, 1995, 23-29.

[24] D.J.Lloyd, Materials Forum Vol. 28, ed. by Nie et al., Institute of Materials Engineering Australasia Ltd, 2004, 107-117

[25] S.Kumar et al., Mat.Sci.Tech., Vol.17, 2001, 113-115.

Serbian Tribology Society

SERBIATRIB '11

12th International Conference on Tribology

Faculty of Mechanical Engineering in Kragujevac

Kragujevac, Serbia, 11 – 13 May 2011

TRIBOLOGY IN BIOMATERIALS DESIGN AND SELECTION

Fatima Zivic[1], Miroslav Babic[1], Slobodan Mitrovic[1], Dragan Adamovic[1], Nenad Grujovic[1]
[1]Faculty of Mechanical Engineering, Kragujevac, Serbia
zivic@kg.ac.rs, babic@kg.ac.rs, boban@kg.ac.rs, adam@kg.ac.rs, gruja@kg.ac.rs

Abstract: *The paper presents review of selected biomaterials that were subject of tribological investigations at Tribology Center of Mechanical Engineering Faculty Kragujevac. Development, design and selection of biomaterials are primary determined by characteristics and nature of the tissue that is being replaced or supplemented. Modern material investigations at micro level loads enable insight into new aspects of material behaviour and offer possibilities for further improvement. Tribological investigations of biomaterials can contribute to their development by offering solutions for wear decrease and wear prediction. Short review is presented of tribological tests of four different biomaterials, namely Ti6Al4V alloy, stainless steel AISI 316LVM, ultrahigh-molecular-weight polyethylene (UHMWPE) and polymethyl methacrylate (PMMA).*

Keywords: *Biomaterials, Ti alloys, Stainless steel AISI 316LVM, UHMWPE, PMMA, Nanotribometer*

1. INTRODUCTION

Advances in biomedical materials research and development have made an enormous impact on the treatment of injury and disease of the human body. Biomaterials scientists and engineers pursue novel techniques and methodologies to study cells, their components, complex tissues and organs and their interactions with natural and synthetic materials and implanted prosthetic devices, as well as to develop and characterize the materials used to measure, restore, and improve physiologic function, and enhance survival and quality of life [1-4]. Biomaterials applications increased rapidly in the late 1800s. The first metal devices to fix bone fractures were used in late eighteenth to nineteenth century; the first total hip replacement prosthesis was implanted in 1938; and in the 1950s and 1960s, polymers were introduced for cornea replacements and as blood vessel replacements [1].

A biomaterial is any matter, surface, or construct that interacts with biological systems. Williams in 1987 defined a biomaterial as: "a nonviable material used in a medical device, intended to interact with biological systems". It is still true today, but the level of interaction of biomaterials with the biological system has changed dramatically. Biomaterial function has advanced from remaining relatively inert in the body to being "bioactive" and assisting with regeneration. Bioactive materials have the capability to initiate a biological response after implantation and research nowadays is aimed towards regeneration of a damaged tissue or whole organ through this interaction.

Multidisciplinary area of biomaterials development, design and selection is today one of the most promising field of research. There is no material suited for all biomaterial applications and new applications are continually being developed as medicine advances. There are number of questions that still need to be answered regarding the biological response to biomaterials and the optimal role of biomaterials in tissue regeneration. The usual approach to regain the function of the lost tissue was to replace it with a simple biomaterial. But as understanding of many aspects of tissues, disease, and trauma improved, the concept of attempting to repair damaged tissues emerged.

Development and application of biomaterials are directly determined by characteristics and nature of the tissue that is being replaced or supplemented. Desired or optimal properties of a biomaterial very much depend on its biomedical application. General strategies for guiding tissue repair by varying the chemistry, structure and properties of biomaterials are subject of many ongoing research projects. Application-specific biomaterials solutions are investigated according to the major organ systems in the body. Important part of biomaterials development is also standardization and regulative to ensure safety and efficiency in this novel scientific area, including many social questions, as well.

Characterization of materials used in medical purposes represents a very complex field which is application dependent. Many interdependent parameters of the observed material are important to study and understand in relation to their material characteristics (thermomechanical processing, microstructural properties), mechanical properties (hardness, modulus of elasticity, tensile stress), corrosion and wear resistance, biocompatibility and osseointegration. It is important to determine their exploitation stability in a longer time, especially for biomaterials used for implants (knee and hip replacement, spinal implants, dental implants etc.) [2]. Investigations in relation to wear behavior, stress/strain development, characteristics such as design and selection of classical or 3D porous structure, grain orientation, porosity, functional stability (durability, biocompatibility, wear, corrosion) are realised in worldwide laboratories in order to provide quantitative parameters for further evaluation and improvement. Tribological behaviour of material is unavoidable, especially from aspect of wear. Tribological investigations by taking into account variation of contact materials and contact conditions can efficiently contribute to improvement of existing biomaterials and validation of newly developed.

Table 1. Materials and their medical use

Class of Material	
Metal	
Stainless steel	Joint replacements, bone fracture fixation, heart valves, electrodes
Titanium and titanium alloys	Joint replacements, dental bridges and dental implants, coronary stents
Cobalt-chrome alloys	Joint replacements, bone fracture fixation
Gold	Dental fillings and crowns, electrodes
Silver	Pacemaker wires, suture materials, dental amalgams
Platinum	Electrodes, neural stimulation devices
Ceramics	
Aluminum oxides	Hip implants, dental implants, cochlear replacement
Zirconia	Hip implants
Calcium phosphate	Bone graft substitutes, surface coatings on total joint replacements, cell scaffolds
Calcium sulfate	Bone graft substitutes
Carbon	Heart valve coatings, orthopedic implants
Glass	Bone graft substitutes, fillers for dental materials
Polymers	
Polymethylmethacrylate (PMMA)	Bone cement, intraocular lenses
Polyethylene (PE); Ultra-high-molecular-weight polyethylene (UHMWPE)	Hip and knee implants, artificial tendons and ligaments, synthetic vascular grafts, dentures, and facial implants
Polyvinylchloride (PVC)	Tubing, facial prostheses
Nylon	Surgical sutures, gastrointestinal segments, tracheal tubes
Silicone rubber	Finger joints, artificial skin, breast implants, intraocular lenses, catheters
Polyester	Resorbable sutures, fracture fixation, cell scaffolds, skin wound coverings, drug delivery devices
Natural Materials	
Collagen and gelatin	Cosmetic surgery, wound dressings, tissue engineering, cell scaffold
Cellulose	Drug delivery
Chitin	Wound dressings, cell scaffold, drug delivery
Ceramics or demineralized ceramics	Bone graft substitute
Alginate	Drug delivery, cell encapsulation
Hyaluronic acid	Postoperative adhesion prevention, ophthalmic and orthopedic lubricant, drug delivery, cell scaffold

Characterization of the surface layers on observed materials, to study local phenomena on the micro- and nano-scale, is realised by advanced microscopy techniques such as scanning electron microscopy (SEM), atomic force microscopy (AFM) or scanning force microscopy (SFM), transmission electron microscopy (TEM), auger electron spectroscopy (AES), etc. It is usually accompanied with chemical analysis such in case of Raman microscopy, or EDS analysis (Energy-dispersive X-ray spectroscopy (EDS or EDX), which is often integral part of SEM microscope. Wear mechanisms and microstructural characteristics can be determined by using these microscopy techniques.

Some estimates on biomaterials use [1]:

- Total hip joint replacements: 448,000
- Knee joint replacements: 452,000
- Shoulder joint replacements: 24,000
- Dental implants: 854,000
- Coronary stents: 1,204,000
- Coronary catheters: 1,328,000

Materials selection for a medical device is complicated. The selection depends on a number of factors, including the mechanical loading requirements, chemical and structural properties of the material itself, and the biological requirements. Generally, materials used for interaction with biological systems can be: metals (Ti-based alloys, stainless steel), polymers (Polymethyl methacrylate**,** PMMA, Ultra-high-molecular-weight polyethylene, UHMWPE, Polylactic acid, PLA), ceramics (Al_2O_3, Hydroxyapatite), composites and many more. Classes of material current uses for biomedical purposes are shown in Table 1 [1].

2. TITANIUM ALLOYS

Titanium and titanium alloys has broad applications in a field of medicine [1-5]. Extensive research activities in relation to different ways of Ti alloys manufacturing and its further treatments and surface modifications are aimed at characteristics improvement. Ti alloys are applied in cases when high strength and low density are of primary importance [1], even though they posses low sliding wear resistance due to its low resistance to plastic shearing. They are particularly interesting for biomedical applications because of their excellent biocompatibility, relatively low Young's modulus and high corrosion resistance [5-14]. Elastic modulus of titanium based materials vary from 55 GPa (Ti-29Nb-13Ta-7.1Zr alloy) to 112 GPa (Ti6Al4V alloy) [2], what is lower compared to 316L stainless steel (200 GPa). Elastic modulus of the bone is approximately 30 GPa and development of new alloys is aimed at achieving elastic modulus close to that of the bone. Metal alloy of nickel and titanium, nickel titanium (NiTi), also known as nitinol, is one of the novel shape memory biomaterials having elastic modulus of approximately 48 Gpa. Titanium based materials are often used for joints (e.g. femoral stem in hip replacements).

Ti6Al4V alloy becomes osteointegrated in a very short period when in contact with a bone. Despite their good mechanical and chemical properties and low density ($4.5 g/cm^3$) the use of Ti alloys for structural applications is prevented by their poor wear resistance what is attributed mainly to two reasons: low resistance to plastic shearing what as a consequence has weak counteracting of material to wear mechanisms (adhesion, abrasion, delamination); and high flash temperatures induced by friction during dry sliding implying forming of surface oxide which greatly influences frictional and wear behaviour of the observed system [2-10]. Due to this, many surface modification techniques are applied in order to improve tribological behaviour of Ti alloys [12-14]. However, the acting wear mechanisms during sliding wear of titanium alloys have not been sufficiently addressed and understood and needs further study [6, 7, 15].

Laboratory simulations regarding biomaterial behaviour can be conducted in different ways. If wear behaviour is considered, tribological investigations are usually performed with reciprocating sliding tester with high contact pressures (e.g. ball-on-flat sliding wear test), in dry conditions or with some solutions simulating body fluids (Ringer solution, distilled water etc.). Investigations on influence of the contact load, sliding speed and environment variation offer valuable information on Ti alloy behaviour.

Real time diagrams of friction coefficient Ti6Al4V alloy sliding against alumina (Al_2O_3) under dry and lubricated conditions for selected regimes of normal force and maximum linear speed are shown in Figs. 1 and 2. Optical micrographs of worn scars are also shown in Figs. 1 and 2. Maximum penetration depth of the ball into the observed sample is also given in Figs. 1 and 2, as recorded on nanotribometer. Tribological tests were realised on the CSM Nanotribometer and linear reciprocating sliding mode was used. Static body was 1.5 mm diameter alumina ball. Moving body was flat rectangular Ti6Al4V alloy sample. Testing was done with 0.5 mm stroke (0.25 mm half amplitude) in dry conditions and with Ringer's solution, in ambient air (temperature of 25 °C). Five values of normal force were selected (100 mN, 250 mN, 500 mN, 750 mN, 1000 mN) and three values of sliding speed (4 mm/s, 8 mm/s, 12 mm/s). The values of estimated maximum contact pressure were 0.68, 0.93, 1.17, 1.34 and 1.47 GPa, respectively. Duration of one test was 30000 cycles, whereat distance of two strokes represents one cycle. Selected sliding velocities corresponds to the range of speed characteristic for hip joints testing (0–50 mm/s) [16].

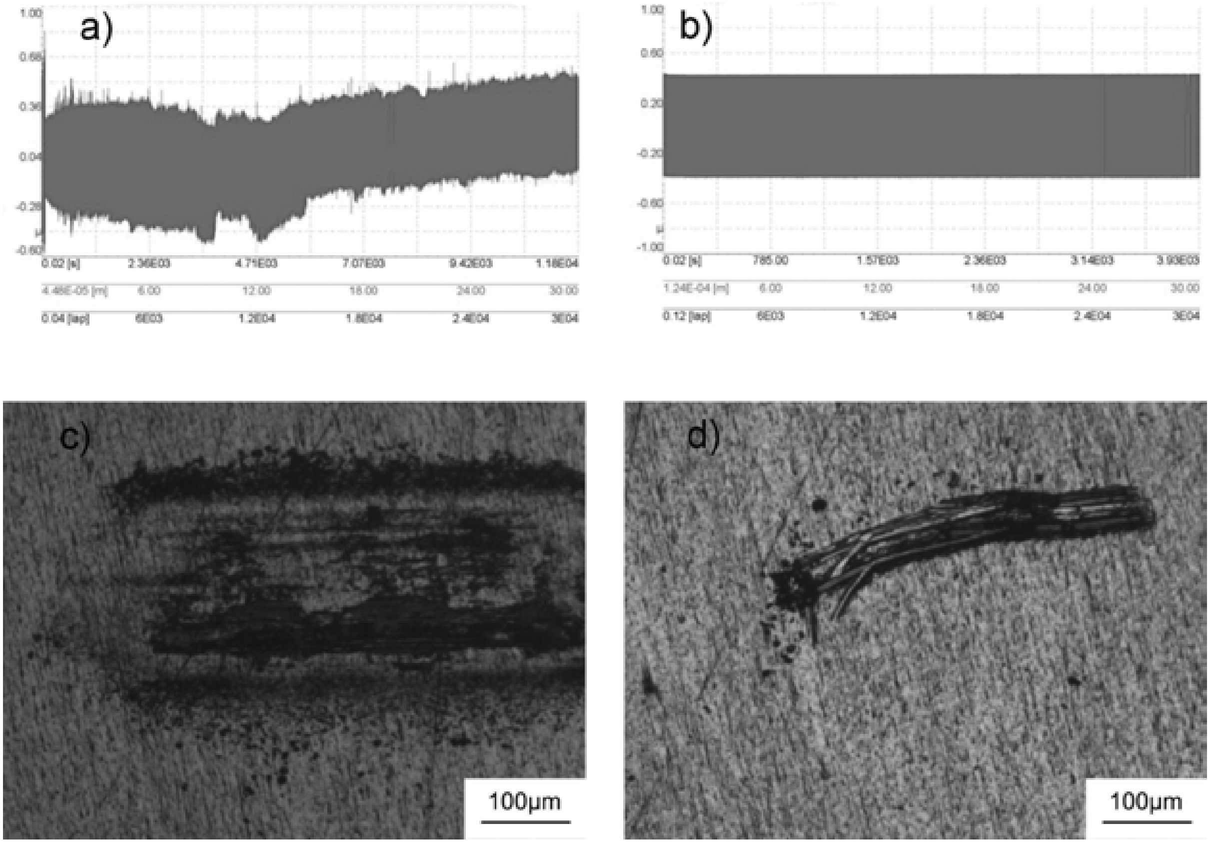

Figure 1. Diagrams of friction coefficient and optical micrograph showing wear track on Ti6Al4V sample:
a), c) Dry, v=4 mm/s; F_N=100mN; Penetration depth: 2.7μm;
b), d) Dry, v=12 mm/s; b F_N=1000mN; Penetration depth: 18.0μm;

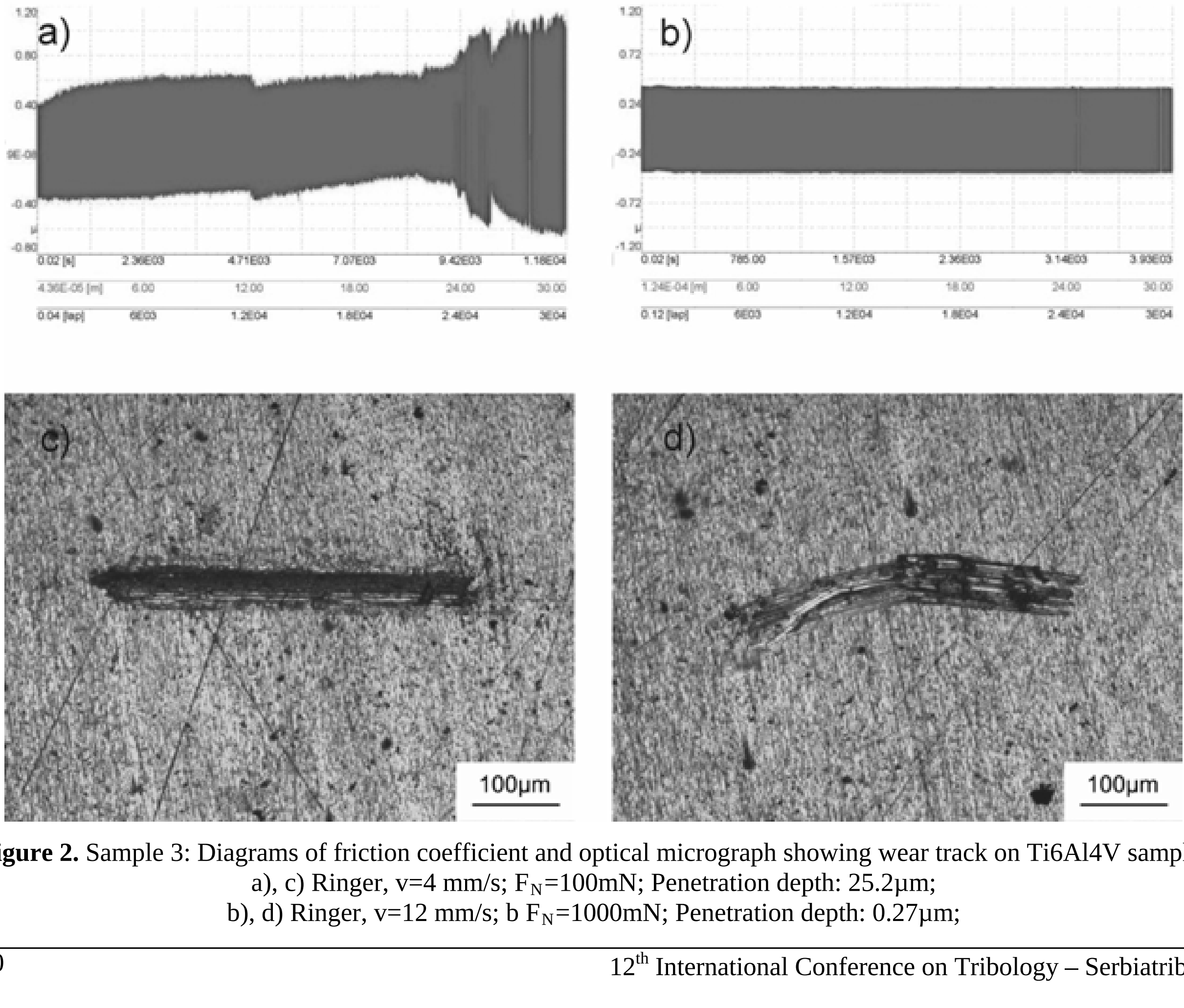

Figure 2. Sample 3: Diagrams of friction coefficient and optical micrograph showing wear track on Ti6Al4V sample:
a), c) Ringer, v=4 mm/s; F_N=100mN; Penetration depth: 25.2μm;
b), d) Ringer, v=12 mm/s; b F_N=1000mN; Penetration depth: 0.27μm;

It can be clearly seen (Figs. 1 and 2) that change of contact conditions (load, sliding speed, dry sliding or with Ringer’s solution) produced significant change in tribological behaviour of Ti6Al4V samples. It is obvious that some regimes should be avoided when using Ti6Al4V alloy. Low sliding speed produced variation of the friction coefficient (Figs. 1a, 2a). In case when Ringer’s solution was present, friction coefficient curve started to rise after approximately 24000 cycles, indicating further change of the behaviour. High sliding speed produced steady friction coefficient during the whole test (Figs. 1b, 2b). Worn tracks are of rather smaller dimensions at 4 mm/s sliding speed than at 12 mm/s sliding speed, especially in case of dry sliding (Figs. 1c, 1d and Figs. 2c, 2d). If optical micrographs were compared in cases of dry sliding and sliding with Ringer’s solution (Figs. 1c, 2c and Figs. 1d, 2d), it can be noticed that worn tracks are significantly smaller at sliding with Ringer’s solution. Presence of the Ringer’s solution produced lowering of the wear level, in comparison with dry sliding.

3. STAINLESS STEEL

Application of metals as biomaterials is based on their high strength and resistance to fracture and design to resist corrosion. Many orthopedic devices are made of metal, such as stents, hip and knee joint replacements. Out of the eight coronary stents approved by the US Food and Drug Administration (FDA), seven are made from 316L stainless steel [17]. Plates and screws that hold fractured bone together during healing also are made of metal. They are sometimes retrieved after successful healing, but in other cases they are left in place. Metallic devices are also used to fuse segments of the spine together when the disk has degenerated and as dental root prosthetic implants.

Metals as biomaterials have advantages over ceramics or polymers because they are strong, tough, and ductile (or deformable, particularly as compared to ceramics). However, they are susceptible to corrosion [18] causing adverse effects on the healing process, which led to application of alloys of titanium or cobalt-chrome. Biocompatibility is an issue with metal implants and allergic reactions can occur. Metals also exhibit high density and much greater stiffness than most natural materials they replace, leading to undesirable stress shielding. For instance, after implantation of metal joint replacements loss of adjacent bone has been observed because the bone is not exposed to normal levels of mechanical loading. Solution to these problems has been investigated by application of shape memory alloys (e.g., nitinol) that can be bent or deformed and still return to their original shape when the stress is released.

Stainless steel AISI 316LVM is a Molybdenum alloyed vacuum remelted stainless steel for the production of both temporary and permanent implants. Chemical composition of AISI 316LVM steel is given in Table 2. ASTM F138-03 defines standard specification for wrought 18 chromium-14 nickel-2.5 molybdenum stainless steel bar and wire for surgical implants. DIN standard designation of the steel is DIN: X 2 CrNiMo 18 15 3. It is a vacuum melted to achieve the extremely high levels of purity and cleanliness required for surgical implants. Elastic modulus of AISI 316LVM stainless steel is approximately 200 GPa.

Table 2. Chemical composition of AISI 316LVM steel

C max	Si	Mn	P max	S max	Cr	Ni	Mo	Cu max	N max
0.025	0.6	1.7	0.025	0.003	17.5	14	2.8	0.10	0.10

Stainless steel AISI 316LVM has a very good resistance in physiological environments to general and integranular corrosion due to high purity and low ferrite content; pitting and crevice corrosion due to the high molybdenum content. However, it is highly susceptible to localized forms of corrosion [19]. Many authors investigated possibilities to predict, prevent or lower corrosion of biomedical grade 316LVM stainless steel surface [18, 19, 20].

Real time diagrams of friction coefficient of AISI 316LVM stainless steel sliding against alumina (Al_2O_3) under dry and lubricated conditions for selected regimes of normal force and linear speed are shown in Figs. 3 and 4. Optical micrographs of worn scars are also shown in Figs. 3 and 4. Penetration depth of the ball into the observed sample (Figs. 3 and 4), as recorded on nanotribometer (minus sign) indicated that wear debris was accumulated within the contact zone, during the sliding.

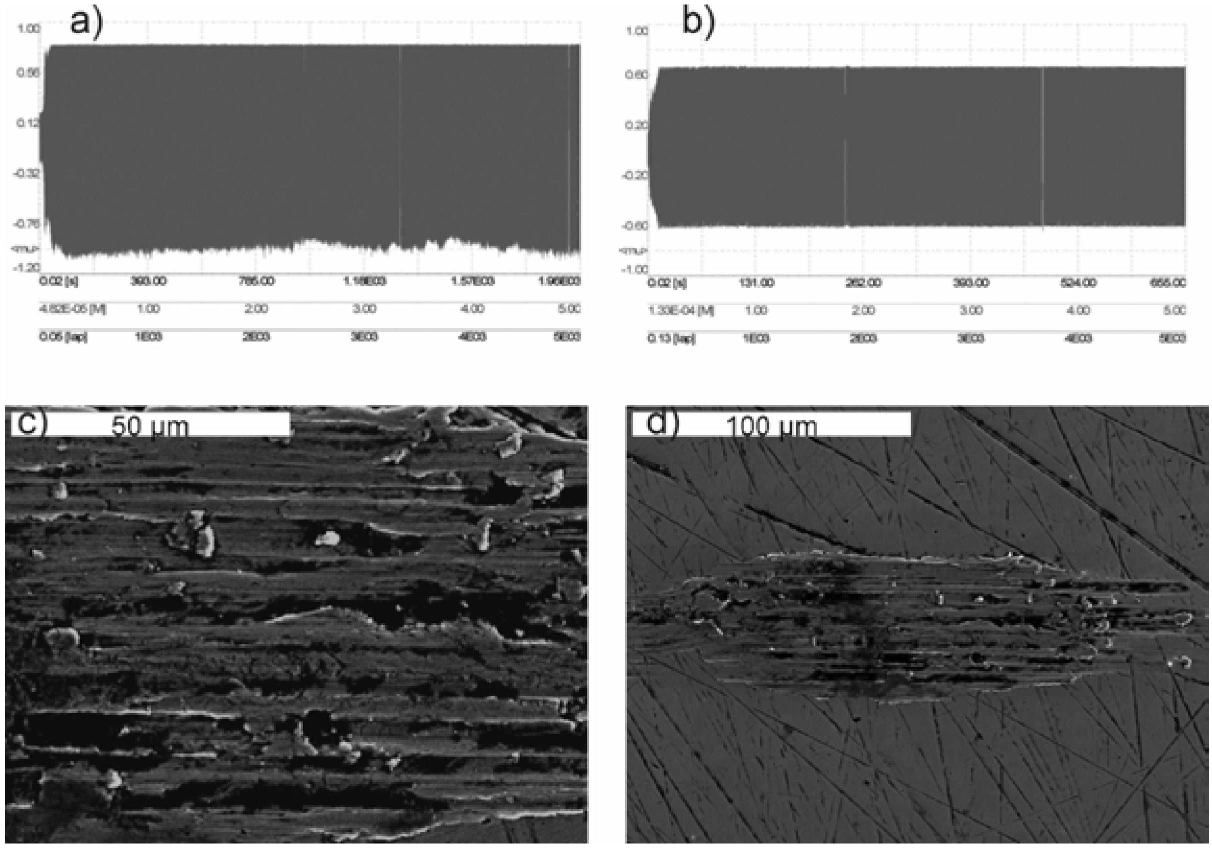

Figure 3. Diagrams of friction coefficient and optical micrograph showing wear track on AISI 316LVM sample in dry conditions: a), c) v=4 mm/s; F_N=100mN; Penetration depth: -1.9µm; b), d) v=12 mm/s; b F_N=750mN; Penetration depth: -0.7µm;

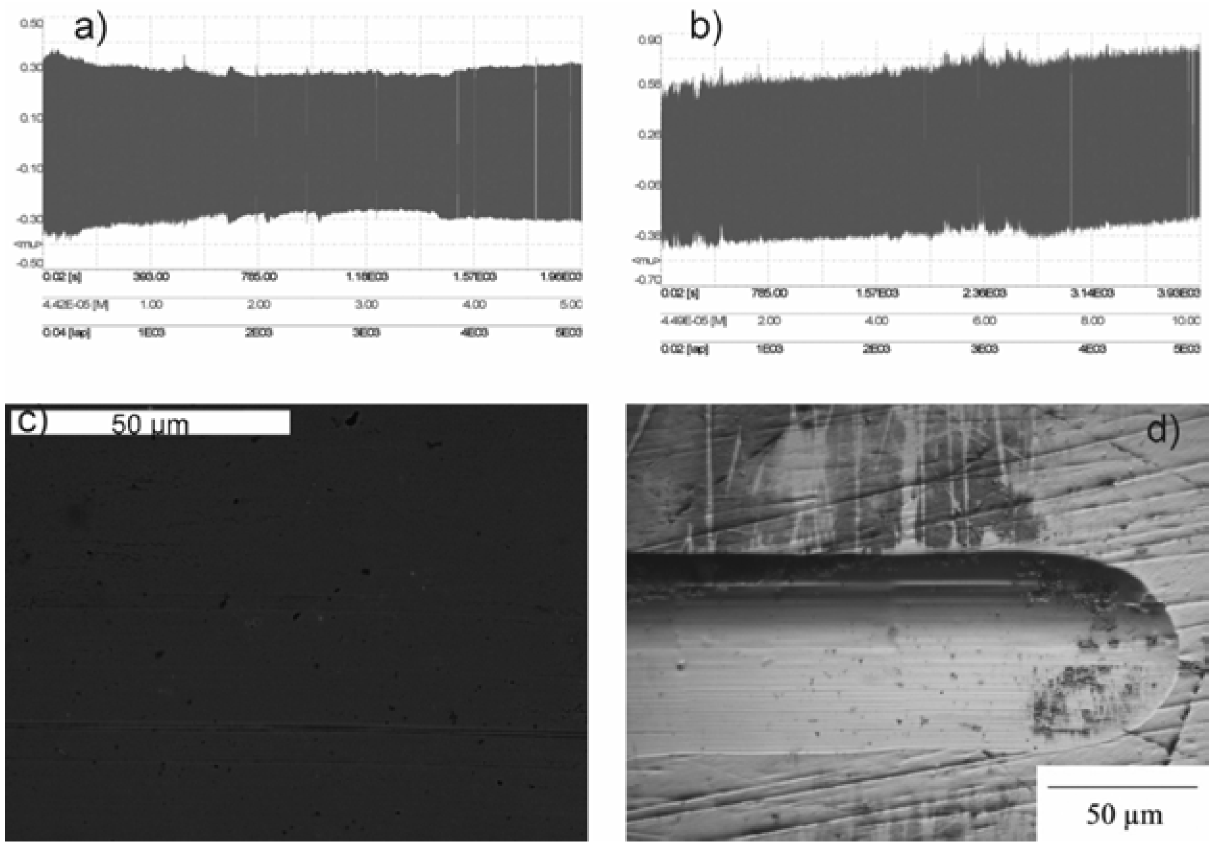

Figure 4. Diagrams of friction coefficient and optical micrograph showing wear track on AISI 316LVM sample: a), c) Ringers' solution; v=4 mm/s; F_N=1000mN; Penetration depth: 0.2µm; b), d) Ringers' solution with PMMA particles; v=12 mm/s; b F_N=750mN; Penetration depth: 3.6µm;

Tests were conducted in dry conditions and with presence of two different solutions: Ringer’s solution and Ringer’s solution with particles of Polymethylmethacrylate (PMMA), in order to simulate human body environment in which implanted component function. It can be clearly seen (Figs. 3 and 4) that change of contact conditions (load, sliding speed, dry sliding, sliding with Ringer’s solution or with presence of Ringer’s solution with PMMA particles) produced significant change in tribological behaviour of AISI 316LVM samples. Abrasive wear mechanism can be clearly seen, accompanied with adhesive wear and pitting. Samples sliding in the presence of pure Ringers’ solution exhibited smooth worn tracks (Fig. 4c) in comparison to all other conditions. It can be clearly seen that presence of PMMA particles produced severe forms of pitting corrosion at leading zones of the worn track (Fig. 4d). This is in consistence with findings of other authors who reported development of localized attack types of pitting corrosion [19]. Severe effects of wear debris on bone regarding biological response have been studied, but it is clear that component also would exhibit worsening of its surface properties leading to further unwanted forms of wear. Pitting corrosion can adversely affect both biocompatibility and mechanical strength of the implant and even lead to complete mechanical failure of the component [19, 20].

4. POLYMERS: ULTRA-HIGH-MOLECULAR-WEIGHT POLYETHYLENE (UHMWPE)

Polymers are large molecules synthesized from smaller molecules, called monomers. Plastics are polymers that are rigid solids at room temperature and generally contain additional additives. Some common plastics used in biomedical applications are polymethyl methacrylate (PMMA) for intraocular lenses, and ultrahigh-molecular-weight polyethylene (UHMWPE) for the articulating surfaces of orthopedic implants. Over the years, ultra-high-molecular-weight polyethylene (UHMWPE) has emerged as the material of choice for fabricating one of the bearing components in various arthroplasties, such as acetabular cups, acetabular cup liners, tibial inserts, etc. [21]. Components made of UHMWPE have performed admirably in vivo. The only major concern is wear and the effect of the wear particles on the in vivo longevity of the prosthesis.

UHMWPE is a linear, low-pressure, polyethylene resin. It has both the highest abrasion resistance and highest impact strength of any plastic. Combined with abrasion resistance and toughness, the low coefficient of friction of UHMWPE yields a self-lubricating, non-stick surface. Static and dynamic coefficients are significantly lower than steel and most plastic materials. Elastic modulus of UHMWPE is approximately 0.69 GPa. ASTM F648-00 defines standard specification for Ultra-High-Molecular-Weight Polyethylene powder and fabricated form for surgical implants.

Despite its superior mechanical performance, the standard UHMWPE is subject to fatigue failure and it produces too many wear particles, leading to shortening of the component life and revision surgeries. It can also absorb small amounts of fluids or retain small amounts of air in the microscopically small pores (about 0,1 volume percent) that can cause great deterioration of the material during the long years in the patient’s body. The main problem is production of wear particles from the UHMWPE surfaces. The wear particles enhance inflammatory reaction and eventually lead to development of osteolysis (bone dissolving disease). Along with the extensive application of UHMWPE, the understanding of polymer tribology is becoming increasingly important. Many authors have investigated tribological performance of UHMPWE [21-25].

Many strategies for reducing wear of this material have been investigated [25]. Widely accepted approach is crosslinking of the polymer. The cross-linked UHMWPE has been introduced in clinical practice in 1998, although it was known since 1960’s that irradiation of UHMWPE increases its wear resistance. In the process called cross-linking, the irradiation "glues" the long polyethylene molecules to keep together. On the other hand this process deteriorates mechanical characteristic of the material and above a certain limit (maximal irradiation dose) it becomes brittle and unusable for mechanical applications. Understanding wear mechanisms occurring during the contact of UHMWPE with other biomaterials is important to be able to predict in-vivo life of the component. Small number of reports has been published regarding a correlation between in vitro and in vivo wear rate results [21].

The effect of different types of lubricant environment and varied regimes (normal load and sliding speed) on the tribological performance of UHMWPE against Al_2O_3 was examined with a reciprocating sliding setup of the nanotribometer (Figs. 5 and 6).

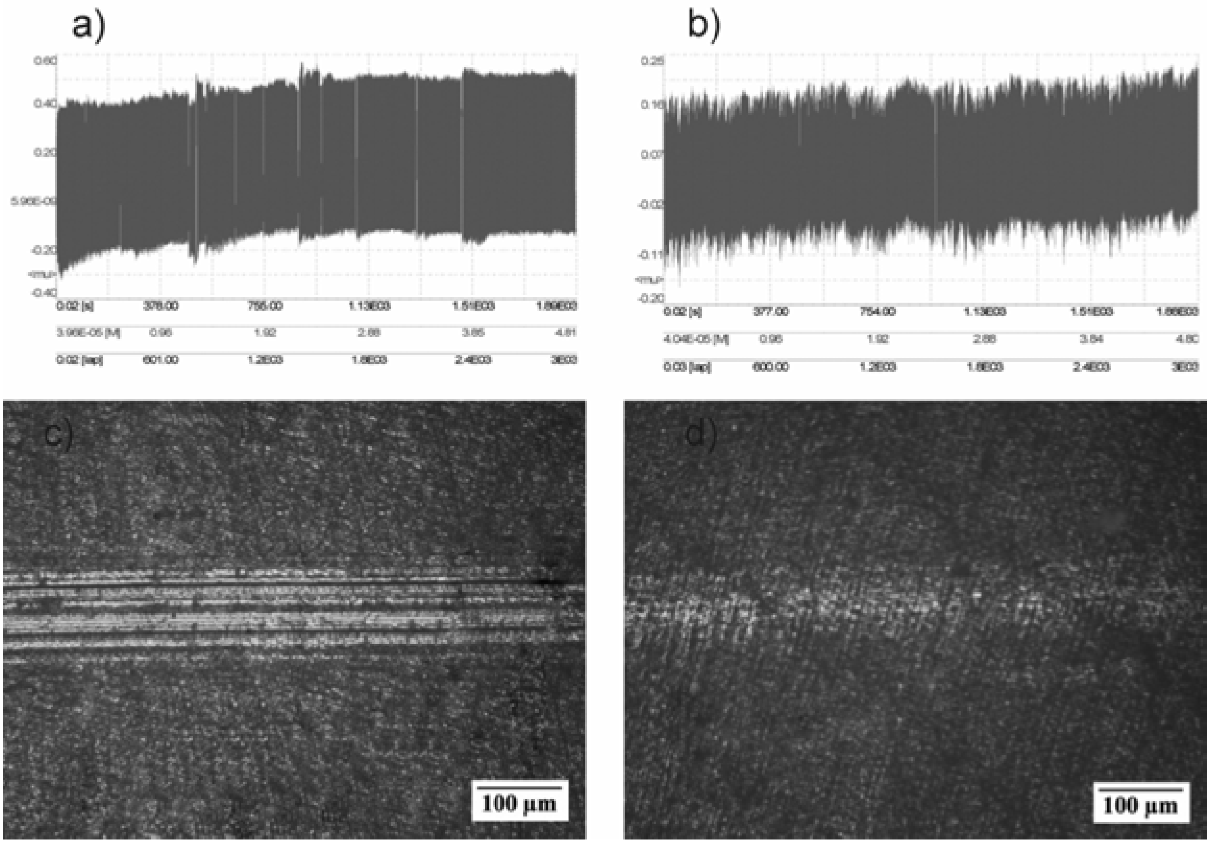

Figure 6. Diagrams of friction coefficient and optical micrograph showing wear track on UHMWPE sample: a), c) Ringers' solution with PMMA particles; v=4 mm/s; F_N=100mN; Penetration depth: 39.0µm; b), d) Distilled water; v=4 mm/s; b F_N=100mN; Penetration depth: 0.2µm;

Tests were conducted in dry conditions and with presence of distilled water and two different solutions: Ringer's solution and Ringer's solution containing particles of PMMA, in order to simulate human body environment in which implanted component function. It can be clearly seen (Figs. 5 and 6) that change of contact conditions (load, sliding speed, environment) produced significant change in tribological behaviour of UHMWPE samples. It can be clearly seen that the highest wear was produced for sliding with Ringer's solution containing particles of PMMA. Final penetration depth recorded by tribometer in that case was 39.0µm in comparison with other testing environments: 1.5µm, 2.5µm and 0.2µm respectively in cases of dry sliding and sliding with Ringer's solution and distilled water.

5. POLYMERS: POLYMETHYL METHACRYLATE (PMMA)

Bone cements have been used very successfully to anchor artificial joints (hip joints, knee joints, shoulder and elbow joints) for more than half a century. Artificial joints are anchored with bone cement. The bone cement fills the free space between the prosthesis and the bone and plays the important role of an elastic zone. This is necessary because the human hip is acted on by approximately 10-12 times the body weight and therefore the bone cement must absorb the forces acting on the hips to ensure that the artificial implant remains in place over the long term. Bone cement chemically is polymethyl methacrylate (PMMA). PMMA was used clinically for the first time in the 1940s in plastic surgery to close gaps in the skull. Comprehensive clinical tests of the compatibility bone cements with the body were conducted before their use in surgery. Also, until recently, the only polymer used to replace or augment bone itself (as opposed to the articulating surfaces) was polymethylmethacrylate (PMMA), or bone cement.

The ready bone cement is a compound consisting of 90 % of polymethylmetacrylate**,** (PMMA), the rest are mainly crystals of barium sulfate or Zirconium oxide that make the resulting product radio-opaque. The microscopic structure of bone cement is made by two substances glued together. One substance are the small particles of pre-polymerized PMMA so called "pearls". These pearls are supplied as a white powder. The other substance is a liquid monomer of MMA (MethylMetacrylate). Both substances are mixed together at the operation table with added catalyst that starts the polymerization of the monomer fluid. Polymer's properties can be predicted and explained by understanding the polymer structure on the atomic, microscopic, and macroscopic scale. Amorphous polymers such as PMMA are brittle, hard plastics at room temperature [26]. It is isotropic and very bioinert material. Elastic modulus is up to 2.65GPa.

The primary functions of bone cement, when used to anchor artificial joints, are to secure the orthopedic implants to bone and transfer mechanical loads from the implant to the bone. The femoral stem and acetabular cups are cemented, screwed or press fit into place. Approximately 50% of all orthopedic implants utilize bone cement to achieve implant fixation [27]. PMMA is the most commonly used bone cement. Local tissue damage due to chemical reactions during polymerization, the high shrinkage of the cement after polymerization, the stiffness mismatch between bone and the cement are some drawbacks associated with PMMA-based bone cements [27]. Loose cement particles also mediate osteolysis of the bone and are highly unwanted to occur.

On the other hand, when PMMA is used to replace or augment bone itself, sliding contacts with different biomaterials become even more important to study, especially under micro-level forces. Many studies have been conducted focused on solving problems of PMMA application [28-33]. The effect of different environment on the tribological performance of PMMA against AISI 316LVM stainless steel at reciprocating sliding setup of the nanotribometer is shown in Fig. 7. These results are part of the investigation where five values of normal force were selected (100 mN, 250 mN, 500 mN, 750 mN, 1000 mN) and three values of sliding speed (4 mm/s, 8 mm/s, 12 mm/s).

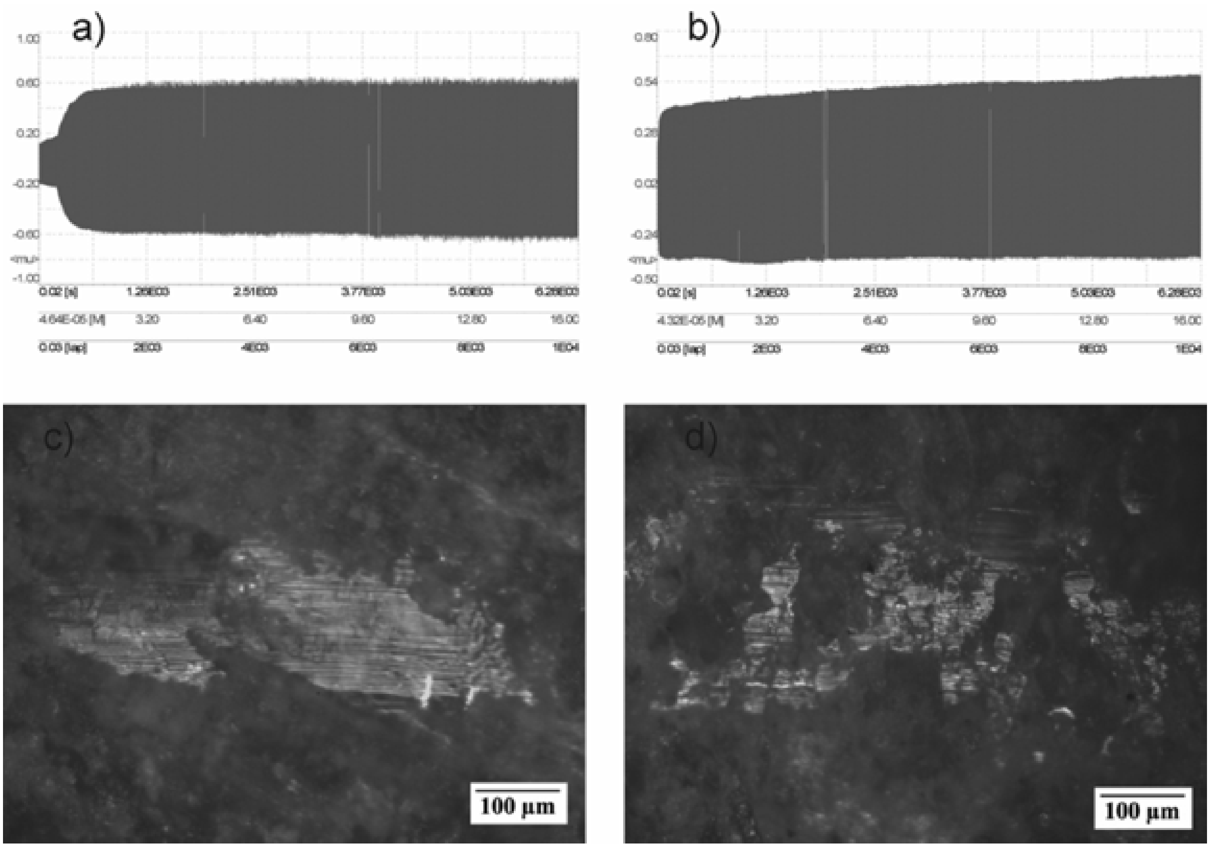

Figure 7. Diagrams of friction coefficient and optical micrograph showing wear track on PMMA sample: a), c) Dry; v=4 mm/s; F_N=500mN; Penetration depth: -0.5µm; b), d) Ringers' solution; v=4 mm/s; b F_N=500mN; Penetration depth: 0.8µm;

It can be clearly seen that the wear behaviour of a PMMA substrate sliding against AISI 316 steel ball is different for dry conditions if compared to sliding with Ringers' solution (Fig. 7). Many studies have been focused on understanding wear mechanisms in relation to polymer sliding contacts, also in case of microwear process. According to [29, 30] microwear process of PMMA involves three distinct stages. First, there is a plateaulike upheaval during which no wear takes place. This is followed by distortion of the surface to produce projections, again involving no wear. Finally, the surface is subjected to wear and wear particles are produced. A special feature of PMMA is that the deformation rapidly proceeds to destruction. This is in consistence with findings of our study. It can be clearly seen that plateaus can be defined throughout the worn track (Fig. 7d), what is more distinctively exhibited for sliding with Ringers' solution than for dry sliding. This phenomenon was also more pronounced for higher normal load applied than for low loads. It is also proved by other authors [30] that wear and fatigue crack growth of PMMA sliding against steel, are very sensitive to organic fluids, related to the absorption of the liquid into the polymer, which, in turn, could result in surface plasticization or reduction of the minimum stress for the onset of cracking. Results of our study also showed that more cracks appeared in case of sliding with Ringers' solution. In case of dry sliding, larger regions with clear abrasive wear were produced. Ringers' solution produced decrease of wear in all cases of observed sliding speeds and normal loads.

6. CONCLUSION

Nowadays, technological innovation has progressed at such an accelerated pace that it is has permeated in almost any aspect of our lives. It is especially pronounced in a field of medicine, by integrating engineering that offer tools for advancement in health care (biomaterials, biosensors, image processing, etc.). Multidisciplinary area of biomaterials research comprises and blends number of research fields, aiming to achieve ultimate goal from prosthetics to regeneration. There are still many challenges to address, from manufacturing of biomaterials and their characterization, to design and selection of material for specific use in medicine and biomaterial interactions with human tissues. Important demand from all biomaterials in use today, is to prevent process of wear or at least to minimize it to the highest possible extent. Tribological investigations can offer valuable insight in material behaviour thus contributing to advances in this complex field of research.

ACKNOWLEDGEMENTS

This study was financed by Ministry of Science and Technological Development, Serbia, project No.35021. We express our appreciation to company Narcissus (Ada, Serbia) for the support, advise and provision of the stainless steel AISI 316LVM and ultrahigh-molecular-weight polyethylene (UHMWPE) test samples.

REFERENCES

[1] J. D. Enderle, J.D. Bronzino, S. M. Blanchard., Introduction to biomedical engineering, Elsevier Academic Press, 2005

[2] M.Geetha, A.K. Singh, R. Asokamani, A.K. Gogia, Ti based biomaterials, the ultimate choice for orthopaedic implants – A review, Progress in Materials Science 54 (2009) 397–425

[3] B. Bhushan, E.K. Her, Fabrication of Superhydrophobic Surfaces with High and Low Adhesion Inspired from Rose Petal, Langmuir, 26 (11), pp 8207–8217, 2010

[4] J. Black, G. Hastings, Ed., Handbook of Biomaterial Properties, Chapman & Hall, 1998

[5] M. Masmoudi, M. Assoul, M. Wery, R. Abdelhedi, F. El Halouani, G. Monteil, Friction and wear behaviour of cp Ti and Ti6Al4V following nitric acid passivation, Applied Surface Science 253 (2006) 2237–2243

[6] A. Molinari, G. Straffelini, B.Tesi, T.Bacci, Dry sliding wear mechanism of the Ti6Al4V alloy, Wear 208 (1997) 105-112

[7] G. Straffelini, A. Molinari, Dry sliding wear of Ti–6Al–4V alloy as influenced by the counterface and sliding conditions, Wear 236 (1999) 328–338

[8] M. Long, H.J. Rack, Friction and surface behavior of selected titanium alloys during reciprocating-sliding motion, Wear 249 (2001) 158–168

[9] H. Dong, T. Bell, Tribological behaviour of alumina sliding against Ti6Al4V in unlubricated contact, Wear (1999) 874–884

[10] P.S. Walker, G.W. Blunn, P.A. Lilley, Wear Testing of Materials and Surfaces for Total Knee Replacement, Journal of Biomedical Materials Research (Applied Biomaterials), Vol. 33, 159-175 (1996), John Wiley & Sons Inc.

[11] W. Osterle, D. Klaffke, M. Griepentrog, U. Gross, I. Kranz, Ch. Knabe, Potential of wear resistant coatings on Ti–6Al–4V for artificial hip joint bearing surfaces, Wear 264 (2008) 505–517

[12] M.J. Jackson, W. Ahmed, Surface Engineered Surgical Tools and Medical Devices, Springer, 2007

[13] P.A. Dearnley, Tribology, Meeting tribological challenges with surface engineered materials, Vol.1 No.1, W. S. Maney & Son Ltd, 2007

[14] H. Dong, T. Bell, Tribological behavior of alumina sliding against Ti6Al4V in unlubricated contact, Wear 225–229 (1999) 874–884.

[15] Gispert, M.P., Serro, A.P., Colaco, R., Saramango B.: Friction and wear mechanisms in hip prosthesis: Comparison of joint materials behaviour in several lubricants, Wear 260 (2006) 149-158

[16] G. Mani, M.D. Feldman, D. Patel, C. M. Agrawal, Coronary stents: A materials perspective, Biomaterials, 28 (2007) 1689-1710

[17] P.A. Dearnley, G. Aldrich-Smith, Corrosion–wear mechanisms of hard coated austenitic 316L stainless steels, Wear, 256 (2004) 491-499

[18] A. Shahryari, S. Omanovic, J.A. Szpunar , Electrochemical formation of highly pitting resistant passive films on a biomedical grade 316LVM stainless steel surface, Materials Science and Engineering: C, 28 (2008) 94-106

[19] A. Shahryari, Jerzy A. Szpunar, S. Omanovic , The influence of crystallographic orientation

distribution on 316LVM stainless steel pitting behavior, Corrosion Science 51 (2009) 677-682

[20] G. Lewis, Properties of crosslinked ultra-high-molecular-weight polyethylene, Biomaterials, 22 (2001) 371-401

[21] S. W. Zhang, State-of-the-art of polymer tribology, Tribology International 31 (1998) 49-60

[22] P.A. Williams, I.C. Clarke, Understanding polyethylene wear mechanisms by modeling of debris size distributions, Wear, 267 (2009) 646-652

[23] S. Ge, S. Wang, N. Gitis, M. Vinogradov, J. Xiao, Wear behavior and wear debris distribution of UHMWPE against Si_3N_4 ball in bi-directional sliding, Wear, 264, (2008) 571-578

[24] V. Banchet, V. Fridrici, J.C. Abry, Ph. Kapsa, Wear and friction characterization of materials for hip prosthesis, Wear, 263, (2007) 1066-1071

[25] M. Kutz, Editor, Biomedical Engineering and Design Handbook, Vol. 1, McGraw-Hill, 2009

[26] P.A. Revell, Editor, Joint replacement technology, Woodhead Publishing Limited, 2008

[27] Lu Z, McKellop H., Effects of cement creep on stem subsidence and stresses in the cement mantle of a total hip replacement, Journal of Biomedical Materials Research, 34 (1997) 221–226

[28] B. J. Briscoe, A. Chateauminois, T. C. Lindley, D. Parsonage, Contact damage of poly(methylmethacrylate) during complex microdisplacements, Wear, 240 (2000) 27-39

[29] T. A. Stolarski, H. Williams, Mode of loading and contact configuration effects in the wear of polymers, Journal of Applied Polymer Science, 61 (1996) 1217–1222

[30] D. Arola, K. A. Stoffel, D. T. Yang, Fatigue of the Cement/Bone Interface: The Surface Texture of Bone and Loosening, Journal of Biomedical Materials Research Part B: Applied Biomaterials, Vol. 76B (2005) 287-297

[31] G. Lewis, Fatigue testing and performance of acrylic bone-cement materials: State-of-the-art review, Journal of Biomedical Materials Research Part B: Applied Biomaterials, Vol. 66B (2003) 457–486

[32] M. Dammak, A. Shirazi-Adl, M. Schwartz, Jr., L. Gustavson, Friction properties at the bone–metal interface: Comparison of four different porous metal surfaces, Journal of Biomedical Materials Research, Vol. 35, 329–336 (1997)

[33] B. J. Briscoe, A. Chateauminois, T. C. Lindley, D. Parsonage, Fretting wear behaviour of polymethylmethacrylate under linear motions and torsional contact conditions, Tribology International, 31 (1998) 701-711

Serbian Tribology Society

SERBIATRIB '11

12th International Conference on Tribology

Faculty of Mechanical Engineering in Kragujevac

Kragujevac, Serbia, 11 – 13 May 2011

TRIBOLOGICAL PROPERTIES OF SHOT PEENED SURFACES OF 36NiCrMo16 ALLOYED STEELS IN DRY SLIDING CONDITION

Miroslav Babić[1], Dragan Adamović[1], Slobodan Mitrović[1], Fatima Živić[1], Dragan Džunić[1], Marko Pantić[1]

[1] Faculty of Mechanical Engineering, Sestre Janjic 6, Kragujevac, Serbia

babic@kg.ac.rs, adam@kg.ac.rs, boban@kg.ac.rs, dzuna@kg.ac.rs, pantic@kg.ac.rs

Abstract: *For right choice of final operation procession, in tribological sense, it is necessary to know the legality of manifesting influences of certain types of processing, as well as regime parameters and conditions of their performance on relevant surface topography parameters (height, cloud, and micro-geometry structure), physical-mechanical state and residual voltages of surface layer. Shot peening method is used to increase both statics, and dynamics hardness of work piece. The result of this method is not only surface layer characteristic change of certain piece but also tribological characteristics change of such processed piece.*

The results of laboratory tests, which correspond and analyse together in work, refer to effects of shot peening use, as final processing by surface plastic deforming, in the example of alloyed steel 36NiCrMo16,with their tribological valorisation of friction and wear tests. Tribological studies show that overall effects of final shot peening processing have positive effect on tribological behaviour of processed elements and may contribute to improvement of tribological element level of tribomechanical systems.

Keywords: *Shot Peening, Friction coefficient, Wear, Alloyed Steels*

1. INTRODUCTION

Methods of reinforcement using balls beam is very widespread and generaly accepted in all industries. The static hardness of work piece as well as dynamic is increased by this method. The advantage of this method, of all the other surface reinforcement methods, is that the appliance expenses of this method are relatively small and that it could be very easily integrated into any production process.

Influence of shot peening on properties of work piece surface layers could be valued only from the aspect of their behaviour in exploitation conditions. Considering that, the key position belongs to tribological characteristics in conditions of sliding friction. Namely, acceptance overview of surface deforming by shot peening, by steel balls beam, as final operation of contact surfaces unavoidably must contain also friction and wear issues.

Micro geometry of contact surfaces represents very important aspect which is often neglected during specification of shot peening parameters [1,2]. Tiresome characteristics are influenced by surface topography which originates from production process. Depending on sensitivity of material, this influence is more or less important [3].

Shot peening can eliminate or mitigate negative effect of surface defects, if the size of balls is properly adjusted to surface topography. If the balls are too big, they cannot remove the traces of tools and the influence of shot peening is weak. The surface appearing after shot peening is anisotropic surface [4].

Besides micro geometry change, resulting from shot peening, in the same time it usually also comes to material reinforcement of surface layer, that is to say hardness increase. Therefore, it also comes to elasticity increase of peak or contact points, through which the surface is "carried", which plays an important role. When relative motion exists between two surfaces, the peaks shall be, in the beginning, elastically deformed without sliding into contact points. The risk of particles separation is reducing with increased limit of elasticity [5,6].

Due to highly concentrated load in the roughness peak, and due to broken balls hitting the surface, the micro-cracks could be conceived, and they can expand, therefore creating large cracks, that may develop into pits. If the surface is exposed to varying loads over times (fretting) it may come to the creation of larger pitting.

Although the residual compressive voltages are the most important consequence of shot peening in order to reduce fretting, the typical roughness (bumps and pitting), created after shot peening, also has important positive effect [7].

Geometrical characteristics, regardless of their importance, can not completely characterize the contact surface quality of tribomechanical elements and their exploitation properties. Physical-mechanical state of contact layers has the crucial influence. Namely, the physical-mechanical state indicators of contact layer, such as the structure, micro-hardness, and residual surface voltages, directly influence the intensity of development wear process [8,9].

2. EXPERIMENTAL TESTING

EN 10083-3: 36NiCrMo16 alloyed steel was selected for testing. Chemical composition of 36NiCrMo16 steel is given in Table 1.

Table 1. Chemical composition of 36NiCrMo16 steel

	Percentage content							
	C	Si	Mn	Cr	Ni	Mo	P max	S max
36NiCrMo16	0.34	0.28	0.48	1.88	4.21	0.58	0.013	0.010

Mechanical characteristics of thermally treated (improved) samples of 36NiCrMo16 steel are given in Table 2.

Table 2. Guaranteed values of mechanical characteristics of 36NiCrMo16 steel

R_p, MPa	R_m, MPa	A_5, %	Z, %	$KU_{300/3}$, J
1050	1420	9	40	30

Microstructure of the tested steel consists of inter-phase structure – trustit with martensite participation. Austenite grain size, determined according to SRPS C.A3.004 (ISO 643, EURONORM 103 and ASTM E-112), using method of comparison with ASTM etalons, is N°8, which belongs to a group of small austenite grains. Investigation of non-metallic inclusions content was realised by comparison with SRPS C.A3.013 (ASTM - E45, DIN 50602) scale, using method according to Jernkontoret chart. It was determined that 36NiCrMo16 steel has non-metallic inclusions from area A1 (mean index of 0.43) and D2 (mean index of 1.25).

Samples for tribological testing were made by cutting them from samples aimed for fatigue test. Cutting was realised by machine saw with intensive cooling in order to avoid changes of surface layers, due to high temperature.

Shot peening of samples by steel balls was realised at shot peening machine of ES-1580-1 model, PANGBORN. Machine is designed for controlled surface strengthening by shot peening for parts of different configurations and dimensions.

Wanted effects of shot peening is obtained if selection of shot peening parameters is realised correctly, such as: ball diameter, Almen intensity, subjected area size coverage and shot duration of shot peening. Shot peening was realised using balls of d=0.8 mm (S330) diameter and 48 - 55 HRC hardness. Manufacturer of balls is Wheelabrator Corporation (USA).

Based on literature recommendations, for 15 mm thickness of the sample, Almen intensity of 16A was chosen. The largest effects of shot peening occur when the whole area is covered. Hence, coverage of P=1×98% was chosen. Duration of shot peening, necessary to achieve wanted Almen intensity (16A) was determined by Almen test strip, by creating saturation curve. Pressure of 4 bar and shot peening time of 5 min correspond to wanted shot peening intensity (16A).

Surface coverage on shot peened sample was observed by the magnifying glass with 10x magnification. It was determined that coverage was 98 % (complete coverage) with shot peening time of 5 min. Appearance of the surface before and after the shot peening is shown in Figure 1.

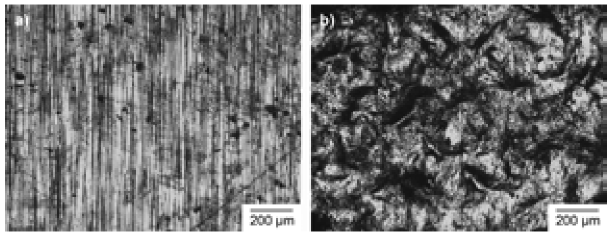

Figure 1. Appearance of the surface before (a) and after (b) shot peening

Required assumptions for sample shot peening was made, by determination of shot peening time and conditions for achieving Almen intensity of 16A. Shot peening was realised under the same conditions that provide aforementioned Almen intensity.

Wear test were carried out in a computer aided block-on-disk sliding wear testing machine with the contact pair geometry in accordance with ASTM G 77–05. A schematic configuration of the test machine is shown in Figure 2a. More detailed description of the tribometer is available elsewhere [10,11].

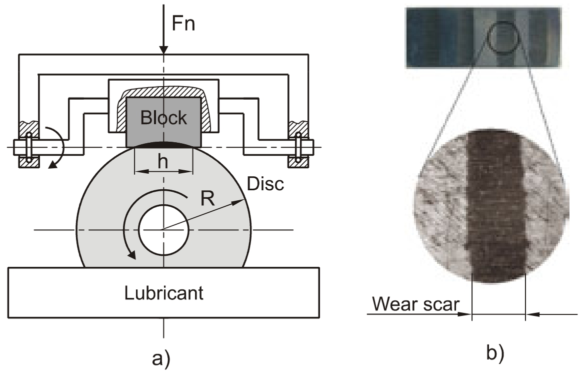

Figure 2. The scheme of contact pair geometry

The test blocks (6.35x15.75x10.16 mm) were prepared from EN 10083-1: 36NiCrMo16 steel with polished and shot peened surfaces. The counter face (disc of 35 mm diameter and 6.35 mm thickness) was made of EN: HS 18-1-1-5 tool steel of 62HRC hardness. The roughness of the ground contact surfaces was R_a=0.45 µm. The tests were performed under lubricated sliding conditions at different sliding speeds (0.25 m/s, 0.5 m/s, 1 m/s) and applied loads (10 N, 30 N, 50 N). The duration of sliding was 60 min. Each experiment was repeated five times.

The tests were performed at room temperature. The wear behavior of the block was monitored in terms of the wear scar width (Figure 2b). Using the wear scar width and geometry of the contact pair the wear volume and wear rate (expressed in mm^3) were calculated.

3. TEST RESULTS

The objective assessment of geometrical parameters of mechanical parts surface should include the characteristics of macro-geometry, micro-geometry, and sub micro-geometry, considering the nature and mechanism of geometric imperfections education. Standard parameters of surface roughness, R_a (middle arithmetic roughness aberration) and R_z (middle roughness height), are insufficient as the characteristic, of not only exploitation but also geometric properties of the surface, because they do not give any information about shape and distribution of the roughness. For the dynamic hardness, for example, it is very important the absence of deep grooves and micro-cracks on the surface, because they act as voltage concentrators and become the focus of the fracture. Therefore, micro-geometry, with that point of view, is not only characterized as middle parameters (such as R_a and R_z), but also as local parameters of micro-geometry, for example: depth and radius of bottom profile surface roundness, step of roughness and others. Local parameters of geometry, which describe the height and shape of unit roughness, depth and shape of pitting between them, and distribution of material by height, are very important in friction and wearing.

Roughness measurement was carried on one ground and one shot peened tube, in the direction perpendicular to the direction of grinding.

Besides numerical values of roughness parameters, obtained results are graphically illustrated by appropriate profilometer examples (figure 3a and b).

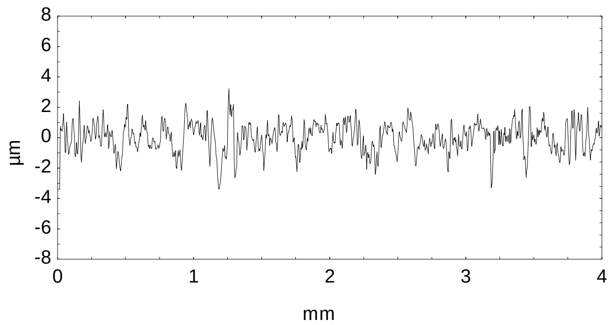

a)

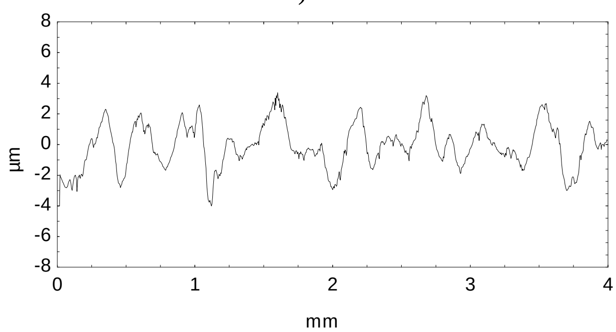

b)

Figure 3. Surface profile sample figure made of steel 36NiCrMo16 in abraded (a) shot peened (b) state

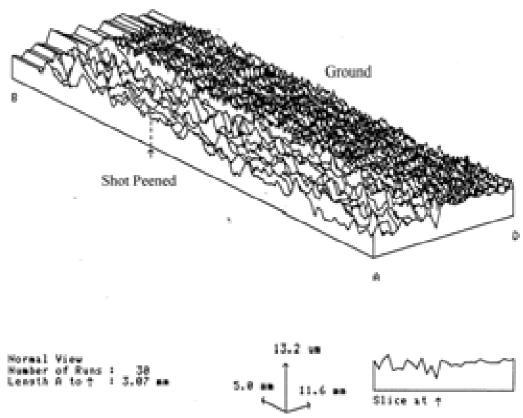

Figure 4. Comparative 3D surface sample figure made of steel 36NiCrMo16 in ground (a) shot peened (b) state

Comparative 3D surface sample figure made of steel 36NiCrMo16 in ground (1) shot peened (2) state is shown in Figure 4.

Profile figure of ground surface is shown in Figure 4a, and completely changed topography regarding height, shape, step and statistics, by which the shot peened processing is resulting, is illustrated by profilometer in figure 4b.

It is obvious that during the shot peening there was very expressed increase of all roughness height parameters (R_a, R_q, R_p, R_v, R_y, R_{tm}, R_{pm}n), in comparison to the initial state obtained by grinding. A higher degree of coverage corresponds to a higher degree of roughness increase.

Besides the parameter increase which represents the height of micro-roughness, shot peened processing by beam of steel balls also influences great parameter increase of step roughness, as it is also visible in appropriate profile records.

Surface roughness (R_a) for steel 36NiCrMo16 in ground state is R_a=0.62μm and in shot peened state is R_a=1.11μm.

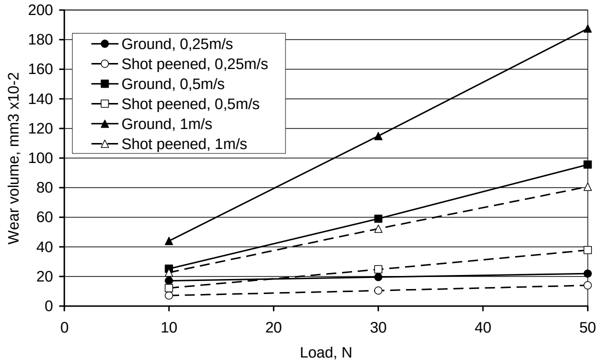

Figure 5. Wear volume change with normal load change for different sliding speeds (0.25, 0.5, 1 m/s) in conditions without lubrication

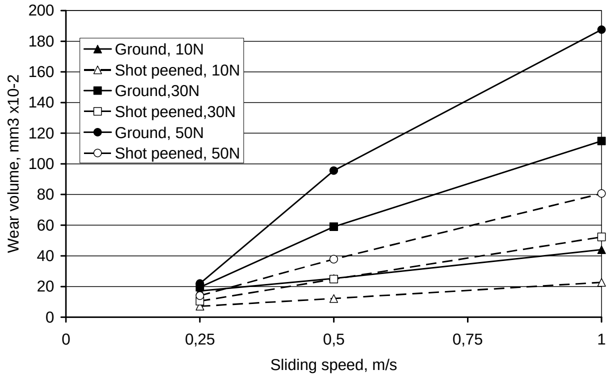

Figure 6. Wear volume change with sliding speed change for different values of normal load (10, 30, 50 N) in conditions without lubrication

Figures 5 and 6 graphically represent the wear volume dependence on normal load value change (fig. 5) and sliding speed value (fig. 6). In Figure 5 it is clear that increase of normal load value leads to, almost linear, increase of wear volume. Also, increase of sliding speed value leads to increase of wear volume value. It should be pointed out, that in all tested conditions, smaller wear volume values are measured for shot peened surfaces in comparison to ground surfaces, which is the consequence of hardness increase in surface layer of shot peened surfaces.

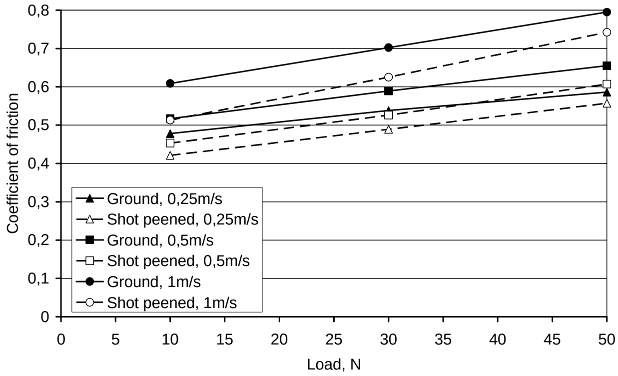

Figure 7. Coefficient friction change with normal load change for different sliding speeds (0.25, 0.5, 1 m/s) in conditions without lubrication

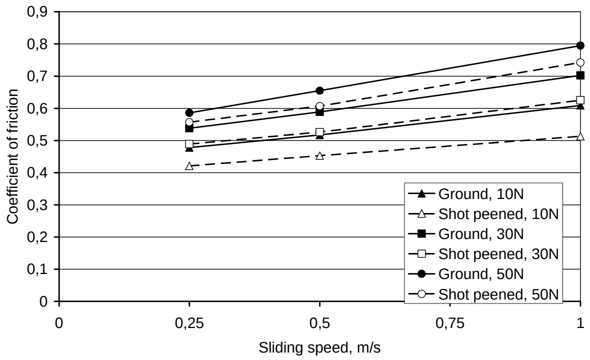

Figure 8. Coefficient friction change with sliding speed change for different values of normal load (10, 30, 50 N) in conditions without lubrication

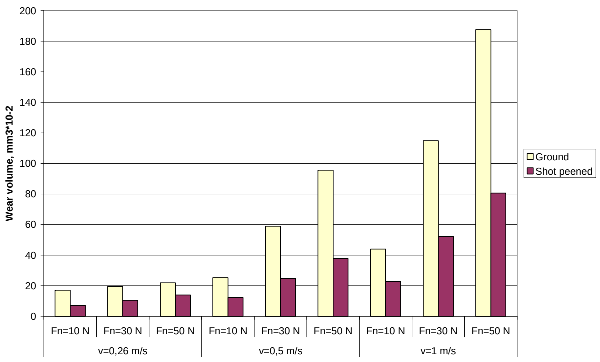

Figure 9. Histogram display of wear volume dependence on speed sliding and normal contact load in conditions without lubrication

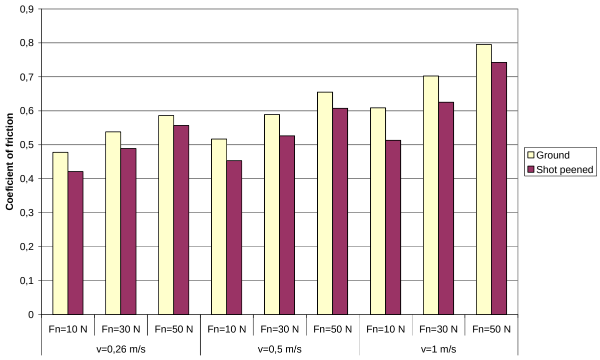

Figure 10. Histogram display of coefficient friction dependence on speed sliding and normal contact load in conditions without lubrication

Figures 7 and 8 graphically represent the coefficient friction dependence on normal load value (fig. 7) and sliding speed value (fig. 8). Increase of normal load value and sliding speed leads to linear increase of coefficient friction value, where it should be pointed out that, in all contact conditions, smaller coefficient friction values are measured for shot peened surfaces in comparison to ground surfaces. The reason for these results could be found in greater hardness of surface layer shot peened surfaces, and partially in the way of making contacts.

Figure 9 on quantitative way represents measured wear volume values, where it is clear that wear of shot peened surfaces in all contact conditions is significantly smaller in comparison to ground surfaces, and the difference itself becomes more apparent with speed increase. Figure 10 represents histogram display of measured coefficient friction values, where shot peened surfaced have 8-10% less coefficient values in comparison to ground surfaces.

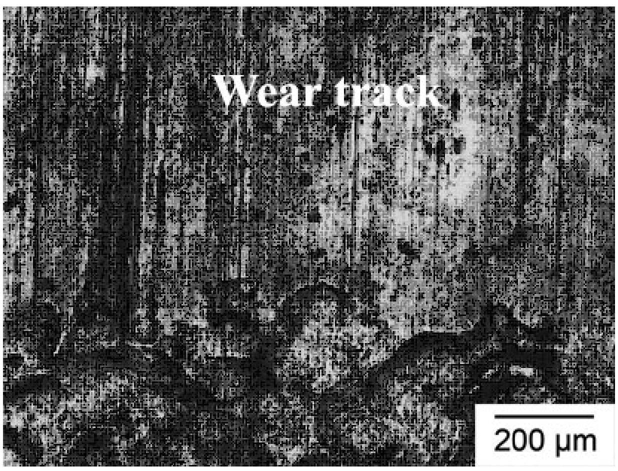

a)

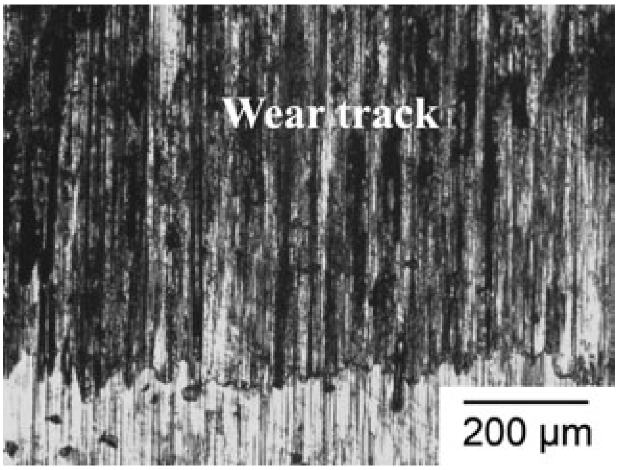

b)

Figure 11. Wear traces display on contact without lubrication for steel 36CrNiMo16 in ground (a) and shot peened state (b)

Figure 11 represents wear traces display of tested samples. Figures shows that dominant wear mechanism in contact conditions without lubrication with both tested surfaces is identical, that is to say abrasive wear is dominant.

4. CONCLUSION

Based on performed tests we may conclude following:

- Shot peening eliminates tool traces and surface defects, by modifying surface roughness, and the surface that occurs after shot peening is anisotropic.
- With mentioned parameters performance of shot peening causes deterioration both in height and structural roughness parameters in comparison to initial state acquired by grinding. That is the consequence of small initial roughness and slightly bigger balls diameter which are used in shot peening processing.
- During shot peening surface tests, the smaller values of wear volumes and coefficient friction of shot peened surfaces are measured in the conditions without lubrication of shot peened surfaces in comparison to ground surfaces. However, it should be noted that improvements are more pointed out in terms of resistance to wear, than in terms of coefficient friction value. In addition, histogram displays refer about that, where it is shown that at higher sliding speed values (0.5 and 1m/s) the wear volume values are less than 50% in comparison to ground surfaces.
- Dominant wear mechanism in these tested conditions (dry sliding, block-on –disc) is abrasive wear which can be seen in wear traces display.
- Numerous comparative tribological studies

show that overall effects of final shot peening processing have positive effects on tribological behavior of certain elements and may contribute to improvement of tribological element level of tribo-mechanical systems.

ACKNOWLEDGMENT

This study was financed by Ministry of Science and Technological Development, Serbia, project No.35021.

REFERENCES

[1] Adamović D., Babić M., Jeremić B.: Influence of Shot Peening on Roughness Parameters, Tribology in Industri, Volume XVI, No 2, Kragujevac, June 1994. pp. 52-56.

[2] Babić M., Adamovic D., Jeremic B., Milić N.: Tribological Characteristics Surfaces Machined by Shot Peening, Tribology in Industri, Volume XVIII, No 3, Kragujevac, September 1996. pp. 93-97.

[3] Adamovic D., Babic M., Jeremic B.: Shot Peening Influence on Tribological Characteristics of Surfaces, ICSP-7, Warsaw, Poland, 1999., pp. 350-358.

[4] Higounenc O.: Correlation of shot peening parameters to surface characteristic, ICSP-9, Paris, France, 2005, pp. 28-35

[5] Kirk D.: Review of Shot Peened Surface Properties, The Shot Peener, Vol 21/Issue 4, Fall, 2007, pp. 24-30

[6] Le Guernic Y.: Shot Peening Retards “Freting”, ICSP-4, Tokyo, Japan, 1990. pp. 281-296.

[7] Vaxevanidis N.M., Manolakos D.E., Koutsomichalis A., Petropoulos G., Panagotas A., Sideris I., Mourlas A., Antoniou S.S.: The Effect of Shot Peening on Surface Integrity and Tribological Behaviour of Tool Steels, AITC-AIT 2006, International Conference on Tribology, Parma, Italy, 20-22 September 2006, pp. 1-8

[8] Adamović D., Jeremić B., Babić M.: Shot Peening, Monograph, Faculty Mechanical Engineering, Kragujevac, 1995. (in Serbian)

[9] M. Babić, D. Adamović, B. Jeremić, S. Mitrović: Tribological Effects of Shot Peening Surface Treatment, 3rd International Conference on Manufacturing Engineering (ICMEN), 1-3 October 2008, Chalkidiki, Greece, pp. 657-664

[10] Babic M., Mitrovic S., Jeremic B.: The Influence of Heat Treatment on the Sliding Wear Behavior of a ZA-27 Alloy, Tribology International Volume 43, Issues 1-2, 16-21 (2010).

[11] Babic M., Mitrovic S., Dzunic D., Jeremic B., Bobic I.: Tribological Behavior of Composites Based on Za-27 Alloy Reinforced With Graphite Particles, Tribology Letters 37, 401-410 (2010).

SERBIATRIB '11

12th International Conference on Tribology

Serbian Tribology Society

Faculty of Mechanical Engineering in Kragujevac

Kragujevac, Serbia, 11 – 13 May 2011

WEAR BEHAVIOUR OF TIN COATINGS FOR COLD FORMING TOOLS UNDER DRY SLIDING CONDITIONS

Slobodan Mitrović[1], Miroslav Babić[1], Dragan Adamović[1], Fatima Živić[1], Dragan Džunić[1], Marko Pantić[1]

[1] Faculty of Mechanical Engineering, Sestre Janjic 6, Kragujevac, Serbia

babic@kg.ac.rs, adam@kg.ac.rs, boban@kg.ac.rs, dzuna@kg.ac.rs, pantic@kg.ac.rs

Abstract: *TiN coatings are very common themes of scientific works and are largely used in industry in metal cutting and cold forming processes; This work on quantitative way represents improvement, in terms of wear resistance, which is obtained by depositing of PVD TiN coating on foundation material. Wear testing is done on tribometer with block –on –disc contact geometry at sliding sample contact coated by TiN coat with steel disc. Testing was performed in conditions without lubrication at variable value of contact parameters (normal load, sliding speed). PVD TiN coatings in all contact conditions show smaller values of wear degree.*

Keywords: *TiN coating, Surface roughness, Dry sliding, Wear,*

1. INTRODUCTION

Intensive developing of complex physical-chemical processes in surface layer represents main cause of losing work capabilities of technical systems, energy and material wasting. Optimal choice is surface layer of high quality on basic material, of lower value and price, which directly refer to coating technology. Since 70s of the last century, when intensive development of this kind of surface modification has begun, a large number of coatings have been developed, as well as technologies for their application. Thin hard coating applied on soft foundation proved as tribological very suitable. First commercial tribological TiN coatings are applied by CVD technology on the tools. In 1980s, with PVD technology development, their commercial growth begins. They were primarily used for cutting tools of high speed steel, but were soon used in other tribological applications, such as the case of drawing tools, bearing, seals, as well as protection layer of erosive wear combination materials.

Tribological characteristic studies of TiN coatings are the subject of numerous studies both before and today. Number of papers containing „TiN coating“ in its title is over 35 000 and it grows intensively, which only tells about scientific and technological potential of these coatings.

In this way, suitable mechanical, physical, and chemical properties can be obtained, using thin and hard one-layer or more-layers coatings over conventional constructional material [1]. One of the biggest advantages of PVD method is relatively low temperatures necessary for TiN coating. That makes this method suitable for materials whose hardness can be affected by uncontrolled annealing in the coating chamber such as reinforced and high speed steels [2].

Numerous factors affect tribological coating characteristics, staring with foundation material on which the coating is being applied, the way of final foundation processing, chosen way of deposition, while these two factors directly affect the third one, also very important factor, adhesion between foundation material and the coating itself.

The primary objective of TiN coating is to reduce wear and extend the life of the tool, therefore great number of papers refer to wear in different exploitation conditions. A large number of parameters have influence on both wear mechanism, and quantitive wear value. Influence of certain procedures of coating depositing and their parameters on tribological characteristics, especially on wearing, is the subject of numerous studies [3-6].

Very influential factor, both on mechanical and tribological characteristics, is the material on which the coating is being deposited, as the way of its previous preparation [7]. P. Harlin has presented the influence of surface roughness of TiN coating on tribological characteristics [8].

Having a constant distribution of titanium interlayer thickness is not necessarily the best solution to achieve maximum performance in terms of wear resistance and hardness. The residual stress distribution along the thickness is unlikely to be constant with the inner layers being more stressed due to a greater amount of thermal differential strain. Influence of thickness on tribological characteristics is shown in E. Bemporad’s paper [9], where it was concluded that thick coatings (i.e. >10 μm) were achieved by alternate multi-layering of TiN with Ti inter-layers, leading to a tougher and less-stressed film.

Material of counter-bodies has huge influence on wearing [10-11], primarily on wear mechanism, that is to say, on tribo-chemical procedures, which in combination with other parameters, under which the contact is achieved, come to the force.

The aim of this paper is to present the benefit in the sense of reducing tool wear in processing of metal deforming using PVD TiN coatings. Therefore, when choosing contact parameters of sliding speed and normal load it should be taken into account to match real exploitation conditions of these tools. The steel X165CrMoV12 is taken as the foundation on which the coating is being deposited and it is often used for tool making in processing of metal deforming. The paper presents the influence of PDV TiN coating on reducing wear values in comparison to foundation material in conditions without lubrication, as well as the influence of contact parameter change (normal load and sliding speed) on the value of wear degree.

2. EXPERIMENTAL

2.1 Material

Contact pairs are made of alloy tool steel with great toughness and hardness, label X165CrMoV12. This steel is wear resistant and scheduled to work on cold. Hardening in oil and loosening were done before mechanical grind processing. Mechanical characteristics are given in Table 1, and chemical composition in Table 2.

Table 1. Mechanical characteristics of alloy tool steel X165CrMoV12

Hardness after soft annealing HB max	Tensile strenght after soft annealing MPa max	Hardness after hardening in oil and loosening HRC	Measured hardness on the used tool HRC
250	830	57-65	58-63

Table 2. Chemical composition of alloy tool steel X165CrMoV12

C	Si	Mn	P max	S max	Cr	Ni max	Mo	V	W
~1.65	~0.30	~0.30	0.035	0.035	~12.0	0.25	~0.60	~0.10	~0.50

In order to test them, the samples were coated with hard coating of titan-nitride (TiN). It should be pointed out that the substrate was heat-treated alloy tool steel X165CrMoV12.

TiN coating is done by RTB Bor PVD (Physical Vapour Deposition) technique – high-vacuum plasma deposition technology of hard layers depositing on contact surfaces.

Characteristics and conditions of applying TiN coating are as follows:

- Micro-hardness: ≈2000 HV,
- Layer thickness: 3-4 μm,
- Adhesive force: over 50 N,
- Application speed: 6-7 min/μm,
- Time of application: 21 min,
- Application temperature: 450 °C,
- Gold coating.

2.1 Tribological test

The specimens were tested using a block-on-disc sliding wear testing machine with the contact pair geometry in accordance with ASTM G 77-83. A schematic configuration of the test machine is shown in Fig. 1. The test block was loaded against the rotating steel disc. This provides a nominal line contact Hertzian geometry for the contact pair.

The test blocks (6.35x15.75x10.16 mm) were prepared from tool steel X165CrMoV12, while one part of the samples is TiN coated. The values of surface roughness were measured on the prepared samples before and after depositing of coating. Measuring of surface roughness was done on Talysurf 6 device and appearance of material layout in surface layer on referent length l=1.2mm, is shown in Figures 1 and 2.

Surface roughness of sample, without coating was Ra=0.01μm, and with TiN coating was Ra=0.02μm, which suggests that after deposition there was no serious change of surface roughness.

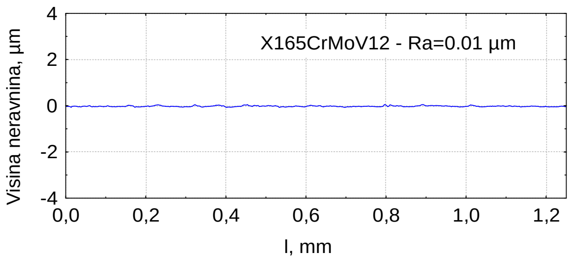

Figure 1. Surface profilometer X165CrMoV12,

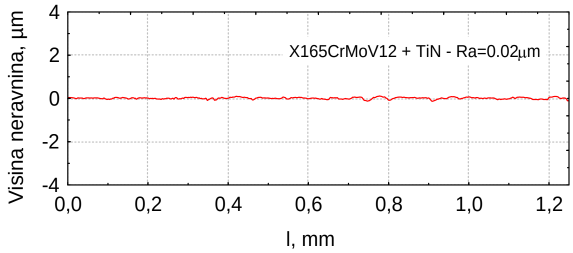

Figure 2. Surface profilometer X165CrMoV12 + TiN

A schematic configuration of the test machine is shown in Fig. 3. More detailed description of the tribometer is available elsewhere [12]. The wear behavior of the block was monitored in terms of the wear scar width - h (Fig. 4). Using the wear scar width and geometry of the contact pair the wear volume (in accordance with ASTM G77-05) and wear rate (expressed in mm^3) were calculated. The repeatability of the results for replicate tests was found as satisfactory (variation of wear scar width was under 5%).

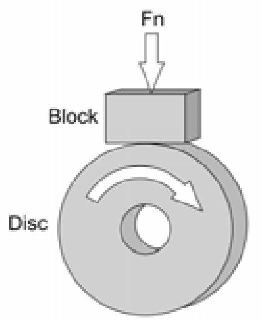

Figure 3. The scheme of contact pair geometry

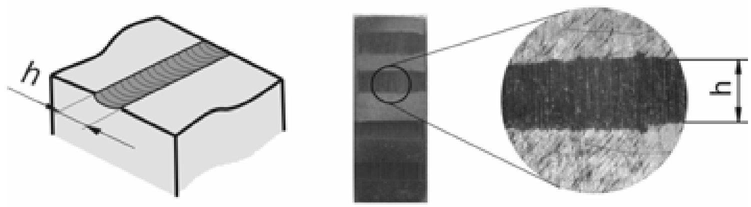

Figure 4. Wear scar

The counter face (disc of 35 mm diameter and 6.35 mm thickness) was made of EN: HS 18-1-1-5 tool steel of 62HRC hardness. The roughness of the ground contact surfaces was R_a=0.45 μm. The tests were performed in dry sliding conditions at sliding speeds (0.25 – 1m/s) and applied loads (10-30 N). Each experiment was repeated five times. Sliding road for all tested samples was 200 m.

3. RESULTS AND DISCUSSION

In the paper steel samples are tested with and without coating in order to qualify the improvement of coating resistance to wearing in relation to foundation material. Prepared samples are tested in conditions without lubrication, with varying values of sliding speed and normal load. Sliding speed in contact was taking three values 0.25, 0.5 and $1ms^{-1}$.

The normal load value also had three values 10, 20 and 30N during the tests. The normal load values are selected to avoid coating perforation during the testing, which was achieved.

Figure 5 shows diagram of wear degree dependence on change of normal load value with constant sliding speed value in contact zone. The Figure clearly shows that, with increase of normal load in contact zone, the wear degree of all tested samples increases. It is also clear that wear degree of TiN coatings in relation to the samples without coatings for the same values of tested parameters is always smaller. Wear degree values for steel samples at the highest speed of $1ms^{-1}$ stand out among the results. At this speed with increase of load it comes to certain increase of wear degree, based on which we can conclude that further increase of normal load would very quickly cause catastrophic wearing of tool material in processing of metal deforming.

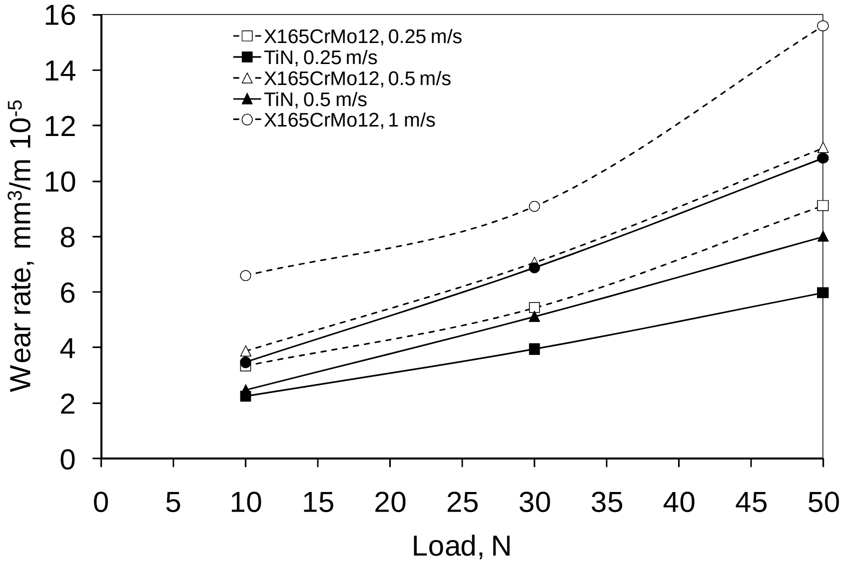

Figure 5. Wear degree dependence of tested samples on the normal load value (10, 20 and 30N)

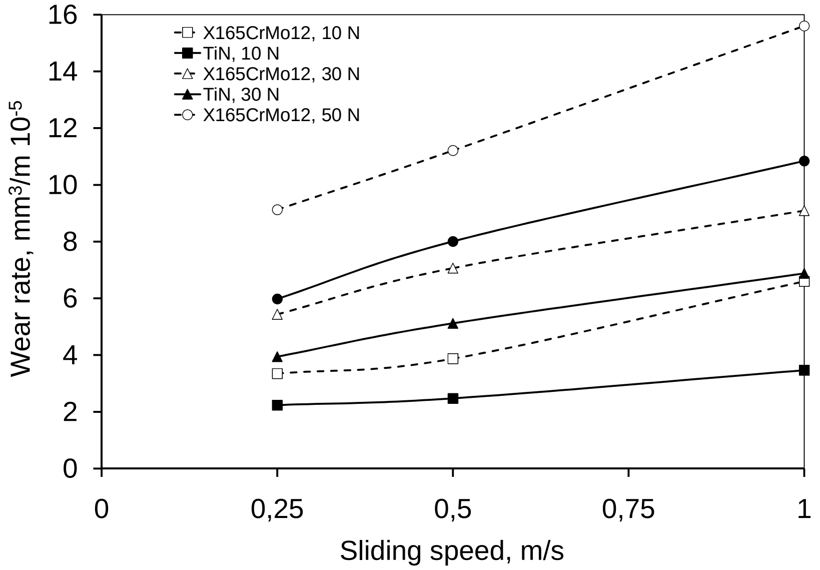

Figure 6. Wear degree dependence of tested samples on sliding speed (0.25, 0.5 and 1ms^{-1})

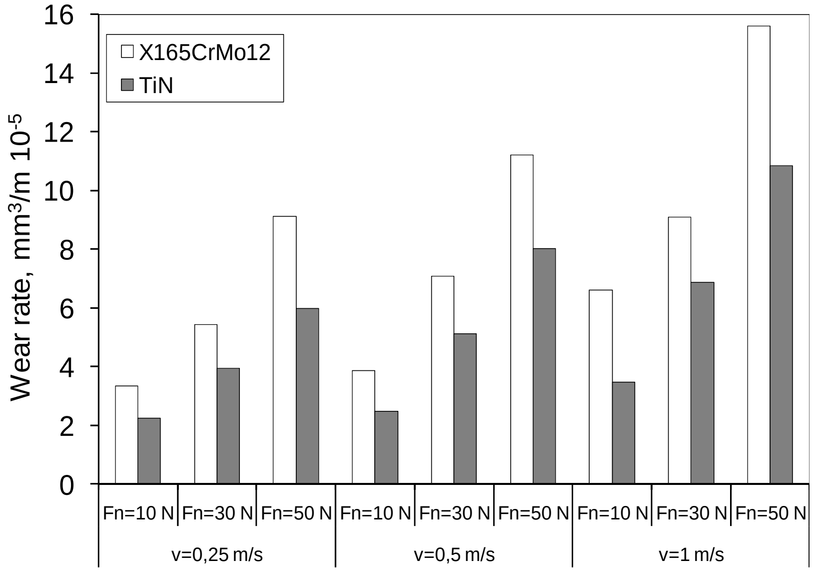

Figure 7. Histogram display of wear degree value for tested samples

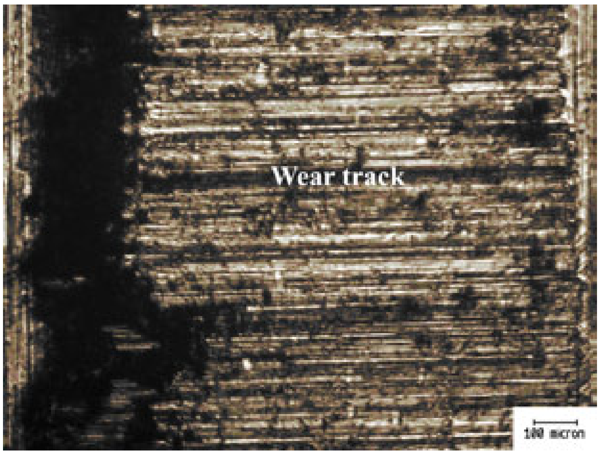

a)

b)

Figure 8. Display of wear traces after sliding road of 200m, normal load value of 30N and sliding speed of 1ms^{-1} a) without coating; b)TiN coating.

Figures 8 show typical wear traces of tested samples in conditions without lubrication. Regardless of the value of contact parameters there was no coating penetration, which can be seen in these figures. Based on the appearance of wear traces at samples with and without coating we may say that the basic wear mechanism is abrasive wearing. At the very beginning of making contact we can talk about adhesive wearing, which is the consequence of contact block-on-disc, or high contact pressures which appears when contact is achieved only on the peaks of prominences. With further development, the wearing from linear contact passes into contact on surface where the oxides are the ones that appear when contacted with steel if they come in the contact zone and act as abrasive.

4. CONCLUSIONS

The results of wear studies, carried out to quantify the influence of TiN coatings on material resistance in processing of metal deforming on wearing, showed that in all contact conditions TiN coatings have lesser wear degree values in comparison to the material without coating. Based on the results, we can conclude that advantages of TiN coating in terms of resistance to wearing, in conditions without lubrication, in comparison to material without coating, come to the force at sliding speed values higher than 0.5ms^{-1} and normal load value higher than 20N.

These results are consequences of expected, by numerous studies confirmed, mechanical and tribological characteristics of TiN coatings. Based on that we can conclude that by TiN coating of material, the significant increase of tool life in processing of metal deforming is acquired, which is expressed at higher values of contact load and sliding speed.

In the conditions of making contact without lubrication, TiN coatings have proven as economically payable which is reflected in decreasing wear degree of tools, in some cases up to 40% in comparison to surfaces without coating.

ACKNOWLEDGMENT

This study was financed by Ministry of Science and Technological Development, Serbia, project No.35021.

REFERENCES

[1] K. D. Bouzakis, N, Widakis: Advanced Physically Vapor Deposited Coatings - State of The Art, Innovations and Future Trends Tribology In Industry, Volume 20, No.3, (1998).
[2] Spur, G. Byrne G., Bienia, B.: The performance of PVD coated High Speed Steel indexible inserts in the milling of ductile materials, ICMC17, San Diego, B 2-6, (1992).
[3] M. Diesselberg, H-R. Stock, P. Mayr: Corrosion protection of magnetron sputtered TiN coatings deposited on high strength aluminium alloys, Surface and Coatings Technology, 177 –178, 399–403 (2004).
[4] Branko Skoric, Damir Kakas, Natasa Bibic, Milan Rakita: Microstructural studies of TiN coatings prepared by PVD and IBAD, Surface Science, 566–568, 40–44 (2004).
[5] F. Borgioli, E. Galvanetto, F.P. Galliano, T. Bacci: Sliding wear resistance of reactive plasma sprayed Ti–TiN coatings, Wear, 260, 832–837 (2006).
[6] ZHAO Hui, WANG Xiao-hui, LIU Qiu-lei, CHEN Li-jia, LIU Zheng: Structure and wear resistance of TiN and TiAlN coatings on AZ91 alloy deposited by multi-arc ion plating, Transactio of Nonferrous Metals Society of China, 20, 679-682 (2010).

[7] S.V. Hainsworth, W.C. Soh: The effect of the substrate on the mechanical properties of TiN coatings, Surface and Coatings Technology, 163 –164, 515–520 (2003).
[8] P. Harlin, P. Carlsson, U. Bexell, M. Olsson: Influence of surface roughness of PVD coatings on tribological performance in sliding contacts, Surface & Coatings Technology, 201, 4253–4259 (2006).
[9] E. Bemporad, M. Sebastiani, C. Pecchio, S. De Rossi: High thickness Ti/TiN multilayer thin coatings for wear resistant applications, Surface & Coatings Technology, 201, 2155–2165 (2006).
[10] S. Wilson, A.T. Alpas: TiN coating wear mechanisms in dry sliding contact against high speed steel, Surface and Coatings Technology, 108–109, 369–376 (1998).
[11] E. Badisch, G.A. Fontalvo, C. Mitterer: The response of PACVD TiN coatings to tribological tests with different counterparts, Wear, 256, 95–99 (2004).
[12] Babic M., Mitrovic S., Jeremic B.: The Influence of Heat Treatment on the Sliding Wear Behavior of a ZA-27 Alloy, Tribology International Volume 43, Issues 1-2, 16-21 (2010).

Serbian Tribology Society

SERBIATRIB '11

12th International Conference on Tribology

Faculty of Mechanical Engineering in Kragujevac

Kragujevac, Serbia, 11 – 13 May 2011

STRACH EPOXY COMPOSITES
A STUDY OF STARCH AMOUNT INFLUENCE

Igor Roman[1], Victor Ungureanu[1], Vasile Bria[1],
Adrian Circiumaru[1], Iulian-Gabriel Birsan[1]
1"Dunarea de Jos" University Galati, Romania, www.ugal.ro

Abstract: *It is well known that starch reticulates when solved into a liquid. Based on this observation might be possible that starch to form its own network inside a thermosetting polymer volume (a network of polymeric chains) acting as a reinforcement if it is solved into the pre-polymer solution. Starting with this idea and taking into account the fact that starch may be easily functionalized it might be possible to use this powder to "place" other atoms or other chemical radicals inside the polymer to change its properties. These are the reasons for which this study is carried out in order to exhaustively characterize the starch epoxy materials realized from epoxy system EPIPHEN RE 4020 / EPIPHEN DE 4020 and corn starch (for food purposes) with weight rations starting with 1:100 till 50:100. For this paper dimensional stability and tribological behaviour are taken into account. The tribological tests were performed with pin-on-disk (with rectangular pins made of filled composites and steel disk) in order to identify the maxim amount of starch to be used without critical effects on the final materials properties.*

Keywords: *starch, epoxy, thermal behavior, tribological behavior, wear..*

1. INTRODUCTION

Filling the polymer with various substances in various forms (powders, whiskers, and flakes) was, at the beginning, a way to reduce the amount of polymer used to form a structure but this method became a way to modify the basic properties of the polymer leading to improvements regarding thermal, electro-magnetic or tribological properties.

The researchers had spent much time on modelling the properties of a particulate composite on the basis of its components' properties and many solutions were purposed [1-3]. For all the models some simplifying assumptions had to be made limiting the models' predictions. For instance, there are not models regarding the connection between the nature and dimensions of dispersed particles and the nature and the properties of the polymer. In the case of thermoplastics the fillers are dispersed into the melt of the polymer and it is possible to control the dispersion conditions by controlling the temperature of the mixture [4]. In the case of thermosetting materials the powders (it is the most important case) are dispersed into a pre-polymer mixture allowing a possible chemical interaction between the polymer and powders molecules. Some of the powder materials could absorb some of the pre-polymer mixture (such as CNT) leading to more dense materials. Generally thermosetting materials are bi-component systems which have to be mixed in certain amounts to polymerize. This fact is making possible three different ways to disperse the powders – into a component, into the other, or in the pre-polymer mixture – leading to different properties of formed material [5].

Regarding the powder fillers another aspect is more important, namely they may create nanostructures inside the matrix [6, 7] if they chemically interact with the thermosetting components. In this regard it has to be said that generally the powder's particles tend to aggregate inside the polymer volume alterating the polymer quasi-continuous structure and leading to worst mechanical properties. A way to solve this problem is to treat the powders in order to make them more dispersible inside the pre-polymer volume; another way is to use two fillers one as dispersant and the other one to change de properties. In this category talc and clay might be included with benefits regarding the fire resistance and wear resistance of formed polymers [8, 9].

The mixing rule [10, 11] is giving some information regarding the amplitude of a property if the properties of the components and their ratios are known. But the mixing rule works for micron dimensions of dispersed particles and in such dispersion the particles act as defects inside the polymer matrix leading to poor mechanical properties. Since the particles' dimensions are decreased other aspects have to be taken into account. If at micron level it might be said that the interaction is solid-liquid type which may be described in terms of adhesion and cohesion forces at nano level the interaction might be at the level of molecules leading even to nano-structures with significant changes of formed material's properties.

2. MATERIALS

This study started with the idea that starch is a special compound which is developing its own structures when is dispersed into a liquid. Thinking this way it would be possible that starch to constitute a network inside the polymer network which means that the polymer is nano-reinforced. For such answers a SEM analysis is required and this is next level of the study.

Mean time starch is very easy to functionalize with different complex compounds. It is possible, this way, to use starch as vector to implant positive or negative ions inside the polymer network. The advantage of this receipt consists in easiness and elegance but involve a study regarding the amount of starch which might be placed into the polymer without changing its mechanical properties. Having ions inside the polymer it is possible to increase electrical conductivity, and even to control it.

Another aspect is connected with the fact that starch is an excellent dispersant so it might be used to avoid aggregation of other powders' particles such as CNT, ferrite etc which are electro-magnetic active and could be used to control electro-magnetic response of the formed material.

The EPIPHEN RE 4020 – DE 4020 was used as matrix and corn starch as filler to form particulate composites with volume ratios starting with 1% and ending with 50%; from 1% to 5% the increment is one unit while from 5% to 50% the increment is five units. As dispersing technique in all the cases the amount of starch was mechanically dispersed for 30 minutes into the pre-polymer mixture (EPIPHEN RE 4020 – DE 4020). The named epoxy system has 45 minutes gel time so the mixture was moulded while its viscosity was not too high. After the polymerization (24 hours) the samples were extracted from moulds and they were thermally treated according to producer's recommendations in order to reach their best properties (8 hours at 60 ^{o}C, 2 hours at 90 ^{o}C and 2 hours at 120 ^{o}C – to ensure a higher value of glass transition of the polymer).

Samples for thermal and tribological analysis were extracted from formed plates by using a high pressure water jet machine to avoid edge effects and thermal changes of the materials.

3. MEASUREMENTS AND RESULTS

Thermal properties of formed materials were investigated in order to identify the effects of starch filling over the epoxy matrix. Also a goal of this study is to determine the maximum starch concentration for which the basic properties of the epoxy resin are not changed allowing the use of starch as dispersant for other active powders. In this regard is not taken into account the initial dispersion technique which might influence the results.

The specific weight of formed materials is showed in Figure 1. Represented values are the ones after the thermal treatment. For the lowest starch ratios the material density is lower than epoxy's one due to the air which is introduced into the polymer volume together with the starch powder. At 10% the material density is just a little bit higher than the epoxy's one and at higher ratios the material specific weight becomes higher that the one of the base polymer.

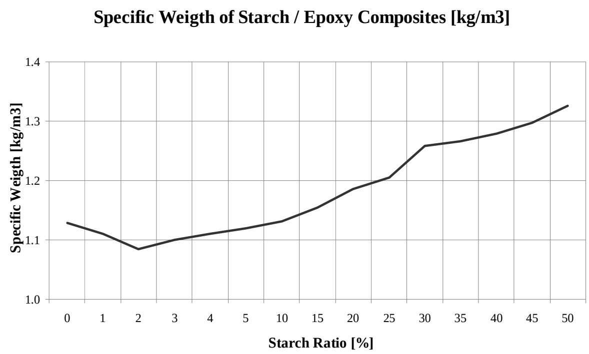

Figure 1. Specific Weigth of Starch/Epoxy Materials

The TMA-SDTA 840 from *Mettler Toledo* was used to determine the coefficient of thermal expansion by means of dedicated software Star***e*** also from *Mettler Toledo*. It is noticeable that in the case of 10% and 20% starch ratios the peak corresponding to the glass transition of epoxy resin is moved to the right with about 5^{o}C signalizing a structural change. Due to the air inside the polymer at low starch ratios the coefficient of thermal expansion is higher than the epoxy's one while for higher ratios it decreases. At 10% starch ratio the coefficient of thermal expansion shows almost the same value for epoxy and for starch/epoxy, Figure 2.

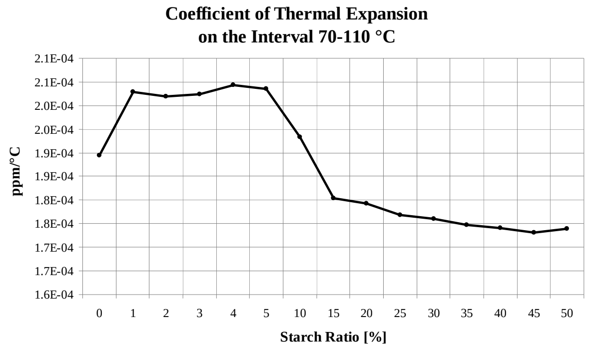

Figure 2. Coefficient of thermal expansion

The tribological behaviour and the wear behaviour had been studied on the same machine *Multi-Specimen Test System - UMT from CETR* in the fixture pin-on-disk with pin made of stratified material and steel disk and with the disk covered with abrasive paper P 400(abrasive tests).

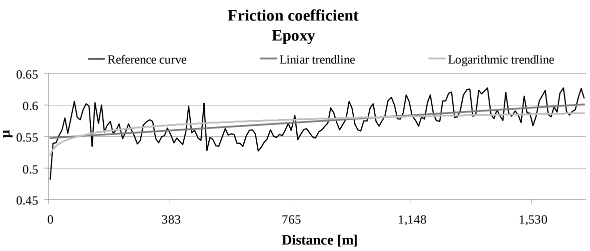

Figure 3. Friction coefficient of epoxy resin

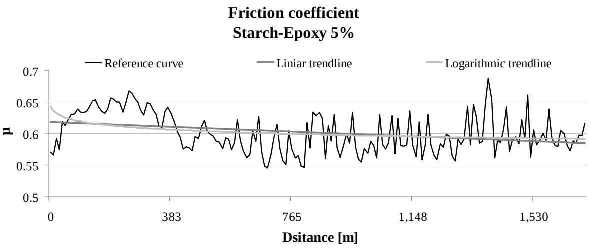

Figure 4. Friction coefficient of starch/epoxy (5%)

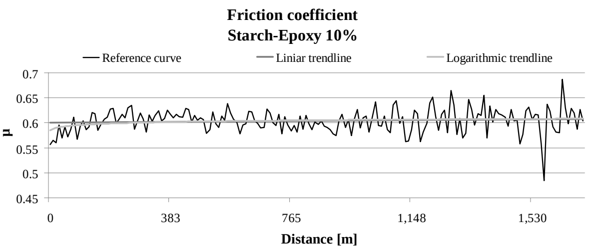

Figure 5. Friction coefficient of starch/epoxy (10%)

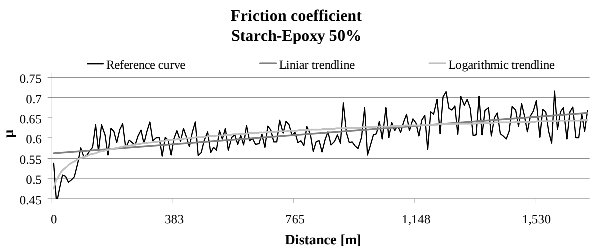

Figure 6. Friction coefficient of starch/epoxy (50%)

The friction condition for the tribological study were set at: normal loading 10 N, sliding distance 1700 m and sliding speed 0.942 m/s for all the materials and in figures 3 to 6 some of acquired data and their trends are presented.

Generally the averaged friction coefficient shows three tendencies: decreasing during tests (for low starch concentrations 1% to 5%; remaining almost constant during tests (10% to 25% starch ratio); increasing during the tests (for concentrations of 30% and above).

For studied materials the frictional wear rate was evaluated and the results are presented in fig. 7.

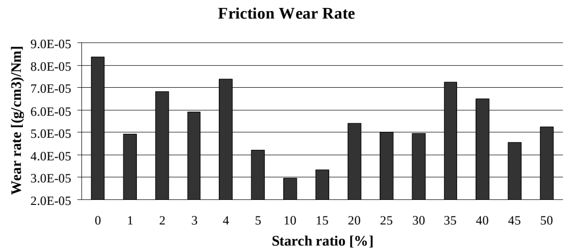

Figure 7. Friction wear rate of starch/epoxy composites

The best friction wear resistance is reached in the case of 10% material but is noticeable that adding starch into the matrix the frictional wear rate decreases. Taking into account also the specific weight of materials it is expected that at high concentrations the frictional wear rate to be higher due to the large amount of material which is lost during test. The high resistance means that adding starch the frictional properties are improved by ensuring a better package of the polymer chains and limiting the weight loss by making the matrix less breakable.

The abrasive tests were performed at a normal loading of 2 N and three different sliding speeds as it might be noticed in fig. 8.

Almost all the materials show abrasive wear rates higher than epoxy's one the few exceptions appear randomly and are explainable just by defects inside the matrix. These defects may appear as a consequence of forming technique or may be caused by mechanical defects of samples as cracks.

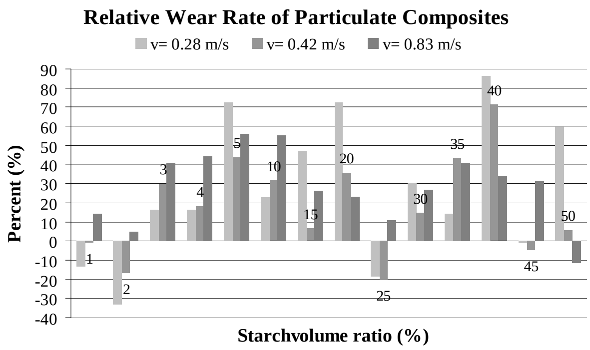

Figure 8. Relative abrasive wear rate

4. CONCLUSIONS

Even the design problem is a complex one the presented results are encouraging further studies regarding filled polymers and reinforced materials with filled polymer matrix to achieve more advantages when forming a material. Another aspect is connected with the description of particulate composite's properties in terms of powder and polymer properties. The mixing rule does work for micron dimensions and is not taking into account possible interaction between fillers' particles and polymer's components. For this study the starch was dispersed directly into the pre-polymer mixture and it is expected that none interaction took place, the starch particles were covered by polymer chains. In this hypothesis the air (or other gaseous chemical compounds) presence inside the matrix is normal but this situation could be improved by using anti-foaming products or by changing the way of dispersion.

The aim of this study was to establish the highest starch concentration which is not changing the epoxy's basic properties. It seems that the answer is 10% from specific weight, thermal stability and frictional properties but is not good enough from the abrasive behaviour point of view. Anyway the study is just a preliminary analysis before using starch just to disperse other fillers which generally tend to aggregate as CNT or ferrite or to use functionalized starch to transport at the polymer chains level some positive or negative ions able to improve the electrical conductivity.

In this regard all the materials have to be studied by SEM and XR means to point out eventual structural changes. Also mechanical properties of materials have to be studied being useless to improve other properties if the mechanical ones are damaged. All the analysis have to be repeated for each material formed with dispersant starch or functionalized starch because even a concentration of 10% will be used it is possible that active fillers' particles to change the properties due to their presence or equally it is possible that complex combinations used to functionalize the starch to chemically interact with the polymer components.

Using filled matrix it is possible to design and form reinforced materials with certain properties only by means of type and amount of the filler. Also using the lay-up method of forming with pre-polymer or filled pre-polymer mixture it is possible to obtain materials with certain properties at different depths inside the material (high electric conductivity at external layers, high magnetic properties in the core etc) but having the same type of polymer chains in all the volume and ensuring by this a right transfer of efforts inside the material.

Using fabrics to reinforce such composites (instead of pre-pregs) it is also possible to obtain polymer bridges through reinforcement layers and not only between them as in the case of laminates.

The presented results are encouraging the continuation of the studies not only in the two above mentioned directions but also in using starch filled epoxy to form laminae and stratified materials to point out also the changes induced in electro-magnetic, thermal, mechanical and tribological properties in the case of reinforced materials

REFERENCES

[1] Torquato, S., Hyun, S., Donev, A., Optimal design of manufacturable three-dimensional composites with multifunctional characteristics, Journal of Applied Physics, 94, pp. 5748-5755, 2003.

[2] Torquato, S., Modeling of physical properties of composite materials, International Journal of Solids and Structures, 37, pp. 411 – 422, 2000.

[3] Feng, X.-Q., Tian, Z., Liu, Y.-H., Yu, S.-W. (2005), Effective Elastic and Plastic Properties of Interpenetrating Multiphase Composites, Applied Composite Materials, 11, pp. 33-55, 2005.

[4] Milton, G. W., Bounds on the Electro-magnetic, Elastic, and Other Properties of Two-Component Composite, Physical Review Letters, 46, pp 542 – 545, 1981.

[5] Fetecau, C., Dobrea, D.-V., Postolache, I., Overmolding Injection Injection Simulation of Tensile Test Specimen, International Journal of Modern Manufacturing Technologies, ISSN 2067–3604, Vol. II, No. 2, pp. 45 – 50, 2010.

[6] Circiumaru, A, Birsan, I.-G., Bria, V., Andrei, G., Dima, D., A comparatie study of particulate epoxy composites, to be published in Journal of Polish Society for Composite Materials, ISSN 1641-8611, 2011.

[7] Winey, I. K., Vaia, A. R. (eds.), Polymer Nanocomposites, MRS Bulletin, Vol. 32, pp. 314 - 322, 2007.

[8] Lefebvre, J.-M., Nanocomposites, Polymer-Clay, in Mark, H.F. (ed.), *Encyclopedia of Polymer Science and Technology*, John Wiley & Sons, Inc., vol. 3, pp. 336 – 352, ISBN: 978-0-471-27507-7, 2004.

[9] Pukanszky, B., Mineral-filled polymers, in Mortensen, A. (ed.), *Concise Encyclopedia of Composite Materials*, Elsevier, pp. 516 – 519, ISBN-13: 978-0-08-045126-8, 2007.

[10] Birsan, I.-G., Circiumaru, A., Bria, V., Ungureanu, V. (2009), Tribological and Electrical Properties of Filled Epoxy Reinforced Composites, in Tribology in industry, 31, No. 1-2, pp. 33-36, ISSN: 0354-8996, 2009.

[11] Callister, W. D. Jr., *Materials Science and Engineering*, 7th ed., John Wiley & Sons, ISNB-10:0-471-73696-1, 2007.

Serbian Tribology Society

SERBIATRIB '11

12th International Conference on Tribology

Faculty of Mechanical Engineering in Kragujevac

Kragujevac, Serbia, 11 – 13 May 2011

TRIBOLOGICAL AND WEAR PROPERTIES OF MULTI-LAYERED MATERIALS

Vasile Bria[1], Dumitru Dima[1], Gabriel Andrei[1], Iulian-Gabriel Birsan[1], Adrian Circiumaru[1]

[1]"Dunarea de Jos" University Galati, Romania, www.ugal.ro

Abstract: *The usage of fabrics as reinforcements in composites is spreading due to fabrics' properties. The use of fabrics allows obtaining of sinuous surfaces, for instance, unlike the use of pre-pregs. Using fabrics as reinforcements it is also possible to obtain laminate-like materials having the same matrix in all their volume. In the case of pre-pregs usage always it is necessary to discuss about the bonding between individual plies. For this study eight materials were formed. The forming method consisted in placing the pre-polymer imbued fabric pieces into a mould to obtain plates of composites. Two types of fabric were used: one simple type of untwisted tows of carbon fibres and the second one simple type of alternated untwisted tows of carbon and aramide fibres. Both fabrics were prepared in order to ensure the matrix adherence. The polymer matrix is realised from epoxy system EPIPHEN RE 4020 / EPIPHEN DE 4020 filled with clay and talc in equal amounts of 5% (weight ratio). The use of clay and talc were meant to improve the thermal dimensional stability of final materials. Tribological properties of formed materials were studied using pin-on-disk method with steel disk and pins made of materials. Both orientation of reinforcement fibres relative to friction direction were taken into account. Results are encouraging further studies in order to identify the best solution of forming a multi-component material with more than one designable property.*

Keywords: *fiber fabrics, epoxy, clay, talc, wear.*

1. INTRODUCTION

Powders are used as fillers in order to obtain bi-components composites [1, 2, 3]. There is no structural order in such a filled composite, the most important aim being the uniform distribution of particles in matrix. If the fillers' particles are arranged into the polymer volume is possible to change the electro-magnetic behavior of the obtained composite making this one to act as a meta-material [4, 5]. The powders can be dielectric as talc, clay or ferrite can be magnetic active as ferrite, or electric active as CNT or carbon nano-fibers. All these powders, added to the polymeric matrix, have effects on the electro-magnetic, thermal and mechanical properties of the composite [6, 7]. What about using all of them, based on partially changes induced by each one? There exist many models regarding the mathematic description of electromagnetic properties of the bi-component composites. Also there are studies regarding the bounds of models. Taking into account that not only the electromagnetic properties are important but also the mechanical and thermal properties the design problem becomes almost impossible.

The use of fabrics as reinforcements for polymer matrix composites is recommended by their ability to form sinuous and complicated surfaces keeping the regulated distribution of the fibers. The lay-up method of forming allows materials with the same matrix in all the volume unlike the laminated composites where the bonds between layers are very important. Stratified materials with the same polymer in all the volume responds different from laminated at all the external solicitations – thermal, electrical, mechanical etc. For this study epoxy resin was used as matrix and two types of fabrics as reinforcement to form layered materials with various orientations of fabric layers and with different distributions of the two fabrics inside the material.

The aim of this study is to identify the tribological changes induced by fillers when they are used to form a stratified fabric reinforced material with different fillers in different layers.

2. MATERIALS

Two types of fabric were used during this study; first type is simple fabric made of untwisted tows of carbon fibers while the second is a simple fabric made of alternating untwisted tows of carbon and aramide fibers. From the beginning the two fabrics were choose because of the intrinsic properties of fibers (electromagnetic and mechanical in the case of carbon fiber, shock and thermal in the case of aramide fiber). Two problems had to be solved before forming the multi-component composites: the fabrics' stability – because during the cutting the tows are slipping one on each other leading to structural defects of fabric with consequences in mechanical properties of the composite; the second problem is about the low epoxy adhesion to the two types of fiber which leads to discontinuities at the interface level with consequences in all the composite's properties. The two fabrics were specially prepared before they had been used as reinforcements.

The fabrics treatment has two phases: a chemical one meant to increase the specific area of fibers and to ensure the matrix adhesion consists in treatment with 50% hypochlorite aqueous solution and then with 20% NaOH aqueous solution; the second phase meant to stabilize the tows consists in covering the fabrics with o thin film of PNB rubber and then with a thin film of epoxy. Both the rubber solution and polymer's components solutions were filled with small amounts of clay and carbon black in order to enlarge the specific area of the fabrics and to improve the electrical behavior of materials.

The matrix is realized from the mentioned epoxy with: clay (5%), talc (5%), CNT (0,5%) for first two reinforcement layers; clay (5%), talc (5%), CNT (1%) and ferrite (5%) for next two layers; clay (5%), talc (5%), CNT (0,5%), ferrite (5%) for other two layers; clay (5%), talc (5%), CNT (0,5%), ferrite (2%) and Wolfram carbide (5%) for last two layers (respecting the molding order) – all the ratios are expressed in weight terms. This type of matrix will be denoted as s for all the information below. The other matrix, denoted with h, represents a homogeneous matrix filled with 5% clay and 5% talc for all the reinforcement sheets. All the powders were mechanically mixed and then dispersed into the right amount of A component of the epoxy system, the amount of B component was added and the fabrics were imbued with the filled pre-polymer mixture.

The presence of both clay and talc leads to a material which acts as a liquid with very high viscosity because the ordered zones surrounding the clay or talc particles are connected through typically polymer bonds. It is expected that the particulate composite to show lower mechanical properties but higher dimensional stability. The use of Ferrite is intended to change the magnetic properties of the final composite while the use of CNT for changing its electric behavior [8]. As per Wolfram carbide, despite its high specific weight, it can be used to change the tribological properties of the composite. It is taken into account not the frictional behavior but the wear resistance under the action of a flux of abrasive particles (as sand) in order to increase the lifetime of components exposed to such factors.

For this study materials were formed in order to point out the influence of reinforcements and matrix on final properties of formed materials. For each formed material the reinforcement consist in eight sheets of fabric. The reinforcement sheets were cut parallel to weft and yarn of the fabric (0) or at 45 reported to the warp and yarn of the fabric (45). The two types of fabrics are denoted as C, for carbon fiber fabric or K for mixed fabric such as each reinforcement's sheet may be described as C(0), C(45), K(0) or K(45). The reinforcement's structure of each material is presented in Table 1 and Table 2.The Epoxy system RE 4020 – DE 4020 was used as matrix and clay, talc, CNT, ferrite and Wolfram carbide as fillers. Each of the fillers is used on a certain purpose connected to the final properties of the composite.

Table 1. Stratified materials' structure - A

	Reinforcement structure - A
1	C(0^o) C(45^o) K(0^o) K(45^o) K(45^o) K(0^o) C(45^o) C(0^o)
2	C(0^o) C(45^o) C(45^o) K(0^o) K(45^o) K(0^o) C(45^o) C(0^o)
3	C(0^o) C(45^o) C(0^o) K(45^o) K(0^o) C(45^o) K(45^o) C(0^o)
4	C(0^o) C(45^o) C(45^o) C(0^o) C(0^o) C(45^o) C(45^o) C(0^o)
5	C(0^o) K(45^o) C(0^o) K(45^o) C(0^o) K(45^o) C(0^o) K(45^o)

Table 2. Stratified materials' structure - B

	Reinforcement structure - B
1	K(0^o) K(45^o) C(0^o) C(45^o) C(45^o) C(0^o) K(45^o) K(0^o)
2	K(0^o) K(45^o) K(45^o) C(0^o) C(45^o) C(0^o) K(45^o) K(0^o)
3	K(0^o) K(45^o) K(0^o) C(45^o) C(0^o) K(45^o) C(45^o) K(0^o)
4	K(0^o) K(45^o) K(45^o) K(0^o) K(0^o) K(45^o) K(45^o) K(0^o)
5	K(0^o) C(45^o) K(0^o) C(45^o) K(0^o) C(45^o) K(0^o) C(45^o)

3. MEASUREMENTS AND RESULTS

The tribological behavior and the wear behavior had been studied on the same machine *Multi-Specimen Test System - UMT from CETR* in the fixture pin-on-disk with pin made of stratified material and steel disk and with the disk covered with abrasive paper (abrasive tests).

In both cases two situations were taken into account: parallel sliding counter-face with the sliding velocity parallel with the yarn tows of materials' first layer and perpendicular sliding counter-face with the sliding velocity perpendicular on yarn tows of materials' first layer.

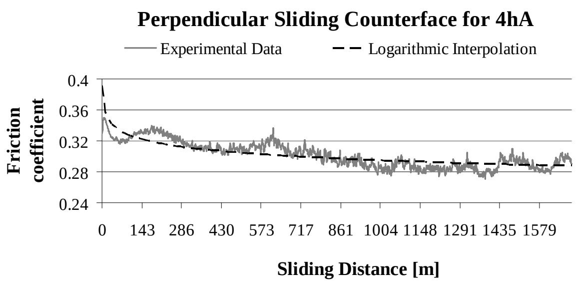

Figure 1. Friction coefficient of 4hA material

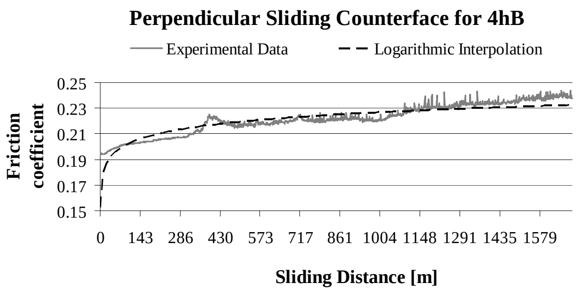

Figure 2. Friction coefficient of 4hB material

From fiber concentration point of view all the materials lie between 100% carbon fiber (4_A) and 50% carbon fiber and 50% aramide fiber (4_B) while from fiber orientation point of view all the materials are identical having 50% fibers perpendicular on the disk and 50% fibers oriented at $\pm 45^{o}$ reported to the disk surface. Materials tribological behavior lies between 4_A and 4_B behavior. In Fig. 1, 3, 5, 7 friction coefficient for 4_A on steel disk with smooth variation during test due to the small fragments of carbon fiber which are acting as dry lubricant. The 4_A represents an extreme being realized only from carbon fiber fabric as reinforcement (100% carbon fiber).

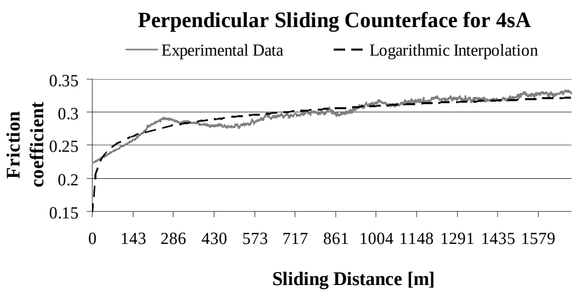

Figure 3. Friction coefficient of 4sA material

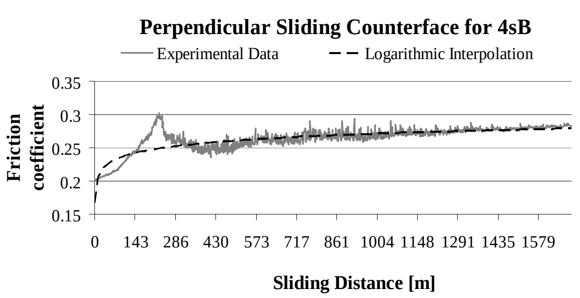

Figure 4. Friction coefficient of 4sB material

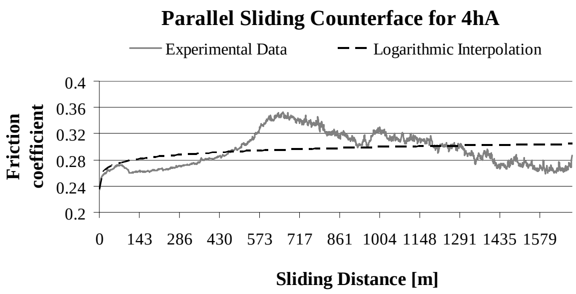

Figure 5. Friction coefficient of 4hA material

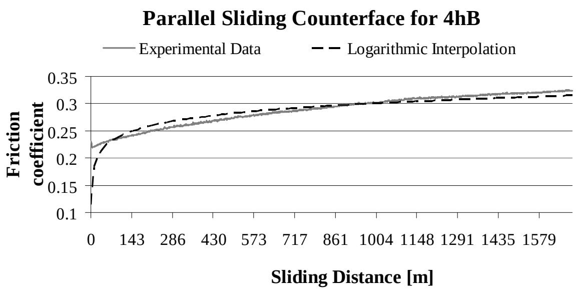

Figure 6. Friction coefficient of 4hB material

In the same figures it might be noticed that the curve realized from data acquisition shows relative flat peaks corresponding to matrix and fibers breaking. The small pieces of matrix are cutting the carbon fibers easier than aramide fibers which are more resistant leading to sharp peaks as it might be noticed in Fig. 2, 4, 6, 8. The 4_B materials are reinforced with 50% carbon fibers and 50% aramide fibers and show the lowest value of friction coefficient both on perpendicular sliding and parallel sliding due to the properties of aramide fibers. Also it is noticeable that in all the data curves these materials show sharp peaks corresponding to aramide fibers extraction from tows.

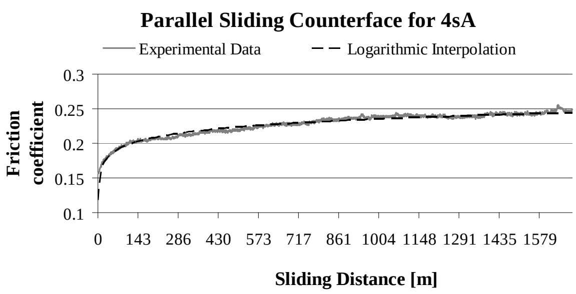

Figure 7. Friction coefficient of 4sA material

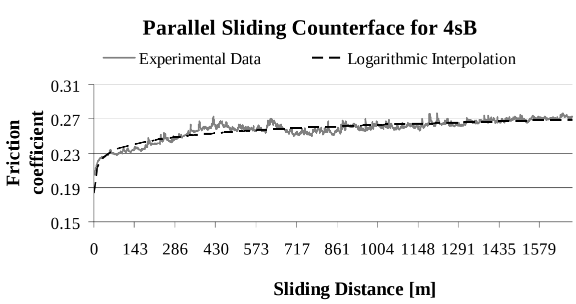

Figure 8. Friction coefficient of 4sB material

All the tested sample were extracted from initial plates of materials such as their edges are parallel with warp tows (the length of friction sample) and weft tows (the width of friction sample) of the first fabric layer (Table 1 and Table 2) such as at the contact with the disk – in the case of perpendicular sliding tests – there are 25% fibers from yarn tows of first layer and from the ones with the same orientation (0^o) - both perpendicular on disk and on sliding direction; 25% fibers from fill tows of first layer and from the ones with the same orientation - parallel with the disk and perpendicular on sliding direction); 50% fibers from yarn and fill tows of fabric layers oriented at (45^o) - being oriented at ($+45^o$) or ($–45^o$) relatively to disk and perpendicular on sliding direction. The last ones are ensuring the dry lubricant. Due their position they are breaking first unlike the fill tow fibers which are taking the interaction on their length. In the case of 4_B material the amount of each fiber is the same so in above described positions there will exist both carbon and aramide fibers with the last ones more resistant and leading to a lower friction coefficient. The aramide fibers are not chopped during the tests but they are separated from tows and remain on the disk (the ones from fill tows) or are pulled out from matrix.

In case of parallel sliding tests (Fig. 5-8) once again the behavior might be explained by fibers' positions relative to the disk and to sliding direction [8 – 11].

The three positions of tows in this case are: warp tows perpendicular on disk and perpendicular on sliding direction (but in this situation their width is parallel with sliding velocity while in previous case their width was perpendicular on sliding velocity); weft tows are parallel to the disk and parallel to sliding direction (their length is on sliding direction); inclined tows are oriented at ($\pm 45^o$) relative to disk and ($\pm 45^o$) relative to sliding direction. In the perpendicular sliding case all the fibers are exposed to interaction leading to a significant amount of chopped fibers acting as lubricant (in the case of perpendicular sliding the friction coefficient is decreasing for carbon fiber 100% and is increasing for 50% carbon fiber – 50% aramide fiber due to the resistance of last ones). In the case of parallel sliding there are fibers which are not affected (the warp tows) and their friction with the disk is lubricated by carbon fiber small pieces and frictional behavior of materials might be identical.

Regarding the friction wear rate it might be noticed that highest values for perpendicular sliding are reached for 4hA and 5sB in the first case due to the carbon fibers which are fragile and are cut by the matrix pieces becoming the dry lubricant while in the case of 5sB material the behavior might be explained by the fact that having all the mixed fabric layers at 0^o and all the carbon fibers layers at 45^o the amount of dry lubricant is low the friction involves a large number of aramide fibers which are milled by the abrasive particles (ferrite, Wolfram carbide) from matrix pieces.

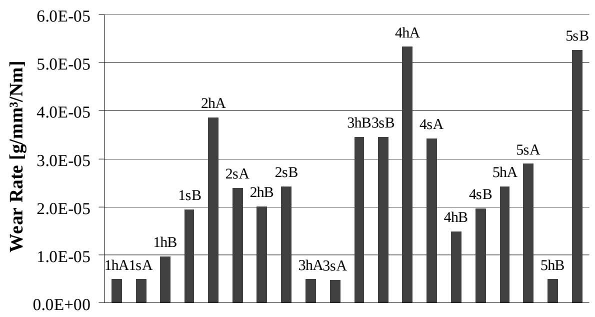

Figure 9. Friction wear rate – perpendicular sliding

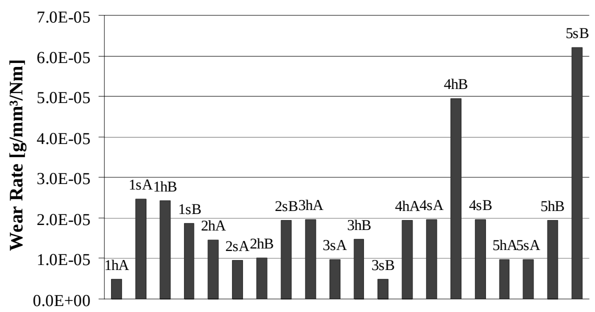

Figure 10. Friction wear rate – parallel sliding

Another aspect might be noticed analyzing both above figures namely: the materials having compact structures (sequences of two or three layers of same fabric) have almost the same behavior both for homogenous matrix and for stratified matrix in both sliding positions.

In the case of abrasive tests (Figures 11 – 14) the wear rate measurements were realized at three different values of sliding speed and as expected the wear rate directly depends on the sliding speed.

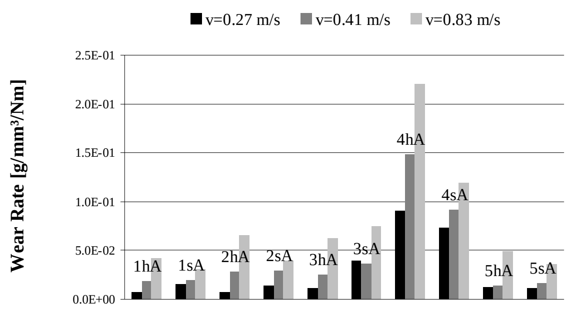

Figure 11. Abrasive wear rate, A materials - perpendicular

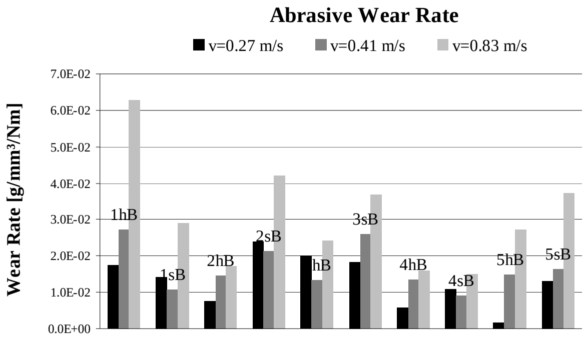

Figure 12. Abrasive wear rate, B materials - perpendicular

As in the case of friction wear rate the position of fibers relative to the disk are important to explain the behavior of materials. The aramide fibers are not milled at the abrasive contact but they are pulled out from matrix together with attached pieces of matrix leading to a high weight loss and as consequence to a higher wear rate.

For all the materials it seems that for stratified matrix ensures a lower wear rate both for perpendicular and parallel sliding but the B materials still show lower values.

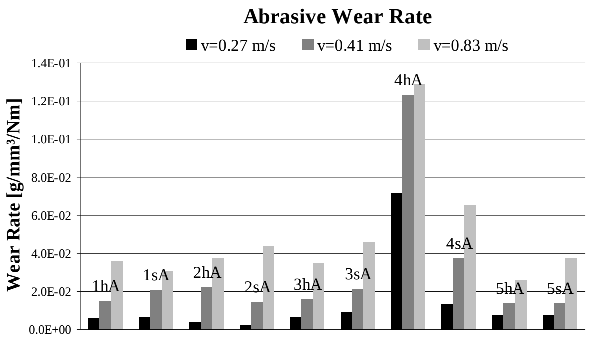

Figure 13. Abrasive wear rate, A materials - parallel

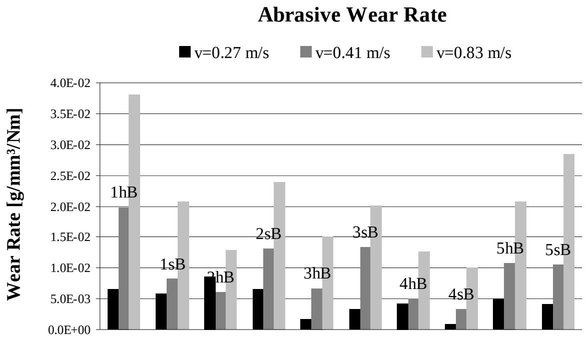

Figure 14. Abrasive wear rate, B materials - parallel

4. CONCLUSIONS

The friction and abrasive behavior of stratified composites had been analyzed in the geometry of pin-on-disk with pin made of studied material and with steel disk or abrasive disk. The results emphasize the role of aramide fibers on increasing the wear resistance of materials while the graphite particles appearing from carbon fibers breaking acts as dry lubricant. The most balanced materials regarding friction coefficient, friction wear rate and abrasive wear rate seems to be the ones with 75% carbon fibers and 25% aramide fibers with symmetrical distribution of fabric layers.

Further studies have to be carried out to investigate the third direction of sliding – the one in which the fabric layer is parallel with the disk in order to get valuable information to design a stratified structure with improved tribological and wear properties on all the directions.

REFERENCES

[1] Pham, H.Q., Marks, M.J., Epoxy resins, in Mark, H.F. (ed), *Encyclopedia of Polymer Science and Technology*, John Wiley & Sons, Inc., vol. 9, pp. 678 – 804, ISBN: 978-0-471-27507-7, 2004.

[2] Tsou, A.H., Waddell, W.H., Fillers, in Mark, H.F. (ed), *Encyclopedia of Polymer Science and Technology*, John Wiley & Sons, Inc., vol. 10, pp. 1 – 20, ISBN: 978-0-471-27507-7, 2004.

[3] Lu, D., Luo, S., Wong, C.P., Conductive Polymer Composites, in Mark, H.F. (ed), *Encyclopedia of Polymer Science and Technology*, John Wiley & Sons, Inc., vol. 5, pp. 653 – 697, ISBN: 978-0-471-27507-7, 2004.

[4] Lau, A.K.T., Lu, J., Varadan, V.K., Chang, F.K., Tu, J.P., Lam, P.M., Multi-functional Materials and Structures, Advanced Materials Research, vol. 47-50, at http://www.ttp.net/0-87849-378-6.html, 2008.

[5] Winey, I. Karen, Vaia, A. R. (eds), Polymer Nanocomposites, MRS Bulletin, Vol. 32. pp. 314 – 322, 2007.

[6] Ciricumaru, A. *et al.*, Thermo-mechanical and electrical properties of high filled epoxy composites, EUROMAT Galsgow, Scotland, 2009.

[7] Circiumaru, A., Birsan I.-G, Bria, V., Postolache, I., Clay/Epoxy Composites, in The Annals of „Dunarea de Jos" University of Galati, Fascicle VIII, Tribology, year XV, ISSN 1221-4590, 2009

[8] Tsukizoe, T., Ohmae, N., Friction and Wear Performance of Unidirectionally Oriented Glass, Carbon, Aramid and Stainless Steel Fibre-Reinforced Plastics, in Friedrich, K. (ed.) *Friction and Wear of Polymer Composites*, Amsterdam, Elsevier, pp. 205-231, 1986.

[9] Friedrich, K., Wear of Reinforced Polymers by Different Abrasive Counterparts, in Friedrich, K. (ed.) *Friction and Wear of Polymer Composites* Amsterdam, Elsevier, pp. 233-287, 1986.

[10] Mathias, P. J., Wu, W., Goretta, K.C., Routbort, J.L., Groppi, D.P., Karasek, K.R., Solid Particle Erosion of a Graphite-Fibre-Reinforced Bismaleimide Polymer Composite, Wear, Vol. 135, pp. 161-169, 1989.

Serbian Tribology Society

SERBIATRIB '11

12th International Conference on Tribology

Faculty of Mechanical Engineering in Kragujevac

Kragujevac, Serbia, 11 – 13 May 2011

TRIBOLOGICAL COMPARISON OF SOME PARTICULATE COMPOSITES

Victor Ungureanu[1], Igor Roman[1], Vasile Bria[1], Iulian-Gabriel Birsan[1],Adrian Circiumaru[1]

[1]"Dunarea de Jos" University Galati, Romania, www.ugal.ro

Abstract: *Using powders to fill a polymer some of its properties might be improved and some other properties might be damaged. The presence of filler's particles inside the polymer volume reduces and limits the polymer chains with consequences on mechanical behaviour of the final material. It is above any discussion that the nature of the powder and the dimensions of powder particles have strong effects on the final material. In the case of a thermosetting material arises another problem connected with the way in which the filled pre-polymer is realized. For this study the epoxy system EPIPHEN RE 4020 / EPIPHEN DE 4020 was used. The named epoxy allows a 45 minutes gel time, long enough to mould valuable materials and long enough to allow three different way of powders dispersion. For each powder three materials were formed (all of them with a volume ratio powder : polymer of 2:100) by dispersing the powder alternatively in the two components or epoxy system or directly into the pre-polymer solution. Mechanical properties of formed materials were investigated together with a tribological investigation performed with pin-on-disk method (with rectangular pins made of particulate composites and steel disk).*

Keywords: *epoxy, clay, talc, starch, CNT, friction, wear.*

1. INTRODUCTION

Epoxies are one of the most versatile classes of polymers with diverse applications such as metal can coatings, automotive primer, printed circuit boards, semiconductor encapsulants, adhesives, and aerospace composites. Most cured epoxy resins provide amorphous thermosetting with excellent mechanical strength and toughness; outstanding chemical, moisture, and corrosion resistance; good thermal, adhesive, and electrical properties; no volatiles emission and low shrinkage upon cure; and dimensional stability - a unique combination of properties generally not found in any other plastic material. These superior performance characteristics, coupled with outstanding formulating versatility and reasonable costs, have gained epoxy resins wide acceptance as materials of choice for a multitude of bonding, structural, and protective coatings applications [1].

As a general rule the polymer composites, as well as ceramic or metal matrix composites, are imparted in particulate (filled) and reinforced or combinations of them. In each case the composite material is formed to solve a problem, to maximize a property for a certain application [2-5]. Carbon fiber reinforced polymers, for instance, are used and formed for low weight and high strength especially for motor sports but in this case it might be done more due to the electrical properties of carbon fiber; namely it might be possible to achieve information about structure's state via electrical resistivity of carbon fibers (or tows).

Complex polymer materials (reinforced with filled matrix) may solve more than one or two problems due their components properties. In this case some problems may occur because by increasing the number of components the forming technique becomes more complicated. However, to form reinforced composites with regulated distribution of fibers is difficult and leaded to pre-preg solution; to form particulate composites with uniform dispersion of fillers' particles is also difficult; to form a polymer composite with a regulated distribution of fibers and uniform dispersion of fillers' particles is more complicated.

This study is just a part of a larger one regarding complex polymer composites reinforced with fibers fabrics and with particulate matrix meant to reach more capabilities for final material. The use of fabrics ensures the fibers spatial distribution and use of fillers solves physical properties (electrical and/or thermal conductivity, dimensional stability etc). In this case it has to be known the way each filler reacts with the polymer aside the necessity of ensure the interface between fibers and polymer. Due an appropriate forming technique (layer-by-layer, for instance) it is possible to obtain laminated-like materials having other fabric in each reinforcement layer and other filler in each polymer layer but keeping the same polymer bonds into material's volume.

2. MATERIALS

The Epoxy system RE 4020 – DE 4020 was used as matrix to form particulate composites with Clay, Talc, Starch, CNT, Aluminum titanate and Lithium titanate. Each of the fillers is used on a certain purpose connected to the final properties of the composite.

The use o Clay is recommended by its capacity to generate nanostructures inside the matrix each nano-plate of clay acting as a crystallization germ and changing, locally, the normal polymer structure with effects on mechanical properties of the final material due to the soft transfer of the loadings between the crystalline and amorphous phases [6]. Another aspect is about the fact that Clay presence in the pre-polymer mixture allows a better dispersion of CNT's which generally tend to aggregate [7, 8]. The clay powder used to form the particulate composites is one of cosmetic application so it contains organic substance aside the mineral one.

The presence of the Talc inside a polymer matrix increases the fire resistance and contributes to better mechanical properties. The presence both of Clay and Talc leads to a material which act as a liquid with very high viscosity because the ordered zones surrounding the Clay or Talc particles are connected through typically polymer bonds. It is expected that the particulate composite to show lower mechanical properties but higher dimensional stability.

Starch is known as a good dispersant and also is known for its capability to form structures inside liquid phases. Starch also may be easily functionalized with various ions and it might be used to transport transitional metals' ions, via complex combinations, inside the polymer structure solving in reasonable limits the problem of electrical conductivity (and not only).

The use of CNT is intended for changing electric behavior [9]. As per Aluminum titanate and Lithium titanate, they are used due their capacity to form nano-structures inside the polymer matrix. Taken separately each of the fillers may be used to obtain a benefit but the problem is to use all of them to fill the same matrix. This type of filled polymer might be also used as matrix for a reinforced composite (with long fibers or fabrics) such as, at least, one design problem to be solved in one layer of the hybrid composite. For instance the external layer has to show high electrical conductivity and good wear resistance, while the other properties of the structure might be set in the internal layers by using glass fibers – for strength, protected by aramide fibers for shock resistance. Using various polymers in various layers it is more possible to control the design of composite materials or composite structures.

For each of above mentioned fillers three types of materials were formed with a volume ratio of 2% filler/polymer. The first type (denoted as A) consists in mechanical dispersion of fillers' particles into the liquid component A of epoxy system (bisphenol A) followed by adding of right amount of B component (aliphatic amine complex). The second type (denoted as B) consists in mechanical dispersion of filler into the liquid component B of the epoxy system while the third type (denoted as P) consists in dispersion of filler into the pre-polymer mixture of right amounts of A and B components of epoxy system.

All the samples were thermally treated to reach their best properties, according to the producer's recommendations. The thermal treatment develops at relatively low temperatures such as the fillers are not affected, except the organic substance from clay powder.

The mixing rule is giving the same result regarding the specific weight for all three types of materials (A, B or P) and it is not taking into account the interactions. Table 1. shows the specific weight values for powders, epoxy and particulate composites, as well as the theoretical value as it results through application of mixing rule [10, 11]. Some differences between measured and evaluated values might be noticed.

Table 1. Specific Weight of Components and Materials

Component		Mixing rule	A type	B type	P type
Epoxy	1.128				
Starch	0.588	1.118	1.090	1.165	1.240
Talc	0.763	1.121	1.113	1.160	1.087
Clay	0.608	1.118	1.145	1.212	1.125
Lithium titanate	1.210	1.130	1.180	1.208	1.132
Aluminum titanate	1.913	1.144	1.231	1.180	1.068
CNT	0.047	1.107	1.146	1.163	1.125

3. MEASUREMENTS AND RESULTS

The tribological behaviour and the wear behaviour had been studied on the same machine *Multi-Specimen Test System - UMT from CETR* in the fixture pin-on-disk with pin made of stratified material and steel disk and with the disk covered with abrasive paper (abrasive tests) – Figure 1.

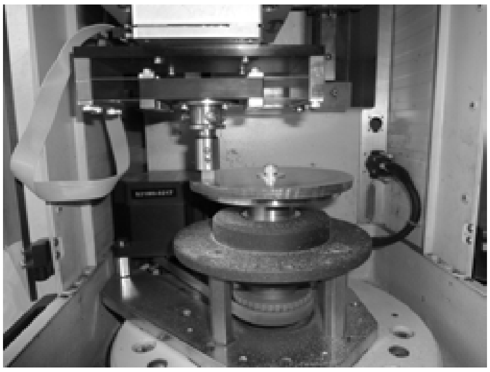

Figure 1. The Multi-Specimen Test System

Analysis was performed at different sliding speed values and different loadings but generally the friction behaviour may be placed into three categories: medium powders (starch and CNT), hard powders (Aluminium titanate and Lithium titanate) and soft powders (talc and clay) as can be noticed in figures below.

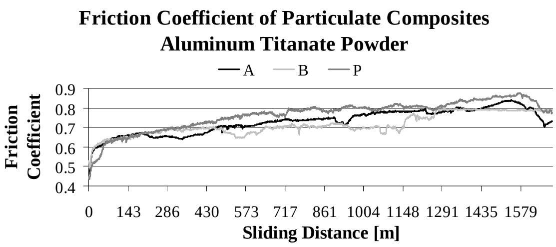

Figure 2. Friction coefficient for hard powders

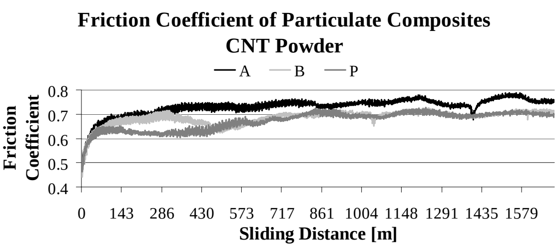

Figure 3. Friction coefficient for soft powders

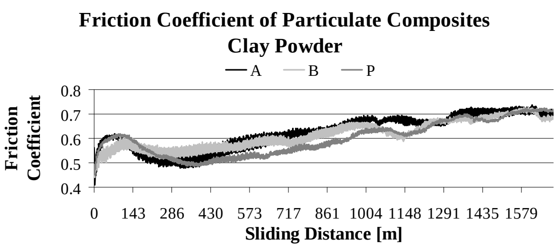

Figure 4. Friction coefficient for soft powders

The hard powders determine low variations of friction coefficient during testing while the soft powders induce large variations of friction coefficient.

The wear rates both at friction and abrasion were evaluated according [12, 13] and the results are presented in figures below. In each case the relative wear rate is presented having as reference the wear rate of epoxy resin and it might be noticed (Figure 5) that generally filling the polymer the wear resistance is increased [14-16] but the dispersion method influence the results. All the values were computed on the basis of measured specific weight. Significant improvements correspond to the clay, talc and CNT filled polymer but for clay and CNT the highest values are related to pre-polymer dispersion while in the case of talc the highest value corresponds to first dispersion method.

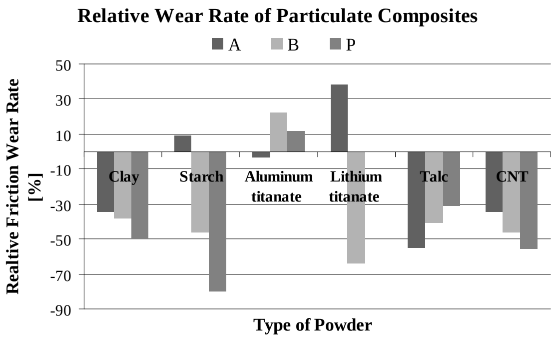

Figure 5. Relative friction wear rate of materials

The abrasive wear tests were performed on the same machine but the steel disk was covered with abrasive paper P400. Presence of clay ensures a higher abrasive wear resistance while presence of talc reduces the resistance (Figure 6).

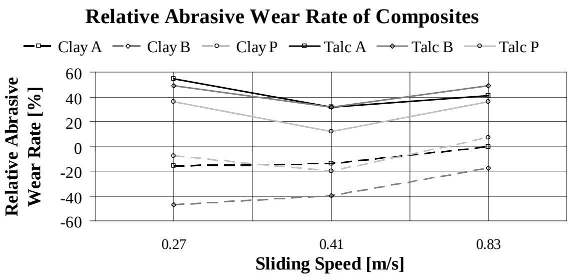

Figure 6. Relative Abrasive Wear Rates - soft powders

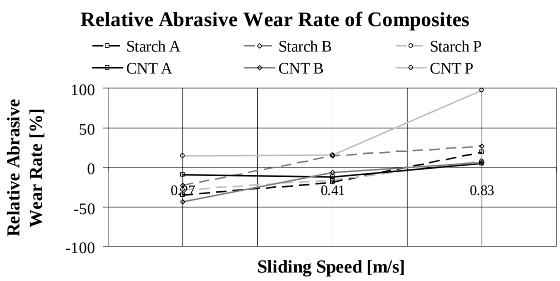

Figure 7. Relative Abrasive Wear Rates - medium powders

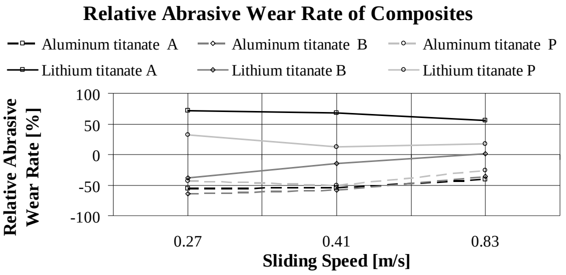

Figure 8. Relative Abrasive Wear Rates - hard powders

In the case of medium powders the benefits are not too important while in the case of hard powders the results are imparted again as in the case of soft powders with the Aluminium titanate increasing the abrasive wear resistance and with Lithium titanate lowering it.

4. CONCLUSIONS

The aim of this study was to identify the effect of dispersion method on the tribological and abrasive properties of particulate composites. The entire study is centred on 2% volume ratio of filler but the analysis has to be performed for other concentrations.

In the case of use of such filled polymers as matrix to form reinforced composites it is necessary to know the way in which the forming technique (the dispersion) is influencing the final properties. Mechanical, thermal and electrical analysis has to be performed to offer accurate information about the presented filled polymers. Even the basic constituents are the same it is easy to notice that is possible to set various properties in various ways leading to the possibility to form a reinforced material based on the same polymer and same filler but having various behaviour in various matrix or reinforcement layers.

Using a layer by layer forming technique the final material will have the same polymer as matrix showing the same type of polymer bonds in all its volume so the loadings will affect the matrix as a bulk material avoiding the inter-laminar problems.

Just few aspects were presented but it is reasonable to imagine a CNT filled polymer matrix fabric reinforced composites with a certain distribution of matrix specific weight based just on the CNT's dispersion technique into the polymer. Such a material could have a better electrical conductivity at the surface combined with a high density (required by tribological behavior).

REFERENCES

[1] Pham, H.Q. & Marks, M.J., Epoxy resins, in Mark, H.F. (ed), *Encyclopedia of Polymer Science and Technology*, John Wiley & Sons, Inc., vol. 9, pp. 678 – 804, ISBN: 978-0-471-27507-7, 2004.

[2] Gay, D., Hoa, S. V., Tsai, S. W., *Composite Materials* – Design and Applications, CRC Press, Boca Raton, USA, ISBN: 58716-084-6, 2003

[3] Daniel, I & Ishai, O., Engineering Mechanics of Composite Materials, Oxford University Press, New York, USA, ISBN: 019515097X, 2006.

[4] Jones, R.M., *Mechanics of Composite Materials*, Taylor&Francis Inc., Philadelphia, USA, ISBN: 1-56032-712-X, 1998.

[5] Vasiliev, V. V. & Morozov, E. V., *Mechanics and Analysis of Composite Materials*, Elsevier, ISBN: 0-08-042702-2, 2001.

[6] Winey, I. Karen & Vaia, A. R. (ed), Polymer Nanocomposites, MRS Bulletin, Vol. 32, 2007.

[7] Ciricumaru, A. et al., Thermo-mechanical and electrical properties of high filled epoxy composites, EUROMAT 2009, Galsgow, Scotland, 2009.

[8] Andrei, G., Dima, D., Birsan, I., Andrei, L., Circiumaru, A., Effect of Ferrite Particles on the Mechanical Behaviour of Glass Fibers Reinforced Polymer Composite, Materiale Plastice, 46, Nr. 3, 284-287. ISSN 0025-5289, 2009.

[9] Andrei, G., et al., Selected mechanical properties of fabric reinforced composites with talc and carbon black filled matrix, in Journal of Polish Society for Composite Materials, Quaterly, 9, Nr.4/2009, 347-351 pp, ISSN 1641- 8611, 2009.

[10] Torquato, S., Modeling of physical properties of composite materials, International Journal of Solids and Structures, 37, 2000.

[11] Callister, W. D. Jr., *Materials Science and Engineering*, 7th ed., John Wiley & Sons, ISNB-10:0-471-73696-1, 2007.

[12] El-Tayeb, N.S.M., Two-body abrasive behaviour of untreated SC and R-G fibers polyester composites, Wear, (266), pp. 220-232, 2009.

[13] Mimaroglu, A., Sen, U., Unal, H., Abrasive Wear Volume Maps for PA6 and PA6 Composites Under Dry Working Condition, Appl. Compos. Mater., (15), pp. 13-25, 2008.

[14] Tsukizoe, T., Ohmae, N., Friction and Wear Performance of Unidirectionally Oriented Glass, Carbon, Aramid and Stainless Steel Fibre-Reinforced Plastics, in Friedrich, K. (ed.) *Friction and Wear of Polymer Composites*, Amsterdam, Elsevier, pp. 205-231, 1986.

[15] Friedrich, K., Wear of Reinforced Polymers by Different Abrasive Counterparts, in Friedrich, K. (ed.) *Friction and Wear of Polymer Composites* Amsterdam, Elsevier, pp. 233-287, 1986.

[16] Mathias, P. J., Wu, W., Goretta, K.C., Routbort, J.L., Groppi, D.P., Karasek, K.R., Solid Particle Erosion of a Graphite-Fibre-Reinforced Bismaleimide Polymer Composite, Wear, Vol. 135, pp. 161-169, 1989.

Tribological of Machine Elements

12th International Conference on Tribology – SERBIATRIB '11

11 – 13 May 2011, Kragujevac, Serbia

Serbian Tribology Society

SERBIATRIB '11

12th International Conference on Tribology

Faculty of Mechanical Engineering in Kragujevac

Kragujevac, Serbia, 11 – 13 May 2011

INFLUENCE OF POWER TRANSMITTER DYNAMIC LOAD ON PHYSICAL AND CHEMICAL PROPERTIES OF USED LUBRICANT

A. Ilić[1], D. Josifović[1], L. Ivanović[1], S. Savić[1]

[1]Faculty of Mechanical Engineering, University of Kragujevac, Kragujevac, Serbia,
gilic9@sbb.rs ; danaj@kg.ac.rs ; lozica@kg.ac.rs ; ssavic@kg.ac.rs

Abstract: *The tribologycal conditions within gear power transmitters as a real tribomechanical system are quite complex and are conditioned to a large extent with the characteristics of used lubricant. Complexities of the conditions are determined by temperature of the elements in contact, current properties of the used lubricant, external load in reference to specific pressures in contact zone, dynamic nature of contact creating, transfer of power and movement. The aim of this paper is to establish the influence of power transmitters' dynamic load to its lubricant degradation. Also, the basic elements of analytical approach to lubricant film behavior under the dynamic loaded conditions were given in this paper. Variations in exploitative conditions lead to variations in load of elements in contact and provoked variation of friction coefficient, so as temperature and pressure decrease. By the means of all listed, those variations lead to changes of lubricant characteristic and its degradations. Furthermore, the intensive wearing and damages of power transmitter elements are provoked. All of the listed facts imposed the great importance of lubricant's current chemical composition, real behavior and its acting mechanisms. Beside all, stability of lubricant's physical and chemical properties during working life is key element of power transmitters' safety and reliability. Experimental procedure shown in this paper refers to testing of power transmission properties and its lubricant properties subjected to dynamic load. Lubricant sampling in exploitation provide very important data of current lubricant condition through its properties testing. Experimentally obtained results point out the necessity of considering the lubricant's present properties as timely depended constructive element. Paper conclusions bring the proposals for reduction of the unwanted consequences due to lubricant degradation. In that way, minimal losses of material and energy, so as decrease of maintenance coasts and minimal ecological impact can be done.*

Keywords: *dynamic load, power transmitter, lubrication, pressure, temperature*

1. INTRODUCTION

Power transmitters and especially gear power transmitters are very dependent on properties of the lubricants for their lubrication. Distinctive close correlation of gear power transmitters properties with the characteristics and properties of lubricants, make this type of power transmitters the most interesting for examining the influence of dynamic load of power transmitters on the physical-chemical properties of its lubricants. In addition to this aspect, the complexity of tribological processes in the gear power transmitters represents one more reason for observing this type of power transmitter during the examination of the influence of dynamic loads of power transmitters on the physical-chemical properties of lubricants [1].

During exploitation, power transmitters are exposed to time variable, dynamic and unsteady loads which represent the functions of a range of factors. Operating regime changes lead to changes in working loads of elements, force and friction coefficient of contact surfaces, increase in operating temperature, and with all these, to changes of properties and lubricant degradation, intensive wear and damage to power transmitter elements. In order to reduce friction and wear, and thereby prevent damage and prolong the life of the power transmitter, various types of lubricants are used. Selection of lubrications for power transmitters depends on the type and construction of the transmitter, materials of which the elements are made, the type and level of loads, working conditions, lubrication method, operating regime and the like [2]. Lubricants should be seen as a constructural element and is therefore very important to know their composition, properties and mechanisms of action. This is illustrated by the fact that many analyses of failure causes of power transmitters have shown that they occurred as consequences of the use of lubricants of poor or inadequate properties [3]. Also, the stability of physical and chemical properties of used lubricant during exploitation is very important. Moreover, by lubricant sampling, very important information about the current condition of lubricants in the system can be obtained, and further, its physical and chemical properties can be examined and an assessment can be provided of whether it is necessary to replace it. The proactive system maintenance with a regular review of functional parameters has a significant role in it [4, 5 and 6].

2. THEORETICAL APROACH – HYDRODYNAMIC THEORY OF LUBRICATION

The usual considerations of some real problems refer to the approach that uses the approximate differential equations of viscous liquids flow that are obtained from the full differential equations by neglecting nonlinear inertial members while retaining the members who are conditioned by viscosity. Further improvement of development the approximate solving methods is based on differential equations that are obtained from the Navier - Stokes equations when some members who are conditioned by viscosity except the nonlinear inertial members are ignored. A very important technical problem of lubrication gave the impulse for the development of approximate method based on these differential equations [7].

The founder of the hydrodynamic theory of lubrication is the Russian scientist Petrov who considered the possibility of direct application of Newton's hypothesis of stress and displayed the solution in case of shaft and bearing surfaces being coaxially cylindrical. In order to confirm the theoretical conclusions, Petrov has performed a large number of experiments which didn’t only confirm the basic assumptions of his theory but also contributed to explanation of the problems related to the mineral oil use.

Circular flow of parts of viscous fluid between two cylinders that rotate around axes which correspond, Petrov has observed under conditions of partial fluid sliding along the walls, unlike the approach that includes complete liquid sticking to the walls. On the basis of experiments and further development of theories that deal with these problems, it was found that the basic links that Petrov obtained correspond to borderline case, of shaft rotation with a large number of revolutions, whereby the shaft carries a relatively small load. For this borderline case the shaft axis creates only a small deviation from the bearing axis, so that this deviation without loss of generality can be neglected. Under normal conditions of exploitation, however, the bearing axis does not correspond with the shaft axis. This kind of eccentric shaft position in the bearing leads to forces that balance the shaft load. Lubrication theory for the eccentric shaft position was developed by Zhukovsky and Chaplygin [7].

By comparison of the Reynolds differential equations for the lubricant film with the Navier - Stokes equations it is shown that for their production there is a need to disregard not only all the non-linear inertial members but also the members who are conditioned by viscosity. With the assumption of differential equations solutions in the form of rows and by comparison of the members with the same degrees, the row of differential equations systems is obtained, with the first system of this row being the Reynolds equation, while the other system contains Laybenson’s equations for the lubricating film [7].

3. PROPERTIES OF THE USED LUBRICANT

The physical properties of lubricating oil are density, colour, viscosity, fire point, the point of hardening and flow, blurring point, specific heat and thermal conductivity, volatility, emulsivity and de-emulsivity, foaming, air separation ability (deaeration) and more. Viscosity is one of the most important properties of lubricants from the tribological aspect and it represents a measure of internal friction. Viscosity occurs as the result of action of the intermolecular forces in the lubricant and as forces grow stronger the viscosity grows higher. Viscosity shows its greatest impact during total lubrication, because film thickness, temperature increase and losses due to friction depend on it. Lubricants behave as Newtonian or non-Newtonian fluids, depending on whether the link between shear stress and velocity gradient is linear or not. Viscosity can be viewed through the dynamic and kinematic viscosity. Dynamic viscosity is obtained by applying Newton's law that connects the shear stress in the fluid and velocity gradient. Kinematic viscosity is the ratio of dynamic viscosity and fluid density. With lubricants that behave as Newtonian fluids, viscosity is a function of temperature and pressure. Oil viscosity decreases with temperature increase by a certain regularity that is increases with temperature drop. During the exploitation viscosity change tends to be as small as possible. Change of viscosity with temperature change is expressed through the dimensionless number - viscosity index. With non-Newtonian fluids, viscosity is not constant at the given temperature and pressure, but depends on the change of shear velocity. Emulsions, suspensions and multigrade oils are among the non-Newtonian fluids. Apparent viscosity is the measurement of viscosity at the specific shear gradient, while the structural viscosity represents the viscosity drop due to increase of shear velocity. Apparent viscosity describes the behaviour of oil at low temperatures. At the beginning of growth of shear velocity, multigrade oils retain their Newtonian character. Non-Newtonian area, which then follows, features a dramatic drop of viscosity. By continuing growth of shear velocity, oil re-enters the Newtonian area, which differs from the previous one. In this area, the present polymer molecules are no longer deformed. The relative viscosity drop increases with temperature lowering and pressure growth at amounts to 10-70 %. Typical example of a complex tribomechanical system with gear power transmitter operating in very changeable conditions of exploitation is the vehicle’s gearbox transmission. Transmission of the vehicle consists of the elements of power transmission and motion (gears and grooved shafts), the elements of information transfer (leverage), elements of conduct (guides) and seals (gaskets). Each of these elements of the transmission can be analyzed as a set of special tribomechanical systems, such as gear pairs, bearings, etc. Also, each gear pair can be further analyzed as a single element which makes the contact. And finally each gear tooth flank or ball of roller bearing can be seen as a basic unit of tribomechanical system. This analysis suggests the fact that the tribological characteristics of a complex tribomechanical system can not be seen in a simple matter and that it is not possible to establish reliable methods and determine the diagnostic parameters for assessing the state of an observed system. Direct participation of lubricant in the contact processes of gear transmitter as tribomechanical system, with the main task to prevent the direct contact of surface elements, provides the lubricant with a special role from the aspect of testing. The lubricant is the carrier of information about the state of gear transmitter as a whole, with attention specially paid to the processes that affect the functionality and reliability. The importance of this information is expressed in monitoring and system diagnosis, because lubricant analysis can point to signs of potential problems that lead to failure, as well as to provide consideration of lubricant influence on the system operation [4, 5 and 6].

4. EXPERIMENTAL TESTING OF OIL PROPERTIES AND THEIR CHANGES DURING THE EXPLOITATION

The subject of testing in this paper is the experimental determination of property changes of gear oil during operation depending on the dynamic properties of loads. The oil SAE 80W-90 of API GL-5 quality was tested which was used in gear group of working machines whose main properties are shown in Table 1. During the testing, the oil was tested that belonged to the gear group of working machines which were used in real conditions of exploitation [6].

Table 1. The values of basic physical - chemical properties of the new oil SAE 80W-90

Properties	**Value**
Appearance	clear
Color	ASTM 5.0
Density	0.902
Viscosity at 40^0C, $\frac{mm^2}{s}$	212.5
Viscosity at 100^0C, $\frac{mm^2}{s}$	18.27
Viscosity index, %	97
Level of combustion, ^{0}C	216
Level of solidification, ^{0}C	-18
Foaming (sequence I, II and III)	0/0
Corosity to Cu, 100^0C/3	1^a
TAN, mgKOH/gr	0.9
Humidity, %	0

Allowed quantities of certain elements in used gear oil and allowed values of deviations in physical - chemical properties of new and used oil are given in Tab.2.

Table 2. Allowed values of deviations in physical - chemical properties of oil

Physical-chemical properties of oil and wearing products	**Maximum deviation allowed**
Viscosity at 40^0C, $\frac{mm^2}{s}$	15%
Viscosity at 100^0C, $\frac{mm^2}{s}$	15%
Viscosity index, %	$\pm$5%
Total Acid Number (TAN), mgKOH/gr	3 mgKOH/gr
Insoluble residue in toluene, %	0.50%
Wearing products – Fe content, ppm	500 ppm

Table 3. Values of the tested physical and chemical properties of used gear oil SAE 80W-90, API classification GL – 5 during exploitation

Properties	**Value after period of exploitation, *h***												
	Sample	Gearbox 1				Gearbox 2				Gearbox 3			
		42	111	217	349	42	111	217	349	42	111	217	349
Color	ASTM 5.0	Black	Black	Black	Black	Black	Black	Black	Black	Black	Black	Black	Black
Density	0,902	0,903	0,907	0,909	0,913	0,905	0,908	0,91	0,915	0,906	0,911	0,916	0,919
Fire point, ^{0}C	216	218	221	225	227	220	224	229	230	222	226	230	231
Level of solidification ^{0}C	-18												
Humidity, %	0	0	0	0	0	0	0	0	0	0	0	0	0
Foaming	0/0												
Viscosity at 40^{0}C, $\frac{mm^2}{s}$	212,5	215,2	223,8	226,1	229,6	216,3	224,7	226,6	230,3	223,6	224,9	227,2	231,1
Viscosity at 100^{0}C, $\frac{mm^2}{s}$	18,27	18,53	18,96	19,16	20,15	18,76	19,12	19,56	20,34	19,05	19,63	20,04	20,71
Viscosity index, %	97	97	96	96	96	98	95	96	96	98	97	96	96
TAN, mgKOH/gr	0,9	1	1,25	2	2,6	1,1	1,7	2,4	2,7	1,2	1,9	2,5	2,75
Insoluble residue in toluene, %	0	0,03	0,06	0,08	0,15	0,05	0,07	0,1	0,17	0,09	0,13	0,19	0,25
Fe content, ppm	0	25	41	270	349	76	260	375	670,5	112	335	536,5	873,4

Experimental testing included determining the color, density, viscosity at 40^{0}C and 100^{0}C, determining viscosity index, fire point and compressibility, TAN, foaming control, humidity content control, control of the insoluble residue in toluene and content control of wear products - iron. The oil of three gearboxes after various intervals of exploitation was tested out [6]. The results of experimental testing are presented in Table 3. Experimental testing was carried out in accordance with manufacturer specifications and proper standards by using the necessary equipment.

Figure 1. shows the change in density of the tested oils during exploitation.

Besides determining the impact of dynamic load characteristics on changes in the physical and chemical properties of oil, the goal of experimental testing was also the checking of the oil replacement intervals, checking the choice of lubricant and monitoring the oil quality.

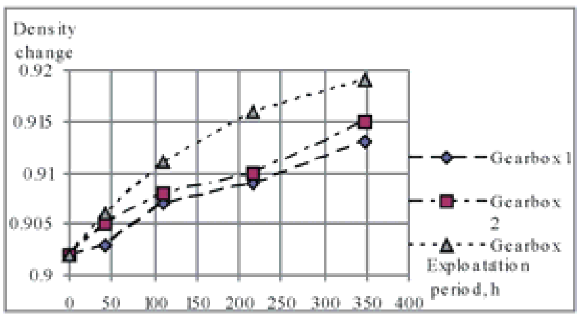

Figure 1. Density change of sampled gear oils

Besides determining the impact of dynamic load characteristics on changes in the physical and chemical properties of oil, the goal of experimental testing was also the checking of the oil replacement intervals, checking the choice of lubricant and monitoring the oil quality. Density change has a trend of slight growth expressed during whole period of exploitation [6]. Figure 2. presents the change of temperature of fire of the tested oil.

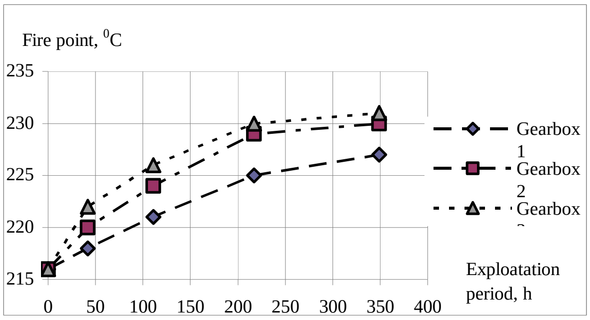

Fig.2. Change of fire point of sampled oil

The growth of fire point indicates the oxidation (aging) of oil or evaporation of easily volatile components. Oil on which sampling was conducted, has a trend of continuous growth (Figure 2.) of fire point, which is another inevitable indicator of oil oxidation due to dynamic load characteristics. Figure 3 shows viscosity change of the tested oil at temperature of 40^{0}C, while figure 4 shows viscosity change at temperature of 100^{0}C.

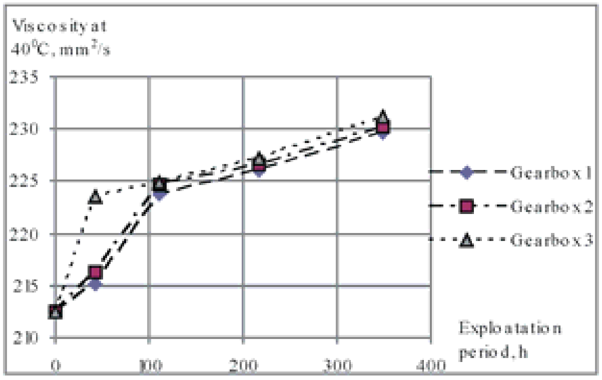

Figure 3. Viscosity change at 40^{0}C of tested oils

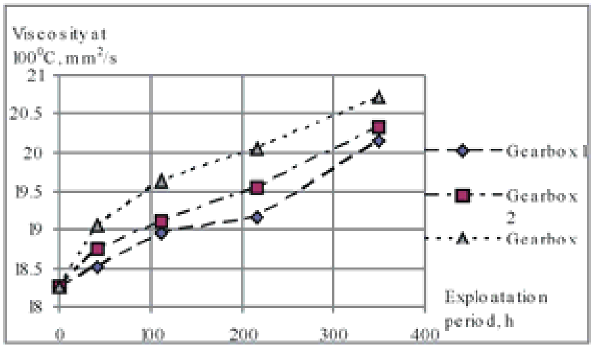

Figure 4. Viscosity change at 100^{0}C of tested oils

In the figure 3. and figure 4. there is an evident trend of constant viscosity growth during exploitation. This increase in viscosity is a consequence of properties change of tested oils due to dynamic loads during exploitation. The increase in viscosity indicates the process of oil oxidation as well or oil contamination with water and dirt, as well as wears products. In the analyzed oil there was no oil contamination with water, because during the analysis of the tested samples water did not show. This conclusion is suggested by the fact that in the examined samples there was no foaming, given that one of the reasons for foaming is the presence of water. It is concluded that one of the main reasons for the increase of viscosity oil oxidation, and contamination of oil by wear products. Water is an undesirable contaminant in the oil, and it is the most present liquid contaminant of lubricating oil and originates from the environment or it is the result of condensation. Water was not the cause of oil degradation in terms of oxidation, the destruction of the oil film, causing corrosion, deposit formation and hydrolysis of certain additives. Particles that got into the oil caused an increase in the intensity of oxidation processes in which process acidic compounds and insoluble products are formed that are internal contaminants. Also, these products neutralize the additive polar molecules in the oil, particularly anti-wear and EP additives, corrosion inhibitors and dispersants. Furthermore, very fine solid particles in stable oil suspension cause an increase in oil viscosity. In regard to the fact that allowed deviations of viscosity at 40^{0}C and 100^{0}C amount to a maximum of 15% to initial values it can be concluded that tested oils meet this criterion. Viscosity drop may be due to mixing with the oil of lower viscosity or due to lower concentration of viscosity improver. Causes of this process can also be high temperature, load, long exploitation interval, insufficient quantity of oil, inefficient cooling and the like. As shown in the figure 5. TAN have trend of increase which indicates oil degradation.

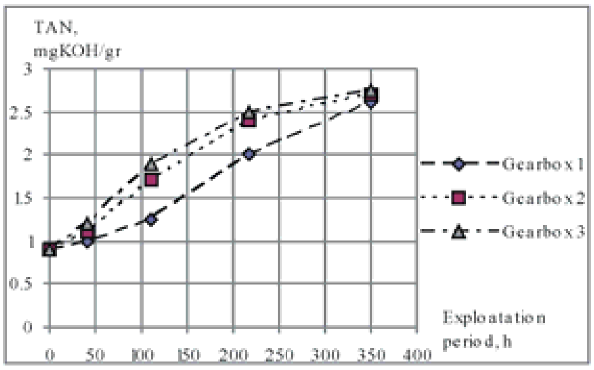

Figure 5. Change of TAN for sampled gear oils

During the exploitation testing of the change in TAN the values were reached which were in within the permissible range of values according to an appropriate standard and specifications of manufacturers. With mineral oils with fewer additives TAN grows rapidly, while with oils that has high additive content, in the initial period of exploitation it decreases, and then receives a growing character. By degradation of oil during exploitation, certain types of polymeric insoluble residues are formed. The content change of these insoluble residues during exploitation is shown in Figure 6 [6].

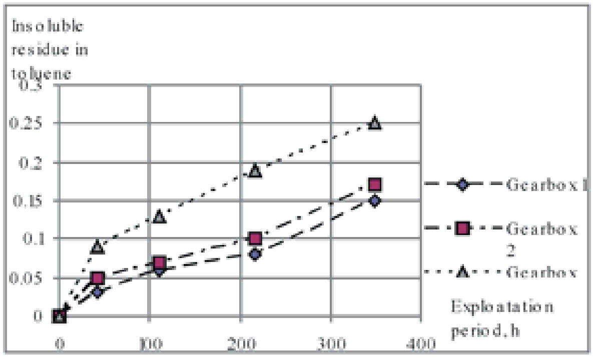

Figure 6. Insoluble residues in toluene of the sampled oils

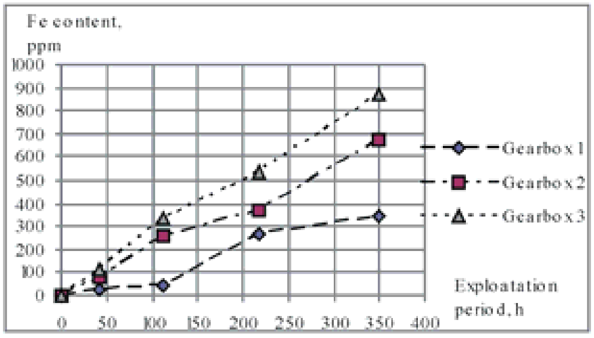

Figure 7. Content changes of wear products of sampled oils

During the testing, observed oils are considered to meet the criterion change of the insoluble residue amount in toluene. Wear products caused the contamination of oil well above the permissible limit and now an intensive degradation of oil starts that will be more intense due to their catalytic action. Also, it can be concluded that this strong growth of the concentration of iron, as wear products, leads to failure of gearbox elements which are mutually located in relative motion.

5. ANALYSE OF EXPERIMENTALLY OBTAINED RESULTS

During the exploitation, the analyzed oil has achieved its primary function and meets the intended replacement interval, which was determined by analysis of characteristic physical - chemical properties and concentration of wear products during exploitation. The increase in viscosity occurred during the examination period of exploitation. Maximum viscosity growth during the oil exploitation is less than 15% of allowed value. Degradation of oil during the testing was analyzed by an increase in TAN and the increase of insoluble residues (in toluene). Both features showed changes that are within the maximum permitted levels. Oil fire point has a trend of constant growth pointing to the process of oil oxidation (aging). The content of wear products in oil came out of the limits of maximum value allowed, indicating the need for check of functional characteristics and oil change interval. In the tested samples of oil there has been no occurrence of water or foaming. By conducted experimental analysis of changes of oil properties during exploitation, a great influence of dynamic load characteristics was proved [4, 5, 6].

6. CONCLUSION

Testing of physical and chemical properties of oil in the function of determining the state of gearbox group as a complex tribomechanical system aims to identify mechanisms of change in the system elements. By appropriate sampling and testing during exploitation, based on the model presented it is possible to identify the state of system elements and predict its future behaviour in exploitation [7]. The conditions in which the of gearbox group elements are found as the real tribomechanical system are complex and are determined to a large extent by oil properties. Complexity of the conditions is determined by temperature of elements in contact, temperature and properties of oil, external load, that is the specific pressure in the contact zone, the dynamic character of contact and transfer of power and movement, etc. During exploitation the gearbox group is exposed to time variable, dynamic and unsteady loads that represent the function of a range of factors. Dynamic loads conditioned complex physical-chemical processes that cause changes in oil. The amplitude as well as frequency of load primarily affect the change in pressure and temperature in the contact zone and thus cause a change in physical-chemical structure of oil. Processes created this way are manifested through unwanted effects that can be identified through the loss of material, energy, movement, functionality and reliability, reduced life cycle and increase in maintenance costs. Gearbox group is a set of very complex tribomechanical systems composed of series of subsystems that are also complex tribomechanical systems. Requirements regarding the oil properties, the type of use and their replacement interval are becoming stricter because designers of gearbox groups continually put before oil manufacturers new and more difficult conditions in terms of improving performance and efficiency [8, 9 and 10]. This inevitably leads to reformulating existing and creating new kinds of oils that are different in chemical composition, exploitation properties and viscosity grading. Direct participation of oil in the contact processes in tribomechanical systems with the main task to prevent direct contact of surfaces of elements gives it a special role in terms of maintenance. This role becomes more important since the oil is carrier of information about the state of the whole system in which process the particular attention is paid to the processes that affect the functionality, reliability and durability. The importance of this information comes into play in monitoring and system diagnosis, because oil analysis can point out to signs of potential problems that lead to failure, as well as to provide an insight into the influence of oil on the functioning of the gearbox group. The current state of the gearbox group system can be analyzed by examining oil without disrupting exploitation. Also, the conditions of exploitation, especially the dynamic characteristics of the load gearbox groups can be analyzed [11, 12 and 13]. Full understanding of the theoretical basis of the oil dynamics of oil and lubricants as a viscous incompressible fluid with the experimental testing of properties allows an adequate evaluation and application of results obtained by modern software packages such as Ansys, Fluent, FlowTech, PowerFlow, Flovent and the like, that use this kind of numerical algorithms for solving the adequate system of equations. Usage of these software packages for Computational Fluid Dynamics provides relevant information about the oil behaviour that can be used in the design, improvement and optimization of complex tribological systems within the gearbox group [14 and 15]. Numerical approach to oil dynamics includes consideration of the global geometry of elements, establishment of finite elements and establishment of shapes and sizes of oil particles and their conditions, as well as global boundary conditions so that the results obtained by analysis of numerical models created in this way, verified experimentally, are the important parameter that must be taken into consideration for solving the problems of lubrication of modern gearbox group.

REFERENCES

[1] D. Josifović: Examinations of mechanical construction I, Faculty of Mechanical Engineering in Kragujevac, 2000 (in Serbian).

[2] S. Tanasijević: Power transmitters, Yugoslav tribology society, Kragujevac, 1995 (in Serbian).

[3] S. Tanasijević: Tribology basic on machine elements, Scientific book, Beograd, 1989 (in Serbian).

[4] M. Trbojević, M. Janković, J. Vukdelija, S. Ivković, L. Latinović: Power transmitters, Scientific book, Beograd, 1988 (in Serbian).

[5] Z. Vukadinović: Examination of lubricant influence on durability of synchrony system of gearbox, Magister thesis, Faculty of Mechanical Engineering in Kragujevac, 2003 (in Serbian).

[6] S. Perić: Influence of exploitation conditions of gearbox on physical and chemical properties of used lubricant, Magister thesis, Faculty of Mechanical Engineering in Beograd, 2006 (in Serbian).

[7] V. Saljnikov: Dynamics of viscous fluid, Faculty of Mechanical Engineering in Beograd, 1969 (in Serbian).

[8] T. J. Chung: Computational Fluid Dynamics, Cambridge University Press, England, 2010 (in English).

[9] J. Denis, J. Briant, J.-C. Hipeaux: Lubricant Properties Analysis and Testing, Editions Technip, France, 2000 (in English).

[10] R. E. Haycock, J. Hillier, J. E. Hillier: Automotive Lubricants Reference Book, Wiley, John & Sons Inc., England, 2005 (in English).

[11] T. Mang, W. Dresel: Lubricants and Lubrication, Wiley-VCH, USA, 2007 (in English).

[12] B. R. Höhn: Europe Trends in Transmission Development, Tagung Antriebstechnik / Zahnradgetriebe, TU Dresden, Dresden, 2000 (in German).

[13] D. Josifović: Influence of Lubricants on Tribological Characteristics of Contact Surfaces and Working Life of Gears by Power Transmission and Elements of Synchronization System of Motor Vehicles, COST 532 – TS 16 Project, Final Report, Brussels, 2008 (in English).

[14] G. E. Totten: Handbook of Lubrication and Tribology: Application and maintenance, CRC Press, USA, 2006 (in English).

[15] G. E. Totten, L. D. Wedeven, M. Anderson, J. R. Dickey: Bench Testing of Industrial Fluid Lubrication and Wear Properties Used in Machinery Applications, ASTM International, USA, 2001 (in English).

Serbian Tribology Society

SERBIATRIB '11

12th International Conference on Tribology

Faculty of Mechanical Engineering in Kragujevac

Kragujevac, Serbia, 11 – 13 May 2011

MULTICRITERIA OPTIMIZATION OF PANETARY GEAR TRAIN USING EVOLUTIONARY STRATEGIES

B. Rosić[1], Lj. Janković[2], M. Milojević[1]

[1] University of Belgrade, Serbia, Faculty of Mechanical Engineering, e-mail:brosic@mas.bg.ac.rs

[2]Grupa Zastava Vozila, Kosovska 4, Kragujevac, Serbia

Abstract: *Planetary gear trains take a very significant place among the gear transmissions which are used in many branches of industry. This power transmission unit can handle larger torque loads relative to its compact size than any other gear combination in standard transmission. With regard to the growing requirements concerning the economical consumption of energy, the utilization ratio represents a very significant qualitative and quantitative performance of gears. This paper gives the utilization ratio analyze of planetary gear train, starting from kinematics of contacted gears and gear profiles, including sliding and rolling losses resulting from the formation of EHD lubrication, with the numerical results of the instantaneous efficiency of a gear pair with internal gearing. Geometric and operating constraints for internal and external gears and whole planetary gear trains are defined. A method is described to solve a nonlinear parameter optimization problem with several objective functions. For the defined multi-objective optimisation model of the planetary gear train, a computer program based in interactive dialogue is developed. The results showed that the genetic algorithm is useful and applicable for optimization of planetary gears design. The genetic algorithm is an efficient search method which is inspired from natural genetics selection process to explore a given search space.*

Keywords: *planetary gear train, efficiency, sliding, losses, Pareto-optimal, Genetic Algorithm*

1. INTRODUCTION

Planetary gear trains take a very significant place among the gear transmissions which are used in many branches of industry. Planetary gear trains have a number of advantages as compared to the transmission with fixed shafts. Under similar operating conditions the planetary transmissions serve longer and produce less noise compared to the fixed shaft transmissions. This power transmission unit can handle larger torque loads relative to its compact size than any other gear combination in standard transmission.

In articles [1] – [12] authors analyzed similar subject based on planetary gear design. Topics of articles [13] – [14] are related to numerical analyses based upon genetic algorithm and neural networks.

The design of planetary gear trains requires a whole range of geometrical and kinematics conditions in order to perform the mounting and an appropriate meshing of the gears during their work. It is necessary to express the above requirements in terms of the corresponding functional constraints, whereby all the relevant values of the gears and planetary gear trains as a system are defined.

Multi objective optimization techniques generally give a set of compromise solutions, a so-called Pareto-optimal set. The definition of Pareto optimality states that the vector is chosen as optimal if no criterion can be improved without at least one other criterion. Genetic Algorithms are nondeterministic stochastic search/optimization methods that utilize the theories of evolution and natural selection to solve a problem within a complex solution space.

2. PLANETARY GEAR TRAIN EFFICIENCY

According to their kinematics structure, planetary gear trains are complex toothed mechanisms which can be decomposed into external and internal toothed gears with the corresponding interaction. This means that in formulating an optimization model for a planetary gear train, it is necessary, first of all, to define the functional constraints and criteria functions both for the external and internal gears, and then for the planetary gear train as a mechanical system.

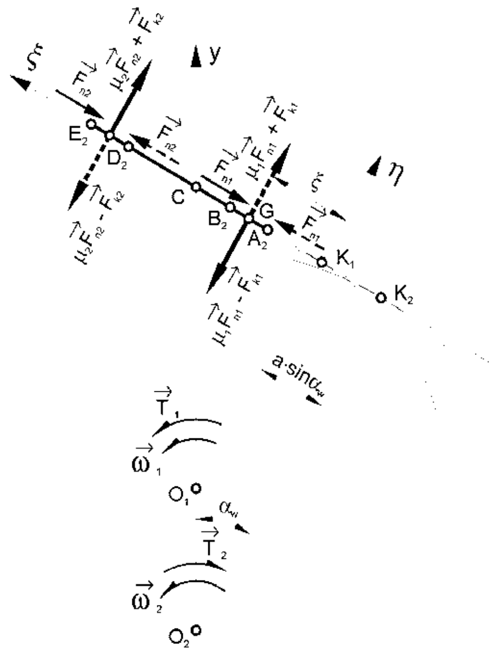

Figure 1. Forces between gear teeth.

In order to ensure the mounting as well as the correct meshing of the gears, it is necessary to fulfill the requirements regarding their alignment, the clearance between the planetary gear trains and their meshing with the sun gear. It is necessary to express the above requirements by the corresponding functional constraints, and based upon them, to identify all relevant values together with the areas of their practical applications.

The analysis considers sliding losses, which are the result of friction forces developed as the teeth slide across each other, rolling losses resulting from the formation of an elasto -hydrodynamic film. The instantaneous efficiency for internal gear at any particular instant, from the relevant T1 input torque, is determined according to the expression:

$$\eta_i = \frac{T_2}{T_1} = \frac{1}{u_{gb}^H} \tag{1}$$

Sliding and rolling losses were evaluated by numerically integrating the instantaneous values of these losses across the path of contact. Contact starts at the intersection of the tip diameter of the internal gear with the path of contact at A_2. The path of contact is tangent to the base circles of two gears. Contact ends at the intersection of the tip diameter of the external gear with the path of contact at E_2.

The overall efficiency for gearing under consideration may be written:

$$\eta_{gb}^H = \frac{1}{l} = \int_{A_2}^{E_2} \eta_i d\xi \tag{2}$$

The instantaneous frictional force due to sliding of two gear teeth against each other is:

$$F_\mu(\xi) = \mu(\xi) F_n K_\alpha(\xi) \tag{3}$$

The friction coefficient is calculated by the method of Benedict and Kelley for mineral oil:

$$\mu(\xi) = 0{,}0127 \log\left(\frac{\frac{29{,}66}{b} F_n}{\eta v_{ki} v_{ko}^2}\right) \tag{4}$$

The instantaneous force due to build up of the EHD film is

$$F_R = Chb \tag{5}$$

The gear contact minimum film thickness is calculated by the method of Dowson and Higginson

$$h(\xi) = 1{,}6\alpha^{0,6} (\eta v_{ko})^{0,7} E^{0,003} \frac{R^{0,43}}{F_n^{0,13}} \tag{6}$$

In order to evaluate the efficiency of an internal gear pair it must be considered equilibrium of the gears. Fig. 1 shows the normal forces F_n, the rolling friction forces F_R, and the sliding friction forces F_μ, with suffices 1 for teeth in the path of approach and 2 for teeth in the path of recess. One pair of teeth is in contact at point G and the other at point H. For convenience the output torque of the train is assumed constant. From the equilibrium of gears, it comes:

$$F_{n1} = \frac{T_1 - p_1 F_{R2} - \xi F_{R1}}{db_1 + \mu_2 P_1 - \mu_1 \xi} \tag{7}$$

$$T_2 = F_{n1} d_{b2} + p_2(\mu_2 F_{n1} - F_{R2}) - (\mu_1 F_{n1} + F_{R1}) p_3 \tag{8}$$

where

$$p_1 = \xi + p_b \tag{9}$$

$$p_2 = a \sin \alpha_w \xi + x + p_b \tag{10}$$

$$p_3 = a \sin \alpha_w + \xi \tag{11}$$

On the basis of the models developed for a gear pair with external and internal gearing, the efficiency of a planetary gear train may be expressed as:

$$\eta_{aH}^{b} = \frac{1-\eta_{ab}^{H}u_{ab}^{H}}{1-u_{ab}^{H}} \qquad (12)$$

where

$$\eta_{ab}^{H} = \eta_{ab}^{H}\eta_{gb}^{H} \qquad (13)$$

3. FORMULATION OF OPTIMIZATION MODEL

The criteria regarding the desired performances are expressed by the criteria functions, which, for the best planetary gear train design, should reach the extreme:

$$\underset{x \in D}{extr}\ f(x) \qquad (14)$$

The function criteria for a one-stage planetary gear train can be written in the form of the following relations for:

Eq. [15] – [23] are called objective functions. In addition, it is also necessary to include the functional constrains in the form of the inequalities:
Eq. [24] – [31] are called inequality constrains for objective functions.
Eq. [32] – [34] are called equality constrains for objective functions.

Based upon the objective functions given and upon the functional constraints, all the relevant values of the planetary gear train have also been identified.

- centre distance $$f_1 = \frac{m_n z_a}{\cos\beta}(1+u_{a-g}^{H})\frac{\cos\alpha_t}{\cos\alpha_w} \qquad (15)$$

- efficiency $$f_2 = \frac{1-\eta_{ab}^{H}u_{ab}^{H}}{1-u_{ab}^{H}} \qquad (16)$$

- contact ratio $$f_3 = \varepsilon_{\alpha_{a-g}}(x) \qquad (17)$$

- pressure angle $$f_4 = \alpha_{w_{a-g}}(x) \qquad (18)$$

- safety factor for bending stress $$f_5 = S_{F1}(x) = \frac{[\sigma_F]M_1}{\sigma_{F1}} \qquad (19)$$

- safety factor for contact stress $$f_6 = S_{H1}(x) = \frac{[\sigma_H]M_1}{\sigma_{H1}} \qquad (20)$$

- volume of material used for gears $$f_7 = V(x) \qquad (21)$$

- safety factor for bending stress $$f_8 = S_{F3}(x) = \frac{[\sigma_F]M_3}{\sigma_{F3}} \qquad (22)$$

- outer diameter $$f_9 = D_{out}(x) \qquad (23)$$

- bending stress $[\sigma_F]$ $$g_1 = \frac{[\sigma_F]M_1}{\sigma_{F1}} - S_F > 0 \qquad (24)$$

$$g_2 = \frac{[\sigma_F]M_2}{\sigma_{F2}} - S_F > 0 \qquad (25)$$

$$g_3 = \frac{[\sigma_F]M_3}{\sigma_{F3}} - S_F > 0 \qquad (26)$$

- contact stress $[\sigma_H]$ $$g_4 = \frac{[\sigma_H]M_4}{\sigma_{H4}} - S_H > 0 \qquad (27)$$

$$g_5 = \frac{[\sigma_H]M_5}{\sigma_{H5}} - S_H > 0 \qquad (28)$$

- tip interference $$g_6 = \delta > 0 \qquad (29)$$

- radial interference $$g_7 = \Delta x > 0 \qquad (30)$$

- space requirements $$g_8 = 2a\sin(\frac{\pi}{n_w}) - f - d_{a-g} \geq 0 \qquad (31)$$

- specific sliding $$h_1 = (u_{a-g}^{H})^2 \rho_E \rho_A - \rho_A \rho_E = 0 \qquad (32)$$

- shaft alignment $$h_2 = \frac{z_a + z_g}{\cos\alpha_{wb-g}} - \frac{z_b + z_g}{\cos\alpha_{wb-g}} = 0 \qquad (33)$$

- condition for assembly $$h_3 = \frac{z_a z_b}{n_w D(z_g z_b)} - INT = 0 \qquad (34)$$

4. OPTIMIZATION PROCEDURE USING MULTI OBJECTIVE GENETIC ALGORITHM

GAs is one type of EAs, which was developed by John Holland in the early 1970s. Every genetic algorithm has its basic components shown as the flowchart in Fig. 2. Simple GA has three basic operators: Selection, Crossover, Mutation.

Each member in this population is evaluated and assigned a fitness value. In the selection procedure, some selection criterion is applied to select a certain number of strings, namely parents, from this population. Parent pairs are randomly chosen from the selected population and the kind of merging depends on the crossover operator used.

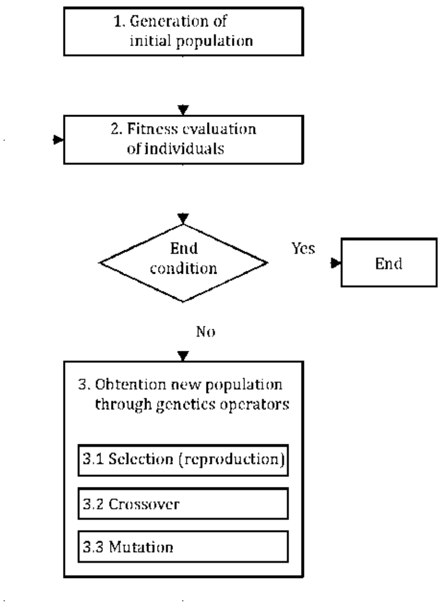

Figure 2. Simple genetic algorithm flowchart.

Mutation simply changes one bit 0 to 1 and vice versa, at a position determined by some rules. Mutation is simple but still important in evolution because it further increases the diversity of the population members and enables the optimization to get out of local optima.

The genetic algorithm (GA) is an optimization and search technique based on the principles of genetics and natural selection. A GA allows a population composed of many individuals to evolve under specified selection rules to a state that maximizes the "fitness" (i.e., minimizes the cost function).

Some of the advantages of a GA include that it
- Optimizes with continuous or discrete variables,
- Doesn't require derivative information,
- Simultaneously searches from a wide sampling of the cost surface,
- Deals with a large number of variables,
- Is well suited for parallel computers,
- Optimizes variables with extremely complex cost surfaces (they can jump out of a local minimum),
- Provides a list of optimum variables, not just a single solution,
- May encode the variables so that the optimization is done with the encoded variables, and
- Works with numerically generated data, experimental data, or analytical functions [15].

The basic idea of the approach is to start with a set of designs, randomly generated using the allowable values for each design variable. Each design is also assigned a fitness value, usually using the cost function for unconstrained problems or the penalty function for constrained problems. From the current set of designs, a subset is selected randomly with a bias allocated to more fit members of the set.

The process is continued until a stopping criterion is met. In the following paragraphs, some details of implementation of these basic steps are presented and explained. First, it shall be defined and explain various terms associated with the algorithm.

5. NUMERICAL RESULTS AND DISCUSSION

In the binary algorithm, after defining the initial population each unknown variable must be encoded and as such must be treated by the end of the process. When the algorithm finds the optimal value, it must be decoded before the end of the process, so that the optimization results was presented as a numerical value. This optimization problem has 8 inequality constraints and 3 equality constraints. Binary coding of specimens is based on the range limits.

Table 1. GA coding of design variables.

Design variables vectors	Vectors	Random binary digits	String length l
Module m_n	x_1	10101	5
Number of teeth z_a	x_2	1101	4
Number of teeth z_g	x_3	11010	5
x_a	x_4	11100	5
x_g	x_5	11100	3
x_b	x_6	111	3
a_1	x_7	11101	5
n_w	x_8	11111	5
H	x_9	101	3
r_{ct}	x_{10}	1111	4
A single 42-bit individual (chromosome)	101011101110101110011100 111111011111111011111		

For example, let the only variables be x_1, x_2, x_3. And let the constraints are in the form of equity, for all three variables from range [1,2]. Then, each of the three variables can take only integer values from 1 and 2 and that means that for their binary encoding are sufficient only two binary digits. One of the possible solution to the optimization problem must have all three variables, and individual genetic algorithm has a total of 6 binary digits. For example, if a solution has this formula:

$$x_1 = 0 x_2 = 0 x_3 = 1,$$

in binary, that means 000001.

In this paper, because of nature of the problem and the conditions of the constraints variables x_5, x_6, x_9 are coded with 3 binary digits, x_2, x_{10} are coded with 4 binary digits and $x_{1,} x_{3,} x_4, x_7, x_8$ are coded with 5 binary digits. That means that one possible solution must be coded in 42-digit binary code. The way of coding the variables is shown in the Table 1.

Following parameters are selected to be used for performing operation of genetic algorithm:

-a binary encoding,
-proportional selection,
-crossover around one point,
-the population size of $\mu = 10$ individuals
-the probability of crossing $p_c = 0{,}8$,
-probability of mutation $p_m = 0{,}01$,
-maximum number of generations $g_{\max} = 500$.

Table 2. A sample case at first generation regarding satisfaction of constraints.

First generation	m_n	z_a	z_g	x_a	x_g
36758890.1	1.25	24	70	0.33	0.54
15648796.1	1.45	26	49	0.55	0.54
13376868.7	1.60	25	69	0.67	0.46
23478909.2	5.0	35	56	0.6	0.58
59890097.1	2.0	23	57	0.82	0.52
13478976.8	2.0	23	50	0.25	0.40
65784634.8	2.0	21	56	0.27	0.68
23768965.5	1.5	20	45	0.48	0.62
34897453.5	1.25	10	66	0.70	0.62
5515354.8	1.5	17	60	0.60	0.67
First generation	x_b	a_1	n_w	h	r
36758890.1	0.65	0.603	1	4.22	0.367
15648796.1	0.66	0.620	2	2.46	0.246
13376868.7	0.64	0.614	5	4.66	0.135
23478909.2	0.50	0.601	7	2.56	0.234
59890097.1	0.36	0.604	6	4.70	0.145
13478976.8	0.36	0.602	5	5.52	0.256
65784634.8	0.45	0.606	2	2.54	0.234
23768965.5	0.45	0.607	1	3.2	0.123
34897453.5	0.51	0.601	8	2.7	0.143
5515354.8	0.53	0.620	7	3.80	0.156

Table 3. A sample case at last generation regarding satisfaction of constraints.

Last generation	m_n	z_a	z_g	x_a	x_g
6214.87	2.0	30	54	0.252	0.064
6214.87	2.0	30	54	0.252	0.064
6214.87	2.0	30	54	0.252	0.064
6214.87	2.0	30	54	0.252	0.064
6214.87	2.0	30	54	0.252	0.064
6214.87	2.0	30	54	0.252	0.064
6214.87	2.0	30	54	0.252	0.064
6214.87	2.0	30	54	0.252	0.064
6214.87	2.0	30	54	0.252	0.064
6214.87	2.0	30	54	0.252	0.064

Last generation	x_b	a_1	n_w	h	r
6214.87	0.320	0.57	2	6.67	0.17
6214.87	0.320	0.57	2	6.67	0.17
6214.87	0.320	0.57	2	6.67	0.17
6214.87	0.320	0.57	2	6.67	0.17
6214.87	0.320	0.57	2	6.67	0.17
6214.87	0.320	0.57	2	6.67	0.17
6214.87	0.320	0.57	2	6.67	0.17
6214.87	0.320	0.57	2	6.67	0.17
6214.87	0.320	0.57	2	6.67	0.17
6214.87	0.320	0.57	2	6.67	0.17

After doing all the settings of the genetic algorithm starts process. Criteria to stop the process are achieved or the maximum number of generations or achieved stall time.

Phases of process are binary coded, selection, reproduction, mutation, crossover and migration. The genetic algorithm starts by generating a random initial population. In the example under consideration, each population has 10 individuals and one choice is shown in the table 2. Genetic algorithm stopped in 201th generation, and achieved solution which are given in table 3.

The table 3 contains integer values for 10 variables and appropriate values for objective function for each gene from population in selected last generation.

As it is shown in table 3 each gene from population of 10 genes has the same values for variables and the objective functions.

6. CONCLUSIONS

Multi objective modeling reflects very well the design process in which usually several conflicting objectives have to be satisfied such as the efficiency of planetary gear trains and the distance between centers of sun gear and planetary gear. In the present study, an optimization approach based on Genetic Algorithms is proposed to improve gear performances. Bounding parameters values are very important in GA and directly affects solutions.

Optimization of gear train was accomplished using GA. Results accomplished using GA are less than results that are found using analytical method. Results shown in tables 4 and 5 showed that GA is better method analytical method to obtain gear train minimum.

REFERENCES

[1] J. C. Rawers, J. H. Tylczak, D. E. Alman, Wear Evaluation of High Interstitial Stainless Steels, Tribology transactions, Volume 51, Issue 4, pp. 515 – 525.

[2] Joslyn Hili, Andrew V. Olver, Simon Edwards; Leon Jacobs,Experimental Investigation of Elastohydrodynamic (EHD) Film Thickness Behavior at High Speeds, Tribology transactions, Volume 53, Issue 5, pp. 658 – 666

[3] Faruk M., Tamer B., Kurtulus B., Fatih E. B. Optimization of module, shaft diameter and rolling bearing for spur gear through genetic algorithm. Expert Systems with Applications; 37(12):8058-8064; 2010.

[4] Arora J.S. Introduction to optimum design. McGraw-Hill; 1989.

[5] A.Marinković, B.Rosić, G. Petropoulos: Analysis and optimization of dynamically loaded porous metal sliding bearings under conditions of elastohzdrodynamic lubrication,International Jounal for Computer-Aided Engineering and Software, Vol.24 No.3,2007.

[6] Rosić B.: Multicriterion Optimization of Multistage Gear Train Transmission, The Scientific Journal FACTA UNIVERSITATIS, Series: Mechanical Engineering, Vol. 1, No 8, 2001.

[7] A. Marinković, B. Rosić, M. Janković: Optimum Design for Porous Metal Bearing, International Journal of Applied Mechanics and Engineering, 2001, Volume 6, Number 1, Technical University Press Zielona Gora, Poland.5.

[8] Rosić B.: Multicriterion optimization of planetary gear train, Proceedings of the International Gearing Conference, Newcastle, 1994, (195-199).

[9] Ristivojević M., Rosić B., Laćarac V.: The influence of gearing parameters on damaging of gear flanks, Proceedings of the abstracts of the papers from the World Tribology Congress, London, England, 1997, page 763.

[10] Rosić B.: An automatic design optimization procedure for compact gear sets, Proceedings of the International conference on engineering design, Dubrovnik, august 1990., Volume 4 (1896 – 1889).

[11] Vulić A., Rosić B.: The analysis of the factors influencing the harmonic transmitters utilization, Proceedings of the International Conference on Tribology and EUREKA Brokerage Event, Thessaloniki, Greece, 1996., (471-477).

[12] Rosić B., A. Marinković, D. Urošević: Dynamic parameters Analysis of planetary transmission structure, The 2nd International conference “Power Transmissions ’06” Novi Sad, Serbia, 2006., (159-162).

[13] Tripathi V.K, Chauhan H.M. Multi objective optimization of planetary gear train. Lecture Notes in Computer Science (including subseries Lecture Notes in Artificial Intelligence and Lecture Notes in Bioinformatics); 6457:578-582; 2010.

[14] Bonori G, Barbieri M, Pellicano F. Optimum profile modifications of spur gears by means of genetic algorithms. Journal of Sound and Vibration; 313(3-5):603-616; 2008.

[15] Haupt R.L, Haupt S.E. Practical Genetic Algorithms. John Wiley and Sons, INC. Publication, 2004.

SERBIATRIB '11

Serbian Tribology Society

12th International Conference on Tribology

Faculty of Mechanical Engineering in Kragujevac

Kragujevac, Serbia, 11 – 13 May 2011

FAILURE ANALYSIS OF THE TIMING BELT DRIVES

Blaža Stojanović[1], Slobodan Tanasijević[1], Nenad Marjanović[1], Mirko Blagojević[1]
[1]Faculty of mechanical Engineering from Kragujevac, Serbia, blaza@kg.ac.rs

Abstract: *This paper refers to testing of timing belt drives. Timing belt drives are relatively young drives that originate from 1950's. Considering the larger and larger use of timing belts and their limited lifetime, their testing is justified. A large number of factors have influence on timing belt drive's lifetime: wear, amount of transmitted power, operating environment, coaxiality of shafts and belt pulleys, handling before and during assembly and others. Failure most frequently occurs because of damage of belt's and belt pulley's teeth or damage of tractive element due to wear. The paper presents the results of experimental testing of wear and failure of timing belt drives originating from change in their geometrical dimensions. Gained experimental results fully coincide with theoretical assumptions and similar tests around the world.*

Keywords: *wear, failure analysis, timing belt drive, friction*

1. INTRODUCTION

Timing belt drive is relatively new conception of power transfer, accepted in all areas of industry today. They are flat belts with series of equal spatial teeth inside addendum diameter.Timing belt transfers the torque by means of its shape. The teeth, equally spaced at inner side of timing belts, contact the belt pulley's teeth with their hollows between teeth and, thus, by conjugate gear action, achieve the meshing between the belt and the belt pulley and transfer the torque.

Considering their purpose and very important role in transmission of power and motion, it is necessary to adequately know tribological characteristics of timing belt drives.

In spite of advantages in operation, timing belt drives have only recently achieved great application. It was yet after their application as IC engine's camshaft drive, that their purposefulness of application had become obvious. Popularity of timing belts in automotive industry has accelerated their use in other branches of industry [1-5].

2. FAILURE OF TIMING BELT DRIVE

A large number of factors have influence on the working life of the timing belt drives:

- friction and wear in the belt - belt pulley contact,
- the belt's tension,
- coaxiality of the shaft and the belt pulley,
- working environment and
- other.

2.1 Influence of friction and wear

Basic tribomechanical systems in timing belt drive are: belt's tooth - belt pulley's tooth (1), belt's face – flange (2), space between teeth of the belt – apex of the belt pulley's tooth (3) (Figure 1). Analysis of these tribomechanical systems shows that the influence of the friction forces that occur in them may not be neglected and directly influences the power and motion transmission and working life of the drive [3,6].

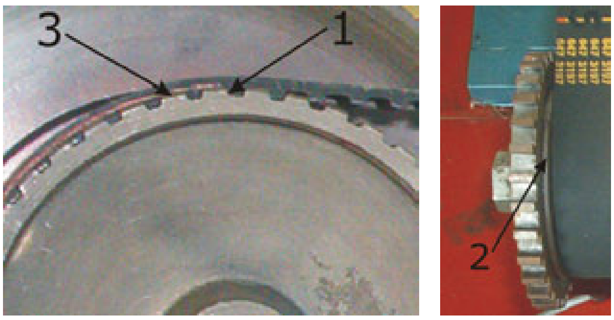

Figure 1. Timing belt drive and basic tribomechanical systems

Values of the friction force are different for all three analyzed tribomechanical systems. Friction force has the largest values at the side surface of the belt's and the belt pulley's teeth. Friction force has somewhat smaller values between belt's face surface and flange, while the lowest values are between the apex of the belt pulley's teeth and the space between belt's teeth. Direction, sense and intensity of these forces are related to kinematics of couplings in timing belt drives.

2.2 Influence of the belt's tension

The belt's tension has an important part in design of the timing belt drive. Proper belt's tension provides normal coupling between the belt and the belt pulley, minimal losses in the drive, smaller wear in bearings and smooth operation of the drive. The belt should be pretensioned according to the producer's recommendations. Checking of the belt's tension is done by tensiometer. Inadequate belt's tension reflects as insufficient or exaggerated belt's tension.

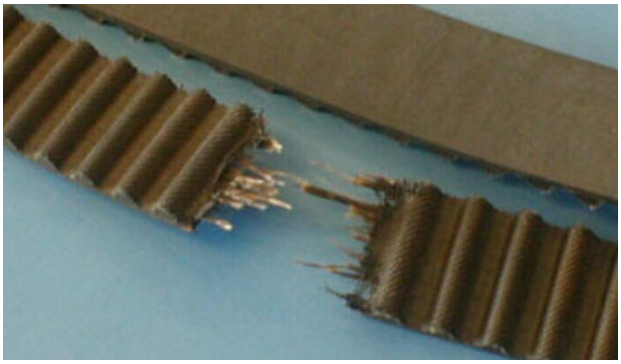

Figure 2. Cracking of the drive element

Exaggerated tension of the belt leads to increase of power losses at idle speed and reduces the efficiency. In addition, if the belt is over-tensioned, drive element's fibres are additionally loaded in view of their strength, which leads to sooner cracking of the drive element (Figure 2). Increase in belt's tension directly influences the kinematics of coupling between the belt and the belt pulley. Hence, cracks appear in the belt's tooth root on the side, which is in contact with the belt pulley's tooth.

The crack in the root of the firstly loaded tooth spreads towards the apex of the tooth and leads to its shearing (cracking) (Figure 3). Besides, the teeth's contact surface decreases, which additionally loads neighbouring teeth on which the cracks in the roots have appeared. Due to over-tension, there is more intensive wear of the belt's surface layer, until the driving element becomes visible.

Over-tension, as well as insufficient tension of the belt, may lead to too early failure of the timing belt drive.

Figure 3. Crack in the belt tooth root

Namely, when the power transmitted by the timing belt is rather large, there may be teeth skipping during operation of the loose belts. Insufficient tension reduces the contact surface between the belt and the belt pulley, which increases the pressure on the teeth surface. Due to large pressure jump, there appear the cutting off of larger number of the belt's teeth and the belt's failure (Figure 4).

Figure 4. Cutting off of larger number of the belt's teeth

2.3 Coaxiality of the shaft and the belt pulley

Coaxiality of the shaft and the belt pulley has a great influence on the working life of the timing belt drive. If there is no angular coincidence of the axes of the drive's shafts, then the contact surface area between the belt's teeth and the belt pulley's teeth reduces. One side of the tooth is more loaded than the other. This load may lead to appearance of intensive wear of the belt and the belt pulley and to rapid damage or failure of the belt.

Another problem due to lack of coaxiality is related to the belt pulley's design. Namely, if the belt pulleys are manufactured with flanges, then one face of the belt is loaded more. Due to lack of coaxiality, the face surface is firmly leaned against the flange and then there comes the abrupt damage of the face surface of the belt (Figure 5). These damages spread towards the centre of the belt, reduce the contact surface, additionally load the nearby teeth and lead to rapid failure of the belt.

Due to lack of coaxiality of the shafts, there appear the increase of unevenness of drive's operation, increase of noise and vibration and even the falling off of the belt from the belt pulley.

The belt's damage also appears due to the belt pulley, which dimensions deviate from design documentation. If diameters of the belt pulleys or teeth are not manufactured with corresponding tolerances, large damage of the belt appears. These deviations lead to damage of protective surface layer of the belt. Damage appears in all directions, they are not distinctive and they look undefined.

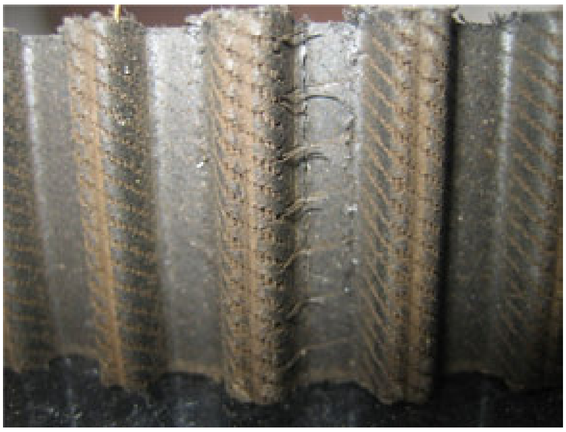

Figure 5. Damage of the face surface of the belt

The increased wear of the belt pulley appears due to over-tension of the belt. Intensive wear of the belt additionally loads the belt pulley's teeth, directly leaving the trace on the belt pulley. Due to extensive wear, the drive element becomes visible and then there is a metal-on-metal contact, which may lead to abrasion and rapid damage of the belt pulley.

2.4 Influence of the environment

The timing belts are especially sensitive to high temperatures, action of chemical compounds and foreign bodies. Materials used for making of the belts are rubber, urethane (polyurethane), neoprene and similar that are more or less not resistant to high temperatures. When rubber belts work at high temperatures for a long period, rubber compounds gradually harden, losing their features. The cracks appear at the back surface of the belt, parallel to space between teeth of the belt. These cracks lead to the cutting off of teeth and to cracking of the drive element.

At urethane and polyurethane belts, the structure, form and shape of teeth change under the effect of temperature and this leads to failure of the belt drive.

Materials of the timing belts are highly sensitive to oils and solvents. There is a large number of chemicals that may come into contact with the belt (antifreeze, fuel, lubricant and similar). Under the action of chemical solvents, the belt reacts similarly as under the action of high temperatures. Rubber compounds harden and the back surface cracks (Figure 6).

Figure 6. Influence of the oil and solvents on belt

The timing belt drives are highly sensitive to the presence of foreign bodies between the belt and the belt pulley. The presence of such bodies leads to heavy damage of the belt, especially the drive element. As soon as the part of the drive element is damaged, the rest is additionally loaded which leads to rapid failure of the belt. Action of the foreign bodies lead to damage of the belt pulley in the form of cuts and scratches, so replacement of the belt pulley is necessary.

3. TESTING OF TIMING BELT DRIVE

Testing of timing belt drive is conducted on a test bench designed on purpose and made at the Laboratory for mechanical constructions an mechanization of the Faculty of mechanical engineering from Kragujevac [7-10]. Test bench operates on a principle of opened loop power.

Basic elements of the test bench are:

1. drive unit (electric motor),
2. cardanic drive,
3. measuring (input) shaft,
4. input shaft's rotational speed transducer,
5. input shaft's torque transducer,
6. tested drive (timing belt drive),
7. output shaft,
8. mechanical brake,

9. tension mechanism and

10. amplifier bridge.

Figure 7 shows the test bench with basic elements.

Mechanical brake provides a given amount of brake torque that is load torque on output shaft of the timing belt drive. Value of the load torque is obtained by readout of a display of digital amplifier bridge which obtains the torque signal from a measuring shaft, through signal preamplifier HBM EV2510A. Rotational speed of input shaft is also read on the amplifier bridge which obtains the signal through inductive sensor and impulse signal receiver of number of revolutions, HBM DV2556. Thus, regime at the input shaft of the driver is defined [10,11].

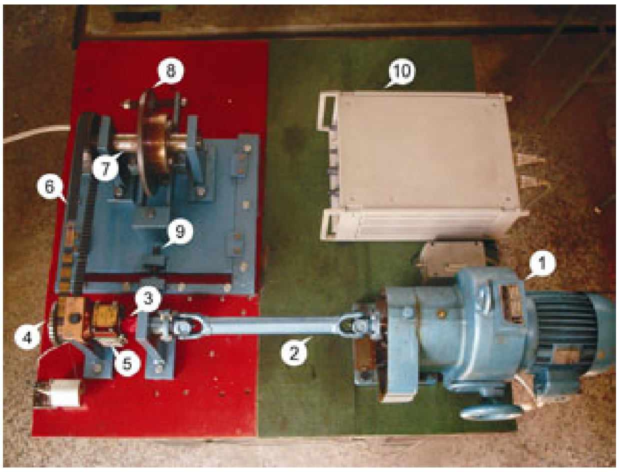

Figure 7. Test bench for testing of timing belt

In order to obtain a true picture on tribological characteristics of the timing belt, measurement of roughness parameters and determination of geometrical values are conducted. Measurement of these values is conducted according to previously determined dynamics.

Table 1. Time intervals of measurement of roughness parameters and belt's geometrical values

Number of measurement	1	2	3	4	5	6	7	8	9	10
Operation time [h]	0	5	10	20	50	100	150	200	250	300

Before the tests began, the state of the contact surfaces and initial values of the belt's geometrical values were established. Further measurements were conducted after a certain operation time and are shown in Table 1.

4. MEASUREMENT OF GEOMETRICAL AND ROUGHNESS PARAMETERS

In addition to measurement of geometrical values, measurement of roughness parameters is conducted during testing of the timing belt.

Measurement of geometrical values of timing belts was conducted on eight belt's teeth. Measurement is conducted on optical microscope ZEISS ZKM01-250C. The following values were measured (Figure 8):

- belt's pitch (t),
- belt's width (b),
- groove's thickness $(h_b = h_s - h_t)$ and
- belt's total height (h_s).

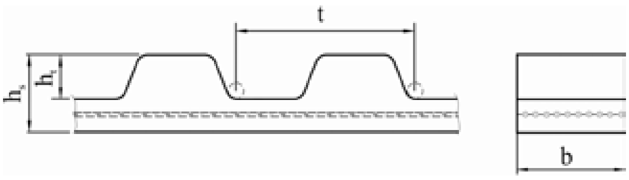

Figure 8. Measured geometrical values of the belt

The following roughness parameters are especially interesting for further analysis:

R_a - mean arithmetic deviation of profile from midline of the profile and

R_{max} - maximal height of roughness along reference length.

Measurement of roughness parameters is performed on three measuring points (Figure 9):

- at the apex of the belt's tooth - 1,
- at the flank of the belt's tooth - 2 and
- at the space between belt's teeth - 3.

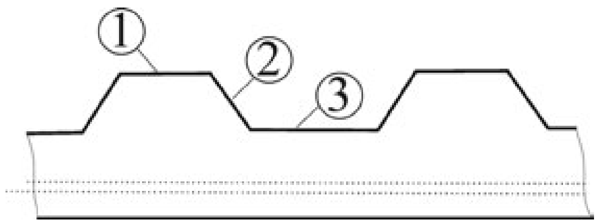

Figure 9. Measuring points on the belt for measurement of roughness parameters

Average values of variation of geometrical values are presented in Figure 10 [9-11].

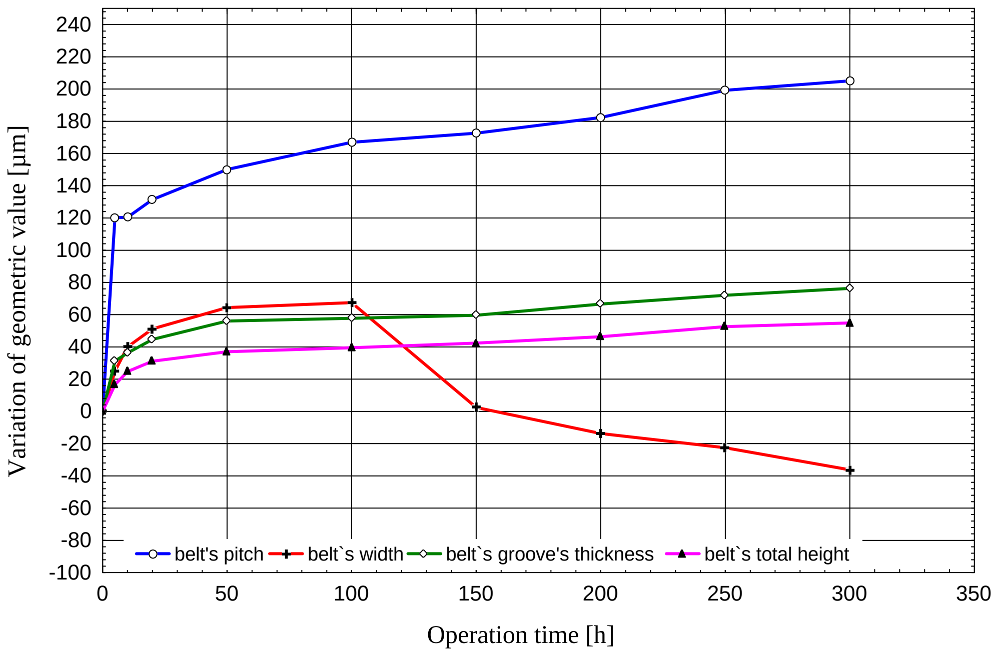

Figure 10. Average values of variations of geometric values

5. ANALYSIS OF THE OBTAINED RESULT

By monitoring the roughness parameters in the period of working out, their decrease after 5 hours of operation may be noticed. Then topography is changed due to transition from technological to exploitation topography. Already in the next phase of the period of working out (5 to 10 hours of operation), monitored roughness parameters increase. In the first 5 hours of operation, the highest roughness peaks are being flattened, so the profile gets more even. However, in the next 5 hours, roller wear already occurs, that is rollers at the belt's tooth are generated. Part of material leaves the belt and then topology of the contact surface is changed, that is roughness parameters grow. Due to this specific form of wear that is characteristic for non-metals, roughness parameters have stochastic variation all the time.

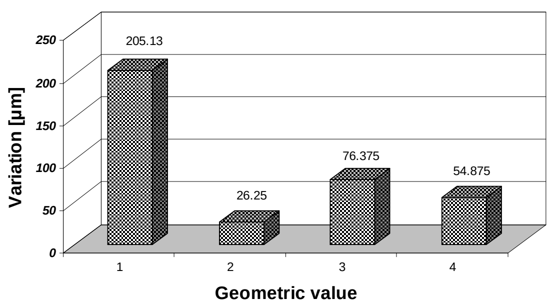

Figure 11. Average values of variations of geometric values

1 - belt' pitch
2 - belt's width
3 - belt's total height
4 - belt groove's thickness

In the period of normal wear which appears after 20 hours of operation, variation of geometrical values is still strong. After 20 hours of operation, the belt's pitch is still increasing. Variation of the belt's pitch is more pronounced in the period from 20 to 50 hours of operation, after which it becomes approximately linear. The results obtained by measurement on all eight teeth almost do not deviate one from another. Absolute average values of variation of geometrical values are presented in figure 11.

6. CONCLUSION

Worn-out belt pulley's teeth induce rearrangement of loads where teeth entering and exiting the coupling have maximal loads. Due to wear of the belt pulley's teeth, nominal contact surface between the belt's teeth and the belt pulley's teeth is reduced. The contact pressure increases, which is the greatest in the belt teeth's groove, according to load distribution along the side surface of the belt's tooth. It all together leads to appearance of the crack in the belts tooth root, which results in separation and cutting off of the teeth. In that case, it is necessary to replace both the belt and the damaged belt pulley.

Reliable and long working life of timing belt drives is possible only under certain conditions:

- belt drive should be isolated from dirt and chemical solvents,
- belt pulleys and belt tensioners should be manufactured and assembled according to technical documentation,

- every lack of coaxiality and existing bending of the axles and belt pulleys should be avoided by control and checking
- belt tensioning should be done according to producer's recommendations and with corresponding devices (tensiometers).

REFERENCES

[1] B. Stojanović, N. Miloradović: Development of timing belt drives, Mobility and Vehicle Mechanics, Vol. 35, No. 2, pp. 29-34, 2009.

[2] Y. R. Case: Timing belt drive, McGraw Hill Book Company, INC, New York, 1954.

[3] B. Stojanović: Characteristics of tribological processes in timing belts (in Serbian), Master's thesis, Faculty of mechanical engineering from Kragujevac, 2007.

[4] T. Johannesson, M. Distner: Dynamic loading of synchronous belts, ASME, J. Mech. Design Vol. 124, pp.79-85, 2002.

[5] T. H. C. Childs, K. W. Dalgarno, M. H. Hojjati, M. J. Tutt, A. J. Day: The meshing of timing belt teeth in pulley grooves. Proc. Instn Mech. Engrs, Part D: J. Automobile Engineering, Vol. 211, pp. 205-218, 1997.

[6] B.Stojanovic, S. Tanasijevic, N. Miloradovic: Tribomechanical systems in timing belt drives, Journal of the Balkan Tribological Association, Vol.15, No.4, pp. 465-473, 2009.

[7] S. Tanasijević: Characteristics of Existence and Development of Machine Element Tribology, Tribology in industry, Vol. 20, No 4, pp. 142-148, 1998.

[8] S.Tanasijević: Tribology in design, Tribology in industry, No. 1, pp. 12-19, 1990.

[9] B. Stojanović, N. Miloradović, M. Blagojević: Analysis of Tribological Processes at Timing Belt's Tooth Flank, Tribology in Industry, Vol.31, No. 3-4, pp. 53-58, 2009.

[10] B. Stojanović, L. Ivanović, M. Blagojević: Friction and Wear in Timing Belt Drive, Tribology in Industry, Vol.32, No. 3, pp. 33-40, 2010.

[11] B. Stojanović, L. Ivanović, N. Miloradović: Testing in Timing Belt Drive, IMK-14, Vol.37, No. 4, pp. 77-80, 2010.

Serbian Tribology Society

SERBIATRIB '11

12th International Conference on Tribology

Faculty of Mechanical Engineering in Kragujevac

Kragujevac, Serbia, 11 – 13 May 2011

TRIBOLOGY ASPECTS OF PROACTIVE MAINTENANCE APPROACH

Branislav Jeremić[1], Ivan Mačužić[1], Petar Todorović[1], Marko Đapan[1], Uroš Proso[1],
[1]Faculty of Mechanical Engineering, Kragujevac, Serbia
bane@kg.ac.rs; ivanm@kg.ac.rs; petar@kg.ac.rs; djapan@kg.ac.rs; urosproso@kg.ac.rs;

Abstract: *There is an increasing need for improved methods of maintenance in order to enable improvement in efficiency, availability, reliability and prolonged lifetime of production and other technical systems. Changing focus of maintenance activities from corrective to preventive ones became main trend in previous period which resulted in much wider appearance of advanced maintenance methods like Condition Based Maintenance and introduction of new ones like Proactive Maintenance. The paper deals with the role of tribology in the large and complex scope of maintenance engineering and the different tribology-aspects related to implementation of proactive maintenance approach.*

Keywords: *tribology, failures, proactive maintenance, condition based maintenance*

1. INTRODUCTION

Tribology development as a scientific discipline causes major changes in thinking and strategic approach to the maintenance problem of technical systems for different purposes [1], [2], [3]. One result of this trend is the introduction a proactive approach of maintenance in the industrial practice.

The term proactivity and generally proactive approach and philosophy have their clear position and role in the broadest area of technical systems maintenance, no matter that concept has not yet been adopted and standardized.

Despite some terminological ambiguity and lack of support in the technical standards related to the term of proactivity, the most of the world's leading scientists and experts in this field agrees with the structure of the basic elements of a proactive approach [4]. In this sense, three elements (modules) of proactive maintenance approach are defined [5], [6]:

- monitoring,
- diagnostics and
- prognostic.

To these elements, or modules are typically joined by a fourth, related to making appropriate decisions.

2. FAILURES IN TECHNICAL SYSTEMS

Failure represents key term which is necessary for understanding the very essence and function of maintenance in modern manufacturing and business systems. Conducted investigation and researches showed that failure intensity curves could be very random and independent of time line. For analysis of failure modes that are not time-specific, besides the time factor, parameters of components or systems condition are also included.

In fact, even when they are not a function of time most failure modes generate certain kinds of signals and information that could be used to monitor the failure. Illustration of such behavior represent so-called "P-F" curve [7] (Figure 1.)

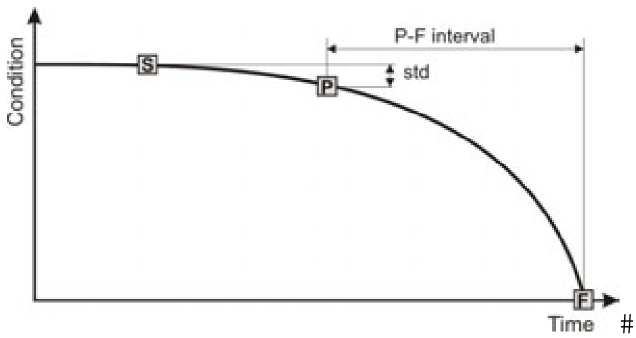

Figure 1. P-F curve

"P-F" curve defines behavior of components or systems from the moment the first symptoms to the failure. This curve has shown great importance in the theory of maintenance and is often used as a starting point for defining the various hypotheses [8], [9]. The analysis of this relatively simple but very important and illustrative diagram can be defined important conclusions and directions for further reflection:

1) Point "S" represents the moment when failure is practically. It is a point that defines the moment in which the projected relations and parameters within components or systems are disturbed to such an extent that further exploitation leads to degradation of states and the outcome of the failure.

From the point of maintenance needs identification of the position of this point on the timeline is very important and identification of the preconditions for its occurrence.

2) The largest number of failures does not occur suddenly, at the time, but has the trend to develop over time and manifests itself first through the various symptoms and finally in its full, functional form. This time delay is defined as the axis interval between points "S" and "F", which allows maintenance personal to take appropriate actions in order to prevent functional failures and all consequences from it arise. The existence of larger or smaller intervals between points "S" and "F" represents basis for the definition and development of various methods, techniques and concepts of maintenance based on condition monitoring of the system or components.

Maintenance activities that are conduct aimed at preventing the progression of degradation of the system or components to point "F" or to extend interval between points "S" and "F" to its maximum.

3) Through the standard maintenance activities precise position of point "S" could not be defined, it may be only a result of modeling or approximation. Therefore, in practical terms point "P" is used that defines time at which we can identify the beginning of failure. This point represents value of condition degradation (condition parameter defining system state) which is measurable by techniques and methods at our disposal (human senses, instruments, measuring equipment).

4) It is very important that point "P" should be located as close as possible to the point "S", which means that identification of potential failures should be performed as soon as its is initialized. In this sense, there are two important factors.

First factor is interval in which condition monitoring, measurements and tests should be performed, because they define the time points where identification of point "P" is possible. There is obvious advantage of continuous monitoring over to measurements at discrete intervals, but it implies much higher costs as is the shortening of the interval between two measurements and increase their number in a given time interval.

Another factor is the minimum value of condition parameter change (in Figure 1 labelled with "std") that could be identified. Application of modern diagnostic methods and precision sensors and instruments leads to early identification of point "P". Also, the methods of measured values processing, understanding of the observed phenomena are of great importance for timely and correct diagnostic and location of point "P".

5) One failure mode can have many symptoms and parameters whose value changes defining point "P". In this sense, for each failure modality it is important to define a number of potential diagnostic parameters and to determine functional dependence system condition in relation to the diagnostic parameters values that define the point "P". Each parameter defines its own point "P" but particularly significant is ones with point "P" closest to the point "S", or those with longest "P-F" the interval.

Since one parameter is often not sufficient to provide a true picture of system condition, and that the error in the process of measuring and testing are always possible, monitoring multiple parameters, or multi-parameter analysis and defining point "P" being imposed as recommended solution.

6) Determination of "P-F" interval length and function of diagnostic parameters change in this interval is problem of primary importance for the maintenance function. Precise time location determination of point "F", or prognosis of "P-F" curve shapes and characteristics is one of the main factors for adequate planning and definition of maintenance activities.

7) Finally, the question that is sort of pushing the boundaries is a problem point "S" origin and in particular, the conditions and phenomena that preceded it. Is it possible to determine or predict the time of point "S" initialization and what are the parameters, symptoms and signs that could help us? If it is possible to determine pre-conditions for initialization of point "S", then it is certainly possible to prolong its origin or even completely eliminate possibility that it occurs, thus all practical dilemmas described above lose their meaning and maintenance function get quite new dimension, shape and significance.

3. PROACTIVE MAINTENANCE AS NEW MAINTENANCE APPROACH

Basic industry standard in the field of maintenance define two basic types of maintenance: Corrective Maintenance (Breakdown Maintenance) and Preventive Maintenance [10]. As part of Preventive Maintenance standard recognizes two methods: Time Based Maintenance (Predeterminated Maintenance) and Condition Based Maintenance (Predictive Maintenance) for total of three standardized maintenance methods.

If we take pre-defined "P-F" curve as a parameter for comparation differences in the approaches of these three models could be clearly observed.

Corrective Maintenance is a reactive approach to failure and it accepts failure as inevitable. This maintenance method has virtually no activity before point "F" and when it occurs (when functional failure occurs) then various activities are performed in order to return system or components condition to state as close as possible to one before failure. The aim is certainly that this level should fully corresponding to point "S" but often this is not quite possible because the occurrence of functional failure leaves some irreversible or long lasting effects.

Preventive Maintenance approach, as the name suggests, is based on principles of prevention activities that are conducted before point "F" in order to prevent, predict or delay its occurrence.

Time Based Maintenance involves the implementation of preventive activities in pre-determinated periods and intervals. Based on experience, technical recommendations, requires of specific technical system and the desired level of reliability, periodic activities are planned and defined in order to restore condition of components or systems to its initial values. These activities are conducted in the interval between points "P" and "F" or "S" and "F". Appropriateness and effect of activities could be significantly decreased as the term of its implementation is closer to the point "S".

Condition Based Maintenance method based itsapproach on the identification of system condition and implementation of relevant activities. It is fully based on previous analysis of "P-F" curves (early defining point "P", forecasting of timeline for point" F", analyzes the modalities of creation point "P"or" S ", the maximum extension of "P-F" interva, etc).

Condition Based Maintenance focuses on methods for monitoring and diagnosis of system condition through measurement of diagnostic parameters whose values are representative of the current state of the system and any disorders. These parameters are divided into direct ones, which include all physical valuess related to opperation processes in system (pressure, flow, force, speed ...) and indirect which primarily include vibration, temperature and wear products.

At the present level of technological development can be said that the method of preventive maintenance according to the state occupied an important place in industrial practice, but room for further improvement and expansion of influence is still huge. This method managed to overcome the gap between theory and practice and to find a real foothold in the minds of technical staff and the general policy of management of business systems, but there is still a significant difference in the expectations and needs of business systems and real, measurable results that can be identified in its implementation [11].

3.1 Proactive Maintenance

The question is should be division on three standardized maintenance methods accepted as final or there is a space for some expansion? Some 20 years ago in a particular engineering literature and magazines that deal with practical aspects of maintenance appeared new term - Proactive Maintenance. In previous period considerable number of different analysis and interpretation of proactivity were published but, up to date, this term is definitely not standardized nor its final place in the theory and technology of maintenance is specified. .

Authors and theorists of the concept of Proactive Maintenance departs their analysis from definition of Preventive Maintenance according to the state under which it is aimed at detecting the early symptoms of failure, or accept it as a possible state of the technical system. On the other hand, Proactive Maintenance is a series of activities and measures aimed at defining, monitoring and elimination of causes of failure.

Proactive Maintenance set its goal that failures or disruptions in the functioning of a component or the whole system does not come, or to provide such conditions of exploitation, which will ideally be an unlimited lifetime guarantee for technical system. According to this interpretation there is a lot of justification which supprot idea that Proactive Maintenance shoul be recognized as a new, independent maintenance method, which falls into the category of preventive and at the same hierarchical level as Time Based Maintenance and Condition Based Maintenance.

An additional argument for this interpretation could be found in previously conducted analysis of "P-F" curve, especially at last of seven conclusions.

Accordin to previous definition Proactive Maintenance put focus of its activities on point "S". Temporal coordinates of points "S" represents the boundary between the Proactive Maintenance and Condition Based Maintenance. All activities that belong to Proactive Maintenance are timely located in period before point "S", while first Condition Based Maintenance activities are related to early detection of point "P".

Another form of recognition of place and role of Proactive Maintenance is based on the views of Condition Based Maintenance through the prism of its broader definition, which established system condtion as basis for any decision and implementation of maintenance activities. According to this interpretation, Proactive Maintenance is assumed as modification and improvement, or a variation of methods of Condition Based Maintenance [5].

An additional argument to this interpretation is that the concept of Proactive Maintenance does not bring any new methods and tools and all methods used in Proactive Maintenance of well-known and already applied in Condition Based Maintenance. Proactive concept just pointing out the importance of certain methods and place them in the foreground. Analysis of numerous diagnostic parameters used in Condition Based Maintenance and their division into those with proactive and those with preventive diagnostic potential, are performed, while certainly there are parameters that can be helpful to use both approaches.

Both interpretations presented have clear grounds and arguments so it is very ungrateful to make definitive conclusions that would be an accepted and others rejected. Regardless of where it ranked, the concept of proactive maintenance represents a new and refreshing theory, which has been confirmed in practice. Bearing in mind the above mentioned facts, it is technically the most correct to use term proactive approach in maintenance, without prejudice to the decision of whether it is a completely new method of or part and modification of Condition Based Maintenance.

4. TRIBOLOGY AND PROACTIVE MAINTENANCE APPROACH

Tribology's contribution to traditional maintenance strategies and methods could be examined in relation to the essential needs of detecting and diagnosing faults before failure occurs. Consequently, it tempts the question as to what tribology can contribute to establishing appropriate prognostic techniques for determining the remaining useful life of failing technical system [12].

In this context, failure could be assumed not only as deterioration in terms of system functionality but also in terms of a reduction in product quality to a level that is unacceptable to the customer.

Through the decades results of tribology investigations and technical development have been used as valuable contribution to maintenance theory and practice. On the basis on focus movement form corrective to preventive measures considerable attention has been given to channelling the fruits of tribological research through improved design methods and manufacture of tribological components and systems that have found application in everyday practice. This has led to marked improvements in the performance and reliability of technical systems [12].

Ways in which tribology contributes to the maintenance activity are shown on Table 1.

Table 1. Tribological inputs to the maintenance activities [12]

Maintenance activity	Tribological input
Corrective Maintenance	Failure examination and diagnosis Designed-out solution
Time Based Maintenance	Lubricant/additive properties Material properties and treatments Surface finish and damage inspection, including internal endoscope surfaces examination
Condition Based Maintenanc	Oil and wear debris analysis Vibration analysis and acoustic emission Preventive diagnostic parameters measurement and monitoring (displacement, temperature measurement)
Proactive Maintenance	Oil analysis (proactive parematers) Root cause analysis Prediction of remaining wear life

As earlier mentioned Condition Based Maintenance could be assumed as corner stone of present advanced maintenance activities. Area of condition monitoring and diagnostic engineering today is an advanced and highly developed field of engineering and multi-technological task, which includes development and application of sophisticated systems to measure changes in performance, data collection, signal processing, diagnostics, prognostics and maintenance engineering, as shown in Figure 2. Tribology as science and technology is fully involved in definition and analysis of failure mechanisms, diagnostic, analysis and prognostic of processes.

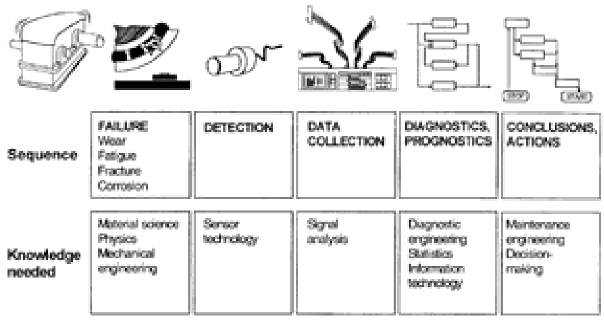

Figure 2. Tribology in Condition Based Maintenance [13]

There is absolutely no doubt that vibration monitoring has enjoyed a far greater presence as the technique of choice for Condition Based Maintenance than any other available (including thermography and oil analysis for instance). There are a number of reasons for this, but one of the main reasons is that oil has always been perceived as a cheap commodity within the maintenance budget by comparison to parts of rotating equipment. A cost justification for predictive maintenance on critical machinery invariably highlights the bearing condition as the main indices to potential system failure, as well as the bearing being a relatively higher cost item to replace. By comparison, the lubricant and industrial oils is a cheap, easily replaced commodity.

Other, very important factor is development of wide range of portable, low – cost instruments for basic vibration measurement together with computerised systems or data collector diagnostic systems with large number of various functions for FFT, CPB, SPM and other complex analysis of vibration signals. All those instruments are capable for real time, on-site and on-line measurements and analysis, while on the other hand analysis of oil and lubricant samples relied on the commercial laboratory services.

Introduction of Proactive Maintenance approach caused significant changes in a way that maintenance experts and technicians think and talk about oil analysis. Corresponding with results that focused oil contamination as major cause of failures in various technical system with oils, importance of oil analysis and related proactive diagnostic parameters become extremely important.

At this time there is no doubt that group of activities named as oil analysis are primary technique of choice for Proactive Maintenance approach. Great numbers of studies and investigations, with illustrative laboratory proofs and field confirmations, have mutual conclusion that oil contamination and corresponding tribological processes are clearly the most common and serious failure culprit.

Wear of components in technical systems with oils should be viewed in two ways:

- development of tribological processes in the system is the most dangerous consequence of contamination of oil and necessarily leads to a change of surface condition and the geometry of the vital parts of components, leaks, reduce efficiency, breakdowns and system failures in the final stage and
- wear parts of components comes to the intensive generating of solid particles, which are a structure much more dangerous to the system of other mechanical particles (dust, fibers, parts of the sealing material).

Bearing in mind previously presented data on significant negative impact of oil contamination on the function, reliability and length of the exploitation period of each technical system with oils, first step in Proactive Maintenance is the implementation of rigorous contamination control programs for lubrication fluids, hydraulic fluids, coolants, air, and fuels.

Contamination control program combines preventive and proactive measures and consists of three basic steps.

The first step is to determine the limits of an allowed contamination levels oils. The limits that we are defining refer to the basic proactive parameters - the concentration of solid particles, the presence of water, oil viscosity and degradation of hydraulic oils. Correctly determining the limits of an allowed contamination levels of hydraulic oils is of great importance for the successful implementation of the program, if the limits set too low (stringent requirements for cleanliness of oil objectively necessary) can lead to increased costs in the following steps. While too high placed limits (requirements for the oil cleanness are not on sufficient level) can disable contamination control program to give the expected results.

The second step in the contamination control program include implementation of a series of activities and measures aimed at reducing levels of contamination to previously defined limits levels and eliminate sources of contamination. This step involves not only the measures relating to oil purification, improved filtration systems and redesign of the hydraulic system in order to eliminate contamination. In addition, this step involves numerous other technical and organizational measures to ensure the proper implementation of routine daily activities in the phases of operation and maintenance of hydraulic systems in order to protect against penetration of any form of contamination.

The third step in the contamination control program includes regular and ongoing activities aimed at monitoring and maintaining the achieved level of contamination. These activities represent the most important part of proactive maintenance, because they provide filtering effectiveness feedback, condition of hydraulic components and oil, the intensity of tribology processes and provide informations that allow proper and timely response and implementation of appropriate measures.

Finaly another asspect of tribology contribution to Proactive Maintenance should be also mentioned. As stated before Proactive Maintenance approach place focus of its activities in on investigation of possibilities for determination of pre-conditions for initialization of point "S" (Fig. 1.) to prolong its origin or even completely eliminate possibility that it occurs. This is very complex and difficult engineering task related with use of numerous sophisticated tools and methods.

For better understanding of mechanisms, functions and methods for failure initialization in components and systems, during exploitation, importance and contribution of tribology is irreplaceable.

In tribology today, it is trend to go to smaller and smaller sizes in the investigation of friction and wear phenomena. In nanotribology, scales are coming down to the very basic dimensions of physical elements such as atoms and molecules. Emerging new technologies opened the possibility to study friction and wear phenomena on a molecular scale [12]. This trend opens quite new and promising directions for advanced failure root cause analysis.

5. CONCLUSION

At today's level of technical development, knowing the rigorous demands of the market in terms of strong economic and general business fluctuations, the proactive approach in defining of maintenance strategy is an essential element. Proactive Maintenance should include all activities aimed at anticipating changes and exploitation characteristics of technical systems.

Innovation of proactive approach is been based on the prediction of degradation and exploitation characteristics of the technical system through the process of prognostics. Prognostics process in a proactive approach aims at early detection of failure causes. Contribution of tribology to those efforts could be examined as very important on several levels and aspects. Oil analysis is recognized as primary tool for proactive maintenance for numerous technical systems.

ACKNOWLEDGMENT

This study was financed by Ministry of Science and Technological Development, Serbia, project No.35021.

REFERENCES

[1] Y. Kimura: Maintenance tribology: its significance and activity in Japan, Wear, Vol. 207, Issues 1-2, pp. 63-66, 1997.

[2] H. Spikes: Tribology research in the twenty-first century, Tribology International, Vol. 34, Issue 12, pp. 789-799, 2001.

[3] Holmberg K., Reliability aspects of tribology, Tribology International, Vol. 34, Issue 12, pp. 801-808, 2001.

[4] L. Swanson: Linking maintenance strategies to performance, International Journal of Production Economics, Vol. 70, pp. 237-244, 2001.

[5] A. Muller, M-C. Suhner, B. Iung: Formalisation of a new prognosis model for supporting proactive maintenance implementation on industrial system, Reliability Engineering & System Safety, Vol. 93, Issue 2, pp. 234-253, 2008.

[6] A. Voisin, E. Levrat, P. Cocheteux, B. Iung: Generic prognostic model for proactive maintenance decision support: application to pre-industrial e-maintenance test bed, Journal of Intelligent Manufacturing Vol. 21, pp. 177-193, 2010.

[7] Moubray J., Reliability-Centered Maintenance – RCM II, Industrial Press Inc, 1992.

[8] Tsang A.H.C., Strategic dimensions of maintenance management, Journal of Quality in Maintenance Engineering, Vol. 8, No. 1, 2002, pp. 7-39

[9] Takata S., Kimura F., Houten van F. J. A. M., Westkamper E., Shpitalni M., Ceglarek D., Lee J., Maintenance: Changing Role in Life Cycle Management, CIRP Annals - Manufacturing Technology, Vol. 53, Issue 2, 2004, pp. 643-655

[10] British Standard BS EN 13306:2001, Maintenance terminology

[11] Dunn S., Condition Monitoring in the 21st Century, Plant Maintenance Resource Center, 2005.

[12] Roylance B. J., Machine failure and its avoidance: What is tribology’s contribution to effective maintenance of critical machinery?, Donald Julius Groen Prize Lecture 2002.

[13] Holmberg K., Reliability aspects of tribology, Tribology InternationalVol. 34, 2001., pp.801–808

[14] Kimura Y., Maintenance tribology: its significance and activity in Japan, Wear Vol. 207, 1997, pp 63-

Serbian Tribology Society

SERBIATRIB '11

12th International Conference on Tribology

Faculty of Mechanical Engineering in Kragujevac

Kragujevac, Serbia, 11 – 13 May 2011

PROGNOSTIC OF TRIBOLOGY PROCESSES IN HYDRAULIC EQUIPMENT

Ivan Mačužić[1], Petar Todorović[1], Uroš Proso[1], Marko Đapan[1], Branislav Jeremić[1]
[1]Faculty of Mechanical Engineering, Kragujevac, Serbia
ivanm@kg.ac.rs; petar@kg.ac.rs; urosproso@kg.ac.rs; djapan@kg.ac.rs; bane@kg.ac.rs

Abstract: *The paper consider possibilities for performing of prognostic for tribology processes in hydraulic equipment. Oil contamination is the biggest threat to hydraulic system as solid particles in hydraulic oil. cause different serious problems. To extend lifespan of hydraulic equipment we used extrapolation procedure of prognostic process to assess remaining time to failure or risk of presence or occurrence of one or more failure modes in the future. This type of procedure can predict the next failure of technical system with significantly accuracy. Experimental tests were performed in laboratory conditions.*

Keywords: *tribology processes, hydraulic equipment, prognostic, extrapolation*

1. INTRODUCTION

When defining a strategy to maintain hydraulic systems we need to take into account their specific characteristics that dictate something modified approach in relation to other mechanical components and systems. Generally, for majority of of modern technical systems there is tendency to shift the focus of activities to the wider introduction of preventive maintenance activities and reduce the share of corrective maintenance. Hydraulic systems use preventive/proactive measures as an extremely important and there is a clear need and a lot of justification that they take dominant position within the defined maintenance strategy.

Introduction of a such approach in hydraulic system maintenance is significantly easier by the fact that the main cause of failure is recognized, clearly defined and described. That applies to all types and forms of contamination in the hydraulic systems that, in all conducted research and analysis, the cause of at least 70% of failures.

The term contamination in hydraulic systems include all processes that lead to temporary or permanent changes of exploitation characteristics of hydraulic oil (in terms of changes in its physical and chemical characteristics, and structural and functional degradation). The most significant contaminants of hydraulic systems are mechanical particles, water and products of oil degradation.

The biggest threat to the hydraulic system is the contamination by solid particles in hydraulic oil. They cause excessive abrasive wear, creating sheets on the surfaces of components, slow motion and could lead to stuck of moving parts. Solid particles can also have the effect of erosion on the valve command edges where disruption of command edge geometry resulted in decreasing of valves function efficiency [1].

Due to the multiple harmful effects on the system, the content of solid particles in the hydraulic oil should be restricted to a certain level. The level of contamination of hydraulic oil is defined by an appropriate standard [2].

2. PROGNOSTICS IN MAINTENANCE

Prognostics is a set of activities aimed at assessing the remaining time to failure for a particular technical system or risk of presence or occurrence of one or more failure modes in the future [3]. In this case, we will take the hydraulic system as a technical system.

Prognostics efficiency can be quite satisfactory for the failure modes that are relatively well-known and repeating time characteristics, followed by progressive degradation of key exploitation characteristics. In cases of failure modes with random and unexpected events, prognostics is a very difficult task with uncertain results.

Defining the Estimated Time To Failure - ETTF is done using the diagnostic parameters which are subject to condition monitoring of technical systems. Results of condition monitoring present a picture of the current condition and its monitoring over a longer period of time its possible to establish a database on condition history of technical system.

Prognostics output is to define the parameter values that determine the starting failure point or aggravation of exploitation characteristics of the system to the limit of its uselessness [3].

Compared to that maximum allowed value, we can define the set of limit values that represent landmarks and guidelines for all future maintenance actions. It's been recommended to define three limits (three levels):

- level of compulsory stops,
- alarm level and
- warning level.

In addition, the level of compulsory stops and the alarm level are often encompassed in practice. Defining these values, or level increasing and decreasing, is done depending on a range of factors such as the characteristics and importance of technical systems, reliability, prognostics, production requirements, efficiency and organization of the maintenance function, the time for delivery of spare parts, etc.

Trend of changing certain failure parameters in the future can be predicted using extrapolation and projection procedures (figure 1).

Extrapolation represents curve adjustment (fitting) of specific failure parameter based on existing known parameter values (the current time and history of the technical system), also represents a relatively simple mathematical procedure.

Projection involves estimating of future parameter value and fitting a curve based on these estimated values. The projection includes mathematical modeling of the parameter behavior and defining the equations that will determine the speed and nature of the change of parameters in time for the defined exploitation conditions of the technical system and set limits for changes influencing factors.

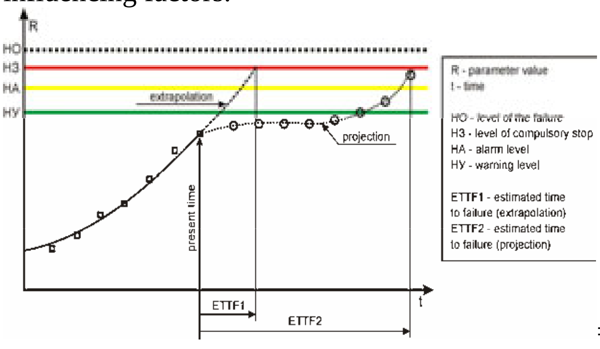

#

Figure 1. Extrapolation and projection in prognostic [15]

Depending on the characteristics of a technical system, failure modes and its parameters, the difference between extrapolated and projected curve can be significant and therefore the difference in the values of the estimated time to failure (ETTF2 - ETTF1). If it is possible to perform projection or to define equations which describes behavior of diagnostic parameters in time, then results of projection is certainly more accurate than the extrapolation ones.

Prognostic can be implemented using one or more parameters of each individual failure modes. Multi-parameter analysis represents simultaneous data display of all parameters in a technical system. This concept has a very important role in prognostic because it enables the overview of mutual correlation and impact parameter and not their separate values.

The main problem with multi-parameter analysis is a way of presenting unified values of different parameters, considering that each parameter has a different unit of measurement and their numerical values can differ. It should also consider that in a number of parameters increasing trend shows deterioration (vibration, temperature, particles in the oil) but there are also those parameters in which zero value represents the failure (pressure or flow in hydraulic systems).

It is necessary to modify the presentation of parameter values where those are projected in the interval from 0 to 100% (regardless of the nature, value and unit of measure) during prognostic. In that case, 0 denotes the initial value of the parameter that corresponds to the new technical system while 100 is the value of the parameter that indicates failure condition.

The parameters that influence the rate of deterioration of failure modes or appearance of new modalities (e.g. load, speed, temperature...) are called influental factors. Each influential factor in general is a symptom of failure modes, but also has an impact on other existing modalities as well as a appearance of new modalities. The parameters that have the characteristics of influential factors must be considered separately, as they may lead to a situation where due to a failure modes with a relative low speed of deterioration occur one or more new failure modes, which have a significantly higher rate of deterioration and lead system to failure in a much shorter time interval.

Initialization of each failure modes should always go back to its cause, which represents a group of parameter values that are the subject of monitornig and defining initial point of the failure modalities, when using multi-parametric analysis techniques. Prognostic accuracy of initialization failure modes depends on whether the techniques used extrapolation or projection to define the trend of change in the value of related parameters in the future (figure 2).

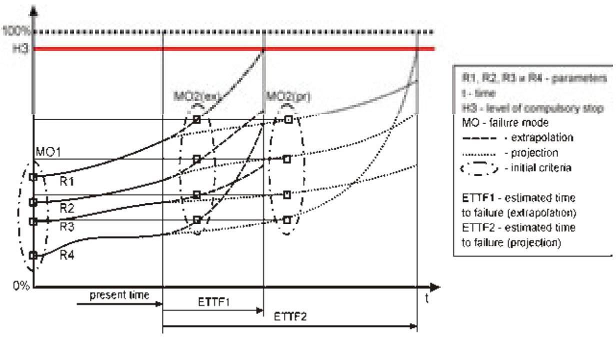

Figure 2. Prognostic of initialization failure modes [3]

The prognostic process involves the implementation of four main phases [4]:

- preparatory activities,
- prognostic of existing failure modes,
- prognostic of future failure modes and
- final activities.

2.1 Prognostic approaches and tools

In the literature, it can be find different proposals for defining the basic approach of prognostic process. Thus, for example in [6] citing [7] or in [4] identified prognostic approaches based on experience, the model or data. Review article [5] also defines three categories of access statistics, model and approach based on the application of artificial intelligence.

Proposed approaches has obvious match and overlap and use different names for, in principle, the same approaches so that the classification proposed in [8] is the most appropriate classification approach to prognostic of future conditions of a technical system:

- prognostic based on the model,
- prognostic based on the measurement results and
- combined approach.

One of modern engineering and mathematical tools that are widely used for prognostic are the different types of artificial neural networks, independently or in combination with using elements of fuzzy logic which are used primarily for prognostic based on the model.

Prognostic based on the measurement results includes the use of various mathematical tools for monitoring and predicting, such as for example, Kalman filter and its simplified version known as alpha-beta-gamma filter (α-β-γ tracking filter).

3. EXPERIMENTAL POSSIBILITY ANALYSIS OF CARRYING OUT THE PROGNOSTIC PROCEDURE

The objective was to simulate tribological processes in the laboratory conditions on the model of tribomechanical system with hydraulic oil. Collected data were used for analysis of possibilities of applying methods and tools for prognostic of condition and evaluate their effectiveness in conditions that simulate the real processes in hydraulic systems. In this sense, extrapolation was performed with polynomial curves of contamination of hydraulic oil at different operating regimes.

3.1 Extrapolation prognostic

Extrapolation curves of oil contamination, in particular case, means the following. Setting a suitable polynomial, based on the known values measured until specific period, we will be able to extrapolate the next value level of contamination. In addition, by placing a tangent to a certain number of points defined by a polynomial we can determine the variation in the rate of trend change, or whether the process is increasing, decreasing or constant. The obtained value of coefficient tangent direction at a point (K) has such a double diagnostic significance and value. Its positive value indicates an increasing trend, the negative decreasing trend while value close to zero indicates trend of constant value.

On the other hand, the coefficient of the tangent line in the final point of extrapolation polynomial multiplied by a time interval in which measurement is performed (cycles, hours, weeks, months) give the expected increase value of the parameter values of contamination in the future.

The next part is an example of the implementation extrapolation process of certain real measurement results of oil contamination in tribological experiments. The curves that are measured continuously (one measurement every 20 seconds) there are many points, and some tests were performed with a reduction in the number of points through which the polynomial is set (every fifth, tenth, twentieth point is taken).

The initial number of points to set the polynomial was three (it is practically possible to set polynomial with two points but the result usually has significant error). After each new measured point, there is redefinition of the polynomial, which practically runs through all points in history of system condition.

Principle of polynomial extrapolation is shown in figure 3.

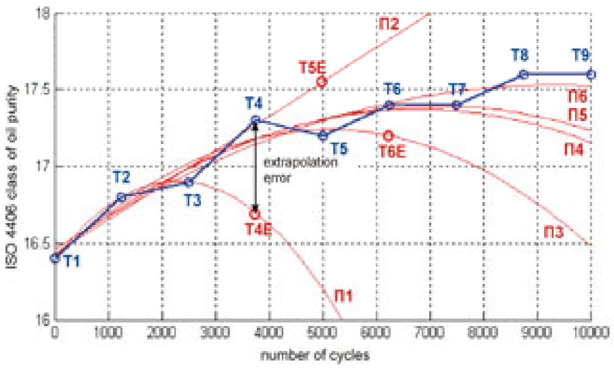

Figure 3. Extrapolation procedure

The first polynomial, P1 runs through the first three points (T1-T3). Based on the values of the polynomial parameters, we can calculate extrapolated value of the next point (T4E). When we measure the real value of that point (T4), it can be calculated extrapolation error in that point.

The procedure continues by running the new polynomial P2 through the points T1 - T4, determine new extrapolated values (T5E) and the new error estimation, and so on.

Example of polynomial extrapolation process for real data obtained by tribological experiment with monitoring of changes in oil contamination level is given on figure 4.

Error of extrapolation process is also calculated and given in separate diagram. It is obvious that for tribological process of continually increased contamination maximal error is less than 0.2 of ISO 4406 contamination code class, which should be examined as fully acceptable.

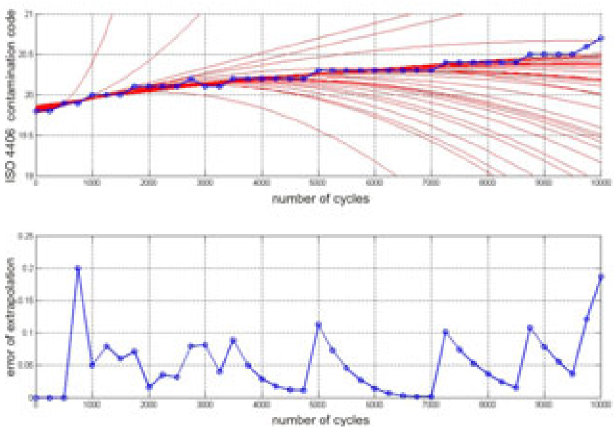

Figure 4. Example of extrapolation procedure

It is obvious that the accuracy of the extrapolation procedure depends on several factors. There are significant differences in the intensity of impact of these factors on extrapolation process as following:

- existence of sudden value jumps and sudden changes in trends,
- value deviations in measured signal,
- integration of the real trend with used extrapolation polynomial profile and
- the number of points through which the extrapolation is done.

4. CONCLUSION

Application of prognostic procedures for tribology processes in hydraulic systems in a term of proactive approach of maintenance has multiple benefits. In addition to the mentioned extension of the exploitation of technical systems, the use of prognostic could lead to reduction of possible level of production failures (breakdowns) and total maintenance cost.

ACKNOWLEDGMENT

Research presented in this paper was supported by Ministry of Science and Technological Development of Republic of Serbia, Grant TR-35021.

REFERENCES

[1] J.C. Fitch: What Particles Mean and Why They Need To Be Monitored and Controlled, in Proceedings of the Reliability Week Conference, September, 1998.

[2] International Standard ISO 4406:1999: Hydraulic fluid power - Fluids - Method for coding the level of contamination by solid particles.

[3] International Standard ISO 13381-1:2004: Condition monitoring and diagnostics of machines – Prognostics -, Part 1: General guidelines, 2004.

[4] D.A. Tobon-Meijia, K. Medjaher, N. Zerhouni: The ISO 13381-1 Standard's Failure Prognostics Process Through an Example, IEEE Prognostics & System Health Management Conference, PHM 2010, Macao, China, 2010.

[5] A.K.S. Jardine, D. Lin, D. Banjevic: A review on machinery diagnostic and prognostic implementing condition based maintenance, Mechanical Systems and Signal Processing, Vol 20, Issue 7, pp.1483-1510, 2006.

[6] K. Medjaher, N. Zerhouni: Residual-based failure prognostic in dynamic systems, 7th IFAC Symposium on Fault Detection, Supervision and Safety of Technical Processes, SAFE PROCESS'09, Barcelona, Spain, 2009.

[7] G. Vachetsavanos, F.L. Lewis, M. Roemer, A. Hess, B. Wu: Inteligent Fault Diagnostic and Prognosis for Engineering Systems, Wiley & Sons, New Jersey, 2006.

[8] J. Lee, J. Ni, D. Djurdjanovic, H. Qiu, H. Liao: Intelligent prognostic tools and e-maintenance, Computers in Industry Vol. 57, Issue 6, pp. 476-489, 2006.

SERBIATRIB '11

Serbian Tribology Society

12th International Conference on Tribology

Faculty of Mechanical Engineering in Kragujevac

Kragujevac, Serbia, 11 – 13 May 2011

INFLUENCE OF FRICTION ON THE FORCE DISTRIBUTION AT CYCLOIDAL SPEED REDUCER

Mirko Blagojević[1], Nenad Marjanović[1], Blaža Stojanović[1], Zorica Đorđević[1], Milorad Kočić[2]
[1]Faculty of Mechanical Engineering in Kragujevac, Serbia, mirkob@kg.ac.rs
[2]Institute Gosa, Smederevska Palanka, Serbia, milorad.kocic@institutgosa.rs

Abstract: *Cycloidal speed reducer belong to the generation of modern planetary gears. Their main features are: high transmission ratio, compact design, long and reliable working life, high efficiency, possibility of accepting big short-term overloads, wide application in various industries,...*
The main element of cycloidal speed reducer is certainly cycloid disc whose profile is equidistant of shortened epitrochoid. Analysis of the forces which act on the cycloid disc when friction is taken into account is presented in this paper. Comparative review of calculated forces in the presence and absence of friction is presented.
The main conclusion arising from the results of of this study are that the phenomenon of friction has an important and unavoidable impact on the load distribution in cycloid speed reducer.

Keywords: *cycloidal speed reducer, cycloid disc, force analysis, friction*

1. INTRODUCTION

Cycloidal speed reducers, have very wild area of application: at conveyors, food machinery, robots, mixers, recycling machines, automotive plants, steel mills, etc. Their main features are: high efficiency, compact design, quite and reliable operation, great gear ratio, minimal vibration, low noise, low backlash, etc. Single-stage cycloidal speed reducer is shown in Figure 1.

M. Lehmann [1] is described the procedure for force distribution at cycloidal speed reducer for theoretical case (when friction don`t exist) in detail. Malhotra [2] is defined some simplified model for force analysis but without friction, too. Distribution of loads at cycloidal speed reducer with modified profile of cycloid disc is presented in papers [3, 4]. Complete geometric and kinematic analysis of cycloid disc tooth profile is described in papers [5, 6, 7]. Gorla, Davoli and other [8] give out the results of theoretical and experimental analysis of cycloidal speed reducer efficiency. Kosse [9] presented the results of experimental study of the hysteresis phenomenon at cycloidal speed reducer and damping properties derived from dickey curves under torsion impact load. Equations for stress, efficiency and moment of inertia of cyclo drives are derived in paper [10]. Stress and strain state at cyclo speed reducer elements is presented in papers [11,12,13]. Meng and other [14] defined a mathematical model of transmission performance of 2K-H pin-cycloid planetary mechanism including the friction.

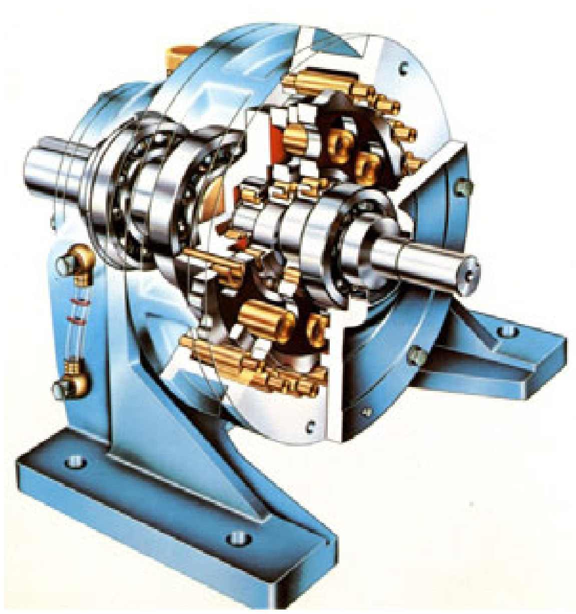

Figure 1. Single-stage cycloidal speed reducer

In this paper is analyzed force distribution at cycloidal speed reducer including the friction.

2. FORCE DISTRIBUTION AT CYCLOIDAL SPEED REDUCER WITHOUT FRICTION

Cycloid disc is the most important element of the cycloidal speed reducer due to its complex geometry and complex stress and strain state. In the first step it is necessary to define forces which act upon it. Cycloid disc with contact elements (housing rollers and output rollers) is shown in Figure 2.

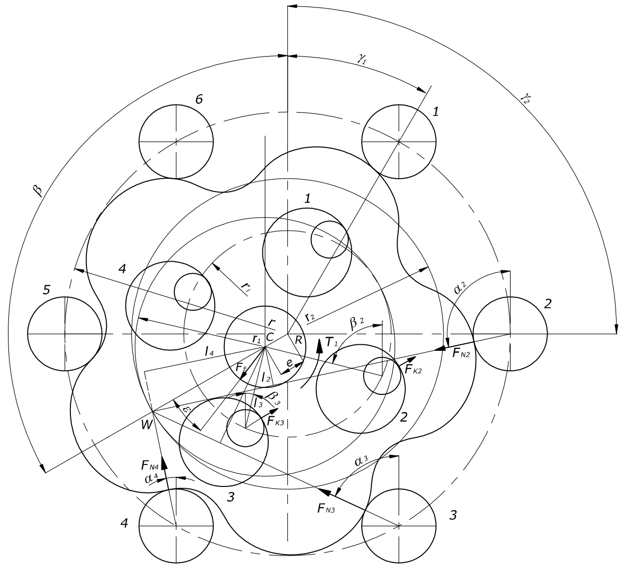

Figure 2. Cycloid disc in contact with housing rollers and output rollers

Forces on cycloid disc are:

F_E – bearing reaction,

F_{Ni} – force between housing roller *i* and cycloid disc,

F_{Kj} – force between output roller *j* and cycloid disc,

T_1 – input torque.

The following equations can be expressed, based on Figure 2:

$$T_1 = F_E\, e \cos(\beta + \varepsilon) \tag{1}$$

$$T_1 = \frac{r_i}{z} \sum_{j=1}^{q} F_{Kj} \sin(\beta_j + \beta) \tag{2}$$

$$-\sum_{i=1}^{p} F_{Ni} \sin\alpha_i + \sum_{j=1}^{q} F_{Kj} \sin\beta - F_E \sin(\beta + \varepsilon) = 0 \tag{3}$$

$$-\sum_{i=1}^{p} F_{Ni} \cos\alpha_i - \sum_{j=1}^{q} F_{Kj} \cos\beta - F_E \cos(\beta + \varepsilon) = 0 \tag{4}$$

$$\sum_{i=1}^{p} F_{Ni}\, l_i - \sum_{j=1}^{q} F_{Kj}\, r_i \sin(\beta_j + \beta) = 0 \tag{5}$$

where:

e – eccentricity,

β – swivel angle of the input shaft,

ε – angle between the force F_E and eccentricity direction,

r_i - radius of output rollers pitch circle,

z - number of teeth of cycloid disk (gearing ratio of the cycloidal speed reducer),

β_j – angular position of the output roller – j ,

α_i – angle which force F_{Ni} makes with vertical,

l_i - lever arm of force F_{Ni},

p - number of the housing rollers that carry the load,

q - number of the output rollers that carry the load.

Values α_i and l_i are calculated according to Figure 2, based on the following expressions:

$$\alpha_i = \operatorname{arctg} \frac{\sin\beta + \frac{r}{r_2}\sin\gamma_i}{\cos\beta - \frac{r}{r_2}\cos\gamma_i} \tag{6}$$

$$l_i = r_1 \sin(\alpha_i - \beta) \tag{7}$$

Angle γ_i (angular position of the housing rollers) is calculated based on the following expression:

$$\gamma_i = \frac{360(2i-1)}{2(z+1)} \tag{8}$$

r - radius of housing rollers pitch circle,

r_1 - base circle radius of the cycloid disc,

r_2 - base circle radius of the housing rollers.

Forces F_{Ni} and F_{Kj} are proportional to their respective distances from the centre of rotation:

$$\frac{F_{Ni}}{l_i} = const. \tag{9}$$

$$\frac{F_{Kj}}{\sin(\beta_j + \beta)} = const. \tag{10}$$

Only for ideal (theoretical) case all cycloid disk teeth are in contact with appropriate rollers and half of them carry load. In reality, cycloidal speed reducer has machining tolerances due to which number of teeth in contact is lower than in ideal case, that is, the load per one tooth is increased.

3. FORCE DISTRIBUTION AT CYCLOIDAL SPEED REDUCER WITH FRICTION

Influence of friction on load distribution at real gear drives is very important. It is the same at cycloidal speed reducer. There are three main areas where friction exist:

- in contact of cycloid disc and central bearing rollers,
- in contact of cycloid disc and output rollers and
- in contact of cycloid disc and stationary ring gear rollers.

Model with friction in contact of cycloid disc and stationary ring gear rollers is analyzed in this paper. Friction in other areas is neglected.

Cycloid disc in contact with output rollers and stationary ring gear rollers (housing rollers) in the presence of friction is presented in Figure 3.

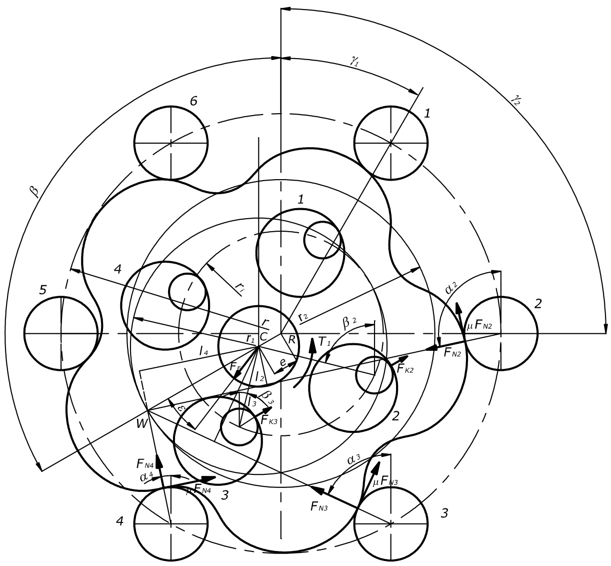

Figure 3. Cycloid disc in contact with housing rollers and output rollers in the presence of friction

The following equations can be expressed, based on Figure 3:

$$-\sum_{i=1}^{p} F_{\mathrm{Ni}} \sin\alpha_{\mathrm{i}} + \sum_{j=1}^{q} F_{\mathrm{Kj}} \sin\beta - F_{\mathrm{E}} \sin(\beta+\varepsilon) - \\ -\mu \sum_{i=1}^{p} F_{\mathrm{Ni}} \cos\alpha_{\mathrm{i}} = 0 \quad (11)$$

$$-\sum_{i=1}^{p} F_{\mathrm{Ni}} \cos\alpha_{\mathrm{i}} - \sum_{j=1}^{q} F_{\mathrm{Kj}} \cos\beta - F_{\mathrm{E}} \cos(\beta+\varepsilon) + \\ +\mu \sum_{i=1}^{p} F_{\mathrm{Ni}} \sin\alpha_{\mathrm{i}} = 0 \quad (12)$$

$$\sum_{i=1}^{p} F_{\mathrm{Ni}}\, l_{\mathrm{i}} - \sum_{j=1}^{q} F_{\mathrm{Kj}}\, r_{\mathrm{i}} \sin(\beta_{\mathrm{j}}+\beta) - \mu \sum_{i=1}^{p} F_{\mathrm{Ni}}\, a_{\mathrm{i}} = 0 \quad (13)$$

where:

μ – coefficient of friction.

Values a_{i} are calculated according to Figure 3, based on the following expression:

$$a_{\mathrm{i}} = r_1 \cos(\alpha_{\mathrm{i}} - \beta) \quad (14)$$

4. ANALYSIS OF THE INFLUENCE OF FRICTION FORCE ON LOAD DISTRIBUTION FOR CONCRETE CYCLOIDAL SPEED REDUCER

Analysis of the influence of the friction force on load distribution was done for concrete one-stage cycloidal speed reducer with next characteristics:

Input power: $P = 1{,}1\,\mathrm{kW}$

Input rpm: $n = 1410\,\mathrm{min}^{-1}$

Gear ratio (number of cycloid disc teeth): $u = 5$ ($z_1 = 5$)

input torque: $T_1 = 3{,}725\,\mathrm{Nm}$

The most critical case of meshing is analyzed in this paper – single meshing.

Based on equations presented in this paper (1-14), calculation of contact force was done. There are four cases: no friction, coefficient of friction $\mu = 0{,}05$; coefficient of friction $\mu = 0{,}1$; coefficient of friction $\mu = 0{,}2$. Results of these calculation are presented in Table 1.

Table 1. Values of contact force

	Contact force F_{N}, N
Without friction	1750
$\mu = 0{,}05$	2109
$\mu = 0{,}1$	2653
$\mu = 0{,}2$	5478

The same results are presented on Figure 4, too.

Based on contact force values for different coefficient of friction (Table 1 and Figure 4), it is clear to see that friction is very important for load distribution at cycloidal speed reducer. With increasing of coefficient of friction, contact force increase, too.

For the real influence of friction on the load distribution it is necessary to take into account and friction between cycloid disc and central bearing rollers and cycloid disc and output rollers.

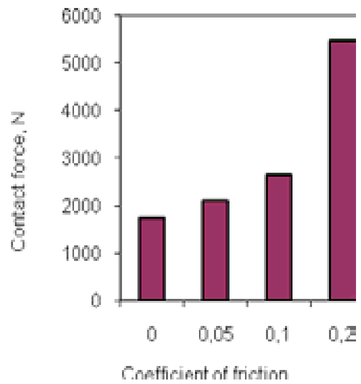

Figure 4. Influence of coefficient of friction on contact force

Taking into account the real lubrication conditions at cycloidal speed reducer, it can be considered that real value of coefficient of friction is $\mu = 0,05$. Further, it means that increasing of contact force for single meshing when friction exist is about 20%.

5. CONCLUSION

Regardless of good lubrication conditions, influence of friction on load distribution is very important. Analytical model for calculating of forces when friction exist is developed in this paper. Friction between cycloid disc and ring gear rollers was analyzed, while friction in other areas was neglected. Some expressions for calculating of contact forces were defined, too.

Calculating of contact force for the most critical case – single meshing for concrete one stage cycloidal speed reducer was done, too. Coefficient of friction is varied in interval 0 to 0,2. The results indicate the occurrence of increasing of contact force with increasing of coefficient of friction.

In the next investigations, it will be interesting to take into account the friction in all areas. It would be very interesting to do the stress and strain analysis with the newly obtained contact forces values.

REFERENCES

[1] M. Lehmann: Calculation and measurement of forces acting on cycloidal speed reducer (in German), PhD Thesis, Technical University Munich, Germany, 1976.

[2] S.K. Malhotra, M.A. Parameswaran: Analysis of a cycloidal speed reducer, Mechanism and Machine Theory, Vol.18, No 6, pp. 491-499, 1983.

[3] L. Lixing, L. Xin, H. Weidong, Q. Yuanmei: Profile modification and accurate force analysis on cycloid drive, in: 4th World Congress on Gearing and Power Transmission, 1999, Paris, France, Vol. 3, pp. 1141-1146.

[4] M. Chmurawa, A. Lokiec: Distribution of loads in cycloidal planetary gear (CYCLO) including modification of equidistant, in: 16th Europian ADAMS user conference, Berchtesgaden, Germany, 2001.

[5] B.K. Chen, T.T. Fang, C.Y. Li, S.Y.Wang: Gear geometry of cycloid drives, Science in China Series E: Technological Sciences, Vol. 51, No. 5, pp. 598-610, 2008.

[6] Y.W. Hwang, C.F. Hsieh: Geometry design and analysis for trochoidal-type speed reducers: with conjugate envelopes, Transactions of the CSME/de la SCGM, Vol. 30, No. 2, pp. 261-278, 2006.

[7] C. Chen, X. Zhang, J. Angeles: Kinematic and geometric analysis of a pure-rolling epicyclic train, Journal of Mechanical Design (ASME), Vol. 129, pp. 852-857, 2007.

[8] C. Gorla, P. Davoli, F. Rosa, C. Longoni, F. Chiozzi, A. Samarani: Theoretical and experimental analysis of a cycloidal speed reducer, Journal of Mechanical Design (ASME), Vol. 130, pp. 112604-1-112604-8, 2008.

[9] V. Kosse: Using hysteresis loop and torsional shock loading to asses damping and efficiency of cyclo drives, 14th International Congress on Sound and Vibration, 9-12. July, 2007, Cairns, Australia.

[10] J. Sensiger: Unified Approach to Cycloid Drive Profile, Stress, and Efficiency Optimization, Journal of Mechanical Design (ASME), Vol. 132, pp. 024502-1-024502-5, 2010.

[11] M. Blagojevic, N. Marjanovic: The force distribution on two stage cyclo speed reducer with new concept, in: 9th International Conference on Accomplishements in Electrical and Mechanical Engineering and Information Technology, Banja Luka, pp. 51-56, 2007.

[12] M. Blagojevic: Stress and strain state of cyclo speed reducer`s elements under dynamic loads, PhD Thesis, Faculty of Mechanical Engineering Kragujevac, Serbia, 2008.

[13] M. Blagojevic, V. Nikolic, N. Marjanovic, Lj. Veljovic: Analysis of cycloid drive dynamic behavior, Scientific Technical Review, Vol.LIX, No. 1, pp. 52-56, 2009.

[14] Y. Meng, C. Wu, L. Ling: Methematical modelling of the transmission performance of 2K-H pin cycloid planetary mechanism, Mechanism and Machine Theory, Vol. 42, pp. 776-790, 2007.

Serbian Tribology Society

SERBIATRIB '11

12th International Conference on Tribology

Faculty of Mechanical Engineering in Kragujevac

Kragujevac, Serbia, 11 – 13 May 2011

GRAPHICS WHICH CONNECT BASIC ROUGHNESS PARAMETERS IN FINISH TURNING FOR TWO KIND OF STEEL

Sava St. Sekulic[1], Nemanja Tasic[1], Branislav Bogojevic[1]

[1]Department of Industrial Engineering and Management, Faculty of Technical Sciences, University of Novi Sad, Serbia, bane.bogojevic@gmail.com

Abstract: *The relationship between individual roughness parameters of a machined surface is approximately given by tables. More accurate relationships between maximal roughness height and mean aritmetic deviation of the profile from mean line and bearing ratio mean aritmetic deviation of the profile from mean line in exponential and linear form are also given. Expremental results were processed, for statistical valid sample N = 78 > 50, pointed strong correlation between roughness parameters.Combined graphics between all three parameters based on previous models are given, in the paper.*

Keywords: *Roughness, Maximal roughness, Mean roughness, Bearing ratio.*

1. INTRODUCTION

Relationship between particular parameters of roughness is given very often in simplified form. Independent of kind of process and work piece material, and another conditions which follow the process.

For example relationship between the maximal roughness height and arithmetic deviation of the profile feom the mean line, i.e. their numerical values, is given in the table (German standard DIN 4767/70) and relationship of the mean height is ten points and the aritmetic deviation of the profile from the mean line according to Yugoslav JUS M.A1.020/79, with a remark on the approximation.

Relationship between maximal height of the roughness and the mean arithmetic deviation of the profile from the mean line $R_{max} = f(R_a)$, in exponential form.

$$R_{max} = 6{,}1595\, R_a^{\;0{,}98}$$

is given independent on the conditions which follow the process. However, that the exponent in the last equation is approximatly one, it can be concluded that, between maximal roughness height and mean arithmetic deviation of the profile, there is a proportionality, i.e.

$$R_{max} = 6{,}16\, R_a$$

The correlation between bearing ratio and mean roughness height, for finish turning for a statistically valid sample, in exponential

$$R_{max} = B\, R_a^{\;a}$$

$$p_n = B\, R_a^{\;a}$$

and linear form

$$R_{max} = aR_a + b$$

$$p_n = B\, R_a^{\;a}$$

have been used, in this paper.

2. EXPERIMENTAL INVESTIGATION

The material of the work pieces was: 1. constructional steel C.0645 (JUS) (DIN St60). According to JUS standard, the chemical composition is provided as follows: 0,43% C, 0,29% Si, 0,79% Mn, 0,015% P and 0,001% S, and mechanical charasteristics: tensile strenght of material σ_m = 740 N/mm^2 yield strenght σ_v = 360 N/mm^2 and elongation δ_5 = 17%, 2. constructional steel for the improvement C.4732 (JUS) (DIN 22CrMo4). Chemical composition: 0,42% C, 0,27% Si, 0, 63% Mn, 11% Cr, 0,16 % Mo, 12% P and 0,010 S. Mechanical charasteristics: tensile strenght of material σ_m = 680 N/mm^2.

The experiments were performed on the universal lathe "Potisje – Morando" PA21, motor power 10kW and number of spindle revolutions from 20 to 2000 rev/min. As a cutting tool the cutter for finish turning JUS K.C1.052/65 (ISO 3), holder cross sectional area 12x20 mm^2, with insert A10 (JUS K.C1.006), back rake angle $\gamma = 12^o$ and noes radius r = 0,5 , 0,9 and 1,6mm, was used.

The roughness parameters were measured using the Perth-O-Meter, type "Universal".

For the purpose of giving providing enough reliable relationships between varialbe values for both of investigated materials, the statistically valid sample of N = 78 > 50, are taken.

Standard data processing, using the least squere method next relationships

$$R_{max} = AR_a{}^{b} \qquad p_n = aR_a{}^{b}$$

$$R_{max} = CR_a + D \qquad p_n = cR_a{}^{d}$$

i.e., for steel C.0645

$$R_{max} = 6{,}16320 \qquad R_a{}^{0{,}93606} \qquad (r=0{,}92)$$

$$R_{max} = 5{,}1968\ R_a + 2{,}\ 3992 \qquad (r=0{,}88)$$

$$p_n = 145{,}5030\ R_a{}^{-0{,}58961} \qquad (r=0{,}92)$$

$$p_n = -\ 7{,}2778\ R_a + 106{,}1370 \qquad (r=0{,}90)$$

steel C.4732

$$R_{max} = 5{,}87092R_a{}^{0{,}96249} \qquad (r=0{,}96)$$

$$R_{max} = 5{,}1928\ R_a + 2{,}0800 \qquad (r=0{,}88)$$

$$p_n = 149{,}0265\ R_a{}^{-0{,}5578} \qquad (r=0{,}93)$$

$$p_n = -\ 7{,}50003\ R_a + 109{,}0871 \qquad (r=95)$$

are given.

By them we have high correlations coefficient. Combining Figure 1. and Figure 2., so to coner scale R_a, graphics which connect all three parameters R_{max}, R_a, p_n, Figure 3., are given. So, if the one roughness parameter is known we can determine another two.

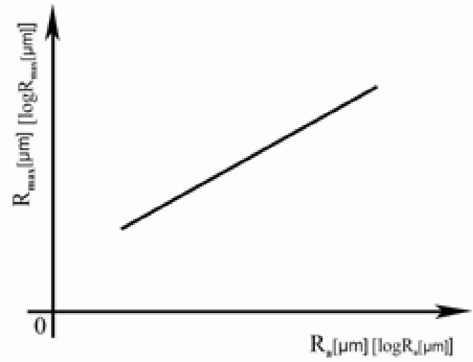

Fig. 1

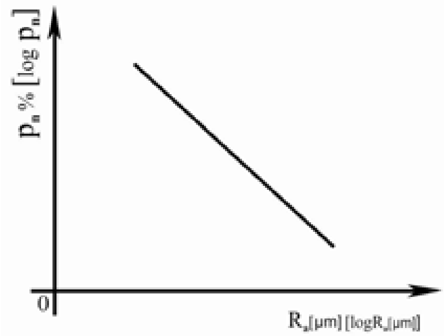

Fig. 2

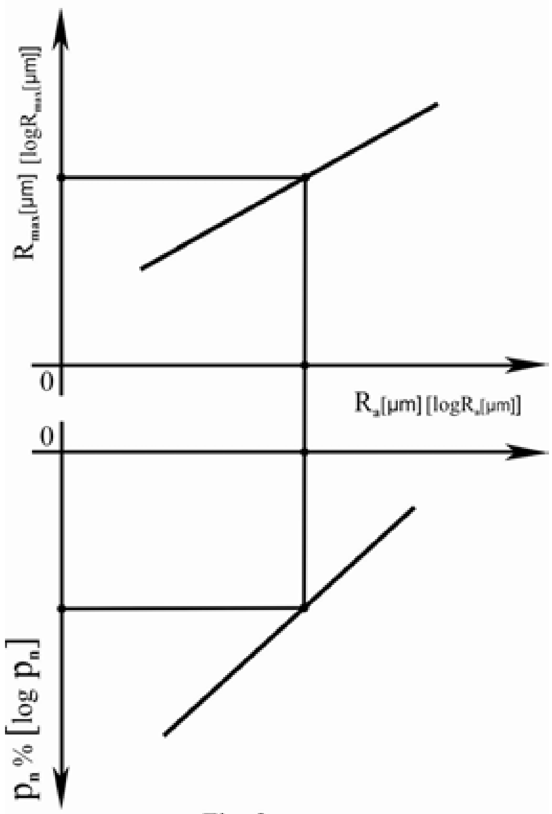

Fig. 3

For the previously work pieces of two materials, we have on Figure 4. to Figure 7. graphics in exponential and linear coordinates.

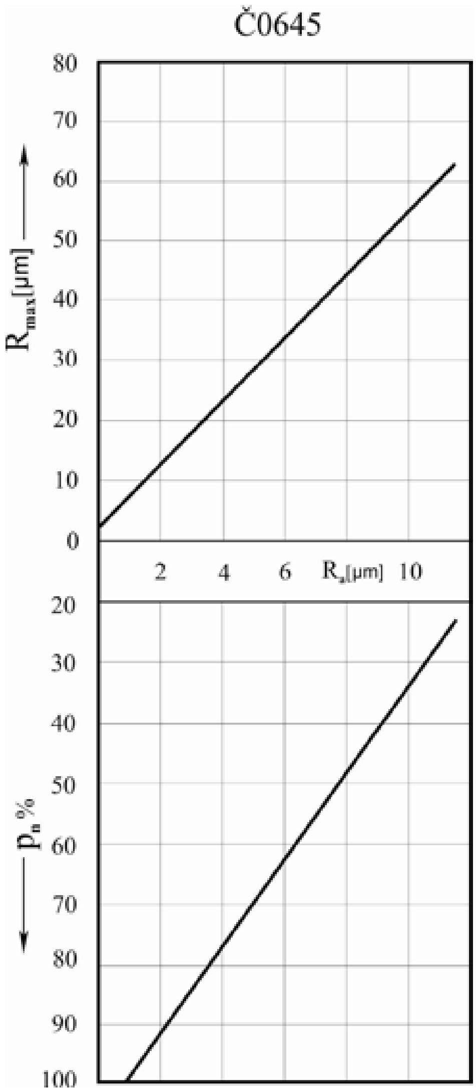

Figure 4

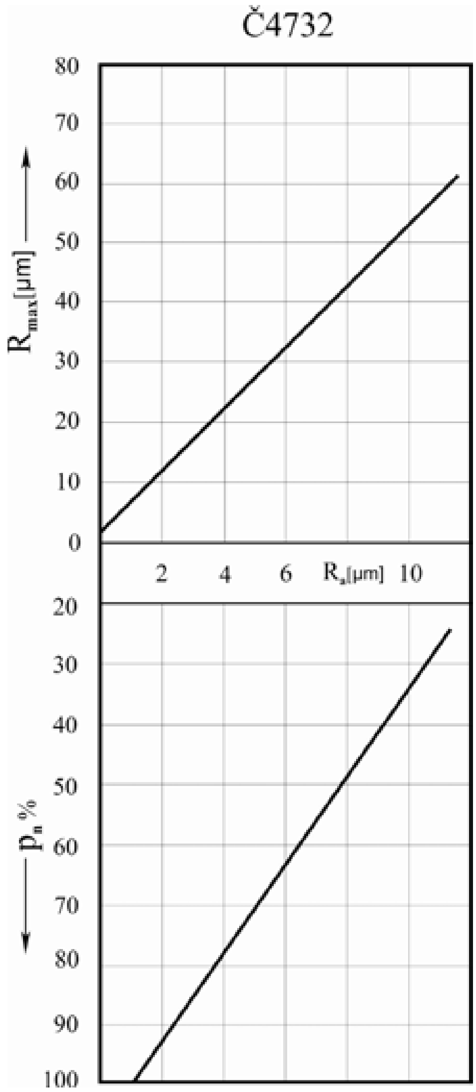

Figure 6

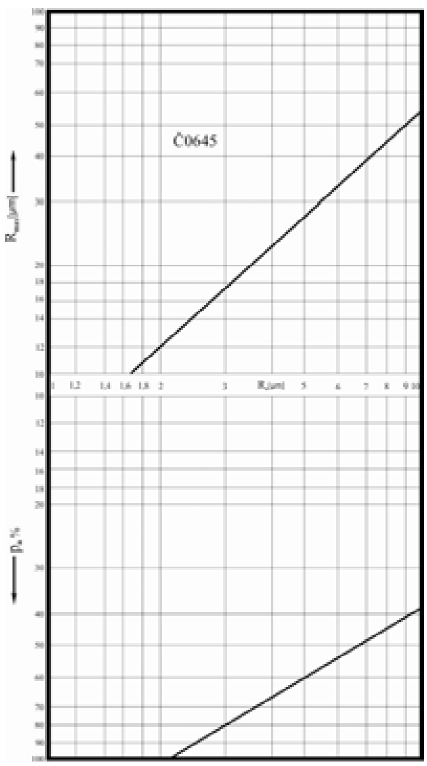

Figure 5

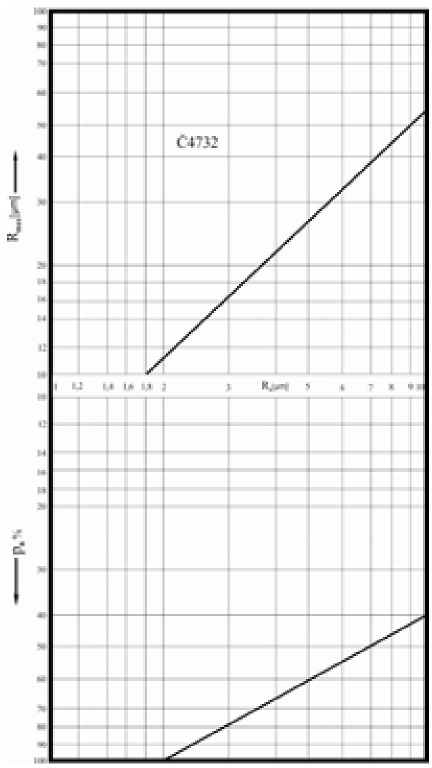

Figure 7

3. CONCLUSION

Refering to the above mentioned we conclude:

- combine graphics which connect all three roughness parameters if one of them is known that other two can be directly easy determined.
- graphics in exponential and linear form can be equaly used, but linear is more appropriate.

REFERENCES

[1] Dyachenko, P.E., and all., About elaboration International standard of machined surface roughness Surface Quality machine elements, Papers of Seminar of the surface quality Proceedings A, Edition AN SSSR Moscow, 1959. (in Russian)

[2] Sekulic, S., Kovac, P., Correlation between the maximal roughness height and aritmetic deviation of the profile from the mean line of machined surface in finish turning, Tribology in Industry, vol. VIII, No.1, 1986. (in Serbian)

[3] Sekulic, S., Kovac, P., Correlation between bearing ratio and mean aritmetic deviation of profile from mean line of machined surface. Proceedings International Conference on Advanced Manufacturing and Technology – AMST 187, October, 1987., Opatia (in Serbian)

[4] Sekulic, S. Correlation between the maximal roughness height and aritmetic deviation of the profile from the mean line of machined surface in finish turning, Abstracts of the papers of the World Tribology Congress, London, September, 1997., p.791.

[5] Sekulic, S., Correlation between some roughness parameters of the machined surface in finish turning, Proceedings of the conference: Situation and Perspective of Research and Development in Chemical and Mechanical Industry, Book 1: Mechanical Engineering, 22-24, 10, 2001, Krusevac, pp. 364-369.

[6] Sekulic, S., Correlation between roughness parameters of the machined surface in finish turning in Proceedings VIII International Symposium INTERTRIBO 2002, 14-17, 10, 2002, Stara Lesna – Tatarska Lomnica, 2002, pp. 85-88.

Serbian Tribology Society

SERBIATRIB '11

12th International Conference on Tribology

Faculty of Mechanical Engineering in Kragujevac

Kragujevac, Serbia, 11 – 13 May 2011

ABOUT THE INFLUENCE OF FRICTION COEFFICIENT ON HEAT GENERATION DURING FRICTION STIR WELDING

Miroslav Mijajlović[1], Dušan Stamenković[1], Miroslav Đurđanović[1], Dragan Milčić[1]
[1] Faculty of Mechanical Engineering Niš, Serbia
mijajlom@masfak.ni.ac.rs; dusans@masfak.ni.ac.rs; djurdjan@junis.ni.ac.rs; milcic@masfak.ni.ac.rs

Abstract: *Friction Stir Welding uses mechanical energy and heat as welding process's activation energy. Mechanical energy is given to the welding tool by welding machine and great portion of that energy is consumed in heat generation on or near the contact between welding tool and base metal. Many studies on FSW processes imply duality of generated heat appearance: it is a direct product of sliding and sticking processes that happen during FSW. Moreover, it is shown that frictional processes dominate in all processes included in heat generation. Almost 20 years after first application of FSW, friction remains unclear and hard to explain tribological phenomenon. Serious studies on FSW point out the necessity of friction demystification as a need for heat generation explanation. Paper gives brief state of the art analysis on influence of friction to the FSW, especially on heat generation process. Numerous studies propose contact and boundary conditions of processes that appear during FSW but very few loudly propose explanations of frictional processes. Since heat and friction are depending and changing one from another, paper will give ideas and experimental researches that show the dependency of heat and friction and might help in further work on heat generation explanation.*

Keywords: *Friction Stir Welding, Friction Coefficient, Heat Generation*

1. INTRODUCTION

As a solid state welding procedure, Friction Stir Welding (FSW) [1] uses pure mechanical energy as welding process activation energy and distributes it from the welding machine to the base material (welding plates) over a specialized, profiled welding tool. However, only one part of the mechanical energy is used directly as a mechanical energy while the rest of it is transformed in other types of energy: into heat, light, electricity, radiation etc. Researches, experience and engineering practice have shown that, as a result of any kind of energy transformation, direct or indirect product of energy use is transformation of input energy into heat, partially or almost completely. This is a phenomenon that appears during the FSW process as well: mechanical energy given to the welding tool is dominantly transforming into the heat, some of it stays mechanical and the rest of it is transformed in other types of energy (Figure 1).

Transformation of power happens on the intimate contact between welding tool and welding plates or in a thin layer of the softer material (in this case it is the material of welding plates).

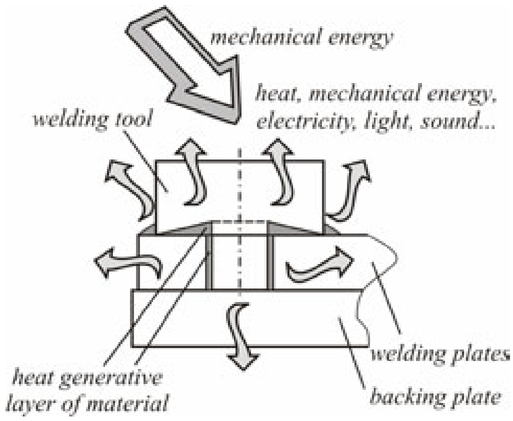

Figure 1. Power transformation during FSW

Recognizing the fact that almost all mechanical power given to the welding process (input power) transforms into the heat[1], also assuming:

[1] The common phrase that explains transformation of the mechanical power into heat is "heat generation".

- heat generated by rotation of the welding tool (Q_{rot}) is far greater than the heat generated by translation of the welding tool (Q_{tran}) and translation heat is equal to the $Q_{tran} \approx 0$ W,
- contact condition between welding tool and welding plates can be defined as pure adhesion, pure deformation and partial adhesion – deformation[2],

Colegrove [2] and Schmidt [3] have proposed equations for estimation of generated heat on a contact surface of the welding tool, influenced by rotation, $Q_{surf,\,rot}$:

$$Q_{surf,rot} = \omega \cdot S_{surf} \cdot \tau_{contact}, \tag{1}$$

where:
ω [rad/s] – angular speed of the welding tool,
S_{surf} [m^3] – voluminous constituent of the generated heat, dependable from the shape of the contact surface (probe tip, probe side, shoulder tip, basic active surfaces on the FSW welding tool [4]), For example, voluminous constituent of the generated heat for the probe tip – *pt* (Figure 4) surface of the welding tool [4] can be defined as:

$$S_{pt} = \frac{2}{3} \cdot \pi \cdot \left(\frac{d}{2}\right)^3, \tag{2}$$

d [m] – diameter of the probe on the welding tool [4], and
$\tau_{contact}$ [N/m^2] – shear stress on contact between welding tool's surface and welding plates.

Angular speed of the welding tool ω and voluminous constituent of the generated heat S_{surf} are pure technological and geometrical parameters of the FSW process and their influence on amount of the generated heat is not so complicated to explain: the greater values of ω and S_{surf} are, the greater value of the generated heat $Q_{surf,\ rot}$ is. However, there is indirect influence of these parameters on other parameters that involve heat generation. Tribological parameter of the generated heat, defined as shear stress on contact between welding tool and welding plate $\tau_{contact}$ is, in fact, describing the true nature of the generated heat by describing the contact condition.

2. CONTACT CONDITION

While rotating and moving along the joint line in the welding phase of FSW [4] welding tool induces contact pressure and contact shear stress in the layer of welding plates [2, 4]. Based on assumed dual nature of the contact condition (adhesion – deformation what is terminologically equal to sliding – sticking), contact shear stress can be estimated as:

$$\tau_{contact} = \begin{cases} \mu(t, p, T, \omega...) \cdot p_m(t) & \text{- sliding} \\ \tau_{yield}(T, \varepsilon) = \dfrac{\sigma_{yield}(T, \varepsilon)}{\sqrt{3}} & \text{- sticking} \end{cases} \tag{3}$$

where:
μ (t, p, T, ω …) = μ – friction coefficient on the contact of the welding tool's surface and welding plates,
t [s] – time,
p [N/m^2] – contact pressure,
T [°C] – temperature,
p_m (t) [N/m^2] – time dependent median contact pressure,
τ_{yield} (T, ε) [N/m^2] – temperature and strain dependent yield shear strength of welding plates,
ε [-] – strain rate,
σ_{yield} (T, ε) [N/m^2] – temperature and strain dependent yield shear strength of welding plates.

This means that heat is generated while welding tool presses and slides over the material of welding plates and while deforms the particles of welding plates; these heat generation processes happen mutually, simultaneously, and dependable one from another.

3. INFLUENCE OF THE FRICTION COEFFICIENT ON HEAT GENERATION

Equation 3 shows that the friction coefficient on contact μ (t, p, T, ω …) influences the contact shear stress $\tau_{contact}$ when pure or partial sliding condition appears. Sliding is a dominant contact mechanism and it is always present in contact problems, when relative movement appears [2, 4]. Basically, friction coefficient is always influencing the contact condition between welding tool and welding plates.

However, relationship between contact condition – friction coefficient – heat generation is not purely one sided nor single parametrically influenced. For example, if some analyze only previously mentioned tribo – parameters (e.g. p, T, ω, $\tau_{contact}$) and neglect all other tribo – parameters (surface hardness, surface roughness, surface corrosion, lubrication, cleanness etc.) that might influence heat generation or friction coefficient, graph of mutual relationships between parameters will get a bit difficult to follow (Figure 2).

For example, following the graph given in Figure 2, and symbolic representation of influences and relationships between parameters[3], S_{surf} is

[2] Also can be found as pure sliding, pure sticking and partial sliding – sticking.

[3] Relationship between parameters ① and ② can be:

directly influencing μ but μ is not influencing S_{surf}; μ is directly influencing p and p is directly influencing μ; μ is directly influencing $\tau_{contact}$ and $\tau_{contact}$ is directly influencing Q_{surf}, *rot, so* μ is indirectly influencing Q_{surf}.

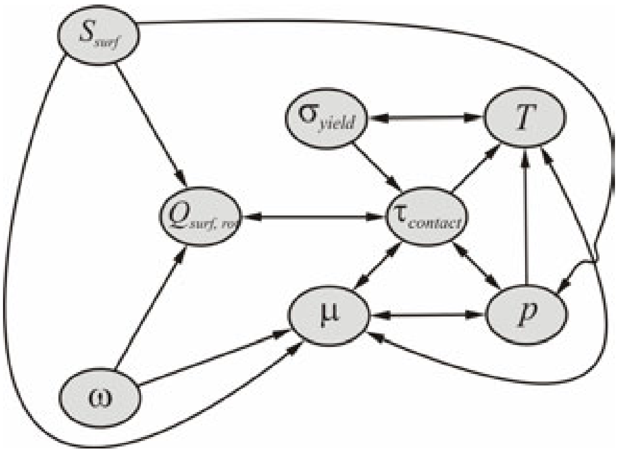

Figure 2. Graph of mutual relationships between some of the tribo – parameters

Analyzing the graph in Figure 2, one can say that friction coefficient μ is directly depending from the most of FSW parameters (technological, geometrical or/and tribological) and indirectly depending from all other (tribological) parameters. This conclusion returns the analysis to the beginning: friction coefficient is a tribological parameter whose value is relatively easy to measure but whose nature is difficult to explain.” [5].

When researchers from TWI [1] patented the Friction Stir Welding as a novel welding procedure they were fully aware of the importance of the “friction” processes / phenomena in application of their patent so they used it for name of the procedure. With such a great number of influencing parameters, with complex relationships between parameters and still present ambiguity of the FSW process itself, friction coefficient in FSW is not at all a value easy to measure and even more hard to explain. Without any doubt, TWI researchers had no idea what a challenge will they make to the FSW researches around the globe with the word “friction” in FSW.

Early researches on the FSW were based on the “try and error” principle and aimed to the optimal geometry of the welding tool retrieval, technological parameters (speed and rotation of the machine) selection and proper materials usage (as well for the welding tool, as well for the welding plates). When usable results were found, researches have extended to the increase of weld’s quality, stress and strain analysis, and material flow, thermal influences on welding plates and welding tools, heat generation during FSW etc. At the beginning, friction coefficient was not of interest in researches. However, when researches aimed into FSW modelling (heat, temperature fields, stress and strain, material flow, residual stresses etc.), friction coefficient became interesting and necessary to be estimated. As one of the pioneers in this area, Schmidt et al [3, 6, 7] has researched analytical thermomechanical model in FSW with a goal to understand material disposal during rotation of the welding tool in a qualitative manner. Friction coefficient was a necessity for the analysis made in ABAQUS / Explicit software used in this work, and authors have used the value of 0.3 for the complete process. In the following works, friction coefficient was mentioned as an important parameter that takes values from 0.3 to 0.4 for the welding phase of the FSW [6]. Results were not confirmed analytically or experimentally – they were predicted due to the experimental setup of conducted experiments [3].

Chen et al. [7] used a theoretical approach on friction coefficient estimation and calculated that the coefficient of friction cannot be greater than 0.577 in FSW. Duffin et al. [9] experimentally determined the friction coefficient exceeds 0.57 during friction welding processes (not FSW), and reported the coefficient of friction to be 1.5, 1.9, 2.1 and 2.7 for the welding of mild steel. Similar results were reported by Reid [10] for the welding of pure copper. Heurtier et al. [11] has modelled material flow around the welding tool and showed thermal history of the flown material with application of the friction coefficient of 0.2 to 0.9. Values of the friction coefficient were assumed.

Numerous authors [6 – 25] have experimentally and analytically worked on problems of heat generation during FSW, thermal modelling, stress distribution, deformation and material flow and they have suggested that friction coefficient in FSW varies from 0.1 to 1.6 dependably on contact pressure, temperature, materials etc. However, none of them has experimentally measured friction coefficient or analytically estimated the value of friction coefficient. Furthermore, no one has suggested that friction coefficient changes its value. All of the mentioned results were assumptions due to the results from similar researches, guesses or analogies with the machining processes – milling, drilling etc.

Summarization of the friction coefficient: it varies from 0.1 to 2.7 in friction welding processes (FSW and other frictional welding processes, for welding of aluminium, steel, copper etc.).

There are only few works that have reported experimental estimation of the friction coefficient.

“①→②” what means: ① is influencing ②, no vice versa effect; “①↔ ②” what means: ① is influencing ② and vice versa, “① ②” what means: no relationship between ① and ②.

Main reasons for such a lack of researches on friction coefficient lays in complexity of the process, difficult measuring task and ambiguity of the process itself.

However, Kumar et al. [26] reported experimentally estimated values of the friction coefficient during plunging and the first dwelling phases of the FSW welding process. Experiment is based on the well known equation for the friction coefficient:

$$\mu = F_t(t)/F_n(t). \tag{4}$$

To determine friction coefficient μ, it is necessary to measure tangential force F_t (t) and normal force F_n (t) = F_z (t) that appear during experiment.

Experimental setup that measures normal and tangential forces applied on the welding tool is given in Figure 3.

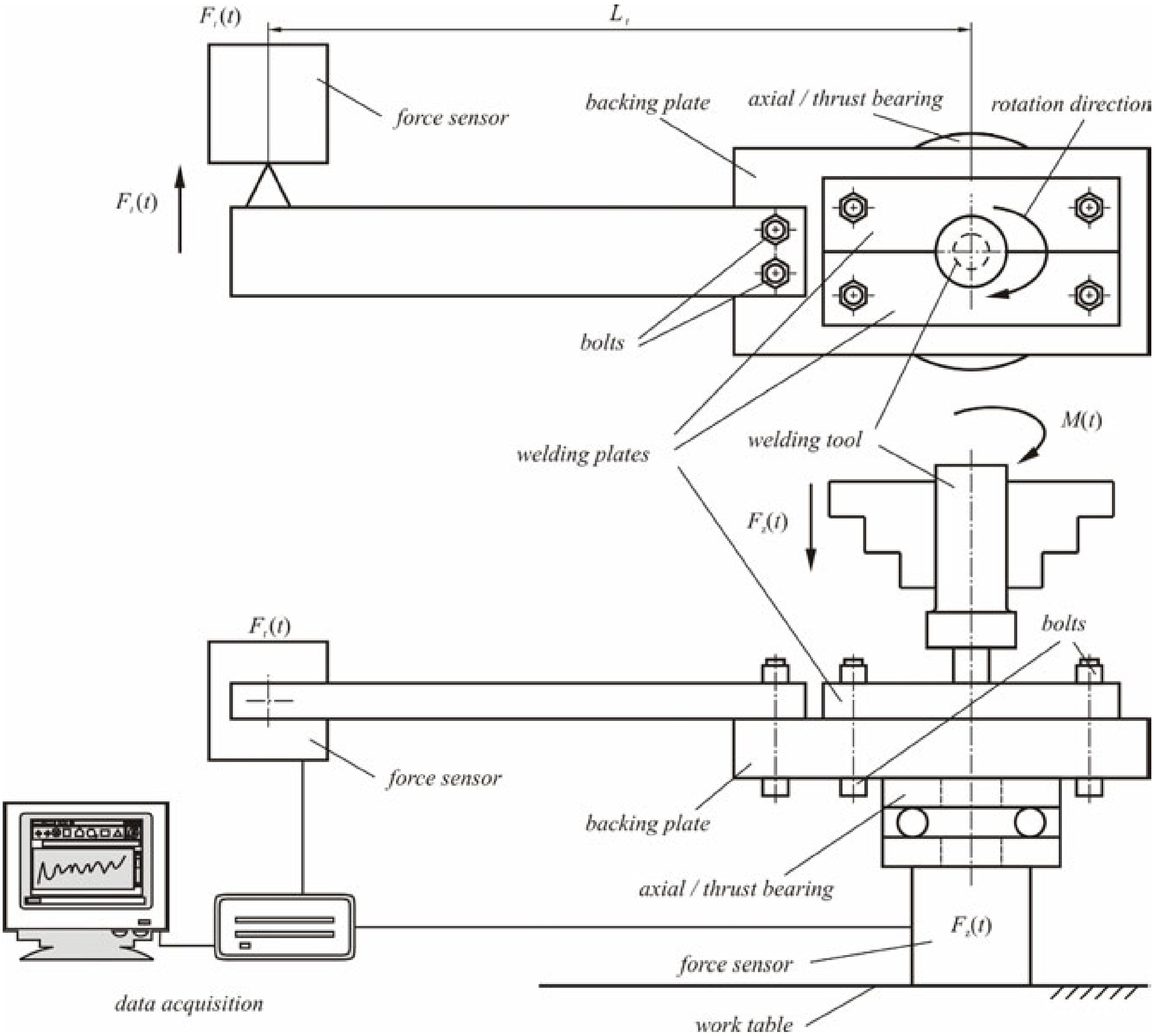

Figure 3. Scheme of the experimental setup for friction coefficient estimation during plunging and first dwelling phases of the FSW process

Following the Equation 4 and analyzing contact mechanics, Galin [27] proposed a dependency between torque M (t), friction coefficient μ and normal force F_z (t) between two solid bodies (semi-rigid punch and elastic half space) in contact:

$$M(t) = \frac{1}{3} \cdot \mu \cdot F_z(t) \cdot d(t) \tag{5}$$

where: d (t) [m] – is diameter of the punch, value dependable on time t and the phase of the FSW process [28]. Transformation of the Equation 5 gives the friction coefficient:

$$\mu = \frac{3 \cdot M(t)}{F_z(t) \cdot d(t)} = \frac{3 \cdot F_t(t) \cdot L_t}{F_z(t) \cdot d(t)}. \tag{6}$$

Kumar has proposed results for a set of conducted experiments where he changed value of contact pressure (normal force), angular rotation of the welding tool and plunging time. Friction coefficient varied from 0.2 to 1.6 (during phases of the FSW and for different technological parameters of the FSW process) [25]. His results are comparable with the results of other presented works.

However, despite the relatively simple construction of monitoring system and excellent results that can be used for further researches Kumar's model has some flaws:

1) it can be used only for the first two phases of the FSW process – plunging and first dwelling phases, due to the rigidity and immovability of the monitoring system;
2) friction coefficient calculated according to the Kumar's model has to be treated as approximate since Galin's equations [27] are usable only for the punch (in this case: probe tip of the welding tool) not for the side of the punch. During these experiments probe side (punch side) is actively involved FSW process and this influences the accuracy of Equations 5 and 6.
3) Kumar's model does not recognize active surfaces of the welding tool [4] nor active surface engagement (ASE, Figure 4) in FSW. Active surfaces of the welding tool are in contact with the welding plates and they generate heat, convey weld, stir and depose material etc. and how much they involve in FSW depends on the ASE. Without concern on the ASE, friction coefficient in FSW by Kumar can be considered only as median value, what is, in most of the cases satisfactory.

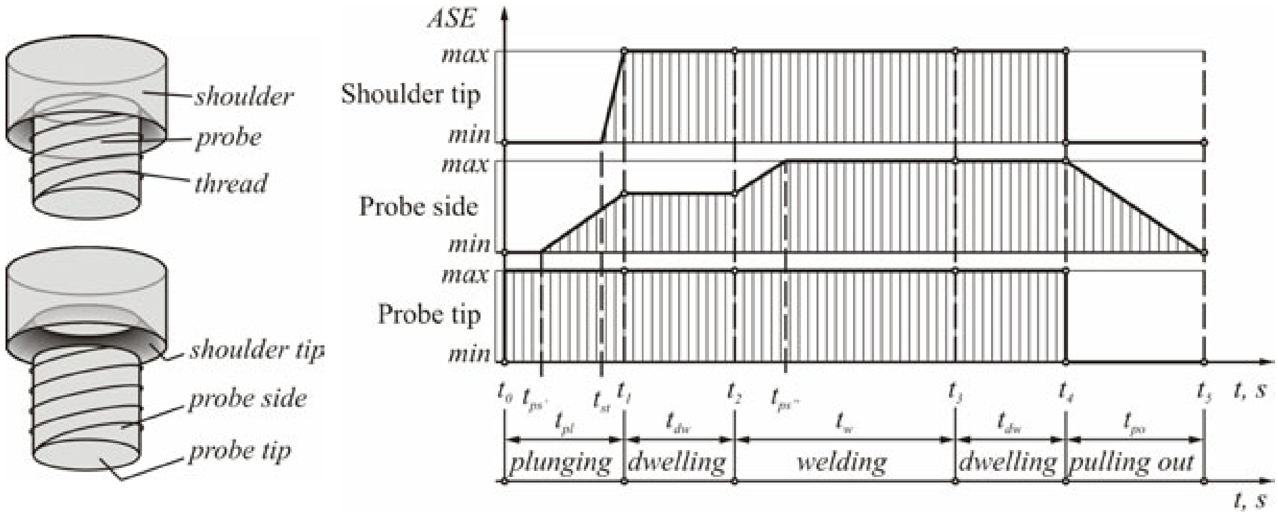

Figure 4. Active surfaces of the welding tool and active surface engagement (ASE) during FSW welding process

4. CONCLUSIONS

Two decades away from the first application of the FSW in industry, friction process stays the least investigated parameter / phenomenon of the FSW process. All published researches about the FSW imply the importance of the friction in every aspect of this welding process's application but do not provide adequate experimental background or mathematical models that will take the influence of the friction (coefficient) in the process of frictional welding. Friction phenomenon or simply – the friction coefficient is considered to be a single value (in most of the researches), mostly from 0.3 to 0.7.

Furthermore, the influence of the friction coefficient to the heat generation process(es) is very poorly investigated or not investigated at all.

Generally speaking, increase of the friction coefficient increases the amount of the generated heat, what implies that mechanical power delivered to the welding tool by machine has to increase. Decrease of the friction coefficient delivers decrease in heat generation and decrease in power consumption during welding process. Problem is simple: friction coefficient is not some technological parameter (such angular rotation is) which can be altered manually / automatically for the purpose of process improvement. So, influence of the friction coefficient on heat generation is in relationship with all other parameters of the FSW and they have to be investigated in depth and mutually.

Understanding the nature of friction coefficient and its relationships with other parameters / phenomena in FSW process is a difficult task and requires in – depth analysis of all parameters that influence friction.

ACKNOWLEDGMENT

The paper presents pre – results of the research project TR35034 – "The research of modern non – conventional technologies: applications in manufacturing companies with the aim to increase efficiency of use, product quality, reduce of costs and save energy and materials". Project is *supported by the Ministry of Science and Technological Development of the Republic of Serbia.*

REFERENCES

[1] Thomas W M et al. 1991 Friction stir butt welding International Patent Application No PCT/GB92/02203; Thomas W M et al. 1995 Friction stir butt welding GB Patent Application No 9125978.8; Thomas W M et al. 1995 Friction stir butt welding UP Patent No 5 460 317.

[2] Colegrove P 2000 2nd Int. Symp. on Friction Stir Welding (Gothenburg, Sweden).

[3] Schmidt H, Hattel J, Wert J: An analytical model for the heat generation in Friction Stir Welding, Modeling Simul. Mater. Sci. Eng. 12 No 1 (January 2004) p. 143-157, PII: S0965-0393(04)69225-4.

[4] Đurđanović. M., Mijajlović, M., Milčić, D., Stamenković, D.: Heat generation during friction stir welding process. SERBIATRIB '09, 11th International Conference on Tribology, Beograd, 13-15 May 2009, pp. 135-140.

[5] Bowden, F.P. and Tabor, D. Friction – An Introduction to Tribology, Anchor Press / Doubleday, Reprinted 1982, Krieger Publishing Co., Malabar 1973.

[6] H. Schmidt, J. Hattel: A local model for the thermomechanical conditions in friction stir welding, Modelling Simul. Mater. Sci. Eng. 13 (2005) 77–93.

[7] H. Schmidt, J. Hattel: Thermal modeling of friction stir welding, Scripta Materialia, Volume 58, Issue 5, Pages 332-337, 2008.

[8] Chen, Z.; Thomson, P.F. Wear 1996, 201, 221–232.

[9] Duffin, F.D.; Bahrani, A.S. Wear 1973, 26, 53–74.

[10] Reid, J.V.; Schey, J.A. Adhesion of copper alloys. Wear 1985, 104, 1–20.

[11] Heurtier P., Jones M.J., Desrayaud C., Driver, J.H. Montheillet F., Allehaux D.: Mechanical and thermal modelling of Friction Stir Welding, Journal of Materials Processing Technology 171 (2006) 348–357.

[12] Chen, C. M.; Kovacevic, R. Finite element modeling of friction stir welding - thermal and thermomechanical analysis, Int. J. Mach. Tool. Manu., v.43, p.1319-1326, 2003.

[13] Ulysse, P. Three-dimensional modeling of the friction stir-welding process, Int. J. Mach. Tool. Manu., v.42, p.1549-1557, 2002.

[14] Colegrove, P.A.; Sherclif, H. R. 3-Dimensional CDF modelling of flow round a threated friction stir welding tool profile, J. Mater. Process. Tech., v.169, p.320-327, 2005.

[15] Nandan, R. et al., Numerical modelling of 3D plastic flow and heat transfer during friction stir welding of stainless steel, Science and Technology of Welding and Joining, v.11, p.526-537, 2006.

[16] Nandan, R. et al., Three-dimensional heat and material flow during friction stir welding of mild steel, Acta Materialia, v.55, p.883-895, 2007.

[17] Song, M.; Kovacevic, R. Thermal modeling of friction stir welding in a moving coordinate system and its validation, Int. J. Mach. Tool. Manu., v.43, p.605-615, 2003.

[18] Santiago, Diego; Urquiza, Santiago; Lombera, Guillermo and Vedia, Luis de. 3D modelling of material flow and temperature in Friction Stir Welding. Soldag. insp. (Impr.) 2009, vol.14, n.3, pp. 248-256.

[19] Gould, J.E.; Feng, Z. Heat flow model for friction stir welding of aluminum alloys, J. Mater. Process. Manu., v.7, 1998.

[20] Chao Y J and Qi X 1999 1st Int. Symp. on Friction Stir Welding (Thousand Oaks, CA, USA).

[21] Frigaard Ø, Grong Ø and Midling O T 2001 Metall. Mater. Trans. A 32 1189–200.

[22] Frigaard Ø, Grong Ø, Bjørneklett B and Midling O T 1999 1st Int. Symp. on Friction Stir Welding (Thousand, Oaks, CA).

[23] Russell M J and Shercliff H R 1999 1st Int. Symp. on Friction Stir Welding (Thousand Oaks, California, USA).

[24] Shercliff H R and Colgerove P A 2002 Math. Modelling Weld. Phenom. 6 927–74, Reynolds A P, Deng X, Seidel T and Xu S 2000 Proc. Joining of Advanced and Specialty Materials (St Louis,, MO, ASM International) pp 172–7.

[25] Xu S, Deng X and Reynolds A P 2001 Sci. Technol. Weld. Joining 6 191–93.

[26] Kumar, K., Kalyan, C., Kaias, Satish V., Srivatsan, T. S., An Investigation of Friction During Friction Stir Welding of Metallic Materials, Materials and Manufacturing Processes, 24:4,438 — 445, 2009.

[27] Galin, L.A.: Contact Problems; The legacy of L.A. Galin, Series: Solid Mechanics and Its Applications, Vol. 155, Galin, L. A., Gladwell, G.M. (Ed.), Original Russian edition published by Nauka, Moscow, Russia, 1953, 1980, 2008, XIV, 318 p., Hardcover, ISBN: 978-1-4020-9042-4.

[28] Mijajlović, M., Milčić D., Stamenković D., Živković, A. :Mathematical Model for Generated Heat Estimation During Plunging Phase of the FSW Process, Journal: Transactions of Famena, Faculty of Mechanical Engineering and Naval Architecture, Zagreb, Croatia, XXXV-1/2011, April 2011.

Serbian Tribology Society

SERBIATRIB '11

12th International Conference on Tribology

Faculty of Mechanical Engineering in Kragujevac

Kragujevac, Serbia, 11 – 13 May 2011

SELECTION OF THE MOST APPROPRIATE TECHNOLOGY OF REPARATORY HARDFACING OF WORKING PARTS ON UNIVERSAL CONSTRUCTION MACHINERY

V. Lazić[1], M. Mutavdžić[2], D. Milosavljević[1], S. Aleksandrović[1], B. Nedeljković[3], P. Marinković[3], R. Čukić[1]

[1)] Faculty of Mechanical Engineering, Kragujevac, Serbia
[2)] Road Company Kragujevac, Kragujevac, Serbia
[3)] Zastava automobiles, Kragujevac, Serbia

Abstract: *The aim of this work is to analyse the possibility to increase the service life of working parts on construction machinery exposed to intensive wear, such as steel blades of the rotary device for roadside vegetation maintenance and grass cutting. A special attention is paid to characteristic working conditions and complex wear mechanisms. In order to select the most appropriate reparation technology, both model and real investigations were conducted. The aim of the model investigations was to select the most appropriate procedure, filler materials and hardfacing technology. Worn cutting edges of the blades were hardfaced and sharpened by grinding to the shape and dimensions of new blades. Then, both new and repaired blades were alternately mounted on the rotor of the machine. Their wear was monitored under the same working and weather conditions. The repaired blades have proven more resistant to wear than the new ones, which is due to better properties of the hardfaced layers.*

Key words: *hardfacing, construction machinery, wear, hardness, microstructure.*

1. INTRODUCTION

Almost all working parts of construction machinery are exposed to complex tribological processes during operation. Sometimes, one type of wear is dominant, but in practice, combined wear is much more common. A typical example of combined wear is seen in blades of the device for roadside vegetation maintenance and grass cutting. These parts are exposed to abrasive, impact and fatigue wear as well as corrosion.

Working parts have relatively short service life, they increase machine downtime, it takes a long time to replace them, they decrease machine utilization rates, etc. However, reparatory hard facing can reduce or eliminate these problems. Hardfacing also offers an opportunity to determine wear resistance of different filler materials.

Our investigations [1-12] and investigations of other authors [13-15] have shown that worn and new parts can be successfully hard-faced. However, both reparatory and production hardfacing can be performed only in specialized facilities with expert staff and adequate equipment.

2. MACHINE AND DEVICE DESCRIPTION

The device for cutting grass and other vegetation is mounted on a universal machine Unimag (Fig. 1). This is a multipurpose vehicle on which thirty-two different devices can be mounted and operated. In addition to grass and vegetation cutting, it can be applied for snow clearing, aggregates spreading, land clearing and levelling, preparing soil or aggregate substrate for concrete or asphalt laying, digging holes in the ground, cutting and removal of trees, load lifting, trench digging for utility installation, etc.

Figure 1. Machine and device for vegetation maintenance and grass cutting

The device for vegetation maintenance is powered by the vehicle. The torque is transferred through the output spline shaft connected to the hydraulic pump and hydro motor, and the device is controlled by hydraulic system. V-belt transmission protects the device allowing some slippage in order to prevent overloading and damages. The number of rotations of the output shafts is in the range from 540 to 1000 min^{-1}.

Forty blades (Fig. 2) are mounted in four rows on the holder of the output spline shaft. The blade mass is 0.30 kg, and all the blades are made of quenched and tempered (Q+T) steel Č4732 (JUS) – 42 CrMo4 (DIN). The connection between the rotary device and blades is mechanical, and blades are mounted on a special holder via screws. Whilst in operation the blades come into contact not only with grass, vegetation and soil, but also with rocks. In order to protect the blades, a protective roller is mounted. It rolls on the ground in front of the working part keeping the device at the same distance from the ground. Behind the working part, there is a curtain that prevents grass, vegetation and aggregates from sticking to the blades, which ensures safety of the vehicle operator and other participants in the traffic.

Figure 2. A new blade for vegetation and grass cutting

3. SELECTION OF THE MOST APPROPRIATE REPARATORY TECHNOLOGY

3.1 Introduction

In order to select the most appropriate reparatory technology, both model and real investigations were conducted. [1-6]. The models, made to be geometrically similar to the real parts, were used for trial hard facing with different filler materials and under different hard facing regimes. From these models, metallographic samples were prepared for hardness measurements, microstructure analysis and tribological investigations of wear resistance. The reparatory technology selected on the models was then applied to the real parts. New and differently hard faced blades were monitored under real working conditions with the aim to compare time in operation and degree of wear between the new and the hard-faced blades and to provide final estimate of justification of reparatory hard facing.

The base material of the blades was Č4732 (JUS) – 42CrMo4 (DIN), while the following filler materials were used for hardfacing: ABRADUR 58, E DUR 600, CrWC 600 and E Mn17Cr13 [1, 2, 4, 18]. Hardfacing of the models and real parts was performed by manual metal arc welding method. Worn blades were hardfaced in three passes to restore the lost - worn part, and then they were sharpened by grinding to restore the shape. The mass of the repaired blades was similar to the mass of new blades.

3.2 Base and filler materials

The spectrographic analysis of the base material revealed that the blades were made of low-alloy quenched and tempered steel Č4732. We used one worn blade to prepare metallographic samples for hardness measurements and microstructure analysis of the base material. The maximum measured hardness was 298 HB, while the microstructure was estimated as an interphase structure of the quenching and tempering. This microstructure is not especially resistant to intensive abrasive wear, so these parts become worn rather quickly [16, 17]. For this reason, we decided to try to extend their service life by hardfacing. Tables 1 and 2 [18, 19] give the chemical composition and the most important mechanical properties of the steel Č4732.

Table 1. The chemical composition and applications of the steel Č4732

B. M.	Chemical composition, %							Application
Č4732	C	Si	Mn	Cr	Mo	P	S	For manufacturing of heavily loaded machine parts after heat treatment
Prescribed	0.38-0.45	0.15-0.40	0.50-0.80	0.90-1.20	0.15-0.30	0.035	0.035	
Analysed	0.45	0.40	0.80	1.20	0.30	0.035	0.035	

Table 2. Mechanical properties and microstructure of the steel Č4732

Notation		Mechanical properties and hardness						Microstructure
JUS	DIN	R_m, MPa	R_{eH}, MPa	A_5, %	Z, %	KV, J	Hardness, HB	Interphase tempered structure (mainly sorbite)
Č4732	42CrMo4	1100-1300	900	10	40	34 (20°C)	298*	

*Measured hardness of the sample after the thermal treatment of the Q+T

The following electrodes were chosen as filler materials: E DUR 600, CrWC 600, ABRADUR 58 and E Mn17Cr13 [1, 2, 4, 18]. Based on the manufacturer's recommendations, hardfaced layers obtained using these electrodes have a high wear resistance, favourable toughness and can endure high impacts during operation. Hardfaced layers can be mechanically treated only by grinding. These electrodes are especially recommended for hardfacing of parts exposed to friction and metal-to-mineral wear, such as bulldozer blades, excavator bucket teeth, excavator shovels, conveyor elements, parts of crushing machines, blades and mixers in processing industry etc. For interlayer welding, a 3.25 mm diameter electrode INOX B 18/8/6 (JUS) - E 188 MnB10+ (DIN) [1-6, 9, 18] was used.

3.3 Estimate of basic material weldability

Due to its content of carbon and alloy elements, steel Č4732 belongs to conditionally weldable steels, which means that it requires a special technology of welding. However, it is possible to improve its weldability by preheating or depositing a plastic austenite interlayer. There are different methods to calculate the preheating temperature based on KH diagrams, but in this case, it was determined using the Seferian formula (Table 3) [2, 11, 13].

Table 3. Determination of the preheating temperature using the Seferian formula

Applied method	Formula	Thickness, s, mm	Preheating temperature, T_p, °C	
			Calculating	Adopted
Seferian formula	$CE = CE_h + CE_s = CE_h \cdot (1 + 0.005 \cdot s)$, % $CE_h = C + \frac{Mn + Cr}{9} + \frac{Ni + 7Mo}{18}$, % $T_p = 350 \cdot \sqrt{CE - 0.25}$, °C	10	≈ 266	≈ 300

Preheating is recommended for hardfacing with filler materials E DUR 600, ABRADUR 58 and CrWC 600, while it is not recommended for hardfacing using the electrode E Mn17Cr13 because this filler material belongs to austenite steels which are well hardfaced on materials with high potential hardness increase. Sometimes expensive preheating can be eliminated by application of interlayer austenite electrodes.

3.4 Model investigations

As mentioned before, we prepared physical models geometrically similar to real parts. The models were made of 10 mm thick low-carbon steel Č0361 (JUS) – S 235 JRG2 (EN 10025). The steel Č4732, of which the blades were made, was not used because Č0361 can be welded without preheating and it provides the same conditions for hardfacing with different filler materials. In this way, hardfaced layers obtained with different filler materials can be compared and analysed. The idea was to use Č0361 for manufacturing of new parts of construction machinery and to hard face the edges with layers resistant to wear [2, 4, 5, 14]. The models were hardfaced by MMA procedure in the laboratory, and technological hardfacing parameters were chosen in compliance with literature recommendations [1-9, 13, 18] (Table 4).

The width of one-pass hardfaced layer was 6.0-10 mm, and its height ranged from 3.0 to 3.2 mm. The way of deposition, the order and number of the deposited layers and the model itself are shown in Figure 3. Prior to each pass, slag was removed with steel brush. The other layers were also deposited in this way (the second - Fig. 3b and the third - Fig. 3c). Figure 3d shows a sample for metallographic and tribological investigations, and Figure 3e shows hardfaced sample models.

Table 4. Technological parameters of the model hardfacing by MMA procedure [2]

Thickness O.M. s, mm	Fiprom-Jesenice electrode	Electrode core diameter, d_e, mm	Hardfacing current, I, A	Working voltage, U, V	Hardfacing speed, v_z, cm/s	Input heat q_l, J/cm	Melting zone depth, mm
10	Sample 1: E DUR 600	3.25	120	25	0.124	19355	2.24-3.73
	Sample 2: CrWC 600	3.25	125	25	0.116	21552	2.36-3.94
	Sample 3: ABRADUR 58	3.25rup	130	25	0.124	20968	2.33-3.88
	Sample 4: E Mn17Cr13	3.25	130	25	0.152	17105	2.10-3.51

Hardness measurements (in direction I-I, Fig. 3d) and analysis of the newly formed structures in the characteristic hardfaced layer zones were performed on metallographic samples shown in Figure 3. The most important results of hardness and microstructure distribution are given in Figures 4, 5, 6 and 7 [1-9].

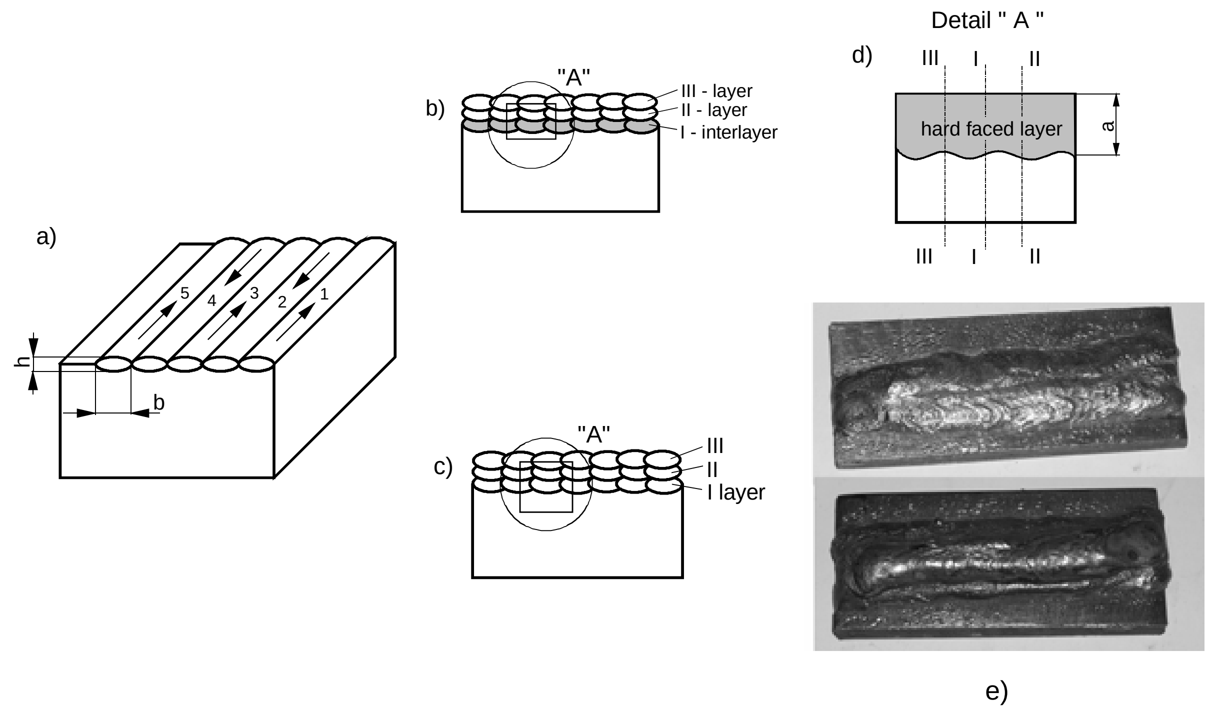

Figure 3. Order of hardfaced layers deposition: a - 1st layer, b - 2nd layer, c - 3rd layer, d-metallographic block and e – hardfaced sample models (model photos)

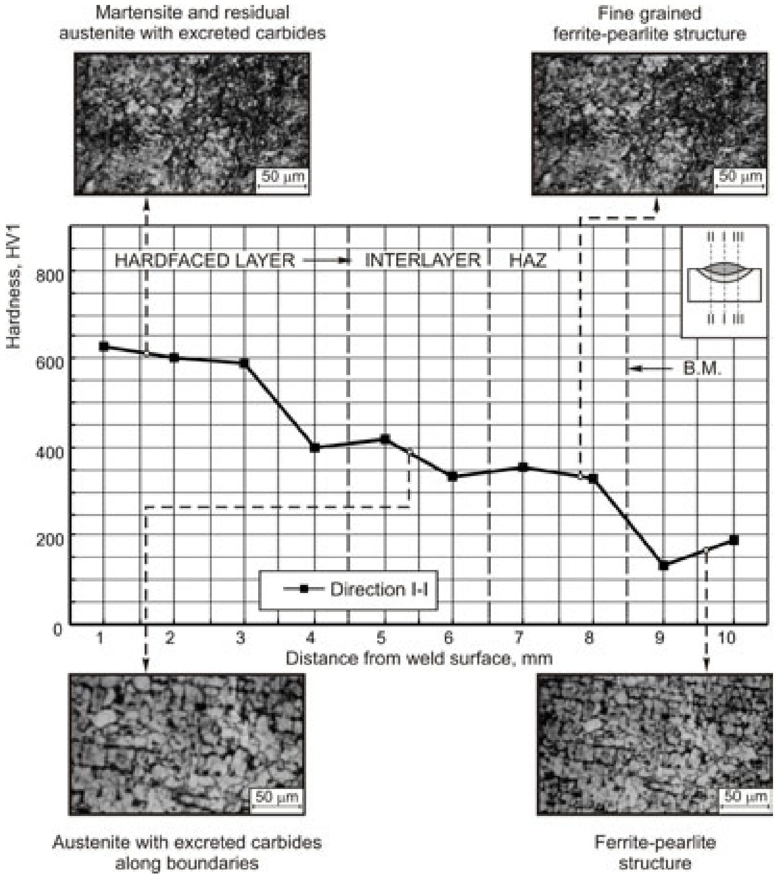

Figure 4. Microstructure of the hardfaced metal zones: B.M. - Č0361, interlayer - INOX B 18/8/6 and hardfaced layer - E DUR 600

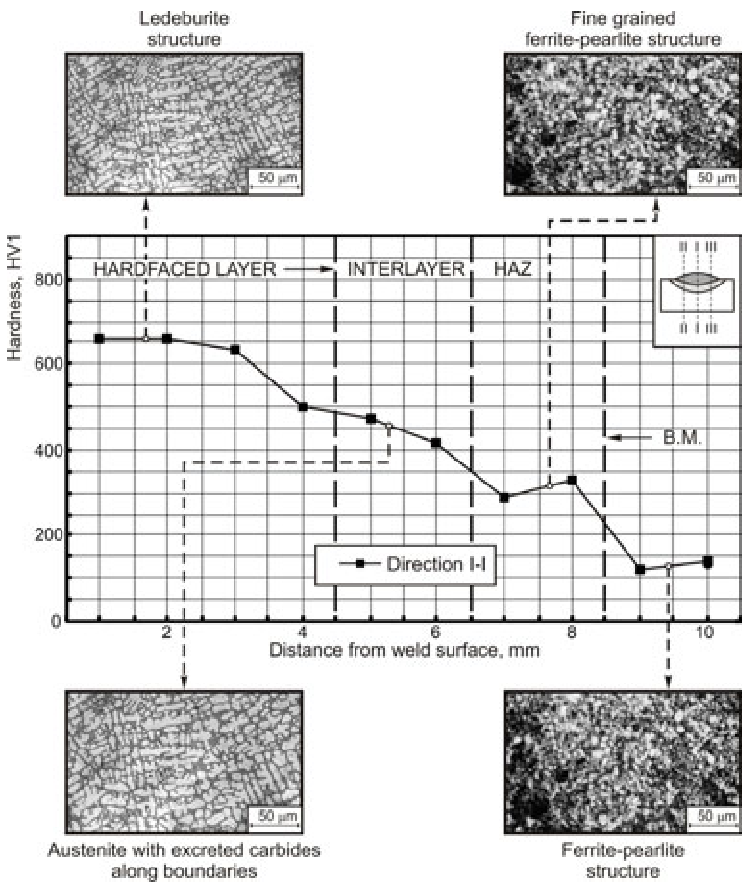

Figure 5. Microstructure of hardfaced layer zones: B. M. - Č0361, interlayer - INOX B 18/8/6 and hardfaced layer - CrWC 600

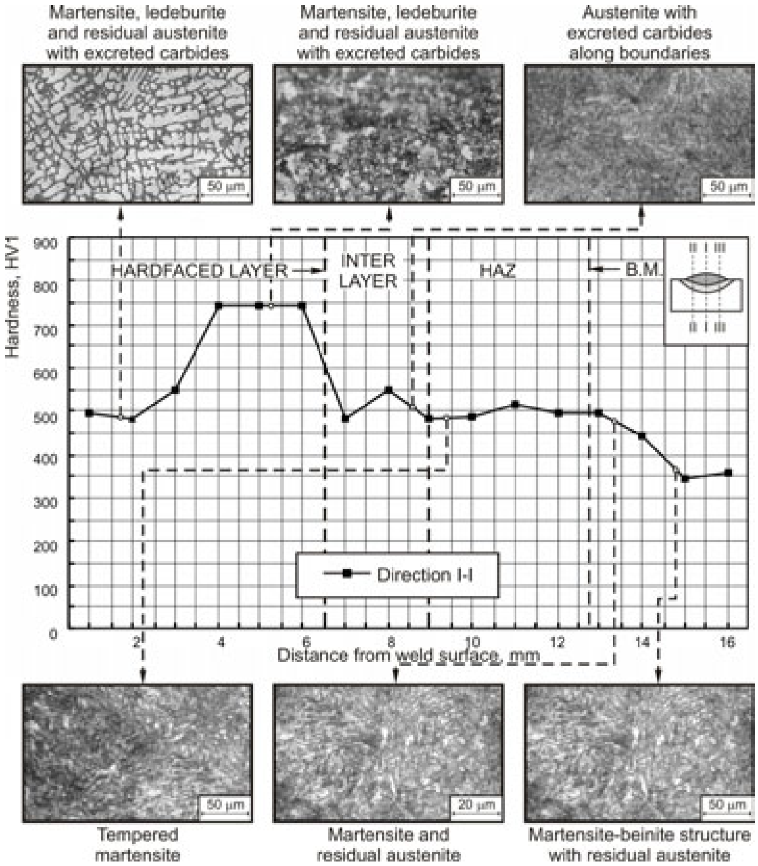

Figure 6. Microstructure of hardfaced layer zones: B. M. - Č0361, interlayer - INOX B 18/8/6 and layer - ABRADUR 58

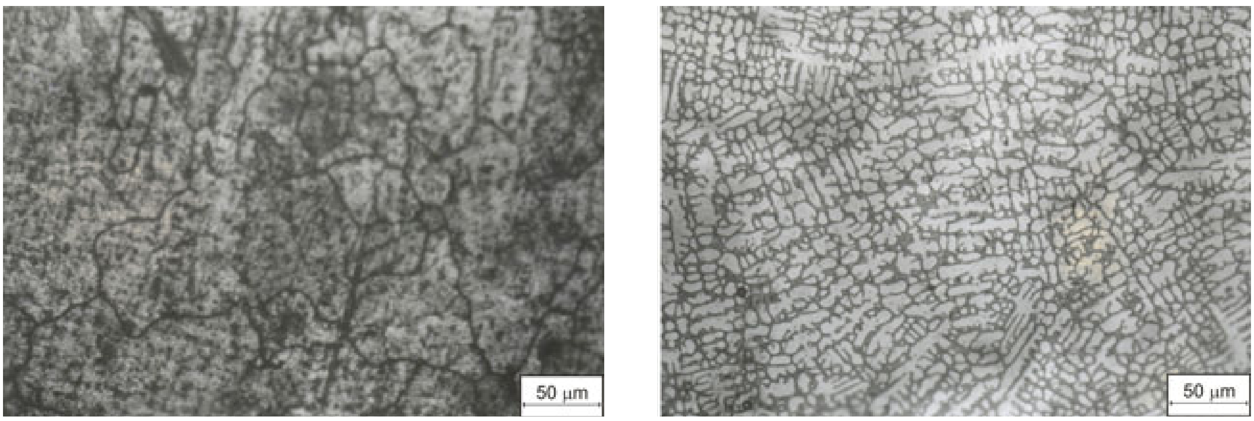

a) b)

Figure 7. Microstructure of the hardfaced layer: (a) E Mn17Cr13 (200×) and (b) INOX B 18/8/6 (200×)

3.5 Tribological investigations

For tribological investigations, it was necessary to prepare blocks whose dimensions were compatible with the tribometer installed at the Faculty of Mechanical Engineering. Five blocks were prepared - four of them from the hardfaced layer (E DUR 600, CrWC 600, ABRADUR 58 and E Mn17Cr13) and one from the base material (Č4732). The blocks were grinded until their dimensions were 6.3×15×10 mm so that they could be placed on the tribometer holder and come into contact with the disc of standard dimensions [2]. During the investigation, a line contact "block on disk" was realized. Outer variables were: contact force, slide speed and lubricant.

Prior to each investigation, the contact surfaces of the discs were grinded to remove the wear traces so that their roughness could be measured and compared to the contact surface roughness of the tested blocks. Table 5 shows the technology of the sample preparation for tribological investigations of the hardfaced layers and base materials. The coupled pairs “disc- block” were lubricated with the motor oil GLX 2 SAE 15 W-40.

Table 5. Technology of the sample preparation for tribological investigations (blocks and disks) [2]

Sample number	Substrate material	Hardfaced layer material	Number of the hardfaced layers	Height of the hardfaced layer, mm	Blocks and discs
1.	Č0361	Interlayer-INOX B 18/8/6 Hardfaced layer -E DUR 600	3*	4.2-5.6	
2.	Č0361	Interlayer -INOX B 18/8/6 Hardfaced layer -CrWC 600	3*	4.5-6.0	
3.	Č0361	Interlayer -INOX B 18/8/6 Hardfaced layer -ABRADUR 58	3*	3.0-3.5	
4.	Č0361	Hardfaced layer -E Mn17Cr13	3	6.2-8.0	
5.	Č4732	-	-	-	

*) The first layer is a plastic interlayer of F. M. - INOX B 18/8/6, while the second and the third layers are made of F. M.–ABRADUR 58, E DUR 600 and CrWC 600.

The aim of these investigations is to determine the wear resistance of the base and filler materials and to estimate how appropriate these filler materials are for reparatory hardfacing of blades and other parts of construction machinery exposed to combined wear.

Prior to investigations, topography of the disc and block surfaces was measured on the computer measuring system Talysarf 6. Then, the contact was realized. The normal force of F_N = 300 N and the sliding speed of v_{kl} = 1 m/s were adopted. During the contact of ≈ 60 min, a change of the friction coefficient was registered (Fig. 8, 9, 10, 11 and 12). When the contact was terminated the topography of the disc and block surfaces was studied i.e., the wear scare area of the block was measured (Fig. 13). In this way, tribological characteristics were determined. The wear scare width was measured using a universal microscope UIM-21, with magnification of 50 times.

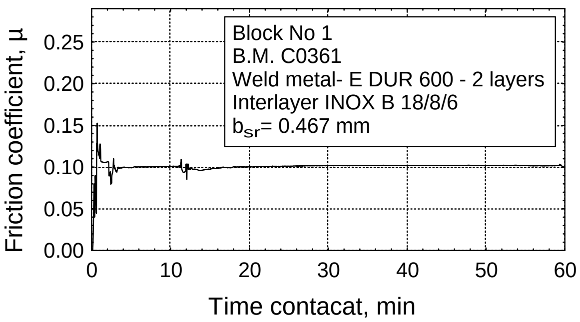

Figure 8. Change of the friction coefficient during the contact of 60 min

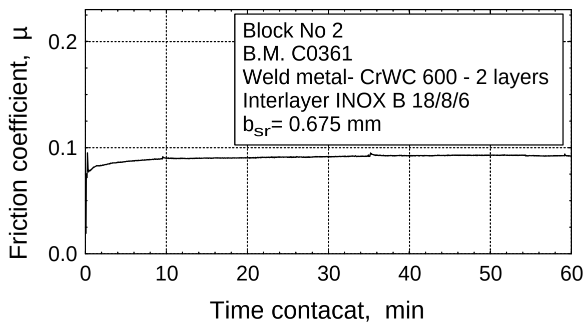

Figure 9. Change of the friction coefficient during the contact of 60 min

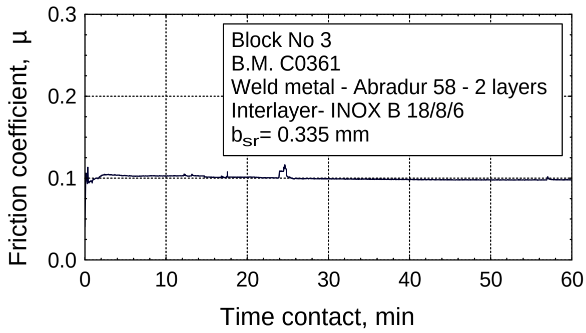

Figure 10. Change of the friction coefficient during the contact of 60 min

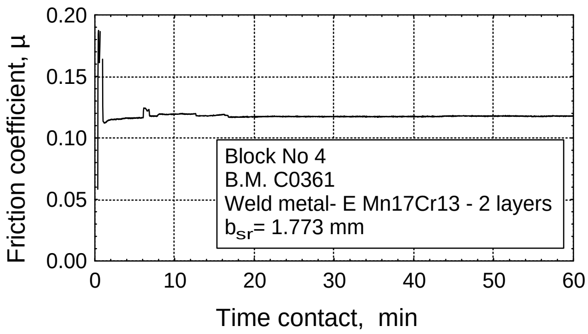

Figure 11. Change of the friction coefficient during the contact of 60 min

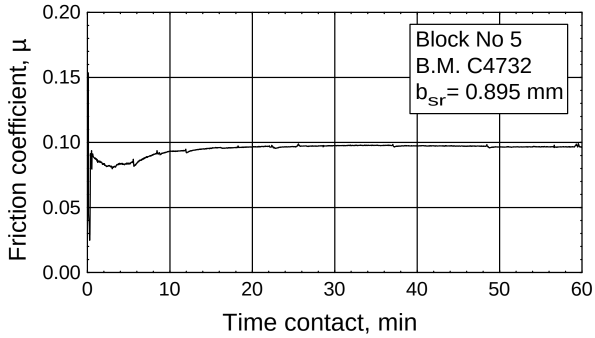

Figure 12. Change of the friction coefficient during the contact of 60 min

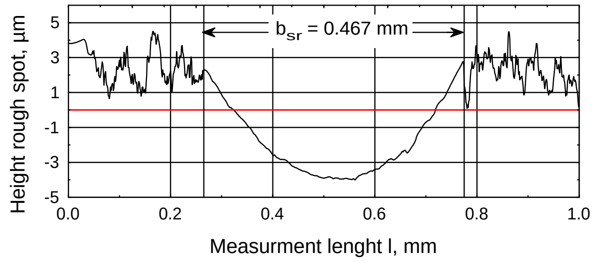

Figure 13. Layout of the wear scare - block No 1 (after the contact of 60 min)

Figure 14a gives a graphical presentation of mean values of the friction coefficient, and Figure 14b shows mean wear scare area widths of the investigated blocks.

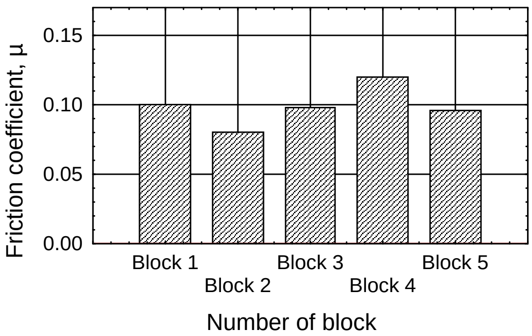

a)

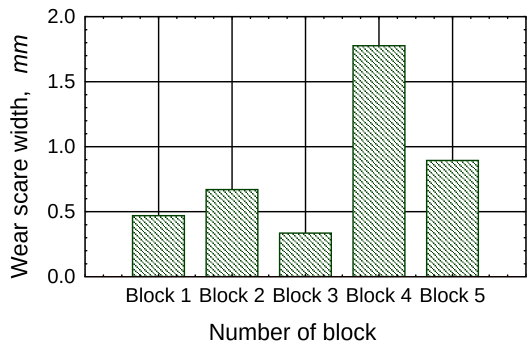

b)

Block 1-E DUR 600, Block 2-CrWC 600, Block 3-ABRADUR 58, Block 4- E Mn17Cr13, Block 5-Č4732

Figure 14. Histograms of the mean values of friction coefficients (a), and wear scare widths (b) after the contact of 60 min

Measurements of the wear scare width have revealed that the hardfaced layers have a significantly higher resistance to wear compared to base material of the blades. This particularly applies to the hard-faced layers obtained using the electrode ABRADUR 58, with application of the interlayer electrode and without preheating. It illustrates how complicated it is to select hardfacing technology and filler materials for real technological working conditions of the construction machinery.

4. HARDFACING OF REAL PARTS

The technology selected on model investigations was applied to the real parts. For investigations under real conditions, 10 blades were hardfaced. Two blades were hard-faced with electrodes E DUR 600 and E Mn17Cr13, and three blades were hardfaced using the electrodes ABRADUR 58 and CrWC 600. Cutting blade edges were hardfaced along the back and front angle sides of the blade, lengthwise. The width of the hardfaced layer was about 25 mm. The hardfaced blades (Fig. 15) were sharpened by grinding and then they were finally ready.

Figure 15. Blades repaired with different filler materials

Thus repaired and sharpened blades were mounted together with new blades on the device and their performance was monitored under real working conditions. The mass of the blades before mounting was 0.30 kg. The wear process was monitored during 120 hours of effective work. Then the devices were cleaned and washed and all the blades were dismounted. Figure 16 shows the mass losses of new and hardfaced blades.

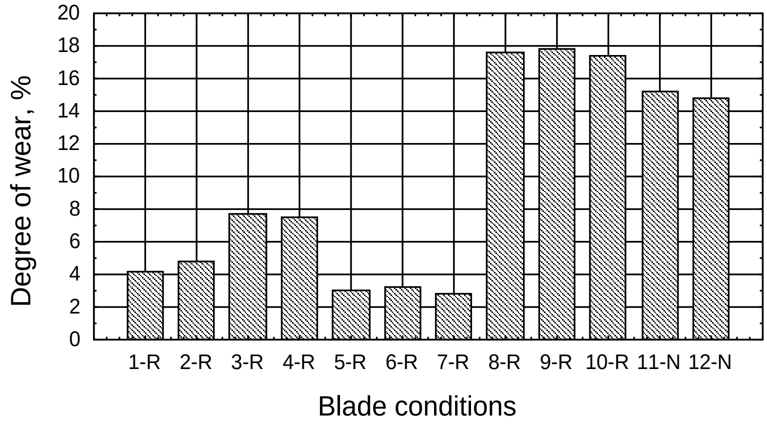

1-R and 2-R – **ABRADUR 58**; 3-R and 4-R – **CrWC 600**; 5-R, 6-R and 7-R – **E DUR 600**; 8-R, 9-R and 10-R – **E Mn17Cr13**; 11-N and 12-N – **NEW BLADES** (**B. M**.)

Figure 16. Graphical presentation of the degree of wear of the blades after 120 hours of effective work

Based on the material mass losses of the studied samples, it can be concluded that, under the same working conditions, the hardfaced blades have in general shown better resistance to wear compared to new, not hardfaced blades. The same conclusion can be drawn for the blades hardfaced with ABRADUR 58, CrWC 600 and in particular with E DUR 600, while the blades hardfaced with E Mn17Cr13 exhibited significantly less resistance to wear, even compared to new blades. This is the result of the working conditions and impossibility of austenite to transform into martensite in shallow surface layers of the hard-faced metal. Therefore, it can be concluded that manganese austenite steel or Hadfield steel is not suitable for the given working conditions [2, 6, 9].

5. CONCLUSION

Having conducted investigations on models and real working parts, the following important conclusions have been drawn:

- Blades can be successfully repaired by hardfacing with or without preheating but with application of austenite interphase filler materials;
- Results obtained in tribological model investigations are in good compliance with the results obtained in investigations on real parts;
- Reparatory hardfacing of blades with hard electrodes can significantly extend their service life;
- The most suitable filler material for reparatory hardfacing of blades is E DUR 600, with service life of 1200 h of effective work compared to 240 h of new blades,
- The costs of reparatory hardfacing are lower than the cost of new blades;
- Multiple reparations of worn blades have been proven possible;
- These methods of reparation can also be applied to other types of construction machinery operating under similar working condition.

6. REFERENCES

[1] Nedeljković, B., et al.: Reparatory hard facing of the rotational device knives for terrain leveling, Journal of the Balkan Tribological Association, Vol. 16, No 1. 2010, pp. 46-75.

[2] Mutavdžić, M.: Reparatory hard-facing of the machine parts and devices in the civil engineering industry mechanization, Master's thesis, Faculty of Mechanical Engineering, Kragujevac, Serbia, 2007. (in Serbian)

[3] Nedeljković, B., et al.: Influence of the carbide type on tribological properties of the hard-faced layers, Metalurgija – Journal of Metallurgy, Vol 16, No 2, 2010, pp. 77-90.

[4] Mutavdžić, M., et al.: Reparatory hard facing of the rotational device knives for terrain leveling del investigations of the filler materials for regeneration of the damaged parts of the construction mechanisation, Tribology in Industry, 3&4/2008., pp. 3-9.

[5] Lazić, V., et al.: Choosing the most suitable technology of hard facing of mixer blades used in asphalt bases, Tribology in Industry, 1&2/2008., pp. 3-10.

[6] Mutavdžić, M., et al.: Selection of the optimum technology of reparatory hard facing of the impact beams of the rotational crushing mills, Welding & welded structures, (2/2007), pp. 55-67.

[7] Lazić, V., et al.: Carbide type influence on tribological properties of the hard faced steel layer – part I – theoretical considerations, Tribology in Industry, Vol. 32, No. 2, 2010., pp. 11-20.

[8] Lazić, V., et al.: Carbide type influence on tribological properties of the hard faced steel layer – part II – experimental results, Tribology in Industry, Vol. 32, No. 3, 2010, pp. 3-12.

[9] Lazić, V., et al.: Estimate of the wear resistance of the hard-faced layers deposited by the manganese electrode, Tribology in Industry, Vol. XXII, No.3&4, Kragujevac, Yugoslavia 2002, pp. 10-17. (in Serbian)

[10] Lazić, V., et al.: Reparation of damaged mallet for hammer forging by hard facing and weld cladding, Tehnical Gazete, Vol. 16, No. 4, 2009., pp. 107-113.

[11] Lazić, V., et al.: Theoretical-experimental determining of coolinig time ($t_{8/5}$) in hard facing of steels for forging dies, Thermal science, Vol. 14, No. 1, 2010, pp. 235-246.

[12] Lazić, V., et al.: Energetic analysis of hard facing and weld cladding of an air powered drop hammer damaged ram, Thermal science, Year 2010, Vol. 14, Suppl.,. pp. S269-S284.

[13] Dziubinski, J., Klimpel, A.: Napawanie i natryskiwanie ciepline, Wydanictwa Naukovo - Techniczne, Warsawa, 1985., (in Polish).

[14] Smith, D.: Welding skills and technology, New York, 1984., (translated by R. Lučić), Belgrade, 1994., (in Serbian)

[15] Wasserman, R.: How to save millions by reparatory welding in machine maintenance, Castolin Eutectic, Institute for advancement of reparatory welding technique and welding technique in machine maintenance, Bor, 2003., (in Serbian).

[16] Gierzynska, M.: Tarcie zužycie i smarowanie w obrobce plastycznej metali, Wydawnictwa Naukowo-Techniczne, Warszawa, 1983., (in Polish).

[17] Ivković, B., Rac, R.: Tribologia, Yugoslav Society for Tribology, Kragujevac, 1995., (in Serbian).

[18] Catalogues and Prospects of Electrode Materials Manufacturers**:** FEP-Plužine, Elvaco-Bijeljina, Železarna-Jesenice, Bohler-Kapfenberg, Messer Griesheim-Frakfurt am Main, Esab- Göteborg, Lincoln Electric-USA, etc.

[19] Standards: JUS, UNI, DIN, IVECO, ASTM etc.

Serbian Tribology Society

SERBIATRIB '11

12th International Conference on Tribology

Faculty of Mechanical Engineering in Kragujevac

Kragujevac, Serbia, 11 – 13 May 2011

SPECIFIC SLIDING OF THE TROCHOIDAL GEARING AT THE GEROTOR PUMP

Lozica Ivanović [1], Danica Josifović[1], Andreja Ilić[1], Blaža Stojanović[1]
[1] Faculty of Mechanical Engineering, Kragujevac, Serbia,
lozica@kg.ac.rs, danaj@kg.ac.rs, gilic9@sbb.rs, blaza@kg.ac.rs)

Abstract: *In the paper is given the method to determination of the gear geometrical dimensions at the gerotor pump on the base of the specific sliding equality in the point with the greatest sliding velocity. The gerotor pumps are the rotated pumps with internal trochoidal gearing. The pump working process is followed with mechanical losses as a consequence of the wearing between the surfaces of the meshing tooth profiles. To reduce these unwanted effects and taking out the gear active tooth surfaces wearing is necessary to realize minimum of the film oil between contact surfaces. Minimum oil film thickness is in function from the numerous different factors and in this paper are analyzed only geometrical and kinematical characteristics of the meshing tooth profile surfaces. At first are defined the geometrical and functional working limits for the gears. It is developed the mathematical model in form of the parameter equations which is following the change of the relative velocities in contact, sliding velocity, rolling velocity and specific sliding of the gear tooth profiles in the contact point. They are defined the conditions for the equality of the specific sliding in the critical contact points. To the observed geometrical-kinematical model of the gerotor pump is developed the computer program and on the base of the obtained results are chosen the values of the parameters to the realisation of the concrete teeth pairs of the gerotor pump with the better tribological characteristics.*

Keywords: *gerotor pump, trochoidal gearing, sliding velocity, specific sliding.*

1. INTRODUCTION

The basic components of the most contemporary machines are gears and oft their quality defined the life time and reliability of machine. The often causes of the functional incorrectness at the gear pairs are different types of the toot flanks wear. From this point of view is very important that to the exploitation and technological demands it is necessary to be chosen corresponding gearing profile at the applied gears, which would be most suitable to its construction form taking into consideration contact stresses and tooth flanks wear. To reduce these unwanted effects and taking out the gear active tooth surfaces wearing is necessary to realize minimum of the film oil between contact surfaces. Minimum oil film thickness is in function from the numerous different factors and in this paper are analyzed only geometrical and kinematical characteristics of the meshing tooth profile surfaces.

In the present time are using most often the gears with involute gearing that besides the great technical and economical advances has also many deficiencies. The main deficiency is the relative small carrying capacity of the tooth flanks and the great contact stresses and it comes to the crease of the efficiency coefficient. The good base to the solutions of the most problems of the gear pair is giving trochoidal gearing. Using this gearing in contemporary constructions can be supplied the basic functional characteristics: needed efficiency coefficient and working life with minimum weight and dimensions. Also at the trochoidal gearing is realised in the same time contact of the all tooth with them can be attained better caring capacity.

In the last time engineers and researches indicated the great interesting to the development and application of the trochoidal form. The most known examples of the trochoidal profiles application are: rotated pumps, rotated motors, rotated compressors, expanders and cycloreducers.

Ansdale and Lokley have done the equations that defined geometry of trochoidal profile, used in construction of Wankel motor [1]. Litvin is applied the gearing theory for generating cycloidal gearing [2]. Maiti has given the detailed analyze of geometrical, kinematical and functionality characteristics of rotated machines with the gerotor mechanism [3]. Beard and other authors investigated the kinematical and geometrical relations between the gear and the cutting tool during the profile generation process is the same relation [4]. Mancò and other authors are developed the computer method for generating gerotor lubricating pump [5].

The existing construction solution on the lubrication pump gears is given in Fig.1. The main part of the gerotor pump is a gear pair which is assembled to the main shaft by a gear key. The pump body has fluid outlets which are connected to pump suction line and delivery line. The cover is on the front side. Both gears rotate counterclockwise. During the gear rotation the inlet chambers are in the area where the teeth are coming out from the tooth space and the outlet chambers where they are coming in contact in the teeth space.

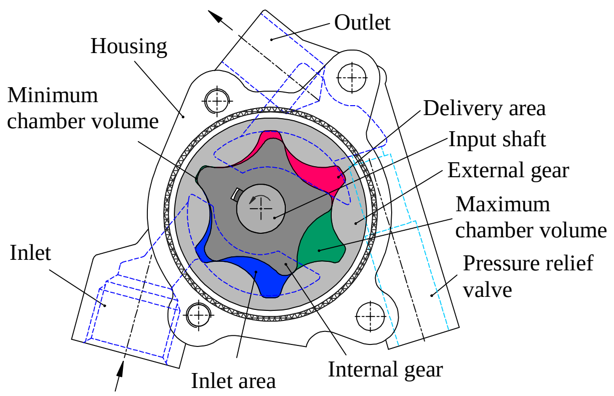

Figure 1. The scheme of the pump model

The functional characteristics of the pump are significantly influenced by the gear pair parameters. This paper will analyze the influence of geometrical and kinematical parameters of the gear pair profile on the pump functional characteristics and their influence on the specific sliding.

2. GEOMETRYCAL PARAMETERS AND LIMITS

At the pump projection is given usually constructive parameters: eccentricity e, teeth number of the external gear z and radius of the root circle of the external gear r_{fa} of the mashing envelope (Fig.2). it is necessary to be defined the limit value of the radius r_c which at the given value trochoid coefficient λ, does not come to the undercutting and interference of the toot profile [..].

This analyze will be done on the base of the geometrical relations given in the Figure 2.

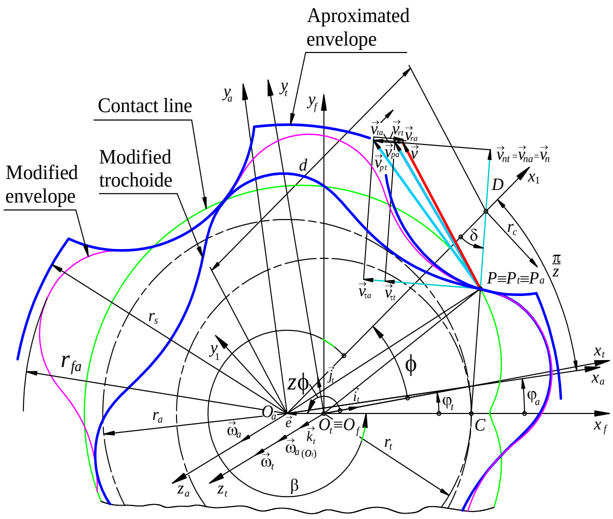

Figure 2. Geometrical and kinematical parameters of the trochoidal gear pair

Starting of equations that defined coordinates of the contact point P in coordinate system of trochoide:

$$\begin{aligned} x_t &= e(\cos z\phi + \lambda z \cos\phi) - r_c \cos(\phi+\delta) \\ y_t &= e(\sin z\phi + \lambda z \sin\phi) - r_c \sin(\phi+\delta) \end{aligned}, \qquad (1)$$

by them δ is leaning angle defined to the following form:

$$\delta = \arctan \frac{\sin(z-1)\phi}{\lambda + \cos(z-1)\phi}. \qquad (2)$$

To be realized meshing gear regulation of the trochoidal tooth pairs is necessary to be filled numerous geometrical and kinematical conditions. In this part of paper are analyzed the conditions that come to the appearance undercutting and interference of tooth profiles.

Criteria for the choice of equidistant radius, to eliminate the phenomenon of tooth profile undercutting is

$$c < z\sqrt{\left(\frac{3}{z+1}\right)^3 (\lambda^2 - 1)(z-1)}, \qquad (3)$$

where c is equidistante coeficient $c=r_c/e$, and condition for elimination of interference of neighboring tooth profiles of external gear is given

$$c \le z\lambda \sin\frac{\pi}{z}. \qquad (4)$$

To be realized the regular meshing of the convex profile part of the modified trochoide in the root area of the meshing envelope that is approximated with circular arc, it is necessary to be filled condition for:

$$r_s > r_{fa}\,, \tag{5}$$

by them is

$$r_{fa} = e(\lambda z + 2) - r_c\,. \tag{6}$$

Taking in coefficient $S_{fa} = r_{fa}/e$ from equation (6) can be defined radius of the equidistance in form

$$c = \lambda z + 2 - S_{fa}\,. \tag{7}$$

To be got correct manufacturing and montage it is needed that r_s is less than $d = e\lambda z$ and can be expressed with following condition:

$$c > 2\,. \tag{8}$$

The value of the radius equidistance for the given constructive parameters is chosen from interval

$$c_{\min} < c < c_{\max}\,, \tag{9}$$

by them is taken for $c_{\min}$ more value from the values obtained to the formulae (7) and (8), and for $c_{\max}$ is taken less value from the values obtained to the formulae (3) and (4),

Starting from analytical relations realized for given geometrical limits can be defined domain of the practical application analyzed geometrical parameters for the internal gear pairs with modified trochoidal gearing.

3. KINEMATICAL PARAMETERS

To the kinematical analyzes of the meshing profiles is considerate the complex moving of the point P_t on the internal gear profile and the point P_a on the external gear profile. There is supposition that is contact in some moment at the points P_t and P_a in the point P on the contact line, as is shown in the Figure 2. For the correct meshing and their continuality is necessary to be realized the condition about equality of the absolute velocities of the meshing profiles in the contact point as also their components in the common normal direction.

From gearing theory it is known that only centroide can realize rolling without sliding. According to, profile sliding is inevitable because they are formed with the curves which are different of centroide. The sliding velocity of the meshing profiles $\vec{v}_{ta}$ in the observed contact point is the velocity of the contact point at the relative profile moving and it is defined with the difference at the transfer velocity vectors, regard to

$$\vec{v}_{ta} = \vec{v}_{pt} - \vec{v}_{pa}\,. \tag{10}$$

The angular frequency of the internal and external gear are defined with the vectors $\vec{\omega}_t$ and $\vec{\omega}_a$. To determination of the relative moving velocity $\vec{v}_{ta}$ vector $\vec{\omega}_a$ is coming through the parallel moving in the point O_t [2]. As the result of reduction is obtained vector $\vec{\omega}_{a(O_t)}$, which is acting in the point O_t, and the vector moment is defined the following vector equation:

$$\vec{m}_a^{(t)} = \vec{e} \times \vec{\omega}_a\,, \tag{11}$$

by them is $\vec{e}$ radius vector of point trough which is acting vector $\vec{\omega}_a$ in the coordinate system $O_t x_t y_t z_t$ (Fig. 2), which can be written in the form:

$$\vec{e} = -e\cos\varphi_t \vec{i}_t + e\sin\varphi_t \vec{j}_t\,. \tag{12}$$

Transfer velocity vectors of the point P_t can be done in form of relation:

$$\vec{v}_{pt} = \vec{\omega}_t \times \vec{r}_t = \begin{vmatrix} \vec{i}_t & \vec{j}_t & \vec{k}_t \\ 0 & 0 & \omega_t \\ x_t & y_t & 0 \end{vmatrix} = -y_t\omega_t\vec{i}_t + x_t\omega_t\vec{j}_t\,. \tag{13}$$

by them are $\vec{i}_t$, $\vec{j}_t$, $\vec{k}_t$ unit vectors of the coordinate system of the trochoide $O_t x_t y_t z_t$.

Transfer velocity vectors of the point P_a can be shown in the form:

$$\begin{aligned} \vec{v}_{pa}^{(t)} &= \vec{\omega}_{a(O_t)} \times \vec{r}_t + \vec{e} \times \vec{\omega}_a = \\ &\begin{vmatrix} \vec{i}_t & \vec{j}_t & \vec{k}_t \\ 0 & 0 & \omega_a \\ x_t & y_t & 0 \end{vmatrix} + \begin{vmatrix} \vec{i}_t & \vec{j}_t & \vec{k}_t \\ -e\cos\varphi_t & e\sin\varphi_t & 0 \\ 0 & 0 & \omega_a \end{vmatrix} = \\ &= (-y_t + e\sin\varphi_t)\omega_a\vec{i}_t + (x_t + e\cos\varphi_t)\omega_a\vec{j}_t \end{aligned} \tag{14}$$

According to, the vector of the profile sliding of the internal in relation to external gear, to the equation (10), in coordinate system of trochoide can be given in the form of vector equation:

$$\begin{aligned} \vec{v}_{ta}^{(t)} &= \left\{-e(\sin z\phi + \lambda\sin\phi) + \frac{r_c}{z}\sin(\phi+\delta)\right\}\omega_t\vec{i}_t \\ &+ \left\{e(\cos z\phi + \lambda\cos\phi) - \frac{r_c}{z}\cos(\phi+\delta)\right\}\omega_t\vec{j}_t \end{aligned}\,. \tag{15}$$

Intensity of the profile sliding velocity in the contact point is:

$$v_r = |\vec{v}_{ta}| = \left\{(1 + \lambda^2 + 2\lambda\cos\beta)^{\frac{1}{2}} - \frac{c}{z}\right\}e\omega_t\,, \tag{16}$$

where

$$\beta = (z-1)\phi \,. \tag{17}$$

Except the sliding velocity for the analyzing of the phenomenon of wear significant is the summary rolling velocity [5]. Intensity of summary rolling velocity can be written in the form:

$$v_{\Sigma} = \left\{ \left(1+\lambda^2+2\lambda\cos\beta\right)^{\frac{1}{2}} - \frac{c}{z}\left(1+2\delta'\right) \right\} e\omega_t \,, \tag{18}$$

where

$$\delta' = \frac{(z-1)(1+\lambda\cos\beta)}{1+\lambda^2+2\lambda\cos\beta} \,. \tag{19}$$

The formulae to determination the specific sliding of the meshing profiles in the contact point can be defined on the base of the obtained equations.

4. SPECIFIC PROFILE SLIDING

The sliding existence in the sliding in the meshing profiles process comes to their wear by that the sliding velocities define the friction forces direction and intensity which take effect on the meshing profiles of the gears. By them the friction force is in direction opposite to the relative motion velocity in the contact point. So the direction of the sliding velocity $\vec{v}_{ta}$ is in agreement with the direction of the friction force which take effect on the profile of the external gear profile, but the direction of $\vec{v}_{at}$ is the same the direction of the friction force on the trochoidal profile [12].

It is necessary to know, at the analysis of the meshing profiles sliding, except the sliding velocity in the contact point also its distribution of their change in relation to corresponding relative velocity of the contact point. Specific sliding is relation between the sliding velocity and relative velocity of the contact point of the meshing profiles [7]. After the substitution of the corresponding formulae for the velocities is obtained finally formulae for the specific sliding on the tooth profile of the internal gear:

$$\xi_t = \frac{z\left(1+\lambda^2+2\lambda\cos\beta\right)^{\frac{1}{2}} - c}{z\left(1+\lambda^2+2\lambda\cos\beta\right)^{\frac{1}{2}} - c\left(1+\delta'\right)} \,, \tag{20}$$

and analogical for external gear:

$$\xi_a = \frac{z\left(1+\lambda^2+2\lambda\cos\beta\right)^{\frac{1}{2}} - c}{c\delta'} \,. \tag{21}$$

Specific sliding is positive on the profile point, where the directions of sliding and relative velocities are in agreement, and where are not in agreement – negative.

4.1 Conditions for the uniform teeth wear

Influence of geometrical and kinematical parameters on the sliding value and intensity of the teeth profile wear is analyzing through the specific profile sliding [7], [8]. The aim of constructer is that with the corresponding choice of geometrical parameters can be realized the uniform wear of the meshing gear teeth in the meshing process. From this aspect is necessary that it is realized equality of the specific sliding in the points with the greatest of the pitch point of the relative velocities. Starting from the formulae (20) and (21), taking in also (19), comes that for the given values of the teeth number z and coefficient of trochoide λ the uniform wear of the tooth profile can be realized when is filled condition about equality of the relative velocities, in regard to, when is chosen value of the coefficient of equidistant radius equal:

$$c = \frac{z\left(1+\lambda^2+2\lambda\cos\beta\right)^{\frac{3}{2}}}{\lambda^2-1+2z(1+\lambda\cos\beta)} \,. \tag{22}$$

This condition can be written for the points with the greatest sliding velocity, and they are the points on the top of the trochoide profile (β=0), in the form:

$$c = \frac{z(1+\lambda)^2}{2z+\lambda-1} \,. \tag{23}$$

5. NUMERICAL EXAMPLES

On the base of the realized analyze as result of the developed methodology for the identification of the optimal geometrical parameters of the trochoidal pump [9], are proposed the solutions with the parameter which are given in the Table 1.

Tabela 1. Parameters of various pump models

Pump parameters	Number of pump chambers			
	z=6			z=5
Trochoid coefficient, λ	1.375	1.575	1.675	1.85
Equidistant radius coefficient, c	2.75	3.95	4.55	3.75

In the Fig. 3 are given alternative solutions of the gear pairs.

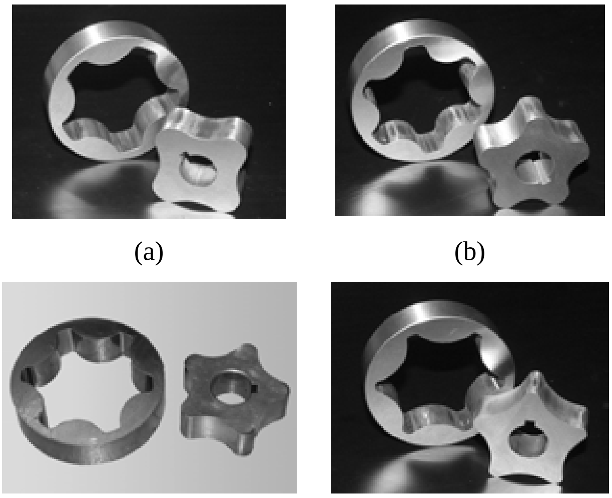

Figure 3. Alternative solutions of the gear pairs theoretical profiles: a) GP-850, b) GP-375, c) GP-575 (commercial) and d) GP-675

This part will present some of the results of the kinematical analysis of trochoidal gearing on the concrete examples of gear pairs of the investigated pump models.

In the Figure 4 are shown diagrams of the sliding velocity v_r and in the Figure 5 summary rolling profile velocity v_Σ in relation of the angle β. Because that the trochoide is cyclical curve with the symmetrical branches, by them is one half generated in angular interval $0 \leq \beta \leq \pi$, that is mean that the obtained diagrams give the clear picture about distribution of the velocity changing along the profile, by them for the top of the trochoidal profile is corresponding angle β=0, and in the root $\beta = \pi$.

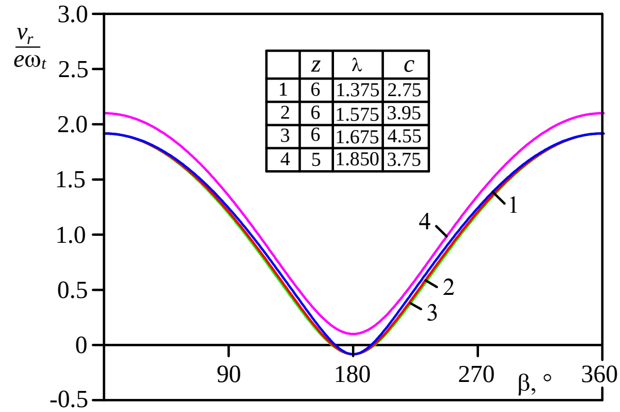

Figure 4. Sliding velocity v_r of the contact point of trochoidal profiles for different teeth number z, values of the trochoid coefficient λ and coefficient of equidistant radius c

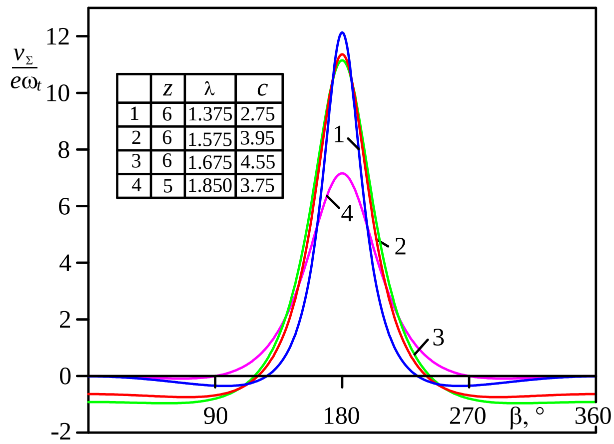

Figure 5. Summary rolling velocity v_Σ of the contact point of trochoidal profiles for different teeth number z, values of the trochoid coefficient λ and coefficient of equidistant radius c

On the base given graphical interpretation obtained results can be defined the following conclusions:

- At the model with z=6 the sliding velocity v_r monoton decrease from maximal (on the top), is equal zero in the moment when the profile are in contact in pitch point abd by them comes to the sign change;
- At the model with z=5 the sliding velocity v_r monoton decrease from maximal (on the top) to the minimal value (in the root of the profile);
- Summary rolling velocity v_Σ has aproximate constant value, near zero (on the convex part of the profile), and after that abruptly increases to the maximal value (in the root of the concave part of the profile).

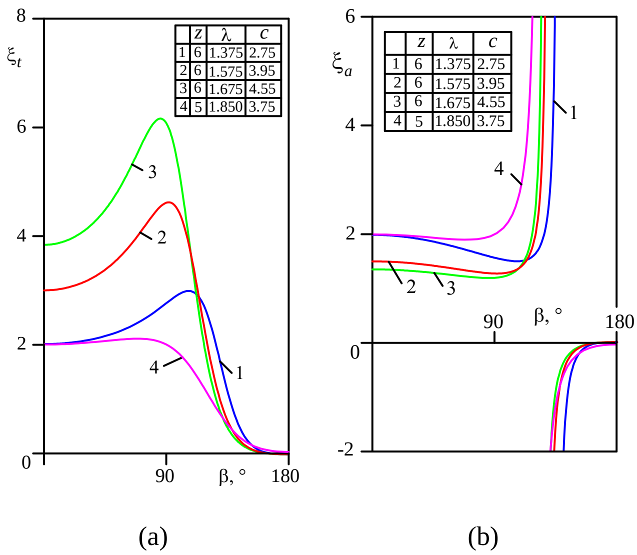

Figure 6. Comparative diagrams of specific sliding of trochoid profiles

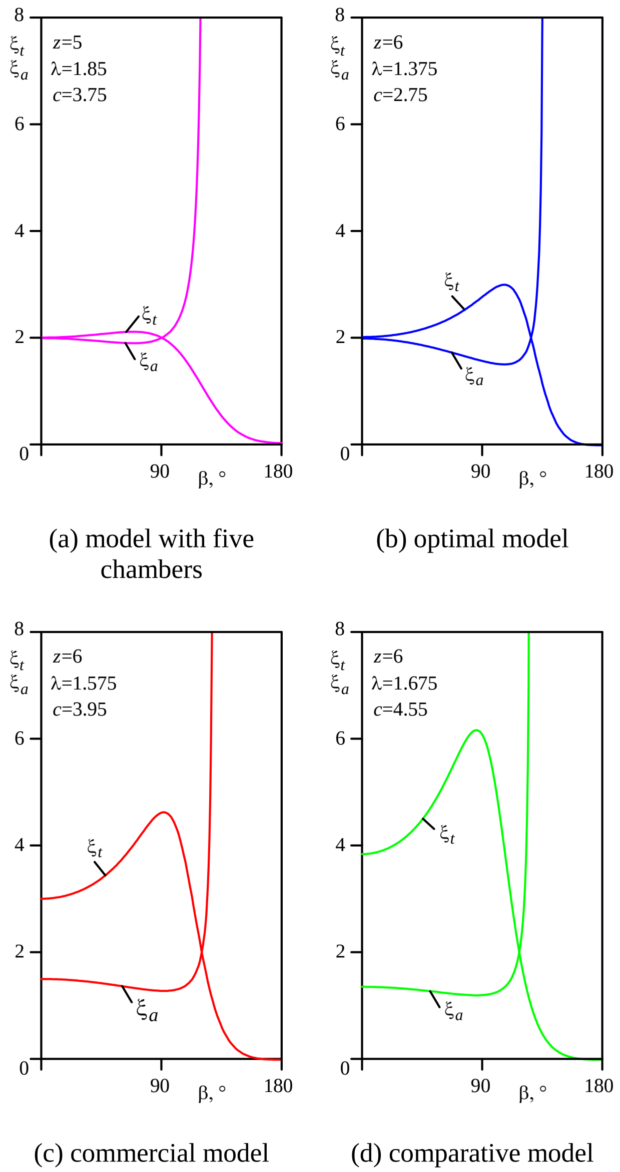

Figure 7. Diagrams of specific sliding trochoid profiles

The sign change of the sliding velocity and the summary rolling velocity has influence on the direction change of the moment of the force sliding friction and the force of the rolling friction at the determination of the mechanical power losses [9].

Figure 6 and 7 illustrates comparative diagrams of specific sliding profile, on the basis of which the following conclusions can be drawn. Specific sliding on the convex part of trochoidal profile significantly decreases at the chosen solutions, while with the circular profiles of external gears it increases at the top part, at the chosen solutions. It is verified that the conditions for even wear of profiles at the point with the highest sliding velocity are met at the chosen solutions, from the aspect of equality of specific sliding.

6. CONCLUSION

In this paper are defined the limits at the profile generating to the aim to establish domains of the practical application of the geometrical parameters of the gear pair. From this aspect are considered conditions that come to appear of undercutting and interference of the profile as at their manufacturing so that in the process of meshing.

In the paper is given a analysis of the kinematical parameters of the trochoidal gearing. There are defined the formulae to calculation of the sliding and rolling velocities in the contact points of the meshing profiles. The paper also gives a analysis of specific sliding at the contact points of the meshing profiles, as well as the relations for its determination. In the choice of the geometrical parameters of the conditions for appearing friction and wear of the contact gear surface specific sliding is one of the more important limiting factors. Based on mutual relations of the sliding and rolling velocities values, conclusions can be made about the changing of the friction conditions during the meshing of profiles.

Except that, in this paper is shown that with the corresponding choice of the geometrical parameters can be realized the equality of the specific sliding in the points with the greatest sliding velocity, in regard to, from the kinematical aspect, ensured the uniform teeth wear of the meshing gears in the process of the meshing profiles.

The developed kinematical model is most helpful in designing, contact and stress analyzing, manufacturing and optimizing internal trochoidal gear pairs.

REFERENCES

[1] R. F. Ansdale, D. J. Lockley: The Wankel RC Engine, Iliffe Books Ltd., London, 1970.

[2] F. L Litvin: Theory of gear meshing, Nauka, Moscow, 1968. (in Russian)

[3] R. Maiti, G. L. Sinha: Kinematics of active contact in modified epitrochoid generated rotary piston machines, Mechanism and Machine Theory, 23, No 1, 39-45, 1988.

[4] J. E. Beard, D. W. Yannitell, G. R. Pennock: The effects of the generating pin size and placement on the curvature and displacement of epitrochoidal gerotors, Mechanism and Machine Theory 27 (4), pp. 373-389, 1992.

[5] G. Mancò, S. Mancò, M. Rundo, N. Nervegna: Computerized generation of novel gearings for internal combustion engines lubricating pumps, The International Journal of Fluid Power, 1, No. 1 - ISBN 1493-9776, 49-58, March 2000.

[6] G. Niemann, H. Winter, Maschinenelemente, Band II, Springer-Verlag, Berlin, 1989.

[7] V. A. Gavrilenko: Gear transmitter in mechanical engineering, Mashgiz, Moskva, 1962. (in Russian)

[8] V. M. Shanikov: Planetary transmitter with the outcentroidal meshing, Mashgiz, Moscow, 1948. (in Russian)

[9] L. Ivanović: Identification of the Optimal Shape of Trochoid Gear Profile of Rotational Pump Elements, PhD dissertation, The Faculty of Mechanical Engineering in Kragujevac, Kragujevac, 2007 (in Serbian)

[10] L. Ivanović, D. Josifović: Specific Sliding of Trochoidal Gearing Profile in the Gerotor Pumps, FME Transactions, 34, No 3, 121-127, 2006.

[11] D. Josifović, L. Ivanović: Kinematical analysis of trochoidal gearing by IC engines lubricating pumps, in: Monograph, Mobility and Vehicles Mechanics, 119-132, Kragujevac, 2005 (in Serbian)

[12] L. Ivanović, D. Josifović, G. Devedžić: Modeling of trochoidal gearing from the aspect of uniform teeth wear, Tribologia, Teoria i praktyka, Vol 40, No 1/2009, pp. 63-75, 2009.

Serbian Tribology Society

SERBIATRIB '11

12th International Conference on Tribology

Faculty of Mechanical Engineering in Kragujevac

Kragujevac, Serbia, 11 – 13 May 2011

LUBRICATING ENGINE OILS FOR SPECIFIC MARINE APPLICATIONS

Anca-Gabriela Marin[1], Ortansa Florea[2], Ion Petre[2]

[1]SC Georom Inspect Consulting SRL Ploieşti, Romania, anca.marin@georomserv.ro
[2]SC ICERP SA Ploieşti, Romania, oflorea_305@icerp.ro

Abstract: *Marine or oceanic ships have different engines types with specific characteristics that require special lubricants. Depending on capacity and purpose, ships are provided with one or two powerful propulsion engines, three or more auxiliary engines, emergency engines and several low power engines for lifeboat. In order to formulate adequate lubricating oils for marine engines must take into account the fuels quality with high sulfur content, the special working conditions in humid and salt environment and the specific operating conditions at constant load and speed. Furthermore, the crankcase lubricating oils for marine engines, cooled with sea water, may form emulsions by accidentally inmoving of cooling water in the oiling circuit. Therefore, these lubricants must have fast desemulsioning capability, condition not required for other engine oils.*

The paper presents the formulation of lubricating oils for two stroke low speed marine engines and four stroke medium speed marine engines, the physico-chemical characteristics of these, the performances level resulted from laboratory stand tests and the real working conditions results. For lubrication of two-stroke marine engines two different types of oils were elaborated and for medium-speed trunk piston engines, two oils were also elaborated, corresponding to the fuels sulphur content.

All the obtained lubricating oils exhibit a very good working behaviour and satisfy all the requirements imposed by specified operating conditions..

Keywords: *lubricants, engine oil, marine, two strokes, four strokes.*

1. INTRODUCTION

Marine lubricants are oil formations with proper additives, that are used in various machinery located on different types of ships.

Depending of capacity and purpose, ships are provided with one or two powerful propulsion engines, three or more auxiliary engines, emergency engines and several low power engines for lifeboat. The most used for propulsion are two cycle low speed engines with crosshead, which need two lubricating oils:

- cylinder lubrication oil, consumed by burning
- bearings and crosshead lubrication oil, changed periodically

The rest of ships engines, such as auxiliary, emergency lighting and lifeboat engines call for a single type of lubricating oil.

In order to formulate adequate lubricating oils for marine engines must take into account the fuels quality with high sulphur content, the special working conditions in humid and salt environment and the specific operating conditions at constant load and speed. Furthermore, the crankcase lubricating oils for marine engines, cooled with sea water, may form emulsions by accidentally in moving of cooling water in the oiling circuit. Therefore, these lubricants must have fast water separation properties, condition not required for other engine oils.

From total among of annual worldwide lubricants needs, only 5% are marine engines oils [1], (Figure 1), but quantities are important and the consumption is constant.

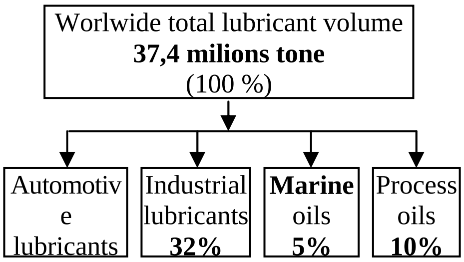

Figure 1. Worldwide marine lubricants consumption from total lubricants

2. EXPERIMENTAL

Our proposal was to formulate and test four types of lubricating oils for oceanic and marine ships:

- system lubricating oil **NL 30-8**, used in crankcases for oiling and cooling the cross-head and bearings of engine; this lubricant is similar to conventional oils used in automotive engines and it is periodically changed.
- cylinder oil **NC 50-70,** with a very high alkalinity level for neutralisation of the acid products resulted from fuel combustion; this lubricant is use up and burn completely in burning room.
- four-strokes engine lubricating oil **NS 40-12**
- four-strokes engine lubricating oil **NS 40-25**

Both four-stroke engine lubricating oils are formulated for medium-speed trunk piston engines, corresponding to fuels sulphur level.

The above oils are designed for lubrication of all types of ships that require different types of Diesel fuels, from gas oils or marine Diesel oils with sulphur content lower then 1,5% to intermediate fuel oils" and up to bunker fuel oils with sulphur content higher then 2,5 % (used on low speed two cycle engines).

2.1 Characteristics and performances of new formulated lubricants

The characteristics of obtained lubricants are presented in Table 1 and Table 2.

Table 1. Two-stroke marine engine lubricating oils

Characteristics	Lubricating oil types		Test methods ASTM D
	NL 30-5	NC 50-70	
Viscosity grade, SAE J 300	30	50	-
Quality level, API	CC	-	-
Kinematic viscosity at 100°C, cSt	11,3	18,6	445
Viscosity index	95	85	2270
Flash point, °C	225	245	92
Pour point, °C	- 21	- 15	97
Total base number, mg KOH/g	5,2	70	2896
Sulphated ash, %	0,75	9,5	874
Copper corrosion, 3hrs/ 100°C	1b	1b	130
Wear scar diameter (4 ball test, 1hr at 40 daN), mm	0,40	0,32	4171

Table 2. Four stroke marine engine lubricating oils

Characteristics	Lubricating oil types		Test methods ASTM D
	NS 40-12	NS 40-25	
Viscosity grade, SAE J 300	40	40	-
Quality level, API	CD	CF	-
Kinematic viscosity at 100°C, cSt	14,7	15,2	445
Viscosity index	90	90	2270
Flash point, °C	230	230	92
Pour point, °C	- 21	- 21	97
Total base number, mg KOH/g	12	25	2896
Sulphated ash, %	1,75	3,5	874
Copper corrosion, 3hrs/ 100°C	1b	1b	130
Wear scar diameter (4 ball test, 1hr at 40 daN), mm	0,39	0,37	4171
Foam properties, tendency-stability, ml - seq. I - seq. II - seq. III	5-0 30-0 5-0	0-0 20-0 10-0	892

All the new lubricating oils was formulated from parafinic base and special high performance additives.

The performances of formulated oils were tested on special laboratory stands (Table 3) related to antioxidant, anticorossion and antiwear properties, the varnish / carbon deposit and rings sticking tendency, as follows:

- oxidation resistance, on Labeco stand, measured by Cu - Pb bearing weight loss, set to max. 40 mg and the lake deposits formed on the piston skirt limited to min. 9.0;
- detergent-dispersant properties, evaluated on Petter AV-B stand by engine cleanliness at the end of the performed test;
- no deposit properties of oils were evaluated on MWM KD 12 E stand, assessed by the degree of freedom of the segments in piston channels and by the amount of carbon deposits formed on the piston;
- lubrication and antiwear properties were evaluated on Caterpillar 1-G_2 stand.

Analyzing the results it is found that the tested oils behaved properly and the data obtained are registered in the acceptable limits of international methods used for certifying their performance levels.

Cylinder oil **NC 50-70** was tested in collaboration with the manufacturer and supplier of additives on a two-stroke, slow speed cross-head engine, type K 6 SZ 90/160° with six-cylinder. The engine lubricating system allowed the separate supply of each cylinder, which made it possible to simultaneously use different oils.

Table 3. Results from special laboratory stand testing

Test stand label	Limits	Labeco L-38			Petter AV-B			MWM KD 12 E			Caterpillar 1G$_2$		
Test methods		ASTM D5119			CEC L-24-A-78			CEC L-05-A-78			ASTM STP 509A		
Marine lubricating oil type		NL 30-5	NS 40-12	NS 40-25	NL 30-5	NS 40-12	NS 40-25	NL 30-5	NS 40-12	NS 40-25	NL 30-5	NL 40-12	NL 40-25
Cu-Pb bearing weight loss, mg	max. 40	22,0	27,6	29,5									
Piston skirt varnish, merit note	min. 9,0	9,3	9,1	9,8									
Deposit, merit note: -on ring grooves					8,9	9,2	9,5						
- on ring land					9,3	9,4	9,3						
- on piston skirt					9,6	9,9	9,7						
Total evaluation notes	min. 70				79	85	83						
Deposit, merit note – on piston skirt								8,9	9,3	9,2			
- on piston crown								9,0	9,2	9,4			
Total evaluation notes	min. 70							89	90	92			
Deposit on superior ring groove, %	max. 80										64	68	75
Reduction of piston-ring gap, μm	max. 12,7										11,0	11,8	12,0
Total cleanliness evaluation notes	max. 300										211	217	228
Tested properties	-	oxidation stability			detergency-dispersancy			anti-deposit properrties			lubricity and antiwear properties		

The NC 50-70 oil was used at the lubrication of cylinders 1,3,5 and 6 in parallel with a reference oil, used in cylinders 2 and 4 in the same operating conditions.

At the end of testing, engine pistons have been removed and then visually examined and measured with micrometer. The results are presented in Table 4 comparatively with standard oil.

Table 4. Results from cylinder oil testing

Evaluation parameters	Cylinder no.					
	1	2	3	4	5	6
Mobility of piston rings	free	free	free	free	free	free
Cylinder surface aspect, note	9	10	7	11	8	12
Cleanliness of space among rings, %	100	97	98	96	97	98
Deposit on cylinder port, % vol.	14,0	15,0	14,0	14,0	14,0	15,0
Oil consumption for cylinders lubrication, g/kWh	1,16	1,17	1,10	1,11	1,13	1,07

From the analysis of presented data, indicates that the oil cylinder NC 50-70 tested behaved similarly to the reference oil, the difference being made due to the cylinders operating conditions (temperature control, fuel oil), quality oils and / or allowable evaluation errors.

2.2 Evaluation of demulsification properties

Besides physico-chemical characteristics presented in Table 1, common to all engine lubricants, marine oils have to meet a very important condition that refers to their ability to separate the contained water. The water can often get into marine engine crankcase oil in significant amounts through the cracks from heat exchangers due to corrosion or under normal atmospheric from condensation of atmospheric wateriness.

This water can lead to oil emulsification, as well as to hydrolysis and precipitation of additives, with worsening of the conditions of lubrication and engine protection. Therefore water must be evacuated as soon as possible from oil for not having time to contribute to the hydrolysis, precipitation and elimination of contained additives. The most used means of removing water from oil is centrifuging, but with water you can remove a part of the additives. Therefore, in the manufacture of marine oils should be used additives with high water resistance, that does not hydrolyse rapidly, to allow removal of therein water, without altering the lubricant quality.

To evaluate the capacity of oil-water separation, ie demulsification were used two laboratory methods,

One according to ASTM D 1401, with static action of separation and the other, according to OMD 113, with dynamic action of separation. In both tests the water quantity is an indication of the capacity of oil-water separation. The OMD 113 is closer to the conditions of oil-water separation from existing marine engines and vessels so that test is more appropriate for evaluating, while ASTM D 1401 is more easily to apply.

NC 50-70 cylinder oil has no such condition because it is fully consumed durring lubrication process and does not come in direct contact with water.

In Table 5 are presented the results of demulsification for tested oils, obtained by the two methods .

Table 5 Results from demulsification tests

Testing methods	Lubricating oil types		
	NL 30-5	**NS 40-12**	**NS 40-25**
OMD 113 (dynamic conditions, 10 minutes, 2 ml sample) - oil - water (ml) - sediment (ml)	 0,7 1,3 0	 0,9 1,6 0	 0,5 1,5 0
ASTM D 1401 (static conditions, 60 minutes, 40 ml sample) - oil (ml) - water (ml) - emulsion or cloudy oil (ml)	 40 39 1	 40 36 4	 40 37 3

2.3 Testing in real working conditions

The oils testing real operating conditions was conducted in collaboration with maritime operators, on engines vessels provided by these.

Oil cylinder NC 50-70 and crankcase oil NL 30-5 were tested on two propulsion engines K 6 SZ 90/160 A for a duration of 1000 hours of operation. Engine cylinders were examined periodically during the experiment, at each 100 hours of operation to assess the deposits formed in the exhaust windows and spaces between the rings. Results from cylinder oil testings are presented in Table 4.

The oil NL 30-5 introduced in the same engine crankcase was periodically investigated by laboratory methods for setting the service life and in terms of the cleanliness of the engine parts.

Physico-chemical characteristics of oil were in the allowable limits throughout the investigation, as shown by the data in Table 6.

Table 6. Results from crankcase oil NL 30-5 testing

Physico-chemical characteristics	Fresh oil	After 1000 hours	Test method ASTM-D
Density at 20 ºC,g/cm3	0,890	0,895	1298
Kinematic viscosity at 100°C, cSt	11,3	13,3	445
Viscosity index	95	90	2270
Flash point, COC, °C	225	224	92
Pour point, °C	- 21	-23	97
Total base number, mg KOH/g	5,2	4,0	2896
Total acidity number, mg KOH/g	2,1	4,7	664
Copper corrosion, 3hrs/ 100°C	1 b	-	130
Sulphated ash, %	0,75	1,30	874
Water content,%	0	0,20	95
Toluene insoluble, %	-	1,80	893

The results obtained both through periodic evaluation of the oil and the final examination of the engines after their partial removal, showed that the oil NL 30-5 behaved normally.

NS 40-12 oil was tested on two types of propulsion engines four-strokes SKL 82 D 72/48 AL-1, taking into account periodic and final examination at the engine and oil. As shown by the data in Table 6, oil characteristics have changed during the experiment, as follows:

- increased oil viscosity due to oxidation products formed in the oil and from fuel combustion;
- total acidity number grew to 2.6 mgKOH / g due to the combustion products;
- basicity number decreased after neutralizing the acids resulted from the fuel combustion.

However, the highlighted changes sign up in acceptable limits for lubricanting engine oils.

Table 7. Results from NS 40-12 oil testing

Physico-chemical characteristics	Fresh oil	After 1000 h	Test method ASTM-D
Density at 20 ºC,g/cm3	0,890	0,910	1298
Kinematic viscosity at 100°C, cSt	14,7	16,3	445
Viscosity index	90	-	2270
Flash point, COC, °C	232	224	92
Pour point, °C	- 23	-	97
Total base number, mg KOH/g	12,2	7,0	2896
Total acidity number, mg KOH/g	1,1	4,7	664
Copper corrosion, 3hrs/ 100°C	1 b	-	130
Sulphated ash, %	1,85	1,70	874
Water content,%	0	0,20	95
Toluene insoluble, %	-	1,54	893

The results of the periodic investigations of oil and the final examination of the engine concluded that the lubricant behaved similarly with reference oil experienced the same conditions.

Oil NS 40-25 was tested on a vessel equipped with two propulsion engines type MAN L 52/55 A: at the portside of the vessel was equipped with a reference oil and at starboard with the tested oil. The obtained results are similar (Table 8).

Table 8. Results from NS 40-25 oil testing and reference oil

Physico-chemical characteristics	Portside Oil		Starboard oil	
	fresh	used	fresh	used
Density at 20 ºC,g/cm3	0,905	0,912	0,925	0,911
Kinematic viscosity at 100°C, cSt	14,30	15,30	15,19	15,80
Viscosity index	90	92	90	95
Flash point, COC, °C	238	232	230	225
Pour point, °C	-15	-15	- 21	-21
Total base number, mg KOH/g	22	14	27,00	16,19
Total acidity number, mg KOH/g	-	-	3,5	5,8
Copper corrosion, 3hrs/ 100°C	1 b	-	1 b	-
Sulphated ash, %	2,8	-	3,3	-
Water content,%	0	0,6	0	1,2
Toluene insoluble, %	-	2,0	-	1,9

3. CONCLUSION

The tests carried out showed that marine lubricants made from paraffinic base oils and additives, fit in terms of quality imposed by the service areas.

From laboratory investigations data by physico-chemical characterisation and special stands as well as from testing in real working conditions, the following conclusions were drawn:

- the formulated lubricating oils covers the engines lubrication conditions from commercial and fishing shipping vessels;
- selected additives were found appropriate, including their demulsification ability;
- the formulation of above lubricants were taken into account construction and operating characteristics of engines and the types of fuel used;
- the obtained oils provide proper engine lubrication in all operating conditions of the vessel;
- the formulated crankcase oils NL 30-8, NS 40-12, NS 40-25 and the cylinder oil NC 50-70 for marine engines exhibit good working behaviour and satisfy all the requirements imposed by these special operating conditions.

REFERENCES

[1] D.T. Mang, W. Dresel: Lubricants and Lubrication, Lubricants and their Market, pp.2, e-books Willey 2007;

[2] A.G. Marin, I. Petre, L. Bogatu: Vegetable Oils in Engine Lubricants Formulations, Proceedings of the Conference on Materials Engineering and Technologies, Mitech ’07, 26 – 27 June 2007, Prague;

[3] *, “A rationalized additive package for marine trunk piston engine oils and crosshead system oils”, Infineum UK Limited, Oxfordshire, 1997, England;

[4] Pevzner, L., “Aspects of Marine Low-Speed, Cross-Head Diesel Engine Lubrication” J. of the Society of Tribologists and Lube. Eng., June 1998, 16-21.

SERBIATRIB '11

Serbian Tribology Society

12th International Conference on Tribology

Faculty of Mechanical Engineering in Kragujevac

Kragujevac, Serbia, 11 – 13 May 2011

SLIDE BEARING FOR ELECTRIC MOTORS IN TESLA'S LEGACY

Aleksandar Marinković[1], Bratislav Stojiljković[2], Miloš Stanković[1]

[1]Mechanical Engineering Faculty University of Belgrade, Serbia
amarinkovic@mas.bg.ac.rs, milos.b.stankovic@gmail.com
[2]Nikola Tesla Museum Belgrade, Serbia, bratislav.stojiljkovic@tesla-museum.org

Abstract: *Nikola Tesla (1856-1943) made numerous inventions and discoveries in the field of electricity, which are the basis of new scientific and technological breakthroughs, started in the late 19th century, and without which our present life could not be imagined. Tesla's work in mechanical engineering has been less studied and published so far, and therefore deserves special attention and interest not only by scientists but also by a chronicler of his life. Besides numerous saved archival documents, personal and technical objects, monographs and serial publications, some samples of slide bearings for electric motors were also found in his legacy.*
The aim of the paper is to present these samples and describe their place in designs of electric motors from that historical period. Authors also provide CAD models based on original samples including some indications of their lubrication and assumed way of operation in electric motor exploitation.

Keywords: *slide bearing, electric motor, lubrication, Tesla, Tesla's legacy, Nikola Tesla Museum.*

1. INTRODUCTION

Nikola Tesla, scientist and inventor, lived and worked in the period that covers both the 19th and 20th century. He belongs to those rare inventors whose inventions for more than a hundred years have not ceased to attract the attention of many scientists and researchers. It was a series of new discoveries, from those in the field of electrical engineering, lighting technology, radio technology, to numerous applications of high-frequency currents in industry and medicine and unusual, original inventions in mechanical engineering and aviation [1].

Thanks to his specialist knowledge and exceptional creativity he was able to solve some technical problems in mechanical engineering and to realize a wide range of new inventions and constructive solutions based explicitly on physical laws. More than twenty years of Tesla's work in the early 20th century is dedicated to the research in this area. Often, without using well established engineering principles, he found his own way to come to genuine and interesting solutions for new design of pumps, turbines, speedometer or fountains. Of particular importance is his contribution to the development of new types of paddleless turbo machines, initiated by the original idea of energy exchange between the fluid in the circuit and turbine discs based on viscous friction [2].

Several original technical exhibits, as well as several articles in newsletters and journals, preserved as a part of Tesla's legacy in the Nikola Tesla Museum in Belgrade, point to the possibility that Nikola Tesla in one period of his life worked on the construction of radial slide bearings for particular types of electric motors. It may be assumed that Tesla was also occupied with the ways and conditions of lubrication of the bearings in the given operational conditions. Preserved specimens of slide bearings and advertising catalogs for electric motors of some U.S. companies from this period lead to this assumption.

2. DESCRIPTION OF ELECTRIC MOTORS AND BEARINGS FOR ELECTRIC MOTORS IN TESLA’S AGE

Thanks to Tesla's discovery of rotating magnetic field the induction motor was designed and a new technology of energy transfer to great distances was introduced, based on the application of polyphase alternate currents [3], [4].

Between the first Tesla's alternate current motors and the present-day ones there is a great difference with regard to their sizes and ratio of weight to power. However, it is only a consequence of the use of better materials and optimization of design and control, while the technical concept remain the same as founded by Tesla' patents more than hundred and twenty years ago.

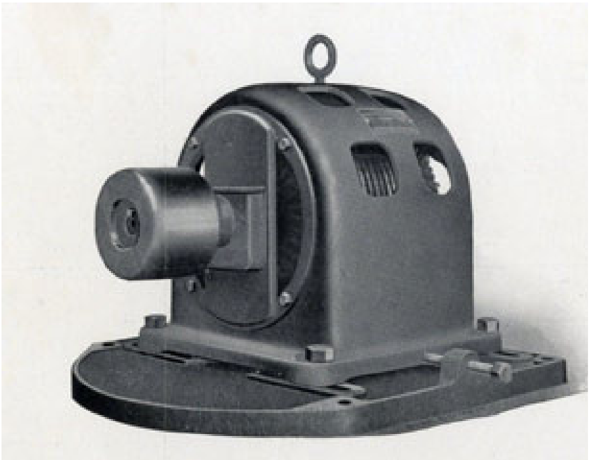

Figure 1. Type EB Induction Motor

Reliability, high average efficiency, long wearing life and low depreciation are obtained by combining correct mechanical design with correct electrical design and by using only the highest quality of materials placed in ample proportion where needed to secure low heating and corresponding capacity for continuous severe service.

They are manufactured as open motors with as much protection to the active parts as is consistent with proper openings for inspection, free ventilation, and adjustment of brushes. They are also furnished with solid enclosing covers or with ventilated or semi-enclosing covers to meet special conditions. These machines can be furnished for suspension from side walls or ceiling by turning the bearing brackets. All parts are interchangeable and the design is rugged, compact, simple and adaptable to any sort of work where reliable electric motor is required.

At the time of Nikola Tesla, the electric motor shafts were supported by slide bearings. Bearings are of composite bearing metal, snugly fitted and secured in bearing brackets and lubricated by multidisc ring oilers which convey oil to the surface of revolving shaft from the recessed pockets in the bearing brackets.

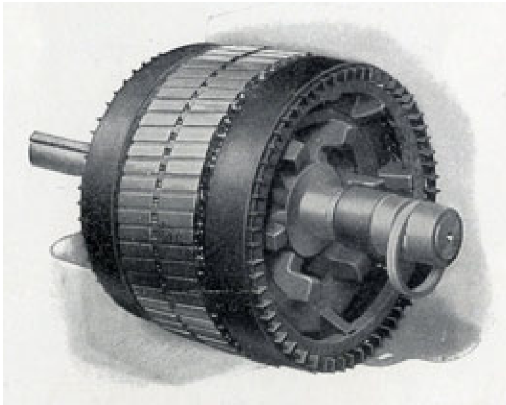

Figure 2. Rotor of Standard Induction Motor

Nowadays slide bearings are phosphor bronze sleeves, adequately grooved for oil circulation, and are interchangeable end for end. Brass oil rings of special design and large diameter feed an abundant supply of fresh oil constantly to the shaft, thereby assuring minimum wear on shaft and bearings. The principle of lubrication of those bearings is shown at the Figure 3.

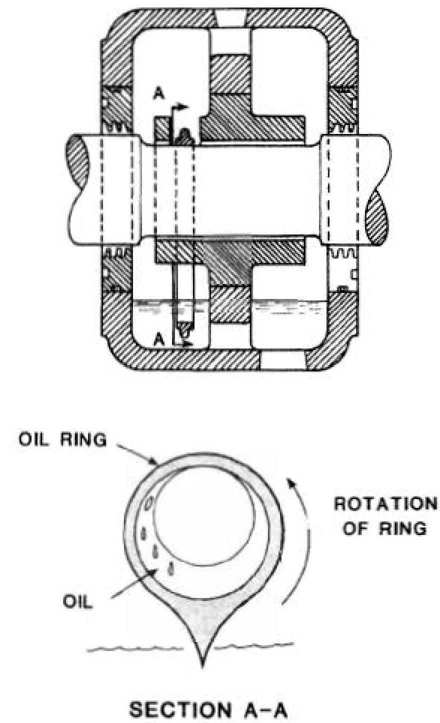

Figure 3. Lubrication of bearing by means of an oil ring

3. EXAMPLES OF SLIDE BEARINGS IN TESLA'S LEGACY

Tesla's estate represents a unique entirety which is preserved, investigated and studied within the bounds of three basic collections of the Nikola Tesla Museum: Archives, Collections and Library.

Tesla' personal assets and technical objects are not only a historical nad material evidence of Inventor's life and work but also a first-class source for the study of the history of technical and technological progress at the end of 19th century and the beginning of 20th century in the Europe and USA.

The preserved technical objects are arranged in four of ten collections of the Museum. These are: Electrical engineering collection, Mechanical engineering collection, Chemical engineering collection, and Collection of minor technical objects. In other words, technical collections of the Museum are organised in accordance with the scientific disciplines in which the objects were either used or represented the results of research performed [5].

In the Mechanical engineering collection there are three original objects, which indicate the possibility of Tesla's interesting in the area of tribology. Two preserved objects, items No. T.23.103 and No. T.23.104, represent machined pieces for manufacturing a slide bearing for electric motors of that period. Both pieces are made of brass by turning on the lathe. We assume that these were experimental pieces which had to enable a realization of Tesla's subsequent modifications and improvements, devised in order to ascertain optimum final characterictics and design of a radial slide bearing.

Their dimensions are almost equal: inner diameter is 15.9 mm, outer diameter 27 mm, while maximum outer diameter of both machined pieces is 28.6 mm. A slight difference in dimensions of these pieces is expressed only in their overall lengths: 44.6 mm at T:23.103 vs. 44.5 mm at T:23.104.

Figure 4. Machined piece for slide bearing T:23.103 (Collection of Objects from the Field of Mechanical Engineering)

However, the main difference between these two pieces is a hole of 5.1 mm diameter and 2.2 mm depth, bored additionaly on the outer surface of one of these pieces (T:23.104). Boring of this hole points to Tesla's initial considerations about the choice of an adequate design which would secure a more uniform delivery of oil into all parts of the shaft of electric motor.

Figure 5. Machined piece for slide bearing T:23.104 (Collection of Objects from the Field of Mechanical Engineering)

The third preserved object is registered in the same collection as item No. T: 23.102. It represents Tesla's design of radial slide bearing, by its shape and other characteristics typical for mounting into the electric motors of that period. Confirmation of their similarity we can find in the advertising catalogues, published by "Diehl Manufacturing Company", Elisabethport, New Jersey, preserved in Tesla's estate. These catalogues, together with catalogues of other American manufacturers of electric motors, suggest that Tesla was paying a thorough attention to the research and development in the fields of science and engineering relevant for his activity [6], [7].

Tesla's slide bearing T: 23.102 are made of brass, by turning on lathe and milling. Its dimensions, except the overall length of 44.2 mm, are identical with those of pieces T: 23.103 and T: 23.104. It suggests that all the three pieces represent a result of a research carried out on a specific type of radial slide bearing.

On the outer curved surface of Tesla's radial slide bearing, next to the opening for oil ring, there are also two smaller circular holes of different radii. Looking on the opening for oil ring, the greater hole, 5.7 mm diameter, is positioned at the left side of the curved surface of the bearing. The smaller hole, 2.3 mm diameter, is placed on the rear side of the curved surface. These two holes, with regard to their diameters and positions on the curved surface of the slide bearing, had to secure maintaining the level of lubricant at the proper height, and on the other hand, to prevent the possible excess of oil to penetrate into the interior of an electric motor and come into contact with its windings.

By comparison of Tesla's design, with holes bored on the curved surface of his slide bearing, with similar design of slide bearings built into electric motors made by Diehl Manufacturing

Company, a clear distinction with regard to the position of holes can be made. At Tesla's design, the greater hole is placed on the left side of the curved surface, at one-third of the bearing height, looking from the opening for oil ring. At the slide bearing of the American manufacturer, however, a hole of similar dimensions, bored for the same purpose, is placed on the top of the curved surface of the bearing, behind the opening for the oil ring. (Precise data are not given in the advertising catalogues). As to the hole with smaller diameter, which is placed on the rear side of Tesla' slide bearing, an adequate comparison was not possible, because the hole of similar dimensions could not be found on the photographs and drawings in the advertisings of the manufacturer.

On the inner surface of Tesla's radial slide bearing, along its axis, two spiral.shaped grooves, each one of 1mm width and approximately 1 mm depth, are cut. Their purpose is to render a more uniform delivery of oil into all parts of the motor shaft and to return excess oil into the central tank.

Figure 6. Model of Tesla's radial bearing for electric motors, T:23.102 (Collection of Objects from the Field of Mechanical Engineering)

However, the original oil ring of Tesla's slide bearing T.23.102 has not been preserved. Lack of this ring makes impossible a complete comprehension of Tesla's design and ascertainment of its performances in terms of lubrication.

Generally speaking, oil rings have the purpose to enable a continuous delivery of fresh oil to slide bearings and shaft, and in this way to secure their minimum wearing during the operation of electric motors. Due to this purpose, oil rings are of greater diameter and of specific design. They are mounted on the outer side, at the opening cut in the curved surface of the slide bearing. In this way, they continuously adhere to the shaft, rotate together with it, lubricating it with a considerable quantity of oil. Oil rings are made of brass or a similar material. In the advertising material printed by Diehl Manufacturing Company we can find photographs of slide bearings with an oil ring of a particular design.

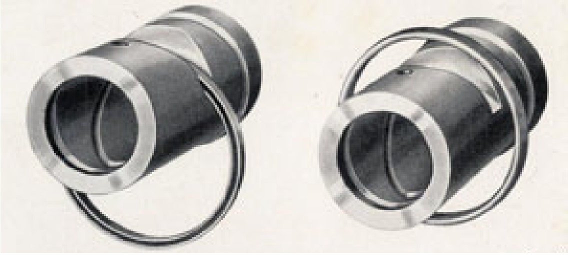

Figure 7. Type of Bearings Used on Diehl Polyphase Induction Motors

4. 3D CAD MODELS OF TESLA'S SLIDE BEARINGS

To have better insight into the samples, CAD models have been designed using CATIA V5 R18 software. Besides giving faithful representation of samples, these models can be used for further analysis in terms of stresses and deformations. This can be the subject of subsequent investigation.

Figure 8. 3D CAD model of the machined piece T:23.103

Figure 9. 3D CAD model of the machined piece T:23.104

Figure 10. 3D CAD model of Tesla's radial slide bearing T: 23.102

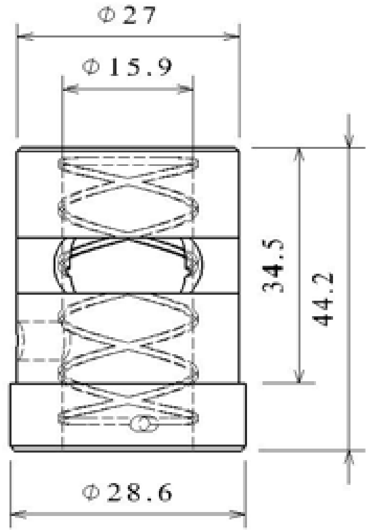

Figure 11. 3D CAD (transparent) model of radial bearing, dimensioned.

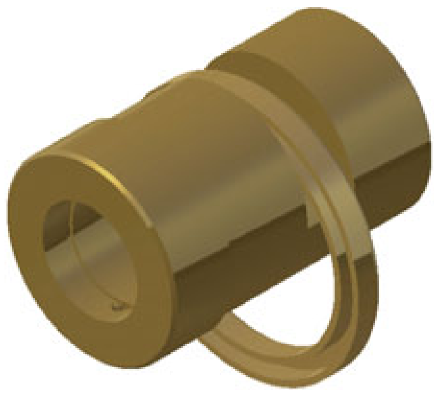

Figure 12. Presumed assembly of bearing and oil ring

5. CONCLUSION

This paper gives types and operational performances overview of sliding bearings that were common in use during the last century when Nikola Tesla investigated and studied electric motors and also their construction and application. Some of those original sliding bearing samples that are keeping in Nikola Tesla Museum in Belgrade are presented following with corresponding CAD models made in CATIA software.

Although we cannot say for sure that Tesla designed the bearings, the fact that they stayed at his heritage forces us to consider this possibility and examine all the features of these cases.

Taking into account that more than 50% of electric motors failures was due to improper lubrication of bearings, analysis of bearings from Tesla's heritage can lead to clearing his thinking in the area of Tribology, as well his contribution in engineering in general. The role of bearing those are current applied in electric motors are more significant, where besides sliding, also rolling bearings are frequently applied. Most electric motors do not contain “special” bearings. The only differences between an electric motor bearing and any other bearing are the higher noise standard and possible electric insulation to prevent electric current passage through the bearing. To reduce noise, process tolerances are much closer, which keeps the bearing running quieter.

AKNOWLEDGEMENT

This work has been performed within the projects TR-35021 and TR-35011. Those projects are supported by the Republic of Serbia, Ministry of Science and Technological Development, which financial help is gratefully acknowledged.

REFERENCES

[1] B. Jovanovic: Tesla – Spirit, Work, Vision, Freemental, Belgrade, 2001.

[2] Tesla III Millennium, The Fifth International Conference, Proceedings, 15-18.10.1996. Belgrade,

[3] Burke Electric Company, Bulletin 119, Direct Current Motors and Generators, Erie, Pennsylvania, USA, September 1917.

[4] Burke Electric Company, Bulletin 120, Polyphase Induction Motors, Erie, Pennsylvania, USA, May 1918.

[5] Nikola Tesla Museum 1952-2003, Nikola Tesla Museum, Belgrade, 2006,

[6] Diehl Manufacturing Company, Bulletin No. 1653, Diehl Direct Current Motors and Generators, Elizabeth, New Jersey, USA,

[7] Diehl Manufacturing Company, Bulletin No. 1672, Diehl Alternating Current Polyphase Induction Motors, Elizabeth, New Jersey, USA.

Serbian Tribology Society

SERBIATRIB '11

12th International Conference on Tribology

Faculty of Mechanical Engineering in Kragujevac

Kragujevac, Serbia, 11 – 13 May 2011

DAMAGE OF THE Co-Cr-Mo FEMORAL HEAD OF A TOTAL HIP PROSTHESIS AND ITS INFLUENCE ON THE WEAR MECHANISM

Lucian Capitanu[1], Liliana Laura Badita[2], Dumitru Catalin Bursuc[3]
[1]Institute of Solid Mechanics of Romanian Academy, Bucharest, Romania,
[2]Micro and Nanomechatronic Technolologies Laboratory, National Institute for Research and Development in Mechatronics and Measurement Technique Bucharest, Romania, badita_l@yahoo.com
[3]Military Technical Academy, Bucharest, Romania

Abstract: *Co-Cr alloy is one of the most used alloys for artificial hip joints and offers a good combination of mechanical properties, corrosion resistance and biocompatibility. To increase its resistance to wear are commonly used hard coating thin layers of Co-Cr-Mo. Analyzing a femoral head of a Co-Cr modular total hip prosthesis coated Co-Cr-Mo, we found peeling coating, abrasion of the substrate, but and hardening of abrasion traces against subsurface initial hardness. This paper presents an analysis by the Student test, of the microhardness peeling a portion of a scratch from a femoral head explant covered with Co-Cr-Mo, and that demonstrate the transformation of wear mechanism from three bodies abrasion in two bodies abrasion.*

Keywords: *total hip prostheses, Co-Cr-Mo coating, spalling, three-bodies abrasion, hardening, two-body abrasion.*

1. INTRODUCTION

Total hip prostheses are among the most successful medical devices. Sir John Charnley, the "father" of modern hip artificial joints, he called "the programmed failure medical devices", now they funcionand generally without problems in the human body for over 12-15 years. Expanding surgical procedure total hip replacement and in younger patients, with intense physical activity, required to find technical and technology solutions to increase the lifespan of total hip prosthesis. However their durability is limited by the wear resistance of the joint bearing femoral head - acetabular cup. In addition, long-term cyclic mechanical loading of the femoral head of a total hip prosthesis, leads to deformation of the femoral head [1]. Scientific and technological advances have made today will be used for a wide range of modular hip prostheses, alloy or ceramic biocompatible, very resistant to wear. If the exception the prosthesis metal / metal have recently been reconsidered, total hip prostheses most used are of the femoral head of Co-Cr-Mo alloy or Ti-6Al-4V, which acts against acetabular cups of ultra-high weight polyethylene molecular (UHMWPE).

The base material of the femoral head provides the taking over mechanical loading, and hard coating on the femoral head provides (or should) wear resistance. There are several methods of thin and multilayer coating of the femoral heads, suitable of the coating material and the substrate. The most common PVD coating process is suitable both Co-Cr-Mo alloy, and Ti-6Al-4V. Ti-6Al-4V alloy has an excellent corrosion resistance, a very high biocompatibility, high strength relative to weight and also a great tenacity, for these reasons he is an alloy widely used for advanced biomedical applications [2].

However, the tribological properties of these alloys are known to be weak, especially in abrasive and sliding conditions [3]. High friction coefficient and severe adhesive wear occurs frequently when Ti-6Al-4V alloy sliding against other engineering materials. Were studied several surface treatments to modify the tribological properties of this alloy, including plasma nitriding [4], ion implantation by plasma immersion [5], laser nitriding and physical vapor deposition (PVD) [6]. Among various processes, PVD can produce coating layers at lower temperatures of the process and therefore, it has the advantage of fewer adverse effects on mechanical properties of the substrate. In the literature many studies are present Ti-6Al-4V alloy coated with either a single coating [7,8] or by duplex approach, aimed at increasing the loading on substrate: nitration / TiN [9], HVOF WC -Co / TiN [10], nitration / DLC [11], deep hardening oxygen / DLC [12].

The friction properties of a tribosistem strongly depend of the matched material properties, the external environment and the nature of the wear particles generated during sliding [20]. The way that deforms a surface will dictate the nature of the wear particles generated, which in turn can significantly influence the wear behavior of materials. Tribofilms and wear particles generated during sliding are known to influence the behavior of the materials friction [21]. The macro-mechanical tribological mechanisms describe friction and wear phenomena by taking into account the distribution stresses - strains in the entire contact, total elastic and plastic deformations, formation process of wear debris and its dynamics [22,23].

Recently, the effect of different mating materials on friction behavior of TiN coatings with different crystallographic orientations was studied [24]. It was noted that the formation of a titanium oxide layer on the surface, lead to a lower value of friction. Much research has been aimed at studying the tribological behavior of pure titanium metal and titanium alloys [25,26]. But reports on the wear behavior of Ti thin films are rare.

Since titanium nitrides are hard biocompatible materials [27,28,29] with excellent resistance to abrasion, have been developed more advanced processing methods in order to achieve a nitrided layer on the surface of materials. At the nitriding in plasma [30], nitrogen atoms diffuse into the titanium matrix, forming a layer of TiN and Ti_2N compounds, usually followed by a deeper diffusion layer. This layered structure produces a continuous profile of hardness, thus providing adequate support of the coating [28,31]. However, the physical properties of treated surface are highly dependent on plasma coating technique and processing parameters.

Co-Cr-Mo alloy is one of the most used implant alloys for artificial joints and offers a good combination of mechanical properties, good corrosion resistance and high biocompatibility [37,38]. There are several types of materials currently used CoCrMo. Each material has a different microstructure and thus different properties optimized for a design or specific function [39]. The microstructure and alloy composition affect the corrosion behavior of simulated body fluids due to changes in surface chemistry. Hiromoto et. al., [34], observed that the passive film composition depends on the solution chemistry and limits grain growth results in a decrease of corrosion resistance of weak alloys forged Ni-Co-Cr-Mo.

It is also well known that these changes affect the mechanical properties and microstructural properties of wear [42-44]. Dobbs and Robertson [24] showed that heat treatment improved the mechanical properties of the alloy, without loss of corrosion resistance. Similarly, Cawley et. al., [43] analyzed the mechanical properties and hardness of a Co-Cr-Mo alloy heat-treated and have found a correlation between carbide volume fraction and wear rate, but they did not observe any influence on the mechanical properties.

We analyzed a series of eight total hip prosthesis with modular femoral head of Ti-6Al-4V alloy and Co-Cr alloy PVD coated with TiN and Co-Cr-Mo respectively, recovered following revision surgery, finding scratching, cracking, peeling and tribocorrosion of thin layers coating. Considering our previous experience regarding the investigation of surface state of explanted total hip prosthesis, we undertook detailed research on these recovered femoral heads.

This paper presents an analysis based on Student test of the case increase microhardness a peeling portion of the coated Co-Cr-Mo femoral head explanted of a total hip prosthesis, demonstrating the transformation of wear mechanism, by three body abrasion in two body abrasion.

2. EXPERIMENTAL METHODS

The femoral head - acetabular cup joints of eight explant total hip prostheses analyzed and presented in Figure 1, have been studied in terms of femoral head damage, which led to wear femoral cups. From beginning to be noted that all joints had various degrees of wear, some of them even catastrophic.

Figure 1. Retrieved total hip prostheses were analyzed.

The investigated hip prosthesis were numbered from left to right starting from 1 to 8. The prosthesis 1 was an alloy Ti-6Al-4V, with alumina ceramic femoral head, of 28 mm diameter.

The prostheses 2-8 were modular head femoral prosthesis with a diameter of 28 or 32 mm, Co-Cr-Mo alloy and Ti-6Al-4V with different surface coatings, polished and ground.

The prosthesis 2 was with Co-Cr alloy femoral head, coated with Co-Cr-Mo alloy, the three prosthesis has titanium alloy femoral head coated with Ti-6Al-4V, 4 prosthesis had a Co-Cr alloy head, femoral head prosthesisfive had alloy Ti-6Al-4V coated with TiN, 6 and 7 had prosthetic heads Co-Cr alloy coated with Co-Cr-Mo, and 8 had a prosthetic femoral head of 32 mm Ti alloy coated with Ti-6Al-4V. All of the prostheses had acetabular cup of high molecular weight polyethylene (UHMWPE).

Joints femoral head - acetabular cup were first photographed, investigated in terms of deviations from roundness with a profilometer Talirond Rank Taylor Hobson, Leicester, UK, and the surface microhardness was investigated with a ultrasound microdurimeter, without contact, Sonotec (KRAUTKRAMER GmbH, Germany).

Surface condition was investigated by optical microscopy, using a microscope type Epiquant (Karl Zeiss Jena GmbH, Germany) and on an atomic force microscopy NanoLaboratory AFM Probe NTEGRA NT - MDT, Russia.

3. RESULTS AND DISCUSSION.

In this paper the we refer to prosthesis no. 7, of a PVD coated Co-Cr femoral head with a layer of Co-Cr-Mo alloy, whose joint components is shown in Figure 2.

a b

Figure 2. Femoral head and acetabular cup of THP 7.

Microhardness measurements of femoral head were made circumferential on three parallel (one located at 5 mm below the pole, one at the equator and another at 5 mm below the equator) as shown in plotting of Figure 3.

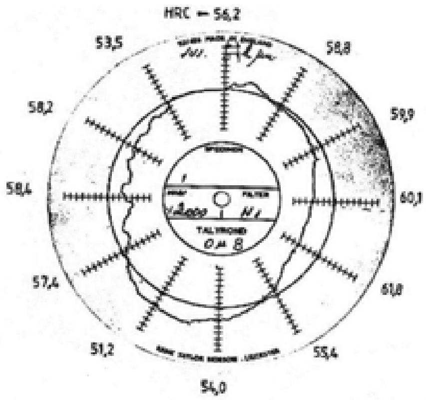

Parallel located at 5 mm below the pole

Figure 3. Femoral head surface deformation and microhardness on parallel situated at 5 mm below the pole.

Were made primarily five measurements on the flat part of the head, and their average was considered as reference value, close to the initially microhardness, because this area is less influenced by cyclical loading status. The result is a hardness of 57 HRC. The roundless records show a serious distortion of the femoral head, especially on parallel located 5 mm below the pole (Figure 3).

Note the ovoid shape of the head in the this plane with the two zones and two expanded areas, diametrically opposed. In the squeezed opposite areas, the microhardness increase in values between 58.4 and 61.8 HRC, while in the expanded areas fell to 54.0 HRC value. There are severe variations from initial microhardness, which could be due to the cold hardening material cyclc compressed.

After inspection of optical microscopy were detected coatings areas completely destroyed (Figure 4)

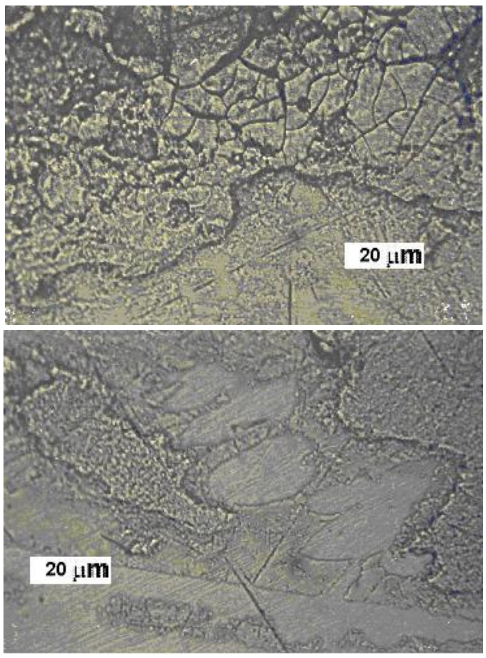

a)

b)

Figure 4. Optical microscopy images of relevant areas on the surface of the femoral head 7.

The investigation by FEM surface condition of the femoral head, showed a relatively uniform roughening of the femoral head surface, with higher R_a values, but without too much dispersion, only very few deep scratches.

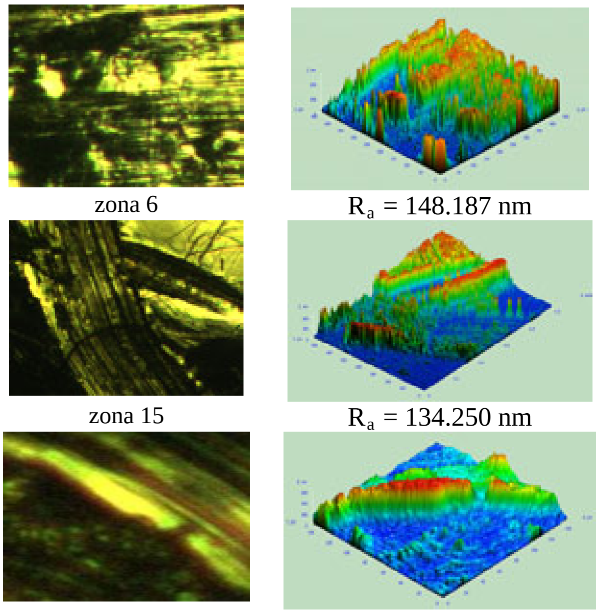

zona 6 — R_a = 148.187 nm

zona 15 — R_a = 134.250 nm

zona 16 — R_a = 119,696 nm

Figure 5. Analiza unor imagini AFM - cap femural 7

R_a values for three randomly chosen areas, are 148.187 nm, 134.250 nm and 119.696 nm respectively (Figure 5). They are approximately 2.5 - 3 times higher than the initial surface Ra values of 0.05 mm, provided by ISO 7206-2, but in a more uniform range than the other studied femoral head, which was surprising.

To elucidate this finding, we used an original tribometru (Figure 6) the ball on the plan type, with reciprocal sliding motion (Figure 6b) for studying resistance of thin layers.

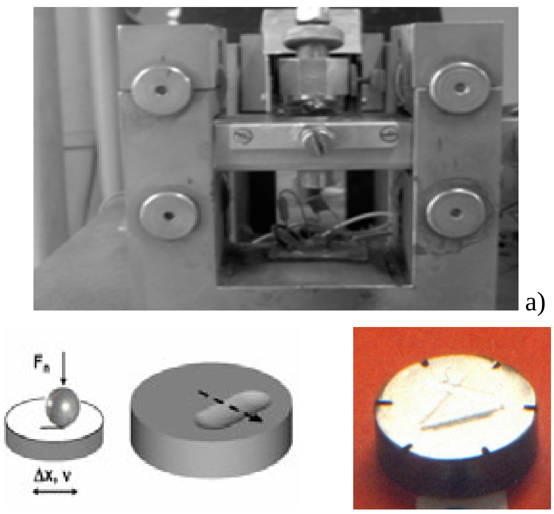

a) b c

Figure 6. Tribometer ball on plane, with sliding reciprocal movement (a), the scheme of motion (b) and one of the samples used (c).

I tested with this tribometer five disk samples C120 alloy with HRC 59 hardness and Rp 3 tool steel with hardness 62 HRC. The alumina ball was 6 mm in diameter, with higher hardness than the tested materials. They used loads of 1-5 N, to have various contact efforts, at a speed of 1, 85 cm / s.

Was quantify the volume of material removed by wear, using the "imprint method", imprint length split into ten equal parts, mathematic calculation of each wear sector based on the transverse profile of the imprints in this area, averaging these sectoral volume of material removed by wear, and by dividing the length of the test or friction course, determining the wear rate (mm / h or mm / km). Initial growth was observed between 1 and 2 N load, followed by a sudden drop of it between 2 and 4 N, then the decline has almost flattened. Before carrying out the wear tests, a check was made of the distribution normality of hardness measurements. For this purpose we made on each sample every 36 indentation at loads of 1-5 N. Microhardness imprints were made by Vickers method, using a PMT 3 microdurimeter. Imprints were made at equal distances inside a square with sides of 0.5 mm, as shown in Figure 7.

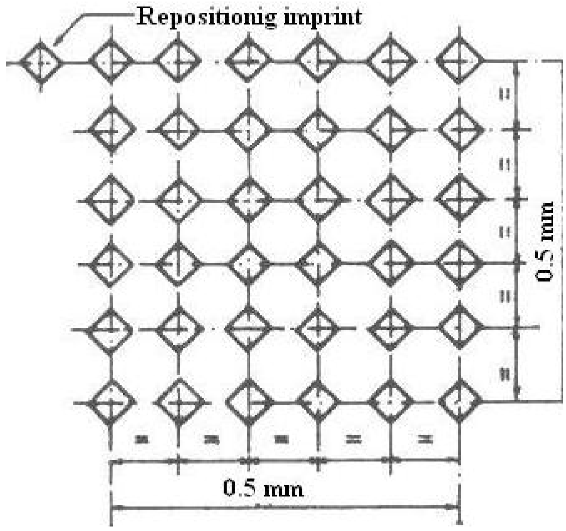

Figure 7. Schema location of microhardness imprints made with an microdurimeter PMT 3.

Microhardness values measured on a sample of C 120 steel, hardened to 62 HRC are shown in table 1, in the order they appear in the field that were performing the tests. To check the normality of the distribution microhardness values, we used Shapiro - Wilk test [13]. This test, based on order statistics is for the verification very small selections of ($3 \le n \le 50$) in terms of normality. Applying this test requires first ordering feature values, upwards, between the minimum value x_i and maximum value x_n:

$$x_1 \le x_2 \le x_3 \le ..... \le x_n \qquad (1)$$

Table 1 shows the microhardness values of the field study.

Table 1. Microhardness values of studied field.

660	636	686	713	686	648
670	670	686	629	686	629
686	670	686	694	728	648
660	660	648	670	694	694
686	670	660	713	670	713
636	660	670	660	648	694

Ordering microhardness values presented in Table 1, we obtain the following sequence of order statistics:

629	629	636	636	636	648	648	648	648
660	660	660	660	660	660	670	670	670
670	670	670	670	686	686	686	686	686
686	694	694	694	694	713	713	713	728

Calculated average and dispersion of above values, was obtained:

$$\overline{x} = \frac{1}{n}\sum_{i=1}^{n} x_i = \frac{1}{36}\sum_{i=1}^{36} x_i = 671.3055 \quad \text{si} \quad (2)$$

$$S^2 = \sum_{i=1}^{n}\left(x_i - \overline{x}\right)^2 = \sum_{i=1}^{36}\left(x_i - \overline{x}\right)^2 = 22{,}054 \quad (3)$$

W_{calc} test statistic was calculated in accordance with equation (10) [13]:

$$W_{calc} = b^2 / S^2, \quad (4)$$

where b is expressed as:

$$b = a_n\left(x_n - x_1\right) + a_{n-1}\left(x_{n-1} - x_2\right) + \ldots\ldots + a_{n-k+1}\left(x_{n-k+1} - x_k\right) \quad (5)$$

In equation (5), $k = n / 2 = 16$ (for n even), and coefficients a_n, a_{n-1} ... a_{n-k+1} depend on the size of selection and are tabulated [13]. Calculation of test statistics is shown in Table 2. On the basis of relation (5) and data from Table 2, results:

$$b^2 = (146)^2 = 21529.89$$

Table 2. Calculul statisticii testului Shapiro – Wilk.

i	x_{n-k+1}	x_k	$\omega_k = x_{n-k+1} - x_k$	σ_{n-k+1}	$\sigma_{n-k+1}.\omega_k$
1	728	629	99	0,4068	40,28
2	713	629	84	0,2813	23,63
3	713	636	77	0,2410	18,56
4	713	636	77	0,2121	16,34
5	694	636	58	0,1883	10,93
6	694	648	46	0,1678	7,72
7	694	648	46	0,1496	6,88
8	694	648	46	0,1331	6,13
9	686	648	38	0,1179	4,48
10	686	660	38	0,1036	3,94
11	686	660	26	0,0900	2,34
12	686	660	26	0,0770	2,02
13	686	660	26	0,0645	1,68
14	686	660	26	0,0523	1,36
15	670	660	10	0,0404	0,41
16	670	670	0	0,0287	0
17	670	670	0	0,0172	0
18	670	670	0	0,0057	0
Σ	-	-	-	-	146,70

Table 3. Determination of microhardness on the samples disk alloy C 120.

Load (N)	SAMPLE HARDNESS					IMPRINT HARDNESS				
	d (div.)	H_i	H_{med}	$H_{med} - H_i$	$\sigma_{H med}$	d (div.)	H_i	H_{med}	$H_{med} - H_i$	$\sigma_{H med}$
		(N / mm^2)					(N / mm^2)			
1	488	788		8		491	769		6	
1	479	808		28		488	779		4	
1	494	760	780	20	± 11.2	492	766	775	9	± 3.41
1	498	748		32		486	785		10	
1	483	795		15		489	775		0	
2	498	775		22		462	869		2	
2	473	829		32		465	858		9	
2	473	829	797	32	± 14.4	441	873	867	6	± 4.80
2	483	795		2		459	880		13	
2	495	757		40		466	854		13	
3	483	795		4		489	775		7	
3	468	847		56		488	779		3	
3	498	748	791	43	± 17.9	490	772	782	10	± 5.29
3	495	757		34		487	782		0	
3	479	808		17		481	802		20	
4	482	798		5		602	512		17	
4	465	859		65		580	551		22	
4	496	754	793	39	± 19.7	600	515	529	14	± 11.2
4	497	751		42		575	561		32	
4	480	805		12		605	507		22	
5	485	788		7		580	551		28	
5	481	892		7		595	524		1	
5	390	772	795	23	± 7.82	575	561	523	38	± 15.0
5	479	808		14		525	476		47	
5	477	815		20		600	515		8	

Table 4. Determination of microhardness on the samples disk steel Rp 3.

Load (N)	SAMPLE HARDNESS					IMPRINT HARDNESS				
	d (div.)	H_{i} (N / mm^2)	H_{med}	H_{med} - H_{i}	$\sigma_{H\ med}$	d (div.)	H_{i} (N / mm^2)	H_{med}	H_{med} - H_{i}	$\sigma_{H\ med}$
1	489	775	775	0	± 3.40	486	785	766	19	± 14.0
1	492	766		9		488	779		13	
1	488	779		4		498	748		18	
1	491	769		6		482	798		32	
1	486	785		10		507	721		45	
2	510	713	745	32	± 24.8	520	686	745	59	± 26.2
2	485	788		43		487	782		37	
2	476	818		73		482	798		53	
2	508	719		26		485	788		43	
2	520	686		59		525	673		72	
3	486	785	766	19	± 14.0	500	742	697	45	± 18.3
3	488	779		13		520	686		11	
3	498	748		18		531	658		39	
3	482	798		32		503	733		36	
3	507	721		45		532	655		42	
4	497	748	780	32	± 11.2	540	636	674	38	± 17.5
4	423	788		8		641	634		40	
4	483	795		15		517	694		20	
4	479	808		28		523	678		4	
4	494	760		20		505	727		53	

For the test statistics, results in accordance with equation (5), the value:

$$W_{calc} = 21520.89 / 22054 = 0{,}976$$

The test statistics W_{calc} is between the values $W_{0.50}$ = 0.970 and $W_{0.90}$ = 0.984 of the statistics Shapiro - Wilk test, for normality checking [13].

The above two values correspond to the normality of the distribution probability of 50% and 90%. By performing a linear interpolation of value W_{calc} between values $W_{0.50}$ and $W_{0.90}$, results for the probability of a normal distribution of microhardness, the value:

$$p = 0.50 + (0.90 - 0.50)\frac{0.976 - 0.970}{0.984 - 0.970} = 0{,}67.$$

Therefore, it can be appreciated that the values obtained by microhardness imprints belong to a 67% probability of a normal distribution, because the condition W_{067} $W_{0.50}$ is satisfied. The specimens of alloy C 120 and Rp 3 steel ones, such as having verified normal distribution, the values of microhardness, were conducted the wear tests, at normal sarcuni ranging between 1 and 5 daN.

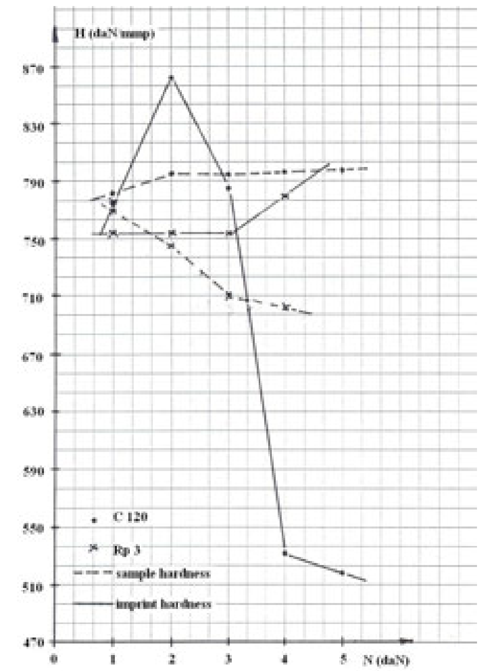

Figure 8. Microhardness variation between contact area and normal load.

On the results wear imprints and on unused portion of the samples were then conducted with five microhardness measurements at equal distances from each other, calculating both microhardness average and standard deviation.

The results are presented in Tables 3 and 4. On this basis, in Figure 8 is illustrated the correspondence between the variation of microhardness contact area of the metallic specimen, function of normal load. Figure 8 illustrates a relatively quick increasing of contact area initial hardness, which results in a low wear rate, until a certain load (contact pressure), then show a sharp decreasing.

The analysis presented above illustrates that the action of normal load (contact pressure), causing cold hardening of metallic material. This happens only to a certain amount of contact stress, then harden layer is destroyed, and the wear rate increases catastrophically. We believe that the same phenomenon happens when explanted the femoral head of total hip prosthesis subject of this paper.

4. CONCLUSION

Due to strong cyclic loading during the patient's current activities (eg the resulting force is about four times the body weight), femoral head is subjected to cyclic deformation plus the aggressive action of the body fluid. As a result, due to the relative speed between head and cup, the wearing process takes place, amid tribocorrosion cracking induced by synovial fluid.

Tribocoroziunea occurs in the micropores and microcracks in hard coating Co-Cr-Mo, exfoliation resulting in the appearance of wear particle. They promote abrasive wear mechanism that leads to three bodies grinding thin coating of the femoral head.

We believe that the small particles resulting from wear damage coating are embedded in the cup bearing surface, still acting as a tool for grinding outer spherical surface, strong loading of femoral head and cold hardening the substrate. In this way the mechanism of wear of the femoral head surface is transformed from three-body abrasion, in a two-body abrasion process, the acetabular cup acts as an outer spherical grinding tool with abrasive particles embedded in the ultra high molecular weight polyethylene surface. Also consider that insufficient adherence to the thin film coating to base material, favors the tribocorossion cracking and peeling coating.

We believe that in case of Co-Cr alloy, strong mechanical loading of femoral head surface leads to cold hardening began of the base material (Co-Cr). This causes a relatively mild wear of coating, manifested by tarnishing it.

REFERENCES

[1] Capitanu L., Onisoru J., Iarovici A., Tiganesteanu C. Scratching mechanisms of hip artificial joints, Journal of the Balkan Tribology Associatiation, Vol. 15, No. 2, 280-291, 2009.

[2] Osterle W, Klaffke D, Griepentrog M, Gross U, Kranz I, Knabe Ch. Potential of wear Resistant coatings on Ti–6Al–4V for Artificial hip joint bearing surfaces. Wear 2008; 264:505–17.

[3] Wilson A D, Leyland A, Matthews A. A comparative study of the influence of plasma treatments PVD coatings and ion implantation On the tribological performance of Ti–6Al– 4V. Surf Coat Technol 1999; 114:70 – 80.

[4] Bemporad E, Sebastiani M, Staia M H, Puch I Cabrera E. Tribological studies on PVD / HVOF duplex coatings on Ti6Al4V substrate.Surf Coat Technol 2008; 203:566–71.

[5] Avelar-Batista J C, Spain E, Fuentes G G, Sola A, Rodriguez R, Housden J. Triode Plasma Nitriding and PVD coating: a successful pre-Treatment combination to improve the wear resistance of DLC coatings on Ti6Al4 alloy. Surf Coat Technol 2006; 201:4335–40.

[6] Zhang Z X, Dong H, Bell T, Xu B S. The effect of deep-case oxygen hardening on the Tribological Behaviour of a-C:HDLC Coatings on Ti6Al4V alloy. JAlloys Compd 2008; 464:519–25.

[7] Varenberg M., Halperin G., Etsion I., Different aspects of the role of wear debris in fretting wear, Wear 252 (2002) 902–910.

[8] Zhou Z., Rainforth W.M., Tan C.C., Zeng P., Ojeda J.J., Romero-Gonzalez M.E., Hovsepian P.Eh., The role of tribofilm and roll-like debris in the wear of nanoscale nitride PVD coatings, Wear 263 (2007) 1328–1334.

[9] Holmberg K., A concept for friction mechanisms of coated surfaces, Surf. Coat. Techn. 56(1992) 1-10.

[10] Holmberg K, Matthews A., Ronkainen H.,Coatings tribology-contact mechanisms And surface design, Tribol. Int. 31 (1998) 107–120.

[11] Tanno Y., Azushima A., Effect of counter materials on coefficients of friction of TiN coatings with preferred grain orientations, Wear 266 (2009) 1178– 1184.

[12] Valero Vidal C, Igual-Munoz A. Corrosion Science 2008; 50:1954–61.

[13] Chelliah N., Kailas S.V., Synergy between tribo-oxidation and strain rate response on governing the dry sliding wear behaviour of titanium, Wear 266 (2009) 704–712.

[14] Iliescu D. V., Vodo V. G., Statistics and clearances. Technical Press, Bucharest, 1977 (in Romanian).

Serbian Tribology Society

SERBIATRIB '11

12th International Conference on Tribology

Faculty of Mechanical Engineering in Kragujevac

Kragujevac, Serbia, 11 – 13 May 2011

LOSS MECHANISMS AND EFFICENCY OF PUSHING METAL BELT CVT

Milan Banić[1], Dušan Stamenković[1], Vojislav Miltenović[1], Jelena Milisavljević[1]
[1] Faculty of Mechanical Engineering, University of Niš, Niš, Serbia
banicmilan@hotmail.com; dusans@masfak.ni.ac.rs;
vojamiltenovic@yahoo.com; jelena.milisavljevic@masfak.ni.ac.rs

Abstract: *The paper describes the loss mechanisms that occur due to friction within the belt drive as well as belt-slip losses due to friction between metal belt and the pulleys. Paper gives an over review of current models of friction caused losses in metal belt CVT drives as well as the advantages and drawbacks of described models. Paper also discusses impacts of lubricating oils on the transmission efficiency of CVTs as well as effects of metal–metal friction characteristics on the efficiency of a metal V-belt type CVT under various running conditions. The paper summarizes results of investigation of clamping force, lubrication and transmission ratio on the efficiency of metal belt CVT.*

Keywords: *Continuously variable transmission, friction, lubrication, loss modeling.*

1. INTRODUCTION

Continuously variable transmission (CVT) has been used for many years in diverse industries. The continuous adjustment of the output speed at constant driving speed is required in many applications. Usage of CVT is especially in the automotive industry as they offer the potential for an improvement in fuel economy relative to discrete ratio transmissions. This arises from the ability to match the engine operating point more beneficially to vehicle requirements as a result of the continuous ratio range. There are many kinds of CVTs [1]: Spherical CVT, Hydrostatic CVT, E-CVT, Toroidal CVT, Power-split CVT, Belt CVT, Chain CVT, Ball-type toroidal CVT, Milner CVT, NUVinci, etc. The review of possible CVT concepts is given on Fig.1. However, belt and push metal belt (or chain) types are the most commonly especially in automotive applications.

Metal push belt CVT consists of cone disks enveloped by a power-transmitting device like belt or chain. Power transmission is done through friction between the disc and chain.

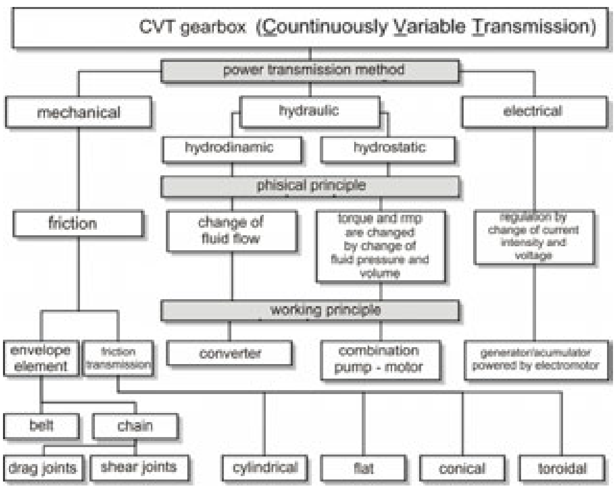

Figure 1. *Review of possible CVT concepts [1]*

Varying of transmission ratio is achieved by different position of disc on input and output shaft (Fig.2), i.e. by changing the diameter at which there is direct contact between metal belt and discs. Required pressure force between compressed elements of the chain and working surface is usually achieved by hydraulics via a special hydro aggregates.

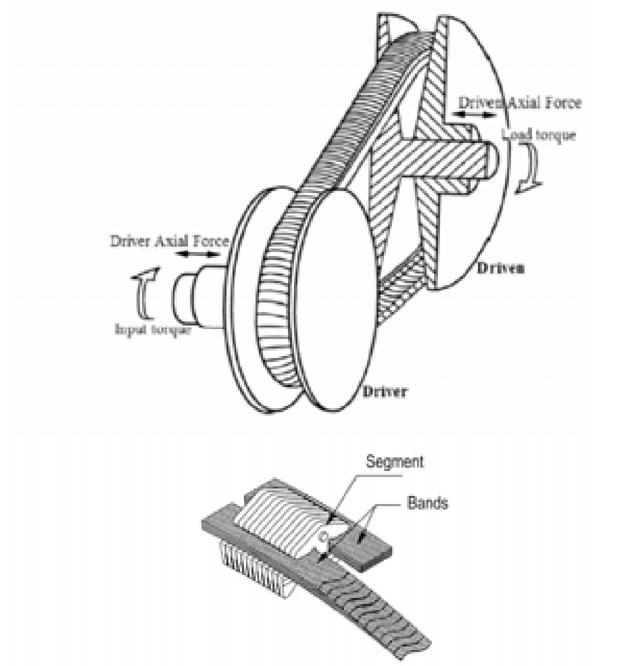

Figure 2. *Schematic diagram of a metal-pushing CVT, or a metal V-belt drive*

Metal belt CVTs have been on the market for a number of years now, but so far did not manage to show the improved fuel economy over discrete ratio transmissions with equivalent torque capacity, which was predicted. This deficiency has three main contributing factors. First, engine cannot always be operated at its most fuel efficient condition, even though the transmission ratio could achieve this, due to constraint on the operating point of the engine in the high acceleration level scenarios. The second reason is the lower efficiency of the CVT (0.87 - 0.93) relative to the efficiency of a discrete ratio transmission (0.96 - 0.99) [2]. The inefficiency of CVT has been linked, amongst number of possible inherent losses, to torque losses within the belt mechanism itself and belt slip. Finally, the control logic has not been accurate enough to deliver a desired shifting behaviour. Almost all models for CVT control design assume CVT to be a pure integrator, which is not the best approach for capturing and controlling the dynamics associated with the various components of a CVT system. Moreover, such models would also be inadequate (or rather inaccurate) for the purpose of optimizing fuel economy and acceleration performance of a vehicle [3].

2. REVIEW OF METAL BELT CVT FRICTION INDUCED MODELS

Numerous authors investigated the function of the pushing metal belt CVT, while some of them proposed the mathematical models concerning the loss mechanism of a metal belt CVT.

The first significant model, after the pioneer work by Gerbert and Becker was by Micklem et al. [4]. Micklem evolved its model from the first papers concentrating on specific torque loss mechanisms within the belt, over proposal of a viscous shear film between any belt components having a relative motion, to proposal of an elastohydrodynamic lubrication (EHL) regime between the segments and the pulleys to model a belt-slip phenomenon. The final model had a good agreement between measured and calculated slip values between the belt and the pulley.

Kobayashi et al. [5] analysed the slip mechanism by focusing on the distribution of the gaps occurring between the segments, and simulation predicted the slip-limit torque at which the slip ratio increases sharply. The authors analysed the slipping behaviour at the reduction speed ratio and the maximum torque condition, but they did not refer to the transmission efficiency of CVT under a realistic scenario.

Karam and Play [4] adopted a numerical approach to derive global equilibrium equations from the equations of the elements that form the metal belt. They, for the first time proposed that the steel bands actively participate in torque transmission. Noted authors also introduced simplifications regarding assumption that the band segments are always in compression and thus an initial tension exists in the steel bands when at rest, as well as the assumption that the bands are rigid, so their length doesn't change during CVT operation. Simplifications in their work proved to be significant by later work of different authors. Noted authors also developed a concept of dividing the contact path about pulleys into two zones, the adherence zone and the sliding zone. The adherence zone is defined in places where segment and pulley forces are constant, while the sliding zone is defined in a region where compressive forces between segments rise (driving pulley) or fall (driven pulley).

Lee and Kim follow the work of Karam and Play and further divide the pulleys contact paths into three regions: region of constant compressive force and band tension, region of band tension change only and region of variable compressive force and band tension. The noted author's main goal was to further understand the clamping force required for torque transmission in order to improve the efficiency of the transmission. The authors proposed the calculations of clamping forces for specific torque and transmission ratio combinations and calculated the required clamping force in boundary operating regimes. One of the most important conclusion of the noted authors is that in order to have a functional model which is in agreement with experimental data it necessary to implement the variable coefficient of friction between the segments and the pulleys. The coefficient of friction increases linearly with the decrease of transmission ratio.

Kanehara et al. [5] focused on the investigation of effects of friction forces between the steel bands and belt segments. The noted authors indentified six friction coefficients that may be varied to achieve agreement between the model and the experimental data.

Akehurst et al. [4], as well as the investigated the loss mechanisms that occur within the belt drive due to relative motion between the bands and segments and between the pulleys and the belt due to pulley deflection effects.

Narita and Priest [5] focused on investigation of losses between all the contact pairs.

The last two models are the most comprehensive and propose improved models that predict both the tension and compression change phenomena in belt elements.

3. LOSS MECHANISMS IN PUSH METAL BELT CVT

Figure 3 shows the ideal metal belt geometry. It is clear from the figure that the expression for the length of the belt can be written as:

$$L = R_p \cdot \beta_p + R_s \cdot \beta_s + 2\sqrt{[a^2 - (R_s - R_p)^2} \; . \qquad (1)$$

where:

$$\beta_p = 180 - 2\alpha$$
$$\beta_s = 180 + 2\alpha \qquad (2)$$
$$\sin\alpha = \frac{R_s - R_p}{a}$$

The push metal belt CVT transmission ratio can be defined in geometric terms as:

$$I = \frac{R_s}{R_p} \; . \qquad (3)$$

Transmission ratio greater than 1 corresponds to the reduction ratio, while transmission ratios lower than 1 corresponds to the overdrive ratio.

In loaded operation, the CVT runs at a slightly reduction speed ratio. This difference is known as the slip ratio between the belt and pulley, S_R:

$$S_R = \frac{(I_L - I)}{I} \times 100(\text{percent}) \; . \qquad (4)$$

where I_L is the speed ratio at a loaded condition.

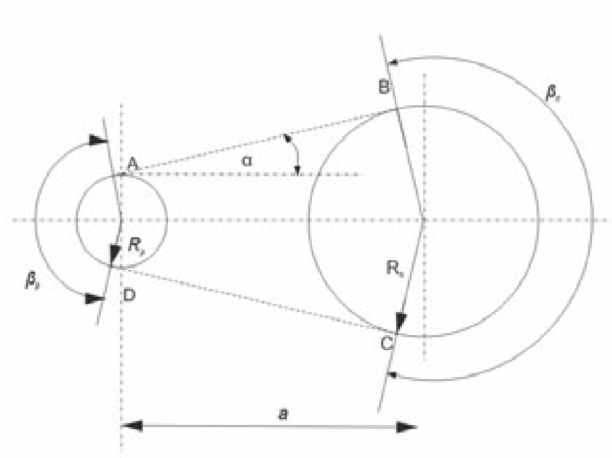

Figure 3. *Schematic of ideal metal belt geometry*

As the friction related power losses are one of the main reasons of CVT inefficiency, it is necessary to investigate where the losses are likely to occur. In order to have a power loss a relative motion has to exist between two or more components with resistive force acting between them. Therefore, the following relative motion pairs were indentified in a push metal belt CVT system:

- between the segment side and the pulley
- between the segment and the outermost bands
- between the bands
- between the neighbouring segments

All of these contact pairs with relative motion has to be investigated in order to assess the value of total torque loss.

Friction force between the neighbouring segments as well as the torque losses associated with it can be neglected as assumption can be made that no radial movement is allowed [4].

3.1. Friction loss between segment side and the pulley

The friction loss between segment side and the pulley that occurs is based on the relative slipping and contact load between the segments side and the pulley surfaces on both sides of the segment. The noted friction loss Q_{sp} is thus:

$$Q_{sp} = 2 \times \mu_{sp} \times F_{sp} \times V_{sp} \; . \qquad (5)$$

where μ_{sp} is friction coefficient, F_{sp} the normal load and V_{sp} the relative slipping speed. The subscript sp refers to the segment side/pulley contact pair.

The coefficient of friction μ_{sp} can be calculated from the equation for maximum torque capacity of push metal belt CVT in specific tribological conditions defined by lubricant type (M_{max}) [5]:

$$\frac{F_{ax}}{\cos(\lambda)} = \frac{M_{\max}}{2\times\mu_{sp}\times R_p}. \qquad (6)$$

The F_{ax} is the axial clamping force on a pulley and λ is half the pulley edge angle. Clamping force on a pulley consists of the static clamp force which is calculated by multiplying the hydraulic pressure by the apply piston area and the centrifugal force generated due to rotation of the piston.

As no slip occurs when the drive torque is at no load, the relative slipping velocity V_{sp} may be calculated from [6]:

$$V_{sp} = \frac{V_s \times S_R}{100}. \qquad (7)$$

Relative slipping between the belt and the pulley occurs on the pulley with the smaller active arc with the belt because there are larger gaps between the neighbouring segments on a smaller arc pulley, due to the smaller radius of curvature, and the gaps facilitate slipping [7]. Thus, slipping occurs on the primary pulley in the case of a reduction speed ratio and on the secondary pulley in the case of an overdrive speed ratio. Slipping occurs mainly on a smaller active arc pulley which was experimentally confirmed in [5].

3.2. Friction loss between and the outermost bands

The bands in contact with the segment slide relative to the segment shoulder both in the arc part of the belt and in the straight part of the belt. The friction loss Q_{br} based on this phenomena is [4]:

$$\begin{aligned} Q_{sb} &= Q_{sb-a} + Q_{sb-st} \Rightarrow \\ Q_{sb} &= \mu_{sb}\cdot N_{sb-a}\cdot V_{sb-a} + \mu_{sb}\cdot N_{sb-st}\cdot V_{sb-st} \end{aligned} \qquad (8)$$

where N is normal load and μ is the friction coefficient. Subscripts *sb-a* and *sb-st* refer to the segment shoulder/outermost band interfaces in the arc part of the belt and in the straight part of the belt.

The normal load N_{sb-a} between the segment shoulder/outermost band in the active arc part is obtained [5]:

$$N_{sb-a} = -\frac{T_1}{\mu_{sb}}\cdot\left[e^{-\mu_{sb}\beta_s} - 1\right] + \frac{m_b V_b^2}{\mu_{sb}}\cdot\left[e^{-\mu_{sb}\beta_s} - 1\right] \qquad (9)$$

where m_b is the mass per unit of length of a band.

The normal load N_{br-st} between the segment shoulder/outermost band in the straight part of the belt can be determined as:

$$N_{sb-st} = (T_1 + T_2)\cdot\tan\alpha \qquad (10)$$

where T_1 and T_2 are the band tensions in upper side of the belt and lower side of the belt, respectfully. In order to simplify the estimation of the friction induced losses, band tensions T_1 and T_2 are considered as constant independent of the drive torque.

The difference in band tensions can be determined from the transmitted torque by:

$$\frac{M}{R_p} = (T_2 - T_1) + C_1. \qquad (11)$$

while the constant C_1 can be obtained from:

$$C_1 = \frac{\left[(M/R_p) + (\mu_{sb}\mu_{sp}/\mu')(F_{ax}/\cos\lambda) + m_s V_s^2 \mu_{sb}\beta_s\right]}{(1-\mu_{sb}\beta_s)} \qquad (12)$$

The actual values of band tension can be determined in last point of contact arc where $T_2 = 0$.

The relative slipping tangential velocity V_{sb-a} of the segment shoulder to the outermost band in the arc part of the segment can be calculated as:

$$V_{sb-a} = V_s\cdot d_R\cdot\left|\frac{1}{R_s} - \frac{1}{R_p}\right|. \qquad (13)$$

where d_R is the distance from the contact circle to the segment shoulder.

Relative slipping tangential velocity V_{sb-st} of the segment shoulder to outermost band in the straight part of the belt can be calculated as:

$$\begin{aligned} V_{sb-st} &= V_s\cdot\frac{d_R}{R_p},\ (I<1), \\ V_{sb-st} &= V_s\cdot\frac{d_R}{R_p},\ (I>1) \end{aligned}. \qquad (13)$$

3.3. Friction loss between the bands

Band set in of a push metal belt is usually composed of 12 sheets of thin steel. The sum of the friction loss Q_{bb} arising from relative slip between the bands in contact is given by [5]:

$$\begin{aligned} Q_{bb} &= Q_{bb-a} + Q_{bb-st} \Rightarrow \\ Q_{bb} &= \mu_{bb}\cdot\sum_{n=2}^{12}\left[N_{bb-a}(n)\cdot V_{bb-a}(n)\right] + \\ &+ \mu_{bb}\cdot\sum_{n=2}^{12}\left[N_{bb-st}(n)\cdot V_{bb-st}(n)\right]\ (2\le n\le 12) \end{aligned} \qquad .(14)$$

where N is normal load and μ is the friction coefficient. Subscripts *bb-a* and *bb-st* refer to the band/band contact in the arc part of the belt (defined by warping angle) and the straight part of the belt.

The normal load $N_{bb-a}(n)$ acting on the n^{th} band in the arc part can be expressed by:

$$N_{bb-a}(n)=\sum_{i=n}^{12}\left\{\begin{array}{l}-\dfrac{T_{1(i)}}{\mu_{sb}}\left[e^{-\mu_{sb}\beta_s}-1\right]+\\+\dfrac{m_b(i)V_b^2}{\mu_{sb}}\left[e^{-\mu_{sb}\beta_s}-1\right]\end{array}\right\}(2\le n\le 12)\ .(15)$$

Constant $T_1(n)$ is given by

$$T_1(n)=\frac{13-n}{12}T_1 \quad . \qquad (16)$$

The normal load $N_{bb2st}(n)$ between the bands in the straight part of the belt can be written as:

$$N_{bb-st}(n)=\sum_{i=n}^{12}\left[T_1(i)+T_2(i)\right]\cdot\tan\alpha \ \ (2\le n\le 12)\ .(17)$$

Relative slipping tangential velocity $V_{bb-a}(n)$ between the bands in the arc part of the belt can be expressed as:

$$V_{bb-a}(n)=V_s t\left|\frac{1}{R_s}-\frac{1}{R_p}+\frac{d_R\,t}{R_sR_p}+\frac{(n-2)t^2}{R_sR_p}\right|(2\le n\le 12)\ (18)$$

Relative slipping tangential velocity $V_{bb-st}(n)$ between the bands in the straight part of the belt can be expressed as:

$$\begin{array}{l}V_{bb-st}(n)=V_s\cdot\dfrac{t}{R_p},\ \ (I<1),\\ V_{bb-st}(n)=V_s\cdot\dfrac{t}{R_p},\ \ (I>1)\end{array}\quad . \qquad (19)$$

In both expressions t denominates band thickness.

3.4. Friction coefficients

Determination of values of μ_{sb} and μ_{bb} during the operation of push metal belt CVT is very difficult. Those values can be determined experimentally on a ring to disk tribometer [5] in which frictional conditions (contact pressure and slipping velocity) are similar to frictional condition of an actual CVT. Values of μ_{sb} and μ_{bb} are determined according to the values of slipping velocities V_{bb} and V_{sb}. If experimental values of friction coefficient are not available they can be selected between 0.08 and 0.14 [5].

Value of friction coefficient primarily depends on clamping force value (which defines the contact pressure), oil type, transmission ratio, slipping velocity and oil temperature. It is observed that lubricants which enable higher overall efficiency tend to lower values of friction coefficient [5]. Moreover, it is also observed that in low contact pressure scenario there is little influence of contact pressure value on friction coefficient. So, to improve the efficiency of push metal belt CVT it is necessary to establish the lower value of the friction coefficient under a lower contact pressure condition.

Although most of the authors use classic Coulomb friction law to describe band segment and band to band contact such models lack the flexibility to adjust the speed relationships of the bands on the driver and driven pulleys to meet the requirement that each band effectively shares part of the load torque. Much better results are obtained via the creep-rate-dependent law [8].

4. EFFICENCY INFLUENCE PARAMETERS

As already noted, values of clamping force and transmission ratio, as well as the oil type and its temperature has an effect to friction coefficient, belt slip and thus system efficiency. Noted influence parameters cannot be considered independently as numerous experimental investigations show strong correlations between them. For instance applying higher torque capacity oil to CVT units could contribute to reduce the maximum required pulley clamping force, and thus lower losses in hydraulic pump which is one of the main contributors to overall losses.

The clamping force has to be precisely controlled in order to achieve maximal efficiency. For a given clamping force there is a maximum limit due to friction at which no slip occurs. If this frictional force is overcome then the belt begins to slip over the pulley surface. Further increasing the torque continues to increase the rate of slip. In low load scenario it is desirable to decrease the clamping force and thus improve efficiency.

Push metal belt efficiency is at maximum at transmission ratio equal to 1. For optimal clamping force the decrease of efficiency is roughly the same in reduction and overdrive operating regimes. With increase of over clamping the decrease of efficiency is grater in the reduction regime than in overdrive. The difference gets larger as the clamping force rise.

The oil type affects not only the efficiency, but torque capacity as well. Experimental investigations showed that lower viscosity index oils have a greater torque capacity, but lower efficiency. From the viewpoint of the improvement of transmission efficiency, it is clarified that the priority for the performance of push metal belt CVT should be focused on the higher transmittable torque capacity.

Metal belt CVT operate in boundary lubrication regime. Friction surfaces are practically in direct contact, thus the load is transferred by the surfaces roughness and waviness elements. This causes deformation of contact surfaces which has also effect on efficiency [4].

5. CONCLUSIONS

Paper indentifies the reasons of friction related losses in push metal melt CVT. Friction loss is caused by slipping between the belt and pulley, the segment and band, and between the bands, while the slipping between the segments can be neglected.

It also gives review of models for modelling the push metal belt CVT as a tribological system.

A model of assessment of friction related losses in push metal belt CVT is also presented as well as the main influence parameters on efficiency.

REFERENCES

[1] A. Miltenović, M. Velimirović, M. Banić, M. Milovančević: Modern trends in development and application of CVT, Konstruisanje mašina - Journal of Mechanical Engineering Design, Vol. 11, No1, pp.14-22, 2009.

[2] V. Miltenović, M. Velimirović, M. Banić, A. Miltenović: Increase of Energy Efficiency of Windturbines by Application of CVT, in: *Proceedings of International conference on Gears - Gears 2010*, 04-06.10.2010, Munich, pp. 1095-1106.

[3] N. Srivastava, I. Haque: A review on belt and chain continuously variable transmissions (CVT): Dynamics and control, Mechanism and Machine Theory, Vol. 44, No 1, pp 19-41, 2009.

[4] S. Akehurst, N. D. Vaughan, D. A. Parker, D. Simner: Modelling of loss mechanisms in a pushing metal V-belt continuously variable transmission. Part 1: torque losses due to band friction, Proceedings of the Institution of Mechanical Engineers, Part D: Journal of Automobile Engineering, Vol. 218, No 11, pp 1295-1306, 2004.

[5] K. Narita, M. Priest: Metal–metal friction characteristics and the transmission efficiency of a metal V-belt-type continuously variable transmission, Proceedings of the Institution of Mechanical Engineers, Part J: Journal of Engineering Tribology, Vol. 221, No 1, pp 11-26, 2007.

[6] C. Morgan, R. Fewkes: Development of a belt CVT fluid test Procedure using the VT20/25E belt box for the DEX-CVT specification, SAE paper 2002-01-2819, 2002.

[7] T. A. Stolarski: Tribology in machine design, Batterworth-Heinemann, Oxford, 1990.

[8] S. Akehurst: An Investigation Into the Loss Mechanisms Associated with a Pushing Metal V-Belt Continuously Variable Transmission, PhD thesis, Department of Mechanical Engineering, University of Bath, Bath, 2001.

[9] K. Narita, J. Deshimaru, M. Kato: The influence of lubricating oil on the performance of a metal V-belt-type continuously variable transmission, in: *Proceedings of JSME International Conference on Motion and power transmissions*, 2001, Fukuoka, pp.730-735.

[10] D. Stamenković, M. Đurđanović: The possibility of static friction coefficient calculation, in: *Proceedings of 5th International Conference on Tribology*, 2005, pp. 465-469.

Tribometry

Serbian Tribology Society

SERBIATRIB '11

12th International Conference on Tribology

Faculty of Mechanical Engineering in Kragujevac

Kragujevac, Serbia, 11 – 13 May 2011

FLAMMABILITY TESTS ON HOT SURFACE FOR SEVERAL HYDRAULIC FLUID

Lorena Deleanu[1], Sorin Ciortan[2], Constantin Georgescu[2]

[1]University “Dunarea de Jos”, Galati, Romania, lorena.deleanu@ugal.ro

[2] University “Dunarea de Jos”, Galati, Romania, sorin.ciortan@ugal.ro

Abstract: *Industrial equipment using hydraulic fluids are design to accept higher load and speed, implicitly higher temperatures, including for fluids. Leakages from enclosures like gear boxes or hydraulic systems could increase the risk of fluid reaching hot surfaces, thus producing fires hard to be controlled and isolated. The designer have to evaluate the flammability of fluids and they should select several solutions for a particular application in order to estimate the costs of different solutions and to mitigate the risk of having accidental fires due to a specific fluid grade.*

The tests were done with the help of an original equipment allowing a dedicated soft assistance in order to protect the operator and to sustain reproducibility, according to the standard SR EN ISO 20823:2004 Petroleum and related products. The determination of the flammability characteristics of fluids in contact with hot surfaces - Manifold ignition test. There were tested the following grades of hydraulic oil HLP 68 X-Oil, HFC Prista, MHE 40 Prista (100% oil), a rapeseed oil (obtained after a dewaxing process) and an emulsion oil-in-water (5% vol. MHE 40 Prista). There were identified distinct behaviours of these fluids under the test conditions.

Keywords: *fluid flammability, hot surface, SR EN ISO 20823:2004, emulsion oil-in-water, hydraulic fluid.*

1. INTRODUCTION

European directives [2-4, 7] and other documents [1,6, 8] emphasis the necessity of reducing the flammability risk when using industrial fluids (hydraulic fluids, lubricants, processing fluids like those used in steel treatment and cutting etc.), especially in explosive atmosphere. Thus, “in particular, where fluids are used, machinery must be designed and constructed for use without risks due to filling, use, recovery or draining.” [7]. Risk assessment implies a complex analysis of design, equipment, procedures and operators. Thus, the same document [7] underlines that “machinery must be designed and constructed to avoid all risk of fire or overheating posed by the machinery itself or by gases, liquids, dust, vapours or other substances produced or used by the machinery.”

Both manufacturers and users ask for tests that could certify fluid flammability characteristics, preferring ISO or ASTM standards [1, 10, 20, 21]. Many documents, including EU Directives, give recommendations to use standardised tests for estimating flammability of fluids [1-4, 6-8, 14-16]. The evaluation of fire resistance of a hydraulic fluid cannot be done by one test only and the aspects of fire resistance have to be pointed out by several tests, including those simulating on small scale the worst scenario that could happen in real applications using hydraulic fluids [11, 17]. Many of these tests give a result as “pass” or “not pass” [8, 20, 21]. The fluid that passed a particular test or, better, a set of tests, is included in recommendations or approvals, but these ones are specific to regional or national reglementations [1, 6, 8, 13].

2. TESTING PROCEDURE

The tests were done with the help of an original equipment (Fig. 1) [27] allowing a dedicated soft assistance in order to protect the operator and to sustain reproducibility, according to the standard SR EN ISO 20823:2004 Petroleum and related products. Determination of the flammability characteristics of fluids in contact with hot surfaces - Manifold ignition test. This test simulates an accident or the hazardous event when a fluid drops on a hot surfaces: 10 ml of fluid is dropped during 40…60 seconds on a manifold kept heated at a constant temperature, from a distance of 300±5 mm above the manifold surface. For each temperature and fluid there were done 3 tests. The highest temperature for which the fluid does not burn or ignite, was established is the same “verdict” was obtained for all the three tests. All the temperature values given in this study have the accuracy given in Figure 2. The equipment is controlled and assisted by a PC with a dedicated soft in order to protect the operator from being near the heated zone. Figure 2 presents the display of soft.

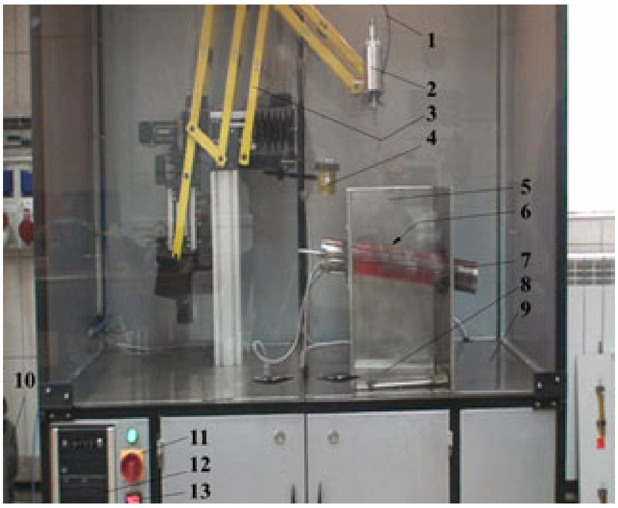

Figure 1. The equipment for testing the fluid flammability on hot surface. 1 – piping for cooling system of the dispenser, 2 – dispenser with cooling mantle, 3 – 2D robot, 4 – glass for the tested fluid, 5 – metallic box, 6 – temperature gauge protected by a welded case, 7 – the heated manifold having inside an electric resistance, 8 – tray for collecting the drops, 9 – ventilated enclosure, 10 – air compressor, 11 – the main switcher, 12 – the hard of the assisting PC, 13 – display for the manifold temperature

There are several reasons of fluid leaking [11, 16]:

- fatigue of the system elements, under normal or severe exploitation (cracks, creep, ageing), or due to an adequate maintenance,

- cyclic or accidental thermal expansions, bolts stretch;

- changes of fluid properties due to exploitation, especially temperature rising that makes the fluid to become thinner,

- the efficiency loss of seals and hoses in time, due to their modifications produced by long exposure to temperature or/and chemicals, but also by trapping “foreign” particles (solid, liquid, gaseous or mixtures of them);

- screw-up operations: a controlled mounting and preventive maintenance decrease the leak probability under functioning conditions. It is also important to respect procedures for starting and stopping the equipment;

- operator faults; regular trainings could significantly reduce these events [8, 11].

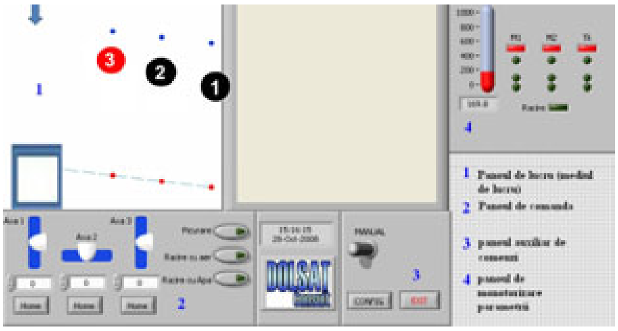

Figure 2. Positions 1 are 2 could be heated at the test temperature with the high accuracy imposed by standard (±5ºC). The accuracy for position 3 is (±6.3ºC).

There were tested the following grade of hydraulic oils HLP 68 X-Oil [25], HFC Prista [23], Shell Irus Fluid DR 46 [22], a rapeseed oil (obtained after a dewaxing process) [9] and an emulsion 5% MHE 46 in water as recommended by Prista producer [24]. There were identified distinct behaviours of these fluids under the test conditions.

Shell Irus Fluid DR46 is a tri-aryl phosphate ester fire resistant hydraulic fluid. It contains carefully selected additives to give superior oxidation and hydrolytic stability. Shell Irus Fluid DR46 should be used in hydraulic systems operating in close proximity to potential ignition sources. This includes equipment such as die-casting machines, billet loaders, electric arc furnaces, forging presses and others operating in fire hazard situations.

PRISTA HFC is a fully synthetic fire resistant water-glycol based hydraulic fluid blended with an additive package to improve the anti-wear properties and corrosion protection of the finished product [23].

HLP 68 X-Oil [25] is an optimized alloyed hydraulic oil with a high performance level and a broad field of industrial application. It especially distinguishes with good viscosity-temperature behaviour, high ageing stability and reliable corrosion protection. Additives provide an excellent wear protection under extreme loads, too. The behaviour against sealing materials is neutral.

Prista MHE-40 is used as 5% working fluid in oil-in-water emulsion for hydraulic systems with high risk of flammability [24]. The tests were done on the fully mineral oil and for the emulsion 5% MHE 40 (vol.) in water.

Table 1. Flammability characteristics of the tested oils

Fluid	Flammability characteristics		
	Flash point	Fire point	Refe-rences
Shell Irus Fluid DR46	245	335	[22]
HLP68-XOIL	238		[25]
Rapeseed oil	270	216...346	[26]

From Table 1 one may notice that the two characteristics, the flash point and the fire point, do not give any starting point for evaluating the flammability on hot surfaces [12, 18, 19]. For instance, the fire point value for Shell Irus Fluid DR 46 is included in the range also reported for rapeseed oils [26], but the first one does not burn on hot surfaces even at the maximum test temperature imposed by the ISO standard (700°C±5°C), the tested rapeseed oil burning when being dropped on a surface heated at 551±5°C.

3. RESULTS AND DISCUSSION

Analysing the recorded films of the tests (Figs. 3-10), the authors noticed the followings: there were stages when the fluid only evaporates or change structure without ignition, these being useful in establishing the time response of fire/security sensors.

The hydraulic fluids HFC Prista, Shell Irus Fluid DR 46 and the emulsion 5%MHE Prista in water does not burn even for the highest tested temperature (700°C±5°C), a temperature also included as imposed for hydraulic fluids with the best behaviour under the conditions of EN ISO 20823:2003. The other two tested fluids burn. The rapeseed oil has 551°C the highest temperature at which it does not burn for repeated test (at least three) and HLP 68 X-Oil has for the same parameter the value of 500°C.

36th second 37th second 38th second

Figure 3. Three consecutive seconds from the film recorded for the fluid HLP 68 X-Oil, tested at 515°C

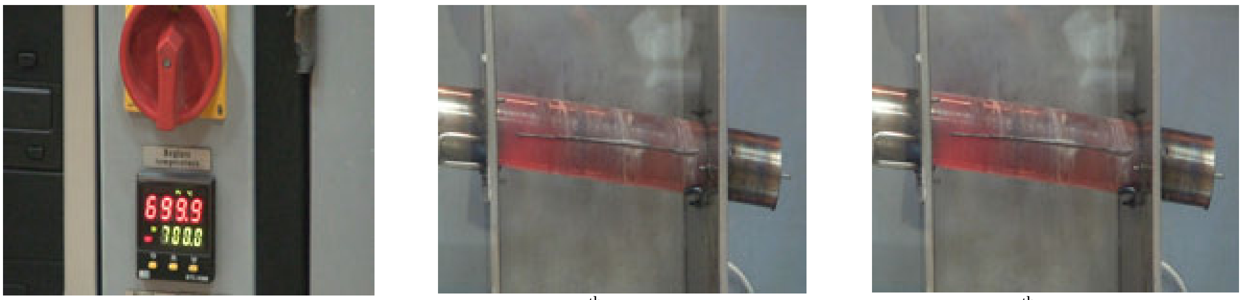

50th second 52th second

Figure 4. Images from the film recorded for the fluid Shell Irus DR 46, tested at 700°C

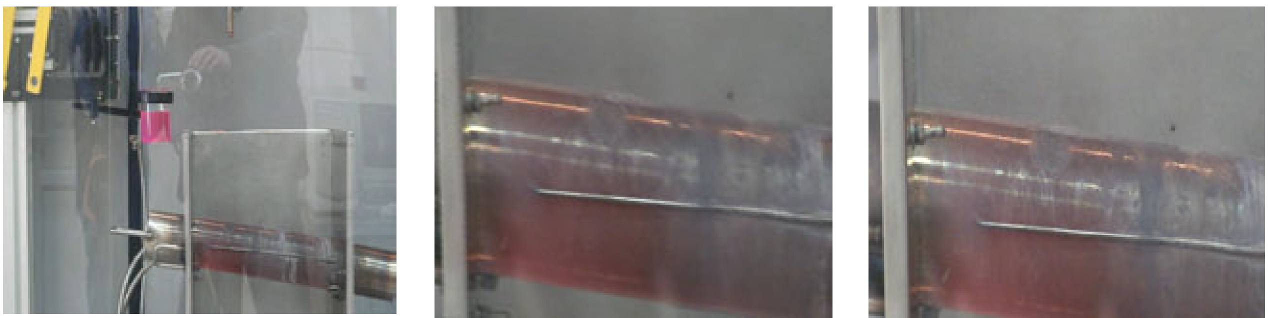

20th second 21th second 23th second

Figure 5. Consecutive images from the film recorded for the fluid HFC Prista, tested at 700°C

2^{th} second (first drop) | 3^{th} second | 7^{th} second

Figure 6. Three images from the film recorded for the mineral oil MHE 40 Prista tested at 450°C

2^{th} second (first drop) | 5^{th} second | 40^{th} second

Figure 7. Images from the film recorded for the mineral oil MHE 40 Prista tested at 460°C

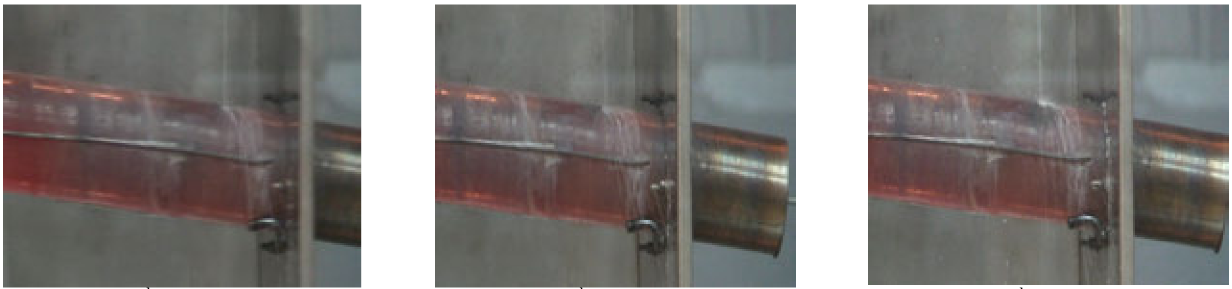

4^{th} second | 5^{th} second | 10^{th} second

Figure 8. Images from the film recorded for the oil-in-water emulsion (5% MHE 40 Prista oil vol. in water), tested at 700°C

38^{th} second | 46^{th} second | 47^{th} second

Figure 9. Images from the film recorded for the rapeseed oil (dewaxed grade) tested at 551°C

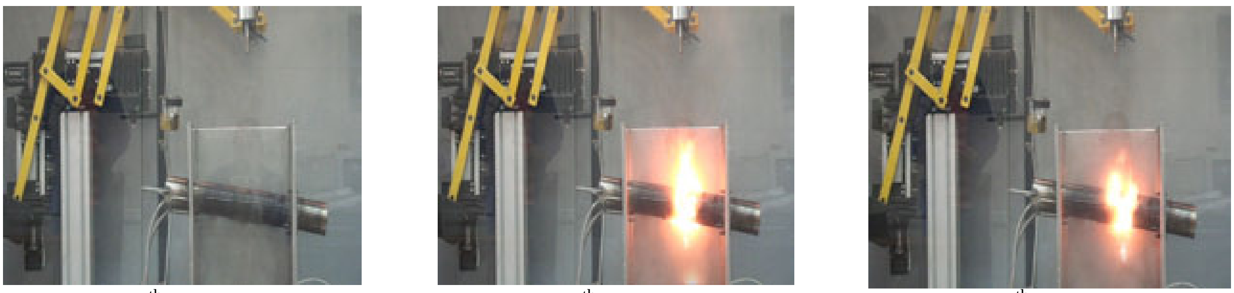

38^{th} second | 39^{th} second | 40^{th} second

Figure 10. Three consecutive seconds from the film recorded for the rapeseed oil (dewaxed grade) tested at 574°C

The behaviour of this rapeseed oil (dewaxed grade) [9] under the testing conditions imposed by SR EN ISO 20823:2003 could be grouped in the following ranges, characterised by temperatures for which the fluid behaviour is the same :

1. a temperature range for which there are repeatedly obtained the same results when testing the fluid on hot manifold (200…551ºC, the fluid does not burn);

2. a temperature range for which the test results is randomly different (in one test the fluid does not burns, but in the following one it is burning and so on): 551…557ºC; in practice it could be included in the range for which the fluid burns and the use of the fluid in this range is strongly not recommended;

3. The temperature range for which the fluid burns, $\theta > 560$ºC.

Any test is irrelevant for the temperature range 552…562ºC for the dewaxed rapeseed oil because the difference (10°C) is the same to the allowance range (±5°C).

The flammability risk could be substantially reduced by using emulsions as that one obtained from 5% vol. MHE 40 in water. The authors noticed that this emulsion does not burn on the surface heated at 700°C, but the mineral oil – 100% MHE 40 Prista does burn at a much lower temperature of 450°C and it is very sensitive to the surface quality. The authors also noticed that the test done at this temperature of 450°C gives inconsistent results. From 9 tests, during 6 ones, the fluid ignited and burnt when it was dropped on the clean surface of the heated manifold. When the test was done on the same manifold, but dirty from previous tests, the temperature of ignition of the same fluid was even lower: 415°C. This is a conclusion that could be the subject of a further investigation, as in practice many surfaces could be far for being clean due to the technological process or, worse, due to the “leak” of operators’ responsibility or an inadequate maintenance.

The designer has two possibilities for reducing the flammability risk: to use a fluid that does not burn or to change the design in order to have a better protection against hazardous events that could cause fluid ignition. Of course, the first solution is better especially when the equipment works in a particular environment, including mining metallurgy, glass industry etc. The designer has to select the hydraulic fluid from families like the synthetic, mineral or that of emulsions. The synthetic ones have some advantages, but they are still expensive. The engineer has to balance the advantages and disadvantages of each group. For instance, the emulsions could be much less expensive, but they have to be circulated in systems (piping, pumps etc.) exhibiting a good corrosion resistance or at least an acceptable resistance for a particular application.

4. THE COLOUR CODE

The authors proposed a code of colours to be written on the oil label in order to emphasis the flammability on hot surfaces [28]: blue for the temperature range the fluid does not burn and red for the temperature range the fluid ignites and burns. Figure 11 presents such possible labels for the tested fluids. Of course the label includes the standard procedure used for testing the flammability (SR EN ISO 20823)

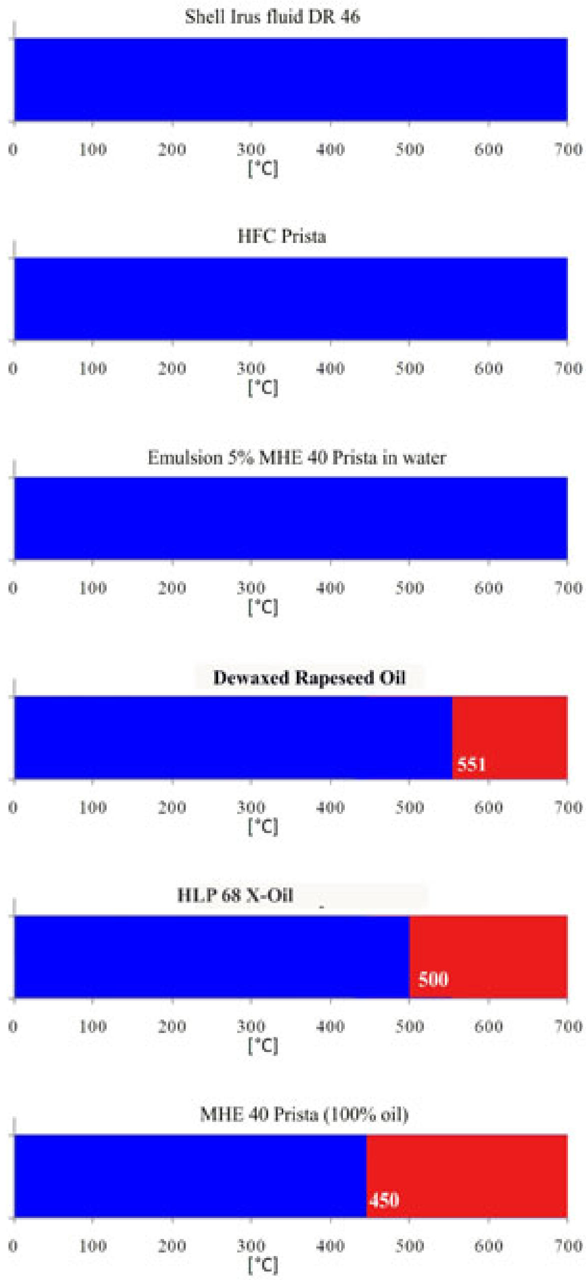

Figure 11. The label proposed by the authors for the tested fluids

5. A RISK INDEX RELATED TO FLUID FLAMMABILITY ON HOT SURFACE

In some cases the designer could apply risk index method, calculating a risk index, as:

$$I_{risk} = \sum_{j=1}^{n} a_j \cdot r_j \qquad (1)$$

where a_j is the attribute *j* related to risk evaluation (for instance, ignition temperature on hot surface, smoke production, electrical ignition sources etc), $j=1,\dots,n$, and r_j is a value associated to likelihood of occurrence and consequences. r_j may have the following values: 0 – the occurrence is not credible, 1 – unlikely, 2 – medium probability, 3 – highly likely [9, 13]. The attribute of ignition on hot surfaces could be related to the ignition temperature of the fluid involved, but in an indirect proportionality to this one. For instance, if the engineer had to select an industrial fluid among several with different hot surface ignition temperatures, $T_1 \langle T_2 ... \langle T_n$, after tested under the procedure of ISO 20823, he would calculate the attribute a_j as following:

$$a_j = T_n / T_j \qquad (2)$$

T_n could be the maximum temperature for which the test for flammability on hot surface is recommended in SR EN ISO 20823 (700±5°C).

It is obviously that a lower value of this attribute (even 1 for fluids that do not burn at 700°C) is desired for a safe functioning and for a very low probability of hazardous events. The problem to be solved is the compromise between the initial costs and the performances of the selected fluid. Several decades ago the ratio between high security fluids and hazardous fluids was as great as 5...3 to 1. A fluid-power system will be more expensive when using water-based fluids due to the materials involved in designing (especially corrosion resistant steels, sealings etc.) as compared to a system with similar performances but using mineral oils. As the tests proved, a safe solution is to use oil-in-water emulsions, but the designer has to balance very well the advantages and disadvantages of this solution and to know the consequences of using such a hydraulic fluid class, including compatibility of emulsions with all the materials they come into contact (steel parts, sealings, other fluids, operators etc.), supplementary furniture for maintaining the emulsion characteristics (dispersion quality, concentration etc.).

6. CONCLUSIONS

There is no test ensuring a high level of safety for fire resistance but a particular set of tests, selected after a well-documented risk assessment could give a better solution.

The determination of fluid flammability on hot surfaces imposes particular solutions for improving the security of the designed system, including fluid selection, avoiding scenarios with hot surfaces near piping and hoses etc.

The list of hydraulic fluids possible to be selected and the tests that these fluids have to pass, will have to be known and set even in the design stage of the equipment. It is also important to analyse similar accidents related to the real applications in order to notice possible improvements in equipment, process and environment control and for workers' training.

These analyses may be useful for designers in order to better assess the risk and to estimate costs of different solutions implying different grades of hydraulic fluids.

AKNOWLEDGEMENT

This research was supported by National Authority for Scientific Research (ANCS), Minister of Education and Research Romania, under the grant CEEX-M4-452 "Adoption and Implementation of Test Methods for Lubricant Conformity Assessment."

REFERENCES

[1] Approval Standard for Flammability Classification of Industrial Fluids (Class 6930), Factory Mutual Global, January, 2002.

[2] Council Directive 92/104/EEC of 3 December 1992 on the minimum requirements for improving the safety and health protection of workers in surface and underground mineral-extracting industries (twelfth individual Directive within the meaning of Article 16 (1) of Directive 89/391/EEC), OJ L 404, 31/12/1992 P. 0010 – 0025.

[3] Directive 94/9/EC of the European Parliament and the Council of 23 March 1994, on the approximation of the laws of the Member States concerning equipment and protective systems intended for use in potentially explosive atmospheres, (OJ L100, 19.4.1994, 1), amended by Regulation (EC) No 1882/2003 of the European Parliament and of the Council of 29 September 2003, OJ L284 1 31.10.2003, Corrected by Corrigendum, OJ L21, 26.1.2000, 42 (94/9/EC), Corrigendum, OJ L304, 5.12.2000, 19 (94/9/EC).

[4] Directive 1999/92/EC of the European Parliament and of the Council of 16 December 1999 on minimum requirements for improving the safety and health protection of workers potentially at risk from

explosive atmospheres (15th individual Directive within the meaning of Article 16(1) of Directive 89/391/EEC), OJ L 23, 28.1.2000

[5] ATEX Guidelines. Guidelines to the application of Directive 94/9/EC of the European Parliament and the Council of 23 March 1994 on the approximation of the laws of the member states concerning equipment and protective systems intended for use in potentially explosive atmospheres, 3rd Edition, June 2009, available online at the address: ec.europa.eu/.../atex/guide/atexguidelines_june2009_en.pdf

[6] The 7th Luxembourg Report, Doc. No. 4746/10/91, Requirements and Test Applicable to Fire-Resistant Hydraulic Fluids used for Power Transmission and Control; L-2920m, Luxembourg, Commission of the European Economic Communities DG\E\4, 1994.

[7] Directive 98/37/EC of the European Parliament and of the Council of 22.06.1998 on the approximation of the laws of the Member States relating to machinery (OJ L 207, 23.7.1998, p. 1) Amended by: Directive 98/79/EC of the European Parliament and of the Council of 27 October 1998, Corrected by: Corrigendum, OJ L 16, 21.1.1999, p. 36 (98/37/EC), Corrigendum, OJ L 22, 29.1.1999, p. 75 (98/79/EC), Corrigendum, OJ L 6, 10.1.2002, p. 70 (98/79/EC).

[8] HSE Approved specifications for fire resistance and hygiene of hydraulic fluids for use in machinery and equipment in mines, (M) File L11.6/3, 1999.

[9] L. Deleanu, S. Ciortan, L. C. Şolea, Rapeseed oil flammability on hot surface, Proceedings of the Intern. Conf. on Diagnosis and Prediction in Mechanical Engineering Systems (DIPRE'09), 22-23 October, Galati, Romania, 2009.

[10] M. J. Goode, D. W. Phillips, R. D. Winkeljohn, Fire-Resistant hydraulic Fluids and the Potential Impact of New Standards for general Industrial Applications, Proceedings of the 48th National Conf. on Fluid Power, paper 100-1.12, 2000.

[11] .Y. Hatamura, Structure and Expression of Failure Knowledge Database, Failure Knowledge Database Project, Japan Science and Technology Agency, 2011, http://shippai.jst.go.jp/en/Contents?fn=1&id=GE0719

[12] A. Hamins, P. Borthwick, C. Presser, Suppression of ignition over a heated metal surface, Proceedings of Int. Conf. on Fire research and Engineering, Sept. 10-15, Orlando, SUA, 1990.

[13] S. F. Jagger, A. Nicol, J. Sawyer, A. M. Thyer, The incorporation of fire test data in a risk-based assessment of hydraulic fluid fire resistance, Proceedings of INTERFLAME, pp. 569-576, 2004.

[14] M. Khan, Spray Flammability of Hydraulic Fluids and Development of a Test Method, Technical Report FMRC J.1 0T0W3.RC, Factory Mutual Corporation, Norwood, MA, 1991.

[15] W. D. Phillips, The Development of a Spray Ignition Test for European Hydraulic Fluid Specifications, Symposium of Fire-Resistant Test Methods, ASTM D02 N. 06 Meeting, Tampa, Florida, 2004.

[16] J. V., Shermann, Current Standards for Certification of Fire-Resistant Hydraulic Fluids Used in General Industrial Applications, Fluid Power Journal, pp. 2-9, 2005.

[17] A. Tewarson, Thermophysical and fire properties of automobile plastic parts and engine compartment fluids, Technical Report, FM Global, Project ID 0003018009-3, 2005.

[18] N. Toy, V. I. Nenmeni, X. Bai, P. J. Disimile, Surface ignition on a heated horizontal flat plat, Proceedings of 4th Intern. Aircraft & Cabin Safety Research Conference, 2004.

[19] L. Yuan, Ignition of hydraulic fluid sprays by open flame and hot surfaces, Journal of Loss Prevention in Process Industry, vol. 19 (4), pp. 353-361, 2006.

[20] M. D. Zinc, Fire Resistant Hydraulic Fluids: Shifting Definitions and Standards, Proc. of the 48th National Conf. on Fluid Power, paper 105-8.3, 2000.

[21] ISO/TC 28 Petroleum products and lubricants, ISO/TC 28N 2139, Results of voting ISO/CD 20823 Petroleum and related products – Determination of the flammability characteristics of fluids in contact with hot surfaces / Manifold ignition test, 24.10.2001.

[22] Datasheet for the hydraulic fluid Irus DR 46, www.maquipesa.com/images/Industria/Shell%20Irus%20Fluid%20DR.pdf

[23] Datasheet for Prista HFC, http://www.prista-oil.com/en/product/prista-hfc-34.html

[24] Datasheet for Prista MHE 40, datasheet, http://www.simbolauto.ro/index.php/pg/produse_unu/pin/421

[25] Datasheet for HLP 68, X-Oil, http://www.xoil.ro/lubrifianti/uleiuri_pentru_motoare/62/

[26] Rapeseed oil for sale, http://www.greenerpro.com/RSO.html

[27] Patent proposal, no. A/00201, 06.05.2010, Instalaţie automatizată pentru testarea inflamabilităţii fluidelor pe suprafeţe calde, OSIM, Romania

[28] Patent proposal, no. A/00200, 06.05.2010, Simbolizare prin cod de culori a inflamabilităţii fluidelor tehnice pe suprafeţe calde, OSIM, Romania

Serbian Tribology Society

SERBIATRIB '11

12th International Conference on Tribology

Faculty of Mechanical Engineering in Kragujevac

Kragujevac, Serbia, 11 – 13 May 2011

COMPARISON OF ADDITIVE'S PROTECTIVE LAYER ON THE CYLINDER LINER SURFACE USING DIESEL ENGINE AND PIN ON PLATE TEST RIGS

Dilek BEKTAS[1], Hakan KALELI[2]
[1]Piri Reis University, Istanbul, bektasdilek@yahoo.com
[2]Yildiz Technical University, Istanbul, kalelih@yahoo.com

Abstract: *In this research, the layer formation of additives on the surface of cylinder liner (single cylinder Diesel engine liner operated 22 h) were examined by using binocular, optical, scanning electron microscope and energy dispersive x-ray spectra and were compared to the plates tested in reciprocating pin on plate tribotest machine. The additive materials such as Ca, Zn, P, and S displayed a significant presence in TDC (Top Dead Center), but relatively less so in MC (Middle Center) and no additive elements were found in the BDC (Bottom Dead Center). Six plates (A, B, C, D, E and F) were tested in tribotest machine and some of them showed surprisingly similar results on their rubbed surfaces as in cylinder liner of Diesel engine during microscopic examination. Additives were detected as islands in both Diesel engine cylinder liner and tested plates. Almost the same additives such as Ca, Zn, P and S detected in Plate A and B as well as in Diesel engine's TDC, MC. Plate C revealed also the presence of P and S elements. Most of the machining marks still remained on the surface of cylinder liner and plates.*

Keywords: *Engine Cylinder Liner, Plates, Additive's Layer, Microscopic Surface Examination.*

1. INTRODUCTION

To meet tough automotive competition and stringent government regulations, more efficient engine components and improved engine oils have been developed within the automotive industry. As part of the overall performance evaluation of these developments, the tribological performance of the piston ring-cylinder bore system must be determined [1]. In an internal combustion engine, piston rings and cylinder bore play very important roles in achieving desired engine performance and durability [2].

Ever since the invention of the internal combustion engine lubricant oils have been an essential component. Over the last century, an increasing range of additives have been incorporated into lubricating oils to confer improved performance [3]. Modern engine lubricants contain a wide range of additives which are blended with base oils to form a complete package capable of meeting demanding performance requirements.

The performance of additive mixtures results in detergency, wear protection, oxidation inhibition and corrosion inhibition in the bulk and on surfaces. Additives are used to reduce thermal and oxidative degradation, reduce deposits, change viscosity characteristics, minimize rust and corrosion, control frictional behavior, reduce wear, prevent destructive metal-metal contact, and control foaming. Additives may modify physical properties (viscosity, pour point, foaming) and chemical behavior (detergency, oxidation, corrosion, wear, extreme pressure resistance) of lubricating formulations [4].

Base oils are hydrocarbons and they tend to oxidize, thermally decompose, and polymerize [5]. The oxidation process is initiated by the formation of free radicals. The free radicals take part in a circular reaction pattern in which hydrocarbons are oxidized. The reaction slows down as the concentration of hydrocarbon is reduced, and free radicals react with each other to yield uncreative species. The reaction is thus halted. In short, the free radical mechanism can be described as follows:

creation of free radicals, radical chain reactions, chain branching, chain termination [6].

The accumulation (i.e. formation and removal) of deposits on the cylinder liners is a complex process. In the marine sector it is generally agreed that it is dependent on interactions among the fuel composition, lubricant formulation and engine design and loading [7]. There is general agreement amongst the sources that formation and accumulation of deposits appears dependent on the interaction between fuel composition, lubricant formulation, engine design and loading.[8]

Liner deposits are reported to consist of inorganic material that is derived from lubricant additives [6]. The inorganic material may constitute 80% of the deposit by weight, most of which reportedly are salts of Zn and Ca [9]. The deposits also typically consist of organic material that is believed to be polymerized hydrocarbon.

There is a great influence of the surface degradation and high temperature on the formation of the protective additive layers. The main mechanical conditions to obtain additive's layers on the surface are a small amount of oil, slight surface degradation and high temperature in boundary lubrication [10].

The purpose of this paper is to determine the additives on TDC, MC and BDC of 22 hour operated Diesel engine cylinder liner and to compare with the plates tested on reciprocating pin on plate test rig.

2. EXPERIMENTAL DETAILS

The both tests were run with commercial "Ribua TIR 6400" 15W40" mineral oil which belongs to Total-Turkey Ltd. Oil Company. Specifications of lubricating oil are listed in Table 1 where the additives content was given under their permission.

Table 1. Specifications of lubricating oil

Specification	Initial values (Method)
SAE Grade	SAE 15W 40
API service class	CH-4 / SJ (ACEA : E3)
TBN	9,7 mgKOH/g ASTM D 2896
Viscosity at 100 °C	14 cSt ASTM D 445
Viscosity index	130 ASTM D 2270
Flash point	>200°C ASTM D 92
Pour Point	-27 °C
Specific gravity at 15 °C	0,871 g/cm^3
Ca content (ppm)	Min 2580 Max 3036
Zn content (ppm)	Min 1363 Max 1610
Mg content (ppm)	Min 298 Max 336
P content (ppm)	Min 1250 Max 1474

2.1 Diesel engine test rig

The tests were carried out on a single cylinder, four stroke, air cooled type Diesel engine. Table 2 shows engine specifications and Figure 1 shows the image of test bench. It is located in the laboratory of Piri Reis University in Istanbul-Turkey.

Figure 1. (a) Control panel and (b) engine test rig

Table 2. Technical specifications of test engine

Engine Manufacturer	Anadolu Motor Co. Turkey
Model	Diesel 4LD820
Type	4-stroke air-cooled Diesel
Aspiration	Naturally aspirated
Number of cylinders	1
Bore x Stroke (mm)	102x100
Cylinder Volume (cm^3)	817
Compression ratio	17:1
Crankcase oil capacity (l)	2.6
Speed range Max (rpm)	(2600)3000
Fuel injection pressure (bar)	134
Rated power and torque at 1600 rpm (kW-Nm)	13 - 48

The test engine was manufactured by Anadolu Motor (Antor Motor) Corporation and the model description is 4LD820. Performance test were performed via varying the load from control panel. During 22 hours of test, engine operated at 2270rpm corresponding to 100% of full load, this load point was determined by considering the stable operation of engine. Engine test conditions are shown in Table 3. At the beginning of the test, engine was installed with new oil filters and was flushed with new oil.

Table 3. Engine testing conditions

Specific Fuel Consumption (g/kWh) and Speed (rpm)	270 at 2270
Load %	100
Lubricating oil temperature (°C)	65
Ambient temperature (°C)	24
Duration (h)	22

At the end of the engine test, the cylinder liner was dismantled and cut accurately without damaging the rubbed surface, cleaned ultrasonically with hexane and then dried before and after the tests for microscopic examination. This gives the possibility to examine real protective additive's layers formed on the rubbed cylinder liner surfaces (see Figure 2).

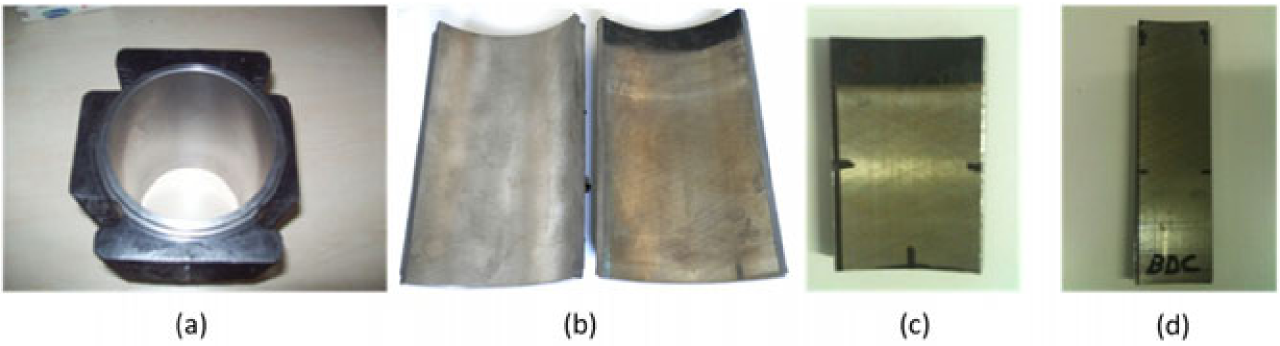

Figure 2. (a) Cylinder and liner before operation, (b) liner specimens cut from new cylinder (left) and cylinder of Diesel engine (right) operated 22h respectively, (c) liner specimen for TDC, (d) liner specimen for MDC (upper side) and BDC (down side)

2.2 Reciprocating pin on plate test rig

Reciprocating pin on plate test rig is used for the test of plates. Test rig is located in the laboratory of INSA in Lyon, France. A schematic diagram showing the main features of the test rig is given at Figure 3(a). In first step of the test procedure, three small drops of oil (approx. 1ml each of them) were dropped in the left, center and right of the wear track then unified those three points as a thin line with the extremity of the pipette before starting the tests. Then 100 N of load is applied on a single way of sliding direction.

Six plates (A, B, C, D, E and F) were tested in tribotest machine and three of them which are Plate A, Plate B and Plate C showed surprisingly similar results on their rubbed surfaces as in cylinder liner of Diesel engine during microscopic examination. The stroke and speed were controlled to produce a wear track length of 60 mm at constant load of 100 N, testing duration of 42 min, with a reciprocating velocity of 0,03 - 0,06 m/s and at the temperature of 95 °C. The only differences between plates were among the piston rings which changes the contact pressures. Plate A and B tested under Cr coated piston rings and Plate C tested under non-Cr coated piston ring. The contact pressure was 0,014 GPa for both Plate A and C, 0,0083 GPa for Plate B. For the test, fresh samples of piston rings and plates were assembled in the test machine and the bath was heated to the required temperatures and allowed to stabilize during test. The tests were run with the same sliding directions (see Figure 3(b)) for both types of piston rings.

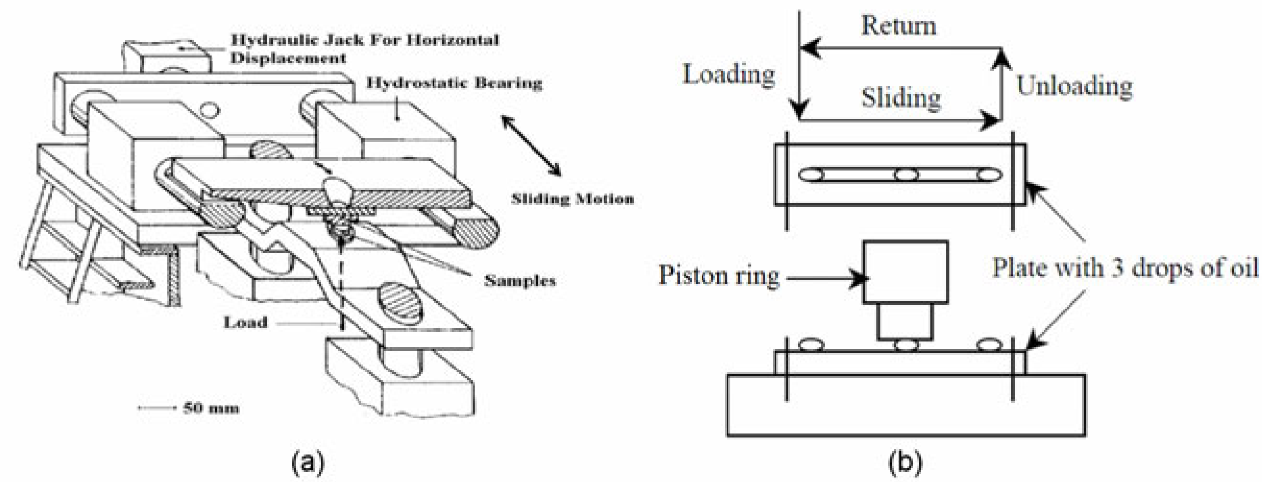

Figure 3. (a) Reciprocating pin on plate test rig, (b) Single way sliding direction of the pin (piston ring) configuration on the plate

Before the tests of the plates, the cylinder liner was cut accurately (for dimensions see Figure 4) without damaging the rubbed surface, cleaned ultrasonically with hexane and then dried before and after the tests for microscopic examination. This gives the possibility to examine the real protective additive's layers remained on the wear track.

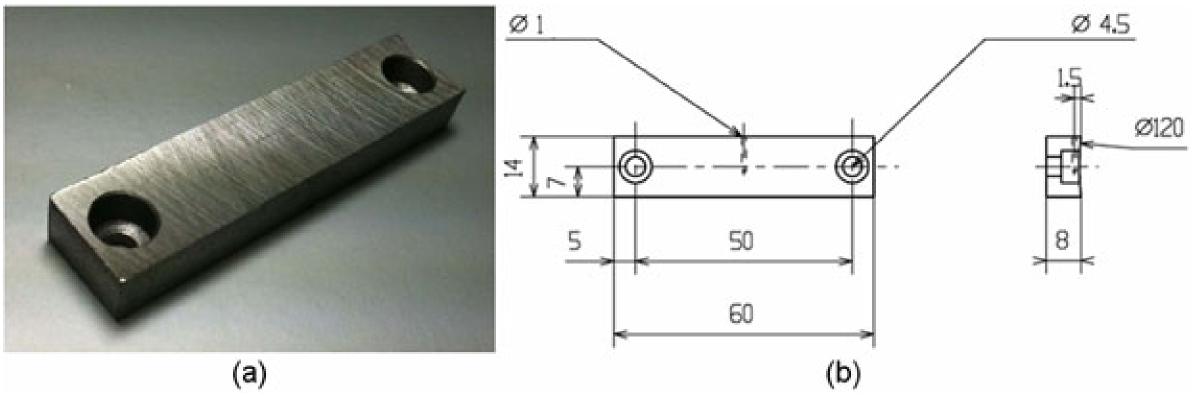

Figure 4. (a) Perspective view and (b) technical drawing of plates prepared for tests

3. COMPARISON OF THE 22H OPERATED ENGINE CYLINDER LINER (TDC, MC AND BDC) AND PLATES (A, B AND C) TESTED ON RECIPROCATING PIN ON PLATE TEST RIG

Optical, Scanning Electron Microscopy and X-Ray Spectra of the non-operated (new) cylinder liner surface is shown at Figure 5. The cylinder liner and plate material is cast iron that consists of Fe, C, Mn and Si and these are the main components which constitute the surface.

Figure 6 shows the TDC of the cylinder liner surface and Plate A tested on reciprocating pin on plate test rig in five different magnifications. For each magnification, six points are measured and examined. Black part at the top of the image identifies the line between the combustion chamber and TDC. Below 800 μm of that line is colorful and shows that the additives were covered the surface as islands.

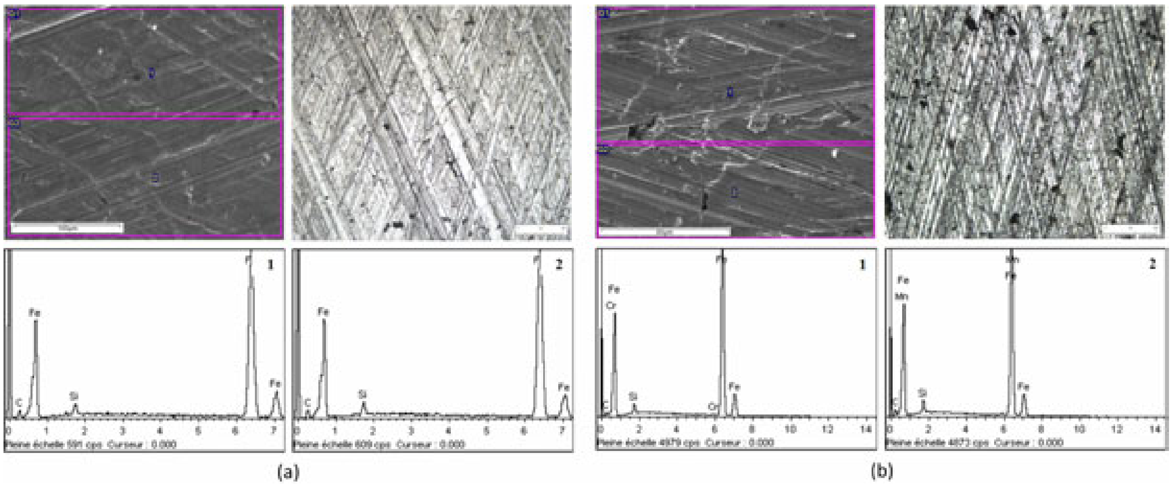

Figure 5. Optical, Scanning Electron Microscopy and X-Ray Spectra of the (a) New Cylinder Liner and (b) unused plate

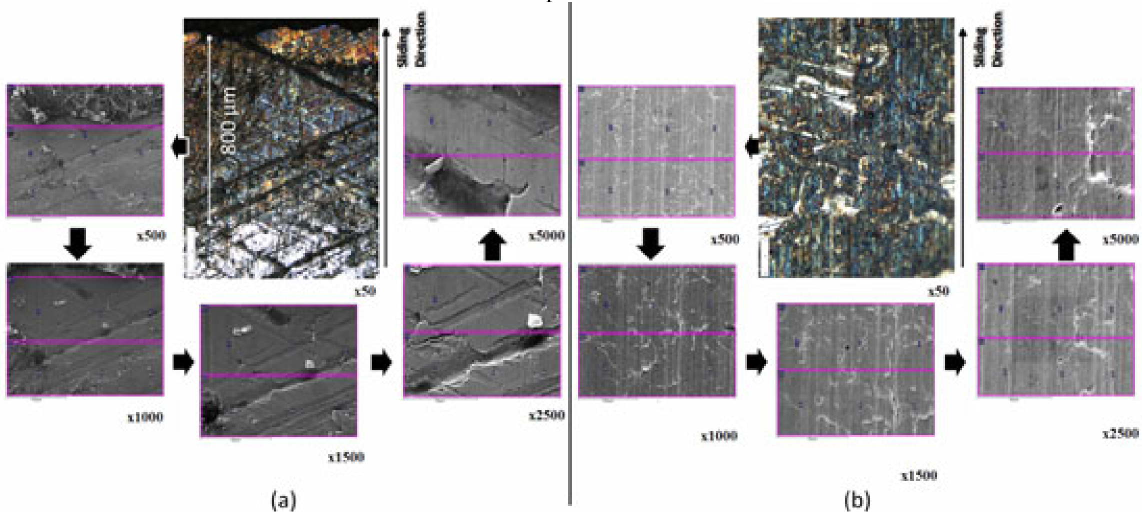

Figure 6. Optical and scanning electron microscopy of the TDC of the (a) engine cylinder liner operated 22h and (b) Plate A in five different magnifications such as x500, x1000, x1500, x2500 and x5000 respectively

Figure 7 is the identification of three points (3, 4 and 5) in x500 magnification of cylinder liner at TDC and two points (2 and 5) in x2500 magnification of Plate A. Ca, Zn, P and S are the main elements detected at the TDC and Plate A comparing to the new cylinder liner in Figure 5. All additives (Ca, Zn, P and S) are observed at the points 3, 4 and 5 and only element P is detected at the points 1, 2 and 6 of TDC. At Plate A points 2 and 5 contains all additive elements (Ca, Zn, P and S), point 1 contains P, point 3 contains Zn and P, point 4 and 6 contains P and S.

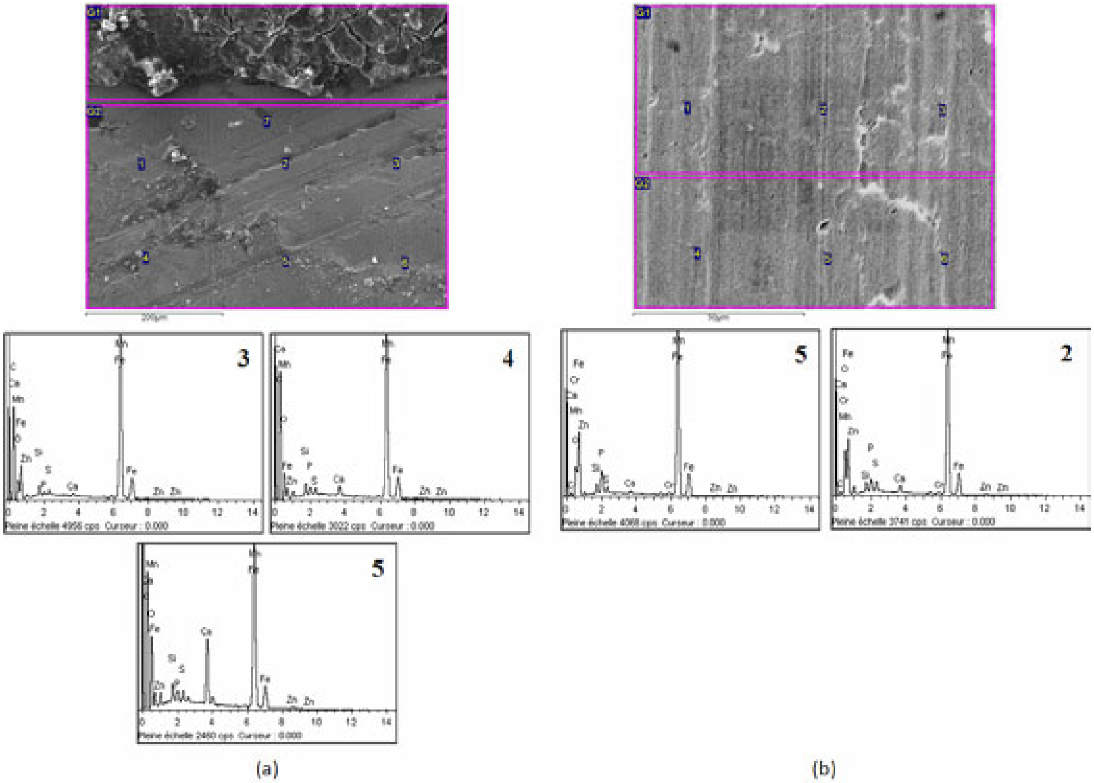

Figure 7. Scanning electron microscopy and X-ray spectra of the (a) cylinder liner TDC in x500 magnification of three points (3, 4 and 5) and (b) Plate A in x2500 magnification of two points (2 and 5)

Figure 8 shows the MC of the cylinder liner surface in five different magnifications and Plate B in three different magnifications tested on reciprocating pin on plate test rig. For each magnification, six points are measured and examined. For both cylinder liner MC surface and Plate B the honing machining marks can be observed. Optical images show that the color of the surface of MC and Plate B are less colorful than TDC and Plate A.

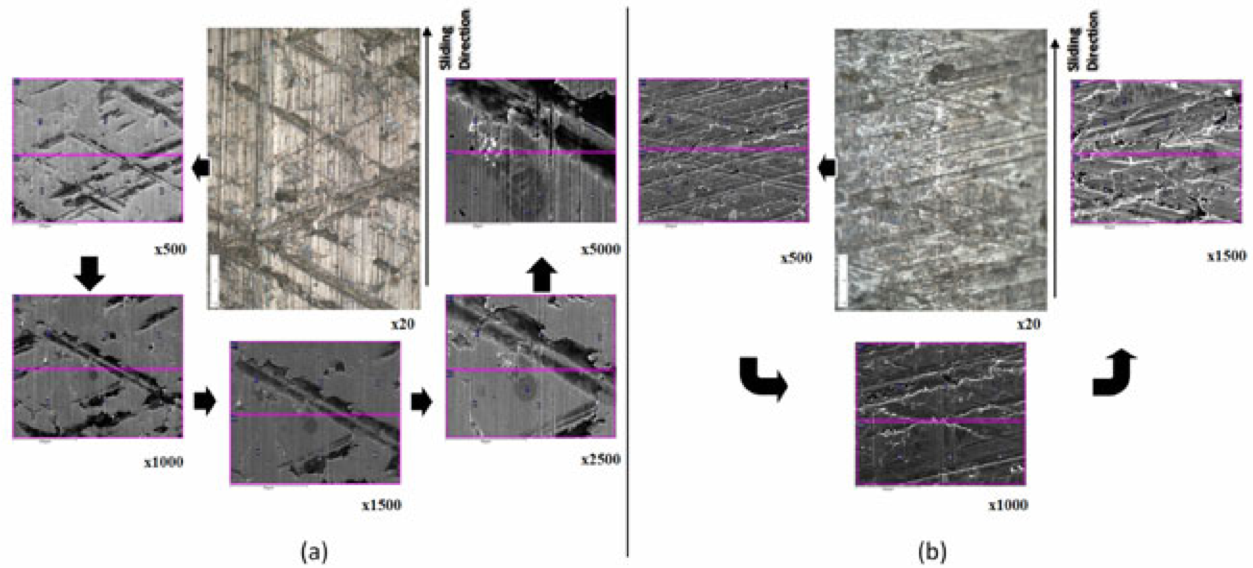

Figure 8. Optical and scanning electron microscopy of the MDC of the (a) engine cylinder liner operated 22h in five different magnifications such as x500, x1000, x1500, x2500 and x5000 respectively and (b) Plate B in three different magnifications such as x500, x1000 and x1500

Figure 9 presents the MC in magnification x1000 of the cylinder liner surface (points 1, 5 and 6) and Plate B in magnification x500 (point 1). Same additives such as Ca, Zn, P and S were detected at the MC and Plate B comparing to the new cylinder liner in Figure 5. All additives (Ca, Zn, P and S) are observed at points 1, 5 and 6 of MC and point 2 of Plate B. For both MC and Plate B, the points which all additives are observed are located in honing grooves as seen in Figure 9. Also, no additives found at points 2, 3 and 4 of MC and at points 1, 3, 4, 5 and 6 of Plate B. The points including additives which were detected in Figure 9 are less than in Figure 7.

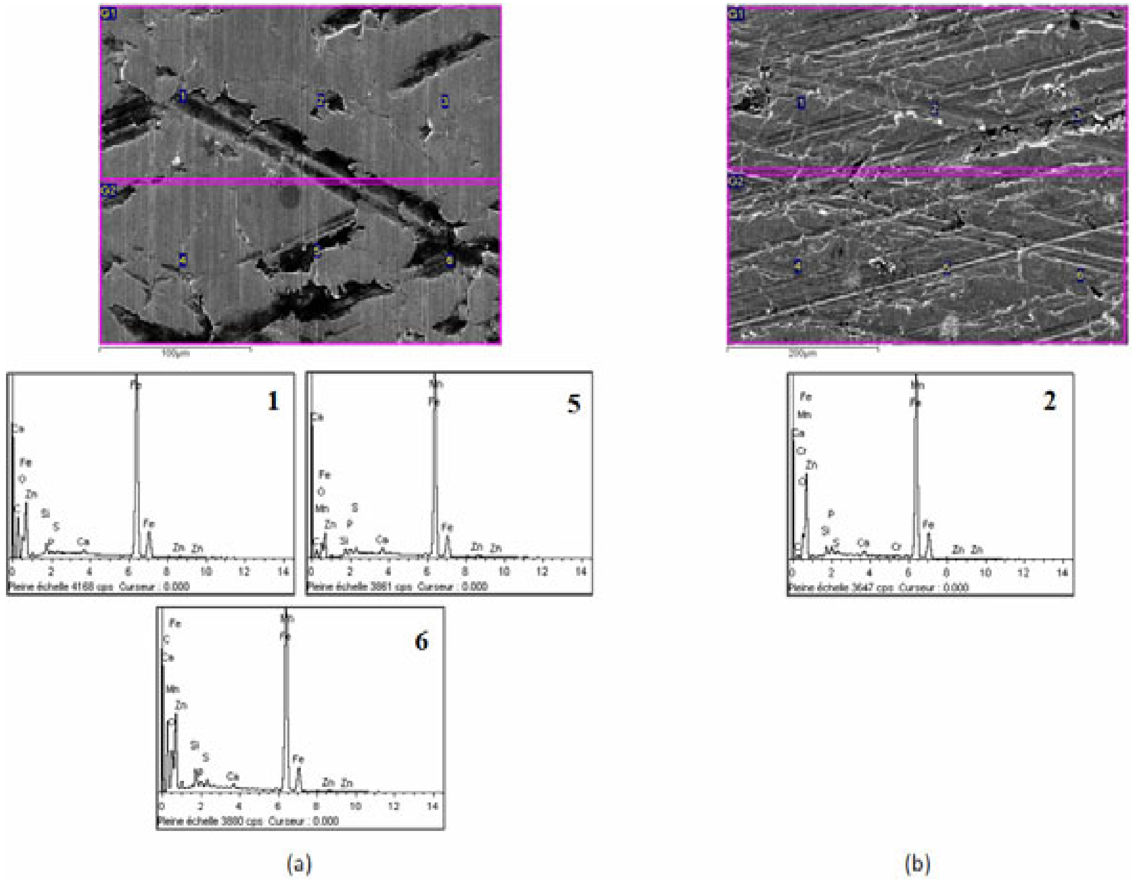

Figure 9. Scanning electron microscopy and X-ray spectra of the (a) cylinder liner MC in x1000 magnification of three points (1, 5 and 6) and (b) Plate B in x500 magnification of one point (2)

Figure 10 is the optical and SEM images of the BDC of the bore surface and Plate C. For each magnification, six points are measured and examined. The honing machining marks are remarkable on the rubbed area during sliding direction as shown in the optical images. BDC and Plate C were investigated in two different magnifications.

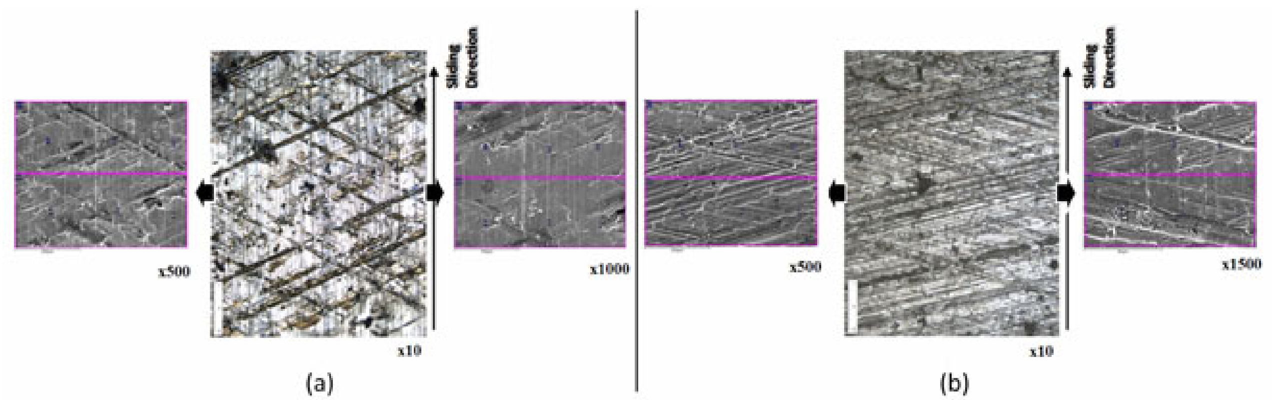

Figure 10. Optical and Scanning Electron Microscopy of the BDC of the (a) engine cylinder liner operated 22h and (b) Plate C in two different magnifications such as x500 and x1000; x500 and x1500 respectively

Figure 11 is the identification of one point in x500 magnification of cylinder liner at BDC (point 1) and used Plate C (point 3). The wear track BDC does not contain any additive's elements. Plate C contains P at points 3 and 6; S at point 3 and no additives found at other points. Point 3 and 6 of Plate C are located in honing grooves.

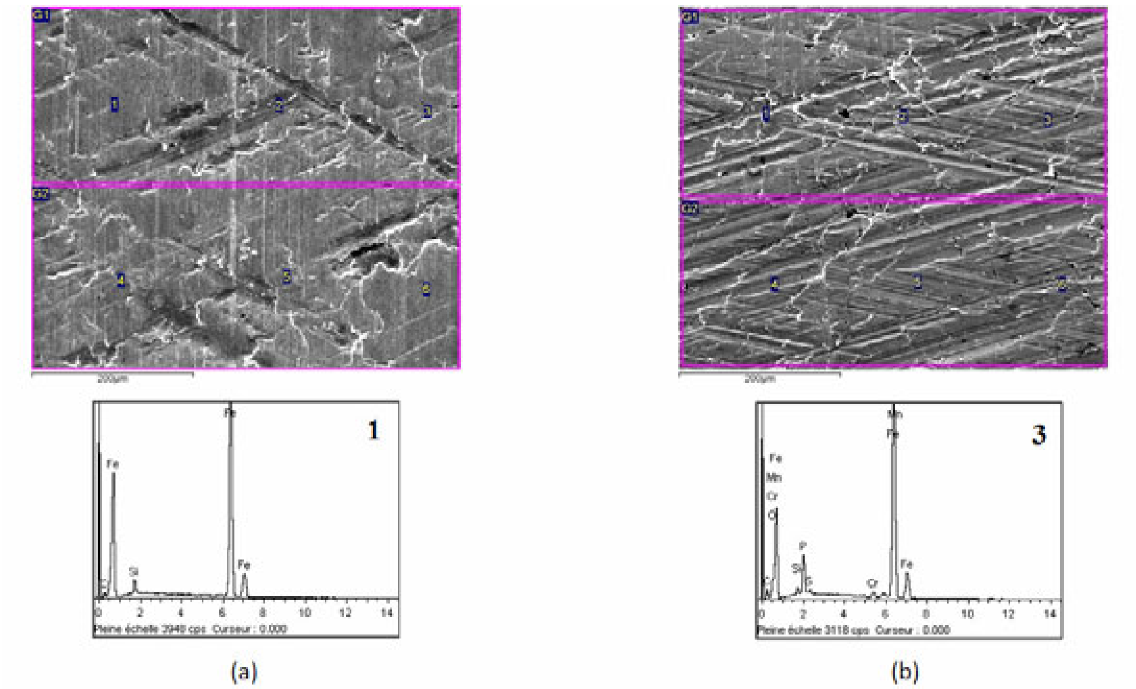

Figure 11. Scanning electron microscopy and X-ray spectra of the (a) cylinder liner BDC and (b) Plate C in x500 magnification of one point (1 and 3 respectively)

4. RESULTS AND DISCUSSION

The profile of the cylinder bore and the protective layer were observed at the same time of acquisition and acceleration of tension to clearly point out the differences between atomic percentage values of the additives in three areas (Top, Middle and Bottom Dead Center) and in plates (A, B, C) as an average of six points at five different magnifications such as x500, x1000, x1500, x2500 and x5000. Six considerable points were also emitted by X-Ray in each magnification and the average value of additives elements is calculated. It can also be seen from X-Ray spectra that the peaks of Ca, Zn, P and S are clearly detected in the protective layer area which is determined by the microscopic wear map. P and Zn are key elements of zinc-dialkyl-dithiophosphate (ZDDP) which is a typical anti-wear additive in engine oils. Ca is supplied by the oil detergent additive (calcium sulfonate). C, O and S are stemming from oil and fuel [7]. It is well known that ZDDP reacts with ferrous and chromium alloys to form a protective boundary film under thermo-mechanical stresses in tribotesting [11].

The comparison of the X-Ray spectra data (as an average of six points) taken from Top, Middle and Bottom Dead Centers of 22h operated cylinder liner [12] and Plate A, B and C in several different magnifications are shown in Table 4.

The graphs shown in Figure 12, 13, 14 and 15 are related to the values of Table 4.

Distribution of additive elements which were observed is shown in Figure 12. Additive elements mostly found at TDC, relatively less at MC and no additives found at BDC [12]. The deposits were distributed in the top regions of all the liners investigated pointing to the high temperature being the dominant factor for their accumulation [6,7]. It can be seen that Zn has the minimum value for each magnification group at TDC. Observed atomic percentages of P for all magnifications are approximately equal to each other for TDC. Measured atomic percentages of S are almost equal at magnifications x500, x1000 and x2500 for MC.

For both TDC and Plate A, the graph that illustrates the additive percentages of the surfaces is shown in Figure 13. Mostly same additive elements observed in each five different magnifications for both TDC and Plate A. Generally the amount of the additives of Plate A is higher than TDC of the wear track. As seen in Figure 13, Zn has the minimum value for each magnification on Plate A except x1500 which is similar to the TDC of 22h operated cylinder liner. P has the highest values comparing to the other additive elements for each magnification in Plate A.

Table 4. Values in atomic % of the wear track of cylinder liner from X-Ray at Top, Middle and Bottom Dead Centers in five different magnifications as x500, x1000, x1500, x2500 and x5000 respectively

		22H CYLINDER			PIN ON PLATE TRIBOTEST MACHINE		
		Values in Atomic % of the layer at TDC	Values in Atomic % of the layer at MC	Values in Atomic % of the layer at BDC	Values in Atomic % of the layer at PLATE A	Values in Atomic % of the layer at PLATE B	Values in Atomic % of the layer at PLATE C
X-Ray Spectra x500	Ca	1,00	0,13	0,00	0,53	0,75	0,00
	Zn	0,22	0,16	0,00	0,47	0,37	0,00
	P	0,41	0,09	0,00	0,95	0,61	1,41
	S	0,28	0,20	0,00	0,84	0,77	0,52
X-Ray Spectra x1000	Ca	0,30	0,22	0,00	0,00	0,59	-
	Zn	0,09	0,28	0,00	0,00	0,00	-
	P	0,41	0,36	0,00	4,57	0,79	-
	S	0,13	0,20	0,00	0,63	0,51	-
X-Ray Spectra x1500	Ca	0,65	0,00	0,00	0,00	0,86	0,00
	Zn	0,33	0,10	0,00	0,38	0,00	0,00
	P	0,41	0,00	0,00	0,95	1,35	1,22
	S	0,57	0,00	0,00	0,00	0,47	0,00
X-Ray Spectra x2500	Ca	0,31	0,24	0,00	0,72	-	-
	Zn	0,00	0,08	0,00	0,50	-	-
	P	0,44	0,42	0,00	3,57	-	-
	S	0,31	0,21	0,00	0,96	-	-
X-Ray Spectra x5000	Ca	0,44	0,11	0,00	0,59	-	-
	Zn	0,19	0,12	0,00	0,44	-	-
	P	0,43	0,00	0,00	3,14	-	-
	S	0,49	0,00	0,00	0,88	-	-

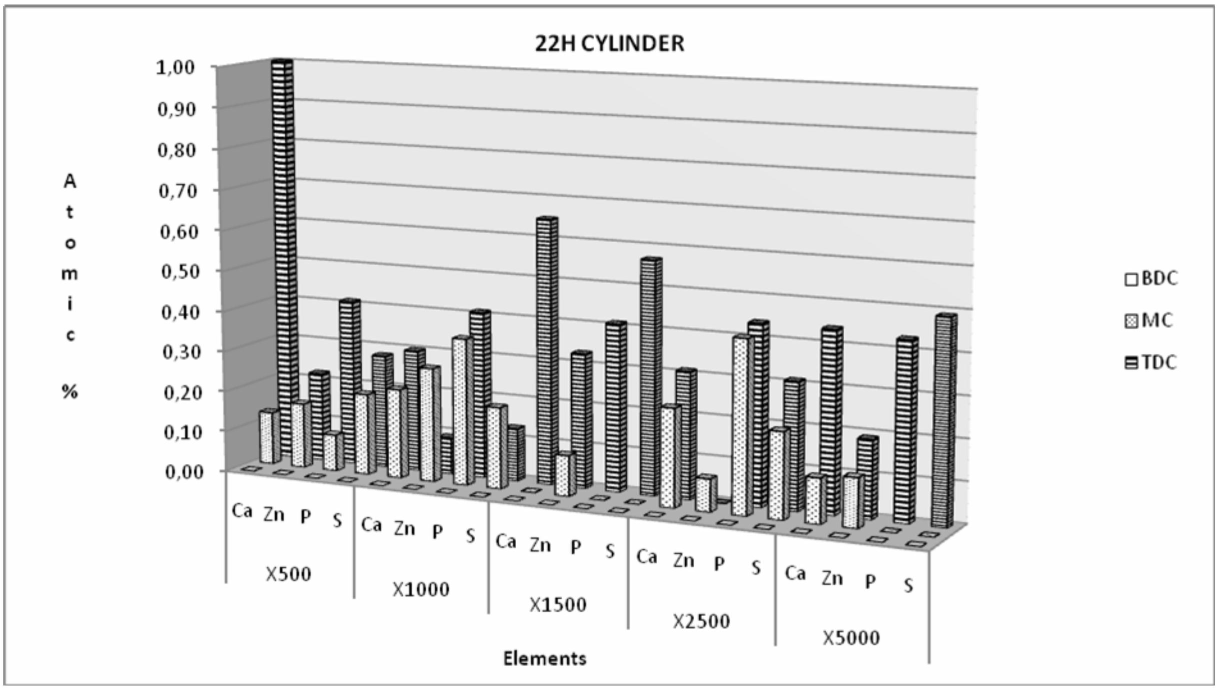

Figure 12. Elemental analysis in atomic % of additive's elements Ca, Zn, P and S in five different magnification x500, x1000, x1500, x2500 and x5000 from X-Ray Spectra of the cylinder liner from Top, Middle and Bottom Dead Centers

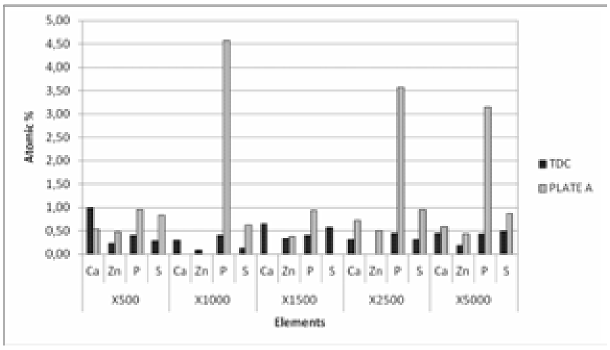

Figure 13. Elemental analysis in atomic % of additive's elements Ca, Zn, P and S in five different magnification x500, x1000, x1500, x2500 and x5000 from X-Ray Spectra of the cylinder liner from TDC and Plate A

The additive percentages of the MC and Plate B are shown in Figure 14. The graph indicates that the Plate B and MC have similar characteristics of additive distribution depending on atomic percentages. Generally amount of the Plate B's additives are higher than MC. It can be observed in Figure 14 that S has the highest atomic percentages comparing to the other additives for both MC and Plate B at the magnification x500. At the magnification x1000, P has measured more than other additive elements for both MC and Plate B. For all magnifications except x500 Zn atomic percentages are nil for Plate B.

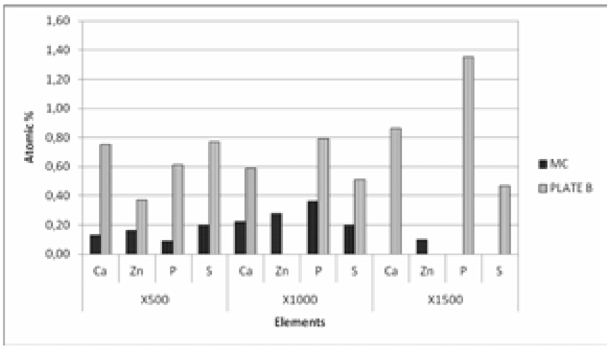

Figure 14. Elemental analysis in atomic % of additive's elements Ca, Zn, P and S in three different magnifications x500, x1000 and x1500 from X-Ray Spectra of the cylinder liner from TDC and Plate B

For both BDC and Plate C, the graph that illustrates the additive percentages of the surfaces is shown at Figure 15. At Plate C, as additive elements Ca and Zn values are nil for magnifications x500 and x1500. Also S value is nil for magnification x1500 at Plate C.

For both 22h Diesel engine cylinder liner and plates, additives are observed as islands. Also, Kaleli and Berthier observed that the steel stub 51115 provides high percentage of protective additive's layers and to cover uniformly the whole wear track in boundary lubricated conditions [13]. According to J. Keller et. al., the reason for additives to cover surface as islands is the microstructure of cast iron, as a result of experiments there was no film is formed on phosphorous eutectics, neither on carbides [14].

The average of all additive atomic percentage values for each 6 measurement points, in each magnification and for plates and cylinder liners (A, B, C and TDC, MC, BDC) are taken and illustrated at Figure 16. Mean additive values are decreasing from Plate A to C and cylinder liner TDC to BDC, which shows similar characteristics relatively.

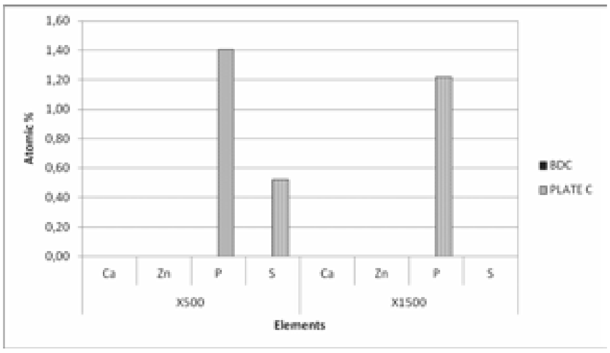

Figure 15. Elemental analysis in atomic % of additive's elements Ca, Zn, P and S in two different magnifications x500 and x1500 from X-Ray Spectra of the cylinder liner from BDC and Plate C

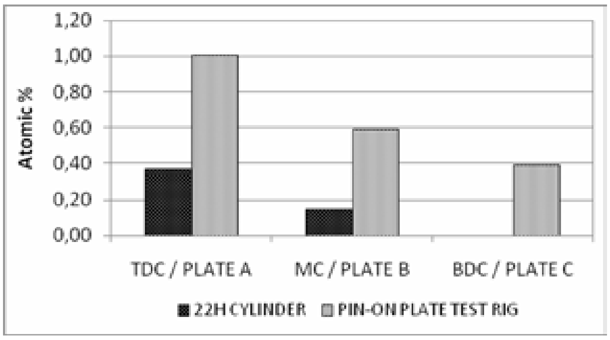

Figure 16. Additive characteristic comparison of plates (A, B and C) and cylinder liner (TDC, MC and BDC)

5. CONCLUSION

The following similarities found between plates (A, B and C) tested on reciprocating pin on plate test rig and 22h operated Diesel engine cylinder liner (TDC, MC, and BDC). Plate A and TDC, Plate B and MC, Plate C and BDC has similar surface characteristics surprisingly.

Most of the machining marks still remained on the surface of cylinder liner and plates.

Additive elements mostly found in the honing grooves of the cylinder liner and plates.

As surface characteristic similarity, it is also observed that the additives of Plate A and TDC, Plate B and MC, Plate C and BDC are similar surprisingly.

For both 22h operated Diesel engine cylinder liner and plates tested on reciprocating pin on plate tribotest machine, additives are covered the surface as islands.

Almost the same additives such as Ca, Zn, P and S detected in Plate A and Plate B as well as in Diesel engine's TDC, MC. There is no additive elements found in BDC. Plate C revealed also the presence of P and S elements.

ACKNOWLEDGMENTS

The authors would like to express their thanks to the elf-total ltd. in Turkey for their support of providing crankcase oil and fuel, to INSA Lyon-France for microscopic examination and pin on plate test rig and to Piri Reis University for providing Diesel engine bench test during this research project.

REFERENCES

[1] S. C. Tung, Y. Huang: Modeling of abrasive wear in a piston ring and engine cylinder bore system, Tribology Transactions, Vol. 47, pp. 17-22, 2004.

[2] L. Gara, Q. Zou, B.P. Sangeorzan, G.C. Barber, H.E. McCormick, M.H. Mekari: Wear measurement of the cylinder liner of a single cylinder diesel engine using a replication method, Wear, Vol. 268, pp. 558-564, 2010.

[3] Ullmann's encyclopaedia of industrial chemistry, vol 20, sixth edition, chapter 6, p 118 Jürgen Braun and Jürgen Omeis. *format düzenlenecek.

[4] Z. Pawlak: Tribochemistry of Lubricating Oils, Elsevier – Tribology and Interface Engineering Series, Poland, 2003.

[5] S. M. Hsu, R.S. Gates: Boundary lubricating films: formation and lubrication mechanism, Tribology International, Vol. 58, pp. 305-312, 2005.

[6] O. Buhaug: Deposit formation on cylinder liner surfaces in medium-speed engines, PhD thesis, Faculty of Engineering Science and Technology, Norwegian University, Trondheim, 2003.

[7] Z. Dimkovski, L. Bååth, S. Rosén, R. Ohlsson, B. G. Rosén: Interference measurements of deposits on cylinder liner surfaces, Wear, Vol. 270, pp. 247-251, 2011.

[8] R.W. Allen: The influence of Marine Fuel Quality on Lubricating Oil Performance, Castrol International, 1995.

[9] Cannon, MJ, Logtenberg, J, Dilks, A. Cylinder liner lacquering in high output medium speed diesel engines. Shell Marine Service Publication. <Not dated>.

[10] H. Kaleli: Additive's layer formation in engine crankcase oil using two different types of tribologycal test rigs, Industrial Lubrication and Tribology, Vol. 56, No. 3, pp. 158-170, 2004.

[11] M.A. Nicholls, T. Do, P.R. Norton, M. Kasrai, G.M. Bancroft: Review of the lubrication of metallic surfaces by zinc dialkyl-dithiophosphates, Tribology International, Vol. 28, pp. 15-39, 2005.

[12] H. Kaleli, D. Bektas: Effect of Additive Level on the Surface of Diesel Engine Cylinder Liner, Journal of the Balkan Tribological Association, *Lubrication section*, Book 1, 2011, pp.139, ISSN 1310-4772.

[13] H. Kaleli, Y. Berthier: Tribomechanical-Chemical Effects And Visualisation Of Additive's Layer Formation In Engine Crankcase Oil Between Sliding Pairs, World Tribology Congress III, 12-16.09.2005, Washington, D.C., USA.

[14] J. Keller, V. Fridrici, Ph. Kapsa, S. Vidaller, J.F. Huard: Influence of chemical composition and microstructure of gray cast iron on wear of heavy duty diesel engines cylinder liners, Wear, Vol. 263, pp. 1158-1164, 2007.

Serbian Tribology Society

SERBIATRIB '11

12th International Conference on Tribology

Faculty of Mechanical Engineering in Kragujevac

Kragujevac, Serbia, 11 – 13 May 2011

NEUTRAL RADIUS VALUE DETERMINATION BY NUMERICAL SIMULATION METHOD AT RING UPSETTING TEST

Marko Vilotić[1], Damir Kakaš[1], Pal Terek[1], Lazar Kovačević[1], Aleksandar Miletić[1]
[1]DPE, Faculty of Technical Sciences, University of Novi Sad, Serbia,
markovil@uns.ac.rs; kakasdam@uns.ac.rs; terekpal@gmail.com; lazarkov@uns.ac.rs; miletic@uns.ac.rs

Abstract: *Ring upsetting represents a basic operation for bulk forming process and has particular significance since it is used for contact friction determination.*
At ring upsetting by flat dies, metal flow depends upon tribological conditions present at contact surface. Thereby, two variants of metal flow are possible:
a) two-way flow from neutral radius that is present at lower friction coefficient values, followed by ring's inner radius reduction and ring's outer radius increase. In such circumstances, neutral radius is found between inner and outer radius.
b) one-way flow that occurs at higher friction coefficient values, where neutral radius is lower than ring's inner radius.
This paper is presenting the results of determination of relation between neutral radius value and friction coefficient. Such relation is determined by numerical simulation, by using Simufact.Forming software. Experimental verification of neutral radius position is conducted by metallographic analysis, for two friction coefficient values. Friction coefficient values are determined by ring upsetting by using dies, where in one case of ring upsetting, contact surfaces were ion implanted with nitrogen.

Keywords: *neutral radius, friction coefficient, ring upsetting, ion implantation.*

1. INTRODUCTION

For a correct tool design it is necessary to analyse the stresses at the tool–workpiece interface with a high degree of accuracy in order to use the process at the limit and to avoid early tool damage. In this analysis friction plays a central role because it is strongly influenced by the existing distribution of the contact variables at the tool–workpiece interface. Moreover, these contact conditions have a great influence on the material flow [1].

One of the most essential problems of technology of plasticity are metal flow across die and cavity filling. These problems are especially associated with tribological state that is present on contact surface between die and workpiece. Since plastic deformation take place in a state of a high contact stresses, which can result in a high tangential stresses too, it is very important to lower the friction coefficient. In this manner it is possible to shape complex parts and lowers the amount of required operations and production cost.

As universal method for friction coefficient measurement in bulk metal forming processes, ring upsetting by flat plates (dies) have been used [2, 3, 4].

2. MATERIAL FLOW AT RING UPSETTING

Key phenomenon required for understanding the subject of wear and friction is material flow across die's surface during plastic deformation. In this paper material flow is analyzed through ring upsetting process by flat dies since upsetting is also used for friction coefficient determination. Material flow phenomenon is investigated by direct measurement of microstructural changes in workpiece at deformation process. Nowadays, modern software packages are also being used for material flow process simulation.

Ring upsetting represents a fundamental operation of bulk forming process and it is a phase in multiphase plastic forming process. This process is particulary interesting from an aspect of possible material flow variants, which depends on a friction coefficient.

According to figure 1 there are three types of material flow at ring upsetting.

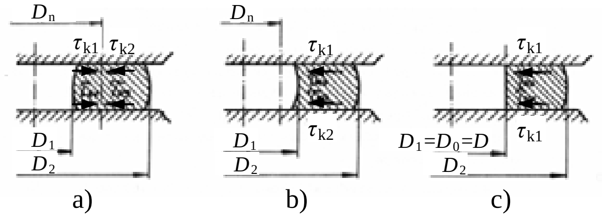

a) b) c)

Figure 1. Types of material flow in ring upsetting [5]

In first type (fig. 1a), material flows in opposite directions respecting neutral radius R_n. Inner diameter decreases D_1, while outer diameter increases D_2. In this case neutral diameter is within the range $D_1<D_n<D_2$. Direction of tangential stress is opposite of material flow direction which affect normal contact stresses too (fig. 2b). This type of material flow occurs at lower friction coefficient values.

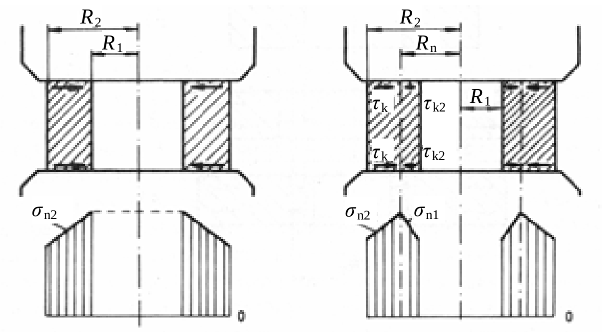

a) b)

Figure 2. Contact stresses distribution depending on material flow [5]

In second type of material flow, both, inner D_1 and outer D_2 diameter increases. In this case, neutral diameter is smaller than inner diameter $D_n<D_1$ (fig. 1b). Contact stresses distribution is shown on figure 2a.

Third type of material flow is featured by one-way material flow with no change of inner diameter. In this case the inner diameter is equal to the neutral diameter $D_1=D_n$.

Second and third type of material flow appears with higher values of friction coefficient.

Based on the presented three types of material flow at ring upsetting it is possible to conclude that the direction of material flow is characterized by the contact friction coefficient value. Furthemore, nature of material flow is also defined by neutral radius. Its magnitude can be determined theoretically, numerically and experimentally.

3. RING UPSETTING EXPERIMENT

Contact friction coefficient was determined experimentally by ring upsetting method (fig. 3).

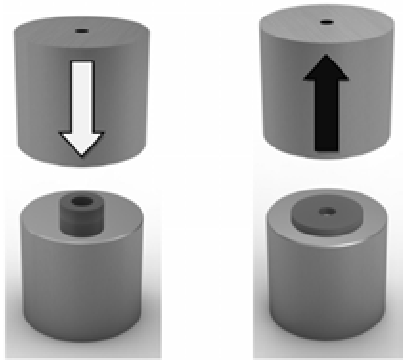

Figure 3. Ring upsetting method

Method consists of establishing the dependence between deformation of inner ring's diameter and ring's height. This dependence is taken into etalon chart and compared with existing within the chart.

Ring upsetting has been performed incrementally, with a height deformation around 10%. After each upsetting stage ring's dimensions were measured. Incremental upsetting has been carried out until total deformation of the ring's height has reach around 70%.

Once the ring upsetting has been completed deformation of the ring's inner diameter and deformation of the ring's height has been calculated for each upsetting increment. By connecting all the pairs of height and inner diameter deformation curve was defined.

In order to find the friction factor for the completed upsetting process it is necessary to compare the curve with an existing ones from the etalon diagram.

Ring upsetting has been carried out with two different pairs of dies. One pair of dies has been grinded, polished and ion implanted with $2 \cdot 10^{17}$ N^+ 50 keV, while another pair of dies has not been ion implanted. Dies were made of X210Cr12 cold work tool steel (Č.4150) with dimensions ø50×45 mm. Rings were made of Ck15 unalloyed carbon steel (Č.1221) with initial dimensions D_2:D_1:h=18:9:6 mm. Hardness of the dies was 58+2 HRC, while hardness of the ring upset with nonimplanted dies was 167 HV-10 and hardness of the ring upset with implanted dies was 161 HV-10.

4. RING UPSETTING SIMULATION BY FINITE ELEMENT METHOD

After friction factors were obtained from ring upsetting, their values were used for ring upsetting simulation. Ring upsetting simulation was performed by Simufact.forming software that is based on FEM. In forming processes this kind of software can provide detailed information about stresses, strains, material flow, friction factors and many more.

Simulation was carried out with following input data which accurately as possible describes actual experimental conditions:

- simulated process: cold upsetting,
- analysis type: 2D, axisymmetrical,
- initial workpiece dimensions: D_2:D_1:h=18:9:6 mm,
- workpiece material: Ck15 (Č.1221), flow curve σ_{avg}=max(0, 276.44+397.715$\cdot\varepsilon_{avg}^{0,317096}$,
- finite element size: 0,1 mm, rectangular shape,
- die dimensions: ø50×45 mm,
- die material: rigid body,
- die, workpiece and environment temperature: 20°C,
- friction type: constant (plastic shear friction),
- friction factors: m=0.11 (for implanted dies) and m=0.15 (for nonimplanted dies),
- upper die stroke: 4.2 mm.

5. RESULTS

5.1 Ion implantation simulation by SRIM software

In order to ensure successful ion implantation into X210Cr12 steel, SRIM simulation software was used to evaluate the effect of $2\cdot10^{17}$ N^+ 50 keV ion implantation into die's surface. As it can be seen from figure 4, ion implantation depth was around 100 nm. For the convenience, SRIM simulation on figure 4 was completed with 10000 ions.

Based on the results of simulation, ion implantation of the dies has been carried out in Institute of Nuclear Sciences "Vinča".

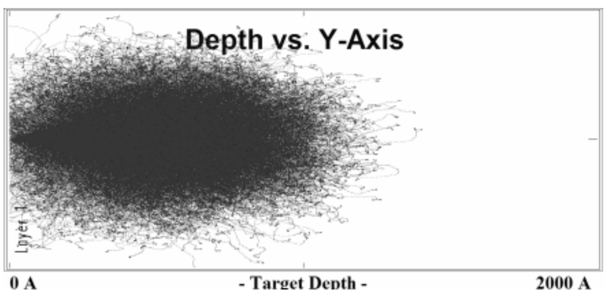

Figure 4. SRIM simulation of ion implantation into steel

5.2 Ring upsetting – contact friction coefficient

Figure 5 shows comparison of friction factors obtained from a ring upsetting experiment.

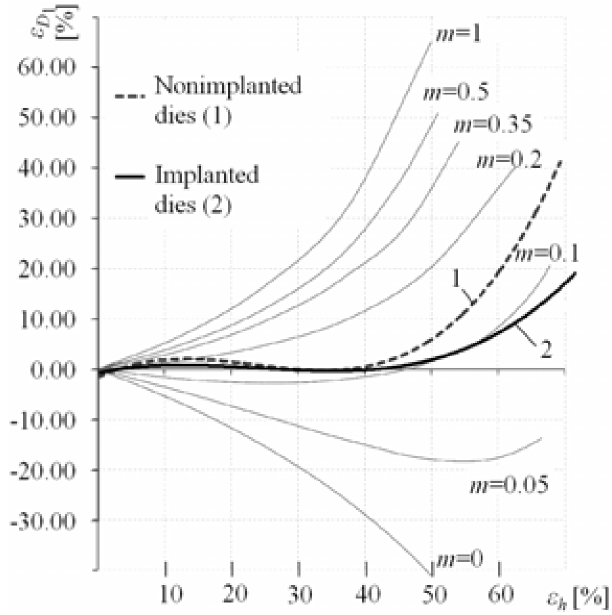

Figure 5. Comparison of friction factors for rings upset with implanted (2) and nonimplanted dies (1) [4]

Table 1 shows friction factors and friction coefficients values obtained in ring upsetting experiment.

Table 1. Friction factors and friction coefficients for rings upset with implanted and nonimplanted dies

Dies	Friction factor (m)	Friction coefficient (μ)
Nonimplanted	0.15	0.087
Implanted	0.11	0.064

5.3 Contact stress distribution

Figures 6 to 8 display tangential contact stress distribution across ring's surface obtained from Simufact.forming simulation at ring upsetting with nonimplanted dies.

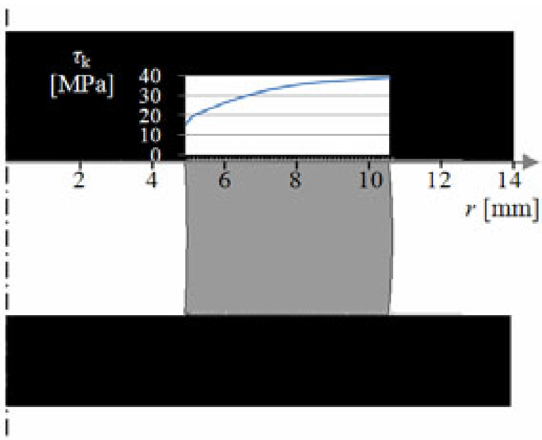

Figure 6. Tangential contact stress distribution, die stroke 1.72 mm

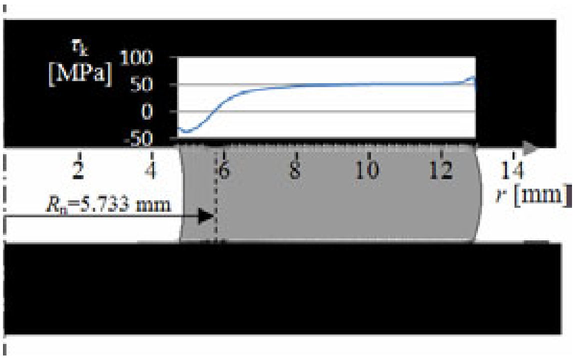

Figure 7. Tangential contact stress distribution, die stroke 3.4 mm

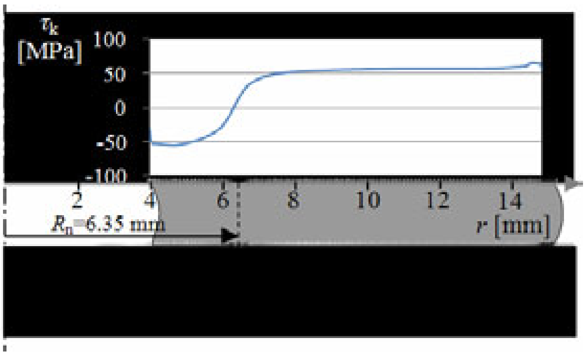

Figure 8. Tangential contact stress distribution, die stroke 4.2 mm

Figures 9 to 11 display tangential contact stress distribution across ring's surface obtained from Simufact.forming simulation. Ring has been upset with implanted dies.

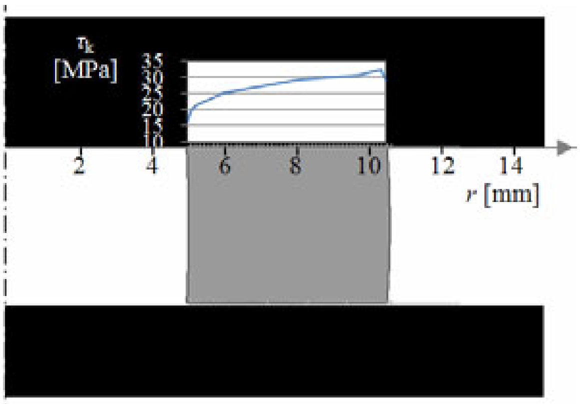

Figure 9. Tangential contact stress distribution, die stroke 1.72 mm

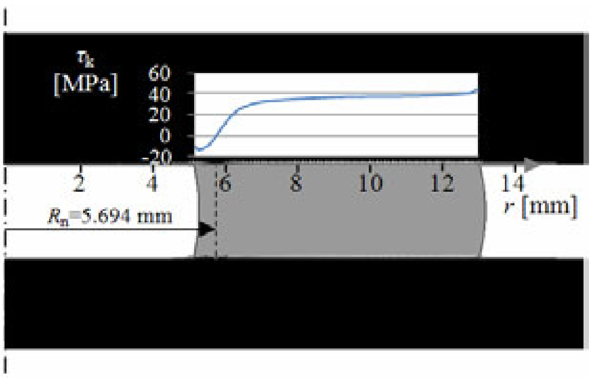

Figure 10. Tangential contact stress distribution, die stroke 3.4 mm

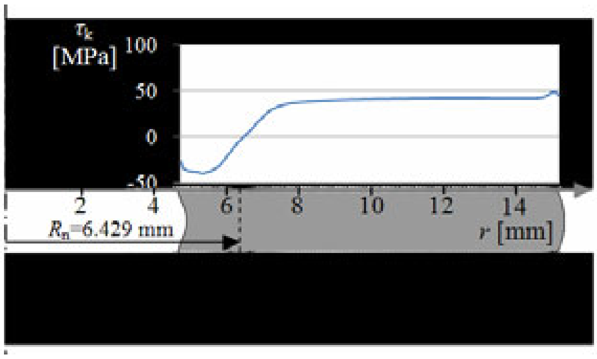

Figure 11. Tangential contact stress distribution, die stroke 4.2 mm

Figures 12 to 14 display normal contact stress distribution across ring's surface obtained from Simufact.forming simulation. Ring has been upset with nonimplanted dies.

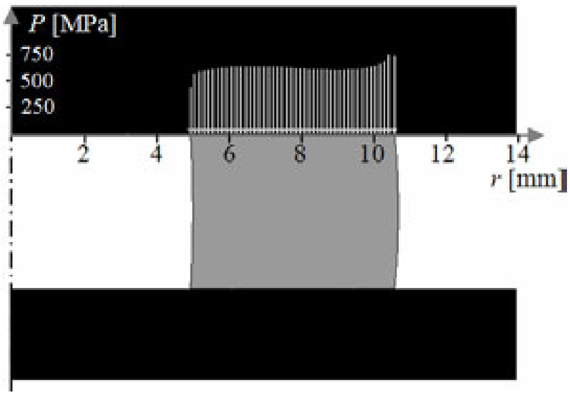

Figure 12. Normal contact stress distribution, die stroke 1.72 mm

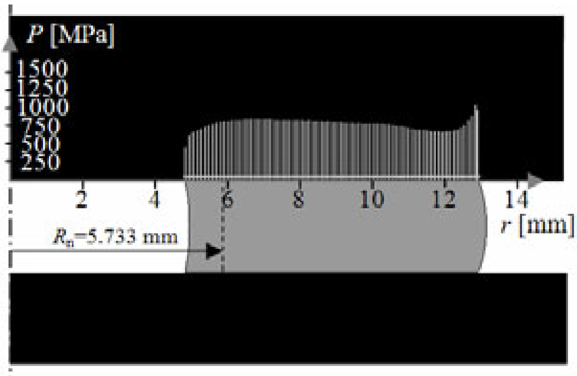

Figure 13. Normal contact stress distribution, die stroke 3.4 mm

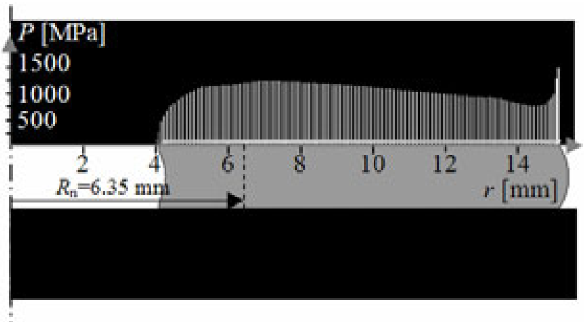

Figure 14. Normal contact stress distribution, die stroke 4.2 mm

Figures 15 to 17 display normal contact stress distribution across ring's surface obtained from Simufact.forming simulation. Ring has been upset with implanted dies.

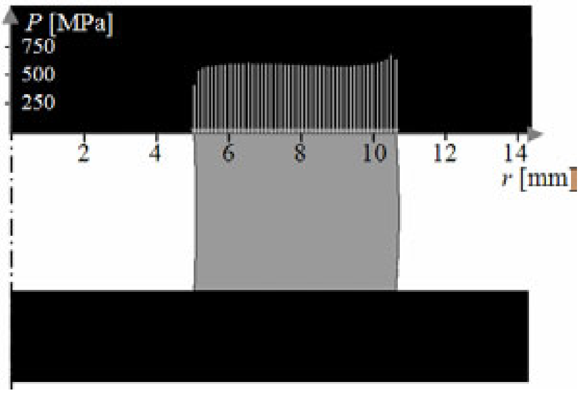

Figure 15. Normal contact stress distribution, die stroke 1.72 mm

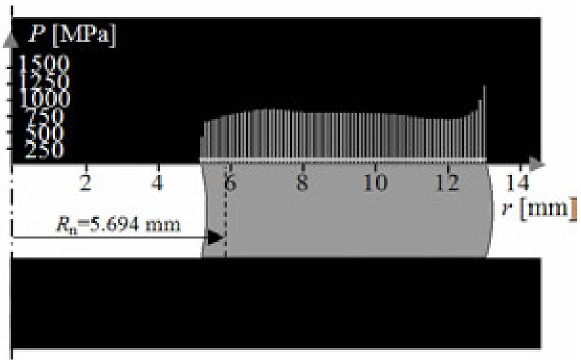

Figure 16. Normal contact stress distribution, die stroke 3.4 mm

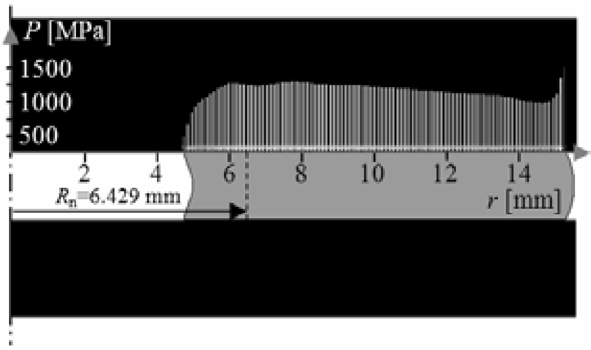

Figure 17. Normal contact stress distribution, die stroke 4.2 mm

5.4 Metallographic analysis

In order to evaluate results of neutral radius determination by numeric simulation, metallographic analysis was used.

Figures 18 and 19 present metallographic image of the ring upset with nonimplanted and implanted dies respectively and calculated neutral radius.

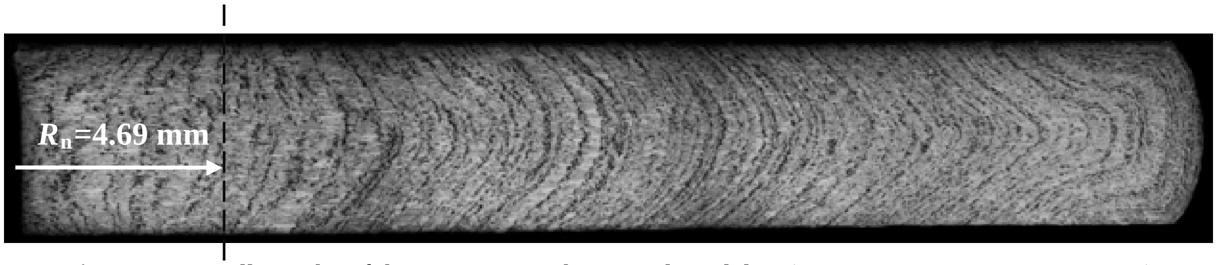

Figure 18. Metallography of the ring upset with nonimplanted dies (R_n=4.69 mm, D_1=5.1, D_2=28.75)

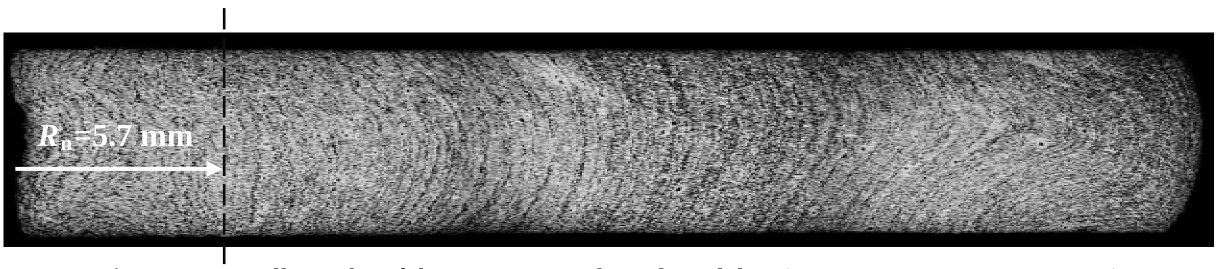

Figure 19. Metallography of the ring upset with implanted dies (R_n=5.7 mm, D_1=7.2, D_2=29.7)

6. DISCUSSION

It is evident from diagram (figure 5) that ion implantation has influence on friction coefficient and therefore friction influences deformation of the ring's inner diameter.

Small differences in neutral radius values determined by numerical simulation and metallographic analysis can be explained with simulation's inability to take into account the real deformation conditions of material.

Neutral radius position at each upsetting phase in numerical simulation is determined from the distribution of tangential and normal contact stresses (figures 6 to 17).

The magnitude of neutral radius depends on the friction coefficient. Based on figures 14, 17, 18 and 19 it can be concluded that at lower friction coefficient values neutral radius value is higher than at higher friction coefficient values. Also, by increasing die stroke the neutral radius is increased.

7. CONCLUSION

Based on the results presented in this paper, it can be concluded that ion implantation can reduce the friction coefficient and thus improve the process of material flow and filling of complex cavities at bulk forming process. Moreover, Simufact.forming simulation can be used for neutral radius determination since it provides approximately accurate values of neutral radius.

More comprehensive determination of the neutral radius at ring upsetting requires detailed micro-structural analysis of the rings at each deformation phase.

ACKNOWLEDGEMENTS

This paper is a part of research included into the project “Project TESLA: science with accelerators and accelerator technologies”, financed by Serbian Ministry of Science and Technology. The authors are grateful for the financial support.

REFERENCES

[1] A. Behrens, H. Schafstall: 2D and 3D simulation of complex multistage forging processes by use of adaptive friction coefficient, Journal of Materials Processing Technology, 80-81, pp. 298-303, 1998.

[2] J. Schey: Metal Deformation Processes: Friction and Lubrication, Marcel Dekker Inc, New York, 1972.

[3] K. Lange: Handbook of Metal Forming, McGraw-Hill, Inc, 1985.

[4] M. Plančak, D. Vilotić: Tehnologija plastičnog deformisanja, Fakutlet tehničkih nauka, Univerzitet u Novom Sadu, Novi Sad, 2003.

[5] V. Vujović: Obrada deformisanjem u mašinstvu 1. Deo, Fakultet tehničkih nauka, Novi Sad, 1977.

Serbian Tribology Society

SERBIATRIB '11

12th International Conference on Tribology

Faculty of Mechanical Engineering in Kragujevac

Kragujevac, Serbia, 11 – 13 May 2011

INVESTIGATION OF ACTION MECHANISM OF ADDITIVES FROM MINERAL RAW MATERIALS

Lyubchenko Elena[1], Aksyonova Svetlana[1]
[1]National Technical University "KPI", Ukraine, Kharkov
e_lyubchenko@ukr.net; saksyonova@gmail.com

Abstract: *The structural changes of friction surfaces and assosiated changes of main tribological characteristics (coefficuient of friction, weight wear) taking place as a result of introduction of additive into the lubricating oil were investigated. It is shown that the mechanism of additive action is based on its specific composition and dispersity. The positive effect of the additive is demonstrated by structural examinations with the help of scanning electron microscopy (SEM), profile recording and microhardness measurements as well as by tribological tests conducted using the pair of "cast iron - chromium" (typical friction pair of the cylinder-piston assembly in the most modern engines).*

Keywords: *coefficient of friction, wear, additive, lubricating oil, surface structure, scanning electron microscopy, profile recording, microhardness.*

1. INTRODUCTION

Lubricating oils with specialized and highly advanced additives made of mineral raw materials have wide distribution in the modern technological world. The use of such additives promotes the optimization of friction processes, reduces wear and friction coefficient, prevents the seizure of mechanisms, provides good running-in ability and, consequently, increases the service life of friction pairs, reduces fuel consumption and improves environmental impact [1]. There are two promising ways of such additive creation, namely, 1) use the various minerals (chiefly, having layered crystallographic structure) and their mixtures in dispersed state, and 2) use the powders of metals and non-metals oxides and salts obtained from mineral raw materials due to their specific treatment.

In the first case the improvement of the tribological characteristics, in particular, the coefficient of friction and wear-out decrease, is arisen from the ability of layered minerals to serve as boundary lubricants, specifically, to form so-called "slickensides" [2]. Such additives actually play the role of running-in coatings, which facilitate the processes of structural adaptation of metallic materials by formation of the surface structures that have boosted strength properties and hardness in comparison to the base metal.

In the second case, when the mixtures of salts and oxides of metals and nonmetals are used, the friction surface modification results from the formation of "servovite" (Latin: "servo" – conserve, vita – life, i.e., "life supporting") ceramic-metal films under the action of high temperatures and pressures in sites of friction parts contact.

The purpose of this study was to use both of the mechanisms at a time for improvement of tribological characteristics of friction pairs.

2. RESULTS

2.1 Additive composition and manufacturing process

The additives which action mechanism was investigated in this work were made by complicated manufacturing process.

The original composition of additive [3] includes the environmentally safe components each one playing the specific roles in realization of required qualities of the additive operation. The additive consists of a powder made by special processing of mineral natural raw materials having in their composition Aluminium, Silicon, Magnesium, etc., that capable to form ceramic-metal servovite films on the rubbing surfaces under the conditions taking place in friction zone. The additive composition also includes chlorides and silicates of Tin and Magnesium that additionally serve as a material for ceramic-metal film creation and carry out plating action, smoothing of working surfaces and protecting the juvenile surfaces of contacting parts.

The original multistage method of raw materials processing includes milling, annealing, mechanical activation, fine grinding and provides required properties of the additive at all stages of a friction process.

Investigated additive is the mixture of solid nano-particles of different types and compositions placed in viscous carrier (thickened mineral oil). Before introducing into friction zone, additive is admixed with lubricating oil (usually in concentration 1:1000).

2.2 Samples and test methods

To reveal the influence of additive on the coefficient of friction and wear we carried out the test using friction machines 2070 СМТ-1 and СМЦ-2. Our testing method was similar to ASTM G77, Ranking Resistance of Materials to Sliding Wear, Modified.

The tribological tests were carried out using the friction pair “cast iron (moving disc) - chrome (chromium-plated fixed disc or block)”. This friction pair was chosen for test due to its wide usage in the friction nods, particularly, in the cylinder-piston groups of modern internal combustion engines.

We used testing schemes showed in Fig.1.

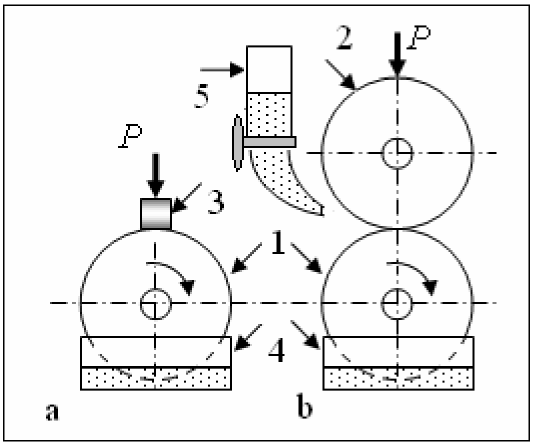

Figure 1. Test scheme: 1–moving disc, 2–fixed disc, 3–fixed block, 4, 5–containers for lubricating oil

Mobile specimens (discs) were made of the alloy grey cast iron castings. Microstructure was the pearlite with lamellar graphite and phosphide eutectic; hardness – HRB 100 - 105 (240 - 245 HB). To relieve stresses due to the mechanical processing the discs were tempered according to the following scheme: charging into a furnace at 300oC, heating at the rate 100o/hour to 600oC, soaking during 3 hours; cooling to 300oC at the rate 100o/hour, and further air cooling. This treatment regime is corresponded to the treatment regime for the cylinder sleeves of diesel locomotive engines.

Immobile sample (blocks or disks) were of two types – either the segments of piston rings (Fig.1, a) or cast iron discs (Fig.1, b).They were made of the high-strength inoculated magnesium cast iron with spheroidal graphite (hardness HB 105 – 108). Their working surfaces were covered by chromium of the thickness 200-220 µm by means of electrolytic technique. Microhardness of chromium coating was HV_5 790-850 (7-7.5 GPa), $H_{\mu\ 100}$880-1000.

The working surface of the cast iron discs in the initial state was of the 8th surface finishing class (the average height of the roughness R_y was ~0.6-0,8 µm).

Lubricating was made by two methods: either by oil drops from upper container (Fig.1, b) or by dipping of moving disc into container (4 in Fig. 1) with oil.

The speed of moving disc (Ø 50 mm) was 1.3 mps. Frictional sliding was 25%.

The testing procedures were following:

- for coefficient of friction measurements: 15 min of run-in at the load of 0.2 kN, then 4 steps of loading (the step was 0.2 kN up to the load of 1 kN; 2 min on each step), off-loading and 15 min at 0.2 kN, and recycling;
- for wear measurements: tests during 1, 5 or 10 hours at the permanent loading of 0.5 kN.

For the friction torque registration the inductive data unit of friction machine СМЦ-2 was used. The coefficient of friction f was calculated according to the formula:

$$f = 2M/(d \cdot P),$$

where M is the friction torque, d is the diameter of mobile specimen, P is the loading magnitude.

The beginning of fretting was determined as the fast growth of the torque magnitude and the appearance of the scores on the working surfaces. The errors in torque and coefficient of friction determination were from 9% at P = 0.2 kN to 2% at P = 1.0 kN.

The wear magnitude was found by weighting on high-accuracy weighing machine before and after the tests with the accuracy ± 0.1 mg.

The investigation of the working surfaces was carried out by means of binocular microscope

МБС-9 using the magnifications x8…50 and by means of scanning electron microscope (SEM) РЭММА 101-А in magnification range x30…1000.

Microhardness of the material was determined:

- on the friction surfaces in the zones with different failure level;

- on the surfaces situated far away from the friction zones (initial state).

Microhardness measurement was made by means ПМТ-3 device at the loading 50 g.

The surface topography analysis was performed on all tested specimens including the specimen not subjected to any friction, using TR200 profile recorder. The following measurements were taken: R_y – sum of the height of the highest peak and the depth of the biggest trench relating to the median in the base length limits; R_p – height of the highest peak relating to the median; R_m – depth of the deepest trench of the profile relating to the median.

2.3 Results of tribological tests

The typical dependences of coefficient of friction on the load during step loading for friction pair "cast iron – chrome" are shown in Figure. 2 and 3. Tests were carried out using mineral oil Shell Helix 15 W-40 (MO), synthetic oil Shell Helix Plus 5W-40 (SO) and these oils with additive in concentration (1000:1).

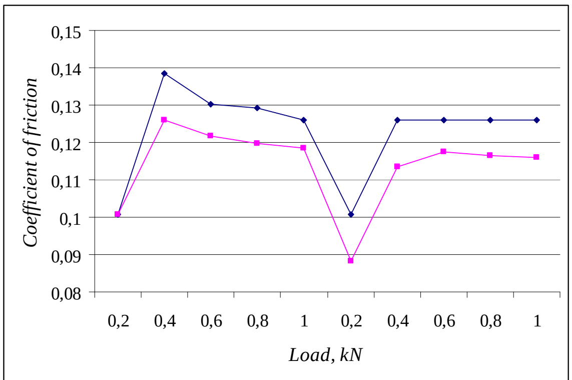

Figure 2. Coefficient of friction vs. load for step loading at friction in mineral oil with and without additive (lower and upper lines, respectively).

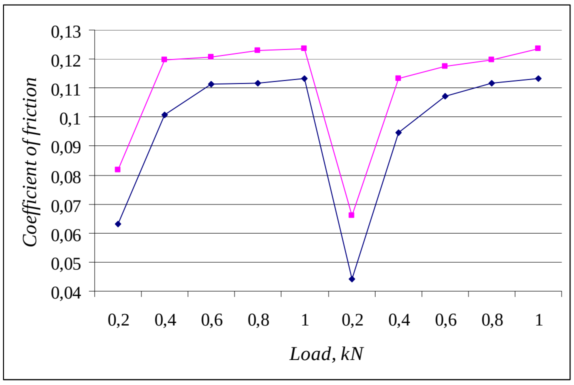

Figure 3. Coefficient of friction vs. load for step loading at friction in synthetic oil with and without additive (lower and upper lines, respectively)

The average improvement of coefficient of friction due to additive introduction was about 8-11% depending on load level and oil type.

The additive introduction into lubricating oil helps to reduce the weight wear both of the discs and blocks. The most clearly this effect was manifested at the analysis of total wear of friction pairs (Fig. 4), i.e. the sum of weight losses of disc and block.

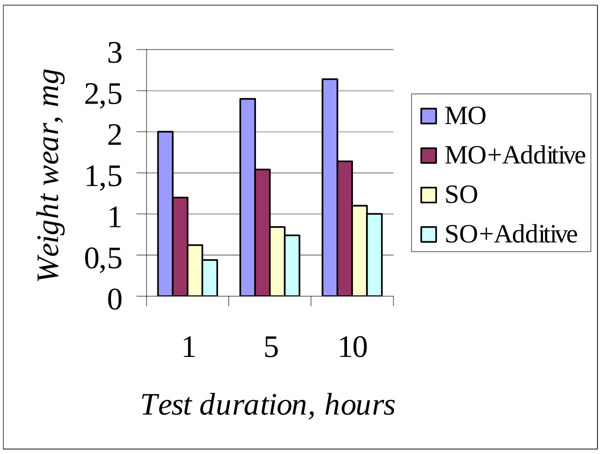

Figure 4. Total wear of friction pairs tested in mineral (MO) and synthetic (SO) oils with and without additive.

The obtained test results make the positive effect of additive introduction into lubricating oil obvious.

2.4 Changes of the surface structure and composition

To explain the reasons of friction characteristics improvement at additive introduction into lubricant the investigations of the friction surfaces and subsurface layers have been conducted. The carried out SEM investigations [4] showed that there are three types of surfaces: initial (untreated) surfaces and surfaces after friction in oil without and with additive (fig. 5). The surface of the initial untreated metal specimen is characterized by striation due to machining tool motion at machining work. There are two systems of striations: with small and big spacings (~300 and 5-20 μm, respectively). They can be seen on Fig. 5, a. Friction in oil (Fig. 5, b) shows the depletion of the surface topography, its smoothing out. However, the main features of relief formed by mechanical treatment, particularly, the systems of striations with different spacings are still present but they are less clearly defined. Interstriation spacings show significant dispersion.

Use of lubricating oil with additive brings on an intensive smoothening of the surface (Fig. 5, c). The relief of mechanical treatment can only be traced. Mainly the striations with large spacing are present. Large areas demonstrate the absence of contrast related to orientated ledges, and, what is more important, to trenches. The structure of these areas is similar to the surface structure of samples manufactured by powder metallurgy, i.e. by sintering of ultra-dispersive powders.

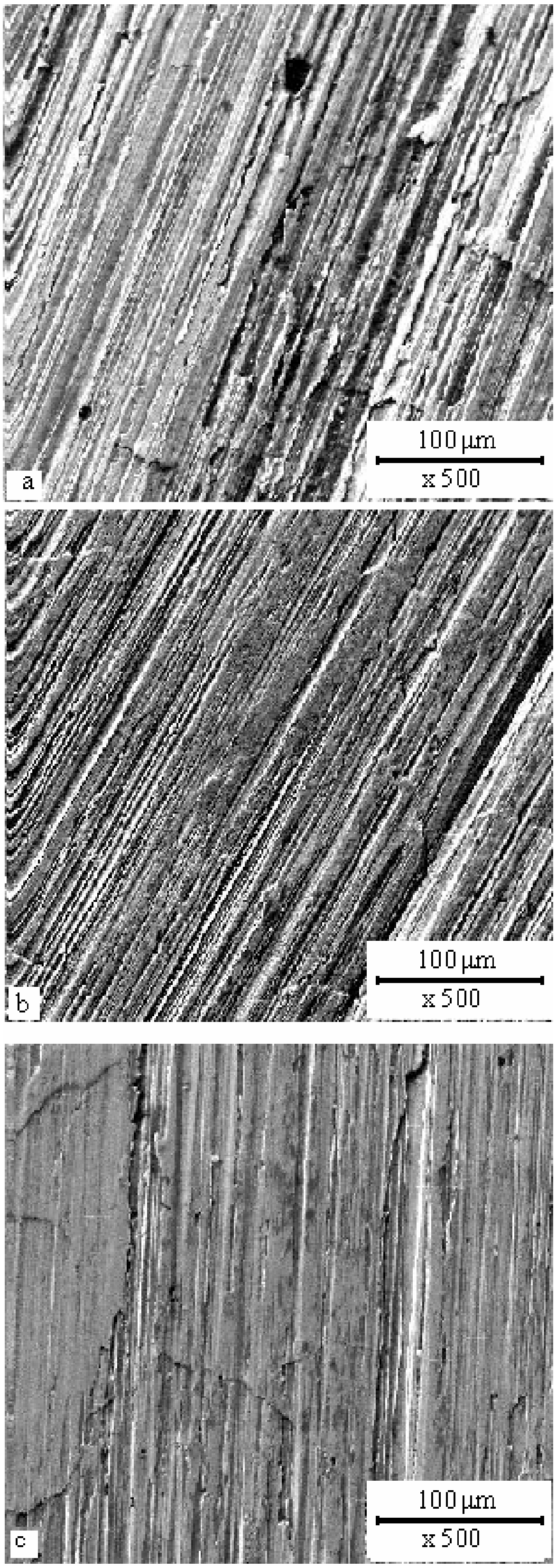

Figure 5. SEM images of initial surface (a) and surfaces after friction in oil (b) and in oil with additive (c)

We believe that this surface secondary structure was formed also by sintering of nano-particles of additive.

The results of profile recording are demonstrated by bar graph (Fig.6). It was observed that additive utilization helps to reduce the roughness of the surfaces. Smoothing of the surface at additive use is realized not only for the mechanical cutting of the surface peaks but due to the filling of cavities by additive ingredients.

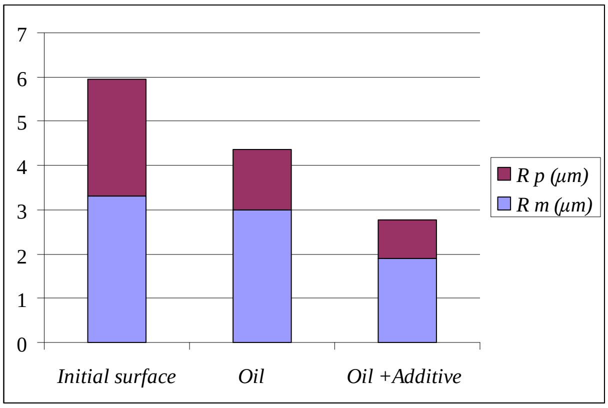

Figure 6. The relief measurements in tested specimens (blue – values for R_m, purple – values for R_p, bar height is the R_y value)

Measurements showed that microhardness of discs and blocks was increased after friction processes due to the mechanical hardening of rubbing surfaces (Table 1). The most significant increase of microhardness was revealed for tests in the lubricating oil with additive. We suppose that this fact reflects the contribution into the surface hardening process of the metal-ceramic film formed due to the additive action.

Table 1. Results of microhardness measurements

Lubricant	Microhardness, GPa			
	Disc		Block	
	before	after	before	after
MO	3.45	4.3	7.0	10.1
MO+Additive	3.50	6.8	7.2	15.2
SO	3.55	4.5	7.5	11.3
SO+Additive	3.4	7.1	7.3	16.8

2.5 Additive action mechanism

Conducted investigations found out that used additive consisted of at least two types of nano-particles: the particles of ingredient with the layered crystallographic structure and the particles of metals and non-metals salts and oxides. Each type of particles at getting into the friction zone plays the specific role. The particles with layered structure at the initial stages of rubbing act similar to classical layered modifiers of friction, for example, the graphite, facilitating the friction due to slickensides creation.

Another mechanism of additive action based on the process of surface modification. The dispersive particles of metals and non-metals oxides and salts together with the lubricating oil get into the friction zone. During the friction pair operation these particle presence leads to the course of the following processes:

- removal of adsorption and oxidation products from the friction surface;
- activation of the surface layers of the rubbing parts;
- mechanical activation of solid particles of additive;
- baking (sintering) of the additive particles under the action of the high temperatures and pressures in the friction zone and, as a result, the formation of the servovite ceramic- metal film.

The optimal complex of the secondary structure properties is stipulated by the composition and dispersity of additive particles. It is very important that the dosed introduction of Mg- and Sn-containing components provides the plastic properties of forming film. The presence of Cl-containing component provides the protective function of chloric films in the instants and in the sites of destruction of metal-ceramic film that prevents the contact of juvenile surfaces and development of dripping processes. Ultra-dispersive state of the additive ensures easy flowing of the sintering process when the particles of oxides are baking at the temperatures and pressures that are realized occasionally in the sites of rubbing surfaces contact. Thin servovite ceramic-metal film (thickness about 0,10…0,15 μm) is in a dynamic state, i.e., it is intermittently formed and destroyed on the rubbing surfaces.

3. CONCLUSION

The additive created and tested in this investigation manifests several mechanisms of its action in friction zone. Due to that the following results of additive effect were observed:

- modification of the topography of friction surface, decrease of the roughness and smoothing of its relief;
- increase of the microhardness of the friction surfaces;
- minimization of the damageability of friction surface due to ceramic-metal film formation in comparison to the properties of secondary structures forming during the operation in the oils without additive;
- minimization of the wear processes: the hydrogen wear minimization – due to the decrease of temperature in friction zone and, as the consequence, of the oil decomposition process; the corrosion wear minimization - due to avoiding of intense oxidation of the rubbing materials; the abrasive wear minimization – due to the cermet-metal film formation, etc.

Introduction of investigated additive into the lubricating oils influences positively on the following operational characteristics of friction nods: coefficient of friction and wear, fuel consumption, working temperature in friction zone, and intensity of lubricating oils decomposition.

REFERENCES

[1] Lubricant Additives: Chemistry and Applications, Editor Leslie R. Rudnick, 2nd edition, Chemical Industries/124, CRC Press, Taylor &Francis Croup, NY, 2009.

[2] В.Н.Кузьмин, Л.И.Погодаев: Смазочные материалы с добавками, Трение, износ, смазка, Т.11, №38, 2009.

[3] Tananko D., Lyubchenko E., Aksyonova S., etc. Nano-particle metal treatment composition for creating a ceramic-metal layer. US Patent 7,304,020, 2007.

[4] Любченко Е., Аксенова С.: Исследование морфологии поверхностей трения методом растровой электронной микроскопии, Тезисы докладов XXIII Российской конференции по электронной микроскопии, Черноголовка, ИПТМ РАН, 2010, с.113.

Serbian Tribology Society

SERBIATRIB '11

12th International Conference on Tribology

Faculty of Mechanical Engineering in Kragujevac

Kragujevac, Serbia, 11 – 13 May 2011

BEHAVIOR OF THE SINTERED CARBIDE PINS UNDER SIMULATED WORK CONDITIONS - EXPERIMENTAL STUDY

Adrian Neacsa[1], Doru Bogdan Stoica[1], Niculae Napoleon Antonescu[1]
[1]Petroleum-Gas University from Ploiesti, Romania
adnea@upg-ploiesti.ro; dstoica@upg-ploiesti.ro; nnantonescu@upg-ploiesti.ro

Abstract: *The pins are sub-assemblies of tree-cone drilling bits used to dislodge the rock. Pin head may have different shapes (chisel, hemisphere, etc.) according to the intended nature of the rock. The pin body has a cylindrical shape and serves to hold (embed) them into the body rolls. The pins are made by sintered carbide that combines the best contradictory properties such as hardness and toughness. Because the sintered metal carbides break after suffering a very small plastic strain, they are classified as brittle materials. In the following, the authors present results of studies conducted under conditions that partially reproduce the actual conditions (lack of drilling fluid however acute test conditions), on the cutting structures of the three-cone drill bits for making it clear that in these subsets, the tensions while working at the base of the drilling hole do not exceed the strength of materials that they are made of.*

Keywords: *three-cone drill bits, cutting structures (pins), strength, sintered carbide, simulated conditions*

1. INTRODUCTION

The latest types of three-cone drill bits used teeth (pins) shapes that are of upright design, made of sintered carbides, tougher and more resistant to wear buttons with elastomeric seals watertight, small tolerances and high resistance in conformity with requests, adding a robust package of protection jaw and cone bits, all that characteristics providing the equipment integrity both during drilling operations and rotary table at the bottom engine [1], [2].

The implementation of new types of drill bits have in advance a program of research and testing in order to examine the design and composition, cutting structures, in terms of increasing the reliability/durability of such complex machines.

The technological redesign of the three-cone drill bits, as a result of laboratory tests and production, has adopted five major changes:

- use of new types of sintered carbides denture;
- protection with pins made of the same types of carbide sintered cone surface, counter-cones and crown pins;
- new forms of teeth recovered from the cones;
- new design flexibility at the baseline of the crown;

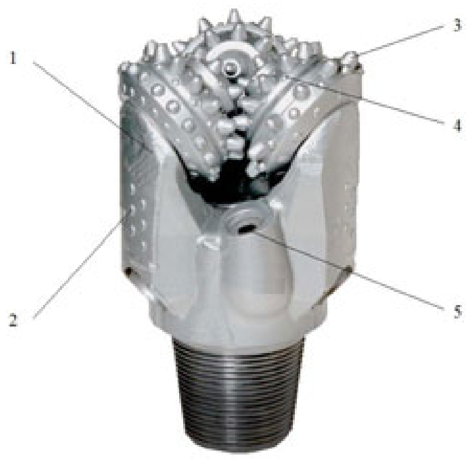

Figure 1. Three Cone Drill Bit
1. Loading jaws with sintered carbide for limiting the influence of wear while keeping integrity; 2. Jaw protecting with sintered carbide pins; 3. Change the shape of pins recovery; 4. Protective pins for cones surface and counter cones with crown pins protection; 5. New nozzles geometry for drilling fluid circulation.

- choosing a new geometry of positioning to the nozzles for drilling fluid circulation.

The studies have been performed on the cutting structures (pins), for roll 3, from a drilling bit type

SM - 8 3 / 8 KGJ, crowns II and III (Figure 2), C - 12 x 14 type (Figure 3).

The rolling pins are made from a mixture obtain by tungsten carbide powder and cobalt powder as a binder.

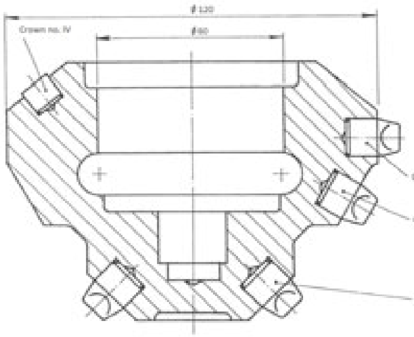

Figure 2. Role no. 3 from Three Cone Drill Bit

Given the multiplicity of tests performed on these cutting structures, from the sintered carbides types: K30-ISO; TIZIT WC-Co-TaC/87,75-12-0,25 type; TIZIT WC-Co-TaC/90,25-9,5-0,25 type; UGINE-CARBONE WC-TiC-Co/87,7-0,3-12, type the latest version of powder was chosen for this study because the subassemblies made by its sintering procedures, have the highest resistance to time requests.

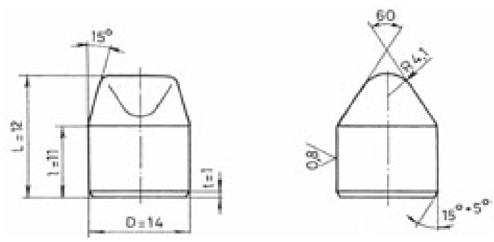

Figure 3. Pin type C - form and dimensions

The mixture of metal powders (UGINE-CARBONE type WC-TiC-Co/87,7-0,3-12 subtype) is ready for pressing and its technical characteristics are, as follows:

- Chemical composition:

- total carbon = 5,37 %;
- free carbon = 0,01 %;
- cobalt =11,40 %;
- titanium = 2 %;
- iron = 0,04 %;
- tungsten carbide = balance

- Physical-mechanical characteristics:

- powder will be ready for pressing granular grain size = 120 µm;
- the conventional of average Fisher size = 1,25µm;
- specific weight = 14,32 g/cm^3;
- Vickers hardness = 1050 HV;
- bend strength = 2250 N/mm^2;
- material strength = 2850 N/mm^2;
- paraffin content = 1,5%;
- pressing load = 115 N/mm^2;
- pre-sintering temperature = 900 ^{0}C;
- sintering temperature = 1410 ^{0}C;
- contraction = 23 %.

The manufactured pins, in full compliance with manufacturer specifications and parameters for the sequence of technological operations, were the study subject realized at the test stand conducted by the Petroleum-Gas University from Ploiesti.

It has also been observed the way of fits achieved between the pins that were tested and the clamping device testing stand (made from the same steel as the body screed – 17NiMo14-2 according to EN 10027-1:2006), thus simulating real restraint of body roll pin in the three-cone drill bits.

The stand construction, the testing methodology and the way of data acquisition is presented in the next chapter.

2. EXPERIMENTAL STUDY UNDER SIMULATED EXPLOITATION OF SINTERED CARBIDE PINS

The stand, shown in figure 4, can be used to study behaviour in simulated conditions similar to those while in operation, of the sintered carbide pins used at three-cone drill bits by using a system of reading and recording data, the request levels where those are subject to check .

The stand construction depends of the specific operation in the sintered pins drilling wells (figure 4.a), namely:

- the rotation motion is performed by the rock sample, the rotations number being checked with a tachometer (figures 4.b, 4.c) and fixed pin is mounted on a shaft (figure 4.i) performing with a hydraulic system (figure 4.g) for the advance and retreat movement that simulates its contact with the foot probe;
- variable speed range is being done by a lever system (figure 4.j) controlling the support of electric drive motor speed where the rock sample is fixed (and the rock is chosen properly to the type of drilling- low-medium hardness);
- the pin application on the workload is performed using a tensioning bolt axis (figure 4.e), while the force is applied towards the axial direction (given the remoteness and the proximity to the rock sample) using a hydraulic system acted by a solenoid (figure 4.d);
- the frequency of advance and retreat movements on the longitudinal direction is given by an adjustable signal generator connected to a 24 volt power source (figure 4.h), acting the solenoid (figure 4.d);
- the acquisition data for the controlled parameter values (pressure on the pin F ≅ 30000 N,

the action pressures for the cylinder that provides an reciprocating movement of the shaft where is fixed the pin and the axial tensions σ_x, σ_y, σ_z) is created using strain marks connected to a computer through two SPIDER 8 acquisition systems connected in series, and as interface uses the licensed software CATMAN 5.0. Those two products are genuine and were purchased from the German concern HBM®.

a.

b.

c.

d.

e.

f.

g.

h.

j.

k.

Figure 4. Testing Stand for Sintered Carbide Pins

Stand operation can be described briefly as:

➢ it is mounted on the bench with a driving steel shaft 17NiMo14-2 (Figure 5), by pressing pin carbide sintered to achieve full compliance with the conditions prescribed for fit (they were mounted in order to raise the minimum and maximum levels for more pins of the same type);

➢ hydraulic piston is actuated at the actuation pressure required (20 bar). The previous stroke is tensioned by a threaded rod to a force of about 30000 N, force which is usually recorded on pin in the process of drilling. The solenoid is actuated using a signal generator to simulate the rock numbers of contacts per time unit (contact frequency is 6 contacts/minute).

➢ the rotation motion whose speed is adjusted using a lever operated system, is performed using an electromotor and transmitted by a chain attached to the device where the rock sample is fixed. For the experiment we adopted the same rotational speed like in the real case, 50 rot/min.

Figure 5. Fixture of sintered carbide pins

➢ the only stand disadvantage is represented by the lack of drilling fluid as a coolant between the sintered carbide pin and the rock sample. For this reason, after about 30 minutes of operation, it no longer shows the fit tight, the main cause is the defects appearance (shock cracks in the pin fastening device). In future, we shall adapt a system of drilling fluid cooling circulation, with a precise role of cooling the pin.

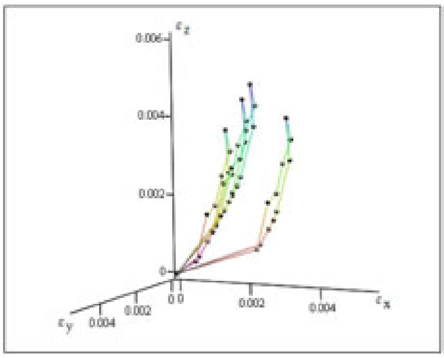

a.

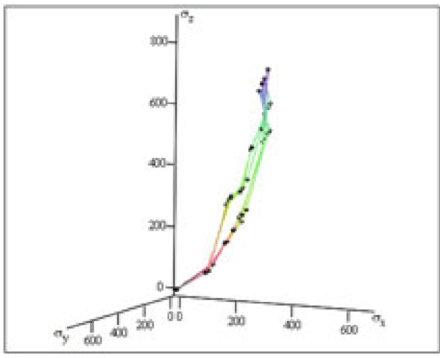

b.

Figure 6. Tri-axial displacements and strengths (absolute values)

a. Displacements [mm]; b. Strengths [N/mm^2].

In figures 6a, 6b it is presented in graphical form, the results and summary from the resulting files generated by CATMAN 5.0 for tests on the bench for a C 12 x 14 pin-type, chisel, manufactured of sintered carbide under normal operation conditions of the drill bits, described above. It should also be noted that, when presented results we used data from a sample of four consecutive rotations (of the approximately 6000 turns of the experiment), full-catcher (equivalent to four turns of the drill bits), corresponding to the highest values of stress and strain recorded [3], [4].

After carrying out tests on several cutting structures the conclusions presented below have been highlighted.

3. CONCLUSION

Using the stand presented before, which can be studied under simulated conditions of the similar behaviour to operation conditions (less presence of the drilling fluid) of the sintered carbide pins, equipping the three cones drill bits, we examined the level of stress undertaken. Also, using appropriate fixtures other parts made of sintered carbides can be studied, which are imposed by the construction and operation conditions of the stand.

The demands faced by the cones are variable, and the dynamic load varies in a short period of time, due to shock characteristics, which led to the conclusion that the same phenomenon is presented at all sintered carbides pins. It was developed the similar way of pin performance at the test stand as for those working during the real operating process.

During working experiments, under the similar drilling conditions, it was noticed that the wear teeth are working on the central shock and they are bending under the action of the body which teeth are forming by compressive stress and tensile. For this reason it has been shown that tooth are developing wear due to cyclic stresses to shock and abrasive wear.

As a result of the experiments it was also concluded the fact that tooth is developing wear due to the plastic deformation of the surface with detachment particles from the teeth surface, coming together with the sliding wear pins on the well foot.

The sintered pins in contact with the drill hole are not uniformly strained, the main cause being stresses combined with shocks.

When the pushing force is taken by a single sintered pin under intermittent contact with the foot probe, the resulted maximum effort value at which it is tested is about 1450 N/mm^2.

Studying the average values of the recorded efforts on the stand for sintered carbide pins, which are as follows:

- static test - 950 N/mm^2 and
- dynamic test - less than 900 N/mm^2,

it is observed that none of the values are exceeding the materials strength values that the two components of the fit are designed for.

REFERENCES

[1] A. Neacsa, D. B. Stoica: Aspects concerning the software applications in order to determine the technological systems reliability, OPROTEH 2007, The 13th International Conference of Fracture Mechanics, Bacau, pp. 155-158, ISSN 1224-7480, 2007;

[2] A. Neacsa: Study on Reliability of Three Cone Drilling Bits and Improvement Possibilities, PhD thesis, Mechanical and Electrical Engineering Faculty, Petroleum-Gas University from Ploiesti, Ploiesti, Romania, 2007;

[3] A. Neacsa, N.N. Antonescu, D. B. Stoica: Software Applications for Complex Technological Systems Reliability, Journal of the Balkan Tribological Association, Vol. 15, No. 1, pp. 45-51, 2009;

[4] F.C. Estes: Selecting the Proper Rotary Rock Bit, Journal of Petroleum Technologies, November, 1997.

Serbian Tribology Society

SERBIATRIB '11

12th International Conference on Tribology

Faculty of Mechanical Engineering in Kragujevac

Kragujevac, Serbia, 11 – 13 May 2011

RESEARCH REGARDING THE ANTICOROSIV PROTECTION OF ATMOSPHERIC AND VACUUM DISTILLATION UNIT THAT PROCESS CRUDE OIL

Marius Morosanu, Marius Gabriel Petrescu, Niculae Napoleon Antonescu
Petroleum-Gas University from Ploiesti, Romania,
marius.morosanu2003@gmail.com; pmarius@upg-ploiesti.ro; nnantonescu@upg-ploiesti.ro

Abstract: *Due to high boiling temperature, organic acids are present in the warmer areas of metal equipment from atmospheric and vacuum distillation units and determine, increased corrosion processes in furnace tubes, transfer lines, metal equipment within the distillation columns etc. In order to protect the corrosion of metal equipment from atmospheric and vacuum distillation units, against acids, de authors researched solution which integrates corrosion inhibitors and selecting materials for equipment construction. For this purpose, we tested the inhibitor PET 1441, which has dialchilfosfat in his composition and inhibitor based on phosphate ester . In this case, to the metal surface forms a complex phosphorous that form of high temperature and high fluid speed. In order to form the passive layer and to achieve a 90% protection, we initially insert a shock dose, and in order to ensure further protection there is used a dose of 20 ppm.The check of anticorrosion protection namely the inhibition efficiency is achieved by testing samples made from steel different.*

Keywords: *corrosion, atmospheric and vacuum distillation units, anticorrosive protection, distillation colum, corrosion inhibitor*

1. INTRODUCTION

In order to assure the anticorrosion protection of metal equipment from VAD installations, produced by various (organic) corrosive compounds or that from crude oil processing, a there was researched solution that integrates the use of corrosion inhibitors and selection of machinery construction materials. For this purpose, there was tested the, inhibitor that has in its composition phosphate ester. In this case, on the surface of the metal, it is formed a phosphor complex that can resist at high temperature and speed of the movement of technologic fluid.

In order to achieve a high anticorrosion protection by forming passivating layer, there is initially inserted, a shock dose, and for further insurance of the fim stability of is being used a dose of 20 ppm.

Checking the anticorrosion protection and the inhibition efficiency is achieved by testing samples of corrosion of authentic steel and martensitic steel-ferrite in corrosion-sensitive areas. Corrosion speeds measured on retractable and electro immune samples of authentic steel X6CrNiMoTi17-12-2 takes very small values. By applying an effective anti-corrosion treatment with corrosion inhibitors, the cladding material of martensitic - ferrites steel columns X6CrA113 is sufficiently resistant to corrosion.

2. AIMS AND BACKROUND

Crude oil which is processed in plants VAD has a corrosive action on the metallic equipment that comes into contact, because of the presence of corrosive agents in its composition, of compounds resulting the process and of some chemicals introduced to improve its quality.

In the refinery of our country crude oil is being processed, with high content of chlorine / organic acid content and low in sulfur compounds and crude oil imports, which has low chlorine content, but high in sulfur compounds.

If crude oil is processed in the mixture, the corrosion processes are more pronounced than if a single variety of crude oil processing. The choice of machinery building materials is made in consideration of these issues.

Due to high boiling temperature, naphthenic acids are present in the warmer areas of metal equipment from VAD pants and determine in furnace's tubes, transfer lines, metal equipment inside the distillation columns, etc.. increased corrosion processes.

In addition to the corrosive effect is noted erosion phenomena, which occurs in areas with high-speed of the fluid, in pipe elbows and heads, where fluid changes its direction.

Also, upper and lower organic acids act on metal surfaces where the temperature falls below the dew point temperature, forming aqueous acid (AD and VD tip columns, condensers, vessels, reflux, etc.)

VAD anticorrosive treatment facility is the introduction of corrosion inhibitors with neutralizing action in the top atmospheric distillation columns (C1), desgasolisaton(C2), stabilization (C3) and vacuum distillation (C5). Also Sulzer filling from columns C1 and C5 built from authenitic stainless steel X6CrNiMoTi 17-12-2 and X2CrNiMo 17-12-2 is protected by naphthenic corrosion inhibitors (Fig. 1 and 2)

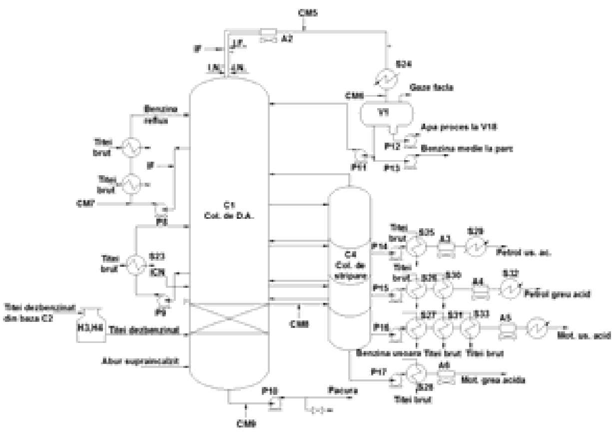

Figure 1 The technological scheme of the atmospheric distillation of crude oil plant

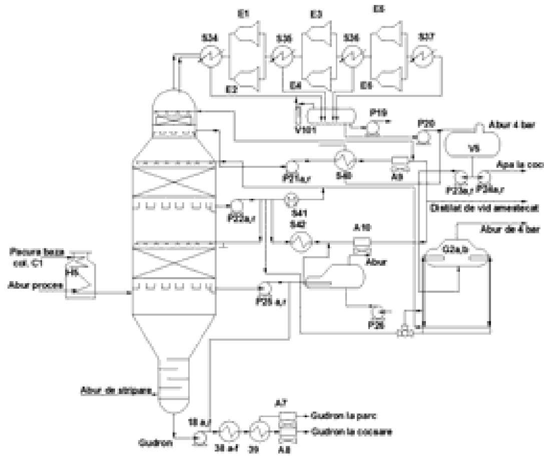

Figure 2 The principle technological scheme of of the installation of oil vacuum

In order to prevent and reduce the corrosion processes, there has been designed a monitoring program for VAD plant that processes crude oil with hing organic acidity. The program consist in the installation of samples in the plant, in ares likely to corrosion. Corrosion samples are mounted on retractable rods, wich can be extracted when needed or the momentary speed of corrosion is measured using portable devices (electroimmune). Their research leads to information on the types and intensity of corrosion.

3. EXPERIMENTAL

Experimental determinations of corrosion behavior of ferrous metalic materials, as a result of aggressive action of crude oil and distillate products from naphthenic crude oil were conducted in an industrial VAD plant. Specimens made of carbon steel S235JR (EN10027-2)- ferritic stainless martensitico steel X6CrAl13 (SR-2 EN10088-2: 1588) and austenitic stainless steels X6CrNiTi18-10, X6CrNiMoTi 17-12-2 and X2CrNiMo17-12-2 (SR EN10216 SR -2:2005) have the composition shown in Table 1.

For the experimental measurements there were used electrical resistances as samples and cylindrical retractable samples.

After preparation (machining followed by pickling and drying), the samples were tested under industrial conditions (immersion in the technological environment) and after original observations that were made on the condition of corrosion surfaces and quantitative determinations.

Table 1 Chemical composition of steels investigated

No	Steel mark	The concentration of elements, %								
		C	Mn	Si	Cr	Ni	Ti	Mo	P	S
1	S235jR	0,22	0,67	-	-	-	-	-	0,049	0,035
2	X6CrAl13	0,06	0,89	0,86	13,5	-	-	-	0,032	0,014
3	X6CrNiTi 18-10	0,07	1,18	0,85	18,5	11,2	0,40	-	0,035	0,015
4	X6CrNiMoTi17-12-2	0,06	1,85	0,78	18,3	12,4	0,42	2,5	0,031	0,013
5	X2CrNiMo 18-14-3	0,03	1,72	0,83	18,1	13,7	-	3,0	0,032	0,015

Retractable samples (Fig. 3) had Φ = 10 mm diameter and length of l = 25mm.

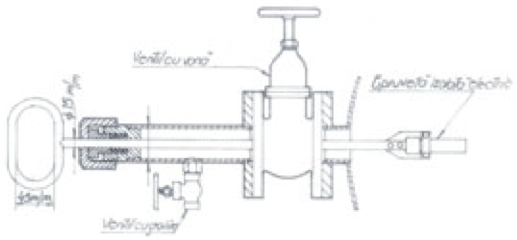

Figure 3. Device with retractable probe for corrosion measurement

The advantages presented by these samples consist in the determination of the corrosion rate at a given time, which can continue tracking the behavior of anticorrosion protection system applied.

The electrical resistance following exposure reduces its cross section and suitably modifying the electrical resistance, according to the relation:

$$R = \rho\ l/s \qquad (1)$$

When:
R – electrical resistance
ρ - specific resistivity of the metal Ω mm2 / m
l – the length of the probe, m
s - probe cross section, mm2

The resistance of the tested sample is compared with the resistance of the reference sample (uncorroded).

Resistances can be measured by Wheatstone method, and the obtained values are converted into units of penetration (mm / year) or gravimetric (g/m2h).

Wiring diagram of principle of the device for measuring rate corrosion by varying the electrical resistance is shown in Figure 4.

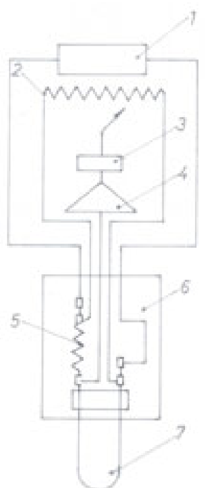

Figure 4 Wiring diagram of principle of the device for measuring the corrosion rate by determining the change in electrical resistance.

4. RESULTS AND DISCUSSION

For the protection against corrosion, inside the atmospheric distillation column C1 and vacuum distillation C5 naphthenic corrosion inhibitor is introduced through the reflux period, in column AD-C1, respectively over the three filling machines SU / ZC5, column C5, made by pump P9, shock dose of 1000 ppm for 4 hours. The result consists in forming on the metal surface of a phosphor complex that resists high temperatures and high speed of technologic fluid, insoluble in hydrocarbons.

For forming the passive layer and achieving the corrosion protection greater than 90% there is being initially inserted a shock inhibitor dose (Table 2).

Table 2. Inhibitor naphthenic shock doses

No	Column	Area of inhibitor introduction	Inhibitor dosage		
			Quantities, ppm	Time, hours	Frequency, No. dosage/ day
1	AD–C1	Sulzer pack	1000	6	1/30
2	VD-C5	Upper Sulzer pack - VDI	800	6	1/30
		Medium Sulzer pack - VDII	800	6	1/30
		Lower Sulzer pack - VDIII	1000	6	1/30

In order to ensure continuity and compactness of the passive layer there is inserted below a maintenance dose of 20 ppm inhibitor.

Also, in order to monitor the naphthenic corrosion protection and corrosion samples there were introduced in the form of Retractable electrical resistance (ER) to the column, stainless steel and carbon steel.

Corrosion specimens electrical resistance (ER) X6CrNiMoTi 17-12-2 austenitic stainless steel mounted in the heavy gas oil from crude oil atmospheric distillation column C1 had the corrosion rate of 0.0014 mm / year after 30 days / 720 hours of testing, of 0.0009 mm / year after 60 days /1440 hours (Table 3). Instead carbon steel corrosion rate S325JR is 9 times higher. 13% Cr Steel (X6CrAl13) is the corrosion rate of 0.0059 to 0.0080 mm / year.

Austenitic stainless steels and X2CrNiNb X6CrNiMoTi 17-12-2 17-12-2 packages are built from Sulzer packing vacuum distillation column C5 of fuel oil are stable working environment in the column, with corrosion rates in the range 0, 0003 to 0.0042 mm / year (Tables 4,5,6) in the presence of corrosion inhibitor naphthenic-based phosphate ester. ER transducers are highly efficient, giving momentary value of corrosion rate, so you can act immediately, as there is a disturbance in the plant.

Table 3 Speed corrosion of the samples monnted on heany diesel pipe Sulzer packing vaccum.

No.	Monitoring specimen	Steel mark	Type of test days / hours	The corrosion rate	
				Kg, g/ m^{2}h	P, mm /year
1	CM8	S235JR	30/720	0,0120	0,0130
			60/1440	0,0082	0,0091
2	CM8	X6CrAl13	30/720	0,0053	0,0059
			60/720	0,072	0,0080
3	CM8	X6CrNiMoTi 17-12-2	30/720	0,0013	0,0014
			60/1440	0,0008	0,0009

Table 4. The corrosion rate of specimens mounted vacuum distillate I (P114) from the upper output Sulzer packing.

No	Monitoring specimen	Steel mark	Type of test days / hours	The corrosion rate	
				Kg, g/ m^{2}h	P, mm/ an
1	CM13	X6CrNiMoTi 17-12-2	25/600	0,00027	0,0003
2	CM13	X6CrNiMoTi 17-12-2	29/696	0,00044	0,00049
3	CM13	X6CrNiMoTi 17-12-2	30/720	0,00045	0,0005
4	CM13	X6CrNiMoTi 17-12-2	35/840	0,00063	0,0007
5	CM13	X2CrNiMo 17-12-2	31/744	0,00081	0,0007
6	CM13	X2CrNiMo 17-12-2	32/768	0,00047	0,00052

Table 5. The corrosion rate of electrorezistive specimens mounted at the output of the I vacuum distillate output (P113) of the average Sulzer packing

No	Monitoring specimen	Steel mark	Type of test days / hours	The corrosion rate	
				Kg, g/ m^{2}h	P, mm/an
1	CM14	S235JR	27/648	0,421	0,468
2	CM14	S235JR	50/1200	0,831	0,923
3	CM14	X6CrNiMoTi 17-12-2	15/360	0,00081	0,0009
4	CM14	X2CrNiMo 17-12-2	29/696	0,0012	0,0013
5	CM14	X2CrNiMo 17-12-2	57/1368	0,0014	0,0016
6	CM14	X2CrNiMo 17-12-2	70/1680	0,0016	0,0018
7	CM14	X2CrNiMo 17-12-2	96/2304	0,0020	0,0022
8	CM14	X2CrNiMo 17-12-2	124/2976	0,0029	0,0032

Table 6. The corrosion rate of specimens mounted at the output of the vacuum out distillate III (P116) of the lower envelope stuffing Sulzer

No.	Monitoring specimen	Steel mark	Type of test days / hours	The corrosion rate	
				Kg, g/ m^{2}h	P, mm/an
1	CM15	S235JR	31/744	0,158	0,176
2	CM15	S235JR	32/768	0,166	0,185
3	CM15	S235JR	34/816	0,186	0,207
4	CM15	S235JR	35/840	0,177	0,197
5	CM15	S235JR	48/1152	0,178	0,198
6	CM15	S235JR	61/1464	0,162	0,180
7	CM15	X6CrNiMoTi 17-12-2	34/816	0,0028	0,0031
8	CM15	X2CrNiMo 17-12-2	42/1008	0,0038	0,0042

From the presented data it results that the austenitic steel, leaves well in technological environment of the vacuum distillation column C5, the corrosion rates having with very low values. The samples from the top of the column have lower corrosion rate than that in the column. S235JR carbon steel is not sufficiently protected by the inhibitor introduced, having high corrosion rates, which makes manufacturing packages filled neutralized Sulzer

5. CONCLUSION

The crude oil processed in the atmospheric distillation of crude oil fuel and vacuum (VAD) is aggressive action on the metal equipment by the presence of corrosive agents in the actual composition of the compounds resulting in processing of petroleum and chemicals introduced results to improve product quality

The paper deals with a combined method of corrosion inhibitors, corrosion protection and selection of materials for the construction of metallurgical equipment for processing crude oil with high content of naphthenic acids.

Corrosion protection monitoring program of the VAD plant that processes crude oil with high organic acid content is achieved through: a) analysis and high quality crude oil and aqueous condensate wave of reflux, b) installation of the corrosion samples in areas susceptible to corrosion; c) valves and pipe wall thickness measurement using ultrasound; d) penetrant nondestructive method e) determination of metals (Fe, Ni, V) of heavy crude oil, vacuum distillate I, II and III, f) inspection equipment during servicing.

Industrial tests were performed with samples and electroreizstente retractable corrosion of carbon steel and austenitic stainless steels.

For corrosion protection package filler made of steel Sulzer X6CrNiMoTi X2CrNiMo 17-12-2 and 17-12-2, within the atmospheric crude distillation column DA and DV vacuum distillation of fuel oil was used on a corrosion inhibitor ester on the metal surface a protective layer of phosphor.

The polarization curves of steel in condensate X6CrNiMoTi 17-12-2 at the top of by the atmospheric distillation column C1 there is found that the presence of 1% naphthenic acid corrosion is 0.004 mA/cm2 current and corrosion potential 120 mV, which correspondie to a corrosion rate of 0.0047 mm / year (figure 5).

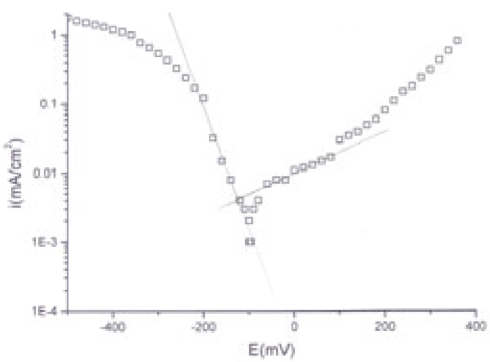

Figure 5 Polarization curves of steel in the austenitic X6CrNiMoTi 17-12-2 condensate from the top 1% DV column naphthenic acids.

At the addition of the naphthenic acids there is found that at a temperature of 250 C, there is caned the inhibition of corrosion processes by forming a protective film of iron naphthenate and corrosion inhibitor.

The condensate from the tip of the vacuum distillation column C5, an ionization occurs first and then distilling the metal protective film formation. The corrosion current is 0.00037 mA/cm^2,and the corrosion rate is of 0.0042 mm / year (Figure 6).

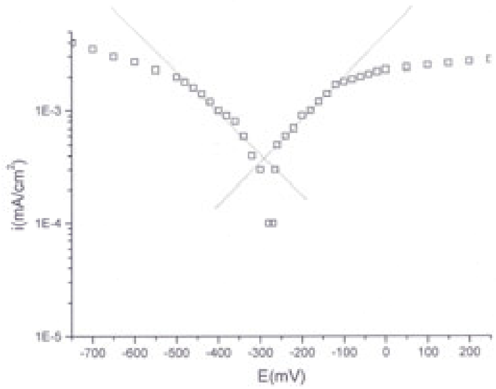

Figure 6 Polarization curves of austenitic steel X6CrNiMoTi 17-12-2 in condensation on top of the column with 1% DV naphthenic acids.

REFERANCES

[1] B. Hopkinson, L. Penueta, Stainless steels versus naphthenic acid corrosion in petroleum refining, Stainless steel world 99 conference, SSW99-005, p. 549-553;

[2] N. Petkova, M. Angelova, P. Petkov, Establishing the reason and type of the enhanced corrosion in the crude oil atmospheric distillation unit, Petroleum & coal 51(4), 2009, p.286-292;

[3] A. Groysman, N. Brodsky, J. Penner, A. Goldis, N. Savchenko, Corrosivness of Acidic Crude Oil and its Fractions, Materials Performance April 2005, NACE International, Vol.44, No.4, 2005 p.34-39;

[4] D. Ramojo , M. Ravicule, R. Benini, S. Marquez Damian, M. Storti, N. Nigro, Diagnose and prediction of erosion-corrosion damage in a pipeline transporting reduced crude oil from the heater to the vacuum distillation tower, Mecanica Computacional vol. XXVIII, Argentina 3-6 Noviembre 2009 p. 1621-1639;

[5] A. Groysman, N. Erdman, A studi of Cormsion of Mild steel in Mixtures of Petroleum Distillate and Electrolytes, Corrosion, vol 56, No 12, NACE International Corrosion Engineering Section, 2000, p.1266-1271

[6] N.N. Antonescu, M. Morosanu, M.G. Petrescu, O. Georgescu, Issues on corrosion equipment in installation by distribution DAV naphthenic acids from crude oil, EUROCORR 2010, the European Corrosion Congres, European federation of Corrosion 13-17 september 2010 Moscow, Rusia.

SERBIATRIB '11

Serbian Tribology Society

12th International Conference on Tribology

Faculty of Mechanical Engineering in Kragujevac

Kragujevac, Serbia, 11 – 13 May 2011

APPLICATION OF MOBILE DEVICE FOR OIL ANALYSIS

Petar Todorović[1], Ivan Mačužić[1], Aleksandar Brković[2], Branislav Jeremić[1]
[1]Faculty of Mechanical Engineering in Kragujevac, S. Janjić 6, 34000 Kragujevac, Serbia, petar@kg.ac.rs
[2]Tetra Pak Production d.o.o, Obilazni put bb, 32300 Gornji Milanovac

Abstract: *For years, the implementation of the oil analysis was limited to a specialized laboratories, but the emergence of proactive maintenance concept, cause intensive development of devices and sensors that strive in direction of miniaturization, automation, performance enhancement and creation of multi-functional diagnostic systems. Proactive maintenance strategy involves continuous monitoring and control of the basic failure causes, among which oil contamination stands out as the most common, serious and generally widely accepted cause of failures in the industry. In this paper is shown part of measurement results obtained with mobile device for oil analysis, which allows us to determine the concentration of wear particles and water in oil. All measurements are done on pin on plate reciprocating tribometer. There are shown results for 4 characteristic working regimes.*

Keywords: *Oil contamination, oil analysis, wear particle, water in oil, reciprocating tribometer*

1. INTRODUCTION

For a number of years oil analysis was widely accepted as one of the standard methods for the condition monitoring of technical systems, primary focused on determining the optimal replacement point for lubricants and oils [1]. As almost changeless factor, there was accepted that oil analysis is mainly laboratory based activity, owing to the complexity of the equipment and expertise of staff that carried out the analysis and interpret test results. Practical experiences in our country shows that this classic concept of oil analysis in industry, based on the use of specialized laboratory services, had a relatively limited use, usually only for special and highly responsible systems, and it failed to become viable as a widely accepted practice [2].

The appearance of proactive maintenance concept caused significant changes in the way that maintenance experts treat oil analysis. Proactive maintenance is focused on identification of failure root causes instead on early signs and symptoms of failures, like predictive maintenance. Although the number of potential failure root causes is large, it is shown that only 10% of all root causes is responsible for over the 90% of failures [3]. With clear identification of failure root causes it is possible to eliminate or minimize the causes that lead to a failure. The result is extended service life of technical systems and significant reduction in maintenance costs. In that sense, any activity aimed on determining the failure root cause is considered as a proactive.

There are a very few mechanical systems that do not require any lubrication. A large number of surveys and studies conducted in laboratory or in industrial surrounding have a unique conclusion, that the degradation of contact surfaces will cause a failure of technical systems in more than 70% of cases [2]. These results are a cause of complete redefinition of the oil analysis position in modern industrial practice. It got one of the central places within the concept of proactive maintenance strategy. Oil analysis has became one of the key tools in monitoring of occurrence, intensity and development of tribological processes within complex technical systems, as well as for diagnosis and monitoring of various forms of oil and lubricant contamination in industry.

Global industry development in last decade is characterized by initiating various projects and programs focused at defining, achieving and maintaining the low levels of industrial oil and lubricant contamination. The results are greater savings, achieved by reducing downtime, extending component and system life and significantly reduced oil consumption [4-7,10]. This period is characterized by intensive development of devices and sensors that strive in the direction of miniaturization, automation, performance enhancement and creation of multifunctional diagnostic systems. It should also be noted that the main manufacturers of instruments and equipment have a leading position not only in practical, but also in the theoretical and scientific work. They have strong research teams that constantly move the limits and make improvements and enhancements. The fact that the basic standards and regulations in this area are changed very frequently present sufficient evidence on the dynamics of changes and the existence of a space for further research and development.

2. OIL CONTAMINATION

The term contamination in hydraulic systems includes all the processes that lead to temporary or permanent changes of exploitation characteristics of hydraulic oil, in terms of changes in its physical and chemical properties, structural and functional degradation. Any unwanted and harmful element (in solid, liquid or gaseous state) located in the hydraulic oil has negative consequences for the system and its called contaminant [11]. Oil spreads contamination particles to all components in hydraulic systems and, depending on the severity level, inevitably causes minor or major damages and functional disorders in the entire hydraulic system.

Main contaminants of hydraulic systems are:

- mechanical particles,
- water and
- products of chemical reactions and fluid degradation.

Among these basic contaminants there is a strong cause - effect connection. For example, increasing of the water content in the working fluid directly affects the dynamics and intensity of chemical processes, where the solid particles in a fluid behave as catalysts. On the other hand, water in hydraulic system causes the development of corrosion process, which results in the creation of mechanical particles. Water also affects the reduction of oil viscosity and leads to intensive wear processes. Mechanical particles and water are external contaminants that are entered into the system from the environment. Products of chemical reactions are generated within the system itself. Presence of these contaminants in hydraulic oil leads to degradation of its basic characteristics, which also results in increasing the intensity of wear process and secondary contaminants origination.

This paper describes development and application of a mobile device for oil analysis which allows us to monitor two of three main contaminants in hydraulic system, namely: mechanical particles and water.

3. MOBILE DEVICE FOR OIL ANALYSIS

The basic idea for development of a mobile device (Figure 1) for on-line and in-line analysis of industrial oils contamination is essentially based on the use of currently available sensing elements to determine the concentration of solid particles and water in oil, as the most important diagnostic parameters. Mobile device for oil analysis (MDOA) contain two sensors:

- Automatic Particle Counter (APC), with laser diode as light source (light blockage type of APC) which perform quantification and measure concentration of solid particles in oil giving result according to ISO 4406 standard cleanness codes for 4, 6, 14 μm and additionally for 21 μm, with resolution of 0.1 ISO code. Result could also be presented in form of cumulative number of particles for each size range.
- Capacitance sensor for water in oil monitoring which measure water content relative to the saturation concentration. Its output is a_w parameter (water activity, ie. water in oil saturation level) as measure of saturation level in the range of 0 to 100%. (0% absence of water, 100% fluid is fully saturated with water).

Complete controlling of MDOA is done using a miniature touch panel PC with Windows CE operating system. Detailed description of MDOA is given in [7,10].

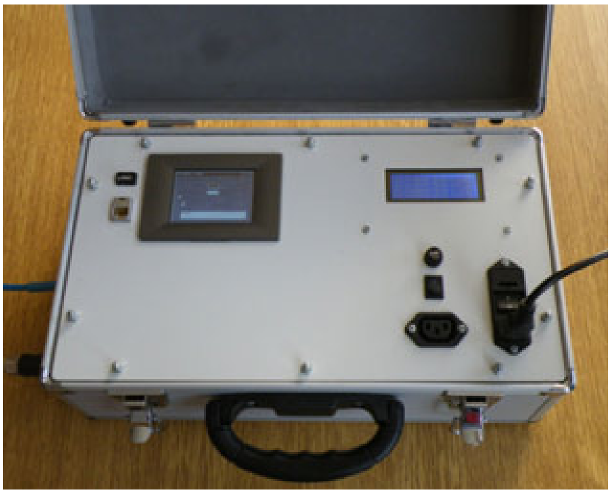

Figure 1. Mobile device for oil-analysis

```
% Comment
%
% Time[s]  Ch1iso  Ch2iso  Ch3iso  Ch4iso  Cumul1  Cumul2  Cumul3  Cumul4  Temp1[C]  Temp[C]  aw[%]
-----------------------------------------------------------------------------------------------------
     0.00   22.70   20.00   18.00   16.50   34000    5150    1317     494        30    24.53  39.91
    10.00   22.70   20.00   18.00   16.40   34000    5100    1286     465        30    24.69  40.04
    20.00   22.70   20.00   18.00   16.30   35000    5036    1298     436        30    24.69  40.17
    30.00   22.70   20.00   17.90   16.30   34000    5025    1254     436        30    24.69  40.17
    40.00   22.70   19.90   17.80   16.20   34000    4847    1175     408        30    24.69  40.17
    50.00   22.60   19.90   17.70   16.20   32000    4762    1143     389        30    24.69  40.17
    60.00   22.70   20.00   17.90   16.40   34000    5068    1271     461        30    24.69  40.29
    70.00   22.60   19.90   17.90   16.30   33000    4879    1241     444        30    24.69  40.29
```

Figure 2. Form of the output text file with measurement results

The measurements results are saved as a text file (Figure 3) which is adopted to the format that can be further processed in appropriate software for advanced data analysis (Excel, Matlab...). Columns in the file contains data about measurement time, ISO 4406 codes and corresponding cumulative numbers of particles, oil temperature value and saturation parameter of oil with water.

4. MEASUREMENT RESULTS

Results of oil contamination measurements using MDOA will be shown through laboratory test examples on tribometer with reciprocating motion, type pin-on-plate (Figure 3) [7].

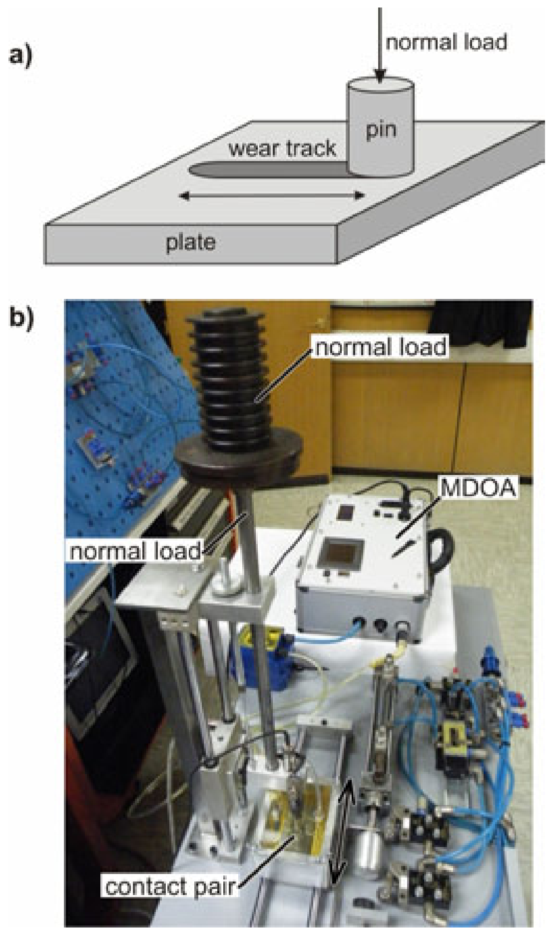

Figure 3. a) Contact type pin-on plate, b) used reciprocating tribometer

Normal load in the vertical direction was 20 N. The lever which was used to transfer the normal load to the pin on the plate is constructed in that way that also represents the dynamometer to measure the force of friction in the contact zone. Reciprocating motion is provided by a pneumatic cylinder and accompanying pneumatic installation. The tribometer is complete with a pneumatic cycle counter.

Contact pair is in the aluminium container with volume of 500 ml, which is filled with oil to 1/3 of its height. In the transparent cover are mounted suction and discharge pipes which allow oil circulation in the container. Suction line takes oil from the bottom of the container, while the returning line back oil to the surface, providing a mix of oil during the experiment. Peristaltic pump generates circulation of oil through the system (contact pair – container – MDOA). The pump is constructed in the way that its functioning does not introduce additional contamination of the tested oils.

Material of the pin and plate is 1.0501 according to standard EN 10027. Pin is circular in cross section area, P=160 mm^2. The material is not heat-treated and has a hardness of 25-30 HRC. Contact surfaces are grinded (Ra = 0.4μm).

This experiment shows results of oil contamination parameter measurements in next characteristic working regimes:

- running-in regime,
- regime of increased contamination by solid particles,
- regime of decreased contamination by solid particles and
- regime of increased contamination by water

4.1 Running-in regime

Work in the running-in regime is characterized by intensive tribological processes and higher internal generation of contamination. Experiment is held for 20,000 cycles. Figure 4 shows the diagram of friction coefficient and the curve that shows the change of oil contamination by solid particles.

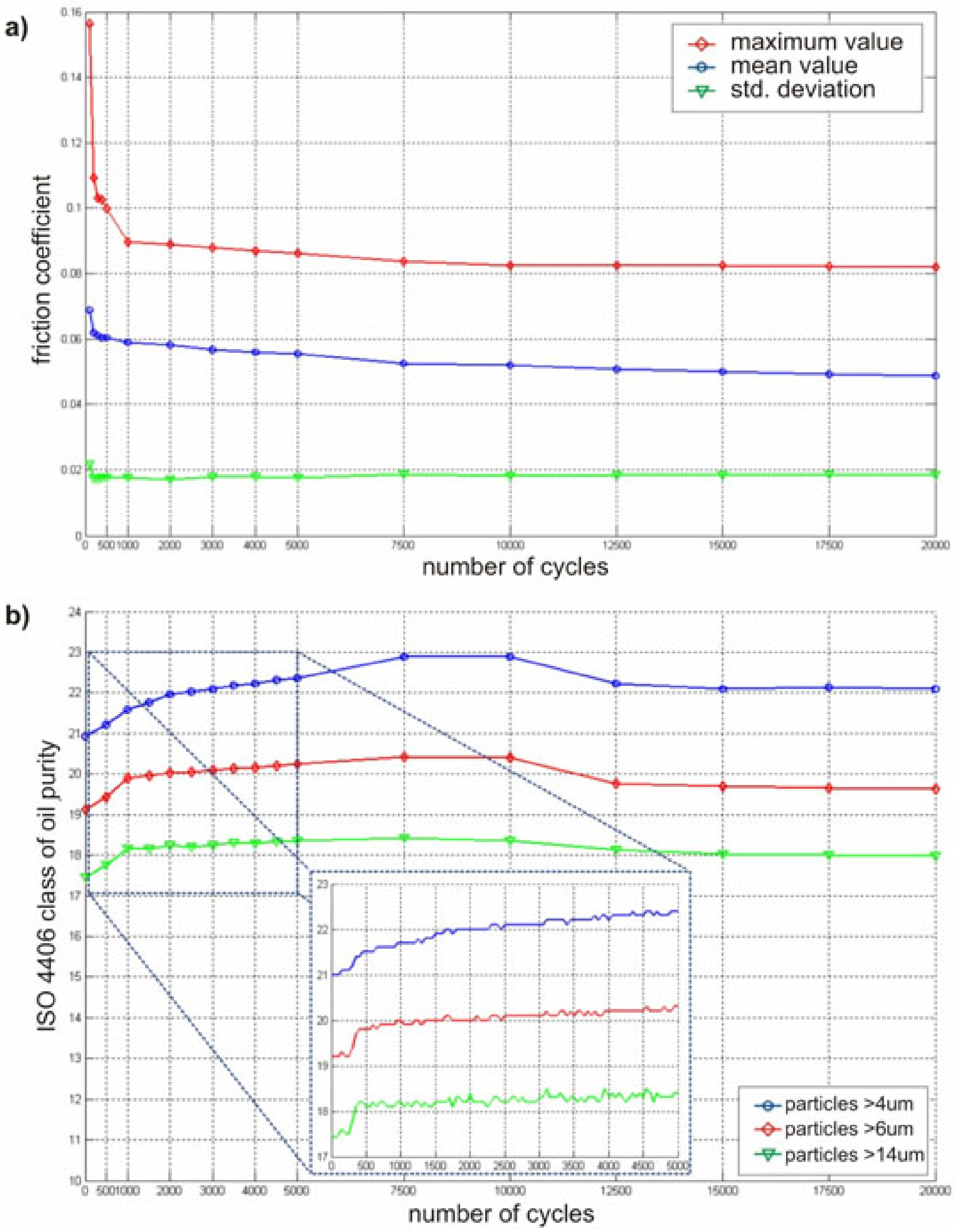

Figure 4. Running-in regime, a) friction coefficient, b) diagram of oil contamination by solid particles

Start of the testing and contact of new tribological pair is characterized by higher values of friction coefficient. Trend parameters of the friction coefficient change, exponentially decrease until the middle test period, after which they keep almost constant value.

As was expected, oil contamination by solid particles has trend of rapid increment at the start of the experiment, as a result of intensive wear during running-in process of tribological pair. After reaching the maximum value of contamination (between 7,500 and 10,000 cycles), there can be noticed a trend of slight decrease in the level of contamination, until it achieve a stable value at the end of the test. This leads to deposition of particles generated during the experiment.

4.2 Regime of increased contamination by solid particles

Contamination of the system by solid particles was performed by direct addition of abrasives in the contact zone of tribological pair. As a source of contamination, an industrial abrasive with declared grit size of 5 μm was used.

Contaminated oil prepared in this was gradually added to the oil in the system and followed by constant monitoring of contamination increase. Figure 5 shows an example of the contamination increment process in the system by the addition of contaminated oil (Added 3 times).

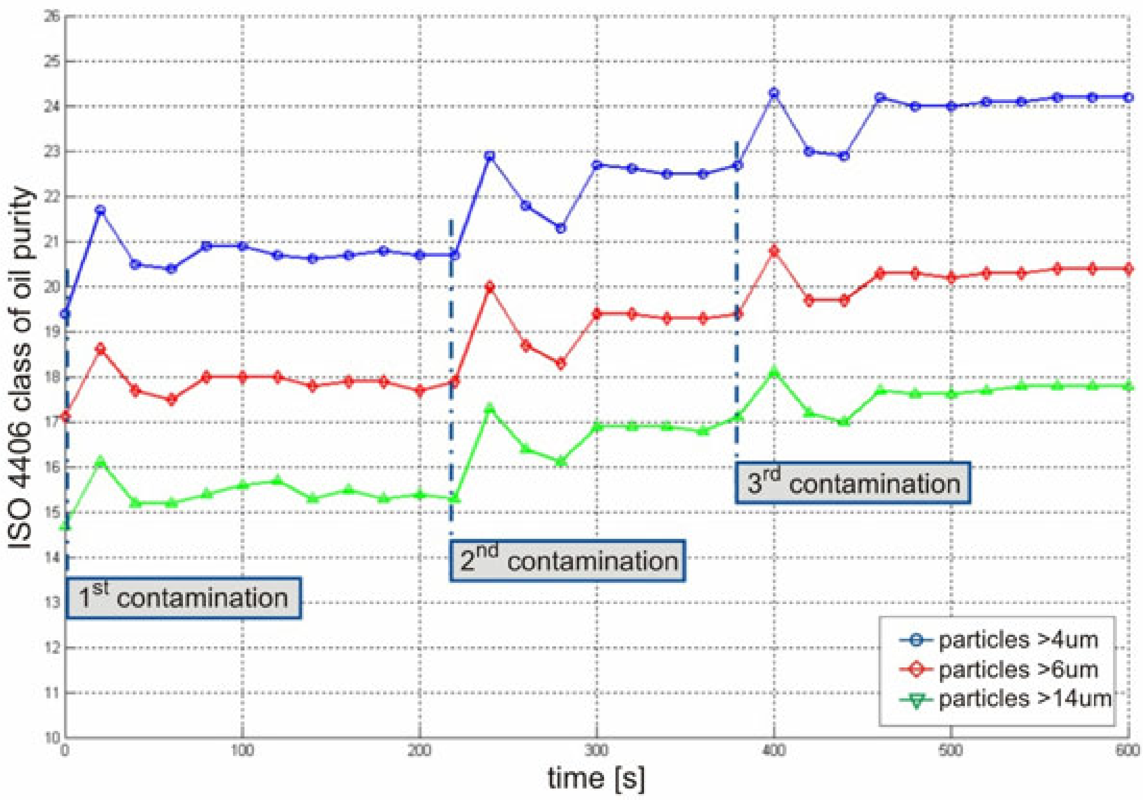

Figure 5. Process of increased oil contamination in the system

4.3 Regime of decreased contamination by solid particles

Reduction of the level of oil contamination by solid particles is done by placing oil filters in the system. Measurement of oil contamination during this regime is shown in Figure 6 and the results show that filtering decreases contamination from level 29.0/23.1/21.2 down to level 19.0/14.4/13.2 during the 4000 cycles.

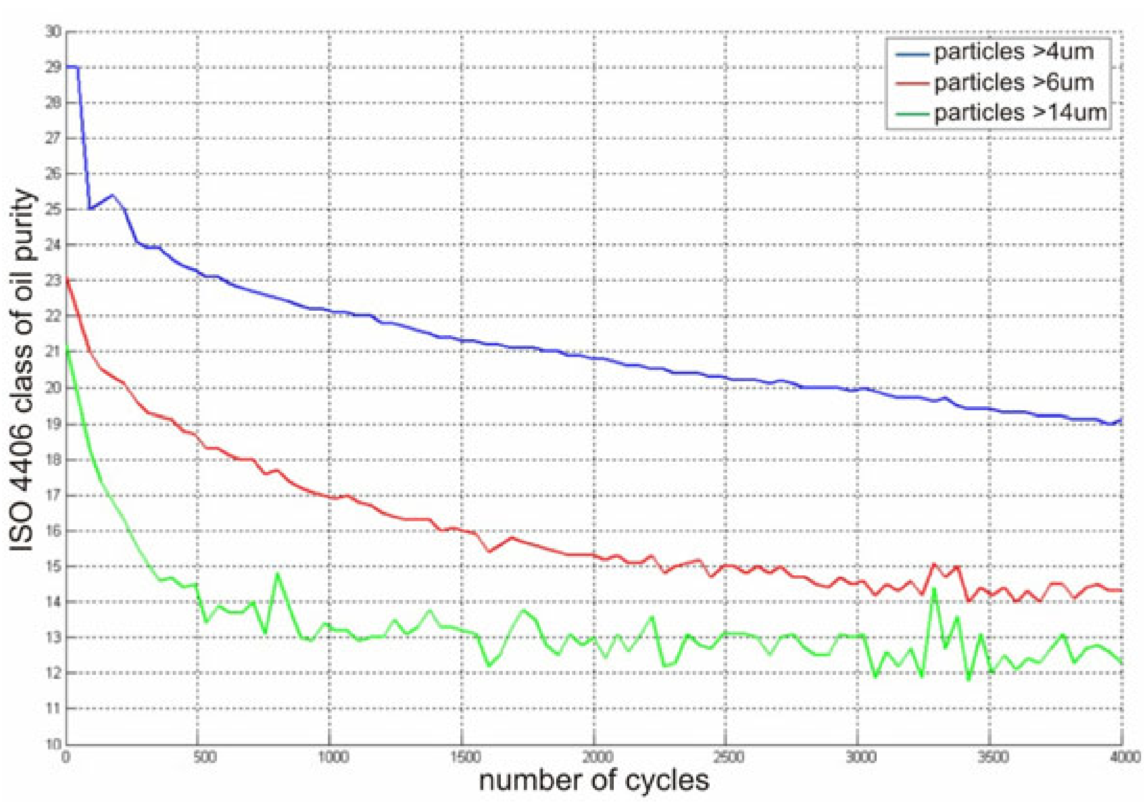

Figure 6. Diagram of changes in oil contamination by solid particles in the filtration regime

4.4 Regime of increased contamination by water

This testing considered intensive increment of system contamination by water with response monitoring of measured parameters. Previously prepared 50 ml of 10% mixture of pure oil and regular water (45 ml oil and 5 ml of water) which was then slowly added to the system. Total entry into the system was 40 ml of this suspension, accordingly 4 ml of water. In this way, by the end of the test, total concentration of water in oil was raised to about 2%, which is 10 times of the recommended maximum allowable value.

Raising level of oil contamination with water was followed with parameter a_w, which is called water in oil saturation level. Changes in diagram of this parameter during testing are shown in Figure 7.

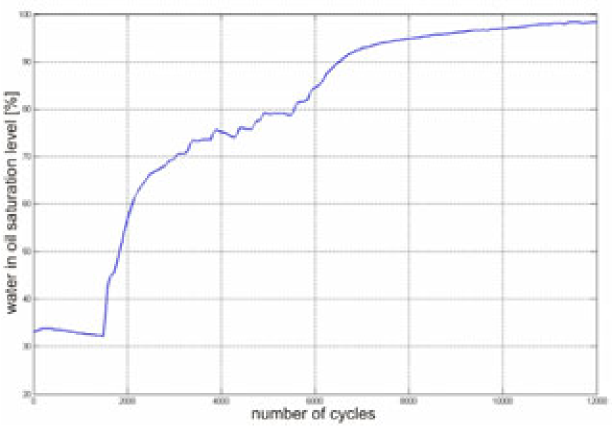

Figure 7. Diagram of changes of water in oil saturation level - a_w

5. CONCLUSION

Presented results of experimental studies show that the level of oil contamination by solid particles and water in oil saturation level are the parameters that have adequate and timely response to the occurrence of any change in the system. Considering the nature of these parameters and their sensitivity to any changes, proactive maintenance strategy can be achieved by following of their changes.

In addition, mobile device for oil analysis has enabled the measurement of selected parameters with high precision, repeatability and high response speed, so that all phenomena and processes are clearly and unambiguously identified.

Acknowledgment

The results of this paper are realized through the National Project TR 35021 financially supported by the Ministry of Science of the Republic of Serbia (coordinator of Project Prof. Dr. Miroslav Babić).

REFERENCES

[1] P. Girdhar, C. Scheffer, Oil and particle analysis, Practical Machinery Vibration Analysis and Predictive Maintenance, Newnes, Oxford, 2004, Pages 168-220

[2] I. Mačužić, B. Jeremić: Proactive Approach to Oil Maintenance Strategy, Tribology in Industry, Volume 26, No. 1&2, 2004

[3] J. C. Fitch, Proactive Maintenance Can Yield More Than a Ten-Fold Savings Over Conventional Predictive/Preventive Maintenance Programs, in: 1992 Predictive Maintenance Indaba Proceedings, South Africa, September, 1992.

[4] J. C. Fitch, What Particles Mean and Why They Need To Be Monitored and Controlled, in: Reliability Week Conference Proceedings, September, 1998.

[5] I. Mačužić, B. Jeremić: Modern Approach to Problems of Transformer Oil Purification, Tribology in Industry, Volume 24, No. 3&4, 2002

[6] I. Mačužić, B. Jeremić, P. Todorović: On-site oil analysis and purification in proactive maintenance strategy, in: Proceedings of the 2nd International Conference on Manufacturing Engineering (ICMEN), 5-7 October 2005, Kallithea - Chalkidiki, Greece, pp. 623-629

[7] I. Mačužić: Proactive approach in hydraulic systems maintenance strategy, PhD Thesis (in Serbian), 2011.

[8] Y.-C. Chiou, R.-T. Lee, C.-Y. Tsai, An on-line Hall-effect device for monitoring wear particle in oils, Wear, Volume 223, Issues 1-2, December 1998, Pages 44-49

[9] M. K. Williamson, A Low Cost On-Site Oil Analysis Strategy, Entek IRD International.

[10] I. Macuzic, B. Jeremic, P. Todorovic, M. Djapan, U. Proso, A. Brkovic: Mobile device for on-line oil analysis, Technical Solution, Faculty of Mechanical Engineering, University in Kragujevac, 2010

[11] Totten G.E., Handbook of Lubrication and Tribology, Volume I: Application and Maintenance, Taylor & Francis, 2006.

Serbian Tribology Society

SERBIATRIB '11

12th International Conference on Tribology

Faculty of Mechanical Engineering in Kragujevac

Kragujevac, Serbia, 11 – 13 May 2011

LINEAR RECIPROCATING TRIBOMETER – EXAMPLES OF AN OBTAINED INVESTIGATION RESULTS

Ivan Macuzic[1], Uros Proso[1] Branislav Jeremic[1], Petar Todorovic[1], Marko Đapan[1],
[1]Faculty of Mechanical Engineering in Kragujevac, S. Janjić 6, 34000 Kragujevac, Serbia
ivanm@kg.ac.rs; urosproso@kg.ac.rs; bane@kg.ac.rs; petar@kg.ac.rs; djapan@kg.ac.rs

Abstract: In present stage of development, hydraulic systems are often used solution in power transmission production and control processes. In order to carry out laboratory investigations of phenomena which characterize the processes of contamination in hydraulic systems, special form of tribometer is developed, which allows simulation of different real conditions in hydraulic and other similar systems that use lubrication oils, as well as monitoring of a defined group of diagnostic parameters. Some examples of an obtained investigation results are also presented in this paper.

Keywords: *Linear reciprocating tribometer, oil contamination, friction coefficient*

1. INTRODUCTION

Hydraulic power systems today are standard and often used solution in power transmission, production and control processes. Continuous improvement of performance of these systems is carried out primarily in order to increase the accuracy and reliability, improve efficiency coefficients, increase degree of performance control, increase strength, speed, pressure, flow, to expand area of use and enable longer life cycle. All this is followed by application of new materials and new methods of construction, reducing the dimensions of hydraulic components, increased production precision, introduction of electric and electronic components and its integration with hydraulics [1].

Conditions of tribological processes in real hydraulic systems are very complex and their full simulation in laboratory conditions could be a very complicated technical problem. Some conditions, such as, for example, pressure in the system (a few tenth to several hundred bars) are practically unattainable when using standard models and types of tribometers. Also, the different hydraulic components have considerable variation regarding the types and characteristics of wear contacts and their basic parameters. In literature can be find information on a number of specific laboratory tests conducted related to modelling of tribological contacts and specific conditions in hydraulic components [3], [4].

2. EXPERIMENTAL EQUIPMENT

The starting point for defining the type and concept of tribometer was an analysis of typical tribological pairs of hydraulic components (pumps, motors, cylinders and valves) and characteristics of wear processes that occur in them.

Coming from the fact that linear, alternately sliding movement, in condition of presence of oil, is dominant form of movement in hydraulic components and that abrasive wear mechanism is the most important one, tribometer type pin-on-plate (pin on the board) was selected where the pin slides on the board (cyclic and straight line) in oil's environment (Figure 1) [2], [5].

In addition, this tribometer should enable definition and control of basic parameters of tribology investigation. In this case those are: load in tribological contact, sliding speed, slide length or pin step in one cycle and the number of cycles.

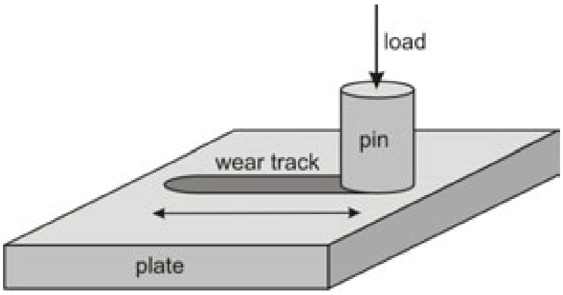

Figure 1. Basic principle of *pin-on-plate* tribometer

Special attention is devoted to the integration of measuring equipment and systems that allow continuous and simultaneous measurement of multiple parameters which characterize the dynamics and phenomena of tribological processes in the contact pair and which could be used as diagnostic parameters.

Result of laboratory prototype of pin-on-plate tribometer with a linear reciprocating motion development is shown in Figure 2.

Constructive solution is based on container with a plate and oil (1), placed on a horizontal linear guides (2), moving alternately, while pin is stationary. Pin bracket (3) is set to vertical linear guides (4) and given loads on the pin passed through the bar, which is also a dynamometer for measuring of friction force. Drive system for reciprocation motion is pneumatic (5) with pneumatic cycle counter (6).

On container with a plate (1) displacement transducer is fixed (7), with function to measure, in real time, container position and thus enable the accurate determination of velocity and moments when container change movement direction. On a tribometer base plate surface there is a connection panel for this transducer (8).

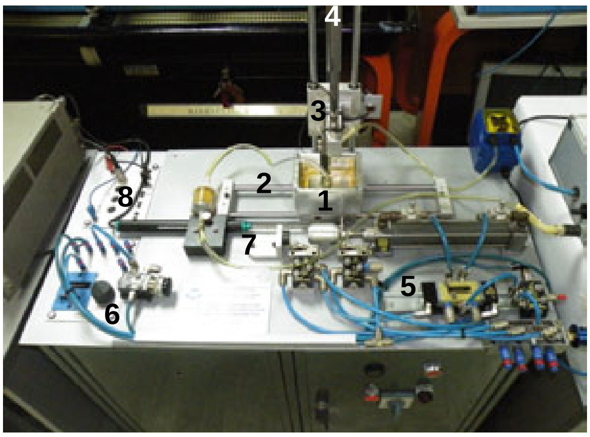

Figure 2. Tribometer *pin-on-plate* with linear reciprocating motion

Pneumatic system for tribometer (Figure 3 a)) consists of pneumatic cylinder (1), air-operated distribution valve 5/2 (2), two pneumatic limit switches (3), pneumatic logic valve 3/2 (4), pneumatic cycle counter and the reset button (6) (Figure 2). Limit switches limit stroke of cylinder piston which is fixed to container. Switches are fixed and the stroke length is determined by varying the length of a cylindrical end part of cylinder (7) which activated limit switches. At both command lines, which bring compressed air to the cylinder, set of throttle valves that regulate the speed of the cylinder (and consequently the bowl with the board) in both directions.

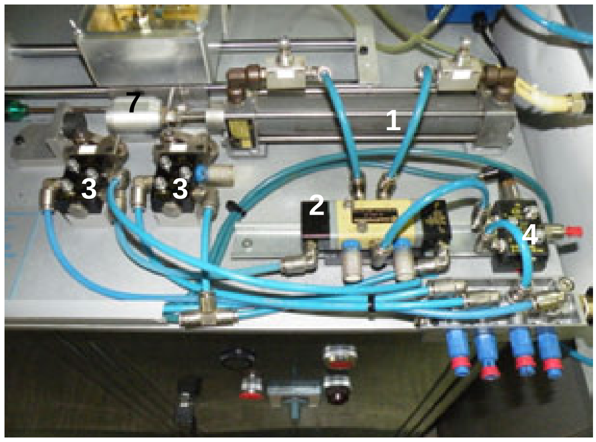

Figure 3. Pneumatic drive system

Normal load, and corresponding value of normal force in the contact zone (Figure 4) is defined by calibrated weights (1) where the forces transferred through the shaft (2) with a spherical end is to the pin bracket (3) (Figure 4). Compensation of own mass elements which are located on the pin bracket is performed through a spring with a threaded spindle (4) (Figure 4).

On pin bracket (3) set the single-axis piezoelectric vibration sensor (6) which measures vibrations in the tribological contact in the vertical direction.

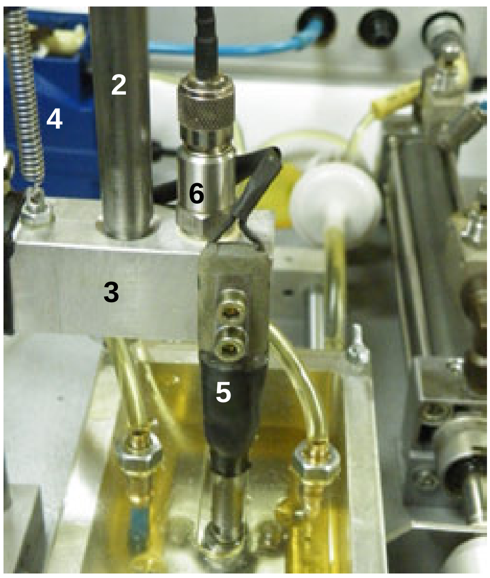

Figure 4. System for setting load and force measurement

At bottom of aluminium container (1) (Figure 5) plate (2) is attached. Pin (3) has cone top that fits into a spherical end of the dynamometer bar (4) and thus carries the normal force evenly over the entire surface of contact. Container (1) has a volume of 500 ml and is filled oil up with oil to about 1/3 of its height. Container is covered with a transparent cover on which there are connections for oil circulation - suction (5) and return (6).

Suction line takes oil from the bottom of container on one side and returns oil back to the surface on the other side of container. This is to ensure adequate oil mixing during circulation.

Oil suction pipe lead to peristaltic pump (7) (Figure 5 b)) that provides oil circulation through tribomechanical system in tribometer and through mobile device which measure contamination of oil by solid particles and water (8). Oil that passes through the device returns back to tribometer where can optionally pass through a filter or cartridge with water absorbent (9) or go directly into the container without filtration or dehydration.

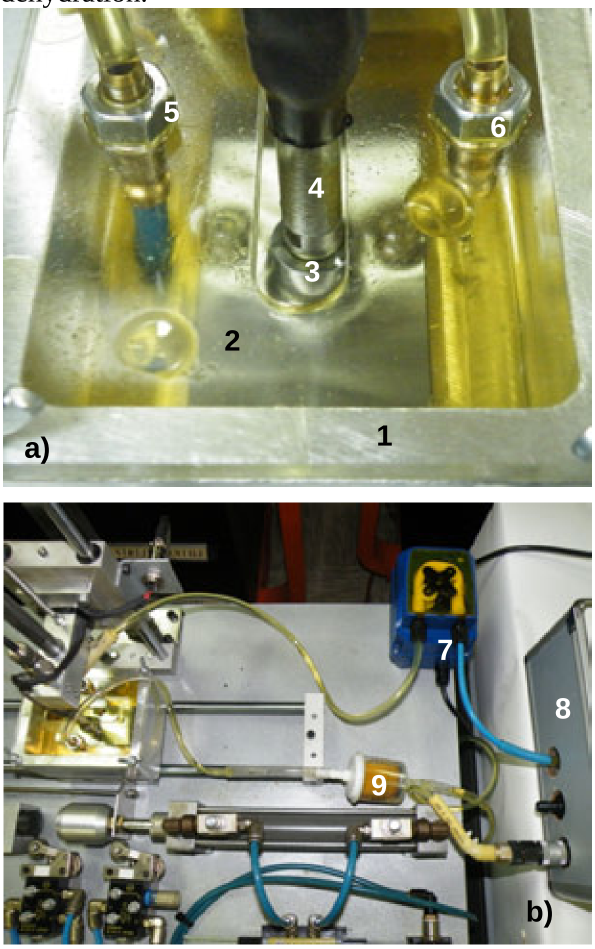

Figure 5. System for oil circulation

Complete laboratory installation (Figure 6) consists of the previously described tribometer with connected measuring equipment (1), laptop PC with A/D converter, software for data acquisition and measurement bridges for measuring vibration and friction forces (2) and mobile devices for control of oil contamination (3) for monitoring of oil contamination by solid particles and water.

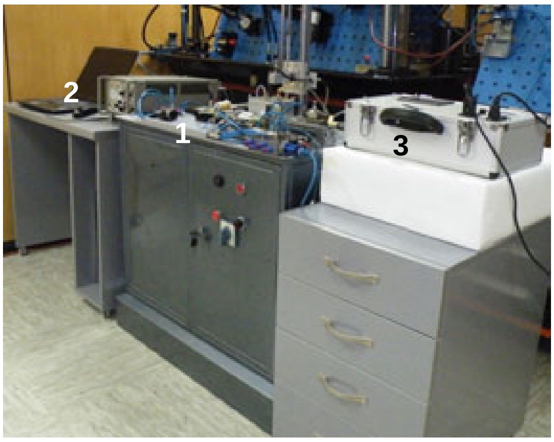

Figure 6. Complete tribometer installation

3. EXAMPLES OF OBTAINED INVESTIGATION RESULTS

In these chapter examples of typical results of performed laboratory tests of wear will be presented. Parameters monitored during tribological tests have specific, periodic diagrams that could not be used for conducting analysis and making conclusions in its original form. Therefore mathematical and statistical signal processing was carried generating of new parameters that indicate a nature and characteristics of wear process in more details.

Figure 7 shows the original shape of the measured signal of friction force (1), container displacement (2) and vibration in the tribological contact (vibration acceleration (3) and vibration velocity (4)). Marked parts on diagrams correspond to one whole cycle.

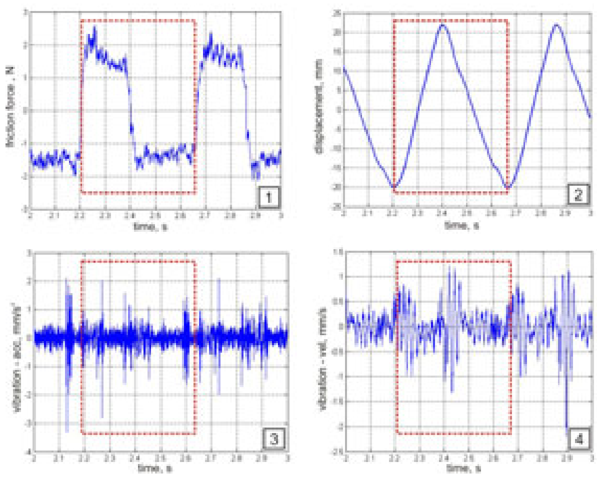

Figure7. Original shape of signals for one cycle

According to periodic repetition of measured signals it was necessary to determine the parameters that will describe the trend of change in friction force (friction coefficient). For each cycle maximum value of the friction (both positive and negative part), was determined, then mean value and standard deviation. The obtained values for each cycle were averaging for measuring intervals of 50 seconds or about 100 cycles. These three parameters were used to define trend of friction coefficient during conducted tribological experiments.

The shape of the measured vibration signals was not suitable for direct analysis in time domain or frequency analysis. Besides the mean-square value of vibration (RMS), an analysis was also amplitude in one cycle and are defined by the parameters of maximum and mean "peak to peak" values for one cycle. Figure 8 shows the part of the signal spectrum that corresponds to the time interval of 0.05 seconds with marked local maximum and minimum values - peaks.

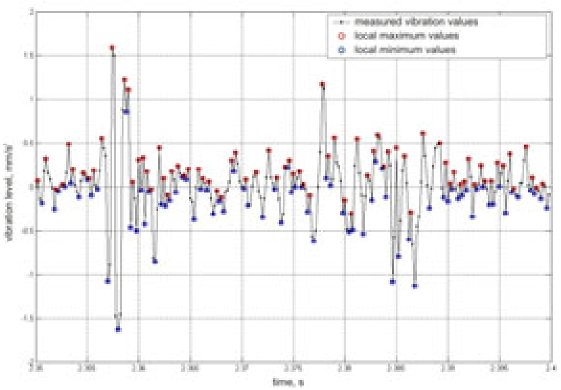

Figure 8. Identification of local peaks values in vibration signal

Typical results of one tribological test are presented below. Test lasted for 20,000 cycles. Figure 9 shows trend parameters of friction coefficient in the regime of running-in

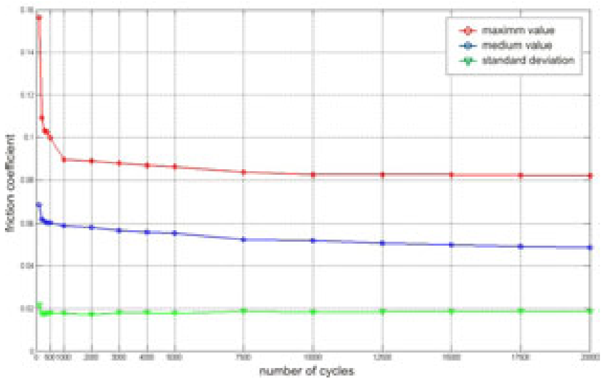

Figure 9. Trend parameters of friction coefficient

Figure 10 shows the original shape of measured values for friction coefficient for this regime.

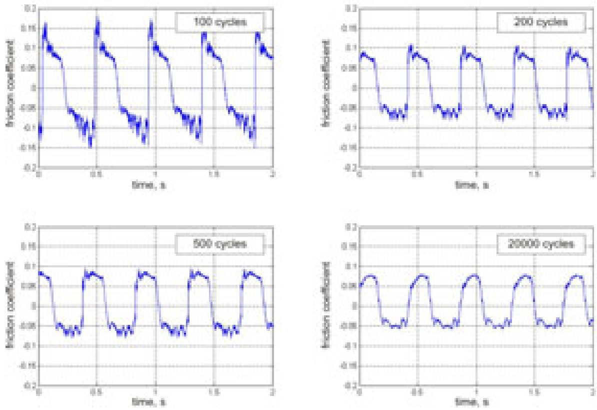

Figure 10. Original signals of friction coefficient

4. CONCLUSION

Presented tribometer has been developed to simulation linear motion that occurs in hydraulic systems as well as monitoring of tribological parameters in different testing conditions.

Some examples of an obtained investigation results are presented. Results are presented in their original form and after statistic analyses of measured signals.

REFERENCES

[1] Majmudar S.R., Majmudar S.: Oil Hydraulic Systems: Principles and Maintenance, McGraw-Hill, 2001.

[2] C.B. Mohan, C. Divakar, K. Venkatesh, K. Gopalakrishna, K.S. Mahesh Lohith, T.N. Naveen: Design and development of an advanced linear reciprocating tribometer, Bengaluru 562112, India 2009.

[3] Nilsson D., Prakash B., Investigation into the seizure of hydraulic motors, Tribology International, Vol. 43, Issues 1-2, 2010,pp. 92-99

[4] Olsson H., Ukonsaari J., Wear testing and specification of hydraulic fluid in industrial applications, Tribology International, Vol.36, Issue 11, 2003, pp. 835-841

[5] Stackhowiak G.W., Batchelor A.W., Stachowiak G.B., Experimental methods in tribology, Elsevier Science, 2004.

Serbian Tribology Society

SERBIATRIB '11

12th International Conference on Tribology

Faculty of Mechanical Engineering in Kragujevac

Kragujevac, Serbia, 11 – 13 May 2011

MULTIPURPOSE BIODEGRADABLE LUBRICATING GREASES

Ortansa Florea[1], Anca-Gabriela Marin[2], Vasile Matei[3]
[1]SC ICERP SA Ploieşti, Romania, oflorea_305@yahoo.com; oflorea_305@icerp.ro
[2]SC Georom Inspect Consulting SRL Ploieşti, Romania, anca.marin@georomserv.ro
[3] Petroleum-Gas University of Ploiesti, Romania, vmatei@upg-ploiesti.ro; vmatei@yahoo.com

Abstract: *Lubricants represent a large and diffuse pollution source both on soil and in water. Conventional lubricants, based on mineral oils contain toxic and non-biodegradable substances. Biodegradable lubricants represent the technical and ecological alternative for conventional lubrication. Lubricating greases are considered as colloidal dispersions of a thickener in a lubricating fluid. Their biodegradable properties and their lubricating ability depend both on the base oil and thickener.*
Soybean oil, rapeseed oil, sunflower oil, castor oil are the most used vegetable oils in biodegradable lubricants formulations. The lithium hidroxystearate thickener was selected to prepare the multipurpose ecological greases. For obtain good performances greases we used a technological method to form the thickener in the absence of base oil. The soap based greases with vegetable oils made by our proprietary technology are rapidly biodegradable (over 85% by equivalent CEC method.
To improve the EP and antiwear properties of the vegetable oils based greases sulfurizated vegetable oils was used. Ultrafine calcium carbonate has major improving on EP/AW properties, even it is not an usually additive for lubricants.

Keywords: *greases, biodegradability, additives, calcium carbonate, vegetable oils, thickener.*

1. INTRODUCTION

Lubricants facilitate the effective operation of mechanical equipment, reducing friction and wear, but in the same time they represent a large and diffuse pollution source both on soil and in water. Biodegradable lubricants represent the technical and ecological alternative for conventional lubrication. These lubricants are mostly required for equipment used in some resources industries such are forestry, mining, petroleum exploration and production or in cases when they might come in the contact with the environment.

Lubricating greases are considered as colloidal dispersions of a thickener in a lubricating fluid. Their biodegradable properties and their lubricating ability depend both on the base oil and thickener. Lithium greases are the most widely used, but Calcium, Aluminum, Polyurea, and organo-clay are also used.

Multipurpose biodegradable lubricating greases are high temperature, anti-wear extreme pressure (EP), greases with very high load carrying capacity and high dropping point engineered for machines and equipment subjected to extreme loads under wet or humid conditions at low and elevated temperatures.

2. BASE FLUIDS FOR BIODEGRADABLE LUBRICATING GREASES

Oil is considered to be readily biodegradable if minimum 70% of the hydrocarbons are removed after 21 days according with CEC L-33-A-94 test. Generally, the biodegradability of the vegetable oils and synthetics esters is over 90%, while that of the mineral oils is 20-40%. In table 1 we present the biodegradability of the most used lubricating oils.

Table 1 Biodegradability of the most used lubricants [6]

Lubricant	Biodegradability, %
Mineral Oils	15-35
White oils	25-45
Vegetable lubricants	70-100
Polyalphaolefins (PAO)	5-30
Polyether	0-25
Polyisobutylene (PIB)	0-25
Phthalate & Trimelitate Esters	5-80
Polyol Esters& Diesters	55-100

Soybean rapeseed-canola, sunflower, corn, peanut, olive, palm, castor oil are the most used vegetable oils in biodegradable lubricants formulations [1, 3, 5]. There are many applications for vegetal oils in the lubrication field, especially for fluid lubricants, such as hydraulic fluids, compressor oils, transformer coolant, two-stroke engine oils, metal working fluids and as the main component of lubricating greases. Due to their triglyceride molecular structures these vegetable oils have poor thermal, hydrolytic and oxidation stability. The presence of water even in small amounts can induce foaming and degradation problems. Also a great disadvantage of vegetable oils is their low cold-flow abilities. On the other hand the polar nature of these oils confers good lubricating capacity.

The stability of vegetable oils can be increased by the chemical modification of the oils in order to reduce the content of conjugated double bonds. There are many different ways to modify the multifunctional vegetable oils. Some reported changes that address the polyunsaturated problem include alkylation, acylation, hydroformylation, oligomerization, epoxidation, the hydrogenation of the conjugated double bonds by selective catalysts in specific conditions, the reaction of the oil with unsaturated esters, the reaction of unsaturated esters with aromatics, in the condition of Friedel-Crafts. Their sensitivity to hydrolysis and oxidation of the vegetal oils can be reduced by different methods like hydrogenation of the conjugated bonds, which also reduces the iodine number of the oil. The structure of the fatty acids of the vegetal oil determines the lubricating properties. An excess composition of certain saturated fatty acids leads to poor cold flowing characteristics of the lubricant. On the contrary, certain polyunsaturated fatty acids impart unfavorable oxidation and chemical stability at high temperatures. The level of oleic acid also influences the oxidative stability. A higher content in oleic acid also determines a lower change in viscosity - Table 3.

Table 2. Iodine value of vegetal oils.

Oil Types	Iodine Value, g/100g I_2
Rapeseed	94…106
Soybean	103…109
Castor	82…90
Sunflower	127…136
Olive	80…85

Table 3. Oleic acid content, viscosities and changes in viscosities of different vegetal oils.

Oil	Oleic acid, %	Kinematic Viscosity, cSt		Δ Visc. @40°C* cSt
		40°C	100°C	
Rapeseed	32	51	10	21
Soybean	27	28.5	7.5	43
Castor	3	293	20	78
Linseed	20	30	7	46
Palm	40	32	6.5	13

* (1000 hrs, 3 l/h, 93°C)

Genetic modifications can also increase their thermal and oxidative stability [1, 7].

Synthetic biodegradable lubricants include diesters and polyalkylene glycols which are rapidly biodegradable. The synthetic esters in lubricants improve the following properties: thermal stability, hydrolytic stability, solvency, lubricity, and biodegradability [4].

To obtain good performances synthetics esters, selected branched alcohols and pure oleic acids are used. The branched alcohols improve the flow properties at low temperatures and in the same time the hydrolytic degradation is inhibited [1]. The synthetic esters in lubricants improve the following properties: thermal stability, hydrolytic stability, solvency, lubricity, biodegradability. These types of fluids exhibit longer service life then vegetal oils [4]. The selection of the acids and alcohols allows combining biodegradability with the very good performance properties. Diesters and phthalates are the most used synthetic esters in lubricating greases formulation. In Table 4 some of their properties are presented.

Table 4. Properties of some synthetic esters.

Properties	Diesters	Phthalates
Viscosity at 40°C, cSt	6…46	29…94
Viscosity at 100°C, cSt	2…8	4…9
Viscosity Index	90…170	40…90
Pour Point, °C	-70 to -40	-50 to -30
Flash point, °C	200…260	200…270
Thermal stability	good	very good
Biodegradability, %	75…100	46…88

Another class of synthetic oils is Polyalkylene Glycols- PAGs. PAGs can be either polyethylene or polypropylene oxide-based. Their water solubility can be differed according to the type. Polyethylene glycols are highly water soluble, present poor miscibility with mineral oils and are very polar structure. Their water solubility helps to provide biodegradability, but also provide some disadvantage as lubricants, due to their frequently free water contamination tends.

3. EXPERIMENTAL

3.1 Manufacturing process and equipment

The process of manufacture the biodegradable lubricating greases must take into account the particularities of components and do not affect the functionality, toxicity and biodegradability of the final product. An important factor is that many biodegradable fluids are readily saponifiable and in some cases (such as soybean oil, castor oil, other vegetable oils) are much time reactive than the fatty acids used to manufacture soap based greases [7]. For obtain good performances greases we used a technological method to form the thickener in the absence of base oil.

The usual equipment is satisfactory for the manufacture of biodegradable greases, but this must be properly cleaned to prevent contamination with conventional greases and their components.

3.2 Test Methods

The experimental greases were characterized using the following test methods:

Table 5. Test Methods

Characteristics	Test Methods
Dropping point	ASTM D 2265
Penetration, 25°C, 1/10mm	ASTM D 217
Mechanical stability, 10000 strokes	ASTM D 217
Oil Separation, 30 hours, 100°C, %	ASTM D 972
Evaporation loss, 30 hours, 100°C, %	ASTM D 972
Colloidal stability, % oil separated	STAS 3793
Biodegradability, %, 21 days	CEC L-33-A-94
Bomb oxidation test	ASTM D 942

3.3 Greases formulated with vegetal oils

The lithium hidroxystearate thickener was selected to prepare the soap based greases with vegetal oil. We present bellow the characteristics of biodegradable greases made with soybean oil - Table 6, and mixture of soybean oil and rapeseed oil (grease 6 in Table 7) and also mixtures of soybean and castor oil (greases 4, 5 in Table 7). The greases made with vegetal oils by authors' technology are rapidly biodegradable (over 85% by CEC L-33-A-94 test). They present high dropping points (over 185°C) and good physico-mechanical characteristics. However, it must be mentioned that a high content of thickener for the same class of consistency is required as comparing to conventional greases.

3.4 Greases formulated with synthetic esters

The rapidly biodegradable greases containing diesters (di-octyl adipate – DOA and di-octyl-sebacate – DOS) and organo-clay [1, 3] were made by a new technology which consists in adding the polar solvent dispersant in two steps. This method confers to the final product higher mechanical and storage stability values than those of the similar greases obtained by classical technologies. The characteristics of the greases containing di-octyl sebacate (7, 8, and 9) and di-octyl adipate (10, 11, and 12) as base fluid are shown in Table 8 and 9. The characteristics of the greases R1 and R2 made by classical technology from di-octyl sebacate and di-octyl adipate are comparatively presented.

Table 6. The characteristics of soybean greases.

Characteristics	Grease		
	A 1	B 2	C 3
Dropping point	190	196	197
Penetration, 25°C, after 60 strokes, 1/10mm	294	275	250
Roll stability, % change	2.1	0	0
Oil Separation, 30 h, 100°C, %	2.4	1.9	1.7
Evaporation loss, 30 hours, 100°C, %	0.3	0.24	0.2
Biodegradability, %, 21 days	87	86	85

Table 7. The characteristics of greases made with vegetal oils mixtures.

Characteristics	Grease		
	D 4	E 5	F 6
Dropping point, °C	193	188	185
Penetration, 25°C, after 60 strokes, 1/10mm	241	279	306
Roll stability, % penetration changes after 10000 strokes	1.7	0.8	9
Oil Separation, 30 h, 100°C, %	0	0.84	1.2
Evaporation loss, 30 h 100°C, %	0.58	0.10	0.61
Biodegradability, %, 21 days	85	87	87
Type of base oil, %	Soybean, Castor	Soybean, Castor	Soybean, Rapeseed

Table 8. The characteristics of DOS greases.

Characteristics	**Greases**			
	G **7**	**H** **8**	**I** **9**	**R1**
Dropping point, °C	>260	>260	>260	>260
Penetration, @ 25°C, 60 strokes, 1/10mm,	278	265	246	262
Mechanical stability, penetration change after 10000 strokes	5.2	4.8	4.6	12.6
Colloidal stability, % oil	2.8	2.3	1.6	9.6
Biodegradability, %, 21 days	86	86	86	-

Table 9. The characteristics of DOA greases.

Characteristics	Greases			
	J 10	K 11	L 12	R2
Dropping point	>260	>260	>260	>260
Penetration, @ 25°C, 60 strokes, 1/10mm,	265	270	324	282
Mechanical stability, penetration change after 10000 strokes	3.9	4.3	4.8	13.2
Colloidal stability, % oil	3.2	4.4	4.6	10.6
Biodegradability, %, 21 days	80	80	80	-

The biodegradability of greases prepared with synthetic oils (DOS and DOA) and bentone tested by the CEC method is 86% and 80%, respectively. Their dropping point, over 260°C are specific for this type of lubricants. The values of mechanical stability measured by penetration change, after 10000 strokes are higher than those of the greases made by adding the polar solvent in a single step. Using this new technology the authors obtained high stability storage products (shown by the values of colloidal stability in accordance to Romanian test method).

3.5 Some additivation aspects in multipurpose biodegradable lubricating greases

Additivation is the solution to improve the properties of the biodegradable greases. The polarity of the vegetal oils and synthetic esters can generate competitive reactions on metallic surfaces [9]. To obtain similar properties as mineral oil based greases a higher proportion of additives is necessary. On the other hand it must be taken into account the biodegradability of the additives, too [1, 8]. In a finished lubricant, additives normally constitute a sufficiently low fraction that their function can be the primary consideration, rather than their environmental behavior.

An additive consisting of sulphurizated soybean oil – Table 11, was used to improve the EP and antiwear properties of biodegradable grease made with the same base oil – Table 11.

Table 10. The characteristics of the sulphurizated soybean oil, used as EP/AW additives.

Characteristics	Values	Method
Density @ 20 °C	1.05	ASTM D1298
Suphur content, %,	20	ASTM 4294
Saponification Number, mg KOH/g,	118	ASTM D1962
Biodegradablity, %, 21 days	78	CEC

Table 11. The effect of sulphurized soybean oil on the biodegradable greases containing vegetal oils.

Characteristics	Greases	
	M 13	N 14
Dropping point°C	196	192
Penetration, @ 25°C, 1/10mm, after 60 strokes	282	297
Roll stability, % change	0	2.4
Oil Separation, 30 hours, 100°C, %	1.9	2.4
Evaporation loss, 30 hours, 100°C, %	0.24	0.36
Biodegradability, %, 21 days	85	85
Four ball test: -Wear scar diameter, mm, -at 40 daN / 60 min -at 150 daN / 1 min -Welding load, daN	 0.86 - 150	 0.62 1.12 280

The sample 13 is non-adittivated grease while the grease grade 14 contains 3.5% sulphurizated soybean oil. The sulphurizated soybean oil improves the antiwear and EP properties of the vegetal base greases – Table 11. The oxidation stability of biodegradable greases made with vegetal oil can be improve using α-tocoferol acetate (pressure drops only 0.22 psi after 100 hours-Table 12). The additive α- tocoferol acetate (vitamine E) used as antioxidant is a pharmaceutical grade product, 30% active substance in sunflower oil.

Table 12. The antioxidant effect of the α-tocoferol acetate in biodegradable lithium greases.

Characteristics	Greases	
	O 15	P 16
Dropping point	196	190
Penetration, 25°C, 1/10mm -unworked -after 60 strokes	 275 282	 280 304
Bomb oxidation test, Δp, psi	0.35 after 25h	0.22 after 100h

3.6 Behaviour of calcium carbonate in Polyurea greases

Due to their suitable properties, the polyurea greases made with high purity white oils, or poly alpha-olefins as base stocks are frequently used in food processing. More over, polyurea greases formulated with suitable oils present very high biodegradability. These type of greases provide high protection for the equipment in the food processing industries (which requirement lubrication under hot and wet conditions) such as conveyor in bakery ovens, in canneries, dairies, beverage and fish processing plants. Polyurea greases have outstanding resistance to oxidation. The oxidation resistance of these products is attributed to the absence of metals. Generally, soap base thickener can helps the promotion of oxidation of the greases. By comparison, a polyurea-base thickener system offers temperature range limits similar to the soap-thickened grease, but additionally it has antioxidant and antiwear properties confer by thickener itself. Polyurea thickeners might become wide used, but they are difficult to manufacture, requiring the handling of several toxic materials. Some polyurea lubricating grease was formulated using preformed thickener (16%) which has no toxicity.

Precipitated calcium carbonate, even it isn't a biodegradable material can be considered a suitable additive, which improve the extreme pressure and anti wear properties of ecological greases. Its non toxicity confer this material, very good attribute to be use in food grade bio-lubricants formulation. Precipitated calcium carbonate used in ours formulation consisted in a mixture of all three polymorphs of calcium carbonate, obtained using two nonionogene additives: polyoxyethylen sorbitan monolaureate, (Tween 20) and polyoxyethylen sorbitan trioleate (Tween 85). In the $CaCO_3$ precipitation process these additives behave as block copolymers with only one hydrophilic group (polyglycolic group). Usually the presence of an electric charged functional group (R^+ or R^-) induces polymorph selectivity. Their absence in Tween 20 (85) structural formulate explains the mixture of polymorphs. They may influence only the particles size distribution. Optic microscopy analysis of the solid phase and SEM micrographs show needle-like aragonite, plates and dendrite-like vaterite, rhombohedral-like calcite.

Table 13. Characteristics of calcium carbonate used in lubricants formulations

Characteristics	Values
Specific surface area, m^2/cm^3	0.73
Average diameter, μm	20.535
Nature of the solid phase	aragonite, vaterite and calcite

Tabele 14. The influence of calcium carbonate as additives in polyurea greases

Characteristics	Calcium carbonate,%			
	0	2,5	3	3,5
Penetration, @ 25°C, 1/10mm, after 60 strokes	269	267	265	262
Dropping point, °C	>230	>230	>230	>230
Four ball test: - Welding load, daN -Wear scar diameter, at 150 daN / 1 min, mm	 140 -	 150 3,2	 170 1,8	 220 0,7
Colloidal stability, % oil separated	4,26	4,05	4,01	3,8
Mechanical stability: penetration after 10 000 strokes, % change	5,6	4,8	5,02	4,3
Corrosion test (OL, 3 hours at 100°C)	pass	pass	pass	pass
Water resistance, 5 hours at 90°C	Stab.	Stab.	Stab.	Stab.

Table 15. The caracteristics of polyurea greases aditivated with diferent morphologycal types of calcium carbonate, versus molibdenum disulphide

Characteristics	Solide additive			
	a	v	c	MoS_2
Penetration, 25°C, 1/10mm, 60 strokes	270	269	275	290
Dropping point, °C	198	196	199	192
Four ball test: -Welding load, daN -Wear scar diameter, at 150 daN / 1 min, mm	 >300 1,2	 290 1	 290 1,2 5	 290 0,85

a: aragonite; v: vaterite; c: calcite

4. CONCLUSION

The greases made with vegetal oils by authors' technology are rapidly biodegradable (over 85% by CEC L-33-A-94 test). They present high dropping points (over 185°C) and good physico-mechanical characteristics. A higher content of thickener for the same class of consistency is required as comparing to conventional greases.

The rapidly biodegradable greases containing diesters (DOA, DOS) and organo-clay were made by a new technology which consists in adding the polar solvent dispersant in two steps.

To improve the EP and antiwear properties of the vegetable greases sulfurizated vegetable oils was used.

The oxidation stability of vegetable greases was improved using α-tocoferol acetate;

Ultrafine calcium carbonate has major improving on EP/AW properties of polyurea based grease, even it is not an usually additive for lubricants.

REFERENCES

[1] P. R. Grives, The Manufacture of Biodegradable Nontoxic Lubricating Greases, NLGI Spokesman, vol. 63, No. 11, Feb. 2000.

[2] I. Roehrs, T. Roβrucker, "Performance and Ecology-Two Aspects for modern Greases", NLGI Spokesman, 58, 12, (1995), 847-483.

[3] R. L. Goyan, R. E. Melley, P. A. Wissner, and W. C. Ong, "Biodegradable Lubricants", Lub. Eng., 54, 7, (1998), 10-17.

[4] L. Leugner, Biodegradable Oils-How to Apply and Maintain, Machinery Lubrication, 7, 2003.

[5] J. Barriga, A. Aranzabe , P. Galda, Sunflower Based Grease For Heavy Duty Applications, Mecanica Experimental, vol. 13, pp. 129-133, 2006.

[6] Dr. In-Sik Rhee, "21 Century Military Biodegradable Greases", NLGI Spokesman, 64, 1, (2000), 8-17.

[7] Mang, T., "Environmentally Harmless Lubricants", NLGI Spokesman, 57, 6, (1993); 233-239.

[8] Qiu, Sunqing; Dong Junxin; Chen Guoxu; Wear and Frictions Behaviour of $CaCO_3$ Nanoparticles Used as Additives in Lubricating Oils, Lub.Sci., vol. 12, 2000, 205-212

[9] O. Florea, M. Luca, Biodegradable lubricating greases for earth moving equipments, Journal of the Balkan Tribological Association vol, Vol. 13, No. 1, 2007, pp 96-102.

[10] M. A Delgado , Relationship among microstructure rheology and processing of a lithium lubricating grease, Chem. Eng. Res.Des.83, 1085-1092, 2005.

[11] Kyriakopoulos, C., Fully Formulated H1 Aluminium Complex Food Machinery Greases, NLGI Spokesman, Vol. 58, No. 4, July 1994.

[12] M. Mocioi, C.D. Mateescu, R. Isopescu, F. Branzoi, M. Coman, O. Florea “Semi-batch precipitation of calcium carbonate in the presence of organic”, 14th Workshop Ind. Crystalization, Delft, 2006

SERBIATRIB ‘11

Serbian Tribology Society

12th International Conference on Tribology

Faculty of Mechanical Engineering in Kragujevac

Kragujevac, Serbia, 11 – 13 May 2011

MICROINDENTATION OF POLYMETHYL METHACRYLATE (PMMA) BASED BONE CEMENT

F. Živić[1], M. Babić[1], G. Favaro[2], M. Caunii[2], N. Grujović[1], S. Mitrovic[1]
[1]Faculty of Mechanical Engineering, Kragujevac, Serbia
zivic@kg.ac.rs, babic@kg.ac.rs, gruja@kg.ac.rs, boban@kg.ac.rs
[2] CSM Instruments, Switzerland,
Gregory.FAVARO@csm-instruments.com, Mihaela.CAUNII@csm-instruments.com,

Abstract: *Characterization of polymethyl methacrylate (PMMA) based bone cement subjected to cyclical loading using microindentation technique is presented in this paper. Indentation technique represents flexible mechanical testing due to its simplicity, minimal specimen preparation and short time needed for tests. The mechanical response of bone cement samples was studied. Realised microindentation enabled determination of the indentation testing hardness HIT and indentation modulus EIT of the observed bone cement. Analysis of optical photographs of the imprints showed that this technique can be effectively used for characterization of bone cements.*

Keywords: *Biomaterials, Polymethyl methacrylate (PMMA), Bone cement, Microindentation*

1. INTRODUCTION

Polymers are large molecules synthesized from smaller molecules, called monomers. Polymers for medical applications can be divided into three general fields:

1. Polymers for artificial joints
2. Bioabsorbable polymers for surgical applications
3. Adhesives for medical applications

An acrylate polymers, commonly known as acrylics or polyacrylates, belongs to a group of polymers which could be referred to generally as plastics. They are noted for their transparency and resistance to breakage and elasticity. Polyacrylates are based on acrylic acid, methacrylic acid, and their esters. Among them, polymethyl methacrylate (PMMA) is largely used for biomedical applications. The clinical history of polyacrylates began when it was unexpectedly discovered that the fragments of PMMA plastic aircraft canopies stayed in the body of the wounded without any adverse chronic reactions [1]. PMMA has been used as self-polymerising bone cement in orthopaedics since the 1960s. Acrylic bone cement is used to fill the irregular space between prosthesis and bone during total hip replacements in order to keep the prosthesis in place (Fig. 1). The primary functions of bone cement, when used to anchor artificial joints, are to secure the orthopedic implants to bone and transfer mechanical loads from the implant to the bone. Approximately 50% of all orthopedic implants utilize bone cement to achieve implant fixation [2].

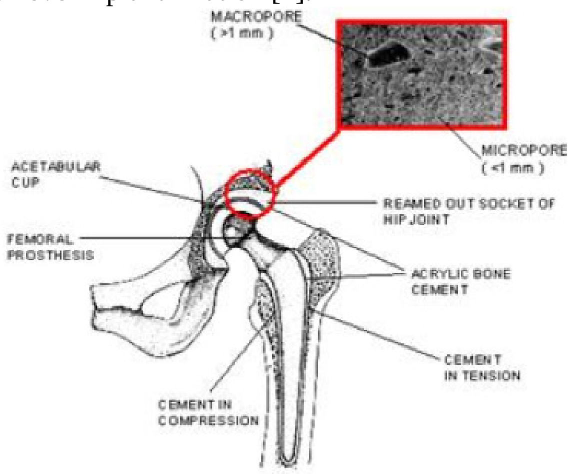

Figure 1. Schematic view of total hip replacement [3]

Some drawbacks associated with PMMA-based bone cements are: local tissue damage due to chemical reactions during polymerization and strong exothermic setting reaction, the high shrinkage of the cement after polymerization, the stiffness mismatch between bone and the cement, toxic effect of the monomer, inability to bond directly to bone causing loosening at the interface and brittle nature [2]. Loose cement particles also mediate osteolysis of the bone and are highly unwanted. Special problems occur at the interfaces due to the different elastic module of the materials (110 GPa for titanium, 2.2 GPa for PMMA, and 20 GPa for bone) [3].

The role of the cement is directly related to the mechanical properties of the cement, especially the resistance to fracture of the cement in the mantle at the cement-prosthesis interface or the cement-bone interface. Method of cement mixing is very important since porosity is one of the crucial characteristics that determine its resistance to fracture. Cement that is inadequately mixed exhibits a high degree of porosity. High porosity means that number of pores is present acting as stress raisers and initiating spots for cracks, further promoting early fatigue failure. Number of types of bioactive bone cements has been investigated to overcome above listed problems.

PMMA is one of the polymeric materials also used as matrix for carbon fibers composites [1]. Carbon fiber has been recognized, recently, as a material with many exciting applications in medicine, since they, when used as a reinforcing material significantly enhance the mechanical properties of the observed system. Orientation and fiber content can be varied in such a way to provide the implant with mechanical property needed for proper functioning. One common feature that implant must satisfy is its resistance to fatigue failure and to be resistant to attacks from the physiological environment [1]. Many new approaches have been tried to enhance mechanical properties of PMMA bone cements [4,5]. Recent methods include addition of reinforcing particle or fiber in order to increase cement stiffness, strength and toughness [4]. Common approach considers improvement of fatigue characteristics, by reinforcement of PMMA with carbon fibers, hydroxyapatite particles, stainless steel fibers, titanium fibers or zirconia particles or fibers, etc.

A recognized issue is that it is not always possible to distinguish the medical-grade polymers from the conventional polymers. They are selected based on clean condition or trace element analysis or mechanical properties. Processing involve clean room conditions and special care not to contaminate the materials.

The ready bone cement is a compound consisting of 90% of polymethylmetacrylate**,** (PMMA), which exists in an amorphous state and is completely transparent. The rest are mainly crystals of barium sulfate or Zirconium oxide that make the resulting product radio-opaque. The microscopic structure of bone cement is made by two substances glued together. One part consists of the small particles of pre-polymerized PMMA (PolyMethylMetaAcrylate), so called “pearls”. These pearls are supplied as a white powder. The other substance is a liquid monomer of MMA (MethylMetacrylate). Both substances are mixed together at the operation table with added catalyst that starts the polymerization of the monomer fluid. Amorphous polymers such as PMMA are brittle, hard plastics at room temperature [6]. It is isotropic and significantly bioinert material. PMMA is attacked by mineral acids but is resistant to alkalis, water and most aqueous inorganic salt solutions [6]. PMMA is also subject to both elastic and viscoelastic (creep) deformation under load [7]. Considering previously stated, it is very important to properly define mechanical characteristics of PMMA bone cements, to be able to further enhance their features.

Characterization of bone cement to cyclical loading is extremely significant and is a subject of many ongoing studies [8-14]. For instance, if total hip replacement is considered, many daily activities involve many cycles of different alternating loading patterns (walking, etc.). Studies showed that one of the main reasons of cement failure mechanism is related to fatigue failure and fatigue crack propagation [8]. Indentation represents flexible mechanical testing due to its simplicity, minimal specimen preparation. It allows selection of loads and tip geometry. Forces can be applied from kilo-newtons down to nano-newtons, but also displacements down to nanometer. Indentation response is related to specific aspects of materials in question (porous structure, biomaterials, etc.) and interpretation of results requires specific knowledge about indentation mechanics and physics of the observed material [15]. The hardness of a material is usually defined as the resistance to local deformation [15]. Until development of instrumentation to accurately measure imprint dimensions (contact area) after unloading, hardness tests were limited to macro scales. However, since great advancements in this area, micro and nano scale optical measurements are widely available thus leading to expansion of indentation interpretation. Devices with depth sensing possibilities, such as CSM Nano Indentation Tester, enable determination of hardness, elastic modulus, plastic stress-strain behavior and/or creep behavior directly using the tester, without the need to measure contact impressions.

2. PRINCIPLE OF INSTRUMENTED INDENTATION TESTING (IIT)

The Nano Indentation Tester uses an already established method where an indenter tip with a known geometry is driven into a specific site of the material to be tested, by applying an increasing normal load. When reaching a pre-set maximum value, the normal load is reduced until partial or complete relaxation occurs. This procedure is performed repetitively; at each stage of the experiment the position of the indenter relative to the sample surface is precisely monitored with a differential capacitive sensor. For each loading/unloading cycle, the applied load value is plotted with respect to the corresponding position of the indenter. The resulting load/displacement curves (Fig. 2) provide data specific to the mechanical nature of the material under examination. Established models are used to calculate quantitative hardness and elastic modulus values for such data.

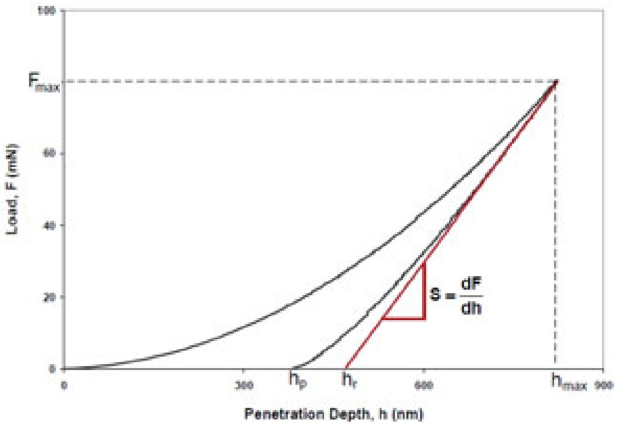

Figure 2. Typical Load/displacement curve

Evaluation of elastic modulus and hardness using instrumented indentation is realised by the method developed and proposed by Oliver and Pharr. It is the most common approach to determine hardness and modulus by interpretation of load - penetration depth (F - h) behavior during indentation (Fig. 1). Oliver and Pharr developed Power Law Method that describes the upper portion of the unloading curve by a power law relationship:

$$F = F_{max}\left(\frac{h-h_p}{h_{max}-h_p}\right)^m$$

where,

F - is the test force,
Fmax - is the maximum applied force,
h - is the indentation depth under applied test force,
hp - is the permanent indentation depth after the removal of the test force,
hmax - is the maximum indentation depth at Fmax,
m - is a power law constant exponent.

The power law exponent *m* is determined by a least squares fitting procedure and is a function of the indenter geometry.

The contact stiffness *S* is given by the derivative at peak load:

$$S = \left(\frac{dF}{dh}\right)_{max} = m \cdot F_{max}\left(h_{max}-h_p\right)^{-1}$$

And the tangent depth, *h*r, is thus given by:

$$h_r = h_{max} - \frac{F_{max}}{S}$$

Where h_r is the point of intersection of the tangent c to curve b at F_{max} with the indentation depth-axis. The contact depth (depth of the contact of the indenter with the test piece at F*max*), h_c, is then:

$$h_c = h_{max} - \varepsilon\left(h_{max} - h_r\right)$$

where ε depends on the power law exponent *m*.

The Indentation Testing Hardness H_{IT} is determined from the maximum load, F_{max}, divided by the projected contact area A_p at the contact depth h_c :

$$H_{IT} = \frac{F_{max}}{A_p(h_c)}$$

Where hc is the depth of the contact of the indenter with the test piece at F_{max}. A_p (h_c) is the projected area of contact of the indenter at distance h_c from the tip. A_p is a function of the contact depth h_c and is determined by a calibration of the indenter tip.

The Vickers Hardness HV is defined by:

$$HV = \frac{F_{max}}{9.81 \cdot A_c(h_c)}$$

Where *Ac* is the developed contact area and can be calculated from the projected contact area A_p and the indenter geometry as:

$$A_c = \frac{A_p}{\sin\alpha}$$

Where α is the angle between the axis of the diamond pyramid and its faces, α = 68° for a Vickers indenter (Fig. 3) and α = 65.27° for a modified Berkovich indenter.

For Vickers indenter: HV = 0.0945 H_{IT}
For modified Berkovich indenter: HV = 0.0926 H_{IT}

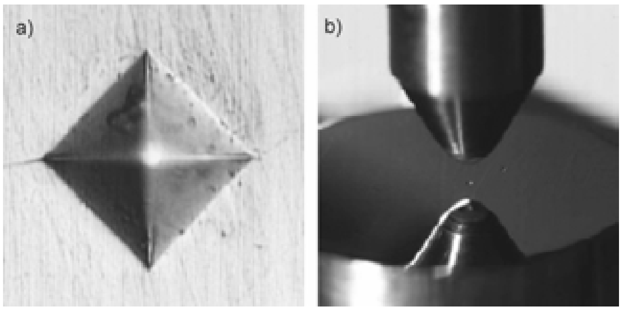

Figure 3. CSM Micro instrumented indentation testing: a) Optical micrograph of a Vickers indentation into a standard steel reference sample; b) Detail of Vickers indenter mounted above sample

Indentation Modulus E_{IT}

The reduced modulus of the indentation contact, E_r, is given by:

$$E_r = \frac{\sqrt{\pi} \cdot S}{2 \cdot \beta \cdot \sqrt{A_p(h_c)}}$$

Where β is a geometric factor depending on the diamond shape (circular: β = 1, triangular: β = 1.034, square: β = 1.012). The Young's modulus of the sample, E_{IT}, can then be obtained from:

$$\frac{1}{E_r} = \frac{1-\nu_s^2}{E_{IT}} + \frac{1-\nu_i^2}{E_i}$$

Where
ν_i is the Poisson's ratio of the indenter.
ν_s is the Poisson's ratio of the sample.
E_i is the modulus of the indenter.

3. EXPERIMENTAL TEST

Bone cement prepared from commercially available type of mixture was used as a sample material for indentation tests. PMMA is isotropic, showing no crystallinity, elasto-viscoplastic solid and amorphous polymer. Several indentations have been performed on each sample using the CSM Micro Indentation Tester (Fig. 4). Indentation test lasted for 300 cycles. Tests were performed with maximum normal load of 15 N, minimum load of 5 N and approach speed of 5000 nm/min.

Vickers indenter was applied with quadratic loading type. There was no pause at maximum load before unloading. Displacement measurements were realised using LVDT sensor which is a part of the tester. Maximum possible indentation depth was limited to 200 μm with displacement resolution of 0.3 nm.

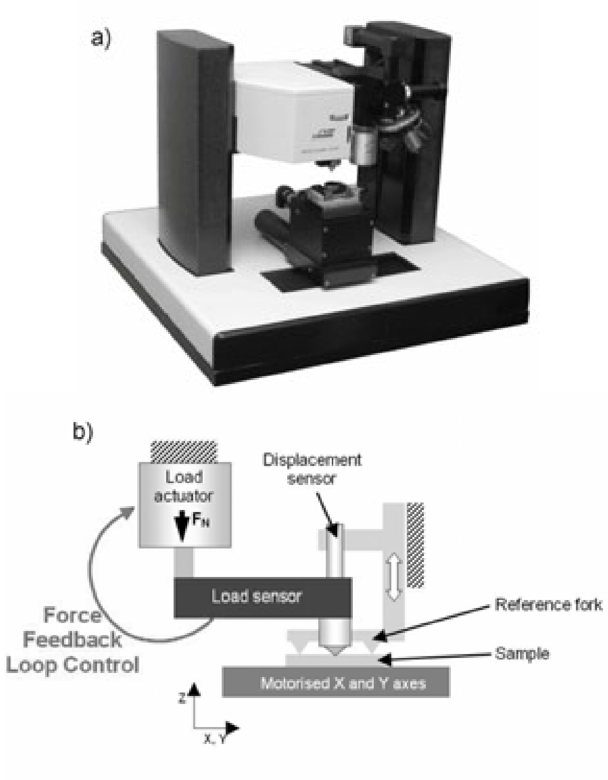

Figure 4. a) CSM Micro Indentation Tester
b) Schematic view of the main elements of Micro Indentation Tester

4. RESULTS AND DISCUSSION

Indentation curve, that is, diagram of the normal force applied during micro indentation as a function of the number of cycles is shown in Fig. 5. This is classical fatigue mode of indentation testing, whereas the force is loaded and unloaded constantly during indentation without a pause. Material is subjected to constant load/unload pattern and is not left to rest, such as in case of indentation mode of testing on creep.

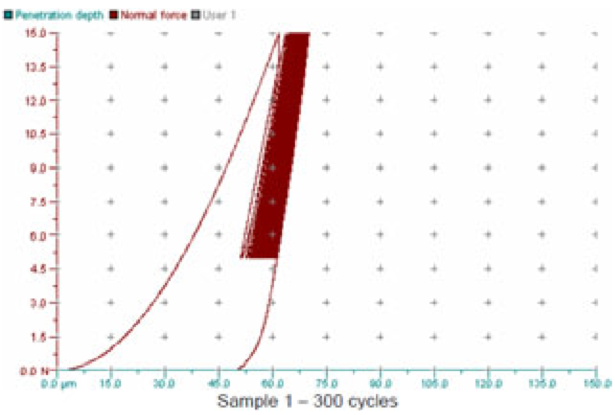

Figure 5. Normal force versus penetration depth curve during micro indentation

Imprint on bone cement sample after indentation lasting for 300 cycles, is shown in Fig. 6. Typical pattern produced by Vickers indentation is clearly seen. Detailed view of the left lower angle is shown in Fig. 6b. The imprint is well shaped with clearly developed edges and no microcracks around angles. This is in consistence with the fact that amorphous materials usually present an elastic behavior up to failure [16]. Permanent deformation occurs due to high shear and compressive stresses which are both present in highly localized area.

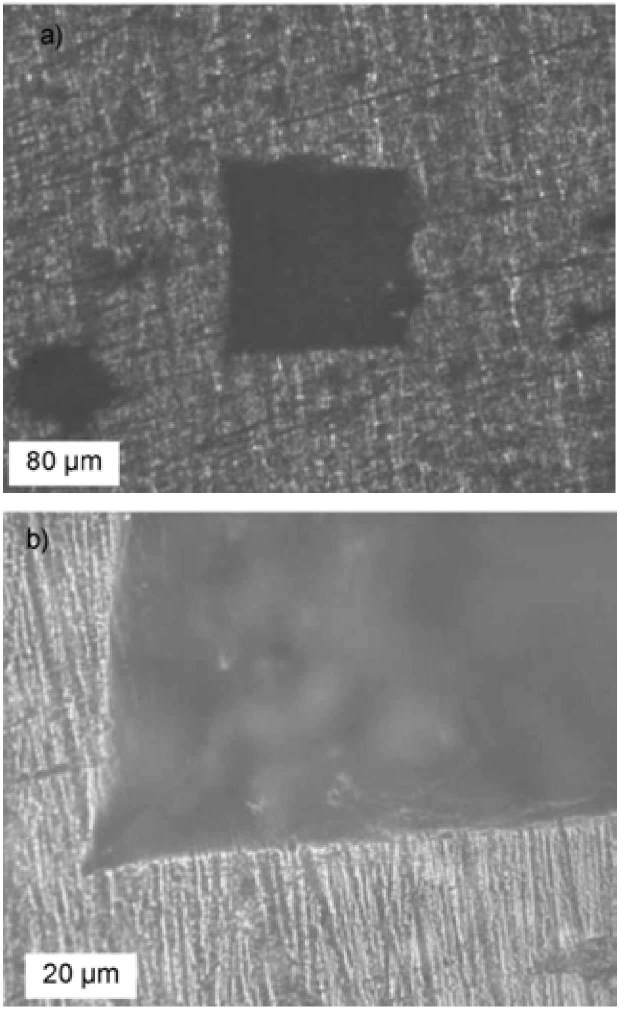

Figure 6. a) Micrograph of the indentation imprint on bone cement after 300 cycles, b) Detail of the indentation imprint on PMMA after 300 cycles (left bottom angle)

Calculated values of hardness H_{IT} and elastic modulus E_{IT} of bone cement sample after 300 cycles obtained by the indentation tester is shown in Table 1.

Table 1. Values of hardness H_{IT} and elastic modulus E_{IT} of bone cement sample after 300 cycles obtained by the indentation tester

	Value for PMMA sample after 300 cycles
Hardness, H_{IT} [MPa]	162.84
Elastic modulus, E_{IT} [GPa]	2.74

Hardness profile and elasticity profile during multicycling loading, unloading and reloading are shown in Fig. 7. Values given in Table 1 are automatically calculated by the tester according to Oliver and Pharr approach, by analysing the unloading curves (Fig. 5). It can be clearly seen that E_{IT} value is rather uniform, whereas hardness has slightly decreasing trend.

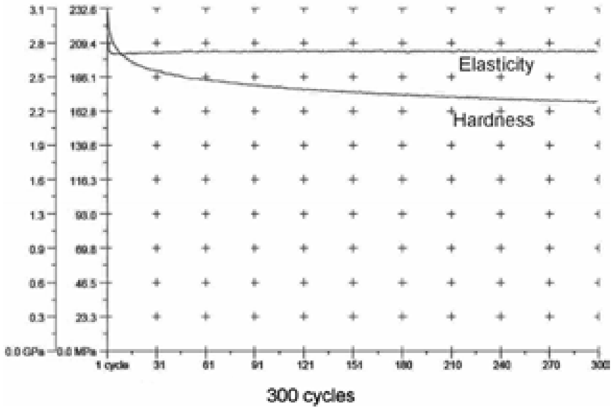

Figure 7. Hardness, H_{IT} and elasticity, as a function of the number of cycles during micro indentation

Loosening is recognized as one of the primary sources of total hip replacement failure. One of the main reasons is considered to be fatigue failure of the implant-bone cement and bone cement - bone interface. That is the reason why characterization of bone cement to cyclical loading is extremely significant and is a subject of many ongoing studies [8-14]. Also, PMMA has been widely used as a model for studies of fatigue and fracture in polymers. Effects of different factors have been investigated, whereas variable amplitude loading offer insight in its behavior from aspects of fatigue and crack propagation. The loading curve in Fig. 5 consists of both elastic and plastic contribution, while the unloading curve is purely elastic and allows calculations of elastic modulus and hardness. Bone cements have a more complicated structure if compared to pure PMMA, with previously polymerised beads in a softer matrix which cures on implantation, and other components such as particles of barium sulphate or zirconia to make the cement visible in radiographs. This microstructural complexity means that the cement may behave very differently from pure PMMA. There are several commercially available bone cement mixtures and they have been comprehensively studied both in laboratory and clinical practice. However, there are still features that need to be enhanced and indentation tests can be used for further understanding of its behavior. Clinical failure of the cement occurs over long time periods, and this implies that the crack growth rate is very low, perhaps as low as 10^{-12} m/cycle. It is clear from Fig. 6 that cracks did not occur in this testing and that edges are smooth and clearly marked with well shaped imprint. Therefore, values of hardness H_{IT} and elastic modulus E_{IT} of bone cement sample can be taken as valid. Micro indentation method can be used for measuring of elastic modulus and hardness of prepared bone cement mixtures in a short period of time.

5. CONCLUSION

Characterization of bone cement to cyclical loading is extremely significant and is a subject of many ongoing studies. Studies showed that one of the main reasons of cement failure mechanism is related to fatigue failure and fatigue crack propagation. Indentation represents flexible mechanical testing due to its simplicity, minimal specimen preparation and short time needed for tests. Devices with depth sensing possibilities, such as CSM Nano Indentation Tester, enable determination of hardness, elastic modulus, plastic stress-strain behavior and/or creep behavior directly using the tester, without the need to measure contact impressions.

Results obtained within this study were fully comparable with the literature data found for PMMA and commercial bone cements. Micro indentation method can be used for measuring of elastic modulus and hardness of prepared bone cement mixtures. Very important feature of CSM Micro indenter is automatic recording of optical photographs of realised imprints.

REFERENCES

[1] J. Black, G. Hastings, Ed., Handbook of Biomaterial Properties, Chapman & Hall, 1998

[2] P.A. Revell, Editor, Joint replacement technology, Woodhead Publishing Limited, 2008

[3] J. D. Enderle, J.D. Bronzino, S. M. Blanchard., Introduction to biomedical engineering, Elsevier Academic Press, 2005

[4] R. J. Kane, W.Y. James, J. Mason, R.K. Roeder, Improved fatigue life of acrylic bone cements reinforced with zirconia fibers, Journal of the Mechanical Behavior of Biomedical Materials, Vol. 3, (2010) 504-511

[5] Y.H. Nien, C. Huang, The mechanical study of acrylic bone cement reinforced with carbon nanotube , Materials Science and Engineering: B, Vol. 169 (2010) 134-137

[6] M. Kutz Editor, Biomedical Engineering and Design Handbook, Vol. 1, McGraw-Hill, 2009

[7] Lu Z, McKellop H., Effects of cement creep on stem subsidence and stresses in the cement mantle of a total hip replacement, Journal of Biomedical Materials Research, 34 (1997) 221–226

[8] S. L. Evans, Fatigue of PMMA Bone Cement, Fracture of Nano and Engineering Materials and Structures, B., Springer, DOI: 10.1007/1-4020-4972-2_133, pp. 271-272, 2006

[9] Arola D, Stoffel KA, Yang DT., Fatigue of the cement/bone interface: the surface texture of bone and loosening, Journal of Biomedical Materials Research Part B: Applied Biomaterials, 76B: 287–297, Wiley Periodicals, 2005

[10] G. Lewis, Fatigue Testing and Performance of Acrylic Bone-Cement Materials: State-of-the-Art Review, Journal of Biomedical Materials Research Part B: Applied Biomaterials, 66B: 457–486, Wiley Periodicals, 2003

[11] D. A. Gorham, A. D. Salman, M. J. Pitt, Static and dynamic failure of PMMA spheres, Powder Technology, Vol. 138, (2003) 229-238

[12] B. J. Briscoe, A. Chateauminois, T. C. Lindley, D. Parsonage, Contact damage of poly(methylmethacrylate) during complex microdisplacements, Wear, 240 (2000) 27-39

[13] T. A. Stolarski, H. Williams, Mode of loading and contact configuration effects in the wear of polymers, Journal of Applied Polymer Science, 61 (1996) 1217–1222

[14] D. Arola, K. A. Stoffel, D. T. Yang, Fatigue of the Cement/Bone Interface: The Surface Texture of Bone and Loosening, Journal of Biomedical Materials Research Part B: Applied Biomaterials, Vol. 76B (2005) 287-297

[15] A. Gouldstone, N. Chollacoop, M. Dao, J. Li, A.M. Minor, Y.L. Shen, Indentation across size scales and disciplines: Recent developments in experimentation and modeling, Acta Materialia, Vol. 55 (2007) 4015-4039

[16] F. Petit, V. Vandeneede, F. Cambier, Relevance of instrumented micro-indentation for the assessment of hardness and Young's modulus of brittle materials, Materials Science and Engineering: A, Vol. 456, (2007) 252-260

Serbian Tribology Society

SERBIATRIB '11

12th International Conference on Tribology

Faculty of Mechanical Engineering in Kragujevac

Kragujevac, Serbia, 11 – 13 May 2011

THE INFLUENCE OF VARIOUS PROCESS PARAMETERS ON COEFFICIENT OF FRICTION ON DIE AT IRONING OF AlMg3 SHEET METALS

D. Adamović[1], M. Stefanović[1], S. Aleksandrović[1], M. Živković[1], Z. Gulišija[2]

[1]Faculty of Mechanical Engineering in Kragujevac, s. Janjic 6, 34000 Kragujevac, Serbia, adam@kg.ac.rs

[2]Institute for Technology of Nuclear and other Raw Materials (ITNMS), Franše d' Eperea 86, 11000 Belgrade, Serbia

Abstract: *Friction coefficient on die side is extremely important in ironing process. Drawing force value, and therefore the power consumed for process performance, will depend on it. That opens up a great number of specific problems, such as: change of friction coefficient on sliding path, significance of tool roughness and its interaction with initial and then varied roughness of material being formed, course of wear process and possible local welding (appearance of "galling"), possibility for lubrication and its quality etc. In the closed system tool-lubricant-material,numerous tribological factors are present, most of which can be varied throughout the process, and during particular interaction, which makes the entire problem extremely complex.*

The obtained results indicate complex influence of selected analysed parameters of ironing process on coefficient of friction on die side.

Key words: *Ironing, Friction coefficient, Dispersion analysis, Aluminium alloys*

1. INTRODUCTION

Friction at cold plastic forming, which occurs on contact surfaces of tool and forming object, is considerably different from sliding friction between different machine elements or other elastically strained couples. Investigation of friction and formulating of particular parameters is of extreme importance, both from the aspect of determining necessary forming forces, forming energy, tool wear intensity and formed parts quality and from the aspect of guiding the process of plastic material flow, distribution of strains which occur, material formability etc. These specific properties mainly arise from the fact that very high working pressures appear on contact surfaces in cold plastic forming processes – much higher pressures than those which occur in hot forming or at relative machine elements travel.

In cold plastic forming, the size of contact surface changes during the process, which means that material parts which were not in contact in the previous phase now come in contact with the tool. This and other circumstances open up a series of specific problems, such as: change of friction coefficient in plastic forming conditions, significance of tool roughness and its interaction with initial and then varied roughness of material being formed, strikingly great differences in mechanical properties of material, course of wear process and possible local welding (appearance of "*galling*"), possibility for lubrication and its quality etc [1,2].

Cold plastic forming processes are characterized by unity of positive and negative influence of outer friction forces; on some areas of contact of tool and material, friction should be intensified (e.g. on movable die surface in indirect extrusion, on punch surface in ironing, etc..), and in some other zones (in general, on almost all surfaces) friction forces must be reduced by lubrication as much as possible. This is possible due to new materials for tools with special coatings of increased hardness and also due to very efficient lubricants.

In the closed system tool-lubricant-material numerous tribological factors are present, most of which are variable during the process and are in a particular interaction, which makes the entire problem extremely complex. These factors can be observed from macro-geometrical, rheological or some other aspect. Some factors which are very important are: properties of tool material and material being formed, thermal problems (temperature, heat transfer, …), micro- and macro-properties of forming process, relation of contact and free surface of the piece, friction properties, lubricant and lubrication method properties, contact surface roughness and its orientation, plasticity, fatigue, adhesion, diffusion, wear, stress and strain distribution, sliding speed, remaining stresses, damages, physical-chemical properties, condition of surface etc [3].

Everything aforesaid indicates that the influence of tribological factors on cold plastic forming process is extremely important and had been the subject of investigations of many researches in the previous period, in both real processes and tribo models [4,5]. Since the investigations in production conditions are considerably more complicated and more expensive in relation to model investigations, they are rarely applied. Modelling of tribological conditions implies satisfying of the minimum of necessary criteria considering the following: similarity of stress-strain properties, temperature-speed conditions, properties of surfaces of tools and forming object and status of their contact during forming, which will be the objective of this paper.

2. EXPERIMENTAL INVESTIGATIONS

The original model of strip ironing device for experimental investigations in this paper has been developed at the Faculty of Mechanical Engineering in Kragujevac. It imitates the zone of contact with die and punch [6] with double-sided symmetry during modelling of ironing. This device enables the realisation of high contact pressures and respects physical and geometrical conditions of real process (material of die and punch, contact surfaces topography, different semi-angle of die cone – α etc). The scheme of strip ironing device, with presentation of forces which act upon the work piece, i.e. die and punch, as well as specimen shape, is shown in Figure 1.

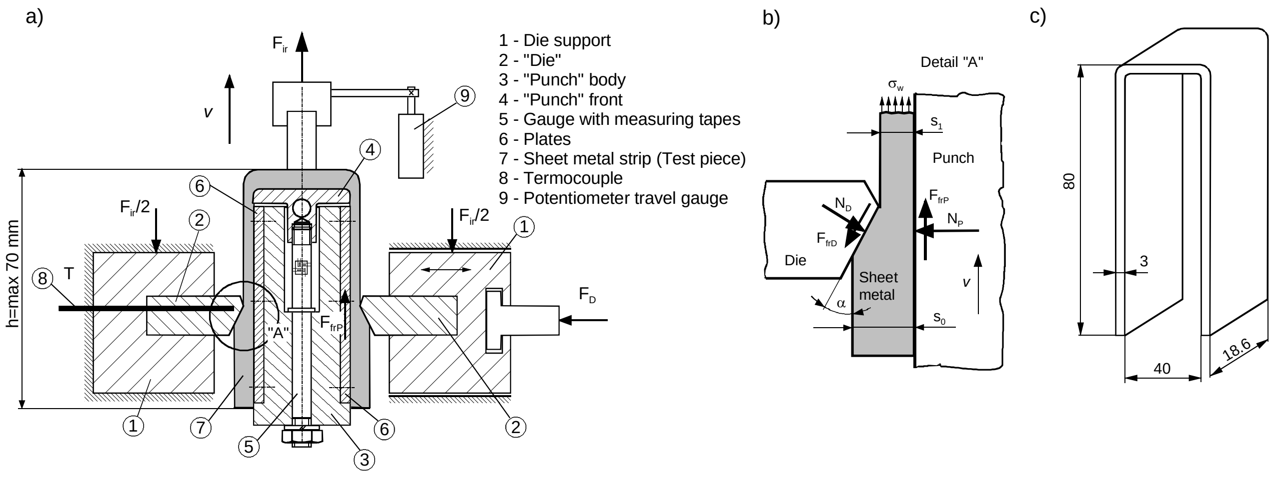

Figure. 1 Scheme of strip ironing device with measuring chain for data acquisition (a), presentation of forces in deformation zone (b) and specimen shape (c)

Strip ironing device is installed on the hydraulic press for investigation of thin sheet metals – ERICHSEN 142/12. The main drive of the machine is used for production of ironing force (force F_{ir}), whereat the second action is the pressure on strip specimen (force F_D). Sheet metal strip 7 is bent (Figure 1c) and placed on the “punch”. Dies 2 are placed in supports, whereat the left support is motionless, and the right one is movable together with the die.

The divided punch consists of body 3 and front 4 which are inter-connected by gauge with measuring tapes 5. The strip is ironed between dies due to the effects of force F on the punch front. Throughout ironing, the outer surface of strip slides over die surface, which is skewed at an angle α. The inner surface of strip slides over plates 6, fixed onto the punch body. During the construction of strip ironing device, the main idea was to enable determining of friction coefficient, both on die side and on punch side at various contact conditions.

Total ironing force F_{ir} represents the sum of friction force F_{frP} between punch and work-piece, and force that acts upon the test specimen bottom, F_w (Figure 1), that is:

$$F_{ir} = F_{frP} + F_w \tag{1}$$

Force F_{ir} is measured on the machine, and friction force on punch side F_{frP}, is registered with the gauge with measuring tapes.

Friction coefficients on punch (μ_P) and die (μ_D) sides can be calculated by equations:

$$\mu_P = \frac{F_{frP}}{2 \cdot F_D} \quad (2)$$

$$\mu_D = \frac{F \cdot \cos\alpha - 2 \cdot F_D \cdot \sin\alpha}{F \cdot \sin\alpha + F_D \cdot \cos\alpha} \quad (3)$$

The process of pieces manufacturing by ironing is influenced by many factors. They can be divided into four main groups [3]:

- Influential factors which depend on forming object (material, dimensions and piece form),
- Influential factors which depend on tools,
- Influential factors which depend on machine, and
- Influential factors that depend on contact conditions (tribological conditions).

By reviewing the forming process and influential factors for all elements which take active participation in the process, the programming of investigation towards optimisation of the production process is performed, both from the aspect of forming object quality and from the aspect of productivity increase and production cheapening.

Considering the large number of influential factors and their interaction, it is not always possible to perceive clearly the individual influence of each factor on output process properties. In laboratory investigations, especially investigations on models, many influential factors cannot be taken into consideration, which requires extreme caution when making conclusions about the influence of particular influential factors.

Based on analysis of researches and preliminary investigations so far, the following factors, which will be the subject of experimental investigations, were selected:

- Type of investigated material (1 level – AlMg3),
- Die gradient angle, α (4 levels - α=5°; 10°; 15°; 20°),
- Tool material (die/punch), (4 levels - TS/TS; Cr/Cr; TiN/TiN; HM/TS),
- Punch roughness, expressed by mean height of roughnesses R_a (3 levels - Ra=0.01; 0.09; 0.4 µm, which corresponds to surface qualities N1; N3; N5 respectively),
- Type of lubricant on die side (1 level – L5 (paraffin based oil with special additives)),
- Type of lubricant on punch side (1 level - L4 (non-emulsifying mineral oil with mild EP properties)),
- Blank holding force (3 levels - F_D = 8.7 ; 17.4 ; 26.1 kN),
- Forming speed (1 level – v = 20 mm/min).

In addition to specified influential parameters, there is a large number of others such as: polishing zone height, punch radius, thickness of work piece bottom, number of dies for drawing, ratio of inner and outer piece diameter, ratio of dies diameters in multistage tool, ratio of height and diameter of work piece etc. [7]. They were not included in this experiment due to objective reasons.

Mechanical properties of aluminium alloy AlMg3 (DIN: AlMg3 F24) are listed in Table 1.

Table 1. Mechanical properties of strip material

Material - AlMg3		
Mechanical properties		
R_p = 201.1 MPa,	R_m = 251.0 MPa,	
R_p/R_m = 0.801,	A = 12.0 %	
n = 0.13545,	r = 0.40510	E = 0.701×10^5 MPa

3. EXPERIMENTAL RESULTS

Friction coefficient on die side is extremely important in ironing process. Drawing force value, and therefore the power consumed for process performance, will depend on it.

Change of friction coefficient on sliding path can be classified into six characteristic types (figure 2):

I. constant,
II. mildly increasing,
III. mildly decreasing,
IV. unstable (wavy),
V. untypical and
VI. intensively increasing

Such classification is in line with the one given in some papers [8,9,10].

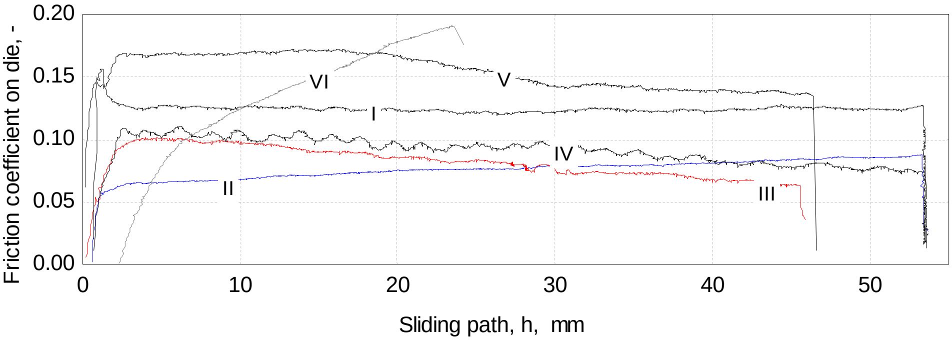

Figure 2. Types of changes of friction coefficient on die

For analysing the influence of all adopted parameters on ironing process, the principle of measuring drawing force and friction force on punch was adopted; therefore, for each investigated sample (test specimen) there is a recorded diagram of change of specified forces in dependence on punch travel (sliding path).

The obtained results were analysed statistically. Since the experiment was performed as multifactor one, dispersion analysis made it possible to determine the influence of particular factors and to determine their interaction towards analysed variable (value). In some cases, further analysis was performed within the very factor in order to determine the best (most favourable) level of that factor for analysed variable (value). The specified additional analysis was performed by comparing mean values by applying Duncan's range test (*Duncan's multiple range test*) [11].

Performed dispersion analysis of the influence of particular factors and their interaction towards friction coefficient on die is given in fig 3. This figure also gives the list of factors whose influence is monitored, as well as the number (in brackets) and mark of the level.

The influence of particular factors and their interaction are estimated based on values of F-test, determined for proper level of credibility (p-level) for which the critical value $\alpha = 0.05$ was taken. This means that one factor or interaction of some factors influences the analysed value of p-level<α=0.05 [11]. The size of influence will be determined by value of F-test, whereat higher value of F-test indicates a stronger influence on analysed value.

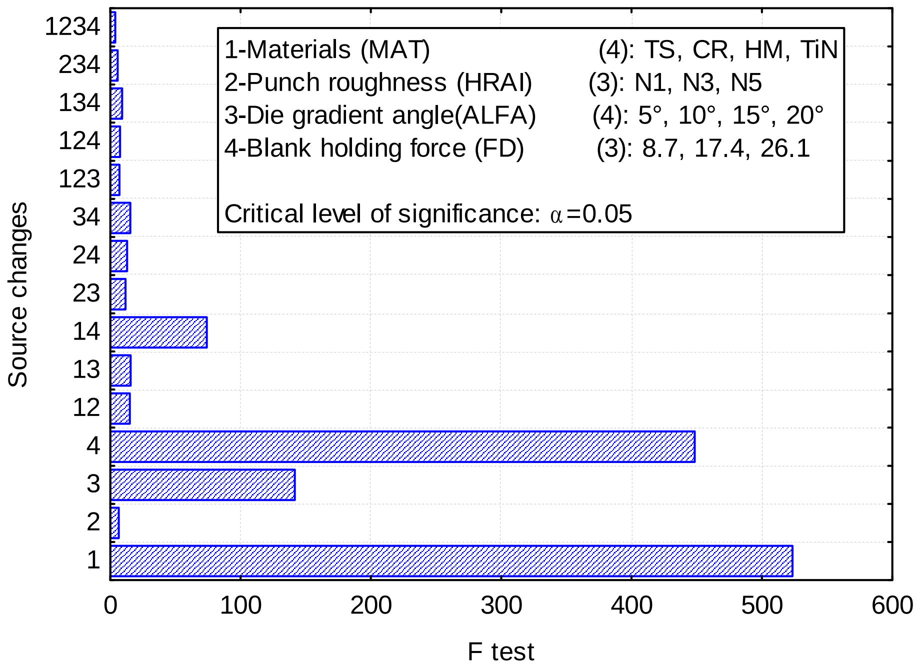

Figure 3. F test

The results of dispersion analysis of factors (tool material, punch roughness, die gradient angle and blank holding force) which influence the friction coefficient on die side (Figure 3), show that the tool material has the biggest influence on friction coefficient on die side (change source 1). The reason for this is the fact that aluminium has a great tendency to adhere to some tool materials. In addition, blank holding force influence is very prominent (change source 4), as well as somewhat smaller influence of die gradient angle (change source 3). Regarding factors interaction, the one between tool material and blank holding force is the most prominent (change source 14). Other interactions are statistically significant, but much smaller. The influence of roughness (change source 2), as shown by dispersion analysis, is very small in comparison with other factors.

The analysis of mean values (table 2) of friction coefficient on die side showed that the smallest value will be obtained by using alloyed tool steel (TS), and the biggest value by using tool with coating TiN. The differences between friction coefficient obtained with hard metal tools (HM) and tools with hard chrome coating (Cr) are statistically insignificant. Considering a very small importance of punch roughness, significant differences were established only between roughnesses N1 (Ra=0.01μm) and N5 (Ra=0.4). In addition to that, Duncan test showed that there are significant differences between all levels of blank holding force and die gradient angle.

Table 2. Analysis of mean values

Duncan test; FRICTION COEFFICIENT ON DIE SIDE - MIM (μ_D)
Mean values analysis
Critical level of significance: α = 0.05

MATERIAL: AlMg3

FACTOR: TOOL MATERIAL (MAT)

	{1} .1027846	{2} .1464502	{3} .1499008	{4} .1872871
AC .... {1}		.000009	.000011	.000003
CR .... {2}	.000009		.106364	.000011
TM .... {3}	.000011	.106364		.000009
TIN .... {4}	.000003	.000011	.000009	

FACTOR: PUNCH ROUGHNESS (HRAI)

	{1} .1499408	{2} .1466464	{3} .1432299
.... N1 .... {1}		.075044	.000426
.... N3 .... {2}	.075044		.064870
.... N5 .... {3}	.000426	.064870	

FACTOR: DIE GRADIENT (ALFA)

	{1} .1431109	{2} .1514303	{3} .1675481	{4} .1243334
.... A1 .... {1}		.000106	.000011	.000009
.... A2 .... {2}	.000106		.000009	.000011
.... A3 .... {3}	.000011	.000009		.000003
.... A4 .... {4}	.000009	.000011	.000003	

FACTOR: BLANK HOLDING FORCE (FD)

	{1} .1780849	{2} .1358248	{3} .1259073
.... D1 {1}		.000009	.000011
.... D2 {2}	.000009		.000009
.... D3 {3}	.000011	.000009	

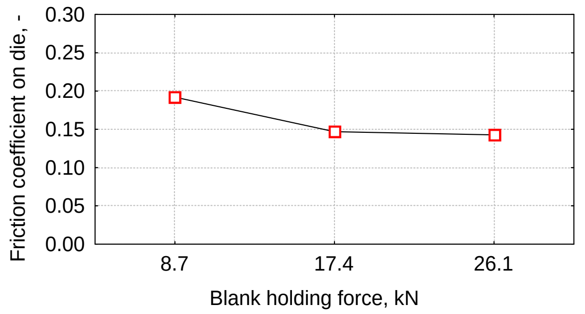

Figure 4. Dependence of friction coefficient on die on blank holding force

The change of mean values of friction coefficient on die side in dependence on blank holding force is shown in figure 4. With the increase of blank holding force, the friction coefficient decreases. That decrease, for bigger blank holding forces, is somewhat less intensive than for smaller blank holding forces.

Dependence of friction coefficient on blank holding force at various levels of analysed factors is shown in figures 5 to 7.

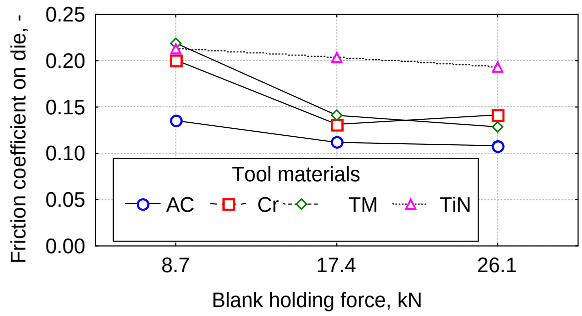

Figure 5. Change of friction coefficient on die in dependence on blank holding force for various tool materials

The change of friction coefficient on die side, in dependence on blank holding force, for different tool materials, is given in figure 5. The smallest friction coefficient was obtained with AC tool, and somewhat higher values were obtained with tools Cr and TM (figure 5). Much higher values were obtained by using TiN tool. It should be mentioned once again that the tool with TiN coating had a partly damaged coating, which could have been the reason for obtaining bigger values of friction coefficient.

As shown previously by Duncan test, significant difference in influence of roughness level on friction coefficient on die (curves in figure 6 for all punch roughnesses almost coincide) was observed only between roughnesses N5 and N1 (figure 6).

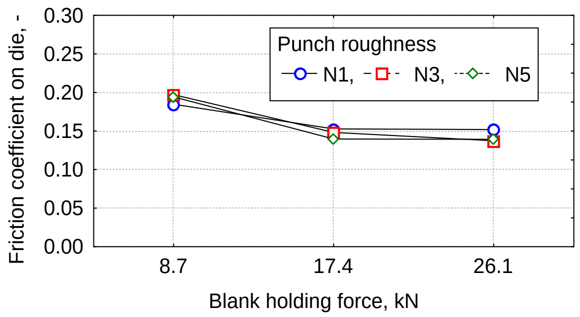

Figure 6. Change of friction coefficient on die in dependence on blank holding force at various punch roughnesses

The smallest friction coefficient, for all blank holding forces, was obtained with die gradient angle of 20° (figure 7).

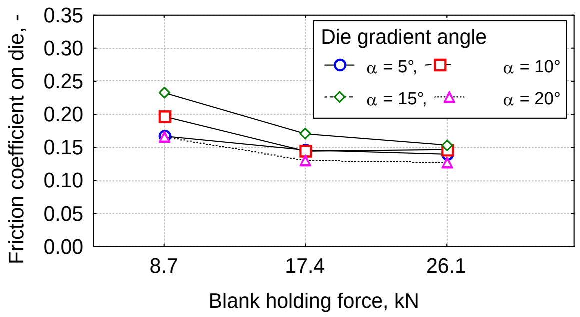

Figure 7. Change of friction coefficient on die in dependence on blank holding force at various die gradient angles

The change of friction coefficient on die, in dependence on die gradient angle, is shown in figure 8. The highest value of friction coefficient is obtained at die gradient angle of 15°.

Figure 8. Change of friction coefficient on die by die gradient angle

Figures 9 to 11 show the change of friction coefficient on die in dependence on die gradient angle at various levels of analysed factors.

Out of all die gradient angles, the best results were obtained for alloyed tool steel die, while somewhat higher values of friction coefficient were obtained with tools with chrome coating and hard metal. Out of all die gradient angles, the worst results were obtained for tool with titanium-nitride coating (Figure 9).

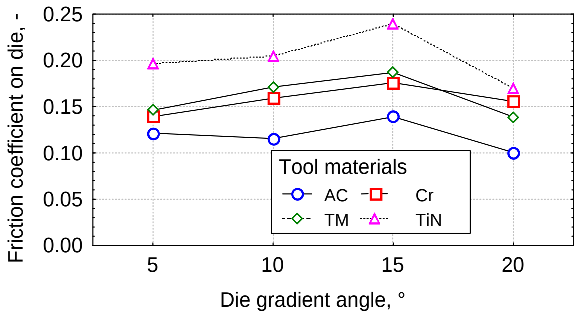

Figure 9. Change of friction coefficient on die in dependence on die gradient angle at various tool materials

The change of friction coefficient in dependence on die gradient angle is shown in figure 10. Here as well, it is obvious that the influence of punch roughness level on friction coefficient is very small.

Diagrams in figure 11 show that higher values of friction coefficient will be obtained at smaller blank holding forces regardless of die gradient angle.

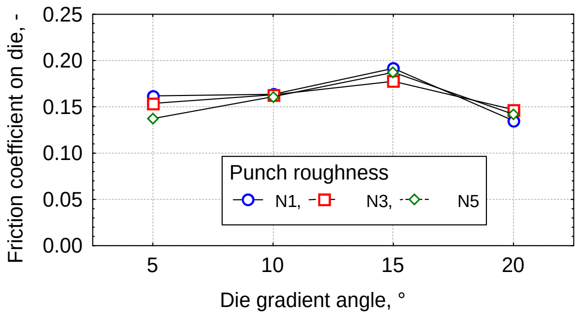

Figure 10. Change of friction coefficient on die in dependence on die gradient angle at various punch roughnesses

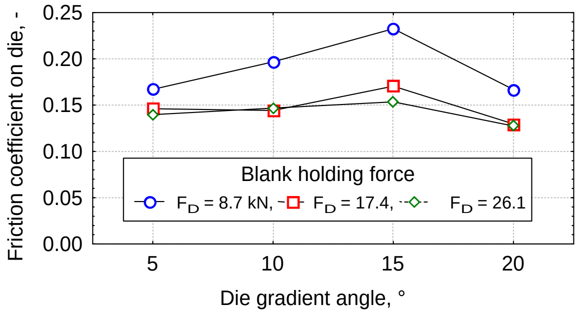

Figure 11. Change of friction coefficient on die in dependence on die gradient angle at various blank holding forces

Friction coefficients for various tool materials are shown in figure 12. The smallest value of friction coefficient was obtained by using tool made of alloyed tool steel. Somewhat higher values of friction coefficient were obtained with alloyed tool steel (TS) and chrome coating (Cr), as well as with hard metal, and the highest values were obtained with tool made of titanium-nitride coating (TiN).

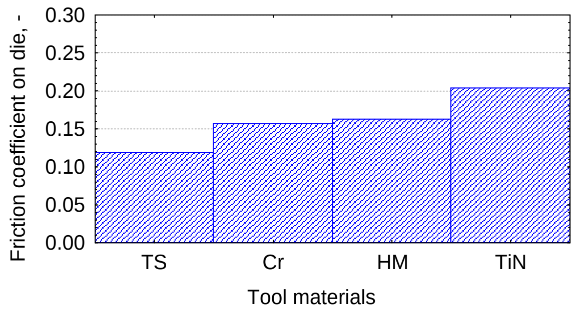

Figure 12. Friction coefficient on die for various tool materials

As established previously by dispersion analysis, friction coefficient will depend on punch roughness very little, which is shown by diagram in figure 13.

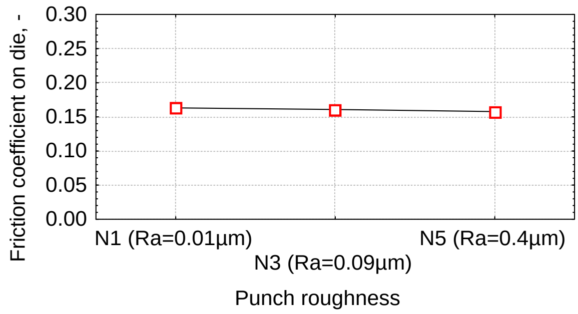

Figure 13. Change of friction coefficient on die in dependence on punch roughness

4. CONCLUSION

Friction coefficient on die side plays an important role in ironing process. Drawing force value, and therefore the power consumed for process performance, will depend on it. The appearance of six different types of change of friction on proper sliding path was observed. Which of those change types will appear depends on the type of tool material, especially type of lubricant and its physical properties.

Performed dispersion analysis shows that tool material has the most prominent influence on friction coefficient on die side. The reason for this is the fact that aluminium has a great tendency to adhere to some tool materials. The influence of blank holding force and die gradient angle is also very prominent here. Regarding factors interaction, the most prominent is the one between tool material and blank holding force. Other interactions are statistically significant but considerably weaker.

REFERENCES

[1] Dohda K. (1990a), Saito M., Saiki H., Kawai N.: Tribology in the Ironing Process of Aluminium Cans, Advanced Technology of Plasticity, Proceedings of Third International Conference on Technology of Plasticity, Vol. 3, Kyoto, 1990., 1191-1198

[2] Kawai N. (1980), Nakamura T., Seko S.: The welding mechanism in drawing of aluminium sheet, Journal of Engineering for Industry, Vol. 102, No 8, 1980., 229-238

[3] D., Adamović, M., Stefanović, V., Lazić: Investigation of Parameters which Influence Ironing Process, DEMI 2002, Banja Luka, pg. 166-171.

[4] D., Adamović, M., Stefanović, M., Živković: Experimental Methods for Determining Friction Coefficient at Ironing, DEMI 2007, Banja Luka, 25.-26. 2007. pg. 199-206.

[5] D., Adamović, M., Stefanović, S., Aleksandrović: Modelling of Tribological Processes in Ironing, DEMI 2009, Banja Luka, 2009

[6] Adamović, D.: Behaviour of Materials in Contact in Cold Plastic Forming Processes with High Working Pressures, Doctoral Thesis, Kragujevac, 2002.

[7] Djukić H., Popović P.: Influential Parameters in Process of Drawing with Wall Thickness Reduction, XIV Conference on Production Engineering of Yugoslavia, Čačak, 1980., 11-19

[8] D., Adamović, M., Stefanović, M., Živković, V., Lazić: Influence of Various Parameters on Drawing Force at Ironing, 31. Conference on Production Engineering, Kragujevac, 19.-21. September 2006. pg. 171-180.

[9] D., Adamović, M. Stefanović, V., Lazić, M., Živković: Investigation of Types of Change of Friction Coefficient on Sliding Path at ironing, YUTRIB '05, Kragujevac, 2005., pg. 738-744.

[10] Kawai N.: Laboratory simulation for galling in metal forming, metal transfer and galling in metallic systems, Proc. Conf. Orlando, Florida, Metal.. Soc. AIME, 1987., 63-86

[11] StatSoft, Inc.: STATISTICA for Windows, Computer program manual, Tulsa, OK, USA, 1995.

Serbian Tribology Society

SERBIATRIB '11

12th International Conference on Tribology

Faculty of Mechanical Engineering in Kragujevac

Kragujevac, Serbia, 11 – 13 May 2011

THE TRAVERSE SPEED INFLUENCE ON SURFACE ROUGHNESS IN ABRASIVE WATERJET CUTTING APPLICATIONS

J.Baralić[1], B.Nedić[2], P.Janković[3]

[1] University of Kragujevac, Technical Faculty Čačak, Serbia, jbaralic@tfc.kg.ac.rs
[2] University of Kragujevac Faculty of Mechanical Engineering, Serbia, nedic@kg.ac.rs
[3] University of Niš, Faculty of Mechanical Engineering, Serbia, jape@masfak.ni.ac.rs

Abstract: *Abrasive water-jet (AWJ) machining is an unconventional method of machining. In all stated options, the machining mechanism is based on erosion of the material uppon which the jet hits. The fact that no major rise in temperature occurs at machining in the processing zone is a huge advantage of this machining method. This study is focused on the surface roughness of abrasive water-jet (AWJ) cut surfaces. In the study is explained the influence of traverse speed on the machined surface roughness. In the presented study, Č4580 was machined under varying traverse speeds of 10 to 70 mm/min by abrasive water-jet machining. After machining, the machined surfaces were examined and surface roughness was measured. The experimental results indicate that the traverse speed is a parameter with significant influence on the surface roughness. It was observed that the surface roughness increases with increasing traverse speed.*

Keywords: *Abrasive water-jet, surface, roughness, traverse speed, Č4580*

1. INTRODUCTION

The faster the development of new production technologies is, the greater challenges face the scientists. Requirements regarding accuracy of shapes and measurements of the final products are becoming more demanding. Furtermore, specific requirements concerning complexity of the shape of the product have recently been set. Therefore, unconventional machining methods have been more frequently applied in modern production. Nowadays, the increasing number of reaserches are conducted in the field of unconventional machining methods with the purpose of obtaining the fastest, the cheapest and high quality machining method.

When selecting the appropriate technology, the most significant features that affect the final decision are the quality of the machined surface and the time required for the design of a product. The quality of the machined surface, during the cutting process, is a complex concept which covers changes of characteristics of material, structure, and size of the defect layer, roughness of the machined surface and geometrical characteristics of the cut. Due to the fact that sometimes it is impossible to satisfy all these criteria in practice, some of them are neglected depending on the required result. The quality of the cutting process can be evaluated through measuring certain characteristics such as roughness of the machined surface, through satisfying demands of tolerance, parallelism of the cut sides and their normality to the base surface [1].

2. ABRASIVE WATER-JET MACHINING

Abrasive water-jet machining is one of the newest unconventional machining methods. This type of machining has significantly changed metal machining industry. Abrasive water-jet makes possible the accurate designing of the parts with complex contours and high quality machined surface in a very short period of time. No temperature increase in the cutting zone, the possibility of complex contours design and no occurrence of residual stress in the cutting zone characterize this machining. Thus, the abrasive water-jet machining has been significantly developed recently. AWJ machining is most frequently applied in profile cutting of various slab-like materials. This machining method is very convenient for the design of different types of materials. Furthermore, abrasive water-jet machining is economic and eco-friendly.

Continuous development of high pressure water-jet machining was initiated in the first half of the twentieth century. However the addition of abrasive material to the water-jet extended the range of machinable materials significantly. Higher machining speed and accuracy as well as higher quality of the machined surface were also achieved.

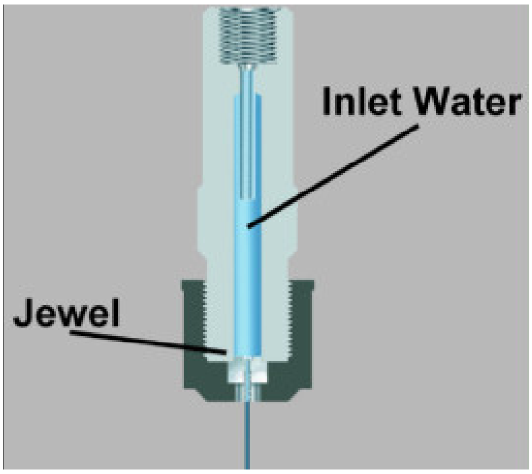

a)

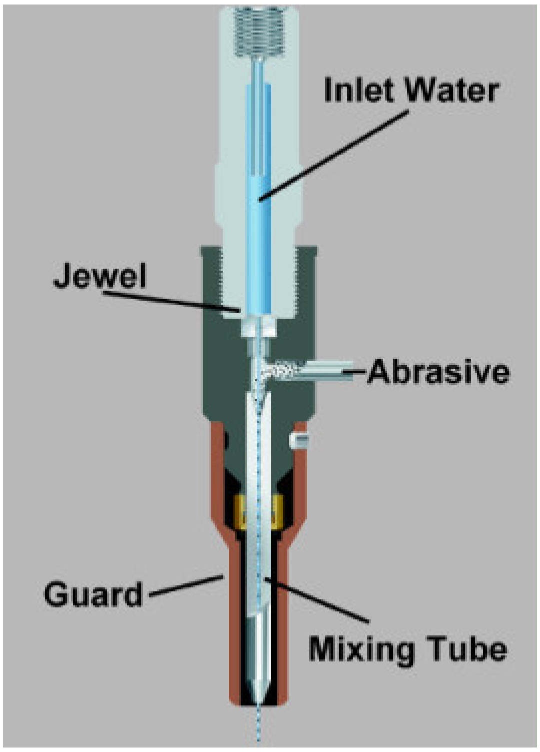

b)

Figure 1. Schematic diagram of water-jet machining without abrasive material a) and with abrasive material b) [2]

The most frequent operations carried out through this type of machining are: cutting, polishing of surfaces, cleaning of surfaces, etc.. In the stated options, the machining mechanism is based on erosion. A particular advantage of this machining method is the fact that no significant temperature increase occurs in the machining zone. A schematic diagram of water-jet machining without abrasive is shown in Figure 1. a), whereas abrasive water-jet machining is displayed in Figure 1 b). Modern installations for abrasive water-jet machining function if the water pressure is above 5000 bar, and the water-jet reaches the speed of 1400 m/s.

Abrasive water-jet machining is based on the erosion process as the main mechanism of the workpiece material removal. Workpiece material removal is a continuous process beginning with the impact between the abrasive particle and the material, which causes the removal of a very small amount of the workpiece material. The number of the abrasive particles striking the workpiece material in one second amounts to ten thousand [3].

3. SURFACE MACHINED WITH ABRASIVE WATER-JET

The biggest problem during abrasive water-jet machining is unevenness of the machined surface quality. The unevenness is manifested in different values of the machined surface roughness parameters, deviations of the machined surface from the vertical plane and the occurrence of the surface waviness and curved lines (striae) on the machined surface. All the above mentioned issues greatly affect limitation on the application of the abrasive water-jet machining. Nevertheless, no study that offers complex estimation of the surface topography depending on the parameters of machining mode has been conducted.

The basic characteristic of the surface machined with abrasive water-jet is the duality of the surface. The upper zone of the surface machined with abrasive water-jet (jet entery side) shows significantly less roughness compared to the lower zone of the machined surface. The end of the upper surface zone is usually called smooth cutting zone. The occurence of waveness, curved lines, and increasing roughness of the machined surface, is more frequent beyond the smooth cutting zone. During the penetration of abrasive water-jet through material, kinetic energy of abrasive particles decreases, which causes retardation of the cutting front of the jet. Y_{ret} (Figure 2). Retardation of the cutting front of the abrasive water-jet and loss of its energy bring about the occurence of curved lines on the machined surface and the change of quality of the machined surface, i.e. the change of the roughness of the machined surface for different depths of the cut.

Roughness of the machined surface, i.e. its change depending on the depth of cut is the most important parameter for the estimation of the effect of certain machining parameters on the quality of the machined surface. Many authors state that the analysis of surface topography provides key informaton about the mechanism of abrasive water-jet machining. Figure 2. shows the characteristic appearance of the surface machined with abrasive water-jet and the quality change in machined surface depending on the depth of cut.

Ra parameter is the main parameter that defines the quality of the machined surface. Figure 3 shows the change of this parameter and the change of the parameters Rq and Rz.

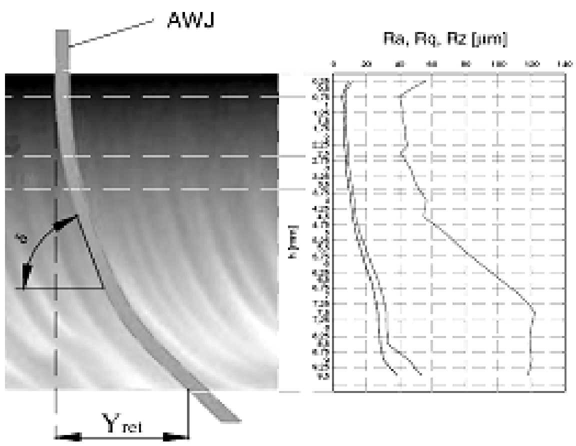

Figure 2. Change in appearance and quality of surface machined by abrasive water-jet for different depth of cut [4]

The quality of the machined surface is affected by cutting modes during abrasive water-jet machining, such as operative pressure, the amount of abrasive, traverse speed, etc.. This machining is also characterised by the change of width of the cut depending on the machining parameters. All the irregularities affect the limited application of this type of machining in industry. Figure 3. shows the appearance of the cut, i.e. the change of the width and conicality of the cut depending on the change of traverse speed.

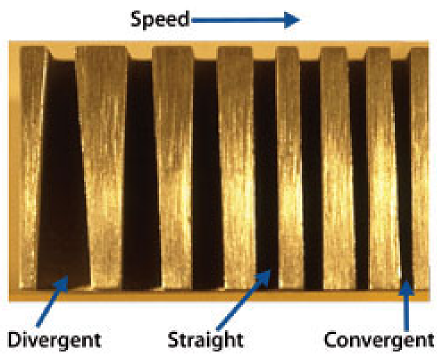

Figure 3. Appearance of cut for different traverse speed [2]

As far as the quality of the machined surface is concerned, five distinctive classification groups can be discerned (Figure 4.). The machined surface which is at Q1 quality level is characteristic for rough cutting of workpieces at high traverse speed. An additional force is necessary to bring about the separation of the cut workpieces. The machined surface requires further machining.

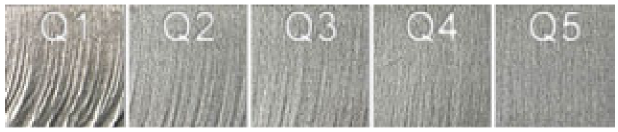

Figure 4. Five characteristics of machined surface quality [2]

Q2 machined surface quality is obtained during the cutting process of workpiece (the parts are completely separated), and in most cases further machining is necessary. Q3 machined surface quality is more demanding than the previous two. In order to reach high quality of the machined surface it is necessary to adjust traverse speed, operating pressure, abrasive water jet speed and the amount of the abrasive material. Such machining modes enable the production of the certain fixed parts, i.e. further machining is not necessary depending on their purpose. Q4 machined surface quality is higher than Q3 machined surface quality. At this quality level, many parts can be designed without additional machining. Q5 machined surface quality is very high and it is achieved in high accuracy parts but at very low traverse speeds wherein the machining time is not the criterion for the selection of the cutting mode. The width of the cut is constant at both upper and lower parts of the machined surface.

4. TRAVERSE SPEED EFFECT ON THE QUALITY OF THE MACHINED SURFACE

All irregularities of the machined surface, obtained either by standard or unconventional machining method (laser, plasma, abrasive water-jet) are characteristics of the machined surface and they are accurately standardized. The subject of the research is roughness of the surface machined with abrasive water-jet and the effect of traverse speed on the machined surface.

The quality of the surface machined by the abrasive water-jet can be influenced by system operational process parameters such as water-jet pressure, abrasive flow rate, standoff distance, depth of cut, angle of cutting, and traverse speed [5]. The effect of certain parameters is different. Majority of authors agree that the greatest impact on the surface quality have traverse speed, operating pressure and amount of abrasive material.

Traverse speed of the jet has a strong effect on the surface finish of the workpiece and material removal rate [6]. Therefore, it is necessary to identify the connection between the quality of the machined surface and traverse speed.

Figure 5. shows the typical relation between traverse speed and machined surface roughness. With an increase of traverse speed, roughness will increase significantly. The diagram refers to the analysis conducted on aluminium [7]. The diagram displays the relation between traverse speed and roughness: at low traverse speed no significant difference in roughness of the machined surface occurs with the change in depth of cut, whereas at higher traverse speed (around 2mm/s), the diffrence becomes obvious.

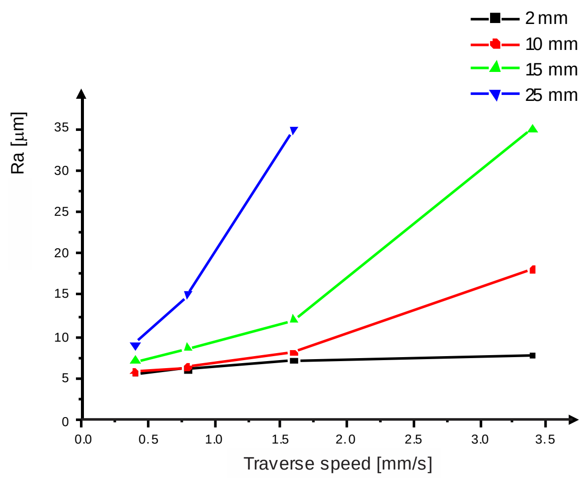

Figure 5. Effect of traverse speed on quality of machined surface [7]

In this paper we analyzed the effect of traverse speed on the quality of the machined surface of Č 4580 (AISI 304) stainless steel. Figure 6. shows the appearance of the machined sample surfaces Č 4580 (30 mm thick), with different traverse speed. The Figure indicates that during machining process at traverse speed of 10 mm/min, no significant difference in quality of the machined surface occurs. Neither surface waviness nor curved lines occur. During machining process, with higher traverse speeds, the difference in quality of the machined surface is more distinct and it varies depending on depth of the cut. In order to observe the difference carefully, we carried out the measurement of roughness of the surfaces machined at different traverse speeds (from 10mm/min to 70mm/min). The recommended traverse speed for Č4580 steel (thickness 30mm and Q3 medium machining quality) is 35 mm/min. The values of the remaining parameters of the machining process were kept constant:

- Operating pressure p = 4130bar
- Abrasive flow Qa = 400 g/min
- Abrasive type – garnet, MASH#80

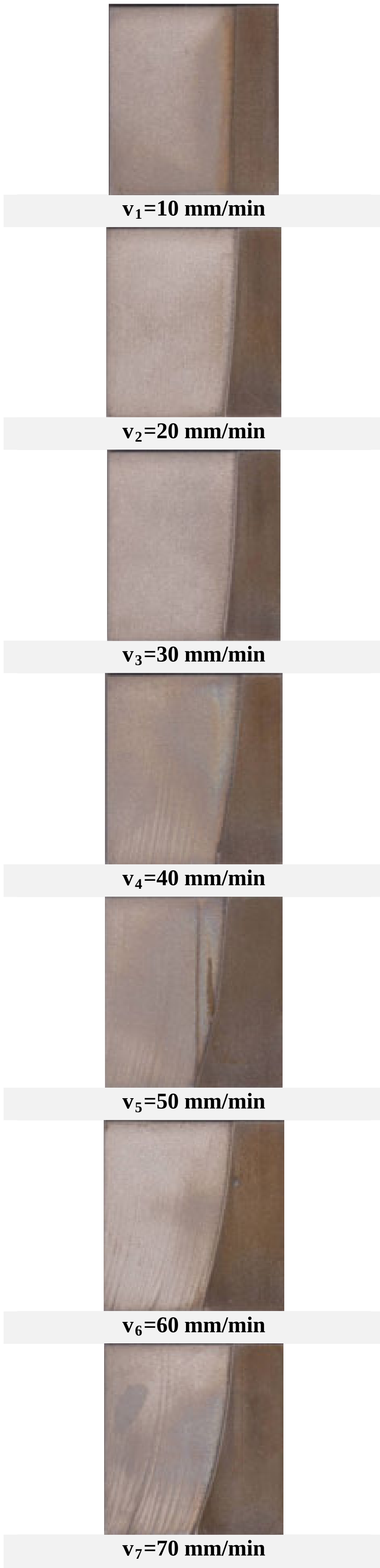

Figure 6. Appearance of machined surface depending on traverse speed

Ra parameter has been considered the most significant for the estimation of machined surface quality. The values of Ra parameter have been measured for different cutting conditions – for 6 different depths of cut: 2,5mm, 7,5mm, 12,5mm, 17,5mm, 22,5mm and 27,5mm, and for 5 different lenghts. Then the mean values of Ra parameter were calculated at the appropriate depth of cut. On the surface machined with traverse speed of 70mm/min, it was impossible to measure Ra. Table 1. displays thus obtained results.

Table 1. Measured values of Ra parameter [µm]

Traverse speed [mm/min]		Depth of measurement [mm]					
		2.5	7.5	12.5	17.5	22.5	27.5
V1	10	1.86	1.57	1.34	1.04	1.29	1.46
V2	20	1.66	1.32	1.35	1.12	1.83	1.64
V3	30	1.43	1.48	1.24	1.43	1.63	1.74
V4	40	1.76	1.56	2.11	2.7	2.76	3.02
V5	50	2.16	1.82	2.89	2.58	2.84	4.52
V6	60	1.94	1.94	2.72	4.34	4.82	5.84
V7	70	1.62	2.32	2.73	4.55		

Thus obtained results are shown in Figure 7. The change in value of Ra parameter has been monitored for different traverse speeds and depths of cut.

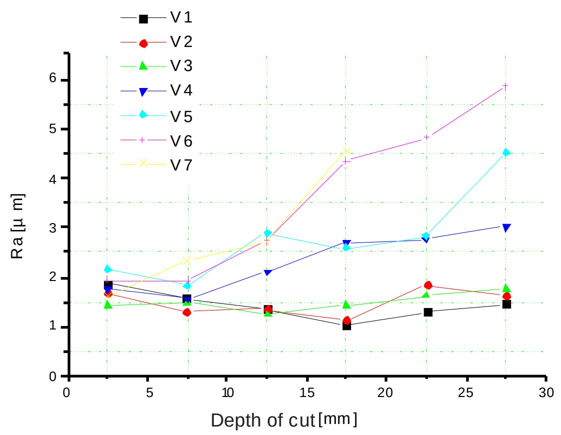

Figure 7. Effect of traverse speed on quality of machined surface of stainless steel Č 4580

Figure 7. indicates that at low traverse speed V1 no significant change in the value of Ra parameter occurs with the change of depth of cut, i.e. Ra parameter is almost constant for every depth of cut and it vaires between 1,04µm and 1,86µm, which can be subsumed under N7 roughness class. During machining process, with higher traverse speed, the change in values of Ra parameter is more distinct and it varies depending on depth of the cut. Furthermore, with low traverse speeds, no significant changes in the value of Ra parameter occur for different traverse speed.

5. CONCLUSION

The paper presents the results of the research concerning the traverse speed effect on the change in surface quality, i.e. the change in Ra parameter. It has been observed that the increase of traverse speed causes the increase in the machined surface roughness. The difference is sharper if the depth of cut is larger, or if the thicker materials are being machined. The value of Ra parameter is almost constant on the entire machined surface, when the traverse speed is low. Therefore, high quality of the machined surface can be achieved through the machining with abrasive water-jet by selecting the appropriate traverse speed.

ACKNOWLEDGMENTS

The authors would like to thank to the Ministry of Science and Technological Development of the Republic of Serbia. Paper is result of technological project TR35034:"The research of modern non-conventional technologies application in manufacturing companies with the aim of increase efficiency of use, product quality, reduce of costs and save energy and materials" which is supported by Ministry of Science and Technological Development of the Republic of Serbia.

REFERENCES

[1] M. Hashish: Characteristics of surfaces machined with abrasive waterjets, J. Eng. Mater. Technol. Trans. ASME, Vol. 113, No. 3, pp.336-354, 1991.

[2] http://www.omax.com/

[3] M. Hashish: A modelling study of metal cutting with abrasive waterjets, J. Eng. Mater. Technol., Vol. 106, pp. 88-100, 1984

[4] J. Valiček, S. Hloch, D. Kozak: Surface geometric parameters proposal for the advanced control of abrasive waterjet technology, Adv Manuf Technol, 41, pp. 323-328, 2009.

[5] J.Valiček, M. Držík, M. Ohlídal, V. Mádr, L.M. Hlaváč: Optical method for surface analyses and their utilization for abrasive liquid jet automation, Proc. of the 2001 WJTA American Waterjet Conference,2001, Minneapolis, pp. 1–11.

[6] E. Lemma: Maximum depth of cut and mechanics of erosion in AWJ oscillation cutting of ductile materials, Journal of Materials Processing Technology, Vol. 160, No. 2, pp.188–197, 2005.

[7] A.W. Momber, R. Kovacevic: Principles of Abrasive Waterjet Machining, Springer, London, 1998.

[8] P. Janković, M. Radovanović: Identifikacija i klasifikacija faktora koji utiču na proces sečenja abrazivnim vodenim mlazom, "IMK-14, istraživanje i razvoj", godina XVI, broj 35, 2/2010, ISSN 0354-6829, Kruševac, Srbija, 2010, s. 71-76

Serbian Tribology Society

SERBIATRIB '11

12th International Conference on Tribology

Faculty of Mechanical Engineering in Kragujevac

Kragujevac, Serbia, 11 – 13 May 2011

RESEARCH ON LIFE PROLONGATION FOR TEMPERATURE SENSORS PLACED IN HIGHLY EROSIVE ENVIRONMENT

Ionescu O.N.[1], Ionescu G.C., Minescu M., Nae I.

[1]Petroleum - Gas University of Ploiesti, Romania, e-mail: ionescu_o_ro@yahoo.com

Abstract: *This study is the results of research on technologies suitable for extending the operational life of temperature sensors placed in highly erosive environment. The need for this research resulted from a request received from a dry mortars factory, operating a sand drying plant. The process of sand drying is automated controlled using the information provided by two temperature sensors. One of these sensors is located inside of the exhaust pipe and was severely eroded in about two months by the quartz sand mixed within the exhaust gases. There it was an attempt to shield the sensor by using a segment of steel pipe; however, the change in the transfer rate of heat generated a significant delay in regulating the system. An alternate solution was studied and the sensor was coated through thermal spray coating with a 0.01 mm layer of Titanium – Zirconium. This solution has been operationally tested and the results showed that there were not troubles due to the heat transfer rate and the operational life of the sensor was prolonged to six months.*

Keywords: *sand drier, abrasion, spray coating, temperature sensors*

1. INTRODUCTION

The sand drying plant used in the commissioned factory uses the phenomenon of fluid bed of material for minimizing the amount of electrical and thermal energy for drying materials. The sand drier see Figure 1 consists of two sections, one for drying the sand (1) and the second for cooling the material (2). The fluid bed of material is generated by a complex system which shakes the bottom part of the drier and realizes a balance between the intake pressure and the exhaust under pressure in each of the section of the sand drier. In the sand drying section the fluid bed is the result of action of the pressure of the hot air generated by the burner (3) and the hot air exhaust fan (4). The hot air is filtered by the first section of the filter plant (5) and released in the atmosphere with content of less than 10000 ppm residues. In the second section, the cooling chamber, the cooling agent is generated by the intake fan (6) and after passing through the cooling chamber it is recycled through the second section of the filter plant and through the fan is used to increase the effectiveness of the burner. The optimum value of the module of the differential pressure which generates the desired fluid bed of material should be established at 1 mbar. The sand drying plant includes an automated control system designed to correlate the temperature of the hot gases into the drying chamber with the quantity of the wet sand feed to the system and to maintain the under pressure required for the fluid bed of material. To protect the filter plant was implemented a system to open a cooling air vane when the temperature is getting over 80 ^{0}C and shutting down the dryer when the exhaust hot gases would reach values over 100 ^{0}C . The sensor used to monitoring the temperature of exhaust gases is PT 100.

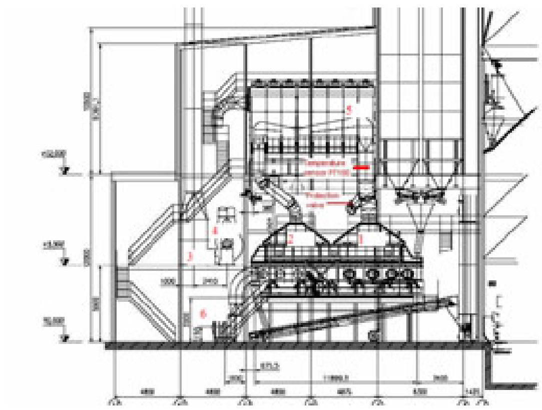

Figure 1. The schematics of Sand drying plant

The experience yielded during the first six months of production and operational tests showed that due to the highly erosive environment the protective tube of PT 100 sensor was severely eroded within 2 months, causing its destruction see Figure 2.

Figure 2. Eroded PT 100 sensor

In order to increase the operational life of the sensor it was studied if possible to add an additional protective tube made off a wear resistant material. To establish the feasibility of this solution the increase of the response time had to be studied. The PT 100 sensor has been already provided with a 4mm protection tube, as presented in Figure 3. According to the PT 100 data - sheet the response time for the 4mm wall thickness protective tube there is a response time of about 6 minutes.

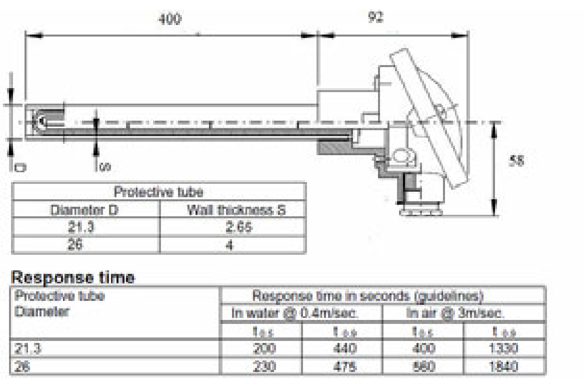

Figure 3. PT 100 temperature sensors technical details [1]

There were conducted mathematical calculations for studying the increase of response time for an additional 4 mm thickness protective tube made of 12Cr 130 (STAS 3583) X 15 Cr 13 (DIN 17440, SEW 400).

Table 1. Chemical composition of steel used for manufacturing the additional shield

Steel	Chemical composition (%)			
	C	Cr	Mn	Si
12Cr130/ X 15 Cr 13	0,09…0,13	12,0…14,0	max. 0,60	max. 0,60

According to the technical documentation [3], there are three methods for calculating heat transmission time, through solid bodies. These methods are considering the main characteristics of heating agent and geometrical characteristics of heated body.

Input data:

a. Thickness of protective tube R = 4 mm;

b. Area of temerature variation for the working environment : $t = (100…400)\ ^0$C;

c. Tipe of material used for protective tube: 12Cr130/ X 15 Cr 13 steel;

1. Calculation method based on heating criterion.

Mathematical formula used for heat transmission time is [3]:

$$\tau_{i,1} = 0.1 \cdot k_f \cdot k_m \cdot k_u \cdot R \text{ (min)} \qquad (1)$$

Where: τ_i is heating time (min), k_f – shape coefficient (based on geometrical shape of studied body – for the studied case- empty cylinder, heated from outside, $k_f = 2$ [3]; k_m – environmental coefficient, characteristic for heating velocity; for this peculiar case the environment consists of gases therefore $k_m = 2$ [3], k_u – coefficient characterizing heating uniformity; for this case $k_u = 1$, [3], R – characteristics related to studied body dimensions (thickness); $R = 4$ mm.

In this specific case heating time calculated with formula (1), is: $\tau_{i,1} = 1.6$ min.

2. Calculation method based on geometrical coefficient of studied body.

Heating time $\tau_{i,2}$ is calculated with formula: [3]:

$$\tau_{i,2} = \frac{(D-d)\cdot l}{4\cdot l + 2\cdot (D-d)} \cdot k_f \text{ (min.)} \qquad (2)$$

Where: D, d are external and internal diameters of cylinder – protective shield - ; in this case D = 34 mm, d = 26 mm, k_f – physical factor characterizing heating, for this case: k_f =35 [3].

In this specific case the result of calculation is: $\tau_{i,2}$ = 6, 93 min

3. Criterial calculation method

Steps of calculations:.

a. Establishment of thermo-phisical parameters as presented in table 2 [2].

Table 2. Value of termo-phisical parameters

Type of material	Value of termo-phisical parameters			
12Cr130 (X15 Cr 13)	Heat transfer coefficient, α $\left(\frac{kcal}{m^2 \cdot h \cdot {}^0C}\right)$	Thermal conductivity λ $\left(\frac{kcal}{m \cdot h \cdot {}^0C}\right)$	Specific heat, C_p $\left(\frac{kcal}{kg \cdot {}^0C}\right)$	Specific weight (density), ρ $\left(\frac{kg}{m^3}\right)$
	13,5	23,8	0,113	7740

b. Calculation of temperature criteria, θ_c [2]:

$$\theta_c = \frac{t_m - t_i}{t_m - t_0} \tag{1}$$

Where: t_m is the temperature of working environment: t_m = 400^{0}C, t_i – temperature at the end of heating cicle: t_i = 200^{0}C; t_0 – initial temperature of heating agent: t_i = 20^{0}C.

Based on these parameters results that: $\theta_c = 0{,}52$

c. Calculation of Biot criteria value, B_i [2]:

$$B_i = \frac{\alpha \cdot R}{\lambda} \tag{2}$$

According to the initial data the value obtained for is: $B_i = 2{,}26 \cdot 10^{-3}$

d. Based on the previously calculated criteria ($\theta_c = 0{,}52$; $B_i = 2{,}26 \cdot 10^{-3}$), the value of is Boussinesq criteria is calculated, B_q = 3,0 [2].

e. Time of heat transmission is calculated with formula [2]:

$$\tau_i = \frac{\lambda^2 \cdot B_q}{a \cdot \alpha^2} \tag{3}$$

For the additional protective tube the increase of the response time will be: $\tau_i = 5{,}75$ min.

The results obtained using all three methods are presented in Table 3.

Table 3. Comparison of results obtained by using the mathematical methods presented.

Nr. crt.	Method of calculation used	Mathematical Formula/results
1	Calculation method based on heating criterion	$\tau_{i,1} = 0.1 \cdot k_f \cdot k_m \cdot k_u \cdot R$ $\tau_{i,1} = 1.6$ min
2	Calculation method based on geometrical coefficient of studied body	$\tau_{i,2} = \frac{(D-d) \cdot l}{4 \cdot l + 2 \cdot (D-d)} \cdot k_f$ $\tau_{i,2}$ = 6,93 min
3	Criterial calculation method	$\tau_{i,3} = \frac{\lambda^2 \cdot B_q}{a \cdot \alpha^2}$ $\tau_i = 5{,}75$ min

Comments

Although the results obtained by using the second and the third algorithms are relatively close, there it is a quite large dispersion of the calculated heating times. Due to the sensitivity of application and in order to protect the filtering cloths there it was decided to verify the mathematical calculation by experimental research.

The calculation was verified by using the One-Dimensional, Transient Conduction Version 3.6b of HTTonedt [3] developed by the staff of Virginia University.

The results showed that the response time would increase from 6 to 11 minutes, which cannot be admissible for this critical application. The exposure of the filter's cloth to temperatures over 100 C ^{0} or long time would destroy the fabric consequently generating environmental issues.

The second option considered was to coat the sensor with a much thinner layer of material which provides a better protection against erosion. One of the most promising alternatives is high velocity oxygen fuel (HVOF) tungsten carbide coatings.

There it was selected the spraying powder produced by Sulzer Metko - WOKA 3901 consisting of 86% Tungsten carbide, 10% Chromium and 4% Chromium. [4].

The coating of the sensor has been performed using the Sulzer Metco Diamond Jet DJ Gun see figure 4 available in the welding laboratory of Petroleum and Gas University. The sensor was coated with a 0.01 mm layer of material.

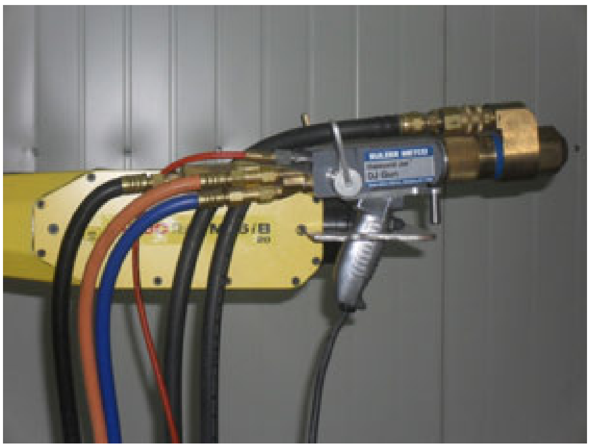

Figure 4. Sulzer Metco Diamond Jet DJ gun

Due to the fact that the thermo-physical parameters of the coating were not known it was not possible to calculate the increase of the response time of the coated sensor. In this regard there were conducted practical measurements using the thermal test chamber ETUVA 100 see Figure 5 housed in the welding laboratory of Petroleum and Gas University. The result of measurements showed that the increase in response time for a 0.01 mm thickness of coating is about 17 seconds.

Figure 5. Thermal test chamber ETUVA 100

2. CONCLUSION

The coated sensor was operationally tested in the sand drying plant. The 0.01 mm thick coating has prolonged the operational life of the sensor to 6 months. Since the increase of the response time due to the 0.01mm coating was relatively small there is still room for applying a thicker layer of Sulzer Metko - WOKA 3901 in order to increase the operational life of sensor.

REFERENCES

[1] http://www.cert-trak.com/literature/ametek/calibrators/SS-FP-1101-US.pdf.

[2] I. Carțiș: Tratamente termice – tehnologie și utilaje, Editura Facla, Timișoara, 1982, pp.6-25.

[3] http://faculty.virginia.edu/ribando/modules/OneDTransient - One-Dimensional, Transient Conduction Version 3.6b of HTTonedt.

[4] WOKA™ Carbide Powder Materials for Thermal Spray Bulletin 10-698.

Serbian Tribology Society

SERBIATRIB '11

12th International Conference on Tribology

Faculty of Mechanical Engineering in Kragujevac

Kragujevac, Serbia, 11 – 13 May 2011

PHYSICAL MODELLING OF VARIABLE CONTACT PRESSURE AND VARIABLE DRAWBEAD HEIGHT INFLUENCE ON DEEP DRAWING OF THIN SHEETS

S. Aleksandrovic[1], T. Vujinovic[2], M. Stefanovic[1] , V. Lazic[1], D. Adamovic[1]

[1] Faculty of Mechanical Engineering, Kragujevac, Serbia, srba@kg.ac.rs

[2] FAM Jelsingrad, Banja Luka, RS BH

***Abstract:** For this experimental research, electro-hydraulic computerised device for sheet metal stripes sliding was made. Its main property is realisation of contact pressure and drawbead height as functions dependent on time, i.e. stripe travel. In addition, it is also possible to measure drawing force, pressure, drawbead displacement etc.*

The paper presents the preliminary results of the investigation of decreasing drawbead height influence in combination with increasing-decreasing contact pressure function. The stripes are made of low-carbon steel sheet metal of 0,8 mm thickness. Contact conditions are influenced additionally in two ways - by mineral oil lubrication and dry surfaces application. Drawbead geometry, with rounding radii of 2 and 5 mm, is also varied.

The results indicate that simultaneous influence of variable drawbead height, variable contact pressure, drawbead geometry and proper friction conditions can influence substantially the plastic flow process.

***Keywords:** deep drawing, variable drawbead height, variable contact pressure.*

1. INTRODUCTION

Due to the significance and complexity of the process of thin sheet metals deep drawing, the tendency to accomplish the control of forming process is the latest trend. In order to succeed in that, it is necessary to select, out of a large number of influential factors, the ones which ca be varied throughout the forming process, thus correcting it until it is completed successfully. There are only two such factors: contact pressure and drawbead height [1].

Process control through active complex (closed-loop) systems requires constant dynamic feedback between the given function of the objective, controlled and controlling variables. The functions of the objective and controlled variable can be different: wrinkle height, thinning in critical zone, flange motion, flange thickness change, friction force, forming force, stress in work piece wall etc. The given objective functions are defined either by computer simulations or by previous experiments. Pressure on flange and drawbead height present the controlling effects. High velocity of reacting to controlled values change and robust controlling hardware and software apparatus are required, which all implies significant investments [2, 3].

There is also the alternative – a much simpler approach – used in this paper. However, first it is necessary to define optimal functions of pressure and drawbead height according to proper criterion (drawing depth, piece quality etc.). This often requires comprehensive experiments [4, 5] in order to identify the character of specified factors influence. With such information, it is possible to form the controlling apparatus for practical application whose main objective is to realise previously defined optimal functions of pressure and drawbead height. Such equipment requires considerably smaller investments regarding hardware and software and is far more accessible to a wide range of users.

Application of constant height drawbeads is still most often applied and well known [6, 7]. The same goes for application of constant blank holding force on flange. The main reasons for this are smaller forming process costs. However, due to the development of new materials of more complex formability properties, in most cases it is not possible to accomplish the satisfactory results by classical methods.

There are also some new ideas, such as application of drawbeads in which the angle between drawbead axis and sheet metal plane is different from 90^o [8]. There is also the increased interest in many numeric simulations and virtual application of drawbeads in processes of complex work pieces forming [9].

The application of blank holding force without draw beads is the subject of separate researches based on the same aforementioned principles [10, 11, 12].

In this paper, the emphasis is on investigation of the character of the connection between drawing force and various influences combinations. They include friction conditions (dry, application of lubricant), drawbead geometry (two rounding radii), one variable function of pressure of increasing-decreasing character, two functions of drawbead of decreasing character and corresponding constant values of both pressure and drawbead height for comparison. The significance of the physical model applied in actual experiments is clearly seen in fig. 1 [7].

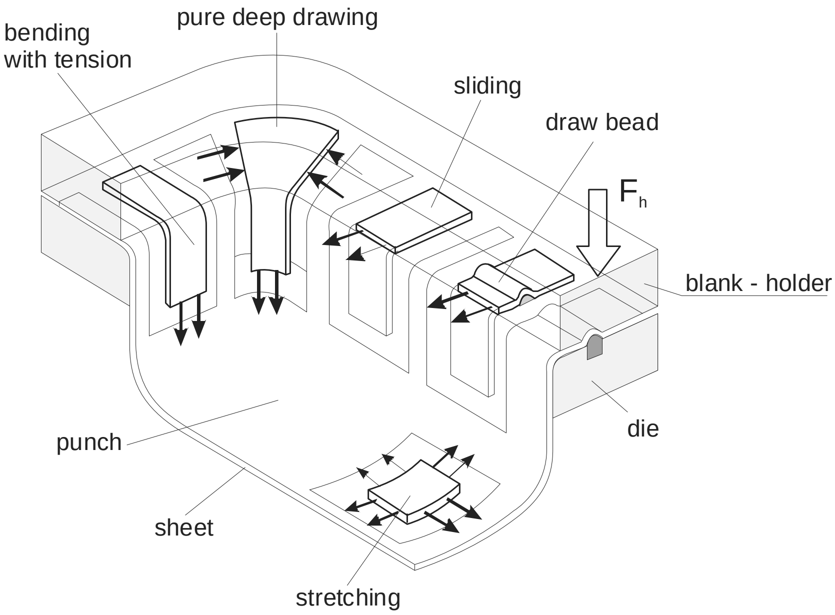

Figure 1. Scheme of physical models at deep drawing of complex geometry parts

2. EXPERIMENTAL CONDITIONS

2.1 Material

The material of which the stripes used in the experiment are made is classic low-carbon steel sheet metal of quality DC04 and 0.8 mm thickness. The main mechanical properties, properties of formability and roughness are given in table 1.

Table 1. Material properties

A. Mechanical properties, DC04					
	R_P, MPa	R_m, MPa	A_{80}, %	n	r
Average	200.2	350.6	36.06	0.235	1.51
Strengthening curve (0^o): $K = 204.9 + 388.9\varphi^{0.448}$, MPa					
B. Roughness properties					
R_a, μm	R_t, μm	R_z, μm	R_p, μm	pike/cm	
0.5	3.9	2.9	1.6	57	

In one case, the friction conditions are dictated by dry surfaces – completely degreased and cleaned by acetone. In the other case, the contact surfaces were richly covered (by sponge) with oil for deep drawing of the following properties at 40^{o}C: kinematic viscosity 45 mm^2/s, dynamic viscosity 42 mPas and density 0,93 kg/dm^3.

Dimensions of applied stripes were: length 250 mm, width 30 mm and thickness 0,8 mm.

2.2 Experimental device

The general scheme of the apparatus is shown in figure 2, and physical appearance in figure 6. Sheet metal stripe is positioned vertically between contact pairs, drawbead and die, which are variable. Drawing force is obtained from laboratory press ERICHSEN 142/12 in range 0-20 kN, as well as stress signal for measuring the force of proper sensor. Hydro-cylinders for drawbead displacement and pressure realization are fed by aggregate ERICHSEN of nominal pressure 100 bars and flow 1,5 l/s. The oil from the aggregate runs through the series of controllable proportional hydro valves to both cylinders.

Measuring and pressure controlling branch consists of pressure sensor which gives the current true value signal and control unit (micro-controller) which receives the given desired value from the software and sends signal D/A to the convertor. The received analogous signal is transmitted to the control card of the proper hydro-valve connected to the pressure cylinder.

In controlling branch, due to drawbead motion, the current true drawbead position is read by rotation encoder. After processing, the signals are sent to the control unit (micro-controller), and then to the card for control of hydro-valve for drawbead cylinder. One signal is related to the direction change, and the other one to the value of drawbead motion function. For measuring and reading the true drawbead position, supporting branch with inductive sensor and proper amplifier is made.

All true values signals are brought into PC computer with integrated A/D card and proper original software, which enables monitoring of all its values, their memorizing, presentation as well as generating of pressure and drawbead motion functions necessary for micro-controller performance.

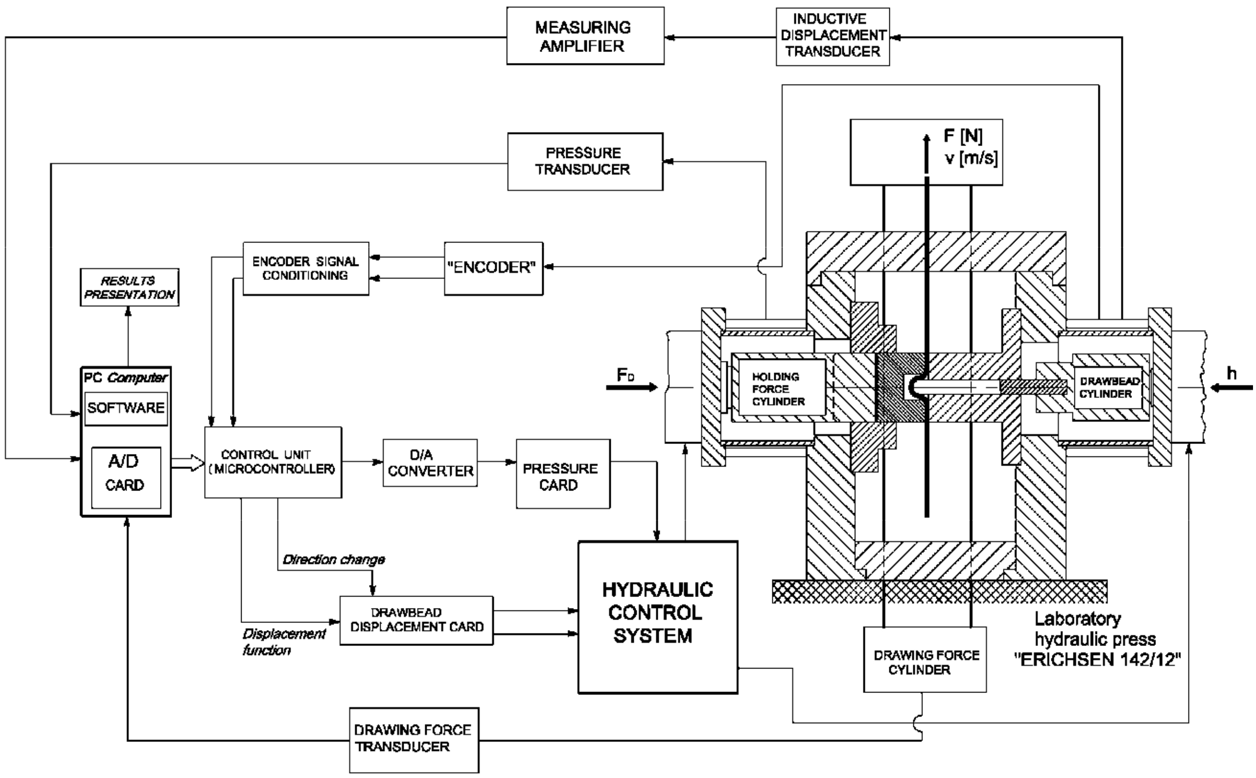

Figure 2. Block scheme of experimental apparatus

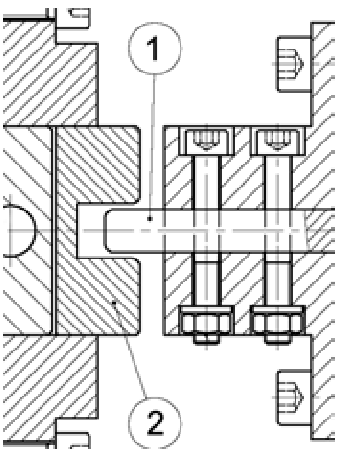

Figure 3. Scheme of drawbead action

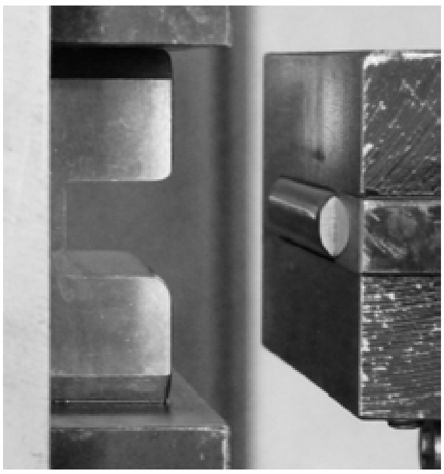

Figure 4. Drawbead and die before contact

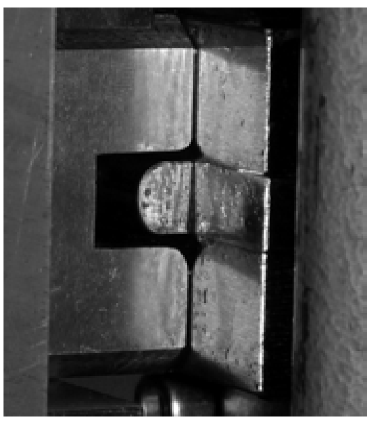

Figure 5. Drawbead and die in contact

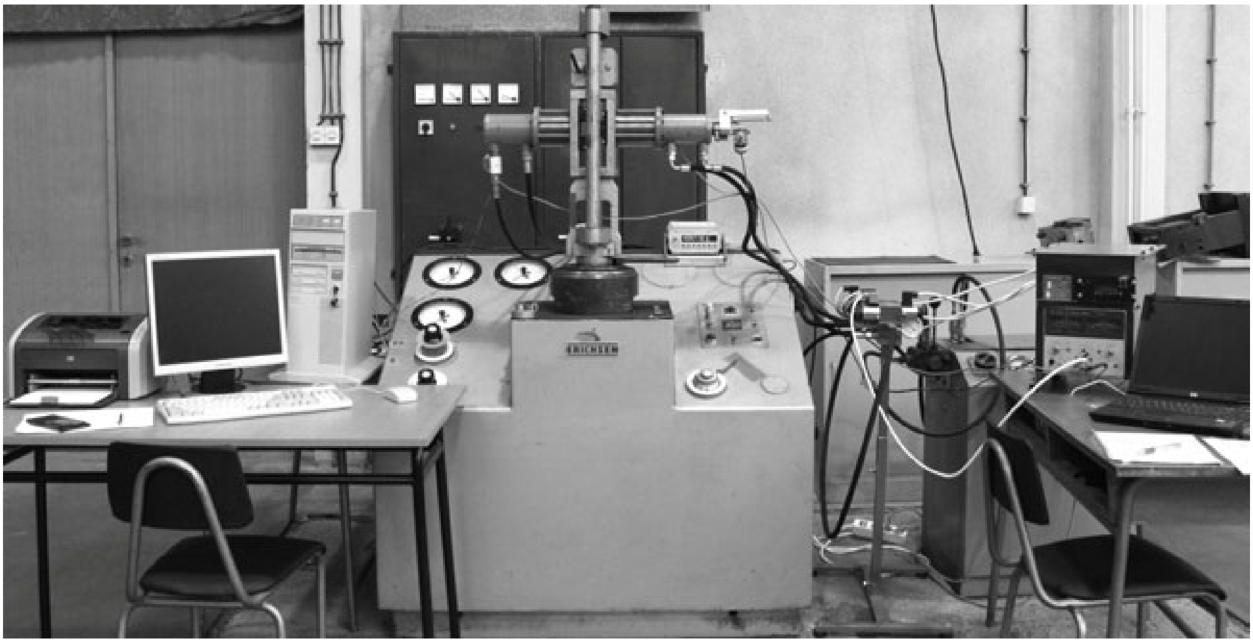

Figure 6. Physical appearance of experimental apparatus

Figure 3 shows the sketch of drawbead (1) and die (2). Drawbead is 10 mm thick and is applied with two radii: 2 mm (shown in the sketch) and 5 mm (shown in the photo, figure 4 and figure 5). Die rounding radius is 2 mm, and die opening is 12 mm. Both drawbead and die can be varied with the aim of monitoring the influence of drawbead geometry change. Active surfaces of drawbead and die are fine grinded and polished.

3. EXPERIMENTAL RESULTS AND DISCUSSION

3.1 Pressure and drawbead displacement functions

For the needs of planned comprehensive experiment, 6 variable dependencies of both pressure and drawbead motions on time, as given functions, were defined. In figures 7 to 12, those functions are marked with numbers 1 to 6. Dependencies 5 and 6 are linear, and 1, 2, 3 and 4 non-linear – parabolic. Functions were defined based on empiric values of minimal and maximal pressure (0-20 MPa) and drawbead height (0-8 mm). Process duration was conditioned by limited stripe displacement and adopted sliding velocity of 20 mm/min. This conditioned maximal process duration of 3 min. Dependency signed from 7 to 10 are related to constant values of pressure and drawbead height.

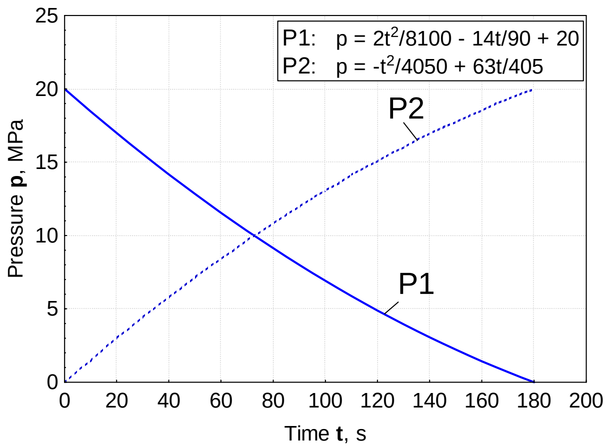

Figure 7. Previously defined dependencies of contact pressure on time

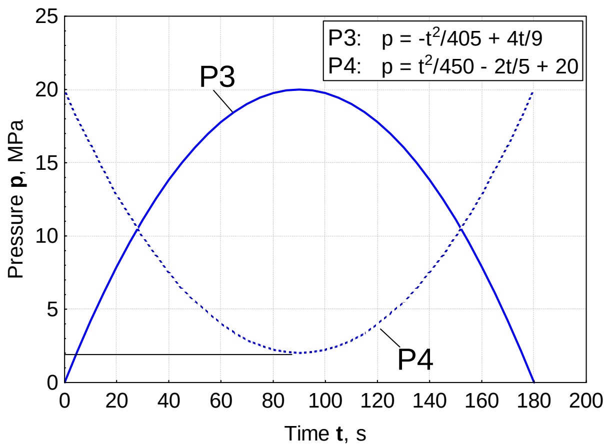

Figure 8. Previously defined dependencies of contact pressure on time

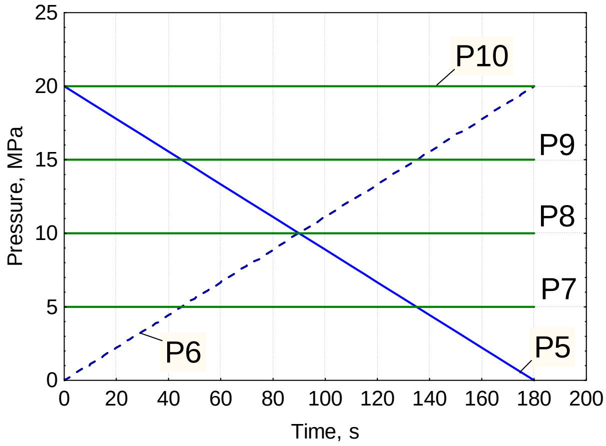

Figure 9. Previously defined dependencies of contact pressure on time

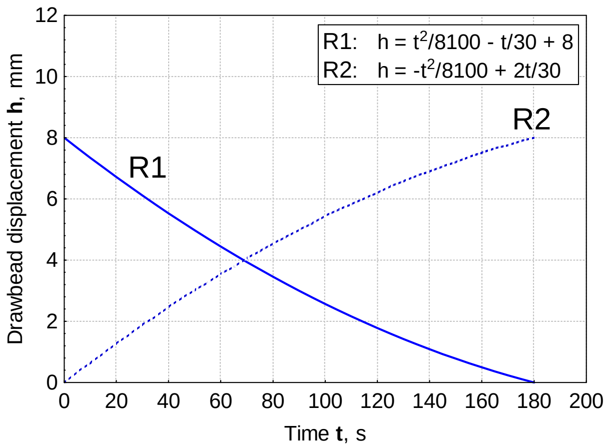

Figure 10. Previously defined dependencies of drawbead height on time

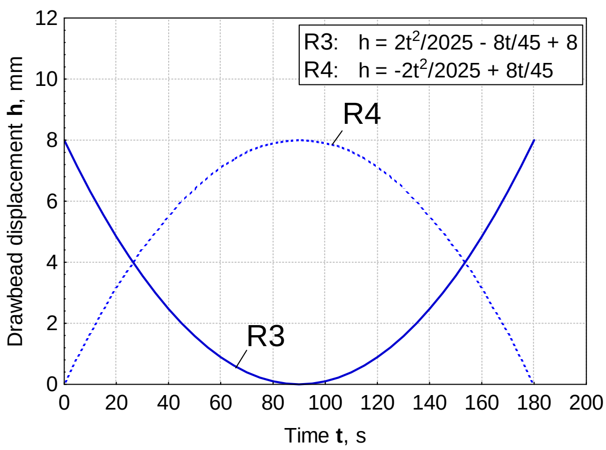

Figure 11. Previously defined dependencies of drawbead height on time

The purpose of so defined functional dependencies, which have different characters, is the inclusion of wide range of possible influences: decreasing, increasing, combined decreasing-increasing and increasing-decreasing, linear and non-linear. Monitoring of the response of drawing force regarding the performance of such dependencies together with friction conditions and drawbead geometry is the most important part of this research.

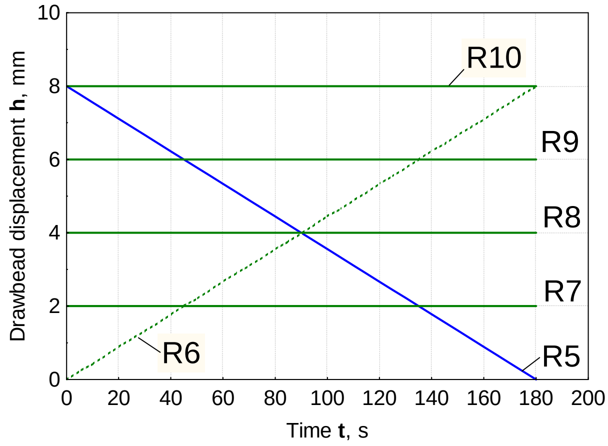

Figure 12. Previously defined dependencies of drawbead height on time

3.2 Measured drawing force values

Figure 13 shows given and truly achieved dependence of pressure P3 change according to marks from figure 8. Figure 14 shows given and truly achieved decreasing dependencies of drawbead height with marks according to figure 10 and figure 12. Truly achieved constant values of pressure according to scheme P8 and constant drawbead height according to scheme R9 are corresponding, with insignificant deviations. Fig. 9 and figure 12 are not shown here. Such a combination was selected with the purpose of checking the response of drawing force to complex increasing - decreasing dependence of contact pressure during the process together with decreasing functions of drawbead height. The investigation of the following combinations was also carried out: constant pressure P8 – decreasing drawbead function R1 and variable pressure P3 – constant drawbead height R9. The purpose of such combinations is the evaluation of separate influences of variable pressure and drawbead height influence. In addition to that, it was necessary to estimate the influence of friction conditions and drawbead geometry.

Figure 15 shows the influence of drawbead functions R1 regardless of variable pressure. Constant pressure was applied according to scheme P8. Drawing force increases until it reaches the critical value, and then it decreases in proportion to drawbead height decrease. Oscillatory phenomena caused by drawing force sensitivity to gradual change of real function R1 can be observed. Drawbead geometry influence exceeds the varying of contact conditions (mixed to dry). The change of drawbead radius from 5 mm to 2 mm makes stripe sliding conditions more difficult than the change of friction conditions caused by oil application on dry surfaces. Curve character L2 (lubrication, r=2 mm) is different compared with curve L5 (lubrication, r=5 mm) and D5 (dry, r=5 mm).

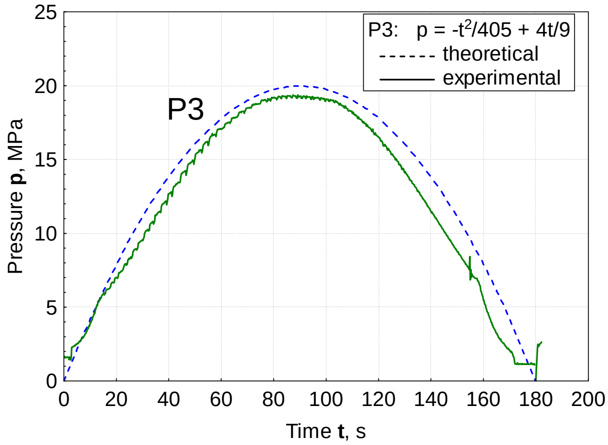

Figure 13. True dependence of pressure on time

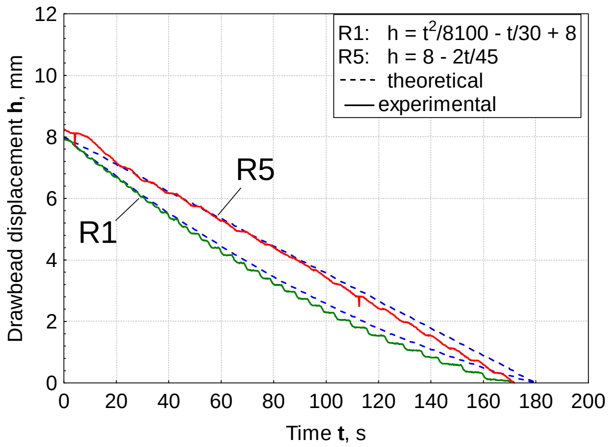

Figure 14. True dependencies of drawbead height on time

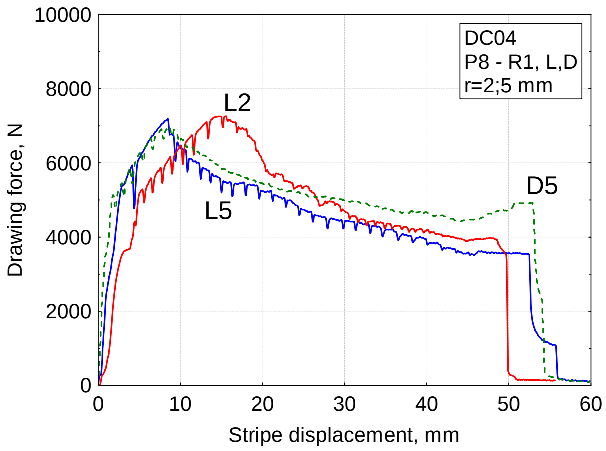

Figure 15. Drawing force dependencies of on stripe displacement

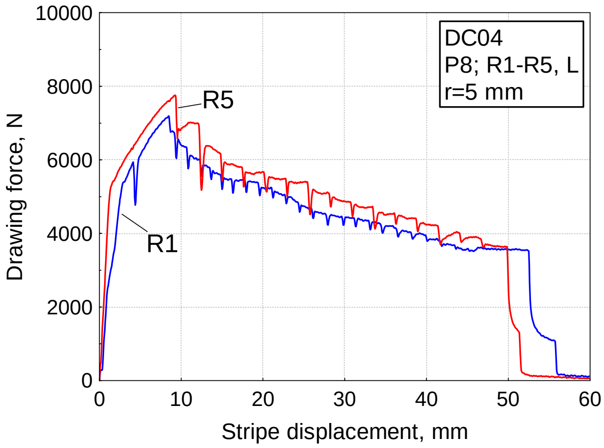

Figure 16. Drawing force dependencies of on stripe displacement

Figure 16 shows the influence of relatively small difference in character and intensity between functions R1 and R5 (figure 14). In line with somewhat higher intensity of R5 change, the reaction of drawing force is obvious and difference in comparison with function R1 application is shown.

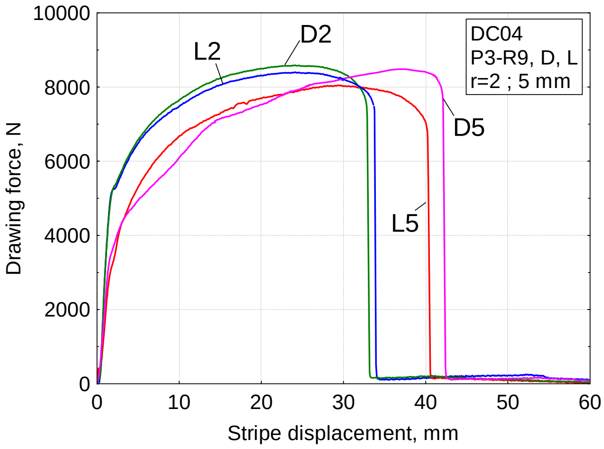

Figure 17. Drawing force dependencies of on stripe displacement

The separate influence of pressure function P3 (at constant drawbead R9 from fig. 12) in all 4 variants is shown in figure 17. The dominant influence of decreased drawbead rounding radius can be seen even more clearly than in fig. 15. Drawing force dependencies for 2 mm radius are separate and of somewhat higher intensity. The change of friction type is noticeable, but it is of smaller intensity. The character of drawing force curves is proportional to the pressure function P3 and is very different from curves in figures 15 and 16.

Figure 18 shows drawing forces at simultaneous actions of pressure functions P3 and drawbead functions R1, i.e. R5.

At 5 mm rounding radius, drawing force curves represent a combination of dependencies from fig.

15 (figure 16) and figure 17. Major part of stripe travel and oscillatory changes were caused by drawbead influence, and general curve form and maximal intensities were caused by pressure influence. By making sliding conditions difficult due to the application of radius r=2 mm, curve form changes and the influence of pressure P3 becomes dominant. Oscillatory disturbance is diminished, and intensity of maximal drawing force somewhat smaller in comparison with figure 17.

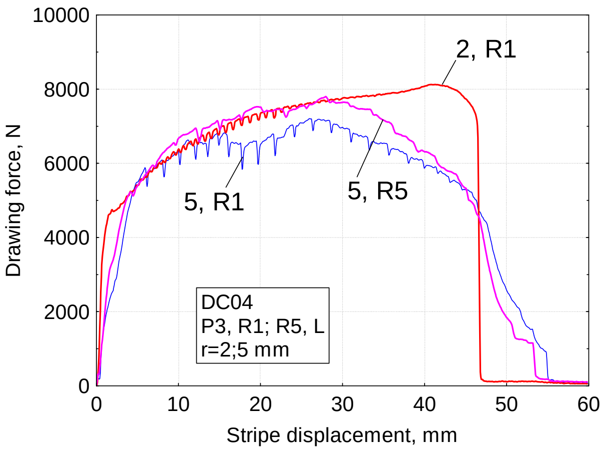

Figure 18. Drawing force dependencies of on stripe displacement

4. CONCLUSION

The presented apparatus for testing the tribological influence on drawing force in the process of stripe sliding over drawbead at variable contact pressure and variable drawbead height enables accurate registering of the influence of drawbead geometry, friction conditions, pressure activity and drawbead height on drawing force.

This paper presents a part of experimental results for the sliding test for low-carbon steel sheet metal stripe. Based on the presented results, the following conclusions can be made:

a) the response of drawing force is approximately equally influenced by simultaneously applied functions of pressure and drawbead height in milder sliding conditions, at larger drawbead rounding radius and smaller friction,

b) in more difficult sliding conditions, at smaller drawbead radius, the influence of pressure function is more significant,

c) drawbead rounding is more influential than friction conditions,

d) reaction of drawing force is registered even at relatively small differences in drawbead height change during the process,

e) the character of drawing force response shows that the favourable combination of simultaneous performance of contact pressure change, change of drawbead height, friction conditions and drawbead geometry makes it possible to control and influence the course of sheet metal forming process

f) by such investigations, with rather simple apparatus, it is possible to define significant data for numerical simulations and immediate application in practice at deep drawing of complex geometry parts.

REFERENCES

[1] S. Wagner: Tribology in drawing car body parts, 11th International colloquium: Industrial and automotive lubrication, Technische Akademie Esslingen, january 1998., Proc. Vol. III, pp. 2365-2372.

[2] M. Liewald: Current Trends in Research on Sheet Metal Forming at the Institute for Metal Forming Technology (IFU) at the University Stuttgart, Papers of the International Conference on ”New Developments in Sheet Metal Forming”, IFU Stuttgart, 2008., pp. 263-288.

[3] C. Blaich, M. Liewald: New Approach for Closed-Loop Control of Deep Drawing Processes, Papers of the International Conference on ”New Developments in Sheet Metal Forming”, IFU Stuttgart, 2008., pp. 363-384.

[4] J. R. Michler, K. J. Weinmann, A. R. Kashani, S. A. Majlessi: A strip-drawing simulator with computer-controlled drawbead penetration and blankholder pressure, Journal of Materials Processing Technology, 43 (1994): pp. 177-194.

[5] S. G. Hu, M. L. Bohn and K. J. Weinmann: Drawbeads and their Potential as Active Elements in the Control of Stamping, Papers of the International Conference on ”New Developments in Sheet Metal Forming”, IFU Stuttgart, 1998., pp. 269-303.

[6] J. A. Waller: Press Tools and Presswork, Portcullis Press Ltd, Great Britain, 1978.

[7] M. Stefanovic: Tribology of deep drawing, monograph, Yugoslav Society for Tribology and Faculty of Mechanical Engineering, Kragujevac, 1994, (In Serbian).

[8] L. M. Smith, Y. J. Zhou, D. J. Zhou, C. Du, C. Wanintrudal: A new experimental test aparatus for angle binder draw bead simulations, Journal of Materials Processing Technology, 209 (2009): pp. 4942-4948.

[9] G.H. Bae, J.H. Song, H. Huh, S.H. Kim, S.H. Park: Simulation-based prediction model of the draw-bead restraining force and its application to sheet metal forming process, Journal of Materials Processing Technology, 187-188 (2007): pp. 123-127.

[10] S. Aleksandrovic, M. Stefanovic and T. Vujinovic: Variable tribological conditions on the blank holder as significant factor in deep drawing process, Tribology in Industry, Faculty of Mechanical

Engineering, Kragujevac, 25 (2003), N^o 3&4, pp. 100-104.

[11] S. Aleksandrovic, B. Nedeljkovic, M. Stefanovic, D. Milosavljevic, V. Lazic: Tribological properties of steel and Al-alloys sheet metals intended for deep drawing, Tribology in industry, Faculty of Mechanical Engineering, Kragujevac, 31 (2009), N^o 3&4, pp. 11-16.

[12] S. Aleksandrovic: Blank holding force and deep drawing process control, monograph, Faculty of Mechanical Engineering, Kragujevac, 2005, (In Serbian).

Serbian Tribology Society

SERBIATRIB '11

12th International Conference on Tribology

Faculty of Mechanical Engineering in Kragujevac

Kragujevac, Serbia, 11 – 13 May 2011

CHARACTERISTICS OF FRICTION IN SHEET METAL SLIDING WITH THICKNESS REDUCTION

Đačić Slaviša[1], Milentije Stefanović[2], Srbislav Aleksandrović[2], Dragan Adamović[2]

[1]Coal Mine A.D., Pljevlja, Montenegro, djale@t-com.me

[2] Faculty of Mecahanical Engineering Kragujevac, Serbia, stefan@kg.ac.rs; srba@kg.ac.rs; adam@kg.ac.rs

Abstract: *Presented in the paper are results obtained in investigation of the effects of tribological conditions in cold metal forming. A characteristically tribo-model is strip ironing between angled die surfaces. Investigated were the changes in ironing force, pressure, friction coefficient in single and multy-phase sliding in the conditions of boundary lubrication. The low carbon mild steel sheet, suitable for plastic forming was used. In course of investigation the so called constant low friction has been realized in condition of high contact pressures. Especially significant are the results of multi-phase sliding, which simulates the moving of piece through dies.*

Keywords: *cold forming, ironing, friction coefficient, sheet metal*

1. INTRODUCTION

In cold metal forming processes, characterized by high pressures, local tool loads, generating of new piece surfaces etc., realisation of the convenient lubrication regime and elimination of micro-welding are of extreme importance. Distribution and intensity of shearing stresses on piece surface influence the possibility for plastic forming, i.e. the size of active force, energy consumption, tool life, piece surface quality etc. Taking into consideration the complexity of specified factors, tribological investigations in MF processes are extremely important and equal with investigations of other forming system segments - machines, tools and materials.

Proper selection of tribological conditions and identification of boundary relations on contact surfaces enables controlled flow in surface layer, whereat this layer has sufficiently lower flow limit than basic material and can be defined without fracture. By combination of main tribo-factors in forming system – speed, load (strain ratio), type of materials in contact (topography, content), preparation of contact surface and lubricant type, it is possible to realise mixed, i.e. boundary friction. In that way, contact between tool and piece material, tearing of softer material particles and rough disruptions of forming conditions are reduced to minimum.

At ironing, pieces of considerable height in relation to diameter are obtained, with bottom thickness larger than wall thickness. In forming, which is most often multi-phase for one stroke, inner diameter slightly changes. Total thinning, i.e. number of rings and geometrical relations of work surfaces of tool elements are important in forming.

2. TRIBOLOGICAL MODEL DESCRIPTION

Modelling of tribological conditions at ironing implies satisfying of the minimum of necessary criteria considering the similarity in stress strain properties, temperature-speed conditions, properties of tools surface and material. In researches, the results of which are presented in this paper, the basic ironing model, which imitates zone of contact with die with biaxial symmetry, was used as tribo-model, fig.1. This is a classical model, which enables realisation of high contact pressure and takes into account real geometrical conditions of forming process. It was used in many researches, especially in the area of tribology of stainless steel sheet metals and in Al- alloys forming [1] , [2].

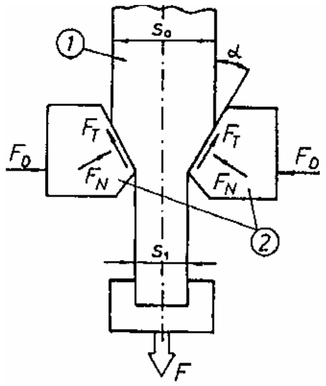

Figure 1. Scheme of the tribo-model

Model applied in paper, according to fig.1, requires measuring of holder force F_D and drawing-sliding force F. If the test-specimen dimensions and die angle are known, it is possible to determine friction coefficient and average pressure in contact:

$$\mu = \frac{\dfrac{F}{2F_D} - tg\alpha}{1 + F\dfrac{tg\alpha}{2F_D}} \tag{1}$$

$$\overline{p} = \frac{F\sin^2\alpha + 2F_D\sin\alpha\cos\alpha}{b_0(s_0 - s_1)} \tag{2}$$

where is:

b_0 - specimen width,

s_0 - initial test-specimen thickness ,

s_1 - thickness after drawing.

3. EXPERIMENTAL RESEARCHES

Ironing is realised in conditions close to plane stress state. The investigated material is low-carbon steel sheet metal of quality DC04, convenient for plastic forming. Mechanical and other properties are specified in Table 1. Dimensions of test-specimen being investigated are: *b_0 x s_0 x length = 20 x 2,5 x 200 mm.*

Table 1. Material properties

R_p, MPa	R_m, MPa	A, %	r	n
185,2	284,5	35,3	1,68	0,215

Contact pair is made of tool steel, hardness 60 HRC, highly-polished to mean roughness Ra =0,06 µm. Gradient angle is $\alpha=10^0$, as recommended in literature. Drawing speed is 20 mm/min. In investigations, mineral oil for cold forming was used [3].

In dependence on specified conditions, it is possible to carry out certain classification of friction types, taking as a criterion the value and change of friction coefficient and appearance of test-specimen surface after investigation [1]:

I - constant low friction,

II - increase of friction after realisation of type I,

III - constant increase of friction,

IV - constant high friction.

Proper contact surfaces have the following descriptions:

- flat (smooth)
- lightly polished
- with abrasions
- lightly scratched
- heavily scratched

At drawing at sliding length of 60 mm, there are no changes in friction character, as a rule. In addition, drawing force records at successive investigations are shown, with shorter sliding paths. Dependence of force on sliding path practically remains constant during investigation period, which corresponds to I friction type. Dependence of drawing force on travel at various working pressures is shown in Fig.2. Total drawing force consists of friction force and "ideal" forming force which depends exclusively on strain ratio [3].

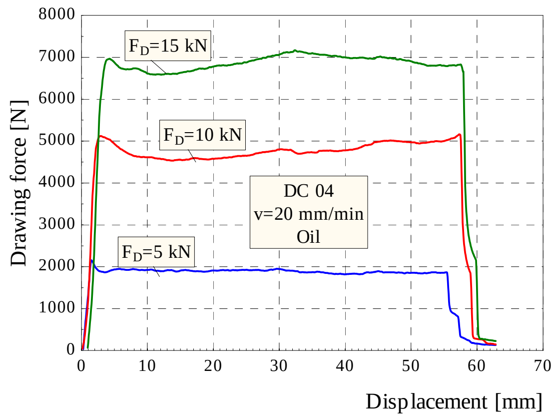

Figure 2. Change of drawing force for different F_D

Sheet metal thinning at the same compression force F_D does not depend on tribological conditions in contact [4]. Increase of the number of drawings worsens the lubrication conditions, which corresponds to real process of drawing through numerous dies- rings, Fig.3.

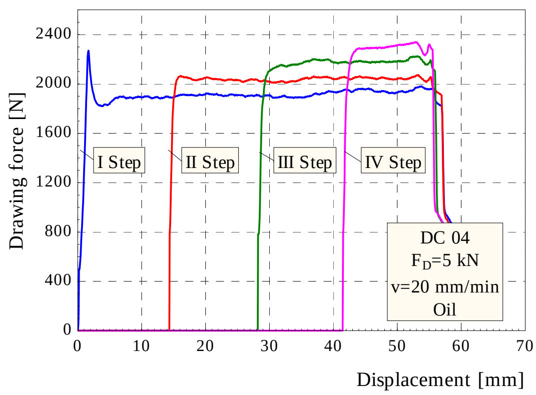

Figure 3. Change of ironing force at multiphase drawing at F_D=5 kN

Important changes in contact occur in the first and second forming phase, and then the process becomes stationary in the subsequent phases, if friction conditions do not change, Fig.4.

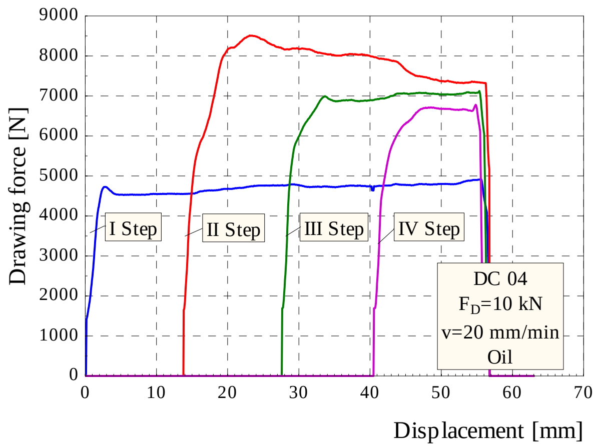

Figure 4. Change of ironing force alt multiphase drawing at F_D=10 kN

By using formula (1), it is possible to determine friction coefficient in dependence on experimental conditions, Fig.5.

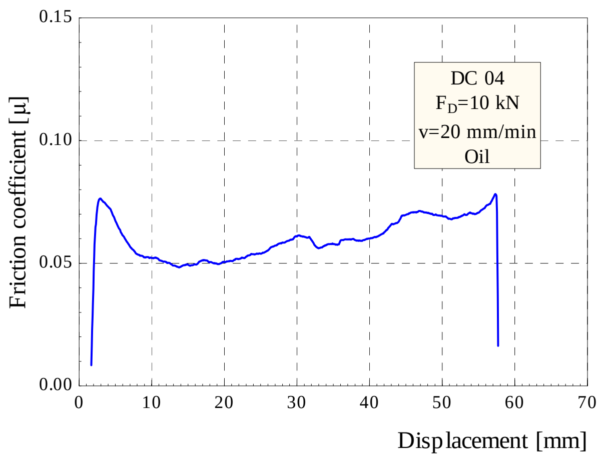

Figure 5. Change of friction coefficient with sliding path at F_D=10 kN

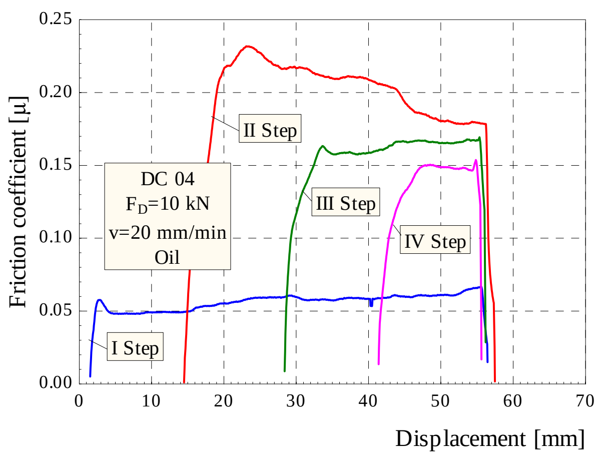

Figure 6. Change of friction coefficient at multiphase drawing at F_D=10 kN

Due to faster increase of contact surface in dependence on compression force, at bigger F_D forces, smaller pressures are realised and vice versa. By using formula (2), it is possible to determine average contact pressure in sliding zone. Dependence of contact pressure on travel at F_D=10 kN is shown in Fig. 7.

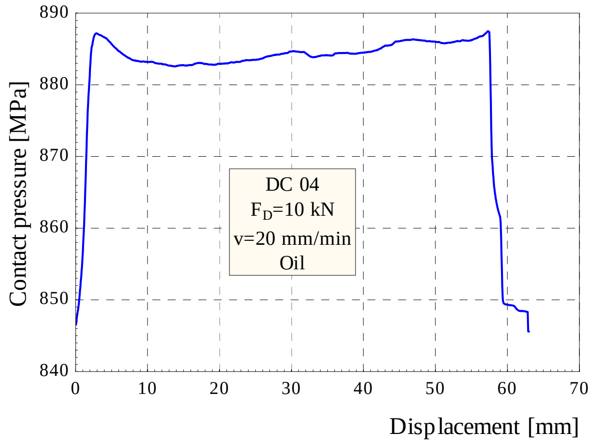

Figure 7. Change of contact pressure at F_D=10 kN

4. CONCLUSION

At model investigations of ironing, presented in the paper, stationary process with "constant low friction" was realised in conditions of high contact pressure. Friction coefficient values are the lowest at the first drawing and do not depend on sliding length.

At consecutive drawing-sliding, specific pressure in contact increases with the constant holder force, with realisation of boundary friction.

In the course of investigation, a new surface is generated, so the total length of test-specimen is increased.

At sliding lengths that are considerably larger than those in the experiment, the appearance of friction force increase is possible, as well as the appearance of the third or fourth friction type. a conclusion may review the main points of the paper, do not replicate the abstract as the conclusion. A conclusion might elaborate on the importance of the work or suggest applications and extensions.

REFERENCES

[1] M.Stefanovic, D.Adamovic, Characteristics of Constant Low Friction in Testing Sheet Metal by Ironing, Yutrib 89, Faculty of Mechanical Engineering Kragujevac, Proceed. pp. 177-182.,

[2] N. Bay, D.D. Olsson, J.L. Andreasen Lubricant test methods for sheet metal forming e Tribology International, Volume 41, Issues 9-10, September-October 2008, Pages 844-853

[3] D.Adamović, M.Stefanović, M.Živković, F.Živić, Investigation of Influence of Tribological Conditions on Friction Coefficient During Multiphase Ironing for Steel and Aluminium Sheet Metal, Tribology in industry, Kragujevac, Vol.28, No 3&4, 2006, pp.29-34.

[4] D.Adamović, M.Stefanović, M.Plančak, S.Aleksandrović, Analysis of Change of Total Ironing Force and Friction Force on Punch at Ironing, Journal for Technology of Plasticity, Novi Sad, Vol.33(2008), N^{o}1-2, pp.23-38.

Serbian Tribology Society

SERBIATRIB '11

12th International Conference on Tribology

Faculty of Mechanical Engineering in Kragujevac

Kragujevac, Serbia, 11 – 13 May 2011

ANALYSIS OF CHANGES OF BULK MODULUS OF MINERAL OIL – EFFECTS ON THE DYNAMIC BEHAVIOR OF HYDRAULIC ACTUATORS

Darko Knežević[1], Aleksandar Milašinović[2], Zdravko Milovanović[3], Vladimir Savić[4]

[1]Faculty of Mechanical Engineering Banja Luka, BiH – RS, E-mail: darkokn@blic.net

[2]Faculty of Mechanical Engineering Banja Luka, BiH – RS, E-mail: acom@blic.net

[3]Faculty of Mechanical Engineering Banja Luka, BiH – RS, E-mail: mzdravko@urc.rs.ba

[4]Faculty of Technical Science Novi Sad, Serbia, E-mail: savicv@uns.ac.rs

Abstract: *When setting up the equations that describe the dynamic behavior of hydraulic actuators, it is important to know the physical properties of working fluid and the mathematical description of change of these properties with changing pressure and temperature. Although the compressibility of liquids in the practical analysis of the flow can usually be ignored, in dynamic analysis of work of hydraulic components fluid must be viewed as an elastic medium which is deformed at rest with changing pressure and temperature. In addition to the dynamic behavior of hydraulic actuators largely influenced by the presence undissolved air in the hydraulic fluid. Even in very small quantities, which can not be avoided in hydraulic systems, usdissolved air in the hydraulic fluid significantly changes the elastic properties of the working fluid, affects the transmission speed of pulses of change of pressure, leading to delay response of actuators and others.*

In this paper, change of value of effective bulk modulus of mixture of mineral oil and dissolved air is given on the basis of data obtained from manufacturers and experimental data obtained in the analysis of decompression of oil in the hydraulic cylinders.

Keywords: *bulk modulus, pressure, temperature, undissolved air, decompression, dynamic behaviour*

1. INTRODUCTION

Besides the basic functions that transmit energy in the hydraulic system from the place of transformation of mechanical into hydraulic energy (pump) to a place of transformation hydraulic into mechanical energy (cylinder, rotary or oscillating motor), hydraulic oils and fluids, perform a few extra features such as lubrication of all places contacts within the hydraulic components, corrosion protection, download the generated heat and, later, its transmission to the environment, and others.

In accordance with the requirements for hydraulic fluid that sets components, system, environment and conditions of exploitation has formulated a series of structural and quality different hydraulic fluids. In practice, as hydraulic fluids are commonly used mineral oils. They are classified into six qualitative levels (HH, HL, HM, HR, HV and HG), but now in the hydraulic systems used exclusively oils classes HM and HV. This is essentially the same quality class of oil, noting that in oil class HV value of viscosity index increased relative to oil HM.

The value of the bulk modulus of mineral oils for hydraulic systems depends primarily on the chemical composition of base oil. [1]

Mineral base oils are composed of complex molecules of carbon-hydrogen. According to the domination of the representation of certain carbon-hydrogen in oil, mineral oil can be divided into paraffinic, naphthenic and mixed. Hydraulic oil is almost completely derived from base oil of paraffinic structure, and the naphthenic oil, because of reduced availability, used only in special conditions of application. [1]

Paraffin carbon-hydrogens can be straight (n-paraffins) and branchy (iso-paraffins) and have the general formula C_nH_{2n+2}.

Molecular structure and weight carbon-hydrogens affect the physical and chemical behavior of mineral oil. Molecules of carbon-hydrogens in paraffin oil contain 20-50 carbon atoms and have the average molecular weight of 350-550. [2]

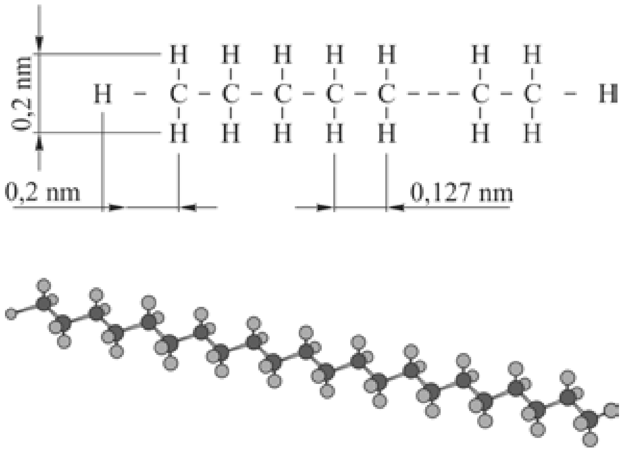

Figure 1. N-paraffins

In Figure 2.1 are given the distance between atoms, in nanometers, into paraffin molecules of carbon-hydrogen. Given the number of carbon atoms in a molecules can be calculated that the length of the molecules n-paraffin 3-6.75 nm (0.003-0.00675 μm). In iso-paraffin molecules length is smaller (because a certain number of atoms of carbon and hydrogen form lateral chains), but the width is higher than the n-paraffins.

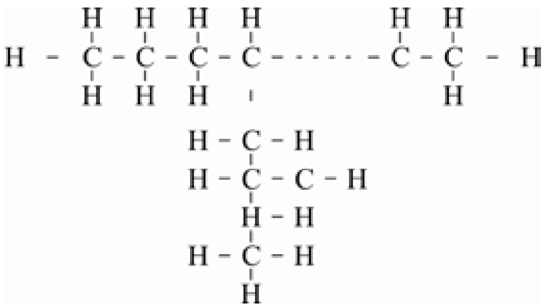

Figure 2. Iso-paraffins

The value of bulk modulus in this paper is given for mineral hydraulic oil HM 46. As the value of the bulk modulus depends almost exclusively on the chemical structure of liquids, this oil can serve as a representative for a wide range of mineral hydraulic oils used in practice. [3]

The accuracy of this statement is confirmed by experimental data obtained by measurements in the analysis process decompression of mineral oils in the cylinders of hydraulic presses. [4]

2. COMPRESSIBILITY – THE ELASTICITY OF HYDRAULIC FLUID

Compressibility of fluid are quantitatively expressed in differential form,

$$\frac{dV}{V} = -\frac{dp}{K}, \qquad (1)$$

where K is a bulk modulus (volumetric elastic modulus) and for the hydraulic oil without undissolved air its value depends on the pressure, temperature and thermodynamic method of process.

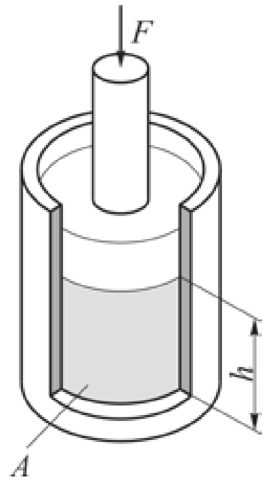

Figure 3. Compressibility of fluid

Elastic properties of liquids can be expressed by the coefficient of elasticity which can be generally given pattern,

$$c = -\frac{dF}{dh} = -\frac{Adp}{dh} = \frac{A\frac{dV}{V}K}{dh} = \frac{KA}{h} = \frac{KF}{hp}, \qquad (2)$$

where:

h – height of column of fluid in the cylinder (a cylindrical container),

p – pressure,

$F = pA$ – pressure force.

3. ISOTHERMAL BULK MODULUS OF MINERAL OIL

Isothermal bulk modulus characterizes a change of density (volume) of fluid at constant temperature

$$K_T = \rho\left(\frac{\partial p}{\partial \rho}\right)_T = -V\left(\frac{\partial p}{\partial V}\right)_T. \qquad (3)$$

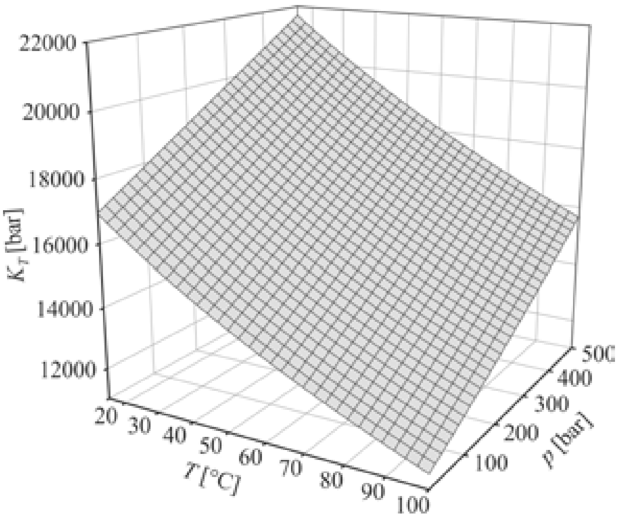

Figure 4. Isothermal bulk modulus of mineral oil

Change the isothermal bulk modulus as function of pressure and temperature, in Figure 4, is given for mineral hydraulic oil viscosity class HM 46, based on data obtained from the manufacturer. [3]

4. ADIABATIC BULK MODULUS OF MINERAL OIL

Adiabatic bulk modulus characterizes a change of density (volume) of fluid in thermodynamic processes without exchange of heat. Unlike the isothermal or static bulk modulus, which is significant for relatively slow processes of compression, adiabatic bulk modulus is important for analysis of the speed of propagation of the pulses of pressure, sudden relief of chambers under pressure, and other processes where a change in oil condition occurs relatively quickly

$$K_S = \rho \left(\frac{\partial p}{\partial \rho} \right)_S = -V \left(\frac{\partial p}{\partial V} \right)_S , \tag{4}$$

$$K_S = \frac{c_p}{c_v} K_T , \tag{5}$$

where:
c_p – specific heat at constant pressure, and
c_v – specific heat at constant volume.

Change the adiabatic bulk modulus as function of pressure and temperature, in Figure 5, is given for mineral hydraulic oil viscosity class HM 46, based on data obtained from the manufacturer. [3]

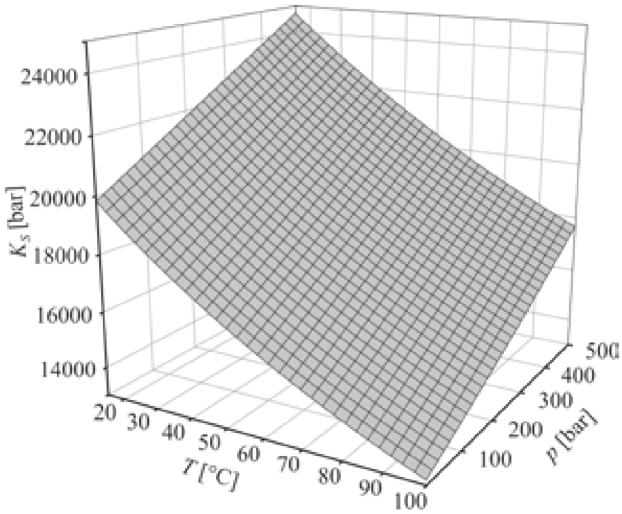

Figure 5. Adiabatic bulk modulus of mineral oil

5. SPEED OF PROPAGATION OF SMALL DISTURBANCES (SPEED OF SOUND) IN MINERAL OIL

Speed of response on the change of pressure in the hydraulic system is very important in a very dynamic process, where significant speed and accuracy of the positioning of hydraulic actuators.

Speed of propagation of the pulses of pressure through a fluid is equal to the speed of sound through the fluid and depends on adiabatic bulk modulus and fluid density

$$c_z = \sqrt{\frac{K_S}{\rho}} . \tag{6}$$

Based on data for the adiabatic bulk modulus K_S and density ρ were calculated data for the velocity of sound for mineral oil HM 46 and give the following diagram.

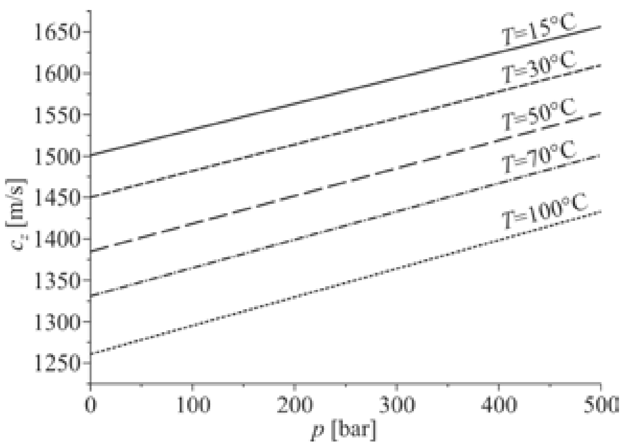

Figure 6. Speed of sound in mineral oil

6. EFFECTIVE BULK MODULUS OF THE MIXTURE OF MINERAL OIL AND UNDISSOLVED AIR

Increased flexibility of working fluid due to the presence undissolved air in the oil will be greater because of the higher volume undissolved air, regardless of the size of air bubbles.

The analysis will be done on the example of a hydraulic cylinder, noting that the results obtained for equivalent compression module does not depend on the type chamber under pressure. Effective bulk modulus of the mixture of oil and air, at a given pressure, can be determined using the analogy of the mechanical model, dividing the total space of the cylinder pressure chamber to the part that meets the oil and the part that meets the undiluted air. As an effective bulk modulus serves to describe the elastic properties of the working fluid, in the case of a mixture of oil and undissolved air, the equivalent stiffness of the working fluid can be defined as the equivalent stiffness of two serially connected springs.

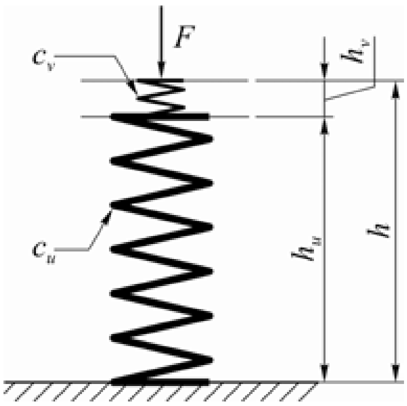

Figure 7. Mechanical model for calculating the equivalent stiffness of the mixture of oil and air

The stiffness (coefficient of elasticity) oil is given by pattern

$$c_u = \frac{K_u A}{h_u}, \tag{7}$$

where:
K_u – bulk modulus of oil,
A – the cross-section of the cylinder and
h – height of the cylinder chamber that is filled by oil,
while the stiffness (elasticity coefficient) air is given by

$$c_v = \frac{K_v A}{h_v}, \tag{8}$$

where:
K_v – bulk modulus of air and
h_v – height of the cylinder chamber that is filled by air.

The equivalent stiffness is given by

$$\frac{1}{c_e} = \frac{1}{c_u} + \frac{1}{c_v}. \tag{9}$$

As

$$c_e = \frac{K_E A}{h}, \tag{10}$$

substituting expressions (2.23) (2.24) and (2.27) into (2.25), we get

$$K_E = \frac{K_u K_v}{K_u \dfrac{V_v}{V} + K_v \dfrac{V_u}{V}}, \tag{11}$$

where:
K_E – effective bulk modulus (mixture of oil and air),
V_u – part of the volume of the cylinder chamber that is filled by oil,
V_v – part of the volume of the cylinder chamber that is filled by air and
V – total volume chamber cylinder.

7. AN EXAMPLE OF EFFECTIVE BULK MODULUS OF MIXTURE OF HYDRAULIC OIL AND UDISSOLVED AIR UNDER ADIABATIC CHANGE OF STATE OIL AND ISOTHERMAL CHANGE OF STATE UNDISSOLVED AIR

Experiments carried out to analyze the process of decompression mineral hydraulic oil in hydraulic presses have shown that due to relatively rapid changes in the conditions of process, change of state of oil can be considered adiabatic. Regardless of the adiabatic change of state, because of the significant heat capacity, oil temperature is slightly changed, so that the change of state of dispersed undissolved air bubbles in oil can be considered isothermal. [4]

If the change of state of undissolved air is isothermal, then the volume of undissolved air in oil, depending on the pressure, given by

$$V_v = \left(\frac{p_a}{p}\right) V_{va}. \tag{12}$$

The effective bulk modulus of the mixture of oil and undissolved air, by inserting the expression (12) into (11), is

$$K_E = \frac{K_S\, p}{K_S \frac{\left(\frac{p_a}{p}\right)V_{va}}{\left(V_u + \left(\frac{p_a}{p}\right)V_{va}\right)} + p\frac{V_u}{\left(V_u + \left(\frac{p_a}{p}\right)V_{va}\right)}} . \quad (13)$$

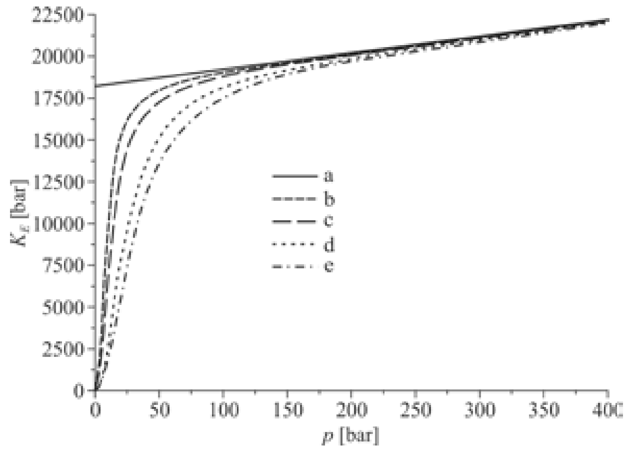

Figure 8. Effective bulk modulus at oil temperature of 30°C: a) the absence of undissolved air, b) 0.5% undissolved air, c) 1% undissolved air, d) 3% undissolved air; e) 5% undissolved air

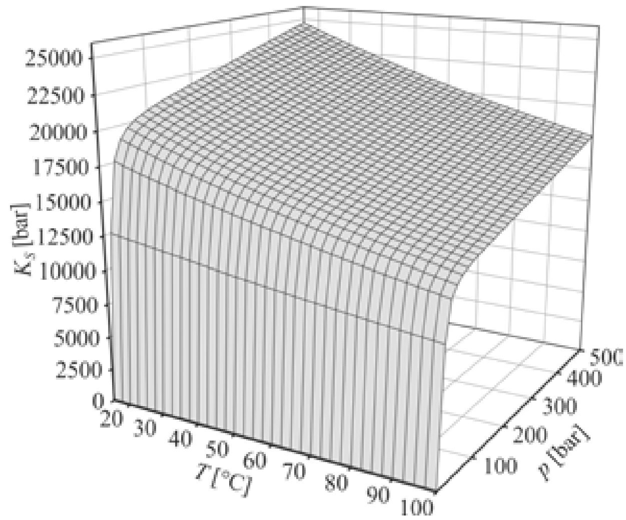

Figure 9. Effective bulk modulus depending on the pressure and temperature in the presence of 1% undissolved air in mineral oil

8. APPLICATION OF VALUE EFFECTIVE BULK MODULUS IN THE ANALYSIS PROCESS DECOMPRESSION (UNLOADING) OF OIL IN THE HYDRAULIC CYLINDERS

Theoretically analyzes the process of unloading of hydraulic cylinders controlled by draining the oil that is released through the relief nozzle-shaped openings with sharp edges. In parallel experimental study was carried out of the process. Experiments were carried out with mineral hydraulic oil HM 22, 32, 46 and 64 and HV 46, the common values of pressure in the hydraulic systems (up to 350 bar) and standard operating temperature (from 15 to 70°C).

Experimental verification of the theoretical model, in which the value of the effective bulk modulus was calculated by the formula (13), was shown that the process of decompression of mineral hydraulic oil can mathematically be described with great accuracy, even for small pressure when the impact undissolved air in the elasticity working fluid very large. Although during the compression and decompression of oil in the hydraulic cylinders are occurred complex processes of gradual dissolution undissolved air in the oil during compression and extraction of dissolved air from the oil during decompression, the experimental data showed that the analytical description can be counted with the presence undissolved air in the hydraulic oil from a to 3% of the total volume of the cylinder at atmospheric pressure.

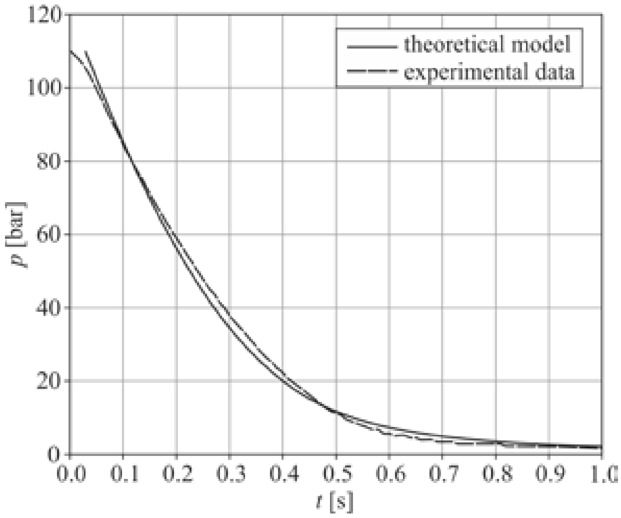

Figure 10. Change of pressure during the process of decompression of mineral oil which content 3% undissolved air at atmospheric pressure (oil temperature is 30 °C)

Figure 10 is an example of comparing experimental results with theoretical model description of the process of decompression, in which the value of the effective bulk modulus calculated by the formula (13). The experimental results in Figure 10 are provided for hydraulic cylinder diameter of 140 mm and length of stroke of 1000 mm. [4]

Controlled load shedding is done by draining the oil through a nozzle with a sharp edge diameter 2 mm. The theoretical model was calculated with undissolved air content of 3% in oil, at atmospheric pressure.

9. CONCLUSION

The value of the bulk modulus of hydraulic fluid has a large impact on the efficiency of the hydraulic system. It affects:

- Speed of propagation of the pulse pressure change in the system,
- Positioning accuracy of hydraulic actuators,
- Volumetric efficiency of pumps,
- The stability of the system according to its own fluctuations,
- The intensity of the hydraulic shock.

This paper gives the values of bulk modulus which are representative for mineral oil for hydraulic systems. The data are presented in the form of a diagram as a function of temperature and pressure. Data were checked indirectly, experimental measurements change of pressure during process decompression of mineral oil in the hydraulic cylinders.

Experimental results show that it is not possible to avoid the presence of undissolved air in the work of hydraulic systems. Comparing experimental data with theoretical model shows that in determining the effective bulk modulus can be count content of undissolved air in mineral oil in quantities of 1 to 3% at atmospheric pressure.

REFERENCES

[1] JUGOMA – Group of Authors, Lubricants and Lubrication, The Union of Yugoslav Societies for Application of Fuels and Lubricants, Zagreb, 1986.

[2] Keith P., Hodges B., Hydraulic Fluids, Arnold, London, 1996.

[3] Frauenstein M., Guide for Fluid Under Pressure for Constructors, Mobil Oil, 1979.

[4] Kneževic D., Analysis of Decompression of Hydraulic Oil in Cylinders of Hydraulic Presses, M.Sc. Thesis, Faculty of Technical Sciences Novi Sad, 2002.

Serbian Tribology Society

SERBIATRIB '11

12th International Conference on Tribology

Faculty of Mechanical Engineering in Kragujevac

Kragujevac, Serbia, 11 – 13 May 2011

EFFECT OF CHANGES OF VISCOSITY OF MINERAL OIL IN THE FUNCTION OF PRESSURE ON FLOWING THROUGH A LONG RADIAL CLEARANCE

Darko Knežević[1], Aleksandar Milašinović[1], Zdravko Milovanović[1], Vladimir Savić[2]
[1]Faculty of Mechanical Engineering Banja Luka, BiH – RS
darkokn@blic.net; acom@blic.net, mzdravko@urc.rs.ba,
[2]Faculty of Technical Science Novi Sad, Serbia; savicv@uns.ac.rs

Abstract: *Radial clearance in hydraulic components (but also in motor vehicles, etc) has multiple roles: it allows relative movement of elements to achieve the given functions, provides the sealing function between the space with different levels of pressure, and also serves as hydrostatic or hydrodynamic bearing according to the forces within the component. Common values of radial clearance is approximate in the range from 1 μm (minimum values for servo valves) to 50 μm (maximum value for axial piston pumps).*
It is common that when calculating the flow rate of mineral oil through clearances, constructors calculate with a constant value of viscosity for given working temperature. In this paper is analyzed the error because of acceptance of such assumptions.

Keywords: *pressure, viscosity, radial clearance, overlap, volumetric flow rate*

1. INTRODUCTION

Mineral oils are the most common type fluid used in the hydraulic systems (over 90% of the total use). To be able to achieve the projected functions, in the hydraulic systems are used many control and regulatory components in which they appear radial clearances.

In the analysis of the hydraulic systems are usually not taken into account change of viscosity of mineral oil with a change of pressure, because that change is far smaller than change of viscosity with changes in temperature. However, as the work of well-designed hydraulic system usually takes place at approximately constant operating temperature of working fluid, this neglect may lead to significant errors in calculations.

In practical calculations, it is common that the volumetric flow rate of fluid through radial clearance is calculated using the following formula

$$Q = \frac{d\pi c_r^3 \Delta p}{12\mu_0 L}, \qquad (1)$$

where:

d – diameter;
c_r – radial clearance;
Δp – pressure drop;
μ_0 – dynamic viscosity at the atmospheric pressure;
L – length of overlap.

Experimental measurements show that the volumetric flow rate through radial clearance calculated by formula (1) is differed from the measured values.

2. PRESSURE DEPENDENCE OF VISCOSITY OF MINERAL OIL

Viscosity of oil is increased with growth of pressure. Chemical composition greatly influences on viscosity-pressure characteristics of a hydraulic fluids.

The best known equation, which describes viscosity-pressure behavior of mineral hydraulic fluids, is Barus equation: [1]

$$\mu = \mu_0 e^{\alpha p}, \qquad (2)$$

where:
μ – dynamic viscosity at the pressure 'p' [Pas];

μ_0 – dynamic viscosity at the atmospheric pressure [Pas];

α - pressure-viscosity coefficient, which dependence of pressure and temperature [1/Pas].

To adopt experimental data by a mathematical model, the so-called "Modulus Equation" was used. "Modulus Equation" is based on Barus equation. The model comprises the pressure, p [bar], and temperature, T [°C], dependence of the dynamic viscosity [2]

$$\mu(p,T) = \mu_0 e^{\left[\frac{p}{a_1+a_2T+(b_1+b_2T)p}\right]}. \quad (3)$$

Dependence pressure-viscosity coefficient, α, of pressure and temperature is given by equation

$$\alpha(p,T) = \frac{\ln\mu - \ln\mu_0}{p - p_a} = \frac{1}{a_1 + a_2T + (b_1 + b_2T)p}. \quad (4)$$

The parameters a_1, a_2, b_1, b_2 represent the oil behavior and have to be calculated from experimental data. In accordance with the data given by the mineral oil producers ([3]), by using method of identification unknown parameters of mathematical model, are calculated constants from equation (4).

Table 1. Parameter values for pressure-viscosity coefficient, α [4]

	a_1 [bar]	a_2 [bar/°C]	b_1	b_2 [1/°C]
Mineral oil of paraffinic base structure	334	3.2557	0.026266	0.000315

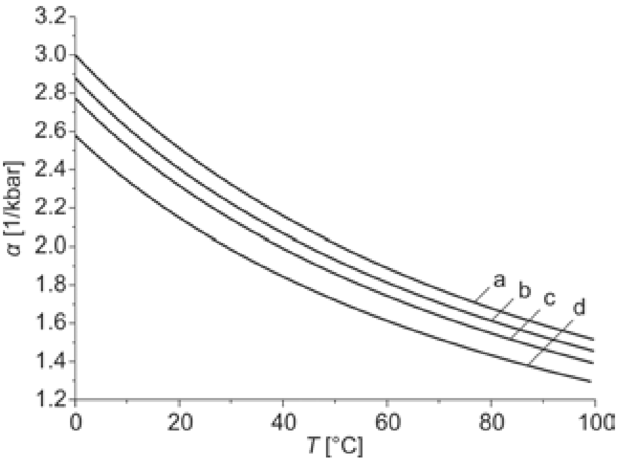

Figure 1. Pressure-viscosity coefficient of mineral oil paraffinic base structure: a) $p = p_a$; b) p = 500 bar; c) p = 1000 bar; d) p = 2000 bar

Example:

For the pressure of 350 bar and temperatures of 20.5 and 40°C, values of pressure-viscosity coefficient, are calculated by using of formula (4):

$$\alpha\left(p = 350\ \text{bar},\ T = 20.5^{\circ}\,\text{C}\right) = 0.002426\ \text{bar}^{-1}$$

and

$$\alpha\left(p = 350\ \text{bar},\ T = 40^{\circ}\,\text{C}\right) = 0.0020928\ \text{bar}^{-1},$$

and values of dynamic viscosity, are calculated by using of formula (3):

$$\mu\left(p = 350\ \text{bar},\ T = 20.5^{\circ}\,\text{C}\right) = 2.3375 \cdot \mu_0$$

and

$$\mu\left(p = 350\ \text{bar},\ T = 40^{\circ}\,\text{C}\right) = 2.08 \cdot \mu_0.$$

Value of dynamic viscosity, at pressure of 350 bar and temperature of 20.5°C (40°C), is for 2.3375 (2.08) times higher then value of dynamic viscosity at atmospheric pressure and the same temperature.

Figure 2 shows values of dynamic viscosity of some hydraulic oil at 50 °C, for different values of working pressure.

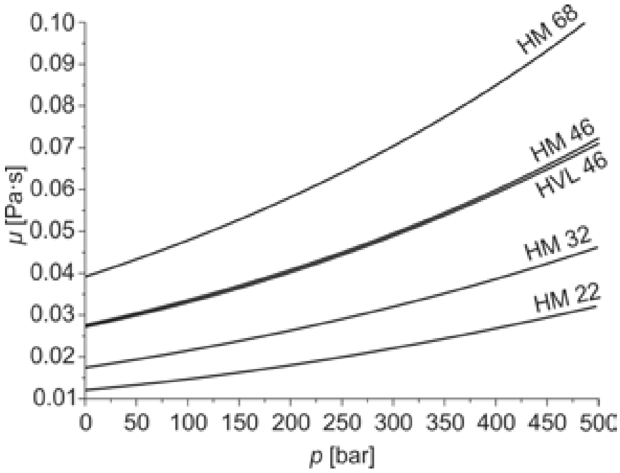

Figure 2. Change of viscosity of some mineral hydraulic oils with the change of pressure (temperature 50 °C) [4]

3. FLOW OF MINERAL OIL THROUGH LONG RADIAL CLEARANCES

Under the long clearance is understood such clearance whose length overlap (the length of leakage path) L is such that the hydraulic fluid is slightly warmed at flowing through the clearance. [4]

In this case, change of state of mineral oil at flowing can be considered isothermal. Such cases flow through the clearance is processed in the literature, but with one flaw: they ignore change of viscosity of oil with a change of pressure. This neglect can lead to the calculated flow rate is up to 50% higher than the actual flow rate (depending on value of working pressure in the hydraulic system).

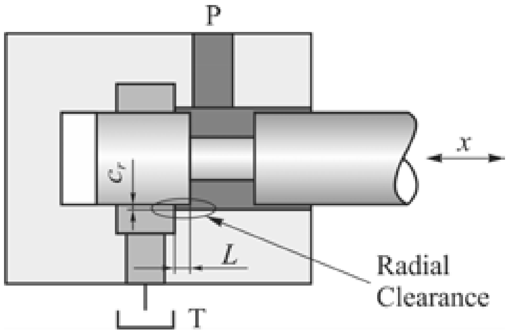

Figure 2. Flow of hydraulic fluid through long radial clearance

The flow of fluid through radial clearance can be described by the Navier-Stokes equations.

For steady flow of incompressible fluid, taking into account the change of viscosity along clearance, the vector form of these equations is

$$\rho \frac{D\mathbf{v}}{Dt} = \rho \mathbf{f} - \mathbf{grad} p + \Delta(\mu \mathbf{v}). \tag{5}$$

where:

$\rho \frac{D\mathbf{v}}{Dt}$ - inertial force per unit volume on elementary particle of fluid;

$\mathbf{grad} p$ - pressure force per unit volume on elementary particle of fluid,

$\Delta(\mu \mathbf{v})$ - viscous force per unit volume on elementary particle of fluid.

Following analysis will be carried out for symmetrical radial clearance because of in real conditions at flowing of oil through the radial clearance within the hydraulic component, pressure seeks to hold piston in concentric (coaxial) position in relation to the cylinder.

Cross sectional area through which fluid flows through the clearance is

$$A = \frac{\left(d_2^2 - d_1^2\right)\pi}{4}, \tag{6}$$

where:

d_2 - inner diameter of cylinder,

d_1 - diameter of piston.

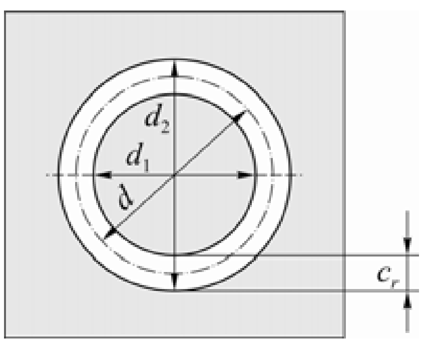

Figure 3. Symmetric radial clearance

As trajectories of fluid particles straight and parallel, fluid flow through radial clearance can be seen as flow between flat parallel surfaces which width are L, and the distance between them is c_r.

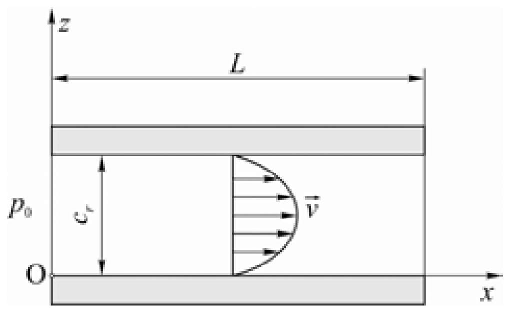

Figure 4. The flow of fluid between parallel plates

Can be written

$$d_1 = d - c_r, \tag{7}$$

and

$$d_2 = d + c_r. \tag{8}$$

Substituting equations (7) and (8) in equation (6), we get

$$A = d\pi c_r = wc_r, \tag{9}$$

where w is defined as the width of rectangular opening.

During steady rectilinear parallel flow there is only longitudinal component of velocity u, while components v and w are equal zero. Profile of velocity for this case of flow does not change along clearance.

Continuity equation in differential form is given by

$$\frac{\partial u}{\partial x} + \frac{\partial v}{\partial y} + \frac{\partial w}{\partial z} = 0. \tag{10}$$

As v and w equal zero, from equation (10) follows $\partial u / \partial x = 0$, why $u = f(z)$.

Since the influence of mass forces (**f**) are negligible, the Navier-Stokes equations are reduced to form

$$\frac{dp}{dx} = \frac{d^2(\mu u)}{dz^2}. \tag{11}$$

Dynamic viscosity of fluid that flowing through clearance, for the specific operating tepmerature, is given by the Barus's equation (2).

As pressure is function of longitudinal coordinate x, and the dynamic viscosity depends on pressure, then the dynamic viscosity is function of coordinates x, so we can write

$$e^{-\alpha p}\frac{dp}{dx}=\mu_0\frac{d^2u}{dz^2}. \qquad (12)$$

As the left side of equation (12) depends only of *x* and the right side equation (12) depends only of *z*, it follows that both sides of the equation (12) must be equal to a constant *C*.

General solution of equation (12) is

$$u=\frac{C}{2\mu_0}z^2+C_1z+C_2. \qquad (13)$$

The constant *C* can be determined from the boundary conditions for pressure:

$$\text{for } x=0, \qquad p=p_0, \qquad (14a)$$

and

$$\text{for } x=L, \qquad p=0. \qquad (14b)$$

From the condition that the left side of equation (12) is equal to constant *C*, ie.

$$e^{-\alpha p}\frac{dp}{dx}=C, \qquad (15)$$

putting

$$e^{-\alpha p}\frac{dp}{dx}=-\frac{1}{\alpha}\frac{d}{dx}e^{-\alpha p}. \qquad (16)$$

equation (15) can be directly integrated, and we get

$$e^{-\alpha p}=-\alpha Cx-\alpha C_3. \qquad (17)$$

Incorporating the boundary conditions (14) in equation (17), we get

$$C_3=-\frac{1}{\alpha}e^{-\alpha p_0}, \qquad (18)$$

and

$$C=\frac{e^{-\alpha p_0}-1}{\alpha L}. \qquad (19)$$

Using equations (16) and (19), from equation (15), we can get the law of change of pressure along clearance

$$p=-\frac{1}{\alpha}\ln\left(e^{-\alpha p_0}+\frac{1-e^{-\alpha p_0}}{L}x\right). \qquad (20)$$

As an example, in Figure 5 is shown the change of pressure through the clearance that length of overlap is 10 mm and working pressure 350 bar. In Figure 5 is given an overview of changes of pressure through the clearance: at neglect of influence of pressure on the value of dynamic viscosity, and curves of pressure change which are calculated by formula (20), for different operating temperatures (20°C and 50°C). The working fluid is a mineral hydraulic oil HM 46.

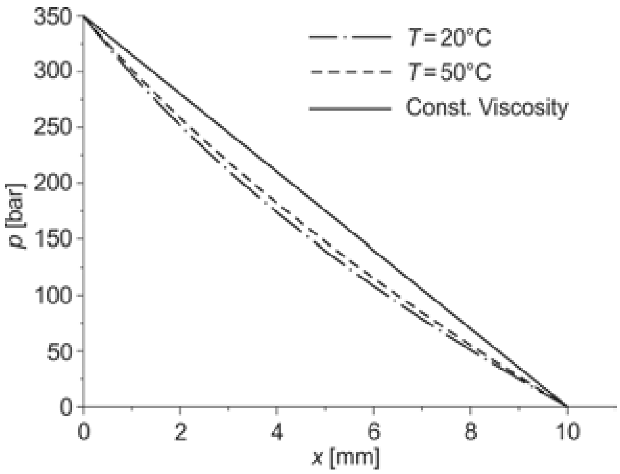

Figure 5. Change of pressure along the clearance

The boundary conditions for velocity are:

$$\text{for } z=0, \qquad u=0, \qquad (21a)$$

and

$$\text{for } z=c_r, \qquad u=0. \qquad (21b)$$

Substituting conditions (21) in equation (13), we get

$$C_2=0, \qquad (22)$$

and

$$C_1=-\frac{C}{2\mu_0}c_r. \qquad (23)$$

Incorporating the constants C_1 and C_2 in equation (13), we get expression for the velocity profile in the cross section of clearance

$$u=\frac{1-e^{-\alpha p_0}}{2\alpha\mu_0 L}\left(c_r z-z^2\right). \qquad (24)$$

Volumetric flow rate through clearance is

$$Q=\frac{1-e^{-\alpha p_0}}{\alpha}\cdot\frac{d\pi c_r^3}{12\mu_0 L}. \qquad (25)$$

4. ORIENTATION (BASED ON RESULTS OF EXPERIMENTS) CRITERIA FOR THE DIVISION CLEARANCES BETWEEN SHORT AND LONG CLEARANCES

Based on the experimental results, it was determined border length L_g for application of the formula (25) [4]

$$L_g=-\lambda\frac{c_r}{\ln 0.9}=9.5\lambda c_r, \qquad (26)$$

where:

λ - coefficient determined from experimental data.

For the lengths of overlap L that are greater than L_g, flow rate through the radial clearance is calculated using the formula (25).

Coeficient λ can be determined from expression ([4]):

$$\lambda = \frac{\sqrt{p_0}}{25 \cdot \beta}. \quad (27)$$

Viscosity-temperature coefficient β can be calculated from equation ([4])

$$\beta = \frac{1}{\Delta T} \ln \frac{\mu_0}{\mu}. \quad (28)$$

where

- $\Delta T = T - T_0$ [°C] - temperature increase,
- μ and μ_0 - values of dynamic viscosity at temperature T and T_0, at atmospheric pressure,
- p_0 – working pressure.

In Figure 6 are given the value of the coefficient β for some oils used in experimental research. [4]

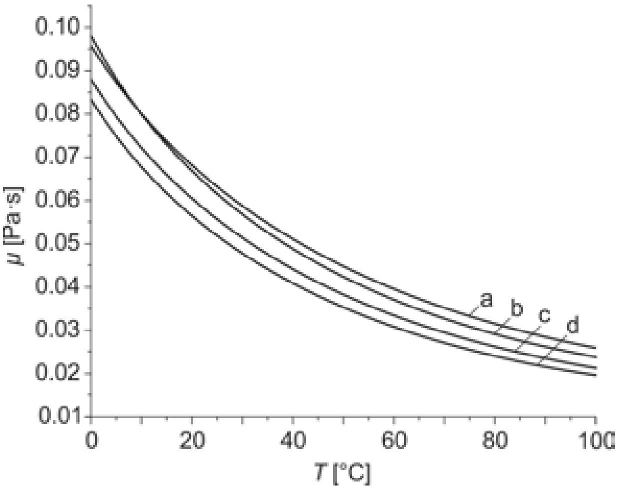

Figure 6. Temperature-viscosity coefficient of hydraulic oil: a) HM 68; b) HM 46; c) HM 32; d) HM 22

5. EXPERIMENTAL VERIFICATION OF THEORETICAL MODEL

In this paper is given an example of check theoretical model at measurement of flow rate through the radial clearance size $c_r = 17$ μm and diameter of the piston $d = 10$ mm. Working pressure was 350 bar. It was used mineral oil HM 46 [4]

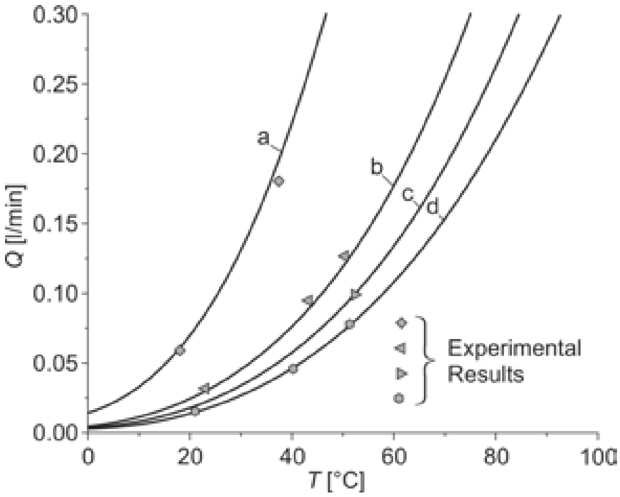

Figure 7. Theoretical curves: a) overlap 2 mm, b) overlap 6 mm; a) overlap 8 mm; a) overlap 10 mm

Table 2. The numerical values of the experimental results in Figure 7 and corresponding values calculated by the theoretical model (Equation 25)

L [mm]	T [°C]	Volumetric flow rate [l/min]	
		Experiment	Theoretical model
2	18	0.058	0.06
	37	0.18	0.19
6	23	0.031	0.028
	43	0.0936	0.087
	50	0.125	0.12
8	52	0.098	0.098
10	21	0.015	0.0148
	40	0.045	0.045
	51	0.0767	0.075

It should be noted that this example provides an illustration. The measuring of the flow rate was carried out for different diameters of pistons, various sizes of radial clearance and various kinds of mineral oils. Results of measurements were showed good agreement between experimental results and those obtained using the theoretical model.

6. CONCLUSION

As the efficiency of components with non-contact sealing clearances depends on the construction, types and characteristics of working fluid, and working pressure and temperature, the results of this study have the following scientific contributions:

- In this paper is presented a detail description of change of viscosity in function of change of pressure for mineral oils (especially mineral hydraulic oils). It is shown that the precise mathematical modeling of the fluid properties are necessary for research phenomena within components in which there are radial clearances;

- It is given mathematical model of flow through long radial clearances, taking into account change of viscosity mineral oil with change of pressure, for given working temperature;
- The derived formulas can be applied for flow through radial clearances with the lengths of overlap that are greater than those given formula (26), and for radial clearances whose size is larger than 10 µm. For radial clearances whose size is less than 10 µm, there is the effect of obliteration, which is not analyzed in this paper.

REFERENCES

[1] JUGOMA – Group of Authors, Lubricants and Lubrication, The Union of Yugoslav Societies for Application of Fuels and Lubricants, Zagreb, 1986.

[2] Schmidt A., Viscosity-Pressure-Temperature Behaviour of Mineral and Synthetic Oils, 12th International Colloquium Tribology 2000., Stuttgart, Germany, 2000.

[3] Frauenstein M., Guide for Fluid Under Pressure for Constructors, Mobil Oil, 1979.

[4] Kneževic D., PhD Thesis, Influence Clearances Geometry in Hydraulic Components of Automation Control on Efficiency of Hydraulic Systems, Novi Sad, 2007.

Serbian Tribology Society

SERBIATRIB '11

12th International Conference on Tribology

Faculty of Mechanical Engineering in Kragujevac

Kragujevac, Serbia, 11 – 13 May 2011

THE BEHAVIOUR OF SOME ADDITIVATED COMPOSITE MATERIALS AT SLIDING INDENTATION TEST

Constantin Spanu[1], Sorin Ciortan[1], Vasile Bria[1], Igor Roman[1]
[1]"Dunarea de Jos" University of Galati, Romania
constantin.spanu@ugal.ro; sorin.ciortan@ugal.ro; vasile.bria@ugal.ro; igor.roman@ugal.ro

Abstract: *The polymeric composite materials with epoxidic resin base and multi-walled carbon nano-tubes (MWCNT) can be used, due their electrical properties, as covering layers for parts subjected to electrical fields, in order to avoid electrostatic charges.These materials also present a brittle behaviour, being subjected to surface cracks development if the loading overcome certain levels. The material's surface response to dynamic loadings has a deirect influence on its tribological properties. A method for characterization of brittle behaviour is the sliding indentation. The paper presents the results obtained by performing indentation and sliding indentation tests on a epoxidic resin based composite, additivated with MWCNT. The tests show that the mixing order of the components have an influence on mechanical properties of the composite.*

Keywords: *MWCNT composite, sliding indentation, mechanical properties.*

1. INTRODUCTION

The composites, as macro-level combination of several materials in order to obtain a new material, with different properties [1], are new opportunities for designers allowing the optimization of products by better matching with technical requirements. By proper choosing of the components, the physical and mechanical properties of the composite can be predicted and obtained, accordingly with the requirements.

Even the composites properties are predicted from the mixing stage, a complete set of tests are required in order to establish the full applications possibilities. Among other classical tests for mechanical properties assessment, the indentation and the sliding indentation can provide useful information about the material behaviour under high loadings rising up until the plastic deformation appear.

Indentation is a mechanical testing method much easier than others (traction, for example), requiring simple samples and providing with satisfactory precision values of specific material's stresses (like ultimate tensile stress and yield tensile stress) [2,3].

The sliding indentation method, [4,5], where to the normal indentation force a tangential one is added, is more difficult to put in practice but provide a more complex state of stress in the sample than simple indentation [6,7].

The present paper is focused on the investigation of the behaviour of some composites based on epoxidic resin with 2% multi-walled carbon nano-tubes (MWCNT), taking into account the obtaining method. Both indentation methods are used for the establishing of cracking force and corresponding pressure values.

2. EXPERIMENTAL SETUP

The tests were performed on several flat samples of a composite with the same ingredients but obtained through different mixing technologies.

2.1 Studied materials

The subject of investigation was a composite based on bi-component epoxidic resin (component A - Ephiphen RE 4020 and component B - Ephiphen DE 4020) with additivated 2% MWCNT. This material should be used as covering layer for parts subjected to electrical fields, in order to avoid static charges. As consequence, some properties like: light weight, good mechanical resistance and electrical conductivity are required.

The system RE 4020/DE 4020 was chosen based on its properties: polymerization at room temperature, high thermal, UV and humidity resistance, transparency and low toxicity.

The added MWCNT should provide the required electrical conductivity and mechanical strength.

The obtaining technologies for composites based on epoxidic resins require the mixing of the additive with the resin's components. This can be done in several ways:

- first mixing all the additive quantity only with component A. The obtained mixture is then mixed with component B and polymerized;
- first mixing all the additive quantity only with component B. The obtained mixture is then mixed with component A and polymerized;
- first component A and B are mixed and all the additive quantity is before polymerization.

The performed tests try to determine which mixing method (Table 1) is most appropriate in order to obtain a composite material showing, beside required electrical properties, the best mechanical ones.

Table 1. Tested samples

Code	Mixing order
CNT-A	MWCNT additive mixed with component A
CNT-B	MWCNT additive mixed with component B
CNT-AB	MWCNT additive mixed with A-B mixture

2.2 Sliding indentation test rig

The tests were performed on a dedicated test rig [8,9,10,11], Figure 1, with a sliding speed v=0.172 mm/s. For simple indentation, a null speed was imposed.

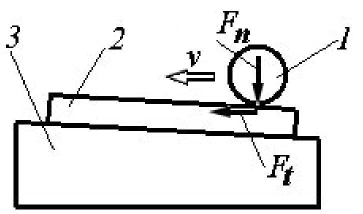

Figure1. The test rig: 1- indenter, 2 - sample, 3- inclined plane, v- horizontal sliding speed, F_t - tangential force, F_n - indentation force

As indenter, a 12.675 mm diameter ball was used. The ball material is hardened Romanian steel RUL-1 (SREN ISO 683-17:2002). The holder doesn't allow the ball rotation and for each test, a new ball was used.

In sliding indentation method case, the normal force value's increasing is obtained by mounting the sample on an inclined plane with angle value 2° (Figure 1), associated with a horizontal sliding speed of the indenter. This mounting leads to increasing rate of normal force (indentation force) depending on both plane angle and sample toughness. Keeping the same angle value for all tested samples, the only one dependency is with sample toughness. Both normal force and tangential force values were monitored and recorded using stress gauges and corresponding electronic amplifier connected to a personal computer.

3. TESTING RESULTS

The results of performed tests allowed analyzing of the composite mechanical behaviour. Several samples from every mixing method were tested and the corresponding results values were averaged.

3.1 Simple indentation

The average normal forces values, leading to samples' cracking are presented in Table 2.

Table 2. Numerical results

Average normal cracking force [N]		
CNT-A	CNT-B	CNT-AB
3039.20	2761.00	2295.64
Average indenter impression diameter [mm]		
CNT-A	CNT-B	CNT-AB
2.484	2.049	2.214
Average cracking pressure [MPa]		
CNT-A	CNT-B	CNT-AB
156.779	209.242	149.20

In order to evaluate the corresponding cracking pressure values, the indenter impression on the sample were measured (Figure 2) using a dedicated image analysis software package.

Figure 2. Indenter impression with lateral cracks

Due to radial cracks and material plastic deformation, aberration from circular shape of the impression was observed, requiring a measurement strategy: circle generation through three points placed on the largest un-cracked arc.

Averaged values of impressions' diameters for each sample category are presented in Table1.

Based on normal force values and measured diameters the corresponding average cracking pressure values can be computed, Table1.

The average calculi for all categories were checked with Grubbs statistical test.

In Figure 3 is presented a graphical comparison between average cracking pressure values.

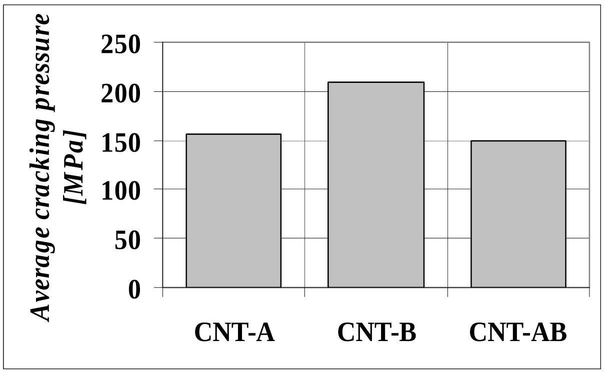

Figure 3. Comparison between average cracking pressure values.

The presented data shows that CNT-B mixing method leads to the highest cracking resistance, comparing to CNT-A and CNT-AB methods.

3.2 Sliding indentation

During sliding indentation process, due to constant normal force increasing, the indenter leaves on the sample surface tracks with a characteristic shape, Figure 4. At beginning and at the ending of the sliding track, areas with higher deformation can be observed. In these areas, due to the sample and indenter manipulation time, a simple indentation effect occurs.

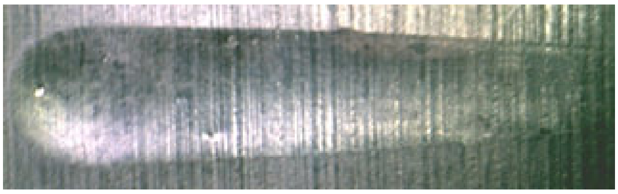

Figure 4. Characteristic tracks during sliding indentation.

The tests want to establish the increasing rate of normal force, as an indicator of material's hardness. As higher is the rate, as harder the material is. With this aim of the normal force variation was monitored and recorded.

In Figure 5 is presented, as an example, the corresponding variation for sample CNT-A.

In order to avoid erroneous results, the recorded data corresponding to areas of sliding beginning and ending are removed.

It can be observed that the graph is stepped shaped; this can be explained by appearance of oscillatory phenomenon due to accumulating-releasing of elastic deformation during sliding process.

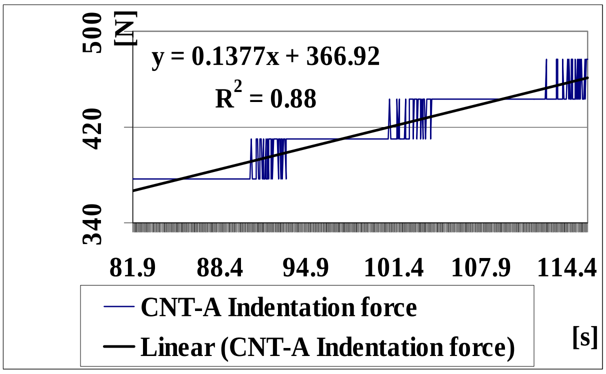

Figure 5. The increasing rate of indentation force for CTA-A sample

Regarding to the increasing rate of the indentation force $\mathbf{F_n}$, the obtained curves was approximate with a straight line, using Trendline facility in MS Excel. Even the R-squared coefficient presents relatively low values, indicating that there is another better approximation; this was preferred, allowing a more facile comparison between the samples. On the chart can be seen also the line equation and the corresponding R-squared coefficient values.

The values for normal force increasing rate obtained from regressing lines that correspond to all materials are presented in Table 3.

Table 3. Normal force increasing rate

Increasing rate [N/s]		
CNT-A	CNT-B	CNT-AB
0.1377	0.1448	0.0965

In Figure 6 is presented a comparison between all three regression lines.

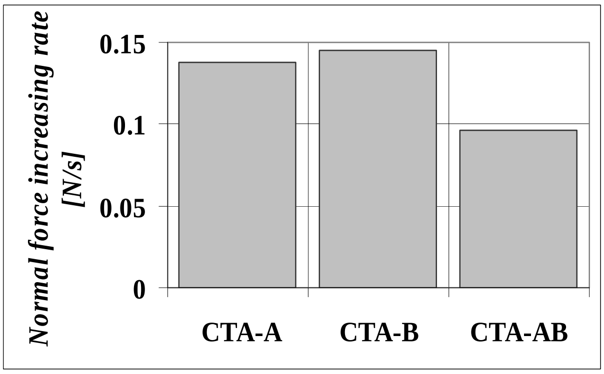

Figure 6. Comparison of normal force increasing rates for tested samples

It can be observed that normal force increasing rate, is biggest in CNT-B case. This observation is coherent with simple indentation results, Figure 3.

4. CONCLUSIONS

The paper presents the results obtained after indentation and sliding indentation tests performed on an epoxidic resin – MWCNT composite. Three mixing methods were sampled, in order to establish the best one from mechanical resistance point of view.

The results show that:

- simple indentation test can stand as a affordable and easy method to establish the toughest material, as being the one which require the biggest cracking pressure value;
- with sliding indentation method, as complementary test, the validation of simple indentation results can be done;
- composites based on epoxidic resin with added MWCNT show, beside the electrical properties, good mechanical properties, making these materials appropriate for using as cover layers.

REFERENCES

[1] R.M. Jones: Mechanics of composite materials, Taylor & Francis, 1992.

[2] I.M. Hutchings: The contributions of David Tabor to the science of indentation hardness, J.Mater.Res., Vol. 24, No. 3, 2009.

[3] B. Janakiraman: Mechanical property measurement by indentation techniques, PhD.thesis, http://repository.tamu.edu/bitstream/handle/1969.1/3111/etd-tamu-2004c-meennakir.pdf?sequence=1, 2011.

[4] K.L. Johnson: Contact mechanics, Cambridge, 1985.

[5] S.J. Sharp, M.F. Ashby, N. F. Fleck: Material response under static and sliding indentation loads, Acta Metallurgica et Materialia, Vol. 41, No. 3, pp. 685-692.

[6] D.A Hills: Mechanics of elastic contacts, Butterworth - Heinemann ltd., Oxford, 1993.

[7] A. Sackfield, D.A. Hills: Some useful results in the tangentially loaded hertzian contact problem, Journal of Strain Analysis, Vol. 18, pp. 107-110, 1983

[8] C. Spânu: Studies and researches on tribomodels as regards surface layer plastic deformation under rolling and sliding, Ph.D. Thesis, Galaţi, 2002.

[9] C. Spânu, C. Teletin, I. Crudu, V. Mereuţă: Sliding indentation behaviour of the x 65 hydrogenate steel. in: Proceedings of International Conference on Diagnosis and Prediction in Mechanical Engineering Systems (Dipre'09) 22-23.10.2009, Galati, Paper 34.

[10] C. Spânu: Calculus of temperature for sliding indentation, The annals of Dunarea de Jos University of Galati, fascicle viii, Tribology, pp. 288-290, 2003.

[11] C. Spânu: Tribomodel, specimen and device for the study of deformation into superficial layer during free rolling, The annals of Dunarea de Jos University of Galati, fascicle viii, Tribology, pp. 102-104, 1997.

Serbian Tribology Society

SERBIATRIB '11

12th International Conference on Tribology

Faculty of Mechanical Engineering in Kragujevac

Kragujevac, Serbia, 11 – 13 May 2011

THE INFLUENCE OF THE RELATIVE SLIDING ON THE SURFACE QUALITY

Nicolae Diaconu, Lorena Deleanu, Florentina Potecaşu, Sorin Ciortan
”Dunarea de Jos” University, Romania, nicolae.diaconu@ugal.ro

Abstract: *This paper presents a study on the surface quality pointing out the influence of relative sliding on the topography parameters. Traditional roughness parameters as Ra and Rq, deal only with relative high of the asperities to the mean line and they give no information on shape, slope and asperities magnitude, on their appearance frequency on the profile length. The authors analysed a set of 3D parameters including the amplitude ones (Sa, Sku, Ssk and St) and functional parameters as Svk, Sk and Spk as calculated with a dedicated soft from the bearing area. Tests were done on roller-roller tribotester lubricated with the grease grade UM185Li2EP (general purpose grease for rolling bearings), the temperature of the environment being kept at 80°C. There was studied the influence of relative sliding speed on the skewness and the kurtosis of the surface topography, but also on common parameters as Sa and St. Such a study may be used for selecting a suitable surface quality and to evaluate the surface topography degradation in time, after tests under severe conditions, very close to the actual ones.*

Keywords: *roller-roller tribotester, relative sliding, profilometry, functional 3D parameters.*

1. INTRODUCTION

Traditional roughness parameters as *Ra* and *Rq*, deal only with relative high of asperities to the mean line and they give no information on shape, slope and asperities magnitude, on their appearance frequency on the profile length.

3D profilometry offers the opportunity for a deeper and more accurate analysis of the surface quality [3-5].

Multiple measurements in different areas on the sample can produce results within a large range, due to variations of the surface texture across the sample surface. Consequently, the results of any single measurement may not be representative of the overall surface quality [3, 4] and specialists recommend methods to be applied for a more accurate characterisation of the surface, more often for manufactured parts, and rarely for evaluating how the surface quality evolved in actual exploitation.

The parameters involved in this study are briefly described below. The analysed amplitude parameters are: the roughness average, *Sa* [μm], the root mean square *Sq* [μm], the surface skewness, *Ssk* [-], the surface kurtosis, *Sku* [-], the peak-peak height, *St* [μm].

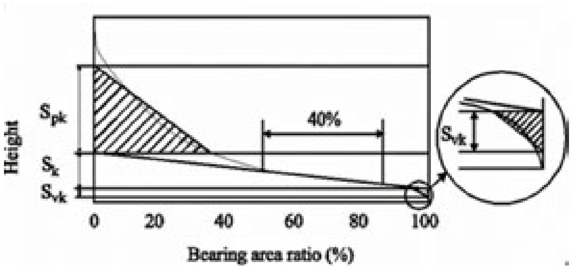

Figure 1. Bearing curve illustrating the calculation of *Spk*, *Sk* and *Svk* [6]

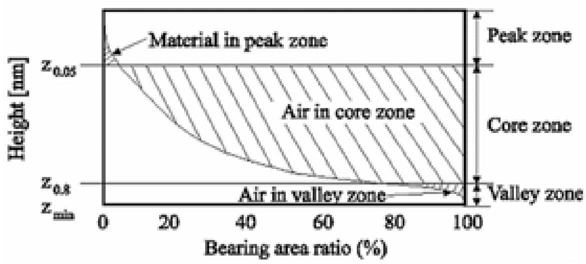

Figure 2. Bearing curve illustrating the calculation of *Sbi*, *Sci* and *Svi* [6]

The functional parameters are described graphically in Figures 1 and 2.

The surface bearing index, *Sbi* [μm], is defined as:

$$Sbi = \frac{Sq}{Z_{0.05}} \quad (1)$$

where $Z_{0.05}$ is the distance from the top of the surface to the height at 5% bearing area.

The core fluid retention index, *Sci* [μm], is defined as:

$$Sci = \frac{\dfrac{V_v(h_{0.05}) - V_v(h_{0.080})}{(M-1)(N-1)\delta x \cdot \delta y}}{Sq} \quad (2)$$

where $Vv(Z_x)$, is the void area over the bearing area ratio curve and under the horizontal line Z_x.

The valley fluid retention index, *Svi* [μm], is defined as:

$$Svi = \frac{V_v(h_{0.80})}{(M-1)(N-1)\delta x \cdot \delta y} \quad (3)$$

For relations (1)…(3), *M* is the number of lines of the investigated area and *N* are the number of points on each line.

The reduced summit height, *Spk*, is the height of the upper left triangle [6]. The core roughness depth, *Sk*, is the height difference between the intersection points of the found least mean square line. The reduced valley depth, *Svk*, is the height of the triangle drawn at 100% (Figure 1).

2. TESTING METHODOLOGY

Tests were done on a roller-roller tribotester (Fig. 1) [2]. The test conditions were: normal load Q=1.0 kN, enclosure temperature θ=80°C, rolling speed (for ξ=0%) v=1.09 m/s, testing period t=240 minutes, lubricant: grease grade UM185Li2EP (general purpose grease for rolling bearings), diameter of rollers for pure rolling D=42.0 mm, contact width B=10 mm ($B_{Roller1}$=10 mm, $B_{Roller2}$=12 mm)

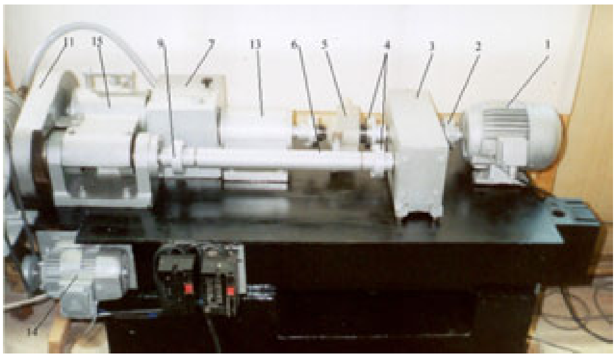

Figure 3. The testing machine 1– driving electric engine; 2, 4, 9– rigid coupling; 3– gear transmission; 5– torque transducer; 6– intermediate shaft; 7– thermoisolant box; 8 – tested rollers (in box 7); 10– force transducer; 11– reducing gear box.

The relative sliding between rollers was pointed out by the sliding coefficient, calculated as:

$$\xi = \frac{2(v_1 - v_2)}{v_1 + v_2} \cdot 100\ [\%] \quad (4)$$

v_1 and v_2 being the peripheral speeds for the roller 1 and 2, respectively. ξ=0 is for pure rolling.

The roller geometry allows running the test with three values for the relative sliding: ξ=0% (pure rolling), ξ=16.3% and ξ=33.5%.

Rollers were made of heat-treated high-quality carbon steel. All rollers were grinded and the topography parameters are given in all figures as for unworn surfaces. The rollers 3A, 5C, 1E and 4A are made of steel grade OLC25 (0.25% C) and the rollers 3B, 5D, 1F are made of steel grade OLC45 (0.45% C). The investigated pairs of rollers are: 3A-3B, 5C-5D, 1E-1F and 4A-4B.

There were investigated square areas of 500μm x 500μm, in the central zone of the wear track with the help of a CETR contact profilometer. The vertical range was set up to 500 μm as wear tracks had visible traces in the sliding direction and the scan speed was set at 35 μm/s. This research was done for 200 points per line and the step between lines was selected at 5 μm. All parameters are calculated from the raw profiles that “rebuild” the actual surface [6]. The stylus equivalent loading force was set at 28 mg for all measurements.

A single 3D measurement is usually insufficient for the grading of a surface, if a specific parameter value is desired. It is recommended a standard number of five sampling length for 2D parameters [7, 8] and the number of line samples are 100 for all three measurements on each wear track, but someone could say these are too “concentrated” in a small area of the surface of interest. It was found that it is often necessary to perform at least 5 measurements to obtain a stable mean value for many roughness parameters while others need a larger number as there is often one or few measurements diverging from the expected normally distributed result [1, 4, 8].

For worn surfaces the number of measurements will be established depending on surfaces to be investigated. Here the authors did 3 measurements for each roller and there were calculated the average values of the 3D amplitude parameters and several functional parameters as obtained from raw (non-filtered) (examples are given in table 1 and Figure 9). $As\%(S_x)$ is the percentage of up-deviation from the calculated average value:

$$As\%(S_x) = \frac{Max(S_x) - Average(S_x)}{Average(S_x)} 100 = \frac{As(S_x)}{Average(S_x)}\ [\%] \quad (4)$$

$Ai\%(S_x)$ is the percentage of the inferior deviation from the calculated average value:

$$Ai(S_x) = \frac{Min(S_x) - Average(S_x)}{Average(S_x)} 100 = \frac{Ai}{Average(S_x)} [\%] \quad (5)$$

In relationships (4) and (5), S_x is one of the parameters *Sa*, *Sq*, *St*, *Sku*, *Ssk*, *Sbi*, *Sci*, *Svi*, *Sk*, *Spk*, *Svk*. $Max(S_x)$ is the maximum value of all measurements for parameter S_x, $Min(S_x)$ is the minimum value of all measurents for parameter S_x and $Average(S_x)$ is the average value of all measurements for parameter the same S_x.

Filtered profiles could disturb the values [3, 4], especially for high peaks and deep valleys that are important to be pointed out on worn surfaces.

3. CONCLUSION

Figure 4 presents the amplitude parameters *Sa*, *Sq* and *St*. As mentioned in [1, 3, 4] *Sa* is not a reliable parameter for assessing the surface quality, especially for worn surfaces. For all investigated surfaces *Sa* is lower than the value obtained for grinded (unworn) surfaces and even *Sq* seems to have the same tendency and both ones could be considered less sensitive to relative sliding. *St* has a clear trend to be reduced for both rollers under pure rolling, but at ξ=16.3%, there were recorded the highest values meaning that this value could generate the highest peaks. These are dangerous especially for lubricated contacts because they incapacitate for generating a continuous film of lubricant and increase the probability of direct contacts among asperities.

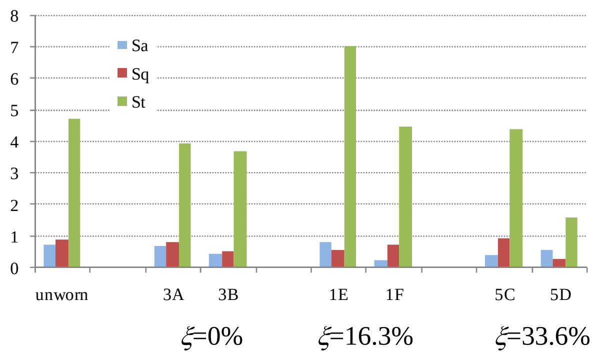

Figure 4. Amplitude parameters *Sa*, *Sq* and *St* for the tested rollers

Sku increases for all tested surfaces, but especially for rollers with relative sliding, meaning that the relative sliding could generate a distribution with rare but narrow peaks. The values are much lower for the steel grade OLC45 and for this steel grade the influence of relative sliding seems to be almost linear under the test conditions. For the steel grade OLC 25 both values of relative sliding have generated close values for this parameter. *Sku* has the largest spread range, about 8...9 times greater than the initial value. Figure 8 presents images of the worn surfaces as being rebuilt based on the measured coordinates and these images reveal isolated deep valleys.

The negative values for *Ssk* point out there are holes in the surface topography, deeper for ξ=16.3% and for this test, for the roller made of steel grade OLC25.

Ssk has a similar trend for the highest relative slide (ξ=33.5%). Due to this value the asperities are "micro-grinded" and *Ssk* is similar to the initial ones. High relative changes of these two parameters (*Ssk* and *Sku*) for the worn surfaces are also reported by Krzyzak in [5].

If one analyses only the average parameter *Sa*, he will notice that it remains close to the initial value, or even lower, but the conclusion that surface become smother is a "false friend" and additional information is necessary for describing it. For instance, *St* – the maximum peak-to-valley value on the investigated areas, increases for roller tested under relative sliding, but for the rollers under pure rolling, the parameters like *Sa*, *Sk* and *St* are smaller with 20...25%. Even *Sa* for all tested rollers remains in a range considered good for further exploitation, the higher values for *St* offers the motivation of harder damages on rollers 5C-5D and 1E-1F.

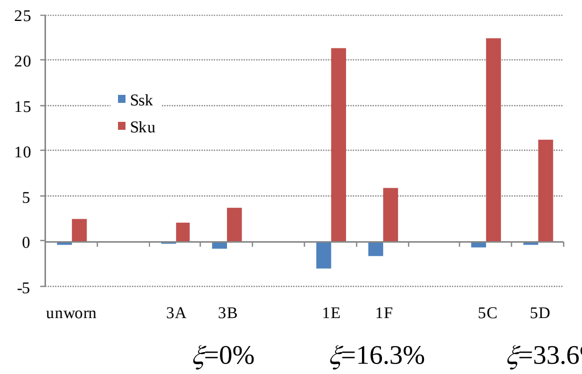

Figure 5. Amplitude parameters *Ssk* and *Sku* for the tested rollers

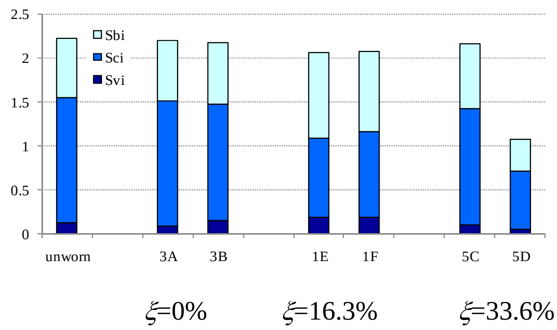

Figure 6. Functional parameters *Sbi*, *Sci* and *Svi* for the tested rollers

Table 1. Example of data for the roller 5C.

3D parameter	Sample 5C_1	Sample 5C_2	Sample 5C_3	Average	MAX	MIN	As	Ai	As (%)	Ai (%)
Sa	0.371	0.376	0.373	**0.373**	0.376	0.371	0.003	-0.002	0.68	-0.59
Sq	0.489	0.601	0.537	**0.542**	0.601	0.489	0.058	-0.053	10.787	-9.74
Ssk	-0.676	1.770	-2.939	**-0.615**	1.770	-2.939	2.385	-2.324	-387.84	377.92
Sku	7.188	39.160	21.375	**22.574**	39.160	7.188	16.586	-15.386	73.47	-68.15
St	6.268	13.290	7.030	**8.863**	13.290	6.268	4.428	-2.595	49.95	-29.27
Spk	0.634	4.367	0.135	**1.712**	4.367	0.135	2.655	-1.577	155.09	-92.10
Sk	1.099	0.829	0.804	**0.910**	1.099	0.804	0.189	-0.107	20.72	-11.74
Svk	0.618	0.685	0.919	**0.741**	0.919	0.618	0.178	-0.123	24.08	-16.59

Table 1 contains the results with 3 digits after point for easy reading, all operations being done with 5 digits after point.

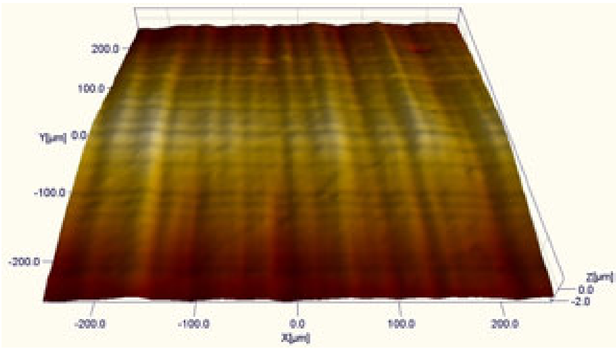

Roller 3A (ξ=0%)

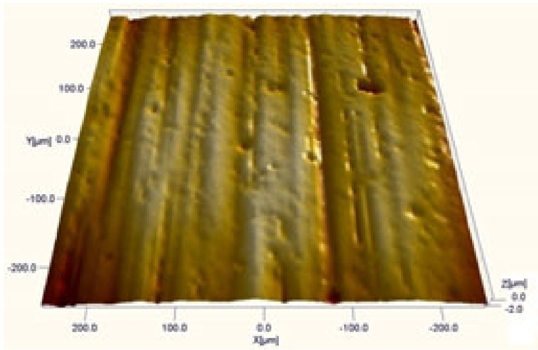

Roller 3B (ξ=0%)

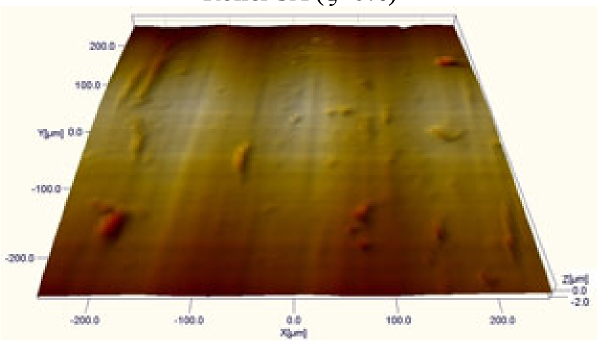

Roller 1E (ξ=16.3%)

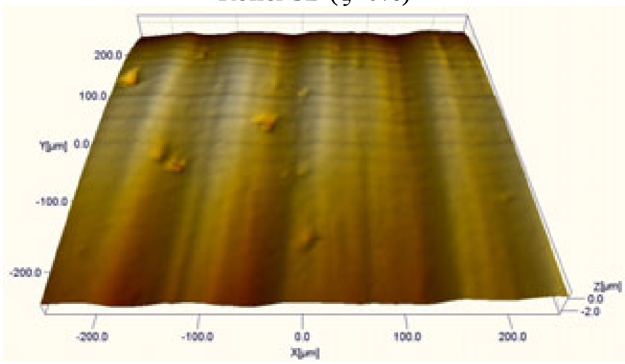

Roller 1F (ξ=16.3%)

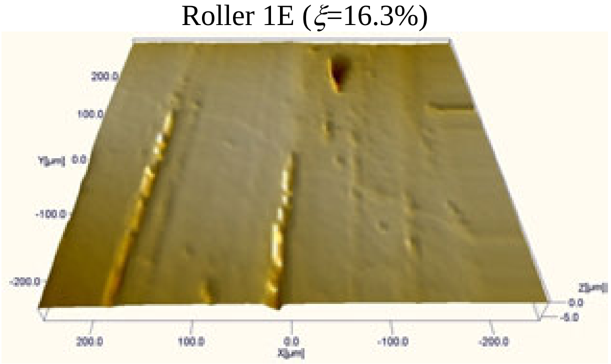

Roller 5C (ξ=33.5%)

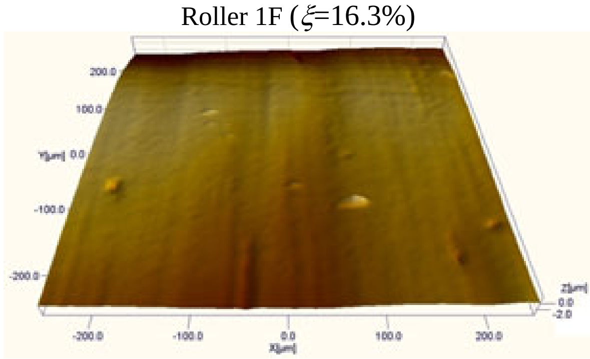

Roller 5D (ξ=33.5%)

Figure 8. Virtual images of the investigated surfaces

Large *Sbi* indicates a good bearing property. Only for the higher relative sliding there was noticed a decrease of *Sbi* and *Sci*. Large values of *Sci* indicate that the void volume in the core zone is large. For the tests with pure rolling the change of these parameters and their sum value are insignificant, but for ξ=33.5% the sum is slightly reduced and *Sbi* increases. Small values of *Svi* indicate small void volumes in the valley zone (correlate Figure 6 to virtual images in Figure 8).

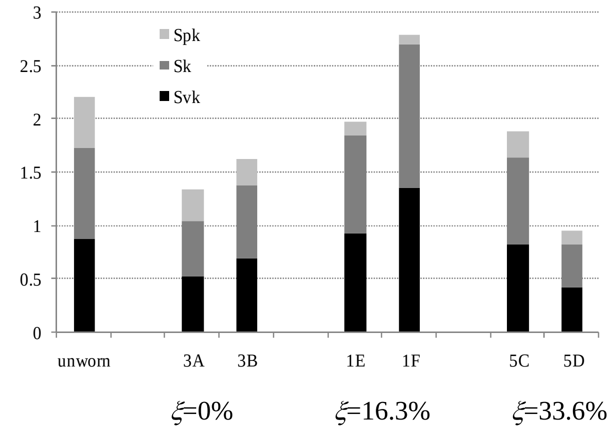

Figure 7. Functional parameters *Spk*, *Sk* and *Svk* for the tested rollers

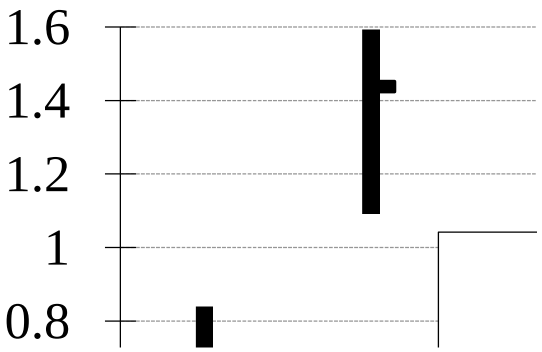

Figure 9. The spread range for functional parameters for roller 5C (three measurements on 500 x 500 μm each)

For ξ=0% and ξ=33.6% the functional parameters *Svk*, *Sk* and *Spk* are reduced as compared to the initial surface, but for ξ=16.3% the sum of these parameters is higher, *Svk* and *Sk* being much higher as compared to the unworn surface (Figure 7).

A comparative study of the surface topography, obtained by changing a single parameter during the tests, may reveal at least a qualitative influence of this parameter that could be useful for practicians.

There could be noticed two groups of parameters:

- parameters less influenced by the relative sliding, including *Sa*, *Sq*,
- parameters bearing a greater influence, these being *Ssk* and *Sku* and the functional parameters.

Taking into account the ranging of the calculated parameters, one may notice that *Sa*, *Sq*, *Svk* and *Sk* have a narrow spreading range, a second group may include parameters with a range similar to the parameter value (50…100%), e.g. *St* and *Sku*. A special attention has to be paid to *Ssk* that could have the spreading range much greater as compared to the average value.

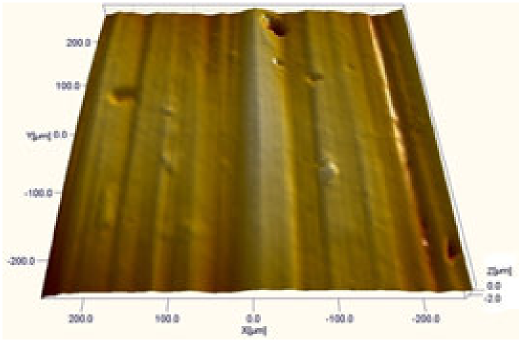

Roller 4A

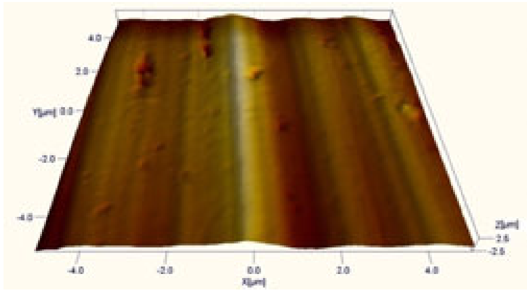

Roller 4B

Figure 10. Virtual rebuilding of the tested surfaces for *Q*=0.7 kN, pure rolling

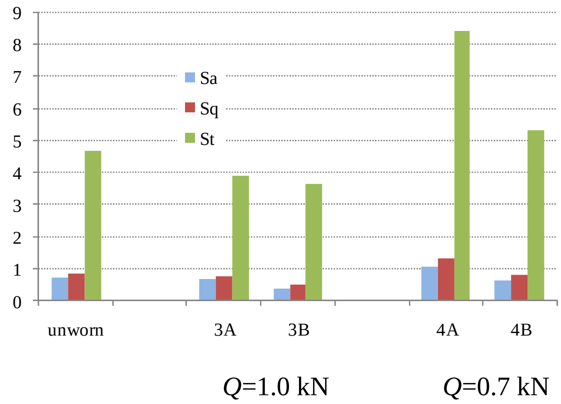

Figure 11. Amplitude parameters *Sa*, *Sq* and *St* for the roller surfaces under pure rolling

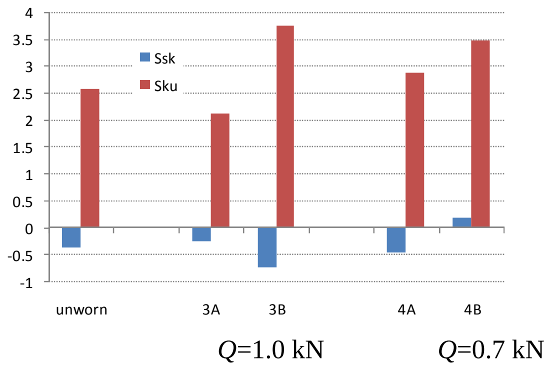

Figure 12. Amplitude parameters *Ssk* and *Sku* for the roller surfaces under pure rolling

For pure rolling an increase of the normal load from 0.7 kN to 1.0 kN modifies the functional parameters as given in Figures 11-13, reducing the sum of these parameters as compared to the value obtained on unworn surface and that of tested at *Q*=0.7 kN.

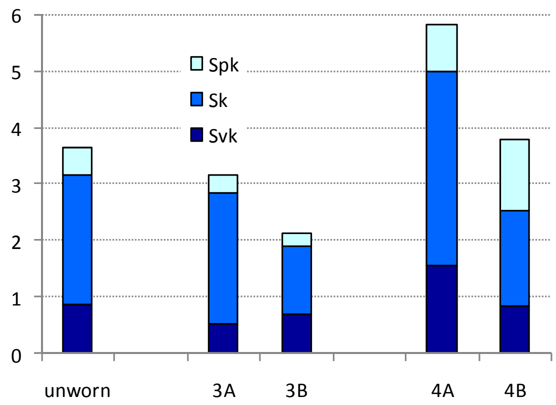

Q=1.0 kN *Q*=0.7 kN

Figure 13. Functional parameters *Sk*, *Spk* and *Svk* for roller surfaces under pure rolling

Comparing images from Figure 8 (rollers 3A and 3B) and Figure 10 (rollers 4A and 4B), one may notice that the damaging processes of the surface are similar, but more intense for the rollers bearing *Q*=1.0 kN. The higher load reduced the amplitude parameters like *Sa*, *Sk* and *St* (Figure 11). *Ssk* remains in the negative range for *Q*=1.0 kN, but for *Q*=0.7 kN there were recorded values giving a positive average (Figure 12). Under this load and pure rolling, the higher isolated peaks may be less damaged as compared to those under a rolling-sliding motion. It could also be the consequence of adhesive wear (isolated high peaks above the surface could be seen in Figure 10, suggesting wear debris adhered on the roller surface).

Taking into account the surface quality, steel grade OLC45 is more appropriate for application with similar conditions as those involved in these tests as compared to the steel grade OLC 25, because many of the surface parameters have only a small increase, meaning the surfaces could continue to work under those conditions. A similar qualitative evaluation was obtained by analysing the virtual images of the tested surfaces as given by a dedicated soft of the 3D profilometer.

REFERENCES

[1] N. Diaconu, Influence of the testing parameters on the surface quality of steel roller-roller system under grease lubrication, paper 25347, Proceedings of the 10th Biennial Conference on Engineering Systems Design and Analysis, ESDA10, July 12-14, Istanbul, Turkey, 2010

[2] N. Diaconu, Study on the Influence of the Working Environment on the Behaviour of Several Greases Used in Rolling and Rolling-Sliding Tribosystems (in Romanian), PhD thesis, “Dunarea de Jos” University of Galati, 2001

[3] L. Blunt, X. Jiang, Advanced techniques for assessment surface topography development of a basis for 3D surface texture standards "surfstand", London; Sterling, VA, Kogan Page Science, Elsevier, 2003.

[4] Whitehouse D.J., Handbook of Surface and Nanometrology, University of Warwick, Institute of Physics Publishing, Bristol and Philadephia, 2003

[5] Z. Krzyzak, P. Pawlus, ‘Zero-wear’ of piston skirt surface topography, Wear 260, pp. 554–561, 2006.

[6] **** The Scanning Probe Image Processor SPIP™, Version 4.7 (2008).

[7] **** SR EN ISO 12085:1999 Geometrical Product Specifications (GPS). Surface texture: Profile method. Motif parameters and SR EN ISO 12085:1999/AC:2009 Geometrical product specifications (GPS). Surface texture: Profile method. Motif parameters

[8] **** SR EN ISO 13565-2:1999 Geometrical Product Specifications (GPS). Surface texture: Profile method; Surfaces having stratified functional properties. Part 2: Height characterization using the linear material ratio curve

Serbian Tribology Society

SERBIATRIB '11

12th International Conference on Tribology

Faculty of Mechanical Engineering in Kragujevac

Kragujevac, Serbia, 11 – 13 May 2011

APPLICATION OF CONTEMPORARY INFORMATION TECHNOLOGIES IN NANOTRIBOMETRY

Milan Erić[1], Slobodan Mitrović[1], Fatima Živić[1], Marko Pantić[1]

[1] Faculty of Mechanical Engineering, Sestre Janjic 6, Kragujevac, Serbia

Abstract: *Relevant and timely information is of crucial importance in scientific investigations and understanding of the phenomena should be precise and explicit. Among other, phases of scientific investigations comprise data acquisition and their structuring into database and data warehouse, followed by their analysis in order to find laws and patterns and comparison with similar data. These activities are aimed at data to become information and for information to grow into knowledge and to further use that knowledge to formulate decisions and to anticipate future events and possibilities. However, simple analysis of information and responses to what already happened are not any longer satisfactory enough. Therefore, proactive approach is needed, that is technologies, skills and tools are needed that will assist in rapid decision making and forecasting. The paper presents architectures for data acquisition, developed databases and reporting, as well as, contemporary information technologies used for tribological investigations in area of nanotribometry.*

Keywords: *Information technologies, database, software tool, data conversion, tribological investigations, nanotribology*

1. INTRODUCTION

We live in time of dynamic, dramatic, complex and unpredictable changes, in a period which is marked by different terms as: digital revolution, information age, digital economy, internet economy, web economy, knowledge economy, knowledge society, post-industrial society, discontinuity society, society of unpredictability, third wave etc. Information and knowledge growth are becoming more and more essential development and economy resources. We have been living in digital technologies era for three decades now and Internet and Intranet environments fundamentally change the way of communications, availability, accessibility and data/information exchange. Relevant and timely information is of crucial importance in scientific investigations and understanding of the performed event should be precise and explicit. Among other, phases of scientific investigations comprise data acquisition and their structuring into database and data warehouse, followed by their analysis in order to find laws and patterns and comparison with similar data. These activities are aimed at data to become information and for information to grow into knowledge and to further use that knowledge to formulate decisions and to anticipate future events, Fig. 1 [1].

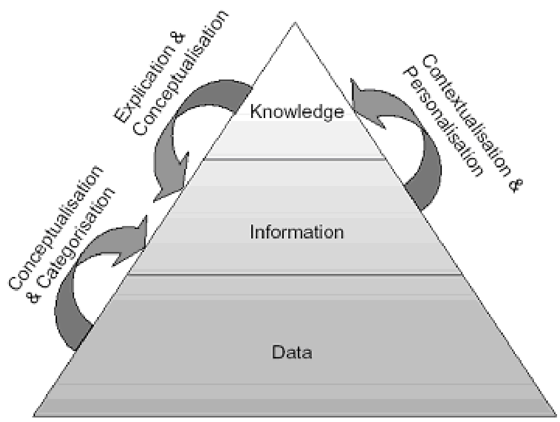

Figure 1. Data-Information-Knowledge

Data alone are rather hardly usable. Only after they have been processed, when relevance in certain context and in specific way is given to them, they become information. Data conversion into information relatively mechanical process and is realised using information technologies that categorize, process and storage them. Role of information is to lower uncertainty in scope of some critical area. Collection of data that has been processed and presented in a certain way, combined with experience and intuition constitute knowledge. Information becomes knowledge when it is processed in a mind of a person. Such knowledge again becomes information when it is transferred to other persons in a form of a text, picture or graphics. Knowledge is sustainable and unlimited resource accumulated through experience. It is embedded in persons who create, develop, enhance, use and transfer it.

2. DATA-TO-INFORMATION CONVERSION PROCESS

Potentially the interpretation of data into information is a very complex issue. One of many possible scenarios of conversion process of data obtained from different resources is shown in Fig. 2 (e.g. from the embedded sensors on the machines, from maintenance database, from manually input working conditions and experimental laboratory investigations into information [2]. Data is obtained from several resources and further transformed into multiple-regime features by selecting the appropriate computational tools for signal processing and feature extraction. In the feature space, indices are calculated by statistically detecting the deviation of the feature space from the baseline by choosing the appropriate computational tools for assessment / evaluation [3].

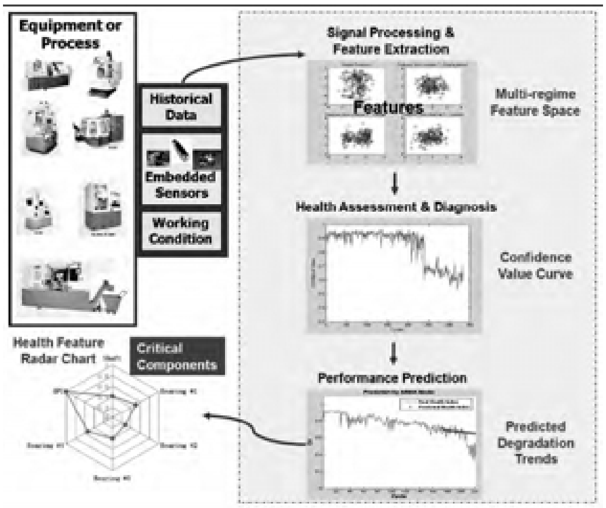

Figure 2. Data-to-information conversion process

In case of tribological investigations, conversion process is realised by data acquisition process whose block diagram is shown in Fig 3 [4]. Data acquisition system must convert real practice signals, such as amplitude, level, voltage, current intensity, temperature, pressure, weight, time period etc., which are not in a format acceptable for computer. It converts them into format understandable for computer, that is, into format that can be registered in databases. Data acquisition system of modern design consists of: analog - digital converter multiplexer, digital - analog transformer (D/A), sampling circuit (Sample/Hold), amplifier, timer (time circuits) and other specific circuits. One of the most important characteristics of the data acquisition system is that computer integrates them all into one compatible system. When appropriate software is added upon it, system is obtained that does not need detailed knowledge to use it. It is necessary to get acquainted with main problems in this area in order to make selection of such a system.

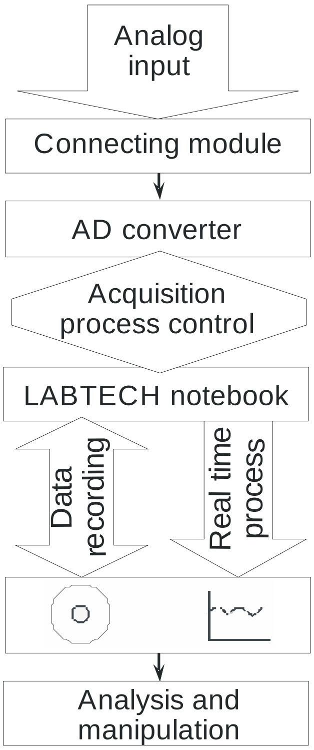

Figure 3. Block diagram of data acquisition process

Database was designed to storage data obtained by data acquisition during tribological investigations and its concept (logic) schema is illustrated in Fig. 4 as entity relationship diagram. Conceptual schema, tha is, logical frame of the model, is done using DeZign for Databases CASE tool. DeZign for Databases is software for database creating and working with them by using entity relationship diagram. Software enables easy and simple work for a user in all database development phases: database creation, documenting, program code generation etc. [5].

By using DeZign for Databases, logical data model is created, in a form of a graphical diagram of entity relationships. Each entity has attributes that describe it and they are linked to each other by relationships. This software tool utilizes simple technique "show and click" to add entities into diagrams and to define their relationships. DeZign for Databases can automatically create schematic view of database from diagram of entity relationships, after they had been defined. The following database formats are supported: Oracle, InterBase, IBM DB2, MySQL, MaxDB, Paradox, MS SQL Server, MS Access, SQLAnywhere, Sybase, Informix, Pervasive, Advantage DB, DBISAM 3 i 4, FoxPro, PostgreSQL [6]. Databases are generated in MS SQL Serveru Express Edition, Microsoft development environment that enables very easy transfer to commercial versions.

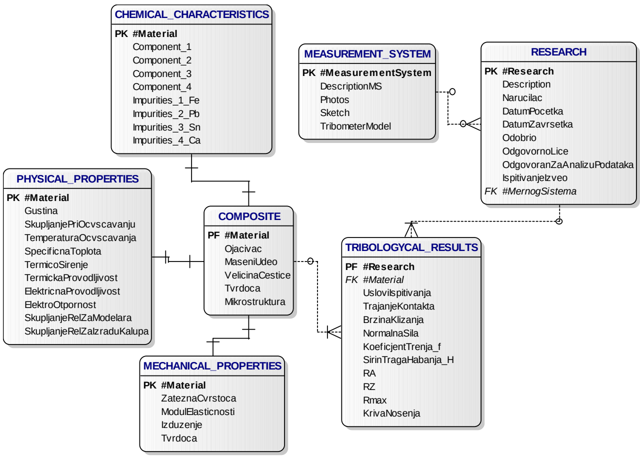

Figure 4. Relationship diagram

Database FIZICKE_OSOSBINE comprises data on tested materials such as: density (g/cm^3) at 20^{o}C, shrinkage during hardening (%), hardening temperature (^{o}C), specific heat (J/kgK) at 24-92^{o}C, thermal emission (m/mK) at 20-100^{o}C, thermal conductivity (W/mK) at 24^{o}C, electrical conductivity (%) IACS, electrical conductivity resistivity (μΩcm) at 20^{o}C, shrinkage relevant for modeling (mm/m) and shrinkage relevant for die making (mm/m). This database enables comparison and comparative commenting on materials according to their physical properties. Database HEMIJSKE _KARAKTERISTIKE contains data on material chemical composition, mainly concerning alloys used in investigations, that is, percentage composition of aluminium, copper, zinc and magnesium, as well as maximum share of impurities such as iron, cadmium, lead and tin. Database MEHANIKCKE_OSOBINE contains data related to mechanical characteristics of used materials such as: tensile strength (MPa), elasticity modulus (GPa), elongation (%), hardness (HB). Database KOMPOZIT contains data related to type of reinforcements, mass share, particles size, hardness, as well as microstructure photograph. Databases MERNI_SISTEM and ISPITIVANJE contains basic data about created measurement system for investigations, its structure and elements, schema and photography of the measurement system; investigation description, client description, beginning date, and end date, who approved test, who performed test, who realised analysis, etc. These are all data related only to the investigation itself. Database REZULTATI_TRIBOLOSKIH_ISPITIVANJA contains data about conditions and results of tribological investigations: test conditions (with or without lubrication), contact duration (min), sliding speed (m/s), normal force (daN), friction coefficient, width of the wear scar (mm), arithmetical mean roughness of a surface, Ra, mean asperities height, Rz, maximum asperities height, Rmax, bearing curve of a profile. Previously described databases with defined logical structure and interrelationships are suitable for analysis of tribological characteristics according to different criteria.

The term, data mining is in literature mainly related to support process to conclusions and decision making, with application of certain statistical techniques on transactional data (note: data created by data acquisition can be considered as transactional data) in order to deliver foreseeable trends and rules. Data mining is precise mathematical area (SQL Server supports certain techniques in this area comprised by Query), but in any case it does not comprise all analytical purposes for which data warehouse is used. Analysis of data organized in OLAP (On-Line Analytical Processing) cube can be done using PivotTable (dynamic table with integrated data from some database) service that enables data access to OLAP Cube. Two ways of data access in OLAP Cubes is shown in Fig. 5, using software tools Microsoft Excel and Statistica (as tools with main role being data analysis) or by creating custom user application through so called ADO mechanism.

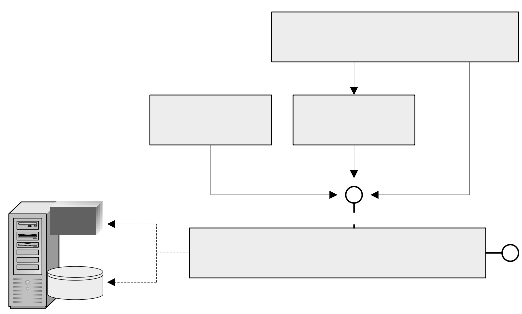

Figure 5. Access to OLAP Cube

Analysis of data organized in OLAP cubes in Excel and Statistica is done by creation of so called pivot tables. MS Excel and Statistica enable analysis by using additional tools which are part of this software. User is provided with the possibility to directly do report printing for specified time interval, for selected level of details and dimensions distribution.

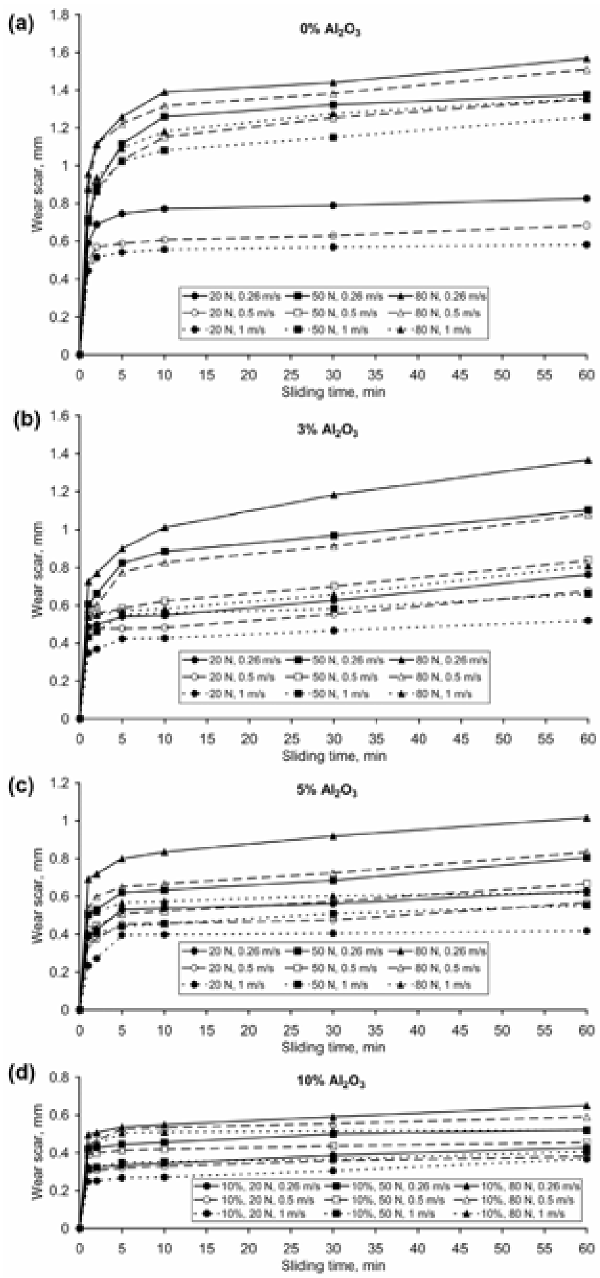

Figure 6. Wear curves of: (a) ZA-27 matrix alloy, (b) MMC 3% Al_2O_3 (c) MMC 5% Al_2O_3 (d) MMC 10% Al_2O_3

Pivot table represents dynamic table with integrated data from some database. It is used for tabular representation of number of data types/dimensions. It enables for resulting data to be presented in any selected level of details. Pivot Table Wizard in MS Excel and Statistica is used to create pivot tables.

Reporting is the last and crucial step of long and complex process of collecting, storing, transforming and manipulating data. Report creating represents presentational layer of working with databases, a layer that leads to generation of knowledge from data. Fig. 6 [4] shows data on wear scar width in time (wear curves) as diagrams, and comparative histogram view of wear of tested materials, obtained from database in MS Excel, is given in Fig. 7 [4]. By using software tool Statistica, data from databases is used for 3D view and determination of analytical relations (using regression function) with high correlation factor. Fig. 8 [4] illustrates report of tribological investigations realised in Statistica, and it shows multidimensional relationships between wear, mass weight of the reinforcements, sliding speed, and normal load.

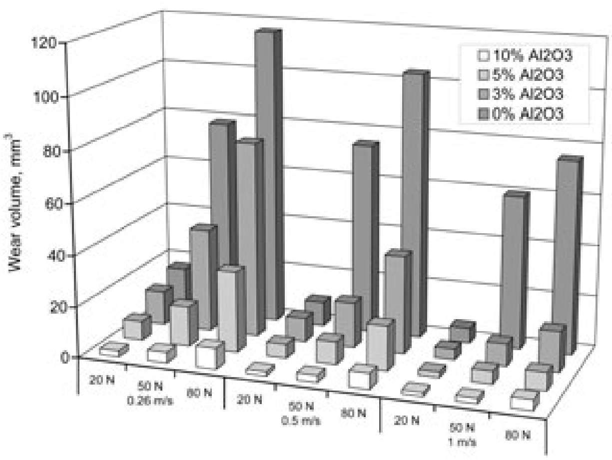

Figure 7. Wear volume of tested materials at different applied loads and sliding speed

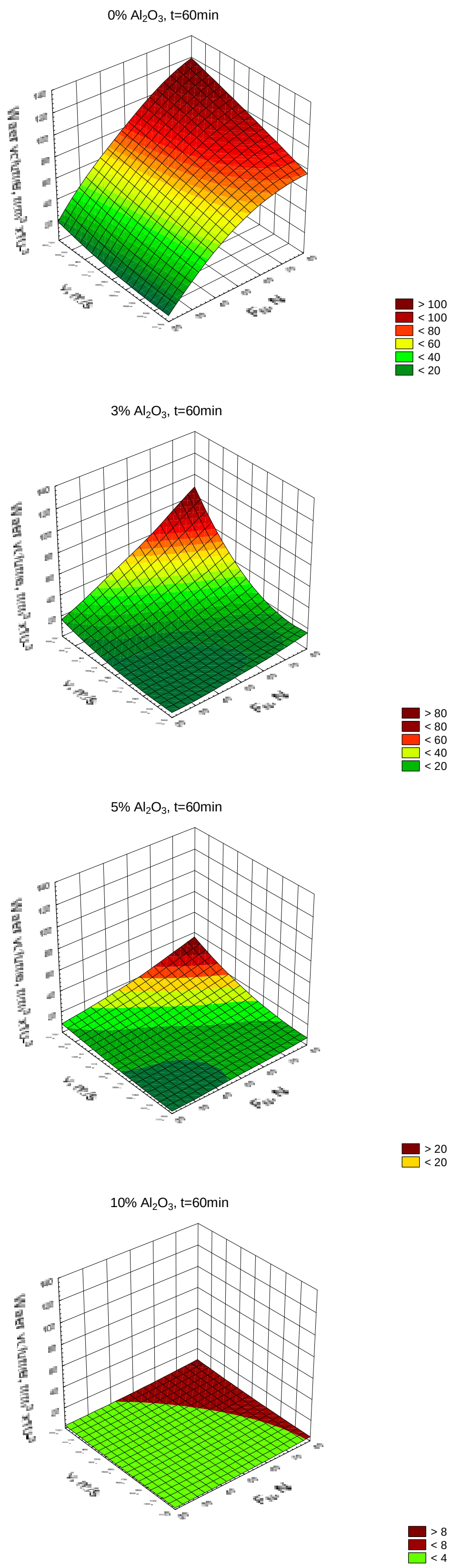

Figure 8. Relationships between wear scar width and normal load and sliding speed, for different mass weight of the reinforcements

3. CONCLUSION

Data structuring, finding adequate information and knowledge gaining are the pre-conditions to understanding and making appropriate and quality conclusions and decisions. During that, it is important that processing and analysis of information make constant process which is adapted to changes in time. New software technologies, such as open service architectures (SOA- Service Oriented Architecture), open data exchange standards (Open Standards for Data Exchange) and similar significantly influence data conversion into information to be introduced as a part of the scientific research work. For such a concept, Internet is especially important, as broad data resource and as a system for exchange of data that should be structured and exchanged in unique way.

ACKNOWLEDGMENT

This study was financed by Ministry of Science and Technological Development, Serbia, project No.35021.

REFERENCES

[1] Sydanmanaka P., An Intelligent Organization: Integrating performance, Competence and Knowledge Management, Capstone, Oxford, 2002.

[2] Jay Lee, Linxia Liao, Edzel Lapira, Jun Ni and Lin Li, Informatics Platform for Designing and Deploying e-Manufacturing Systems, Springer, 2009.

[3] Anthony Cleve, Jean Henrard and Jean-Luc Hainaut, Co-transformations in Information System Reengineering, Electronic Notes in Theoretical Computer Science 137, 2005.

[4] Mitrović S., Tribological characteristics of composites based on ZnAl alloys, PhD thesis (in Serbian), 2007.

[5] Jean-Marc Hick, Jean-Luc Hainaut, Database application evolution: A transformational approach, Data & Knowledge Engineering 59, 534–558, 2006.

[6] Erić M. et al.., References Document Model, QF2006, 95-98, Kragujevac, 2006.

SERBIATRIB '11

Serbian Tribology Society

12th International Conference on Tribology

Faculty of Mechanical Engineering in Kragujevac

Kragujevac, Serbia, 11 – 13 May 2011

DEVELOPMENT OF TRIBOMETER AND MEASUREMENT RESULTS OF STATIC COEFFICIENT OF FRICTION SLIDING AND COEFFICIENT OF ROLLING FRICTION BY PRINCIPLE STEEP PLANE

Tadić[1] B., Jeremić[1] B., Vukelić[2] Đ., Mitrović[1] S., Erić[1] M.
[1]Faculty of Mechanical Engineering Kragujevac
[2]Faculty of Technical Science Novi Sad

Abstract: *The paper presents a solution of new developed tribometer intended measuring that static coefficient of friction sliding and static coefficient of rolling friction materials of various types. Principles of measurement are theoretically analyzed, presented the basic of structural solutions and some results of measurements. Tribometer is based on the principle of the steep plane and provides a rotation angle of the steep plane with an accuracy of one minute, which provides high precision of measurements. From the point of the possible values of the load contact pairs developed tribometer belongs to a class of micro and nano tribometers.*

1. INTRODUCTION

Tribology as a science and technology largely allows the solution of many global problems related to consumption of materials, energy, reduces costs and increases reliability of complex technical systems [8]. Tribology in the field of tribo-diagnostics and development of modern measuring systems at the present time is experiencing a full expansion. The reasons are primarily in the fact that the analysis and quantification of complex tribological processes are necessarily reliable on measuring devices and machines. Due to the complexity of processes occurring in the zones of contacts tribology is largely based on experimental research methods. Modern methods of experimental research, in addition to required reliability of measurement system, are placing a number of other complex requirements and restrictions. All this imposes a constant need for developing new and improving existing measurement devices and machines, not only in the specific field measuring system and accompanying software, but also in the field of measurement and the very principles of physics processes. Tribological studies of experimental type at the present time are not only the needs of research institutions but also production of many companies who recognize that due to their survival in the market that this is necessary.

Research in the field of modern equipment tribo-diagnostics deals with many global and specialized institutes. In short, research has been pointed to the improvement and standardization of existing solutions and development of new solutions of tribometers. A large number of existing global solutions of tribometers is standardized (ASTM and ISO standards) under the terms of making contact. Today, these structures of tribometers are improved the most in terms of software solutions and improve the technical characteristics (increased levels of stress, increase speed skating, rolling, an increase of temperature, vacuum chambers, etc.).. In many cases the already standardized solutions of tribometers arise tribometer in a highly improved performance that is designed research to a much wider range of load, speed skating, rolling, operating temperature, lubrication conditions, the presence of abrasives etc. There is also a number of solutions of tribometers covering several types of contacts. These solutions are more universal in character and are often designed in a modular system design. There are also a number of special solutions (structures) tribometers intended tribological tests of gear pairs, hard coatings, plastics and other materials. The world has developed a number of dedicated testing tribometers, tribological properties of materials in a vacuum, and tribometers intended for testing in conditions of extremely high temperatures and pressures of contact pairs. The development of nano tribometers as a special field of tribology, initiated the development of a large number of highly sophisticated solutions of nano tribometers. Development of new solutions of tribometers, largely, initiated the development of new materials and coatings, special loading conditions, hostile environments and other specific conditions.

A large number of papers in leading journals is treating the static coefficient of friction. In this regard it should be noted that research moved in more directions, such as: a) research on the design of the topography of contact surfaces that provides the maximum value of static coefficient of friction [2], b) Research related to development and tribological tests of composite biomaterials [3] c) Research related to identification and quantification of the impact of various factors on the size of the static coefficient of friction in systems for rail equipment for metal processing [6], d) Investigations related to the impact of vibration, humidity and other factors on the bearing capacity of the connection that has generated friction [7] e) The development of devices for measuring the static coefficient of friction, the initial moment of motion detection and measurement of adhesion forces [1]. f) development of theoretical models for calculating the value of static coefficient of friction of certain materials [4]. From this partial review of the literature can be concluded that the area of research related to the static coefficient of friction is very topical. Given the topic of the paper should emphasize that the research on the measurement of coefficient of friction on the principle of the plane is also very relevant [5] particularly in terms of comparing the results with those obtained by measuring the static friction coefficient by other methods.

Within the Center for the revitalization of the industrial system and the center for tero-technology Mechanical Engineering in Kragujevac was designed a new tribometer, designed for determining the static coefficient of friction sliding and rolling friction. Tribometer operates on the principle of the plane and is characterized by high precision measurements. Since, the world realized tribometers solutions of this kind, that developed tribometer has advantages and can be one of the current program of domestic metal industry.

2. MEASURING COEFFICIENT OF FRICTION ON THE PRINCIPLE OF THE PLANE

The principle of measuring the coefficient of friction over the plane (figure. 1) is essentially based on the power of the earth's gravity. Sliding friction coefficient, is well known ,represents ratio of friction force and the force perpendicular to the surface of contact. In the limiting case of sliding friction is true equality:

$$\mu = \frac{T}{N} = \frac{G \cdot \sin\alpha}{G \cdot \cos\alpha} = tg\alpha ,$$

where the:

$\mu -$ size of static friction coefficient; T -friction; G -gravitation force; α -angle of the plane.

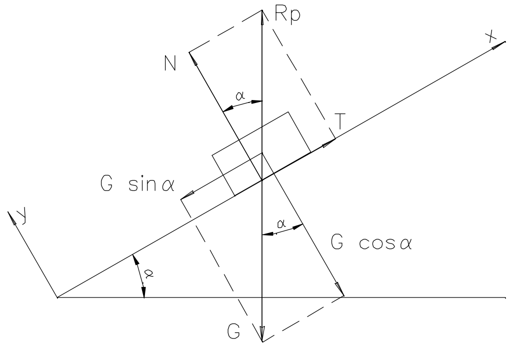

Figure 1. The balance of the body on a steep plane

In the case of friction rolling borderline case (figure 2a and 2b) rolling friction coefficient follows from the following equation:

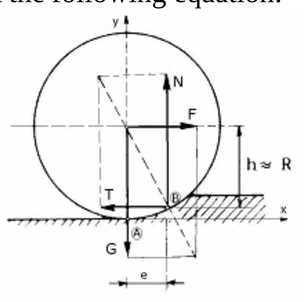

a)

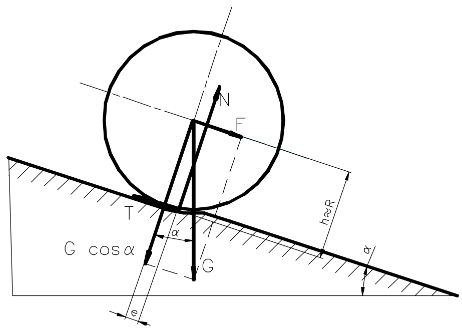

b)

Figure 2. *The balance of the body when rolling*

$$\sum M_A = 0 \Rightarrow N \cdot e - F \cdot R = 0$$

In the limiting case of drive torque $M_K = N \cdot e$ must be equal to the moment of resistance which is

$$M_P = F \cdot R$$

From this dependence follows:

$T = F = N \cdot \dfrac{e}{R} = f \cdot N$ apropos:

$f = \dfrac{e}{R} = tg\alpha,$ which follows from the equations of equilibrium body rolling down an inclined plane (figure.2b.),
apropos:

$$\sum F_i(y) = 0 \Rightarrow N = G \cdot \cos\alpha$$

$$\sum M_A = 0 \Rightarrow G \cdot \sin\alpha \cdot R = N \cdot e = G \cdot \cos\alpha \cdot e \Rightarrow \frac{e}{R} = tg\alpha$$

where the:
f – static coefficient of friction rolling;
e – coordinates,which determines the position of the resultant reaction N; R – radius of the body to roll; α – angle of the plane

3. DESCRIPTION OF THE REALIZED SOLUTION OF TRIBOMETER

Completed (Presented) tribometer is designed to measure the static and rolling coefficient of friction of all kinds materials. Figure 3. is schematically showing construction design of this tribometer.

In the base (position1) are set out specially designed screws (item 11) which are used for leveling the base of tribometer. Leveling is performed through a specially prepared vials for leveling in two planes. Support plate (position 2) slides on the prepared groove on the base. On the support plate (position 2) is attached nut (position 12), and zero-point position pointer (position 19.). On the base (position 1) the bearing plate are attached, (position 6) in which are placed radio-axial bearings (position 7). Screw spindle (position 9) of step 1 mm coupled with a nut (position 12), and nonius (position 8) through which the movement is read with an accuracy of one minute. On the support plate (position 2) dug a groove through which enables vertical movement of shift pins (position 5) on which are on both sides affixed two ball bearings (position 10). Ball bearings are indented in discs (positions 3 and 4). On disk (position 3) is engraved angle scale in degrees and feature two pins (position 14). On the inside of the disc (position 3.) two boundary balls are attached (position 13). Contact pair (positions 15 and 16) with a weight (position 17) which is attached to separate connection for the sample (position 16) are placed on the pins (position 14). Turning nonius (position 8) support plate (item 2) moves in a straight line, while disks (positions 3 and 4) rolling on the top of the base (position 1) and thus swing plane fits the contact pairs (positions 15 and 16) for the desired angle. Additional load can be added via changeable weights (position 17)

Figure 4 give photographic overview of the device and sets of samples while in figure 5 presents details of the leveling device and nonius scale.

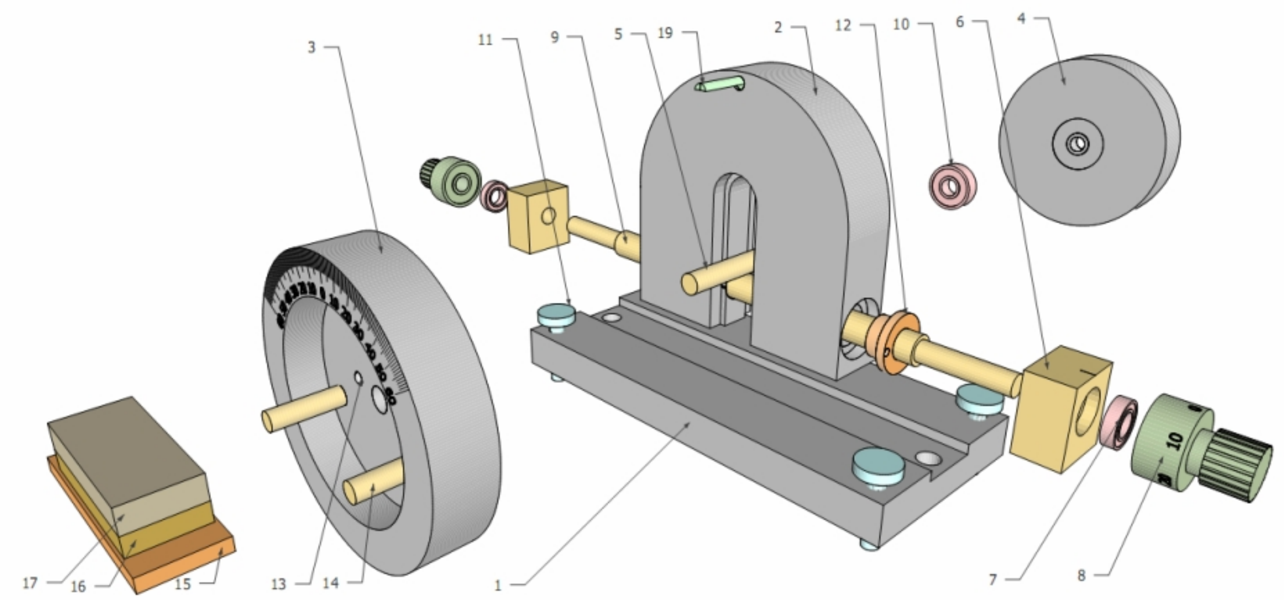

Figure 3. Schematic of tribometer

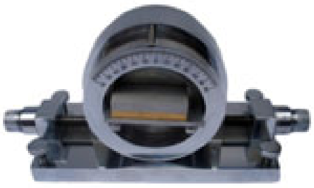

a) sliding friction

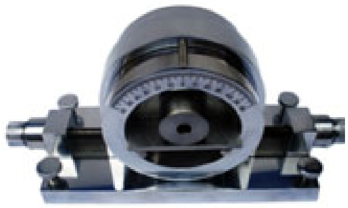

b) rolling friction

Figure 4. The initial positions of contact pairs and a set of contact pairs of samples

Figure 5. Details related to leveling devices and nonious scale

4. MEASUREMENT RESULTS

For the described device, measurements were made of the coefficient of friction sliding and rolling friction coefficient of various metallic and nonmetallic materials with various loads. Investigated metal materials (steel, cast iron, aluminum, brass and bronze) determined the mechanical properties were brought grinding to approximately the same value of the arithmetic mean deviation in the amount of profile. For the observed non-metallic materials (glass, wood, plastic, leather and rubber) which are closer to specific mechanical properties and friction coefficient measurements were made in a part of these materials to have a comparative character. In figure 6. diagram gives the results of measurements of static coefficient of friction sliding. Each measurement was performed with 20 repetitions on the basis of which they calculated the mean value and dispersion coefficient of friction. The diagram as a background pattern that indicated in figure 3 defines the position15 while the other contact pair is marked as a template (position 16 to figure 3).

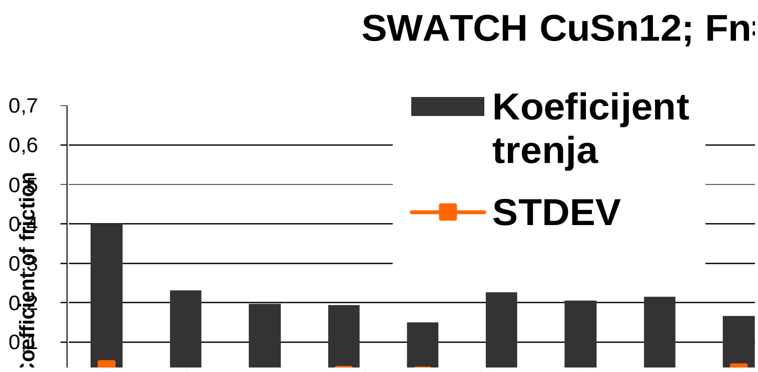

Figure 6. Histogram report on the results of measurement of static coefficient of friction sliding of materials.

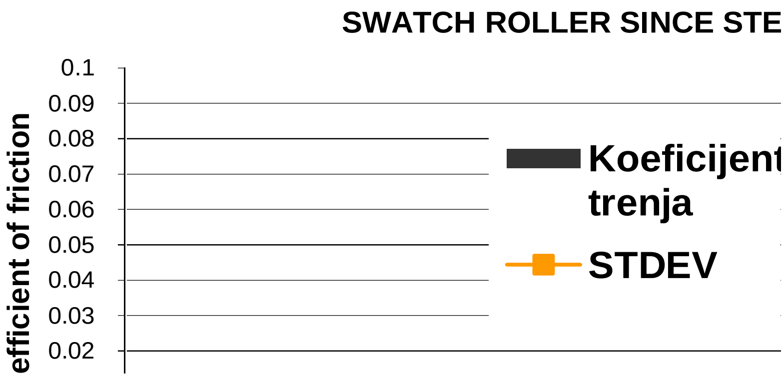

Figure 7. Histogram of results of measurements of static coefficient of friction rolling various materials.

In figure .7. presents some results of measurements related to measuring the static coefficient of friction rolling.

5. CONCLUSIONS

Based on the above we can conclude the following:

- Results of the analysis of literature sources indicate that the theoretical and experimental research in the field of static friction are current problems. The research is focused in many directions. Some current areas of research are: a) research on the design of the topography of contact that provides the maximum value of static coefficient of friction [2], b) Research related to development and tribological tests of composite biomaterials [3], c) Research related to identification and quantification of impact various factors on the size of the static coefficient of friction in systems for rail equipment for metal processing [6], d) Investigations related toinfluence of vibration , humidity and other factors on the bearing capacity of the connection that is generated by friction [7]e) The development of devices for measuring the static friction coefficient , the initial moment of motion detection and measurement of adhesion forces [1]. f) development of theoretical models for calculating the value of static coefficient of friction of certain materials [4].
- Given the topic of the paper should emphasize that the research on the measurement of coefficient of friction on the principle of the plane is also very relevant [5] particularly in terms of measuring devices and compare the results with those obtained by measuring the static friction coefficient by other methods.
- Developed a device for measuring static coefficient of friction sliding and rolling friction is zero-the plane is designed to allow very precise determination of the static coefficient of friction. Error reading angle value is less than one minute so that, in this regard, the error measured values of sliding friction coefficient is negligible. When it comes to measuring the coefficient of friction rolling maximum error of measurement does not exceed 5%, which is quite acceptable given the very low value of coefficient of friction rolling and measurement errors on the different kinds of devices.
- The results of measuring the static coefficient of friction sliding and static friction coefficient of rolling various materials obtained by using the realized devices are supported by the literature.

REFERENCES

[1] Habib S. Benabdallah, Static friction coefficient of some plastics against steel and aluminum under different contact conditions, Tribology International 40 (2007) 64–73

[2] Lars Hammerstr , Staffan Jacobson, Designed high-friction surfaces—Influence of roughness and deformation of the counter surface, Wear 264 (2008) 807–814

[3] S.H. Teoh , R. Thampuran, W.K.H. Seah, Coefficient of friction under dry and lubricated conditions of a fracture and wear resistant P/M titanium-graphite composite for biomedical applications, Wear 214 (199s) 237-244

[4] E.L. Deladi, M.B. de Rooij, D.J. Schipper, Modelling of static friction in rubber–metal contact, Tribology International 40 (2007) 588–594

[5] Na Jin Seoa, Thomas J. Armstrongb, Philip Drinkaus, A comparison of two methods of measuring staticcoefficient of friction at low normal

forces, Ergonomics, Vol. 52, No. 1, January 2009, 121–135

[6] W. Xie, E.C. De Meter, M.W. Trethewey, An experimental evaluation of coefficients of static friction of common workpiece–fixture element pairs, International Journal of Machine Tools & Manufacture 40 (2000) 467–488

[7] Mohammad Asaduzzam Chowdhurya, Md. Maksud Helali, The effect of frequency of vibration and humidity on the coefficient of friction, Tribology International 39 (2006) 958–962

[8] 8. Ivkovic, B, Tribology in the industry on the threshold of the twenty-first century, Tribology in the industry, H1/4, Kragujevac, 1999.

Trenje, habanje i podmazivanje

12th International Conference on Tribology – SERBIATRIB '11

11 – 13 May 2011, Kragujevac, Serbia

Serbian Tribology Society

SERBIATRIB '11

12th International Conference on Tribology

Faculty of Mechanical Engineering in Kragujevac

Kragujevac, Serbia, 11 – 13 May 2011

REZULTATI EKSPERIMENTALNIH ISPITIVANJA TRIBOLOŠKIH KARAKTERISTIKA ULJA IZ MOTORA I MENJAČA VOZILA

Perić Sreten[1], Nedić Bogdan[2]

[1]Vojna akademija, Beograd, Srbija, sretenperic@yahoo.com
[2]Mašinski fakultet Kragujevac, Srbija, nedic@kg.ac.rs

Apstrakt: *Motori i menjački prenosnici vozila predstavljaju složene tribomehaničke sisteme. Uslovi u kojima se nalaze elementi tribomehaničkih sistema su veoma složeni i određeni su u velikoj meri odgovarjućim karakteristikama maziva. Složenost uslova je određena: temperaturom elemenata u kontaktu i temperaturom maziva, spoljašnjim opterećenjem (odnosno specifičnim pritiskom u zoni kontakta), dinamičkim karakterom ostvarivanja kontakta, prenosa snage i kretanja i dr.*
Postupak ispitivanja triboloških karakteristika ulja za podmazivanje u toku eksploatacije se sastoji u sledećem:uzorkovanje ulja iz realnog tribomehaničkog sistema, utvrđivanje učešća produkata habanja u ulju i merenje triboloških karakteristika tribomehaničkog sistema u modelskim uslovima uz korišćenje uzorkovanog ulja kao maziva.
Analiza uzoraka ulja koja u sebi sadrže čestice nastale habanjem omogućava da se u ranim fazama korišćenja sistema oceni stanje triboloških svojstava.
U ovom radu će biti prikazani rezultati eksperimentalnih istraživanja triboloških karakteristika uzorkovanih ulja iz motora i menjača vozila Mercedes O 345, PUCH 300GD i PINZGAUER 710M koja su bila u eksploataciji. Realizovanim ispitivanjima konstatovano je da dolazi do promena triboloških karakteristika ulja za podmazivanje u motorima i menjačima vozila. Ove promene su u direktnoj zavisnosti od stanja svih elemenata tribomehaničkog sistema, odnosno u zavisnosti od njihovih funkcionalnih karakteristika.

Ključne reči: *tribološke karakteristike, tribomehanički sistem, analiza ulja, podmazivanje.*

1. UVOD

Težište eksperimentalnog istraživanja, realizovanog u ovom radu, stavljeno je na mazivo, kao nosioca informacija o stanju sistema u celini. Ispitivanja sprovedena na većem broju različitih tehničkih sistema, koji su identifikovani kao tribomehanički, pokazala su da se u najvećem broju slučajeva promena funkcionalnosti elemenata i kompletnog sistema iskazuje kroz promene osobina maziva. To potvrđuje da se promena triboloških karakteristika uljnog punjenja može usvojiti za ocenu stanja sistema.

U cilju potpunog sagledavanja ponašanja ulja i davanja konačne ocene njegovog uticaja na performanse sistema, izvršena su tribološka ispitivanja maziva, koja se svrstavaju u grupu modelskih ispitivanja. Prilikom realizacije modelskih ispitivanja vrši se uzorkovanje ispitivanog elementa (ulja) iz realnog sistema i simuliraju uslovi kontakta. Ovim putem moguće je doći do velikog niza podataka koji sa dovoljnom pouzdanošću ukazuju na stanje sistema i daju predviđanje njegovog daljeg ponašanja. Jednoveremeno, kod modelskih ispitivanja moguće je obezbediti ponovljivost postupka uzorkovanja i ispitivanja, a na osnovu toga i uporedljivost rezultata i ocenu istog elementa u različitim laboratorijama. Realizacija ovih ispitivanja ne zahteva izradu skupih prototipova, pa su i sa tog aspekta pogodna.

Program eksperimentalnog ispitivanja uticaja maziva na motore i prenosnike snage motornih vozila obuhvatio je definisanje uslova ispitivanja navedenih elemenata, formiranje mernog lanca (slika 1), tribološka ispitivanja ulja i obradu dobijenih rezultata. Ispitivanja triboloških karakteristika ulja vršena su u Laboratoriji za obradu metala i tribologiju Mašinskog fakulteta u Kragujevcu.

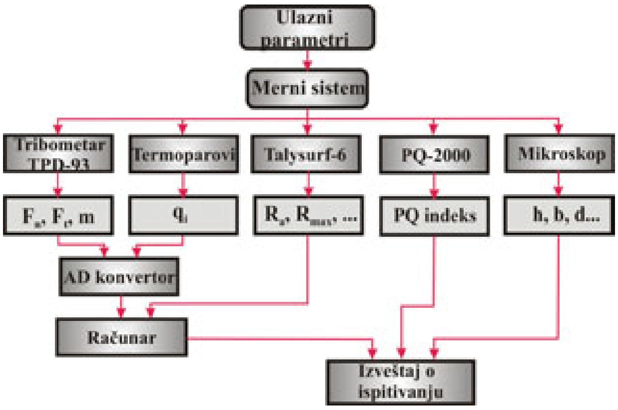

Slika 1. Blok šema mernog sistema

Pri realizaciji ovih ispitivanja neophodno je prethodno odrediti uslove ostvarivanja kontakta: geometriju kontakta; intenzitet i karakter spoljašnjeg opterećenja; vrstu opterećenja (kontinualno, ciklično i dr.) i brzinu kretanja; temperaturu elemenata u kontaktu; način podmazivanja itd.

Detaljnom analizom realnog tribomehaničkog sistema utvrđuju se prethodno definisani parametri i formiraju elementi kontaktnih parova. Pri ovome potrebno je da elementi kontaktnih parova budu tačno definisanih svojstava (materijal, tvrdoća, stanje površina itd.).

Svi ovi merni lanci se sastoje od odgovarajuće merne opreme koju čine merni senzori, pojačavači signala od senzora, sistemi za akviziciju podataka u računar, softver za monitoring signala merene veličine i računarska oprema za čuvanje podataka i formiranje i prezentaciju izveštaja merenja.

Ispitivanje je sprovedeno na uljima uzorkovanim iz motora i menjačkih prenosnika sledećih vozila: PINZGAUER 710M (PINZ), PUCH 300 GD (PUCH), autobus MERCEDES O 345. Zbog ograničenosti obima rada, nisu prikazivni tabelarni podaci vezani za tehničke karakteristike razmatranih motora i menjača, kao i podaci o karakteristikama korišćenih maziva.

2. REZULTATI TRIBOLOŠKIH ISPITIVANJA ULJA

U okviru ovog dela prikazani su rezultati eksperimentalnih ispitivanja triboloških karakteristika motornih i menjačkih ulja.

Ispitivanje je realizovano periodičnim uzimanjem uzoraka ulja iz motora i menjača navedenih vozila. Osim svežeg ulja („nulti“ uzorak), uzeti su uzorci nakon određenog broja pređenih km, u tačno definisanim periodičnim intervalima.

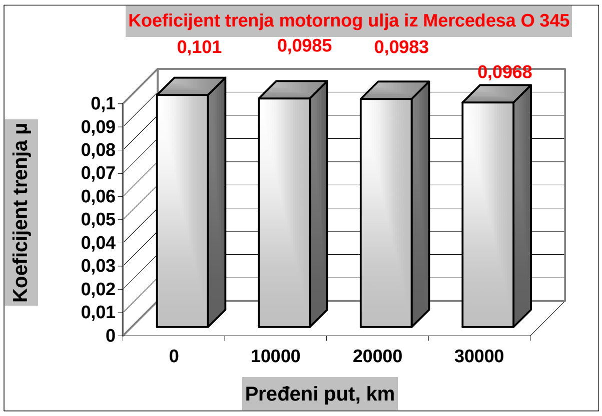

Slika 2. Koeficijent trenja motornog ulja Mercedesa [3]

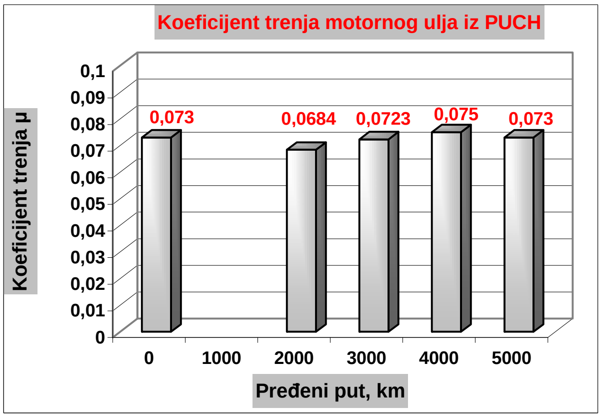

Slika 3. Koeficijent trenja motornog ulja iz PUCH[3]

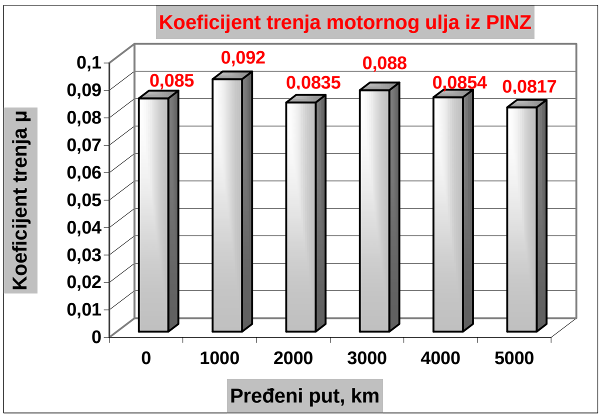

Slika 4. Koeficijent trenja motornog ulja iz PINZ[3]

Na slikama 2, 3 i 4 prikazani su dijagrami promene koeficijenta trenja uzorkovanih motornih ulja u funkciji od pređenog puta vozila. Može se zaključiti da se srednje vrednosti koeficijenta trenja između bloka i diska pri korišćenju ispitivanih motornih ulja kod svih vozila kreću u granicama od 0,0684 do 0,101. Takođe se može zaključiti da sa povećanjem pređenog puta koeficijent trenja kod motornog ulja iz Mercedesa O 345 (SAE 10W-40, API klasifikacije CF) postepeno pada, kod motornog ulja iz PUCH (SAE 10W-40, API SG/CE) u početku pada, dok je kasnije prisutan rast. Kod motornog ulja iz PINZ (SAE 30/S3) koeficijent trenja u početku raste, a zatim pada.

Veliki koeficijent trenja (μ=0,101) kod svežeg motornog ulja (nulti uzorak) SAE 10W-40, API klasifikacije CF (autobusi Mercedes O 345), koji je veći nego kod korišćenih ulja potiče od sastava ulja koje sadrži ZnDDP (cinkdialkilditiofosfat), čija formulacija je različita od formulacije kod menjačkih ulja, zbog prirode i uslova kontakta koji vladaju u motoru. ZnDDP kao aditiv vrši tri značajne funkcije i to kao aditiv *antioksidant*, *protiv korozije* i *protiv habanja*. Njegovo delovanje kao antioksidanta je u uslovima relativno niskih temperatura (do 100 °C), a ukoliko se primenjuje kod viših temperatura (slučaj u motornim uljima) dolazi do termičke razgradnje, usled čega svi produkti nastali na ovaj način deluju vlastitim mehanizmom kao inhibitori oksidacije.

Na slikama 5, 6 i 7 prikazani su dijagrami promene širine traga habanja uzorkovanih motornih ulja u funkciji od pređenog puta vozila.

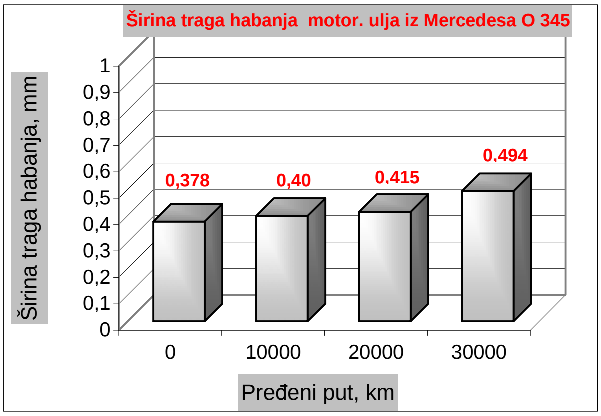

Slika 5. Širina traga habanja motornog ulja Mercedes [3]

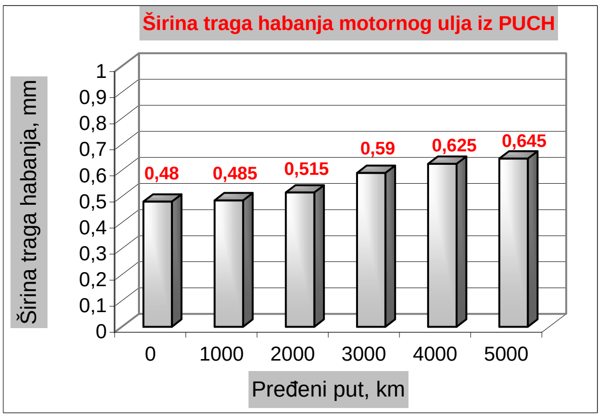

Slika 6. Širina traga habanja motornog ulja iz PUCH[3]

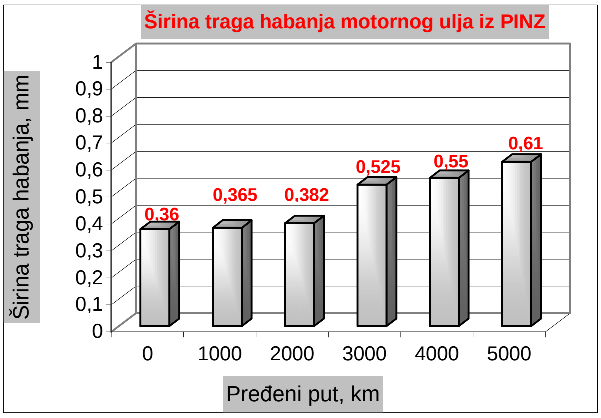

Slika 7. Širina traga habanja motornog ulja iz PINZ[3]

Sa povećanjem pređenog puta širina pojasa (traga) habanja diska raste kod ispitivanih motornih ulja iz sva tri vozila i to: kod ulja iz Mercedesa O 345 do vrednosti 0,494 mm; kod ulja iz PUCH do vrednosti 0,645 mm i kod ulja iz PINZ do vrednosti 0,61 mm. Porast širine traga habanja u početnom periodu se može objasniti uhodavanjem diska i bloka, a u stvarnosti bi odgovaralo početnom korišćenju vozila sa novim uljem.

Približan konstantan rast širine habanja diska, u funkciji pređenog puta, može se tumačiti uticajem povećanja produkata habanja u ulju i promeni podmazujućih karakteristika ulja (usled postepene degradacije ulja) u toku ispitivanja.

Pre početka realizacije eksperimenta izvršena su merenja hrapavosti površina diskova i blokova pomoću uređaja Talysurf. Parametri topografije površine bloka i diska, koji se mere navedenim uređajem, prikazani su u tabeli 1.

Tabela 1. Parametri topografije površine (Talysurf–6)

Rt1-Rt5, μm	Maksimalne visine profila na referent. dužinama, na dužini ocenjivanja
Ra, μm	Srednje aritmetičko odstupanje profila na dužini ocenjivanja
Rq, μm	Srednje kvadratno odstupanje profila na dužini ocenjivanja
Ry, μm	Maksimalna visina profila, maksimalna Rti vrednost
Rtm,μm	Srednja Rti vrednost
Rv, μm	Najveća dubina udubljenja profila
Rp, μm	Najveća visina ispupčenja profila
Sm, μm	Srednji korak ispupčenja profila
Δq, °	Srednji kvadratni ugao nagiba profila
Rsk	Koeficijent asimetrije profila, mera simetrije krive raspodele amplituda
Rku	Kurtosis, mera zaoštrenosti krive raspodele amplituda
S, μm	Srednji korak lokalnih ispupčenja profila
R3z, μm	Srednja vrednost rastojanja trećeg po visini ispupčenja i trećeg po dubini udubljenja na referent. dužini profila
Rpm, μm	Srednja vrednost Rpi određenih na referent. dužin.
R3y, μm	Najveće rastojanje trećeg po visini ispupčenja i trećeg po dubini udubljenja na referentnoj dužini.

Parametri topografije površina novog diska i bloka, kao i diskova na kraju ispitivanja uzoraka motornog ulja prikazani su u tabeli 2. Dobijene vrednosti srednjeg aritmetičkog odstupanja označene su sa Ra.

Tabela 2. Parametri topografije površina novog diska i bloka na referentnoj dužini i diskova na kraju ispitivanja uzoraka motornog ulja

Veličina	Novi disk	Na kraju eksperimenta (ispitivanja)			Novi blok
		disk Merc.	disk PUCH	disk PINZ	
Rt1	2.0	2.5	2.1	3.0	2.45
Rt2	1.8	2.3	3.5	3.5	1.66
Rt3	2.1	2.1	2.6	2.1	1.77
Rt4	2.3	2.1	2.4	3.4	1.23
Rt5	1.9	2.9	2.9	3.2	1.48
Ra	0.48	0.36	0.41	0.41	0.357
Rq	0.61	0.46	0.54	0.55	0.429
Ry (Rmax)	2.3	2.9	3.5	3.5	2.45
Rtm	2.0	2.4	2.7	3.0	1.72
Rv	1.4	1.8	1.9	2.1	1.07
Rp	2.1	1.3	1.7	2.1	1.38
Sm	62	40	64	50	202
Δq	3.0°	4.5°	3.8°	4.6°	1.7°
Rsk	0.5	-0.5	-0.2	-0.1	-0.3
Rku	3.1	3.4	4.0	4.3	2.5
S	17	18	24	21	4.1
R3z	1.6	1.8	2.0	2.3	1.23
Rpm	1.2	1.0	1.0	1.3	0.92
R3y	1.8	2.0	2.6	2.8	1.49

Na slikama od 8 do 12 su prikazane topografije površina novog bloka i diska na referentnoj dužini, kao i diskova na kraju ispitivanja motornog ulja iz razmatranih vozila.

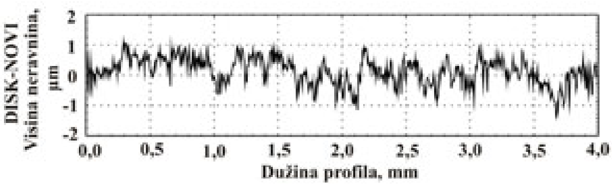

Slika 8. Topografija površine novog diska [3]

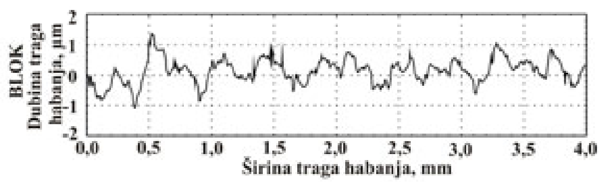

Slika 9. Topografija površine novog bloka [3]

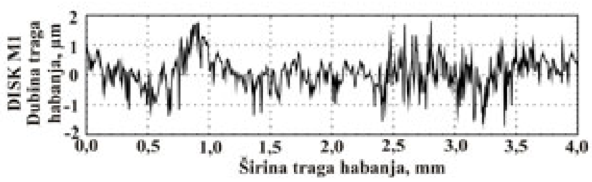

Slika 10. Topografija površine diska na kraju ispitivanja motornog ulja iz Mercedesa [3]

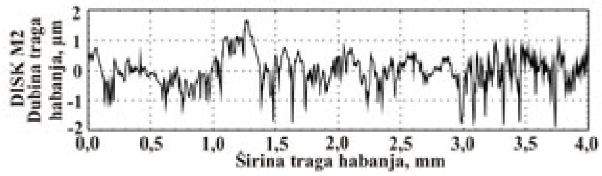

Slika 11. Topografija površine diska na kraju ispitivanja motornog ulja iz PUCH [3]

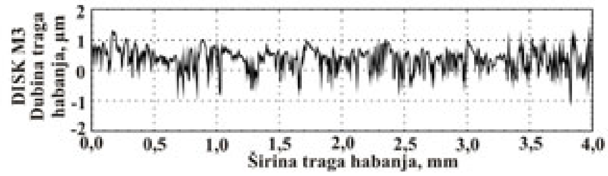

Slika 12. Topografija površine diska na kraju ispitivanja motornog ulja iz PINZ [3]

Na slikama 13, 14 i 15 prikazani su dijagrami promene koeficijenta trenja uzorkovanih menjačkih ulja u funkciji od pređenog puta vozila.

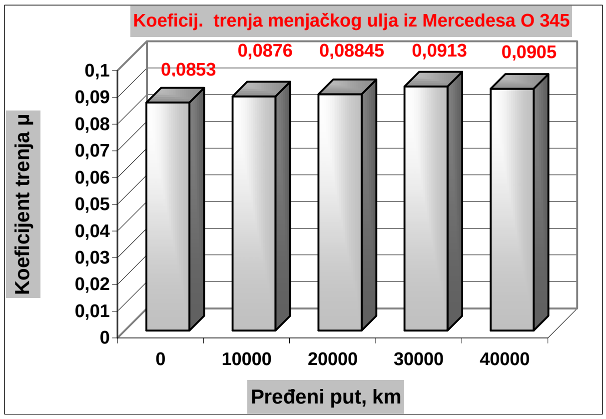

Slika 13. Koeficijent trenja menjačkog ulja Mercedes [3]

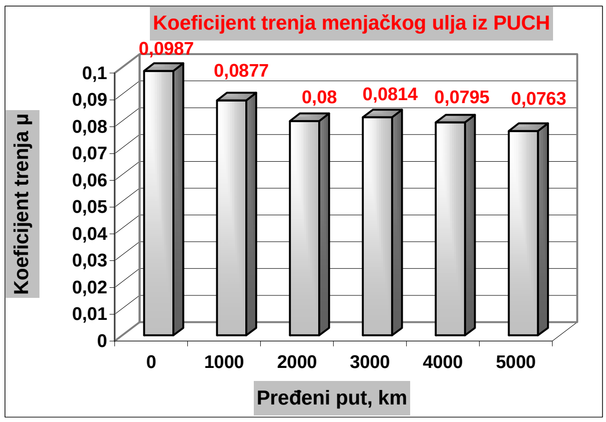

Slika 14. Koeficijent trenja menjačkog ulja iz PUCH[3]

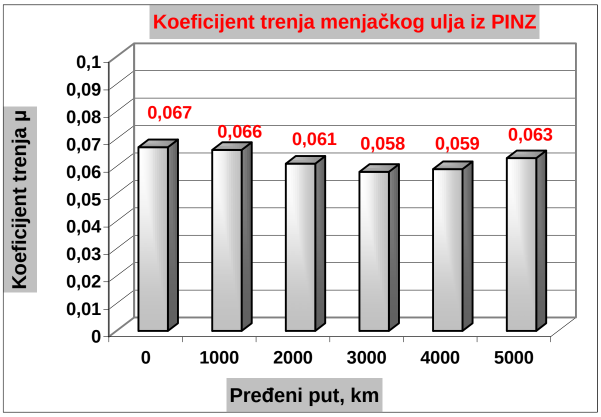

Slika 15. Koeficijent trenja menjačkog ulja iz PINZ [3]

Srednje vrednosti koeficijenta trenja između bloka i diska pri korišćenju ispitivanih menjačkih ulja kod svih vozila kreću se u granicama od 0,058 do 0,0987.Sa povećanjem pređenog puta koeficijent trenja kod menjačkog ulja iz Mercedesa O 345 (PRISTA ATF) postepeno raste, kod menjačkog ulja iz PUCH (UAMS) postepeno pada. Kod menjačkog ulja iz PINZ (HIP 90) koeficijent trenja u početku pada, a zatim raste.

Dijagram na slici 13 pokazuje da je koeficijent trenja kod uzoraka rabljenog menjačkog ulja Prista ATF (iz Mercedesa O 345) veći od koeficijenta trenja nultog uzorka (sveže ulje). Na povišenim radnim temperaturama dolazi do reakcije između aditiva iz ulja i površine koja se podmazuje, raspadanja ZnDDP (cinkdialkilditiofosfat) i njegovog prelaska u oblik slobodnog radikala. Na ovaj način se usporava proces oksidacije ulja u menjaču tokom njegovog rada.U korišćenom menjačkom ulju Prista ATF nalaze se, na opisan način formirani slobodni radikali, koji zbog funkcije ZnDDP (antioksidant) ne utiču na smanjenje trenja i habanja.

Uticaj degradacije menjačkog ulja i povećanja koncentracije produkata habanja ogleda se, za vreme triboloških ispitivanja, u većem koeficijentu trenja i habanju.

Analizom dijagrama na slici 14 može se uočiti da je koeficijent trenja pri ispitivanju nultog (svežeg) uzorka menjačkog ulja UAMS (iz PUCH) veći nego pri ispitivanju sa rabljenim uzorcima. Uzrok ovakvog koeficijenta trenja treba tražiti u samoj strukturi ulja, koja je formulisana sumpor-fosfornim bespepelnim EP antihabajućim aditivom. Fosfor ima osobinu da pri kontaktnoj temperaturi od 700°C reaguje sa metalom i gradi metal–fosfid koji kao hemijska prevlaka štiti površinu od habanja, dok sumpor na temperaturi od 900°C pri reakciji sa metalom gradi metal–sulfid koji se odlikuje velikom tvrdoćom i ne dozvoljava habanje površine. Posledica formiranja hemijskih slojeva velike tvrdoće na dodirnim površinama je veliko trenje iskazano koeficijentom trenja.

Rabljeno menjačko ulje UAMS sadrži u sebi polarna jedinjenja nastala reakcijom aditiva i metala usled oksidacije (posebno izražena kod povišenih radnih temperatura). Na taj način formirana polarna jedinjenja se, prilikom triboloških ispitivanja, vezuju za metalne površine bloka i diska i obrazuju sloj koji predstavlja metalni sapun. Na taj način oformljeni mazivi sloj sprečava kontakt površina bloka i diska, usled čega se stvaraju uslovi da početno granično podmazivanje prelazi u elastohidrodinamičko podmazivanje. Posledica toga je manji koeficijent trenja i manje habanje, kao i mogućnost da dođe do proklizavanja površina.

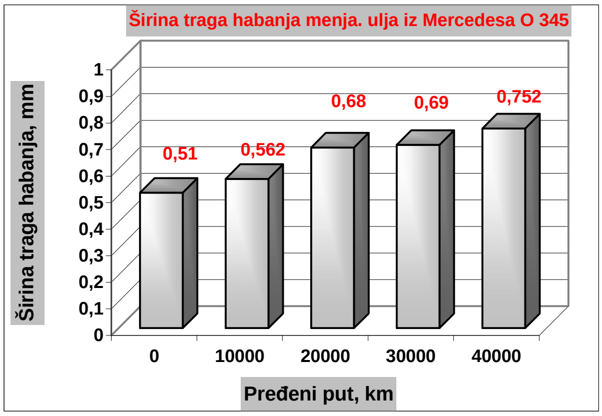

Slika 16. Širina traga habanja menjač. ulja Mercedes [3]

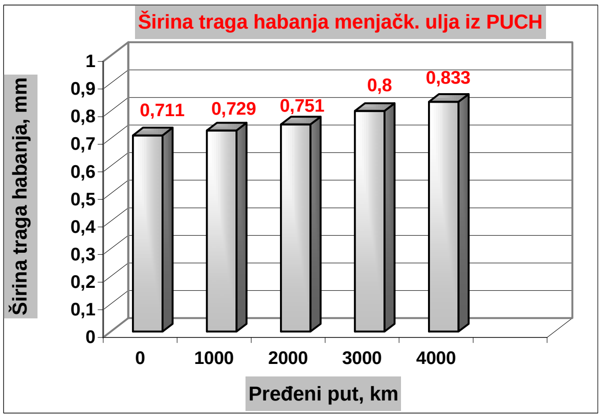

Slika 17. Širina traga habanja menjač. ulja iz PUCH[3]

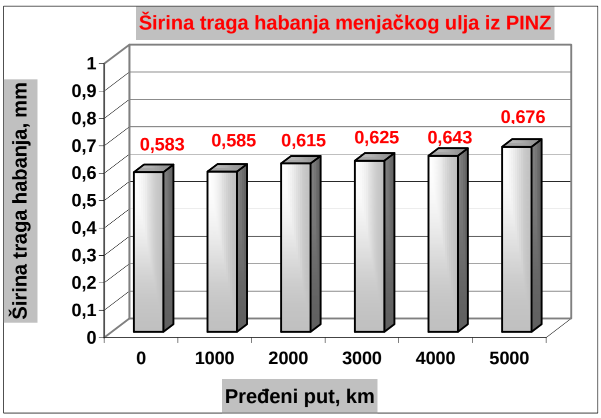

Slika 18. Širina traga habanja menjačkog ulja iz PINZ[3]

Na slikama 16, 17 i 18 prikazani su dijagrami promene širine traga habanja uzorkovanih menjačkih ulja u funkciji od pređenog puta vozila.

Sa povećanjem pređenog puta širina pojasa habanja diska raste kod ispitivanih menjačkih ulja iz sva tri vozila i to: kod ulja iz Mercedesa O 345 do vrednosti 0,752 mm; kod ulja iz PUCH do vrednosti 0,833 mm i kod ulja iz PINZ do vrednosti 0,676 mm. Vidljiv je konstantan rast širine habanja diska, u funkciji od pređenog puta, što je posledica uticaja povećanja produkata habanja u ulju i promene podmazujućih karakteristika ulja (usled postepene degradacije ulja) u toku ispitivanja.

Pre početka ispitivanja mereni su parametari topografije diskova i blokova radi provere njihove hrapavosti. Ukoliko hrapavost nekog elementa značajno odstupa od ostalih, on se ponovno brusi ili se izostavlja iz ispitivanja.

Parametri topografije površina novog diska i bloka, kao i diskova na kraju ispitivanja uzoraka menjačkog ulja prikazani su u tabeli 3.

Tabela 3. Parametri topografije površina novog diska i bloka na referentnoj dužini i diskova na kraju ispitivanja uzoraka menjačkog ulja

Veličina	Novi disk	Na kraju eksperimenta (ispitivanja)			Novi blok
		Disk Merc.	Disk PUCH	Disk PINZ	
Rt1	1.6	4.8	2.	1.1	1.82
Rt2	2	3.7	1.3	1.0	1.13
Rt3	2.3	5.0	1.1	1.2	1.67
Rt4	1.9	4.2	1.3	1.0	1.24
Rt5	1.9	3.7	1.4	1.0	1.63
Ra	0.28	0.54	0.2	0.17	0.303
Rq	0.35	0.75	0.26	0.22	0.375
Ry	2.3	5.0	2.1	1.2	1.82
Rtm	2.0	4.3	1.4	1.0	1.5
Rv	1.4	3.7	1.6	0.7	1.04
Rp	1.0	1.7	0.6	0.5	0.99
Sm	36	64	45	41	168
Δq	3.3°	4.9°	2.3°	1.9°	0.9°
Rsk	-0.2	-1.1	-1.2	-0.4	0.1
Rku	3.0	5.6	6.1	2.9	2.6
S	15	23	16	16	51
R3z	1.4	2.7	1.0	0.9	0.99
Rpm	0.8	1.4	0.5	0.4	0.74
R3y	1.6	3.9	1.1	0.9	1.15

Na slikama od 19 do 23 su prikazane topografije površina novog bloka i diska na referentnoj dužini, kao i diskova na kraju ispitivanja menjačkog ulja iz razmatranih vozila.

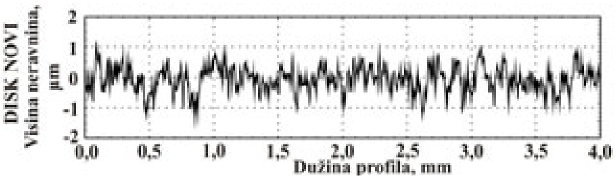

Slika 19. Topografija površine novog diska [3]

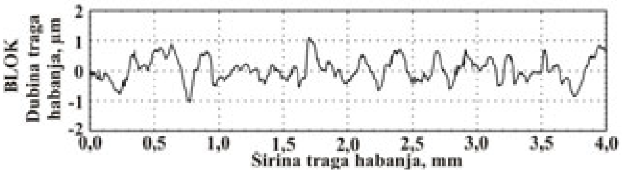

Slika 20. Topografija površine novog bloka [3]

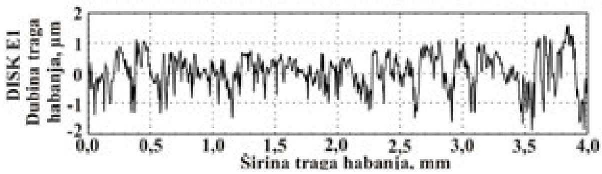

Slika 21. Topografija površine diska na kraju ispitivanja menjačkog ulja iz Mercedesa [3]

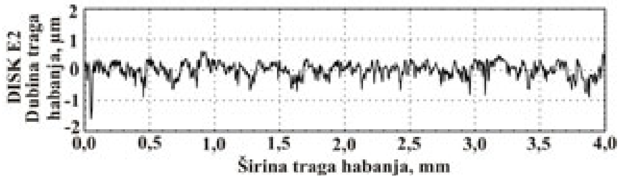

Slika 22. Topografija površine diska na kraju ispitivanja menjačkog ulja iz PUCH [3]

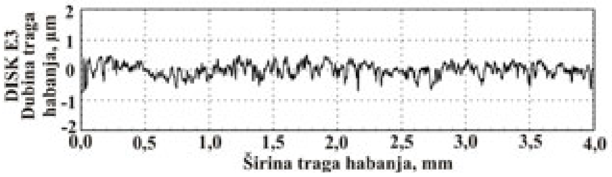

Slika 23. Topografija površine diska na kraju ispitivanja menjačkog ulja iz PINZ [3]

3. ZAKLJUČAK

Rezultati koji su dobijeni tokom ispitivanja sadrže informacije o koeficijentu trenja, sili trenja, širini i dubini traga habanja, obliku habanja kontaktne površine bloka, promeni koeficijenta trenja i temperature u toku vremena ostvarivanja kontakta, parametre topografije površine bloka i diska pre i posle ispitivanja, trag habanja na bloku i disku i dr. Radi ispitivanja dinamike procesa ostvarivanja kontakta vršen je kontinualni zapis signala sile i koeficijenta trenja radi kasnije obrade.

Na osnovu realizovanih ispitivanja dobijeni su odgovarajući histogrami promene koeficijenta trenja mereni nakon određenog vremena ostvarivanja kontakta na tribometru u zavisnosti od uzorka ulja, odnosno pređenog puta vozila, kao i širine pojasa habanja bloka.

Sprovedena ispitivanja i dobijeni rezultati omogućili su da se identifikuju određene tribološke pojave koje se događaju u motorima i menjačima razmatranih vozila. Identifikovane su tribološke pojave koje se odnose na trenje preko koeficijenta trenja, pojave habanja preko širine pojasa habanja i dubine habanja.

Realizovanim ispitivanjima konstatovano je da dolazi do promena triboloških karakteristika ulja za podmazivanje u motorima i menjačima vozila. Navedene promene su u direktnoj zavisnosti od stanja svih elemenata tribomehaničkog sistema, odnosno u zavisnosti od njihovih funkcionalnih karakteristika.

LITERATURA

[1] B. Ivković, A. Rac: Tribologija, Jugoslav Tribology Society, Kragujevac, 1995.

[2] M. Babić: Monitoring ulja za podmazivanje, Kragujevac, 2004.

[3] S. Perić: Doprinos razvoju metoda dijagnostike stanja sa aspekta fizičko hemijskih i triboloških karakteristika ulja kod motornih vozila, doktorska disertacija, Beograd, 2009.

[4] S. Perić: Uticaj načina eksploatacije menjačkog prenosnika guseničnog vozila na fizičko-hemijske karakteristike sredstva za podmazivanje, Magistarski rad, Mašinski fakultet Beograd, 2006.

[5] S. Perić, B. Nedić: „Monitoring oil for lubrication of tribomechanical engine assemblies", Journal of the Balkan tribological association, Volume 16, pages 242-257, University of Sofia, Bulgaria, 2010.

[6] S. Perić, B. Nedić, M. Vuruna: Monitoring Physical and Chemical characteristics Oil for Lubrication, Journal Tribology in industry, Volume 31, No 3-4, December 2009, pp. 59-66, University of Kragujevac - Faculty of Mechanical Engineering.

[7] Perić S., Nedić B., Vuruna M., Pešić Z.: Contribution to diagnostics of technical condition tribology assemblies transmitters of vehicles, 6th International conference on tribology, BALKANTRIB ′08, 12-14 June 2008, Sozopol, Bulgaria, pages BT-095-1 - BT-095-4.

[8] A. E. Yousif, Liquid-Solid Lubricants I Conditions Pertinent to Isothermal Elastohydrodynamic Line Contact Lubrication, Tribology in Industry, vol. 31, No. 1&2, pp. 23-31, p. 47-52, 2009.

[9] M. Ripa, C. Spanu, S. Ciortan, Characterisation of Hydraulic Oils by Shear Stability and Extreme Pressure Tests, Tribology in Industry, vol. 30, No. 3&4, pp. 23-31, p. 48-57, 2008.

[10] L. V. Markova, N.K.Myshkin, C.V. Ossia, H. Kong Fluorescence Sensor For Characterization Of Hydraulic Oil Degradation, Tribology in Industry, vol. 29, No. 1&2, pp. 23-31, p. 33-36, 2007.

RESULTS OF EXPERIMENTAL RESEARCH TRIBOLOGICAL CHARACTERISTICS OIL FROM ENGINES AND POWER TRANSMITTERS OF VEHICLES

Abstract: *Engines and power transmitters of vehicles are complex tribomechanical systems. Conditions of the elements of tribomechanical system are very complex and determinate great deal by the adequate characteristics of lubricants. Complexity of conditions is determinated by: temperature of elements in contact and temperature of lubricant, outer load (specific pressure in contact zone), dynamic character of making contact and power and motion transmission.*

Investigation procedure of tribological characteristics of lubricant during exploitation consists of following: oil sampling from real tribomechanical system; establishing of wear products participation in oil and measuring tribological characteristics of tribomechanical system in model conditions using sampled oil as lubricant.

Analysis of oil samples which contain particles, created as results of wear, enable evaluation of system tribology condition in different phases of system exploatation.

In this project, it will be presented results of experimental research tribological characteristics oil was sampled from engines and power transmitters of vehicles, Mercedes O 345, PUCH i PINZGAUER 710M, that were exploited. During realized investigations it was concluded that changes in tribological characteristics of lubricant in engine and power transmitters appear. These changes directly depend on condition of all elements of tribomechanical system, from their functional characteristics.

Keywords: *tribological characteristics, tribomechanical systems, Oil Analysis, lubrication.*

Serbian Tribology Society

SERBIATRIB '11

12th International Conference on Tribology

Faculty of Mechanical Engineering in Kragujevac

Kragujevac, Serbia, 11 – 13 May 2011

UTICAJ TEMPERATURE NA MEHANIČKE KARAKTERISTIKE ČESTIČNIH ZA27/Al_2O_3 KOMPOZITA

I. Bobić [1], M. Babić [2], S. Mitrović [2], A.Vencl[3], B. Bobić [4]

[1] INN "Vinca", Univerzitet u Beogradu, Beograd, Srbija, ilijab@vinca.rs

[2] Mašinski fakultet u Kragujevcu, Kragujevac, Srbija, babic@kg.ac.rs, boban@kg.ac.rs

[3] Mašinski fakultet u Beogradu, Beograd, Srbija, avencl@mas.bg.ac.rs

[4] IHIS R&D Centar, Beograd, biljanabobic@gmail.com

Izvod: *Mehaničke karakteristike ZA27 legure pogoršavaju se sa povećanjem temperature. Da bi se ublažio ovaj problem, pristupilo se izradi kompozita sa osnovom od navedene legure. U ovom radu ispitan je uticaj povišenih temperatura (od 70˚C do 170˚C) na mehaničke karakteristike (izražene vrednošću pritisne granice popuštanja) kompozita sa osnovom od ZA27 legure. Kompoziti su dobijeni kompokasting postupkom, uz infiltraciju različitih udela (3, 8 i 16 mas. %, respektivno) krupnih čestica Al_2O_3 (veličine 250 μm) u metalnu matricu. Ispitivanje mehaničkih karakteristika dobijenih kompozitnih materijala na povišenim temperaturama izvršeno je sa ciljem da se oceni mogućnost njihove primene u takvim radnim uslovima*.

Ključne reči: *ZA27 legura, čestični kompoziti, , kompokasting, pritisna granica popuštanja*

1. UVOD

ZA27 legura na sobnoj temperaturi poseduje dobru kombinaciju mehaničkih karakteristika (čvrstoća i tvrdoća) i tehnoloških osobina (livkost, mašinska obradivost), kao i visoku otpornost prema habanju i otpornost prema koroziji [1-4]. Legura je pogodna je za termičku obradu i plastičnu preradu, tako da je moguće naknadno uticati na mehaničke osobine dobijenh proizvoda. Legura ZA27 koristi se za izradu čaura i kliznih ležaja raznih veličina (za građevinske mašine, traktore, prese, strugove) i u tom pogledu uspešno zamenjuje skuplje materijale (mesing, bronze).

Poznato je da su za komercijalne ležajne legure pritisne osobine na sobnoj i povišenim temperaturama (oko 100ºC) od velikog značaja [5]. ZA27 legura pripada grupi niskotopivih legura, pa se sa povišenjem temperature njene mehaničke osobine pogoršavaju već na temperaturi od oko 80ºC [6]. Da bi se ublažio taj nedostatak, sredinom 80-tih godina prošlog veka otpočeli su eksperimenti na dobijanju kompozita sa osnovom od ZA27 legure, sa ciljem da se proširi polje njene primene u uslovima povećanih radnih temperatura (iznad 100ºC) [6] pod dejstvom spoljnjih opterećenja.

Za dobijanje kompozita sa osnovom od aluminijumskih legura, kao i kompozita sa osnovom od ZA legura [7-9], može se primenjuje kompokasting postupak [10], koji se zasniva na infiltraciji čestica ojačivača u metalnu matricu, koja se nalazi u poluočvrslom stanju. Razvoj kompozitnih materijala sa osnovom od ZA27 legure, uz dodatak čestica ojačivača (Al_2O_3, SiC [7-9] i ZrO_2 [10]), pokazao je da se, u odnosu na matričnu leguru, povećavaju modul elastičnosti, tvrdoća, otpornost prema habanju, koeficijent linearnog termalnog širenja i gustina dobijenih kompozita, dok se vrednosti izduženja i zatezne čvrstoće smanjuju.

Rezultati triboloških ispitivanja kompozitnih materijala sa osnovom od ZA27 legure, u koju su infiltrirane krupne čestice Al_2O_3 (veličine 250 μm) [11,12], ukazuju na poboljšanje triboloških karakteristika kompozita u odnosu na tribološke osobine osnove (matrice).

S obzirom na nedostatak konkretnih rezultata istraživanja uticaja povišenih temperatura na mehaničke osobine kompozita sa osnovom od ZA27 legure, predmet ovoga rada je ispitivanje pritisnih karakteristika kompozita sa osnovom od ZA27 legure u koju su infiltrirane krupne Al_2O_3 čestice. Ispitivanje mehaničkih karakteristika kompozita, odnosno određivanje vrednosti pritisne granice popuštanja, izvršeno je na sobnoj i povišenim temperaturama (do 170ºC), sa ciljem da se oceni mogućnost primene dobijenih kompozitnih materijala na povišenim temperaturama.

2. EKSPERIMENTALNI RAD

2.1 Kompokasting postupak

Osnovna, ZA27 legura napravljena je u Laboratoriji za materijale Instituta u Vinči. Prva faza kompokasting postupka (priprema rastopa, infiltracija čestica ojačivača i promešavanje do željenog rasporeda čestica u masi osnovne legure) izvršena je primenom aparature prikazane ranije [13].

Prva faza kompokasting postupka predstavlja mešanje poluočvrslog rastopa ZA27 legure u temperaturnom intervalu između likvidus i solidus temperature. Infiltracija krupnih Al_2O_3 čestica (250 μm) u poluočvrsli rastop legure vršena je kontinuirano, uz mešanje. U metalnu osnovu (leguru) dodato je 3, 8 i 16 mas. % Al_2O_3 čestica, respektivno. Tako su dobijeni odgovarajući kompozitni materijali. Keramičke čestice su unošene u zonu neposredno uz vratilo aktivnog dela mešača. Radna temperatura na kojoj je vršena infiltracija čestica, kao i vreme unošenja čestica, prilagođeni su masenom udelu Al_2O_3 čestica, što je prikazano u Tabeli 1.

Tabela 1. Uticaj masenog udela čestica Al_2O_3 na temperaturu i vreme infiltracije

ZA27/ Al_2O_3 kompoziti			
δ (μm)	250		
G (%)	3	8	16
t_r (°C)	461	464	468
τ_{inf} (min)	3	4	5
τ_{uk} (min)	30		

Gde je:

δ (μm) - prosečna veličina čestica Al_2O_3, G (%) - maseni udeo čestica Al_2O_3, t_r-radna temperatura mešanja poluočvrslih rastopa kompozita (°C), τ_{inf}- vreme infiltracije čestica ojačivača uz mešanje (min), τ_{uk} - ukupno vreme mešanja poluočvrslih kompozitnih masa (min) .

Po završetku procesa, poluočvrsli rastop kompozita izliven je u čeličnu kokilu predgrejanu na 300°C. Tako su dobijeni odlivci-kompoziti, cilindričnog oblika, prečnika 36 mm, visine oko 120 mm.

Toplo presovanje svih kompozitnih materijala vršeno je na temperaturi od 230°C, pri radnom pritisku od 250 MPa.

2.2. Strukturna i mehanicka ispitivanja

Pored optičke mikroskopije ("Zeiss") i skening-elektronske mikroskopije, primenjena je i SEM/EDS analiza ("Philips") u cilju praćenja raspodele hemijskih elemenata u pojedinim mikrokonstituentima legure, odnosno kompozita.

Uzorci legure i kompozita su mašinski isečeni iz dobijenih otpresaka, a zatim brušeni i polirani. Brušenje je izvedeno pomoću brusnog papira finoće 80, 360 i 600, a poliranje primenom polir tkanine "Buehler" uz dodatak polir paste sa Al_2O_3 česticama veličine 1 do 5 μm.

Pritisna ispitivanja osnovne legure u livenom stanju, kao i dobijenih kompozitnih materijala izvršena su na 20, 70, 120 i 170º C, respektivno. Ispitivanja su izvršena na uzorcima cilindričnog oblika, prečnika 4 mm i visine 6 mm. Za ispitivanja je korišćena kidalica ("Instron") sa toplom komorom, u kojoj je održavana radna temperatura sa tačnošću od ± 1ºC. Uzorci su pre izlaganja pritiskivanju bili progrevani 20 minuta. Sva pritiskivanja izvršena su brzinom od 1 mm/min.

Merenje tvrdoće uzoraka osnovne legure i kompozita izvršeno je na sobnoj temperaturi pomoću uređaja "Karl Frank GMBH". Vrednosti tvrdoće izražene su u Vikersovim jedinicama (HV).

3 REZULTATI I DISKUSIJA

3.1 Strukturna ispitivanja

Na slici 1 prikazan je izgled površine poliranog uzorka kompozita sa osnovom od ZA27 legure u koju su infiltrirane Al_2O_3 čestice (250 μm), u količini od 3 mas. % Al_2O_3.

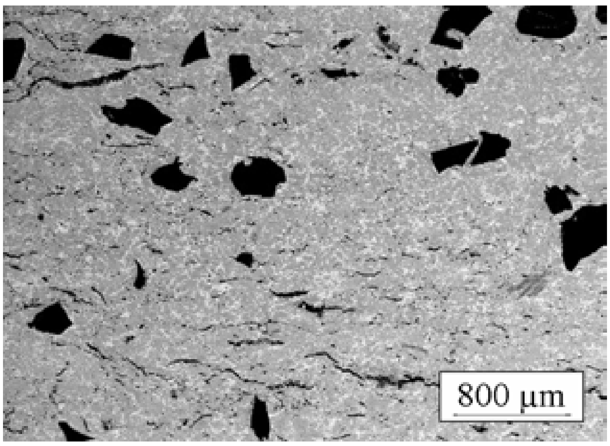

Slika 1. Kompozit ZA27 + 3 mas. % Al_2O_3 (250μm), polirano, (SEM)

U strukturi kompozita vidljiva je povoljna raspodela čestica Al_2O_3. Nije primećena segregacija ovih čestica, niti njihovo međusobno dodirivanje. Takođe, uočava se odsustvo tendencije Al_2O_3 čestica ka stvaranju nakupina.

Opšte je poznato da se dobra distribucija čestica ojačivača u matrici javlja kao zahtev pri razvoju bilo kog postupka za dobijanje kompozita**.** Pored raspodele čestica ojačivača, na mehaničke osobine kompozita značajno utiče i veličina čestica. Pri povoljnoj distribuciji čestica, bolje mehaničke osobine postižu se sa smanjenjem veličine čestica ojačivača [14,15]. Najveći broj istraživanja strukturnih i mehaničkih osobina kompozita sa osnovom od ZA27 legure, uz dodataka tvrdih (SiC, Al_2O_3, ZrO_2 [7,8, 16,17,]) i mekih čestica (grafit, coke dust [19,20]) rađen je sa česticama veličine od 5 do 150 μm. Nema radova sa česticama većim od 200 μm. U našem ranijem radu [9] vršena su poređenja strukturnih i mehaničkih osobina kompozita sa osnovom od ZA27 legure koja je ojačana sa 3 mas. % Al_2O_3 čestica, veličine 12 μm i 250 μm, respektivno. Primećena je znatno veća tendencija ka stvaranju nakupina kod kompozita koji su ojačani manjim česticama. Sitnije čestice (12 μm) bile su raspoređene u obliku nakupina, koje odgovaraju nakupinama tipa B, kako ih je definisao Tszeng [20]. Krupnije čestice (250 μm) bile su ravnomerno raspoređene u osnovi [9].

Na osnovu rezultata ranijeg rada [21], povećanjem masenog udela čestica Al_2O_3 sa 3 mas.% na 8 i 16 mas. % nije se pogoršala raspodela čestica na mikro nivou. Došlo do smanjenja zapremine matrice bez čestica.

Pored rasporeda čestica ojačivača, na slici 1 (malo uvečanje) vide se i mikroprsline u strukturi matrice i primećuju fragmenti čestica Al_2O_3 znatno manji od 250 μm. Pri većem uvećanju [21] jasnije se vidi granica čestica/matrica (osnova) i inicijalne prsline, koje polaze od čestica ojačivača ka matrici (A), kao i duž granice čestica/matrica (B). Pri ovom uvećanju ne uočava se poroznost na granici čestica/matrica. Sve zapažene mikroprsline, koje napreduju kroz zonu matrice, nalaze se u oblasti η faze [21].

Uočena je i pojava čestica ojačivača manjih od 250 μm (slika 1), koje su nastale, najverovatnije usled loma krupnijih čestica u nekoj od faza kompokasting postupka. Prema našim eksperimentalnim zapažanjima, lomljenje čestica je najviše zastupljeno kod kompozita koji sadrže 16 mas. % Al_2O_3 čestica (u odnosu na kompozite sa 3 i 8 mas. % čestica). Lomljenje čestica ojačivača je nepoželjno, jer dovodi do stvaranja nakupina čestica. Ovo negativno utiče na mehaničke osobine kompozita. Naime, pod dejstvom spoljnih opterećenja takva nakupina ponaša se kao izvor inicijalnih prslina koje se dalje šire kroz matricu i mogu izazvati lom materijala pri opterećenjima koja su niža od predviđenih. Prsline u matrici i polomljene čestice ojačivača u strukturi kompozita mogu biti izazvane prekomernom silom primenjenom za vreme toplog presovanja ili pojavom zaostalih naprezanja (residual stress) u fazi hlađenja otpresaka posle presovanja.

Rezultati SEM/EDS analize, prikazani na slici 2 a i b.

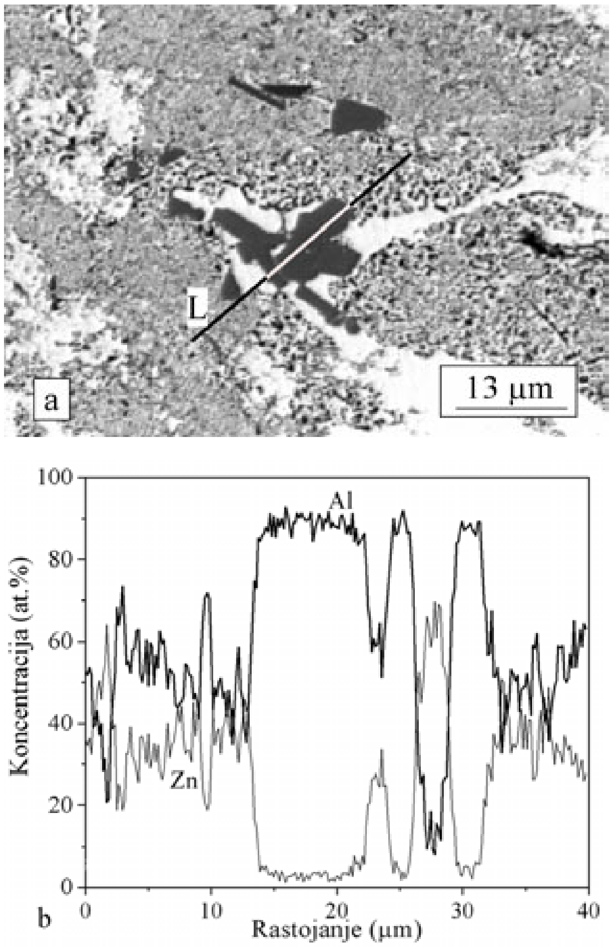

Slika 2. Kompozit ZA27 + 16 mas. % Al_2O_3. (250 μm), SEM/EDS analiza. A-položaj linije L u mikrostrukturi, b- Promena hemijskog sastava duž linije L

Analiza slike 2 a i b omogućava uvid u stanje granične površine čestica/matrica (eventualna pojave neke hemijske reakcije između metalne osnove kompozita i čestica ojačivača), kao i raspodelu hemijskih elemenata po fazama (u matrici i kroz česticu Al_2O_3). Linija L, čiji je položaj u strukturi dat na slici 2a, polazi iz oblasti α+η dvofazne smeše, ulazi u oblast η faze, prolazi kroz Al_2O_3 česticu, zatim kroz kratku zonu η faze i završava u smeši α+η faza. Po značajnom skoku koncentracije aluminijuma na prikazanom dijagramu jasno je da linija nailazi na česticu Al_2O_3. Nije primećeno prisustvo reakcionog sloja, koji bi ukazivao na hemijsku reakciju između čestica ojačivača i osnove. Ovo ukazuje na postojanje mehaničke veze između ojačivača i matrice.

Ovim je dokazano da su, u primenjenom radnom intervalu temperaturnom intervalu kompokasting postupka, čestice Al_2O_3 hemijski i termodinamički stabilne, tj, da je moguće formirati samo mehaničku vezu ojačivač-matrica.

3.2 Mehanička ispitivanja

Uporedni rezultati pritisnih ispitivanja livenih uzoraka ZA27 legure, kao i uzoraka kompozita, prikazani su na dijagramu na sl. 7 Ispitivanja su izvršena na sobnoj i povišenim temperaturama, u temperaturnom intervalu od 20 do 170ºC, sa korakom od 50°C. Kao pogodan pokazatelj promene pritisnih osobina sa temperaturom uzeta je vrednost pritisne granice popuštanja.

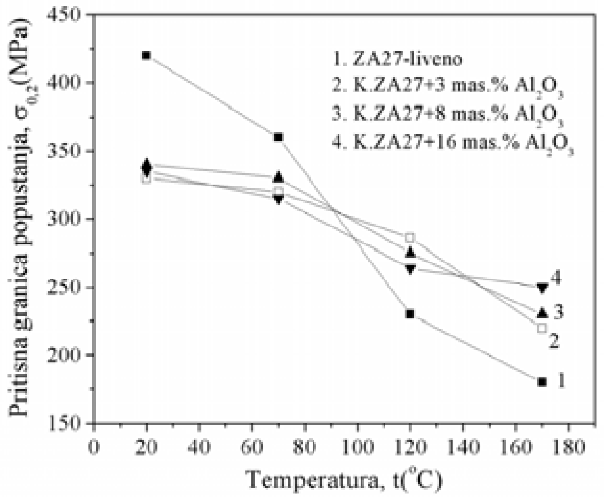

Slika 3. Promena pritisne granice popuštanja pri povećanju temperature livene ZA27 legurei kompozita sa njenom osnovom

Kao što se vidi sa pregledom dijagrama na sl. 3, osnovna, ZA27 legura (matrica) u livenom stanju, od sobne do temperature od 70ºC, pokazuje veće vrednosti pritisne granice popuštanja, u odnosu na kompozitne materijale. Sa povećanjem temperature iznad 70ºC dolazi do brzog pada vrednosti granice popuštanja livenih uzoraka, u odnosu na vrednosti granice popuštanja za kompozite. Počev od temperature od oko 90°C pa do kraja primenjenog radnog intervala (170ºC), kompozitni materijali pokazuju bolje mehaničke osobine, nezavisno od veličine udela čestica ojačivača. Promene vrednosti pritisne granice popuštanja kompozita sa 3 i 8 mas. % Al_2O_3 su vrlo slične. U odnosu na ove kompozite, vrednosti granice popuštanja kompozita sa 16 mas.% Al_2O_3 su manje na nižim temperaturama, dok na temperaturama iznad 130ºC postaju veće od vrednosti granice popuštanja kompozita sa nižim masenim udelima čestica ojačivača.

Vrednosti izmerenih tvrdoća na sobnoj temperaturi, za ZA27 leguru u livenom stanju, kao i vrednosti tvrdoće dobijenih kompozita prikazane su u Tabeli 2.

Tabela 2. Tvrdoća ZA27 legure i kompozita na sobnoj temperaturi

Materijal/Stanje	Tvrdoća (HV)
ZA27, liveno	115
ZA27 + 3 mas.% Al_2O_3	92
ZA27 + 8 mas.% Al_2O_3	117
ZA27 + 16 mas.% Al_2O_3	125

Mehaničke karakteristike kompozinih materijala sa osnovom od legura cinka do sada nisu standardizovane, pa su rezultati mehaničkih ispitivanja sličnih materijala drugih autora bili osnovna orijentacija za ocenu rezultata naših istraživanja. Pored toga, korišćen je i standard [22].

Ako se ima u vidu Arsenolov (Arsenault) mehanizam [23] ojačanja kompozitnih materijala usled različitih koeficijenata linearnog širenja čestica ojačivača i matrice kompozita, za kompozite dobijene u ovom radu moglo bi se očekivati izvesno povećanje vrednosti pritisne granice popuštanja na sobnoj temperaturi. Naime, vrednost koeficijenta linearnog termalnog širenja ZA27 legure je 26 $\mu m\ m^{-1}\ K^{-1}$ [5], odnosno 3,7 puta veća u odnosu na vrednost tog koeficijenta za Al_2O_3 (7,6 $\mu m\ m^{-1}\ K^{-1}$) [33]. Međutim, kod svih kompozitnih materijala koji su ispitivani u ovom radu (sa 3, 8 i 16 mas. % čestica Al_2O_3 u metalnoj matrici), konstatovano je smanjenje vrednosti pritisne granice popuštanja na sobnoj temperaturi u odnosu na liveno stanje ZA27 legure.

Kada se imaju u vidu rezultati metalografskih ispitivanja, može se pretpostaviti da su mikroprsline (nastale kao posledica postupka dobijanja kompozita) osnovni uzrok smanjenja pritisne čvrstoće kompozita, u odnosu na liveno. Opisana pojava primećena je kod različitih vrsta kompozita [24], a njeno dalje proučavanje je neophodno u cilju poboljšanja mehaničkih karakteristika kompozita sa krupnim česticama, u uslovima eksploatacije na temperaturama do 70ºC.

Poređenjem rezultata merenja tvrdoće kompozita Tabela 2 vidi se da sa povećanjem masenog udela čestica ojačivača povećava tvrdoća. Dok su tvrdoće kompozita sa 3 i 8 mas.% Al_2O_3 približne tvrdoćama uzoraka u livenom stanju, dotle je tvrdoća uzoraka sa 16 mas. % Al_2O_3 veća. Ovo je u skladu sa rezultatima drugih autora [5].

Prema podacima Conrada [25], koji se odnose na čiste metale, pa se mogu uzeti kao orijentacioni u slučaju ZA27 legure (koju praktično čine cink i aluminijum), za vrednosti radnih temperatura $T > 0{,}5\ T_m$, gde je T_m temperatura topljenja metala, pod dejsatvom spoljnih opterećenja, osnovni mehanizam kretanja dislokacija na povišenim temperaturama je uspinjanje (climb). Prema binarnom dijagramu stanja aluminijum-cink [3], temperatura početka topljenja ZA27 legure je 373ºC (T_m = 646 K). Za ZA27 leguru, kritična temperatura, na kojoj, pri opterećenju, dolazi do naglog pogoršanja mehaničkih osobina iznosi oko 100ºC [6], odnosno 80ºC [7]. Ako pretpostavimo da je uzorak od ZA27 legure opterećen pri radnoj temperaturi od 100ºC (T_r = 373º K), tada je T_r = 0,57 T_m . U slučaju Zn25Al3Cu legure, može se pretpostaviti da se na temperaturama preko 80ºC, pod dejstvom opterećenja, odvija intenzivni transport atoma, što ima za posledicu brzo smanjenje vrednosti mehaničkih osobina kod uzoraka u livenom i tiksokasting stanju. Prema rezultatima prikazanim na sl. 7, vrednosti pritisne granice popuštanja za kompozite sporije opadaju iznad temperature od 80ºC. Ovo je, najverovatnije, posledica prethodnog porasta gustine dislokacija i povećanja broja subzrna (prema Arsenolovom mehanizmu), odnosno otežanog kretanja dislokacija, čime se usporava smicanje atomskih ravni. Sa povećanjem masenog udela čestica ojačivača u kompozitu, umnožava se i gustina dislokacija, tako da su opisani efekti veći. U slučaju kompozita ZA27 + 16 mas.% Al_2O_3, ovi efekti su u punoj meri izraženi kada je temperatura viša od 130ºC.

Zajednički uticaj parametara presovanja i zaostalih naprezanja, tokom hlađenja otpresaka dobijenih kompozitnih materijala, negativno se odrazio na mehaničke osobine uzoraka dobijenih kompokasting postupkom. Imajući ovo u vidu, potrebno je izvršiti modifikaciju ove faze kompokasting postupka u cilju dobijanja kompozita sa minimalnim brojem prslina

Upoređivanjem vrednosti pritisne granice popuštanja nekoliko komercijalnih legura za izradu kliznih ležaja [5] sa odgovarajućim vrednostima za kompozite koji su dobijeni u ovom radu, može se konstatovati da kompozitni materijali poseduju bolje mehaničke karakteristike. Pored toga, rezultati triboloških ispitivanja kompozita sa osnovom od ZA27 legure uz dodatak čestica Al_2O_3 veličine 250 μm [11,16], ukazuju na povećanu otpornost prema habanju kompozita u odnosu na liveno stanje ZA27 legure.

5. ZAKLJUČCI

1. Primenom opisanog kompokasting postupka dobijeni su kompoziti sa dobrom raspodelom krupnih čestica ojačivača (Al_2O_3 čestice, veličine 250 μm), na makro i mikro nivou, u matrici ZA27 legure. Primenom toplog presovanja, smanjena je poroznost, ali je prisutna pojava prslina u matrici kompozita, nezavisno od masenih udela čestica ojačivača.

3. Mehaničke osobine kompozitnih materijala, izražene vrednošću pritisne granice popuštanja, bolje su u odnosu na osobine osnovne ZA27 legure u livenom stanju, za temperature više od 80ºC. Na nižim temperaturama, mehaničke osobine kompozita su lošije u odnosu na liveno i tiksokasting stanje matrične legure.

4. Na osnovu izloženog, smatramo da je potrebno nastaviti istraživanja vezana za poboljšanje strukturnih i mehaničkih osobina kompozita sa osnovom od ZA27 legure u koju su infiltrirane krupne čestice ojačivača, u smeru dobijanja i primene jeftinih kompozitnih materijala sa dobrim mehaničkim osobinama na nižim temperaturama (ispod 80˚C).

LITERATURA

[1] M Durman, Z. Metallkd. 89 (1998.),6, p.417-423,

[2] J. Hallen-Lopez, J.I. Dickson, L. Handfield, R.J. Barnhurst, AFS Transactions 88-121, (1988), p.633-644

[3] E. Gervais, R.J. Barnhurst, C. A. Loong, Journal of Metals, (1985), p. 43-47,

[4] V. G. S. Mani, P. Sriram, N. Raman, S. Seshan, AFS Transactions, 88-100, (1988.), p.525-532,

[5] A. G. Guy , Element of Phisical Metallurgy, Addison-Wesley, inc, USA, july 1960, p. 360,

[6] E. J. Kubel, Advanced materials & Processes inc. Metal Progress 7, (1987.) p. 51-57,

[7] I. A. Cornie, R. Guerriero, L. Meregalli, I. Tangerini, Cast Reinforced Metal Composites, ASM International USA, (1988.) p. 155-165,

[8] N. Karni, G.B. Barkay, M. Bamberger, J. Mater. Sci. Lett., 13, (1994.) p. 541-544,

[9] I. Bobic, M. T. Jovanovic, N. Ilic, Materials Letters 57, (2003), p. 1683 – 1688,

[10] R. Mehrabian, R. G. Riek, M. C. Flemings, Metall. Trans. vol. 5, (1974.).p. 1899-1905,

[11] S. Mitrović, PhD, Thesis. Kragujevac 2007.

[12] S. Mitrovic, M. Babic, I. Bobic, Tribology in Industry, vol. 29, No 3 & 4, (2007),p.35-41

[13] I. Bobić, M. Babić, S. Mitrović, B. Bobić, M.T. Jovanović, Proceedings of the 3rd International Conference on Manufacturing Engineering (ICMEN), 1-3 October 2008, Chalkidiki, Greece, 363-373.

[14] T. J. A. Doel, P. Brown, Composites Part A, 27 A (1996.), 655-665

[15] R. M. Aikin, JOM, vol 49, (1997.), p. 35-39

[16] S. C. Sharma, B. M. Girish, D.R. Someshekar, B.M. Satish, R. Kamath Wear 224, (1999.), p. 89-94

[17] K. Seah, S. Sharma, P. R. Rao, B. Girish, Materials & Design, vol. 16, 5 (1995.), 277-281,

[18] K. H. W. Seah, S. C. Sharma, B. M. Girish, Materials & Design, vol.16, 5 (1995.), 271-275,

[19] A. Madronero, J. Cruz, C. Foruria, J. Coleto, JOM, vol. 49, (1997). 46-48,

[20] T. C. Tszeng, Composites, Part B, 29 B, (1998), p. 299-308,
[21] B. Bobić, M. Babić, S. Mitrović, N. Ilic, I. Bobić, M.T. Jovanović, Int. J. Mat. Res (formerly Z. Metallkd.) 101 (2010)12, p. 1524-1531
[22] EN 12844 (1998), Zinc and zinc alloys. Castings. Specifications.
[23] R. J. Arsenault, L. Wang, C. R. Feng, Acta Metall. Materialia, vol.39, No1, (1991) p. 47-57, [24] Fundamentals of Metal-Matrix Composites, Edited by S. Suresh, A.
[24] Mortenson, A. Needleman, Ch.13, A. Neesleman, S. Nutt, S. Suresh, V. Tvergaard,.Butterworth–Heineman, (1993.)
[25] H. Conrad, Journal of Metals 7,(1964), p. 582-588,

Serbian Tribology Society

SERBIATRIB '11

12th International Conference on Tribology

Faculty of Mechanical Engineering in Kragujevac

Kragujevac, Serbia, 11 – 13 May 2011

UTICAJ TEHNIČKE DIJAGNOSTIKE NA STANJE ISPRAVNOSTI TEHNIČKIH SISTEMA

Hasan Avdić, Asmir Demirović, Mehmed Hasanović
RMU – Banovići, d.d. Banovići, BiH, h.avdic@bih.net.ba
Univerzitet u Tuzli, Mašinski fakultet, BiH

Apstrakt: *Dijagnostika je tehnologija koja je,sa jedne strane, vezana za tehničko stanje sistema, odnosno za sam objekat dijagnosticiranja, sa druge strane i za sistem održavanja apliciran na taj objekat radi obezbjeđenja njegovog ispravnog funkcionisanja (obezbjeđenja potrebnog eksploatacionog nivoa pouzdanosti). Alokacija dijagnostike u sistemu održavanja jednog tehničkog sistema proizilazi iz njene dvojne uloge. Ona naime, sa jedne strane služi za to da se utvrdi da li je tehnički sistem u stanju "u radu", stanju "u otkazu", ili nekom drugom međustanju. Ovo, po suštini ima kontrolni, pa time i preventivni karakter. Sa druge strane, ako se prilikom kontrole tehničkog stanja utvrdi da sistem ne izvršava svoju funkciju, onda se od dijagnostike očekuje da ukaže na uzroke neispravnosti, i na prognozu tehničkog stanja sistema u budućnosti.*

S druge strane ispravnost sistema je tehničko stanje sistema pri kom on odgovara svim zahtjevima ispravnosti propisanim normativno-tehničkom dokumentacijom.

U ovom radu su prikazani rezultati eksperimentalnih istraživanja koja su izvedena na opremi (tribološki sklopovi hidrostatičkih prenosnika snage hidrauličnog bagera Liebherr R 9350) u Rudniku mrkog uglja Banovići, dok su laboratorijska ispitivanja uzoraka ulja izvršena u ovlaštenim laboratorijama.

Ključne reči: *tehnička dijagnostika, stanje ispravnosti, tribološki sklop, tehnički sistemi.*

1. UVOD

RMU "Banovići" d.d. Banovići je u proteklih par godina u nabavku i održavanje mehanizacije investirao više nego svi rudnici zajedno u BiH, a vrlo brzo će postati prvi u rudarstvu ali i cjelokupnoj industriji na ovim prostorima koji je modernizovao proces održavanja u cjelosti.

Da bi smanjili zastoje neophodno je bilo preći sa reaktivnog (čekaj i vidi) na proaktivni (otklanjati uzroke umjesto posljedica) pristup održavanju tehničkih sistema. Takav prelaz bio je uslovljen nabavkom savremenih dijagnostičkih uređaja.

Nakon što je stigla dijagnostička oprema izvršena je obuka dijagnostičara i počelo se sa njenom primjenom.

2. TEORIJSKA ISTRAŽIVANJA

2.1 Pojam i zadaci tehničke dijagnostike

Pod ovim pojmom danas se podrazumijevaju sve aktivnosti koje se sprovode sa ciljem ocjene trenutnog tehničkog stanja sistema (sa rastavljanjem i bez rastavljanja sistema) radi preduzimanja planiranih aktivnosti održavanja ili davanja prognoze tehničkog stanja sistema u budućnosti [1].

Tehnička dijagnostika, kao sastavni dio procesa održavanja prema stanju, treba da utvrdi tehničko stanje sastavnog dijela sistema sa određenom tačnošću u određenom trenutku vremena. To je zapravo nauka koja se bavi prepoznavanjem tehničkog stanja sistema [1].

Zadaci tehničke dijagnostike su :

- provjera ispravnosti tehničkog stanja sistema,
- provjera radne sposobnosti tehničkog sistema,
- provjera funkcionalnosti,
- istraživanje otkaza (mjesto, oblik i uzrok otkaza).

Osnovni postupci tehničke dijagnostike

- Subjektivni,
- Objektivni.

2.2 Ispravnost tehničkih sistema

Tehnički sistemi predstavljaju organizovan skup elemenata i relacija između njih i njihovih karakteristika povezanih i objedinjenih međusobno u cjelinu, sa istom funkcijom cilja. Različiti tehnički sistemi imaju različite funkcije cilja.

Ispravnost sistema je tehničko stanje sistema pri kome on odgovara svim zahtjevima ispravnosti propisanim normativno tehničkom dokumentacijom [1].

Kada se tehnički sistem proizvede i uključi u eksploataciju, može biti u jednom od dva moguća stanja: stanju "U RADU" i stanju "U OTKAZU". Ako je tehnički sistem ispravan i izvršava propisani zadatak, na propisan način i u propisanom vremenu, on je u stanju "U OTKAZU". Ako nije ispravan, zadatak se ne izvršava na propisan način, i nalazi se u stanju "U OTKAZU".

2.3 Tribologija, tribološki sistemi i procesi

″Tribologija je naučna i tehnološka oblast (teorija i praksa) koja izučava međusobna dejstva površina u kontaktu pri njihovom relativnom kretanju″ [ITC]. Kontakt dva elementa sa trećim elementom koji ih u manjoj ili većoj mjeri razdvaja naziva se TRIBOLOŠKI SISTEM (TS).

Unutrašnji proces tribološkog sistema zove se TRIBOLOŠKI PROCES (TP) koji najčešće obuhvata trenje i trošenje površina u kontaktu. Proučavanje uzorka ulja, koje sadrži čestice nastale habanjem, omogućava da se u ranim fazama korištenja ocijeni stanje TS [2].

2.4 Dijagnostika stanja hidrauličnog ulja

Dijagnostika stanja hidrauličnog ulja podrazumijeva skup aktivnosti kojima se, u toku eksploatacije ulja u hidrauličnom sistemu, vrši procjena stanja radnog fluida u smislu njegovih osnovnih funkcionalnih karakteristika. Dijagnostika stanja ulja ima za cilj da se ulje u sistemu koristi što duže i da hidraulični sistem radi u optimalnim uslovima u odnosu na radni fluid. Najkompletniji i svakako najpouzdaniji, prilaz dijagnostici stanja hidrauličnog ulja je metoda periodičnog uzorkovanja uljnog punjenja i laboratorijskih analiza osnovnih fizičko-hemijskih karakteristika i prisustva mehaničkih nečistoća.

Analiza uzoraka ulja tokom njegove eksploatacije predstavlja dijagnostički alat za određivanje stanja ulja i stanja mehaničkog sistema u cjelini. Analiza pomaže da se identifikuje stanje normalne eksploatacije hidrauličnog ulja, odnosno habanja mehaničkog sistema i trenutak kada se pojavljuje potencijalno ozbiljan problem.

Ako se neka karakteristika obuhvaćena ispitivanjem nađe izvan dopuštenih granica, smatra se da su nastale izvjesne promjene uljnog punjenja i da je ulje potrebno češće kontrolisati, odnosno smanjuje se period uzorkovanja ulja [1].

3. EKSPERIMENTALNA ISTRAŽIVANJA

3.1 Plan istraživanja

Istraživanje je obavljeno na površinskom kopu „Grivice“, Rudnika mrkog uglja „Banovići“ d.d. Banovići, na hidrauličnom bageru Liebherr R9350 Litronic, koji je u martu mjesecu 2010. god. nabavljen, montiran i pušten u rad.

Za realizaciju funkcije cilja urađeno je slijedeće:

- definiran tehnički sistem,
- definiran tribološki sistem,
- definirani parametri istraživanja i metode ispitivanja ulja,
- definirana prihvatljiva ograničenja,
- definiran vremenski interval uzimanja uzoraka ulja,
- ispitivanje ulja, obrada i analiza rezultata izmjerenih veličina, komparacija sa graničnim vrijednostima,
- zaključna razmatranja.

3.2 Definiranje tehničkog sistema

Hidraulički bager Liebherr R9350 spada u klasu teških hidrauličkih rudarskih bagera, projektovan je za rad u najtežim uslovima i svim vrstama miniranog okruženja. Ukupna radna težina bagera je 3225 kN. Bager je opremljen sa čeonom kašikom zapremine 18 m^3, i pogonskim elektromotorom snage 1200 kW. Izgled i tehničke karakteristike bagera prikazani su na slici 1. i tabeli 1.

Slika 1. Hidraulički bager Liebherr R9350

Tabela 1. Tehničke karakteristike bagera

Pogonski elektromotor izlazne snage	1200 kW
Čeona kašika (SAE 2:1) kapaciteta	18 m^3
Maksimalna sila kopanja	1300 kN
Maksimalna sila kidanja	1060 kN
Širina papuča gusjeničnog lanca	850 mm
Radna težina bagera	3225 kN
Pritisak na podlogu	$2{,}7 \cdot 10^5$ Pa
Ukupna količina ulja u hidrauličnom sistemu	4200 litara
Kapacitet hidrauličnog rezervoara	3000 litara
Maksimalni radni pritisak	$320 \cdot 10^5$ Pa
Maksimalni pritisak u transportu	$370 \cdot 10^5$ Pa
Maksimalni pritisak u kružnom kretanju	$350 \cdot 10^5$ Pa
Maksimalna brzina okretanja	3,9 o/min
Maksimalna brzina transporta	2,2 km/h

Hidraulični bager Liebherr R9350 sastoji se iz sljedećih podsistema :

- Pogonski modul (elektromotor, reduktor, pumpe),
- Upravljački modul,
- Mehanizam kopanja (kašika, cilindri),
- Mehanizam kružnog kretanja,
- Mehanizam transporta,
- Sistem podmazivanje svih komponenata bagera.

Kao radni fluid, u hidraulični sistem je usuto motorno ulje za hidraulične sisteme tip SAE 20W-20.

3.3 Definiranje tribološkog sistema

Hidraulični bager je sačinjen iz više triboloških sistema. Problem koji je analiziran u ovom radu je dio mehanizma kružnog kretanja, konkretno obrađen je problem na pumpi kružnog kretanja i tribološkom procesu koji se odvija unutar same pumpe. Pumpa je prikazana na slici 2.

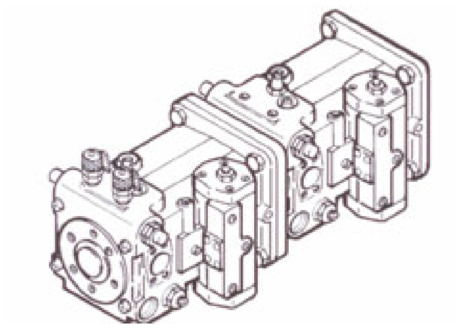

Slika 2. Pumpa kružnog kretanja

3.4 Definiranje parametara istraživanja i metoda ispitivanja ulja

U ovom radu je vršeno istraživanje sljedećih parametara :

- promjena fizičko – hemijskih karakteristika ulja (kinematska viskoznost, indeks viskoznosti, tačka paljenja, totalni bazni broj, neutralizacioni broj)
- sadržaj metala po vrsti i količini (Fe, Cu, Al, Pb)

Metode korištene pri određivanju promjena fizičko-hemijskih karakteristika ulja su:

- Kinematska viskoznost [mm^2/s] na temperaturama 40 °C i 100 °C (ispitivanje izvršeno prema standardu BAS ISO 3104 i DIN 51562),
- Indeks viskoznosti (ispitivanje izvršeno prema standardu BAS ISO 2909 i ASTM D2207),
- Tačka paljenja (ispitivanje izvršeno prema standardu ISO 2592 i ASTM D 92),
- Totalni bazni broj (TBN) [mgKOH/g] (ispitivanje izvršeno prema standardu BAS ISO 3771),
- Neutralizacioni broj (TAN) [mgKOH/g] (ispitivanje izvršeno prema standardu ASTM 664),

Sadržaj metala (Fe, Cu, Al, Pb) [mg/kg – ppm]

- ispitivanje izvršeno prema standardu ASTM D5863 odnosno primjenjena je atomska apsorpciona spektrometrija.

3.5 Definiranje graničnih vrijednosti

U tehničko-tehnološkoj dokumentaciji bagera, proizvođač bagera je definisao granične vrijednosti fizičko-hemijskih karakteristika ulja i prisustva mehaničkih nečistoća koje su prikazane u tabelama 2 i 3.

Tabela 2. Granične vrijednosti fizičko hemijskih karakteristika

Wear Metals	Monitor	Caution	Action
Viskoznost na 40 °C (mm^2/s)	min 52 - max 60	min 50 - max 62	min 48 - max 66
Viskoznost na 100 °C (mm^2/s)	min 8.2 – max 8.6	min 8.0 – max 9.0	min 7.7 – max 9.3
Indeks viskoznosti	min 100 – max 110	min 95 – max 115	min 90 – max 125
TBN (mgKOH/g)	novo ulje -0.2 / +0.3	novo ulje -0.2 / +0.4	novo ulje -0.2 / +0.5
Klasa onečišćenja	19/16/13	20/17/14	22/18/15

Tabela 3. Granične vrijednosti prisustva mehaničkih nečistoća

Wear Metals	Monitor	Caution	Action
Fe	10	12	15
Cu	8	10	18
Al	2	3	5
Pb	3	5	7

3.6 Definiranje vremenskog intervala uzimanja uzoraka ulja

Uzimanje uzoraka je osnovni preduslov za dobijanje pouzdanih rezultata ispitivanja. Uzorci ulja treba da omogućavaju dobijanje prosječnog sastava ukupnog ulja; osim toga, svi se uzorci moraju uzimati po istom postupku.

Proizvođač bagera je tehničkom dokumentacijom preporučio vremenski interval za uzimanje uzoraka ulja od 500 radnih sati. Preporučeni interval zamjene kompletnog ulja hidrauličnog sistema bagera je 2000 radnih sati. U slučaju pozitivnih rezultata analize ulja, interval korištenja ulja može biti produžen do 5000 radnih sati ili maksimalno 3 godine rada.

Vremenski interval zamjene hidrauličkih filtera koje preporučuje proizvođač bagera je 1000 radnih sati za filtere povratnog voda hidraulike i servo filtere, dok je za filtere visokog pritiska 5000 radnih sati.

Zbog mogućih oštećenja na hidrauličkim komponentama, konstrukciono su na bageru postavljena tri nivo zaštite :

- Prvi nivo (Svaka od hidrauličkih pumpi ima senzor onečišćenja, kao prvi signal trošenja i prisustva metalnih opiljaka u pumpi),
- Drugi nivo (Filteri visokog pritiska, predstavljaju zaštitu izvršnih organa i upravljačkih jedinica od onečišćenja nastalog u samim pumpama),
- Treći nivo (Magnetna klipnjača na filterima povratnog voda hidraulike, zaštita rezervoara ulja od onečišćenja nastalih u izvršnim organima i razvodnim ventilima).

Kako bi se omogućilo nesmetano uzimanje uzoraka i onečišćenje uzorka ulja svelo na minimum, proizvođač bagera je konstrukciono postavio odgovarajuće ispusne ventile. Mjesto za uzimanje uzoraka ulja prikazano je na slici 3.

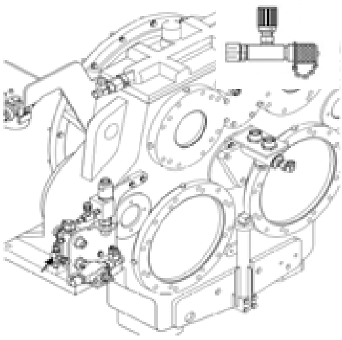

Slika 3. Mjesto predviđeno za uzimanje uzoraka ulja

3.7 Ispitivanje ulja, obrada i analiza rezultata

U skladu sa preporukama izvršeno je uzorkovanje i ispitivanje ulja u ovlaštenim laboratorijama. Rezultati ispitivanja ulja su prikazani tabelarno i pomoću histograma (tabela 4, slike 3 i 4).

Tabela 4. Rezultati analize ulja

Datum uzimanja uzorka	11/10/10	18/08/10	07/07/10	17/06/10	04/05/10	20/04/10	15/03/10
Broj sati mašine	2870	1790	1287	883	516	218	0
Broj sati ulja	866	1790	1287	883	516	218	0
Viskoznost na 40 °C (mm²/s)	50,03	49,89	49,99	50,16	50,37	51,16	50,4
Viskoznost na 100 °C (mm²/s)	8,05	8,1	8,09	8,07	8,13	8,18	8,24
Indeks viskoznosti	132	134	133	132	133	132	136
TBN (mgKOH/g)	10,13	10,07	10,06	9,99	9,89	9,82	10,34
Tačka paljenja (°C)	237	237	237	248	243	247	248
Fe	28,78	3,91	3,44	3,49	8,18	4,38	1,47
Cu	5,99	5,42	4,73	4,74	3,69	1,97	1,15
Al	0	9,98	9,31	5,8	78,3	0	0
Pb	0	3,86	0	0	1,37	0	0
Klasa zaprljanosti							
4 µm (c)		19	20	20	21	21	
6 µm (c)		16	17	17	16	17	
14 µm (c)		12	12	13	11	12	

Slika 4. Histogram trenda prisustva mehaničkih nečistoća

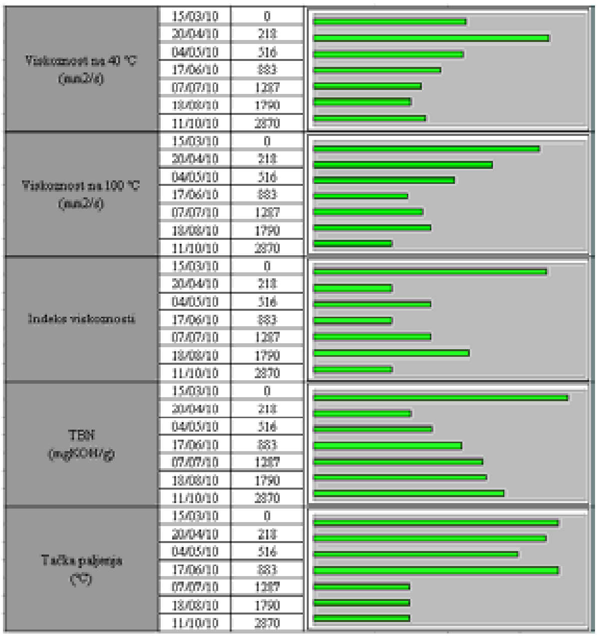

Slika 5. Histogram trenda fizičko hemijskih karakteristika ulja

Sa slike broj 4, jasno se uočava trend rasta prisustva mehaničkih nečistoća u ulju sa povećanjem broja sati rada bagera. Izmjerene vrijednosti bakra (Cu) su u stalnom porastu ali su još uvjek unutar dopuštenih vrijednosti (na histogramu zeleno područje). Vrijednosti željeza su u prva tri mjerenja bile u porastu, da bi nakon trećeg mjerenja vrijednost pala. Razlog pada vrijednosti leži u zamjeni filtera povratnog voda hidraulike (filteri u tanku bagera) koji se prema preporukama proizvođača mijenjaju svakih 1000 radnih sati.

Nedopušteno velika vrijednost prisustva aluminija (Al) kao i upozoravajuća vrijednost prisustva olova (Pb) u uzorcima ulja ukazivale su na loše tribološke procese trošenja određenih triboloških elemenata unutar hidrauličkih pumpi hidrauličkog sistema bagera.

Na slici 5., prikazan je djelimičan presjek pumpe kružnog kretanja, na kojoj su izdvjene pozicije 3 i 4 koje skupa sa uljem čine jedan tribološki sistem unutar kojeg se odvija tribološki proces.

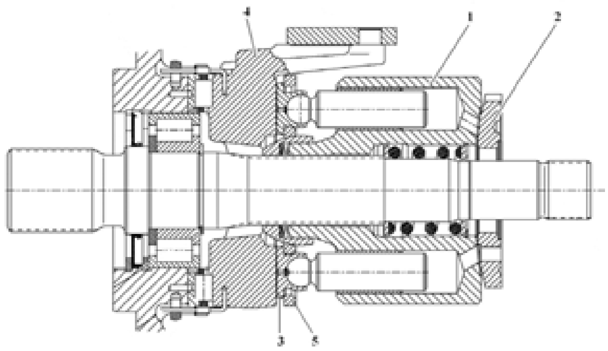

Slika 5. Presjek hidraulične pumpe kružnog kretanja

Demontažom i defektažom pumpe kružnog kretanja, konstatovana su oštećenja elemenata pumpe (pozicije 3, 4 i 5). Izled oštećenja prikazan je na slici 6.

Slika 6. Oštećenja na komponentama pumpe

Slika 7. Metalni opiljci pronađeni u filterima fisokog pritiska

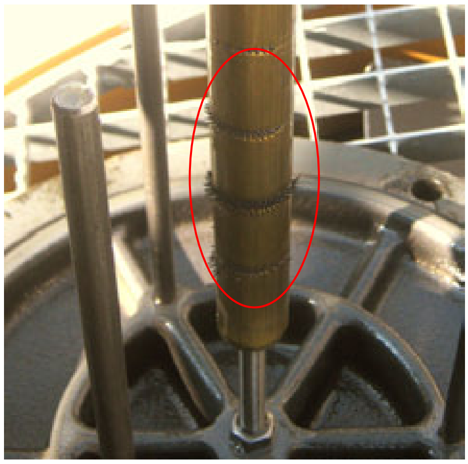

Slika 8. Metalno onečišćenje na magnetnoj klipnjači filtera ulja

4. ZAKLJUČAK

Rudnici mrkog uglja Banovići d.d. Banovići, pri eksploataciji mineralne sirovine, koriste visoko produktivne tehničke sisteme. Zastoji ovih tehničkih sistema izazivaju zastoje u procesu proizvodnje što dovodi do visokih ukupnih troškova a posebno indirektnih.

Stanju ispravnosti ovih tehničkih sistema u fazi eksploatacije mora se posvetiti posebna pažnja. To se, između ostalog, može postići primjenom tehničke dijagnostike (teorija, metode i uređaji) na organizovan način.

U ovom radu je prikazana primjena metoda tehničke dijagnostike u cilju utvrđivanja stanja triboloških sklopova jednog od visoko produktivnih tehničkih istraživanja.

Istraživanja su pokazala da se tehnička dijagnostika ne primjenjuje na organizovan način što je dovelo do ovakvih oštećenja triboloških sklopova još u ranoj fazi primjene tehničkog sistema.

Daljna istraživanja treba usmjeriti na izradu programa primjene metoda i uređaja radi utvrđivanja stanja tehničkih sistema i prognoze ponašanja u budućnosti što i jeste najvažiji zadatak tehničke dijagnostike.

LITERATURA

[1] Adamović Ž.: Tehnička dijagnostika, Zavod za udžbenike i nastavna sredstva, Beograd, 1996.,

[2] Ekinović S.: Osnovi tribologije i sistema podmazivanja, Mašinski fakultet u Zenici, Zenica, 2000.,

[3] Babić M.: Monitoring ulja za podmazivanje, Mašinski fakultet u Kragujevcu, Kragujevac, 2004.,

[4] Avdić H, Tufekčić Dž.: Tereotehnologija I, Univerzitet u Tuzli, Mašinski fakultet, Tuzla, 2007.

TEHNICAL DIAGNOSTIC INFLUENCE ON AN ACCURACY CONDITION OFF TECHNICAL SYSTEMS

Abstract: *Diagnostics is a technology that is, on the one hand, related to the technical condition of the system, apropos to the object of diagnostic, on the other side to the maintenance system which is applied to that object because of ensuring its proper functioning (providing the required reliability level of exploitation). Allocation of diagnostics in the system of maintaining a technical system stems from its dual role. In a fact, on the one hand, it is used to determine whether the system is technically able "to work" condition, "in failure" condition, or another intermediate condition. This, in essence, has a control and preventive character. On the other hand, if during a control of technical condition determines that the system does not perform its function, then the diagnosis is expected to show the causes of failure, so as the prediction of technical condition of the system in the future. On the other hand, the correctness of the system is a technical condition of the system that meets all safety requirements prescribed by the normative-technical documentation. This paper will present results of experimental studies which were performed on equipment (tribological circuits hydrostatic power transmission of hydraulic excavator Liebherr R 9350) at coal-mine Banovici, while laboratory tests of oil samples were performed in accredited laboratories.*

Keywords: *Tehnical diagnostics, correct state, tribology system, tehnical systems.*

SERBIATRIB '11

Serbian Tribology Society

12th International Conference on Tribology

Faculty of Mechanical Engineering in Kragujevac

Kragujevac, Serbia, 11 – 13 May 2011

PRIMJENA TRIBOLOŠKI ISPRAVNOG KONSTRUIRANJA NA RJEŠAVANJU PROBLEMA TROŠENJA (U CILJU SMANJENJA GUBITAKA I TROŠKOVA ODRŽAVANJA)

Vlatko Marušić [1], Goran Rozing[2], Luka Marušić[3], Željko Ivandić[4]

[1]Strojarski fakultet Slavonski Brod, Hrvatska, vlatko.marusic@sfsb.hr, [2] Elektrotehnički fakultet Osijek, Hrvatska, goran.rozing@etfos.hr, [3]Industrijsko-obrtnička škola Slavonski Brod, Hrvatska, calubeatz@gmail.com, [4]Strojarski fakultet Slavonski Brod, Hrvatska, zivandic@sfsb.hr

Apstrakt: *Na primjeru dijelova pužnih presa za cijeđenje ulja i turbopuhala motora SUI analizirana su nova konstrukcijska rješenja. Snimanjem stanja utvrđeno je prebrzo trošenje i oštećivanje dijelova nosive konstrukcije pužne preše, a na turbopuhalu učestala pojava zaribavanja osovine propelera. Izvršena su metalografska i mehanička ispitivanja materijala kao i dimenzionalna kontrola. Analizirani su direktni i indirektni gubici. Zaključeno je da se pomoću polukarika može postići značajno smanjenje troškova sanacije oštećenih jarmova cjedila pužne prese, a da bi kod turbopuhala ugradnja odgovarajućeg senzora temperature u značajnoj mjeri smanjila opasnost zaribavanja osovine.*

Ključne reči: *tribološki ispravno konstruiranje, pužna presa, turbopuhalo motora SUI, triboloških gubici*

1. UVOD

Tribologija „nije neka znanost radi znanosti“ [1] nego se znanstvenim pristupom bavi rješavanjem mogućnosti produljenja vijeka dijelova izloženih trošenju u cilju smanjenja troškova-gubitaka tribonaravi [2].

Na novijoj konstrukcijskoj izvedbi pužnih presa za cijeđenje ulja, kapaciteta 100 i više tona/dan uljnog sjemenja, razvijenoj tijekom protekle decenije, uočena je pojava neuobičajeno brzog oštećivanja ne samo radnih dijelova nego i nosivih. Radni dijelovi prese su noževi cjedilne korpe i segmenti pužnice. Nosivi dijelovi konstrukcije prese su vratilo, na koje se navlače segmenti i formiraju pužnu zavojnicu, te polutke cjedila na čije se jarmove slažu noževi radi formiranja cjedilne korpe. Noževi cjedilne korpe i segmenti pužnice dominantno se troše abrazijom uslijed djelovanja SiO_2 x nH_2 O sadržanog u ljusci [3].

Izvršena je međusobna usporedba rezultata ispitivanja dijelova presa, različitih kapaciteta i proizvođača. ali i usporedbom sa starijim presama manjeg kapaciteta.

Konstatirano je da na novim presama velikog kapaciteta konstrukcijska izvedba elemenata tribopara vratilo/segmenti pužnice uzrokuje njihovo (pre)brzo oštećivanje. Isto je uočeno i na kućištu vratila kao i na dosjednim površinama kontakta kućišta reduktora s jarmovima. Na temelju metalografskih pretraga je zaključeno da do otkaza dolazi uslijed gotovo istovremenog djelovanja abrazije, adhezije, umora i tribokorozije [4].

Na jednom tipu automobila poznate marke, sa dizelskim agregatom od 1,9 l raspona snage od 66 do 77 kW, koji je proizvođen od 2004. godine do 2008. godine, snimanjem stanja je utvrđeno učestalo oštećivanje osovine turbopuhala. Jedan ovlašteni distributer i ujedno serviser je u RH od 2004. do 2008. godine ukupno prodao 101 vozilo analiziranog tipa. Vozila u toj grupaciji su u to vrijeme imala jamstvo dvije godine od dana preuzimanja-kupovine. Na temelju podataka o aktiviranju jamstva i servisiranja došlo se do informacije da je do 2010. godine zamjenjeno 21 turbopuhalo. S obzirom na to da se radi o 20-tak % od ukupnog broja prodanih vozila ukazala se potreba za analizom tribosustava turbopuhala. Ispitivanjem je trebalo obuhvatiti radne parametre i dijelove turbopuhala: kućište, kompresorski impeler, turbinski rotor, zazor osovine te njenu dimenzionalnu kontrolu, analizu kemijskog sastava, metalografske pretrage i mjerenja tvrdoće. Cilj je naći uzroke oštećivanja a pomoću njih mogući pristup kako bi se smanjili troškovi ali i indirektni gubici.

Prikupljeni rezultati analiza i međusobnih usporedbi poslužili su kao osnova za pristup rješavanju problema primjenom mjere poznate kao tribološki ispravno konstruiranje [5,6]. Cilj je smanjenje ne samo direktnih nego i indirektnih troškova-gubitaka u promatranim tribosustavima.

2. SNIMANJE STANJA RADA PRESE ZA PREDPREŠANJE

Prva neuobičajena trošenja na presi uočena su već nakon tri godine od ugradnje, a pristup produljenju vijeka sastojao se, prvo u navarivanju površina jarmova cjedila [7]. Nakon 5 godina rada s navarenim jarmovima uočeno je da je došlo do njihovog ponovnog oštećivanja. Konstatirano je da je nanošenjem dodatnog materijala, tvrdoće oko 400 HB, postignuto produljenje vijeka jarmova za skoro 70 %.

Na slici 1 prikazana je pužna presa. Glavni nosivi dijelovi prese su prijenosnik snage i gibanja i kućište (reduktora), vratilo pužnice i jarmovi cjedila, a radni dijelovi su segmenti pužnice i noževi cjedilne korpe.

Pužnica je sastavljena od pužnih segmenata i konusnih prstenova koji su nanizani na vratilo. Vratilo je izrađeno u pet stupnjeva različitih promjera. Na reduktoru promjer vratila je najveći i iznosi 160 mm a najmanji promjer vratila je na izlazu iz prese i on iznosi 151,4 mm. Treba istaknuti da je vratilo (ukupne dužine 4355 mm) uležišteno samo kod reduktora tako da pužnica ustvari „pliva“ u cjedilnoj korpi okružena mlivom.

Cjedilna korpa se formira slaganjem noževa na nosače "jarmove" koji, nakon sastavljanja polutki čine zatvorenu korpu oko pužnice. Noževi su konstrukcijski izvedeni tako da nakon slaganja i formiranja plašta košare, između njih ostaje odgovarajući zazor (0,75 mm na ulazu u prešu, pa do 0,17 mm na izlazu iz prese). Kroz te zazore se cijedi ulje. Veličina zazora definira tzv. radna polja kojih u presi ovoga tipa ima ukupno 7. Pomoću konusnih segmenata postiže se da pritisak raste od ulaza prema izlazu iz prese, a zbog stupnjevite izvedbe pužnice pritisak lokalno doseže vrijednosti 450 do 500 bara.

Utvrđeno je da je do prestanka funkcionalnog rada prese došlo zbog:
- oštećivanja kućišta reduktora,
- oštećivanja dosjednih površina cjedila, i
- oštećivanja jarmova.

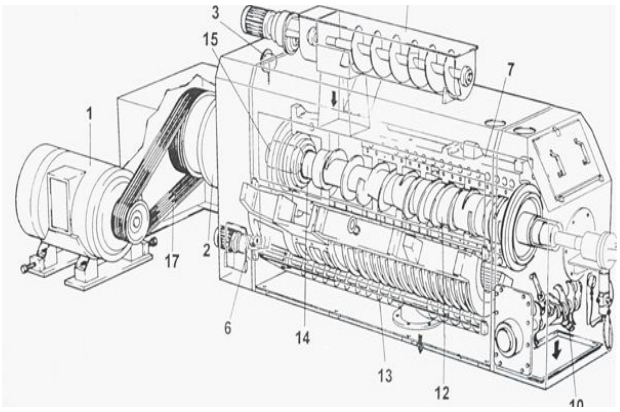

Slika 1. Prikaz dijelova prese tip EP 16

1-elektromotor, 2-reduktor, 3-termometar, 4-dozirni puž, 6,7-jarmovi, 10-lomač pogače, 12-pužnica, 13-sabirni puž, 14-brtveni prsten, 15-vratilo, 17-klinasto remenje

2.1 Oštećivanje kućišta reduktora

Na slici 2 prikazan je detalj najoštećenijih površina kućišta reduktora. Kontrolom pomoću prijenosnog spektrometarskog kemijskog analizatora utvrđeno je da je kućište izrađeno od čeličnog Cr-Mo lijeva, a kontrolom prijenosnim (umjerenim) tvrdomjerom konstatirano je da se tvrdoća njegove površine kreće između 210 i 235 HB.

Detaljnom kontrolom površina konstatirano je da je oštećivanje izazvano djelovanjem agresivnog medija (kisele supare) a manifestiralo se pojavom tribokorozije na zaptivnim i dosjednim dijelovima reduktora koje su u kontaktu s dosjednim površinama cjedila.

Slika 2. Trobokorozijom oštećene površine kućišta reduktora

Oštećivanje kućišta reduktora je za posljedicu imalo nedozvoljeno ekscentrično "njihanje" cjedila.

2.2 Oštećivanje cjedila pužne prese

Oštećivanje cjedila drugi je razlog prestanka funkcionalnog rada prese. Na dijelu cjedila koji se nalazi u dosjedu s kućištem reduktora uočeni su tragovi koji ukazuju na oštećivanje ulijed ekscentričnog gibanja u kontaktu površina na zaporu kućište/cjedilo, ali i tragovi koji se mogu pripisati tribokoroziji, slika 3.

Slika 3. Oštećenje dosjedne površine na ulazu u cjedilo

Oslonci noževa (jarmovi) trošeni su erozijom abrazivnim česticama mliva koje s uljem intenzivno prolazile kroz zazore između djelomično istrošenih noževa. Vizualnim pregledom jarmova uočeno je da ta oštećenja imaju neujednačene vrijednosti, ne samo po radnim poljima nego i po obujmu jarmova, slika 4. U uvjetima ovako oštećenih jarmova nemoguće je izvršiti geometrijski pravilno slaganje nove garniture noževa na mjesto istrošenih [7]. Materijal cjedila je Cr-Mo čelični lijev, sličnog kemijskog sastava kao i kućište reduktora. Tvrdoća dosjednih površina cjedila i osnovnog materijala jarmova kreće se u rasponu od 170 do 225 HB. Izmjerene vrijednosti tvrdoća pri sanaciji navarenog (površinskog) sloja na jarmovima iznosile su od 380 d0 430 HB.

Slika 4. Karakteristični tragovi trošenja površina jarmova s navarenim slojem

3. PRISTUP RJEŠAVANJU PROBLEMA TROŠENJA PUŽNIH PRESA

Težište pristupa stavljeno na smanjenje indirektnih gubitaka. Razlog se nalazi u činjenici da zastoj zbog potrebe zamjene oštećenih dijelova traje od pet do šest tjedana, a rad s djelomično istrošenim radnim površinama dovodi do smanjenog iskorištenja instaliranog kapaciteta prese. Na izbor toga pristupa utjecala je relativna usporedba visina direktnih triboloških gubitaka s indirektnim u koje ulaze dužina trajanja zastoja, smanjeno iskorištenje instaliranog kapaciteta i smanjena efikasnost cijeđenja ulja.

3.1 Produljenje vijeka dosjednih površina reduktora

S obzirom na to da je dominantni mehanizam oštećivanja dosjednih i zaptivnih površina reduktora tribokorozija, kao varijantni (eksperimentalni) materijal odabran je Cr Ni nehrđajući kiselootporni čelik.

Nakon utvrđivanja razlike između istrošenih i nazivnih mjera, odabrana je tehnologija (pred)obrade istrošenih i izrade nadomjesnih površina kućišta. Iz varijantnog materijala izrađeni su dijelovi u obliku poluprstenova. Predobrađene dosjedne površine kućišta nadomještene su poluprstenovima izrađenim prema potrebnim konstrukcijskim dimenzijama. Zbog opasnosti prodiranja agresivnog medija („kisele supare“ s visokim udjelom fosfatida) i njegovog korozijskog djelovanja te razvijanja korozije u zaporu, na vanjskoj strani poluprstenova izrađeni su utori u koje su postavljene silikonske brtve. Na slici 5 prikazano je sanirano kućište reduktora (montirano na presu).

Slika 5. Prikaz saniranog i ugrađenog reduktora

3.2 Produljenje vijeka dosjednih površina cjedila

Utvrđivanju nazivnih mjera oštećenih površina nosača noževa cjedilne korpe, tehnologiji obrade i izrade nadomjesnih istrošenih pozicija pristupilo se na isti način kao i u slučaju oštećenog kućišta reduktora. Dosjedne površine koje su u kontaktu s kućištem reduktora nadomještene su poluprstenovima obrađenim na potrebnu konstrukcijsku mjeru, a na pripremljeni osnovni materijal cjedila (slika 6) dotegnute su odgovarajućom steznom napravom.

Slika 6. Poluprstenovi u fazi montaže na dosjedne površine ulaznog dijela cjedila

3.3 Produljenje vijeka jarmova cjedila

S obzirom na to da je dominantni mehanizam oštećivanja površina jarmova erozija abrazivnim česticama kao osnovni materijal nadomjesnih eksperimentalnih materijala odabran je Cr-Mo čelik za poboljšavanje. Iz njega su izrađene polukarike, zakaljene i popuštene na oko 400 HB. Polukarike su konstrukcijski izrađene tako da je njihova zamjena jednostavna. Prije ugradnje izvršena je dimenzionalna kontrola kako bi se tijekom upotrebe u presama moglo utvrditi kolika je otpornost trošenju. Izgled polukarika prikazan je na slici 7.

Slika 7. Polukarike izrađene od eksperimentalnog materijala

4. SNIMANJE STANJA TURBOPUHALA

4.1 Osnovne konstrukcijske karakteristike

Turbopuhalo se sastoji od kompresorskog i ispušnog dijela koji su međusobno povezani istom osovinom. Danas se u pravilu koriste jednostupanjski radijalni kompresori. Za male promjere i niske protoke radijalno turbopuhalo ima veću efikasnost, međutim problemi proizvodnje ograničavaju njezinu primjenu. Radijalna turbopuhala treba lijevanjem izraditi veoma točno iz materijala otpornog na visoke temperature, što zahtjeva skupe kalupe. Na slici 8 prikazani su glavni dijelovi turbopuhala.

Impelari se ljevaju tehnikom vakumskog ljeva te se spajaju sa osovinom tupim zavarivanjem. Budući da je u radu temperatura lopatica veća od temperature kola, mogu se koristiti različiti materijali, primjerice, disk se izrađuje od čelične legure s 13% Cr, ili CrNi čelik 1613, a lopatice se izrađuju iz In-713C. Izbor materijala ovisi o očekivanoj ispušnoj temperaturi motora. Temperatura ispušnih plinova se kod dizelskih motora kreće do max. 450 ÷ 500°C, dok se temperatura ispušnih plinova kod otto motora penje i do 1000°C. Za impelere kompresora mogu se koristiti sljedeći materijali: silumin gamma (lijevano ili kovano), aluforit 47 (lijevano), perunal B (kovano), steel G-x22 CrMoV 121 (lijevano), steel DMU83 (kovano - omekšano popuštanjem), titan 1,33 (kovano) i titan alloy 6AL4V [8,9].

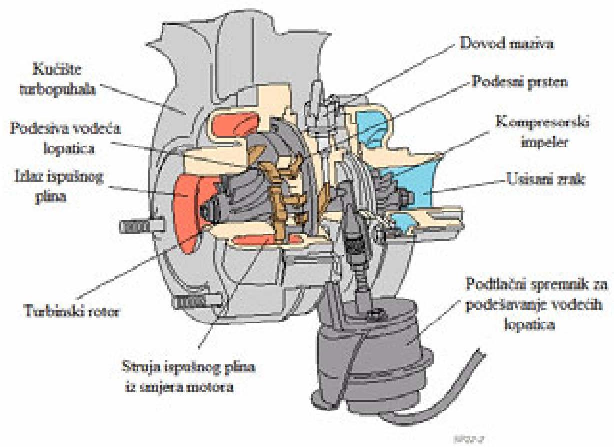

Slika 8. Osnovni dijelovi turbopuhala

Kod turbopuhala se koriste vanjski i unutarnji ležaji. Ako se radi o vanjskim ležajima oni su u paru, a ako se radi o unutarnjim onda je obično samo jedan ležaj. Vanjski ležaji su pretežno kuglični dok su unutarnji ležaji klizni.

Kod manjih turbopuhala se radi o unutarnjim kliznim ležajima koji su spojeni sa uljnim krugom motora. Karakteristično je za njih da imaju smanjeno trošenje kod pravilno konstruiranih ležaja s punim hidromehaničkim podmazivanjem na prevladavajućim niskim naprezanjima i visokim brzinama. Imaju duži vijek trajanja, manje su osjetljivi na udarce i vibracije. Nedostaci su im potreba za većim protokom i višim tlakom ulja koje treba da odvede toplinu proizvedenu trenjem. Potrebno je vršiti predpodmazivanje prije starta motora ali i kontinuirano podmazivanje nakon što je motor zaustavljen pri visokom opterećenju. Razlog se nalazi u tome što toplina koja ulazi u ležaj kroz osovinu pregrijava ulje a može prouzročiti „koksiranje“ ulja.

4.2 Ispitivanje oštećenja na odabranim uzorcima

Od 21 oštećenog turbopuhala slučajnim odabirom za potrebe ispitivanja uzeto je 5. Na njima je nakon rastavljanje obavljen detaljan pregled. Uočeno je sljedeće:
- nema vidljivih oštećenja na kućištu turbopuhala,
- nema vidljivih oštećenja na komprsorskom impeleru,
- nema vidljivih oštećenja na turbinskom rotoru,
- zazor osovine nije povećan, i
- daljnom demontažom ustanovljeno da je osovina promjenila boju, boja osovine je od tamno crvene do ljubičaste, slika 9.

Slika 9. Karakteristična promjene boje osovine turbopuhala

Po promjeni boje je jasno da je došlo do pregrijavanja materijala, uzrok pregrijavanja je nedovoljno hlađaenje, osovina se hladi uljem. Uzrok oštećenja je loše podmazivanje ili prekid podmazivanja. Prekid podmazivanja uzrokuje povećavanje temperature u kliznom ležaju te veće trošenje materijala, kao posljedica nastaje debalans rotirajućih tijela: oštećenja rotora i impelera.

Kemijska analiza matrijala spektrometrom je pokazala da je osovina turbopuhala izrađena od matrijala CrMo čelika za poboljšavanje.

Metalografske pretrage i mjerenja vrdoće HO 0,1 obavljene su na tri presjeka, slika 10. Rezultati metalografskih ispitivanja na osovini turbopuhala su pokazali da je u zoni utjecaja topline došlo do promjene strukture materijala. Dodatna mjerenja tvrdoće u zoni utjecaja povišene temperature su pokazateli da je došlo do značajnijih lokalnih promjena tvrdoće površinskog sloja.

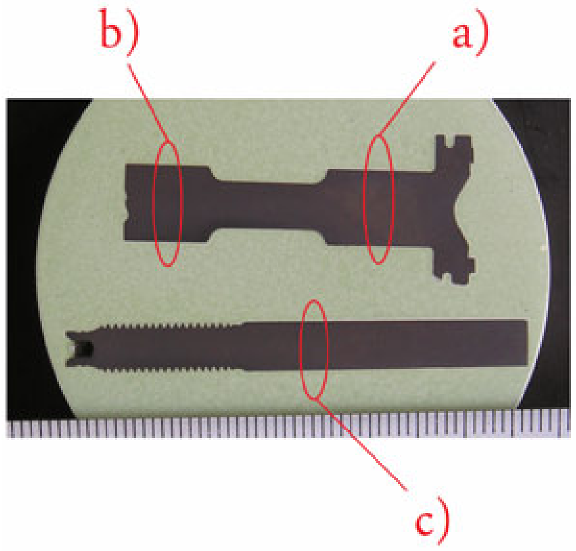

Slika 10. Pozicije snimanja strukture i mjerenja tvrdoće HV0,1

Na dijelovima presjeka „b“ i „c“ tvrdoća se kreće između 330 i 350 HV 0,1 dok se na presjeku „a“ tvrdoća penje na 420 do 430 HV 0,1 (to je dio osovine na kojemu se uočava promjena boje u ljubičastu).

Ispitivanje radnh uvjeta temperature pri normalnom opterećenju je pokazalo da temperatura ne prelazi ekstremne granice. Ispitivanja su obavljena na radnom stolu, slika 11, pri opterećenju turbopuhala: 3440 o/min (slika12).

Slika 11. Ispitivanje na radnom stolu

Temperatura zagrijanosti rashladne tekućine u motoru dosegla je 90 °C, a temperatura na kućištu kliznog ležaja iznosila je 219,2 °C. Iz sigurnosnih razloga, broj okretaja motora nije više podizan, ali iz izvedenog ispitivanja je vidljivo da se temperatura rapidno povećava ovisno o broju okretaja. Maksimalan broj okretaja iznosi 6000 o/min.

Mazivo (koje preporuča proizvođač za podmazivanje kliznog ležaja se koristi i za podmazivanje motora.

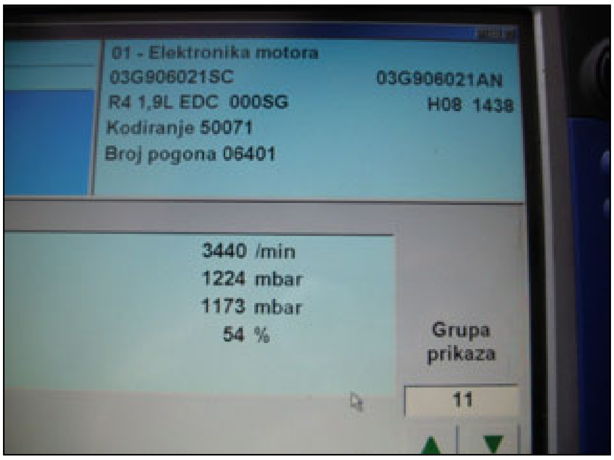

Slika 12. Tlak i temperatura pri 3440 o/min

Kritična temperatura na kojoj se ulje počinje raspadati na lake konponente i koks je vrlo niska, tek 360 °C što ne zadovoljava. Naime, rezultati ispitivanja na probnom stolu, ukazuju na to da u ekstremnim uvjetima temperatura turbopuhala može prekoračiti dopuštenu temperaturu.

4.3 Analiza mogućih konstrukcijskih rješenja

Da bi se izbjegao utjecaj promjene temperature na turbopuhalu, napravljena je analiza mogućih konstrukcijskih rješenja:

1. Senzor za temperaturu turbo puhala koji ne bi dozvolio gašenje pogonskog agregata dok se ne snizi temperature turbopuhala na prihvatljivu vrijednost.
2. Zasebni sustav podmazivanja kliznog ležaja koji nije vezan na sistem podmazivanja pogonskog agregata, sa prilagođenim sredstvom podmazivanja te da ima zasebno hlađenje i pogonsku pumpu koja nastavlja rad nakon zaustavljanja pogonskog agregata.
3. Hlađenje kućišta turbopuhala tekućinom s kojom se hladi i pogonski agregat. U ovom rješenju je problem taj što je temperatura rashladne tekućine morora 90 °C a temperatura kućišta turbopuhala puno veća pa je potrebna prilagodba sistama hlađenja s većim hladnjacima i većom količinom rashladnog sredstva.

5. ZAKLJUČAK

Direktni troškovi u promatranom slučaju oštećivanja pužne prese su troškovi demontaže i rastavljanja oštećenih dijelova, transporta i usluge strojne obrade za pripremu istrošenih dijelova, kao i za izradu novih poluprstenova i polukarika te steznih naprava. Zastoj u radu prese u trajanju od pet do šest tjedana, zbog potrebe zamjene i/ili sanacije oštećenih površina, doprinosi veoma visokom iznosu indirektnih triboloških gubitaka. Naročito je to izraženo ako neplanirano dugi zastoji nastupe za vrijeme kampanje.

S obzirom na to da se izborom materijala i zaštitnog sloja radnih dijelova prese može direktno utjecati na njihov eksploatacijski vijek, težište pristupa stavljeno je na tribološki ispravno konstruiranje. U ovom slučaju odabran je pristup kojim se odgovarajućim konstrukcijskim rješenjem treba omogućiti ne samo veća otpornost dominantnom mehanizmu trošenja nego se olakšava i zamjena istrošenih dijelova. Prethodna laboratorijska ispitivanja uzoraka-dijelova i njihova usporedba s rezultatima koji će se dobiti njihovim praćenjem u realnim uvjetima trebaju poslužiti kao pokazatelj mogućnosti i opravdanosti ovakvog tribološkog pristupa.

Rezultati ispitivanja uzoraka turbopuhala ali i snimanja stanja ukazuju na to da kod vožnje na dužim relacijama i pri većim brzinama dolazi do ekstemnog zagrijavanja turbopuhala a da uslijed prekida podmazivanja kod gašenja agregata dolazi do oštećenja kliznih površina ležajeva. S vremenom može doći do pojave debalansa rotirajućih dijelova, a kao posljedica tog debalansa I do oštećenja turbinskog rotora i kompresorskog impelera.

Da bi se izbjegao utjecaj promjene temperature na turbopuhalu, napravljena je analiza mogućih konstrukcijskih rješenja.

Kao najpovoljnije u ovom trenutku ističe se rješenje sa senzorom koji ne bi dopustio gašenje pogonskog agregata sve dok se ne snizi temperature turbopuhala na prihvatljivu vrijednost.

LITERATURA

[1] R Zgaga: Tribologija u cementnoj i srodnim industrijama, Zbornik savjetovanja o tribološkoj problematici u cementnoj i srodnim industrijama, Split, 1987, 1-5

[2] V. Marušić, D. Štrucelj, Ž. Ivandić: Povećanje učinkovitosti prerade sjemena suncokreta primjenom novih postupaka zaštite za smanjenje intenziteta trošenja dijelova pužnih preša, 53, Kemija u industriji, 9 (2004), 393-400

[3] V. Ivušić, V. Marušić, K. Grilec: Abrasion resistance of surface layers, VTT Symposium 180 & COST 516 Tribology Symposium: proceedings, Ronkainen, H., Holmberg, K., (ur.). VTT Technical Researche Centre of Finland, 1998. 201-210

[4] V. Marušić, D. Krumes, S. Marušić: Sva četiri osnovna mehanizma trošenja u jednom tribosustavu, Zbornik radova Međunarodnog savjetovanja MATRIB 2008, Hrvatsko društvo za materijale i tribologiju, Zagreb, 2008. 191-197

[5] B. Nedić: Merna oprema za tribološka ispitivanja, Monografija Mašinskog fakulteta Kragujevac 2007

[6] V. Marušić, F. Rozing, D. Krumes, S. Marušić: Problem održavanja pužnih preša u uvjetima trošenja uzrokovanog konstrukcijskim rješenjem,

Zbornik 14. Međunarodnog savjetovanja Održavanje 2008, Šibenik, 2008, 169-174

[7] V. Marušić, R. Popović, S. Marušić: Mogućnost sanacije jarmova cjedila pužne preše u cilju povećanja efikasnosti rada prešaone, 37, Uljarstvo, 1-2 (2006), 29-36

[8] M. Grljušić, Mirko: Motori s unutrašnjim izgaranjem, Fakultet elektrotehnike, strojarstva i brodogradnje sveučilišta u Splitu, Split 2000.. str. 301-346

[9] SP_209_19litarski_motor_sa_sustavom_ubrizgavanja_p umpamlaznica_2, URL: https://www.group-training-online.com, 04.03.10. PDF, str. 14,15,16,17,18

APPLICATION OF TRIBOLOGICALLY ACCURATE CONSTRUCTION ON WEAR PROBLEMS SOLUTION (TOWARDS LOSSES AND MAINTENANCE COSTS DECREASE)

Abstract: *The possibility of applaying tribological corrextly design of the example pieces of worm process for squeezing oil and turbochargers internal combustion engines were analyzed. Recording status:to fast wear and damage to parts of the bearing structure screw presses,and the turbocharger frequent seizure propeller shaft. Metallographic and mehanical testing of materials and dimenzional controls were carried out. The direct and indirect lossers were analyzed.We came to the conclusion when the construction and installation of a removable semi rings can achive a significant reduction in a rehabilitation costs of damage yokes strainers. The cheapest solution were to install appropriate temperature sensor by turbochargers,which would not be allowed off the drive unit until the temperature lowers to an acceptable vaule of turbochargers.*

Keywords: *tribological correctly design, cavity press, turbochargers, internal combustion engines, tribological losses*

Serbian Tribology Society

SERBIATRIB '11

12th International Conference on Tribology

Faculty of Mechanical Engineering in Kragujevac

Kragujevac, Serbia, 11 – 13 May 2011

TEHNOLOŠKO NASLEĐE POVRŠINA TRIBO-MEHANIČKIH SISTEMA REGENERISANIH NAVARIVANJEM

Svetislav Lj. MARKOVIĆ[1], Tatjana LAZOVIĆ[2], Aleksandar MARINKOVIĆ[3], Slobodan TANASIJEVIĆ[4], Danica JOSIFOVIĆ[5]

[1]Visoka tehnička škola Čačak, svetom@open.telekom.rs
[2]Mašinski fakultet Beograd, tlazovic@mas.bg.ac.rs
[3]Mašinski fakultet Beograd, amarinkovic@mas.bg.ac.rs
[4]Mašinski fakultet Kragujevac, irmes2004@kg.ac.rs
[5]Mašinski fakultet Kragujevac, danaj@kg.ac.rs

Apstrakt: *U istraživanjima tribologa i mašinaca uočava se sve veće interesovanje za ispitivanje tehnološkog nasleđa i njegove veze sa eksploatacionim svojstvima mašinskih elemenata i sistema. Različite studije pokazuju da je životni vek mašinskog sistema određen još u fazi konstruisanja. Međutim, nema sumnje da postoji ogroman uticaj tehnologije i parametara obrade na tribološka svojstva obrađenih površina elemenata tribo-mehaničkih sistema. Pojava takozvanog tehnološkog nasleđivanja nastalog pri operacijama obrade rezanjem ili deformisanjem pokazuje uticaj na tribološki relevantne parametre obrađenih površina. To su zaključci koji se nameću kada je u pitanju izrada novih mašinskih elemenata. Ali, tehnološko nasleđe ima znatno veći uticaj na tribološke karakteristike i vek trajanja regenerisanih površina nego što je to slučaj kod nove izrade. Osnovni cilj modelskih ispitivanja prikazanih u ovom radu je komparacija triboloških karakteristika prevlaka nanetih pri regeneraciji navarivanjem i osnovnog materijala, koje su dobijene ispitivanjima pri istim radnim uslovima, što približnijim eksploatacionim uslovima rada zupčanika.*

Ključne reči: *regeneracija, navarivanje, tribo-mehanički sistemi, tehnološko nasleđe, mikrostruktura, tribološka ispitivanja.*

1. UVOD

Fizičko-hemijsko-metalurške karakteristike kontaktnih slojeva u tribo-mehaničkim sistemima zavise od uslova pod kojima su nastale radne (kontaktne) površine. To je razlog što se sve više razmatra uticaj postupaka obrade i režima rezanja, korišćenih pri formiranju kontaktnih površina, na razvoj procesa habanja elemenata u dodiru. Tako su razvijene takozvane teorije tehnološkog i eksploatacionog nasleđa, kojima su i ovi problemi obuhvaćeni.

Većina pojava nastalih u procesu izrade mašinskih elemenata značajno utiče na proces gubitka radne sposobnosti mašinskih sistema u eksploatacionim uslovima. Otuda je za obezbeđenje neophodnog nivoa kvaliteta i pouzdanosti rada mašina potrebno analizirati sve pojave koje prate proces izrade i eksploatacije mašinskih sistema i njima pripadajućih delova. Tehnološko nasleđe se izražava međusobnom zavisnošću geometrijskih i fizičko-mehaničkih parametara proizvoda formiranih kroz prethodne i završne tehnološke operacije. Pojava eksploatacionog nasleđa se odražava vezom parametara procesa gubitka radne sposobnosti proizvoda, vrednosti radnog resursa i predistorijom opterećenja. Uslovi i režim rada mašina određuju, uglavnom, oblik habanja kontaktnih površina, veličinu i oblik zazora sklopova i slično. To se u određenom odnosu odražava na krutost sistema i veličinu specifičnih pritisaka između kontaktnih površina. Sve to u velikoj meri utiče na intenzitet habanja u narednom periodu rada i predstavlja pojavu eksploatacionog nasleđa. Istovremeno, intenzitet habanja radnih površina zavisi i od makro i mikrogeometrije kontaktnih površina, mikrotvrdoće, strukture i naponskog stanja površinskih slojeva, formiranih u procesu izrade. Prema tome, povezanost tehnološkog i eksploatacionog nasleđa je potpuna, a proučavanje ove zavisnosti omogućuje ne samo uzimanje u obzir datih pojava u procesu konstruisanja, već i upravljanje procesom gubitka radne sposobnosti mašinskih elemenata.

2. EKSPERIMENTALNO ODREĐIVANJE TRIBOLOŠKIH KARAKTERISTIKA POVRŠINA REGENERISANIH NAVARIVANJEM

Tribološke karakteristike (pre svega koeficijenti trenja) navara dobijenih odabranim postupcima navarivanja određivne su na tribometru. Ispitivani su modeli bloka navarenog odabranim dodatnim materijalom spregnuti sa diskom od čelika Č4321, cementiranim i kaljenim.

Probni uzorci za ispitivanje na tribometru po metodi „block on disc" izrađeni su od čelika za cementaciju oznake Č4321, čiji hemijski sastav je dat u tabeli 1. Uzorci su izrađivani tako da simuliraju uslove rada spregnutih zubaca konkretnih zupčanika u uslovima kakvi su u uređaju za eksploataciona ispitivanja.

Tabela 1. Hemijski sastav čelika za izradu uzoraka

Legirajući elementi (%)					
C	Si	Mn	P_{max}	S_{max}	Cr
0,17-0,22	0,15-0,40	1,1-1,4	0,035	0,035	1,0-1,3

Diskovi dimenzija $\phi 60x10$ mm izrađeni su od navedenog čelika (slika 1). Posle mašinske obrade na strugu, oni su gasno cementirani, kaljeni i otpuštani, a zatim brušeni. Pošto su svi diskovi od istog materijala (iz jedne šarže), obrađivani podjednakim režimima mašinske obrade i zajedno cementirani i termički tretirani, imaju i gotovo identičnu površinsku tvrdoću. Njihova tvrdoća kretala se u granicama 56÷56,2 HRC.

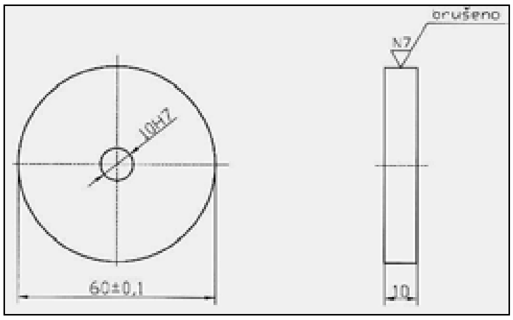

Slika 1. Konstrukcija diska za tribološka ispitivanja

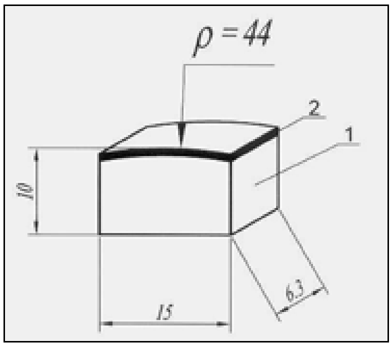

Slika 2. Uzorci ispitivani na tribometru (1 – osnovni materijal, 2 – navareni sloj; ρ - radijus krivine zupca)

Radi tačnijeg određivanja relevantnih pokazatelja tehnološkog nasleđa regenerisanih površina navarivan je veći broj uzoraka (blokova) izrađenih od navedenog materijala, pri čemu su varirane vrste dodatnog materijala, režimi navarivanja i naknadne termičke obrade. Ukupno je pripremljeno devet vrsta blokova za ispitivanje, koji se prema načinu izrade mogu podeliti u tri grupe:

- U prvoj grupi su blokovi navarivani „tvrdim" dodatnim materijalima. Urađeno je pet različitih vrsta uzoraka, a tehnologija pripreme prikazana je u tabeli 2. Temperatura predgrevanja bila je 230^{0}C, a elektrode su sušene četiri časa na temperaturi od 350^{0}C. Posle navarivanja uzorci su vraćani u peć, gde su zagrevani na temperaturu predgrevanja i hlađeni u njoj do sobne temperature.

Tabela 2. Tehnologija pripreme uzoraka „tvrdim" navarivanjem

Redni broj uzorka	Osnovni materijal	Termička obrada pre navarivanja	Navarivanje		Termička obrada posle navarivanja
			Dodatni materijal	Postupak navari-vanja po AWS	
1	Č4321	Predgrevanje	Inox 18/8/6 + EDur 600	SMAW (111)	Niskotemperaturno otpuštanje
2		Predgrevanje	Castolin 2	SMAW (111)	Niskotemperaturno otpuštanje
3		Predgrevanje	DUR 600-IG	GTAW (TIG) (111)	Niskotemperaturno otpuštanje
4		Predgrevanje	UTP 670	SMAW (111)	Niskotemperaturno otpuštanje
5		Predgrevanje	Tooldur	SMAW (111)	Niskotemperaturno otpuštanje

- Drugu grupu čine blokovi navareni „mekim“ dodatnim materijalom, koji su, potom, cementirani, kaljeni i otpuštani. Takvih uzoraka je urađeno tri različite vrste, navarivani tehnologijom koja je prikazana u tabeli 3. Postupci predgrevanja i navarivanja su identični. Razlika je u tome što su navareni blokovi meko žareni, gasno cementirani, kaljeni i otpuštani.

Tabela 3. Tehnologija pripreme uzoraka „mekim“ navarivanjem

Redni broj uzorka	Osnovni materijal	Termička obrada pre navarivanja	Navarivanje		Termička obrada posle navarivanja
			Elektroda	Postupak navari-vanja po AWS	
6	Č4321	Predgrevanje	EVBCrMo	SMAW (111)	Meko žarenje + cementacija + kaljenje + otpuštanje
7		Predgrevanje	EVB2CrMo	SMAW (111)	Meko žarenje + cementacija + kaljenje + otpuštanje
8		Predgrevanje	Phönix 120K/E	SMAW (111)	Meko žarenje + cementacija + kaljenje + otpuštanje

- U trećoj gupi su blokovi koji nisu navarivani, već su gasno cementirani, kaljeni i nisko otpuštani. Ovakvi blokovi su simulirali rad novoizrađenih (neregenerisanih) zubaca zupčanika.

Svi dodatni materijali su nanošeni u smeru upravnom na pravac klizanja u jednom sloju. Izuzetak je navarivanje uzoraka označenih rednim brojem 1, kod kojih je prvo navarivan međusloj elektrodom Inox 18/8/6 pa, nakon otklanjanja troske i čišćenja, elektrodom EDur 600.

Posle navarivanja i termičke obrade, navarene površine blokova su brušene na brusilici za obimno brušenje. Radijus zaobljenja bloka (slika 2) odgovara računskoj vrednosti srednjeg poluprečnika zubaca zupčanika koji se regenerišu:

$$\rho = R_1 \cdot \sin\alpha = 129 \cdot \sin 20^0 \cong 44 \text{ mm}$$

Oznake korišćenih dodatnih materijala, njihove dimenzije (prečnik, D) i jačina struje (J) navarivanja dati su u tabeli 4.

Tabela 4. Karakteristike korišćenih dodatnih materijala

R. br.	Oznaka po		Oznaka DM po DIN 8555 (po AWS-u)	Proizvođač	Oznaka postupka po	D (mm)	J (A)
	DIN	AWS					
1.	E-6-UM-55G	/	EDur 600	Jesenice (Slovenija)	SMAW (111)	2,5	70
2.	/	/	Castolin 2	Castoline Eutectic (Švajcarska)	SMAW (111)	3,25	92
3.	MSG-6-GZ-60	/	DUR 600-IG	BÖHLER (Nemačka)	GTAW (TIG) (141)	1,2	76
4.	E-6-60-UM	/	UTP 670	UTP (Nemačka)	SMAW (111)	3,25	90
5.	E-4-UM-60-65-S	EFe5-B	Tooldur	Jesenice (Slovenija)	SMAW (111)	2,5	80
6.	ECrMo1B26	E8018-B2	EVBCrMo	Jesenice (Slovenija)	SMAW (111)	2,5	75
7.	ECrMo2B26	E9018-B3	EVB2CrMo	Jesenice (Slovenija)	SMAW (111)	2,5	75
8.	/	/	Phönix 120 K/E 425 B/E7018-1	Tüssen (Nemačka)	SMAW (111)	2,5	72
9.	E18.8.Mn6B20+	E307-15	Inox 18/8/6	Jesenice (Slovenija)	SMAW (111)	2,5	70

3. ISPITIVANJA MIKROSTRUKTURE

Metalografska ispitivanja su sprovedena na kvantitativnom optičkom metalografskom mikroskopu tipa „Polyvar-Met“ („Reichert-Jung“) pri povećanjima od 20 do 2000 puta. Mikrostrukturna analiza slike izvođena je na uređaju „Leica Q500MC“, dok su slikanja i merenja izvršena u kompjuterskom programu „Qwin“.

Mikrostruktura površinskog i potpovršinskog sloja (cementiranog sloja i jezgra) novoizrađenog uzorka prikazana je na slici 3. Osnovni mikrokonstituent cementiranog sloja je otpušteni martenzit (tamna polja sa slici 3). U mikrostrukturi se zapaža manji udeo zaostalog austenita. U površinskoj zoni, do dubine 0,2-0,3 mm, prisutni su pojedinačni krupniji karbidi legirajućih elemenata. Na osnovu martenzitnih iglica zaključuje se da materijal ima sitnozrnastu strukturu, što ukazuje da je proces termičke obrade pravilno izveden.

Mikrostruktura jezgra cementiranog uzorka sa krupnijim iglicama prelaznih struktura (bejnit) i poljima ferita prikazana je na slici 4.

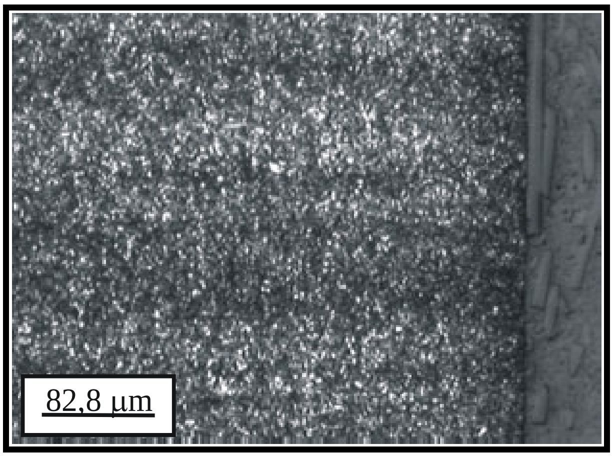

Slika 3. Mikrostruktura cementiranog sloja

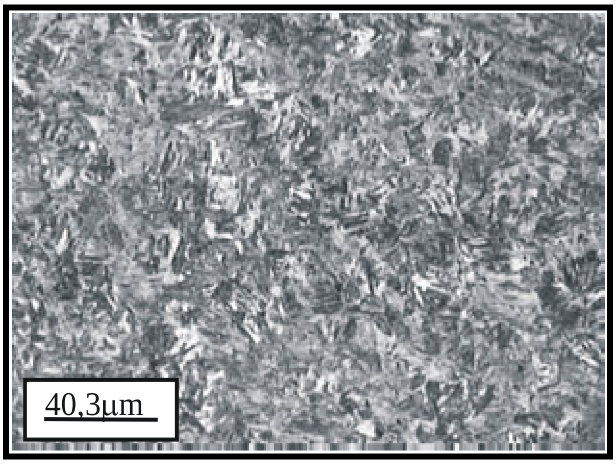

Slika 4. Struktura jezgra cementiranog uzorka

Mikrostruktura navara sa dva različita dodatna materijala (Inox 18/8/6 i Edur 600) data je na slici 5. Na levoj strani slike zapaža se stubičasta dendritna struktura navara sa „tvrdom“ elektrodom EDur 600. U centralnom delu slike sa slabije izraženom dendritnom strukturom nalazi se navar sa elektrodom Inox 18/8/6. Linija spoja navara sa DM Inox 18/8/6 i ZUT-a (osnovnog materijala) je relativno jasno izražena i prilično neravna.

Prema slici 6, navar sa dodatnim materijalom Castolin 2 odlikuje se izrazitom dendritnom strukturom. Prosečna širina dendritnih iglica je 10-15 µm, što je veoma povoljno. Međutim, dendriti se odlikuju dosta izraženom nehomogenošću, što se pokazuje različitom nagriženošću površine istih. U navaru sa DM Castolin 2 prisutna je karbidna faza (primarni karbidi) izlučena pretežno po granicama dendrita. Rast dendrita je uglavnom upravan na površinu uzorka.

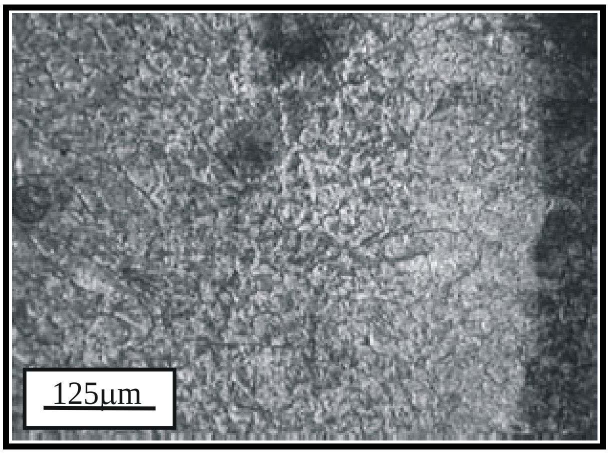

Slika 5. Mikrostruktura ZUT i navara sa dva DM Inox 18/8/6 + EDur 600 (EDur 600 – levo; Inox 18/8/6 – u sredini; ZUT – desno)

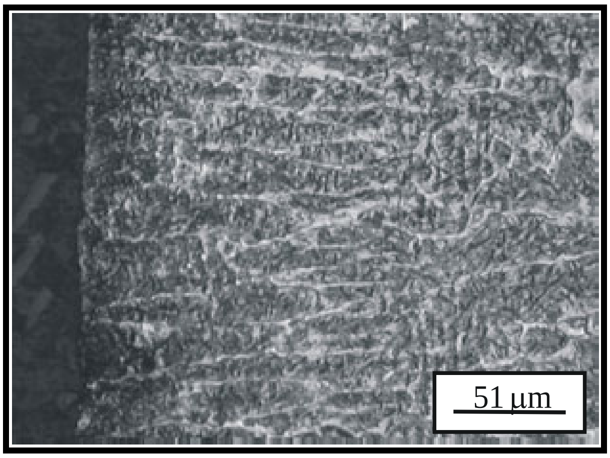

Slika 6. Mikrostruktura navara sa DM Castolin 2

Na slici 7 prikazana je izdužena dendritna struktura navara nanetog postupkom TIG navarivanja u zaštiti argona sa dodatnim materijalom DUR 600-IG do same površine reparaturno navarenog uzorka. Uočava se da su u navarenom sloju prisutni dendriti, čiji je pravac rasta upravan na radnu površinu. Na ivicama dendrita (tamne linije) uglavnom se izlučuju nečistoće, karbidna faza i slično.

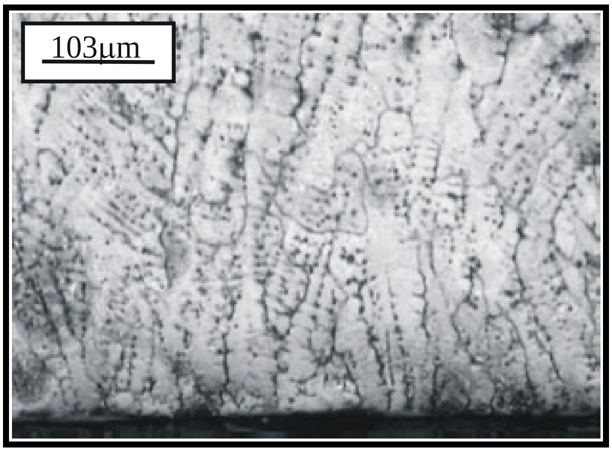

Slika 7. Izdužena dendritna struktura navara dobijenog TIG postupkom sa DM DUR 600-IG

Uzorak navaren dodatnim materijalom UTP 670 ima srednje do krupnu strukturu navara (sa širinom pojedinih dendritnih stubića od 30 do 80 μm). U strukturi je prisutan visok udeo karbidne faze (svetla polja na slici 8), koja je izlučena po granicama zrna, ali najvećim delom u samim kristalnim zrnima.

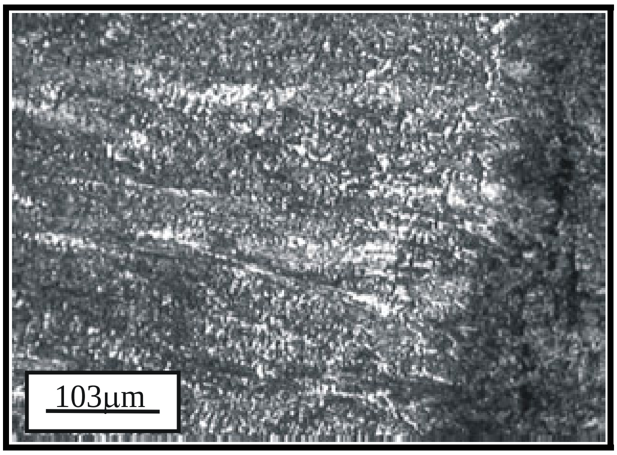

Slika 8. Mikrostruktura navara sa DM UTP 670 (svetla zona) i ZUT-a (tamna zona)

Navareni sloj sa dodatnim materijalom Tooldur odlikuje se izrazito dendritnom strukturom. Poredeći mikrostrukture svih navarenih slojeva dobijenih prilikom izrade eksperimentalnog rada može se zaključiti da je kod navara sa ovim DM prisutan najveći udeo karbidne faze (slika 9). Kod navara sa DM Tooldur najveći udeo karbidne faze prisutan je u navaru neposredno do ZUT-a, gde je ona izlučena po granicama zrna i u samom kristalnom zrnu. Manji udeo karbidne faze je prisutan u drugim zonama navara i pri površini, gde je ova faza uglavnom izlučena po granicama dendrita i kristalnih zrna.

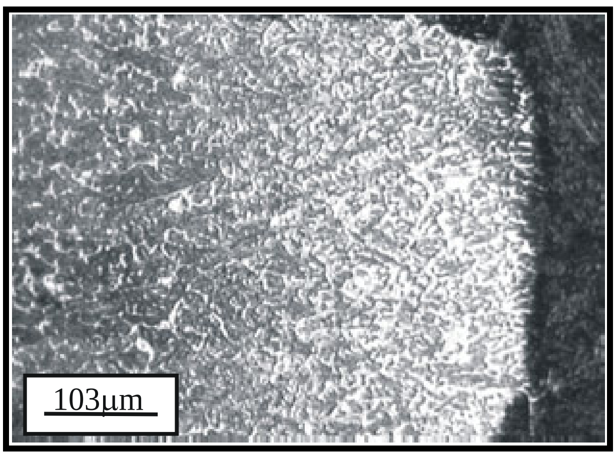

Slika 9. Mikrostruktura navara sa DM Tooldur (svetla zona) i ZUT-a (tamna zona)

Na slici 10 prikazana je mikrostruktura u oblasti prelaza između cementiranog sloja u navaru sa dodatnim materijalom EVBCrMo (sitnozrnasta struktura) i prelazne zone cementacije, koja se takođe nalazi u navaru. Osnovni mikrokonstituent u strukturi je otpušteni martenzit sa manjim udelom karbidne faze i zaostalog austenita. Veličina martenzitnih iglica je relativno sitnozrnasta, što ukazuje da su proces mekog žarenja posle navarivanja i naknadni procesi hemijsko-termičke i termičke obrade pravilno izvršeni.

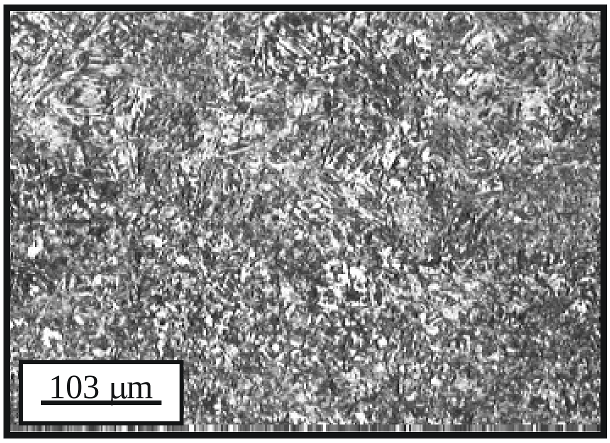

Slika 10. Mikrostruktura prelaza između cementiranog sloja i prelaznog sloja u navaru sa DM EVBCrMo, hemijsko-termički obrađenom

Mikrostruktura cementiranog sloja u navaru sa dodatnim materijalom EVB2CrMo prikazana je na slici 11. Cementirani pa termički obrađeni sloj se odlikuje nešto većom nehomogenošću u odnosu na sloj navaren sa DM EVBCrMo. Osnovni mikrokonstituent u zoni navarenog sloja je otpušteni martenzit. Navareni sloj je svetlo polje, a osnovni materijal (odnosno zona pod uticajem toplote) tamno polje. Na osnovu razlike u stepenu nagrizanja u osnovnom materijalu i navaru može se zaključiti da postoji izraženija razlika u pogledu njihovih hemijskih sastava.

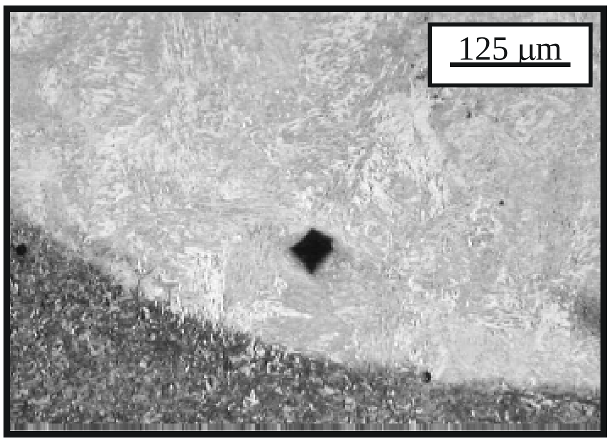

Slika 11. Mikrostruktura prelaza između navara sa DM EVB2CrMo (svetlo polje) i osnovnog materijala (ZUT-a); stanje: navareno + meko žareno + cementirano + termički obrađeno

Na osnovu analize mikrostrukture navara sa dodatnim materijalom Phönix zapaža se da navar poseduje srednje do sitnozrnastu mikrostrukturu.

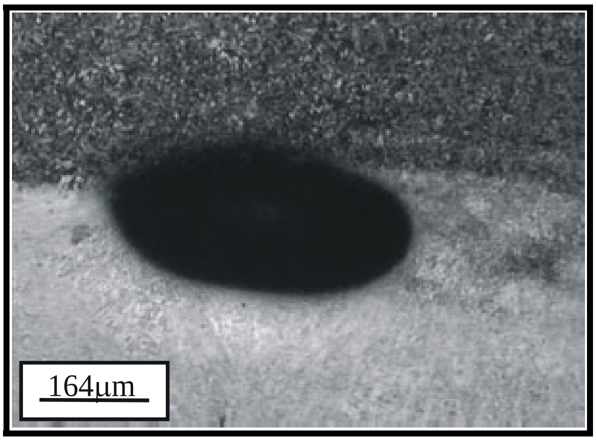

Slika 12. Mikrostruktura prelaza navara sa DM Phönix i ZUT-a sa pojavom gasnog mehura

Na osnovu razlike u stepenu nagrizanja utvrđuje se različitost hemijskih sastava osnovnog i dodatnog materijala. Pored toga, na istoj slici (12) prikazan je i primer pojave pojedinačnog gasnog mehura na liniji spoja osnovni materijal – dodatni materijal.

4. ISPITIVANJA TVRDOĆE I MIKROTVRDOĆE

Veoma bitan pokazatelj otpornosti na habanje regenerisanih uzoraka svakao je tvrdoća radnih površina. Pored površinske i makrotvrdoće neophodno je proveriti i njihovu mikrotvrdoću po preseku. U okviru izrade eksperimentalnog dela ovog rada izvršena su merenja površinske tvrdoće metodom Rokvela.

Površinska tvrdoća je merena na uređaju „Leitz Wetzlar“ metodom Rokvel (HRC) na navarenim blokovima u pet tačaka. Prosečne vrednosti tvrdoće po Rokvelu unošene su u tabelu 5. Zapaža se da najveću tvrdoću imaju novoizrađeni zupci, ali svakako najvažniji zaključak je da se površinska tvrdoća svih navara nalazi u zahtevanim granicama (58±3 HRC).

Tabela 5. Površinska tvrdoća i makrotvrdoća navarenih i novoizrađenih uzoraka

R. br.	Metod regeneracije	Tvrdoća HRC	Makrotvrdoća	
			$HV_{30/15}$	Odgovara HRC
1.	REL navarivanje DM Inox 18/8/6 + EDur 600	57,5	780	63,3
2.	REL navarivanje DM Castolin 2	58	752	62,2
3.	REL navarivanje TIG postupkom DM DUR 600-IG	56,5	775	63,1
4.	REL navarivanje DM UTP 670	55,5	782	63,4
5.	REL navarivanje DM Tooldur	56	792	63,7
6.	REL navarivanje DM EVBCrMo + C + TO	57	775	63,1
7.	REL navarivanje DM EVB2CrMo + C + TO	56	763	62,6
8.	REL navarivanje DM Phönix 120 K/E 425 B/E7018-1+ C + TO	56,5	763	62,6
9.	Novoizrađen (Č4321 + C + TO)	59	763	62,6

5. MODELSKA TRIBOLOŠKA ISPITIVANJA

Na tribološke procese utiču mnogi faktori, koji se uočavaju u kompleksnim međusobnim odnosima i, manje ili više, definišu mehanizme habanja. Mogu se svrstati u pet grupa [10]:

- _Geometrijski faktori_ (odnosno topografija kontaktnih površina), koji se odnose na: makrogeometriju površina u kontaktu, koja definiše da li je kontakt površinski, linijski ili tačkasti; mikrogeometriju kontaktnih površina, određenu preko hrapavosti, valovitosti, linijske i površinske nosivosti; koeficijent neregularnosti profila; deformacije makro i mikro zona kontakta i površinu stvarnog kontakta.
- _Kinematski faktori_, koji su određeni preko karaktera i vrste kretanja, brzine i vremena trajanja kontakta.
- _Dinamički faktori_, definisani preko raspodele i veličine normalnih pritisaka i karaktera i promene opterećenja.
- _Fizičko-hemijski faktori_, koji zavise od vrste materijala od kojih su izrađeni parovi trenja, hemijskog afiniteta kristalne građe materijala kontaktnih parova, vrste oksida nastalih u procesima kovanja osnovnog materijala i njegove regeneracije i vrste maziva primenjenih pri eksploataciji.
- _Energetski faktori_, vezani za temperature mikro zona kontakta, toplotne bilanse u makro i mikro zonama kontakta i slično.

Za tribološka ispitivanja prezentirana u ovom radu usvojen je linijski kontakt između diska i bloka. Da bismo što više približili modelska ispitivanja eksperimentalnim, blokovi su izrađivani sa radijusom zaobljenja koji odgovara radijusu krivine zupca ρ=44 mm, dok je disk prečnika ϕ60 mm. Ovakvi polupričnici nisu slučajno odabrani, već oni odgovaraju radijusima krivina zubaca u kontaktu u određenim trenucima perioda sprezanja, odnosno u početku kontakta i izlasku iz sprege, kada je i najveće klizanje.

Osim toga, mereni su i parametri hrapavosti svakog bloka i diska pre početka i posle ispitivanja, čime je omogućeno da se prati njihov uticaj na koeficijent trenja delova u kontaktu.

Usvojen je polazni linijski kontakt između diska i bloka, koji je nakon elastičnih i plastičnih deformacija elemenata prerastao u površinski. Pri tome je i jedinični kontaktni pritisak od ekstremno velikog, u početku kontakta, pao na nivo merljivog – radnog pritiska.

Realan kontakt zubaca se ostvaruje uz kretanje (praćeno klizanjem) oba zupca – i pogonskog i gonjenog zupčanika. Ovde je zbog tehničkih ograničenja ispitnog uređaja uzeto da se samo jedan uzorak kreće (disk rotira sa brojem obrtaja n=885 o/min), dok drugi (blok) miruje. Praćen je uticaj brzine klizanja (koja je bila konstantna i približna maksimalnoj brzini klizanja zubaca u paru) i vremena trajanja kontakta na promenu koeficijenta trenja, odnosno širinu pojasa habanja.

U procesu sprezanja radni delovi profila zubaca se kotrljaju i klizaju jedan po drugom. Brzine klizanja su najveće u krajnjim tačkama sprezanja, odnosno na početku i kraju perioda sprezanja jednog para zubaca. Klizanja u kinematskom polu nema. Pri prolasku spregnutog para zubaca kroz kinematski pol brzina klizanja menja znak. Maksimalna brzina klizanja spregnutih zubaca konkretnih zupčanika pri eksperimentalnim ispitivanjima na uređaju bila je v_{kl}=2,86 m/s (imala je istu vrednost na početku i kraju perioda sprezanja). Brzina klizanja u tribološkom paru blok-disk pri ovim ispitivanjima bila je v_{kl}=2,93 m/s, što predstavlja odstupanje od oko 2,5%.

Poznato je da koeficijent trenja nema linearnu zavisnost od opterećenja [9] i da pri veoma velikim pritiscima taj koeficijent izrazito raste.

Pri tribološkim ispitivanjima pokušavali smo (i uspevali u priličnoj meri) da normalnu (radnu) silu održavamo konstantnom. Ali, njena vrednost (F_n=250 N) daleko je niža od obimne sile na realnim ispitivanim zupčanicima. Ova normalna sila odgovara normalnoj sili zupčanika koji bi bili ispitivani sa obrtnim momentom od T=32,25 Nm. Potrebno opterećenje se ne može postići na tribometru, što je jedan od bitnih nedostataka modelskih ispitivanja.

Pored toga, zupci u sprezi se kotrljaju uz klizanje jedan po drugom, dok je pri ovim ispitivanjima prisutno samo klizanje, uz činjenicu da je jedan element (blok) nepokretan, a kod zupčaste sprege oba elementa (zupca) se kreću. Sve to predstavlja odstupanje stvarnih uslova sprezanja zubaca zupčanika od modelskih ispitivanja.

Jedan od glavnih zadataka eksperimenata sprovedenih pri izradi ovog rada odnosio se na izbor osnovnog materijala i dodatnih materijala za reparaturno navarivanje spregnutih zubaca. Kako se radi o teškoopterećenim zupčanicima kao materijal za izradu izabran je čelik za cementaciju Č4321. Zahtevala se tvrdoća veća od 55 HRC. Svi diskovi su izrađeni od ovog čelika i imali su zahtevanu tvrdoću. Blokovi, izrađeni od istog materijala, navarivani su na dva principski različita načina (što je ranije opisano). I oni su imali zahtevane tvrdoće.

Tvrdoća je, svakako, jedan od najuticajnijih činilaca što se tiče karakteristika otpornosti na habanje površina u kontaktu. Naime, smatra se da metalne površine veće tvrdoće imaju bolje tribološke karakterisitke. To je i razlog navedenog izbora dodatnih materijala pri reparaturnom navarivanju: dodatni materijali koji daju veliku površinsku tvrdoću i dodatni materijali koji omogućavaju da se njihova tvrdoća odgovarajućom naknadnom termičkom obradom podigne na željeni nivo.

Podmazivanje ima izuzetno važnu ulogu pri tribološkim procesima. Ovde nije analiziran uticaj pojedinih sredstava za podmazivanje na vrednosti koeficijenta trenja, već je za podmazivanje korišćeno isto ulje kao i kod realnih zupčanika (HIPOL B SAE 90). Podmazivanje je izvođeno potapanjem diska u korito sa uljem.

Trenje, posmatrano sa energetskog aspekta, predstavlja proces transformacije mehaničke energije u druge oblike energije (pre svih u toplotnu). Takođe, energetska teorija trenja ukazuje da se spoljašnje trenje ne može razmatrati odvojeno od unutrašnjeg trenja u kontaktnim slojevima [11].

Ispitivanje triboloških karakteristika navarenih blokova i cementiranih diskova izvedeno je na tribometru TPD-93. Disk se obrće ugaonom brzinom ω=92,7 s^{-1}, blok je nepokretan, čvrsto postavljen u posebno konstruisanom nosaču (slika 13). Podmazivanje je izvođeno zahvatanjem određene količine ulja pomoću donjeg dela diska. Podmazivanje je granično. Linijski kontakt se ostvaruje dodirom čeone površine bloka i obimne površine diska.

Blokovi su označeni na sledeći način:

- 1 – blok REL navaren DM Inox 18/8/6 + EDur 600,
- 2 – blok REL navaren DM Castolin 2,
- 3 – blok navaren TIG postupkom DM DUR 600-IG,
- 4 – blok REL navaren DM UTP 670,
- 5 – blok REL navaren DM Tooldur,
- 6 – blok REL navaren DM EVBCrMo, pa cementiran i termički obrađen,

- 7 – blok REL navaren DM EVB2CrMo, pa cementiran i termički obrađen,
- 8 – blok REL navaren DM Phönix 120 K/E 425 B/E7018-1, pa cementiran i termički obrađen,
- 9 – blok cementiran i termički obrađen (bez nanošenja navara).

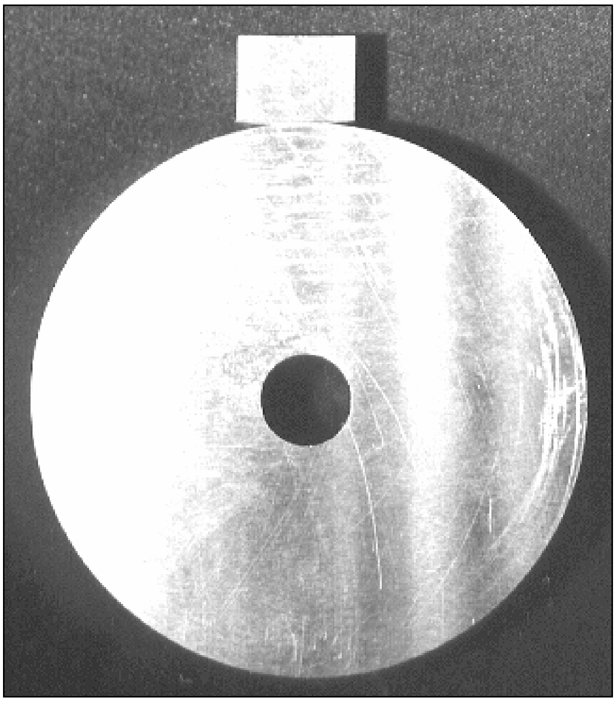

Slika 13. Blok i disk pripremljeni za modelska-tribološka ispitivanja

Diskovi su posle obrade cementirani i termički obrađeni, a nose oznake blokova sa kojima su bili u kontaktu.

Primarni cilj triboloških ispitivanja je određivanje otpornosti na habanje nanetih prevlaka–navara i osnovnog materijala. Zbog toga je ostvarivan kontakt „block on disc“, pri čemu su promenljivi parametri bili ispitivani materijali. Bolje rečeno, interesovali su nas parametri habanja (koeficijenti trenja i širina pojasa habanja) blokova reparaturno navarenih različitim vrstama dodatnog materijala. Iz tih razloga kao nepromenljivi faktori pri tribološkim ispitivanjima uzeti su:

- sila kontakta: F=250 N,
- brzina klizanja: v=2,93 m/s,
- podmazivanje: granično (ulje HIPOL B SAE 90),
- vreme kontakta: t=30 min.

Istovremeno, varirani su sledeći tehnološki parametri:

- vrsta dodatnog materijala,
- tehnološki postupak izrade (navarivanje pre ili posle termičke obrade),
- režimi termičke obrade.

Na osnovu sprovedenih triboloških ispitivanja određivani su srednji koeficijenti trenja (μ_{sr}), čije vrednosti su date u tabeli 6 i na dijagramu prikazanom na slici 14. Najzad je određena topografija površina ispitivanih blokova merenjem pojasa pohabanosti. Širina pojasa habanja merena je na univerzalnom mikroskopu UIM-21, a rezultati su prikazani u tabeli 6 i na dijagramu na slici 15.

Tabela 6. Koeficijenti trenja (μ_{sr}) i širine pojasa habanja za različite dodatne materijale

Disk		Blok			Koeficijent trenja μ_{sr}	Širina pojasa habanja (mm)
Materijal	Tvrdoća HRC	Oz-naka	Dodatni materijal	Postupak navarivanja		
Č4321	55-58	1	Inox 18/8/6 + EDUR 600	SMAW (111)	0,064	0,960
		2	Castolin 2	SMAW (111)	0,115	1,028
		3	DUR 600-IG	GTAW (TIG) (141)	0,100	1,020
		4	UTP 670	SMAW (111)	0,090	0,955
		5	Tooldur	SMAW (111)	0,072	1,118
		6	EVBCrMo	SMAW (111)	0,110	1,130
		7	EVB2CrMo	SMAW (111)	0,106	1,198
		8	Phönix 120 K/E 425 B/E7018-1	SMAW (111)	0,108	1,200
		9	Č4321	/	0,077	0,751

Analizirajući rezultate određivanja koeficijenta trenja navedenih dodatnih materijala može se zaključiti da se navarivanjem kombinacijom dodatnih materijala Inox 18/8/6 + EDUR 600 dobijaju najniže vrednosti koeficijenta trenja. Pored ovog dodatnog materijala i navar izveden DM Tooldur daje manji koeficijent trenja nego cementirani i kaljeni blokovi (naravno, svi su u kontaktu sa cementiranim i kaljenim diskovima od Č4321). Najveće koeficijente trenja daju blokovi navareni DM Castolin 2, a potom navari „mekim“ dodatnim materijalima (EVBCrMo, Phönix 120 K/E 425 B/E7018-1 i EVB2CrMo), koji su potom cementirani i termički obrađeni.

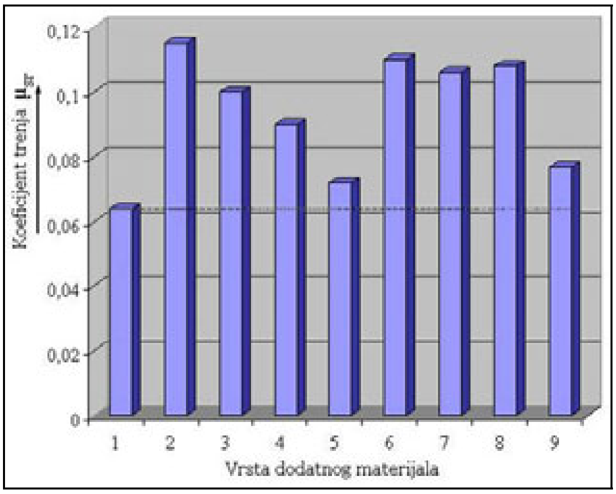

Slika 14. Uporedne vrednosti srednjeg koeficijenta trenja različitih dodatnih materijala

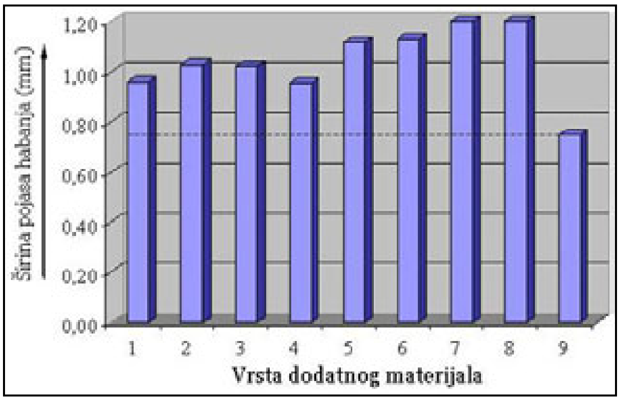

Slika 15. Uporedne vrednosti širine pojasa habanja različitih dodatnih materijala

Što se tiče veličine pojasa habanja (što je od izuzetnog značaja) daleko najmanju širinu pohabanosti imaju cementirani i kaljeni blokovi. Od navarenih blokova najbolje su se pokazali navari UTP 670 i Inox 18/8/6 + EDUR 600. I sa ovog aspekta najslabiji su navari „mekim“ dodatnim materijalima Phönix 120 K/E 425 B/E7018-1 i EVB2CrMo.

Pri izboru načina navarivanja zubaca opredelilo nas je to što je najveća širina pohabanosti od „tvrdih“ DM bila kod navara elektrodom Tooldur, dok je kod „mekih“ DM najslabiji navar bio sa dodatnim materijalom Phönix 120 K/E 425 B/E7018-1. To je i osnovni razlog zašto za navarivanje zubaca zupčanika ove dve vrste dodatnih materijala nisu korišćene.

6. ZAKLJUČAK

Na osnovu sprovedenih triboloških ispitivanja (modelskih ispitivanja na tribometru) došlo se do zaključka da je sa aspekta otpornosti na habanje (najmanje širine traga habanja) najpovoljniji osnovni materijal (Č4321), a potom navar sa dodatnim materijalom UTP 670. Sa energetskog aspekta (minimalnog koeficijenta trenja) navari sa dodatnim materijalom Inox 18/8/6 + EDur 600 i DM Tooldur su povoljniji čak i od osnovnog materijala.

Na bazi analize svih mikrostruktura može se pretpostaviti da:

- u pogledu otpornosti na habanje bolje rezultate trebalo bi očekivati kod navara ostvarenih „tvrdim“ dodatnim materijalima i novoizrađenih uzoraka,
- sa stanovišta otpornosti na lom najbolje karakteristike trebalo bi da imaju novoizrađeni uzorci.

Metalografskom analizom u navarenim slojevima i ZUT-u nisu otkrivene tople ili hladne prsline, nastale kao posledica navarivanja i prateće termičke obrade. Pored toga, nije zapaženo ni prisustvo neprovara, uključaka troske i slično. Utvrđeno je kod nekih navarenih uzoraka prisustvo pojedinačnih gasnih pora u zoni spoja navara sa osnovnim materijalom, što ne može izrazitije uticati na eksploataciono ponašanje ovih slojeva.

LITERATURA

[1] Josifović D., Marković S.: Diagnostics and Regeneration of the Wear Damaged Teeth Gears, First World Tribology Congress, London, 1997.

[2] Marković S., Josifović D.: Regeneracija zupčanika, monografija, Jugoslovensko društvo za tribologiju, Kragujevac, 1998.

[3] Marković S.: Uticaj vrste navarivanja na radne karakteristike regenerisanih zupčanika, doktorska disertacija, Mašinski fakultet, Kragujevac, 2003.

[4] Marković S.: Tribological characteristics of gears reparatorily hardfaced wit „hard“ and „soft“ additional materials, Proceedings 11th International Research/Expert Conference „Trends in the Development of Machinery and Associated Technology“ TMT 2007, Hammamet, Tunisia, 5÷9. September 2007.

[5] Marković S., Josifović D.: Comparative characteristics of gear teeth regenerated by hard facing, Tribologia – teoria i praktyka, rok XXXIX, nr 1/2008 (217), „Simpress“, Warszawa, Polska.

[6] Marković S., Josifović D.: Determination of specific tribological and mechanical characteristics of the gear teeth subjected to reparatory hard facing with „hard“ and „soft“ additional materials, 13th Nordic Symposium on Tribology, NORDTRIB 2008, Proceedings, Tampere, Finland, 10÷13 June 2008.

[7] Marković S.: The influence of hereditary characteristics on tribological properties by hard facing of the regenerated gear teeth, 9th International Conference „Research and Development in Mechanical Industry“ RaDMI 2009, Proceedings, Vrnjačka Banja, Serbia, 16÷19. September 2009, p. 269÷276.

[8] Marković S., Josifović D., Tanasijević S., Jovičić S.: Comparative parameters of the teeth roots strength of the gears regenerated by two different methods, Proceedings of the 3rd International

Conference Power Transmissions ´09, 1÷2. October 2009, Kallithea–Chalkidiki, Greece, p. 589÷594.

[9] Ortmann R., Nestler S.: Werkstoffe zum Verschleiβschutz, Thyssen Edelst. Techn. Ber. 14, Band 1988, Heft 2.

[10] Forrest P. G.: Fatigue of metals, Pergamon press, Oxford-London-New York-Paris, 1962.

[11] Winter H.: Die wesentlichen Einfluesse auf die Tragfaehigkeit von Zahnradgetrieben, Dresden, 1983.

TECHNOLOGICAL HERITAGE OF THE TRIBO-MECHANICAL SYSTEMS REGENERATED BY WELDING

Abstract: *In the tribology research and mechanical engineering there has been a growing interest for technological heritage analysis and examination of its links with the exploitation properties of mechanical parts and systems. Various studies show that the life expectancy of machine systems is determined even in the design stage. However, there is no doubt that there is great impact of technology and processing parameters on the tribological properties of treated surfaces of the tribo-mechanical systems. The phenomenon of the so-called technological inheritance resulting from the operations of the cutting treatments or distortions shows the influence on the tribological relevant parameters of the processed surfaces. All those conclusions are reached when it comes to the development of new mechanical components. But technological heritage has a much greater influence on the tribological characteristics and a lifetime of the regenerated area than is the case with new constructions. The main objective of the model testing presented in this paper is the comparison of tribological properties of coatings sprayed in the regeneration process of surfacing and base materials, which are obtained in the same working conditions as similar as possible to the exploitation conditions of gears.*

Keywords: *regeneration, surfacing, the tribo-mechanical systems, technological heritage, microstructure, tribological tests.*

ACKNOWLEDGMENT

This work has been performed within the project TR 35011. This project is supported by the Republic of Serbia, Ministry of Science and Technological Development, which financial help is gratefully acknowledged.

Authors Index

tribology in industry

Journal of Serbian Tribology Society
Mechanical Engineering Faculty
University of Kragujevac

Tribology in industry - 32 Years With You

Tribology in industry is the official journal of the Serbian Tribology Society. First issue of the Journal dates back to 1979 when The Council of Faculty of Mechanical Engineering in Kragujevac brought a decision to start publishing the Journal. At the beginning the Journal was just on Serbian language but since 1996 it is published on English language, as well.

Tribology in industry publishes experimental and theoretical papers on all aspects of the science of friction, wear and lubrication.

Subjects:

• Friction • Wear • Lubricants • Surface characterization • Surface engineering
• Nanotribology • Contact mechanics • Wear resistant materials • Coatings • Alloys
• Composites • Tribology of friction pairs • Bearings • Tribological design • Biotribology

The Journal tribology in industry all these years was, and still is, the only scientific Journal, from the area of Tribology, in Serbia and on wider former Yugoslavian spaces.

More information about the Journal and download of the full papers, from all the issues, could be found at the official web page of the Journal:

www.tribology.mfkg.kg.ac.rs

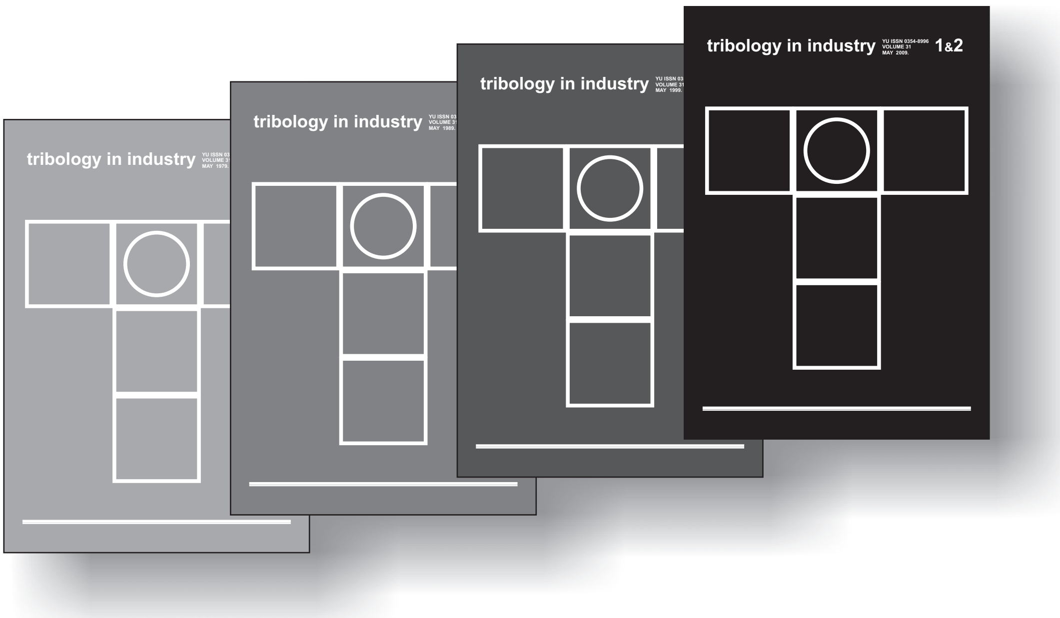

Serbian Tribology Society

SERBIATRIB '11

Faculty of Mechanical Engineering
University of Kragujevac

SERBIATRIB '11

12th International Conference on Tribology

11 – 13 May, 2011, Kragujevac, Serbia

PROTECTIVE LAYER IN CARPET EXHIBITION

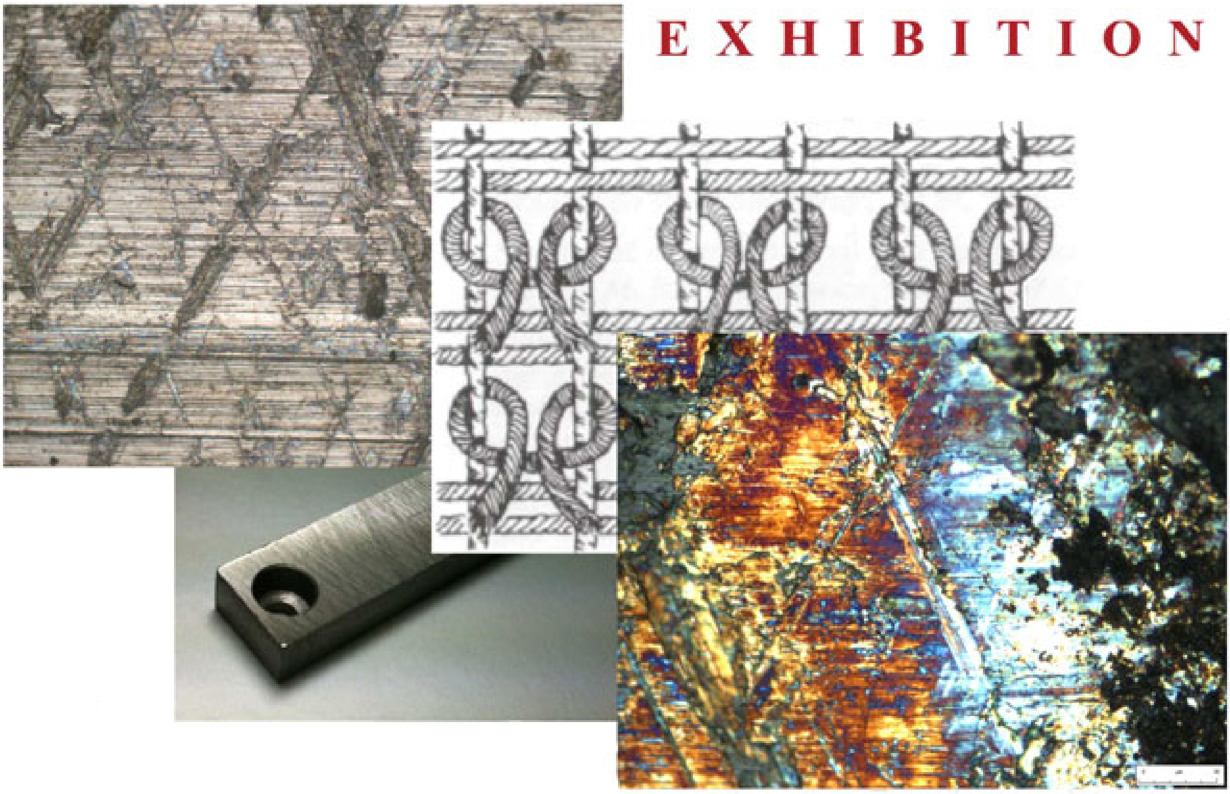

Lecturer Zeynep ÇAVDAR KALELİ*

*SAKARYA UNIVERSITY
FINE ARTS FACULTY
TRADITIONAL TURKISH HAND ART DEPARTMENT
SAKARYA / TURKEY

Nano & Micro Indenters

up to 500mN or upto 20N

- Hardness
- Modulus
- Modulus vs Depth
- Hardness vs Depth
- Dynamic Indentation
- Matrix of Indents

Nano Tribometer

from μN, -25 to 1100° C

- Ball/pin on disk
- Multiple in-situ sensors
- Nano and Micro tribology
- Depth resolution in nm range
- Rotary and reciprocating wear
- Tribo-corrosion

Scratch tester

up to 500mN or upto 20, 200N

- Scratch test
- Linear Wear
- Scratch adhesion
- Scratch hardness
- Coating delamination
- Scratch-corrosion

Heavy Duty Tribometer

up to 1200 N, -25 to 1100° C

- Block on ring
- Ball/pin on disk
- Multiple In-situ sensors
- Tribo- corrosion module
- Four ball and cross cylinder
- Fretting and linear reciprocating

1717 Dell Avenue, Campbell, CA 95008 info@cetr.com
WORLD LEADERS IN MECHANICAL AND TRIBOLOGY TEST INSTRUMENTATION, WWW.CETR.COM

SERBIATRIB '11